

OTTAWA • CANADA  
**icpeac**  
**2023**

## Book of Abstracts

XXXIII International Conference on Photonic, Electronic  
and Atomic Collisions

July 25 - August 1, 2023, Ottawa, Canada

# Preface

This Book of Abstracts is a compilation of all contributions accepted and scheduled for poster presentations at the XXXIII International Conference on Photonic, Electronic and Atomic Collisions, held in Ottawa, Ontario from July 25 to August 1, 2023 (ICPEAC 2023). All abstracts submitted by March 19, 2023 were reviewed by the ICPEAC General Committee. Post-deadline abstracts were reviewed by the Local Organizing Committee of ICPEAC 2023. All abstracts included in this volume are also listed in the Conference Program distributed to ICPEAC 2023 participants and available online. Those abstracts listed there but absent here were withdrawn by the authors after the Conference Program went into print. The contributions included here are scheduled for presentation in four poster sessions throughout the conference, as indicated by their identifiers. Those whose titles are marked by a star were selected for oral Special Reports.

As a new element, in addition to purely scientific abstracts we invited “In Memoriam” abstracts meant to pay tribute to colleagues who passed away since we last met in person in 2019 and the ICPEAC-related physics they championed and helped move forward. Four such abstracts were received. Together with nine abstracts from authors based in Ukraine they form the special section **Absent Friends** (AF001 – AF013). These abstracts are included here as well, and the posters are on display throughout the conference.

We take this opportunity to express our gratitude to our partners, exhibitors, and friends and, most importantly, to all participants for their support of and contributions to ICPEAC 2023.

## Tom Kirchner

Chair of the Local Organizing Committee



## André Staudte

Co-Chair



## François Légaré

Co-Chair





# Sponsors

We thank our Partners, Exhibitors and Friends for generously supporting ICPEAC 2023!

## Partners



## Exhibitors



## Friends of ICPEAC



# Committees

## Executive Committee

**Friedrich Aumayr** Austria  
Chair

**Emma Sokell** Ireland  
Secretary

**Stefan Schippers** Germany  
Treasurer

**Kiyoshi Ueda** Japan  
Past Chair

**Dajun Ding** China  
Vice Chair

**Dominique Vernhet** France  
Past LOC Chair (ICPEAC 2019)

**Olivier Dulieu** France  
Past LOC Co-Chair (ICPEAC 2019)

**Lamri Adoui** France  
Past LOC Co-Chair (ICPEAC 2019)

**Tom Kirchner** Canada  
LOC Chair

**André Staudte** Canada  
LOC Co-Chair

**Michael Meyer** Germany  
LOC Co-Chair (ICPEAC 2027)

**Robin Santra** Germany  
LOC Co-Chair (ICPEAC 2027)

**Toshiyuki Azuma** Japan  
LOC Chair (ICPEAC 2025)

**Kenichi Ishikawa** Japan  
LOC Co-Chair (ICPEAC 2025)

**Masahiko Takahashi** Japan  
LOC Co-Chair (ICPEAC 2025)

**Jimena Gorfinkel** UK  
Member

**Till Jahnke** Germany  
Past NLOC Chair (VICPEAC 2021)

**Ann Orel** USA  
Member

**James Sullivan** Australia  
Member

## Local Organizing Committee

**Tom Kirchner** York University  
Chair

**André Staudte** NRC Canada/University of  
Ottawa  
Co-Chair

**François Légaré** INRS  
Co-Chair

**Ravi Bhardwaj** University of Ottawa  
Member

**Thomas Brabec** University of Ottawa  
Member

**Paul Corkum** University of Ottawa  
Member

**Daniel Fischer** Missouri S&T  
Member

**T.J. Hammond** University of Windsor  
Member

**Allison Harris** Illinois State University  
Member

**Marko Horbatsch** York University  
Member

**Heide Ibrahim** INRS  
Member

**Chitra Rangan** University of Windsor  
Member

**Joseph Thywissen** University of Toronto  
Member

**David Villeneuve** University of Ottawa  
Member

**Amar Vutha** University of Toronto  
Member

**Zong-Chao Yan** University of New Brunswick  
Member

## General Committee

**Diego Arbó** Argentina  
**Dariusz Banas** Poland  
**Sadia Bari** Germany  
**Iva Brezinova** Austria  
**Paola Bolognesi** Italy  
**Michael Bromley** Australia  
**Romarly Costa** Brazil  
**Xiangjun Chen** China  
**Jan Marcus Dahlström** Sweden  
**Alicja Domaracka** France  
**Nirit Dudovich** Israel  
**Ilya Fabrikant** USA  
**Juraj Fedor** Czech Republic  
**Gleb Gribakin** UK  
**Rosario González-Férez** Spain  
**Elena Gryzlova** Russia  
**Alexandre Gumberidze** Germany  
**Yasushi Kino** Japan  
**Holger Kreckel** Germany  
**Edwin Kukk** Finland  
**Allen Landers** USA  
**Heather Lewandowski** USA  
**Chetan Limbachiya** India  
**Igor Litvinyuk** Australia  
**Philippe Martin** France  
**Takashi Mukaiyama** Japan  
**Nobuyuki Nakamura** Japan  
**Antonio Picon** Spain  
**Francoise Remacle** Belgium  
**Daniel Rolles** USA  
**Henning Schmidt** Sweden  
**Thomas Schlathöler** Netherlands  
**Lucas Sigaud** Brazil  
**Olga Smirnova** Germany  
**Lokesh Tribedi** India  
**Katalin Varju** Hungary  
**Oleg Vasyutinskii** Russia  
**Zong-Chao Yan** Canada  
**Jianmin Yuan** China  
**Shaofeng Zhang** China

# Posters

## Schedule

Topics	Wed, July 26	Thu, July 27	Fri, July 28	Mon, July 31
Absent Friends	AF001 – AF013	AF001 – AF013	AF001 – AF013	AF001 – AF013
Photon Atom/Ion	We001 – We027	Th001 – Th025	Fr001 – Fr025	Mo001 – Mo025
Photon Molecule/Cluster	We028 – We055	Th026 – Th053	Fr026 – Fr054	Mo026 – Mo053
Photon Surface/Solid	We056 – We065			Mo054 – Mo064
Photon Other			Fr055 – Fr066	
Lepton Atom/Ion	We066 – We082	Th054 – Th070	Fr067 – Fr082	
Lepton Molecule/Cluster	We083 – We098	Th071 – Th086	Fr083 – Fr098	Mo065 – Mo080
Lepton Surface/Solid				Mo081 – Mo085
Heavy Atom/Ion	We099 – We109	Th087 – Th098		Mo086 – Mo096
Heavy Molecule/Cluster	We110 – We120	Th099 – Th109	Fr099 – Fr109	Mo097 – Mo106
Heavy Surface/Solid			Fr110 – Fr127	
Low-Energy to Ultracold		Th110 – Th127		Mo107 – Mo122
Structure & Spectroscopy	We121 – We133	Th128 – Th132	Fr128 – Fr135	
Experimental Developments				Mo123 – Mo132
Post Deadline	We134 – We141	Th133 – Th143	Fr136 – Fr140	Mo133 – Mo142

# Posters

## Absent Friends

### a. Posters from Ukraine

- [AF001](#) **Electron-impact ionization of the 5p<sup>6</sup> subshell in barium** • Oleksandr Borovik
- [AF002](#) **Photoluminescence of L-valine irradiated with 12.5 MeV electrons** • Yu. Bandurin, A. Zaviropulo, V. Maslyuk, N. Svatiuk
- [AF003](#) **Investigation of photoluminescence of glucose and fructose in the powder form** • Yu. Bandurin, A. Zaviropulo, V. Maslyuk, N. Svatiuk
- [AF004](#) **Studies of the VUV luminescence excited by electron impact on the gas-phase glycine and alanine** • H. Bohachov, R. Tymchyk
- [AF005](#) **The near-threshold electron-impact resonance excitation of the In<sup>+</sup> ion** • A. N. Gomonaj, V. Jonauskas, S. Kučas, V. Roman, A. I. Gomonai, Yu. Hutysh, V. Zvenihorodsky
- [AF006](#) **Ramsauer-Townsend minima in the low-energy integral cross sections of elastic electron scattering by Sb, Xe and Bi, Rn atoms** • V. I. Kelemen, E. Yu. Remeta
- [AF007](#) **High-energy critical minima in differential cross sections of elastic electron scattering by Sb, Xe and Bi, Rn atoms** • V. I. Kelemen, E. Yu. Remeta
- [AF008](#) **Elastic and charge transfer cross sections for low energy H<sup>+</sup> + H collisions: Quantal and semiclassical calculations** • Mykhaylo V. Khoma
- [AF009](#) **Ionization of outer shells in the K atom by electron impact** • V. Roman

### b. In Memoriam

- [AF010](#) **Electron Atom/Molecule Scattering and its Applications: A Tribute to Michael Brunger** • Stephen Buckman, Oddur Ingólfsson, Dragana Maric, Ronald White
- [AF011](#) **Electron Swarms as a Bridge Between Atom/Molecule Collisions and Gas Discharges: A Tribute to Robert W. Crompton** • Zoran Petrović, Stephen Buckman
- [AF012](#) **Multiphoton ionization and detachment of atoms and negative ions: A tribute to Anthony F. Starace** • Jean Marcel Ngoko Djiokap, Ilya I. Fabrikant
- [AF013](#) **In memoriam of past ICPEAC chairs and stalwarts** • Emma Sokell

# Posters

Wednesday, July 26

Photon – Atom/Ion

- [We001](#) **Inner-shell ionization of low-charged silicon and iron ions** • Stefan Schippers, Alfred Müller, Simon Reinwardt, Michael Martins, Stephan Fritzsche for the PIPE collaboration
- [We002](#) **Relativistic and correlation effects in np photoionization Cooper minima of high-Z atoms** • S. Baral, J. Jose, P. C. Deshmukh, S. T. Manson
- [We003](#) **Angular distribution, spin polarisation and time delay studies of the potassium 4s orbital in the vicinity of Cooper minimum** • Nishita M. Hosea, Pranawa C. Deshmukh, Jobin Jose, Hari Varma Ravi, Steven T. Manson
- [We004](#) **New source for tuning the effective Rabi frequency in multiphoton ionization** • Dongdong Zhang, Wankai Li, Yue Lei, Xing Li, Tao Yang, Mei Du, Ying Jiang, Jialong Li, Aihua Liu, Lanhai He, Pan Ma, Sizuo Luo, Dajun Ding
- [We005](#) **Non-classical properties of light after strong-laser field processes in atomic and solid-state systems\*** • Javier Rivera Dean, Philipp Stammer, Andrew S. Maxwell, Theocharis Lamprou, Andrés F. Ordóñez, Emilio Pisanty, Paraskevas Tzallas, Maciej Lewenstein and Marcelo F. Ciappina
- [We007](#) **Lorentz-force shifts in strong-field ionization with mid-IR laser fields** • Stephan Fritzsche, Birger Böning, Danish F. Dar
- [We008](#) **An atomic magnetometer to detect the oscillating magnetic field based on twisted light atom interaction** • S. Ramakrishna, R.P. Schmidt, A.A. Peshkov, A. Surzhykov, S. Fritzsche
- [We009](#) **Time-resolved Kapitza-Dirac effect** • Kang Lin, Maksim Kunitski, Sebastian Eckart, Alexander Hartung, Qinying Ji, Lothar Ph. H. Schmidt, Markus S. Schöffler, Till Jahnke, Reinhard Dörner
- [We010](#) **Pulse length effects in long wavelength driven non-sequential double ionization** • H. Jiang, M. Mandrysz, A. Sanchez, J. Dura, T. Steinle, J. S. Prauzner-Bechcicki, J. Zakrzewski, M. Lewenstein, F. He, J. Biegert, M. F. Ciappina

# Posters

Wednesday, July 26

Photon – Atom/Ion

- [We011](#) **Ultrafast excitation dynamics for noble gas atoms subject to intense femtosecond laser fields** • S. P. Xu, M. Q. Liu, W. Quan, W. Becker, J. Chen, X. J. Liu
- [We012](#) **Visualization of a complex electron wavefunction in momentum space using an attosecond pulse** • Hiromichi Niikura, Takashi Nakajima, Tasuku Shinoda, D. M. Villeneuve
- [We013](#) **First commissioning results of the AMO endstation at the Shanghai soft X-ray free-electron laser facility** • Ruichao Dong, Xincheng Wang, Yuliang Guo, Jinze Feng, Mingjie Zhang, Hailong Guo, Yuhai Jiang
- [We014](#) **PCI effects following 2p double ionization of argon atoms** • Laura Sommerlad, Sven Grundmann, Florian Trinter, Max Kircher, Andreas Pier, Dennis McGinnis, Leon Kaiser, Jan Kruse, Angelina Geyer, Nils Anders, Niklas Melzer, Till Jahnke, Reinhard Dörner
- [We015](#) **Gauge-invariant absorption of light by coherent superposition states** • Axel Stenquist, Felipe Zapata, Marcus Dahlström
- [We016](#) **Few-photon single ionization of cooled rubidium in the over-the-barrier regime** • H. Y. Ma, X. Wang, L. X. Zhang, Z. H. Zou, J. Y. Yuan, Y. X. Ma, R. J. Lv, Z. J. Shen, T. M. Yan, M. Weidemüller, D. F. Ye, Y. H. Jiang
- [We017](#) **Carrier-Envelope-Phase Effects for Multiphoton and Tunnel Excitation of Argon** • D. Chetty, R.D. Glover, X.M. Tong, B.A. deHarak, H. Xu, N. Haram. K. Bartschat, A.J. Palmer, A.N. Luiten, P.S. Light, I.V. Litvinyuk, R. T. Sang
- [We018](#) **Attosecond time delay during resonance-enhanced multiphoton ionization of noble gases in strong laser fields** • Lanhai He, Xing Li, Xuanhong Gao, Sizuo Luo, Song-Feng Zhao, Dajun Ding
- [We020](#) **Rescattering sequential multiple ionization of cold Rb** • Z. H. Zou, J. Y. Yuan, X. C. Wang, H. Y. Ma, M. Weidemüller, Y. H. Jiang
- [We021](#) **Autoionization of two-electron-excited  $^{88}\text{Sr } 5p_{1/2} n\ell_j$  states** • S. Yoshida, J. Burgdörfer, R. Brienza, G. Fields, F. B. Dunning

# Posters

Wednesday, July 26

Photon – Atom/Ion

- [We022](#) **Ion and Electron Momentum Distributions from Single and Double Ionization of Helium Induced by Compton Scattering** • M. Kircher, L. Sommerlad, F. Trinter, S. Grundmann, G. Kastirke, M. Weller, I. Vela-Pérez, A. Khan, C. Janke, M. Waitz, S. Zeller, T. Mletzko, D. Kirchner, V. Honkimäki, S. Houamer, O. Chuluunbaatar, Y. V. Popov, I. P. Volobuev, M. S. Schöffler, L. Ph. H. Schmidt, T. Jahnke, R. Dörner
- [We023](#) **Progress on a new toroidal spectrometer to measure multiple-path interference from Rb excited and ionized by laser radiation** • Joshua Rogers, Michele Siggel-King, Andrew Murray
- [We024](#) **Unexpected pathway to double-core-hole states in atoms and molecules** • Iyas Ismail
- [We025](#) **Polarization Dependence of Laser Induced recollision and inner-shell excitations** • Yunpei Deng, Zhinan Zeng, Pavel Komm, Yinghui Zheng, Wolfram Helml, Xinhua Xie, Zoltan Filus, Mathieu Dumergue, Roland Flender, Máté Kurucz, Ludovit Haizer, Balint Kiss, Subhendu Kahaly, Ruxin Li, Gilad Marcus
- [We026](#) **Atomic phase delays in  $w - 2w$  above-threshold ionization** • Sebastián López, Joachim Burgdörfer, Diego Arbó
- [We027](#) **Novel semiclassical model for accurate spectra and nondipole effects in multielectron ionization of strongly driven atoms** • Georgios Katsoulis, Matthew Peters, Agapi Emmanouilidou

Photon – Molecule/Cluster

- [We028](#) **Photoionization dynamical parameter for the radicals using B-spline R-matrix method** • Kedong Wang
- [We029](#) **Laser-induced electron diffraction in chiral molecules** • Debobrata Rajak, Sandra Beauvarlet, Omer Kneller, Antoine Comby, Raluca Cireasa, Dominique Descamps, Baptiste Fabre, Jimena D. Gorfinkiel, Julien Higuët, Stéphane Petit, Shaked Rozen, Hartmut Ruf, Nicolas Thiré, Valérie Blanchet, Nirit Dudovich, Bernard Pons, Yann Mairesse
- [We030](#) **Attosecond Delays in Vibrationally Resolved Dissociation of Molecules** • Peipei Ge, Chenxi Hu, Feng He, Yunquan Liu



# Posters

Wednesday, July 26

Photon – Molecule/Cluster

- [We031](#) **Ultraviolet Pump-Probe Photodissociation Spectroscopy of Electron-Rotation Coupling in Diatomics** • Y. R. Liu, V. Kimberg, Y. Wu, J. G. Wang, O. Vendrell and S. B. Zhang
- [We032](#) **Shone and driven, they cool down in femtoseconds but scoot off in attoseconds** • Maia Magrakvelidze, Mohamed Madjet, Esam Ali, Ruma De, Himadri Chakraborty
- [We033](#) **Intensity dependence of the double ionization dissociation of argon dimers in the fields of femtosecond laser pulses** • Pan Song, Xiaowei Wang, Dongwen Zhang, Zengxiu Zhao, Jianmin Yuan
- [We034](#) **Time-Resolved Dynamics on the Giant Plasmon Resonance of C<sub>60</sub>** • Aaron Laforge, D. Mishra, R. Obaid, S. Pathak, F. Trost, H. Lindenblatt, S. Meister, P. Rosenberger, R. Michiels, E. Kukk, S. Biswas, K. Saraswathula, F. Stienkemeier, D. Rolles, F. Calegari, M. Braune, M. Mudrich, M. Kling, T. Pfeifer, U. Saalman, J. -M. Rost, R. Moshhammer, N. Berrah
- [We035](#) **Ultrafast non-adiabatic relaxation of C<sub>60</sub>: In search of efficient MD model** • Ruma De, E. Ali, M. B. Wholey, M. E. Madjet, H. S. Chakraborty
- [We036](#) **Photodissociation of halogen-substituted nitroimidazole radiosensitizers – A pathway towards new radiosensitizer drugs?** • Lassi Pihlava, Marta Berholts, Johannes Niskanen, Anton Vladyka, Kuno Kooser, Christian Stråhlman, Per Eng-Johnsson, Antti Kivimäki, Edwin Kukk
- [We037](#) **Double ionization of S<sub>2</sub>** • Emelie Olsson
- [We038](#) **Intermolecular coulombic decay in an unbound substituted benzene** • Nihar Behera, Saroj Barik, Saurav Dutta, G. Aravind
- [We039](#) **Photoexcited Polycyclic Aromatic Hydrocarbon undergoes Intermolecular Coulombic Decay\*** • Saurav Dutta, Nihar Ranjan Behera, Saroj Barik, G. Aravind

# Posters

Wednesday, July 26

Photon – Molecule/Cluster

- [We040](#) **Time-resolving molecular tunneling dynamics with Free-Electron-Laser-pump and High-Harmonics-Generated-probe transient absorption spectroscopy\***  
• Alexander Magunia, Marc Rebholz, Elisa Appi, Christina Papadopoulou, Thomas Ding, Michael Straub, Gergana Borisova, Florian Trost, Severin Meister, Hannes Lindenblatt, Rui Jin, Juhee Lee, Alexander von der Dellen, Christian Kaiser, Markus Braune, Stefan Düsterer, Skirmantas Ališauskas, Tino Lang, Christoph Heyl, Bastian Manschwetus, Sören Grunewald, Ulrike Frühling, Ayhan Tajalli, Ammar Bin Wahid, Laura Silletti, Francesca Calegari, Uwe Thumm, Uwe Morgner, Milutin Kovacev, Ingmar Hartl, Rolf Treusch, Robert Moshhammer, Christian Ott, Thomas Pfeifer
- [We041](#) **A study of the valence photoelectron spectrum of uracil and mixed water-uracil clusters** • Giuseppe Mattioli, Lorenzo Avaldi, Paola Bolognesi, Anna Rita Casavola, Filippo Morini, Thomas Van Caekenberghe, John D. Bozek, Mattea C. Castrovilli, Jacopo Chiarinelli, Alicja Domaracka, Suvasthika Indrajith, Sylvain Maclot, Aleksandar R. Milosavljević, Chiara Nico-lafrancesco, Christophe Nicolas, Patrick Rousseau
- [We042](#) **Femtosecond timed imaging of rotation and vibration of alkali dimers on the surface of helium nanodroplets** • Henrik Høj Kristensen, Lorenz Kranabetter, Nicolaj Jyde, Constant Schouder, Henrik Stapelfeldt
- [We043](#) **Fragmentation and dynamics of protonated reserpine induced by femtosecond laser excitation** • Richard Brédy, Marius Hervé, Alexie Boyer, Abdul Rahman Allouche, Isabelle Compagnon, Franck Lépine
- [We044](#) **Scaling law on the x-ray induced nonadiabatic transition in aromatic molecules**  
• Kaoru Yamazaki, Katsumi Midorikawa
- [We045](#) **The role of non-local processes in the decay of X-ray induced electronic inner-shell vacancies in weakly bound systems** • Andreas Hans
- [We046](#) **Aromatic cyclo-dipeptides in the gas-phase: photoemission and state-selected fragmentation** • Laura Carlini, Elena Molteni, Paola Bolognesi, Davide Sangalli, Giuseppe Mattioli, Paola Alippi, Annarita Casavola, Manjot Singh, Carlo Altucci, Mohammadhassan Valadan, Mauro Nisoli, Yingxuan Wu, Federico Vismarra, Rocio Borrego Varillas, Robert Richter, Jacopo Chiarinelli, Mattea Carmen Castrovilli, Lorenzo Avaldi
- [We047](#) **NIR-induced fragmentation of VUV-generated molecular cations** • Rico Mayro Tanyag, Flora Aleksandra Kappel Hübschmann, Jan Thøgersen, Henrik Stapelfeldt

# Posters

## Wednesday, July 26

### Photon – Molecule/Cluster

- [We048](#) **Photoionization of polyatomic molecules with ASTRA: a scalable wave-function approach** • Carlos Marante, Juan M Randazzo, Barry I. Schneider, Jeppe Olsen, Luca Argenti
- [We049](#) **Exploring Electron-Nuclear Entangled Dynamics in Hydrogen Molecular Ions using Quantum Computer\*** • Chihiro Osaku, Yuki Orimo, Kenichi L Ishikawa, Yukio Kawashima, Tanvi Gujarati, Takeshi Sato
- [We050](#) **Photoionisation, Rayleigh, and Raman scattering cross sections for the ground and excited vibrational levels of  $H_2^+$**  • Adam Singor, Liam Scarlett, Igor Bray, Dmitry Fursa
- [We051](#) **Attosecond delays of high harmonic emissions from isotopes of molecular hydrogen measured by Gouy phase XUV interferometer** • Mumta Mustary, Liang Xu, Wanyang Wu, Nida Haram, Han Xu, Feng He, Robert Sang, Igor Litvinyuk
- [We052](#) **Experimental determination of thermal electron detachment rates of  $C_7^-$**  • Shimpei Iida, Susumu Kuma, Kei Masuhara, Shouta Masuda, Hajime Tanuma, Klavs Hansen, Haruo Shiromaru, Toshiyuki Azuma
- [We053](#) **Higher multipolar terms on core-level photoemission time delay of homonuclear diatomic molecules** • Yoshiaki Tamura, Kaoru Yamazaki, Kiyoshi Ueda, Keisuke Hatada
- [We054](#) **Dissociation of methanol molecules excited by XFEL studied with molecular frame photoelectron diffraction** • Soki Goto, Manabu Kanno, Hao Xue, Naoki Kishimoto, Fukiko Ota, Keisuke Hatada, Kiyoshi Ueda
- [We055](#) **A theoretical model of depolarized scattering in molecular clusters** • Chitra Rangan, Christopher DiLoreto, M. Sara Moezzi

### Photon – Surface/Solid

- [We056](#) **Selective enhancement of even order harmonics in a monolayer TMDC** • Viacheslav Korolev

# Posters

## Wednesday, July 26

### Photon – Surface/Solid

- [We057](#) **Controlling the polarization and phase of high-order harmonics with a plasmonic metasurface\*** • Sohail A. Jalil, Kashif M. Awan, Idriss A. Ali, Sabaa Rashid, Joshua Baxter, Aleksey Korobenko, Guilmot Ernotte, Andrei Naumov, David M. Villeneuve, André Staudte, Pierre Berini, Lora Ramunno, Giulio Vampa
- [We058](#) **Doping effects in high-harmonic generation from correlated systems** • Thomas Hansen, Lars Bojer Madsen
- [We059](#) **Modelling high-harmonic generation in quantum dots using a tight-binding approach** • Martin Thümmmler, Alexander Croy, Ulf Peschel, Stefanie Gräfe
- [We060](#) **High-order wavemixing during high-harmonic generation in solids** • David Purschke, Alvaro Jimenez-Galan, Thomas Brabec, Andrei Yu Naumov, Andre Staudte, David M. Villeneuve, Giulio Vampa
- [We061](#) **Momentum-resolved dynamics of femtosecond laser ablation with a pump-probe technique** • Aleksey Korobenko, Alan T. K. Godfrey, Andre Staudte, Adam Carew, Alexandre V. Loboda, Paul B. Corkum
- [We062](#) **Theory for ionization rate of dielectrics in two-color strong laser fields** • Mizuki Tani, Kenichi L. Ishikawa
- [We063](#) **XUV absorption spectroscopy of Ti-doped iron oxide** • Miguel Omar Segovia Guzman, Masoud Lazemi, Frank de Groot, Marc J. J. Vrakking, Arnaud Rouzée
- [We064](#) **Laser-based processing of dielectric chips for the generation of nano focused XUV radiation** • Parnia Bastani, Aleksey Korobenko, Giulio Vampa
- [We065](#) **XPS Study in situ of the Diluted Perovskite Nanocrystals Surface's Stability Stoichiometry** • Joel Pinheiro, Arnaldo Brito, Gustavo Bonato, L. Cornetta, O. Bjorneholm, G. Öhrwall, T. Gallo, F. Nogueira

### Lepton – Atom/Ion

- [We066](#) **Effect of transient spatial localization on electron impact excitation and ionization processes in dense plasmas** • Jiaolong Zeng, Jianmin Yuan
- [We067](#) **X-ray studies of atomic processes in the EBIT plasma** • Daniel Sobota, Łukasz Jabłoński, Dariusz Banaś, Paweł Jagodziński, Aldona Kubala-Kukuś, Ilona Stabrawa, Karol Szary, Marek Pajek

# Posters

Wednesday, July 26

Lepton – Atom/Ion

- [We068](#) **Observation of THz-wave-assisted electron scattering by Ar atoms** • Michihiro Kitanaka, Motoki Ishikawa, Reika Kanya, Kaoru Yamanouchi
- [We069](#) **Theoretical investigation of electron-impact ionization of  $W^{8+}$  ion** • Shiping Zhang, D. H. Zhang, L. Y. Xie, X. B. Ding
- [We070](#) **Theoretical investigation of electron-impact ionization of  $W^{6+}$  ion** • Lili Ma, D. H. Zhang, L. Y. Xie, X. B. Ding
- [We071](#) **Theoretical study on the electron collision ionization of  $Sn^{11+}$  ions** • Fangjun Zhang, X. B. Ding, D. H. Zhang, C. Z. Dong
- [We072](#) **The state-resolved integral cross sections for atomic krypton studied by fast electron scattering** • Wanlu Ma, Zhiwei Nie, Linfan Zhu
- [We073](#) **Development of particle detectors for electron-ion collision spectroscopy with highly charged ions at the storage ring CSRe** • Zhongkui Huang, S. X. Wang, W. Q. Wen, H. B. Wang, W. L. Ma, S. Shao, H. K. Huang, D. Y. Chen, S. F. Zhang, L. F. Zhu, X. W. Ma for the DR collaboration@HIRFL
- [We074](#) **First Dielectronic Recombination Measurements at the Cryogenic Storage Ring** • Leonard Isberner, Manfred Grieser, Robert von Hahn, Zoltán Harman, Ábel Kálosi, Christoph H. Keitel, Claude Krantz, Daniel Paul, Daniel W. Savin, Suvam Singh, Andreas Wolf, Stefan Schippers, Oldřich Novotný
- [We075](#) **Electron recombination of deuterated triatomic hydrogen ions at the Cryogenic Storage Ring** • Aigars Znotins, Alexandre Faure, Joshua Forer, Chris Greene, Florian Grussie, Leonard Isberner, Abel Kalosi, Viatcheslav Kokoouline, Marco Pezzella, Damian Mull, Oldrich Novotný, Daniel Paul, Daniel Savin, Stefan Schippers, Jonathan Tennyson, Xavier Urbain, Andreas Wolf, Holger Kreckel
- [We076](#) **Radiative Recombination Studies for Bare Lead Ions Interacting with Low-Energy Electrons** • Binghui Zhu, Alexandre Gumberidze, Günter Weber, Tobias Over, Zoran Andelkovic, Angela Bräuning-Demian, Ruijiu Chen, Dmytro Dmytriiev, Oliver Forstner, Christoph Hahn, Frank Herfurth, Marc Oliver Herdrich, Pierre-Michel Hillenbrand, Anton Kalinin, Felix Martin Kröger, Michael Lestinsky, Yury A. Litvinov, Esther Babette Menz, Wilko Middents, Tino Morgenroth, Nikolaos Petridis, Philip Pfäfflein, M. Shahab Sanjari, Ragandeep Singh Sidhu, Uwe Spillmann, Sergiy Trotsenko, Laszlo Varga, Gleb Vorobyev, Stefan Schippers, Reinhold Schuch, Thomas Stöhlker

# Posters

Wednesday, July 26

## Lepton – Atom/Ion

- [We077](#) **Charge-state distributions after beta decay of  ${}^6\text{He}$  to form  ${}^6\text{Li}^{+*}$**  • Aaron Bondy, Gordon W. F. Drake
- [We079](#) **Near-threshold collisional dynamics in the  $e^-e^+p$  system** • Harindranath Ambalampitiya, Joshua Stallbaumer, Ilya Fabrikant, Ivan Kalinkin, Dmitry Fursa, Alisher Kadyrov, Igor Bray
- [We080](#) **Convergent close-coupling calculations of positron scattering from atomic oxygen** • Nicolas Mori, Liam Scarlett, Igor Bray, Dmitry Fursa
- [We081](#) **Differential positronium-formation cross-sections around zero degrees from atoms and molecules** • Donovan Newson, Michael Shipman, Sam Fayer, Simon Brawley, Rina Kadokura, Andrea Loreti, Gaetana Laricchia
- [We082](#) **Electron elastic scattering by Bk and Cf atoms: polarization effects** • Alfred Z. Msezane Zineb Felfli

## Lepton – Molecule/Cluster

- [We083](#) **Theoretical investigation of bound and resonant states of imidogen radical NH** • Raju Ghosh, Kalyan Chakrabarti, Binayak S. Choudhury
- [We086](#) **Symmetry breaking in dissociative ionization of symmetric molecules by electron impact\*** • Noboru Watanabe, Masahiko Takahashi
- [We087](#) **Isomerization dynamics of triatomic molecules driven by the electron-impact** • Lei Chen, Enliang Wang, Zhenjie Shen, Maomao Gong, Xu Shan, Xiangjun Chen
- [We088](#) **Quantum coherence induced by incoherent free electron scattering** • Akshay Kumar, Suvasis Swain, Vaibhav S. Prabhudesai
- [We089](#) **Cold-target electron-ion-coincidence momentum-spectroscopy study of electron-impact single and double ionization of  $\text{N}_2$  and  $\text{O}_2$  molecules** • S. Jia, J. Zhou, X. Wang, X. Xue, X. Hao, Q. Zeng, Y. Zhao, Z. Xu, A. Dorn, X. Ren

# Posters

Wednesday, July 26

## Lepton – Molecule/Cluster

- [We090](#) **Modelling of the (e,2e) binary collision of water using the distorted wave Born approximation with single center expansion** • Mareike Dinger, Woon Yong Baek
- [We091](#) **Investigation of the valence-shell excitations of CS<sub>2</sub> by high-energy electron scattering** • Zhi-Wei Nie, Shu-Xing Wang, Li-Han Wang, Lin-Fan Zhu
- [We092](#) **Isotopic selectivity in the metastable dication production of benzene** • Lucas Sigaud, W. Wolff, E. C. Montenegro
- [We093](#) **Absolute cross sections for ionization and fragmentation of CO<sub>2</sub> by electron impact** • Ana Beatriz Monteiro-Carvalho, L. Sigaud, E. C. Montenegro
- [We094](#) **Low energy electron interaction with the potential extreme ultraviolet resist material component 2-(trifluoro-methyl) acrylic acid** • Reza Tafrishi, Daniela Torres-Diaz, Lionel Amiaud, Ali Kamali, Anne Lafosse, Oddur Ingólfsson
- [We095](#) **Signatures of ICD from heterocycle dimers and heterocycle-water complexes** • Deepthy Maria Mootheril Thomas, Xueguang Ren, Thomas Pfeifer, Alexander Dorn
- [We097](#) **R-Matrix investigations of low-energy positron scattering from biomolecules\*** • Vincent Graves, Jimena Gorfinkiel
- [We098](#) **An iterative negative imaginary potential applied to the Schwinger multichannel method to model ionization effects** • Alan Guilherme Falkowski, Romarly Fernandes da Costa, Fábris Kossoski, Marco Aurélio Pinheiro Lima

## Heavy Particle – Atom/Ion

- [We100](#) **Interaction of Singly Charged Sodium Ion with Nitrogen Atom: Total and Differential Ionisation Cross Sections** • M. Al-Ajaleen, Karoly Tókési

# Posters

Wednesday, July 26

## Heavy Particle – Atom/Ion

- [We101](#) **Interaction of Protons with Noble Gas Atoms: Total and Differential Ionisation Cross Sections** • M. Al-Ajaleen, Karoly Tókési
- [We102](#) **Experimental study of single electron capture in 150 keV O<sup>5+</sup> + He collisions** • Yong Gao, Ting Cao, Kaizhao Lin, Dalong Guo, Shaofeng Zhang, Xiaolong Zhu, Ruitian Zhang, Shuncheng Yan, Shenyue Xu, Dongmei Zhao, Xinwen Ma
- [We103](#) **Measurements of the single and double electron capture cross sections in O<sup>6+</sup> + He collisions** • Tianming Meng
- [We104](#) **L-MM Auger electron emission in Ar<sup>9+</sup> - Ar Collision** • Rohit Tyagi, S. K. Maurya, L. C. Tribedi, A. H. Kelkar
- [We105](#) **Time evolution of Migdal electrons** • Juan Randazzo, Raul Barrachina
- [We106](#) **Stopping power in lanthanides, from Ce to Lu** • Jesica Peralta, Alejandra Mendez, Diego Arbó, Dario Mitnik, Claudia Montanari
- [We108](#) **Ion-ion collision-induced longitudinal emittance preservation in RF bunching of ions in an electrostatic ion beam trap** • Deepak Sharma, Ryan Ringle, Oded Heber, Daniel Zajfman
- [We109](#) **AEGIS Phase II: Upgrading for collinear antihydrogen production** • Saiva Huck on behalf of the AEGIS collaboration

## Heavy Particle – Molecule/Cluster

- [We110](#) **State selective electron capture study with NO<sup>2+</sup> using Cold Target Recoil Ion Momentum Spectroscopy** • Jibak Mukherjee, Md Abul Kalam Azad Siddiki, Kamal Kumar, Harpreet Singh, Lokesh C. Tribedi, Deepankar Misra
- [We111](#) **Isomerized dissociation dynamics of hydrocarbon dications induced by slow highly charged ion impact** • Baihui Ren
- [We112](#) **Three-body fragmentation dynamics of cyclopropane induced by high-energy ion collisions** • Kaizhao Lin
- [We113](#) **Measurements of subrotational lifetimes of molecular ions: a new experimental technique** • Cholakka Parambath Safvan, Herendra Kumar, Pragya Bhatt, Jyoti Rajput



# Posters

Wednesday, July 26

## Heavy Particle – Molecule/Cluster

- [We114](#) **Measurements of Absolute Electron Capture Cross Sections in He<sup>2+</sup> - He and Ne<sup>8+</sup> - O<sub>2</sub> Collisions** • Pufang Ma
- [We115](#) **Sequential deprotonation of the allene trication produced by He<sup>2+</sup> impact** • Jiarong Wang
- [We116](#) **Merged-beams reactive scattering studies of N<sub>2</sub> + D<sub>3</sub><sup>+</sup> → N<sub>2</sub>D<sup>+</sup> + D<sub>2</sub>** • Dmitry Ivanov, Caixia Bu, Pierre-Michel Hillenbrand, Leonard W. Isberner, Daniel Schury, Xavier Urbain, Daniel Wolf Savin
- [We117](#) **Fully Differential Study of Dissociative Capture in p + H<sub>2</sub> Collisions** • Sujan Bastola, Mhadav Dhital, Basu Lamichhane, Ramaz Lomsadze, Ahmad Hasan, Michael Schulz
- [We118](#) **Observation of recurrent fluorescence from excited anthracene cations** • Jyunnosuke Kusuda, Rihito Fukuzaki, Takuya Majima, Hidetsugu Tsuchida, Manabu Saito
- [We119](#) **Efficient molecular oxidation in collisions with superoxide anions** • Sergio Diaz-Tendero, Carlos Guerra, Sarvesh Kumar, Fernando Aguilar-Galindo, Ana I. Lozano, Mónica Mendes, Paulo Limão-Vieira, Juan C. Oller, Gustavo García
- [We120](#) **Synthesis of N–O–H bearing species in HONO<sub>2</sub> and H<sub>2</sub>O: an infrared spectroscopic study using heavy-ion irradiation of solid samples** • Ana De Barros, A. Bergantini, F. Jandorno, A. Domaracka, H. Rothard, P. Boduch, E. Silveira

## Structure and Spectroscopy

- [We121](#) **Chemical shifts in the carbon core-level of ethanol in water-ethanol mixtures** • Lucas Cornetta, Ricardo Marinho, Hans Ågren, Arnaldo de Brito
- [We122](#) **Observation of the hyperfine transition in hydrogen-like <sup>208</sup>Bi<sup>82+</sup>** • Rodolfo Sánchez, Max Horst, Zoran Andelkovic, Carsten Brandau, Rui Jiu Chen, David Freire Fernández, Christopher Geppert, Jan Glorius, Volker Hannen, Regina Hess, Phillip Imgram, Sebastian Klammes, Kristian König, Guy Leckenby, Sergey Litvinov, Yury Litvinov, Bernd Lorentz, Johann Meisner, Konstantin Mohr, Patrick Müller, Wilfried Nörtershäuser, Stephan Passon, Tim Ratajczyk, Simon Rausch, Jon Rossbach, Shahab Sanjari, Ragandeep Singh Sidhu, Felix Sommer, Uwe Spillmann, Markus Steck, Thomas Stöhlker, Ken Ueberholz, Christian Weinheimer, Danyal Winters

# Posters

Wednesday, July 26

## Structure and Spectroscopy

- [We123](#) **Hyperfine-induced transition in highly charged Ne-like ions studied with the cryogenic electrostatic ion storage ring RICE** • Naoki Kimura, Sakumi Harayama, Chartkunchand Kiattichart, Susumu Kuma, Yuji Nakano, Toshiyuki Azuma
- [We124](#) **Precise determinations of the energy of the  $4s^2 4p \ ^2P_{3/2} - 2P_{1/2}$  transition and the lifetime of the  $4s^2 4p \ ^2P_{3/2}$  level in Ga-like  $Mo^{11+}$**  • Jialin Liu
- [We125](#) **Precision Measurements of the  $^2P_{1/2} - ^2P_{3/2}$  fine-structure splitting in B-like  $S^{11+}$  and  $Cl^{12+}$  at SH-HtscEBIT** • X. Liu, X. P. Zhou, W. Q. Wen, Q. F. Lu, C. L. Yan, J. Xiao, A. V. Volotka, Y. S. Kozhedub, M. Y. Kaygorodov, X. Ma
- [We126](#) **EUV spectra of  $Ge^{4+}$  -  $Ge^{13+}$  ions in laser-produced plasmas** • Y. H. Wu, H. Y. Li, S. Q. He, H. D. Lu, S. Q. Cao, M. G. Su, Chenzhong Dong
- [We127](#) **Ultra-high precision laser spectroscopy of anti-hydrogen\*** • Janko Nauta on behalf of the ALPHA collaboration
- [We128](#) **Development of microwave system for a high-precision Lamb shift spectroscopy of antihydrogen atoms** • Takumi Tanaka on behalf of the GBAR collaboration
- [We129](#) **Radiative lifetimes in atomic negative ions** • Julia Karls, David Leimbach, Moa K. Kristiansson, N. Daniel Gibson, Henning T. Schmidt, C. Wesley Walter, Dag Hanstorp
- [We130](#) **Determination of  $2s^2 2p^5 \rightarrow 2s 2p^6$  transition energy in fluorine-like nickel utilizing a low-lying dielectronic resonance** • Shuxing Wang, Z. K. Huang, W. Q. Wen, H. B. Wang, S. Schippers, Z. W. Wu, Y. S. Kozhedub, M. Y. Kaygorodov, A. V. Volotka, K. Wang, X. Ma, L. F. Zhu for the DR collaboration@HIRFL
- [We131](#) **Breit effect on radiative transition rates of highly charged heavy ions** • Zhimin Hu
- [We132](#) **The QED correction of the transition energy of  $Ne^{7+}$  and  $Ca^{17+}$  ions** • Bingbing Li, Jun Jiang, Lei Wu, D. H. Zhang, L. Y. Xie, D. X. Sun, C. Z. Dong
- [We133](#) **Recent progress of muon catalyzed fusion study: II. new muonic x-ray spectroscopy** • Yuichi Toyama, T. Azuma, D. A. Bennett, W. B. Doriese, M. S. Durkin, J. W. Fowler, J. D. Gard, T. Hashimoto, R. Hayakawa, G. C. Hilton, Y. Ichinohe, K. Ishida, S. Kanda, N. Kawamura, Y. Kino, R. Konishi, Y. Miyake, K. M. Morgan, R. Nakashima, H. Natori, H. Noda, G. C. O'Neil, S. Okada, T. Okumura, K. Okutsu, C. D. Reintsema, K. Sasaki, T. Sato, D. R. Schmidt, K. Shimomura, P. Strasser, D. S. Swetz, T. Takahashi, M. Tampo, H. Tatsuno, J. N. Ullom, I. Umegaki, S. Watanabe, S. Yamada, T. Yamashita

# Posters

Wednesday, July 26

## Post Deadline

- [We134](#) **Photoelectron signature of dressed-atom stabilization in intense XUV field** • Edvin Olofsson, Jan Marcus Dahlström
- [We135](#) **Laser-assisted reduction of graphene oxide coated on melamine sponge for advanced application in electromagnetic interference shielding** • Yitbarek Fitwi Kidane, Lee Hun
- [We136](#) **Quantification of Pressure-Enhanced Electron-Phonon Coupling in  $\text{Bi}_2\text{S}_3$  via Femtosecond Pump-Probe Spectroscopy** • Bowen Guan, Y. Chen, Ruiqi Wu, H. Liu, Y. Jiang, J. Dong, Qingyi Li, M. Jin
- [We137](#) **Fragmentation of pyrene molecules following double ionization by 70 eV electron impact** • Peter Van Der Burgt, Marcin L. Gradziel
- [We138](#) **Reactive collisions of electrons with  $\text{NS}^+$  cation in interstellar media** • Felix-Iosif Iacob, Zsolt Mezei, Ioan F. Schneider, Jonathan Tennyson
- [We139](#) **H assisted Shape Resonance in Negative ion formation of Acetaldehyde** • Surbhi Sinha, Samata Gokhale, Vaibhav Prabhudesai, Y. Sajeev
- [We140](#) **L- and M-subshell ionization cross sections of heavy atoms** • Claudia Montanari, Silvina Segui, Darío Mitnik, José María Fernández-Varea, Michael Dingfelder
- [We141](#) **Fine-structure energy levels, oscillator strengths and lifetimes in chromium** • Vikas Tayal

# Posters

Thursday, July 27

Photon – Atom/Ion

- [Th001](#) **Determination of ionic polarizability by nonsequential double ionization** • Huipeng Kang
- [Th002](#) **Enhancement and Suppression of Nonsequential Double Ionization by Spatially Inhomogeneous Field** • Xuan Luo, Li Guang Jiao, Aihua Liu, Xue-Shen Liu
- [Th003](#) **Internal collision double ionization of Ar driven by co-rotating two-color circularly polarized laser fields** • Xuefeng Li, Yue Qiao, Jun Wang, Fuming Guo, Yujun Yang
- [Th004](#) **Attosecond time-resolved photoemission dynamics in atoms and molecules** • Xiaochun Gong, Kiyoshi Ueda, Jian Wu
- [Th005](#) **Spatially dependent laser assisted photoionization of He** • R. Della Picca, J. M. Randazzo, S. D. López, M. F. Ciappina, D. G. Arbó
- [Th006](#) **Direct confirmation of 164-nm-wavelength superfluorescence from a dense sample of helium ions** • James Harries, Hiroshi Iwayama, Arisa Iguchi, Susumu Kuma
- [Th007](#) **Multiphoton ionization cross sections and photoelectron angular distributions of the helium atom** • Andrej Mihelic, Martin Horvat
- [Th008](#) **Core-resonance line-shape analysis of atoms undergoing strong-field ionization\*** • Maximillian Hartmann, Lynda Hutcheson, Gergana Borisova, Paul Birk, Shuyuan Hu, Andrew Brown, Hugo van der Hart, Christian Ott, Thomas Pfeifer
- [Th009](#) **Carrier-envelope-phase and helicity control of electron vortices and spirals in photodetachment** • Mateusz Majczak, F. Cajiao Vélez, J. Z. Kamiński, K. Krajewska
- [Th010](#) **A time-dependent theory for RABBIT** • Matías Ocello, Sebastián López, Diego Arbó
- [Th011](#) **First-principles simulations of multielectron dynamics in strong laser pulses using the hardware-efficient ansatz on quantum computers** • Yuki Orimo, Kenichi L. Ishikawa, Yukio Kawashima, Tanvi Gujarati, Takeshi Sato
- [Th012](#) **Relativistic calculations of electron-parent ion entanglement using the KRAKEN protocol** • C. Leon M. Petersson, Eva Lindroth

# Posters

Thursday, July 27

Photon – Atom/Ion

- [Th013](#) **Estimating Rare Gas Spectra with a New Theoretical Model for Pump-Probe Spectroscopy** • Miguel Alarcon, Chris Greene, Arvinder Sandhu, Alex Plunkett, James Wood, Dipayan Biswas
- [Th014](#) **Tracking Few-Femtosecond Auger Decay by Synchrotron Radiation** • Tatsuo Kaneyasu, Yasumasa Hikosaka, Masaki Fujimoto, Hiroshi Iwayama, Masahiro Katoh
- [Th015](#) **Phase-resolved photoelectron-imaging of potassium atoms in two-color laser fields** • Wankai Li, Yixuan Wang, Dongdong Zhang, Dajun Ding
- [Th016](#) **Strong-field Effects on Time Delays in Correlated Ionization** • Wei-Chao Jiang, M. -C. Zhong, Y. -K. Fang, S. Donsa, I. Brezinova, L. -Y. Peng, J. Burgdörfer
- [Th017](#) **Experimental fingerprint of the electron's longitudinal momentum at the tunnel exit in strong field ionization\*** • Angelina Geyer, Daniel Trabert, Max Hofmann, Nils Anders, Markus Schöffler, Lothar Schmidt, Till Jahnke, Maksim Kunitski, Reinhard Dörner, Sebastian Eckart
- [Th020](#) **Orbital effects in laser tunneling ionization of Ar and H<sub>2</sub> studied by electron-ion coincidence momentum imaging** • Daimu Ikeya, Hikaru Fujise, Shinnosuke Inaba, Minami Takahashi, Masateru Yamamoto, Takeru Nakamura, Yu Nagao, Akitaka Matsuda, Mizuho Fushitani, Akiyoshi Hishikawa
- [Th021](#) **Coulomb focusing in attosecond angular streaking measurement of strong field tunneling ionization** • Xiaokai Li
- [Th022](#) **Relativistic treatment of hole alignment due to autoionization processes and Cooper minima in noble gas atoms** • Rezvan Tahouri, Asimina Papoulia, Felipe Zapata, Stefanos Carlström, Jan Marcus Dahlström
- [Th023](#) **Interferences due to Auger decay of a doubly excited atomic state** • Matjaž Žitnik, Mateja Hrast, Andrej Mihelič, Klemen Bučar, Janez Turnšek, Ralph Püttner, G. Goldsztejn, T. Marchenko, R. Guillemin, L. Journel, O. Travnikova, I. Ismail, M. N. Piancastelli, M. Simon, D. Ceolin, M. Kavčič
- [Th024](#) **Asymmetry parameters in single ionization of Ne by XUV pulse** • Jianting Lei

# Posters

Thursday, July 27

Photon – Atom/Ion

[Th025](#) **K-shell photodetachment of carbon, oxygen, and silicon anions** • Stefan Schippers, Alfred Müller, Michael Martins, Simon Reinwardt, Florian Trinter, Stephan Fritzsche for the PIPE collaboration

Photon – Molecule/Cluster

[Th026](#) **Vibrationally resolved inner-shell photoexcitation of the molecular anion  $C_2^-$**  • Stefan Schippers, Pierre-Michel Hillenbrand, Alexander Perry-Sassmannshausen, Ticia Buhr, Sebastian Fuchs, Simon Reinwardt, Florian Trinter, Alfred Müller, Michael Martins

[Th027](#) **Investigation of Interatomic Coulombic Decay after inner-shell ionization in heterogeneous rare gas clusters by multi-coincidence spectroscopy** • Catmarna Küstner-Wetekam, Lutz Marder, Dana Bloß, Nils Kiefer, Uwe Hergenbahn, Arno Ehresmann, Premysl Kolorenc, Andreas Hans

[Th028](#) **DFT study of d-electron photoionization of  $x@C_{60}$  with  $x = Cu^+, Cu, Cu^-, Zn$**  • Dalton Forbes, Sanjay Prabhakar, Ruma De, Himadri Chakraborty

[Th029](#) **Photofragmentation of cyclo-dipeptides in the gas-phase and routes to the formation of peptide chains** • Paola Bolognesi, Darío Barreiro Lage, Jacopo Charinelli, Robert Richter, Henning Zettergren, Mark Stockett, Laura Carlini, Sergio Diaz-Tendero, Lorenzo Avaldi

[Th030](#) **Strong evidence for neighbor-induced recapture obtained by electron-photon-coincidence spectroscopy** • Nils Kiefer, Carolin Honisch, Catmarna Küstner-Wetekam, Lutz Marder, Niklas Golchert, Arno Ehresmann, Andreas Hans

[Th031](#) **Probing conical intersection dynamics in the dissociative photoionization of formaldehyde at FLASH** • David Chicharro Vacas, Weiyu Zhang, Hannes Lindenblatt, Florian Trost, Pedro Recio, Alexandre Zanchet, Roger Y. Bello, Jesús González-Vázquez, Ulrike Fruehling, Markus Braune, Sonia Marggi Poullain, Luis Bañares, Thomas Pfeifer, Robert Moshhammer

[Th032](#) **Investigating the UV-Induced Dynamics of Methylated Cyclopentadiene with XUV Photoelectron Spectroscopy at FLASH** • Zane Phelps, Lisa Huang, Tristan Fehl, Dennis Meyer, Fabiano Lever, Stefan Duesterer, Artem Rudenko, Martin Centurion, Adam Kirrander, Peter M. Weber, Markus Guehr, Daniel Rolles

[Th033](#) **Electron-rotation coupling in diatomics by intense UV pulses** • Y. R. Liu, V. Kimberg, Y. Wu, J. G. Wang, O. Vendrell, S. B. Zhang

# Posters

Thursday, July 27

## Photon – Molecule/Cluster

- [Th034](#) **Initial-site characterization of hydrogen migration in ethanol** • Travis Severt, Eleanor Weckwerth, Balram Kaderiya, Peyman Feizollah, Bethany Jochim, Kurtis Borne, Farzaneh Ziaee, Kanaka Raju P., Kevin D. Carnes, Marocs Dantus, Daniel Rolles, Artem Rudenko, Eric Wells, Itzik Ben-Itzhak
- [Th035](#) **Competition of photon and electron emission in the decay of doubly ionized ArKr clusters** • Lutz Marder, Catmarna Küstner-Wetekam, Dana Bloß, Nils Kiefer, Arno Ehresmann, Andreas Hans
- [Th036](#) **Isotope labelling as a tool for atto-chemistry** • Morgane Vacher, Alexie Boyer, Vincent Lorient, Franck Lépine, Saikat Nandi
- [Th037](#) **Time-resolved imaging of an elusive molecular reaction: hydrogen roaming in acetonitrile** • Aaron Laforge, Debadarshini Mishra, Lauren Gorman, Sergio Díaz-Tendero, Fernando Martín, Nora Berrah
- [Th038](#) **Valence photo double ionization of CH<sub>3</sub>OD: Insights into Molecular Dynamics and Electron Correlation** • S. Kumar, M. Shaikh, W. Iskandar, R. Thurston, M. A. Fareed, D. Call, R. Enoki, C. Bagdia, N. Iwamoto, T. Severt, J. B. Williams, I. Ben-Itzhak, D. S. Slaughter, Th. Weber
- [Th039](#) **An ultrafast stopwatch to clock and manipulate molecular dynamics\*** • Shengzhe Pan, Jian Wu
- [Th040](#) **Photoionization dynamics of cyano substituted PAHs in the Vacuum-Ultraviolet range** • Madhusree Roy Chowdhury, Gustavo A Garcia, Helgi Hrodmarsson, Jean-Christophe Loison, Laurent Nahon
- [Th041](#) **High Dose-Rate MeV Electron Beam from a Tightly-Focused Femtosecond IR Laser in Ambient Air: A Radiation Safety Issue** • Simon Vallières, Jeffrey Powell, Tanner Connell, Michael Evans, Marianna Lytova, Sylvain Fourmaux, Stéphane Payeur, Philippe Lassonde, François Fillion-Gourdeau, Steve MacLean, François Légaré
- [Th043](#) **Femtosecond laser assisted chemical ionization mass spectrometry** • Tao Cao, Shaozhen Liu, Qi Xu, Karry Hu, Zhou Li, Kun Chen, Teng Guo, Ping Cheng, Jiahui Peng
- [Th044](#) **VUV photoelectron spectroscopy of vibrationally-excited CO<sub>2</sub> molecules** • Masamitsu Hoshino, Akihiro Yodo, Naoki Hishiyama, Takeshi Odagiri, Junichi Adachi
- [Th045](#) **Imaging the nuclear wavepacket dynamics of multiply charged Ar<sub>2</sub> using a two-color laser field** • Arnab Sen, M. J. J. Vrakking, A. Rouzée



# Posters

Thursday, July 27

## Photon – Molecule/Cluster

- [Th046](#) **Carrier envelope phase sensitivity of photoelectron circular dichroism** • V. Hanus, S. Kangaparambil, M. Richter, L. Haßfurth, M. Dorner-Kirchner, G. G. Paulus, X. Xie, A. Baltuška, S. Gräfe, M. Kitzler-Zeiler
- [Th047](#) **Capturing electron-driven molecular chirality** • Vincent Wanie, Etienne Bloch, Erik P. Månsson, Lorenzo Colaizzi, Krishna Saraswathula, Sergey Ryabchuk, Andrea Trabattoni, Valérie Blanchet, Nadia Ben Amor, Marie-Catherine Heitz, Yann Mairesse, Bernard Pons, Francesca Calegari
- [Th049](#) **Time-resolved Imaging of CH<sub>4</sub> Fragmentation in Strong Laser Fields** • Weiyu Zhang, David Chicharro Vacas, Thomas Pfeifer, Robert Moshhammer
- [Th050](#) **Camphor: Dynamics post C 1s ionisation and interaction with shaped laser pulses** • Sanket Sen, Abhisek Sinha, Haritha Venugopal, Suddhasattwa Mandal, Arnab Sen, Ram Gopal, Ltaief Ben Ltaief, Stefano Turchini, Daniele Catone, Nicola Zema, Marcello Coreno, Robert Richter, Marcel Mudrich, Sivarama Krishnan, Vandana Sharma
- [Th052](#) **Dissociative Photoionization of EUV Lithography Photoresist Models** • Fabian Holzmeier, Marziogiuseppe Gentile, Marius Gerlach, Robert Richter, Michiel van Setten, John S. Petersen, Paul van der Heide
- [Th053](#) **Accurate molecular ab initio calculations in support of strong-field attosecond physics experiments** • Giorgio Visentin, Bo Ying, Gerhard G. Paulus, Stephan Fritzsche

## Lepton – Atom/Ion

- [Th054](#) **Effect of the Breit interaction on the angular distribution of Auger electrons following electron-impact excitation of Be-like ions** • Zhongwen Wu, Yong Li, Zhouwang Tian, Chenzhong Dong, Stephan Fritzsche
- [Th055](#) **Linear polarization and angular distribution of the Lyman- $\alpha_1$  line following electron-impact excitation of H-like ions** • Zhongwen Wu, Zhongmang He, Zhouquang Tian, Zhongwen Dong, Stephan Fritzsche
- [Th056](#) **Classical description of the ionization of carbon by electron impact** • N. Bachi, S. Otranto, Karoly Tókési
- [Th057](#) **Impact Parameter and Kinematic Information for Differential Ionization of Argon by 1 keV Positrons and Electrons** • Karoly Tókési, R. D. DuBois



# Posters

Thursday, July 27

Lepton – Atom/Ion

- [Th058](#) **Convergent close-coupling calculations of positron scattering from carbon** • Nicolas Mori, Liam Scarlett, Igor Bray, Dmitry Fursa
- [Th059](#) **Low-energy elastic scattering of positrons by helium** • Xian-Jun Li, M. -S. Wu, J. Jiang, J. -Y. Zhang, Z. -C. Yan, K. Varga
- [Th060](#) **Laser-assisted positron-H scattering in reduced quantum mode** • Xiao Hu Ji, Li Guang Jiao, Aihua Liu
- [Th061](#) **Low-energy total cross-sections of positronium scattering from the inert atoms** • Donovan Newson, Simon Brawley, Rina Kadokura, Andrea Loreti, Michael Shipman, Gaetana Laricchia
- [Th062](#) **Collective effects in positronium formation from rare gas atoms** • Paul-Antoine Hervieux, Adrien Andoche, Kévin Lévêque, Himadri Chakraborty
- [Th063](#) **Calculation and Wigner law analysis of scattering cross sections for collisions of antihydrogen atom with excited positronium** • Takuma Yamashita, Yasushi Kino, Emiko Hiyaama, Svante Jonsell, Piotr Froelich
- [Th064](#) **Electron impact excitation of Na-like Ar<sup>7+</sup>, Kr<sup>25+</sup> and Xe<sup>43+</sup>** • Aloka Kumar Sahoo, Shikha Rathi, Lalita Sharma
- [Th065](#) **Electron impact excitation of Ar-like Kr XIX** • Aloka Kumar Sahoo, Nitish Ghosh, Lalita Sharma
- [Th066](#) **Ionization cross section and plasma density effects** • Djamel Benredjem, Jean-Christophe Pain
- [Th067](#) **M $\beta$  photon self-attenuation across the M<sub>5</sub> edge for elements with 70 ≤ Z ≤ 80** • Silvina Segui, Silvina Limandri, María Torres Deluigi, Claudia Montanari, Darío Mitnik, Alejo Carreras, Gustavo Castellano, Jorge Trincavelli
- [Th068](#) **Indirect ionization of the Mo<sup>14+</sup> ion in EBIT** • Cunqiang Wu, Xiaobin Ding, Denghong Zhang, Ke Yao, Yang Yang, Yunqin Fu, Chenzhong Dong
- [Th069](#) **Theoretical investigation of KLL dielectronic-recombination processes of highly charged Cu ions** • Jianhu Deng, Shengbo Niu, Wenliang He, Yulong Ma, Luyou Xie, Chenzhong Dong

# Posters

Thursday, July 27

Lepton – Atom/Ion

[Th070](#) **Laser-assisted radiative attachment in short laser pulses** • Deeksha Kanti, Jerzy Kamiński, Liang-You Peng, Katarzyna Krajewska

Lepton – Molecule/Cluster

[Th071](#) **Positron annihilation spectra and binding energies for heterocyclic molecules** • Eugene Arthur-Baidoo, James Danielson, Daniel Witteman, Soumen Ghosh, Clifford Surko

[Th072](#) **Measurements of positron and electron scattering from biomolecules** • David Stevens, Zoe Cheong, Tamara Babij, Josh Machacek, James Sullivan

[Th073](#) **Quantum Monte Carlo study on positron binding to atomic anion dimers** • S. Ito, D. Yoshida, Y. Kita, T Shimazaki, M. Tachikawa

[Th074](#) **Low-energy positronium scattering from O<sub>2</sub>** • Donovan Newson, Rina Kadokura, Harriet Allen, Samuel Fayer, Simon Brawley, Michael Shipman, Gaetana Laricchia, Robyn Wilde, Ilya Fabrikant, László Sarkadi

[Th075](#) **Production of O<sub>2</sub><sup>+</sup> following the double ionization of CO<sub>2</sub><sup>\*</sup>** • Ana Beatriz Monteiro-Carvalho, L. Sigaud, E. C. Montenegro

[Th076](#) **Observation of ultrafast proton and energy transfer in hydrated pyrrole dimers induced by electron impact\*** • J. Zhou, S. Jia, X. Xue, X. Hao, Q. Zeng, X. Ren

[Th077](#) **Development of atomic momentum spectroscopy of polyatomic molecules** • Satoru Kanaya, Yuuki Onitsuka, Noboru Watanabe, Hirohiko Kono, Masahiko Takahashi

[Th078](#) **Development of a new molecular spectroscopy technique: mapping atomic motions and elemental composition analysis of a molecule** • Yuuki Onitsuka, Yuichi Tachibana, Satoru Kanaya, Hirohiko Kono, Masahiko Takahashi

[Th079](#) **Velocity slice imaging probed for kinematically complete measurements of dissociative electron attachment to OCS molecule** • Narayan Kundu, Vikrant Kumar, Dhananjay Nandi

[Th080](#) **Fragmentation dynamics of BrCN<sup>q+</sup> (q = 2-6) induced by 1-keV electron impact** • Wenchao Zhao

# Posters

Thursday, July 27

## Lepton – Molecule/Cluster

- [Th081](#) **Elastic scattering and rotational excitation of H<sub>2</sub> by electron impact: Convergent close-coupling calculations** • Liam Scarlett, Una Rehill, Mark Zammit, Nicolas Mori, Igor Bray, Dmitry Fursa
- [Th082](#) **Resonances in electron scattering from SO<sub>2</sub>** • Peter Bingham, Jimena Gorfinkiel
- [Th083](#) **Comparison of electron induced reactions of (CH<sub>3</sub>)AuP(CH<sub>3</sub>)<sub>3</sub> under single collision conditions and its deposition composition in UHV FEBID** • Ali Kamali, Elif Bilgilişoy, Alexander Wolfram, Thomas Xaver Gentner, Gerd Ballmann, Sjoerd Harder, Hubertus Marbach, Oddur Ingólfsson
- [Th085](#) **Dynamics of Dissociative Electron Attachment to Acetylacetone\*** • Surbhi Sinha, Vaibhav Prabhudesai

## Heavy Particle – Atom/Ion

- [Th087](#) **AEGIS: Synthesis of mid-heavy antiprotonic atoms at CERN** • Adam Linek on behalf of the AEGIS collaboration
- [Th088](#) **Nonradiative electron capture in collisions of fast Xe<sup>54+</sup> with Kr and Xe\*** • Bian Yang
- [Th089](#) **An improved short-range description for CDW-EIS model with dressed projectiles** • Nicolás Esponda, Michele Quinto, Roberto Rivarola, Juan Monti
- [Th090](#) **Target atomic number dependence of the electron capture and excitation process for the relativistic hydrogen-like Cs ions** • Caojie Shao, H. Q. Zhang, B. Yang, D. Y. Yu, Z. Y. Song, P. F. Li, H. Yuan, Z. D. Cheng, S. Ha, H. W. Zhang, Y. S. Kozhedub, W. Wang, M. W. Zhang, J. L. Liu, Y. L. Xue, C. L. Wan, Y. Cui, K. Yao, Z. H. Yang, X. H. Cai, R. Schuch, X. M. Chen
- [Th091](#) **State-selective single-electron capture in 1 keV/u Ar<sup>2+</sup>-Ar collisions** • Shucheng Cui
- [Th092](#) **State-selective single electron capture in 9 keV N<sup>+</sup>-He collisions** • Da Xing

# Posters

Thursday, July 27

## Heavy Particle – Atom/Ion

- [Th093](#) **Fully Differential Study of Non-PCI Higher-Order Contributions to Ionization of Helium by Proton Impact** • Shruti Majumdar, Sujan Bastola, Ramaz Lomsadze, Ahmad Hasan, Michael Schulz
- [Th094](#) **Energy and angular distributions of electrons produced in intermediate-energy proton-helium collisions** • Kade Spicer, Corey Plowman, Shukhrat Alladustov, Ilkhom Abdurakhmanov, Igor Bray, Alisher Kadyrov
- [Th095](#) **Single ionization of helium by protons in the parabolic quasi-Sturmians approach** • Sergey A. Zaytsev, Darya S. Zaytseva, Alexander S. Zaytsev, Lorenzo Ugo Ancarani, Konstantin A. Kouzakov, Yuri V. Popov
- [Th096](#) **A 22-pole RF ion trap experimental setup to study the ion-neutral and ion-photon interactions relevant to astrophysical environments** • Roby Chacko, Nihar Ranjan Behera, Saurav Dutta, Saroj Barik, Aravind Gopalan
- [Th097](#) **Upcoming atomic physics studies of ion-ion collisions** • Mariette Jolly, Emily Lamour, Alain Méry, Angela Bräuning-Demian, Alain Dubois, Jean-Yves Chesnel, Alexandre Gumberidze, Christoph Hahn, Michael Lestinsky, Stéphane Macé, Christophe Prigent, Jean Marc Ramillon, Jimmy Rangama, Patrick Rousseau, Uwe Spillmann, Sébastien Steydli, Thomas Stöhlker, Martino Trassinelli, Dominique Vernhet
- [Th098](#) **Three-particle one-dimensional model for ionization collisions: A simple laboratory to test perturbative approximations** • T. Guarda, V. D. Rodríguez, Raul Barrachina

## Heavy Particle – Molecule/Cluster

- [Th099](#) **Dissociation pathways of methane dication** • Jyoti Rajput, Diksha Garg, A. Cassimi, A. Mery, X. Flechard, J. Rangama, C. P. Safvan
- [Th100](#) **Fragmentation upon collision-induced activation of cysteine–water cluster cations\*** • Lukas Tiefenthaler, Paul Scheier, Ewa Erdmann, Néstor F. Aguirre, Sergio Díaz-Tendero, Thomas F. M. Luxford, Jaroslav Kočíšek
- [Th101](#) **Swift heavy ion irradiation of water, carbon monoxide, and methanol mixture in the solid phase** • Ana De Barros, C. Mejía, A. Domaracka, P. Boduch, C. P. da Costa, H. Rothard, E. F. da Silveira
- [Th102](#) **Probing the fragmentation pathways of an Argon dimer in slow ion-dimer collisions** • Md Abul Kalam Azad Siddiki, Lokesh C. Tribedi, Deepankar Misra

# Posters

Thursday, July 27

## Heavy Particle – Molecule/Cluster

- [Th103](#) **Single-electron capture and ionisation in He<sup>2+</sup> - H<sub>2</sub> collisions** • Akshit Kotian, Corey Plowman, Igor Bray, Alisher Kadyrov
- [Th104](#) **Differential ionisation in proton collisions with molecular hydrogen** • Corey Plowman, Ilkhom Abdurakhmanov, Igor Bray, Alisher Kadyrov
- [Th105](#) **Role of different electron capture mechanisms in fragmentation of CO<sub>2</sub><sup>3+</sup> into O<sup>+</sup> + C<sup>+</sup> + O<sup>+</sup>** • Kamal Kumar, Md Abul Kalam Azad Siddiki, Jibak Mukherjee, Deepankar Misra
- [Th106](#) **Giant quadrupole plasmon resonance in C<sub>60</sub> in high perturbation collisions** • Lokesh Tribedi, S. Kasthurirangan, E. Suraud
- [Th107](#) **Lifetime measurement of collision-induced delayed fragmentation from singly charged intermediate ions** • Tomohiko Nakao, Riyon Takasu, Siyao Li, Hidetsugu Tsuchida, Manabu Saito, Takuya Majima
- [Th108](#) **Ion molecule reaction dynamics of the radical anion O<sup>-</sup> with deuterated methane CD<sub>4</sub> and methyl iodide CH<sub>3</sub>I** • Atilay Ayasli, Tim Michaelsen, Arnab Khan, Thomas Gstir, Fabio Zappa, Roland Wester
- [Th109](#) **Survival of Interstellar Carbon Knockout Fragments** • Naemi Florin, Michael Gatchell, João Ameixa, MingChao Ji, Mark Stockett, Ansgar Simonsson, Suvasthika Indrajith, Peter Reinhed, Stefan Rosén, Henrik Cederquist, Henning Schmidt, Henning Zettergren

## Low Energy to Ultracold

- [Th110](#) **Cold molecular dynamics and chemical reactions of H<sub>2</sub> (D<sub>2</sub>) in strong laser fields\*** • Lianrong Zhou, J. Qiang, H. Ni, Z. Jiang, W. Jiang, W. Zhang, P. Lu, K. Lin, H. Stapelfeldt, J. Wu
- [Th111](#) **Collective electron dynamics in large ultracold atomic ensembles** • Mario Großmann, Julian Fiedler, Jette Heyer, Amir Khan, Markus Drescher, Klaus Sengstock, Philipp Wessels-Staarmann, Juliette Simonet
- [Th112](#) **Magneto-optical trap reaction microscope for strontium atoms** • Shushu Ruan

# Posters

Thursday, July 27

## Low Energy to Ultracold

- [Th113](#) **Microwave Spectroscopy of high- $n$  low- $l$   $^{84}\text{Sr}$  Rydberg states in a cold gas** • Robert Brienza, Yi Lu, Chuanyu Wang, Soumya Kanungo, Thomas Killian, Barry Dunning, Shuhei Yoshida, Joachim Burgdörfer
- [Th114](#) **Cold collisions of atomic and molecular hydrogen with astrochemically relevant anions** • Christine Lochmann, Sruthi Purushu-Melath, Markus Nötzold, Robert Wild, Francesco A. Gianturco, Roland Wester
- [Th115](#) **Theoretical Studies of Mutual Neutralization** • Ann Orel, Åsa Larson
- [Th116](#) **Theoretical studies of reactive scattering processes involving the  $\text{H}_2$  reaction complex** • Johan Hörnquist, Patrik Hedvall, Åsa Larson, Ann E. Orel
- [Th117](#) **Mutual neutralization of  $^{1,2}\text{H}^-$  with  $\text{Li}^+$ ,  $\text{O}^+$ ,  $\text{N}^+$  and  $\text{C}^+$  at DESIREE\*** • Alice Frederike Schmidt-May, G. Eklund, S. Rosén, M. C. Ji, J. Grumer, P. S. Barklem, H. Cederquist, H. Zettergren, H. T. Schmidt
- [Th118](#) **Mutual neutralization in collision of  $\text{Na}^+$  with  $\text{O}^-$  and  $\text{S}^-$**  • Antoine Aerts, Arnaud Dochain, Jacky Liévin, Xavier Urbain, Nathalie Vaeck
- [Th119](#) **Charge transfer in Sodium Iodide collisions** • Patrik Hedvall, Michael Odelius, Åsa Larson
- [Th120](#) **Molecular-rotation-induced splitting of the binary ridge in the velocity map of sub-eV  $\text{H}^+$  ( $\text{D}^+$ ) ions ejected from  $\text{H}_2$  ( $\text{D}_2$ ) molecules by ion impact** • Zoltán Juhász, Sándor T. S. Kovács, Violaine Vizcaíno, Péter Herczku, Sándor Demes, Richárd Rácz, Béla Sulik, Sándor Biri, Nicolas Sens, Duncan V. Mifsud, Gergő Lakatos, Rahul K. Kushwaha Jean-Yves Chesnel
- [Th122](#) **Two-photon optical shielding of collisions between ultracold polar molecules\*** • Charbel Karam, Mara Meyer zum Alten Borgloh, Romain Vexiau, Maxence Lepers, Silke Ospelkaus, Nadia Bouloufa-Maafa, Leon Karpa, Olivier Dulieu
- [Th123](#) **Emergent s-wave dimers near a p-wave Feshbach resonance in a strongly confined Fermi gas\*** • Kevin Xie
- [Th124](#) **Resonant processes and their impact in many-body dynamics\*** • Robin Côté
- [Th125](#) **Dynamical instabilities and macroscopic quantum self-trapping in a rotating Bose-Einstein condensate** • Denise Kamp, Duncan, O'Dell

# Posters

Thursday, July 27

## Low Energy to Ultracold

- [Th126](#) **Observation of Sequential Tunneling in Driven Optical Lattices** • X. X. Ma, X. Y. Tong, N. C. Zhang, X. Zhang, K. K. Huang, Xuanhui Lu
- [Th127](#) **Two-Dimensional Turbulence in dipolar Bose-Einstein condensate** • Sabari Subramaniyan, Ramavarmaraja Kishor Kumar, Lauro Tomio

## Structure and Spectroscopy

- [Th128](#) **Electronic  $K$  x rays emitted from muonic atoms: an application of density functional theory** • X. M. Tong, D. Kato, T. Okumura, S. Okada, T. Azuma
- [Th129](#) **High precision theory for the Rydberg states of helium up to  $n = 24$ : test of a  $7\sigma$  discrepancy with experiment** • Gordon Drake, Aaron Bondy, Eric Ene, Evan Petrimoulx, Lamies Sati
- [Th130](#) **Theoretical study on radii of neutral atoms and singly charged negative ions** • Mingmin Luo, Guangxin Min, Guannan Guo, Xuemei Zhang
- [Th132](#) **The planetary states of the Sr atom** • Matthieu Génévriez, Ulli Eichmann

## Post Deadline

- [Th133](#) **Table-top setup for independent phase and timing control of XUV pulse pairs** • Sarang D. Ganeshamandiram, Ronak N. Shah, Fabian Richter, Ianina Kosse, Jahanzeb Muhammad, Lukas Bruder, Frank Stienkemeier, Giuseppe Sansone
- [Th134](#) **Intensity variation of  $N_2$  and CO in the presence of two-color ultrafast pulses** • Madhusudhan P, Rajesh Kumar Kushawaha
- [Th135](#) **Ultrafast Imaging of Molecular Chirality with Photoelectron Vortices** • Xavi Planas, Andres Ordóñez, Maciej Lewenstein, Andrew Maxwell
- [Th136](#) **Ionization dynamics of  $CO_2$  in intense XUV and strong IR pump/probe at REMI end station FLASH2** • Atia Atia Tul Noor
- [Th137](#) **Geometry dependence of photoionization asymmetry parameter of  $CH_3I$**  • Paresh Modak, Loren Greenman
- [Th138](#) **Molecular ion time-dependent rotational relaxation dynamics probed by photo-electron in an ion trap** • Abhishek Shahi, Deepak Sharma, Sunil Kumar, Saurabh Mishra, Igor Rahinov, Oded Heber, Daniel Zajfman

# Posters

Thursday, July 27

## Post Deadline

- [Th139](#) **Cusp-electron production in collisions of open-shell  $O^{6+}(1s2s)$  ions with He** • Stefanos Nanos, N. J. Esponda, P. -M. Hillenbrand, A. Biniskos, A. Laoutaris, M. A. Quinto, N. Petridis, E. Menz, T. J. M. Zouros, Th. Stöhlker, R. D. Rivarola, J. M. Monti, E. P. Benis
- [Th140](#) **Suppression of three-body loss near a p-wave Feshbach resonance in a quasi-1D ultracold fermionic system** • Kenta Nagase, Z. Xu, N. Takahashi, T. Mukaiyama
- [Th141](#) **Precise measurement of the electron affinity of  $C_{60}$**  • José Eduardo Navarro Navarrete, P. Martini, M. Kristiansson, S. Indrajith, M. Björkhage, S. Rosén, A. Simonsson, P. Reinhed, J. D. Alexander, M. Gatchell, H. Cederquist, H. T. Schmidt, H. Zettergren
- [Th142](#) **X-ray spectra of highly charged Nd in an EBIT plasma: line identifications and effect of metastable states on ionization balance** • Adam Hosier, Joseph Tan, Timothy Burke, Dipti, Galen O'Neil, Endre Takacs, Yuri Ralchenko
- [Th143](#) **CollisionDB: An online repository of plasma collisional data sets** • Christian Hill, Dipti, Martin Haničinec



# Posters

Friday, July 28

Photon – Atom/Ion

- [Fr001](#) **Characterization of the longitudinal gas density profile in the microfluidic gas cell** • Janez Turnšek, Klemen Bučar, Matjaž Žitnik, Marcello Coreno, Anna Gabriella Ciriolo, Rebeca Martinez Vazquez
- [Fr002](#) **Laser cooling experiments at the CSRe: explanation for the observed wide deceleration range on a coasting ion beam by a cw laser** • Dongyang Chen, H. B. Wang, W. Q. Wen, Y. J. Yuan, D. Winters, S. Klammes, Th. Walther, U. Schramm, M. Bussmann, X. Ma and Laser Cooling Collaboration
- [Fr003](#) **Quantum Holography in Above Threshold Ionization** • Sebastián López, Diego Arbó
- [Fr004](#) **First principles simulation of high harmonic generation using quantum computer** • Hiroki Gi, Yuki Orimo, Kenichi L. Ishikawa, Yukio Kawashima, Tanvi Gujarati, Takeshi Sato
- [Fr005](#) **Impact of nondipole corrections on photoelectron rescattering off atomic targets in intense midinfrared laser pulses** • Resad Kahvedzic, Stefanie Gräfe
- [Fr006](#) **Attosecond-resolved Non-dipole Electron Dynamics** • Jintai Liang, Meng Han, Yijie Liao, Jia-bao Ji, Leung Chung Sum, Wei-Chao Jiang, Kiyoshi Ueda, Yueming Zhou, Peixiang Lu, Hans Jakob Wörner
- [Fr007](#) **Multi-photon double ionization of helium by ultrashort XUV pulses: probing the role of electron correlations** • Wei-Chao Jiang, M. Ederer, S. Donsa, J. Feist, I. Brezinova, J. Burgdörfer
- [Fr008](#) **Precise control of intracycle interference with a phase-stabilized polarization-gated laser pulse** • Yanlan Wang
- [Fr010](#) **Twisted attosecond pulse trains driven by amplitude-polarization pulses** • E. G. Neyra, D. Biasseti, F. Videla, L. Rebón, M. Ciappina
- [Fr011](#) **Tailoring the spectral phase of attosecond pulse trains generated by intense, femtosecond, two-color fields** • Trevor Olsson, Spenser Burrows, Swapneal Jain, Jody Davis, Scott Chumley, William Medlin, Guillaume Laurent
- [Fr012](#) **Study of the effect of higher-order dispersions on photoionisation induced by ultrafast laser pulses** • István Márton, László Sarkadi
- [Fr014](#) **Carrier-phase envelope control of nondipole effects in ionization** • Julia Derlikiewicz, Mihai C. Suster, Jerzy Z. Kaminski, Katarzyna Krajewska

# Posters

Friday, July 28

Photon – Atom/Ion

- [Fr016](#) **Spin-polarized electron vortices generated in single-photon ionization of atoms** • Yibo Hu, Qiangfei Ma, Kunlong Liu
- [Fr017](#) **Measuring the photoelectron angular distribution after nonlinear interaction of two photons with two active electrons in helium** • Michael Straub, Thomas Ding, Marc Rebholz, Gergana D. Borisova, Alexander Magunia, Hannes Lindenblatt, Severin Meister, Florian Trost, Yimeng Wang, Steffen Palutke, Markus Braune, Stefan Düsterer, Rolf Treusch, Chris H. Greene, Robert Moshhammer, Thomas Pfeifer, Christian Ott
- [Fr018](#) **Multi-sideband interference structures observed via high-order photon-induced continuum-continuum transitions in helium** • Divya Bharti, Hemkumar Srinivas, Farshad Shobeiry, Robert Moshhammer, Thomas Pfeifer, Kathryn R. Hamilton, Aaron T. Bondy, Soumyajit Saha, Klaus Bartschat, Anne Harth
- [Fr019](#) **Extended RPAE method for cross sections and delays** • A. Ljungdahl, J. Vinbladh, C. L. M. Petersson, S. Saha, J. Sörngård, Eva Lindroth
- [Fr020](#) **Disentangling interferences in the photoelectron momentum distribution from strong-field ionization** • Tian Wang, Zack Dube, Yonghao Mi, Giulio Vampa, David M. Villeneuve, Paul B. Corkum, Xiaojun Liu, Andre Staudte
- [Fr021](#) **Energy variation of double K-shell photoionization of Ne** • T. W. Gorczyca, S. T. Manson, S. H. Southworth, S. Li, D. Kouletianos, G. Doumy, L. Young, D. A. Walko, R. Püttner, D. Céolin, R. Guillemin, I. Ismail, O. Travnikova, M. N. Piancastelli, M. Simon
- [Fr022](#) **R-matrix with time dependence theory for double photoionization of general atoms** • Gregory Armstrong, Martin Plummer, Andrew Brown, Hugo van der Hart
- [Fr023](#) **Angular Distributions of Attosecond Time Delay in the Photoionization of ns Subshells of Atomic Systems: Relativistic and Nondipole Effects** • R. Hosseini, P. C. Deshmukh, Steven Manson
- [Fr024](#) **Singlet/triplet branching ratios in core-valence double photoionization of neon** • Takeshi Odagiri, Yuma Sugawara, Tatsuo Kaneyasu, Jun-ichi Adachi, Hirokazu Tanaka, Isao H. Suzuki, Sakura Suzuki, Yasumasa Hikosaka
- [Fr025](#) **Photoionization of a quantum grating formed by a single atom** • Shaofeng Zhang, B. Najjari, X. Ma

# Posters

Friday, July 28

Photon – Molecule/Cluster

- [Fr026](#) **Recurrent fluorescence rates of tetracene cations  $C_{18}H_{12}^+$  measured at two electrostatic Storage Rings: DESIREE and Mini-Ring** • Jérôme Bernard, MingChao Ji, Suvasthika Indrajith, Mark H Stockett, José E. Navarro Navarrete, Naoko Kono, Henrik Cederquist, Serge Martin, Henning T Schmidt, Henning Zettergren
- [Fr027](#) **Resonant intercluster Coulombic decay in the photoionization of  $Na_{20}$  confined inside  $C_{240}$**  • Rasheed Shaik, Kuldeep Prajapat, Hari Varma Ravi, Himadri S. Chakraborty
- [Fr028](#) **Efficient indirect interatomic Coulombic decay induced by photoelectron impact excitation in large pure He nanodroplets** • Ltaief Ben Ltaief, Keshav Sishodia, Suddhasattwa Mandal, Subhendu De, Sivarama Krishnan, Cristian Medina, Nitish Pal, Robert Richter, Thomas Fennel, Marcel Mudrich
- [Fr029](#) **The primary steps of ion solvation in helium nanodroplets** • Simon Høgh Albrechtsen, Jeppe Christensen, Constant Schouder, Albert Muñoz, Manuel Barranco, Marti Pi, Henrik Stapelfeldt
- [Fr030](#) **Carrier-envelope-phase measurement of sub-cycle UV pulses using angular photofragment distributions** • X. X. Dong, Y. R. Liu, V. Kimberg, O. Vendrell, Y. Wu, J. G. Wang, J. Chen, S. B. Zhang
- [Fr031](#) **Chiral Molecular Frame Photoelectron Angular Distributions in achiral formic acid** • Dimitrios Tsitsonis, Florian Trinter, Till Jahnke, Reinhard Dörner, Markus Schöffler
- [Fr032](#) **Ultrafast imaging of molecular chirality via low-order nonlinear interactions** • Josh Vogwell, Laura Rego, Olga Smirnova, David Ayuso
- [Fr033](#) **Revealing the wave-function-dependent zeptosecond birth time delay in molecular photoionization** • Xuanyang Lai, S. P. Xu, S. G. Yu, M. W. Shi, Y. L. Wang, W. Quan, X. J. Liu
- [Fr034](#) **Time-Resolved Images of Intramolecular Charge Transfer in Organic Molecules** • Francisco Fernández-Villoria, Jesús González-Vázquez, Alicia Palacios, Fernando Martín
- [Fr035](#) **Theory of molecular photoionization time delays** • Adrian J. Suñer-Rubio, Roger Y. Bello, Christoph Lemell, Joachim Burgdörfer, Alicia Palacios, Fernando Martín

# Posters

Friday, July 28

Photon – Molecule/Cluster

- [Fr036](#) **Ultrafast competition between  $H_2^+$  and  $H_3^+$  formation via roaming  $H_2$  mechanism** • Krishnendu Gope, Itamar Luzon, Dror Bittner, Ester Livshits, Roi Baer, Daniel Strasser
- [Fr037](#) **Ionization Dynamics in  $H_2$  by Interference of One- and Two-Photon Pathways employing VUV FEL Pulses** • Fabian Holzmeier, Alberto Gonzalez-Castillo, Thomas Baumann, Carlo Callegari, Michele Di Fraia, Matteo Lucchini, Michael Meyer, Danielle Dowek, Oksana Plekan, Kevin Prince, Eleonore Roussel, Rene Wagner, Alicia Palacios, Fernando Martin, Danielle Dowek
- [Fr038](#) **Chiral photoelectron angular distributions from ionization of achiral atomic and molecular species** • Andreas Pier, Kilian Fehre, Sven Grundmann, Isabel Vela-Perez, Nico Strenger, Max Kircher, Dimitrios Tsitsonis, Joshua B. Williams, Arne Senftleben, Thomas Baumert, Markus S. Schöffler, Philipp V. Demekhin, Florian Trinter, Till Jahnke, Reinhard Dörner
- [Fr039](#) **The Big, the Small & the Shoulder: Controlling OCS post-Ionization Dynamics\*** • Tomoyuki Endo, Karl Michael Ziem, Martin Richter, Akiyoshi Hishikawa, Stefanie Gräfe, François Légaré, Heide Ibrahim
- [Fr040](#) **Exploration of VUV photodissociation of aniline as a source of astronomically important  $HC_2N$**  • S. Muthumirthambal, S. Arun, K. Ramanathan, R. Richter, N. Pal, P. Bolognesi, L. Avaldi, M. V. Vinitha, C. S. Jureddy and U. Kadhane
- [Fr041](#) **Differentiating Molecular Structures using Laser-induced Coulomb Explosion Imaging\*** • Huynh Van Sa Lam, Anbu Selvam Venkatachalam, Surjendu Bhattacharyya, Keyu Chen, Vinod Kumarappan, Artem Rudenko, Daniel Rolles
- [Fr042](#) **Fully differential double photoionization of linear molecules beyond  $H_2$**  • Frank Yip, R. R. Lucchese, T. N. Rescigno, C. W. McCurdy
- [Fr043](#) **First principle approach to the simulation of attosecond XUV pump XUV probe spectra for small organic molecules** • Gilbert Grell, Jesús González-Vázquez, Piero Decleva, Alicia Palacios, Fernando Martín
- [Fr044](#) **Sub-cycle resolved tunnel ionization of chiral molecules** • Max Hofmann, Angelina Geyer, Daniel Trabert, Nils Anders, Jan Kruse, Jonas Rist, Lothar Schmidt, Till Jahnke, Maksim Kunitski, Markus Schöffler, Sebastian Eckart, Reinhard Dörner

# Posters

Friday, July 28

Photon – Molecule/Cluster

- [Fr045](#) **UV-induced ring-opening dynamics investigated by time-resolved Coulomb explosion imaging** • Keyu Chen, Surjendu Bhattacharyya, Anbu Venkatachalam, Huynh Lam, Kurtis Borne, Sergey Usenko, Björn Senfftleben, Daniel Rivas, Terence Mullins, Thomas Baumann, Benjamin Erk, Aljoscha Rörig, Philipp Schmidt, Sharath Sasikumar, Simon Dold, Tommaso Mazza, Michael Meyer, Basile Curchod, Mike Ashfold, Felix Allum, Alice Green, Emily Warne, Joseph McManus, Michael Burt, Mark Brouard, Ruaridh Forbes, Pedro Nunes, Martin Centurion, Peter Weber, Arnaud Rouzee, Rico Tanyag, Henrik Stapelfeldt, Kang Lin, Rebecca Ingle, Enliang Wang, Florian Trinter, Till Jahnke, Rebecca Boll, Daniel Rolles, Artem Rudenko
- [Fr046](#) **Resonant Double-Core Excitation of N<sub>2</sub>** • Eetu Pelimanni, Adam Fouda, Phay Ho, Thomas Baumann, Alberto De Fanis, Simon Dold, Iyas Ismail, Dimitris Koulentianos, Tommaso Mazza, Michael Meyer, Maria Novella Piancastelli, Ralph Püttner, Daniel Rivas, Björn Senfftleben, Marc Simon, Linda Young, Gilles Doumy
- [Fr047](#) **Metrology of Attosecond Soft X-ray Pulses at European XFEL** • Markus Ilchen, Sadia Bari, Thomas M. Baumann, Rebecca Boll, Markus Braune, Günter Brenner, Francesca Calegari, Alberto De Fanis, Kristina Dingel, Stefan Düsterer, Felix Egun, Arno Ehresmann, Benjamin Erk, Lars Funke, Andreas Galler, Gianluca Geloni, Gesa Goetzke, Tais Gorkhover, Jan Grünert, Patrik Grychtol, Marc Guetg, Andreas Hans, Arne Held, Ruda Hindrikson, Moritz Hoesch, Till Jahnke, Fini Jastrow, Reinhard Kienberger, Stephan Kuschel, Joakim Laksman, Mats Larsson, Jia Liu, Jon Marangos, Lutz Marder, David Meier, Michael Meyer, Najmeh Mirian, Jacobo Montano, Terence Mullins, Valerija Music, Christian Ott, Thorsten Otto, Yevheniy Ovcharenko, Christopher Passow, Thomas Pfeifer, Nils Rennhack, Daniel Rivas, Daniel Rolles, Artem Rudenko, Patrick Rupprecht, Sara Savio, Albert Schletter, Frank Scholz, Jörn Seltmann, Svitozar Serkez, Philipp Schmidt, Evgeny Schneidmiller, Bernhard Sick, Richard D. Thomas, Kai Tiedtke, Sergey Usenko, Jens Viefhaus, Peter Walter, Vincent Wanie, Niclas Wieland, Lasse Wülfing, Mikhail Yurkov, Vitali Zhaunerchyk, Wolfram Helml
- [Fr048](#) **XUV-induced dynamics in complex molecular ions in the gas phase** • Richard Brédy, Alexie Boyer, Marius Hervé, Isabelle Compagnon, Franck Lépine
- [Fr049](#) **Mass spectrometry at the limits of biological objects: viruses, bacteria and amyloid fibers** • Sylvain Maclot, Rodolphe Antoine, Philippe Dugourd
- [Fr050](#) **Observation of H<sub>3</sub><sup>+</sup> formation from molecular hydrogen dimers** • Yonghao Mi, Enliang Wang, Zack Dube, Tian Wang, Andrei Naumov, David Villeneuve, Paul Corkum, Andre Staudte

# Posters

Friday, July 28

## Photon – Molecule/Cluster

- [Fr051](#) **Coincidence Measurements of Photodouble Ionization of Thiophene** • Nicholas Wong, Jason Howard, Emma Sokell, Paola Bolognesi, Lorenzo Avaldi
- [Fr052](#) **On the role of isomerisation in the photo dissociation of PANHs : A casestudy with methyl amidogen abstraction** • Subramani Arun, Karthick Ramanathan, S. Muthuamirthambal, Robert Richter, Nitish Pal, J. Chiarinelli, Paola Bolognesi, Lorenzo Avaldi, M. V. Vinitha, Chinmai Sai Jureddy, Umesh R. Kadhane
- [Fr053](#) **Diatomic molecular vibrations in a strong infrared laser field: an analytic treatment of the laser-dressed Morse potential** • Szabolcs Hack, Sándor Varró, Gábor Paragi, Péter Földi, Imre Ferenc Barna, Attila Czirják
- [Fr054](#) **Fragmentation of methanol molecules after valence photoexcitation studied by negative-ion positive-ion coincidence spectroscopy** • Hanan Sa'Adah, Antti Kivimäki, Christian Stråhlman, Kevin C. Prince, Richard D. Thomas

## Photon – Other

- [Fr055](#) **Unexpected enhanced terahertz radiation in two-foci cascading plasmas** • Jingjing Zhao
- [Fr056](#) **Realtime tracking of ultrafast dynamics in liquid water\*** • Gaia Giovannetti, Sergey Ryabchuk, Ammar bin Wahid, Hui-Yuan Chen, Erik Petter Maansson, Andrea Trabattoni, Vincent Wanie, Hugo Marroux, Majed Chergui, Francesca Calegari
- [Fr057](#) **Enhanced cutoff energies in strong-field photoelectron emission of plasmonic nanoparticles** • Erfan Saydanzad, J. A. Powell, A. Rudenko, Uwe Thumm
- [Fr058](#) **Nonadiabatic Tunneling of Photoelectrons Induced by Few-Cycle Near-Fields** • B. Lovász, Václav Hanus, P. Sándor, G. Z. Kiss, B. Bánhegyi, Z. Pápa, J. Budai, C. Prietl, J. R. Krenn, P. Dombi
- [Fr059](#) **Photoionization of H Debye plasmas in strong field approximation** • Yugang Yang, Li Guang Jiao, Aihua Liu
- [Fr060](#) **Shake-up and shake-off satellites as probe of ultrafast charge delocalization in liquid water\*** • Florian Trinter, B. Winter, S. Thürmer

# Posters

Friday, July 28

Photon – Other

- [Fr061](#) **High-order harmonic generation and confinement in artificial atoms** • Harshitha Nandiga Gopalakrishna, Raktim Baruah, Christian Hünecke, Viacheslav Korolev, Martin Thümmel, Alexander Croy, Ulf Peschel, Stefanie Gräfe, Maria Wächtler, Daniil Kartashov
- [Fr062](#) **Studying the Optical Properties of 1-decanol for Ultrashort Pulse Generation** • Nathan Drouillard, TJ Hammond
- [Fr063](#) **Supercontinuum amplification for nonlinear optics** • Nathan Drouillard, Sagnik Ghosh, TJ Hammond
- [Fr064](#) **Application of LIBS spectral data fusion in quantitative analysis of Astragalus** • P. Zhao, W. W. Han, D. X. Sun, G. D. Zhang, Maogen Su
- [Fr065](#) **Experimental and theoretical study on the extreme ultraviolet radiation behavior of laser-produced Al-Sn alloy plasmas** • Maogen Su, H. Y. Li, Y. B. Fu
- [Fr066](#) **Analysis of 4p-5s spectral characteristics in laser-produced Ag plasmas in the EUV region** • M. J. Li, Maogen Su, C. Z. Dong

Lepton – Atom/Ion

- [Fr067](#) **Commissioning of a new energy-scan system for electron-impact ionization experiments and first results for La<sup>1+</sup>** • Michel Döhring, Alexander Borovik Jr., Felix Gocht, Kurt Huber, Alfred Müller, Stefan Schippers
- [Fr068](#) **High-resolution dielectronic recombination of Pb<sup>78+</sup> ions at the ultra-cold electron cooler of the CRYRING@ESR storage ring** • S. Fuchs, Z. Andelkovic, D. Banas, A. Borovik Jr., C. Brandau, M. Fogle, S. Fritzsche, Z. Harman, F. Herfurth, C. Kozhuharov, C. Krantz, M. Lestinsky, E. Lindroth, X. Ma, E. B. Menz, A. Müller, R. Schuch, U. Spillmann, A. Surzhykov, M. Steck, M. Trassinelli, G. Vorobyev, S. X. Wang, T. Stöhlker, Y. Zhang, S. Schippers for the SPARC Collaboration
- [Fr070](#) **Continuous injection of metallic elements into an electron-beam ion trap using an electron-beam evaporator** • Naoki Kimura, Genichi Kiyama, Daiki Ito, Nobuyuki Nakamura



# Posters

Friday, July 28

Lepton – Atom/Ion

- [Fr071](#) **Recombination processes in He-like oxygen ions measured at CRYRING@ESR electron cooler** • Weronika Biela-Nowaczyk, Pedro Amaro, Carsten Brandau, Sebastian Fuchs, Filipe Grilo, Michael Lestinsky, Esther Babette Menz, Stefan Schippers, Thomas Stöhlker, Andrzej Warczak
- [Fr072](#) **Plasma screening effects on dielectronic satellites** • Nigel Badnell, Kata Benedek
- [Fr073](#) **The effect of electron correlation on trielectronic recombination rate coefficients for Be-like argon\*** • Chunyu Zhang, Chongyang Chen, Nigel Badnell
- [Fr074](#) **Theoretical study on Dielectronic recombination process and X-ray line polarization of B-like Ar ion** • Shengbo Niu, Luyou Xie, Jianhu Deng, Wenliang He, Yulong Ma, Chenzhong Dong
- [Fr075](#) **Measurement of Dielectronic Recombination of Ne<sup>2+</sup> at CRYRING@ESR** • Esther Babette Menz, Michael Lestinsky, Sebastian Fuchs, Weronika Biela-Nowaczyk, Alexander Borovik Jr., Carsten Brandau, Claude Krantz, Gleb Vorobyev, Bela Arndt, Alexandre Gumberidze, Pierre-Michel Hillenbrand, Tino Morgenroth, Ragandeep Singh Sidhu, Stefan Schippers, Thomas Stöhlker
- [Fr076](#) **Theoretical investigation of dielectronic satellite spectra of Au<sup>69+</sup> -Au<sup>65+</sup> ions** • Wenliang He, Luyou Xie, Shengbo Niu, Jinglin Rui, Yulong Ma, Chenzhong Dong
- [Fr077](#) **Electron Scattering Cross Sections for Neutral and Doubly-Charged Tin** • Haadi Umer, Dmitry Fursa, Yuri Ralchenko, Igor Bray
- [Fr078](#) **Electron impact ionization of atoms and molecules: an improved BBK model** • Maroua Attia, T. Khatir, S. Houamer, K. Bechane
- [Fr079](#) **Laser-assisted ionization of atomic hydrogen by the impact of a twisted electron beam** • Neha Neha, Nikita Dhankhar, Rakesh Choubisa
- [Fr080](#) **Helical structures of alignment angle function in the electron-atom collision studies** • Mariusz Piwinski, Lukasz Klosowski
- [Fr081](#) **A binary (e, 2e) study on Ne at incident electron energies up to 4 keV: Asymptotic behavior of the (e, 2e) cross section to its high energy limits** • Isao Nakajima, Masakazu Yamazaki, Yuri Popov, Salim Houamer, Masahiko Takahashi



# Posters

Friday, July 28

Lepton – Atom/Ion

[Fr082](#) **Low to intermediate energy (e,2e) measurements from Krypton in the perpendicular plane** • Joshua Rogers, Andrew Murray

Lepton – Molecule/Cluster

[Fr083](#) **FEBID of  $[(\text{CH}_3)_2\text{AuCl}]_2$  and its fragmentation through low energy electron interaction under single collision conditions** • Elif Bilgilişoy, Ali Kamali, Alexander Wolfram, Thomas Xaver Gentner, Gerd Ballmann, Sjoerd Harder, Hubertus Marbach, Oddur Ingólfsson

[Fr084](#) **Triple ionization and fragmentation of benzene trimers following ultrafast intermolecular Coulombic decay** • J. Zhou, X. Yu, S. Luo, X. Xue, S. Jia, X. Zhang, Y. Zhao, X. Hao, L. He, C. Wang, D. Ding, X. Ren

[Fr085](#) **Computed total and partial cross sections for direct electron and positron impact ionization** • Vincent Graves

[Fr086](#) **Convergent close-coupling calculations of electrons scattering on  $\text{HeH}^+$**  • Liam Scarlett, Mark Zammit, Igor Bray, Barry Schneider, Dmitry Fursa

[Fr087](#) **Probing electron projectile coherence with twisted electron collisions** • Allison Harris

[Fr088](#) **Valence-shell electronic excitations of nitrogen dioxide studied by fast electron scattering** • Qiang Sun, Shu-Xing Wang, Lin-Fan Zhu

[Fr089](#) **Theoretical electronic excitation cross sections of  $\text{CCl}_4$**  • Noboru Watanabe, Masahiko Takahashi

[Fr090](#) **Absolute Electron Impact Ionization Cross Sections of Carbon Dioxide** • Weizhe Huang, Xu Shan, Xiangjun Chen

[Fr091](#) **R-matrix calculation of electron collisions with interhalogen compounds** • Jasmeet Singh, Jonathan Tennyson

[Fr092](#) **Comparison of Theoretical Methods to Calculate Electron-Impact Ionization Cross-Sections of Benzene Derivatives** • Anirudh Krishnadas, Nidhi Sinha, Hans Jürgen Lüdde, Tom Kirchner, Bobby Antony

[Fr093](#) **Electron impact ionization cross sections of tyrosine** • Suriyaprasanth S, Dhanoj Gupta

# Posters

Friday, July 28

## Lepton – Molecule/Cluster

- [Fr094](#) **Electron-electron-ion coincidence studies for electron impact ionization of small water clusters** • K. Hossen, S. Jia, J. Zhou, X. Xue, X. Ren, Alexander Dorn
- [Fr095](#) **Cross sections for ionization of liquid water by electron impact** • M. L. de Sanctis, M. -F. Politis, R. Vuilleumier, C. Stia, O. Fojón
- [Fr096](#) **Novel results for the electron-impact recombination and excitation of molecular cations: the role of the core-excited bound resonances** • Zsolt Mezei, Andrea Orbán, Jeoffrey Boffelli, Frederic Gauchet, Riyad Hassaine, Nicolina Pop, Felix Jacob, Mehdi Ayouz, Viatcheslav Kokoouline, Jonathan Tennyson, Ioan Schneider
- [Fr097](#) **Dissociative recombination of ArH<sup>+</sup> at the Cryogenic Storage Ring\*** • Abel Kalosi, Manfred Grieser, Leonard W. Isberner, Daniel Paul, Daniel W. Savin, Stefan Schippers, Viviane C. Schmidt, Andreas Wolf, Oldrich Novotny
- [Fr098](#) **AMOS Gateway: A Portal for Research and Education in Atomic, Molecular, and Optical Science** • Kathryn R. Hamilton, Klaus Bartschat, Igor Bray, Andrew C Brown, Nicolas Douguet, Charlotte Froese Fischer, Jesus G. Vasquez, Jimena D. Gorfinkiel, Robert Lucchese, Fernando Martin, Sudhakar Pamidighantam, Barry I. Schneider, Armin Scrinzi

## Heavy Particle – Molecule/Cluster

- [Fr099](#) **Two- and three-body dissociations of C<sub>3</sub>H<sub>6</sub> isomer dications investigated by 4 keV/u Ar<sup>8+</sup> impact** • Dalong Guo, K. Z. Lin, X. L. Zhu, R. T. Zhang, Y. Gao, D. M. Zhao, X. B. Zhu, S. F. Zhang, X. Ma
- [Fr100](#) **Ionization of oxygen in collisions with 2.5-MeV/u Si<sup>12+</sup> ions** • Sanjeev Maurya, Debasmita Chakraborty, Abhijit Bhogale, Chandan Bagdia, Laszlo Gulyás, Lokesh Tribedi
- [Fr101](#) **Classical-trajectory Monte Carlo calculations for ionizing proton-ammonia-molecule collisions: the role of multiple ionization** • Alba Jorge, Marko Horbatsch, Tom Kirchner
- [Fr102](#) **Alpha particle transport modeling in a biological environment with TILDA-V** • Alexandre Larouze, Mario Enrique Alcocer-Avila, Nicolas Esponda, Michele Arcangel Quinto, Juan Manuel Monti, Roberto Daniel Rivarola, Elif Hindie, Christophe Champion

# Posters

Friday, July 28

## Heavy Particle – Molecule/Cluster

- [Fr103](#) **Fragmentation Dynamics of a Carbon Dioxide Dication Produced by Ion Impact** • Hang Yuan, S. Xu, E. Wang, Jiawei Xu, Y. Gao, X. L. Zhu, D. L. Guo, B. Ma, D. Zhao, S. F. Zhang, S. Yan, R. T. Zhang, Y. Gao, Z. F. Xu, X. Ma
- [Fr104](#) **Gas-phase collision studies as a tool to investigate molecular mechanisms underlying radiation damage** • Wen Li, Oksana Kavatsyuk, Wessel Douma, Xin Wang, Ronnie Hoekstra, Dennis Mayer, Matthew Robinson, Markus Gühr, Mathieu Lalande, Marwa Abdelmouleh, Michal Ryszka, Jean Christophe Pouilly, Thomas Schlathölter
- [Fr105](#) **Characterization of collision-induced dissociation of deprotonated dAMP in an ion funnel** • Uma Namangalam, Salvi M, Hemanth Dinesan, S. Sunilkumar
- [Fr106](#) **Temperature of  $H_3^+$  produced in the  $H_2 + H_2^+$  reaction** • Moana Astigarreta, Lucas Sigaud, Eduardo Montenegro
- [Fr107](#) **Exploring Three Body Fragmentation of Acetylene Trication** • Jatin Yadav, C. P. Safvan, Pragya Bhatt, Pooja Kumari, Jasmeet Singh, Jyoti Rajput
- [Fr108](#) **Formation and elongation of polyglycine via unimolecular reactions in the gas phase** • Michel Farizon, Hector Lissillour, Laura Parrado Ospina, Denis Comte, Léo Lavy, Paul Bertier, Peter Calabria, Raphaël Fillool, Florent Calvo, Isabelle Daniel, Bernadette Farizon, Tilmann D. Märk
- [Fr109](#) **Dissociation dynamics in Tetrachloromethane molecule induced by ion impact** • Nirmallya Das, Sankar De, Pragya Bhatt, C. P. Safvan, Abhijit Majumdar

## Heavy Particle – Surface/Solid

- [Fr110](#) **Effect of vanadium implantation on the structure of glassy carbon** • O. S. Odutemowo, T. Fodor, Karoly Tókési, J. B. Malherbe
- [Fr111](#) **Collisions between solar wind ions and the lunar surface** • Johannes Brötzner, Herbert Biber, Noah Jäggi, Paul S. Szabo, Christian Cupak, Andre Galli, Peter Wurz, Friedrich Aumayr
- [Fr112](#) **Can the ion charge state be observed while travelling within a solid?** • Richard Wilhelm, Anna Niggas, Friedrich Aumayr
- [Fr113](#) **Study of charge state distribution for Si projectile with carbon target** • Deepak Swami, Sarvesh Kumar, S. Ojha, R. K. Karn

# Posters

Friday, July 28

## Heavy Particle – Surface/Solid

- [Fr114](#) **Fast heavy-ion-induced anion–molecule reactions on the droplet surface\***  
• Takuya Majima, Yuki Mizunami, Taichi Takemura, Takahiro Teramoto, Hidetsugu Tsuchida, Manabu Saito
- [Fr115](#) **Amorphous and crystalline pyridine ices irradiated by MeV ions** • Cintia Da Costa, Anna Bychkova, Philippe Boduch, Ana de Barros, Ignace Bouchard de La Poterie, Zuzana Kaňuchová, Hermann Rothard, Alicja Domaracka
- [Fr116](#) **Spin-dependent metastable He ( $2^3S$ ) atom scattering from  $Fe_3O_4(100)$  surfaces**  
• Haruka Maruyama, Mitsunori Kurahashi, Kanta Asakawa, and Atsushi Hatakeyama
- [Fr117](#) **Progress on observation of radiative double-electron capture (RDEC) with  $F^{9,8+}$  on graphene** • David La Mantia, K. Bhatt, S. Dutta, T. D. Ulrich, U. Abesekera, M. J. Hall, H. Weerathne, J. A. Tanis, A. Kayani
- [Fr118](#) **A versatile 3D transmission setup for ion–solid interaction studies using keV ion energies at Uppsala University** • Radek Holenak, Svenja Lohmann, Eleni Ntemou, Daniel Primetzhofer
- [Fr119](#) **Characterization of a double torsion pendulum for detecting torque exerted by the spins of gaseous atoms** • Runa Yasuda, Atsushi Hatakeyama
- [Fr120](#) **Detecting sample surface magnetism with highly charged ions** • Perla Dergham, Emily Lamour, Stéphane Macé, Christophe Prigent, Sébastien Steydli, Dominique Vernhet, Martino Trassinelli
- [Fr121](#) **Clocking ultrafast relaxation of Rydberg hollow atoms at surfaces by x-rays\*** • Łukasz Jabłoński, Dariusz Banaś, Paweł Jagodziński, Aldona Kubala-Kukuś, Daniel Sobota, Ilona Stabrawa, Karol Szary, Marek Pajek
- [Fr122](#) **Nanostructures formed on a gold crystal surface by the impact of slow highly charged xenon ions** • Arkadiusz Foks, Dariusz Banas, Ilona Stabrawa, Karol Szary, Aldona Kubala-Kukuś, Paweł Jagodziński, Łukasz Jabłoński, Marek Pajek, Daniel Sobota, Regina Stachura, Milena Majkić, Natasa Nedeljković
- [Fr123](#) **Effect of the accelerator-related materials preparation on the ion stimulated desorption yield** • Sebastien Steydli

# Posters

Friday, July 28

## Heavy Particle – Surface/Solid

- [Fr124](#) **Irradiation of Oxygen-Bearing Ices on Top of Elemental Sulphur Layers: Implications for Astrophysical Sulphur Chemistry** • Duncan V Mifsud, Péter Herczku, Olivier Auriacombe, Sándor T S Kovács, Béla Sulik, Zoltán Juhász, Richárd Rácz, Gergő Lakatos, Rahul K. Kushwaha, Sándor Biri, István Vajda, István Rajta, Robert W McCullough, Sergio Ioppolo, Nigel J. Mason, Zuzana Kaňuchová
- [Fr125](#) **Investigation of the evolution of defect in Si ion implanted GaN after UHPA by means of RBS/channeling and HR-XRD methods** • Karolina Pağowska, Iwona Sankowska, Przemysław Józwik, Kacper Sierakowski, Andrzej Taube, Paweł Prystawko, Michał Boćkowki, Anna Szerling, Izabella Grzegory
- [Fr126](#) **Emission of x rays in collisions of xenon ions with metal surfaces** • Yipan Guo
- [Fr127](#) **Neutron spectra in nuclear hybrid reactors** • J. Garcia-Gallardo, N. Gimenez, Juana Gervasoni

## Structure and Spectroscopy

- [Fr128](#) **Modeling and computation of atomic cascades** • Stephan Fritzsche, Patrick Palmeri, Stefan Schippers
- [Fr129](#) **Separation of the inner and outer electrons for two-electron atoms near the critical bound limit** • Li Guang Jiao, Yew Kam Ho, Stephan Fritzsche
- [Fr130](#) **A community platform for just atomic computations** • Stephan Fritzsche
- [Fr131](#) **The ARTEMIS experiment: Towards high precision g-factor measurements on highly charged ions** • Bianca Reich, Arya Krishnan, Khwaish Anjum, Patrick Baus, Gerhard Birkl, Kanika, Jeffrey Klimes, Wolfgang Quint, Manuel Vogel
- [Fr132](#) **Lifetimes of excited states of the lanthanum negative ion** • C. Wesley Walter, N. D. Gibson, F. E. Vassallo, J. Karls, D. Leimbach, D. Hanstorp, J. E. Navarro Navarrete, M. K. Kristiansson, M. Björkhage, R. D. Thomas, H. Zettergren, H. T. Schmidt
- [Fr133](#) **Toward a new type of gas phase spectroscopy for complex organic ions** • Stav Knaffo

# Posters

Friday, July 28

## Structure and Spectroscopy

- [Fr134](#) **Precision X-Ray Spectroscopy of He-like Uranium employing Metallic Magnetic Calorimeter Detectors\*** • Philip Pfäfflein, Steffen Allgeier, Zoran Andelkovic, Sonja Bernitt, Alexander Borovik, Louis Duval, Andreas Fleischmann, Oliver Forstner, Marvin Friedrich, Jan Glorius, Alexandre Gumberidze, Christoph Hahn, Frank Herfurth, Daniel Hengstler, Marc Oliver Herdrich, Pierre-Michel Hillenbrand, Anton Kalinin, Markus Kiffer, Felix Martin Kröger, Maximilian Kubullek, Patricia Kuntz, Michael Lestinsky, Bastian Löher, Esther Babette Menz, Tobias Over, Nikolaos Petridis, Stefan Ringleb, Ragandeep Singh Sidhu, Uwe Spillmann, Sergiy Trotsenko, Andrzej Warczak, Günter Weber, Binghui Zhu, Christian Enss, Thomas Stöhlker
- [Fr135](#) **Design and Underlying Concepts of a Python Based Quantum Package for High Precision Atomic Structure Calculations** • Vipul Badhan, Bindiya Atora, Bijaya Kumar Sahoo

## Post Deadline

- [Fr136](#) **The spectrum of the vacuum as a primary reference for radiometry** • Samuel Lemieux
- [Fr137](#) **New methods for implementing photon addition with postselection and swift electrons** • Hao Jeng, Jan-Wilke Henke, Germaine Arend, Armin Feist, Claus Ropers
- [Fr138](#) **Fast-ion induced electron emission from nano-structured gold: applications as a radiosensitizer for cancer cell killing in hadron therapy** • Jefferson Shinpaugh, Wilson Hawkins, Nichole Libby, Tristan Gaddis, Eric Maertz, Nathan Carlson, Chris Boyd, Michael Dingfelder
- [Fr139](#) **A numerical approach to the deexcitation of a hollow atom** • M. Werl, Anna Niggas, Thomas Koller, Paul Haidegger, Karoly Tókési, Friedrich Aumayr, Richard A. Wilhelm
- [Fr140](#) **Stopping power of heavy ions under channeling condition** • Radek Holenak, Svenja Lohmann, Eleni Ntemou, Daniel Primetzhofer

# Posters

Monday, July 31

Photon – Atom/Ion

- [Mo001](#) **Generating Ultrafast MeV Electrons with a mJ-class Laser** • Jeffrey Powell, S. Vallières, S. Payeur, S. Fourmaux, S. Jolly, F. Fillion-Gourdeau, H. Ibrahim, S MacLean, F Légaré
- [Mo002](#) **Selective field ionization of Rydberg atoms in a room-temperature vapor** • David La Mantia, A. P. Rotunno, N. Prajapati, M. Simons, C. L. Holloway, E. B. Norrgard, S. P. Eckel
- [Mo003](#) **Momentum of Light in an Atom** • Joshua Hainge, Duncan O'Dell
- [Mo005](#) **Photoelectron holography: an interplay between different interference mechanisms** • Sándor Borbély, Attila Tóth, Ladislau Nagy
- [Mo006](#) **Soft x-ray spectroscopy on non-linear interaction of x-rays with matter at the Small Quantum Systems instrument of European XFEL** • Thomas Baumann, Marcus Agåker, Hans Ågren, Olle Björneholm, Rebecca Boll, John Bozek, Sebastian Cardoch, Sonia Coriani, Lucas Cornetta, Alberto De Fanis, Emiliano De Santis, Simon Dold, Gilles Doumy, Ulli Eichmann, Xiaochun Gong, Johan Gråsjö, Iyas Ismail, Ludvig Kjellsson, Kai Li, Eva Lindroth, Tommaso Mazza, Jacobo Montaña, Terence Mullins, Hongcheng Ni, Joseph Nordgren, Christian Ott, Yevheniy Ovcharenko, Minna Patanen, Thomas Pfeifer, Maria Novella Piancastelli, Ralph Püttner, Nils Rennhack, Nina Rohringer, Cecilia Sánchez-Hanke, Conny Sâthe, Philipp Schmidt, Björn Senfftleben, Marc Simon, Johan Chau Söderström, San-Kil Son, Stephen Southworth, Nicusor Timneanu, Moto Togawa, Kiyoshi Ueda, Sergey Usenko, Hans Jacob Wörner, Weiqing Xu, Zhong Yin, Linda Young, Michael Meyer, Jan-Eric Rubensson
- [Mo007](#) **Fano-ADC(2,2) method for multi-electron decay processes** • Přemysl Kolorenč
- [Mo008](#) **Nonadiabatic Strong Field Ionization of Atomic Hydrogen** • Daniel Trabert, Nils Anders, Simon Brennecke, Markus Schöffler, Till Jahnke, Lothar Schmidt, Maksim Kunitski, Manfred Lein, Reinhard Dörner, Sebastian Eckart
- [Mo009](#) **Nondipole effects in strong-field ionization using few-cycle laser pulse** • Danish Furekh Dar, Stephan Fritzsche
- [Mo010](#) **Nonsequential double ionization of Ne with elliptically polarized laser pulses** • Fang Liu, Zhangjin Chen, Stephan Fritzsche
- [Mo011](#) **Strong field phenomena with sculpted laser pulses** • Allison Harris, Dany Yaacoub

# Posters

Monday, July 31

Photon – Atom/Ion

- [Mo012](#) **Optical tunnelling without a barrier?\*** • Anne Weber, Emilio Pisanty
- [Mo013](#) **Streaked angle-resolved shake-up photoemission from He** • Hongyu Shi, Uwe Thumm
- [Mo014](#) **Circular Dichroism in Multiphoton Ionization of Resonantly Excited Helium Ions near Channel Closing** • Rene Wagner, Markus Ilchen, Nicolas Douguet, Carlo Callegari, Zachary Delk, Michele Di Fraia, Jiri Hofbrucker, Valerija Music, Okasna Plekan, Kevin C. Prince, Daniel E. Rivas, Philipp Schmidt, Alexei N. Grum-Grzhimailo, Klaus Bartschat, Michael Meyer
- [Mo015](#) **Quasi-chirp-free isolated attosecond pulse generation from atoms by optimized two near-infrared pulses and their second harmonic fields** • Jin-Xu Du
- [Mo016](#) **Complete reconstruction of an electron wavepacket generated by absorption of an attosecond pulse** • John Vaughan, Saad Mehmood, Coleman Cariker, Trevor Olsson, Swapneal Jain, Spenser Burrows, Eva Lindroth, Luca Argenti, Guillaume Laurent
- [Mo017](#) **Time-domain investigation of strong-field recollision to measure recombination time delay** • Donghyuk Ko, Chunmei Zhang, Graham Brown, Paul Corkum
- [Mo018](#) **Nondipole study of backward emission of electrons in ionization driven by high-frequency laser pulses** • Mihai Suster, Julia Derlikiewicz, Felipe Cajiao Velez, Jerzy Z. Kaminski, Katarzyna Krajewska
- [Mo019](#) **A comparison study for high-order harmonic generation in helium** • Aaron Bondy, Soumyajit Saha, Nicolas Douguet, Kathryn Hamilton, Andrew Brown, Klaus Bartschat
- [Mo020](#) **Analytical Guidelines to Choose the Right Pressure Profile for High-harmonic Generation in Gas Targets** • Balazs Major, Katalin Varju
- [Mo021](#) **High-order harmonic generation of alkali metals in few-cycle laser pulses** • Chih-Yuan Lin
- [Mo022](#) **Investigation of the spatial distribution of atomic high-order harmonic generation using the bohmian trajectories scheme** • Susu Zhang



# Posters

## Monday, July 31

### Photon – Atom/Ion

- [Mo023](#) **Photoionization of Rydberg atoms out of an optical dipole trap** • Kevin Romans, B. P. Acharya, K. Foster, D. Fischer
- [Mo024](#) **Photoionization of Atomic Sodium Near Threshold** • C. P. Ballance, T. W. Gorczyca, N. R. Badnell, S. T. Manson, D. W. Savin
- [Mo025](#) **Probing Photoelectron Dynamics by Coulomb-distorted Terahertz Radiation** • Ziyang Gan

### Photon – Molecule/Cluster

- [Mo026](#) **Towards understanding the electronic structure of essential medicines: a photoemission study of aspirin, paracetamol, and ibuprofen in the gas phase** • Hanan Sa'Adeh, Kevin C. Prince, Robert Richter, Vladislav Vasilyev, Delano P. Chong, Feng Wang
- [Mo027](#) **Isomer effects and orbital features in the ellipticity dependence of high-order harmonics from C<sub>20</sub> isomers** • A. Dubey, O. Cohen, M. F. Ciappina
- [Mo028](#) **Time-resolved resonant Auger scattering clocks distortion of a molecule** • C. Wang, M. M. Gong, Y. J. Cheng, V. Kimberg, X. J. Liu, O. Vendrell, K. Ueda and S. B. Zhang
- [Mo029](#) **Ultrafast Dynamics in Donor-Acceptor Prototype Molecules by XUV-IR Attosecond Spectroscopy** • Francisco Fernández-Villoria, Federico Vismarra, Rocío Borrego-Varillas, Yingxuan Wu, Daniele Mocci, Lorenzo Colaizzi, Maurizio Reduzzi, Fabian Holzmeier, Laura Carlini, Paola Bolognesi, Robert Richter, Lorenzo Avaldi, Jesús González-Vázquez, Alicia Palacios, José Santos, Matteo Lucchini, Luis Bañares, Nazario Martín, Fernando Martín, Mauro Nisoli
- [Mo031](#) **Scaling laws for the cooling dynamic of catacondensed PAH cations** • Suvasthika Indrajith, Mingchao Ji, Jose E. Navarro Navarrete, Paul Martini, Jerome Bernhard, Serge Martin, Mark H. Stockett, Michael Gatchell, Henrik Cederquist, Henning T. Schmidt, Henning Zettergren
- [Mo033](#) **A new pulsed superfluid helium droplet machine for experiments at a free-electron laser beamline** • James Harries, Arisa Iguchi, Susumu Kuma
- [Mo034](#) **Ion-neutral coincidence experiments to characterize the photofragmentation of cyclo-dipeptides** • Jacopo Charinelli, Robert Richter, Lorenzo Avaldi, Paola Bolognesi

# Posters

Monday, July 31

Photon – Molecule/Cluster

- [Mo035](#) **Visualisation and laser-induced modification of a vibrational wave-packet revival in the excited H<sub>2</sub> molecule** • Gergana D. Borisova, Paula Barber Belda, Shuyuan Hu, Paul Birk, Veit Stooß, Maximilian Hartmann, Daniel Fan, Robert Moshhammer, Alejandro Saenz, Christian Ott, Thomas Pfeifer
- [Mo036](#) **Ultrafast temporal evolution of interatomic Coulombic decay in NeKr dimers** • Florian Trinter, T. Miteva, M. Weller, A. Hartung, M. Richter, J. B. Williams, A. Gatton, B. Gaire, J. Sartor, A. L. Landers, B. Berry, I. Ben-Itzhak, N. Sisourat, V. Stumpf, K. Gokhberg, R. Dörner, T. Jahnke, T. Weber
- [Mo037](#) **Polarization-induced molecular photoionization delays and equivalence of RABITT and streaking dipole-laser coupling** • Jakub Benda, Zdenek Masin
- [Mo038](#) **Photoionization and Resonance Formation in Formic Acid Monomer and Dimer** • Julio Ruivo, Thomas Meltzer, Alex G. Harvey, Jakub Benda, Zdeněk Mašín
- [Mo039](#) **Angular distribution and energy spectra of photoelectrons from tetrahydrofuran illuminated by VUV photon source** • István Márton, Levente Ábrók, Dávid Nagy, Ákos Kövér, László Gulyás, Sándor Demes, Sándor Ricz
- [Mo040](#) **Direct signatures of coherent bending vibrations observed using laser-induced Coulomb explosion imaging** • Huynh Van Sa Lam, Anbu Selvam Venkatachalam, Sina Jacob, Surjendu Bhattacharyya, Keyu Chen, Vinod Kumarappan, Daniel Rolles, Artem Rudenko
- [Mo041](#) **Strong-field-driven dissociation dynamics in CO<sub>2</sub><sup>+</sup>** • Van-Hung Hoang, Uwe Thumm
- [Mo042](#) **Ultrafast dynamics in tryptophan-based peptides controlled by micro-environment** • Richard Brédy, Marius Hervé, Alexie Boyer, Abdul Rahman Allouche, Isabelle Compagnon, Franck Lépine
- [Mo043](#) **Observation of the ions CH<sub>3</sub><sup>+</sup>, SH<sup>+</sup>, SH<sub>2</sub><sup>+</sup> and CH<sub>3</sub>S<sup>+</sup> from thiophene and tetrathiophene by laser radiation at 532, 355 and 266 nm** • Alfonso Guerrero, Ignacio Álvarez, Eladio Prieto, Carmen Cisneros
- [Mo044](#) **Vibrational patterns in dissociative photoionization of H<sub>2</sub> and D<sub>2</sub> molecules by VUV + NIR absorption** • Spenser Burrows, Jan Dvorak, Itzik Ben-Itzhak, Ben Berry, Elio Champenois, Reinhard Dörner, Averell Gatton, Wael Iskandar, Kirk Larsen, Guillaume Laurent, Robert Lucchese, Daniel Metz, Tom Rescigno, Hendrik Sann, Travis Severt, Niranjana Shivaram, Dan Slaughter, Miriam Weller, Joshua Williams, C. William McCurdy, Thorsten Weber

# Posters

Monday, July 31

## Photon – Molecule/Cluster

- [Mo045](#) **How does the solvation affect molecular ultrafast dissociation?** • Debora Vasconcelos
- [Mo047](#) **Impact of the XFEL shot-to-shot variation onto soft X-Ray pump-probe studies of attosecond charge migration in molecules** • Gilbert Grell, Piero Decleva, Alicia Palacios, Fernando Marti n on behalf of the LCLS Attosecond Campaign Collaboration
- [Mo048](#) **Formation of Breathing Ions via Coherent Shake-Up** • James Tarrant
- [Mo049](#) **Real-time first-principles simulations of molecules in intense laser fields using the erf-gau potential** • Yuki Orimo, Takeshi Sato, Kenichi L. Ishiakwa
- [Mo050](#) **Absolute photodetachment cross-section of deprotonated indole using a 16-pole ion trap** • Salvi M, Uma N N, Abheek Roy, Hemanth Dinesan, S. Sunil Kumar
- [Mo051](#) **Late recollisions in dissociative strong-field ionization of D<sub>2</sub>** • Sebastian Hell, Matthias Kübel
- [Mo052](#) **Time-dependent multicomponent optimized coupled-cluster method for nonadiabatic electro-nuclear dynamics** • Takeshi Sato, Chihiro Osaku, Yuki Orimo, Kenichi L. Ishikawa
- [Mo053](#) **Quantitative broadband coherent anti-Stokes Raman scattering microscopy based on a simple laser source** • Zhou Li, Tao Cao, Kun Chen, Qi Xu, Jiahui Peng

## Photon – Surface/Solid

- [Mo054](#) **Attosecond chronoscopy of the photoemission of a layered system** • D. Potamianos, M. Schnitzenbaumer, C. Lemell, P. Scigalla, F. Libisch, E. Scheck-Schmidtke, M. Haimerl, M. Schäffer, J. T. Kühle, J. Riemensberger, Y. Cui, U. Kleineberg, J. Burgdörfer, J. V. Barth, P. Feulner, F. Allegretti, R. Kienberger
- [Mo055](#) **Features of the grazing interaction of microfocal bremsstrahlung with the surface edge** • Vladimir Smolyanskiy, M. M. Rychkov, V. V. Kaplin
- [Mo056](#) **Ultrafast THz Magnetic Field Generation Using Quantum Interference Control of Semiconductor Currents** • Kamallesh Jana, Yonghao Mi, Søren H. Møller, Shawn Sederberg, Paul. B. Corkum

# Posters

Monday, July 31

## Photon – Surface/Solid

- [Mo057](#) **MsSpec-DFM (Dielectric function module): Towards a multiple scattering approach to plasmon description** • Aditi Mandal, S. Tricot, R. Choubisa, D. Sebilliau
- [Mo058](#) **Pressure-dependent Photoluminescence of 0D/2D Heterostructures** • Ruiqi Wu, Bowen Guan, Y. Jiang, H. Liu, Qingyi Li, M. Jin
- [Mo059](#) **Electron excitation dynamics in silicon irradiated by femtosecond double pulses of different wavelength combination** • Eiyu Gushiken, Mizuki Tani, Kenichi Ishikawa
- [Mo060](#) **Visualization of ultrafast plasmon by nonlinear multi-photon photoemission electron microscopy** • Boyu Ji, Peng Lang, Yang Xu, Xiaowei Song, Jingquan Lin
- [Mo061](#) **Orbital perspective of high-harmonic generation in ReS<sub>2</sub>** • Álvaro Galán, Chandler Bossaer, Guilmoet Ernotte, Andrew Parks, Rui Silva, David Villeneuve, André Staudte, Thomas Brabec, Adina Luican-Mayer, Giulio Vampa
- [Mo062](#) **Characterizing high harmonics using frequency resolved optical switching** • Saadat Mokhtari, Mayank Kumar, Tristan Guay, Giulio Vampa, Francois Légaré
- [Mo063](#) **Tunable spectral shift of high-order harmonic generation in atoms by a plasmon-assisted shaping pulse** • Yuan Wang, Qingyi Li, Zhou Chen, Jun Wang, Fuming Guo, Yujun Yang
- [Mo064](#) **Far-ultraviolet (FUV) emission from laser-produced plasma of Al, Fe, Cu and Inconel** • Shuichiro Tamaki, Hiroki Ohnishi, Yoko Shiina, Yuji Nakano

## Lepton – Molecule/Cluster

- [Mo065](#) **Recent progress of muon catalyzed fusion study: I. new kinetics model with muonic molecular resonances** • Takuma Yamashita, Yasushi Kino, Kenichi Okutsu, Yuichi Toyama, Shinji Okada, Motoyasu Sato
- [Mo066](#) **Recent progress of muon catalyzed fusion study: III. Alternative measurement of nuclear fusion reaction in muonic molecule** • K. Okutsu, T. Yamashita, Yasushi Kino, R. Nakashima, R. Konishi, K. Sasaki, K. Miyashita, Y. Toyama, S. Okada, M. Sato, T. Oka, N. Kawamura, S. Kanda, K. Shimomura, P. Strasser, S. Takeshita, M. Tampo, S. Doiuchi, Y. Nagatani, H. Natori, S. Nishimura, A. D. Pant, Y. Miyake, K. Ishid

# Posters

Monday, July 31

Lepton – Molecule/Cluster

- [Mo067](#) **Triple-differential cross sections in three-dimensional kinematics for electron-impact-ionization dynamics of tetrahydrofuran at 250-eV** • X. Xue, D. M. Mootheril, E. Ali, M. Gong, S. Jia, J. Zhou, E. Wang, J. Li, X. Chen, D. H. Madison, A. Dorn, and X. Ren
- [Mo068](#) **Molecular ionization cross-sections using complex Gaussian representations of the continuum** • Abdallah Ammar, Arnaud Leclerc, Lorenzo Ugo Ancarani
- [Mo069](#) **Many-body theory and calculations of  $\gamma$  spectra for low-energy positron annihilation in polyatomic molecules** • Andrew Swann, Sarah Gregg, Jack Cassidy, Jaroslav Hofierka, Brian Cunningham, Charlie Rawlins, Charles Patterso, Dermot Green
- [Mo070](#) **Many-body theory calculations of positron binding to halogenated hydrocarbons** • Jack Cassidy, Jaroslav Hofierka, Brian Cunningham, Charlie Rawlins, Charles Patterson, Dermot Green
- [Mo071](#) **Low-energy positron collisions with tetrachloroethylene (C<sub>2</sub>Cl<sub>4</sub>) molecule** • Rafael O. Lima, Alessandra S. Barbosa, Márcio H. F. Bettega, Sérgio d`A. Sanchez, Giseli Moreira
- [Mo072](#) **Electron and Positron impact ionisation of few biologically relevant molecules for coplanar and perpendicular plane emission of electrons** • Alpana Pandey, Ghanshyam Purohit
- [Mo073](#) **Electronic excitation of benzene by electron impact: a theoretical and experimental investigation** • Alan Guilherme Falkowski, Romarly Fernandes da Costa, Marco Aurélio Pinheiro Lima, Alexi De Avila Cadena, Ronald Pocoroba, Murtadha A. Khakoo, Fábio Kossoski
- [Mo074](#) **Scaled Born approximation for electron impact excitations of N<sub>2</sub> molecule** • Jorge Lino
- [Mo075](#) **Electron Impact Induced Fragmentation of ND<sub>3</sub><sup>+</sup>** • M. O. A. El Ghazaly, J. J. Jureta, Ola Al-Hagan, P. Defrance
- [Mo076](#) **Elucidating geometrical features of e-C<sub>60</sub> interaction from their elastic scattering spectra** • R. Aiswarya, Jobin Jose, Rasheed Shaik, Hari Varma Ravi, Himadri S. Chakraborty
- [Mo078](#) **Tracing the expansion of molecular plasma with electron collision** • Guangqing Chen, Zonglin Yao, Xu Shan, Xiangjun Chen

# Posters

## Monday, July 31

### Lepton – Molecule/Cluster

[Mo079](#) **Oscillator strengths and cross sections of the valence-shell excitations of HBr studied by fast electron impact** • Jian Hui Zhu, S. X. Wang, L. F. Zhu

[Mo080](#) **Effects and data of electron collisions on various molecules for medical applications** • Yeunsoo Park, Mi-Young Song, Mareike Dinger, Woon Yong Baek

### Lepton – Surface/Solid

[Mo081](#) **Oscillator model applied to calculations of energy loss in anisotropic 2D materials\*** • Silvina Segui, Juana L. Gervasoni, Zoran L. Miskovic, Néstor R. Arista

[Mo082](#) **Secondary electron emission & detection of low-energy charged particles impacting channel electron multipliers** • Donovan Newson, Simon Brawley, Michael Shipman, Rina Kadokura, Tamara Babij, David Cooke, Dawn Leslie, Gaetana Laricchia

[Mo083](#) **Determination of Electron Inelastic Mean Free Path and Stopping Power of Hafnium Dioxide** • J. M. Gong, Karoly Tókési, X. Liu, B. Da, H. Yoshikawa, S. Tanuma, Z. J. Ding

[Mo084](#) **Energy Loss Function of Samarium determined from the reflection electron energy loss spectroscopy spectra** • T. F. Yang, R. G. Zeng, L. H. Yang, A. Sulyok, M. Menyhárd, K. Tókési and Z. J. Ding

[Mo085](#) **Focusing an electron beam by the self-arranged formation of a quadrupole-like electrostatic field inside a quartz capillary of square cross section** • Hongqiang Zhang, Reinhold Schuch

### Heavy Particle – Atom/Ion

[Mo086](#) **Wave-packet continuum discretisation approach to dressed carbon ion collisions with atomic hydrogen** • Nicholas Antonio, Corey Plowman, Ilkhom Abdurakhmanov, Igor Bray, Alisher Kadyrov

[Mo088](#) **Quantum vortices in the fully differential cross section for the ionization of atoms by the impact of protons and positrons** • Tamara Guarda, Francisco Navarrete, Raul Barrachina

[Mo089](#) **Direct determination of the fully differential cross section of the ionization by the wave function** • Zorigt Gombosuren, Khenmedekh Lochin, Aldarmaa Chuluunbaatar

# Posters

## Monday, July 31

### Heavy Particle – Atom/Ion

- [Mo090](#) **Quadrupole l-changing collisions** • Nigel Badnell, Evangelia Deliporanidou
- [Mo091](#) **Towards determination of absolute cross sections for excitation of hydrogen-like uranium in collisions with neutral atoms** • G. Weber, Alexandre Gumberidze, D. B. Thorn, A. Surzhykov, C. J. Fontes, M. O. Herdrich, R. Martin, U. Spillmann, S. Trotsenko, N. Petridis, Th. Stöhlker
- [Mo092](#) **M X-ray Production Cross-Sections in  $_{70}\text{Yb}$  Induced by Nitrogen Ions** • Balwinder Singh, Shehla, Anil Kumar, Deepak Swami, Ajay Kumar and Sanjiv Puri
- [Mo093](#) **Interaction between highly charged ions near the Bohr velocity energy region and laser-produced plasmas** • S. Q. Cao, R. Cheng, M. G. Su, L. L. Shi, Z. Wang, Z. X. Zhou, S. Q. He, Y. H. Wu, H. D. Lu, Q. Min, D. H. Zhang, C. Z. Dong
- [Mo094](#) **Probing the formation of quasi-molecules in collisions of  $\text{Kr}^{q+}$ -ion with Pb and Bi** • C. V. Ahmad, K. Chakraborty, R. Gupta, D. Swami and P. Verma
- [Mo095](#) **Efficiency enhancement of the dynamical capture of ion bunches by instantaneous ion-mode coupling** • Stefan Ringleb, Markus Kiffer, Sugam Kumar, Manuel Vogel, Wolfgang Quint, Thomas Stöhlker, Gerhard G. Paulus
- [Mo096](#) **Resonance-Enhanced Electron Capture in the Laser-Assisted Proton-Hydrogen Collision** • S. Gao, F. Zhu, L. G. Jiao, Aihua Liu, U. Thumm

### Heavy Particle – Molecule/Cluster

- [Mo097](#) **Development of electrospray ion source and setup for collision induced dissociation experiments of large molecules** • Kamal Kumar, Md Atiqur Rehman, Deepankar Misra
- [Mo098](#) **Dissociation dynamics in Chloroform molecule induced by ion impact** • Nirmallya Das, Sankar De, Pragya Bhatt, C. P. Safvan, Abhijit Majumdar
- [Mo099](#) **Excitation processes in collisions of  $\text{He}^+$  ions with  $\text{N}_2$ ,  $\text{O}_2$  molecules** • Malkhaz Gochitashvili, Ramaz A. Lomsadze, Roman Ya Kezerashvili, Michael Schulz



# Posters

Monday, July 31

## Heavy Particle – Molecule/Cluster

- [Mo100](#) **Ionization of molecules by bare ions impact: dynamic effective charge in the residual-target continuum state** • Maria Fernanda Rojas Barillas, M. A. Quinto, N. J. Esponda, R. D. Rivarola, J. M. Monti
- [Mo101](#) **A travelling-wave ion-mobility system for preparation of conformationally pure molecular targets for collision experiments** • Marcelo Goulard, Klaas Bijlsma, Martje Nieuwenhuis, Jente Damm, Thomas Schlathölter
- [Mo102](#) **Ultrafast rotational energy transfer initiating by Coulomb explosion in two-body dissociation of  $\text{CO}_2^{3+}$**  • Weiqing Xu, Ruichao Dong, Xincheng Wang, Yuhai Jiang
- [Mo103](#) **Statistical Analysis of X-ray Spectra of Aqueous Tripeptides** • Eemeli Eronen, Anton Vladyka, Florent Gerbon, Christoph Sahle, Johannes Niskanen
- [Mo104](#) **The role of molecular collisions in the conversions of nuclear spin isomers of methanol gas** • Zhen-Dong Sun
- [Mo105](#) **Combining momentum-space wavefunctions and frontier orbital theory for providing predictive insights into pharmacological activity** • Long Sihan, Y. Onitsuka, S. Nagao, M. Takahashi
- [Mo106](#) **Probing the internal dynamics of homonuclear dimer anions via time-dependent electron detachment inside an electrostatic ion trap\*** • Roby Chacko, Stav Knaffo, Nikolaj Klinkby, Oded Heber, Daniel Zajfman

## Low Energy to Ultracold

- [Mo107](#) **Ultralong-range Rydberg Molecules: Electronic Structure and Rydberg blockade** • D. Mellado-Alcedo, J. Gacia-Garrido, A. Guttridge, D. K. Ruttley, C. S. Adams, S. L. Cornish, H. R. Sadeghpour, R. Gonzalez-Ferez
- [Mo108](#) **Inner-shells effect for positrons and electrons traversing cold matter and plasmas** • Claudio Archubi, Claudia Montanari, Néstor Arista, Diego Arbó
- [Mo109](#) **Stereodynamical control of cold collisions between two aligned  $\text{D}_2$  molecules** • Pablo Jambrina, James F. E. Croft, J. Zuo, Hua Guo, F. J. Aoiz, N. Balakrishnan
- [Mo110](#) **Improved method to treat asymptotic non-adiabatic couplings in scattering processes** • Patrik Hedvall, Åsa Larson



# Posters

Monday, July 31

## Low Energy to Ultracold

- [Mo111](#) **Low-energy collisions between two indistinguishable tritium-bearing hydrogen molecules: HT+HT and DT+DT** • Renat Sultanov
- [Mo112](#) **Mutual neutralization between diatomic cation and atomic anion** • Arnaud Dochain, M. Poline, Ansgar Simonsson, Stefan Rosén, MingChao Ji, Henning Schmidt, R. D. Thomas
- [Mo113](#) **A new approach for measuring the reaction rates of low-energy ion—polar-molecule reactions for astrochemistry** • Kunihiro Okada, Kazuki Sugata, Naoki Kimura, Kazuhiro Sakimoto, Hans A. Schuessler
- [Mo114](#) **Observation of radiative vibrational cooling of  $N_2O^+$  ions using a cryogenic electrostatic ion storage ring: contribution of Fermi resonance** • Sakumi Harayama, S. Kuma, N. Kimura, K. C. Chartkunchand, Y. Nakano, T. Yamaguchi, T. Azuma
- [Mo115](#) **Mutual Neutralization in sub-eV  $C_{60}^+ + C_{60}^-$  collisions** • Raka Paul
- [Mo116](#) **Slow decay processes of molecular anions during long-time storage in a cryogenic storage ring** • Viviane Charlotte Schmidt, Klaus Blaum, Roman Čurík, Paul Fischer, Lisa Gamer, Sebastian George, Jürgen Göck, Manfred Grieser, Florian Grussie, Robert von Hahn, Oded Heber, Mark A. Iron, Ábel Kálosi, Claude Krantz, Holger Kreckel, Evangelos Miliordos, Preeti M. Mishra, Damian Müll, Oldřich Novotný, Felix Nuesslein, Milan Ončák, Daniel Paul, Hendrik B. Pedersen, Lutz Schweikhard, Kaija Spruck, Yoni Toker, Andreas Wolf, Aigars Znotiņš
- [Mo117](#) **X-ray imaging of nanostructures in superfluid helium droplets** • Rico Mayro Tanyag
- [Mo118](#)  **$CO_2$  activation by Cu clusters in superfluid helium nano-droplets** • Olga Lushchikova, M. Gatchell, J. Reichegger, S. Kollotzek, F. Zappa, P. Scheier
- [Mo119](#) **A versatile ion source for cold ions using superfluid helium nanodroplets** • Paul Martini, Henning Zettergren, Henning Schmidt, Michael Gatchell
- [Mo120](#) **Mid-infrared spectroscopy of aromatic molecular cations in helium nanodroplets** • Arisa Iguchi, Susumu Kuma, Hajime Tanuma, Toshiyuki Azuma
- [Mo121](#) **Supersolidity in a quasi-2D spinor Bose-Einstein condensate with SO-coupling** • Pardeep Kaur, Sandeep Gautam, S.K. Adhikari

# Posters

Monday, July 31

## Experimental Developments

- [Mo123](#) **Waterloo/ALLS Reaction Microscope Cold Target Recoil Ion Momentum Spectrometer Endstation** • Kaili Tian, H. Ibrahim, R. Karimi, F. Légaré, A. Staudte, J. Sanderson
- [Mo125](#) **Present and future opportunities at the CAMP instrument at the Free-Electron Laser FLASH** • Benjamin Erk
- [Mo127](#) **Direct measurement of few-cycle electric fields using a lock-in detection** • Ronak Narendra Shah, Jahanzeb Muhammad, Ianina Kosse, Samuel Bengtsson, Riccardo Mori, Mario Niebuhr, Fabio Frassetto, Luca Poletto, Giuseppe Sansone
- [Mo128](#) **A hybrid mode-locking Yb:fiber laser for generations of vector dissipative solitons** • Kun Chen, Tao Cao, Shaozhen Liu, Qi Xu, Zhou Li, Jiahui Peng
- [Mo130](#) **The CSR-ReMi – A cryogenic in-ring reaction microscope** • Felix Herrmann, David V. Chicharro, Robert Moshhammer, Claus Dieter Schröter, Thomas Pfeifer
- [Mo131](#) **The (only) way towards low-energy, heavy, highly charged ions: the HITRAP deceleration facility** • Nils Stallkamp, Zoran Andelkovic, Svetlana Fedotova, Wolfgang Geithner, Frank Herfurth, Max Horst, Dennis Neidherr, Simon Rausch, Sergiy Trotsenko, Gleb Vorobjev
- [Mo132](#) **ErUM-FSP APPA: BMBF Collaborative Research Center at FAIR** • Stefan Schippers, Thomas Stöhlker for the APPA collaboration

## Post Deadline

- [Mo133](#) **A real-time gas monitoring system based on ion mobility spectrometry for high concentration** • Kazunari Takaya, Masayoshi Hagiwara, Shiro Matoba, Mitsutoshi Takaya, Nobuyuki Shibata
- [Mo134](#) **Development of a universal in-ring COLTRIMS Reaction Microscope for CRYRING@ESR** • G. Kastirke, L. Ph. H. Schmidt, T. Jahnke, R. Dörner, M. S. Schöffler
- [Mo135](#) **Novel High Harmonic Beamline Design for Ultrafast X-ray Spectroscopy** • Philippe Burden, Patrick Elten, Andrey E. Boguslavskiy, Claude Marceau, Iain Wilkinson, Arnaud Rouzée, Paul Corkum, Albert Stolow

# Posters

Monday, July 31

## Post Deadline

- [Mo136](#) **The development of marking system of secondary battery anode and cathode using nanosecond laser with in situ tracking module** • Seungsik Ham, Jaesung Park, Taeho Jun, Ho Lee
- [Mo137](#) **Development of Polymer Dispersed Liquid Crystal (PDLC)-based switchable spatial filter using femtosecond laser micro-patterning** • Jaesung Park, JongWook Park, Ho Lee
- [Mo138](#) **Ultrafast electron-stimulated desorption to form ion pulses for time-resolved ion surface collision experiments** • Marius C. Chirita Mihaila, Gabriel L. Szabo, Alexander Redl, Markus Goldberger, Richard Wilhelm
- [Mo139](#) **Development of portable Electron Beam Ion Traps at NIST** • Joseph Tan, David La Mantia, Aung Naing, Albert Henins, Alessandro Banducci, Samuel Brewer
- [Mo140](#) **Toward a new type of gas phase spectroscopy for complex organic ions** • Stav Knaffo, M. L. Rappaport, H. Kreckel, K. Blaum, A. Wolf, Th. Henning, Y. Toker, S. Sunil Kumar, O. Heber, D. Zajfman
- [Mo142](#) **Recent progress of muon catalyzed fusion study: IV. Nuclear reaction processes in the dtu molecule** • Masayasu Kamimura, Yasushi Kino, Takuma Yamashita

## Electron-impact ionization of the $5p^6$ subshell in barium

O Borovik\*

Institute of Electron Physics, Uzhhorod, 88017, Ukraine  
Uzhhorod National University, Uzhhorod, 88000, Ukraine

**Synopsis** Ionization of the  $5p^6$  subshell in Ba atoms has been studied by observing the excitation dynamics of the electron spectra arising from the Auger decay of the  $5p^5n_1l_1n_2l_2$  states. The energy range of incident electrons from the lowest ionization threshold to 600 eV has been investigated. The ionization cross section for the  $(5p^56s^2)^2P_{1/2}$  state has been obtained with the maximum value of  $(3.2 \pm 0.6) \times 10^{-17}$  cm<sup>2</sup> at 132 eV.

Ionization of the  $5p^6$  subshell in Ba atoms is a very efficient process leading to the formation of  $5p^5n_1l_1n_2l_2$  ionic states, most of which are in the energy range between the second ionization limit and lower excited levels  $5p^5(2^0P_{3/2})5d$  of  $Ba^{2+}$  ions ( $E_{exc} \geq 31.677$  eV [1]). In this case, the Auger decay with the formation of  $Ba^{2+}$  ions in the ground state is the only de-excitation channel for  $5p^5n_1l_1n_2l_2$  states. This makes their excitation cross sections proportional to the intensity of the corresponding lines in the Auger spectra (see Figure 1 (a)).

In the present work, we report the first measurements of the ionization cross section for the  $(5p^56s^2)^2P_{1/2}$  state ( $E_{exc}=24.76$  eV), which is well separated from other ionic states. The data were obtained by measuring the intensity of the  $^2P_{1/2}$  line in the Auger spectra at various impact energies. The relative uncertainty in determining the line intensity generally did not exceed 20%. The relative data were put on the absolute scale by using the ratio of intensities of the  $^2P_{1/2}$  Auger line and line 28 reflecting the decay of the  $(5p^55d6s^2)^3D_1$  atomic autoionizing state (see Figure 3 in [2]. The excitation cross section of the latter was calculated at 600 eV in relativistic distorted wave approximation [2].

Figure 1(b) shows the measured ionization cross section for the  $(5p^56s^2)^2P_{1/2}$  state and the ionization cross section of the  $5p^6$  subshell calculated in Born approximation [3]. Comparing both data one can be seen that the growth of the measured cross-section to the maximum value  $(3.2 \pm 0.6) \cdot 10^{-17}$  cm<sup>2</sup> (at 132 eV) occurs much more slowly and its subsequent decrease occurs faster than could be expected for the direct ionization process. A comparison with the ionization cross section for the  $(4p^55s^2)^2P_{1/2}$  state in strontium [4] reveals a similar picture. Currently, the reason for this discrepancy is not clear, and additional experimental and theoretical studies of

doublet states  $^2P_J$  in the  $5p^56s^2$  configuration and low-lying states in the  $5p^55d6s$  and  $5p^55d^2$  configurations are required.

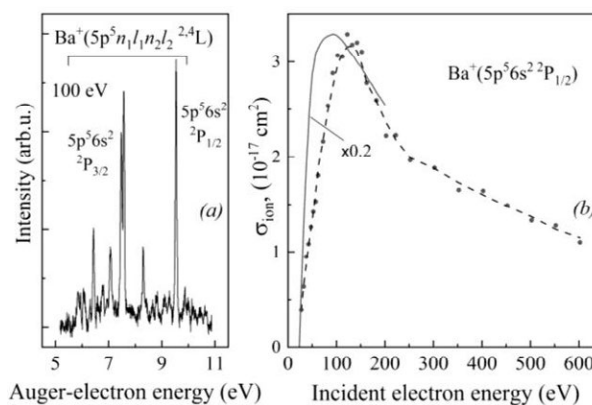


**Figure 1.** (a) – the  $5p^5n_1l_1n_2l_2$  Auger spectrum of Ba atoms at 100 eV impact energy; (b) – ionization cross sections: • present for the  $(5p^56s^2)^2P_{1/2}$  state; — calculated for the  $5p^6$  subshell [3]. The dashed line is used to guide the eye.

This work was funded by the National Academy of Sciences of Ukraine through Projects Nos. 0112U002079, 0117U003239, and by the Ministry of Education and Science of Ukraine under Project No. 0118U000173.

### References

- [1] Kramida A, Ralchenko Yu, Reader J and NIST ASD Team (2022), <https://physics.nist.gov/asd> [2023, March 8]
- [2] Hrytsko V Kerevicius G, Kupliauskienė A and Borovik A 2016 *J. Phys. B* **49** 145201
- [3] Vainshtein L A, Ochkur V I, Rakhovskii V I and Stepanov A M 1972 *Sov. Phys. – JETP* **49** 271
- [4] Borovik O 2022 *J. Phys. B* **55** 245202

\* E-mail: [baa1948@gmail.com](mailto:baa1948@gmail.com)

## Photoluminescence of L-valine irradiated with 12.5 MeV electrons

Yu Bandurin\*, A Zavilopulo, V Maslyuk and N Svatiuk

Institute of Electron Physics, National Academy of Sciences of Ukraine, 88017 Uzhhorod, Ukraine

**Synopsis** The luminescence spectra of powdered L-valine in the spectral region  $\lambda = 400 \div 800$  nm were investigated using a Shimadzu RF-6000 spectrofluorophotometer. Also the samples of L-valine were irradiated by electrons with an energy of 12.5 MeV. Different radiation doses in the range of  $0 \div 100$  kGy were prepared. We obtained nonlinear dose dependence of the photoluminescence quantum yield. The time of irradiation also play an important role in formation of L-valine molecules final state.

About 20% of the human body consists of proteins, which play a decisive role in almost all biological processes in living organisms, and amino acids are their building blocks. Since most of our cells, muscles and tissues are made up of amino acids, they are responsible for a significant number of essential body functions, especially in metabolic processes (metabolism). Amino acids are biologically important organic compounds that are the building blocks of proteins and contain amine ( $-\text{NH}_2$ ) and carboxyl ( $-\text{COOH}$ ) groups. Most proteins consist of a combination of nineteen so-called "primary" amino acids. One of the amino acid - valine ( $\text{C}_5\text{H}_{11}\text{NO}_2$ ) play an important role in formation of tissue cells in living organisms.

We have studied the photoluminescence spectra of powdered L-valine (in the spectral region  $400 \div 800$  nm) excited by photons in the range  $275 \div 380$  nm. The experiment and measurement technique are described in detail in [1]. Here are the results of measuring the photoluminescence spectra of the L-valine, irradiated at room temperature by electrons with an energy of 12.5 MeV (density from  $6.25 \cdot 10^{10}$  to  $4.37 \cdot 10^{11}$  el/cm<sup>2</sup>) on the M-30 microtron. The radiation doses were in the range of  $0 \div 100$  kGy.

The photoluminescence spectra measured by us show two maxima at 445 and 503 nm. The intensity of the luminescence spectrum of irradiated valine differs significantly from that of non-irradiated. The dependence on the radiation dose is non-linear and has a maximum at the doses  $40 \div 50$  kGy. In addition, the spectral intensity distribution changes on the wavelength scale, which may be associated with structural changes in the irradiated valine molecules. This suggests that the final state of valine molecules

after irradiation depends not only on the absorbed dose, but also on the time of irradiation. To test this assumption, we measured the photoluminescence spectra of valine (dose 50 kGy, obtained during 6 min and 15 min). On the figure one can see the difference both in terms of the spectrum shape and in terms of the quantum yield of luminescence.

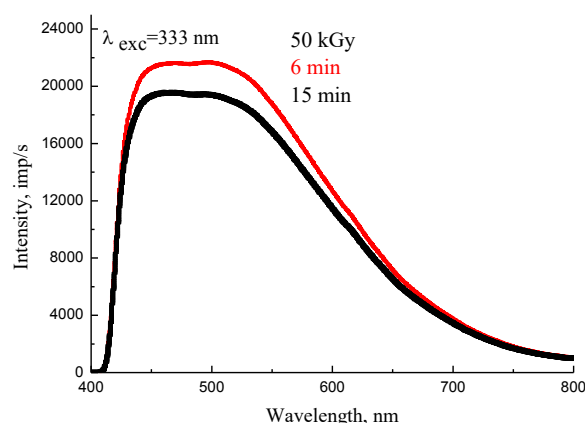


**Figure 1.** The influence of irradiation time

Thus, the final state of irradiated valine molecules depends not only on the absorbed dose, but also on the conditions (beam intensity, irradiation time). In the future, it is necessary to elucidate the role of structure restoration processes due to self-organization, chemical interaction, and clustering of structural segments of the valine molecule.

### References

- [1] Bandurin Yu, Zavilopulo A, Molnar Sh, and Shpenik O 2022 *Eur. Phys. J. D* **76** 9

\* E-mail: [bandurin\\_unc@ukr.net](mailto:bandurin_unc@ukr.net)

## Investigation of photoluminescence of glucose and fructose in the powder form

Yu Bandurin\*, A Zavilopulo, V Maslyuk and N Svatiuk

Institute of Electron Physics, National Academy of Sciences of Ukraine, 88017 Uzhhorod, Ukraine

**Synopsis** The luminescence spectra of glucose and fructose molecules in the spectral region  $\lambda = 400 \div 700$  nm were investigated using a Shimadzu RF-6000 spectrofluorophotometer. The differences were found both in the quantum yield of luminescence of these molecules and in the shape of spectra. Irradiation of glucose by 12,5 MeV electrons with doses 14 and 164 kGy has a significant influence on the luminescent properties of glucose molecules.

The biological and industrial importance of monosaccharides stimulates research into the processes of electrons and photons interaction with their molecules. Understanding the mechanisms of energy dissipation in organic molecules is extremely important both for studying the processes occurring in living organisms and for studying radiation damage to biological objects. The literature mainly presents the results of studies of the photoluminescence of monosaccharides in the form of solutions. We have developed a technique for measuring photoluminescence spectra from the surface of powdered substances [1–2]. A comparison of the glucose and fructose spectra obtained by us [3] shows a significant difference both in the luminescence quantum yield and in the shape of the spectra. Despite the same formula -  $C_6H_{12}O_6$ , glucose and fructose differ in the structure of the molecules. We measured the photoluminescence spectra of powdered glucose samples irradiated on an M-30 microtron. Glucose was irradiated with electrons with an energy of 12.5 MeV. The radiation dose was 14 and 164 kGy. In the wavelength range of 400–700 nm, photoluminescence spectra were measured upon excitation by photons with wavelengths (energies): 380 nm (3.26 eV), 354 nm (3.53 eV), 323 nm (3.83 eV) and 275 nm (4.51 eV).

On fig. Figure 1 shows as an example the spectra measured for the case  $\lambda_{exc} = 354$  nm. The most intense long-wavelength maximum ( $\lambda_{max}=535$  nm in the case of non-irradiated glucose) is associated with the relaxation of excitations occurring in the COH carbonyl group. The shorter wavelength  $\lambda_{max}=445$ -450 nm owes its appearance to excitation processes in the OH radical. A similar maximum in the spectrum of

fructose is located in the longer wavelength region  $\lambda_{max}=551.5$  nm, which is explained by the difference in structure from the glucose molecule. When glucose is irradiated with electrons at a dose of 14 kGy, the molecules are rearranged, and the spectrum becomes similar to that of fructose, both in the shape of the spectrum and in the quantum yield. It seems at this dose of irradiation, glucose becomes ketose. Increasing the dose up to 164 kGy leads to more significant damage to the molecular structure. Most likely, fragmentation of glucose molecules is already taking place, and another maximum appears in the luminescence spectrum.

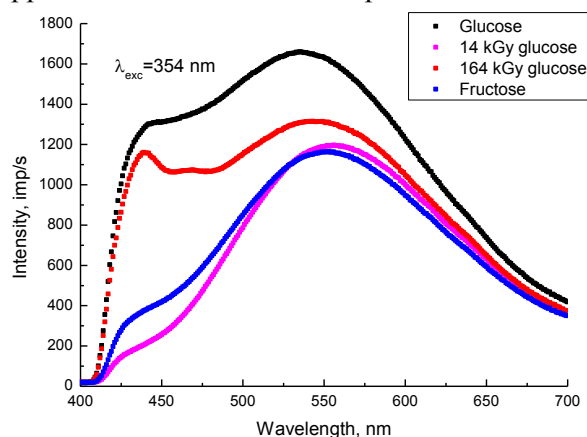


Figure 1. Photoluminescence spectra of glucose and fructose

### References

- [1] Bandurin Yu, Zavilopulo A, Molnar Sh, and Shpenik O 2022 *Eur. Phys. J. D* **76** 9
- [2] Bandurin Yu, Popik T Yu, Zavilopulo A N 2022 *Rep. of the NAS of Ukraine* **1** 58
- [3] Bandurin Yu *et al.* 2023 *J. of Phys. & Opt. Sci.* **5** 1

\* E-mail: [bandurin\\_unc@ukr.net](mailto:bandurin_unc@ukr.net)



## Studies of the VUV luminescence excited by electron impact on the gas-phase glycine and alanine

H. Bohachov\* and R. Tymchyk

Institute of Electron Physics, Universitetska 21, Uzhhorod, 88000 Ukraine

**Synopsis** Biomolecule fragmentation under low-energy electron influence is being studied extensively using the mass-spectrometry technique. However, in this case the role of the fragments produced due to excitation remains not clarified. This work is devoted to studying the VUV luminescence induced by electron impact on glycine and alanine molecules. It could be useful for understanding the fragment excitation role.

The work was carried out using the crossed electron and molecular beam technique applying a 0.5 metre Seya-Namioka VUV spectrometer [1] with the assembly of photon detectors (near-VUV photomultiplier and open electron multichannel-plate multiplier). The beam of the molecules under study was formed from the fine-crystalline amino acid powders under heating in the oven provided with a cylindrical channel. The oven temperature was kept near 50-70°C, i.e. substantially below the glycine and alanine molecules decomposition temperature (292°C and 297°C respectively).

The luminescence spectra for both amino acids were recorded in the 80-215 nm region at the electron energies from 20 to 100 eV. Note that short-wavelength spectra (up to 125 nm) measured with open electron multiplier include only the H Lyman-series spectral lines. The long-wavelength spectra (112-215 nm) measured at the 40 eV energy are shown in Fig. 1. At the energies above 40 eV the resonance H Lyman- $\alpha$  line at 121.6 nm dominates for both amino acids. A number of other emissions comparable by intensity with H Lyman- $\alpha$  line are observed in the spectra in the region 140-170 nm. One can see from Fig.1 evident similarity between glycine and alanine spectra. But noticeable difference between these spectra in intensity distribution take place – in alanine case the emissions are more intensive as well as many weak emissions above 170 nm are present.

Using the compilation data [2], seven of visible emissions in the region 140-170 nm (141.6, 144.6, 147.7, 151.0, 154.2, 156.0, 165.1 nm) could be clearly assigned to the band spectrum of carbon monoxide, namely to the 4<sup>th</sup> positive system ( $A^1\Pi-X^1\Sigma^+$ ) – transitions (4,0), (3,0), (2,0), (1,0), (3,2), (1,1), (3,4) respectively. The emission at 115 nm seemingly correspond to transition (0,0) of the Hopfield-Birge band system ( $B^1\Sigma^+-X^1\Sigma^+$ ).

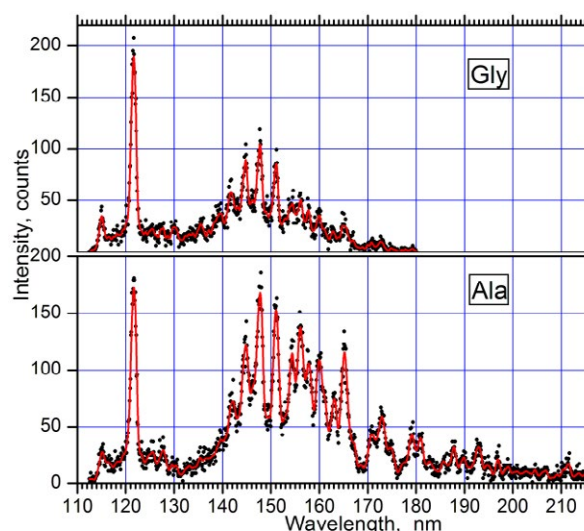


**Fig. 1:** Emission spectra for glycine and alanine recorded at the 40 eV electron energy

The mechanisms of the appearance of the emissions in the spectra are analyzed. It is logically to suppose that formation of excited CO molecules relate to carboxyl group detachment followed by process of detachment / excitation CO fragments. As to formation of excited H atoms, perhaps, a complicated process occurs with target molecules under electron impact – ionization-fragmentation of the target molecule with release of an excited hydrogen atom like it was supposed in the case of tymin target [3].

### References

- [1] Aleksakhin I S, Bogachev G G, Zapesochnyi I P, Ugrin S Yu 1981 *Sov. Phys. JETP*, **53** 1140
- [2] Krupenie P H 1966 *Natl. Std. Ref. Data Series – NBS 5 (US)* 39-41
- [3] Tiessen C J, Trocchi J A, Hein J D, Dech J, Kedzierski W, McConkey J W 2016 *J. Phys. B: At. Mol. Opt. Phys.* **49** 125204

\* E-mail: [bogach\\_gen@gmail.com](mailto:bogach_gen@gmail.com)

## The near-threshold electron-impact resonance excitation of the In<sup>+</sup> ion

A N Gomonai<sup>1</sup>, V Jonauskas<sup>2</sup>, S Kučas<sup>2</sup>, V Roman<sup>1\*</sup>, A I Gomonai<sup>1</sup>,  
Yu Hutych<sup>1</sup> and V Zvenihorodsky<sup>1</sup>

<sup>1</sup> Institute of Electron Physics, Ukrainian National Academy of Sciences, Uzhhorod, 88017, Ukraine

<sup>2</sup> Institute of Theoretical Physics and Astronomy, Vilnius University, Vilnius, LT-01108, Lithuania

**Synopsis** The results of experimental and theoretical investigation of the near-threshold electron-impact excitation cross-section of the  $\lambda 158.6$  nm ( $5s5p\ ^1P_1 \rightarrow 5s^2\ ^1S_0$ ) and  $\lambda 289.0$  nm ( $5s5d\ ^1D_2 \rightarrow 5s5p\ ^1P_1$ ) lines of the In<sup>+</sup> ion is presented.

The dominance of resonance processes in electron-impact excitation of the resonance line  $\lambda 158.6$  nm ( $5s5p\ ^1P_1 \rightarrow 5s^2\ ^1S_0$ ) of the In<sup>+</sup> ion in the near-threshold energy region was studied by us experimentally earlier [1]. However, there were no reliable theoretical calculations of this process for the In<sup>+</sup> ion at that time.

Here we report on experimental and theoretical study of the electron-impact excitation cross section of the  $\lambda 158.6$  nm ( $5s5p\ ^1P_1 \rightarrow 5s^2\ ^1S_0$ ) resonance and  $\lambda 289.0$  nm ( $5s5d\ ^1D_2 \rightarrow 5s5p\ ^1P_1$ ) cascade lines of the In<sup>+</sup> ion from the excitation thresholds up to 30 eV.

The experimental excitation functions were measured by a VUV-spectroscopy method using the crossed monoenergetic electron and ion beams technique which is described in detail in [2]. The electron-impact excitation cross sections are calculated in the distorted wave (DW) approximation using Flexible Atomic Code [3] which implements the Dirac-Fock-Slater approximation. Single and double excitations from the  $5s^2$ ,  $5s5p$ , and  $5s5d$  configurations are considered to build the list of interacting configurations. Populations of the excited levels ( $5s5p\ ^1P_1$  and  $5s5d\ ^1D_2$ ) were studied by considering the direct excitation by electron impact, the excitation to the higher levels followed by radiative cascade, and dielectronic capture to the levels of the In atom with subsequent decay through radiative and Auger transitions. It should be noted that the radiative decay from the higher levels populated by the excitations from the ground level included branching ratios. The determinate uncertainty of the absolute effective excitation cross-section was about  $\pm 30\%$ .

The energy dependences of the absolute emission cross-sections of the  $\lambda 158.6$  nm and

$\lambda 289.0$  nm lines are presented in Fig. 1. The absolute values of the cross-sections are obtained by normalizing the experimental data to that calculated using DW approximation at the energy of 100 eV.

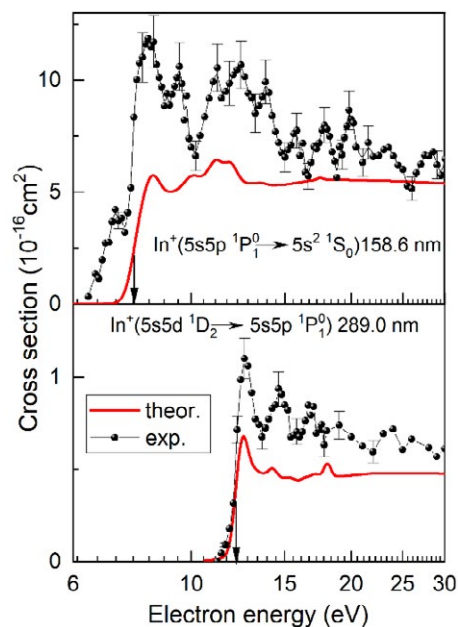


**Figure 1.** Emission cross sections of the  $\lambda 158.6$  nm and  $\lambda 289.0$  nm lines of the In<sup>+</sup> ion.

It is seen that the energy position of the structure maxima in the calculated emission cross-sections rather good agrees with that experimentally observed. At the same time some experimental structural features are missing in the calculated cross-sections.

### References

- [1] Gomonai A *et al.* 2005 *Nucl. Instr. Meth. Phys. Res. B.* **233** 250
- [2] Ovcharenko E *et al.* 2010 *J. Phys. B* **43** 175206
- [3] Gu M 2008 *Can. J. Phys.* **86** 675

\* E-mail: [viktoriyaroman11@gmail.com](mailto:viktoriyaroman11@gmail.com)



## Ramsauer-Townsend minima in the low-energy integral cross sections of elastic electron scattering by *Sb*, *Xe* and *Bi*, *Rn* atoms

V I Kelemen\* and E Yu Remeta†

Institute of Electron Physics, Ukrainian National Academy of Sciences, Uzhhorod, 88017, Ukraine

**Synopsis** The low-energy behavior of the integral cross sections of elastic electron scattering on *Sb*, *Xe*, *Bi* and *Rn* atoms is studied using the relativistic optical potential method. The contribution of *s*-, *p*-, and *d*-partial cross sections is considered and the energies of Ramsauer-Townsend minima are calculated.

The Ramsauer-Townsend (RT) minimum and the maximum following it are the manifestation of the combined action of exchange-polarization interactions [1].

Using relativistic optical potential method without (RSEP) and with (RSEPA) account absorption effects we calculated energy dependences of ICSSs of electron scattering at *Sb*([*Cd*]5p<sup>3</sup>), *Xe*([*Cd*]5p<sup>6</sup>), *Bi*([*Hg*]6p<sup>3</sup>), *Rn*([*Hg*]6p<sup>6</sup>). At energies <30 eV, the energy behavior of ICSSs is similar and irregular – of the maximum-minimum-maximum type.

As an example, the dependences of ICSSs  $\sigma_{el}(E)$  of electron scattering by the *Rn* atom calculated in RSEP and RSEPA are shown in figure 1. In [2] the relativistic nonlocal potential is used, and in [3] the static-exchange-polarization potential with account of absorption effects is used in the Dirac equation.

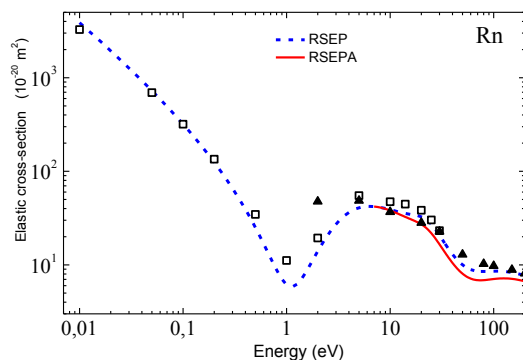


**Figure 1.** Energy dependence of the ICSSs for the electron scattering by *Rn* atom (in units of  $10^{-20} \text{ m}^2$ ). Theory: present calculations – RSEP (blue dashed line), RSEPA (red solid line); [2] (□); [3] SEPA (▲).

The RT minima in CSs is due to the minimum in the *s*-wave partial CSs  $\sigma_0(E)$  (see table 1) and the values of  $\sigma_{el}(E_{RT})$  are a result of combined contribution in general from *s*-, *p*- and *d*-partial CSs. For example, for *Xe* atom at 0.766 eV these contributi-

ons are (%) - 4.2, 10.5, 72.7 and for *Rn* at 1.12 eV - 11.3, 19.6, 62.8. For the Ar atom in the RSEP value  $\sigma_{el}(E_{RT}=0.33 \text{ eV})=2.157 \cdot 10^{-21} \text{ m}^2$  the main contribution is made by the *p*-partial CS (72.2%), whereas the *d*-wave contribution was only 22.8% [4].

**Table 1.** Energy  $E_{RT}$ , ICSSs  $\sigma_{el}(E_{RT})$ , energy  $E_{min}$ , *s*-wave partial cross section  $\sigma_0(E_{min})$  in RSEP.

	$E_{RT}$ , eV	$\sigma_{el}(E_{RT})$ , $10^{-20} \text{ m}^2$	$E_{min}$ , eV	$\sigma_0(E_{min})$ , $10^{-20} \text{ m}^2$
<i>Sb</i>	0.344	2.02	0.43	$2.2 \cdot 10^{-8}$
<i>Xe</i>	0.766	1.25	0.862	$2.9 \cdot 10^{-6}$
<i>Bi</i>	0.60	6.27	0.79	$4.06 \cdot 10^{-4}$
<i>Rn</i>	1.12	5.86	1.41	$9.2 \cdot 10^{-5}$

The low-energy maxima in CSs  $\sigma_{max}(E_{max})$  have such values at the corresponding energies (in  $10^{-20} \text{ m}^2$ ): ***Sb*** –  $\sigma_{max}(5.1 \text{ eV})=49.04$ ; ***Xe*** –  $\sigma_{max1}(8.2 \text{ eV})=37.9$ ,  $\sigma_{max2}(21.1 \text{ eV})=33.67$ ; ***Bi*** –  $\sigma_{max}(4.45 \text{ eV})=49.65$ ; ***Rn*** –  $\sigma_{max1}(6.3 \text{ eV})=42.24$ ,  $\sigma_{max2}(21.3 \text{ eV})=31.60$ .

Maxima in ICSSs for *Sb*, *Bi* atoms and first maxima for *Xe*, *Rn* atoms are primarily a result of combined contribution of *p*- and *d*-partial CSs (%) – ~20-40, 35-55. Second maxima for *Xe* and *Rn* atoms are a result of combined contribution of *p*-, *d*- and *f*-partial CSs (%) – ~20, ~30-54, 40-47.

### References

- [1] Burke P G 1977 Potential scattering in atomic physics. Plenum Press, N.Y. and London
- [2] Sin Fai Lam L T 1982 *J. Phys. B: At. Mol. Phys.* **15** 119
- [3] Neerja, Tripathi A N, Jain A K 2000 *Phys. Rev. A* **61** 032713
- [4] Kelemen V, Dovhanych M, Remeta E 2014 *Ukr. J. Phys.* **59** 569

\* E-mail: [vlad.kelemen@gmail.com](mailto:vlad.kelemen@gmail.com)

† E-mail: [remetoveyu@gmail.com](mailto:remetoveyu@gmail.com)

## High-energy critical minima in differential cross sections of elastic electron scattering by *Sb*, *Xe* and *Bi*, *Rn* atoms

V I Kelemen\* and E Yu Remeta†

Institute of Electron Physics, Ukrainian National Academy of Sciences, Uzhhorod, 88017, Ukraine

**Synopsis** It is established that six high-energy ( $> 100$  eV) critical minima (CM) in differential cross sections (DCSs) of elastic electron scattering by *Sb*, *Xe*, *Bi*, *Rn* atoms from two different periods have approximately the same value of the ratio of the atomic nuclear charge  $Z$  to electron momentum  $k$ . This value is also close to the values  $Z/k$  for the 6 high-energy CM in the DCSs for the *Hg* and *Pb* atoms.

Diffraction and interference of electron partial waves, when electron interact with a target, lead to minima in the angular dependence of the differential cross sections (DCSs) of elastic scattering at all scattering energies.

At critical minima (CM), the magnitude of DCSs is very small ( $\ll 10^{-20}$  m<sup>2</sup>/sr) and the direct amplitude  $f(E, \theta)$  is less than the spin-flip  $g(E, \theta)$ , thus  $|f(E, \theta)|^2 \ll |g(E, \theta)|^2$  [1].

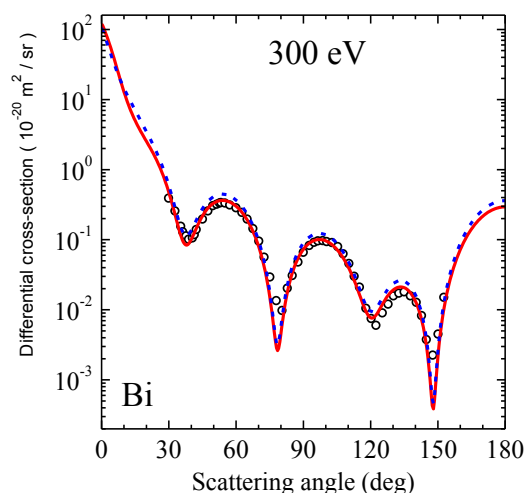


**Figure 1.** Angular dependences of the DCSs of the elastic  $e+Bi$  scattering at an energy of 300 eV close to KM №1. Theory: present calculations - RSEP (blue dashed line), RSEPA (red solid line). Experiment: [2] (o).

Using relativistic optical potential method without (RSEP) and with (RSEPA) account absorption effects we calculated angular dependences of DCSs of elastic electron scattering at *Sb*([*Cd*]5p<sup>3</sup>), *Xe*([*Cd*]5p<sup>6</sup>), *Bi*([*Hg*]6p<sup>3</sup>), *Rn*([*Hg*]6p<sup>6</sup>) atoms. As an example, the DCSs of electron scattering by the *Bi* atom calculated in RSEP and RSEPA are shown in figure 1.

\* E-mail: [vlad.kelemen@gmail.com](mailto:vlad.kelemen@gmail.com)

† E-mail: [remetoveyu@gmail.com](mailto:remetoveyu@gmail.com)

Energies  $E_{cr}$  and angles  $\theta_{cr}$  of CM in the DCSs of electron scattering were determined – *Sb* (15 CM), *Xe* (16) and *Bi* (14), *Rn* (15).

Table 1 shows 6 high-energy CM with close values of critical angles  $\theta_{cr}$  and approximately equal ratio  $Z/k=Z/(2E_{cr})^{1/2}$  (in a.u.) for the same CM numbers. These values,  $\theta_{cr}$  and  $Z/k$ , are approximately equal for the same for the corresponding numbers of 6 high-energy CM for *Hg*([*Xe*]4f<sup>14</sup>5d<sup>10</sup>6s<sup>2</sup>) [3] and *Pb*([*Hg*]6p<sup>2</sup>) [4] atoms.

**Table 1.** RSEPA energies  $E_{cr}$  (eV) and angles  $\theta_{cr}$  (deg.) of high-energy CM.

№	<i>e+Sb</i>		<i>e+Xe</i>	
	$E_{cr}$	$\theta_{cr}$	$E_{cr}$	$\theta_{cr}$
1	87.6	141.23	102.6	141.97
2	142.6	108.59	151.0	110.78
3	146.6	57.06	196.0	58.57
4	233.6	151.08	256.5	151.05
5	341.4	93.72	383.5	94.99
6	727.6	131.89	791.4	133.16
№	<i>e+Bi</i>		<i>e+Rn</i>	
	$E_{cr}$	$\theta_{cr}$	$E_{cr}$	$\theta_{cr}$
1	288.4	148.06	300.8	149.16
2	364.1	118.69	388.3	119.38
3	468.8	70.18	485.1	71.92
4	614.6	152.55	652.9	152.72
5	960.5	100.11	1003.0	101.03
6	1810.8	137.34	1918.8	137.64

### References

- [1] Kessler J 1976 Polarized electrons (Springer-Verlag, Berlin Heidelberg N.Y.)
- [2] Haug R 1968 *Zeit. fur Physik* **215** 350
- [3] Kelemen V, Remeta E 2012 *J. Phys. B: At. Mol. Opt. Phys.* **45** 185202
- [4] Haque A et al 2018 *J. Phys. Commun.* **2** 125013

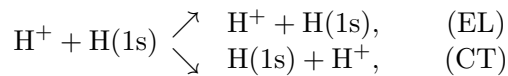
# Elastic and charge transfer cross sections for low energy $H^+ + H$ collisions. Quantal and semiclassical calculations

Mykhaylo V. Khoma \*

Institute of Electron Physics, Ukrainian National Academy of Sciences, Uzhhorod, 88017, Ukraine

**Synopsis** The elastic scattering and charge transfer (spin exchange) cross sections in  $H^+ + H$  collisions are computed for the center-of-mass energy range  $10^{-10} - 1$  eV. Fully quantal and semiclassical approaches are utilized in the present calculations, as are highly accurate electronic potential energy curves. The results are compared with available data.

We present a theoretical study of the elastic scattering (EL) and the symmetric charge transfer (CT)



at proton collision with atomic hydrogen for the center-of-mass energy range  $10^{-10} \leq E_{c.m.} \leq 1$  eV. The integral cross sections of the EL and CT reactions were computed using the elastic scattering approximation and a two-channel (corresponding to the  $1s\sigma_g$  and  $2p\sigma_u$  electronic states of the  $H_2^+$  system) approach [1, 2]. The scattering phase shifts were computed by fully quantal and semiclassical (JWKB) methods. From the phase shifts, the cross sections for the EL and CT reactions have been computed by using both the quantum indistinguishable particles (QIP) and the classical distinguishable particles (CDP) approaches. The results (in atomic units) are given in tables 1 and 2. The digits in brackets refer to the power of ten multiplier.

**Table 1.** The integral cross section for elastic scattering, QIP approach.

$E_{c.m.}$ (eV)	Present, quantal	Results from [1, 2]
		Ref. [1]
1.0(-10)	5.87336(+6)	6.01101(+6)
1.0(-9)	5.69042(+6)	5.72909(+6)
2.0(-8)	3.39329(+6)	3.44225(+6)
1.0(-7)	1.23945(+6)	1.24376(+6)
		Ref. [2]
1.000(-4)	10174.1	10180
3.715(-4)	6249.8	6219
7.244(-4)	5606.7	5595
9.772(-4)	5537.7	5533

\*E-mail: [m.khoma@gmail.com](mailto:m.khoma@gmail.com)

**Table 2.** The integral cross section for charge transfer, CDP approach.

E(eV)	Present, quantal	Present, JWKB
0.1254	205.247	195.32
0.1950	181.147	186.38
0.3	184.318	187.99
0.7	169.275	169.11
1.0	162.251	162.16

In Figure 1 we show the quantal and JWKB results for CT cross section in the energy range of 0.11 – 0.4 eV. Surprisingly, the JWKB results agree well with quantal calculations down to the fairly low collision energy  $\sim 0.11$  eV.

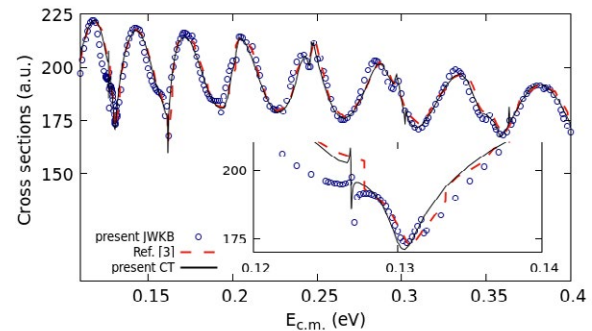


**Figure 1.** The integral cross section for charge transfer: the present results are compared with theoretical work [3]. The inset displays a close-up of the sharp oscillation at  $E_{c.m.} \sim 0.127$  eV.

## References

- [1] Glassgold A E, Krstic P S and Schultz D R 2005 *The Astrophys. Journ.* **621** 808
- [2] Schultz D R, Ovchinnikov S Yu, Stancil P C and Zaman T 2016 *J. Phys. B* **49** 084004
- [3] Tolstikhina I Yu and Kato D 2010 *Phys. Rev. A* **82** 032707

## Ionization of outer shells in the K atom by electron impact

V Roman\*

Institute of Electron Physics, Ukrainian National Academy of Sciences, Uzhhorod, 88017, Ukraine

**Synopsis** The relativistic distorted-wave, Coulomb-Born, and binary-encounter-dipole approximations were employed for calculating the electron-impact single ionization cross-sections of the  $4s$ ,  $3p^6$ ,  $3s^2$  shells for the K atom taking into account both configuration interaction and relativistic effects.

Electron-impact ionization cross-sections are widely used in applications such as modeling of plasma syntheses in tokamaks, modeling of radiation effects for materials, medical research, and aeronomy as well as in basic research in astrophysics, atomic, molecular, and plasma physics. Therefore, the study of ionization of atoms is very relevant today. This is confirmed by a large number of experimental and theoretical studies of the ionization process of atoms, in particular alkali metal atoms [1–4]. Previously, we studied the ionization cross-sections for the rubidium atom [5]. Here we consider the capabilities of the most widely used theoretical approaches, namely relativistic Coulomb-Born (CB), distorted-wave (DW), and binary-encounter-dipole (BED), for the single electron-impact ionization of the K atom in the impact energy range from the  $4s$  threshold up to 700 eV using the standard software package Flexible Atomic Code (FAC) [6].

Figure 1 shows a comparison of the single ionization cross-sections of the  $4s$ ,  $3p^6$ , and  $3s^2$  shells of the K atom calculated in the DW, BED, and CB approximations with the data [4] obtained using the plane wave Born (PWB) approximation. Note that the experimental data are available only for the  $4s$  shell and only below the excitation threshold of the  $3p^6$  shell [1]. In Fig. 1 these data [1] are normalized to the absolute values from Ref. [2] at 500 eV.

The comparison of the ionization cross-sections of the  $4s$  shell shows that the absolute values of the BED data are the best match with the experiment, however the maximum of the cross-section is strongly shifted. As for the maxima position, the CB and DW data are in the best agreement with the experiment. The  $4s$  shell ionization cross-section obtained using PWB approximation [4] shows the largest discrepancy with the experiment regarding the absolute values as well as maxima position.

As for the K atom  $3p^6$  and  $3s^2$  shells, their ionization cross-sections strongly differ between themselves. Unfortunately, one is unable to obtain the experimental cross-section of a specific electron shell. For this reason, we are now calculating the excitation cross-sections of the K atom. This will allow us to isolate this indirect process from the complete ionization cross-section and obtain only the total cross-section of the direct ionization of the potassium atom ( $4s+3p^6+3s^2$ ). This will make it possible to estimate the correct description of both excitation and ionization of the deeper  $3p^6$  and  $3s^2$  shells.

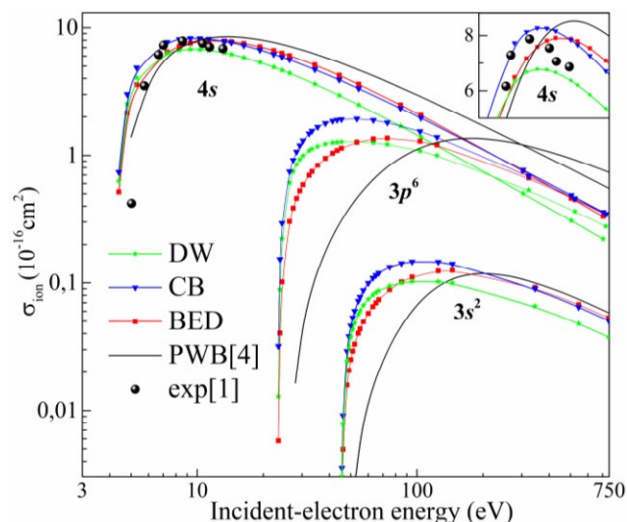


**Figure 1.** The single ionization cross-sections of the  $4s$ ,  $3p^6$  and  $3s^2$  shells of the K atom.

### References

- [1] Tate J, Smith P 1934 *Phys. Rev.* **46** 773
- [2] Mcfarland R *et al.* 1965 *Phys. Rev.* **137** 1058
- [3] Roy B, Rai D 1973 *Phys. Rev. A.* **8** 849
- [4] Bartlett P, Stelbovics A 2004 *Atomic Data and Nuclear Data Tables* **86** 235
- [5] Roman V *et al.* 2015 *J. Phys. B.* **48** 205204
- [6] Gu M 2008 *Can. J. Phys.* **86** 675

\* E-mail: [viktoriyaroman11@gmail.com](mailto:viktoriyaroman11@gmail.com)

## Electron Atom/Molecule Scattering and its Applications: A Tribute to Michael Brunger

S J Buckman<sup>1\*</sup>, O Ingolfsson<sup>2</sup>, D Maric<sup>3</sup> and R D White<sup>4</sup>

<sup>1</sup>Research School of Physics, Australian National University, Canberra 0200, Australia

<sup>2</sup>Department of Chemistry, University of Iceland, 107 Reykjavik, Iceland

<sup>3</sup>Institute of Physics, Pregrevica 118, Beograd, Serbia

<sup>4</sup>College of Science & Engineering, James Cook University, Douglas 4811, Australia

**Synopsis** Michael James Brunger passed away in September 2022 at the tender age of 61. Here we briefly remember and pay tribute to his many contributions to atomic and molecular collision physics and its applications.

Michael Brunger commenced his research career in the early 1980s working on low energy electron collisions with atoms and molecules while a graduate student in Peter Teubner's lab at Flinders University in Adelaide, South Australia. His thesis work involved measurements of differential cross sections and electron-photon coincidence parameters for metal targets, Mg and Na.

Following several years as a Postdoctoral Fellow at the Australian National University, Michael returned to Flinders to work with Erich Weigold on (e,2e) spectroscopy of molecules and, after being appointed to the faculty there, started to work on electron molecule scattering measurements that were relevant across a range of important industrial, medical, environmental and atmospheric applications.

This work, and that throughout his career, is characterised by highly accurate measurements of absolute scattering cross sections for low energy electrons, typically less than 60 eV collision energy. He did not baulk at difficult challenges, as exemplified by his measurements of electron collisions with molecular radical species. This endeavour, which saw him develop a complex multi-chamber vacuum apparatus for the production and characterisation of mixed molecule/radical beams of CF<sub>2</sub> and CF<sub>3</sub>, and their subsequent interaction with a high resolution electron beam, was an experimental *tour de force* and the first of its kind.

He was always driven to measure things that others could use in a variety of applications, and was a well-known figure within the global gaseous electronics community, an interdisciplinary

community that both measure and use atomic and molecular data across a range of industrial, environmental and atmospheric applications. To this end, he and colleagues developed an advanced atmospheric modelling code and used their data, and the data of others, to provide accurate predictions and insight into the behaviour of our atmosphere and the atmospheres of neighbouring planets. It was also through these measurements and models that he developed strong collaborations with quantum scattering and charged-particle transport theorists, many of whom he published with jointly.

Since the early 2000s, Michael also ventured into studies of positron scattering from atoms and molecules and, through all of these activities, he developed an extensive network of more than 100 international collaborators and colleagues, many of whom contributed to his more than 350 academic publications.

Michael was well known and highly regarded by all of his many international colleagues, students and friends, for his academic prowess, his willingness to drive fruitful collaborations, and his eclectic but ever-present sense of humour.

Michael was a strong supporter of ICPEAC and its various satellites for many years. He is a profound loss to us all, and taken way too early.



**Prof. Michael Brunger**

\* E-mail: [stephen.buckman@anu.edu.au](mailto:stephen.buckman@anu.edu.au)



## Electron Swarms as a Bridge Between Atom/Molecule Collisions and Gas Discharges: A Tribute to Robert W. Crompton

Z Lj Petrović<sup>1,2\*</sup> and S J Buckman<sup>3§</sup>

<sup>1</sup>Serbian Academy for Sciences and Arts, Knez Mihailova 35, 11001 Belgrade, Serbia

<sup>2</sup>School of Engineering, Ulster University, Jordanstown, County Antrim BT37 0QB, United Kingdom

<sup>3</sup>Research School of Physics, Australian National University, Canberra 0200, Australia

**Synopsis** Robert (Bob) Woodhouse Crompton passed away in June 2022 at the age of 96. Here we remember and pay tribute to his defining contribution to the physics of electron swarms, and especially their application in atomic and molecular collision physics, during his distinguished career at the Australian National University (ANU).

Bob Crompton's name has become synonymous with the physics of swarms of charged particles, indeed it was Bob who coined the phrase 'swarms'. He pioneered the swarm technique used to determine high accuracy electron scattering cross sections, and the development of experiments that led the scientific world in this field by their precision and interpretation. The term seemed very aptly chosen as electron 'swarms' display collective behavior in the complete absence of any interaction under the influence of external fields.

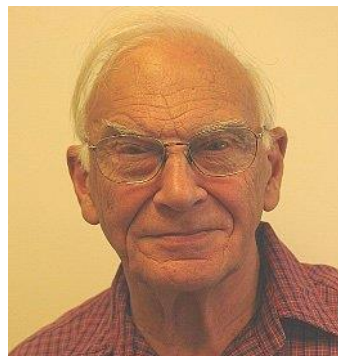
Robert Crompton was born in Adelaide in 1926. He completed his undergraduate and graduate studies at the University of Adelaide, his thesis supervisor being Sir Leonard Huxley, a student of Sir John Townsend.

Over his career Bob developed (often in collaboration with Malcolm Elford and John Gascoigne) the most accurate experimental devices for measurements of drift velocities, characteristic energies ( $D_T/\mu$ ), thermal diffusion coefficients and attachment rates. These transport data are the basis for the swarm analysis, resulting in the determination of electron scattering cross sections.

Bob inspired his colleague Kailash Kumar and PhD student Robert Robson to open a theoretical study of electron transport based on the Boltzmann equation. He oversaw the development of the two-term code as a tool for evaluation of the cross sections. He also organized development of a Monte-Carlo-based code to establish a set of benchmark results to test the two-term theory.

Bob's crowning achievements include the cross section for elastic scattering of electrons from He below the threshold for excitation, which remain to this date amongst the most accurately determined cross sections available.

In addition are the benchmark data for argon and para-hydrogen. Cross sections were also determined for molecular hydrogen, nitrogen and other gases. Last but not the least, attachment rates measured for the room temperature electrons in SF<sub>6</sub> (and other gases) are regarded as the most accurate and are used to normalize the results of relative measurements. Bob was the most persistent of all the swarm physicists in pursuing joint work with binary collision theorists and experimentalists. Indeed, most of the cross section sets available today for the common gases are based, in part, on the data developed by Bob and his group.



Professor Robert W. Crompton

Bob regarded ICPEAC as the most important platform in achieving agreement between swarm-derived cross sections and those calculated and/or measured in binary collision experiments. He was one of the founding members of the Swarm Seminar – an ICPEAC satellite - and also one of the initiators of the merger of this satellite with the Electron Molecule satellite.

Bob was general secretary of the Australian Academy of Science, Head of Atomic and Molecular Physics Laboratories at ANU, and an extremely influential scientist.

\*[zoran1@ipb.ac.rs](mailto:zoran1@ipb.ac.rs) §[stephen.buckman@anu.edu.au](mailto:stephen.buckman@anu.edu.au)

## Multiphoton ionization and detachment of atoms and negative ions A tribute to Anthony F. Starace

J M Ngoko Djio kap<sup>1\*</sup> and I I Fabrikant<sup>1†</sup>

<sup>1</sup>Department of Physics and Astronomy, University of Nebraska-Lincoln, Lincoln, NE-68588-0299, USA

**Synopsis** Anthony F. Starace passed away on September 5, 2019 at the age of 74. We briefly review some of his contributions to the theory of multiphoton ionization and detachment of atoms and negative ions.

One of us started his postdoc under Tony's guidance by developing *ab initio* theoretical tools to study correlated ionization processes that Tony had conceived. TDSE codes treating elliptical polarized XUV light with many-body systems were not available. By adopting the basic principle of the method introduced in 1999 by H.G. Muller, we marshaled tools of quantum physics to build this toolbox [1]. We were then ready to do physics by exploring electron effects and target properties that are not accessible with linearly polarized pulses. **Can the simplest nonlinear dichroic effect be observed?** By detecting back-to-back the two electrons freed from He by an intense elliptically polarized XUV pulse, the linear dichroism vanishes allowing us to isolate the nonlinear dichroism by interference of the 1st- and 2nd-order ionization amplitudes thanks to the at-pulse broad bandwidth [1]. **What new physics emerges when we use two time delayed pulses to produce single ionization of atoms?** By inspecting the photoelectron momentum distribution, we discovered spiral vortex patterns from Ramsey interference, whose arms reflect the number of photons involved in the multiphoton transition [2]. Our prediction, confirmed experimentally, provides an example of wave-particle duality of matter, and has opened a new area of research for potential application.

Together with Tony and the postdoc Katarzyna Krajewska, we contributed to the threshold behavior of strong-field detachment of negative ions by static and time-varying electric fields. Nonperturbative Floquet formalism to study threshold effects in above-threshold detachment (ATD) of H<sup>-</sup> and F<sup>-</sup> was used [3]. Significant changes in the angular distribution and great enhancement of the ATD rates in the high-energy plateau region were found as the

laser intensity passes across ponderomotively shifted multiphoton thresholds. In accordance with the Wigner threshold law, the ATD plateau enhancements are sensitive to the initial state symmetry, with the most pronounced enhancements occurring for an initial state having s or p symmetry in the case of even- or odd-photon channel closings. These studies were then extended to multiphoton ionization of neutral atoms using the threshold law in the case of Coulomb interaction in the final state [4]. Accordingly, the above-threshold ionization rate is nearly constant below and above each multiphoton threshold. Between such thresholds, resonances with laser-field-modified Rydberg states occur.



**Figure 1.** Anthony F. Starace's official 70<sup>th</sup> Birthday photo in front of Newton's Apple Tree which was planted in 1991 when he was UNL physics department Chair.

### References

- [1] Ngoko Djio kap J M, Manakov N L *et al* 2014 Phys. Rev. Lett. **113**, 223002
- [2] Ngoko Djio kap J M, Hu S X, Madsen L B *et al* 2015 Phys. Rev. Lett. **115**, 013004
- [3] Krajewska K, Fabrikant I I and Starace A F 2006 Phys. Rev. A **74**, 053407
- [4] Krajewska K, Fabrikant I I and Starace A F 2012 Phys. Rev. A **86**, 053410

\* E-mail: [marcelngoko@unl.edu](mailto:marcelngoko@unl.edu)

† E-mail: [ifabrikant@unl.edu](mailto:ifabrikant@unl.edu)

## In Memoriam of Past ICPEAC Chairs & Stalwarts

Emma Sokell<sup>1,2</sup>

<sup>1</sup>ICPEAC International Scientific Secretary

<sup>2</sup> School of Physics, University College Dublin, Dublin 4, Ireland

**Synopsis** This poster is to celebrate the particular contributions to ICPEAC that scientific and local chairs and colleagues, who have sadly passed, since we last convened the conference in person in Deauville in 2019, have made over the years.

Benjamin Bederson was the Scientific Chair of the first, second and third ICPEAC meetings held in New York (1958), Boulder (1961) London (1963) and again in 1985 in Palo Alto [1]. As the ICPEAC community well remembers, he said at the second meeting, “This conference is the second in the series of informal meetings organised...in the general field of electronic and atomic collisions. The first such meeting was held at New York University in 1958, and we will probably continue to meet at irregular intervals”. Benjamin was also International Secretary from 1958 until 1971 and continued to support ICPEAC, writing an informal history and attending the 50<sup>th</sup> anniversary celebration in Kalamazoo in 2009.

Born in 1921 in New York, Benjamin passed away at the age of 101 in January 2023. He was a graduate of City College of New York, Columbia University and New York University, he worked at Massachusetts Institute of Technology and was dean at New York University. Among other things he worked on the Manhattan Project, was Editor-in-Chief of Physical Review and a Fellow of the American Physical Society [2].

Chris Brion was Local Co-Chair of the Whistler ICPEAC held in 1995. Chris was born in 1937 and passed away in November 2022. Chris worked in the Chemistry Department at the University of British Columbia (UBC), where he taught for 41 years until he retired to become an emeritus professor [3].

John Tanis was Local Co-Chair of the 2009 ICPEAC meeting held in Kalamazoo. John was born in 1945 in Michigan, graduated from Hope College, the University of Iowa and New York University. John served on the faculty of West-

ern Michigan University for 40 years, before retiring in 2020. John passed away in October 2022 [4].

Derrick Crothers was the Local Co-Chair of the 2011 ICPEAC meeting held in Belfast. He was born in 1942, studied mathematics at Balliol College, Oxford. Derrick obtained his PhD from Queen’s University Belfast, where from 1985 until his retirement in 2007 he held a personal chair in Theoretical Physics. He was also a member of the Royal Irish Academy from 1991 until he passed away in January 2021 [5].

We remember fondly many other ICPEAC colleagues who have passed away since we last met in person in 2019. Including Anthony Starace (Nebraska, Sept 2019), James Walters (QUB, Sept 2020), Oleg Zatsarinny (Drake, March 2021), Don Madison (MST, May 2022), Robert Crompton (ANU, June 2022), Howard Reiss (MBI, Aug 2022), Michael Brunger (Flinders, Sept 2022) and Miron Amusia (the Hebrew University).

### References

- [1] <https://www.ucd.ie/icpeac/historic.html>
- [2] [https://en.wikipedia.org/wiki/Benjamin\\_Bederson](https://en.wikipedia.org/wiki/Benjamin_Bederson)
- [3] <https://vancouver.sunandprovince.remembering.ca/obituary/chris-brion-1086699013>
- [4] <https://www.langelands.com/obituary/DrJohn-TanisPhD>
- [5] <https://www.iop.org/physics-community/obituaries/professor-derrick-crothers#ref>

\* E-mail: [emma.sokell@ucd.ie](mailto:emma.sokell@ucd.ie)



## Inner-shell ionization of low-charged silicon and iron ions

S Schippers<sup>1\*</sup>, A Müller<sup>1</sup>, S Reinwardt<sup>2</sup>, M Martins<sup>2</sup> and S Fritzsche<sup>3,4,5</sup>  
for the PIPE collaboration

<sup>1</sup>I. Physikalisches Institut, Justus-Liebig-Universität Gießen, Germany

<sup>2</sup>Institut für Experimentalphysik, Universität Hamburg, Germany

<sup>3</sup>GSI Helmholtzzentrum für Schwerionenforschung, Darmstadt, Germany

<sup>4</sup>Helmholtz-Institut Jena, Germany

<sup>5</sup>Institut für Theoretische Physik, Friedrich-Schiller-Universität Jena, Germany

**Synopsis** We report on recent experimental and theoretical work on single and multiple L-shell photoionization of low-charged iron ions ( $\text{Fe}^+$ ,  $\text{Fe}^{2+}$ ,  $\text{Fe}^{3+}$ ) and on single and multiple K-shell photoionization of low-charged silicon ions ( $\text{Si}^-$ ,  $\text{Si}^+$ ,  $\text{Si}^{2+}$ ,  $\text{Si}^{3+}$ ). The experiments were carried out at the photon-ion end-station PIPE of beamline P04 of the PETRA III synchrotron light source. Our data are decisive for determining how much of the interstellar iron and silicon is in the gas phase and how much is chemically bound in dust grains.

We report on recent experimental and theoretical work on single and multiple L-shell photoionization of low-charged iron ions ( $\text{Fe}^+$ ,  $\text{Fe}^{2+}$ ,  $\text{Fe}^{3+}$ ) [1, 2, 3] and on single and multiple K-shell photoionization of low-charged silicon ions ( $\text{Si}^-$ ,  $\text{Si}^+$ ,  $\text{Si}^{2+}$ ,  $\text{Si}^{3+}$ ) [4, 5]. The experiments were

carried out at the photon-ion end-station PIPE of the PETRA III synchrotron radiation source operated by DESY in Hamburg, Germany. In addition, Multi-Configuration Dirac-Hartree-Fock calculations were performed that accounted for the complex de-excitation cascades [7] that set in after the creation of an inner-shell hole and that result in a distribution of product-ion charge states.

Figure 1 compares experimentally-derived and theoretical cross sections for the photoabsorption of  $\text{Si}^-$ ,  $\text{Si}^+$ ,  $\text{Si}^{2+}$ , and  $\text{Si}^{3+}$  ions at photon energies around the respective silicon K-edges. Similar results were also obtained for L-shell photoabsorption of  $\text{Fe}^+$ ,  $\text{Fe}^{2+}$ , and  $\text{Fe}^{3+}$ . Such absolute photoabsorption cross sections aid in the derivation of the silicon and iron abundances in the interstellar medium from astrophysical x-ray absorption spectra. In particular, accurate resonance energies are required for being able to discriminate between the various ion charge states and Si/Fe atoms bound in the minerals that make up the interstellar dust.

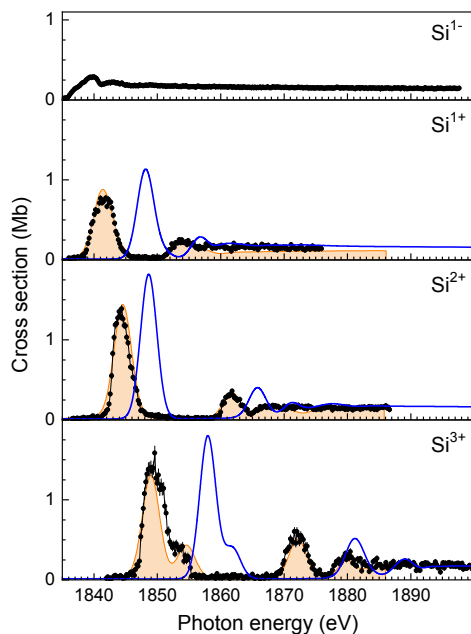


**Figure 1.** Experimentally-derived cross sections (symbols) for K-shell photoabsorption of  $\text{Si}^-$ ,  $\text{Si}^+$ ,  $\text{Si}^{2+}$ , and  $\text{Si}^{3+}$  [4] in comparison with our theoretical photoabsorption cross-sections (shaded curves) [4] and those of Witthoef et al. [6] (blue curves).

\*E-mail: [stefan.schippers@physik.uni-giessen.de](mailto:stefan.schippers@physik.uni-giessen.de)

### References

- [1] Schippers S et al 2017 *Astrophys. J.* **849** 5
- [2] Beerwerth R et al 2019 *Astrophys. J.* **887** 189
- [3] Schippers S et al 2021 *Astrophys. J.* **908** 52
- [4] Perry-Sassmannshausen A et al 2021 *Phys. Rev. A* **104** 053107
- [5] Schippers S et al 2022 *Astrophys. J.* **931** 100
- [6] Witthoef M C et al 2009 *Astrophys. J. Suppl. Ser.* **182** 127
- [7] Fritzsche S et al 2021 *Symmetry* **13** 520

## Relativistic and correlation effects in $np$ photoionization Cooper minima of high- $Z$ atoms

S. Baral<sup>1</sup>, J. Jose<sup>1,†</sup>, P. C. Deshmukh<sup>2,3</sup> and S. T. Manson<sup>4,\*</sup>

<sup>1</sup>Department of Physics, Indian Institute of Technology Patna, Bihta -801103, Bihar, India

<sup>2</sup>Department of Physics, Indian Institute of Technology Tirupati, Tirupati, Andhra Pradesh 517506, India

<sup>3</sup>Department of Physics, Dayananda Sagar University, Bengaluru, 560114, India

<sup>4</sup>Department of Physics and Astronomy, Georgia State University, Atlanta, GA 30303, USA

**Synopsis** Cooper minima of  $np$  subshells in high- $Z$  atoms are investigated to delineate the correlation and relativistic effects using RRPA and DF methodologies.

Photoionization transition matrix elements pass through a zero or attains a minimum that leaves imprints on photoionization parameters like cross-section, angular distribution asymmetry parameter, phase shift and time-delay. This minimum is well-known as Cooper minimum (CM) [1,2]. The CM, in general, are strongly affected by relativistic and correlation effects. In previous works, CM for the  $6p$  subshell photoionization was observed up to  $Z=100$  using the Dirac-Slater method [3,4]. This work both extends the earlier work to  $Z$  up to 120 using more accurate methods; Dirac-Fock (DF) [5] which includes both exchange and relativistic effects, and the relativistic random phase approximation (RRPA) [6] which includes initial and final state correlation. In addition to  $6p$ , the calculations have also been extended for  $5p$  and  $4p$ . To bring out the features, the atoms Rn ( $Z=86$ ), Ra ( $Z=88$ ), No ( $Z=102$ ), Cn ( $Z=112$ ), Og ( $Z=118$ ), Ubn ( $Z=120$ ) are investigated.

As an example, Figure 1 shows the CM location for the  $6p_{1/2} \rightarrow \epsilon d_{3/2}$  channel as a function of atomic number  $Z$ . It is evident that new results are following the trends of earlier calculations. However, the impact of the enhanced spin-orbit coupling effect on the CM is clear.

The work of STM was supported by the US Department of Energy, Office of Science, Basic Energy Sciences under Award Number DE-FG02-03ER15428, JJ by SERB Grant No. CRG/2022/000191.

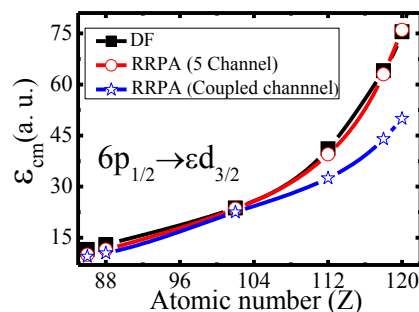


**Figure 1.** Locus of the  $6p_{1/2} \rightarrow \epsilon d_{3/2}$  Cooper minima as a function of photoelectron energy (a. u.). The 5 channel RRPA includes only the  $6p$  channels, while the coupled channel RRPA includes coupling of all of the channels from  $4f$  to the valence subshell for the low  $Z$ 's, with the inclusion of  $4d$  and  $4p$  channels for the higher  $Z$ 's.

### References

- [1] Cooper J W 1962 *Phys. Rev.* **128** 681
- [2] Johnson W R and Cheng K T 1979 *Phys. Rev. A.* **20** 978
- [3] Manson S T, Lee C J, Pratt R H, Goldberg I B, Tambe B R and Ron A 1983 *Phys. Rev. A.* **28** 2885
- [4] Deshmukh P C, Tambe B R and Manson S T 1986 *Austral. J. Phys.* **39** 679
- [5] I. P. Grant, *Relativistic Quantum Theory of Atoms and Molecules: Theory and Computation* (Springer, 2010)
- [6] Johnson W R and Lin C D 1979 *Phys. Rev. A.* **20** 964

\* E-mail: [smanson@gsu.edu](mailto:smanson@gsu.edu)

† E-mail: [jobin.josen@gmail.com](mailto:jobin.josen@gmail.com)

## Angular distribution, spin polarisation and time delay studies of the potassium 4s orbital in the vicinity of Cooper minimum

N M Hosea<sup>1</sup>, P C Deshmukh<sup>2,3</sup>, J Jose<sup>4</sup>, H R Varma<sup>1\*</sup> and S T Manson<sup>5</sup>

<sup>1</sup>Indian Institute of Technology Mandi, Mandi, 175075, India

<sup>2</sup>Dayananda Sagar University, Bengaluru, 560078, India

<sup>3</sup>Indian Institute of Technology Tirupati, Tirupati, 517506, India

<sup>4</sup>Indian Institute of Technology Patna, Patna, 801106, India

<sup>5</sup>Georgia State University, Atlanta, 30302-3965, USA

**Synopsis** Photoionisation cross section, angular distribution, spin polarisation and time delay of 4s orbital of potassium atom in the vicinity of Cooper minimum (CM) is studied.

Determination of the characteristic properties of the photoionisation process can be extracted by a set of carefully defined parameters such as cross section, angular distribution and spin polarisation of photoelectrons that constitutes a complete photoionisation experiment. Theoretically, information about the magnitudes and phases of the transition matrix elements is sufficient to calculate these parameters and it give a complete quantum mechanical description of the process.

Alkali metals have one valence electron in the ns-subshell. The photoionisation cross section of these subshells shows a CM near the threshold. The region of CM is particularly interesting because this is the region where (i) angular distributions undergo rapid variation (ii) the photoelectron spin-polarization is energy dependent [1] and (iii) Eisenbud-Wigner-Smith (EWS) time delay is known to be affected strongly by correlation and relativistic interactions [2].

We present a preliminary study on the photoionisation of 4s subshell of potassium. The bound state wavefunction is calculated using General-purpose Relativistic Atomic Structure Program (GRASP) [3] software which is based on the MCDHF method. The transition amplitudes with their corresponding phases which are required to calculate the cross section, angular distribution, spin polarisation and time delay of the photoelectron are obtained from the Relativistic calculations of Atomic Transition, Ionization and recombination Properties (RATIP)

code [4].

Figure 1, shows our single configuration (SC) calculations of the cross section and asymmetry parameter. Our cross section results are compared with Hartree Fock (HF) calculations [5] which show very good agreement. These studies will be extended for the spin-polarisation parameters and EWS time delay to understand the photoionisation dynamics in detail. Further attempt will be made to calculate these parameters by performing these studies at the multi-configuration level and all of these will be presented at the conference.

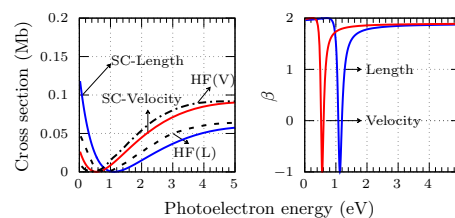


**Figure 1.** Left: Photoionisation cross section, Right: Asymmetry parameter of K 4s.

### References

- [1] Cherepkov N A 1973 *Zh. Eksp. Teor. Fiz* **65** 933
- [2] Ganesan A et al 2020 *J. Phys. B: At. Mol. Opt. Phys.* **53** 225206 (and references therein)
- [3] Parpia F A et.al 1996 *Comput. Phys. Commun.* **94** 249
- [4] Fritzsche S 2012 *Comput. Phys. Commun.* **183** 1525
- [5] Hari P Saha 1989 *Phys. Rev. A* **39** 628

\*E-mail: [hari@iitmandi.ac.in](mailto:hari@iitmandi.ac.in)

## New source for tuning the effective Rabi frequency discovered in multiphoton ionization

D Zhang<sup>1,2\*</sup>, W Li<sup>1,2</sup>, Y Lei<sup>1,2</sup>, X Li<sup>1,2</sup>, T Yang<sup>1,2</sup>, M Du<sup>1,2</sup>, Y Jiang<sup>1,2</sup>, J Li<sup>1,2</sup>, A Liu<sup>1,2</sup>, L He<sup>1,2</sup>, P Ma<sup>1,2</sup>, S Luo<sup>1,2</sup> and D Ding<sup>1,2†</sup>

<sup>1</sup>Institute of Atomic and Molecular Physics, Jilin University, Changchun, 130012, China

<sup>2</sup>Jilin Provincial Key Laboratory of Applied Atomic and Molecular Spectroscopy, Jilin University, Changchun, 130012, China

**Synopsis** The Autler-Townes effect due to near resonance transition between 4s-4p states in potassium atoms is mapped out in the photo-electron-momentum distribution. The energy splitting fits well with the calculated Rabi frequency at low laser intensities and shows clear deviation at laser intensities above  $1.5 \times 10^{11}$  W/cm<sup>2</sup>. An effective Rabi frequency formula including the ionization process explains the observed results.

A detailed account for the Autler-Townes (AT) effect [1] measured in the photoelectron momentum distribution of multiphoton ionization of potassium atoms is presented. Beyond the normal AT splitting, at higher intensities we observe significant deviation from the Rabi frequency. To explain the experimental observations, we treat the 4s-4p as a simple two-level system and the ionization process as a pure loss. The effective Hamiltonian can be written as:

$$H = H_0 + H' \quad (1)$$

where  $H_0 = \begin{pmatrix} 0 & \frac{1}{2}\Omega_{Rabi} \\ \frac{1}{2}\Omega_{Rabi} & 0 \end{pmatrix}$ , and  $H' = \begin{pmatrix} 0 & 0 \\ 0 & i\Gamma \end{pmatrix}$ .  $\Omega_{Rabi}$  and  $\Gamma$  represent the coupling strength of the two-level system with the laser field and the ionization rate, respectively. The energy splitting of such system can be related to the renormalized effective Rabi frequency as:

$$\Delta E = \Omega_{Rabi}^{eff} = \sqrt{\Omega_{Rabi}^2 + (i\Gamma)^2}. \quad (2)$$

The comparison between our model and the experimental results is plotted in Fig. 1. The agreement is excellent.

To summarize, an effective Rabi frequency formulae taking into account the ionization process is derived, which indicates that decay processes causing loss of populations will affect the Rabi frequency which in turn change the coupling strength.

\*E-mail: [dongdongzhang@jlu.edu.cn](mailto:dongdongzhang@jlu.edu.cn)

†E-mail: [dajund@jlu.edu.cn](mailto:dajund@jlu.edu.cn)

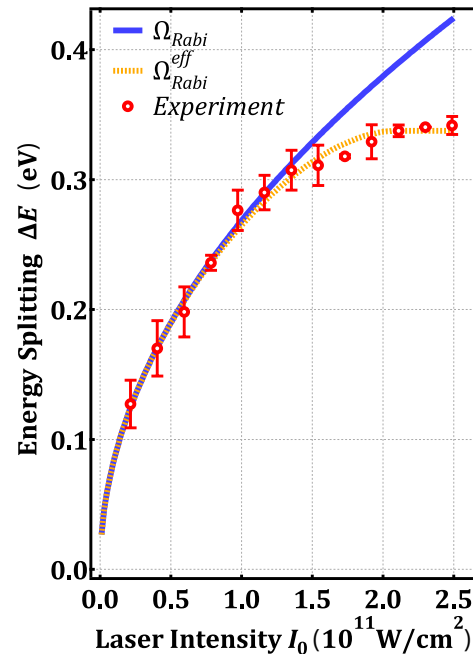


**Figure 1.** The energy separation of the Autler-Townes splitting as a function of laser intensities. The red dots represent the experimentally measured kinetic energy difference of the photoelectron. The error bar is the statistical error from ten individual measurements. The blue line is the Rabi frequency. The orange broken line is the effective Rabi frequency in Eq. 2.

### References

- [1] Autler S H and Townes C H 1955 *Phys. Rev.* **100** 703

## Non-classical properties of light after strong-laser field processes in atomic and solid-state systems

J. Rivera-Dean<sup>1\*</sup>, P. Stammer<sup>1</sup>, A. S. Maxwell<sup>2</sup>, Th. Lamprou<sup>3,4</sup>, A. F. Ordóñez<sup>1</sup>, E. Pisanty<sup>5</sup>, P. Tzallas<sup>3,6</sup>, M. Lewenstein<sup>1,7</sup> and M. F. Ciappina<sup>8,9,10</sup>

<sup>1</sup>ICFO – Institut de Ciències Fotoniques, The Barcelona Institute of Science and Technology, 08860 Castelldefels (Barcelona) <sup>2</sup>Department of Physics and Astronomy, Aarhus University, Dk-8000 Aarhus C, Denmark <sup>3</sup>Foundation for Research and Technology-Hellas, Institute of Electronic Structure & Laser, GR-70013 Heraklion (Crete), Greece <sup>4</sup>Department of Physics, University of Crete, P.O. Box 2208, GR-70013 Heraklion (Crete), Greece <sup>5</sup>Department of Physics, King’s College London, WC2R 2LS London, United Kingdom <sup>6</sup>ELI-ALPS, ELI-Hu Non-Profit Ltd., Dugonics tér 13, H-6720 Szeged, Hungary <sup>7</sup>ICREA, Pg. Lluís Companys 23, 08010 Barcelona, Spain <sup>8</sup>Physics Program, Guangdong Technion–Israel Institute of Technology, Shantou, Guangdong 515063, China <sup>9</sup>Technion – Israel Institute of Technology, Haifa, 32000, Israel <sup>10</sup>Guangdong Provincial Key Laboratory of Materials and Technologies for Energy Conversion, Guangdong Technion – Israel Institute of Technology, Shantou, Guangdong 515063, China

**Synopsis** The quantum optical characterization of strongly driven laser-matter interactions may allow extending current quantum technology platforms to unprecedented time and energy scales. Here, we present some of the recent progress that has been done in this direction, when considering atoms and solids as the matter system. In particular, we study the presence of light-matter entanglement in above-threshold ionization processes in atoms and in high-harmonic generation (HHG) processes in solid-state systems. Furthermore, we characterize the non-classical properties of the quantum optical state obtained after HHG in solid-state media, and study how the different intraband and interband transitions affect the quantum optical state of the field.

The presence of non-classical states of light is usually witnessed by means of negative regions on its Wigner function representation, or by the presence of entanglement when more than one optical mode is considered. Exploiting the non-classical properties of light is crucial for the development of quantum technologies based in quantum optics [1]. However, as well as important is to find experimental setups that allow for the generation of the desired quantum optical states. In this direction, it was recently proved theoretically and experimentally that laser-atom interactions driven by highly intense laser fields, can lead to the generation of non-classical states of light [2–5].

Here, we extend the theoretical approach used in Refs. [2–5] to study above-threshold ionization (ATI) processes in atoms, where photoelectrons with large values of kinetic energy are extracted from the atomic system; and high-order harmonic generation (HHG) processes in solid-state systems, where radiation in form of attosecond bursts with frequencies that range from the mid-infrared to the extreme ultraviolet

are generated. In the first study [6], related to ATI in atoms, we observe that the final state of the light-field is entangled with that of the ionized electron, which allows for the generation of *hybrid-entangled* states, i.e., entangled states between light and matter. Moreover, if we only consider the field modes, we find a coherent state superposition where the amplitude of each coherent state within the superposition depends on the electronic properties: its final kinetic momentum and at what instant of time it has ionized.

In the second study [7], related to HHG in solid-state media, we propose a quantum optical extension of the semiclassical description of HHG proposed in Ref. [8]. This allows us to study how the extra interactions of the electrons in the solid get imprinted in the quantum optical state. Furthermore, and following the same experimental operations as the ones performed in Refs. [2–5], one can find two non-exclusive indications of non-classical behaviors, namely the presence of Wigner function negativities and entanglement features.

\*E-mail: [javier.rivera@icfo.eu](mailto:javier.rivera@icfo.eu)

### References

- [1] O’Brien J L *et al* 2009 *Nature Photon* **3** 687-695
- [2] Lewenstein M *et al* 2021 *Nat. Phys.* **17** 1104-1108
- [3] Rivera-Dean J *et al* 2022 *Phys. Rev. A* **105**, 033714
- [4] Stammer P *et al* 2022 *Phys. Rev. Lett.* **128** 123603
- [5] Stammer P *et al* 2022 *arXiv:2206.04308* (accepted in *Phys. Rev. X Quantum: Tutorial*)
- [6] Rivera-Dean J *et al* 2022 *Phys. Rev. A* **106**, 063705
- [7] Rivera-Dean J *et al* 2022 *arXiv:2211.00033*
- [8] Osika E *et al* 2017 *Phys. Rev. X* **7** 021017

# Lorentz-force shifts in strong-field ionization with mid-IR laser fields

S Fritzsche<sup>1,2,3\*</sup>, B Böning<sup>1</sup> and D F Dar<sup>1,3</sup>

<sup>1</sup>Helmholtz-Institut Jena, Germany

<sup>2</sup>GSF Helmholtzzentrum für Schwerionenforschung, Darmstadt, Germany

<sup>3</sup>Institut für Theoretische Physik, Friedrich-Schiller-Universität Jena, Germany

**Synopsis** Measurements with different infra-red (IR) pulses have shown the crucial role of the magnetic field on the electron dynamics, classically known as the Lorentz force  $\mathbf{F}_L = q(\mathbf{E} + \mathbf{v} \times \mathbf{B})$ , and as it acts upon all particles with charge  $q$  in motion. These measurements also call for new theoretical methods beyond the presently applied ones. We here explain and discuss that several, if not most, observations from strong-field ionization experiments with mid-IR fields can be *quantitatively* explained within the framework of non-dipole SFA, i.e. if the Lorentz force is taken into account by means of non-dipole Volkov states.

If atoms are exposed to visible or near-infrared laser pulses with peak intensities larger than, say,  $10^{13}$  W/cm<sup>2</sup>, various nonlinear optical processes are known to arise, such as above-threshold ionization (ATI), tunneling ionization, high-order harmonic generation, or nonsequential double ionization. All these processes reflect the interaction of weakly-bound electrons with the external field and, more often than not, depend on their laser-driven rescattering at the parent ions and, thus, the Lorentz force [1].

typically restricted to co-propagating plane-wave beams. Until the present, only the non-dipole strong-field approximation (SFA) [2], derived by us, has been found able to support both, discrete and continuous, superpositions of plane-wave beams and, hence, a *spatial* dependence of the laser field for the motion of the electrons in the continuum. This non-dipole SFA for spatially-structured beams also provides a non-zero and observable peak shift  $\Delta p_z$  (of the maxima) in the photoelectron momentum distributions of the ATI spectra in good-to-excellent agreement with experiment [3], cf. Figure 1.

We here explain how *this* non-dipole SFA can be utilized to quantitatively predict the energy and momentum shifts in the observed ATI spectra. Details are discussed for the (peak) shifts of the polar-angle distribution of ATI photoelectrons along the laser propagation, the steering of electron momenta by two not quite collinear laser beams as well as the enhanced momentum transfer to photoelectrons in standing light fields. Moreover, the same formalism promises to explain the generation of high harmonics and other strong-field rescattering phenomena when driven by mid-IR laser fields.

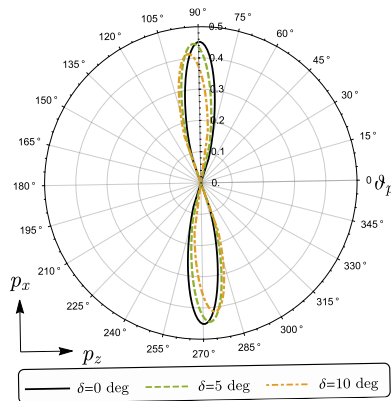


**Figure 1.** PAD of photoelectrons with energy  $E_p = 7.8$  eV  $\approx 5\omega$  as emitted in the ATI with two not quite collinear laser beams ( $I = 10^{14}$  W/cm<sup>2</sup>,  $\lambda = 800$  nm).

Several approaches have been developed to account for major parts of the Lorentz force and, especially, to compute the peak shifts of the photoelectrons along the beam propagation, though

## References

- [1] Fritzsche S and Böning B 2022 *Phys. Rev. Res.* **4** 033031
- [2] Böning B, Paufler W and Fritzsche S 2019 *Phys. Rev.* **A99** 053404
- [3] Böning B and Fritzsche S 2022 *Phys. Rev.* **A106** 043102

\*E-mail: [s.fritzsche@gsi.de](mailto:s.fritzsche@gsi.de)



## An atomic magnetometer to detect the oscillating magnetic field based on twisted light atom interaction

S. Ramakrishna<sup>1,2,3\*</sup>, R.P. Schmidt<sup>4,5</sup>, A.A. Peshkov<sup>4,5</sup>, A. Surzhykov<sup>4,5,6</sup> and S. Fritzsche<sup>1,2,3</sup>

<sup>1</sup>Helmholtz-Institut Jena, Fröbelstieg 3, D-07743 Jena, Germany

<sup>2</sup>GSI Helmholtzzentrum für Schwerionenforschung GmbH, Planckstrasse 1, D-64291 Darmstadt, Germany

<sup>3</sup>Theoretisch-Physikalisches Institut, Friedrich-Schiller-Universität Jena, Max-Wien-Platz 1, D-07743 Jena, Germany

<sup>4</sup>Physikalisch-Technische Bundesanstalt, Bundesallee 100, D-38116 Braunschweig, Germany

<sup>5</sup>Institut für Mathematische Physik, Technische Universität Braunschweig, Mendelssohnstraße 3, D-38106 Braunschweig, Germany

<sup>6</sup>Laboratory for Emerging Nanometrology Braunschweig, D-38106 Braunschweig, Germany

**Synopsis** We present a new theoretical model to detect the frequency and strength of the oscillating magnetic field based on the interaction of twisted light with atoms. In particular, we study the photoexcitation of atoms by vector Bessel beams in the framework of density matrix theory and based on the Liouville-von Neumann equation. We show that the excited state population is sensitive to the position of the atom in the beam cross section of the Bessel light beam. Furthermore, we plot the population of the excited state population for various frequency and strength of the magnetic field.

The Bessel light beam is a twisted light field that has helical wavefronts and carries orbital angular momentum in addition to spin angular momentum as in the case of plane waves. The twisted light fields can be classified into scalar and vector fields depending on the polarization. Over the last decade, twisted light fields, especially vector twisted light, have played an important role in the investigation of the atomic processes [1] and metrology experiments [2].

The detection of moderate oscillating magnetic fields is a cornerstone for the experimental techniques such as Magnetic resonance imaging. Optically pumped atomic magnetometers are one of the promising candidate to measure such magnetic fields [3].

In this work, we analyze the electric dipole transition [ $5s\ ^2S_{1/2} (F=1) \rightarrow 5p\ ^2P_{3/2} (F=0)$ ] in the  $^{87}\text{Rb}$  atoms driven by the vector Bessel beam in the framework of density matrix theory and the Liouville-von Neumann equation. We show that the position of the atoms in the beam cross section influences the response of the atoms to the external magnetic field. Furthermore, we plot the time-averaged population of the excited state in the beam cross section for various frequencies and strength of the external oscillating magnetic field. These time-averaged plots of the population of the excited state (see Figure 1.)

\*E-mail: [shreyas.ramakrishna@uni-jena.de](mailto:shreyas.ramakrishna@uni-jena.de)

can be used to detect the frequency and strength of the external oscillating magnetic field.

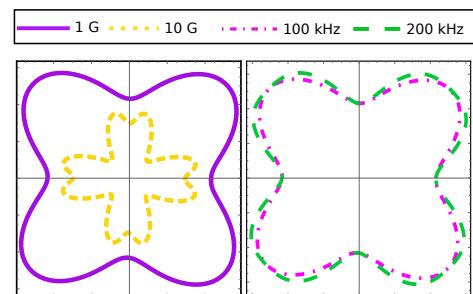


**Figure 1.** Left plot: The time-averaged population of the excited state in the beam cross section of twisted light for a magnetic field strength of 1 G (purple solid line) and 10 G (yellow dashed line) keeping the frequency fixed at  $f = 100$  kHz. Right plot: Time-averaged population plot for  $f = 100$  kHz (magenta dot-dashed line) and  $f = 200$  kHz (green long-dashed line) for 1 G magnetic field.

### References

- [1] S. Ramakrishna *et al.* 2022 *Phys. Rev. A* **105** 033103
- [2] F. Castellucci *et al.* 2021 *Phys. Rev. Lett* **127** 233202
- [3] I.M. Savukov *et al.* 2005 *Phys. Rev. Lett* **95** 063004

## Time-resolved Kapitza-Dirac effect

Kang Lin\*, Maksim Kunitski, Sebastian Eckart, Alexander Hartung, Qinying Ji, Lothar Ph. H. Schmidt, Markus S. Schöffler, Till Jahnke, Reinhard Dörner†

Institut für Kernphysik, Goethe-Universität, Frankfurt, 60438, Germany

**Synopsis** The Kapitza-Dirac effect describes that an electron beam can be diffracted when passing through a light standing wave. Here, a principle new phenomenon, termed as time-resolved Kapitza-Dirac effect, is discovered. We track the spatiotemporal evolution of an electron wavepacket diffracted by an ultrafast femtosecond light standing wave. By scanning the delay between the electron wavepacket and the standing wave, we show that the momentum spacing between diffraction peaks decreases continuously with the delay increasing, which can be fractions instead of integers of two-photon momenta.

In 1933, Kapitza and Dirac suggested that an electron beam can also be diffracted by an immaterial standing light wave. This is termed the Kapitza-Dirac (KD) effect nowadays [1]. With the advent of pulsed lasers, ultrashort laser pulses today provide electric fields of comparable strength to the Coulomb field binding electrons in atoms and molecules. Electrons released by such laser pulses show unique properties different from those produced by collimating a beam from an electron gun. The former is a coherent electron wavepacket while the latter can be approximated by a plane wave. Most importantly, the ultrashort laser pulses offer the possibility to track the ultrafast spatiotemporal evolution of the electron wavepacket. It is widely unclear how an electron wavepacket will be diffracted by an ultrafast light standing wave.

Here, we report on observation of spatiotemporal evolution of an ultrafast electron wavepacket diffracted by an ultrashort standing wave. By scanning the time delay between a strong pulsed standing wave (pump pulse) which launches the electron wavepacket by strong field ionization and a weaker, non-ionizing, ultrashort standing wave (probe pulse), we observe previously illusive interference fringes. We show that the momentum spacing between these diffraction peaks decreases continuously with increasing time delay. Our observation can be well reproduced by performing the one-dimensional time-dependent Schrödinger equation (TDSE) simulation. The time-dependent diffraction pattern results from the dispersion of the electron wavepacket fol-

lowed by spatial phase modulation of the standing wave. Alternatively, from the particle perspective, our classical simulation shows that the diffraction peaks can also be understood as the acceleration or deceleration of the electrons by the position-dependent ponderomotive force of the standing wave. The time-resolved KD effect can serve as a direct optical diagnosis of the electron wavepacket.

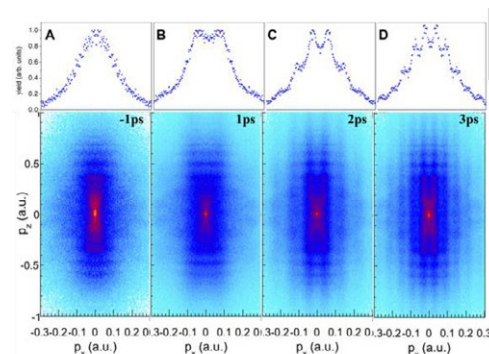


**Figure 1.** (A-D) Experimentally measured two-dimensional momentum distribution in the plane formed by polarization axis ( $p_z$ ) and light-propagation direction ( $p_x$ ) at time delays of -1, 1, 2, and 3 ps. The top panels are one-dimensional momentum distribution along the light-propagation axis by selecting the range of  $p_z$  between [0.65, 0.75] atomic units.

### References

- [1] Kapitza P and Dirac P 1933 Math. Proc. Cambridge Philos. Soc. **29** 297

\* E-mail: [lin@atom.uni-frankfurt.de](mailto:lin@atom.uni-frankfurt.de)

† E-mail: [doerner@atom.uni-frankfurt.de](mailto:doerner@atom.uni-frankfurt.de)



## Pulse length effects in long wavelength driven non-sequential double ionization

H Jiang<sup>1,†</sup>, M Mandrysz<sup>2,†</sup>, A Sanchez<sup>3</sup>, J Dura<sup>3</sup>, T Steinle<sup>3</sup>, J S Prauzner-Bechcicki<sup>2</sup>, J Zakrzewski<sup>4,5</sup>, M Lewenstein<sup>3,6</sup>, F He<sup>1,7</sup>, J Biegert<sup>3,6</sup> and M F Ciappina<sup>8,9,10\*</sup>

<sup>1</sup>Key Laboratory for Laser Plasmas (Ministry of Education) and School of Physics and Astronomy, Collaborative innovation center for IFSA (CICIFSA), Shanghai Jiao Tong University, Shanghai 200240, China

<sup>2</sup>Instytut Fizyki imienia Mariana Smoluchowskiego, Uniwersytet Jagielloński, Łojasiewicza 11, 30-348 Kraków, Poland

<sup>3</sup>ICFO - Institut de Ciències Fòniques, The Barcelona Institute of Science and Technology, Av. Carl Friedrich Gauss 3, 08860 Castelldefels (Barcelona), Spain

<sup>4</sup>Institute of Theoretical Physics, Jagiellonian University in Krakow, Łojasiewicza 11, 30-348 Kraków, Poland

<sup>5</sup>Mark Kac Complex Systems Research Center, Jagiellonian University, Łojasiewicza 11, 30-348 Kraków, Poland

<sup>6</sup>ICREA, Pg. Lluís Companys 23, 08010 Barcelona, Spain

<sup>7</sup>CAS Center for Excellence in Ultra-intense Laser Science, Shanghai 201800, China

<sup>8</sup>Physics Program, Guangdong Technion - Israel Institute of Technology, Shantou, Guangdong 515063, China

<sup>9</sup>Technion - Israel Institute of Technology, Haifa, 32000, Israel

<sup>10</sup>Guangdong Provincial Key Laboratory of Materials and Technologies for Energy Conversion, Guangdong Technion - Israel Institute of Technology, Shantou, Guangdong 515063, China

**Synopsis** We present a joint experimental and theoretical study of non-sequential double ionization (NSDI) in argon driven by a 3100-nm laser source. The correlated photoelectron momentum distribution (PMD) shows a strong dependence on the pulse duration, and the evolution of the PMD can be explained by an envelope-induced intensity effect. This work sheds light on the importance of the pulse duration in NSDI and improves our understanding of the strong field tunnel-recollision dynamics under mid-IR laser fields.

Electron correlations during strong-field double ionization play an instrumental role and have been widely investigated through the correlated photoelectron momentum distribution (PMD) under 800-nm laser fields. However, there exist few studies under mid-IR laser fields [1].

The emitting electrons can be driven back to the nucleus with high rescattering energy by a long wavelength laser field, leading to direct nonsequential double ionization (NSDI) and an asymmetric energy distribution. Thus, a typical near-axis V-shaped structure can be found in the PMD [2]. Our experimental result in Fig. 1 shows that such a structure will be largely influenced by the pulse duration.

In essence, the envelope-induced intensity effect comes from the tunnel-recollision dynamics and we extract the mechanism through a semi-classical model. Considering the travel time after tunneling, the recollision most likely occurs 1.2T later. Thus, the recollision happens further back in the laser envelope with a smaller laser intensity for a shorter pulse, leading to a smaller drift momentum. We further confirm this mechanism

\*E-mail: [marcelo.ciappina@gtiit.edu.cn](mailto:marcelo.ciappina@gtiit.edu.cn)

through quantum mechanical simulations.

Our findings indicate the importance of the pulse length effects for NSDI under quasi-static conditions. The found envelope-induced intensity effect may help to study tunnel-recollision dynamics through the information encoded in the PMDs [3].

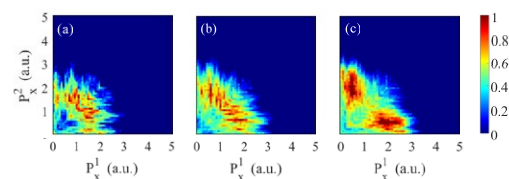


**Figure 1.** Experimental normalized correlated PMD along the polarization direction. The FWHM of the 3100-nm laser is 4T in (a), 6.5T in (b), and 13.5T in (c).

### References

- [1] Wolter B *et al* 2015 *Phys. Rev. X* **5** 021034
- [2] Shaaran T *et al* 2019 *Phys. Rev. A* **99** 023421
- [3] Jiang H *et al* 2023 *New J. Phys.* (in press)

## Ultrafast excitation dynamics for noble gas atoms subject to intense femtosecond laser fields

S P Xu<sup>1</sup>, M Q Liu<sup>2</sup>, W Quan<sup>1\*</sup>, W. Becker<sup>3</sup>, J. Chen<sup>4†</sup> and X.J. Liu<sup>1#</sup>

<sup>1</sup>State Key Laboratory of Magnetic Resonance and Atomic and Molecular Physics, Wuhan Institute of Physics and Mathematics, Innovation Academy for Precision Measurement Science and Technology, Chinese Academy of Sciences, Wuhan 430071, China

<sup>2</sup>College of Physics and Optoelectronic Engineering, Shenzhen University, Shenzhen 518060, China

<sup>3</sup>Max-Born-Institut, Max-Born-Strasse 2a, 12489 Berlin, Germany

<sup>4</sup>Institute of Applied Physics and Computational Mathematics, P.O. Box 8009, Beijing 100088, China

**Synopsis** A unified perspective for the electron dynamics in the laser-driven atoms near the continuum threshold is presented. Our experimental and theoretical investigation reveals that the second-order term of the S-matrix expansion may provide an effective theory for the intense-laser-atom interaction.

S-matrix theory provides an efficient and physically appealing theoretical tool for the study of atomic and molecular dynamics in intense laser fields [1, 2]. For a given process, the S-matrix amplitude is usually expanded into the Born series. The series converges quickly only for a short-range or zero-range binding potential. If a long-range Coulomb potential has to be adopted to reproduce the experimental observations, e.g., the height of the plateau of high-order above-threshold ionization [3] or the low-energy structure [4,5], then the higher-order term may be larger than the lowest-order term and the convergence of the Born expansion becomes questionable.

Based on experimental data and theoretical analysis [6,7], we demonstrate that the second-order term of the S-matrix expansion may provide an effective theory for the intense-laser-atom interaction when the long-range Coulomb potential has to be adopted. Our work relies on experimental and theoretical investigations of ionization and Rydberg-state excitation of an argon atom subject to a strong laser field for various wavelengths. It is shown that the wave-

length scaling law of the measured ratio of Ar<sup>\*</sup> over Ar<sup>+</sup> and the period of its oscillation with respect to laser intensity can be well reproduced by the second-order term of the S-matrix expansion in terms of the Coulomb potential, but not by the lowest-order term. Our work sheds new light on establishing a comprehensive quantum theory for the atomic dynamics in strong laser fields.

### References

- [1] Keldysh L V 1965 Sov. Phys. JETP. 20 1307
- [2] Becker W, Grasbon F, Kopold R et al. 2002 Adv. At. Mol. Opt. Phys. 48, 35
- [3] Milošević D B and Ehlötzky F 1998 Phys. Rev. A 57, 5002
- [4] Guo L, Han S S, Liu X et al. 2013 Phys. Rev. Lett. 110, 013001
- [5] Becker W, Goreslavski S P, Milošević D B and Paulus G G 2014 J. Phys. B 47, 204022
- [6] Liu M Q, Xu S P, Hu S L et al. 2021 Optica 8, 765
- [7] Xu S P, Liu M Q, Quan W et al. 2022 Phys. Rev. A 106, 063106

\* E-mail: [charlywing@wipm.ac.cn](mailto:charlywing@wipm.ac.cn)

† E-mail: [chenjing@ustc.edu.cn](mailto:chenjing@ustc.edu.cn)

# E-mail: [xjliu@wipm.ac.cn](mailto:xjliu@wipm.ac.cn)

## Visualization of a complex electron wavefunction in momentum space using an attosecond pulse

H Niikura<sup>1\*</sup>, T Nakajima<sup>1</sup>, T Shinoda<sup>1</sup> and D M Villeneuve<sup>2</sup>

<sup>1</sup>Department of Applied Physics, Waseda University, Tokyo, 169-8555, Japan

<sup>2</sup>Joint Attosecond Science Laboratory, National Research Council and University of Ottawa, Ottawa, K1A0R6, Canada

**Synopsis** We measure the phase and amplitude distributions of photoelectrons ionized from neon gas by attosecond laser in the presence of an infrared laser field. From these data, we visualize a complex wavefunction.

An electron wavefunction is represented by phase and amplitude distributions over position or momentum space. A recent attosecond technology has enabled us to measure the angular dependence of the photoelectron phase [1]. This work used a three-path interference between photoelectron wavepackets ionized by an attosecond pulse train (XUV) in the presence of the infrared (IR) laser field.

In the present study, we employ a two-path interference for a XUV-IR photoionization process of neon to fully measure the phase and amplitude distributions of photoelectrons in a two-dimensional momentum space [2]. We generate the XUV pulse which consists of both odd and even harmonics. We limit the maximum harmonic number to 14 (H14) whose photon energy slightly exceeds the ionization potential of neon. In this condition, two photoelectron wavepackets,  $\Psi_a$  and  $\Psi_b$ , are produced by one-photon ionization via H14, and two-photon ionization via harmonic 13 (H13) plus one IR photon absorption (H13+IR). These two wavepackets interfere to each other and the intensity is modulated as a function of the XUV-IR delay.

We record a photoelectron velocity map images as a function of the XUV-IR delay. At every photoelectron momentum, we fit the signal modulation by cosine functions to obtain the phases and amplitudes. From the phase and amplitude distributions, we generate a “mapping” complex wavefunction,  $\Psi$ . Figure 1 (a) and (b) plot the measured  $\Psi$  at slightly different experimental conditions. In order to visualize complex values, we use the HSV (*hue-saturation-value*) color map: the phase is represented by *hue* (color) and amplitude is *value* (brightness). We set the saturation to 0.5. In Fig. 1 (a), a six-fold structure is recognized, in which the phase of the upper lobe is different from that in the

lower lobe by  $\pi$  radians. This feature is mainly due to the  $f$ -wave produced by H13 + IR from the  $2p$  ground state of neon. In Fig. 1 (b), another structure is recognized in the momentum  $<0.05$  a.u. Because of using interference, we can resolve a detailed structure of wavefunctions with a momentum resolution less than 0.02 a.u., which is much smaller than the bandwidth of the XUV pulse.

Furthermore, we develop a method to disentangle  $\Psi$  into wavefunctions produced by individual ionization pathways using the relationship  $\Psi = \Psi_a \Psi_b^*$ . Each individual wavefunction is decomposed as a coherent superposition of partial waves,  $s$ - and  $d$ -waves for  $\Psi_a$ , and  $p$ - and  $f$ -waves for  $\Psi_b$ . With this analysis, we obtain the phase and relative amplitude of each partial wave as a function of the radial momentum. The obtained information can be a reference for future theoretical calculations.

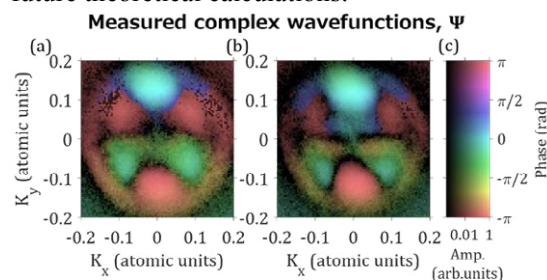


**Figure 1.** (a) (b) The complex electron wavefunctions ionized from neon with two different experimental conditions. (c) The color map for phase and amplitude.

### References

- [1] Villeneuve D M, Hockett P, Vrakking M J J and Niikura H, 2017 *Science*. [356, 1150](#).
- [2] Nakajima T, Shinoda T, Villeneuve D M, Niikura H, 2022 *Phys. Rev. A*. [106, 063513](#).

\* E-mail: [niikura@waseda.jp](mailto:niikura@waseda.jp)

## First commissioning results of the AMO endstation at the Shanghai soft X-ray free-electron laser facility

Ruichao Dong<sup>1,2</sup>, Xincheng Wang<sup>3\*</sup>, Yuliang Guo<sup>3</sup>, Jinze Feng<sup>3</sup>, Mingjie Zhang<sup>1,2</sup>, Hailong Guo<sup>3</sup>, and Yuhai Jiang<sup>3,1,2†</sup>

<sup>1</sup>Shanghai Advanced Research Institute, Chinese Academy of Sciences, Shanghai, 201210, China

<sup>2</sup>University of Chinese Academy of Sciences, Beijing, 100049, China

<sup>3</sup>Center for Transformative Science and School of Physical Science and Technology, ShanghaiTech University, Shanghai, 201210, China

**Synopsis** The Shanghai soft X-ray free-electron laser (SXFEL) aims to provide ultra-intense femtosecond X-ray pulses to five endstations covering a range of 100-620 eV. The reaction microscope (REMI) endstation as one of the five endstations, allows high-resolution and  $4\pi$  solid-angle coincidence detection of ions and electrons. The initial commissioning of the beamline and REMI endstation was carried out and the first experimental results were obtained in January 2023. Here, we report the first commissioning results of the REMI endstation.

X-ray free electron lasers (XFELs) provide a new tool to study how matter responds to ultra-intense femtosecond X-ray radiation, and understanding the new physical processes that arise from this light-matter interaction is important for studying both the few-body quantum world and radiation damage to biomolecules. The Shanghai soft X-ray free-electron laser (SXFEL) is a large scale scientific facility and can provide ultra-fast intense X-ray laser pulses in the water-window for the study of atomic, molecular and cluster science.

Here, the commissioning was finished based on the Seeded line ( $h\nu = 260$  eV, pulse duration  $\sim 150$  fs, intensity  $\sim 10^{13}$  W/cm<sup>2</sup>) of the SXFEL. The FEL beam was optimized so that the intense ultrashort X-ray laser pulses were focused on the gaseous Ar. Then, the relative intensity of each event was collected using a Faraday cylinder device and Fast-ADC, and electrons and ions were detected by using a reaction microscope (REMI) [1]. The time-of-flight spectra of Ar were obtained as shown in Fig. 1. In comparison with the results of synchrotron radiation (SR) facility [2], the percentage of high-valence states in our results were noticeably higher than that from SR facility, indicating the prominent contribution of the nonlinear multiphoton of SXFEL, and the intensity-dependent ion yields were also analyzed. Meanwhile, in comparison with results at 38 eV at FLASH [3], the present results were typical characteristic of inner-shell

ionization, where Ar<sup>2+</sup> is dominating. These results demonstrate the performance of the REMI endstation, which provides an advanced tool for studying the atomic, molecular and cluster reactions of SXFEL.

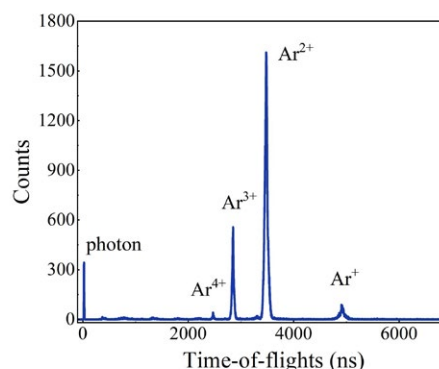


**Figure 1.** Time-of-flight spectrum of Ar in intense X-ray FEL laser fields.

In the future, we will mount an Even-Lavie valve on the REMI endstation to investigate scientific problems, such as the coupling of electron-nuclear dynamics and the fundamental dynamics of energy and charge of molecules and clusters in extreme environments.

### References

- [1] W Jiang *et al* 2022 *Appl. Sci.* **12** 1821
- [2] N Saito *et al* 1992 *Int. J. Mass Spectrom. Ion Processes* **115** 157-172
- [1] R Moshhammer *et al* 2007 *Phys. Rev. Lett.* **98** 03001

\* E-mail: [wangxch1@shanghaitech.edu.cn](mailto:wangxch1@shanghaitech.edu.cn)

† E-mail: [jiangyh3@shanghaitech.edu.cn](mailto:jiangyh3@shanghaitech.edu.cn)

## PCI effects following 2p double ionization of argon atoms

L Sommerlad<sup>1,\*</sup>, S Grundmann<sup>1</sup>, F Trinter<sup>1,2,3</sup>, M Kircher<sup>1</sup>, A Pier<sup>1</sup>, D McGinnis<sup>1</sup>, L Kaiser<sup>1</sup>, J Kruse<sup>1</sup>,  
A Geyer<sup>1</sup>, N Anders<sup>1</sup>, N Melzer<sup>1</sup>, T Jahnke<sup>1</sup> and R Dörner<sup>1,†</sup>

<sup>1</sup>Institut für Kernphysik, Goethe-Universität Frankfurt, 60438 Frankfurt, Germany

<sup>2</sup>Photon Science, Deutsches Elektronen-Synchrotron (DESY), 22607 Hamburg, Germany

<sup>3</sup>Molecular Physics, Fritz-Haber-Institut der Max-Planck-Gesellschaft, 14195 Berlin, Germany

**Synopsis** We have measured energy- and angular resolved momentum distributions of photoelectrons just above the 2p ionization threshold in argon atoms following a photo-double ionization process. The observed energy- and angular shifts can contribute to gain insight into electronic correlations.

Electrons in quantum systems (e.g. atoms) are correlated, i.e., their wave functions are interdependent. As consequence, the absorption of one photon can lead to the emission of two electrons. Such correlations are intriguing quantum-mechanical phenomena which are still subject of modern day research. Although the electron electron correlation is not an observable that can directly be measured, the interaction between the electrons can indirectly be observed. One example is the so-called Post Collision Interaction (PCI), which was first discovered 1974 [1]. The effect occurs typically between a high energetic Auger-electron and a low energetic photoelectron and the Coulomb interaction between both electrons induces distinct shifts in their energy- and angular distributions.

Using a COLTRIMS reaction microscope and synchrotron radiation of the U49/2 PGM1 beamline at Synchrotron BESSY (Berlin, Germany), we were able to create energy- and angular resolved momentum distributions of the photoelectron close to the 2p ionization threshold at 248.63 eV [2] in argon atoms following a double ionization process. We observed that the momentum components of the photoelectron parallel to the momentum of the Auger electron are suppressed. This is shown in Fig. 1 for two photon energies just above the 2p threshold. For both photon energies, the measured distribution of the relative emission angle  $\theta_{12}$  between the photo- and Auger electron has a significant minimum for small values of  $\theta_{12}$ . This effect has already been observed experimentally for neon atoms [3] and could be confirmed for argon atoms with our work. Furthermore, we

discovered that the energy shift of the photoelectron slightly depends on  $\theta_{12}$ . Such an angular dependent PCI effect still lacks theoretical and experimental confirmation and requires further investigations.

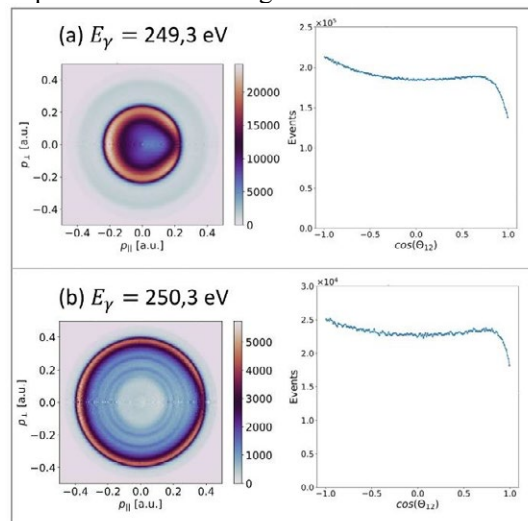


**Figure 1.** (a): The left histogram shows the momentum distribution of the measured photoelectron relative to the emission direction of the Auger electron. The histogram on the right reveals the measured distribution of the angle  $\theta_{12}$  between the photo- and Auger electron. The photon energy was 249.3 eV. (b): The same as in (a) but with a photon energy of 250.3 eV.

### References

- [1] P. J. Hicks et al 1974 *Vacuum*. **24** 573–580
- [2] G. C. King et al 1977 *J. Phys. B*. **10** 2479
- [3] A. Landers et al. 2009 *Phys. Rev. Lett.* **102** 223001

\* E-mail: [Sommerlad@atom.uni-frankfurt.de](mailto:Sommerlad@atom.uni-frankfurt.de)

† E-mail: [Doerner@atom.uni-frankfurt.de](mailto:Doerner@atom.uni-frankfurt.de)



# Gauge-invariant absorption of light by coherent superposition states

A Stenquist<sup>\*</sup>, F Zapata<sup>†</sup> and J M Dahlström<sup>‡</sup>

Department of Physics, Lund University, Lund, 22100 Sweden.

**Synopsis** Absorption of light by an atom in a coherent superposition of states is studied theoretically in both time and energy domains. The atom interacts with an isolated attosecond pulse, which couples both bound and continuum states. The problem is formulated to be gauge invariant and perturbation theory is used to explain different symmetries in absorption due to resonant and off-resonant fundamental processes.

Attosecond transient absorption spectroscopy (ATAS) is used to study electron dynamics with the aim of unravelling ultra-fast phenomena in atoms and molecules. There have been many investigations on ATAS between bound states [1], but few works has focused on the coupling of a prepared bound wave packet to both bound and continuum states [2]. A recent experimental investigation of the physical phenomena in this regime is presented in Ref. [3]. In order to disentangle the fundamental processes in this rich transient absorption regime, we establish a gauge invariant formulation of ATAS based on Yang's energy operator [4]. In the present work [5], perturbation theory is used to study the absorption of a hydrogen atom in an initial superposition state interacting with an attosecond pulse. Absorption is studied in both time and energy domain, resolved over the relative phase of the superposition. The model is validated by numerically solving the time dependent Schrödinger equation. The model allows for disentangling the absorption into fundamental processes of resonant and off-resonant nature, being symmetric and anti-symmetric over phase, respectively, *see* Fig. 1. The off-resonant contribution is found to be significant for states with dipole-allowed transitions to states of lower energy. This yields large regions of emission in the absorption profile of the  $2p + 3p$  superposition, not present in the  $2s + 3s$  case. Additionally, agreement with simulations of helium and neon atoms indicate the applicability of our model to more complex atoms. Using the model we have fully disentangled the ATAS spectra of two-state superpositions in atoms, with coupling to continuum and off-resonant coupling to bound states.

\*E-mail: [axel.stenquist@matfys.lth.se](mailto:axel.stenquist@matfys.lth.se)

†E-mail: [felipe.zapata@matfys.lth.se](mailto:felipe.zapata@matfys.lth.se)

‡E-mail: [marcus.dahlstrom@matfys.lth.se](mailto:marcus.dahlstrom@matfys.lth.se)

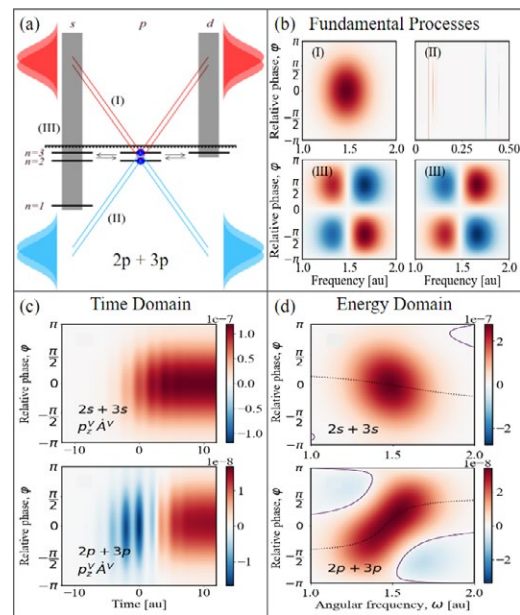


**Figure 1.** (a) Schematic of ATAS absorption processes: resonant continuum (I), resonant bound (II) and off-resonant (III). The energy-domain absorption of these fundamental processes are presented in (b), resolved over the relative superposition phase and Fourier frequency of the pulse, showing absorption in red and emission in blue. (c) and (d) show the absorption for the prepared superpositions  $2s + 3s$  and  $2p + 3p$  in the time and energy domain, respectively.

## References

- [1] M Wu *et al.* J. Phys. B **49**, 062003 (2016)
- [2] J M Dahlström *et al.* J. Opt. **19**, 114004 (2017)
- [3] P Birk *et al.* J. Phys. B **53**, 03 (2020)
- [4] K H Yang Annals of physics **101**, 62 (1976)
- [5] A Stenquist *et al.* <https://arxiv.org/abs/2302.05345>

## Few-photon single ionization of cooled rubidium in the over-the-barrier regime

H Y Ma<sup>1,2,3</sup>, X Wang<sup>1,\*</sup>, L X Zhang<sup>4,5</sup>, Z H Zou<sup>1,2,3</sup>, J Y Yuan<sup>1,2,3</sup>, Y X Ma<sup>1,2,3</sup>, R J Lv<sup>2,3</sup>, Z J Shen<sup>2</sup>, T M Yan<sup>2</sup>, M Weidemüller<sup>6</sup>, D F Ye<sup>4,\*</sup>, and Y H Jiang<sup>1,2,3\*</sup>

<sup>1</sup>Center for Transformative Science and School of Physical Science and Technology, ShanghaiTech University, Shanghai 201210, China;

<sup>2</sup>Shanghai Advanced Research Institute, Chinese Academy of Sciences, Shanghai 201210, China

<sup>3</sup>University of Chinese Academy of Sciences, Beijing 100049, China

<sup>4</sup>Laboratory of Computational Physics, Institute of Applied Physics and Computational Mathematics, Beijing 100088, China

<sup>5</sup>Graduate School, China Academy of Engineering Physics, Beijing 100193, China

<sup>6</sup>Physikalisches Institut, Universität Heidelberg, Im Neuenheimer Feld 226, 69120 Heidelberg, Germany

**Synopsis** In this work, the photoionization of cooled rubidium atoms is investigated both experimentally and theoretically with the 400 nm 35 fs laser pulses at intensities of  $I = 3 \times 10^9 \text{ W/cm}^2 - 4.5 \times 10^{12} \text{ W/cm}^2$ . The recoil-ion momentum distributions (RIMD) are measured for both ground  $5S_{1/2}$  and excited  $5P_{3/2}$  states which coexist in the magneto-optical trap. Along with the ion-yield ratio of the  $5S_{1/2}$  over the  $5P_{3/2}$  states of  $\text{Rb}^+$  ions, we find that the  $5S_{1/2}$  state is completely in the perturbed two-photon ionization while the  $5P_{3/2}$  state transits from perturbed single photon ionization to strong-perturbed single photon ionization with the increase of laser intensity. While the experimental results can be qualitatively explained by numerical simulations that directly solve the time-dependent Schrödinger equation (TDSE), some discrepancies persist, especially for the change of near zero-momentum (NZM) dip in the one-dimensional momentum distribution with respect to the laser intensity, which could stem from the electron-electron correlation that is neglected in the present TDSE simulations.

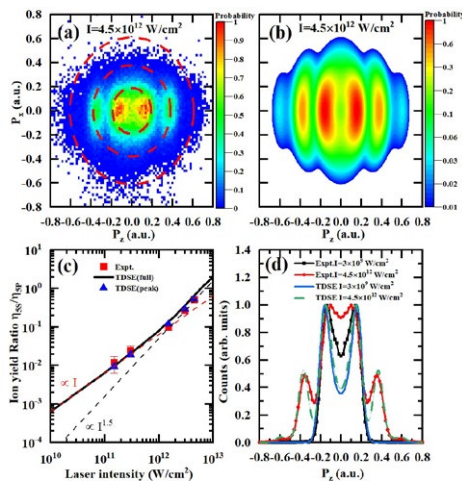


**Figure 1.** Experimental and theoretical results of momentum distribution and ion-yield ratio

In the MOTRIMS [1], in addition to Rb atoms in the  $5S_{1/2}$  state, a certain fraction of excited Rb atoms ( $5P_{3/2}$ ) are effectively populated by the cooling lasers. It is thus possible to compare directly the ionization mechanism of the two

states exposed to the same laser. The measured RIMD in the polarization plane ( $x - z$  plane) of the ionizing laser is presented in Fig.1 (a). RIMD of  $\text{Rb}^+$  exhibits rich ring-like structures and these energies correspond to single-photon ionization of the  $5P_{3/2}$  state ( $p_r = 0.2a.u.$ ), two-photon ( $p_r = 0.39a.u.$ ) and three-photon ionizations of the  $5S_{1/2}$  state ( $p_r = 0.6a.u.$ ), respectively. The corresponding TDSE simulation result shown in Fig.1 (b) can qualitatively reproduce the experimental results. On the other hand, the intensity-dependent scaling law of the ion yields ratio  $\eta_{5S}/\eta_{5P}$  can serve as an indication for the onset of strong-perturbative few-photon ionization, as presented in Fig.1 (c). Although the RIMD and ionization yields obtained by TDSE agree well with the experimental results, there are still noticeable discrepancies in the change of the NZM dip of one-dimensional momentum distribution with the laser intensity, as shown in Fig.1 (d), which will be presented with more details at the meeting.

### References

- [1] Li R Y and Yuan J Y and Wang X C, et al 2019 *J. Instrum.* **14** P02022

\*E-mail: [jiangyh3@shanghaitech.edu.cn](mailto:jiangyh3@shanghaitech.edu.cn)

## Carrier-Envelope-Phase Effects for Multiphoton and Tunnel Excitation of Argon

D. Chetty<sup>1</sup>, R.D. Glover<sup>2</sup>, X.M. Tong<sup>3</sup>, B.A. deHarak<sup>4</sup>, H. Xu<sup>1</sup>, N. Haram<sup>1</sup>, K. Bartschat<sup>5</sup>, A.J. Palmer<sup>1</sup>, A.N. Luiten<sup>2</sup>, P.S. Light<sup>2</sup>, I.V. Litvinyuk<sup>1</sup> and R.T. Sang<sup>1</sup>

<sup>1</sup>Centre for Quantum Dynamic, Griffith University, Nathan, Queensland 4111, Australia

<sup>2</sup>Institute for Photonics and Advance Sensing and the School of Physical Sciences, The University of Adelaide, Adelaide, South Australia 5005, Australia

<sup>3</sup>Centre for Computational Sciences, University of Tsukuba, 1-1-1 Tennodai, Tsukuba, Ibaraki 305-8573, Japan

<sup>4</sup>Physics Department, Illinois Wesleyan University, Bloomington, Illinois 61702-2900, USA

<sup>5</sup>Department of Physics and Astronomy, Drake University, Des Moines, Iowa 50311, USA

**Synopsis** In this paper we present the results a theoretical and experimental investigation of carrier-envelope phase effects in the strong-field excitation of argon. Our study focuses in the intermediate regime where multiphoton and tunneling excitation mechanisms can occur. We demonstrate good agreement between experiment and theory and find a clear boundary for the transition from multiphoton to the tunneling regime.

The excitation of atoms or molecules into excited states is a fundamental physical process with a vast array of applications. In the very high intensity regime, commonly referred to as the strong-field regime, very short pulses of light are used to excite targets. The excitation mechanisms are typically described using either a multiphoton or tunneling explanation. In the multiphoton regime, an excited state can be reached via the absorption of multiple photons whose energy add up. In the tunneling regime, excitation is the result of recapturing tunneled electrons [1]. The dynamics of multiphoton and tunneling plus recapture are very different, however often in experiments, both numerical and physical, the boundary between these processes is broad and frequently in the intermediate regime these models are used interchangeably.

Our work focuses on the effect of the carrier-envelope-phase (CEP) of the exciting laser pulse on the excitation process [2,3] with argon as the target atom. Because excitation is described very differently in the multiphoton

and tunneling regime it is expected that the effect of changing CEP will be observed differently depending on the intensity regime. We explore how the CEP modifies the final bound-state populations and show it is potentially a clear marker for the changing dynamics of the interaction. Our experiments measure the total excitation rate as a function of the CEP and we compare this with numerical simulation. We then extend the simulation to identify how the CEP can be used to show a clear change of the excitation dynamics by observing the bound-state distribution.

### References

- [1] Nubbermeyer *et al*, *Phys. Rev. Lett.* **101**, 233001 (2008)
- [2] Chetty *et al*, *Phys. Rev. Lett.* **128**, 173201 (2022)
- [3] Chetty *et al*, *Phys. Rev. A* **101**, 053402 (2020)

\* E-mail: [r.sang@griffith.edu.au](mailto:r.sang@griffith.edu.au)



## Attosecond time delay during resonance-enhanced multiphoton ionization of noble gases in strong laser fields

Lanhai He<sup>1\*</sup>, Xing Li<sup>1</sup>, Xuanhong Gao<sup>2</sup>, Sizuo Luo<sup>1</sup>, Song-Feng Zhao<sup>2†</sup> and Dajun Ding<sup>1‡</sup>

<sup>1</sup>Institute of Atomic and Molecular Physics, Jilin University, Changchun 130012, China

<sup>2</sup>College of Physics and Electronic Engineering, Northwest Normal University, Key Laboratory of Atomic and Molecular Physics and Functional Materials of Gansu Province, Lanzhou 730070, China

**Synopsis** Phase-dependent photoelectron spectra in resonance-enhanced multiphoton ionization (REMPI) of noble gases, i.e. Ar and Kr, have been obtained by scanning the relative phase of two-color femtosecond lasers. Take Ar as an example, six REMPI channels are resolved and the relative time delays in the attosecond-timescale are extracted, wherein the influences of the resonance width of Rydberg states and the detuning during multiphoton absorption are investigated. Moreover, the possible contribution of laser-induced sub-cycle ac-Stark effect on the delay time during REMPI has been discussed.

Photoionization as one of the most fundamental photon-induced processes occurs after photon absorption by targets. The relevant studies promote the development of quantum physics and bring novel insights for physics, chemistry, and materials science [1-3]. Numerous phenomena, e.g., resonance-enhanced multiphoton ionization (REMPI), tunneling ionization, above threshold ionization, photoelectron diffraction, photoelectron holography, and strong field autoionization have been extensively studied, wherein the real-time electron wavepacket evolution can be traced with attosecond resolution.

In this work, we investigate the relative time delay between different REMPI channels of Ar using phase-stabilized two-color laser fields ( $\omega + 2\omega$ ). Six Freeman-resonant channels (i.e.,  $3d$ ,  $4f$ ,  $5p$ ,  $5g$ ,  $6h$ , and  $7i$  states) are resolved and confirmed from the measured photoelectron spectra. As shown in Fig.1, the relative phase delays (time-delay) with attosecond temporal resolution for different multiphoton resonant channels have been obtained by scanning the phase delay between two-color laser fields. Our results show that the trapping of resonant states and the distortion of the wavepackets by the sub-cycle ac-Stark effect on the effective resonance width of Rydberg state and the detuning during multiphoton absorption have significant contributions to the attosecond time-delay during REMPI process. These findings will bring new insight into the understanding of atomic

and molecular multiphoton ionization in strong laser fields.

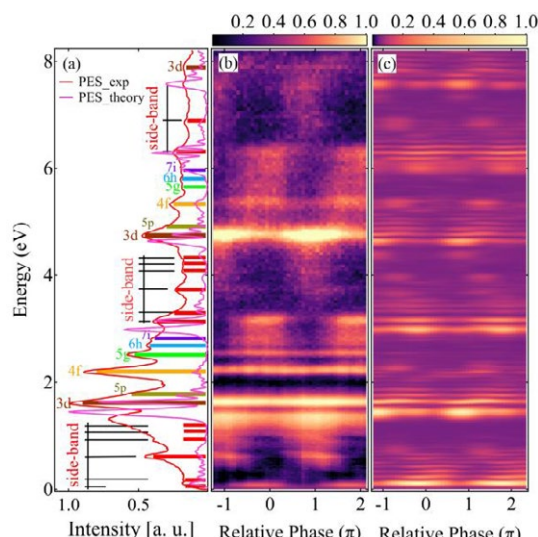


**Figure 1.** Phase-integrated photoelectron energy distribution of the experiment (b) and TDSE simulation (c) at energy under 8eV. Corresponding photoelectron spectra was shown in (a).

### References

- [1] Corkum P B and Krausz F 2009 *Nat. Phys.* **3** 381
- [2] Freeman R R, Bucksbaum P H, Milchberg H, Darack S, Schumacher D, Geusic M E 1987 *Phys. Rev. Lett.* **59** 1092
- [3] Ge P, Han M, Liu M -M, Gong Q, Liu Y 2018 *Phys. Rev. A* **98** 013409

\* E-mail: [helanhai@jlu.edu.cn](mailto:helanhai@jlu.edu.cn)

† E-mail: [zhaosf@nwnu.edu.cn](mailto:zhaosf@nwnu.edu.cn)

‡ E-mail: [dajund@jlu.edu.cn](mailto:dajund@jlu.edu.cn)

## Rescattering sequential multiple ionization of cold Rb

Z H Zou<sup>1,2,3</sup>, J Y Yuan<sup>1,2,3</sup>, X C Wang<sup>1\*</sup>, H Y Ma<sup>1,2,3</sup>, M Weidemüller<sup>4</sup> and Y H Jiang<sup>1,2,3\*</sup>

<sup>1</sup>Center for Transformative Science and School of Physical Science and Technology, ShanghaiTech University, Shanghai 201210, China;

<sup>2</sup>Shanghai Advanced Research Institute, Chinese Academy of Sciences, Shanghai 201210, China

<sup>3</sup>University of Chinese Academy of Sciences, Beijing 100049, China

<sup>4</sup>Physikalisches Institut, Universität Heidelberg, Im Neuenheimer Feld 226, 69120 Heidelberg, Germany

**Synopsis** We report on correlated studies of ionization dynamics of Rb by measuring the yields and momentum distributions from Rb<sup>2+</sup> to Rb<sup>5+</sup> created by 800 nm, 35 fs laser pulses in the intensity range from  $3 \times 10^{14}$  W/cm<sup>2</sup> to  $7 \times 10^{15}$  W/cm<sup>2</sup>. For the ion yields of Rb<sup>2+</sup>, good agreement is achieved between experimental results and Ammosov-Delone-Krainov (ADK) theory, while pronounced “knee” structures can be observed for higher charge states. Moreover, although the momentum distribution of Rb<sup>2+</sup> can be explained by the tunneling picture, the broadening of longitudinal momentum distribution under OBI intensity of higher charge states does not agree with the simple sequential tunneling ionization picture.

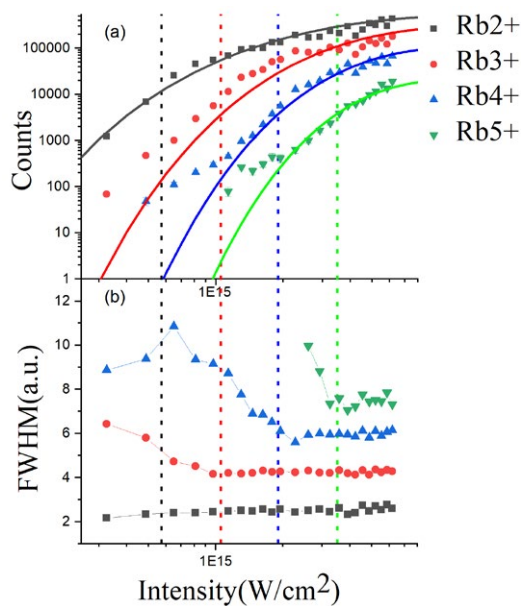


**Figure 1.** The yield and FWHM of different charge states vary with the light intensity. The vertical dash lines represents OBI intensity from Rb<sup>2+</sup> to Rb<sup>5+</sup> and solid lines are calculated result from ADK theory.

In this work, we present a correlational

study of multiple ionization of Cold Rb by intense linearly polarized laser with MOTRIMS [1] (magneto-optical trap recoil ion momentum spectrometer). The ion yield results and the widths (FWHM) of the longitudinal momentum distribution for different charge states are shown in Fig.1 as a function of laser intensity. Experimental results of ion yields from Rb<sup>2+</sup> to Rb<sup>5+</sup> are plotted with various symbols while solid lines are results from ADK theory. Good agreement between experimental result and ADK theory for the Rb<sup>2+</sup> yield is achieved while for higher charge states, typical “knee” structures can be observed, demonstrating the signature of the non-sequential double ionization mechanism (NSDI). The OBI intensities of these charge states are drawn as vertical lines. For the regime between the “knee” structure and OBI intensity, the ion yield can be well reproduced by ADK model, thus it seems that the dominant process in this regime is sequential tunneling ionization. However, the width of momentum distribution increases with decreasing laser intensity, which is not expected in the sequential tunneling picture. A new mechanism is suggested to explain this process and precise theoretical treatment is needed to better explain these results.

### References

- [1] Li R Y, Yuan J Y and Wang X C, et al. 2019 *J. Instrum.* **14** P02022

\*E-mail: [jiangyh3@shanghaitech.edu.cn](mailto:jiangyh3@shanghaitech.edu.cn)

## Autoionization of two-electron-excited $^{88}\text{Sr } 5p_{1/2}n\ell_j$ states<sup>†</sup>

S Yoshida<sup>1\*</sup>, J Burgdörfer<sup>1</sup>, R Brienza<sup>2</sup>, G Fields<sup>2</sup>, and F B Dunning<sup>2</sup>

<sup>1</sup>Institute for Theoretical Physics, Vienna University of Technology, Vienna, Austria, EU

<sup>2</sup>Department of Physics and Astronomy, Rice University, Houston, Texas 77005-1892, USA

**Synopsis** We present a comprehensive experimental and theoretical study of the autoionization of two-electron-excited  $^{88}\text{Sr } 5p_{1/2}n\ell_j$  Rydberg states for low- $\ell$ ,  $0 \leq \ell \leq 5$ . For a given  $\ell$  state the autoionization rate decreases with  $n$  as  $\sim 1/n^3$  mirroring the decrease in the Rydberg electron probability density in the vicinity of the inner  $5p_{1/2}$  electron cloud. This decrease results in a rapid decrease ( $\sim \ell^{-5}$ ) in the autoionization rates for high- $\ell$  states ( $\ell > 3$ ) of given  $n$ . In the low- $\ell$  regime a non-monotonic behavior in autoionization rate is observed.

Autoionization is triggered by energy exchange during collisions between two excited electrons within an atom. It has been used to detect Rydberg atoms (through ionization induced by excitation of the second valence electron) and to obtain information on the time-reversed process, dielectronic recombination, important in many plasmas.

Here we focus on autoionization of  $^{88}\text{Sr } 5p_{1/2}n\ell_j$  levels with  $0 \leq \ell \leq 5$ . For high- $n$  levels the Rydberg electron stays far away from the  $\text{Sr}^+$  ion core and the electron-electron interaction is suppressed. In addition, for high- $\ell$  states the centrifugal barrier keeps the Rydberg electron away from the inner valence electron. Therefore, the interaction is mainly due to the polarization of the  $\text{Sr}^+$  ion core and can be treated well using a perturbative approximation. On the other hand, for low- $\ell$  states, the interaction can be enhanced by penetration of the Rydberg electron into the core ion and by the exchange energy and the perturbative approach breaks down. We analyze the properties of the autoionizing states using an *ab initio* non-perturbative method within a two-active-electron model. The exterior complex rotation (ECR) method enforcing an outgoing boundary condition is used to obtain a more accurate estimate of the auto ionization rate.

New measurements report the autoionization rates and quantum defects of high- $n$  Rydberg states ( $120 \leq n \leq 200$ ). In this regime several autoionization resonances overlap and individual states cannot be resolved. The ECR predictions are used to identify which autoionizing states are

involved in the measured spectra. Both the measurements and the calculations show the autoionization rates scale as  $\Gamma = \Gamma_0/n^3$ . The measured values of the scaled autoionization rate  $\Gamma_0$  as well as those predicted using the ECR method and perturbation theory (PT) are shown in Fig.1. At the higher values of  $\ell$  the ECR, PT, and experimental results are in good agreement, but at low- $\ell$ , PT dramatically overestimates  $\Gamma_0$  due to its neglect of configuration mixing and exchange effects. For high  $\ell$ , the autoionization rate scales approximately as  $1/\ell^5$ . The local maximum at  $\ell \sim 2-3$  is a consequence of phase matching between the bound and scattering wavefunctions.

The ECR predictions are also in good agreement with earlier measurements for  $n \leq 40$  and help illuminate the important role intruder states play in autoionization.

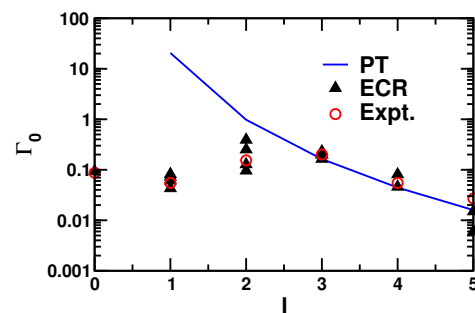


**Figure 1.**  $\ell$  dependence of  $\Gamma_0$ , including the measured values and the ECR predictions. The solid line shows the results of perturbation theory.

<sup>†</sup> Research supported by the NSF and FWF (Austria).

\*E-mail: [shuhei@concord.itp.tuwien.ac.at](mailto:shuhei@concord.itp.tuwien.ac.at)

## Ion and Electron Momentum Distributions from Single and Double Ionization of Helium Induced by Compton Scattering

M Kircher<sup>1\*</sup>, L Sommerlad<sup>1</sup>, F Trinter<sup>1</sup>, S Grundmann<sup>1</sup>, G Kastirke<sup>1</sup>, M Weller<sup>1</sup>, I Vela-Pérez<sup>1</sup>, A Khan<sup>1</sup>, C Janke<sup>1</sup>, M Waitz<sup>1</sup>, S Zeller<sup>1</sup>, T Mletzko<sup>1</sup>, D Kirchner<sup>1</sup>, V Honkimäki<sup>2</sup>, S Houamer<sup>3</sup>, O Chuluunbaatar<sup>4</sup>, Y V Popov<sup>5</sup>, I P Volobuev<sup>5</sup>, M S Schöffler<sup>1</sup>, L Ph H Schmidt<sup>1</sup>, T Jahnke<sup>1</sup> and R Dörner<sup>1†</sup>

<sup>1</sup>Institut für Kernphysik, J. W. Goethe Universität, Max-von-Laue-Str. 1, 60438 Frankfurt, Germany

<sup>2</sup>ESRF, 6 Rue Jules Horowitz, BP 220, 38043 Grenoble Cedex 9, France

<sup>3</sup>LPQSD, Department of Physics, Faculty of Science, University Sétif-1, 19000, Setif, Algeria

<sup>4</sup>Joint Institute for Nuclear Research, Dubna, Moscow region 141980, Russia

<sup>5</sup>Skobel'syn Institute of Nuclear Physics, Lomonosov Moscow State University, Moscow 119991, Russia

**Synopsis** We present a differential study on Compton scattering with  $h\nu = 40$  keV on gas-phase helium. Comparing experimental and theoretical cross sections, we find a strong influence of electron-electron correlations in the final state, thus showing the invalidity of the independent-particle approximation in this energy regime.

A differential measurement of Compton scattering at He with  $h\nu = 40$  keV has been performed [1]. In particular, the double ionization process (DI) was investigated. In about 1% of all cases, due to electron-electron correlations the interaction of one photon results in He DI. The mechanisms responsible are either the shakeoff or the knockoff process. The former is the result of  $e-e$  correlations in the initial state, the latter of  $e-e$  correlations in the final state. For Compton scattering, both these mechanisms do not involve the He nucleus in the interaction, since the momentum of the emitted electrons is balanced by the scattered photon, as opposed to photoionization, where the nucleus has to compensate the electron momenta to ensure momentum conservation. As a consequence, the initial one-electron (for single ionization) or two-electron (for DI) momentum distribution of the initial state is reflected in the momentum distribution of the He ion. For the one-electron initial state, this is known as the Compton profile.

For He DI, we detect the He<sup>2+</sup> ion in coincidence with a low-energy electron utilizing the COLTRIMS technique [2]. In the majority of the cases, the low-energy electron is emitted by the shakeoff or the knockoff mechanism. The results are shown in Fig. 1, together with our theoretical model. To model the results, nonrelativistic calculations with highly correlated initial- and final-state wave functions were required. The initial-state wave function was modeled using a highly correlated trial wave function; the final-state using a wave function which treats  $e$ -nucleus and  $e-e$  interaction on equal footing [3].

In Fig. 1(a), one can see that the nucleus momentum profile of the He ground state (dashed line) is

\*E-mail: kircher@atom.uni-frankfurt.de

virtually identical with the measured (and predicted) He momentum distribution, alluding to the spectator-only role of the nucleus in the Compton scattering DI process.

In Fig. 1(b), the electron momentum distribution is shown, as well as the Compton profile. The continuum electrons produced by Compton scattering DI have significantly smaller momenta than in the initial-state momentum distribution. This is due to the fact that in the shakeoff and the knockoff mechanisms, small energy transfers to the secondary electron are favored.

Our theoretical predictions match excellently with our experimental results. If one neglects  $e-e$  correlations in the initial or the final state, this agreement breaks down.

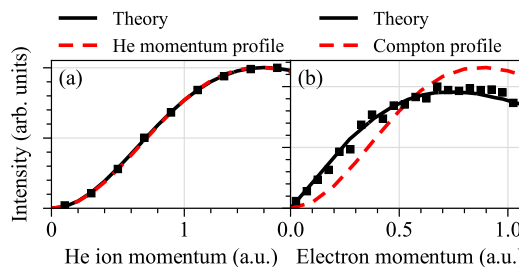


**Figure 1.** Momentum distributions of He<sup>2+</sup> ions (a) and of electrons (b). Experimental data (points) and lines are normalized to their integral, respectively.

### References

- [1] M. Kircher *et al.* Phys.Rev.Lett. **128**, 053001 (2022)
- [2] J. Ullrich *et al.* Rep. Prog. Phys. **66**, 1463 (2003)
- [3] O. Chuluunbaatar *et al.* J. Quant. Spectrosc. Radiat. Transfer **278**, 108020 (2022)

## Progress on a new toroidal spectrometer to measure multiple-path interference from Rb excited and ionized by laser radiation

J P Rogers<sup>1\*</sup>, M R Siggel-King<sup>†</sup>, and A J Murray<sup>1‡</sup>

<sup>1</sup>Photon Science Institute, Dept. of Physics and Astronomy, University of Manchester, Manchester, UK

**Synopsis** A new toroidal spectrometer has been designed to study multiple-path interference from single Rb atoms illuminated by high resolution laser beams. The spectrometer adapts an older instrument designed for photo-electron spectroscopy at Daresbury (TEARES), re-optimised to operate in a lower energy regime (0.1 – 5 eV). Progress on the new instrument is discussed, including the design of a suite of computer controlled supplies that set the operating conditions automatically, based upon simulations of the electron optics in the system.

Experiments in 2019 demonstrated that the excitation and ionization of Rb via different pathways produces interference in the photo-ionization cross-section [1]. Two high-resolution lasers were directed at the atoms to simultaneously excite the 5P state at 780 nm and the 6P state at 421 nm. The 780 nm beam also ionized the 6P state, and the 421 nm beam ionized the 5P state, producing photo-electrons that were detected. Since the ionization pathways cannot be determined by experiment the amplitudes from each must be added coherently, leading to interference in the angular cross-section.

The results were confirmed by calculations from the Halle group [1]. This theory predicts that the interference depends on the laser polarization and target states that are excited. A further prediction is that the introduction of a third laser, whose energy is equal to the sum of the exciting/ionizing beams, will modulate the interference amplitude and phase [2].

The 2019 experiments were extremely time-consuming as the photo-electrons were detected with a hemispherical electron analyser with a narrow angular acceptance. An opportunity arose at this time to obtain a toroidal spectrometer (TEARES) [3] that was being decommissioned at the Daresbury SRS laboratory. This spectrometer is designed to detect photo-electrons over a 270° angular range, allowing measurements to be made far more quickly than using a conventional electron spectrometer.

Figure 1 shows the redeveloped spectrometer. The oven produces a beam of Rb atoms, which is excited by laser beams propagating in the

spectrometer's plane of acceptance. The atomic beam is trapped beyond the interaction region using a cryopump to reduce surface contamination of internal components. The photo-electrons have low energy (0.1 – 5 eV) and so a suite of bespoke computer controlled power supplies drives the electron optics, using data from SIMION simulations of the electrons' trajectories.

A full description of the spectrometer is presented, together with preliminary data from the commissioning of the instrument.

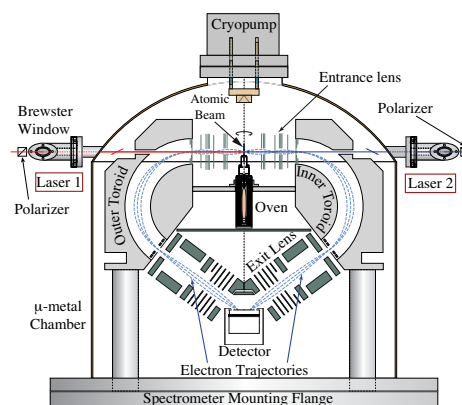


Figure 1. The new toroidal spectrometer.

### References

- [1] Pursehouse J, Murray A J, Watzel J and Berakdar J 2019 *Phys. Rev. Lett.* **122** 053204
- [2] Watzel J, Murray A J and Berakdar J 2019 *Phys. Rev. A* **100** 013407
- [3] Siggel-King M R, Lindsay R, Reddish T J, Secombe D P and Quinn F M 2005 *J. Elect. Spect.* **144-147** 1005

\*E-mail: [joshua.rogers@manchester.ac.uk](mailto:joshua.rogers@manchester.ac.uk)

†E-mail: [michele.siggel-king@stfc.ac.uk](mailto:michele.siggel-king@stfc.ac.uk)

‡E-mail: [andrew.murray@manchester.ac.uk](mailto:andrew.murray@manchester.ac.uk)



# Unexpected Pathway to Double-Core-Hole States in Atoms and Molecules

I ISMAIL<sup>1\*</sup>

<sup>1</sup>Sorbonne Université, CNRS, Laboratoire de Chimie Physique-Matière et Rayonnement, LCPMR, F-75005 Paris Cedex 05, France

## Synopsis

We have studied experimentally and theoretically the formation of double-core-hole (DCH) states in isolated water molecules and neon atoms by the sequential absorption of two X-ray photons. The present study reveals a second important pathway for the population of DCH states, which has almost the same probability but occurs at a lower photon energy compared to the direct  $K^{-1} \rightarrow K^{-2}V$  pathway. This new pathway is observed in both atomic and molecular systems, suggesting that it is a universal phenomenon that can be generalized even to liquids and solids.

Double-core-hole (DCH) states can be produced in atoms and molecules with intense X-rays either by single-photon double ionization [1], in which one photon removes both core electrons, or by two-photon double ionization [2]. Alternatively, monocationic DCH states ( $K^{-2}V$ ) can be produced by photoionization of one core electron with simultaneous resonance excitation of a second core electron. These excited DCH states can be produced by absorption of one [3] or two photons [4]. The signatures of DCH states with very short lifetimes, on the order of a femtosecond or less, can be observed in the subsequent nonradiative relaxation processes, which in the case of cations ( $K^{-2}V$  states) can be considered as resonant Auger decays of the produced DCH states. In these nonradiative decays, an electron from a higher energy level fills one of the two core holes, while another electron, a so-called hypersatellite Auger (HS) KVV1, is emitted into the continuum. The second core hole can be filled by a second step of Auger decay (KVV2). The HS Auger electrons have a higher kinetic energy than those emitted in the Auger decay of the single-core-hole states [5]. Measuring the HS Auger electrons while tuning the photon energy allows us to map the  $K^{-2}V$  resonances.

In this work, we report different DCH excited states of  $H_2O^+$  and  $H_2O^{++}$  ions resonantly

and selectively excited by sequential absorption of X-ray photons from the ground state (GS) via the excitation scheme  $GS \rightarrow O 1s^{-1} \rightarrow O 1s^{-2}V$  or  $O 1s^{-2}$ . In addition to these spectral features where the excitation path is expected, we have found other resonance features with comparable intensity but at lower photon energies. Our calculations have revealed an alternative way to produce  $H_2O^+$  and  $H_2O^{++}$  DCH states with lower photon energies. In this pathway, the core-ionization with the first photon is accompanied by a shake-up of a valence electron. Then, the excitation in the second step consists of promoting the second core-electron into the valence orbital depopulated by the shake process. Revisiting neon as a prototypical atomic system, we have also observed the presence of these unexpected resonance features, suggesting that it is a universal phenomenon that should now be expected.

## References

- [1] Eland, J.H.D., et al. 2010 *Phys. Rev. Lett.* **105** 21
- [2] Berrah, N., et al. 2011 *PNAS USA* **108** 41: p. 16912-16915.
- [3] Püttner, R., et al. 2015 *Phys. Rev. Lett.* **114** 9
- [4] Mazza, T., et al. 2020 *Phys. Rev. X* **10** 4
- [5] Goldsztejn, G., et al. 2016 *Phys. Rev. Lett.* **117** 13

\*E-mail: [iyas.ismail@sorbonne-universite.fr](mailto:iyas.ismail@sorbonne-universite.fr)

## Polarization Dependence of Laser Induced recollision and inner-shell excitations

Y Deng<sup>1</sup>, Z Zeng<sup>2</sup>, P Komm<sup>3</sup>, Y Zheng<sup>2</sup>, W Helml<sup>4</sup>, X Xie<sup>1</sup>, Z Filus<sup>5</sup>, M Dumergue<sup>5</sup>, R Flender<sup>5</sup>, M Kurucz<sup>5</sup>, L Haizer<sup>5</sup>, B Kiss<sup>5</sup>, S Kahaly<sup>5</sup>, R Li<sup>2</sup> and G Marcus<sup>3\*</sup>

<sup>1</sup>SwissFEL, Paul Scherrer Institut, 5232 Villigen PSI, Switzerland

<sup>2</sup>Shanghai Institute of Optics and Fine Mechanics, Chinese Academy of Sciences, 201800, China

<sup>3</sup>Department of Applied Physics, Faculty of Science, Hebrew University of Jerusalem, Jerusalem 91904, Israel

<sup>4</sup>Zentrum für Synchrotronstrahlung, Technische Universität Dortmund, 44227 Dortmund, Germany

<sup>5</sup>ELI-ALPS, ELI-HU Non-Profit Ltd., Wolfgang Sandner utca 3, Szeged 6728, Hungary

**Synopsis** The ability to initiate core-hole excitation with a time precision of sub femtosecond is of paramount important for time resolved studies of such excitations. Here we show the ability to do so by using the process of laser induced electron recollision. We observed x-ray fluorescence from core-hole excitations and tested the fluorescence yield against the laser state of polarization. We found the conditions at which recollision excitation is the dominant process. Such excitations are inherently synchronized with the laser and possibly with attosecond pulses which may probe the excitation dynamics.

We present experimental and theoretical results [1] on soft x-ray emission due to laser-induced recollision and inner-shell excitation. This work summarizes the collected results from two different laser systems: The first laser has a pulse duration of 12 fs at a central wavelength of 1800nm, the second system works with a pulse duration of 60 fs at a central wavelength of 3200 nm. We measured the x-ray emission at right angle to the IR beam propagation direction. Neon and krypton gases were used as targets.

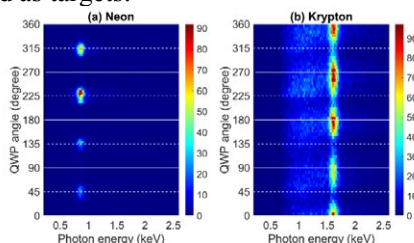


**Figure 1.** (a) The x-ray spectrum generated after inner-shell excitation of neon Vs. the QWP angle (linear polarization approximately at 0, 90, 180 & 270 degree, white solid lines; circular polarization at 45, 135, 225 & 315 degree, white dashed lines) with estimated peak intensity on target  $2.8 \times 10^{15}$  W/cm<sup>2</sup>. (b) The corresponding x-ray spectrum for krypton. Estimated peak intensity  $2.3 \times 10^{15}$  W/cm<sup>2</sup>.

A common practice to separate re-collision related processes, such as high harmonic generation (HHG), from other competing processes is to check the signal against the driving laser state of polarization. As the polarization changes

from linear to elliptical, the electrons' trajectories quickly run away from the parent ion and the re-collision process ceases to exist. Hence, to verify the re-collision mechanism, we checked the fluorescence yield against the laser polarization ellipticity.

The results presented in Fig. 1(b) are similar to those we got in our previous work [2,3], i.e., the yield of the characteristic line in krypton peaks at linear polarization and drops to a minimum at circular polarization, though it does not completely disappear. This picture is more detailed than the previous one and we can see a slight shift between the peak position of the characteristic line and the peak position of the continuum. Contrary to Fig. 1(b), Fig. 1(a) shows a completely opposite behavior: both the characteristic K line and the continuum emission from the neon atoms peak around the circular polarization of the IR laser and reduce to a much lower yield near the linear polarization. In this talk we will discuss these results, the reasons for those differences, and the conditions at which recollision is the dominant process.

### References

- [1]. Deng Y, et al. Opt Express, 2020; 28 :23251–65.
- [2]. Marcus G, et al. Phys Rev Lett. 2012; 108 :023201.
- [3]. Deng et al. Phys Rev Lett. 2016; 116 :073901.

\* E-mail: gilad.marcus@mail.huji.ac.il



## Atomic phase delays in $\omega - 2\omega$ above-threshold ionization

S D López<sup>1</sup>, J Burgdörfer<sup>2</sup>, and D G Arbó<sup>1,3</sup>†

<sup>1</sup>Institute for Astronomy and Space Physics IAFE (CONICET-UBA), C1428ZAA, Buenos Aires, Argentina

<sup>2</sup>Institute for Theoretical Physics, Vienna University of Technology, A-1040 Vienna, Austria, EU

<sup>3</sup>Universidad de Buenos Aires, Facultad de Cs. Exactas y Naturales and Ciclo Básico Común, Buenos Aires, Argentina

**Synopsis** We theoretically explore the extraction of information on the ionization phases in a  $\omega - 2\omega$  setting. We find a very good agreement between our *ab initio* results of the time dependent Schrödinger equation and measured phase delays for Ar atoms [L. J. Zipp, A. Natan, and P. H. Bucksbaum 2014, *Optica* **1**, 361] but significant differences with the strong field approximation even at energies well above the ionization threshold.

Two-color  $\omega$ - $2\omega$  laser fields with well-controlled relative phases have been studied experimentally and theoretically since the last decade of the last century. Recently, they have also been employed as alternative tool to extract information on ionization phases and time delays. One key feature is that the broken inversion symmetry of the  $\omega$ - $2\omega$  field allows for interference between odd and even partial waves of the outgoing photoelectron, which leads to a forward-backward asymmetry of the emission signal. Recently, Zipp *et al* [1] extended the measurement of ionization phases and attosecond time delays to the strong-field multiphoton regime, providing new perspectives on time-resolved strong-field ionization. In this novel  $\omega$ - $2\omega$  interference protocol the role of electron wavepackets emitted by absorption of subsequent harmonics in the RABBIT protocol is replaced by adjacent ATI peaks generated by a strong driving field of frequency  $2\omega$ . The concomitant weaker field opens up interfering pathways to side bands in between neighboring ATI peaks by absorbing or emitting one  $\omega$  photon [2].

In this work, we present a theoretical study of the ionization phase in the multi-photon regime accessible by such a  $\omega$ - $2\omega$  interference protocol for two collinearly polarized laser fields. In Fig. 1 we show *ab initio* results of the energy spectrum calculated within the time dependent Schrödinger equation (TDSE) in the forward direction as a function of the relative phase  $\phi$ . Phase delays have been extracted by fitting the ATI and sideband with the perturbative prediction [3]. We find a very good agreement between our TDSE calculations and the

experiments [1] but strong deviations from the predictions of the strong field approximation (SFA) in dashed vertical lines, clearly indicating that the atomic potential has a crucial influence on the ionization phase of ATI peaks even at energies well above the ionization threshold.

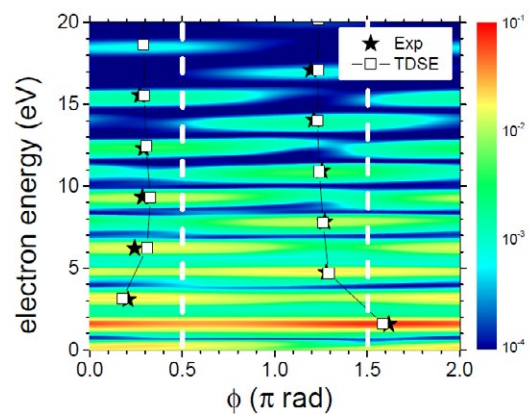


**Figure 1.** TDSE energy spectrum in the forward direction as a function of the relative phase  $\phi$ . Squares: calculated phase delays and the stars: experiments in [1]. vertical dashed lines: SFA.

This work is supported by PICT 2020-01755, 2020-01434, and PICT-2017-2945 of ANPCyT (Argentina), PIP 2022-2024 11220210100468CO of Conicet (Argentina).

### References

- [1] L J Zipp *et al* 2014 *Optica* **1** 361-364
- [2] López S D *et al* 2021 *Phys. Rev. A* **104**, 043113
- [3] Arbó D G *et al* 2022 2021 *Phys. Rev. A* **106**, 053104

† E-mail: [diego@iafe.uba.ar](mailto:diego@iafe.uba.ar)

# Novel semiclassical model for accurate spectra and nondipole effects in multielectron ionization of strongly driven atoms

G P Katsoulis<sup>1\*</sup>, M B Peters<sup>1</sup> and A Emmanouilidou<sup>1†</sup>

<sup>1</sup>Department of Physics and Astronomy, University College London, Gower Street, London WC1E 6BT, United Kingdom

**Synopsis** We formulate a novel 3D semiclassical model as a powerful technique for studying correlated multielectron escape in atoms driven by infrared laser pulses. The model fully accounts for the singularity in the Coulomb potential of any electron and the core and for the Coulomb potential between a recolliding and a bound electron. Using this model, we obtain triple ionization distributions of the sum of the final electron momenta which are in excellent agreement with experiments. Fully accounting for the magnetic field component of the Lorentz force we also identify signatures of nondipole effects.

In atoms driven by intense infrared laser pulses, nonsequential multielectron ionization (NSMI) is a fundamental process governed by electron-electron correlation. However, the theoretical study of NSMI constitutes a big computational challenge for three-dimensional (3D) quantum mechanical studies. Hence, studies employ various approximations such as the dipole approximation, and use lower dimensionality models or soften the Coulomb potential. Most classical models also soften the Coulomb potential to treat unphysical autoionization.

Here, we provide a general 3D classical model of NSMI developed in the nondipole framework that addresses autoionization while including the Coulomb singularity. This is achieved by employing effective Coulomb potentials to describe the interaction between bound electrons (ECBB) [1, 2]. The main premise in our model is that two interactions are most important during a recollision and hence are treated exactly. The Coulomb potential between each electron, bound or recolliding, and the core. Also, the Coulomb potential between each pair of a recolliding and a bound electron and hence the transfer of energy from a recolliding to a bound electron is treated exactly. We determine on the fly whether an electron is bound or recolliding.

We demonstrate that the ECBB model is a powerful tool to study correlated multielectron escape in driven atoms. To do so, we study nonsequential triple ionization (TI) in Ar [1] and Ne [2] driven by infrared pulses. We show that the obtained distribution of the sum of the final elec-

tron momenta is in very good agreement with experiments, see Fig. 1 [2].

Moreover, we use the ECBB model to identify nondipole effects in TI and double ionization (DI) of driven Ne [3]. We find a large positive average sum of the final electron momenta along the direction of light propagation. This momentum offset is zero in the absence of the magnetic field. Most importantly, we show this final electron momentum offset to be a probe of electron-electron correlation by finding a larger momentum offset for TI compared to DI and in the direct versus the delayed pathway of TI and DI [3]. This offset is due to the magnetic field and is related to the sharp change of momentum during the recollision for the recolliding electron [3].

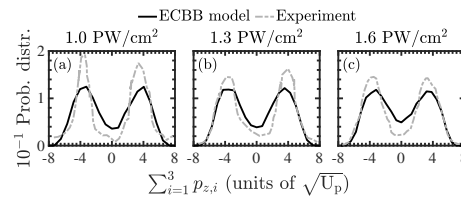


**Figure 1.** For Ne, TI probability distributions of the sum of  $p_z$  obtained with the ECBB model (black lines), and measured experimentally (grey lines).

## References

- [1] Peters M B, Katsoulis G P and Emmanouilidou A 2022, *Phys. Rev. A* **105**, 043102
- [2] Emmanouilidou A, Peters M B and Katsoulis G P 2023 [arXiv:2302.03777](https://arxiv.org/abs/2302.03777)
- [3] Katsoulis G P, Peters M B and Emmanouilidou A 2023 [arXiv:2210.17394](https://arxiv.org/abs/2210.17394)

\*E-mail: [g.katsoulis@ucl.ac.uk](mailto:g.katsoulis@ucl.ac.uk)

†E-mail: [a.emmanouilidou@ucl.ac.uk](mailto:a.emmanouilidou@ucl.ac.uk)

## Photoionization dynamical parameter for the radicals using B-spline R-matrix method

K D Wang\*

Henan Normal University, Xinxiang, 453007, P. R. China country

**Synopsis** Absolute cross sections for the photoionization of radicals are very difficult to measure accurately. There are major discrepancies among several measurements regarding an absolute cross sections for the photoionization of hydroxyl radicals and formyl radicals. To estimate the accuracy of the various results, we carried out accuracy calculations with the B-spline R-matrix method employing the configuration-interaction method to describe electronic correlation.

Measurements of photoionization cross sections (PICSs) for free radicals and transient intermediates are challenging due to the difficulty in producing these species with detectable and quantifiable concentrations. PICSs for free radicals are commonly measured relative to a reference compound that is formed simultaneously with the target free radical in specific molar ratios. For these reasons, the measured absolute PICSs for the radicals from different groups show major discrepancies. Here we carried out accuracy calculations for photoionization of a serial of radicals with the B-spline R-matrix method [1].

1. For photoionization from the OH radical [2], Our results show the Gaussian basis provides a similar quality of description continuum as B-spline base up to 25 eV for ground state, and up to 20 eV for the first excited state. While at higher energy region, oscillatory behavior appearing in the cross section of Gaussian basis indicates it may be not stable. Our predicted positions of resonant peaks agree well with the measured results [3-4]. In general, our total cross sections agree better with the results of Harper *et al.* [4], as shown in Fig. 1.

2. There are major discrepancies between recent [5] and the two early [6-7] measurements regarding an absolute PICS of formyl radicals. We reported accurate cross sections and asymmetry parameters for formyl radicals [8]. The

convergence of the results is checked by changing the partial waves and active spaces. Our smoothed cross section is in close agreement with the experimental measurements of FitzPatrick *et al.* [6] and Shubert *et al.* [7], but are slightly lower than the measurements from Savee *et al.* [5].

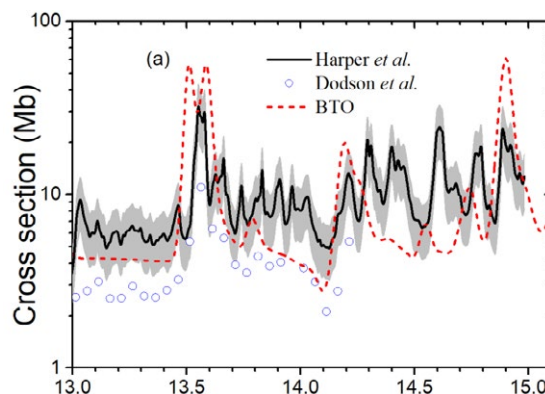


**Figure 1.** The total photoionization cross section of hydroxyl radicals.

### References

- [1] Tennyson J., 2010 *Phys. Rep.* **491** 29
- [2] Wang K. D., *et al.* *Phys. Rev. A* **103** 063101
- [3] Dodson L. G., *et al.*, *J. Chem. Phys.* **148** 184302
- [4] Harper O. J., *et al.*, *J. Chem. Phys.* **150** 141103
- [5] Savee J. D. *et al.*, *J. Phys. Chem. A* **125** 3874
- [6] FitzPatrick B.L. *et al.* *J. Chem. Phys.* **133** 094306
- [7] Shubert V. A. *et al.* *J. Phys. Chem. A* **114** 11238
- [8] Wang K. D., *et al.* *Phys. Rev. A* **105** 042811

\* E-mail: wangkd@htu.cn

## Laser-induced electron diffraction in chiral molecules

D Rajak<sup>1</sup>, S Beauvarlet<sup>1</sup>, O Kneller<sup>2</sup>, A Comby<sup>1</sup>, R Cireasa<sup>3</sup>, D Descamps<sup>1</sup>, B Fabre<sup>1</sup>,  
J D Gorfinkiel<sup>4</sup>, J Higué<sup>1</sup>, S Petit<sup>1</sup>, S Rozen<sup>2</sup>, H Ruf<sup>1</sup>, N Thiré<sup>1</sup>,  
V Blanchet<sup>1</sup>, N Dudovich<sup>2</sup>, B Pons<sup>1</sup>, Y Mairesse<sup>1\*</sup>

<sup>1</sup>Université de Bordeaux – CNRS – CEA, CELIA, UMR5107, 33405 Talence, France

<sup>2</sup>Weizmann Institute of Science, Rehovot 76100, Israel

<sup>3</sup>ISMO, CNRS – Université Paris-Saclay, 91405 Orsay, France

<sup>4</sup>School of Physical Sciences, The Open University, Walton Hall, MK7 6AA Milton Keynes, United Kingdom

**Synopsis** We use strong laser fields to investigate the collision between electrons and oriented chiral molecules. The electron momentum distributions show clear signatures of chiro-sensitive laser-induced electron diffraction.

Chiral molecules exist in two mirror forms, called enantiomers, which interact differently with other chiral objects. For instance the collision of spin-polarized electrons with randomly oriented gas-phase chiral molecules can distinguish two enantiomers [1]. This spin-dependent electron scattering is however a weak effect. Much stronger enantiomeric discrimination was predicted theoretically in the collision between spin-unpolarized electrons and oriented chiral molecules [2]. However the difficulties to orientate the molecules has prevented so far the observation of such chiro-sensitive collision processes. In this work, we overcome this by using strong laser fields.

Strong laser pulses enable probing molecules with their own electrons [3]. The oscillating electric field can tear an electron off a molecule, accelerate it and drive it back to recollide with its parent ion within a few hundreds of attoseconds. The electron-ion collision produces diffraction patterns, encoding the molecular structure and dynamics with Angström and attosecond resolutions [4].

The strong-field ionization probability is very sensitive to the shape of the ionized molecular orbital (here peaking along the CO bond in Fig. 1). As a result, the ionized molecules are an oriented subset of the initial random ensemble. In order to manipulate the direction of the recolliding electrons with respect to the molecular orientation, we use elliptically polarized light. The laser ellipticity controls the electron trajectories in the continuum. We identify two sets of electron trajectories, recolliding from the two ends of the molecules. Measuring the 3D photoelectron momentum distribution shows that the

electron-ion collision is sensitive to chirality. Depending on the handedness of the molecule, the electrons are preferentially diffracted forward or backward along the light propagation axis. This asymmetry can be reversed for electrons recolliding from two ends of the same molecule as shown in Fig. 1.

Our results are in good agreement with calculations using R-matrix data, confirming that laser-induced electron diffraction can be used to investigate collision between electrons and oriented molecules. Such a measurement serves as a new and sensitive probe of the chiral properties of the molecule, opening a new path to resolve ultrafast chiral dynamics.

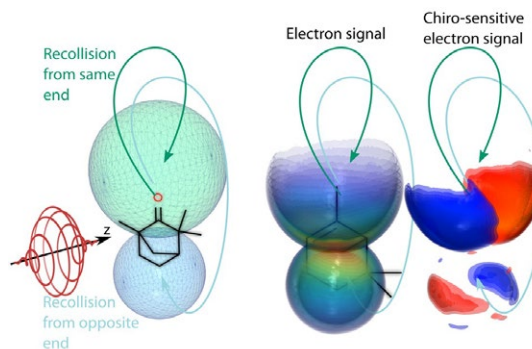


**Figure 1.** Photoelectron distributions from collision between electrons and oriented chiral molecules.

### References

- [1] Mayer S et al. 1995 Phys. Rev. Lett. **74**, 4803
- [2] Busalla et al. 1999 Phys. Rev. Lett. **83**, 1562
- [3] Lin C D et al. 2010 *J. Phys. B* **43** 122001
- [4] Amini K and Biegert J 2020 *Adv. At. Mol. Opt. Phys.* **69**, 163

\* E-mail: [yann.mairesse@u-bordeaux.fr](mailto:yann.mairesse@u-bordeaux.fr)

## Attosecond Delays in Vibrationally Resolved Dissociation of Molecules

Peipei Ge<sup>1\*</sup>, Chenxi Hu<sup>2</sup>, Feng He<sup>2</sup> and Yunquan Liu<sup>†</sup>

<sup>1</sup> Peking University, Beijing, 100871, China

<sup>2</sup> Shanghai Jiao Tong University, Shanghai, 200240, China

**Synopsis** We experimentally measure the time delay of nuclear wave packet in multiphoton dissociative ionization of CO molecules using a sub-laser-cycle pump-probe strategy. We show the vibrationally resolved dissociation channels reveal the time delay of tens of attoseconds. Based on the theoretical calculations, we decouple the delay contribution induced by photoionization of molecules from the measurement, and thus access the settling time of the coherent vibrational motion of CO<sup>+</sup>. Our work sheds new light onto the birth of vibrational nuclear wave packet that is beyond Franck-Condon approximation.

Photoionization of molecules is one of the most fundamental processes in light-matter interaction. It simultaneously triggers the electronic and nuclear vibrational motion. While photoemission dynamics has intrigued scientists for decades [1,2], the other side of the coin, i.e., the nuclear dynamics at the time of ionization, receives much less attention. This is primarily owing to the common adoption of Franck-Condon principle, in which the temporal property of vibrational excitation in molecular ion at the ionization instant has been ignored.

Here, we answer the question: how long does it take to launch a vibrational wave packet composed of different vibrational states? To this end, we study the time delay of vibrational nuclear wave packet in multiphoton dissociative ionization of carbon monoxide (CO) molecules. By performing coincidence measurements in intense linearly polarized laser fields at 400 nm as shown in Figure 1, we are able to clearly identify the vibrationally resolved dissociative transitions during the dissociation of CO. We then introduce a weak probing field with parallel polarization at 800 nm to probe the vibrationally resolved time delay of vibrational wave packet. Strikingly, tens of attoseconds time delays between different vibrational states embedded in the same CO<sup>+</sup> electronic state are revealed, much smaller than the characteristic time scale of the vibrational motion of CO<sup>+</sup>.

Such tiny time delay encodes the temporal dynamics of vibrational wave packet in the two-step dissociation process, i.e., ionization and subsequent dissociation. By extracting the time delay between the parallel and perpendicular dissociative transitions that are initiated from the same CO<sup>+</sup> electronic state, we eliminate the

influence of ionization step and directly access the time delay accumulated in dissociation step, which is of ~12 attoseconds. Moreover, based on the theoretical simulation of the time-dependent evolution of vibrational wave packet, we decouple the delay contribution in ionization step from the measured delays, which scales hundreds to thousands of attoseconds. This delay corresponds to the settling time in the coherent vibrational motion of CO<sup>+</sup> ions before the dissociative transition.

Our results suggest the initial vibrational wave packet needs time to settle on the vibrational states of molecular ion. It sheds light on the birth of vibrational nuclear wave packet that is beyond the Franck-Condon approximation, and would have far-reaching consequences in ultrafast molecular physics and photochemistry.

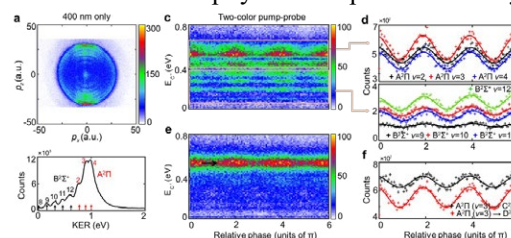


**Figure 1.** (a), (b) Measured momentum distribution of C<sup>+</sup> and kinetic energy release in multiphoton dissociation of CO. (c), (e) Measured two-color phase-dependent energy distributions of C<sup>+</sup> and the corresponding ion yields [(d), (f)].

### References

- [1] Schultze M et al. 2010 Science 328, 1658-1662.
- [2] Biswas S et al. 2020 Nat. Phys. 16, 778-783.

\* E-mail: [gepeipei@pku.edu.cn](mailto:gepeipei@pku.edu.cn) † E-mail: [yunquan.liu@pku.edu.cn](mailto:yunquan.liu@pku.edu.cn)



## Ultraviolet Pump-Probe Photodissociation Spectroscopy of Electron-Rotation Coupling in Diatomics

Y R Liu<sup>1</sup>, V Kimberg<sup>2</sup>, Y Wu<sup>3,4</sup>, J G Wang<sup>3</sup>, O Vendrell<sup>5</sup> and S B Zhang<sup>1\*</sup>

<sup>1</sup>School of Physics and Information Technology, Shaanxi Normal University, Xi'an 710119, China

<sup>2</sup>Department of Chemistry, KTH Royal Institute of Technology, 10691 Stockholm, Sweden

<sup>3</sup>Institute of Applied Physics and Computational Mathematics, Beijing 100088, China

<sup>4</sup>Center for Applied Physics and Technology, Peking University, Beijing 100084, China

<sup>5</sup>Theoretical Chemistry, Institute of Physical Chemistry, Heidelberg University, 69120 Heidelberg, Germany

**Synopsis** The electronic angular momentum projected onto the diatomic axis couples with the angular momentum of the nuclei, significantly affecting the rotational motion of the system under electronic excitations by intense lasers. In this letter, we propose a pump-probe photodissociation scheme for an accurate determination of electron-rotation coupling effects induced by the strong fields. As a showcase, we study  $\text{CH}^+$  molecule excited by a short intense ultraviolet pump pulse to the  $A^1\Pi$  state, which triggers coupled rovibrational dynamics. The dynamics is observed by measuring the kinetic energy release and angular resolved photofragmentation upon photodissociation induced by the time-delayed probe pulse populating the  $C^1\Sigma^+$  state. Simulations of the rovibrational dynamics unravel clear fingerprints of the electron-rotation coupling effects that can be observed experimentally. The proposed pump-probe scheme opens new possibilities for the study of ultrafast dynamics following valence electronic transitions with current laser technology, and possible applications are also discussed.

A UV pump-probe scheme is proposed to study the electron-rotation coupling effects [1]. The proposed scheme uses the presently accessible UV pulse parameters for revealing and manipulating the effects of  $\mathbf{R}-\Omega$  coupling [2] on the rovibrational wavepacket dynamics.

The resonant excitation from ground state  $X^1\Sigma^+$  into the valence excited state  $A^1\Pi$  is triggered by an intense pulse, creating a rovibrational wavepacket, which has imprinted the effect of the  $\mathbf{R}-\Omega$  coupling. The coupled electron-rotational dynamics is unraveled by the weak time-delayed probe pulse, which promotes the system to a higher valence excited dissociative state  $C^1\Sigma^+$ . Our numerical simulations of the dissociation dynamics show a significant effect of the  $\mathbf{R}-\Omega$  coupling on the pump electronic transition for the kinetic energy release (KER) spectra and angular distribution of photofragments (ADP).

Besides revealing the effects of the  $\mathbf{R}-\Omega$  coupling in the angular distributions and rotational wavepackets, the theoretical results indicate that a proper description of this coupling is necessary for accurate consideration of the manipulation and control of rovibrational wavepackets in strong UV fields.

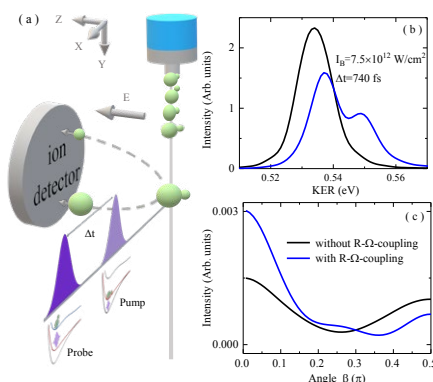


**Figure 1.** (a) Illustration of the dissociative UV pump-probe spectroscopy scheme for  $\text{CH}^+$ ; KER spectra (b) and ADP (c) of the fragments from the dissociative state  $C^1\Sigma^+$ .

### References

- [1] Liu Y R, Kimberg V, Wu Y, Wang J G, Vendrell O and Zhang S B 2021 *J. Phys. Chem. Lett.* **12** 5534
- [2] Liu Y R, Wu Y, Wang J G, Vendrell O, Kimberg V and Zhang S B 2020 *Phys. Rev. A.* **102** 033114

\*E-mail: [song-bin.zhang@snnu.edu.cn](mailto:song-bin.zhang@snnu.edu.cn)

## Shone and driven, they cool down in femtoseconds but scoot off in attoseconds

M Magrakvelidze<sup>1,2</sup>, M E Madjet<sup>2,3</sup>, E Ali<sup>2,4</sup>, R De<sup>2</sup> and H S Chakraborty<sup>2†</sup>

<sup>1</sup> Science Department, Cabrini University, Radnor, Pennsylvania 19087, USA

<sup>2</sup> Department of Natural Sciences, D L Hubbard Center for Innovation, Northwest Missouri State University, Maryville, Missouri 64468, USA

<sup>3</sup> Bremen Center of Computational Materials Science, University of Bremen, Bremen, Germany

<sup>4</sup> Department of Physics, Faculty of Science, University of Benghazi, Benghazi 9480, Libya

**Synopsis** We simulate the electron relaxation dynamics of mid-UV-photon excited  $C_{60}$  and  $Mg@C_{60}$  by non-adiabatic molecular dynamics based on DFT. We also compute intrinsic time delay of XUV ionized photoelectrons from  $C_{60}$  by a linear-response DFT approach. The dramatically different time scales of femtoseconds in the former to attoseconds in the latter arise from the coupling of electrons with the phonon versus the plasmon.

Understanding the photoinduced “hot” electron relaxation dynamics in fullerenes is valuable in photovoltaics and photothermal therapy. While the knowledge of photoelectron emission time delay at fullerene giant plasmon (GP) excitation energies can be beneficial for quantum plasmonics. Of course, both have deep fundamental interests. With easy availability of  $C_{60}$  and advances in the synthesis of endohedral  $C_{60}$  in gas phase, in solution or as films [1], they render natural laboratories to probe ultrafast processes by transient absorption spectroscopy and time-resolved photoelectron spectroscopy.

The relaxation simulation is carried out by electron-phonon coupled non-adiabatic molecular dynamical workflow in a DFT frame [2]. While this method relies on an independent particle approach, a configuration-interaction singles description of the many-body effects produced similar results [2]. The photoemission time delay is computed *via* the Eisenbud-Wigner-Smith (EWS) track employing linear-response time-dependent DFT [3]. This method enables collective many-body effects to couple emerging electrons with plasmon excitations.

Figure 1 (top) presents the decay spectrogram of  $Mg\ 3s \rightarrow 3p$  excitation in  $Mg@C_{60}$  in ten's of femtoseconds (fs), while the following intermediate events persist for longer than 100 fs. The bottom panel captures the profile of EWS delay in attoseconds (as) as a function of the photoelectron energy around GP with its average dephasing time (ADT) of 214 as [4].

This three orders of magnitude quickening of the speed from relaxation to ionization must be due to the coupling of electrons with the phonon

(lattice vibration) in the former, while with the plasmon (giant correlation) in the latter.

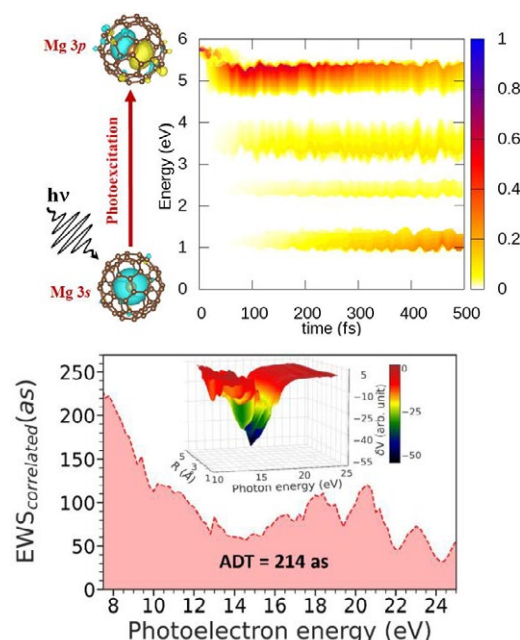


**Figure 1.** (Top) Energy-time spectrogram of  $Mg@C_{60}$  relaxation of excited and transient states. (Bottom)  $C_{60}$  photoelectron delay and GP-induced potential (inset).

Supported by US-NSF Grant PHY-2110318; BARTIK HPC (US-NSF Grant CNS-1624416)

### References

- [1] Popov A 2017 *Nanostr. Sc. Tech. Ser.* Springer
- [2] Madjet M *et al* 2021 *Phys. Rev.Lett.* **126** 183002
- [3] Choi J *et al* 2017 *Phys. Rev. A* **95** 023404
- [4] Biswas S *et al* 2023 (in review) [arXiv](https://arxiv.org/abs/2307.12345)

† E-mail: [himadri@nwmissouri.edu](mailto:himadri@nwmissouri.edu)



## Intensity dependence of the double ionization dissociation of argon dimers in the fields of femtosecond laser pulses

P Song<sup>1</sup>, X W Wang<sup>1</sup>, D W Zhang<sup>1</sup>, Z X Zhao<sup>1</sup> and J M Yuan<sup>2†</sup>

<sup>1</sup>Department of physics, National University of Defense Technology, Changsha 410073, China

<sup>2</sup>Department of Physics, Graduate School of China Academy of Engineering Physics, Beijing 100193, China

**Synopsis** The double ionization dissociation of argon dimer in femtosecond laser fields with different intensities has been investigated experimentally. It is shown that laser intensity significantly modulates the released kinetic energies and the angular distributions of fragmental ions of the dissociation  $\text{Ar}_2^{2+} \rightarrow \text{Ar}^+ + \text{Ar}^+$ . The result suggests that radiative charge transfer after one-site double ionization contributes relatively more to the dissociative double ionization at lower light intensity, but decreases with the increase of light intensity.

The ionization mechanism and fragmentation dynamics of argon dimer in the fields of femtosecond intensive laser pulses has been extensively studied. Double ionization of argon dimer occurs mainly through two-site double ionization. In addition, laser-induced radiative charge transfer after one-site double ionization and frustrated triple ionization have also been observed. Here, we focus on the dissociative double ionization of argon dimer under different laser intensity and measure the released kinetic energy and the angular distribution of fragmental ions generated by coulomb explosion. In the experiment, laser pulses of 25 fs centered at 790 nm and of 10 kHz repetition rate are focused onto argon dimers formed from the supersonic expansion of argon gas through a 30  $\mu\text{m}$  nozzle with 4 bar backing pressure. The laser peak intensity ranges from 100  $\text{TW}/\text{cm}^2$  to 1000  $\text{TW}/\text{cm}^2$ . The fragments from Coulomb explosion of multiply charged ions are then detected with a cold target recoil ion momentum spectrometer (COLTRIMS) [1].

We plot the sum of the released kinetic energy (KER) of the two  $\text{Ar}^+$  ions by the Coulomb explosion under different light intensities in Fig.1. Three-peaks with the KERs of 3.8 eV (A), 5.4 eV (B) and 7.4 eV (C) is shown, indicating three different double ionization mechanism before the Coulomb explosion [2-4]. They are two-site sequential double ionization (A), Single-site double ionization followed by radiative charge transfer after contraction of the dimer bond (B), and frustrated tunnel ionization to  $\text{Ar}_2^{3+}$  (C), respectively. The KER spectra under different light intensities were normalized ac-

cording to the maximum number of events to obtain the changes in KER spectra with light intensity. Fig. 1 clearly show that light intensity can significantly affect the relative intensities of peaks A, B and C and the corresponding double ionization mechanism. The dissociation path corresponding to peak B contributed more to the double ionization dissociation of Ar dimers at low light intensity. When the light intensity increased from 130 to 970  $\text{TW}/\text{cm}^2$ , the contribution change of peak B reached an order of magnitude relatively to peak A.

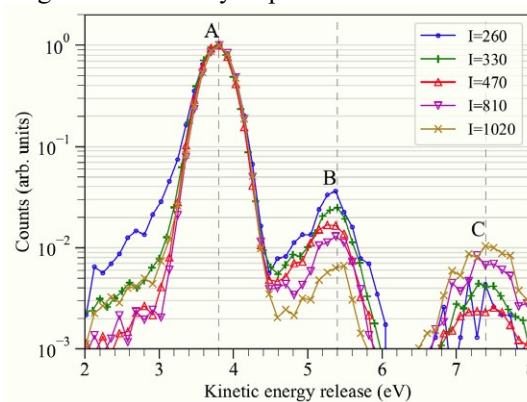


Figure 1. The changes of the KER spectra of  $\text{Ar}^+$  ions with the laser intensities of 260, 330, 470, 810, and 1020  $\text{TW}/\text{cm}^2$ , respectively.

### References

- [1] Song P *et al.* 2022 *Phys. Rev. A* **106**, 023109
- [2] Ulrich B *et al.* 2010 *Phys. Rev. A* **82**, 013412
- [3] Matsumoto J *et al.* 2010 *Phys. Rev. Lett.* **105**, 263202
- [4] Ren X G *et al.* 2015 *Nat. Comm.* **7**, 11093

<sup>†</sup> E-mail: [jmyuan@g scaep.ac.cn](mailto:jmyuan@g scaep.ac.cn)

## Time-Resolved Dynamics on the Giant Plasmon Resonance of $C_{60}$

A C LaForge<sup>1\*</sup>, D Mishra<sup>1\*</sup>, R Obaid<sup>1</sup>, S Pathak<sup>2</sup>, F Trost<sup>3</sup>, H Lindenblatt<sup>3</sup>, S Meister<sup>3</sup>, P Rosenberger<sup>4</sup>, R Michiels<sup>5</sup>, E Kukk<sup>6</sup>, S Biswas<sup>4</sup>, K Saraswathula<sup>7</sup>, F Stienkemeier<sup>5</sup>, D Rolles<sup>2</sup>, F Calegari<sup>7</sup>, M Braune<sup>8</sup>, M Mudrich<sup>9</sup>, M Kling<sup>4</sup>, T Pfeifer<sup>3</sup>, U Saalman<sup>10</sup>, J-M Rost<sup>10</sup>, R Moshhammer<sup>3</sup>, and N Berrah<sup>1</sup>

<sup>1</sup>Department of Physics, University of Connecticut, Storrs, Connecticut, 06269, USA

<sup>2</sup>J.R. Macdonald Laboratory, Department of Physics, Kansas State University, Manhattan, Kansas 66506, USA

<sup>3</sup>Max-Planck-Institut für Kernphysik, 69117 Heidelberg, Germany

<sup>4</sup>Physics Department, Ludwig-Maximilians-Universität Munich, 85748 Garching, Germany

<sup>5</sup>Physikalisches Institut, Universität Freiburg, 79104 Freiburg, Germany

<sup>6</sup>Department of Physics and Astronomy, University of Turku, 20014 Turku, Finland

<sup>7</sup>Center for Free-Electron Laser Science, DESY, 22607, Hamburg, Germany

<sup>8</sup>Deutsches Elektronen-Synchrotron (DESY), 22607 Hamburg, Germany

<sup>9</sup>Department of Physics and Astronomy, Aarhus University, 8000 Aarhus C, Denmark

<sup>10</sup>Max Planck Institute for the Physics of Complex Systems, 01187 Dresden, Germany

**Synopsis** We have studied the ultrafast ionization and fragmentation dynamics of fullerene,  $C_{60}$ , using intense, femtosecond XUV free-electron-laser (FEL) pulses. The FEL was tuned to the giant plasmon resonance, which has a very high absorption cross-section. The dynamics were probed using a single-color XUV pump-probe technique in combination with coincident momentum imaging spectroscopy.

The ultrafast response of a molecule when it is placed in a highly excited state is a fundamental process. FELs have offered new avenues for studying this type of intense light-matter interaction where numerous photons can be absorbed within a few femtoseconds. We will present the time-resolved ionization and fragmentation dynamics of  $C_{60}$  using intense, ultrashort radiation from the FLASH FEL tuned above, on, and below the giant plasmon resonance around 20 eV. The ion dynamics were probed using a one-color XUV pump-probe technique in combination with a reaction microscope. We systematically studied the time-dependent kinetic energies of the atomic and molecular ionic fragments as a function of photon energy and pulse intensity. Comparison with simulations for  $C^+$  and  $C_2^+$  reveal that their measured kinetic-energy distributions are characteristic of neutral fragments, i.e., C and  $C_2$ , which sheds light on the dynamics of neutral light fragments that typically remain unobserved. To show the relevant time-resolved dynamics of interest, we have plotted the kinetic-energy distributions as a function of pump-probe delay for  $C^{2+}$ ,  $C^+$ , and  $C_2^+$  in Fig. 1.

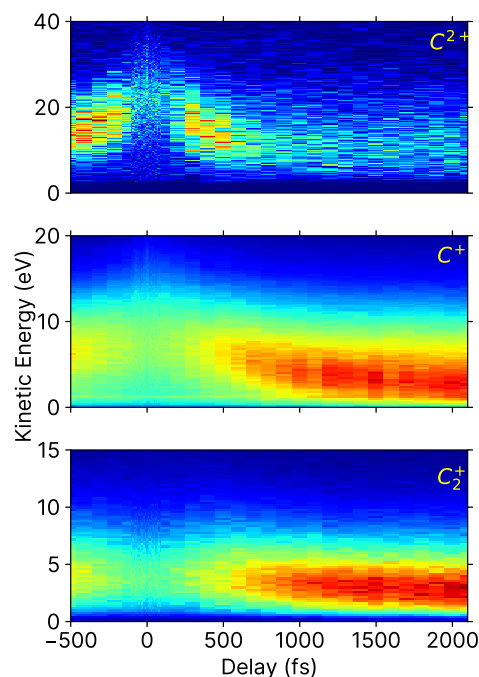


**Figure 1.** Kinetic-energy distributions as a function of pump-probe delay for  $C^{2+}$ ,  $C^+$ , and  $C_2^+$ .

This work is primarily funded by Office of Basic Energy Sciences, Office of Science, US Department of Energy, grant No DE-SC0012376.

## Ultrafast non-adiabatic relaxation of C<sub>60</sub>: In search of efficient MD model

R De<sup>1†</sup>, E Ali<sup>1,2</sup>, M B Wholey<sup>1</sup>, M E Madjet<sup>1,3</sup> and H S Chakraborty<sup>1</sup>

<sup>1</sup> Department of Natural Sciences, D L Hubbard Center for Innovation, Northwest Missouri State University, Maryville, Missouri 64468, USA

<sup>2</sup> Department of Physics, Faculty of Science, University of Benghazi, Benghazi 9480, Libya

<sup>3</sup> Bremen Center of Computational Materials Science, University of Bremen, Bremen, Germany

**Synopsis** Employing non-adiabatic molecular dynamical (NAMD) approaches we simulate the relaxation of C<sub>60</sub> pre-excited by mid-UV photons. Various DFT models to describe the electron dynamics are tested and compared. We study non-DFT extended tight-binding model to seek an inexpensive computing route. To circumvent over-coherence due to classical description of the nuclear motion, a decoherence remedy is tested.

Time-domain spectroscopy of the relaxation of photoexcited electrons in fullerenes are of fundamental interest. These natural processes can be probed by ultrafast transient absorption and time-resolved photoelectron spectroscopy. On the application prospect, non-adiabatic relaxation processes in fullerene materials are relevant in electron transport and cooling which find use in photovoltaics and photothermal therapy. C<sub>60</sub> is commercially available in gas phase, in solution or as films [1].

We use two workflows of electron-phonon coupled non-adiabatic molecular dynamics (NAMD) [2] for simulations. The methodology relies on the fewest-switch stochastic surface hopping approach for the nuclear trajectories in a classical frame [3]. This combines with single-particle DFT description of quantum electron dynamics [3], where different exchange-correlation (xc) models are chosen and compared [4]. Since the DFT approach is expensive, we test with a cheaper extended tight-binding (xTB) framework. Further, to make up for the overestimate in quantum electron-coherence due to classical description of phonon modes, a decoherence correction is examined.

Figure 1 presents the decay spectrogram of C<sub>60</sub> HOMO→LUMO+20 excitation. The workflow includes the software Gamess for geometry optimization, followed by MD with nanoQMflow+cp2k with PBE0 xc to compute non-adiabatic couplings and vibronic Hamiltonian. The femtosecond (fs) populations are obtained using PYXAID package. LUMO+20 is seen to decay in ten's of femtoseconds (fs), while the following intermediate populations

grow, peak and persist for longer than one to several 100 fs.

Fig.1 may be measured in experiments to compare and gain insights. Comparisons among PBE, B3LYP, PBE0 xc's, between DFT and xTB, and with or without decoherence will be presented to optimize the best track for NAMD.

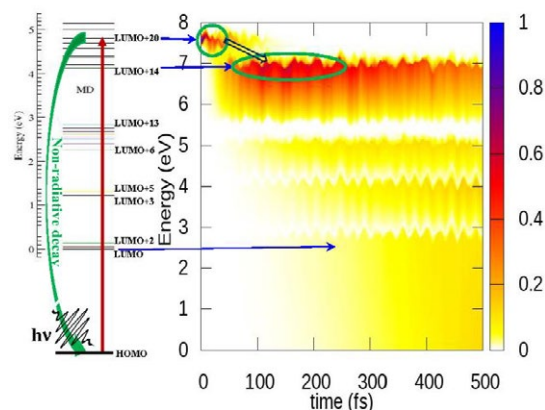


**Figure 1.** Energy-time spectrogram of the relaxation of initial HOMO→LUMO+20 excitation through intermediate states. The cartoon on the left delineates the process.

Supported by US-NSF PHY-2110318; BARTIK HPC (US-NSF CNS-1624416); US-NSF OAC-1919789

### References

- [1] Popov A 2017 *Nanostr. Sc. Tech. Ser.* Springer
- [2] Madjet M *et al* 2021 *Phys. Rev.Lett.* **126** 183002
- [3] Akimov A V and Prezhdo O V, 2013 *J. Chem. Theory Comput.* **9** 11
- [4] Ali E, Madjet M E, De R and Chakraborty H S (*in preparation*)

<sup>†</sup> E-mail: [ruma@nwmissouri.edu](mailto:ruma@nwmissouri.edu)

## Photodissociation of halogen-substituted nitroimidazole radiosensitizers – A pathway towards new radiosensitizer drugs?

L Pihlava<sup>1\*</sup>, M Berholts<sup>2</sup>, J Niskanen<sup>1</sup>, A Vladyka<sup>1</sup>, K Kooser<sup>2</sup>, C Strählman<sup>3</sup>, P. Eng-Johnsson<sup>4</sup>,  
A Kivimäki<sup>5</sup> and E Kukk<sup>1,6</sup>

<sup>1</sup>Dept. of Physics and Astronomy, University of Turku, Turku, 20014, Finland

<sup>2</sup>Institute of Physics, University of Tartu, Tartu, 50411, Estonia

<sup>3</sup>Dept. of Materials Science and Applied Mathematics, Malmö University, Malmö, 20506, Sweden

<sup>4</sup>Dept. of Physics, Lund University, Lund, 221 00, Sweden

<sup>5</sup>MAX IV Laboratory, Lund University, Lund 221 00, Sweden

<sup>6</sup>Laboratoire de Chimie Physique-Matière et Rayonnement, CNRS, Sorbonne University, Paris, 75005, France

**Synopsis** Heavy elements and certain nitroimidazoles both exhibit radiosensitizing properties through different mechanisms. In an effort to investigate the prospect of combining the two in the same molecule, we set out to study the gas-phase photodissociation of halogenated nitroimidazole samples and a halogen-free reference sample utilizing synchrotron radiation and energy-resolved multiparticle coincidence spectroscopy. Although halogenation was observed to somewhat quench the release of important NO<sup>+</sup> fragments, the overall release of fragments capable of mediating cellular damage remained high.

Heavy elements and certain nitroimidazoles are both potential radiosensitizer – they can boost the effectiveness of radiotherapy. The primary sensitization pathway of heavy elements is related to the high x-ray absorption cross sections and to the capability of releasing Auger cascades [1]. Nitroimidazoles are oxygen mimetics [2], whose effectiveness is thought to be related particularly to the release of NO/NO<sup>+</sup> fragments after dissociation.

To explore the potential of heavy-element-enhanced oxygen mimetics, we set out to investigate the gas-phase photodissociation of two brominated nitroimidazole isomers. The results were compared to a normal 2-nitroimidazole molecule. Our work [3] is further motivated by a promising *in vitro* study on iodinated nitroimidazoles [4].

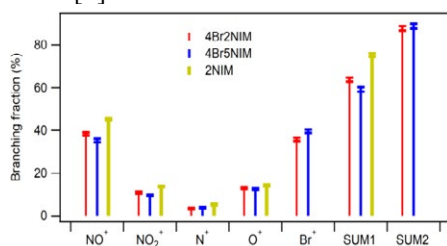


**Figure 1.** Fragment yields of selected ions, all nitro related ions (SUM1) and all likely harmful ions (SUM2) upon dicationic dissociation.

Synchrotron radiation at the FinEstBeAMS beamline of MAX IV was employed for ionization of selected core-level orbitals, which after Auger decay resulted in the creation of dicationic states. The ensuing dissociation was recorded in PEPICO experiments.

We observed dicationic brominated samples releasing notable amounts of ionic fragments capable of mediating damage to cells (Figure 1) and some ionization-site-selective effects on the dissociation. The release of ions originating from the nitro-group was slightly quenched upon bromination, but compensated by the release of reactive Br<sup>+</sup> fragments. Additionally, we estimated that the total x-ray absorption cross section was increased by over a factor of 1.6, accompanied by increase in the free electron release owing to Auger cascades in Br. Consequently, from a physical point of view, halogenation of nitroimidazoles appears to be a viable path towards new multifunction radiosensitizer drugs.

### References

- [1] Kobayashi K *et al.* 2010 MRR 704 123
- [2] Gong L *et al.* 2021 Int J Nanomedicine 16 1083
- [3] Pihlava L *et al.* submitted manuscript
- [4] Krause W *et al.* 2005 Anticancer Res. 25 2145

\* E-mail: [leapih@utu.fi](mailto:leapih@utu.fi)

## Double ionization of S<sub>2</sub>

E Olsson<sup>1</sup>, T Ayari<sup>2</sup>, V Ideböhn<sup>1</sup>, M Wallner<sup>1</sup>, R J Squibb<sup>1</sup>, M Cheraki<sup>2</sup>, J Andersson<sup>1</sup>,  
A Hult Roos<sup>1,3</sup>, J M Dyke<sup>4</sup>, J H D Eland<sup>5</sup>, M Hochlaf<sup>2</sup> and R Feifel<sup>1\*</sup>

<sup>1</sup>University of Gothenburg, Department of Physics, Gothenburg, 412 58, Sweden

<sup>2</sup>Université Gustave Eiffel, COSYS/LISIS, Champs sur Marne, 77454, France

<sup>3</sup>ELI Beamlines, Institute of Physics AS CR, Prague, 182 21, Czech Republic

<sup>4</sup>School of Chemistry, University of Southampton, Highfield, Southampton SO17 1BJ, UK

<sup>5</sup>Oxford University, Physical and Theoretical Chemistry Laboratory, Oxford OX1 3QZ, United Kingdom

**Synopsis** The double ionization spectrum of S<sub>2</sub> and the subsequent fragmentation dynamics of its dication has been investigated using a multi-particle-coincidence time-of-flight technique.

Disulfur, S<sub>2</sub>, is a reactive intermediate molecular species, which is of great interest from both a fundamental perspective, due to its similarity to molecular oxygen, and for a number of applied scientific aspects. In particular, it is astrophysically significant, where it is known to be important in the atmospheres of Jovian planets. Whereas the single ionization photoelectron spectrum of S<sub>2</sub> is known, from the work of Dyke and coworkers [1], the double ionization photoelectron spectrum of S<sub>2</sub> was until now unknown. Previous electron-impact experiments suggests a double ionization energy of 26.2 eV for S<sub>2</sub> [2], in line with our theoretical and experimental results.

Using time-of-flight multiple electron and ion coincidence techniques, in combination with a helium gas discharge lamp and synchrotron radiation, the double ionization electron spectrum and fragmentation dynamics of S<sub>2</sub> are investigated. S<sub>2</sub> was produced by resistively heating mercuric sulfide (HgS), whose vapour at a suitably chosen temperature consists primarily of S<sub>2</sub> and atomic Hg. A multi-particle-coincidence technique is particularly advantageous for retrieving spectra of S<sub>2</sub> from ionization of the vapour. The results obtained are compared with detailed calculations performed with highly correlated ab initio methods, such as CASSCF followed by MRCI for the electronic structure and potential energy curves of S<sub>2</sub>, and RCCSD(T) for total energies and dissociation limits. The experimental vertical double ionization energy at  $27.3 \pm 0.8$  eV strongly agree with these theoretical results [3].

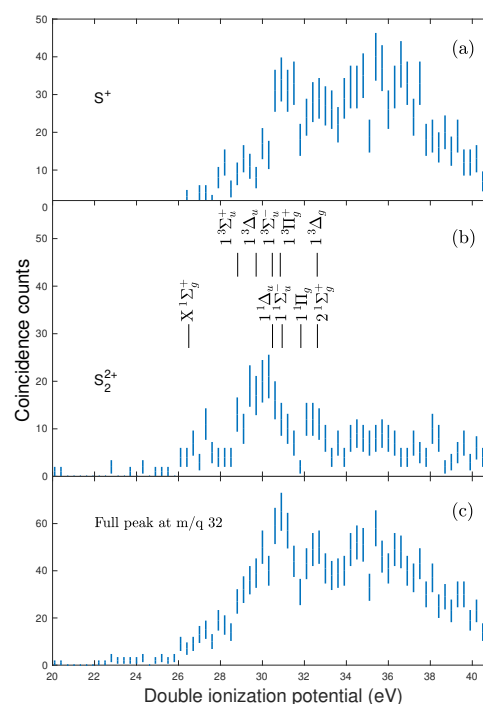


**Figure 1.** Double ionization electron spectra from electron-ion coincidences at the photon energy of 40.81 eV. Each spectrum is based on electron pairs extracted in coincidence with all ions at mass/charge 32 (c), S<sub>2</sub><sup>2+</sup> ion (b) or one of its S<sup>+</sup> fragments (a). The combs in the middle panel shows calculated vertical double ionization energies from the ground state of neutral S<sub>2</sub>.

### References

- [1] Dyke J M et al 1987 *J. Chem. Soc. Faraday Trans. 2* **83** 69
- [2] Zvilopulo A et al 2014 *Tech. Phys.* **59** 951
- [3] Olsson E et al 2022 *Sci. Rep.* **12** 12236

\*E-mail: [raimund.feifel@physics.gu.se](mailto:raimund.feifel@physics.gu.se)



## Intermolecular coulombic decay in an unbound substituted benzene

N R Behera<sup>1</sup>, S Barik<sup>1</sup>, S Dutta<sup>1</sup>, and G Aravind<sup>1\*</sup>

<sup>1</sup>Indian Institute of Technology, Madras, Chennai, 600036, India

**Synopsis** We report a soft ionization mechanism of a substituted benzene neutral that involves intermolecular coulombic decay.

Benzene and substituted benzenes are considered as precursors for the formation of polycyclic aromatic hydrocarbons (PAHs), which account for around 20% of the cosmic carbon [1]. PAHs are ubiquitous in the interstellar medium (ISM) and are proposed to be the source of 3-20 $\mu$ m of unidentified infrared bands (UIB) [2, 3]. So it is very important to study the stability of these neutrals in the astrophysical environment. Here we present the results of our experimental studies of photoionization of a substituted benzene monomer. Different types of cations were formed when unfocused 266 nm laser pulse of intensity  $1 \times 10^5$  to  $1 \times 10^7$   $Wcm^{-2}$  was made to interact with the neutrals (No carrier gas was used) between the repeller and extractor plate of home-built Wiley-McLaren type time of flight spectrometer (TOF). Multiphoton ionization (MPI) and resonance enhanced multiphoton ionization (REMPI) are not expected in this low intensity of laser. A velocity map image recorded for the emitted electrons shows isotropy in the angular distribution, unlike MPI and REMPI where anisotropy in the angular distribution is observed. We propose intermolecular coulombic decay (ICD) between two excited monomer as an underlying process here [4]. An excitation to a  $\pi^*$  state, induces an attractive covalent interaction between two excited units, leading to association. En route to the association, one of the units transfer energy to the other via ICD and eventually ionizes it. The details of the experi-

ment and results will be presented in poster.

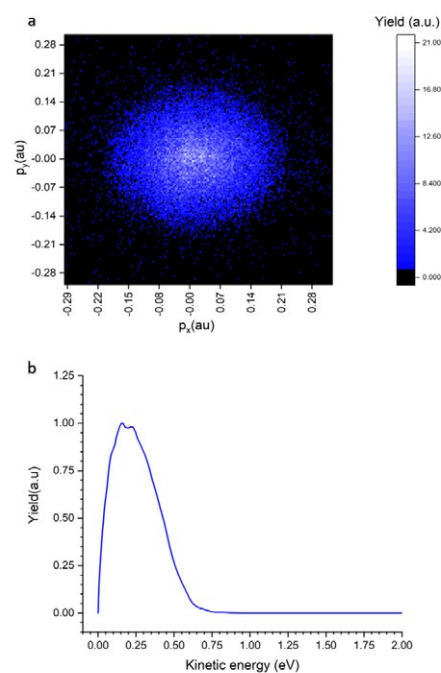


**Figure 1.** (a) velocity map image of emitted electrons due to the interaction between neutrals and 266 nm laser pulse, (b) kinetic energy of the emitted electrons.

### References

- [1] Dwek E et al. 1997, *The Astrophysical Journal*. **475** 565
- [2] Allamandola et al. 1989 *The Astrophysical Journal Supplement Series*. **71** 733
- [3] Peeters E et al. 2011 *Proceedings of the International Astronomical Union*. **7** 149
- [4] Saroj et al. 2022 *Nature chemistry*. **14** 1098

\*E-mail: [garavind@iitm.ac.in](mailto:garavind@iitm.ac.in)

## Photoexcited Polycyclic Aromatic Hydrocarbon undergoes Intermolecular Coulombic Decay

Saurav Dutta<sup>1</sup>, Nihar Ranjan Behera<sup>1</sup>, Saroj Barik<sup>1</sup>, and G Aravind<sup>1\*</sup>

<sup>1</sup>Indian Institute of Technology, Madras, Chennai, 600036, India

**Synopsis** We report Intermolecular Coulombic Decay using low-intensity UV-Visible light in an unbound system of Polycyclic Aromatic Hydrocarbon.

A system where inner valence vacancy is created by a photon it relaxes either by emitting a photon or losing another electron. This latter is known as Auger Decay. In certain cases the Auger Decay channel is energetically forbidden. However, even in such cases, if the same system is embedded in an environment, the emission of valence electrons from the neighbouring system can relax the excitation. This process is called Interatomic or Intermolecular Coulombic Decay (ICD) [1]. In the case of collective ICD, more than atoms or molecules in a cluster is excited simultaneously. The excited atoms or molecules deexcite and transfer their energies to another excited atomic or molecular system in the same cluster and ionizes it [2]. High-intensity sources are required to simultaneously excite that many atoms/molecules in a cluster. Here we report an efficient collective ICD between unbounded Polycyclic Aromatic Hydrocarbon molecules (PAHs) excited at ambient light intensity [3]. The chemical evolution of the photoexcited PAHs gives parent cations and daughter cations fragments.

The gas phase PAHs were released into the interaction region through a solenoidal pulse valve operated at 10 Hz. An unfocused 266 nm photon beam of width 4ns from the 4th harmonic of Nd: YAG pulsed laser operated at 10Hz with intensity  $1 \times 10^5$  to  $1 \times 10^7$  W/cm<sup>2</sup> was employed to photoexcite the molecules. The gas and Laser beam was crossed at this interaction region. The interaction region was the midpoint between the first two plates of the Wiley-McLaren type Time of flight (TOF) mass spec-

trometer, which mass separated the cations' form after light-matter interaction. The  $\pi - \pi^*$  excitation of PAH monomers allows them to undergo a covalent bond-forming association in our experimental condition. Two excited monomers on the way of association exchange energy via ICD resulting in ionization (see Figure 1). The associated dimer cation is unstable and fragments into parent and daughter cations. This observed unusual collective ICD assisted by excited state molecular association implications in environmental chemistry, molecular astrophysics etc. The detailed experiments and results will be presented at the conference.

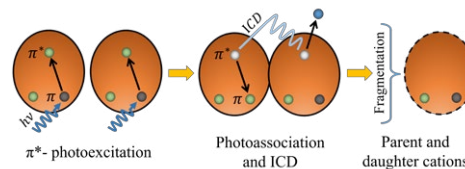


**Figure 1.** Schematic of the mechanism: The excited PAH monomers followed by associative interaction and ICD. The associated dimer cation formation and relaxation by molecular fragmentation are shown.

### References

- [1] Cederbaum L, Zobeley J & Tarantelli F 1997 *Physical Review Letters* **79**, 4778
- [2] Kuleff A, Gokhberg K, Kopelke S & Cederbaum L 2010 *Physical Review Letters* **105**, 043004
- [3] Barik S, Dutta S, Behera N, Kushawaha R, Sajeew Y & Aravind G 2022 *Nature Chemistry*. **14**, 1098-1102

\*E-mail: [garavind@iitm.ac.in](mailto:garavind@iitm.ac.in)



## Time-resolving molecular tunneling dynamics with Free-Electron-Laser-pump and High-Harmonics-Generated-probe transient absorption spectroscopy

A. Magunia<sup>1\*</sup>, M. Rebholz<sup>1</sup>, E. Appi<sup>2</sup>, C. C. Papadopoulos<sup>3</sup>, T. Ding<sup>1</sup>, M. Straub<sup>1</sup>, G. D. Borisova<sup>1</sup>, F. Trost<sup>1</sup>, S. Meister<sup>1</sup>, H. Lindenblatt<sup>1</sup>, R. Jin<sup>1</sup>, J. Lee<sup>1</sup>, A. v. d. Dellen<sup>1</sup>, C. Kaiser<sup>1</sup>, M. Braune<sup>3</sup>, S. Düsterer<sup>3</sup>, S. Ališauskas<sup>3</sup>, T. Lang<sup>3</sup>, C. M. Heyl<sup>3,4,5</sup>, B. Manschwetus<sup>3</sup>, S. Grunewald<sup>3</sup>, U. Frühling<sup>3</sup>, Ayhan Tajalli<sup>3</sup>, A. B. Wahid<sup>6</sup>, L. Silletti<sup>6</sup>, F. Calegari<sup>6</sup>, U. Thumm<sup>7</sup>, U. Morgner<sup>2</sup>, M. Kovacev<sup>2</sup>, I. Hartl<sup>3</sup>, R. Treusch<sup>3</sup>, R. Moshhammer<sup>1</sup>, C. Ott<sup>1†</sup>, T. Pfeifer<sup>1°</sup>

<sup>1</sup>Max Planck Institute for Nuclear Physics, 69117 Heidelberg, Germany; <sup>2</sup>Leibniz University Hannover, 30167 Hannover, Germany; <sup>3</sup>Deutsches Elektronen-Synchrotron (DESY), 22607 Hamburg, Germany; <sup>4</sup>Helmholtz-Institute Jena, 07743 Jena, Germany; <sup>5</sup>GSF Helmholtzzentrum für Schwerionenforschung, 64291 Darmstadt, Germany; <sup>6</sup>Center for Free-Electron Laser Science (CFEL), DESY, 22607 Hamburg, Germany; <sup>7</sup>Kansas State University, 66506 Kansas, USA

We combine XUV-FEL-pump with XUV-HHG-probe pulses in a transient absorption spectroscopy experiment to investigate the dissociation of molecular oxygen. We time-resolve the tunneling of the  $O_2^+$  ( $c^4\Sigma_u^- v=0$ ) state into two channels within picoseconds by identifying absorption resonances of the neutral and ionic fragments.

We introduce an all-XUV FEL-pump—HHG-probe transient absorption spectroscopy scheme (see Fig. 1a), which allows to investigate XUV-initiated molecular dynamics with electronic-state-resolved sensitivity to neutral and ionic fragments. For a first benchmark of this new measurement scheme, we consider the tunneling and pre-dissociation dynamics in oxygen molecules from a specific FEL-excited state by measuring the broadband HHG-probe absorption spectra, covering 10s of characteristic absorption lines from 23 to 35 eV. The FEL-excited  $O_2^+$  ( $c^4\Sigma_u^- v=0$ ) state, which exhibits a local potential-energy minimum in the Franck-Condon region, can dissociate along two parallel pathways, with the rates  $R_{1,2}$ , respectively, 1<sup>st</sup>: the  $O(^3P) + O^+(^4S^0)$  channel or 2<sup>nd</sup>: the  $O(^1D) + O^+(^4S^0)$  channel including the electronically excited state  $O(^1D)$  (see Fig. 1c). We identify these fragments in the time-resolved absorption spectrum ( $\Delta OD$ , Fig. 1b) from well-known resonant atomic transitions and find, in agreement with a rate equation model and theoretical expectations [1–4], all fragments to appear with a common 280 ps time constant.

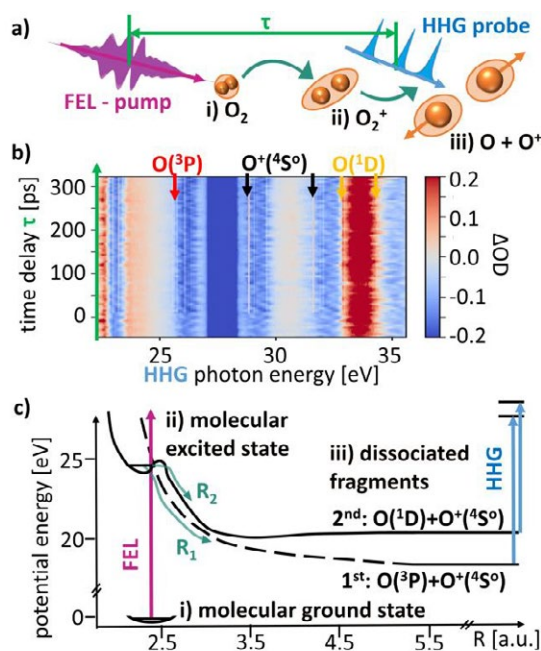


**Figure 1.** a) experimental scheme, b) time-resolved absorption spectrum, c) relevant  $O_2$  potential-energy curves

### References

1. A Ehresmann et al. *J. Phys. B At. Mol. Opt. Phys.* 2004; 37: 4405.
2. P V. Demekhin et al. *Opt. Spectrosc.* 2007 1023 2007; 102: 318-329.
3. H Liebel et al. *J. Phys. B At. Mol. Opt. Phys.* 2002; 35: 895.
4. K Tanaka et al. *J. Chem. Phys.* 1979; 70: 1626.

E-mails: \*[alexander.magunia@mpi-hd.mpg.de](mailto:alexander.magunia@mpi-hd.mpg.de), †[christian.ott@mpi-hd.mpg.de](mailto:christian.ott@mpi-hd.mpg.de), °[thomas.pfeifer@mpi-hd.mpg.de](mailto:thomas.pfeifer@mpi-hd.mpg.de)

## A study of the valence photoelectron spectrum of uracil and mixed water-uracil clusters.

Giuseppe Mattioli<sup>1</sup>, Lorenzo Avaldi<sup>1</sup>, Paola Bolognesi<sup>1</sup>, Anna Rita Casavola<sup>1</sup>, Filippo Morini<sup>2\*</sup>, Thomas Van Caekenberghe<sup>2</sup>, John D. Bozek<sup>3</sup>, Mattea C. Castrovilli<sup>1</sup>, Jacopo Chiarinelli<sup>1</sup>, Alicja Domaracka<sup>4</sup>, Suvasthika Indrajith<sup>4</sup>, Sylvain Maclot<sup>5</sup>, Aleksandar R. Milosavljević<sup>3</sup>, Chiara Nicolafrancesco<sup>3,4</sup>, Christophe Nicolas<sup>3</sup> and Patrick Rousseau<sup>4</sup>

<sup>1</sup>CNR-Istituto di Struttura della Materia, Area della Ricerca di Roma 1, CP 10, Monterotondo Scalo, Italy.

<sup>2</sup>X-lab, Faculty of Sciences, University of Hasselt, Campus Diepenbeek, BE 3590 Diepenbeek, Belgium.

<sup>3</sup>Synchrotron SOLEIL, L'Orme de Merisiers, 91192, Saint Aubin, BP48, 1192, Gif-sur-Yvette Cedex, France.

<sup>4</sup>Normandie Univ, ENSICAEN, UNICAEN, CEA, CNRS, CIMAP, 14000 Caen, France.

<sup>5</sup>Institut Lumière Matière, UMR5306 CNRS, Université Claude Bernard Lyon 1, 69622 Villeurbanne CEDEX, France.

**Synopsis** The outer valence electronic structure of uracil and mixed uracil-water clusters in gas phase have been investigated by photoemission spectroscopy with DFT, NBO analysis and Green's functions calculations.

The valence ionization of uracil and mixed water-uracil clusters has been studied experimentally and by ab initio calculations [1]. In both measurements the spectrum onset shows a red shift with respect to uracil molecule, with the mixed cluster characterized by peculiar features unexplained by the sum of independent contributions of the water or uracil aggregation. To interpret and assign all the contributions, we performed a series of multi-level calculations, starting from an exploration of several cluster structures using automated conformer-search algorithms based on a tight-binding approach. Ionization energies have been assessed on smaller clusters via a comparison between accurate wavefunction-based approaches and cost-effective DFT-based simulations, the latter applied to clusters up to twelve uracil and thirty-six water molecules. The results confirm that i) the bottom-up approach based on a multilevel method [2] to the structure of neutral clusters of unknown experimental composition converges to precise structure-property relationships and ii) the coexistence of pure and mixed clusters in the water-uracil samples. A natural bond orbital (NBO) analysis performed on a subset of clusters highlighted the special role of H-bonds in the formation of the aggregates. The NBO analysis yields a second-order perturbative energy between H-bond donor and acceptor orbitals correlated with the calculated ionization energies as shown in figure 1. This sheds light on the role of the oxygen lone-pairs of the uracil CO group in the formation of strong H-bonds,

with a stronger directionality in mixed clusters, giving quantitative explanation for the formation of core-shell structures.

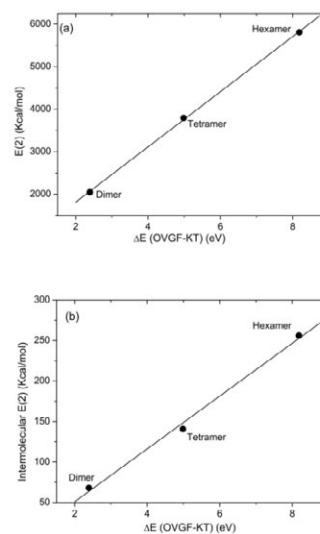


**Figure 1.** Correlation between the  $E(2)$  and the total  $\Delta E$  (OVGF-KT) for the first peak of the OVGF simulated spectra. In (a) the total  $E(2)$  and in (b) only the intermolecular contribution to  $E(2)$  are shown.

### References

- [1] Mattioli G et al. *J. Phys. Chem.* DOI: [10.1063/5.0135574](https://doi.org/10.1063/5.0135574)
- [2] Mattioli G et al. *PCCP* **23** 1859

\* E-mail: [filippo.morini@uhasselt.be](mailto:filippo.morini@uhasselt.be)

## Femtosecond timed imaging of rotation and vibration of alkali dimers on the surface of helium nanodroplets

H H Kristensen<sup>1</sup>, L Kranabetter<sup>2</sup>, N Jyde<sup>2</sup>, C A Schouder<sup>3</sup>, and H Stapelfeldt<sup>2\*</sup>

<sup>1</sup>Department of Physics and Astronomy, Aarhus University, Ny Munkegade 120, DK-8000 Aarhus C, Denmark

<sup>2</sup>Department of Chemistry, Aarhus University, Langelandsgade 140, DK-8000 Aarhus C, Denmark

<sup>3</sup>LIDYL, CNRS, CEA, Université Paris-Saclay, 91191 Gif-sur-Yvette, France

**Synopsis** Na<sub>2</sub> and K<sub>2</sub> on the surface of He nanodroplets are set into rotation and vibration by a moderately intense femtosecond pulse. The time-dependent nuclear motion is recorded via timed Coulomb explosion using a 50-fs pulse. For Na<sub>2</sub> and K<sub>2</sub> in the a <sup>3</sup>Σ<sub>u</sub><sup>+</sup> state, the observed alignment dynamics match predictions from a 2D rigid rotor model, implying that the dimers undergo planar rotation at the surface. For K<sub>2</sub>, 250 periods of a vibrational wave packet in the a <sup>3</sup>Σ<sub>u</sub><sup>+</sup> state is observed in the time-dependent distribution of internuclear distances and appear essentially undisturbed by the He droplet.

Dimers of sodium or potassium, residing on the surface of helium nanodroplets, are set into rotation and vibration, through the dynamic Stark effect, by a moderately intense 50-fs pump pulse. Coulomb explosion of dimers in the singlet X <sup>1</sup>Σ<sub>g</sub><sup>+</sup> and triplet a <sup>3</sup>Σ<sub>u</sub><sup>+</sup> state [1, 2], induced by an intense, delayed femtosecond probe pulse, is used to record the time-dependent nuclear motion.

Concerning rotation, the measured alignment traces show a distinct, periodic structure that differs qualitatively from the well-known alignment dynamics of linear molecules in either the gas phase or dissolved in liquid helium [3]. Instead, the observed alignment dynamics of Na<sub>2</sub> (see Fig. 1a) and of K<sub>2</sub> in the a <sup>3</sup>Σ<sub>u</sub><sup>+</sup> state agree with that obtained from a 2D rigid rotor model, strongly indicating that the rotation of each dimer occurs in a plane – defined by the He droplet surface.

Concerning vibration, the Coulomb explosion probe method enables us to measure the distribution of internuclear distances as a function of time. For K<sub>2</sub> in the a <sup>3</sup>Σ<sub>u</sub><sup>+</sup> state, we observe a distinct oscillatory pattern caused by a two-state vibrational wave packet in the initial electronic state of the dimer (see Fig. 1b). The wave packet is imaged for more than 250 vibrational periods with a precision better than 0.1 Å on its central position and a resolution < 1 Å of its shape. Unlike the rotational motion, the vibration of the dimer is essentially unaffected by the presence of

the He droplet.

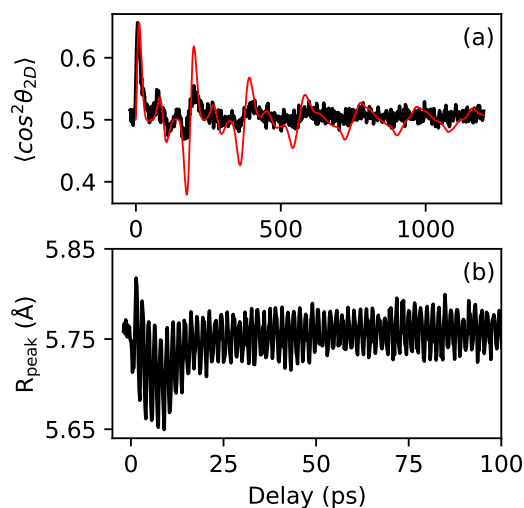


**Figure 1.** (a) Time-dependent degree of alignment for Na<sub>2</sub> in the a <sup>3</sup>Σ<sub>u</sub><sup>+</sup> state (black) and the expected alignment trace from a 2D rigid rotor model (red) with inhomogeneous broadening. (b) Central position  $R_{peak}$  of the distribution of internuclear distances for the first 60 vibrational periods of the vibrational trace for K<sub>2</sub> in the a <sup>3</sup>Σ<sub>u</sub><sup>+</sup> state.

### References

- [1] Kristensen H, *et al.* 2022 *Phys. Rev. Lett.* **128** 093201
- [2] Kristensen H, *et al.* 2023 *Phys. Rev. A* **107** 023104
- [3] Chatterley A S, *et al.* 2020 *Phys. Rev. Lett.* **125** 013001

\*E-mail: [henriks@chem.au.dk](mailto:henriks@chem.au.dk)

## Fragmentation and dynamics of protonated reserpine induced by femtosecond laser excitation

R Brédy<sup>1</sup>\*, M Hervé<sup>1</sup>, A Boyer<sup>1</sup>, A R Allouche<sup>1</sup>, I Compagnon<sup>1</sup> and F Lépine<sup>1</sup>

<sup>1</sup>Univ Lyon, Université Claude Bernard Lyon 1, CNRS, Institut Lumière Matière, F-69622, Villeurbanne, France

**Synopsis** Fragmentation of gas phase protonated reserpine has been investigated using "on-the-fly" femtosecond laser activation in static and time-resolved experiments. These results illustrate the use of ultrafast processes to unveil specific fragmentation patterns with the goal of studying the mechanisms behind fs-laser activation and the dynamics of the involved excited states.

Extracted from the root of *Rauwolfia* species, reserpine is used as drug treatment for hypertension or depression. In analytical sciences, it is routinely employed as a chemical standard to calibrate and evaluate performances of mass spectrometers based on collision induced dissociation (CID) or collisional activation methods [1]. Despite these extensive uses the molecular physics properties of this model molecule are scarce.

The reserpine molecule ( $C_{33}H_{40}N_2O_9$ ,  $M = 608.7$  g/mol) contains 2 aromatic rings that are connected by a molecular bridge. It can therefore absorb UV light efficiently on either one of the chromophore. In its protonated form the proton is located near the N atom of the bridge.

To explore photo-physical properties of protonated reserpine we have performed "on-the-fly" experiments, i.e. without trapping device [2], by coupling electrospray ionization source (ESI) and mass spectrometry (MS) technologies with femtosecond laser at different wavelengths. This configuration ensures that one molecule interacts with one single laser pulse.

In mass spectra of protonated reserpine activated by 25 fs laser pulse at 800 nm (0 to  $3.8 \times 10^{14} \text{W/cm}^2$ ), the observation of doubly charged reserpine and specific fragment  $m/z$  414 show evidence of non-ergodic fragmentation, in contrast to fragmentation observed at 267 nm or CID. This specific fragmentation is attributed to Coulomb repulsion between the native proton site and the extra charge created by ionization in the multiphoton and tunnel regimes [3].

In UV-IR ultrafast pump-probe experiments

we observed non-adiabatic relaxation of the UV excited protonated reserpine through conical intersection in about 4 ps [4]. This shows that the reserpine molecule efficiently converts UV excitation and electronic energy into internal vibrational heating. This result could explain the fluorescence quenching observed in the molecule [5].

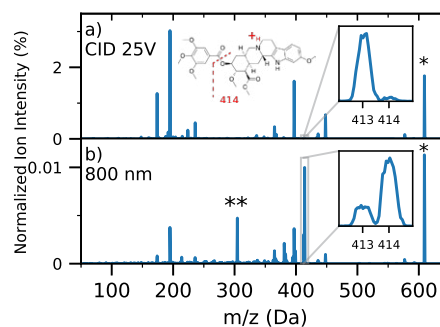


**Figure 1.** a) CID and b) 800 nm ( $3.8 \times 10^{14} \text{W/cm}^2$ ) fs-laser mass spectra of protonated reserpine. Parent ion at  $m/z$  609 is marked by \*, divided by a factor  $10^3$  in b). Doubly charged reserpine not observed in a) is marked by \*\* in b).

### References

- [1] Kumar S *et al* 2016 *J. Pharm. Biomed. Anal.* **118** 183
- [2] Hervé M *et al* 2019 *J. Phy. Chem. Lett.* **10** 2300
- [3] Brédy R *et al* 2022 *Int. J. Mass Spectrom.* **471** 116729
- [4] Hervé M *et al.* 2022 *Adv. Phys.-X* **7** 212328
- [5] Savory B and Turnbull 1983 *J. Photochem.* **23** 171-181

\*E-mail: [richard.bredy@univ-lyon1.fr](mailto:richard.bredy@univ-lyon1.fr)

## Scaling law on the x-ray induced nonadiabatic transition in aromatic molecules

K Yamazaki<sup>1,2\*</sup> and K Midorikawa

<sup>1</sup>RIKEN Center for Advanced Photonics, RIKEN, Wako, Saitama 351-0198, Japan

<sup>2</sup>PRESTO, JST, Kawaguchi, Saitama 332-0012, Japan

**Synopsis** We theoretically investigated the scaling law on the time constant of x-ray induced nonadiabatic transition  $\tau_{\text{NAT}}$  for aromatic molecules. We assumed Fermi's golden rule and linear electronic density of states of x-ray created dicationic states against their excitation energy. We found that  $\tau_{\text{NAT}}$  logarithmically increases as a number of valence electron  $N_v$  as  $\tau_{\text{NAT}} \approx \tau_0 \ln(N_v/N_0)$  ( $\tau_0, N_0$ : constant) for quasi-degenerated electronically excited dicationic states of aromatic molecules. Typical  $\tau_{\text{NAT}}$  for aromatic molecules with one to three aromatic rings is estimated to be  $\sim 160$ - $300$  fs ( $N_v=26$ - $66$ ).

Nonadiabatic transition (NAT) drives x-ray induced radiation damages [1-3] of many bio- and x-ray functional molecules. These molecules contain aromatic rings in their skeleton and the NAT time constant is therefore a fundamental parameter to understand the mechanisms of the radiation damage process.

In this study, we theoretically investigated the scaling law on the time constant of x-ray induced nonadiabatic transition  $\tau_{\text{NAT}}$  for aromatic molecules [4]. We assumed Fermi's golden rule and linear electronic density of states of x-ray created dicationic states against their excitation energy as Hervé *et al.* [5], which has originally been proposed to account for the time constants of the internal conversion (*i.e.* NAT conserving spin multiplicity) among quasi-degenerated electronically excited (QDEE) monocationic states of polyaromatic hydrocarbons. We also considered not only internal conversion but also intersystem crossing (*i.e.* NAT changing spin multiplicity).

We found that  $\tau_{\text{NAT}}$  logarithmically increases as a number of valence electron  $N_v$  as

$$\tau_{\text{NAT}} \approx \tau_0 \ln(N_v/N_0) \quad (1)$$

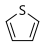
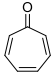
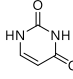
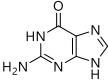
for their QDEE dicationic states.  $\tau_0$  and  $N_0$  represent the NAT time constant and minimum number of valence electron to create QDEE dicationic states in a reference molecule, respectively. We adopted  $\tau_0$  from the experimental value of thiophene molecule ( $\tau_0 = 158 \pm 12$  fs,  $N_v = 26$ ) in gas phase [6] and evaluated  $N_0$  to be  $9.57 \pm 1.03$ . Resultant  $\tau_0$  and  $N_0$  were uniformly used for the subsequent calculations.

The calculated  $\tau_{\text{NAT}} = 226 \pm 18$  fs for tropone ( $N_v = 40$ ) dication reproduces the value obtained by nonadiabatic molecular dynamics simulation

( $\tau_{\text{MD}} = 211$  fs) [4] as shown in Figure 1. This indicates that the scaling law is useful to estimate the NAT timescale of aromatic molecules.

We also applied the eq. (1) to uracil ( $N_v = 42$ ) and guanine ( $N_v = 56$ ). The resultant  $\tau_{\text{NAT}}$  for uracil was  $226 \pm 18$  fs, which is almost the same as tropone ( $N_v = 40$ ) since their  $N_v$  is very similar. Guanine can undergo slower NAT than uracil ( $\tau_{\text{NAT}} = 279 \pm 18$  fs) due to its larger  $N_v$ .

We will discuss the detail on the derivation of eq. (1) and further applications to polyaromatic hydrocarbons in the presentation.

				
	Thiophene (Reference)	Tropone	Uracil	Guanine
$N_v$	26	40	42	56
$\tau_{\text{NAT}}$ (fs)	$158 \pm 12$	$226 \pm 18$	$234 \pm 18$	$279 \pm 18$
$\tau_{\text{MD}}$ (fs)	---	211	---	---

**Figure 1.** Molecular structure, number of valence electrons  $N_v$ , and time constant of nonadiabatic transition in the quasi-degenerated energy region  $\tau_{\text{NAT}}$  for selected aromatic molecules calculated by eq. (1). For tropone, the corresponding time constant obtained by the nonadiabatic molecular dynamics calculations  $\tau_{\text{MD}}$  [6] is also displayed for comparison.

### References

- [1] Li Z *et al.*, 2015 *Phys. Rev. Lett.* **115** 143002
- [2] Liekhus-Schmaltz C. E *et al.* 2015 *Nat. Commun.* **6** 8199
- [3] Li Z *et al.*, 2017 *Nat. Commun.* **8** 453
- [4] Yamazaki K and Midorikawa K 2022 submitted, arXiv:2209.02874
- [5] Hervé M *et al.*, 2021 *Nat. Phys.* **17** 327
- [6] Kukuk E *et al.*, 2021 *Phys. Rev. Res* **3** 013221

\* E-mail: [Kaoru.yamazaki@riken.jp](mailto:Kaoru.yamazaki@riken.jp)



## The role of non-local processes in the decay of X-ray induced electronic inner-shell vacancies in weakly bound systems

A Hans<sup>1\*</sup>, C Küstner-Wetekam<sup>1</sup>, L S Cederbaum<sup>2</sup>, U Hergenhahn<sup>3</sup> and A Ehresmann<sup>1</sup>

<sup>1</sup>Institute of Physics and CINSaT, University of Kassel, Kassel, 34132, Germany

<sup>2</sup>Institute of Physical Chemistry, University of Heidelberg, Heidelberg, 69120, Germany

<sup>3</sup>Fritz-Haber-Institut der Max-Planck-Gesellschaft, Berlin, 14195, Germany

**Synopsis** The response of matter to X-ray impact is dominated by the formation of electronic inner-shell vacancies by the photoelectric effect. Except for energetically very deep vacancies, those holes decay by Auger emission, which creates multiply charged states. In molecules, highly charged states are strongly dissociative due to the Coulomb repulsion, typically leading to rapid fragmentation. We introduce the role of non-local decay of inner-shell vacancies preventing the population of highly charged states in weakly bound prototype systems.

The interaction of matter and light has always been one of the most fundamental subjects in physics. X-rays with energies in the range of the binding energies of inner-shell electrons (typically few hundreds of eV to several keV) are of special interest because of their relevance in many fields, covering fundamental natural science, life science, radiation damage and material characterization.

The creation and decay of electronic inner-shell holes by X-ray photoionization can be thoroughly investigated using spectroscopy of the primary photoelectrons as well as secondary decay products such as photons, electrons, and ions. In the decay of shallow to medium-deep core holes, Auger decay is mostly dominant, i.e., the vacancy is filled by a valence electron and another valence electron is emitted. The spectroscopy of Auger electrons has evolved to a powerful tool in many fields of science.

The Auger final states are doubly or multiply charged, depending on the number of Auger electrons emitted. In atoms, those states may be ground states or relax further by fluorescence. In small molecules, the situation is different because Coulomb repulsion favors charge separation by fragmentation. Consequently, X-ray ionization and subsequent Auger decay leads inevitably to destruction of the molecule, which is an important aspect to be considered in X-ray induced radiation damage.

Due to their localized nature, the influence of the environment in weakly bound matter, such as van der Waals or hydrogen bound clusters, liquids, and solids, has not been considered for a long time. Within the last decades, however,

new environment-enabled decay mechanisms have been discovered, the most prominent of which is interatomic (intermolecular) Coulombic decay (ICD) [1, 2]. ICD is a non-local autoionization, in which one site decays but the electron is emitted from a neighbor.

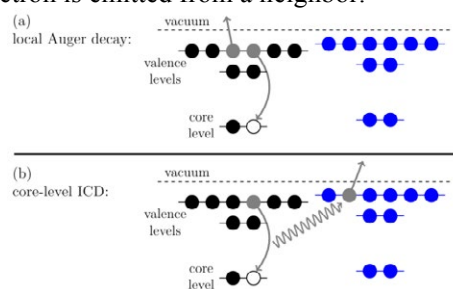


**Figure 1.** a) Auger decay and b) core-level ICD in the relaxation of electronic inner-shell vacancies [3].

For the decay of core-holes, the difference between Auger decay and ICD is illustrated in Figure 1. We review the search for the elusive core-level ICD in rare-gas clusters [3] and outline its impact for radiation biology, where it may dramatically affect the formation of highly charged states and therefore molecular fragmentation, e.g., in an aqueous environment [4].

### References

- [1] Cederbaum LS, Zobeley J, Tarantelli F 1997 *Phys. Rev. Lett.* **79** 4778
- [2] Jahnke T, Hergenhahn U, Winter B, et al. 2020 *Chem. Rev.* **120** 11295
- [3] Hans A, Küstner-Wetekam C, Schmidt Ph, et al. 2020 *Phys. Rev. Research* **2** 012022(R)
- [4] Hans A, Schmidt Ph, Küstner-Wetekam C, et al. 2021 *J. Phys. Chem. Lett.* **12** 7146

\* E-mail: [hans@physik.uni-kassel.de](mailto:hans@physik.uni-kassel.de)

## Aromatic cyclo-dipeptides in the gas-phase: photoemission and state-selected fragmentation

L Carlini<sup>1\*</sup>, E Molteni<sup>1</sup>, P Bolognesi<sup>1</sup>, D Sangalli<sup>1</sup>, G Mattioli<sup>1</sup>, P Alippi<sup>1</sup>, A Casavola<sup>1</sup>, M Singh<sup>2</sup>,  
C Altucci<sup>2</sup>, M Valadan<sup>2</sup>, M Nisoli<sup>3,4</sup>, Y Wu<sup>3</sup>, F Vismarra<sup>3,4</sup>, R Borrego Varillas<sup>4</sup>, R Richter<sup>5</sup>,  
J Chiarinelli<sup>1</sup>, M C Castrovilli<sup>1</sup> and L Avaldi<sup>1</sup>

<sup>1</sup>CNR - Istituto di Struttura Della Materia (CNR - ISM), Area della Ricerca di Roma 1, Monterotondo Scalo, Italy

<sup>2</sup>Università degli Studi di Napoli Federico II, Dipartimento di Fisica, Napoli, Italy

<sup>3</sup>Politecnico di Milano, Dipartimento di Fisica, Milano, Italy

<sup>4</sup>CNR - Istituto di Fotonica e Nanotecnologie (CNR - IFN), Milano, Italy

<sup>5</sup>Elettra, Sincrotrone Trieste S.C.p.A., Trieste, Italy

**Synopsis.** The photoionization of three aromatic cyclo(*c*)-dipeptides (*c*-GlyPhe, *c*-TrpTrp and *c*-TrpTyr) has been studied by valence photoemission (PES), mass spectrometry (MS) and photoelectron-photoion coincidence, PEPICO, measurements at 60 eV photon energy. The comparison between theoretical calculations and experimental PES allowed to determine the ionization potential and to assign the main features in the experimental spectra, while PEPICO experiments provided information on the binding energy selected fragmentation.

Linear (*l*-) and cyclo (*c*-) dipeptides built by two aminoacids via one/two peptide bonds, are the object of widespread interest due to their central role in several scientific as well as practical areas. Among the dipeptides, the ones with an aromatic aminoacid are of interest for the study of the energy and charge transfers<sup>[1]</sup>, relevant processes in bio-systems.

In this work a combined experimental and theoretical study of electronic structure and state-selected fragmentation of *c*-dipeptide cations (*c*-GlyPhe, *c*-TrpTrp and *c*-TrpTyr) has been performed.

A systematic ab-initio study implemented with different computational tools allowed to explore geometry, energy levels, electronic wave-functions and optical properties of the molecules<sup>[2]</sup>. In the calculated as well as experimental valence photoemission (PES) spectra typical features due to the aromatic aminoacid appear, indicating the key role of the side chain in determining the photo-chemical properties of this class of molecules.

Mass spectrometry (MS) and photoelectron-photoion coincidence (PEPICO) measurements provided information on state selected fragmentation. The correlation between the electronic distribution of the molecular orbitals and the fragments yields has been investigated by comparing the PES spectrum and the PEPICO relative ion yields. From the fragment branching ratios the dependence of specific fragmentation pathways on the binding energy (BE) as well as

approximate onset for the production of specific fragments have been obtained. By comparing the most probable fragmentation pathways of the three samples we found that when the dipeptide contains the Trp aminoacid, independently of the ionized orbital, the charge migrates always to the Trp aromatic terminal, which is then lost as a charged fragment during dissociation. Such complete dominance of a single fragment overall the mass spectra and PEPICO measurements has never been observed during our previous studies on *l*- and *c*-dipeptides.

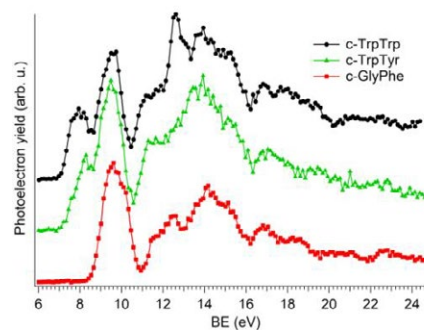


**Figure 1.** The PES spectra of *c*-GlyPhe, *c*-TrpTyr and *c*-TrpTrp dipeptides. The feature at 12.6 eV in the *c*-TrpTrp spectrum (black curve) is due to residual water in the sample.

### References

- [1] R. Weinkauff *et al* 1996 *J. Phys. Chem.* **100** 18567.
- [2] E. Molteni *et al* 2021, *Phys. Chem. Chem. Phys.*, **23**, 26793.

\* E-mail: [laura.carlini@ism.cnr.it](mailto:laura.carlini@ism.cnr.it)



## NIR-induced fragmentation of VUV-generated molecular cations

R M P Tanyag, F A K Hübschmann, J Thøgersen, and H Stapelfeldt

Department of Chemistry, Aarhus University, 8000 Aarhus C, Denmark

**Synopsis** The fragmentation of naphthalene cation, generated by ionization with a femtosecond VUV laser pulse, can be induced and monitored by a 150-ps long NIR pulse, sent at different time delays with respect to the VUV pulse.

Monitoring the fragmentation of a molecular ion is fundamental to many photochemical studies on molecules such as polyaromatic hydrocarbons and biomolecules. However, the molecular ion must first be prepared in a state without exciting intermediary energy levels that could lead to its immediate photofragmentation [1]. Ionization with vacuum ultraviolet (VUV) radiation with a few tens of femtosecond duration is one means, and it creates a “clean” mass spectrum showing mostly the parent ion along with its complexes and clusters (dimers, trimers, and so on) [2, 3]. In contrast, multiphoton or strong-field ionization often causes significant fragmentation. Figure 1(a) shows the difference between single- and multi-photon ionization of naphthalene molecules ( $m/z = 128$ ) in a cold molecular beam with helium as the carrier gas.

In this contribution, we will first describe the generation of a lab-based VUV source by focusing the second harmonic of a 50-femtosecond 800 nm near-infrared (NIR) laser into an argon filled chamber; a process which creates the third harmonic of the 400 nm (133 nm) [4] with a conversion efficiency of less than 1%. Then, a 150-picosecond 800 nm beam was sent to the molecular beam at different time delays with respect to the counterpropagating VUV pulse. Figures 1(b) to (d) demonstrate that fragments are formed only when the VUV arrives before the NIR. We could also demonstrate that heavier fragments appear about 10 to 20 picoseconds after the molecule was ionized, while it takes longer to create lighter fragments. These initial results can possibly be used to follow the relaxation of

the VUV-generated cations and control the pathways of their induced-photofragmentation [5].

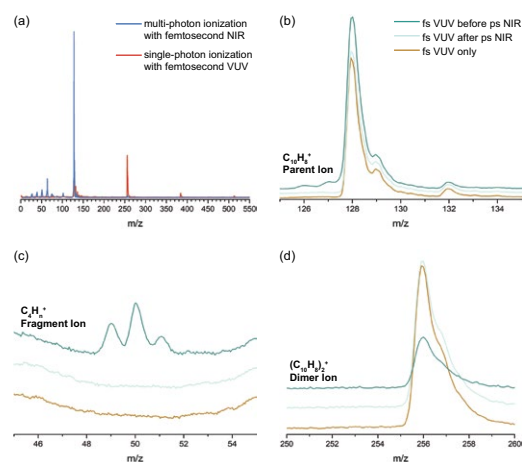


**Figure 1.** Ionization and fragmentation of Naphthalene. (a) A comparison between single- and multi-photon ionization. (b-c) Appearance of different naphthalene cations depending on the delay between the VUV and the NIR.

### References

- [1] Ng C-Y 2002 *Annu. Rev. Phys. Chem.* **53** 101
- [2] Shi YJ and Lipson RH 2005 *Can. J. Chem.* **83** 1891
- [3] Phan TD, Li A, Nakamura H, Imasaka T, and Imasaka T 2020 *J. Am. Soc. Mass Spectrom.* **31** 1730
- [4] Trabs P, Ritzke H-H, and Noack F 2016 in *Conference on Lasers and Electro-Optics, OSA Technical Digest (online)* FM4A.4
- [5] Varvarezos L, Delgado-Guerrero J, Di Fraia M, Kelly TJ, Palacios A, et al. 2023 *J. Phys. Chem. Lett.* **14** 24

## Photoionization of polyatomic molecules with ASTRA: a scalable wave-function approach

C Marante<sup>1\*</sup>, J M Randazzo<sup>2</sup>, B I Schneider<sup>3</sup>, J Olsen<sup>4</sup> and L Argenti<sup>1,5†</sup>

<sup>1</sup>Department of Physics, University of Central Florida, Orlando, Florida 32816, USA

<sup>2</sup>CONICET, San Carlos de Bariloche, Río Negro 8400, Argentina

<sup>3</sup>NIST, Applied and Computational Mathematical Div., Gaithersburg, MD 20899, USA

<sup>4</sup>Department of Chemistry, Aarhus University, Aarhus 8000, Denmark, EU

<sup>5</sup>CREOL, University of Central Florida, Orlando, Florida 32816, USA

**Synopsis** The ASTRA suite is used to study the influence of electronic correlation on the total and partial valence photoionization cross sections of the nitrogen and formaldehyde molecules. ASTRA implements a new efficient approach to the multi-channel molecular electronic continuum, based on high-order transition density matrices between a target correlated ionic states.

Ultrafast laser technologies keep extending the intensity and frequency of attosecond pulses [1, 2]. When impinging on molecular targets, these pulses can produce an electronic excitation in an energy range that comprises multiple ionization thresholds. The coherent electron dynamics so triggered involves entangled photoelectron-photoion states that can be accurately described only within a correlated wave-function approach. We present several ionization observables for a diatomic (nitrogen) and a polyatomic (formaldehyde) molecules, computed with the ASTRA suite of codes [3]. ASTRA implements a new approach to the close-coupling representation of the molecular electronic continuum based on high-order transition density matrices (TDM) between correlated ionic states with arbitrary multiplicity, obtained with an extension of LUCIA, a general large-scale configuration-interaction code [4]. The wave function continuity between the short-range molecular orbitals and the long-range numerical functions that describe the asymptotic photoelectrons is achieved by means of the hybrid Gaussian-B-spline integrals implemented in the GBTO library [5]. The B-splines can be extended to reach quantization boxes of hundreds of atomic units, where complex-absorbing

potentials are used to enforce the outgoing boundary conditions appropriate for photoionization processes and prevent unphysical reflections at the boundary, when solving the time-dependent Schrödinger equation. We study the effect of electronic correlation on the total and partial photoionization cross sections of nitrogen and formaldehyde, which compares well with established benchmarks [6, 7]. The efficient spin-string formalism of TDM's algorithms in LUCIA [8] makes ASTRA scale favorably with molecular size, thus opening the way to study correlated dynamics in complex molecules. This work is supported by the DOE CAREER grant No. DE-SC0020311. Part of the calculations used NERSC resources under the contract No. DE-AC02-05CH11231 and the award BES-ERCAP0024720.

### References

- [1] Duris J *et al* 2020 *Nat. Photon.* **14** 30
- [2] Saito N *et al* 2019 *Optica* **5** 1542
- [3] Randazzo J M *et al* 2022 *arXiv*: 2211.10316
- [4] Olsen J *et al* 1996 *J. Chem. Phys.* **104** 8007
- [5] Masin Z *et al* 2020 *Comput. Phys. Commun.* **249** 107092
- [6] Klinker M *et al* 2018 *J. Phys. Chem.* **9** 756
- [7] Cacelli I *et al* 2001 *Chem. Phys. Lett.* **347** 261
- [8] Olsen J *et al* 1988 *J. Chem. Phys.* **89** 2185

\*E-mail: [carlos.marantevaldes@ucf.edu](mailto:carlos.marantevaldes@ucf.edu)

†E-mail: [luca.argenti@ucf.edu](mailto:luca.argenti@ucf.edu)

## Exploring Electron-Nuclear Entangled Dynamics in Hydrogen Molecular Ions using Quantum Computer

C Osaku<sup>1\*</sup>, Y Orimo<sup>1</sup>, K L Ishikawa<sup>1</sup>, Y Kawashima<sup>2</sup>, T Gujarati<sup>3</sup>, and T Sato<sup>1†</sup>

<sup>1</sup> Graduate School of Engineering, The University of Tokyo, 7-3-1 Hongo, Bunkyo-ku, Tokyo 113-8656, Japan

<sup>2</sup>IBM Quantum, IBM Research Tokyo, Tokyo, 103-8510, Japan

<sup>3</sup>IBM Quantum, IBM Research - Almaden, 650 Harry Road, San Jose, CA 95120, USA

**Synopsis** We have developed a non-adiabatic simulation method for hydrogen molecular ions under an intense laser field using a quantum computer and succeeded in calculating with high accuracy using an actual quantum computer.

The interaction between matter and intense laser fields is of great interest in contemporary physics, with many applications in areas such as plasma physics, materials science, and chemistry. When subjected to intense laser fields, matter can exhibit fascinating and unexpected phenomena. Understanding these phenomena is crucial for designing and controlling material properties. While we have developed first-principles methods for studying molecules in intense laser fields [1], they suffer from the problem of exponentially increasing computational cost with the number of particles.

Therefore, quantum chemical calculations using quantum computers, which can be calculated in polynomial time instead of exponential time, have attracted much attention [2]. In our laboratory, we have developed a quantum-classical hybrid method, the time-dependent optimized unitary coupled cluster method (TD-OUCC), which can incorporate particle correlations using time-dependent orbital functions. However, the application of this technique was limited to electronic systems only.

In this study, we extend the TD-OUCC method to multicomponent systems and use it to calculate the real-space dynamics of one-dimensional molecular hydrogen ions under an intense laser field.

Figure 1 shows the time evolution of the electron and nuclear density when a 1D molecular hydrogen ion model is irradiated by a high-intensity laser. Figure 1(a)(c) was calculated on a classical computer using a quantum circuit simulator, and (b)(d) was obtained using the reduced density matrix calculated on the quantum computer `ibm_kawasaki`, which was in-

stalled in Kawasaki, Japan in 2021. The tunneling ionization and subsequent dissociation, which cannot be described without incorporating the electron-nucleus correlation [3], could be reproduced. It should be emphasized that the results obtained by the quantum computer with noise [Fig. 1(b)(d)] excellently agree with ideal results [Fig. 1(a)(c)] on noiseless classical computers.

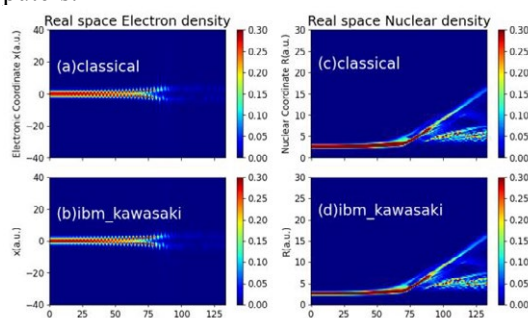


**Figure 1.** Time evolution of the electron(a)(b) and nuclear(c)(d) density of one-dimensional  $H_2^+$  irradiated by a laser pulse with a wavelength of 800 nm, an intensity of  $2 \times 10^{14} \text{ W/cm}^2$ , and the duration of about 50 fs. Comparison of the results of a quantum circuit simulator (a)(c) and `ibm_kawasaki` (b)(d).

### References

- [1] Li Y, Sato T, and Ishikawa KL 2021 *Phys. Rev. A* **104** 043104
- [2] McArdle S, Endo S, Aspuru-Guzik A, Benjamin SC, and Yuan X 2020 *Rev. Mod. Phys.* **92** 15003
- [3] Abedi A, Maitra NT, and Gross EKV 2010 *Phys. Rev. Lett.* **105** 123002

\* E-mail: [sakefake@g.ecc.u-tokyo.ac.jp](mailto:sakefake@g.ecc.u-tokyo.ac.jp)

† E-mail: [sato@atto.t.u-tokyo.ac.jp](mailto:sato@atto.t.u-tokyo.ac.jp)

# Photoionisation, Rayleigh, and Raman scattering cross sections for the ground and excited vibrational levels of $\text{H}_2^+$

A Singor\*, L H Scarlett, I Bray, and D V Fursa

Department of Physics and Astronomy, Curtin University, Perth, Western Australia 6102, Australia

**Synopsis** Photoionisation, Rayleigh, and Raman scattering cross sections have been calculated for the ground and excited vibrational levels of the  $1s\sigma_g$  state of  $\text{H}_2^+$  within the Born–Oppenheimer approximation. The origin of the near–threshold oscillations in the vibrationally–resolved photoionisation cross sections has been investigated.

Photon scattering cross sections have proved essential in many applications, such as modelling opacities and radiative transport, quantum illumination and radar, and Raman spectroscopy, which in particular has important applications in hydrogen storage. Atomic and molecular hydrogen are abundant in the interstellar medium, with  $\text{H}_2^+$  being formed by radiative association of protons and atomic hydrogen, and ionisation of  $\text{H}_2$ . Hence, photon scattering cross sections for  $\text{H}_2^+$  are of particular interest in astrophysics. Given that  $\text{H}_2^+$  exists in a distribution of vibrational levels, cross sections resolved in the initial vibrational level are required.

Photon–molecule scattering processes have been well understood to second order in perturbation theory since the development of the Kramers–Heisenberg–Waller (KHW) matrix element [1, 2] in the mid 1920’s. We have produced a comprehensive set of vibrationally–resolved photoionisation, Rayleigh, and Raman scattering cross sections for the  $1s\sigma_g$  state of  $\text{H}_2^+$  by calculating the KHW matrix elements. The electronic target structure was calculated using prolate spheroidal coordinates. Bound electronic states were obtained by diagonalising the target Hamiltonian in a Sturmian basis while continuum electronic states were generated using our recently developed code for calculation true continuum spheroidal wave functions [3]. Photoionisation cross sections and dipole matrix element curves were produced as a function of internuclear separation, which were then used to calculate the vibrationally–resolved photoionisation, Rayleigh, and Raman cross sections. For Rayleigh and Raman scattering a complete set of intermediate states was included and pole terms arising from integration over the vibrational con-

tinuum were handled using a Gaussian quadrature method to implement principal value integration.

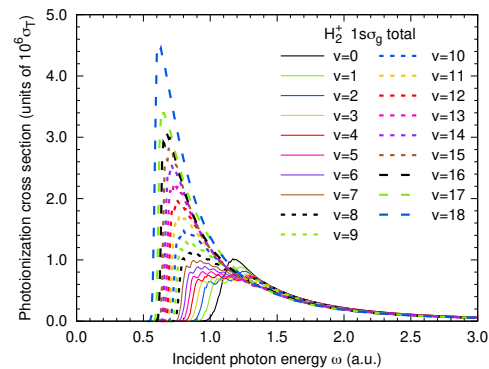


**Figure 1.** Photoionisation cross sections for all bound vibrational levels of the  $1s\sigma_g$  state of  $\text{H}_2^+$  by unpolarised light.  $\sigma_T \approx 6.652 \times 10^{-29} \text{ m}^2$  is the Thomson cross section.

Photoionisation cross sections for the ground and excited bound vibrational states of  $\text{H}_2^+$  are presented in Fig. 1. It was found that the ionisation threshold shifts to lower incident photon energies as the initial vibrational level increases. Oscillations were observed in the near–threshold cross sections for photoionisation from vibrationally excited states. The magnitude of the near–threshold photoionisation cross sections also increases as the initial vibrational level increases.

## References

- [1] Kramers H A and Heisenberg 1925 *Z. Phys.* **31** 681
- [2] Waller I 1929 *Z. Phys.* **58** 75
- [3] Singor A, Savage J S, Bray I, Schneider B I, and Fursa D V 2023 *Comput. Phys. Commun.* **282** 108514

\*E-mail: [adam.singor@postgrad.curtin.edu.au](mailto:adam.singor@postgrad.curtin.edu.au)

## Attosecond delays of high harmonic emissions from isotopes of molecular hydrogen measured by Gouy phase XUV interferometer

M H Mustary<sup>1</sup>, Liang Xu<sup>2,3</sup>, Wanyang Wu<sup>2</sup>, Nida Haram<sup>1</sup>, Han Xu<sup>1</sup>, Feng He<sup>2,4</sup>, R T Sang<sup>1</sup>  
and I V Litvinyuk<sup>1,\*</sup>

<sup>1</sup>Centre for Quantum Dynamics, Griffith University, Brisbane, Queensland 4111, Australia

<sup>2</sup>Key Laboratory for Laser Plasmas (Ministry of Education) and School of Physics and Astronomy, Collaborative Innovation Center for IFSA (CICIFSA), Shanghai Jiao Tong University, Shanghai 200240, China

<sup>3</sup>Shanghai Key Lab of Modern Optical System, University of Shanghai for Science and Technology, 200093 Shanghai, People's Republic of China

<sup>4</sup>CAS Center for Excellence in Ultra-intense Laser Science, Shanghai, 201800, China

**Synopsis** We present a precise measurement of HHG phase difference between two isotopes of molecular hydrogen using the advanced extreme-ultraviolet (XUV) Gouy phase interferometer [1]. The measured phase difference is about 200 mrad, corresponding to  $\sim 3$  attoseconds time delay which is nearly independent of harmonic order. The measurements agree very well with numerical calculations of a four-dimensional time-dependent Schrödinger equation. Numerical simulations also reveal the effects of molecular orientation and intra-molecular two-centre interference on the measured phase differences. This technique enables the observation of subtle effects of molecular structures and nuclear motion on electron dynamics in strong laser fields.

High harmonic spectroscopy can access structural and dynamical information on molecular systems encoded in amplitude and phase of high harmonic generation (HHG) signals<sup>4</sup>. However, measurement of the harmonic phase is a daunting task. Building an interferometer in the XUV region is quite challenging for two reasons: firstly, it is challenging to control the delay of the XUV pulses precisely between the two arms with sub-cycle precision; secondly, the highly reflective XUV optics is yet to be developed. Our passively stabilized Gouy phase interferometer [1,2], on the other hand, is an all-optical direct XUV interferometric technique. It does not require calibration of gas pressures to ensure the same number densities. Additionally, it does not require any XUV optics. The technique provides an elegant way to generate two coherent high harmonic pulses without splitting the driving laser and XUV beams. The two mutually coherent XUV pulses are generated by exploiting the inherent properties (Gouy phase) of a single Gaussian focused laser beam. Its unprecedented resolution of 300  $\mu$ rad ( $\sim 100$  zeptoseconds) is a result of any instability in the distance between the two arms (the gas jets in this case) of the interferometer being determined relative to the Rayleigh length,  $z_R$  of the fundamental laser beam as opposed to the XUV wavelength in a conventional optical interferometer.

Here, we apply the technique to investigate the effect of nuclear dynamics on the electron motion in molecular hydrogen by precise measurement of high harmonic phase difference (and corresponding HHG phase delays) produced in H<sub>2</sub> and D<sub>2</sub>. Since the ionization potentials of H<sub>2</sub> (Ip = 15.43 eV) and D<sub>2</sub> (Ip =

15.46 eV) are almost identical, the difference in the phase accumulated by electron in the continuum is considered to be negligible. However, due to the nuclear mass difference, the evolution of nuclear wave packet while electron propagates in the continuum and then recombines to the ground state may differ substantially. The harmonic intensity from the heavy isotope was shown to be higher compared to the lighter molecule as harmonic emission is sensitive to the nuclear motion, though for D<sub>2</sub> the ionization probability is less than for H<sub>2</sub>. The aim of this work is to measure a small phase difference of HHG signals and to gain an insight into the correlated electron–nuclear dynamics for the two isotopes of molecular hydrogen.

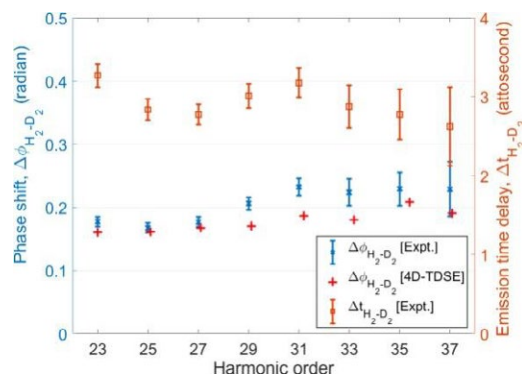


**Figure 1.** Phase differences and delays between H<sub>2</sub> and D<sub>2</sub>.

### References

- [1] Mustary M H et al. *J. Phys. B: At. Mol. Opt. Phys.* 51, 094006 (2018).
- [2] Laban, D. E. et al. *Phys. Rev. Lett.* 109, 263902 (2012).

\*E-mail: [i.litvinyuk@griffith.edu.au](mailto:i.litvinyuk@griffith.edu.au)



## Experimental determination of thermal electron detachment rates of $C_7^-$

S Iida<sup>1</sup>\*, S Kuma<sup>2</sup>, K Masuhara<sup>1</sup>, S Masuda<sup>1</sup>,  
H Tanuma<sup>1</sup>, K Hansen<sup>3</sup>, H Shiromaru<sup>1</sup>, and T Azuma<sup>2</sup>

<sup>1</sup>Department of Physics, Tokyo Metropolitan University, Tokyo 192-0397, Japan

<sup>2</sup>Atomic, Molecular and Optical Physics Laboratory, RIKEN, Saitama 351-0198, Japan

<sup>3</sup>Center for Joint Quantum Studies, Department of Physics, School of Science, Tianjin University, 92 Weijin Road, Tianjin 300072, China

**Synopsis** Thermal electron detachment rate constants of  $C_7^-$  anions were measured. The energy-resolved values were obtained from radiatively cooled ions after 190 ms in an ion storage ring. The measured rate constants are found to be reduced by two orders of magnitude compared to theoretical values. The difference is tentatively assigned to the anharmonicities of the vibrational motion.

Energy resolved electron detachment rates of  $C_7^-$  were measured by observing delayed detachment of photo-excited  $C_7^-$  stored in an electrostatic ion storage ring. The relevant energy distributions are shown in Fig. 1, where the outcomes of radiative cooling and photo-excitation are demonstrated schematically. Hot  $C_7^-$  anions were produced in a laser ablation source (a), and after a preset storage time leaving them to cool radiatively (b), anions were photo-excited above the electron detachment threshold by a resonant two-photon excitation (c). Photo-excitation at 40 ms storage shows that the delayed electron detachment yields are inversely proportional to the time after excitation (power-law decay), reflecting the fact that the energy distribution is still broad, as also revealed in a previous study [1]. On the other hand, the decay profiles obtained by excitation at 190 ms can be fitted well with a single exponential function, indicating that the radiative cooling makes the energy distribution narrow enough to allow a description in terms of a single detachment rate constant. The time constant can be identified with the electron detachment rate constant in this process, because the competing radiative cooling is much slower.

By scanning the wavelength of the laser excitation at 190 ms storage, detachment rate constants were measured. A plot of the obtained rate constants is shown in Fig. 2, together with the theoretical values obtained based on the detailed balance theory assuming that all the molecular vibrations are harmonic. The vibrational cooling rates of the dominantly contributing mode are also depicted to demonstrate that they are negligible. The internal energy is the sum of the two-photon energy and the mean residual internal energy present in the

ion immediately before excitation, estimated to be 0.24 eV. As can be seen in the figure, the experimental values are about two orders of magnitude smaller than the harmonic oscillator theoretical values. Theoretical calculations including anharmonicity are ongoing and expected to explain the source of the disagreement.

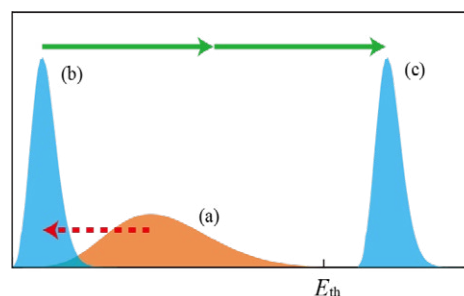


**Figure 1.** Schematic drawing of internal energy distributions, which are continuously pushed to the lower energy side by radiative cooling before photo-excitation.

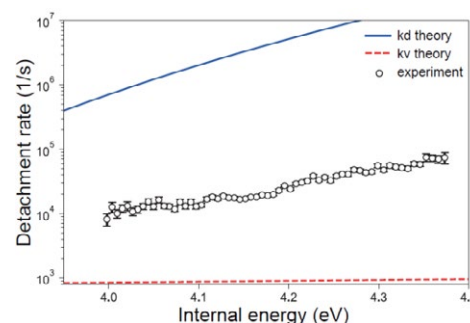


**Figure 2.** Experimental and theoretical electron detachment rates, and vibrational cooling rates of  $C_7^-$ .

### References

- [1] Najafian K et al. 2014 *J. Chem. Phys.* **140** 104311

\* E-mail: [s-iida@tmu.ac.jp](mailto:s-iida@tmu.ac.jp)



## Higher multipolar terms on core-level photoemission time delay of homonuclear diatomic molecules

Y Tamura<sup>1\*</sup>, K Yamazaki<sup>2</sup>, K Ueda<sup>3</sup>, K Hatada<sup>1†</sup>

<sup>1</sup>Department of Physics, University of Toyama, 3190 Gofuku, Toyama 930-8555, Japan

<sup>2</sup>RIKEN Center for Advanced Photonics, RIKEN, 2-1 Hirosawa, Wako, Saitama, 351-0198, Japan

<sup>3</sup>Graduate School of Science, Tohoku University, 6-3 Aramaki Aza-Aoba, Aoba-ku, Sendai 980-8578, Japan

**Synopsis** Zeptosecond time delay due to light propagation between equivalent absorbing atoms appears in the molecular frame core-level photoelectron angular distributions of homonuclear diatomic molecules. We show that the total time delay can be divided into (i) atomic time delay, delays due to (ii) scattering at each atomic site and (iii) propagation of photoelectrons among atoms, (iv) light propagation in the framework of multiple scattering theory accounting non-dipole terms. The effect (iv) is proportional to the time of light propagation between atoms and can be observed in experiments.

Recent developments in core-level photoemission measurement realise to study time delay in atto- and zepto-seconds. The core-level photoemission processes about homonuclear diatomic molecules reflect delocalization of gerade ( $g$ ) and ungerade ( $u$ )  $1s$  core molecular orbitals (MOs) in contrast to heteronuclear ones [1]. This delocalization results in a zeptosecond time delay [2].

In this study, we analytically investigated the delocalization effect on the time delay with higher multipolar terms. We first define the core-level photoemission time delay of a homonuclear diatomic molecule in Rydberg atomic units [1]:

$$t_{g/u}(\mathbf{k}, \hat{\boldsymbol{\epsilon}}, \boldsymbol{\kappa}) \equiv \frac{1}{2k} \frac{d}{dk} \arg \{ \langle \psi^-(\mathbf{k}) | e^{i\boldsymbol{\kappa} \cdot \mathbf{r}} \hat{\boldsymbol{\epsilon}} \cdot \mathbf{k} | \phi_{g/u} \rangle \}, \quad (1)$$

where  $|\phi_{g/u}\rangle$  is the initial state MO and  $|\psi^-(\mathbf{k})\rangle$  is the photoelectron continuum state with incoming boundary condition with momentum vector  $\mathbf{k}$  ( $k = |\mathbf{k}|$ ).  $\hat{\boldsymbol{\epsilon}}$  and  $\boldsymbol{\kappa}$  are the polarization and momentum vectors of the light, respectively. We then describe the delocalized  $|\phi_{g/u}\rangle$  as a linear combination of  $i$   $1s$  atomic orbitals  $\{|\phi_{1s}^i\rangle\}$  as  $|\phi_{g/u}\rangle = (|\phi_{1s}^1\rangle \pm |\phi_{1s}^2\rangle)/\sqrt{2}$ . We employ electric dipole approximation only for the transition matrix element in each atom [3] to include the phase difference of the photoelectrons by the light propagation between the atoms.

We found that the core-level photoemission time delay of a homonuclear diatomic molecule can be divided into four terms using Multiple

scattering theory with Muffin-tin approximation:

$$t_{g/u}(\mathbf{k}, \hat{\boldsymbol{\epsilon}}, \boldsymbol{\kappa}) = t_{\text{abs}}(k) + t_{g/u}^{\text{sc}}(\mathbf{k}, \hat{\boldsymbol{\epsilon}}, \boldsymbol{\kappa}) + t_{g/u}^{\text{path}}(\mathbf{k}, \hat{\boldsymbol{\epsilon}}, \boldsymbol{\kappa}) + t_{g/u}^{\text{nd}}(\mathbf{k}, \hat{\boldsymbol{\epsilon}}, \boldsymbol{\kappa}). \quad (2)$$

Here,  $t_{\text{abs}}$  refers to the time delay of the photoemission of the absorbing atom.  $t_{g/u}^{\text{path}}$  and  $t_{g/u}^{\text{sc}}$  originated from the propagation and scattering of the photoelectrons between atoms, respectively.  $t_{g/u}^{\text{nd}}$  comes from non-dipole terms representing the time delay due to the propagation of the light pulses. We derived it as,

$$t_{g/u}^{\text{nd}}(\mathbf{k}, \hat{\boldsymbol{\epsilon}}, \boldsymbol{\kappa}) = \frac{1}{2} \frac{R}{c} \hat{\boldsymbol{\kappa}} \cdot \hat{\mathbf{R}} \frac{I_2(\mathbf{k}, \hat{\boldsymbol{\epsilon}}) - I_1(\mathbf{k}, \hat{\boldsymbol{\epsilon}})}{2I_{g/u}(\mathbf{k}, \hat{\boldsymbol{\epsilon}}, \boldsymbol{\kappa})}, \quad (3)$$

where  $R/c$  is the travelling time of light with velocity  $c$  along the bond length  $R$ .  $I_{g/u}$  and  $I_i$  are the molecular frame photoelectron angular distributions emitted from the delocalized core MO  $|\phi_{g/u}\rangle$  and localized core  $|\phi_{1s}^i\rangle$ , respectively.

Actual experiments will measure the incoherent sum of  $t_g$  and  $t_u$ :  $t_{\text{sum}} \equiv (I_g t_g + I_u t_u)/(I_g + I_u)$ . Only  $t_{\text{sum}}^{\text{nd}}$  is a term depending on  $\boldsymbol{\kappa}$  after the incoherent sum as,

$$t_{\text{sum}}^{\text{nd}}(\mathbf{k}, \hat{\boldsymbol{\epsilon}}, \boldsymbol{\kappa}) = \frac{1}{2} \frac{R}{c} \hat{\boldsymbol{\kappa}} \cdot \hat{\mathbf{R}} \frac{I_2(\mathbf{k}, \hat{\boldsymbol{\epsilon}}) - I_1(\mathbf{k}, \hat{\boldsymbol{\epsilon}})}{I_2(\mathbf{k}, \hat{\boldsymbol{\epsilon}}) + I_1(\mathbf{k}, \hat{\boldsymbol{\epsilon}})}. \quad (4)$$

### References

- [1] Tamura Y *et al.* 2022 *J. Phys. B* **55** 10LT01.
- [2] Grundmann S *et al.* 2020 *Science* **370** 339.
- [3] Ivanov IA *et al.* 2021 *Sci. Rep.* **11** 21457.

\*E-mail: yoshiakitamura.susa@gmail.com

†E-mail: hatada@sci.u-toyama.ac.jp

## Dissociation of methanol molecules ionized by XFEL studied with molecular frame photoelectron diffraction

S Goto<sup>1</sup>, M Kanno<sup>2</sup>, H Xue<sup>2</sup>, N Kishimoto<sup>2</sup>, F Ota<sup>1</sup>,  
K Hatada<sup>1</sup> and K Ueda<sup>2</sup>

<sup>1</sup>Department of Physics, University of Toyama, Gofuku 3190, Toyama 930-8555, Japan

<sup>2</sup>Department of Chemistry, Tohoku University, 6-3 Aramaki Aza-Aoba, Aoba-ku, Sendai 980-8578, Japan

**Synopsis** During the dissociation of doubly charged methanol molecules created by the Auger decay after irradiation by an XFEL pulse, interesting ultrafast dynamics that involve motions of neutral hydrogen atoms occur. We theoretically show that polarization-averaged molecular frame photoelectron angular distributions (PA-MFPADs) can reveal the directions of the neutral hydrogen atoms around the photo-absorbing O atom as a result of the focusing effect of photoelectron diffraction in high energy regime ( $\gtrsim 100$  eV). H<sub>2</sub> ejection was observed as broken symmetry of a fringe structure due to the interference of photoelectron waves between C and O atoms.

Ultrafast hydrogen migration in a molecule is one of the most important processes in chemistry and biochemistry. Since scattering cross sections of hydrogen atoms are very small compared to the ones by other atoms, it is challenging to trace the dynamics by any scattering methods with a high temporal resolution in  $\sim 1$  fs. In our recent study [1], we revealed that polarization-averaged core-level photoelectron angular distributions in molecular frame (PA-MFPADs) can be used to probe the H migration in ethanol dications. In this work, we demonstrate that molecular hydrogen ejection in CH<sub>3</sub>OH<sup>2+</sup> can also be probed by time-resolved PA-MFPADs.

The dissociation trajectories of CH<sub>3</sub>OH<sup>2+</sup> were explored using Global Reaction Route Mapping and Molecular Dynamics (MD) simulations for triplet and singlet states. For MD simulations, the initial velocities of individual atoms were randomly sampled assuming that the excess vibrational energy of 5 eV was obtained by instantaneous electronic relaxation and the temporal evolution of the nuclear coordinates after the initial time  $t = 0$  was traced for each of 1000 trajectories for both singlet and triplet states.

The O 1s PA-MFPADs were calculated for each of the 200 trajectories for singlet states corresponding to the H<sub>2</sub> ejection and averaged over them. The results for photoelectron kinetic energies of 100 eV and 2500 eV at the delay of 2 fs are shown in Fig. 1, where the center of gravity of OH and C are set at the origin of the coordinate and on the z-axis towards a positive direction, respectively, and OH is in the z-x plane. The O-H bond is also broken in all the 200 trajectories.

The most prominent peaks are oriented in the direction of the C atom due to the focusing effect. The dominant cylindrical symmetry structure appears as a result of interference between photoelectron waves diffracted from C and O, analogous to the Young's double slit fringes [2]. This symmetric structure is broken due to the presence of H in the z-x plane ( $z < 0$ ) and H<sub>2</sub> around the forward scattering peak ( $z > 0$ ). The broken symmetry is more visible at 100 eV than at 2500 eV, since the H scattering cross section is significantly higher at 100 eV. These symmetry-broken structures disappear by elapsing the time since both H<sub>2</sub> and H go away. Thus, we conclude that we can probe the H<sub>2</sub> and H ejections by time-resolved PA-MFPADs.

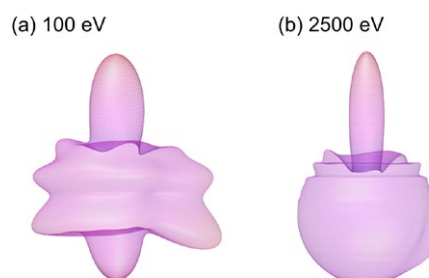


**Figure 1.** PA-MFPADs from O 1s averaged over 200 trajectories, at 2 fs after starting dissociation, with the kinetic energy of the photoelectron is (a) 100 eV and (b) 2500 eV.

### References

- [1] F Ota et al., 2021 *Phys. Chem. Chem. Phys.* **23** 20174
- [2] F Ota et al., 2021 *J. Phys. B: At. Mol. Opt. Phys.* **54** 244002

## A theoretical model of depolarized scattering in molecular clusters

C Rangan<sup>1\*</sup>, C DiLoreto<sup>1</sup> and M Moezzi<sup>1</sup>

<sup>1</sup>Department of Physics, University of Windsor, Windsor, ON N9B 3P4, Canada

**Synopsis** We present a theoretical model for a class of optical, depolarized scattering experiments in which short-duration, linearly-polarized electromagnetic pulses scatter off dielectric liquids.

We present a theoretical model for a class of optical scattering experiments in which short-duration, linearly-polarized electromagnetic pulses scatter off dielectric liquids. The pattern of scattering, particularly in the transverse direction, indicates that significant free currents are generated in the direction orthogonal to the polarization of the incident light. Modelling the target as a dense cluster of two-level systems, we show that transverse free currents are produced by short duration, electric-dipole interactions between proximate molecules, and result in scattering patterns similar to those observed in the experiments. Calculations provide a rationale for why these scattering patterns are not observed in the same molecules at lower densities or with lower field intensities. These features make this model a relevant alternative to proposed transverse optical magnetism theories. Extension of this model to control schemes such as EIT will be presented.

The target is modelled as a dense, spherical cluster of 4000 two-level atoms arranged in a cubic grid pattern. A short (50-200 fs) electromagnetic pulse is incident on the cluster, and scattered. Each atom is illuminated by a combination of the incident linearly-polarized electromagnetic field and the spontaneous emission from nearest-neighbor atoms.

To account for the change in the direction of polarization of the mean field over time, each two-level atom is modelled by 4 basis states --- one ground state, and three degenerate, directional excited states. The dynamics of each atom is modelled by the Liouville Master Equation with the Lindblad term, and is numerically solved by the Runge-Kutta method. Maxwell's equations with the free-current density from each atom acting as source terms are numerically solved by the Pseudospectral Time Domain (PSTD) method using the Yee Algorithm and

an absorbing boundary conditions at the grid boundary.

The emission ratio  $R$ , i.e., the ratio of the intensity of light polarized perpendicular to the incident polarization to the intensity of light polarized parallel to the incident polarization as measured in the transverse scattering direction is calculated. We find that the calculated emission ratio from this model is approximately 0.3, which agrees well with the experimentally measured values of 0.25 – 0.35 for different liquid targets. [1]

Figure 1 shows how the calculated emission ratio varies as a function of the number density of the cluster as well as the intensity of the incident field. [2] This pattern is well-modelled by an effective single particle model where the inter-particle interactions are modelled by decoherences. [1] Recent extensions of this model to other phenomena such as EIT in clusters will be presented.

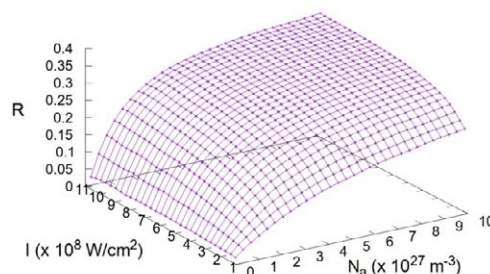


**Figure 1.** Density dependence of the Emission Ratio of an ensemble of molecules as a function of increasing number density in the ensemble. As the number density is increased, the probability of inter-molecular interactions increases, thus increasing the Emission Ratio.

### References

- [1] DiLoreto C and Rangan C 2018 *Phys. Rev. A* **97** 013812
- [2] DiLoreto C and Rangan C 2021 *Frontiers in Physics* **9** 700283

\* E-mail: [rangan@uwindsor.ca](mailto:rangan@uwindsor.ca)

## Selective enhancement of even order harmonics in a monolayer TMDC

V Korolev<sup>1</sup>\*, V Krishna<sup>1</sup>, A Croy<sup>1</sup>, S Gräfe<sup>1</sup>, G Soavi<sup>1</sup> and D Kartashov<sup>1</sup>

<sup>1</sup>Friedrich-Schiller University Jena, Max-Wien-Platz 1, 07743 Jena, Germany

**Synopsis** We report on the results of experimental investigation of high-order harmonic generation in single atomic layer WS<sub>2</sub> and MoS<sub>2</sub> as a function of crystal orientation, laser wavelength and intensity. We observe that even order harmonics show enhancement in a specific spectral window, that is material and orientation dependent, while odd-order harmonics show a standard plateau-cutoff behaviour. We suggest that this enhancement originates from the contribution of multiple band effects.

High-order harmonic generation (HHG) in monolayer TMDC has revealed new peculiar signatures in the resulting harmonic emission due to the distinctive electronic properties of the material [1]. It appears that most of the signatures can be seen on even order harmonics, that are intrinsically related to spatial crystal symmetries and time-reverse symmetry in the generation process.

Recently, enhancement of some even harmonics was observed when the pump laser polarisation is oriented along a zigzag direction of TMDC monolayers [2]. This enhancement was attributed to the band nesting, causing van Hove singularities in the joint density of states and specific for the band structure along zigzag direction. However, enhancement of particular even harmonics near the cut-off region of the spectrum was observed later also for the armchair orientation of the MoS<sub>2</sub> monolayer [3]. As there is no band nesting for the band structure along the armchair orientation, the enhancement was interpreted as a result of spectral interference within the optical cycle mediated by Berry connections.

In this contribution, we experimentally investigate even harmonic enhancement from WS<sub>2</sub> and MoS<sub>2</sub> monolayers, for both armchair and zigzag orientations, in dependence on the laser intensity and wavelength. The dependence of even harmonic intensities, normalized to the absolute maximum value, on the pumping wavelength is shown in Fig.1. This dependence was measured in WS<sub>2</sub> monolayer, oriented along the zigzag direction, at the laser intensity 1.7 TWcm<sup>-2</sup>. We observe that an even harmonic that falls within a spectral window 3.2-3.8 eV is substantially enhanced in comparison to all,

even and odd, harmonics with energies of quanta above the bandgap. For armchair orientation, the enhancement spectral window is shifted to 3.8-4.2 eV region. Similar results are observed in a MoS<sub>2</sub> monolayer. At the same time, odd harmonic intensities show no enhancement but rather standard plateau-cut-off like behavior. It is noteworthy that the enhancement is observed not at the spectral cutoff but rather at the border between two plateau regions, suggesting that the contribution of higher lying conduction band might be responsible for the effect. Finally, the enhancement becomes much more pronounced at longer driving wavelengths.

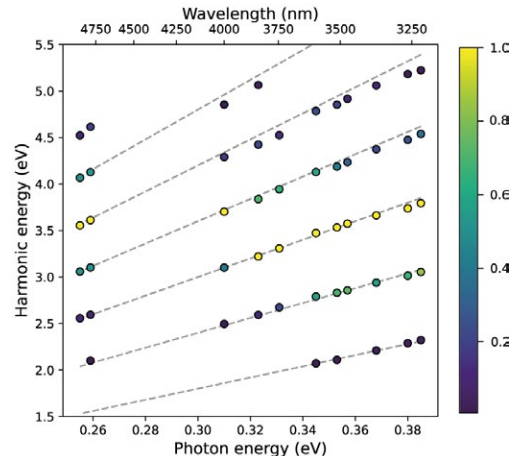


**Figure 1.** Even harmonic intensities as a function of the pump wavelength from a monolayer WS<sub>2</sub>.

### References

- [1] Liu H et al 2017 *Nature Phys.* **13** 262
- [2] Yoshikawa N et al 2019 *Nat Com.* **10** 3709
- [3] Cao J et al 2021 *Opt. Express* **29** 4830

\* E-mail: [viacheslav.korolev@uni-jena.de](mailto:viacheslav.korolev@uni-jena.de)

## Controlling the polarization and phase of high-order harmonics with a plasmonic metasurface

Sohail A. Jalil<sup>1\*</sup>, Kashif M. Awan<sup>2</sup>, Idriss A. Ali<sup>1</sup>, Sabaa Rashid<sup>3</sup>, Joshua Baxter<sup>3,4</sup>, Aleksey Korobenko<sup>1</sup>, Guilmot Ernotte<sup>1</sup>, Andrei Naumov<sup>1</sup>, David M. Villeneuve<sup>1</sup>, André Staudte<sup>1</sup>, Pierre Berini<sup>3,4</sup>, Lora Ramunno<sup>3,4</sup>, AND Giulio Vampa<sup>1†</sup>

<sup>1</sup>Joint Attosecond Science Laboratory, National Research Council of Canada and University of Ottawa, Ottawa, Ontario K1N 0R6, Canada

<sup>2</sup>Stewart Blusson Quantum Matter Institute, University of British Columbia, Vancouver, British Columbia V6T 1Z4, Canada

<sup>3</sup>Centre for Research in Photonics, University of Ottawa, 25 Templeton Street, Ottawa, Ontario K1N 6N5, Canada

<sup>4</sup>Department of Physics, University of Ottawa, 150 Louis Pasteur, Ottawa, Ontario K1N 6N5, Canada

**Synopsis** Recently, metasurfaces have broken new ground in high-field attosecond science. We demonstrate the ability to control recolliding electrons and holes using a plasmonic metasurface, which results in the emission of high harmonics with controlled polarization and phase. Our metasurface enhances circularly polarized harmonics by approximately 43 times compared to unpatterned surfaces.

Nanostructured surfaces, or metasurfaces, offer precise manipulation of optical processes through the modification of electric and magnetic fields near wavelength-scale heterogeneities. In recent years, metasurfaces have made significant strides in high-field attosecond science by amplifying the typically inefficient process of high-order harmonics from femtosecond infrared laser pulses [1-4]. However, control of polarization and phase of the generated harmonics remained elusive.

Here we demonstrate the ability to control the polarization and phase of high harmonics using a plasmonic metasurface [5]. By creating perpendicularly aligned rectangular gold antennas on a silicon crystal, we generate circularly polarized deep-ultraviolet high harmonics from a circularly polarized infrared driver, providing a straightforward means of achieving circular emission from patterned crystals. Typically, circularly polarized drivers do not emit harmonics because electrons and holes are accelerated on trajectories that do not recollide. Our metasurface enhances the circularly polarized harmonics by approximately 43 times compared to the unpatterned surface, where the harmonics are suppressed.

Going forward, circularly polarized high harmonics will prove useful in sensing chiral laser-matter interactions and magnetic materials. This work opens the door to polarization

control at even shorter, extreme ultraviolet wavelengths.

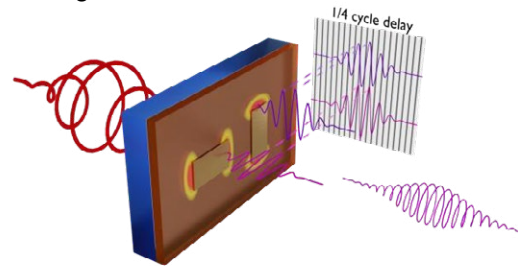


**Figure 1.** Each antenna resonates for the linear component of the incident circularly polarized driving field that aligns parallel to the antenna's major axis, thereby emitting linearly polarized odd-order high-harmonic radiation with half-cycle multiples of one quarter-cycle delay. Interference of pairs of antennas' emission results in circularly polarized high harmonics upon diffraction. The experiments are performed in reflection; however, transmission geometry is shown for clarity.

### References

- [1] Sivilis et al., (2017) *Science* **357** 303-306.
- [2] Vampa et al., (2017) *Nature Physics* **13** 659.
- [3] Zograf et al., (2022) *ACS Photonics* **9.2** 567-574.
- [4] Liu, Vampa et al., (2020) *Comm. Physics* **3.1** 1-6.
- [5] Jalil, Sohail A. et al., (2022) *Optica*, 9(9), 987-991.

\* E-mail: [sohailsulehria@gmail.com](mailto:sohailsulehria@gmail.com)

† E-mail: [gvampa@uottawa.ca](mailto:gvampa@uottawa.ca)



# Doping effects in high-harmonic generation from correlated systems

T Hansen<sup>1\*</sup> and L B Madsen<sup>1†</sup>

<sup>1</sup>Department of Physics and Astronomy, Aarhus University, 8000 Aarhus C, Denmark

**Synopsis** High harmonic generation from correlated systems is a highly non-linear and ultrafast process. Here we present a theoretical study of the effects of doping on the high harmonic generation process in strongly correlated systems. We present a qualitative picture for understanding the changes in the spectra and dynamics using the quasiparticle-based doublon-holon picture.

High harmonic generation (HHG) is an ultrafast ( $10^{-18} - 10^{15}$  s) and highly non-linear process, which is of high interest due to its potential as a spectrographic tool and as a method for producing ultrafast laser pulses. About five years ago Silva et. al. presented the first study of HHG from strongly correlated systems [1]. Since then multiple studies of HHG from such systems has resulted in a qualitative picture of the HHG process based on the doublon-holon picture [2, 3] and sources therein. Doublons and holons being doubly occupied and empty lattice sites, respectively. Such studies have typically been from half filled lattices. However, certain groups of highly interesting materials do not, necessarily, have half filling. One such group is the high- $T_c$  superconducting cuprates. Doping is especially important in strongly correlated materials as half-filling leads to Mott insulating behavior [1, 2].

Here we utilize the Fermi-Hubbard model to simulate such doped materials. We find that for relatively weak correlation, doping has little to no effect on the dynamics nor the HHG spectra. For large degrees of correlation, on the other hand, the dynamics and spectra were heavily dependent on the degree of doping. Those findings are explained through the doublon-holon picture. We use this picture to separate the dynamics into two categories: (i) doublon-holon movement and (ii) doublon-holon pair creation and annihilation. The correlation effects included in this work only directly affect the doublon-holon pair creation and annihilation, not the doublon-holon movement.

At half-filling strong correlation result in groundstates which contains neither doublons nor holons, whereas doped systems do contain either doublons or holons in the groundstate. As doublons and holons can move around the lattice at no correlation-induced energy cost doublon and holon movement is the dominant source of lower-order harmonics in highly correlated doped systems. We thus find that doping effects result in an increase in the harmonic spectrum for low harmonic orders but a decrease in the harmonic gain from higher harmonic orders, which are associated with doublon-holon annihilation, see fig. 1 [3].

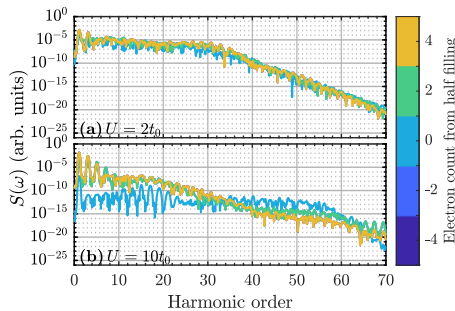


**Figure 1.** HHG spectra for relatively low correlation, (a), and high correlation (b), and various numbers of electrons in the lattice. At half filling, the lattice contains 12 electrons.

## References

- [1] Silva R E F, Blinov I V, Rubtsov A N, Smirnova O, and Ivanov M, 2018 *Nature Photonics* **12** 266
- [2] Murakami Y and Takayoshi S and Koga A and Werner P, 2021 *Phys. Rev. B* **103** 035110
- [3] Hansen T, and Madsen L B, 2022 *Phys. Rev. B* **106** 235142

\*E-mail: [thansen@phys.au.dk](mailto:thansen@phys.au.dk)

†E-mail: [bojer@phys.au.dk](mailto:bojer@phys.au.dk)



## Modelling high-harmonic generation in quantum dots using a tight-binding approach

M Thümmeler<sup>1\*</sup>, A Croy<sup>1</sup>, U Peschel<sup>2</sup> and S Gräfe<sup>1</sup>

<sup>1</sup>Institute of Physical Chemistry, Friedrich Schiller University Jena, Germany

<sup>2</sup>Institute of Condensed Matter Theory and Solid State Optics, Friedrich Schiller University Jena, Germany

**Synopsis** We present a tight-binding model to simulate the recently observed generation of high harmonics in quantum dots in strong laser fields. Our real-space tight-binding approach enables us to take the spatial extension of the quantum dots, as well as ionization effects, into account, while keeping the computational effort manageable.

Very recently, the properties of high-harmonic generation (HHG) in quantum dots (QDs) were experimentally studied by two independent groups in great detail [1, 2]. One of the main observed features is the sharp QD-size dependent drop in the yield of the high harmonics, which onsets for CdSe QD dots at around a diameter of 2 nm. To simulate the HHG, we use a tight binding approach with the following features: (1) We include two-particle effects. (2) We incorporate spatial effects, like finite dot-size and ionization events, which is infeasible in the framework of the usual semiconductor Bloch equations (SBEs)[3]. (3) The computational effort is - even for dot sizes larger than 3 nm - manageable, in stark contrast to real-time dependent density functional theory calculations.

Building on our recently proposed model [4], we have extended it towards three dimensions. Moreover, the model in [4] relied on empirical parameters and included only direct dipole transitions. We set up our model Hamiltonian including hopping on a spatial mesh, as it is depicted in figure 1. The Wannier functions of the bulk material and their overlaps are utilized to describe the QD using an electron-hole picture. The free-space Hamiltonian is obtained by a discretization of the time-independent Schrödinger equation (TISE). The hopping strength of the conduction-band electrons from the QD into free space is estimated by extending the Wannier functions into the free space using the TISE.

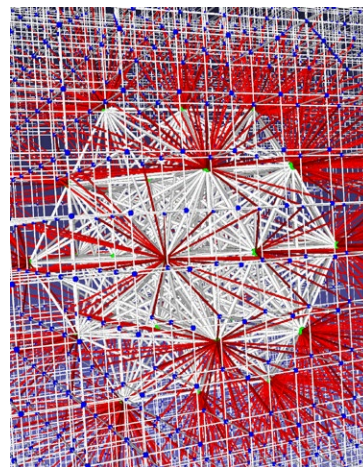


**Figure 1.** Example of a neighbouring graph of the tight binding sites (spheres) of a quantum dot with diameter 1 nm. The white cylinders indicate the hoppings inside the dot and in free space, whereas the red ones show the hoppings between those.

Similar to the derivation of the SBEs, we set up rate equations for the two-particle correlations in the Heisenberg picture, which are then integrated numerically. Inspired by the experimental observations, we present simulation results of HHG spectra in 3D CdSe quantum dots. Specifically, we show the size dependence of the HHG yield and discuss the effect of the polarization of the driving laser on the HHG.

### References

- [1] Gopalakrishna H N, Baruah R et. al. 2023 *Phys. Rev. Research* **5** 013128
- [2] Nakagawa K, Hirori H et. al. 2022 *Nat. Phys.* **18** 874-878
- [3] Golde D, Meier T, and Koch S W 2008 *Phys. Rev. B.* **77** 75330
- [4] Peschel U, Thümmeler M et. al. *Phys. Rev. B* **106** 245307

\*E-mail: [martin.thuemmler@uni-jena.de](mailto:martin.thuemmler@uni-jena.de)

## High-order wavemixing during high-harmonic generation in solids

D N Purschke<sup>1\*</sup>, Á Jiménez-Galán<sup>1,2</sup>, T. Brabec<sup>3</sup>, A Yu Naumov<sup>1</sup>, A Staudte<sup>1</sup>,  
D M Villeneuve<sup>1</sup>, G Vampa<sup>1</sup>

<sup>1</sup>Joint Attosecond Science Laboratory, Ottawa, K1A 0R6, Canada

<sup>2</sup>Max Born Institute, Berlin, D-12489, Germany

<sup>3</sup>University of Ottawa, Ottawa, K1N 6N5, Canada

**Synopsis** We study high-order wavemixing during high harmonic generation (HHG) emitted from a magnesium oxide crystal and a perturbing field at the second harmonic of the driver. We show that the wavemixing efficiencies are governed by the microscopic physics. We develop a microscopic analytic theory of two-color high-harmonic generation that captures the essential aspects of high-order wavemixing. Our theory highlights the photon-mixing aspect of two-color HHG, which we use to explain the striking asymmetry between sum- and difference-frequency pathways in our data.

Two-color fields are used extensively to measure and control attosecond dynamics [1]. Despite operating in a highly non-perturbative regime, the high-harmonic generation (HHG) from two-color fields can be indexed by the underlying wavemixing pathways similarly to perturbative nonlinear optics. These pathways can be isolated experimentally using a non-collinear excitation geometry [2].

Using a strong fundamental field and its weak second harmonic, we apply the non-collinear two-color technique to isolate the high-order wavemixing pathways in magnesium oxide [3]. As in gases, we observe a rich two-dimensional spectrum of the wavemixing pathways that scale perturbatively in the weak field. However, unlike gases, we find that the wavemixing intensities are governed by the microscopic physics, which makes the solid state an interesting platform to study the recollision physics in two-color fields.

We observe a striking asymmetry in the number and amplitude of sum-/difference-frequency peaks (see Figure 1), which is well reproduced by calculations with the semiconductor Bloch equations. To understand the origin of this asymmetry, we develop a microscopic theory of high-order wavemixing within the strong-field approximation that is valid for both solids and gases. Our theory outlines the correct selection rules and perturbative scaling governing the wavemixing pattern and demonstrates how each pathway will diffract to the far field in the non-collinear geometry. It also highlights the photon-mixing aspect of two-color

HHG and shows how the second-harmonic field pushes the spectrum upwards (downwards) in energy for sum (difference)-frequency pathways. The observed asymmetry is thus linked to the inhomogeneous single-color HHG spectrum.

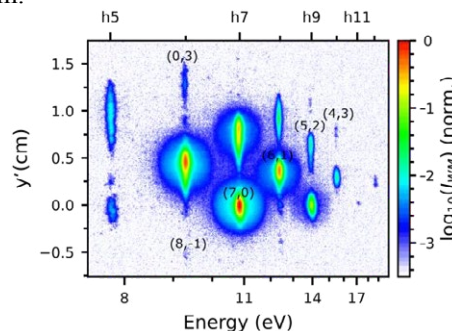


**Figure 1.** Log-scale intensity of the wavemixing pattern from the non-collinear two-color HHG experiment in magnesium oxide. The wavemixing order of several pathways is indicated.

Our work reveals fundamentally new insights into the ubiquitous technique of two-color HHG and shows how it will be a useful new spectroscopy for attosecond dynamics in solids. Furthermore, the bright wavemixing pathways we observe suggests that the sophisticated techniques developed to control gas-phase HHG should be highly effective in solids [4,5].

### References

- [1] Vampa V *et al.* 2015 *Nature* **522**
- [2] Bertrand J *et al.* 2011 *Phys. Rev. Lett.* **106**
- [3] Purschke D N *et al.* 2023 (*in review*)
- [4] Hickstein D D *et al.* 2015 *Nat. Phot.* **8263**
- [5] Kong F *et al.* 2017 *Nat. Commun.* **7180**

\* E-mail: [dpurschk@uottawa.ca](mailto:dpurschk@uottawa.ca)

## Momentum-resolved dynamics of femtosecond laser ablation with a pump-probe technique

A Korobenko<sup>1</sup>\*, A T K Godfrey<sup>1</sup>, A Staudte<sup>1</sup>, A Carew<sup>2</sup>, A V Loboda<sup>2</sup>, and P B Corkum<sup>1</sup>

<sup>1</sup>Joint Attosecond Science Laboratory, National Research Council of Canada and University of Ottawa, Ottawa K1N 7N9, Canada

<sup>2</sup>Standard BioTools Canada Inc., Markham, ON L3R 4G5, Canada

**Synopsis** We propose a pump-probe approach to study femtosecond ablation of solid matter. Spatio-temporal separation of pump and probe beams allows for a full momentum characterization of the ejected fragments.

Femtosecond lasers have been used extensively for micromachining and laser ablation. The focused laser transfers energy into electronic motion inside the focal volume via a single- or multiphoton process. This energy is then exchanged with the lattice, leading to the quick expansion and ejection of the material into the empty space. High density of the expanding matter originating from a condensed state leads to convoluted dynamics, involving recombination of the initially-created plasma. This calls for new tools that would allow better understanding of the ablation process.

Here we report on a pump-probe measurements using two collinear beams. The first one, tightly focused on the sample, leads to its ablation. The ablated matter expands in a free space, and is then reionized with a second beam 25 micrometers away, where its density is substantially decreased, and plasma recombination is suppressed, making it suitable for time-of-flight measurements of ions. Varying the time delay between the two pulses, as well as the relative position of their focal spots, we are able to measure the vectorial momenta of the produced fragments.

We apply our technique to a multilayered sample, consisting of a 100 nm PMMA film on top of a 100 nm indium-tin oxide film on a glass substrate. We demonstrate more than a 500-fold

increase in the ion yield in the presence of the reionizing pulse.

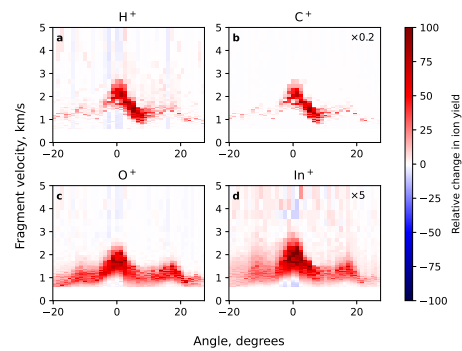


**Figure 1.** Relative change in the ion yield as a function of the ejection angle and velocity for several fragments.

All ablated fragments leave the sample with similar velocities, consistent with their intense interaction during the expansion, quickly decreasing in quantity away from the normal to the surface. Some qualitative difference between the fragments originated from ITO ( $O^+$ ,  $In^+$ ) and PMMA ( $H^+$ ,  $C^+$ ) can be observed, with the latter demonstrating narrower angular distributions.

Our findings will shed light onto the dynamics of femtosecond ablation.

\*E-mail: [akoroben@uottawa.ca](mailto:akoroben@uottawa.ca)

## Theory for ionization rate of dielectrics in two-color strong laser fields

Mizuki Tani<sup>1\*</sup> and Kenichi L Ishikawa<sup>1,2†</sup>

<sup>1</sup>Department of Nuclear Engineering and Management, The University of Tokyo, Tokyo, 113-8656, Japan

<sup>2</sup>Research Institute for Photon Science and Laser Technology, The University of Tokyo, Tokyo 113-0033, Japan

**Synopsis** Expressions are obtained for the ionization probability of dielectrics in two-color strong laser fields whose photon energies are smaller than the bandgap. This enables to calculate ionization rate without solving time-dependent equations. The formula is applied to  $\alpha$ -SiO<sub>2</sub> under  $\omega$ - $2\omega$  strong laser fields, predicts enhancement in ionization rate compared to the single-color case. The results are qualitatively in good agreement with *ab initio* simulation based on the time-dependent density functional theory.

Laser technology has made prodigious progress in decades. Keldysh's pioneering work [1], which is the foundation for the modern theory of tunneling and multiphoton ionization of atoms and ions in low-frequency intense laser fields, has been employed to understand what occurs under state-of-the-art laser lights. Recently, Otobe *et al.* has modified the Keldysh theory to predict ionization rate of solid state dielectrics under single-color strong laser fields [2]. Since two-color pump pulse is widely used for electron excitation in dielectrics [3], here we extend Ref. [2] to derive expressions for the ionization probability of dielectrics in two-color intense laser fields. The derived formula is applied to  $\alpha$ -SiO<sub>2</sub> under  $\omega$ - $2\omega$  bright electromagnetic wave that are oscillating in phase. Our calculation indicates that the ionization rate of  $\alpha$ -SiO<sub>2</sub> is dramatically enhanced in two-color case compared to the single-color case. This analytically supports our recent paper [4], shows good qualitative agreement with those by first principles time-dependent density functional theory (TDDFT) simulation.

We consider an electron system in one-body potential  $V(\mathbf{r})$  and vector potential  $\mathbf{A}(t)$ . The Hamiltonian is given by  $\mathcal{H} = ((\nabla/i + \mathbf{A}(t))^2/2 + V(\mathbf{r}))$ . Suppose the energy gap between conduction and valence bands is given by  $\Delta\varepsilon(\mathbf{k}) = \mathbf{k}^2/2\mu + B_g$ , where  $\mathbf{k}$ ,  $\mu$ , and  $B_g$  denote wave vector, reduced effective mass, and bandgap, respectively. We define the ionization rate  $W$  as transition probability between valence and conduction bands per unit time and space. The expression for linearly polarized  $\omega$ - $2\omega$  laser field  $\mathbf{A}(t) = (0, 0, A_1 \cos \omega t + A_2 \cos 2\omega t)$  is,

$$W \sim \sum_{l=l_0}^{\infty} \sqrt{\kappa_l} \int_{-\infty}^{\infty} d\theta \sin \theta \times [A_1 \{J_{l-1}(\boldsymbol{\eta}) + J_{l+1}(\boldsymbol{\eta})\} + A_2 \{J_{l-2}(\boldsymbol{\eta}) + J_{l+2}(\boldsymbol{\eta})\}], \quad (1)$$

where  $\kappa_l = l\omega - B_g - (A_1^2 + A_2^2)/4\mu$ ,  $\boldsymbol{\eta} = (\eta_1, \eta_2, \eta_3, \eta_4)$ , and  $\eta_1 = A_1 \sqrt{2\kappa_l} \cos \theta / \sqrt{\mu}\omega + A_1 A_2 / 2\mu\omega$ ,  $\eta_2 = A_1^2 / 8\mu\omega + A_2 \sqrt{2\kappa_l} \cos \theta / 2\sqrt{\mu}\omega$ ,  $\eta_3 = A_1 A_2 / 6\mu\omega$ , and  $\eta_4 = A_2^2 / 16\mu\omega$ .  $J_l$  stands for the multivariable Bessel function.

For demonstration in  $\alpha$ -SiO<sub>2</sub> with  $\hbar\omega = 1.55$  eV (corresponding to 800 nm wavelength), bandgap and effective mass are assumed as  $B_g = 9$  eV,  $\mu = 0.3m_0$  where  $m_0$  denotes static mass. Figure 1 shows total intensity dependence of ionization rate calculated by Eq. (1) and TDDFT for single-color cases and half-half two-color case. Both results show similar trend, with ionization rate significantly enhanced by two-color mixing above  $10^{13}$  W/cm<sup>2</sup>.

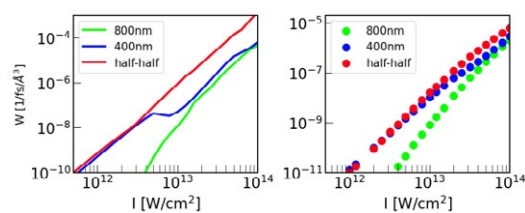


**Figure 1.** Ionization rate calculated by TDDFT (right panel) and Eq. (1) (left panel). Green, blue, and red dots (lines) indicate  $A_2 = 0$ ,  $A_1 = 0$ , and  $A_1 = A_2$  case.

### References

- [1] Keldysh L V 1965 *Sov. Phys. JETP* **20** 1307
- [2] Otobe T, *et al.* 2019 *JPSJ* **88** 0224706
- [3] Yu X, *et al.* 2014 *Opt. Lett.* **39** 5638
- [4] Tani M, *et al.* 2022 *Phys. Rev. B* **106** 195141

\* E-mail: [mzktani@atto.t.u-tokyo.ac.jp](mailto:mzktani@atto.t.u-tokyo.ac.jp)

† E-mail: [ishiken@n.t.u-tokyo.ac.jp](mailto:ishiken@n.t.u-tokyo.ac.jp)

## XUV absorption spectroscopy of Ti-doped iron oxide

M O Segovia-Guzman<sup>1\*</sup>, M Lazemi<sup>2</sup>, F de Groot<sup>2</sup>, M J J Vrakking<sup>1</sup>, and A Rouzée<sup>1</sup>

<sup>1</sup>Max Born Institute, Berlin, 12489, Germany

<sup>2</sup>Utrecht University, Utrecht, 3584, Netherlands

**Synopsis** XUV radiation produced by High Harmonic Generation was used to study XUV absorption spectroscopy at the Fe and Ti M-edges of titanium doped iron oxide. This experimental technique is proposed to study charge carrier dynamics in doped metal oxides.

Hydrogen production through solar water splitting reaction is a clean solution to the actual energy demand. It can be carried out in a photoelectrochemical cell where a photoelectrode absorbs sunlight producing electron-hole pairs, then the charge carriers are collected separately to oxidize oxygen and reduce hydrogen from water. However, the development of this process is still a challenge due to its low efficiency. With its high stability, abundance and strong absorption cross-section in the visible spectral range, hematite ( $\alpha$ -Fe<sub>2</sub>O<sub>3</sub>) is considered a very promising material to serve as photoelectrode in photoelectrochemical cells [1]. However, the overall efficiency for the water splitting reaction based on hematite photoelectrode has been limited. Recent studies have shown that the efficiency can increase substantially when hematite is doped with titanium but the mechanism responsible for the improved efficiency remains to be understood [2, 3].

Here, XUV absorption spectroscopy at the Fe and Ti M-edges is proposed to study the charge carrier dynamics of Ti-doped iron oxide. XUV absorption spectroscopy near the M-edge is particularly well-suited to the investigation of metal oxide materials since XUV radiation covers multiple absorption edges of metals, allowing to study core-to-conduction-band transitions

[4]. The dynamics resulting from the photoexcitation of Ti-doped iron oxide by a 400 nm pump laser pulse can be probed by XUV absorption spectroscopy using a time-delayed XUV pulse obtained by two-color (800 nm + 1300 nm) high harmonic generation that allows to generate a continuous XUV spectrum from 20 eV to up to 200 eV [5]. In this contribution, we will present first the static XUV absorption spectrum of Ti-doped iron oxide obtained using such source showing that the Fe and Ti M-edges can be associated with the conduction band of the material. In addition, using time-resolved XUV absorption spectroscopy we expect to recover the ultrafast charge carrier dynamics of the Ti-doped iron oxide. This results can potentially increase the understanding of photoexcitation dynamics of doped solar materials.

### References

- [1] Lin Y, Yuan G, Sheehan S, Zhou S and Wang D 2011 *Energy Environ. Sci.* **4** 4862
- [2] Kronawitter C X et al. 2014 *Energy Environ. Sci.* **7** 3100
- [3] Deng J et al. 2012 *J. Appl. Phys.* **112** 084312
- [4] Geneaux R, Marroux H J B, Guggenmos A, Neumark D M and Leone S R 2019 *Philos. Trans. R. Soc. A Math. Phys. Eng. Sci.* **377** 2145
- [5] Schütte B et al. 2015 *Opt. Express* **23** 33947

---

\*E-mail: [guzman@mbi-berlin.de](mailto:guzman@mbi-berlin.de)



## Laser-based processing of dielectric chips for the generation of nano focused XUV radiation

Parnia Bastani<sup>\*</sup>, Aleksey Korobenko<sup>1</sup>, Giulio Vampa<sup>1</sup>

<sup>1</sup>Joint Attosecond Science Laboratory, National Research Council of Canada and University of Ottawa, Ottawa, Ontario K1N 0R6, Canada

**Synopsis** Recently, we demonstrated nanofocusing of XUV high harmonics with a nanostructured dielectric target, providing unique opportunities for direct nanoscale laser writing of materials with tailored spectral and temporal characteristics of XUV beam and structured beams. However, contamination of the XUV focus with the strong infrared driver risks to ablate the material to be processed at micron scales. Here we demonstrate a technique that allows to position the Fresnel zone plates, our nanofocusing elements, at the edge of the chip. Irradiating the zone plates with the infrared beam at the Brewster angle allows to position a sample in the XUV nanofocus, free of infrared contamination.

Generating and controlling extreme-ultraviolet (XUV) light with the wavelength shorter than 100nm is crucial in applications in attosecond science and lensless imaging. Although there has been considerable progress in average power, lack of appropriate optical elements is still a main challenge for spatially controlling XUV beams [1,2]. Solids provide a unique opportunity to emit XUV radiation in the form of high harmonics with spatial control by structuring the solid surface. MgO is well known to emit XUV high harmonics. We previously showed a robust and precise method to focus XUV high harmonics at the nanoscale by nanofabricating Fresnel zone-plate patterns on MgO [3].

The contamination of the XUV beam with IR radiation is a major problem in spectroscopy, microscopy, and imaging because it can cause considerable background noise and reduce the spatial resolution in imaging and laser processing with the XUV nanofocus. Besides, the IR radiation can cause unwanted affects to the sample of interest. We propose to illuminate the zone plates at the Brewster angle of the infrared driver, thus removing infrared contamination in the XUV nanofocus.

To be able to position a sample or measure the XUV nanofocus in this reflection geometry, however, the zone plates must be positioned near the edge of the MgO crystal. Direct fabrication on

the edge of chips is not possible, or difficult to achieve, due to some limitation in the fabrication technique such as lack of uniform resist near the edges. Instead, we use a femtosecond laser (1030nm, 100KHz, 20W, 40fs) to cut the MgO crystal at specific distance from the zone-plates.

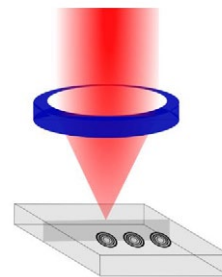


**Figure 1.** The beam of 1030-nm laser is focused with an aspheric lens, 5 $\mu$ m away from 30  $\times$  30  $\mu$ m<sup>2</sup> zone-plates onto a MgO (500 $\mu$ m thickness) crystal. The sheet is drawn with gradient power (600mW-5mW) from back surface to the front surface without damaging the front surface.

### References

- [1] Roscam Abbing et al., *Phys. Rev. Lett* **128** 223902-1 223902-7.
- [2] Korobenko et al., (2021) *Optica* **29** 24161-24168.
- [3] Korobenko et al., (2022) *Phys. Rev. X* **12** 041036-1 041036-7.

\*E-mail: [pabastani100@gmail.com](mailto:pabastani100@gmail.com)



## XPS Study in situ of the Diluted Perovskite Nanocrystals Surface's Stability Stoichiometry

<sup>1\*</sup>J A F Pinheiro, <sup>1†</sup>A N Brito, <sup>1</sup>L G Bonato, <sup>1</sup>L Cornetta,  
<sup>2</sup>O Björnehölm, <sup>3</sup>G Öhrwall, <sup>3</sup>T Gallo, <sup>1</sup>A F Nogueira.

<sup>1</sup>Universidade Estadual de Campinas (UNICAMP) 13083-859 Campinas, SP, Brazil

<sup>2</sup>Ångströmlaboratoriet, Uppsala Universitet, 752 36, Uppsala, Sweden

<sup>3</sup>MAX IV Laboratory and Lund University, 221 00, Lund, Sweden.

**Synopsis** Study Nano Perovskite in a liquid environment had been a challenge, however, this study it is shown the first outcomes from their surface in situ. Along with TEM measurements and DFT calculation, we report Stoichiometric results.

Here we present an investigation of these Lead-Halide Perovskites Nanocrystals (NCs) from two different synthetic methods. The first method to be developed was successful in producing very narrow emission linewidth Protasescu et al. [1], however, the NCs showed slow colloidal and phase stability. The labile bond nature of the OLA<sup>+</sup>, as well as a non-bind nature of the OA/oleate species, are pointed out as responsible for the low colloidal and phase stability of perovskite NCs. Thus to solve these problems, Yassitepe et al. [2] developed a strategy called Amine-free synthesis where only oleic acid was used as a surface ligand. Although the improvement in the colloidal stability of Amine-free CsPbX<sub>3</sub> NCs seems to be related to the absence of OLA<sup>+</sup> species on the NCs surface, there is still a lack of surface chemistry for the material obtained under this condition. The utilization of

X-ray electron spectroscopy (XPS) can help to elucidate the surface structure of the amine-free CsPbX<sub>3</sub> NCs. So far only the OLA<sup>+</sup> method has been studied by XPS together with DFT calculations [3] which were employed solid samples presenting prone to contamination and radiation damage. Recently the liquid microjet starts to change the scenario and studies involving nano-particle interface diluted in aqueous solutions [4], [5]. Moreover, the Perovskite can only be diluted in nonpolar solvents, to the best of our knowledge, all micro-jet XPS studies on NPs or NCs are performed using a polar solvent such as water. In this work, we show the first microjet study of perovskite NCs diluted in a mixture of toluene and hexane. In addition, we introduce experimental evidence supporting that not only Cs are substituted but also Br atoms are substituted in either of the two syntheses.

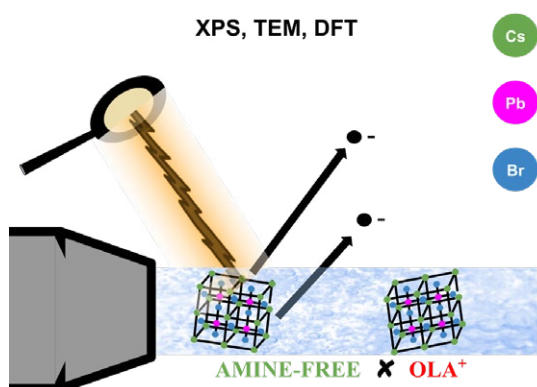


**Figure:** XPS applied on Perovskite NCs in a liquid environment. Combined with TEM and DFT, we obtained information from chemical dynamics, Stechiometry and the below layer apart from the surface.

### References

1. Nano Lett. 2015. <https://doi.org/10.1021/nl5048779>.
2. Adv. Funct. Mater., 2016. <https://doi.org/10.1002/adfm.201604580>
3. J. Phys. Chem. Lett. 2017 <https://doi.org/10.1021/acs.jpcclett.7b02192>
4. Surface Science, ELSEVIER. 2013. <https://doi.org/10.1016/j.susc.2013.01.012>.
5. Chem Sci. 2018. doi: 10.1039/c7sc05156e.

\* E-mail: [j262756@dac.unicamp.br](mailto:j262756@dac.unicamp.br)

† E-mail: [arnaldo@ifi.unicamp.br](mailto:arnaldo@ifi.unicamp.br)

## Effect of transient spatial localization on electron impact excitation and ionization processes in dense plasmas

Jiaolong Zeng<sup>1\*</sup> and Jianmin Yuan<sup>2†</sup>

<sup>1</sup>College of Science, Zhejiang University of Technology, Hangzhou Zhejiang 310023, P. R. China

<sup>2</sup>Graduate school of China Academy of engineering Physics, Beijing 100193, P. R. China

**Synopsis** In dense plasmas, the electron impact excitation and ionization cross sections are in general decreased due to plasma screening compared with those of the isolated ion, although the ionization potential depression results in an increase of ionization cross section near the threshold. Here a mechanism of transient spatial localization is proposed, which enhances the cross sections in dense plasmas. We suggest that this mechanism should be the physical origin of the increased electron-ion collisional ionization cross section observed in the experiment.

In dense plasmas, the electron impact excitation and ionization processes of atoms and ions are of interest both for fundamental science and for practical applications in the interiors of stars, white dwarf and neutron stars [1], as well as for black holes, inertial confinement fusion [2], and high-energy-density plasmas [3]. They determine the charge-state distribution and power balance and can also be used to infer the electron temperature and electron density of plasma.

For rarefied plasmas where the coupling with the plasma environment is trivial, the excitation and ionization probabilities of isolated atoms or ions can be used for practical applications. However, if the plasma density is sufficiently high and the coupling cannot be neglected, plasma screening plays a non-negligible role. The effects of plasma screening on electron-impact processes were investigated using various models. Practical calculations showed that the electron impact excitation cross sections are in general decreased by plasma screening.

Here we propose a concept of transient spatial localization of continuum electrons in dense plasmas [4], which enhance the electron-impact excitation and ionization. Random collisions with free electrons and ions in plasma cause electron matter waves to lose their phase, which results in the partial decoherence of incident and scattered electrons. Such a plasma-induced transient spatial localization of the continuum electron states significantly modifies

the wave functions of continuum electrons, resulting in an enhancement of the electron-ion collisional processes in plasma compared to the isolated ions. A theoretical formulation was developed to calculate the differential and integral cross sections by incorporating the effects of transient spatial localization. The approach is used to investigate the electron-impact ionization of ions in solid-density magnesium plasma, yielding results that are consistent with experiments [5].

Recent experiments have observed much higher electron-ion collisional ionization cross sections and rates in dense plasmas than predicted by the current standard atomic collision theory, including the plasma screening effect. Such an enhancement should originate from the spatial localization of incident and scattered electrons. Our findings provide new insight into collisional excitation and ionization and three-body recombination and may aid investigations of the transport properties and nonequilibrium evolution of dense plasma.

### References

- [1] Booth N, Robinson APL, Hakel P, Clarke RJ Dance RJ et al. 2015 *Nat. Commun.* 6 8742
- [2] Hu SX, Militzer B, Goncharov VN, Skupsky S 2010 *Phys. Rev. Lett.* 104 235003
- [3] Glenzer SH and Redmer R 2009 *Rev. Mod. Phys.* 81 1625
- [4] Liu PF, Gao C, Hou Y, Zeng JL, and Yuan JM 2018 *Commun. Phys.* 1 95
- [5] Zeng JL, Ye C, Liu PF, Gao C, Li YJ, and Yuan JM 2022 *Int. J. Mol. Sci.* 23 6033

\* E-mail: [jlzeng@zjut.edu.cn](mailto:jlzeng@zjut.edu.cn)

† E-mail: [jmyuan@gscaep.ac.cn](mailto:jmyuan@gscaep.ac.cn)

## X-ray studies of atomic processes in the EBIT plasma

D Sobota, Ł Jabłoński, D Banaś, P Jagodziński, A Kubala-Kukuś,  
I Stabrawa, K Szary and M Pajek\*

Institute of Physics, Jan Kochanowski University, 25-406 Kielce, Poland

**Synopsis** X-rays emitted from Xe plasma in the electron beam ion trap (EBIT) were measured in order to investigate the atomic processes determining charge state distribution of trapped ions. The measured x-ray spectra for electron impact energies 3 – 9 keV demonstrates a presence of Xe ( $n\ell \rightarrow n'\ell'$ ) x-ray transitions and the radiative recombination lines for  $n \geq 3$  states for various  $\text{Xe}^{q+}$  ions ( $q \leq 38$ ). In particular, the charge state distribution of highly charged  $\text{Xe}^{q+}$  ions was extracted from the measured radiative recombination x-rays.

The successive electron impact ionization of ions in the EBIT trap [ ] leads to production of highly charged ( $q \gg 1$ ) ions (HCI) having rather wide charge state distribution and various electronic configurations. The atomic processes involved in formation of EBIT plasma include the electron impact ionization/excitation, radiative (RR) and dielectronic recombination (DR), charge exchange (CX) and radiative and Auger deexcitation.

The x-rays emitted from Xe plasma trapped in the EBIT, which was generated by electron beam of energy 3-9 keV, were measured by a silicon drift detector (SDD) separated from the EBIT plasma by 50  $\mu\text{m}$  Be window. The electron beam current was in the range 30-70 mA and pressure was about  $10^{-9}$  mbar. The EBIT trap was operated in the “leaky” mode allowing extraction of  $\text{Xe}^{q+}$  from the trap to be further charge state analyzed in the dipole magnet of the EBIS facility [2]. In this way the charge state distribution of ions extracted from the observed x-rays was confronted with the charge states measured directly by analysis in magnet.

In the measured spectra of x-rays emitted from EBIT the fluorescence x-ray transitions Xe ( $n\ell \rightarrow n'\ell'$ ) and RR lines for  $n \geq 3$  states for various highly charged  $\text{Xe}^{q+}$  ions ( $q \leq 40$ ) are identified as well as the electron bremsstrahlung edges and K-x-ray fluorescence lines of Cr and Fe excited by electrons scattered on the trap walls. Generally, the intensities of various Xe x-rays depend on population of  $n\ell$ -states in the plasma which can be described by radiative-collisional (CR) models [3]

\* E-mail: [pajek@ujk.edu.pl](mailto:pajek@ujk.edu.pl)

solving the system rate equations involving all atomic processes discussed above.

In the present work the charge state distribution of  $\text{Xe}^{q+}$  ions in the EBIT plasma was studied to interpret the observed RR lines, mainly for photorecombination into  $n=3$  states of Xe. The results are discussed in terms of the CR models developed for a low density and temperature non-Maxwellian plasma.

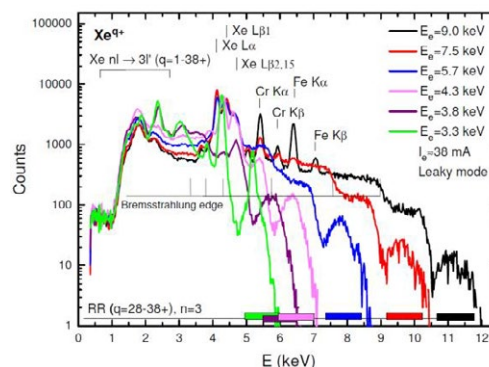


**Figure 1.** The spectra of x-rays emitted from Xe plasma trapped in the EBIT measured for electron impact energies 3.3- 9.0 keV. The energies of x-ray lines for RR into  $n=3$  for different charge states  $q=28-38+$  are indicated by horizontal bars.

### References

- [1] Zschornack G and Kreller M 2008 *Rev. Sci. Instrum.* **79** 02A703
- [2] Banas D et al. 2010 *J. Instrum.* **5** C09005
- [3] Ralchenko Y 2013 *Plasma and Fusion Res.* **8** 2503024

## Observation of THz-wave-assisted electron scattering by Ar atoms

M Kitanaka<sup>1</sup>, M Ishikawa<sup>1</sup>, R Kanya<sup>2,3\*</sup> and K Yamanouchi<sup>1†</sup>

<sup>1</sup>Department of Chemistry, School of Science, the University of Tokyo, Bunkyo-ku, Tokyo 113-0033, Japan

<sup>2</sup>Department of Chemistry, Faculty of Science, Tokyo Metropolitan University, Hachioji-shi, Tokyo 192-0397, Japan

<sup>3</sup>JST PRESTO, Hachioji-shi, Tokyo 192-0397, Japan

**Synopsis** The signals of THz-wave assisted electron scattering (TAES) by Ar are recorded as a first step for ultrafast electron diffraction by the THz-wave streaking. The analysis of the TAES signals obtained using a single-cycle THz-wave field reveals that the scattered electrons gain and lose their energy corresponding to as many as 800 photons of the THz wave. The observed characteristic asymmetries in the azimuth-angle dependence of the energy spectra of the TAES signals show that continuous probing of the structural change of molecules can be achieved by the THz-wave assisted electron diffraction.

Observation of laser-assisted electron scattering (LAES) processes induced by an intense ultrashort laser pulse [1] revealed a unique opportunity of probing ultrafast phenomena in real time by electron scattering. Our recent theoretical study showed that the THz-wave assisted electron diffraction (TAED) using a single-cycle THz wave as a streaking field would give us a unique opportunity to record temporal evolution of geometrical structure of molecules without scanning the pump-probe time delay [2]. In this presentation, we report our measurements of THz-wave assisted electron scattering (TAES) processes [3] and confirm the following theoretically predicted unique features of TAES; (i) a continuous energy spectrum, (ii) extremely high-order energy transfer corresponding to more than  $10^2$ - $10^3$  photons, (iii) an asymmetric scattering-angle distribution, and (iv) asymmetry in the energy gain and the energy loss.

The TAED setup is composed of a home-built single-cycle THz-wave source, generating a THz wave by the tilted-pulse-front technique, and a home-built LAES apparatus with high electron detection sensitivity [4], equipped with an angle-resolved time-of-flight (ARToF) electron analyzer. A 1 keV electron beam pulse is scattered by an Ar gas at the scattering point in the presence of the single-cycle THz wave pulse. The energy distribution and the two-dimensional scattering-angle distribution of the scattered electrons are recorded by the ARToF electron analyzer.

As shown in Fig. 1, the energy shift ( $\Delta E$ ) of the scattered electrons exhibits a continuous spectrum in the whole range of the azimuth an-

gle ( $\phi$ ) and the maximum energy shift is 2 eV, corresponding to the energy of about 800 photons of the THz wave whose central frequency is 0.6 THz. A significant asymmetry of the signal distribution can be seen between the positive and negative ranges of  $\phi$ . The recorded two-dimensional signal distribution is well reproduced by numerical simulations, showing that the ultrafast structural change of molecules can be probed by the TAED measurement.

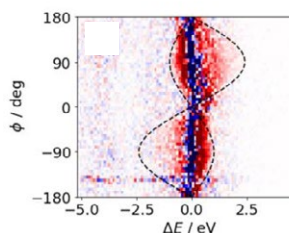


**Figure 1.** An energy and azimuth angle distribution of electrons scattered by Ar obtained by the TAES measurement. The red and blue color represent the signal increase and decrease, respectively, induced by the irradiation of the single-cycle THz wave. The dotted curves represent the theoretically calculated maximum and minimum  $\Delta E$ .

### References

- [1] Kanya R, Morimoto Y, and Yamanouchi K 2010 *Phys. Rev. Lett.* **105**, 123202
- [2] Kanya R and Yamanouchi K 2017 *Phys. Rev. A* **95**, 033416
- [3] Kitanaka M, Ishikawa M, Kanya R, and Yamanouchi R 2022 *Chem. Phys. Lett.* **795**, 139512
- [4] Ishikawa M, Ishida K, Kanya R, and Yamanouchi K 2023 *Instruments* **7**, 4

\* E-mail: [kanya@tmu.ac.jp](mailto:kanya@tmu.ac.jp)

† E-mail: [kaoru@chem.s.u-tokyo.ac.jp](mailto:kaoru@chem.s.u-tokyo.ac.jp)

# Theoretical investigation of electron-impact ionization of $W^{8+}$ ion

S P Zhang\*, D H Zhang†, L Y Xie and X B Ding

Key Laboratory of Atomic and Molecular Physics & Functional Materials of Gansu Province, College of Physics and Electronic Engineering, Northwest Normal University, Lanzhou 730070, China

**Synopsis** Electron-impact single ionization cross sections are calculated for  $W^{8+}$  ion from the ground state using flexible atomic code with the level-to-level distorted-wave approximation. The contributions of the direct ionization and excitation autoionization are included in the present calculation. The present cross sections underestimate the available experimental values. Such underestimation could be improved by including the contribution of the excited states, which are analysed in our further study.

Electron-impact ionization (EII) processes are of critical importance in plasma modeling, as which are essential collisional atomic process in hot plasmas. [1] Tungsten has been considering as a plasma-facing material in fusion reactors. Thus, reliable EII data for tungsten ions is necessary for the spectroscopic modelling and analysis for fusion plasmas. [2]

The EII cross sections are presented for  $W^{8+}$  ion from the ground state ( $[Cd]4f^{14}5p^4$ ), which are calculated using the flexible atomic code (FAC) [3] with the level-to-level distorted-wave method. The contributions of the direct ionization (DI) from  $5p$ ,  $4f$ , and  $5s$  shells and excitation autoionization (EA) channels from  $5p$ ,  $4f$ ,  $5s$ , and  $4d \rightarrow 12l$  ( $l \leq 6$ ) are included. It is found in the present calculations that the  $4f$  ionization and  $4d$  excitation is dominant to the DI and EA processes, respectively.

Figure 1 shows the present total EII cross section including the contribution of DI and EA, which are compared with available experimental results. [4] It is found that the present results are underestimate, comparing with the experimental values. Note that the experimental data unambiguously show an onset of cross-section contributions below the  $4f^{14}5p^4$  ground-state ionization threshold, as indicated by Ref. [4] Which arises from the excited-state configurations  $4f^{13}5p^45d$  and  $4f^{14}5p^35d$ . Therefore, ion-

ization from excited states could contribute to total cross sections, which are included in our further calculations to improve the discrepancies with experimental data.

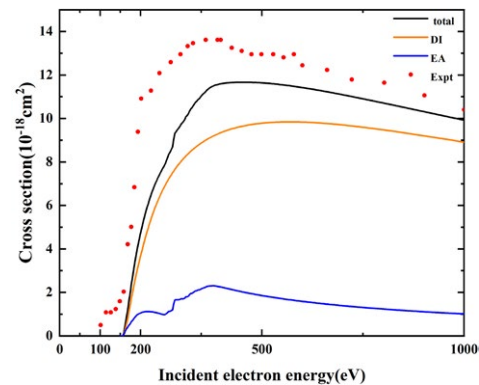


**Figure 1.** (color online) Total cross section including direct ionization (denoted as DI) and excitation autoionization (denoted as EA) cross section are compared with experimental results. [4]

This work has been supported by National Key Research and Development Program of China (20JR5RA541).

## References

- [1] Runjia Bao et al 2022 *atoms*. **100** 30092
- [2] V Jonauskas et al 2019 *Phy. Rev. A*. **100** 062701
- [3] Gu M F et al 2008 *Can. J. Phys.* **86** 675
- [4] M Stenke et al 1995 *J. Phys. B*. **28** 2711

\*E-mail: [transform2021@163.com](mailto:transform2021@163.com)

†E-mail: [zhangdh@nwnu.edu.cn](mailto:zhangdh@nwnu.edu.cn)

## Theoretical investigation of electron-impact ionization of $W^{6+}$ ion

Lili Ma<sup>1\*</sup>, Denghong Zhang<sup>1†</sup>, Luyou Xie<sup>1</sup> and Xiaobin Ding<sup>1</sup>

<sup>1</sup>Key Laboratory of Atomic and Molecular Physics Functional Materials of Gansu Province, College of Physics and Electronic Engineering, Northwest Normal University, Lanzhou 730070, China

**Synopsis** Theoretical investigations of electron-impact ionization of  $W^{6+}$  ion are presented, and the cross sections are calculated using flexible atomic code based on the level-to-level distorted-wave approximation. Contributions from direct-ionization and excitation-autoionization processes are taken into account. Our cross sections are compared with available experimental and theoretical data, and a good agreement is obtained between the theoretical results.

Tungsten is currently a promising plasma-facing material in a fusion reactor because of the preference compromised between its refractoriness against various physical and chemical reactions and strong radiative loss of inherent high-Z impurity [1]. Electron-impact ionization (EII) is an essential collisional atomic process in hot plasma. Therefore, detailed knowledge about atomic processes and about the atomic structure of tungsten in all charged states is necessary for the spectroscopic modelling and analysis for fusion plasma [2].

EII cross sections are performed for  $W^{6+}$  ion using the flexible atomic code (FAC) [3] with the level-to-level distorted wave approximation. In the present calculations, the contributions of the direct ionization (DI) from  $5p$ ,  $4f$ , and  $5s$  shells and excitation autoionization (EA) channels from  $5p$ ,  $4f$ , and  $5s \rightarrow 15l$  ( $l \leq 6$ ) are included. The calculated ionization thresholds of  $4f$ ,  $5p$ , and  $5s$  are determined to be 118.29, 120.20 and 166.43 eV, respectively.

In Fig.1, our calculated EII cross sections are compared with the available theoretical [4] and experimental results [5] from the ground state of  $W^{6+}$  ion. The theoretical results of Pindzola et al were calculated with configuration-average distorted wave approximation. [4] It is found that the present values agree with

theoretical results of Pindzola et al, however, both of which are underestimate, comparing with the experimental values. Such discrepancies between theoretical and experimental results are discussed in our further study.

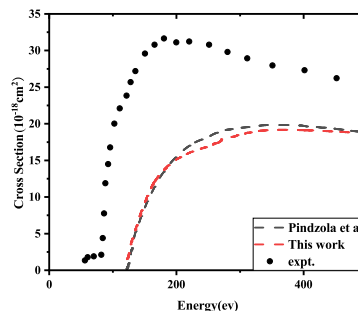


**Figure 1.** present cross sections are compared with available theoretical [4] and experimental [5] data for electron-impact ionization of  $W^{6+}$  ion.

This work has been supported by National Key Research and Development Program of China (20JR5RA541)

### References

- [1] M Mita *et al* 2017 *J. Phys. Conf.Ser.* **875** 012019
- [2] D H Zhang *et al* 2018 *Chin. Phys. B.* **27** 053402
- [3] Gu M F *et al* 2008 *Can. J. Phys.* **86** 675
- [4] Pindzola M S *et al* 1997 *Phys.Rev.A.* **56** 1654
- [5] Stenke M *et al* 1995 *J. Phys. B.* **28** 2711

\*E-mail: [917579871@qq.com](mailto:917579871@qq.com)

†E-mail: [zhangdh@nwnu.edu.cn](mailto:zhangdh@nwnu.edu.cn)



# Theoretical study on the electron collision ionization of $\text{Sn}^{11+}$ ions

F J Zhang,<sup>\*</sup> X B Ding, D H Zhang, and C Z Dong<sup>†</sup>

Key Laboratory of Atomic and Molecular Physics and Functional Materials of Gansu Province, College of Physics and Electronic Engineering, Northwest Normal University, Lanzhou 730070, China

**Synopsis** The cross section for electron-impact single ionization of  $\text{Sn}^{11+}$  ions has been calculated by the level-to-level distorted-wave (LLDW) method using FAC code. The available calculation results are compared with the experimental results in detail. It is found that the present results are in good agreement with the experimental results at high energy, but there are some difference at low energy.

Electron-impact ionization is widely exists in the laboratory and astrophysical plasma environment, which is vital for the creation and maintain of the charge distribution equilibrium of the plasmas [1]. The electron-impact single ionization (EISI) and double ionization has been the focus of many theoretical and experimental studies, especially EISI process. In generally, total EISI cross section is obtained through the direct ionization (DI) and the indirect ionization (excitation-auto-ionization (EA), resonant-excitation double-auto-ionization (REDA)) processes [2].

In recent years, with the rapid development of extreme ultraviolet lithography (EUVL) light source technology, tin is considered to be the most effective radiator of the 13.5 nm emission used in the lithography of nano-structured semiconductor devices [3]. Therefore, it is necessary to theoretically calculate various collision data of tin ion. The total electron-impact single ionization cross section for ground state configuration  $\text{Sn}^{11+}$  ions is calculated by the LLDW method in the present work.

**Table 1.** The energy threshold for direct ionization of  $\text{Sn}^{11+}$  4l subshells.

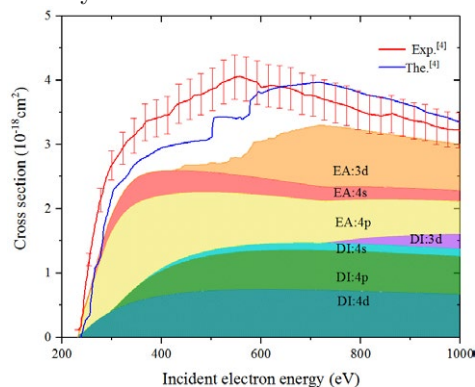
Method	4d	4p	4s
FAC	231.9	296.0	355.4
CADW [4]	231.3		
Exp. [4]	226±1		
NIST	232±2.5		

Table 1 list the energy threshold for the direct ionization of the  $\text{Sn}^{11+}$  4d, 4p, and 4s subshells. The present work were calculated by using the LLDW method and compared with CADW calculation and NIST results. It can be found that the ionization energies calculated in the

\*E-mail: [2018211853@nwnu.edu.cn](mailto:2018211853@nwnu.edu.cn)

†E-mail: [dongcz@nwnu.edu.cn](mailto:dongcz@nwnu.edu.cn)

present work are in good agreement with CADW method by Borovik *et al.* and the NIST data.



**Figure 1.** Total EISI cross section for ground state of  $\text{Sn}^{11+}$  ion.

The DI and EA cross section of each channel are plotted separately in Figure 1, and the contribution of different processes are presented by the labeled shaded curves. It shows that the dominant contribution of DI comes from the 4d and 4p subshells, and the main contribution of EA cross section comes from 3d subshells at high energy. Additionally, we also compare our results with calculations of CADW method and experimental results by Borovik *et al.* The present EISI cross section are in good agreement with the experimental results at high energy, but there are some difference at low energy. This might caused by contribution of metastable state and REDA to the cross section.

This work has been supported by National Key Research and Development Program of China (2022YFA1602500) and National Natural Science Foundation of China (Grant Nos.12274352).

## References

- [1] Liu P F., *et al.* 2014 *Phys. Rev. A.* **89** 042704.
- [2] Zhang D H., *et al.* 2018 *Chin. Phys. B.* **27** 053402.
- [3] Krücken T., *et al.* 2004 *J. Phys. D.* **37** 3213.
- [4] Borovik A., *et al.* 2013 *J. Phys. B.* **46** 175201.

## The state-resolved integral cross sections for atomic krypton studied by fast electron scattering

W. L. Ma<sup>1</sup> Z. W. Nie<sup>1</sup> and L. F. Zhu<sup>1\*</sup>

<sup>1</sup>Department of Modern Physics, University of Science and Technology of China, Hefei, Anhui 230026, China

**Synopsis** The generalized oscillator strengths (GOSs) of the low-lying excited states for atomic krypton have been determined at an impact electron energy of 1500 eV and an experimental resolution of 80 meV. The corresponding optical oscillator strengths (OOSs) were obtained by extrapolating the GOSs to the zero squared momentum transfer. Using the measured GOSs, the corresponding BE-scaled integral cross sections (ICSs) from the threshold to 5000 eV were obtained with the help of the BE-scaling method.

Krypton plays an important role in the plasma diagnostics of the tokamaks and the KrF gas-laser system [1]. From the viewpoint of fundamental research, the excitation mechanism of atomic krypton is also interesting for the theoretical models because of the well-known non-LS coupling. The dynamic parameters, including the GOSs, OOSs, and ICSs, are critical for these applications. Therefore, the GOSs and OOSs for valence-shell excitations of krypton have been reported by some experimental groups [1, 2].

Based on the relative flow technique, we have measured the GOSs for atomic krypton at an impact electron energy of 1500 eV and an experimental resolution of 80 meV. The corresponding OOSs were obtained by extrapolating the GOSs to the zero squared momentum transfer using Lassette formula [3]. The BE-scaled ICSs of the corresponding excitations have been determined in the energy range from the threshold to 5000 eV by using the BE-scaling method [4] and the experimentally derived absolute GOSs, which is normalized with respect to absolute He GOSs. It should be noted that the BE-scaling method is only suitable for the typical dipole-allowed transitions [5]. The derived ICSs data compared with the results from the literature [6] are shown in Fig. 1. Both ICSs data have a good

agreement considering the experimental uncertainties except for the data at 100 eV. The presented ICSs data provide a benchmark for developing and testing the theoretical models.

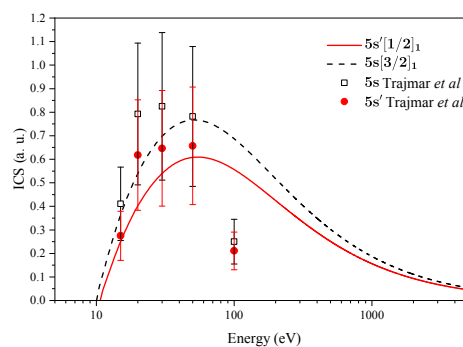


**Figure 1.** The BE-scaled ICSs of the  $5s[3/2]_1$  and  $5s'[1/2]_1$  for atomic krypton as well as the experimental data of Trajmar *et al.* [6]. The uncertainties are 38% for the ICSs data of Trajmar *et al.* [6].

### References

- [1] W. B. Li, *et al.*, *Phys. Rev. A* **67** 062708
- [2] W. F. Chan, *et al.*, *Phys. Rev. A* **48** 858
- [3] E. N. Lassette, *et al.*, *J. Chem. Phys* **50** 1829
- [4] Y. K. Kim, *et al.*, *J. Chem. Phys* **126** 064305
- [5] S. X. Wang, *et al.*, *J. Quant. Spectrosc. Radiat. Transfer* **277** 107988
- [6] S. Trajmar, *et al.*, *Phys. Rev. A* **23** 2167

\*E-mail: [lfzhu@ustc.edu.cn](mailto:lfzhu@ustc.edu.cn)

## Development of particle detectors for electron-ion collision spectroscopy with highly charged ions at the storage ring CSRe

Z K Huang<sup>1\*</sup>, S X Wang<sup>2</sup>, W Q Wen<sup>2</sup>, H B Wang<sup>1</sup>, W L Ma<sup>2</sup>, S Shao<sup>1</sup>, H K Huang<sup>1</sup>, D Y Chen<sup>1</sup>, S F Zhang<sup>1</sup>, L F Zhu<sup>2</sup> and X W Ma<sup>1†</sup> for the DR collaboration@HIRFL

<sup>1</sup>Institute of Modern Physics, Chinese Academy of Sciences, Lanzhou, 730000, China

<sup>2</sup>Department of Modern Physics, University of Science and Technology of China, Hefei, 230026, China

**Synopsis** A new experimental setup for the merged-beams electron-ion collision experiments has been established at the cooler storage ring HIRFL-CSRe. Test experiment with sodium like Kr<sup>25+</sup> has been carried out and nice DR spectra have been obtained.

The electron cooler EC-300 at the experimental Cooler Storage Ring (CSRe) has been upgraded with an embedded electron energy fast detuning system for the merged-beams electron-ion collision experiments. A plastic scintillation detector (PSD) and a multi-wire proportional chamber (MWPC) detector have been developed and installed downstream of the electron cooler to detect the and ionized ions in the electron-ion collision experiments at the CSRe. Both detectors have been tested successfully in a recent dielectronic recombination (DR) experiment of Na-like Kr<sup>25+</sup> ions at the CSRe. In addition, the measured DR rate coefficients for Kr<sup>25+</sup> ions from both detectors were compared with the flexible atomic code (FAC) calculations, and a very good agreement is achieved. The present experimental results demonstrate that the new experimental setups at the CSRe including the electron energy fast detuning system and the particle detectors have high stability and efficiency and meet the needs of the forthcoming electron-ion collision spectroscopy at the CSRe [1].

**Table 1.** Parameters of electron-ion collision experiments at the storage ring and CSRe.

Parameters(units)	Value	
Storage ring	CSRm	CSRe
circumference (m)	161.00	128.80
beam energy (MeV/u)	6-50	25-400
e-coolers	EC-35	EC-300
e-beam energy(keV)	4-35	10-300
electron density(cm <sup>-2</sup> )	10 <sup>5</sup> -10 <sup>7</sup>	10 <sup>5</sup> -10 <sup>7</sup>
detuning range(kV)	-1.5-1.5	-15-15
kT <sub>⊥</sub> (meV)	30	100
kT <sub>∥</sub> (meV)	0.1	1

\*E-mail: [huangzhongkui@impcas.ac.cn](mailto:huangzhongkui@impcas.ac.cn)

†E-mail: [x.ma@impcas.ac.cn](mailto:x.ma@impcas.ac.cn)

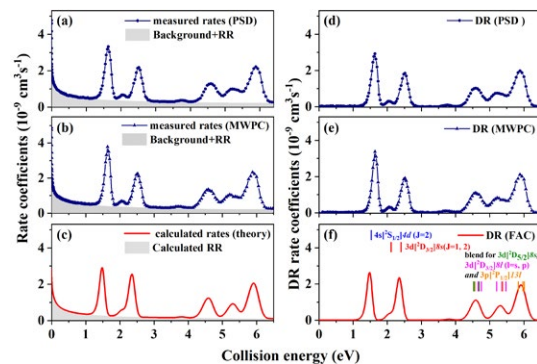


**Figure 1.** (Left) Comparison of the total recombination rate coefficients for Kr<sup>25+</sup> ions at CSRe by (a) PSD (dark blue dotted line + light gray color shaded area), (b) MWPC (dark blue dotted line + light gray color shaded area), and with the (c) theoretical RR (gray color area) + DR (solid red line) rate coefficients, respectively. (Right) Comparison of the pure DR rate coefficients, where (d) represents PSD data (dark blue dotted line), (e) is the MWPC data (dark blue dotted line), and (f) theoretical data by FAC calculation (solid red line), respectively. The vertical bars in (f) with different colors are the DR resonances positions for the indicated configurations, respectively.

### References

- [1] Z. K. Huang, N. Khan, S.X. Wang, et al., *Nucl. Instrum. Methods A* **1040** 167286

## First Dielectronic Recombination Measurements at the Cryogenic Storage Ring

L W Isberner<sup>1,2\*</sup>, M Grieser<sup>2</sup>, R von Hahn<sup>2</sup>, Z Harman<sup>2</sup>, Á Kálosi<sup>3,2</sup>, C H Keitel<sup>2</sup>, C Krantz<sup>4</sup>, D Paul<sup>3,2</sup>, D W Savin<sup>3</sup>, S Singh<sup>2</sup>, A Wolf<sup>2</sup>, S Schippers<sup>1</sup> and O Novotný<sup>2</sup>

<sup>1</sup>I. Physikalisches Institut, Justus-Liebig-Universität Gießen, Gießen, Germany

<sup>2</sup>Max-Planck-Institut für Kernphysik, Heidelberg, Germany

<sup>3</sup>Columbia Astrophysics Laboratory, Columbia University, New York, NY, USA

<sup>4</sup>GSF Helmholtzzentrum für Schwerionenforschung GmbH, Darmstadt, Germany

**Synopsis** We have carried out two measurements for the recombination of free electrons with  $\text{Ne}^{2+}$  and  $\text{Xe}^{3+}$  at the Cryogenic Storage Ring (CSR). In the past, recombination studies on atomic ions have been restricted to ions with a low mass-to-charge ratio ( $m/q$ ) due to the background induced by charge transfer from residual gas. The excellent vacuum conditions in CSR open up new possibilities to investigate recombination with low-charged heavy ions (high  $m/q$ ). Our results demonstrate the feasibility of recombination studies with such low-charged heavy atomic ions at CSR.

The charge state balance in atomic plasmas is governed by competing processes for ionization and recombination. In order to understand and accurately model plasmas in astrophysical environments as well as terrestrial applications, reliable data on recombination of atomic ions with free electrons are needed [1]. With the recent identification of singly charged strontium in a kilonova event, arising from the merger of two neutron stars [2], the need for recombination data on low-charged heavy ions has become even more apparent. As theoretical calculations for these multi-electron systems are challenging, laboratory measurements are crucial.

Electron-ion recombination has been experimentally investigated in magnetic heavy-ion storage rings since the 1990s using the merged-beams technique [3]. A persisting challenge in these experiments is the background signal induced by electron capture from residual gas. Due to the relatively high residual gas pressure in these room-temperature storage rings and the limited magnetic rigidity of the storage ring magnets, experiments were restricted to ions with a high charge-to-mass ratio, which could be stored at sufficiently high energies where the rate coefficient for residual-gas-related electron capture is

low. Experimental data on low-charged heavy ions are still widely missing.

The electrostatic Cryogenic Storage Ring (CSR) [4], located at the Max-Planck-Institut für Kernphysik in Heidelberg, Germany, combines the mass-independent storage of electrostatic storage rings with the excellent vacuum conditions provided by a fully-cryogenic beam environment. CSR is equipped with an electron cooler and an efficient single-particle detector. Thus, CSR provides unique possibilities for the investigation of electron-ion recombination of low-charged heavy ions.

Here, we report on the first recombination studies with atomic ions at CSR. Investigating the dielectronic recombination of  $\text{Ne}^{2+}$  and  $\text{Xe}^{3+}$ , we have observed resonant recombination features in agreement with preliminary theoretical calculations. Our results clearly demonstrate the feasibility of atomic recombination studies with heavy low-charged ion species at CSR.

### References

- [1] Müller A 2008 *At. Mol. Opt. Phys.* **55** 293
- [2] Watson D et al. 2019 *Nature* **574** 497
- [3] Schippers S 2015 *Nucl. Instrum. Methods Phys. Res., Sect. B* **350** 61
- [4] von Hahn R et al. 2016 *Rev. Sci. Instr.* **87** 063115

\*E-mail: [leonard.isberner@mpi-hd.mpg.de](mailto:leonard.isberner@mpi-hd.mpg.de)

## Electron recombination of deuterated triatomic hydrogen ions at the Cryogenic Storage Ring

A Znotins<sup>1\*</sup>, A Faure<sup>2</sup>, J Forer<sup>3</sup>, C H Greene<sup>4</sup>, F Grussie<sup>1</sup>, L W Isberner<sup>5,1</sup>, Á Kálosi<sup>6,1</sup>, V Kokoouline<sup>3</sup>, M Pezzella<sup>7</sup>, D Müll<sup>1</sup>, O Novotný<sup>1</sup>, D Paul<sup>6,1</sup>, D W Savin<sup>6</sup>, S Schippers<sup>5</sup>, J Tennyson<sup>7</sup>, X Urbain<sup>8</sup>, A Wolf<sup>1</sup>, H Kreckel<sup>1</sup>

<sup>1</sup> Max-Planck-Institut für Kernphysik, Heidelberg, 69117, Germany

<sup>2</sup>University Grenoble Alpes, CNRS, IPAG, Grenoble, F-38000, France

<sup>3</sup>Department of Physics, University of Central Florida, Orlando, FL 32816, USA

<sup>4</sup>Department of Physics and Astronomy, Purdue University, West Lafayette, IN 47907, USA

<sup>5</sup>I. Physikalisches Institut, Justus-Liebig-Universität, Gießen, 35392, Germany

<sup>6</sup>Columbia Astrophysics Laboratory, Columbia University, New York, NY 10027, USA

<sup>7</sup>Department of Physics and Astronomy, University College, London, WC1E 6BT, UK

<sup>8</sup>Institute of Condensed Matter and Nanosciences, Louvain-la-Neuve, B-1348, Belgium

**Synopsis** We have carried out dissociative electron recombination studies with  $\text{H}_2\text{D}^+$  and  $\text{D}_2\text{H}^+$  ions at the Cryogenic Storage Ring (CSR). The experiments are combined with state-of-the-art calculations for all relevant processes to understand the evolution of individual rotational states in the cryogenic vacuum of the CSR.

The triatomic hydrogen ion  $\text{H}_3^+$  is one of the most important molecules for the gas phase chemistry of interstellar clouds. As an active proton donor, it is a primary driver of ion-neutral chemistry in interstellar environments. Moreover, as the simplest polyatomic molecule,  $\text{H}_3^+$  is an important benchmark system for theoretical molecular calculations.

Considerable focus has been given to the dissociative electron recombination (DR) of triatomic hydrogen ions, as the rate coefficient for this reaction is crucial in determining the ionization balance of interstellar clouds. Although earlier studies have established that the DR rate coefficients of  $\text{H}_3^+$  and its isotopologues are influenced by rotational excitation, state-selective measurements have not been feasible thus far.

Here we present ongoing efforts aimed at understanding electron collisions and recombination of deuterated variants of triatomic hydrogen – namely  $\text{H}_2\text{D}^+$  and  $\text{D}_2\text{H}^+$  – inside the Cryogenic Storage Ring (CSR) [1]. Radiative cooling models, based on comprehensive line-lists [2], predict that the rovibrational populations of  $\text{H}_2\text{D}^+$  and  $\text{D}_2\text{H}^+$  become confined to a handful of identifiable states after storage times of several hundreds of seconds (see Fig. 1). Our models also include inelastic electron collisions and selective depletion by electron recombination.

\* E-mail: [znotins@mpi-hd.mpg.de](mailto:znotins@mpi-hd.mpg.de)

We will present recent DR experiments performed with cold  $\text{H}_2\text{D}^+$  and  $\text{D}_2\text{H}^+$  ions, combined with new theoretical calculations for all relevant processes.

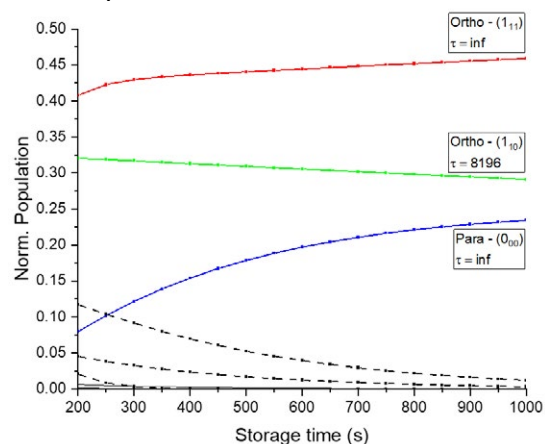


**Figure 1.** Simulated radiative cooling of  $\text{H}_2\text{D}^+$  ions inside the Cryogenic Storage Ring. After 1000 s of storage, essentially only three rotational states remain populated.

### References

- [1] R von Hahn et al., 2016, *Rev. Sci. Instrum.* **87** [063115](#)
- [2] C A Bowesman et al., 2023, *MNRAS* **519** [6333](#)



## Radiative Recombination Studies for Bare Lead Ions Interacting with Low-Energy Electrons

B Zhu<sup>1,2,3</sup>, A Gumberidze<sup>2</sup>, G Weber<sup>1,2</sup>, T Over<sup>1,3</sup>, Z Anelkovic<sup>2</sup>,  
 A Bräuning-Demian<sup>2</sup>, R J Chen<sup>2</sup>, D Dmytriiev<sup>2</sup>, O Forstner<sup>1,2,3</sup>, C Hahn<sup>1,2,3</sup>,  
 F Herfurth<sup>2</sup>, M O Herdrich<sup>1,2</sup>, P-M Hillenbrand<sup>2,4</sup>, A Kalinin<sup>2</sup>, F M Kröger<sup>1,2,3</sup>,  
 M Lestinsky<sup>2</sup>, Yu A Litvinov<sup>2</sup>, E B Menz<sup>1,2,3</sup>, W Middents<sup>1,3</sup>, T Morgenroth<sup>1,2,3</sup>,  
 N Petridis<sup>2</sup>, Ph Pfäfflein<sup>1,2,3</sup>, M S Sanjari<sup>2,5</sup>, R S Sidhu<sup>2</sup>, U Spillmann<sup>2</sup>, S Trotsenko<sup>1,2</sup>,  
 L Varga<sup>2</sup>, G Vorobyev<sup>2</sup>, S Schippers<sup>4,6</sup>, R Schuch<sup>7</sup> and Th Stöhlker<sup>1,2,3</sup>

<sup>1</sup> Helmholtz Institute Jena, Jena, 07743, Germany

<sup>2</sup> GSI Helmholtzzentrum für Schwerionenforschung, Darmstadt, 64291, Germany

<sup>3</sup> Institute of Optics and Quantum Electronics, Friedrich Schiller University Jena, Jena, 07743, Germany

<sup>4</sup> I. Physikalisches Institut, Justus-Liebig-Universität Gießen, Gießen, 35392, Germany

<sup>5</sup> Aachen University of Applied Sciences, Aachen, 52005, Germany

<sup>6</sup> Helmholtz Research Academy Hesse for FAIR, Campus Gießen, Gießen, 35392, Germany

<sup>7</sup> Physics Department, Stockholm University, Stockholm, 106-91, Sweden

**Synopsis** X-ray emission as a result of radiative recombination (RR) at threshold energies in the electron cooler of the CRYRING@ESR was investigated for decelerated bare lead ions at a beam energy of 10 MeV/u. The recorded spectra are dominated by fine-structure resolved Lyman, Balmer and Paschen lines, originating in particular from yrast cascade transitions into inner shells. In addition, a rigorous theoretical model is applied for the interpretation of measured x-ray spectra, and shows a good agreement.

Radiative recombination (RR) is the time-reversed process of photoionization and, therefore, one of the most fundamental processes in atomic physics [1]. Here, we present a pioneering x-ray spectroscopic study of RR for bare lead ions ( $\text{Pb}^{82+}$ ) at the electron cooler of recently re-commissioned CRYRING@ESR at FAIR, Darmstadt [2]. The x-rays emitted following the RR process have been recorded by Ge(i) detectors mounted along the ion beam axis.

For comparison with the x-ray spectra recorded in coincidence with the down-charged hydrogen-like Pb ions, Fig. 1 displays theoretical results based upon our versatile radiative cascade code that takes into account the initial population distribution via RR for all atomic levels up to Rydberg states with principle quantum number  $n = 165$  in combination with time-dependent feeding transitions [3]. One may note practically background free spectra with two groups of x-ray lines: characteristic projectile x-rays and the RR transitions. Prominent features of characteristic radiation incorporate the Lyman lines corresponding to  $nl \rightarrow 1s$  transitions where the state  $n = 2$  is well resolved, as well as two intense Balmer transitions,  $3d_{5/2} \rightarrow 2p_{3/2}$  and  $3d_{3/2} \rightarrow 2p_{1/2}$ , respectively. Also, due to the Doppler blue shift in conjunction with the low

absorption of the x-rays through the beryllium window, Paschen radiation from  $\text{Pb}^{81+}$  ions was observed for the first time at  $0^\circ$  observation geometry with an intensity comparable to the overall line intensities of the Balmer transitions. A detailed comparison between our experimental spectra and theory will be presented elucidating in particular the role of prompt and delayed x-ray emission. Furthermore, the current experiment can be considered as an important prerequisite for future precision x-ray spectroscopy studies at the electron cooler of the CRYRING@ESR.

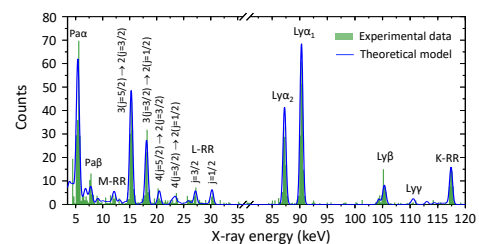


**Figure 1.** X-ray spectroscopy registered by a Ge(i) detector mounted at  $0^\circ$  observation angle [3].

### References

- [1] Eichler J and Stöhlker Th 2007 *Phys. Rep.* **439** 1
- [2] Lestinsky M et al. 2016 *Eur. Phys. J. Spec. Top.* **225** 797
- [3] Zhu B et al. 2022 *Phys. Rev. A* **105** 052804



# Charge-state distributions after beta decay of ${}^6\text{He}$ to form ${}^6\text{Li}^+$

A T Bondy<sup>1\*</sup> and G W F Drake<sup>1,2</sup>

<sup>1</sup>Department of Physics, University of Windsor, Windsor, Ontario, N9B 3P4 Canada

<sup>2</sup>Canterbury College, Windsor, Ontario, N9B 3Y1 Canada

**Synopsis** Projection operators have been developed to treat the double ionization of  ${}^6\text{Li}^+$  following the beta decay of  ${}^6\text{He}$ .

The electron-antineutrino angular correlation coefficient characterizing the beta decay of  ${}^6\text{He}$  has long been studied in searching for physics beyond the Standard Model [1]. At present, there exists a major discrepancy in the amount of double ionization predicted [2] after this beta decay compared with what is observed experimentally [3].

In Ref. [4], we partially resolve this discrepancy; the results are shown in Table 1. The difficulty encountered in previous theoretical works is shown in Figure 1, where the  $E > 0$  region contains overlapping continua where single and double ionization can occur. In order to partition these two outgoing channels of ionization, we have developed projection operators by forming configuration-interaction-like products of one-electron Sturmian functions. These projection operators are then applied to the  $E > 0$  region of the  $\text{Li}^+$  pseudospectrum shown in Figure 1, which is formed variationally using Hylleraas wave functions and is assumed to describe the state of the  ${}^6\text{He}$  system after beta decay in the sudden approximation.

In this poster, we will describe these methods along with their benefits and shortcomings, and offer ideas for the future resolution of this problem within the framework described here.

**Table 1.**  ${}^6\text{Li}^{3+}$  charge-state fractions (in %) for each initial state following beta decay.

	Previous[2]	Present[4]	Exp't.
1 ${}^1S_0$	1.2(1)	0.35(5)	0.018(15) [1]
2 ${}^3S_1$	1.86(7)	0.53(7)	<0.01 [3]

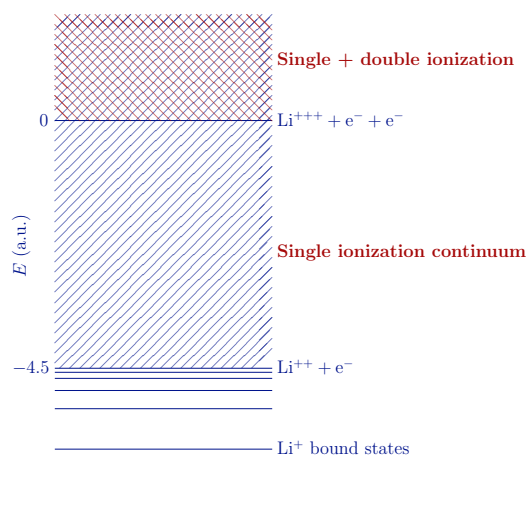


**Figure 1.** Energy level diagram of  ${}^6\text{Li}^+$  following beta decay. The single and double continua overlap for  $E > 0$ .

Work supported by the Natural Sciences and Engineering Research Council of Canada (NSERC) and the Digital Research Alliance of Canada/Compute Ontario.

## References

- [1] Carlson T A, Pleasonton F, Johnson C H 1963 *Phys. Rev.* **129** 2220
- [2] Schulhoff E E and Drake G W F 2015 *Phys. Rev. A* **92** 050701
- [3] Hong R *et al.* 2017 *Phys. Rev. A* **96** 053411
- [4] Bondy A T and Drake G W F 2023 *Atoms* **3** 41

\*E-mail: [bondy11u@uwindsor.ca](mailto:bondy11u@uwindsor.ca)

## Near-threshold collisional dynamics in the $e^-e^+p$ system

H B Ambalampitiya<sup>1</sup>, J Stallbaumer<sup>1</sup>, I I Fabrikant<sup>1\*</sup>, I Kalinkin<sup>2</sup>, D V Fursa<sup>2</sup>,  
A S Kadyrov<sup>2</sup> and I Bray<sup>2</sup>

<sup>1</sup>Department of Physics and Astronomy, University of Nebraska, Lincoln, Nebraska 68588, USA

<sup>2</sup>Curtin Institute for Computation and Department of Physics and Astronomy, Curtin University, GPO Box U1987, Perth, WA 6845, Australia

**Synopsis**  $e^+ - H(n)$  and  $Ps(n) - p$  collisions near the three-body break-up threshold and thresholds for the charge-transfer processes are investigated by the classical-trajectory Monte Carlo simulations and quantum convergent close-coupling method. For the target in the ground state the classical approach works well in the former case and fails in the latter. With increasing degree of excitation of the target both methods converge according to the correspondence principle.

The threshold laws are ubiquitous in collision processes. It is important to understand the role of quantum effects in these laws. In particular, the Wigner threshold law is purely quantum-mechanical. In contrast, the Wannier law for electron-impact ionization of atoms was derived within the framework of classical mechanics and confirmed by the quasiclassical theory. Although there is no formal proof of this law within the framework of quantum-mechanical three-body problem, there is strong evidence that the three-body physics of particles interacting by the Coulomb force, near the threshold of the three-body break-up, is described adequately by classical mechanics. However, until recently, the absence of accurate quantum calculations in the challenging near-threshold region prevented rigorous tests of Wannier physics. Recent convergent close-coupling (CCC) calculations of  $e^+ - H$  and  $Ps - p$  collisions [1, 2, 3] are overcoming this obstacle and allow a detailed verification of the classical approach. On the other hand, with the increasing degree of excitation of reactants, quantum calculations become very challenging computationally whereas classical calculations can be extended for higher states with the same computational efficiency. Moreover, due to the classical scaling laws [4] the volume of the classical trajectory Monte Carlo (CTMC) calculations can be substantially reduced by rescaling results obtained for the ground target state.

In the present work we study  $e^+ - H(n)$  and  $Ps(n) - p$  collisions near the three-body break-up threshold and thresholds for the charge-transfer

processes. We show that CTMC simulations for the three-body break-up agree well in this energy region with quantum-mechanical CCC calculations even if the initial hydrogen atom or positronium atom is in the ground state. The threshold behavior of the three-body break-up cross sections in  $e^+ - H(1s)$  and  $Ps(1s) - p$  collisions agrees with the Wannier law with the Klar's exponent [5] and obeys the classical scaling laws, although some deviation from the Klar-Wannier behavior is observed in the CCC results. Below the threshold the agreement between CTMC and CCC disappears. In particular CTMC method fails completely for the processes of H formation in  $Ps(1s) - p$  collisions and Ps formation in  $e^+ - H$  collisions well below the three-body break-up threshold. For higher initial states the CTMC results below the threshold improve substantially, in accordance with the correspondence principle. This is explained by comparing the quantum-mechanical threshold laws with the classical laws.

### References

- [1] Kadyrov A S, Rawlins C M, Stelbovics A T, Bray I, and Charlton M 2015 Phys. Rev. Lett. **114** 183201
- [2] Kadyrov A S, Bray I, Charlton M, and Fabrikant I I 2017 Nature Commun. **8** 1544
- [3] Charlton M, Ambalampitiya H B, Fabrikant I I, Kalinkin I, Fursa D V, Kadyrov A S, and Bray I 2023 Phys. Rev. A **107** 012814
- [4] Abrines R and Percival I C 1966 Proc. Phys. Soc. **88** 861
- [5] Klar H 1981 J. Phys. B: Atom. Mol. Phys. **14** 4165

\*E-mail: ifabrikant@unl.edu

## Convergent close-coupling calculations of positron scattering from atomic oxygen

N A Mori\*, L H Scarlett, I Bray, and D V Fursa

Department of Physics and Astronomy, Curtin University, Perth, Western Australia 6102, Australia

**Synopsis** The single-centre convergent close-coupling (CCC) method has been utilised to study positron scattering from atomic oxygen. Cross sections have been determined for major scattering processes between threshold and 5000 eV. A complex model potential, scaled to the CCC results, has been used to overcome drawbacks present in this approach. Excellent agreement has been found at high energies with other theories, halved electron/positron O<sub>2</sub> experiment, and electron experiment. However, there are large discrepancies between different theoretical methods at low energies.

The oxygen atom is a fundamental part of life as it composes molecular oxygen (O<sub>2</sub>), water (H<sub>2</sub>O), and many important biomolecules, such as the bases of DNA. Consequently, oxygen is the main component of the human body, comprising approximately 65% of its mass. Positron interactions inside the human body are of great interest due to the applications in the biomedical industry, most notably in positron emission tomography (PET) scans and positron therapy. However, quantifiable data for the scattering processes occurring in these procedures is scarce and largely unknown [1]. Independent atom modelling (IAM) or Monte-Carlo methods require cross sections of independent atomic components to calculate positron scattering from the complex biomolecules within the body. Therefore, accurate calculations of positron scattering upon atomic oxygen are necessary to facilitate such calculations.

Atomic oxygen is also a fundamental part of the Earth's atmosphere, where due to the continuous dissociation of O<sub>2</sub> molecules by ultraviolet radiation it is the main component between 200 and 650km [2]. Positrons are also readily produced in this region through cosmic ray interactions with the atmosphere, terrestrial gamma-ray flashes, or nuclear reactions [3, 4, 5]. Therefore, accurate positron-oxygen cross sections are important for modelling positron transport through this region or in the atmosphere of oxygen-rich bodies such as Venus [6] and Europa [7].

The single-centre convergent close-coupling

(CCC) method has been utilised to perform 1367-state calculations for this scattering system. This method has two main drawbacks; firstly, it cannot be applied at energies between the positronium-formation and ionisation thresholds. Secondly, the positronium-formation and direct ionisation components of the total ionisation cross section are modelled implicitly and therefore combined. We employ a complex potential calculation scaled to the CCC calculation to address these issues. This approach can be used to calculate cross sections between the two thresholds and disentangle the positronium-formation and direct ionisation from the total ionisation cross section.

Beyond ionisation processes, we have also calculated total, bound state excitation, optical emission, elastic, momentum transfer, and stopping power cross sections for this system for energies between threshold and 5000 eV. Low-energy studies have also been conducted to determine quantities such as the scattering length.

### References

- [1] C. Makochekanwa *et al.* 2009 *New J. Phys.* **11** 103036
- [2] H. Richter *et al.* 2021 *Commun. Earth. Environ.* **2** 19
- [3] Adriani *et al.* 2014 *Phys. Rep.* **544** 323
- [4] Gusevet *et al.* 2001 *J. Geophys. Res.* **106** 26111
- [5] Sarria *et al.* 2019 *J. Geophys. Res.* **124** 10497
- [6] G. Keating, J. Nicholson III, and L. Lake 1980 *J. Geophys. Res.* **85** 1941
- [7] C. Hansen, D. E. Shemansky, and A. R. Hendrix 2005 *Icarus* **176** 305

\*E-mail: [nicolas.mori@postgrad.curtin.edu.au](mailto:nicolas.mori@postgrad.curtin.edu.au)

## Differential positronium-formation cross-sections around zero degrees from atoms and molecules

D M Newson\*, M Shipman, S E Fayer, S J Brawley, R Kadokura, A Loreti, G Laricchia†

UCL Department of Physics and Astronomy, Gower Street, London WC1E 6BT, UK

The first experimental study [1] of the absolute differential positronium formation cross-section (DCS) in the forward direction ( $\pm 1^\circ$ ) revealed the propensity for forward emission at intermediate energies ( $> 10$  eV), particularly for helium and molecular hydrogen. More recently, results presented by Fayer *et al.* [2] for the inert atoms showed hints of minima in the forward collimation (differential-to-integral positronium-formation cross-section ratio) when cast in terms of the reduced excess energy. A possible link to quantum vortices was considered — a feature of the velocity field of the collisional wave function that occurs when both the real and imaginary parts are zero [3]. In theoretical investigations, vortices manifest as zero cross-sections for particular scattering angles and projectile momenta, and have been identified in the differential positronium-formation cross-sections of hydrogen [4] and helium [5]. Whilst the vortices, in these cases, occur at scattering angles  $> 0^\circ$ , deep minima, linked to them, are present in the forward direction, as shown in figure 1 for helium.

New experimental determinations of the differential positronium-formation cross-section around zero degrees ( $\pm 1^\circ$ ) will be presented for  $H_2$ ,  $N_2$ ,  $O_2$  and the inert atoms, over an extended energy range. Those in the low-energy region, a few electron volts above the relevant positronium threshold, will be discussed in the context of recent theoretical works on vortices [5]. Trends in the energy-dependence and position of maxima are identified amongst both the atoms and molecules separately, and the differences between these two groups of targets indicated. The statistical nature of positronium formation is highlighted with the aid of the log-normal distribution [7]

and the energy-sharing amongst the degrees of freedom of the collision system is considered.

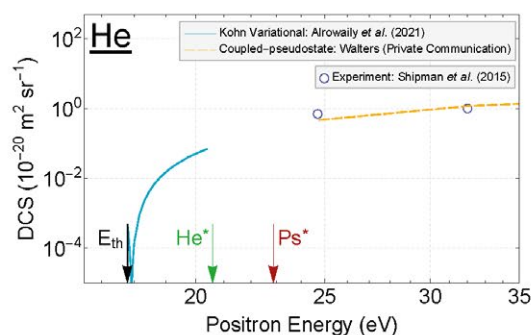


**Figure 1.** Low-energy experimentally determined absolute differential positronium-formation cross-sections of [1] alongside results from the coupled-pseudostate [6] and Kohn variational approaches [5], shown on a logarithmic y-axis. The latter displays a minimum in the forward direction close to the positronium-formation threshold ( $E_{th}$ ). The excitation threshold energies of helium ( $He^*$ ) and positronium ( $Ps^*$ ) are also indicated.

EPSRC (UK) is thanked for financial support (EP/P009395/1, EP/R513143/1).

### References

- [1] Shipman M *et al.* 2015 *Phys. Rev. Lett.* **115** 033401
- [2] Fayer S E *et al.* 2019 *Phys. Rev. A* **100** 062709
- [3] Macek J H *et al.* 2009 *Phys. Rev. Lett.* **102** 143201
- [4] Alrowaily A W *et al.* 2019 *J. Phys. B: At. Mol. Opt. Phys.* **52** 205201
- [5] Alrowaily A W *et al.* 2021 *Atoms* **9** 56
- [6] Walters H R J 2015 Private communication of unpublished data, used in ref [1]
- [7] Laricchia G *et al.* 2018 *Sci. Rep.* **8** 15056

\*E-mail: [ucapdne@ucl.ac.uk](mailto:ucapdne@ucl.ac.uk)

†E-mail: [g.laricchia@ucl.ac.uk](mailto:g.laricchia@ucl.ac.uk)



## Electron elastic scattering by Bk and Cf atoms: polarization effects

A Z Msezane<sup>1\*</sup> and Felfli<sup>1†</sup>

<sup>1</sup> Center for Theoretical Studies of Physical Systems, Clark Atlanta University, Atlanta, Georgia 30314, USA

**Synopsis** Regge pole-calculated low-energy electron elastic total cross sections (TCSs) for actinide atoms are characterized by ground, metastable and excited negative-ion formation, shape resonances (SRs) and Ramsauer-Townsend (R-T) minima. Here we demonstrate the sensitivity of R-T minima and SRs to the electronic structure and dynamics of Bk and Cf atoms, thereby permitting their first ever use as novel validation of the experimental observation that Cf is a transitional element in the actinide series; we also calculate their electron affinities.

The recent experiment [1] using only a single nanogram of the highly radioactive Bk and Cf atoms characterized their structure and dynamics, concluding that indeed Cf is a transitional element in the actinide series. The observation [1] has been validated through the sensitivity of the Regge pole-calculated R-T minima and SRs in the metastable TCSs of Bk and Cf. Namely, the deep R-T minimum in the Bk TCS (see Fig. 1) flips over to a SR appearing very close to threshold in the metastable TCS of the Cf atom [2]

The TCS which embeds fully the essential electron-electron correlation effects [3] is calculated from (atomic units are used)

$$\sigma_{tot}(E) = 4\pi k^{-2} \int_0^\infty \text{Re}[1 - S(\lambda)] \lambda d\lambda - 8\pi^2 k^{-2} \sum_n \text{Im} \frac{\lambda_n \rho_n}{1 + \exp(-2\pi i \lambda_n)} + I(E) \quad (1)$$

In Eq. (1)  $S(\lambda)$  is the S-matrix,  $k = \sqrt{2mE}$ ,  $m = 1$  being the mass and  $E$  the impact energy,  $\rho_n$  is the residue of the S-matrix at the  $n^{\text{th}}$  pole,  $\lambda_n$  and  $I(E)$  contains the contributions from the integrals along the imaginary  $\lambda$ -axis. The TCS calculation uses the ABF potential which accounts for the vital core-polarization interaction

$$U(r) = -\frac{Z}{r(1 + \alpha Z^{1/3} r)(1 + \beta Z^{2/3} r^2)} \quad (2)$$

In Eq. (2)  $Z$  is the nuclear charge,  $\alpha$  and  $\beta$  are variation parameters. The potential has the appropriate asymptotic behavior and accounts correctly at low  $E$  for the polarization interaction.

Fig. 1 presents the TCSs for the Bk atom, typical of those for actinide atoms, showing the deep R-T minimum before it flips over to a SR in the TCSs of Cf. Indeed, they are characterized by ground, metastable and excited negative-ion formation, whose binding energies (BEs) yield the challenging to cal-

culate electron affinities (EAs). These BEs have been compared with the theoretical EAs of Bk and Cf to understand and make sense of those EAs since they are riddled with uncertainties and are difficult to interpret. The results here are also important in guiding theoretical methods on the vital importance of the polarization interaction as demonstrated in the calculation of the EA of the At atom [2].

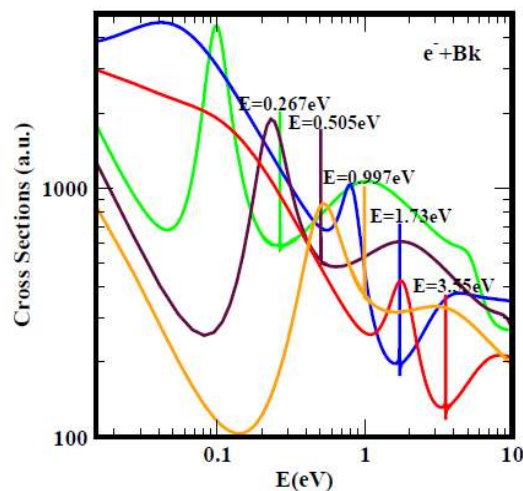


**Figure 1.** Electron TCSs for Bk: red, blue and orange (polarization-induced) curves are respectively for ground and metastable TCSs. Brown and green curves represent excited states. Very sharp peaks denote anionic BEs.

Research was supported by US DOE Office of Basic Energy Sciences, Office of Energy Research.

### References

1. Müller A *et al* 2021 *Nat. Commun.* **12** 948
2. Msezane A Z and Felfli Z 2023 *Atoms* **11**, 47
3. Sokolovski D *et al* 2007 *Phys. Rev. A* **76** 026707

\* E-mail: [amsezane@cau.edu](mailto:amsezane@cau.edu)

## Theoretical investigation of bound and resonant states of imidogen radical NH

R. Ghosh,<sup>1,2,\*</sup> K. Chakrabarti,<sup>3,†</sup> and B. S. Choudhury<sup>2</sup>

<sup>1</sup>Department of Mathematics, Sukumar Sengupta Mahavidyalaya, Keshpur, Paschim Medinipur, 721150, India

<sup>2</sup>Department of Mathematics, Indian Institute of Engineering Science and Technology, Shibpur, Howrah 711103, India

<sup>3</sup>Department of Mathematics, Scottish Church College, 1 & 3 Urquhart Sq., Kolkata 700006, India

**Synopsis** The molecular R-matrix formalism is used to calculate bound and continuum states of the NH molecule. Potential energy curves for the bound states of singlet, triplet and quintet symmetry are obtained for an extended range of inter nuclear distances between 1–9 a.u. Resonance positions and widths for low-lying Feshbach resonances are also obtained for states with singlet and triplet symmetry.

The imidogen radical NH is a very common species in nitrogen chemical reaction patterns in atmospheric or interstellar medium (ISM). NH was discovered in diffuse clouds in the 1990s [1], though the existence of NH was known earlier in the atmosphere of the sun [2], in stellar atmospheres and in the tail of comets [3]. Moreover, it is likely to be present and is a precursor to the formation of ammonia in the ISM. [4].

NH and NH<sup>+</sup> also occur as products during combustion of nitramine compounds in explosives, rocket propellants and emergency escape devices. Many nitrogen plasmas contain NH<sup>+</sup> and NH, therefore, the kinetic modeling and dynamics calculations of the products require not only electronic structure data, but also collision data in the form of Potential energy curves, cross sections and reaction rate coefficients [5].

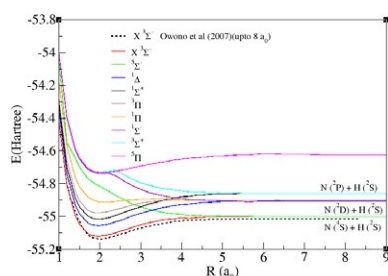


FIG. 1. Potential energy curves of the ground and eight lowest bound states of NH.

Low-energy electron collision calculations have been performed on the imidogen molecular ion (NH<sup>+</sup>) at its equilibrium geometry using the R-matrix method. A suitable model [6] is first built to represent the target ion. Scattering calculations are then performed as a function of geometry between 1-9 a<sub>0</sub> on a moderately dense grid of 50 points to yield the bound states of NH for <sup>3</sup>Σ<sup>-</sup>, <sup>3</sup>Π, <sup>3</sup>Σ<sup>+</sup>, <sup>1</sup>Π, <sup>1</sup>Δ, <sup>1</sup>Σ<sup>-</sup>, <sup>1</sup>Σ<sup>+</sup>, <sup>5</sup>Σ<sup>-</sup>, <sup>5</sup>Π symmetries and resonance parameters for <sup>1</sup>Σ<sup>-</sup>, <sup>1</sup>Π and <sup>3</sup>Π symmetries. To show the relative position of the low-lying states, we show the PECs of the ground and eight lowest states of NH in figure 1. We also compare our ground state with the work of Owono et al 2007 [7]. It is clear that there is a good agreement. Numerous resonances are characterised by the characteristic oscillations in the eigenphase sums of <sup>1</sup>Σ<sup>-</sup>, <sup>1</sup>Π and <sup>3</sup>Π overall symmetries of the e+ NH<sup>+</sup> system. It has been shown that many of the resonances [6] occur in series characterized by their effective quantum numbers  $\nu$ . Many of these resonances also have very narrow widths. These are liable to be on the verge of being bound and hence may be very close to crossing an NH<sup>+</sup> ion curve from above. To find the true picture we are in processing to do the detailed construction of the potential energy curves of the ion and the resonant states as a function of the inter nuclear distance R. These resonant states are expected to be useful for other collisional calculations, in particular for the Dissociative Recombination of the NH<sup>+</sup> ion.

- [1] D. M. Meyer and K. C. Roth, *Astrophys. J. Lett.* **376**, L49 (1991).  
 [2] H. D. Babcock, *Astrophys. J.* **102**, 154 (1945).  
 [3] R. Meier, D. Wellnitz, S. J. Kim, and M. F. A'Hearn, *Icarus* **136**, 268 (1998).  
 [4] E. T. Galloway and E. Herbst, *Astron. Astrophys.* **211**,

- 413 (1989).  
 [5] G. F. Adams and R. W. Shaw, Jr., *Annu. Rev. Phys. Chem.* **43**, 311 (1992).  
 [6] R. Ghosh, K. Chakrabarti, and B. S. Choudhury, *Plasma Sources Sci. Technol.* **31**, 065005 (2022).  
 [7] L. C. O. Owono, N. Jaidane, M. G. K. Njock, and Z. B. Lakhdar, *J. Chem. Phys.* **126**, 244302 (2007).

\* rajughosh152@gmail.com

† kkch.atmol@gmail.com



## Symmetry breaking in dissociative ionization of symmetric molecules by electron impact

N Watanabe<sup>1\*</sup> and M Takahashi<sup>1</sup>

<sup>1</sup> Institute of Multidisciplinary Research for Advanced Materials, Tohoku University, Sendai 980-8577, Japan

**Synopsis** We report experimental evidence of symmetry breaking in electron-impact dissociative ionization of inversion-symmetric molecules. Electron-ion coincidence experiments of CO<sub>2</sub> and N<sub>2</sub> reveal that symmetry breaking appears in the angular distribution of fragment ions. If ionization and dissociation are two separate processes, such asymmetry cannot occur. It follows that electron localization in the molecular ion is induced by the interaction with the slow ejected electron.

Symmetry plays a crucial role in photon- and electron-induced processes in molecules; it provides fundamental insights into the spectroscopic properties and gives strict rules for the angular distributions of the dissociation fragments. For instance, in dissociative ionization (DI) of an inversion-symmetric molecule, such as H<sub>2</sub>, the fragment ion is generally emitted into both directions along the molecular axis with equal probability. However, we have recently found that under some conditions, asymmetric ion emission occurs in electron-impact DI even for symmetric molecules [1]. In this contribution, we provide experimental evidence of the symmetry breaking in electron-impact DI of CO<sub>2</sub> and N<sub>2</sub>, and discuss the underlying mechanism.

Scattered electron-fragment ion coincidence experiments were carried out using an (*e*, *e*+ion) apparatus [2]. An incident electron energy of ~1.4 keV was used in the measurements. From the results, we obtained the angular distributions of the fragment ions with respect to the direction of the momentum transfer vector **K**.

Here we show the results of CO<sub>2</sub>. Figure 1 depicts the angular distributions of CO<sup>+</sup> with kinetic energy of 1.4-2.3 eV, which are plotted as a function of angle between **K** and the recoil direction of CO<sup>+</sup>,  $\phi_K$ . It has generally been assumed that DI consists of two independent steps: firstly, the ionized electron quickly escapes to infinity and subsequently, the molecular ion dissociates. Within this assumption, the probability of CO<sup>+</sup> emission in the direction of **K** should be the same as that in the opposite direction due to the inversion symmetry of CO<sub>2</sub><sup>+</sup>. Indeed, the result at the electron energy loss of  $E = 34-36$  eV is forward-backward symmetric. Nevertheless, unexpected asymmetry has been

observed at  $E = 28-30$  eV: the intensity at  $\phi_K \sim 0^\circ$  is noticeably higher than that around  $180^\circ$ . To get a clue to the origin of this phenomenon, we consider ionization channels associated with the 28-30 eV region. Three channels,  $3\ ^2\Pi_u$ ,  $2\ ^2\Pi_g$ , and  $4\ ^2\Pi_u$ , can contribute to the production of CO<sup>+</sup> with KE  $\geq 1.4$  eV, and their ionization potentials (27.3, 29.7, and 30.5 eV) are close to each other. One may conceive that the Coulomb interaction between the slow ejected electron and CO<sub>2</sub><sup>+</sup> causes mixing of the close-lying  $^2\Pi_u$  and  $^2\Pi_g$  states. The superposition of the gerade and ungerade states leads to asymmetric electron localization in CO<sub>2</sub><sup>+</sup> and therefore breaks symmetry. Such an electron-localization effect should be general in electron-impact DI reactions over a wide impact energy range.

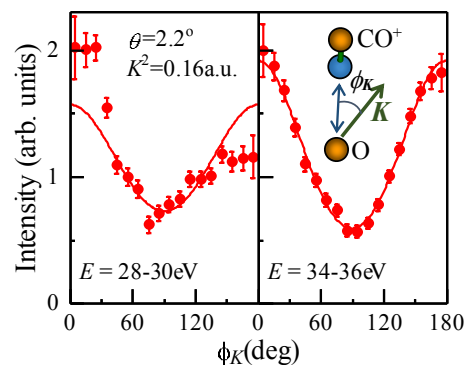


**Figure 1.** Angular distributions of CO<sup>+</sup> at scattering angle of  $\theta=2.2^\circ$ .

### References

- [1] Watanabe N and Takahashi M 2021 *Phys. Rev. A* **104** 032812
- [2] Watanabe N *et al* 2018 *Rev. Sci. Instrum.* **89** 043105.

\* E-mail: [noboru.watanabe.e2@tohoku.ac.jp](mailto:noboru.watanabe.e2@tohoku.ac.jp)

## Isomerization dynamics of triatomic molecules driven by the electron-impact

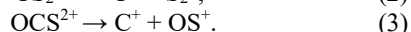
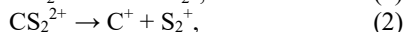
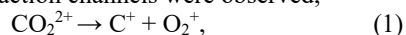
Lei Chen, Enliang Wang<sup>\*</sup>, Zhenjie Shen, Maomao Gong, Xu Shan, and Xiangjun Chen<sup>†</sup>

Hefei National Research Center for Physical Sciences at the Microscale and Department of Modern Physics, University of Science and Technology of China, Hefei 230026, China

**Synopsis** The isomerization dynamics of the dicationic states of CO<sub>2</sub>, CS<sub>2</sub>, and OCS were investigated. The dications were created by a high-energy nanosecond electron pulse and the fragment ions were detected by a momentum imaging time-of-flight spectrometer. The bond rearrangement reactions of C<sup>+</sup> + O<sub>2</sub><sup>+</sup>, C<sup>+</sup> + S<sub>2</sub><sup>+</sup>, and C<sup>+</sup> + OS<sup>+</sup> were identified by the coincident measurement. The kinetic energy releases (KERs) and the potential energy surfaces were studied.

The isomerization of polyatomic molecules by dissociative ionization has attracted interests in recent years since it plays an important role in the fields of chemistry, biochemistry, and astrochemistry. The isomerization of CO<sub>2</sub> [1,2] was considered as a potential mechanism for abiotic oxygen production in the planets' atmosphere.

In this work, we performed a systematic study of the isomerization dynamics of three polyatomic molecules, i.e., CO<sub>2</sub>, CS<sub>2</sub>, and OCS by electron impact double ionization. By means of coincident measurement of the fragment ions, the following bond rearrangement reaction channels were observed,



The corresponding KER distributions were obtained, as shown in Figure 1 (a) – (c) for channels (1) – (3), respectively.

We calculated the potential energy surfaces as a function of the reaction coordinate and the involved transition states. The theoretical investigations showed that the bond rearrangement of CO<sub>2</sub> and CS<sub>2</sub> happen via the decay of the excited dicationic state, while the bond rearrangement of OCS can open on the ground dicationic state.

The different isomerization mechanisms were ascribed to the symmetry effect. For the linear CO<sub>2</sub>, CS<sub>2</sub> molecules, the D<sub>∞h</sub> symmetry results in two terminal charges from the HOMO double ionization which do not correspond to the charge separation channels. And the isomerization channel can only open on the excited dicationic states. For OCS, the HOMO corresponds to the sulfur 3p lone-pair orbital and the double ionization is localized on sulfur atom. The following electron transfer creates a charge state on the carbon. In this way, the ground dicationic state can result in C<sup>+</sup> + OS<sup>+</sup> channel.

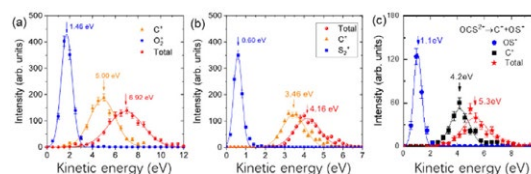


**Figure 1.** The kinetic energy distributions of channel (1) – (3) in (a) – (c), respectively.

### References

- [1] Lu Z, et al., 2014 Science **346** 61.
- [2] Wang X.-D. et al., 2016 Nat. Chem. **8** 258.

<sup>\*</sup> E-mail: [elwang@ustc.edu.cn](mailto:elwang@ustc.edu.cn)

<sup>†</sup> E-mail: [xjun@ustc.edu.cn](mailto:xjun@ustc.edu.cn)

## Quantum coherence induced by incoherent free electron scattering

Akshay Kumar<sup>1\*</sup>, Suvasis Swain<sup>2</sup> and Vaibhav S. Prabhudesai<sup>1†</sup>

<sup>1</sup>Tata Institute of Fundamental Research, Mumbai, 400005, India

<sup>2</sup>Centre de recherche sur les ions les matériaux et la photonique, Caen, France

**Synopsis** Quantum coherence is pivotal in various applications. An example of its manifestation in molecular dynamics is inversion symmetry breaking in the photodissociation of homonuclear diatomic molecules. Here we present, the most general scenario of non-resonant inelastic electron scattering inducing such a quantum coherence in molecular dynamics. The non-resonant nature of this process makes this effect generic and points to the possible prevalent role of such coherence in particle collision processes.

Quantum coherence is observed in photodissociation [1] in which two or more photons create different quantum paths that lead to the same final product and results in quantum interference[QI]. Recently E. Krishnakumar *et. al* [2] have shown the QI in dissociative electron attachment(DEA) that leads to forward-backward asymmetry in angular distribution with respect to the incident electron beam direction. However, both photodissociation and DEA are resonant processes. One of the most general processes is non-resonant electron scattering. Here, we will present how QI can manifest in non-resonant electron scattering of  $e^-$  from H<sub>2</sub>. The induced coherence caused by electron scattering leads to inversion symmetry breaking in the system and causes forward-backward asymmetry in angular distribution (figure 1(a)). The non-resonant nature of this process makes these results more general than the dissociative electron attachment or photodissociation processes that are resonant in nature. We explain this observation using the QI of two paths of opposite parities resulting in ion-pair formation.

The quantum coherence induced by the transfer of odd and even partial waves results in the transition of the molecule to the superposition of the two states from the Q1 band of H<sub>2</sub> with opposite parity and dissociating to the same limit. Being a scattering process, the coefficient of the involved transition has a dependence on the incident electron energy and impact parameter. We have carried out the corresponding simulations and compared the results with the experiment. The estimated asymmetry parameter as a function of incident electron energy and the impact parameter range is shown in figure 1(b) for H<sub>2</sub>. We also show the estimated values

for D<sub>2</sub>, which shows the isotope effect. Figure 1(c) shows the experimentally obtained asymmetry parameters for H<sub>2</sub> at various electron energies. The values match well with those obtained from the model for the typical impact parameter of 1.4 to 1.6 au which is very close to the typical bond length of the H<sub>2</sub> molecule in its ground state.

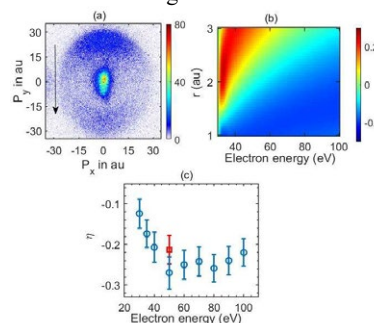


Figure 1. (a) Momentum image of H<sup>-</sup> from H<sub>2</sub> at 50 eV incident electron energy,  $e^-$  direction is from top to bottom. (b) The asymmetry parameter obtained from the model for H<sub>2</sub> as a function of incoming electron energy for various impact parameters. (c) Energy-integrated asymmetry parameters were obtained experimentally for H<sub>2</sub>. Also shown is the asymmetry parameter obtained for D<sub>2</sub> (red circle).

### References

- [1] Shapiro M, and Brumer P 2003 *Rep. Prog. Phys.* **66** 859.
- [2] Krishnakumar E, Prabhudesai V S, and Mason N J 2017 *Nat. Phys.* **14** 149.

\* E-mail: [akshay.kumar\\_167@tifr.res.in](mailto:akshay.kumar_167@tifr.res.in)

† E-mail: [vaibhav@tifr.res.in](mailto:vaibhav@tifr.res.in)

## Cold-target electron-ion-coincidence momentum-spectroscopy study of electron-impact single and double ionization of N<sub>2</sub> and O<sub>2</sub> molecules

S Jia<sup>1</sup>, J Zhou<sup>1</sup>, X Wang<sup>1\*</sup>, X Xue<sup>1</sup>, X Hao<sup>1</sup>, Q Zeng<sup>1</sup>, Y Zhao<sup>1</sup>, Z Xu<sup>1</sup>, A Dorn<sup>2</sup>, and X Ren<sup>1†</sup>

<sup>1</sup>School of Physics, Xi'an Jiaotong University, Xi'an 710049, China

<sup>2</sup>Max-Planck-Institut für Kernphysik, Saupfercheckweg 1, 69117 Heidelberg, Germany

**Synopsis** We report experimental studies of electron-impact ionization of nitrogen (N<sub>2</sub>) and oxygen (O<sub>2</sub>) molecules using a cold target recoil ion momentum spectrometer (COLTRIMS, reaction microscope). The ionization cross-sections for producing the doubly and singly charged parent ions were measured as a function of the incident electron energy ranging from 50 to 600 eV. The projectile energy-loss spectra correlated to the final-state ions were measured, which provide direct evidence of the ionization mechanisms of N<sub>2</sub> and O<sub>2</sub> molecules.

Dications play a significant role in atmospheric escape and ionization induced chemical reactions. The dications can be formed by direct double ionization (DI), in which two outer-valence electrons are ejected simultaneously, or an indirect process via inner-shell ionization and subsequent autoionization, i.e., Auger process.

As the most abundant components of the Earth's atmosphere, nitrogen (N<sub>2</sub>) and oxygen (O<sub>2</sub>) molecules are regarded as two benchmark targets whose ionization cross-sections have been studied extensively for understanding the DI mechanisms. The cross-section measurements generally rely on the detection of ion time of flight (TOF), which is difficult to distinguish the cations with identical mass-to-charge ratios, e.g., O<sub>2</sub><sup>2+</sup> and O<sup>+</sup> or N<sub>2</sub><sup>2+</sup> and N<sup>+</sup> ions. This could be a reason for the considerable discrepancies in the previous O<sub>2</sub><sup>2+</sup> cross-section measurements, and calls for experimental studies with additional methods.

In the present work, electron-impact ionization of N<sub>2</sub> and O<sub>2</sub> molecules is investigated with COLTRIMS. Here, we develop an approach to efficiently suppress the contributions of fragment ions from the intact dications with momentum boundary conditions on both TOF and position spectra (called TOF+POS condition).

The cross-section ratios between doubly and singly charged ions, i.e.,  $\sigma(\text{O}_2^{2+})/\sigma(\text{O}_2^+)$  and  $\sigma(\text{N}_2^{2+})/\sigma(\text{N}_2^+)$ , are presented in Fig. 1(a) and (b) as a function of the impact energy; also included in the figure are the data from previous experiments [1~4]. The distinct differences of  $\sigma(\text{O}_2^{2+})/\sigma(\text{O}_2^+)$  ratios between different experiments are mainly caused by the incomplete

suppression to the contribution of O<sup>+</sup> ions. The energy-loss spectra shown in Figs. 1(c) and (d) provide direct evidence of the ionization mechanisms for the dications. The O<sub>2</sub><sup>2+</sup> dication is produced mainly by Auger process after 2 $\sigma_g$  inner-shell ionization, while the N<sub>2</sub><sup>2+</sup> dication is generated by the direct removal of two electrons from the outermost 3 $\sigma_g$  orbital of N<sub>2</sub>.

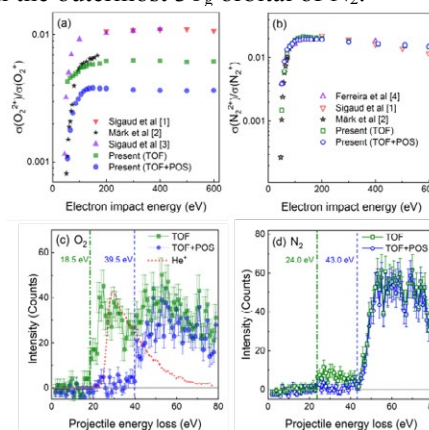


**Figure 1.** (a) Cross-section ratios between doubly and singly charged parent ions as a function of the impact energy for O<sub>2</sub>, and (b) for N<sub>2</sub> molecules. (c) Projectile energy-loss spectra correlated to the detected O<sub>2</sub><sup>2+</sup> and (d) N<sub>2</sub><sup>2+</sup> ions at the incident energy of 120 eV.

### References

- [1] L Sigaud and E Montenegro 2018 Phys. Rev. A. [98 052701](#).
- [2] T Märk 1975 J. Chem. Phys. [63 3731](#).
- [3] L Sigaud et al. 2013 J. Chem. Phys. [139 024302](#).
- [4] N Ferreira et al. 2012 Phys. Rev. A. [86 012702](#).

\* E-mail: [wangxingcn@xjtu.edu.cn](mailto:wangxingcn@xjtu.edu.cn)

† E-mail: [renxueguang@xjtu.edu.cn](mailto:renxueguang@xjtu.edu.cn)

## Modelling of the (e,2e) binary collision of water using the distorted wave Born approximation with single center expansion

M Dinger<sup>1,2\*</sup> and W Y Baek<sup>1</sup>

<sup>1</sup>Physikalisch-Technische Bundesanstalt (PTB), Braunschweig, 38116, Germany

<sup>2</sup>Ruprecht-Karls Universität Heidelberg, Heidelberg, 69117, Germany

**Synopsis** The distorted wave Born approximation was combined with a single center approach to obtain fully differential cross sections of water which showed good agreement with experimental data. Due to the combination of both models it is now possible, to obtain theoretical fully differential as well as integrated ionization cross sections with sufficient accuracy within a matter of seconds or days, respectively.

In radiotherapy accurate electron scattering cross sections are needed to provide optimal treatment planning as secondary electrons deliver a great part of radiation to the tumorous cells. However, due to the difficulties in experimental determinations, these cross sections of human tissue are only sparsely available. As a consequence, dose calculations often model human tissue as water with different densities, leading to higher uncertainties. An inaccurate dose can result in suboptimal treatment plans, which can potentially harm the patient. Therefore, efficient but accurate theoretical models are needed to determine the interaction cross sections for electrons within human tissue.

In this work, triply differential electron ionization cross sections (TDCS) of water (H<sub>2</sub>O) were calculated by the use of a theoretical model based on the distorted wave Born approximation (DWBA) and the single-center expansion (SCE) for the interaction potentials. The (e,2e) reaction is considered as an inelastic scattering between the incident electron and the individual orbitals of the target ground-state. The SCE was performed using the code SCeLib4 [1]. Without losing too much accuracy, the theoretical model employed in this work enables the calculation of fully differential ionization cross sections in reasonable time.

The theoretically obtained TDCS of the combined 3a<sub>1</sub>+1b<sub>1</sub> orbitals of water showed good agreement with the experimental data from Ren et al. [2] in coplanar asymmetric kinematics (see figure 1). In addition, integrating the TDCS over the emission angle of ejected electrons yields results agreeing qualitatively well with the binary

encounter Bethe model (BEB), which is known to be rather accurate at high incident energies.

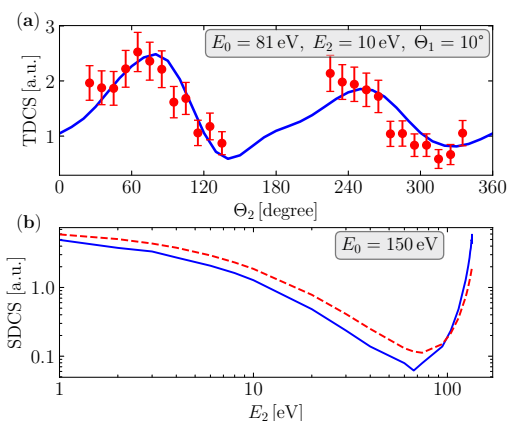


**Figure 1.** (a) TDCS of the combined 3a<sub>1</sub>+1b<sub>1</sub> orbitals in atomic units. The experimental data (●) were taken from [2]. (b) Singly differential cross section (SDCS) of the 3a<sub>1</sub> orbital in atomic units. The SDCS was determined using the DWBA (—) or BEB (---), respectively. The DWBA calculations were normalized to the experimental data or BEB, respectively. All relevant kinematic parameters are given in the figure, where  $E_0$  and  $E_2$  are the energies of the incident and ejected electrons, respectively, and  $\Theta_1$  and  $\Theta_2$  the scattering and emission angles.

### References

- [1] Sanna N, Morelli G, Orlandini S, Tacconi M and Baccarelli I 2020 *Comput. Phys. Commun.* **248** 106970
- [2] Ren X, Amami S, Hossen K, Ali E, Ning C, Colgan J, Madison D and Dorn A 2017 *Phys. Rev. A* **95** 022701

\*E-mail: [mareike.dinger@ptb.de](mailto:mareike.dinger@ptb.de)



## Investigation of the valence-shell excitations of CS<sub>2</sub> by high-energy electron scattering

Zhi-Wei Nie<sup>1</sup>, Shu-Xing Wang<sup>1\*</sup>, Li-Han Wang<sup>1</sup> and Lin-Fan Zhu<sup>1†</sup>

<sup>1</sup>Department of Modern Physics, University of Science and Technology of China, Hefei, Anhui 230026, China

**Synopsis** Absolute generalized oscillator strengths (GOS) of the valence-shell excitations of carbon disulfide (CS<sub>2</sub>) have been determined by a joint investigation of a fast electron impact experiment and an equation of motion coupled cluster with single and double excitations (EOM-CCSD) calculations. Based on the measured GOSs, the integral cross sections (ICS) of the valence-shell excited states from their excitation thresholds to 5000 eV have been obtained by means of the BE-scaling method. The oscillator strengths and integral cross-sections complement the fundamental data of carbon disulfide and can be used for modeling astrophysics and atmospheric observations.

Carbon disulfide (CS<sub>2</sub>) is one of the important species in astrophysical observation, which was identified in the emission spectra of Venus [1] and several comets [2, 3]. Moreover, about 5 tg yr<sup>-1</sup> of OCS in the earth's atmosphere could be generated from CS<sub>2</sub> [4, 5], and CS<sub>2</sub> is the primary precursor of the atmosphere pollutant SO<sub>2</sub> [6]. Therefore, the dynamic parameters of CS<sub>2</sub>, including its optical oscillator strengths (OOS), GOS and ICS are crucial for modeling the astronomically observed spectra and understanding its evolution in the earth's atmosphere.

In this work, the GOSs of the valence-shell excitations of CS<sub>2</sub> were determined at an incident electron energy of 1500eV and an energy resolution of 80meV. Besides, the GOSs for the <sup>1</sup>Δ<sub>u</sub>, <sup>1</sup>Σ<sub>u</sub><sup>+</sup> and 4σ<sub>g</sub><sup>1</sup>Π<sub>g</sub> states were calculated using EOM-CCSD method, which give a cross-check and help to determine the excitation character. The present electron energy loss spectrum at 3.5° and generalized oscillator strength density (GOSD) of CS<sub>2</sub> are shown in Figure 1. The momentum transfer dependence behaviors as shown in Figure 1(b) indicates that the <sup>1</sup>Δ<sub>u</sub> is a typical dipole-forbidden transition, while the <sup>1</sup>Σ<sub>u</sub><sup>+</sup> is a dipole-allowed transition. Moreover, the OOSs have been obtained by extrapolating the GOSs to the limit of the zero squared momentum transfer  $K^2 \rightarrow 0$ , and the ICSs of the valence-shell excitations from the threshold to 5000 eV have been

obtained systematically with the aid of the BE scaling method.

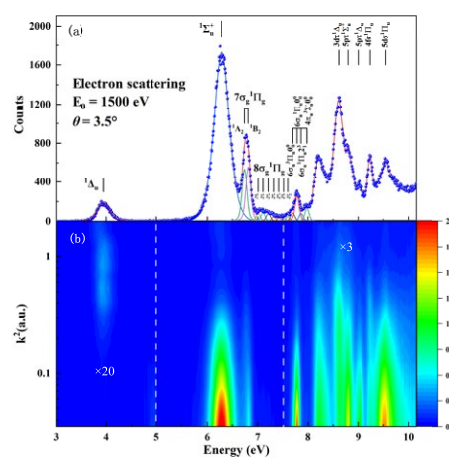


**Figure 1.** Electron energy loss spectrum at 3.5° and GOSD of CS<sub>2</sub>.

### References

- [1] S. S. Limaye et al 2018 *Space Science Reviews* **214** 102
- [2] W. M. Jackson et al 1986 *The Astrophysical Journal* **304** 515
- [3] H. A. Weaver et al 2003 *The Astronomical Journal* **126** 444
- [4] R. P. Turco et al 1980 *Nature* **283** 283
- [5] P. J. Maroulis et al 1980 *Geophysical Research Letters* **7** 681
- [6] J. A. Logan et al 1979 *Nature* **281** 185

\*E-mail: wangshuxing@ustc.edu.cn

†E-mail: lfzhu@ustc.edu.cn



## Isotopic selectivity in the metastable dication production of benzene

L Sigaud<sup>1</sup>\*, W. Wolff<sup>2</sup> and E C Montenegro<sup>2</sup>

<sup>1</sup>Instituto de Física, Universidade Federal Fluminense, Niterói, 24210-346, Brazil

<sup>2</sup>Instituto de Física, Universidade Federal do Rio de Janeiro, Rio de Janeiro, 21941-909, Brazil

**Synopsis** Double ionization of molecules trigger a competition process between fragmentation and stabilization in a molecular dication. We find experimentally that stabilization of benzene following an electron-impact-induced double-ionization is remarkably sensitive to the isotopic replacement of just one <sup>13</sup>C atom in the benzene ring. This result has no analog in dications of smaller molecules.

The double ionization of benzene initiates a competition between its fragmentation, driven by Coulombic repulsion, and its stabilization as a molecular dication. Nevertheless, from the fundamental neutral state to the metastable state with two fewer electrons the molecule undergoes a strong geometrical rearrangement of its constituents, with one of the carbon nuclei leaving the original geometrical plane, as shown in Figure 1.

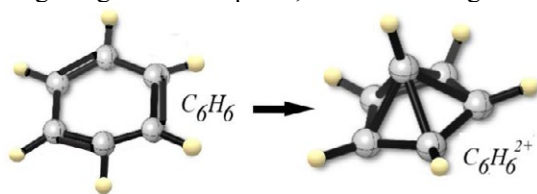


**Figure 1.** Pictorial representation of the change in the molecular geometry of benzene as it becomes a dication.

The mass spectrometry detection of the benzene dication is hindered by the difficulty of disentangling it from the molecular fragment  $C_3H_3^+$ , since both have the same mass-to-charge ratio ( $m/q$ ). Usually, in molecules with an even symmetry (e.g.  $N_2$  and  $O_2$  [1]), this problem is circumvented by means of an isotopic analogue of the molecular dication, providing a  $m/q$  different than the one for the molecule broken in half – in this case,  $^{13}C^{12}C_5H_6$  [2]. With the DETOF technique, the dication production for this class of molecules can be measured directly [3].

In this work, the double ionization of the benzene molecule was studied for electron impact ranging from 30 to 800 eV. Via the DETOF technique, the different kinetic energy distributions present for each peak of the time-of-flight spectra were determined. Thus, the molecular dication of benzene, which retains the same Max-

well-Boltzmann distribution as the parent molecule, can be distinguished from the  $C_3H_3^+$  fragment, which acquires kinetic energy in the break-up process. The dication production for the molecule with an isotopic substitution of <sup>13</sup>C in the aromatic ring was also obtained.

The experimental results [4] show that the stabilization after double ionization of the benzene molecule is extremely sensitive to this single carbon isotopic substitution. A difference of approximately 40% more production of  $^{12}C_6H_6^{2+}$  than that of  $^{13}C^{12}C_5H_6^{2+}$  was observed [4]. Since such discrepancy was never observed for smaller molecules, this result can be attributed to the conformational structural change in the benzene molecule when it loses two electrons. The nuclear rearrangement in the transient period to the new geometry seems to make fragmentation more likely when a mass asymmetry is introduced in the system.

These results represent, therefore, a paradigm shift regarding the use of isotopic analogues for obtaining dication production cross sections for molecules with an even symmetry, in particular when a significant molecular geometry change occurs in the process. This selectivity should be investigated for other isotopically-substituted aromatic compounds.

### References

- [1] Märk T D 1975 *J. Chem. Phys.: Conf. Ser.* **63** 3731
- [2] Wolff W *et al.* 2020 *J. Phys. Chem. A* **124** 9261
- [3] Sigaud L and Montenegro E C 2020 *J. Phys.: Conf. Ser.* **1412** 052007
- [4] Sigaud L, Wolff W and Montenegro E C 2022 *Phys. Rev. A* **105** 032816

\* E-mail: [lsigaud@id.uff.br](mailto:lsigaud@id.uff.br)

## Absolute cross sections for ionization and fragmentation of CO<sub>2</sub> by electron impact

A B Monteiro-Carvalho<sup>1\*</sup>, L Sigaud<sup>1†</sup> and E C Montenegro<sup>2</sup>

<sup>1</sup>Instituto de Física, Universidade Federal Fluminense, Niterói, 24210-346, Brazil

<sup>2</sup>Instituto de Física, Universidade Federal do Rio de Janeiro, Rio de Janeiro, 21941-909, Brazil

**Synopsis** Absolute cross sections for the ionization of CO<sub>2</sub> by electron impact has been the subject of many studies throughout the past decades, but data have shown many discrepancies. In this work we present new results that corroborate some of the previously measured data but expand it to a wider impact energy range.

Carbon dioxide is one of the most studied molecules due to its impact in the Earth's atmosphere, besides its presence in other planets and applications in the industry, such as lasers and low-temperature plasmas devices. In these media, the ionization of the molecule and how it fragments into smaller products play a crucial role to describe the system correctly.

Therefore, many laboratories, throughout the past decades, have housed electron-impact ionization measurements of CO<sub>2</sub>. Different groups (e.g. Rapp and Englander-Golden [1], Orient and Srivastava [2], Straub et al. [3], Lindsay and Mangan [4] and Tian and Vidal [5]) have reported data, but discrepancies among them are shown to be rampant, as one can see in Figure 1. It should be remarked that absolute cross sections for all ionic fragments are constrained to the total cross section values.

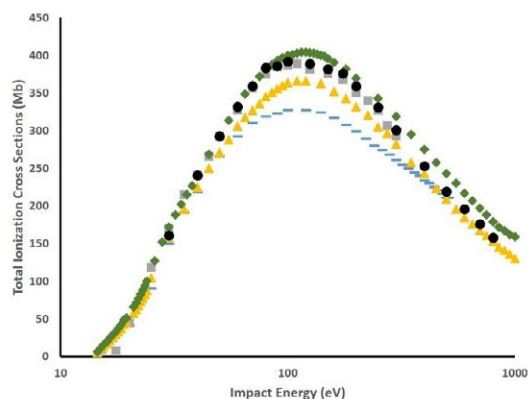


**Figure 1.** Total ionization cross section data for CO<sub>2</sub> by electron impact: black circles, this work; grey squares, Tian and Vidal [5]; green lozenges, Rapp and Englander-Golden [1]; blue traces, Orient and Srivastava [2]; and yellow triangles, Lindsay and Mangan [4], combining low

impact energy data from Rapp and Englander-Golden [1] and renormalized data from Straub et al. [3].

In this work we perform new data collection for the electron-impact ionization of CO<sub>2</sub>. The experimental setup consists of an electron gun operating in the 30–800 eV energy range coupled to a Time-of-Flight mass spectrometer and a pressure-controlled gas cell target. Argon ionization measurements were also performed, for different impact energies, in order to assure the efficiency calibration of the whole apparatus [6].

The new data presented here agrees well with the data from Tian and Vidal [5], as can be seen in Figure 1, who guaranteed that no ions were lost before detection due to fragmentation resulting in fast products leaving the collection area of the spectrometer. We guarantee the same aspect by using the DETOF technique [6], and expand the impact energy range of their data.

Furthermore, fragmentation cross sections for all fragments – including the never before reported O<sub>2</sub><sup>+</sup> – have also been obtained.

### References

- [1] Rapp D and Englander-Golden P 1965 *J. Chem. Phys.* **43** 1464
- [2] Orient O J and Srivastava S K 1987 *J. Phys. B: At. Mol. Phys.* **20** 3923
- [3] Straub H C, Lindsay B G, Smith K A and Stebbings R F 1996 *J. Chem. Phys.* **105** 4015
- [4] McConkey J W, Malone C P, Johnson P V, Winstead C, McKoy V and Kanik I 2008 *Phys. Rep.* **466** 1
- [5] Tian Cechan and Vidal C R 1998 *J. Chem. Phys.* **108** 927
- [6] Sigaud L, de Jesus V L B, Ferreira Natalia and Montenegro E C 2016 *Rev. Sci. Instrum.* **87** 083112

\* E-mail: [anabeatrizcarvalho@id.uff.br](mailto:anabeatrizcarvalho@id.uff.br)

† E-mail: [lsigaud@id.uff.br](mailto:lsigaud@id.uff.br)

## Low energy electron interaction with the potential extreme ultraviolet resist material component 2-(trifluoro-methyl) acrylic acid.

R Tafrishi<sup>1</sup>, D Torres-Diaz<sup>2</sup>, L Amiaud<sup>2</sup>, A Kamali, A Lafosse<sup>2</sup>, O Ingólfsson<sup>1\*</sup>

<sup>1</sup>Science Institute and Department of Chemistry, University of Iceland, Dunhagi 3, 107 Reykjavik, Iceland

<sup>2</sup>Université Paris-Saclay, CNRS, Institut des Sciences Moléculaires d'Orsay, 91405 Orsay, France

**Synopsis** Dissociative ionization and dissociative electron attachment of 2-(trifluoro-methyl) acrylic acid is studied in relation to its potential use as EUVL resist component.

With the current transition from the deep ultraviolet lithography (DUVL) to extreme ultraviolet lithography (EUVL) in chip manufacturing processes, come significant challenges. Many of these are technical in nature as the generation of the 13.5 nm light is not straight forward and its handling is difficult. [1] However, the fact that the current resist materials are optimized for DUV (193 - 248 nm), is also a challenge in this transition.[2] This is particularly true, as the current photoresists are optimized for photochemical response in the DUV wavelengths regime. The 13.5 nm light, on the other hand, is ionizing radiation at a photon energy of 92 eV and the chemistry induced within the resist is electron driven. Moreover, inelastic scattering of the generated photoelectrons within the matrix, leads to a broad electron energy distribution. Correspondingly a significant number of different reaction channels may be open through dissociative ionization (DI), dissociative electron attachment (DEA) and neutral and dipolar dissociation upon electronic excitation (ND and DD, respectively) [3]. The advancement of EUVL resist material is thus critically dependent on funded understanding of the electron induced chemistry triggered within this energy range.

Here we present a study on low energy electron induced fragmentation of 2-(trifluoro-methyl) acrylic acid (TFMAA). This compound is a potential resist component, specifically as fluorination is known to enhance the EUV absorption. Moreover, the fluorination along with the acetic hydrogens at the carboxylic group and the CH<sub>2</sub> side group, allow for H...F intramolecular hydrogen-bonding and cleavage of neutral HF from the respective ionized species. This provides the close to 6 eV bond energy of HF into the dissociation process, and specific-

ly in dissociative electron attachment, the introduction of this channel has been shown to significantly enhance fragmentation [4, 5].

In the current study both DI and DEA in the gas phase under single collision conditions are considered. The appearance energies of individual fragments are determined and quantum chemical calculations at the DFT and coupled cluster level of theory are used to aid the interpretation of the experimental data.

As is to be expected, fragmentation through DI is found to be significantly more extensive than through DEA. In fact, the only significant DEA channel observed is the cleavage of HF from the transient negative ion formed in the attachment process. Loss of neutral HF is also found to play a significant role in DI as well as neutral CO<sub>2</sub> formation, and in general the DI processes are characterized by rearrangements and new bond formations rather than the cleavage of single bonds.

The observed fragmentation reactions are discussed in relation to the underlying reaction mechanisms and potential implications for the suitability of TFMMA as a component of EUVL resist materials.

### References

- [1] Wood OR 2017 J Photopolym Sci Technol. 30(5), 599-604
- [2] De Simone D 2017 J Photopolym Sci Technol. 30(5), 613-617
- [3] Ingólfsson O 2019 Low-Energy Electrons Fundamentals and Applications, Jenny Stanford Publishing, New York.
- [4] Ómarsson B et al. 2013 Phys. Chem. Chem. Phys. 15 (13), 4754-4766
- [5] Cipriani M and Ingólfsson O 2022 Int. J. Mol. Sci. 23 (5)

\* E-mail: [odduring@hi.is](mailto:odduring@hi.is)

## Signatures of ICD from heterocycle dimers and heterocycle-water complexes

D M Mootheril<sup>1\*</sup>, X Ren<sup>1,2†</sup>, T Pfeifer<sup>1</sup>, A Dorn<sup>1‡</sup>

<sup>1</sup>Max-Planck-Institute of Nuclear Physics, Heidelberg, 69115, Germany

<sup>2</sup>School of Physics, Xi'an Jiaotong University, Xi'an, 710049, China

**Synopsis** We study the Coulomb explosion (CE) of thiophene dimers and pyridine-water complexes induced by electron collisions (109 eV) using the (e,2e+ion) coincidence technique. Signatures of intermolecular Coulombic decay (ICD) have been identified in both systems. Comparison of projectile energy loss spectra with theoretical single ionization spectra shows the ICD predominantly proceeds from the C  $2s^{-1}$  inner valence vacancy in thiophene dimers and from the O  $2s^{-1}$  and the N  $2s^{-1}$  inner-valence vacancies in pyridine-water clusters.

Inter-atomic/intermolecular Coulombic decay (ICD) is an important electronic relaxation mechanism after inner-valence ionization of atoms or molecules with weakly bound neighbours. ICD has been experimentally studied in variety of atomic and molecular clusters using electron-ion coincidence spectroscopic techniques. It is known that ICD can mediate radiation damage in biologically relevant molecules. Experimental evidence has identified that ICD can trigger alpha-cleavage in hydrated tetrahydrofuran (THF) after inner valence ionization of the O  $2s^{-1}$  orbital in water and THF [1].

Here, we study ICD following inner valence ionization induced by the collision of electrons with an energy of 109 eV with thiophene dimers and pyridine-water clusters that contain the heteroatoms sulfur and nitrogen, respectively. Experimental results suggest that the energy released after relaxation to the inner valence vacancy is transferred to the neighbouring molecule, predominantly via ICD, and ionizes the outer valence orbital of the neighbor. The dicationic state thus produced, with charges on both neighbouring molecules, induces Coulomb explosion of the dimer. Ionic fragments are detected in coincidence with one of the outgoing electrons using the multi-particle momentum spectrometer 'Reaction microscope,' and the momentum vectors are reconstructed [2].

The electron energy loss spectrum for Coulomb explosion of the thiophene dimer shows an onset at 20 eV, indicating the creation of an inner valence vacancy, C  $2s^{-1}$ , which triggers the

\*E-mail: [deepthy.mootheril@mpi-hd.mpg.de](mailto:deepthy.mootheril@mpi-hd.mpg.de)

†E-mail: [renxueguang@xjtu.edu.cn](mailto:renxueguang@xjtu.edu.cn)

‡E-mail: [alexander.dorn@mpi-hd.mpg.de](mailto:alexander.dorn@mpi-hd.mpg.de)

energy transfer. It is compared with the energy loss spectrum for the monomer inner valence ionization channel, which undergoes fragmentation to produce  $C_3H^+$  ions. The strong resemblance between the spectra suggests energy transfer via ICD to the weakly bound neighbour. Similarly, the energy loss spectrum for CE of pyridine-water dimer, with an onset at 29.5 eV, is comparable to that of the O  $2s$  inner valence ionization of water, which produces  $O^+$  ions. A comparison with the theoretical single ionization spectrum for the pyridine-water complex suggests that an inner-valence vacancy at pyridine (N  $2s^{-1}$ ) close to this energy region can also relax via ICD [3].

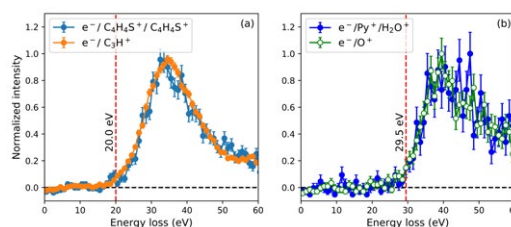


**Figure 1.** Projectile energy loss spectra for (a) Coulomb explosion of thiophene dimer and C  $2s$  inner valence ionization of thiophene monomer and (b) Coulomb explosion of pyridine- $H_2O$  dimer and O  $2s$  inner valence ionization of water.

### References

- [1] X. Ren *et al* 2018 *Nature Physics* **14**(10) 1062-1066
- [2] R. Moshhammer *et al* 1994 *Phys. Rev. Lett* **73** 3371
- [3] A. D. Skitnevskaya *et al* 2023 *J. Phys. Chem. Lett.* **14**(6) 1418-1426

## R-Matrix investigations of low-energy positron scattering from biomolecules

V Graves<sup>1\*</sup>, and J D Gorfinkiel<sup>1</sup>

<sup>1</sup>School of Physical Sciences, The Open University, Walton Hall, Milton Keynes, UK

**Synopsis** When modelling low energy lepton scattering from biomolecules, accurately describing polarization effects is very important. In positron scattering, this description is particularly crucial, since exchange effects are not present. Conventional scattering approaches struggle to model the interaction targets with high polarizability. Here, improvements to this description are investigated.

Modelling low energy lepton scattering from molecules has applications in many areas. Specifically, PET scans used in medicine to provide highly detailed images of biological matter involve the production inside the body. The focus of the work presented here is to provide data on low energy positron collisions which can be used in combination with higher energy data to model positron interactions with biological matter.

We use the R-Matrix method as implemented in the UKRmol+ suite [1]. In this method, the low energy lepton scattering problem is separated into an inner region, where the projectile-target molecule interaction is accurately described, and an outer region, where correlation and exchange can be neglected. Within the R-Matrix method, polarization effects are modelled by including configurations in the expansion of the inner region target + projectile wave function that correspond to excitations from the ground state configuration. These effects are particularly crucial at low scattering energy, when the projectile spends more time in the interaction region of the molecule. For positron scattering, there is no exchange and, as a result, the accuracy of the polarization and correlation/anti-correlation description become crucial.

We have investigated methods for improving the polarization description in R-matrix calculations of positron and electron scattering from highly polarizable biomolecules. These include using the Polarization Consistent Coupled Hartree-Fock method [2] and enhancing the electron-positron attraction integrals [3].

The effect from these methods can be seen in Figure 1 that presents positron scattering from furan which has a spherical polarizability of 48.79 Å. It can be seen that the Static plus

\*E-mail: [vhg7@open.ac.uk](mailto:vhg7@open.ac.uk)

Polarization (SP) calculations, with or without the enhancement factor, as well as the PCCHF approach underestimate the size of the cross section. Inclusion of a Born correction is unlikely to resolve this discrepancy. Note that the step-like shape of the experimental cross section is due to different acceptance angles at different scattering energies.

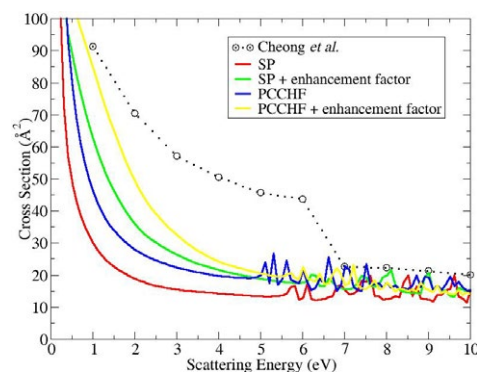


**Figure 1.** Elastic cross section for positron scattering from furan calculated using different models and compared with experimental results [4]. No Born correction is included in the calculations shown. The spikes in the cross sections are pseudoresonances.

### References

- [1] Mašín Z, Benda J, Gorfinkiel J D, Harvey A G, and Tennyson J 2020 *CPC* **249** 107092
- [2] Meltzer T and Mašín Z 2022 *J. Phys. B: At. Mol. Opt. Phys.* **55** 035201
- [3] Franz J, Baluja K L, Zhang R, and Tennyson J 2008 *NIM-B* **3** 266
- [4] Cheong Z, Moreira G M, Bettgega M H F, Blanco F, Garcia G, Brunger M J, White R D, and Sullivan J P 2020 *J. Chem. Phys.* **24** 153



## An iterative negative imaginary potential applied to the Schwinger multichannel method to model ionization effects

A G Falkowski<sup>1\*</sup>, R F da Costa<sup>2</sup>, F Kossoski<sup>3</sup>, M A P Lima<sup>1</sup>

<sup>1</sup>Instituto de Física Gleb Wataghin, Universidade Estadual de Campinas, Campinas, 13083-872, Brazil

<sup>2</sup>Centro de Ciências Naturais e Humanas, Universidade Federal do ABC, 09210-580, Brazil

<sup>3</sup>LCPQ (UMR 5626), Université de Toulouse, CNRS, UPS, France

**Synopsis** In order to mimic the ionization effects in the electron-molecule collisions described with the Schwinger multichannel method, we implemented a negative imaginary potential to act as a sinkhole of probability flux. We employed an iterative procedure to reproduce the ionization cross sections computed with the BEB approach.

The many-body problem (including for instance electron scattering by molecules) is a complicated task to solve since it is theoretically impossible to find the exact wave function for multielectronic systems. A variety of approximations should be made to tackle electron-molecule collisions. The Schwinger Multichannel method (SMC) implemented with pseudopotentials [1], a variational method for the scattering amplitude is one of these approaches. However, to date, only the elastic and electronic excitation channels (involving transitions between bound states) could be addressed within the SMC method. To work around this limitation, we implemented a negative imaginary potential (NIP)  $V = V_0 - iW_0$  to act as a sinkhole of probability flux, where  $V_0$  is the electron-molecule interaction potential and  $W_0$  is the model potential for ionization, as suggested in Ref. [2]. The model potential is a single Gaussian function, parameterized to fit the total ionization cross sections (TICS) as obtained with the Born-Encounter-Bethe (BEB) method [3].

To improve the computed absorption integral cross sections (AICS), that is, the difference between the total cross sections (TCS) and elastic integral cross sections (EICS), we developed an iterative procedure to obtain NIPs such that the computed AICS matches the TICS obtained with the Born-Encounter-Bethe (BEB) method. As the magnitude of  $W_0$  accounts for how much flux probability is stolen through the NIP, we developed a normalization function to scale it as

$$\zeta_N(E_i) = \frac{\sigma_{\text{BEB}}}{\sigma_{\text{a},N-1}} \prod_{j=0}^{N-1} \zeta_j(E_i)$$

where  $N$  is the number of iterations,  $\zeta_0(E_i)$

is a quadratic function of incident electron impact energy  $E_i$ . Also,  $\sigma_{\text{BEB}}$  is the TICS calculated with the BEB approach, and  $\sigma_{\text{a},N-1}$  is the AICS obtained when the NIP is included, at the  $(N-1)$ -iteration. The final form of the potential is  $V = V_0 - i\zeta_N(E_i)W_0$ .

We applied this new technique to investigate the electron scattering by  $\text{H}_2$  molecules at the static-exchange (SE) approximation, as shown in Fig. 1. Preliminary results are encouraging since we observe a drop in the magnitude of the EICS due to the presence of the NIP. This feature stimulates the studying the effect of this strategy on multichannel calculations.

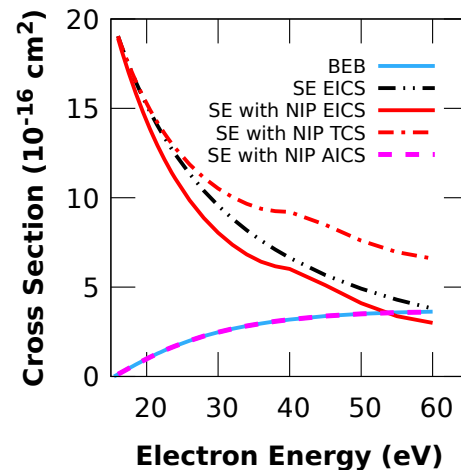


**Figure 1.** Cross sections for electron scattering by  $\text{H}_2$  molecules.

### References

- [1] da Costa R F *et al.* 2015, *Eur. Phys. J. D* **69** 159
- [2] Falkowski A G *et al.* 2021, *Eur. Phys. J. D* **75** 308
- [3] Kim Y-K and Rudd M E 1994, *Phys. Rev. A* **50**, 3954

\*E-mail: [agf18@ifi.unicamp.br](mailto:agf18@ifi.unicamp.br)



## Interaction of Singly Charged Sodium Ion with Nitrogen Atom: Total and Differential Ionisation Cross Sections

M. Al-Ajaleen<sup>1,2</sup>, and K.Tökési<sup>2,3\*</sup>

<sup>1</sup>Institute for Nuclear Research (ATOMKI), Debrecen, 4026, Hungary

<sup>2</sup>University of Debrecen, Doctoral School of Physics, 4032 Debrecen, Egyetem tér 1, Hungary

<sup>3</sup>Centre for Energy Research, Budapest, Hungary

**Synopsis** We present total and differential cross sections for single ionization in collision between  $\text{Na}^+$  ions with  $\text{N}(2p)$  atom. We used the Garvey model potential and the classical trajectories Monte Carlo (CTMC) method to model the collision system. We present total ionisation cross sections in the energy range between 10 keV to 100 MeV and single/double differential cross sections for impact energies of 30, 40, 50 and 60 keV.

The electron processes play a significant role in radiation physics, the study of atomic and molecular structures, fusion plasma, and other research domains. In tokamak, atoms are used as a neutral diagnostic beams, such as helium and nitrogen [1].

In our work, we present total and differential cross sections for single ionization in collision between  $\text{Na}^+$  ions with  $\text{N}(2p)$  atom.

We modelled the collision system as a three body system using Garvey model potential [2]. The target is separated into a single active electron and nitrogen core (i.e., nitrogen nucleus and its remaining non-active electrons), the projectile  $\text{Na}^+$  with its electrons are considered as a single particle. This model potential invokes the effective charge for a given particle, hence, it considers the screening effect of the non-active electrons. The equations of motion of the collisions system are solved numerically using classical trajectories Monte Carlo CTMC method [3].

We present the total ionisation cross section as a function of the impact energy in the energy range between 10 keV to 100 MeV. Moreover, we present the single (SDCS) and double (DDCS) differential cross sections for impact energy range of 30-60 keV as a function of the ejected electron energies and angles.

We found that the dominant contribution of the Double Differential Cross Sections (DDCS) are achieved by electrons with energies below 10 eV and ejection angles under 20 degrees. Moreover, electrons ejected with energies larger than 20 eV have shown very small angular dependence [4].

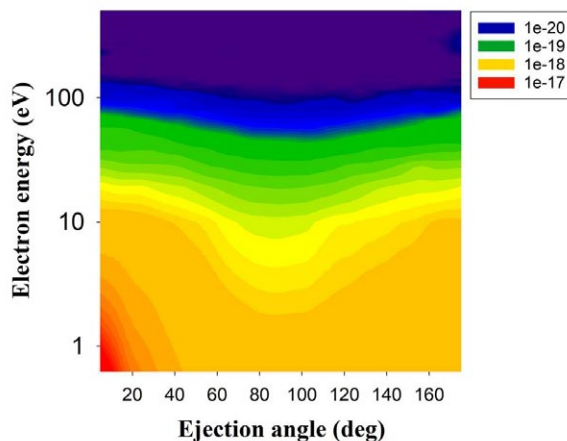


**Figure 1.** Double differential cross section (DDCS) of the single ionization in collision between  $\text{Na}^+$  ions with  $\text{N}(2p)$  atom as a function of the ejected electron energies and ejection angles at impact energy of 30 keV.

### Acknowledgements

This work has been carried out within the framework of the EUROfusion Consortium, funded by the European Union via the Euratom Research and Training Programme (Grant Agreement No 101052200 — EUROfusion). Views and opinions expressed are however those of the author(s) only and do not necessarily reflect those of the European Union or the European Commission. Neither the European Union nor the European Commission can be held existingible for them.

### References

- [1] Patel M et al., 2021 *Vacuum* **192** 110440.
- [2] Garvey R.H. et al., 1975 *Phys. Rev. A* **12** 1144.
- [3] Tökési K. et al., 1994 *Nucl. Instrum. Methods Phys. Res. B: Beam Interact. Mater. At.* **86** 201.
- [4] Al-Ajaleen M and Tökési K, to be published.

\* E-mail: [tokesi@atomki.hu](mailto:tokesi@atomki.hu)

## Interaction of Protons with Noble Gas Atoms: Total and Differential Ionisation Cross Sections

M. Al-Ajaleen<sup>1,2</sup>, and K.Tőkési<sup>2,3\*</sup>

<sup>1</sup>Institute for Nuclear Research (ATOMKI), Debrecen, 4026, Hungary

<sup>2</sup>University of Debrecen, Doctoral School of Physics, 4032 Debrecen, Egyetem tér 1, Hungary

<sup>3</sup>Centre for Energy Research, Budapest, Hungary

**Synopsis** We present total and differential cross sections for single ionisation in the collision of protons with Ne, Ar, Kr and Xe. We used the Garvey model potential and the classical trajectories Monte Carlo (CTMC) method to model the collision system. We present the total ionisation cross sections in the energy range between 10 keV and 100 MeV and the ionisation differential cross sections for an impact energy of 35 keV.

Electron processes have a crucial impact on various fields of study, such as radiation physics, atomic and molecular structures, and fusion plasma research. In the context of tokamaks, neutral atom beams are used as diagnostic tools[1].

The aim of our present work is to provide total and differential cross sections for single ionization in collisions between  $H^+$  with Ne(2p) Ar(3p) Kr(4p), Xe(4d) and Xe (5p).

To model our collision systems we used the 3-body classical trajectory Monte Carlo technique. The interactions among the particles are taken into account with the Garvey model potential [2]. The target was split into a single active electron and the target core consisting of the nucleus and remaining non-active electrons. The projectile  $H^+$  was the third particle. This model potential takes into account the effective charge of the target, incorporating the screening effect of non-active electrons. The classical equation of motions were solved numerically using the adaptive Runge-Kutta method, the step size depends on the initial parameters of all particles [3]. We present results both for the charge transfer and ionisation total cross section as a function of the impact energy. Moreover, we also present single (SDCS) and the double (DDCS) differential cross sections as functions of the ejected electron energies and angles at an impact energy of 35 keV.

We compared our cross sections with the existing experimental data, and with the previous theoretical data like first Born approximation (FBA), Oppenheimer-Brinkman-Kramers (OBK) approximation, and the results of the

two-state two-centre atomic expansion model [4].

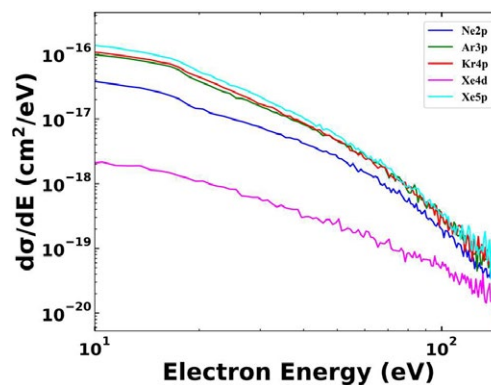


**Figure 1.** Single differential cross section (SDCS) as a function of the ejected electron energies at impact energy 35 keV.

### Acknowledgements

This work has been carried out within the framework of the EUROfusion Consortium, funded by the European Union via the Euratom Research and Training Programme (Grant Agreement No 101052200 — EUROfusion). Views and opinions expressed are however those of the author(s) only and do not necessarily reflect those of the European Union or the European Commission. Neither the European Union nor the European Commission can be held existingible for them.

### References

- [1] Patel M et al., 2021 Vacuum [192 110440](#).
- [2] Garvey R.H. et al., 1975 Phys. Rev. A [12 1144](#).
- [3] Tőkési K. et al., 1994 Nucl. Instrum. Methods Phys. Res. B: Beam Interact. Mater. At. [86 201](#).
- [4] Al-Ajaleen M and Tőkési K, to be published.

\* E-mail: [tokesi@atomki.hu](mailto:tokesi@atomki.hu)

## Experimental study of single electron capture in 150 keV $O^{5+} + He$ collisions

Y Gao<sup>1,2</sup>, T Cao<sup>1,2</sup>, K Z Lin<sup>1,3</sup>, D L Guo<sup>1,2</sup>, S F Zhang<sup>1,2\*</sup>, X L Zhu<sup>1,2</sup>, R T Zhang<sup>1,2</sup>, S C Yan<sup>1,2</sup>, S Xu<sup>1,2</sup>, D M Zhao<sup>1,2</sup>, and X Ma<sup>1,2†</sup>

<sup>1</sup> Institute of Modern Physics, Chinese Academy of Sciences, Lanzhou 730000, China

<sup>2</sup> School of Nuclear Science and Technology, University of Chinese Academy of Sciences, Beijing 100049, China

<sup>3</sup> Hefei National Laboratory for Physical Sciences at Microscale and Department of Modern Physics, University of Science and Technology of China, Hefei, Anhui 230026, China

**Synopsis** We have performed an experiment on single electron capture from He impacted by 150 keV  $O^{5+}$  employing a new reaction microscope with a novel focus method of the time of flight spectrometer (TOF). It is observed that almost all of transfer electrons are captured into M shell of  $O^{5+}$ . By fitting the experimental data, we find that the contribution of the triplet state of  $^3S$  ( $2s3s$ ) is about 3 times that of  $^1S$  ( $2s3s$ ) state.

Charged transfers between highly charged ion (HCI) projectiles and neutral atomic and molecular target gases has been a subject of intense research for a long time because of the fundamental physics interest and the practical application value [1, 2]. To investigate them, we developed a new quasi-longitudinal reaction microscope in Lanzhou, China. Its time-of-flight spectrometer (TOF) uses a new flight time focusing method with two accelerating regions, which can achieve ideal focusing condition without limiting the length ratio of the two accelerating regions for charged fragments with any initial speed. The TOF axis is tilted by an angle of  $12^\circ$  with respect to the ion beam direction to avoid the TOF grid electrodes intercepting projectile ion beam.

We have performed an experiment on single electron capture from He impacted by 150 keV  $O^{5+}$  employing the reaction microscope. In the light of its high momentum resolution, the states with different angular quantum numbers are identified, as showed in Fig. 1. The experimental result reveals that all of transfer electrons are captured into M shell of  $O^{5+}$ . This does not fulfill the classical energy-matching rule [3] which anticipates these electrons to be mainly transferred into N shell of  $O^{5+}$ . Furthermore, the subshells of 3s, 3p and 3d have comparable contributions. The phenomenon implies that angular quantum number does not seem to affect the probability that the captured electrons populate into the subshell for the present reaction. By fitting the experimental data, we find that the contribution of

the triplet state of  $^3S$  ( $2s3s$ ) is about 3 times that of  $^1S$  ( $2s3s$ ) state. The similar conclusion is valid for  $2s3d$  configuration. This means that the probability depends significantly on the spin quantum number in the present collision reaction.

The further understanding of the experimental data expects the accurate calculations of Quantum mechanics.

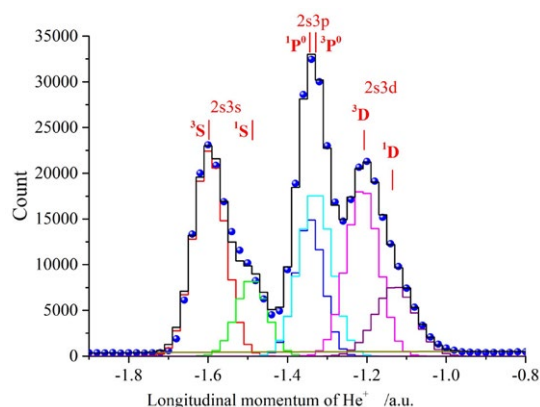


**Figure 1.** The longitudinal momentum of the recoil ion He in 150 keV  $O^{5+} + He \rightarrow O^{4+} + He^+$ .

### References

- [1] Janev R K, Presnyakov L P, 1981 Phys. Rep. [70 1](#)
- [2] Janev R K, Winter H 1985 Phys. Rep. [117 265](#)
- [3] Warczaki A, Liesen D and Liu B 1986 J. Phys. B: At. Mol. Phys. [19 3975](#)

\* E-mail: [zhangshf@impcas.ac.cn](mailto:zhangshf@impcas.ac.cn)

† E-mail: [x.ma@impcas.ac.cn](mailto:x.ma@impcas.ac.cn)

## Measurements of the single and double electron capture cross sections in $O^{6+} + He$ collisions

T Meng<sup>1</sup>, B Ren<sup>1</sup>, Z Xia<sup>1</sup>, P Ma<sup>1</sup>, J Wang<sup>1</sup>, M X Ma<sup>1</sup>, B Tu<sup>1</sup>, Y Zou<sup>1</sup> and B Wei<sup>1\*</sup>

<sup>1</sup> Institute of Modern Physics, Key Laboratory of Nuclear Physics and Ion-Beam Application (MOE), Fudan University, Shanghai, 200433, China

**Synopsis** Single and double electron capture between incident  $O^{6+}$  ions and target He gas are studied with measurements on their total and state-selective cross sections in the energy range of 2.625 – 37.5 keV/u, of which the state-selective ones are measured by a cold target recoil ion momentum spectroscopy at Fudan University.

Electron capture (EC), as an indispensable collision mechanism in low energy region [1], has received close attention from both fundamental physics and applied physics for nearly half a century. Due to the non-negligible abundance in many plasma environments like interstellar medium or tokamak [2, 3] and simple structure for theoretical researches, EC between helium-like  $O^{6+}$  and neutral He are significant study objects.

Based on the Highly Charged Ions Collision Platform at Fudan University constructed with a 14.5 GHz electron cyclotron resonance (ECR) ion source, we have achieved the total and state-selective cross sections for the electron(s) captured into  $O^{5+}(1s^2nl)$  or  $O^{4+}(1s^2nln'l')$  from He( $1s^2$ ) in the energy range of 2.625 – 37.5 keV/u through the growth-rate method [4] and the longitudinal momentum spectrum of recoil He ions [5] measured by a cold target recoil ion momentum spectroscopy (COLTRIMS), respectively.

Figure 1 shows the present experimental results of EC cross sections. In the energy range of 2.625 – 37.5 keV/u, the total cross sections are stable for both single and double EC, while the state-selective ones demonstrate various trends which may provide new insights for collision dynamics. All the results of single EC have been validated through comparisons with correlated data reported by Dijkkamp [6], Iwai [7] and Fritsch [8], which are not shown here because of the format restriction. More details can be found in the poster during the ICPEAC 2023 conference.

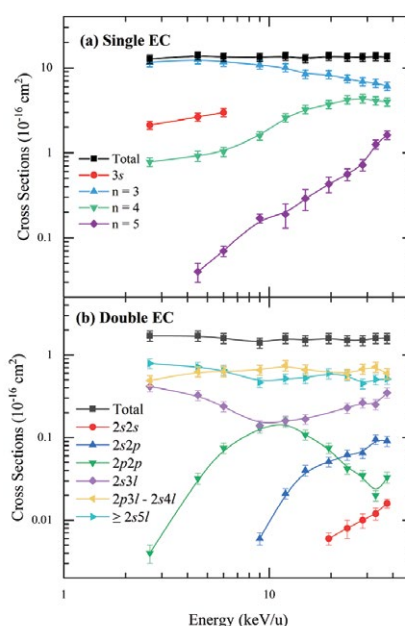


**Figure 1.** The present experimental single and double EC cross sections as a function of impact energy.

### References

- [1] Greenwood J B *et al* 2004 *Phys. Scr.* **2004** 358
- [2] von Steiger R *et al* 2000 *J. Geophys. Res.* **105(A12)** 27217
- [3] Matthews G F 1989 *J. Nucl. Mater.* **162-164** 38
- [4] Han J *et al* 2021 *ApJS* **253** 6
- [5] Xia Z H *et al* 2022 *ApJ* **933** 207
- [6] Dijkkamp D *et al* 1985 *J. Phys. B: Atom. Mol. Phys.* **18** 737
- [7] Iwai T *et al* 1982 *Phys. Rev. A* **26** 105
- [8] Fritsch W and Lin C D 1986 *J. Phys. B: Atom. Mol. Phys.* **19** 2683

\* E-mail: [brwei@fudan.edu.cn](mailto:brwei@fudan.edu.cn)

## L-MM Auger electron emission in Ar<sup>q+</sup> - Ar Collision

Rohit Tyagi<sup>1\*</sup>, S K Maurya<sup>2</sup>, L. C. Tribedi<sup>2</sup> and A. H. Kelkar<sup>1†</sup>

<sup>1</sup> Department of Physics, Indian Institute of Technology Kanpur, Kanpur - 208016, India

<sup>2</sup> Tata Institute of Fundamental Research, 1 Homi Bhabha Road, Colaba, Mumbai - 400005, India

**Synopsis** We have measured the absolute double differential cross section for LM-M Auger emission from atomic Ar in collisions with 15keV/u Ar<sup>q+</sup> ions. The symmetry of the projectile ion-target atom provides Auger peak corresponding to both, target and projectile inner valance ionization. Measurement over a wide angular range reveal kinematic shift in the peak position due to moving projectile. The observed features of the spectra can be described via electron capture to the projectile and outer shell ionization of the target atom.

Electron correlation is the key factor in a number of relaxation processes in an excited atom or molecule. The well-known Auger effect has been used extensively in the past to study these correlations. In this study, we have measured the absolute DDCS for electron emission in Ar<sup>q+</sup>-Ar atom collisions using an electrostatic hemispherical electron energy analyser [1]. Slow highly charged ion beams of Ar<sup>3+</sup> and Ar<sup>6+</sup> were obtained from the ECR ion accelerator (ECRIA) facility at TIFR Mumbai [2]. In addition to measuring the absolute DDCS we have also measured the angular distribution of Auger electrons. It is observed that the electron spectrum consists of peaks due to Auger emission from target atoms as well as projectile ions. The projectile Auger peak energy varies from ~225 eV (forward angle) to ~105 eV (backward angle) as shown in figure 1.

L-MM transitions in Ar produce several peaks which are broadened due to multiplet splitting and fine structure. With the limited resolution of the spectrometer (~6%) we have identified most probable transitions for L<sub>23</sub>M<sub>23</sub><sup>i</sup>-M<sub>23</sub><sup>i+2</sup> with i = 2,3 [3]. Relative contributions from these peaks vary with the projectile energy and charge state [4]. Using energy correction corresponding to kinematic Doppler shift in the laboratory frame we have calculated the projectile Auger peak energy to be ~ 160 eV. We also observe (see figure 1) that this is the most dominant contribution even for target Auger emission. This deviation of Auger peak energy for stationary target atom (~190 eV) indicates charge equilibration during the collision process, where both projectile and target Auger electrons correspond to Ar<sup>q+</sup> ion.

In this poster we shall present the detailed analysis and interpretation of the observed spectrum for Ar<sup>3+</sup> and Ar<sup>6+</sup> projectile.

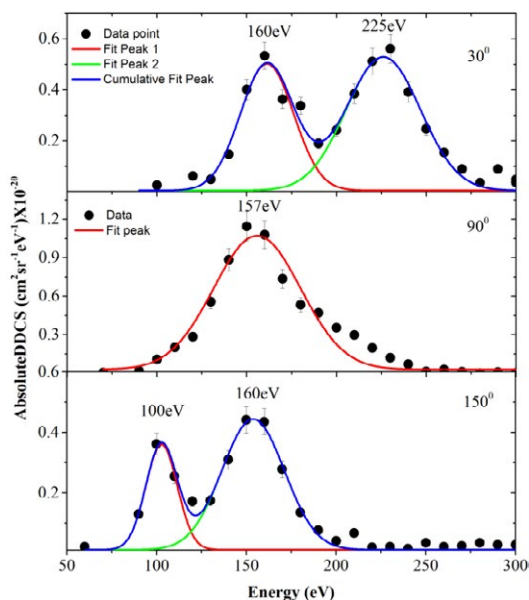


**Figure 1.** Coulomb background subtracted L-MM Auger emission DDCS spectra for 15 keV/u Ar<sup>3+</sup> + Ar.

### References

- [1] Deepankar Misra, *et al* Nucl. Instrum. Meth. Phys. Res. B, **267** (2009), p. 157
- [2] A N Agnihotri *et al* 2011 *Phys. Scr.* **2011** 014038
- [3] SM. E. Rudd, T. Jorgensen, Jr., and D. J. Voltz Phys. Rev. **151**, 28
- [4] N. Stolterfoht, D. Schneider, and H. Gabler Physics Letters A **47** 271
- [5] G. M. Thomson, W. W. Smith, and A. Russek Phys. Rev. A **7**, 168

\* E-mail: [rtiyagi@iitk.ac.in](mailto:rtiyagi@iitk.ac.in)

† E-mail: [akelkar@iitk.ac.in](mailto:akelkar@iitk.ac.in)



## Time evolution of Migdal electrons

J Randazzo<sup>1,2\*</sup> and R O Barrachina<sup>1,2†</sup>

<sup>1</sup>Bariloche Atomic Centre, Comisión Nacional de Energía Atómica, 8400 Bariloche, Río Negro Argentina

<sup>2</sup>Balseiro Institute, 8400 Bariloche, Río Negro Argentina

**Synopsis** We study the Migdal effect, by which an atom is excited or ionized by the sudden and impulsive acceleration of its nucleus. This process can occur by alpha or beta decay, or by the impact of a neutron or even dark matter, a promising option that has gained great notoriety in recent years. We solve the time-dependent Schrödinger equation to analyze the temporal evolution of the electron distribution over a wide range of the nucleus velocities. In particular, the discovery of a quantum vortex should be highlighted.

In 1927, Heisenberg envisioned the possibility that an atom could be ionized by the sudden disappearance of the nuclear charge [1]. Years later, Arkady Migdal showed that this possibility could materialize through the sudden acceleration of the nucleus, either by the impact of a neutron [2] or through alpha or beta decay [3]. This "Migdal effect" was observed in 1954 in the beta decay of <sup>147</sup>Pm [4]. Since then, it represents both a simple and analytical didactic example of the technique of sudden approximation [5], and a research topic of great interest in itself (See, for example, [6-9]). Recently, this effect has gained great relevance in relation to its promising use in the detection of Dark Matter [10]

In all the cases mentioned, where the Migdal effect is triggered by neutrons, dark matter, or alpha or beta decay, it is valid to assume that the setting in motion of the nucleus is "sudden" and impulsive [5,10]. Also, the evaluation of the excitation or ionization transition amplitude of the electrons is similar [2,10], involving the calculation of the matrix element of a translation operator between the initial and final electronic states.

The objective of this work, however, is not to evaluate solely the final state of the system, but its entire temporal evolution, through the resolution of the time-dependent Schrödinger equation for different ranges of the nucleus velocity.

As an example, in Fig. 1 we show the electronic density along the  $z$ - $\rho$  plane at  $t=2$  a.u. after the nucleus suddenly acquired a velocity  $v=2.5$  a.u. in the  $z$  direction. A ring type nodal structure, characteristic of a quantum vortex, is

clearly seen in front of the nucleus, together with a binary-collision ionization structure.

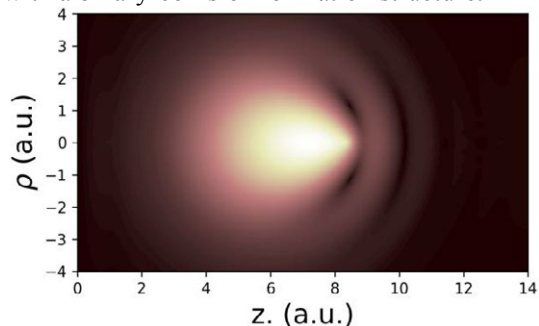


**Figure 1.** Square modulus of the electronic wave function of an Hydrogen atom after a sudden acceleration of its nucleus (see text).

### References

- [1] Heisenberg W 1927 Z. Phys. [43 172](#)
- [2] Migdal A B 1939 Zhurnal Éksperimental'noĭ i Teoreticheskoi Fiziki 9 1163
- [3] Migdal A B 1941 Zhurnal Éksperimental'noĭ i Teoreticheskoi Fiziki 11 207
- [4] Boehm and Wu 1954 Phys. Rev. [93 518](#)
- [5] Migdal A B and Krainov V 1969 *Approximation Methods in Quantum Mechanics* (New York: Benjamin) pp. 71-78
- [6] Lovesey S W, Bowman C D and Johnson R G 1982 Z. Physik B [47 137](#)
- [7] Talman J D and Frolov A M 2006 Phys. Rev A [73 032722](#)
- [8] Lietzer M, Feist J, Nagele S and Burgdörfer J 2012 Phys. Rev. Lett. [109 013201](#)
- [9] Pindzola M S, Lee T G, Abdel-Naby Sh A, Robicheaux F, Colgan J and Ciappina M F 2014 J. Phys. B [47 195202](#)
- [10] Ibe M, Nakano W, Shoji Y and Suzuki K 2018 J. High Energ. Phys. [194](#)

\* E-mail: [juan.randazzo@ib.edu.ar](mailto:juan.randazzo@ib.edu.ar)

† E-mail: [barra@cab.cnea.gov.ar](mailto:barra@cab.cnea.gov.ar)



## Stopping power in lanthanides, from Ce to Lu

J Peralta<sup>1\*</sup>, A M P Mendez<sup>1</sup>, D G Arbó<sup>1</sup>, D M Mitnik<sup>1</sup>, and C C Montanari<sup>1</sup>

<sup>1</sup>Instituto de Astronomía y Física del Espacio, CONICET and Universidad de Buenos Aires, Buenos Aires, Argentina.

**Synopsis** In the last decade, lanthanides have become the subject of multiple studies due to their importance in technological applications. This work aims to systematically study the energy loss of protons on the fifteen lanthanides, from lanthanum to lutetium. Inner-shell and conduction electrons contributions are considered independently. We employ a many-electron model for the former and a combination of perturbative and non-perturbative free electron gas approaches for the latter. Our stopping results for the lanthanide series cover an extended energy range from very low to the MeV region, and cast doubts on the highly used SRIM code.

The knowledge of electronic stopping is important in many fields, from basic physics to technology and medicine. We focused on lanthanides due to its electronic complexity (open 4f-subshell, need of relativistic description [1]); the importance of rare-earth oxides, and discrepancies among experimental data. In this work we perform a systematic study of the stopping cross sections from La ( $Z=57$ ) to Lu ( $Z=71$ ). Fully relativistic atomic structure calculations were developed for the atomic wave functions and binding energies. These values are the only inputs of our full theoretical calculations for bound electrons using the shellwise local plasma approximation [2]. This model uses the Levine-Mermin dielectric function (SLPA-LM), and considers the density of electrons of each shell and the ionization gap [3]. Our results cover an extended energy region by considering separately the free electron gas (FEG) and the bound electrons as in [2].

As example, in Figure 1 we show our results for stopping of proton in Gd, the present results describe nicely the latest experimental data around the stopping maximum. Differences between new data and previous values show the need of new measurements in all Lanthanides [4]. We also compare with other theoretical models, such as DPASS [5] and CasP 6.0 [6]. We will show that the systematic study of all the lanthanides lets us have some doubts about the SRIM predictions for this type of targets. We call attention to the scarcity of measurements in the low and intermediate ranges, and we suggest experimental efforts to shed light on the stopping power of these rel-

evant targets.

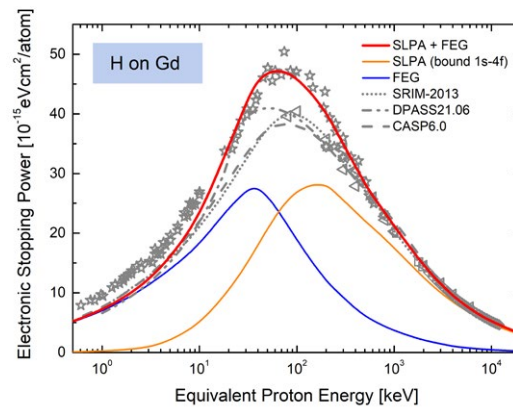


**Figure 1.** Stopping cross-section of Gd for H. Solid curves: present results; total (thick red line), bound electrons (1s-4f) (thin orange line), and FEG (thin blue line). Discontinued curves: SRIM [7] (gray-dotted line), DPASS21.06 [5] (gray-dash-double-dotted line), and CASP6.0 [6] (gray-dashed curve). Symbols: experimental data [8]

### References

- [1] A M P Mendez et al 2019 Nuclear Inst. and Meth in Phys. Res. B 460, 114.
- [2] C C Montanari et al 2017 Phys. Rev. A 96, 012707.
- [3] J P Peralta et al 2022 Phys. Rev. A 105, 062814.
- [4] D. Roth et al (2017) Phys. Rev. Lett. 118, 103401.
- [5] P Sigmund and A Schinner [www.sdu.dk/en/dpass](http://www.sdu.dk/en/dpass).
- [6] G Schiwietz and P L Grande [www.casp-program.org/](http://www.casp-program.org/).
- [7] J.F. Ziegler [www.srim.org/](http://www.srim.org/).
- [8] Electronic Stopping Power of Matter for ions IAEA database [www-nds.iaea.org/stopping/](http://www-nds.iaea.org/stopping/).

\*E-mail: [jpperalta@iafe.uba.ar](mailto:jpperalta@iafe.uba.ar)

## Ion-ion collision-induced longitudinal emittance preservation in RF bunching of ions in an electrostatic ion beam trap

D Sharma<sup>1</sup>\*, R Ringle<sup>2</sup>, O Heber<sup>1</sup> and D Zajfman<sup>1</sup>

<sup>1</sup>Department of Particle Physics and Astrophysics, Weizmann Institute of Science, Rehovot, 761001, Israel

<sup>2</sup>Facility for Rare Isotope Beams, Michigan State University, Michigan, 48823, USA

**Synopsis** Dynamics of ions under an external RF field is studied in an electrostatic ion beam trap (EIBT). The non-linear dependence of synchrotron oscillation on phase amplitude causes phase space filamentation and results in longitudinal emittance growth in RF bucket. Furthermore, a high space charge should enhance the phase space filamentation. We show that the ion-ion collision helps to preserve the emittance growth. The particle-in-cell technique is used to simulate the ion dynamics in the trap.

Storage rings or ion traps are widely used to study the time-dependent dynamics of ions. Electrostatic Ion Beam Trap (EIBT), is a unique device where ions are stored between two sets of electrostatic mirrors by applying appropriate voltages [1]. Depending on the voltage profile of the trap, the trap can be operated in diffusive or synchronization mode. The ion-ion interaction can either enhance the diffusion or the strong correlation between the ions results in the self-bunching of ions [2]. We use the particle-in-cell technique to simulate the ion dynamics in the trap [3].

A bunch of ions injected in a storage ring or ion trap will disperse with time. The ion-ion collisions further increase the dispersion. The most common technique of keeping the ions in a bunch is RF bunching. The synchrotron oscillations of ions in the RF bucket are non-linear and the frequency changes with oscillation amplitude. This gives rise to filamentation in the RF bucket. Figure 1 shows the emittance growth in the RF bucket for different ion densities. Surprisingly, the emittance growth is highly suppressed for high ion density where the ion-ion interaction is strong. This effect is similar to the self-bunching in EIBT [2], where the ion-ion interaction, which is repulsive Coulombic interaction, indeed helps to keep the ions in a bunch.

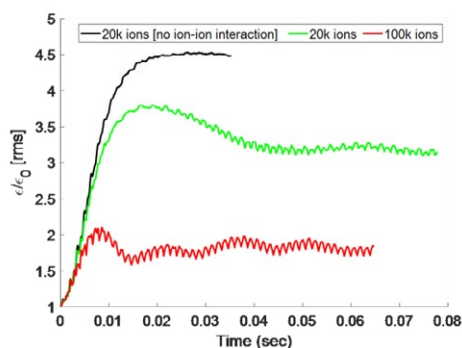


**Figure 1.** RMS emittance growth for different ion densities.

The counterintuitive results can be verified experimentally with the Fourier Transformed (FT) time signal of the ion bunch in the trap. The longitudinal motion of ions bunch results in two sidebands in the FT spectrum [4,5]. The ratio of the height of sidebands to the main peak is higher for high ion density. The preliminary results show the importance of ion-ion collisions and open a window for phase space manipulation of ions in the trap.

### References

- [1] D Zajfman *et al* 1997 *Phys. Rev. A.* **55** R1577
- [2] H B Pedersen *et al* 2001 *Phys Rev Lett* **87** 055001
- [3] D Gupta *et al* 2021 *Phys Rev E* **104** 065202
- [4] Y Toker *et al* 2014 *Journal of Instrumentation* **9** P04008
- [5] K Shaha *et al* 2016 *Review of Scientific Instruments* **87** 113302

\* E-mail: [deepak.sharma@weizmann.ac.il](mailto:deepak.sharma@weizmann.ac.il)

## AEGIS Phase II: Upgrading for collinear antihydrogen production

S Huck<sup>1,2\*</sup>, on behalf of the AEGIS collaboration

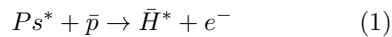
<sup>1</sup>University of Hamburg, Institute for Experimental Physics, Hamburg, 22761, Germany

<sup>2</sup>CERN, EP Department, Meyrin, 1211, Switzerland

**Synopsis** Having successfully established antihydrogen production, AEGIS has been extensively upgraded to improve production efficiency and is now working towards a gravity measurement with antimatter: main improvements and first results are presented.

The AEGIS (Antimatter Experiment: Gravity, Interferometry, Spectroscopy) collaboration [1], based at CERN's Antiproton Decelerator (AD) complex, is working towards a direct measurement of the influence of gravity on antimatter by means of the detection of the vertical deflection of antihydrogen atoms travelling as a horizontal beam. Such a measurement will allow to directly test the Weak Equivalence Principle for antimatter and presents an indirect probe of CPT symmetry.

AEGIS has recently successfully demonstrated the procedure to produce antihydrogen in Rydberg states through a charge exchange reaction (Eq. 1) between cold antiprotons and laser-excited positronium atoms inside a Penning-Malmberg trap, providing very precise knowledge of the formation time of the anti-atoms [2, 3].



Since then, the experiment has entered its second phase and undergone multiple extensive upgrades, including the connection to the new ELENA (Extra Low ENergy Antiproton) decelerator to improve the  $\bar{p}$  trapping efficiency and increase their numbers, the implementation of a completely new control system to provide a full automation of the experimental procedures, and the remodelling of the entire experiment for a collinear antihydrogen production, which is shown in the schematic in Fig. 1. The latter eliminates both the Ps losses due to dynamical field ionization and the need for azimuthal asymmetries in the  $\bar{H}$  production trap.

These upgrades are expected to greatly improve the efficiency of antihydrogen production, yielding several orders of magnitude higher  $\bar{H}$  rates.

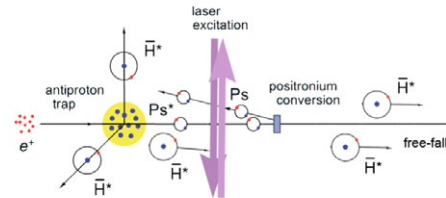


**Figure 1.** Schematic of collinear antihydrogen production in AEGIS.

Having successfully validated and consolidated the new control system and the additional hardware upgrades in the ELENA beam times in 2021 and 2022, AEGIS is now working towards establishing the improved antihydrogen production and eventually forming the horizontal  $\bar{H}$  beam. In 2022, record  $\bar{p}$  trapping efficiencies of 65% have been routinely achieved.

This contribution gives an overview of the recent upgrades in AEGIS with a focus on the conversion to a collinear antihydrogen production and on the new, automated experimental control system as well as subsequent results from the first antiproton beam times with ELENA.

### References

- [1] M. Doser et al. 2012 *Class. Quantum Grav.* **29** 184009
- [2] C. Amsler et al. 2021 *Nature Comms.* **4** 19
- [3] D. Krasnicky et al. 2016 *Phys. Rev. A* **94** 022714

\*E-mail: [saiva.huck@cern.ch](mailto:saiva.huck@cern.ch)

## State selective electron capture study with $NO^{2+}$ using Cold Target Recoil Ion Momentum Spectroscopy

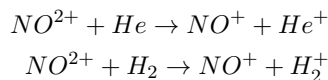
J Mukherjee\*, Md A K A Siddiki, K Kumar, H Singh, L C Tribedi and D Misra†

Department of Nuclear and Atomic Physics, Tata Institute of Fundamental Research, Mumbai, 400005, India.

**Synopsis** We have observed relative cross-section and scattering angle distribution for non-dissociative channels of single electron capture by  $NO^{2+}$  during collision with He and  $H_2$  at 10 keV and 40 keV projectile energies.

State selective electron capture is a dominant processes when an ion collides with an atom or molecule with a velocity less than electron orbital velocity of the target. It is a dynamic many body quantum mechanical problem which is difficult to solve theoretically. Numerous studies are available with atomic ion on atomic and molecular targets. Here we have tried to explore what happens when a dication molecular ion collides with an atom and a diatomic molecule? Some translational energy spectroscopic studies are also available on  $NO^{2+}$ [1]. However, those were restricted to only low energies.

In our experiment we looked for non dissociative channels of



We tried to observe relative cross-sections and scattering angle distributions of resolvable channels and their variation at two different projectile velocities, 0.116 a.u. and 0.232 a.u.

Using home build state-of-the-art Cold Target Recoil Ion Momentum Spectroscopy (COLTRIMS) setup [2] we can measure 3d momentum vector of each recoil ion and hence we can deduce the Q-value spectra and the scattering angle distributions associated with different channels simultaneously. The  $NO^{2+}$  projectile beam was obtained from ECR ion source located at TIFR [3].

With the help of theoretical potential energy curves [4, 5] we have concluded that electron capture is taking place from  $NO^{2+}$  ground electronic state to  $NO^+$  ground and excited electronic states. The relative cross-sections of electron capture to ground state is higher for He tar-

get, but less for  $H_2$  target. We have also observed with increasing projectile velocity there are enhancements in relative cross-sections of excited states transitions for He target but diminution for  $H_2$  target. Scattering angles are found to be decreasing with increasing projectile velocity for both He and  $H_2$  target cases.

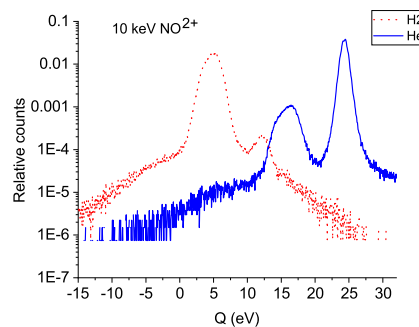


**Figure 1.** Q-value spectrum for 10 keV  $NO^{2+}$  with He and  $H_2$  targets. Dotted curve is for  $H_2$  and solid is for He. The higher Q value peaks are coming from electron capture to ground electronic  $NO^+$  states and lower Q value peaks are coming from capture to excited electronic  $NO^+$  states.

### References

- [1] M Hamdan *et al* 1990 *J. Phys. B: At. Mol. Opt. Phys.* **23** L705
- [2] Md Abul Kalam Azad Siddiki, M. Nriishimhamurty, Kamal Kumar, *et al.* 2022 *Rev. Sci. Instrum.* **93** 11331
- [3] A N Agnihotri *et al.* 2011 *Phys. Scr.* **2011** 014038
- [4] L.G.M. Pettersson, P.E.M. Siegbahn, L. Broström, S. Mannervik, Mats Larsson 1992 *Chemical Physics Letters* **191** 3,4
- [5] D. L. Albritton, A. L. Schmeltekopf and R. N. Zare 1979 *J. Chem. Phys.* **71** 3271

\*E-mail: [jibak.mukherjee@tifr.res.in](mailto:jibak.mukherjee@tifr.res.in)

†E-mail: [dmisra@tifr.res.in](mailto:dmisra@tifr.res.in)

## Isomerized dissociation dynamics of hydrocarbon dications induced by slow highly charged ion impact

B Ren<sup>1,2</sup>, Y Zhang<sup>3</sup>, A-R Allouche<sup>2</sup> and B Wei<sup>1\*</sup>

<sup>1</sup>Institute of Modern Physics, Key Laboratory of Nuclear Physics and Ion-Beam Application (MOE), Fudan University, Shanghai 200433, China

<sup>2</sup>Institut Lumière Matière, Université Claude Bernard Lyon 1, CNRS, Villeurbanne F-69622, France

<sup>3</sup>School of Mathematics, Physics and Information Engineering, Jiaxing University, Jiaxing 314001, China

**Synopsis** To probe the crucial ultrafast isomerization of hydrocarbons, the fragmentations of ethylene and ethane dications were performed utilizing COLTRIMS combined with the transition state and molecular dynamics calculation. Isomerization processes induced by hydrogen migration were revealed.

The isomerization process with hydrogen migration is a critical elementary chemical reaction in chemistry and biochemistry. Such typical atomic movements occurring in tens to hundreds of femtoseconds could open some special dissociation channels. Studying detailed isomerization processes is crucial for understanding ultrafast reaction dynamics. One way to probe the isomerization mechanism of hydrocarbons is by combining the collision experiment with *ab-initio* quantum chemical calculations (e.g., transition state theory (TST) and molecular dynamics (MD)).

In present works, the symmetric and isomerized asymmetric fragmentations of ethane and ethylene dications have been investigated by collisions between 3-keV/u Ar<sup>8+</sup> and C<sub>2</sub>H<sub>6</sub>, 18-keV/u Ne<sup>8+</sup> and C<sub>2</sub>H<sub>4</sub> utilizing the cold target recoil ion momentum spectrum (COLTRIMS) [1,2]. The associated minimum energy path (MEP) of dications with complex isomerization processes was further revealed by the TST.

As shown in Fig. 1(a, c), the kinetic energy release distribution (KERs) of asymmetric fragmentations involving H-migration CH<sub>3</sub><sup>+</sup> + CH<sup>+</sup> and CH<sub>4</sub><sup>+</sup> + CH<sub>2</sub><sup>+</sup> were measured as singlet Gauss structure. With the help of TST calculations, isomerization processes were found to take place prior to C-C bond breakage on both asymmetric channels. For symmetric fragmentation channels in Figs. 1(b, d), two KER peaks were assigned by different complex dissociation evolution paths. In particular, H-induced isomerization also played a special role in the cleavage of CH<sub>3</sub><sup>+</sup> + CH<sub>3</sub><sup>+</sup>. But for fragmentation CH<sub>2</sub><sup>+</sup> + CH<sub>2</sub><sup>+</sup>, no isomerization process was observed.

Moreover, to understand the isomerization and hydrogen migration mechanism of C<sub>2</sub>H<sub>6</sub><sup>2+</sup>, MD calculations of the fragmentation were performed. The two- and three-body fragmentation channels observed in experiments were also observed in MD simulations, on both singlet and triplet states with proper KERs and Dalitz plots. We found that fragmentation processes including transition state and roaming path occurred on time scales from tens to hundreds of femtoseconds.

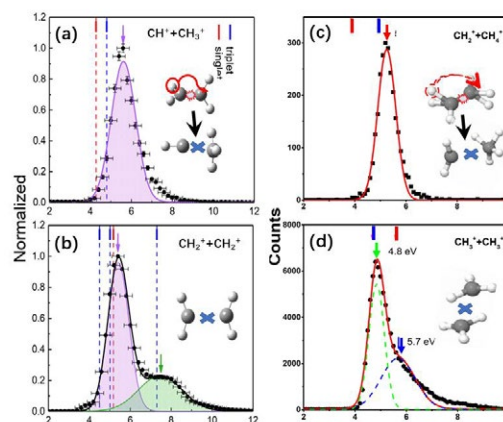


**Figure 1.** Fragmentation sketches and KERs of (a) C<sub>2</sub>H<sub>4</sub><sup>2+</sup> → CH<sub>3</sub><sup>+</sup> + CH<sup>+</sup>, (b) C<sub>2</sub>H<sub>6</sub><sup>2+</sup> → CH<sub>2</sub><sup>+</sup> + CH<sub>2</sub><sup>+</sup>, (c) C<sub>2</sub>H<sub>6</sub><sup>2+</sup> → CH<sub>4</sub><sup>+</sup> + CH<sub>2</sub><sup>+</sup>, and (d) C<sub>2</sub>H<sub>6</sub><sup>2+</sup> → CH<sub>3</sub><sup>+</sup> + CH<sub>3</sub><sup>+</sup>.

### References

- [1] Wei L, Lam C-S, Zhang Y, *et al.* 2021 *J. Phys. Chem. Lett.* **12** 5789
- [2] Ren B, Ma P, Zhang Y, *et al.* 2022 *Phys. Rev. A* **106** 012805

\* E-mail: [brwei@fudan.edu.cn](mailto:brwei@fudan.edu.cn)



## Three-body fragmentation dynamics of cyclopropane induced by high-energy ion collisions

K Z Lin<sup>1,2\*</sup>, D L Guo<sup>2,3</sup>, S F Zhang<sup>2,3</sup>, X L Zhu<sup>2,3</sup>, X B Zhu<sup>2,3</sup>, X Shan<sup>1</sup>, X J Chen<sup>1</sup> and X Ma<sup>2,3</sup>

<sup>1</sup>Department of Modern Physics, School of Physical Sciences, University of Science and Technology of China, Hefei 230026, China

<sup>2</sup>Institute of Modern Physics, Chinese Academy of Sciences, Lanzhou 730000, China

<sup>3</sup>University of Chinese Academy of Sciences, Beijing 100049, China

**Synopsis** The three-body fragmentation dynamics of cyclopropane ( $C_3H_6$ ) induced by  $Ni^{19+}$  ion at an impact energy of 5.8 MeV/u were studied using cold target recoil ion momentum spectroscopy COLTRIMS spectrometer. Three three-body dissociation channels of  $C_3H_6^{3+}$  were identified in the present experiment. Two different sequential mechanisms, depending on which of the two kinds of bonds, i.e., CH and CC, breaks first, are distinguished for these three dissociation channels. Our preliminary analysis indicates that the projectile velocity effect may be responsible for the dominance of the sequential fragmentation processes.

The fragmentation dynamics of molecules have received much attention in recent decades, not only because of their fundamental nature but also because of their various applications in many fields. Among the various molecules investigated in the past, the hydrocarbon molecules, which widely exist in the universe and play an important role in industry, have attracted special interest. While the chain-structure hydrocarbon molecules have been the focus of most of the previous work, the three-body fragmentation of the ring-structure hydrocarbon molecules has been reported only for a few cases [1, 2].

In this work, the three-body fragmentation dynamics of cyclopropane induced by 5.8 MeV/u  $Ni^{19+}$  ion collisions were studied using a COLTRIMS. Three three-body dissociation channels including deprotonation channel  $C_3H_6^{3+} \rightarrow H^+ + CH_2^+ + C_2H_3^+$ , isomerization channel  $C_3H_6^{3+} \rightarrow H^+ + CH_3^+ + C_2H_2^+$  and  $H^{2+}$  formation channel  $C_3H_6^{3+} \rightarrow H^{2+} + CH_2^+ + C_2H_2^+$  were identified. The Dalitz plots, Newton diagrams and the KER distribution spectra are used to study the dissociation mechanisms.

For the channel  $C_3H_6^{3+} \rightarrow H^+ + CH_2^+ + C_2H_3^+$ , two oblique stripe structures marked by red and gray dashed rectangle are observed in the experimental Dalitz plot shown in Fig. 1(a), implying that different fragmentation mechanisms may be involved in this channel. In Fig. 1(b), we show the Newton diagram normalized to the momentum of  $H^+$  (black arrow). A clear circular structure marked by red lines ex-

\*E-mail: lkz666@mail.ustc.edu.cn

hibits in the Newton diagram, which is an evidence of a sequential fragmentation process via  $C_3H_6^{3+} \rightarrow H^+ + C_3H_5^{2+} \rightarrow H^+ + CH_2^+ + C_2H_3^+$ . Another weak circular structure marked by gray dashed semicircles appears in the Newton diagram, indicating that a different sequential fragmentation process occurs in this channel.

It is interesting to note that the Newton diagrams and the Dalitz plots for the other two channels display similar patterns, implying that the dominant dissociation dynamics for these two channels might be similar for the three channels, i.e., only two sequential fragmentation pathways are observed for all the three channels. Our preliminary analysis suggests that the dominance of the sequential fragmentation processes may be attributed to the projectile velocity effect.

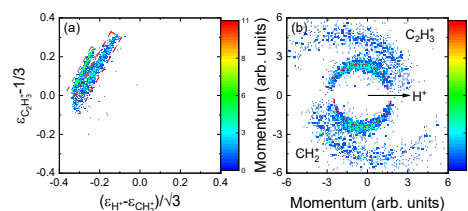


**Figure 1.** (a) Dalitz plot and (b) Newton diagram of channel  $C_3H_6^{3+} \rightarrow H^+ + CH_2^+ + C_2H_3^+$ .

### References

- [1] Attar A R *et al* 2017 *Science*. **356** 54
- [2] Shabnam O *et al* 2017 *Phys. Chem. Chem. Phys.* **19** 19631



## Measurements of subrotational lifetimes of molecular ions: a new experimental technique

C P Safvan<sup>1\*</sup>, Herendra Kumar<sup>2</sup>, Pragma Bhatt<sup>1</sup> and Jyoti Rajput<sup>2</sup>

<sup>1</sup>Inter University Accelerator Centre, Aruna Asaf Ali Marg, New Delhi-110067, INDIA

<sup>2</sup>Department of Physics and Astrophysics, University of Delhi, Delhi-110007, INDIA

**Synopsis** We present a new technique to estimate the lifetimes of multiply charged molecules that are shorter than their rotational periods. Molecular dications formed in three-body sequential breakup of polyatomic molecular precursors are studied using recoil ion momentum spectroscopy. Specifically the lifetime against dissociation of  $\text{SO}^{2+}$  as a fraction of its rotational period is determined by utilizing the “native frames” approach.

The lifetimes of multiply charged molecular ions range from infinity (stable ions e.g.  $\text{N}_2^{2+}$ ) to those that explode immediately due to Coulomb repulsion. Theoretical *ab initio* calculations predict lifetimes from picoseconds to seconds depending on the structure and electronic states of the molecular ions. Conventional techniques have measured lifetimes in the range of nanoseconds to milliseconds and higher. Measurements using femto or attosecond pulses used to study temporal variations are not well suited for such studies. Very short lifetimes, though difficult to access experimentally provide stringent tests for theoretical calculations for effects of electron correlations and the breakdown of Born-Oppenheimer approximation.

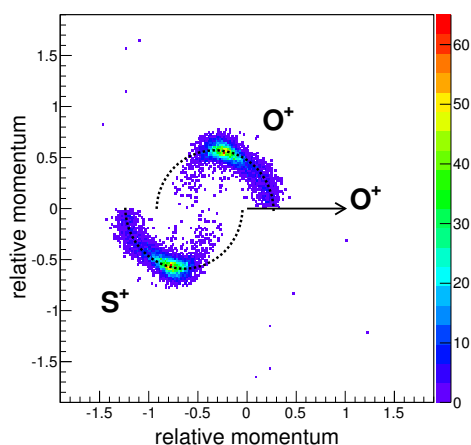
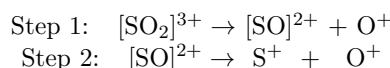


**Figure 1.** Newton plot showing the relative momenta for the fragments in the dissociation of  $\text{SO}_2^{3+}$  into  $(\text{O}^+, \text{O}^+, \text{S}^+)$

\*E-mail: [cp.safvan@gmail.com](mailto:cp.safvan@gmail.com)

In this work, we study the dissociation dynamics of the  $\text{SO}^{2+}$  dication, formed as an intermediate, in the sequential dissociation of  $\text{SO}_2^{3+}$  into  $\text{S}^+$  and two  $\text{O}^+$  ions [1]. The following two steps are observed:



The figure shows the Newton plot generated using the measured momenta of the ions ( $\text{O}^+, \text{O}^+, \text{S}^+$ ). The arc like feature (but not a complete semi-circle) shows the existence of a sequential mechanism that has a lifetime shorter than the rotational time of the intermediate ion.

Further analysis is done using the “native frames” approach [2] to determine the dynamics in the two separate steps, including the determination of the kinetic energy release in the first step, as well as the relative angle between the two dissociation steps in the centre of mass of the trication.

We measured the lifetime of the dicationic state to be around 2 ps which is shorter than the rotational period ( $\approx 16$  ps) of  $\text{SO}^{2+}$ , by combining two powerful techniques, one experimental viz. coincidence momentum imaging and the other, an analysis procedure, the native frames approach. The lifetime of the  $\text{SO}^{2+}$  intermediate is determined to be a fraction of its rotational period.

### References

- [1] J Rajput, H Kumar, P Bhatt and C P Safvan 2020 *Scientific Reports* **10** 20301
- [2] J Rajput *et al.* 2018 *Phys. Rev. Lett* **120** 103001

## Measurements of Absolute Electron Capture Cross Sections in $\text{He}^{2+}$ - He and $\text{Ne}^{8+}$ - $\text{O}_2$ Collisions

P Ma<sup>1</sup>, B Tu<sup>1</sup> †, J Wang<sup>1</sup>, T Meng<sup>1</sup>, Z Xia<sup>1</sup>, B Ren<sup>1</sup>, Y Zou<sup>1</sup> and B Wei<sup>1</sup> \*

<sup>1</sup>Institute of Modern Physics, Key Laboratory of Nuclear Physics and Ion-Beam Application (MOE), Fudan University, Shanghai 200433, China

**Synopsis** To provide an experimental verification of the theoretical calculation and to aid for fusion research and astrophysical X-ray studies, the total electron capture cross sections in collisions of  $\text{He}^{2+}$  - He and  $\text{Ne}^{8+}$  -  $\text{O}_2$  have been studied in the energy range from 3.5 to 50 keV/u and 2.8 to 40 keV/u, respectively.

Electron capture (EC) of charged particles with neutral atoms and molecular species is a fundamental process that occurs in various plasma environments. It affects the ionization balance and leads to spectral line emissions in astrophysical regions or fusion devices. For example, Ne is one of the main impurities, and He is a product in the fusion reactors, both appearing at various relative energies in different ionization stages in the plasmas. Furthermore, the minor presence of  $\text{Ne}^{8+}$  ions as HCIs in solar wind, along with the critical role of He as a constituent of the solar system, adds significant value to EC measurements. As for these applications, there is a strong demand for accurate data on the cross sections of EC.

The experiment is performed on the 150kV highly charged ion collision platform at Fudan University[1]. The HCIs beam, produced by an ECR ion source, collides with neutral gases in a gas cell. In the present work, the EC cross sections are measured with the growth-rate method. The systematic uncertainties of our

experimental and measurement procedures are analyzed in detail, and eventually the experimental error of absolute cross sections of single electron capture (SEC) is reduced to lower than 10%.

The absolute cross sections of SEC and double electron capture (DEC) in collisions of  $\text{He}^{2+}$  with He have been studied in energy ranges from 3.5 to 50 keV/u. The present result of  $\text{He}^{2+}$ - He collision shows good consistency with previous measurements, which verifies the reliability of the experimental system and paves the way for precise measurements of electron capture (EC) cross sections for a variety of ions and neutral gases. On this basis, the absolute cross sections of SEC and DEC for  $\text{Ne}^{8+}$  -  $\text{O}_2$  is performed, filling in the gaps of the EC cross section data in the corresponding energy region. The results of SEC and DEC cross section both diminish with a gentle slope as the collision energy increases from  $4.55 \times 10^{-15} \text{ cm}^2$  to  $3.46 \times 10^{-15} \text{ cm}^2$  and  $1.52 \times 10^{-15} \text{ cm}^2$  to  $1.11 \times 10^{-15} \text{ cm}^2$ , respectively.

### References

[1] J. Han, L. Wei, B. Wang, et al 2021 *Astrophys. J., Suppl. Ser.* **253** 6

\* E-mail: [brwei@fudan.edu.cn](mailto:brwei@fudan.edu.cn)

† E-mail: [bingshengtuo@fudan.edu.cn](mailto:bingshengtuo@fudan.edu.cn)

## Sequential deprotonation of the allene trication produced by He<sup>2+</sup> impact

J Wang<sup>1</sup>, Z He<sup>1</sup>, Y Zhang<sup>2\*</sup>, B Wang<sup>1</sup>, B Ren<sup>1</sup>, L Wei<sup>1</sup>, Y. Zou<sup>1</sup> and B Wei<sup>1†</sup>

<sup>1</sup>Institute of Modern Physics, Key Laboratory of Nuclear Physics and Ion-Beam Application (MOE), Fudan University, Shanghai 200433, China

<sup>2</sup>College of Data Science, Jiaxing University, Jiaxing 314001, China

**Synopsis** The three-body fragmentation channel H<sup>+</sup> + H<sup>+</sup> + C<sub>3</sub>H<sub>2</sub><sup>+</sup> of the allene trication produced by 30-keV/u He<sup>2+</sup> ion impact is investigated using cold-target recoil-ion momentum spectroscopy. The two protons with different kinetic energies are found emitted sequentially from the parent trication, which may result from a major molecular deformation process, e.g., ultrafast hydrogen migration.

The three-body fragmentation of multicharged polyatomic molecules has drawn much attention recently, since it can serve as a diagnostic tool to probe the structural and dynamical information during molecular dissociation, e.g., molecular geometry reconstructed by Coulomb explosion imaging [1] and lifetime of metastable intermediate ions [2]. Allene (CH<sub>2</sub>CCH<sub>2</sub>), as one isomer of C<sub>3</sub>H<sub>4</sub>, possesses a linear carbon skeleton, which ionization and dissociation processes have been investigated to obtain information concerning the isomer effect, fragmentation patterns[3], and intramolecular hydrogen migration [4]. Compared with other two channels, i.e., H<sup>+</sup> + CH<sup>+</sup> + C<sub>2</sub>H<sub>2</sub><sup>+</sup> and H<sup>+</sup> + CH<sub>2</sub><sup>+</sup> + C<sub>2</sub>H<sup>+</sup> under 50-keV/u Ne<sup>8+</sup> collisions [5] and strong laser field ionization, less is known on the two-proton emission pattern in the allene trication fragmentation and on the role of hydrogen-migration-induced isomerization for the H<sup>+</sup> + H<sup>+</sup> + C<sub>3</sub>H<sub>2</sub><sup>+</sup> channel.

We pay attention to the three-body channel H<sup>+</sup> + H<sup>+</sup> + C<sub>3</sub>H<sub>2</sub><sup>+</sup> of C<sub>3</sub>H<sub>4</sub><sup>3+</sup> induced by 30-keV/u He<sup>2+</sup> impact. Utilizing the cold-target recoil-ion momentum spectroscopy technique on the 150-kV highly charged ion collision platform at Fudan University, the complete kinematics of channels of interest are measured [6].

The results are found to be different from previous studies of similar three-body channels because it herein only includes a sequential process, i.e., C<sub>3</sub>H<sub>4</sub><sup>3+</sup> → H<sup>+</sup> + C<sub>3</sub>H<sub>3</sub><sup>2+</sup> → H<sup>+</sup> + H<sup>+</sup> + C<sub>3</sub>H<sub>2</sub><sup>+</sup>, and the concerted deprotonation mechanism is found to be totally absent to form this channel. Such a unique fragmentation pattern suggests that the two resultant protons or corre-

sponding hydrogen atoms are not identical in the structure of the C<sub>3</sub>H<sub>4</sub><sup>3+</sup>. An ultrafast hydrogen migration process might occur immediately after the triple ionization of the allene molecule, which finally leads to the two different proton fragments.

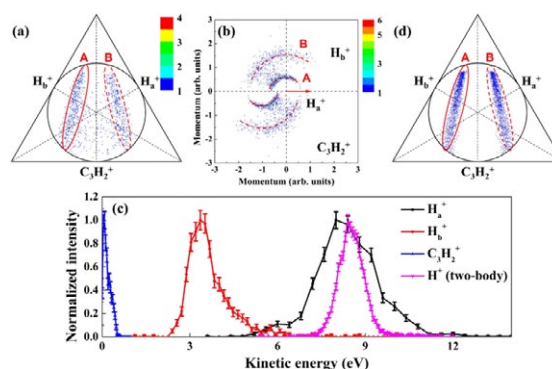


**Figure 1.** (a) (b) Dalitz plot and Newton diagram for the H<sup>+</sup> + H<sup>+</sup> + C<sub>3</sub>H<sub>2</sub><sup>+</sup> channel, respectively. H<sub>a</sub><sup>+</sup> represents the first detected proton, whereas H<sub>b</sub><sup>+</sup> the second one. The momenta of H<sub>b</sub><sup>+</sup> and C<sub>3</sub>H<sub>2</sub><sup>+</sup> are normalized to the momentum of H<sub>a</sub><sup>+</sup>. (c) KE distributions of H<sub>a</sub><sup>+</sup>, H<sub>b</sub><sup>+</sup>, C<sub>3</sub>H<sub>2</sub><sup>+</sup> and H<sup>+</sup> from the two-body dissociation channel. (d) Simulated Dalitz plot for the sequential dissociation process C<sub>3</sub>H<sub>4</sub><sup>3+</sup> → H<sup>+</sup> + C<sub>3</sub>H<sub>3</sub><sup>2+</sup> → H<sup>+</sup> + H<sup>+</sup> + C<sub>3</sub>H<sub>2</sub><sup>+</sup>.

### References

- [1] Hishikawa A et al. 1999 *Phys. Rev. Lett.* **83**, 1127
- [2] Neumann N et al. 2010 *Phys. Rev. Lett.* **104**, 103201
- [3] Scully S et al. 2005 *Phys. Rev. A* **72**, 030701(R)
- [4] Xu H et al. 2009 *J. Chem. Phys.* **131**, 151102
- [5] Ma C et al. 2020 *Phys. Rev. A* **101**, 052701
- [6] He Z C et al, 2022 *Phys. Rev. A* **105**, 022818

\* E-mail: [zyclay@outlook.com](mailto:zyclay@outlook.com)

† E-mail: [brwei@fudan.edu.cn](mailto:brwei@fudan.edu.cn)

## Merged-beams reactive scattering studies of $\text{N}_2 + \text{D}_3^+ \rightarrow \text{N}_2\text{D}^+ + \text{D}_2$

D Ivanov<sup>1\*</sup>, C Bu<sup>1</sup>, P-M Hillenbrand<sup>2</sup>, L W Isberner<sup>2</sup>, D Schury<sup>1</sup>, X Urbain<sup>3</sup>, and D W Savin<sup>1†</sup>

<sup>1</sup>Columbia Astrophysics Laboratory, Columbia University, New York, NY 10027, USA

<sup>2</sup>I. Physikalisches Institut, Justus-Liebig-Universität Gießen, 35392 Gießen, Germany

<sup>3</sup>Institute of Condensed Matter and Nanosciences, Université catholique de Louvain, B-1348 Louvain-la-Neuve, Belgium

**Synopsis** Astronomical observations of  $\text{N}_2\text{D}^+$  and  $\text{N}_2\text{H}^+$  abundances are used to trace the properties of cosmic objects, such as prestellar cores and protoplanetary disks. Interpreting the observations requires an accurate understanding of how these ions are formed through reactions of  $\text{N}_2$  with  $\text{H}_3^+$  isotopologues. In this poster, we present our recent results for  $\text{N}_2 + \text{D}_3^+ \rightarrow \text{N}_2\text{D}^+ + \text{D}_2$ , describe the underlying molecular physics, and discuss some of the astrophysical implications of our findings.

Deuterated molecules are used to infer the temperature, chemistry, and thermal history of cosmic objects such as prestellar cores and protoplanetary disks [1, 2]. In the very dense cold regions found in prestellar cores and the outer mid-plane of protoplanetary disks, most molecules beside hydrogen freeze onto dust grains, leaving HD as the primary deuterium reservoir in the gas phase. The HD can react with  $\text{H}_3^+$  to form deuterated isotopologues of the ion. Subsequent ion-neutral reactions pass on the deuteration to other gas-phase species. Of particular importance is the abundance ratio for  $\text{N}_2\text{D}^+$  and  $\text{N}_2\text{H}^+$ . Their formation occurs near the  $\text{N}_2$  snow line in prestellar cores and protoplanetary disks and they are commonly used to trace the properties of these objects. However, to reliably interpret observations of these ions, an accurate understanding of their formation process is needed.

In this poster, we report our recent absolute measurement of the integral cross section vs. collision energy for  $\text{N}_2 + \text{D}_3^+ \rightarrow \text{N}_2\text{D}^+ + \text{D}_2$ , with an accuracy of about 20%. We have used our dual-source, ion-neutral, merged-fast-beams apparatus, where for our previous work we used photodetachment of fast atomic anions to generate beams of ground-term atomic D, C, and O [3, 4, 5, 6, 7]. For this work, we start with fast  $\text{N}_2^+$  and pass it through a gas cell where a fraction of the beam undergoes nearly resonant electron capture from room-temperature  $\text{N}_2$  to generate the desired fast  $\text{N}_2$  beam. The  $\text{N}_2^+$

is produced in a duoplasmatron source by electron impact ionization of  $\text{N}_2$  via a nearly vertical transition between the vibrational levels of the initial  $\text{N}_2$  and the final  $\text{N}_2^+$ , as they share the same equilibrium geometry and nearly identical vibrational frequencies. Filament sources, such as duoplasmatrons, have been shown to generate  $\text{N}_2^+$  beams with rotational temperatures of  $\sim 600$  K [11], which is expected to be conserved during the nearly resonant electron capture process. Furthermore, previous experimental work has shown that electron capture by  $\text{N}_2^+$  on  $\text{N}_2$  forms an  $\approx 100\%$  ground-term  $\text{N}_2$  beam [8, 9, 10].

This work was supported, in part, by a grant from the U.S. National Science Foundation Division of Astronomical Sciences Astronomy and Astrophysics Grants Program.

### References

- [1] Aikawa Y et al. 2018 *Astrophys. J.* **885** 119
- [2] Sipilä O and Caselli P 2018 *Astron. Astrophys.* **615** A15
- [3] O'Connor A et al. 2015 *Astrophys. J. Suppl. Ser.* **219** 6
- [4] de Ruelle N et al. 2016 *Astrophys. J.* **816** 31
- [5] Hillenbrand P-M et al. 2019 *Astrophys. J.* **877** 38
- [6] Hillenbrand P-M et al. 2020 *Phys. Chem. Chem. Phys.* **22** 27364
- [7] Bowen K P et al. 2021 *J. Chem. Phys.* **154** 084307
- [8] Flannery M R et al. 1973 *J. Chem. Phys.* **59** 5494
- [9] McAfee K B et al. 1981 *J. Phys. B* **14** L243
- [10] McAfee K B 1982 *J. Chem. Phys.* **77** 2399
- [11] Peterson J R et al. 1998 *J. Chem. Phys.* **108** 1978

\*E-mail: [di2224@columbia.edu](mailto:di2224@columbia.edu)

†E-mail: [dws26@columbia.edu](mailto:dws26@columbia.edu)

## Fully Differential Study of Dissociative Capture in $p + H_2$ Collisions

S. Bastola<sup>1</sup>, M. Dhital<sup>1</sup>, B. Lamichhane<sup>1</sup>, R. Lomsadze<sup>2</sup>, A. Hasan<sup>3</sup>, and M. Schulz<sup>1</sup>

<sup>1</sup>Missouri University of Science and Technology, Rolla, MO 65409, USA

<sup>2</sup>Tbilisi State University, Tbilisi, 0179, Georgia

<sup>3</sup>University of United Arab Emirates, Al-Ain, UAE

**Synopsis** Fully differential cross sections were measured for electron capture accompanied by vibrational dissociation as a function of projectile scattering angle.

We have measured fully momentum analyzed protons, emitted in fragmentation of  $H_2^+$ , in coincidence with polar and azimuthal angular resolved neutralized projectiles for 75 keV  $p$  impact. From the data, we extracted fully differential cross sections (FDCS) for dissociative capture [1]. Data were analyzed for two molecular orientations, both of which are perpendicular to the projectile beam direction. One is also perpendicular to the transverse component of the momentum transfer  $q_{tr}$  while the other is parallel to  $q_{tr}$ . Based on the kinetic energy release (KER) we separated dissociation by nuclear excitation to a vibrational continuum state (vibrational dissociation) from dissociation by excitation of the electron to a repulsive molecular state (electronic dissociation).

In the scattering angle-dependence of the FDCS for vibrational dissociation, and selecting the parallel molecular orientation, we observed a pronounced two-center molecular interference pattern. Earlier [2], we reported that this interference pattern was phase-shifted by  $\pi$ . The new data, and employing improved data analysis techniques, revealed that this phase shift is not constant, but rather depends on the scattering angle  $\theta_p$ . However, we did not find any significant dependence on the KER.

A phase shift was observed in previous studies of electronic dissociation for excitation to an anti-symmetric molecular state and convincingly explained by parity conservation [3]. However, in vibrational dissociation the electron is passive and remains in the symmetric ground state so that this explanation does not hold in this case. Based on the observed dependence of the phase shift on  $\theta_p$  and the independence on the KER we have offered a hypothetical explanation for the

phase shift in vibrational dissociation. As the nuclear wave packet is lifted to the vibrational continuum state it can propagate either towards decreasing internuclear separation  $D$  or towards increasing  $D$ . The latter path leads to direct dissociation, for which we do not expect any phase shift. However, for the former path the wave packet first has to be reflected from the molecular potential wall at small  $D$  before dissociation can occur (reflection path). For such a reflection a  $\pi$  phase leap is expected. Depending on which path is stronger, which may depend on  $\theta_p$ , the average phase shift thus can take any value between 0 and  $\pi$ .

If this explanation is correct, one would expect additional interference between the direct and the reflection paths because they are indistinguishable.

The phase angle for such an interference should depend on the KER. Indeed, in the KER dependence of the interference term we did observe an oscillating pattern (see Fig. 1). Therefore, these data are supportive of our explanation, but they do not provide conclusive evidence.

This work was supported by NSF.

- [1] S. Bastola et al., PRA **105**, 032805 (2022)  
 [2] L. Schmidt et al., PRL **101**, 173202 (2008)  
 [3] B. Lamichhane et al., PRL **119**, 083402 (2017)

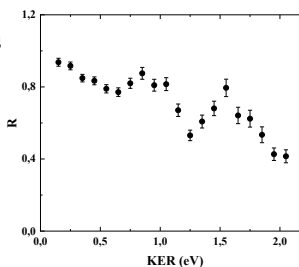


Figure 1 interference term as a function of KER

E-mail: [schulz@mst.edu](mailto:schulz@mst.edu)

## Observation of recurrent fluorescence from excited anthracene cations

J Kusuda<sup>1</sup>, R Fukuzaki<sup>1\*</sup>, T Majima<sup>1</sup>, H Tsuchida<sup>1,2</sup> and M Saito<sup>1,2†</sup>

<sup>1</sup>Department of Nuclear Engineering, Kyoto University, Kyoto, 615-8540, Japan  
<sup>2</sup>Quantum Science and Engineering Center, Kyoto University, Uji, 611-0011, Japan

**Synopsis** The recurrent fluorescence of anthracene cations was investigated using an electrostatic ion beam trap. The photons on the  $D_2 \rightarrow D_0$  transition of the trapped anthracene cations were measured as a function of the storage time. The emission of photons was found to continue until the order of milliseconds, suggesting that our observed photons are the recurrent fluorescent photons.

The electronic excitation energy of molecules isolated in a vacuum is distributed to all vibrational states through internal conversion (IC) in a time range of picoseconds. After the IC process, the vibrationally excited states decay gradually through infrared radiation. The time scale of this vibrational radiative cooling is typically from milliseconds to seconds. Léger et al suggested a faster radiative cooling process in which the vibrational energies are reconverted to the electronic energy (inverse IC) and subsequently emitted as visible fluorescence (recurrent fluorescence) [1]. Recently, we succeeded in directly observing the recurrent fluorescence from naphthalene cations [2]. In this work, we aimed to detect recurrent fluorescence from anthracene cations for which indirect evidence of cooling by recurrent fluorescence has already been reported [3]. Because the cooling time through inverse IC is expected to be long at a time scale of approximately 1 ms, an ion storage technique is required to measure recurrent fluorescence. In this experiment, we used an electrostatic ion beam trap constructed at our laboratory [4]

Excited anthracene cations ( $C_{14}H_{10}^+$ ) were produced using an electron impact ion source from anthracene molecules, which were evaporated from an oven close to the ion source. The ions were extracted from the ion source at a voltage of 1.2 kV. The ion beam was then mass- and charge-analyzed, and only the  $C_{14}H_{10}^+$  ion beam was injected into the trap. The beam was multiply reflected between a pair of mirror electrodes of the trap, resulting in the storage in the trap. The vacuum pressure in the trap was maintained at less than  $2 \times 10^{-7}$  Pa, which is sufficiently low to neglect the decay of excited states due to background gas collisions. The photons

were observed from the direction perpendicular to the reciprocating beam, filtered to a specific wavelength by an optical filter, and detected by a photomultiplier tube. The photon counts as a function of time were recorded by a multi-channel scalar.

Figure 1 shows the photon spectrum as a function of time after the subtraction of dark counts. The photon counts were observed until the millisecond time range. The measured wavelength (724 nm) corresponded to the dipole transition of  $D_2 \rightarrow D_0$  levels of anthracene cations [5], and its spontaneous transition time was estimated to be a sub-microsecond. We consider that the obtained spectrum in millisecond order is attributable to the recurrent fluorescence process.

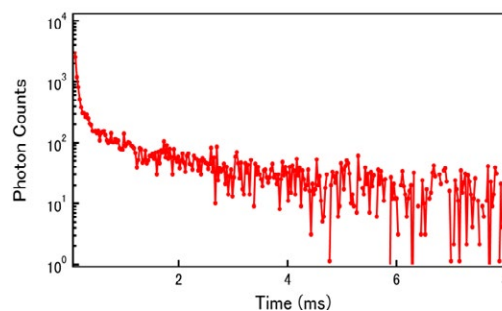


**Figure 1.** Photon spectrum as a function of storage time.

### References

- [1] A. Léger et al. 1988 *Phys. Rev. Lett.* **60** 921
- [2] M. Saito et al. 2020 *Phys. Rev. A* **102** 012820
- [3] S. Martin et al. 2013 *Phys. Rev. Lett.* **110** 063003
- [4] T. Ota et al. 2006 *Jpn. J. Appl. Phys.* **45** 5263
- [5] K. F. Man et al. 1992 *J. Phys. B* **25** 5245

\* E-mail: [fukuzaki.licht.82c@st.kyoto-u.ac.jp](mailto:fukuzaki.licht.82c@st.kyoto-u.ac.jp)

† E-mail: [saito@nucleng.kyoto-u.ac.jp](mailto:saito@nucleng.kyoto-u.ac.jp)



## Efficient molecular oxidation in collisions with superoxide anions

S Díaz-Tendero<sup>1,2,3\*</sup>, C Guerra<sup>4</sup>, S Kumar<sup>5</sup>, F Aguilar-Galindo<sup>1</sup>, AI Lozano<sup>5</sup>, M Mendes<sup>5</sup>, P Limão-Vieira<sup>5</sup>, JC Oller<sup>6</sup>, and G García<sup>4,7†</sup>

<sup>1</sup>Departamento de Química, Universidad Autónoma de Madrid, 28049 Madrid, Spain

<sup>2</sup>Condensed Matter Physics Center (IFIMAC), Universidad Autónoma de Madrid, 28049 Madrid, Spain

<sup>3</sup>Institute for Advanced Research in Chemical Science (IAChem), Univ. Autónoma de Madrid, 28049 Madrid, Spain

<sup>4</sup>Instituto de Física Fundamental, Consejo Superior de Investigaciones Científicas (CSIC), 28006 Madrid, Spain

<sup>5</sup>Atomic and Molecular Collisions Laboratory (CEFITEC), Dep. of Physics, Universidade NOVA de Lisboa, Portugal

<sup>6</sup>Centro de Investigaciones Energéticas Medioambientales y Tecnológicas (CIEMAT), 28040 Madrid, Spain

<sup>7</sup>Centre for Medical Radiation Physics, University of Wollongong, Wollongong, NSW, Australia

**Synopsis** Superoxide anions colliding with benzene molecules at impact energies from 200 to 900 eV are reported to form massive complexes. With the aid of quantum chemistry calculations, we propose a mechanism in which a sudden double ionization of benzene and the subsequent electrostatic attraction between the dication and the anion form a stable covalently bonded  $C_6H_6O_2^+$  molecule, that evolves towards the formation of benzene-diol conformers. These findings lend support to a model presenting a new high energy anion-driven chemistry as an alternative way to form complex molecules.

Benzene is one of the simplest and more stable aromatic ring molecules. It has been considered a prototype for the study of chemical reactions involving biomolecules. On the other hand, oxygen superoxide anion,  $O_2^-$ , is one of the reactive oxygen species (ROS) which are responsible for numerous biochemical processes leading to oxidative damage in living organisms[1]; In particular, 8-oxoguanine is frequently formed by the interaction of ROS with the guanine base in DNA under conditions of oxidative stress, yielding an efficient way of damaging DNA[2]. In this context, oxidative processes in benzene have been extensively studied from different points of view such e.g. in atmospheric reactions[3,4]. However, most of the previous studies fall into the domain of room temperature chemical reactions, i.e. no significant kinetic energy of the reactants is required to trigger such processes. Yet, if the kinetic energy involved in these collisions increases, new channels are open yielding excitation, ionization or even molecular dissociation. Ascenzi et al.[5] showed that oxygen-benzene reactions in atmospheric pressure plasmas induce energetically disfavored chemical processes leading to formation of phenol cations ( $C_6H_5OH^+$ ) and neutral phenol ( $C_6H_5OH$ ). Additionally, relevant ion chemistry processes in the interstellar medium (ISM) have been reported from low-energy anion induced reactions with different

types of hydrocarbons yielding increasingly complex molecules[6].

In this communication, we present gas-phase energetic interactions of a superoxide anion with a benzene molecule leading to an unexpectedly and quite efficient oxidation process of the neutral molecule[7,8]. Under the experimental collision energy range probed (200–900 eV), significant fragmentation of benzene is reported, whilst a comprehensive description of the underlying collision dynamics mechanisms is investigated. The experimental conditions provide binary collisions between the incoming projectile ( $O_2^-$ ) and the neutral target molecule ( $C_6H_6$ ), where no positive ions with higher mass-to-charge ratio ( $m/z$ ) than that of the parent ion ( $m/z=78$  u) are expected to be formed. However, the mass/charge analysis of the collision products reveals the presence of a prominent feature at  $m/z \sim 110$  u for specific impact energies between 200 and 900 eV.

### References

- [1] Marx J 1987 *Science* **235** 529
- [2] Shigdel UK *et al.* 2020 *Nat Commun* **11** 4437
- [3] Norrish RGW 1956 *Proc R Soc London A Math Phys Sci* **234** 160
- [4] Lay TH *et al.* 1996 *J Phys Chem* **100** 6543
- [5] Ascenzi D *et al.* 2006 *J Phys Chem A* **110** 7841
- [6] Larsson M *et al.* 2012 *Rep Prog Phys* **75** 066901
- [7] Guerra C *et al.* 2021 *Sci Rep* **11** 23125
- [8] Guerra C *et al.* 2022 *Int J Mol Sci* **23** 1266

\* E-mail: [sergio.diaztendero@uam.es](mailto:sergio.diaztendero@uam.es)

† E-mail: [g.garcia@csic.es](mailto:g.garcia@csic.es)

## Synthesis of N–O–H bearing species in HONO<sub>2</sub> and H<sub>2</sub>O: an infrared spectroscopic study using heavy-ion irradiation of solid samples

Ana de Barros<sup>1\*</sup>, A. Bergantini<sup>1</sup>, F. Jandorno<sup>1</sup>, A. Domaracka<sup>2</sup>, H. Rothard<sup>2</sup>, P. Boduch<sup>2</sup>, E. Silveira<sup>3</sup>

<sup>1</sup>Department of Physics - CEFET/RJ, Av. Maracanã 229, Rio de Janeiro, 20271-110, Brazil

<sup>2</sup>CIMAP-CIRIL-Ganil, Boulevard Henri Becquerel, CS 65133 14076, Cedex 5 Caen, France

<sup>3</sup>Department of Physics, PUC/Rio, Rua Marquês de São Vicente 225, 22451-900, Rio de Janeiro, RJ, Brazil

The heterogeneous chemistry on surfaces of pure nitric acid and its mixture with water in the troposphere is known to be significant. However, there are currently only a few techniques available for investigating the nature of radiolysis-formed species as well as their chemistry under ion irradiation at lower temperature. We have analyzed the effect of heavy and swift ion irradiation with an astrochemical relevant ice mixture of nitric acid and water (H<sub>2</sub>O:HNO<sub>3</sub>) at 16 K in order to understand the destruction and formation mechanisms of nitric acid and water in astrophysical environments.

When the nitric acid-water film is exposed to ion radiation NO and HONO is produced; moreover, surface-adsorbed nitrogen oxides is converted into astrochemically active N<sub>x</sub>O<sub>y</sub>.

In atmospheric chemistry, nitrogen oxides (NO<sub>x</sub>) refers to nitrogen oxide (NO), nitrogen dioxide (NO<sub>2</sub>), or any mixture of such compounds. In astronomy, however, the term nitrogen oxides may refer to a broader list of chemical species, in which are included small molecules containing only N-O and N-H bonds (e.g., N<sub>x</sub>O<sub>y</sub> and N<sub>x</sub>H<sub>y</sub>), but also some species containing H in addition to N-O, such as HNO (nitrosyl hydride). Nitrogen oxides are thought to have an important role as a nitrogen reservoir in molecular clouds, thus participating in the formation of more complex molecules, such as hydroxylamine (NH<sub>2</sub>OH), a species linked to the formation of prebiotic amino acids in space. Among the N-O-H bearing species of great interest for astronomers and biologists is nitric acid (HNO<sub>3</sub>), a species that greatly resembles nitrogen dioxide, but that has not been detected in the interstellar medium so far [1].

This study was conducted in a high vacuum chamber at the IRRadiation SUD (IRRSUD) beamline at GANIL-France. Nickel heavy ion: <sup>58</sup>Ni<sup>11+</sup> were used to irradiate the ice mixtures at 16 K [2] in two separate experiments. FTIR spectrometer at transmission mode from 4000 to 600 cm<sup>-1</sup> was used for in-situ data gathering.

When the beam was hitting the sample, the chamber pressure was less than 2 x 10<sup>-8</sup> mbar, and IR spectra was collected in different flu-

ences of irradiation, from zero to up to 3 x 10<sup>13</sup> ions.cm<sup>-2</sup> [2] (Fig.1).

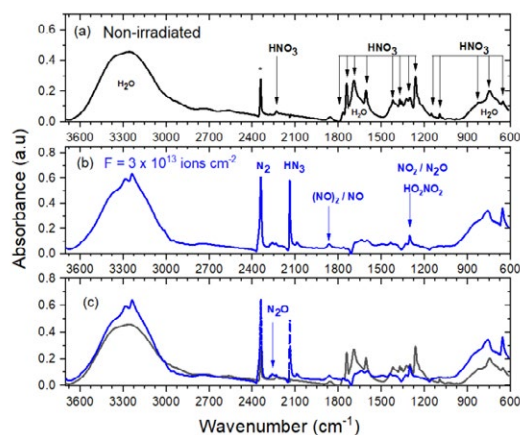


**Figure 1.** Mid-IR spectra of HNO<sub>3</sub>:H<sub>2</sub>O (7:3) mixture: (a) the unirradiated sample; (b) at 3.0 10<sup>13</sup> fluence and (c) a comparison of both spectra.\* can be related to a chemical reaction during deposition of HNO<sub>3</sub> + H<sub>2</sub>O generating NO<sub>2</sub><sup>+</sup> and NO<sub>3</sub><sup>+</sup> [3].

At least 20 bands of HNO<sub>3</sub> are observed before irradiation. During irradiation, 13 new molecules are formed: 5 containing N-O, 1 of H-O, 4 of N-O-H and 3 of N-H. This is the first time that the destruction and formation of these species are analysed.

### References

- [1] Bergantini, A., et al., 2022, *MNRAS*, **511**(1), 31
- [2] de Barros, A.L.F. et al. 2011 *MNRAS*, **418**(2), 1363
- [3] Teranishi, R., & Decius, J. C. 1954. *The Journal of Chemical Physics*, **22**(5), 896-900

\* E-mail: [ana.barros@cefet-rj.br](mailto:ana.barros@cefet-rj.br)

## Chemical shifts in the carbon core-level of ethanol in water-ethanol mixtures

L. M. Cornetta<sup>1,2\*</sup>, R. Marinho<sup>3</sup>, O. Björneholm<sup>2</sup>, H. Ågren<sup>2</sup> and A. N. de Brito<sup>1</sup>

<sup>1</sup>Institute of Physics Gleb Wataghin, State University of Campinas, Campinas, Brazil

<sup>2</sup>Ångströmlaboratoriet, Uppsala University, Uppsala, Sweden

<sup>3</sup>Institute of Physics, University of Brasília, Brasília, Brazil

**Synopsis** X-ray spectroscopy is a powerful tool to investigate chemical environment and several other properties of liquid samples. In this work we report a detailed spectroscopic study of the core level of the ethanol molecule embedded in a liquid water environment. This theoretical and experimental investigation was based on both XPS and resonant Auger decay processes.

The characterization of physical and chemical properties of water-ethanol mixtures at different concentrations are relevant for a number of applications. Several aspects regarding thermodynamics, analysis of configurations, chemical environment, hydrogen bonding distributions, among others, are of central importance when dealing with such mixtures. Besides, ethanol is virtually the simplest system that presents two stable conformers at gas phase - the *anti* and *gauche*. Therefore statistics associated with these two conformers in the liquid phase are also important in such studies.

Spectroscopic signatures in the X-ray range are useful to probe some of the above mentioned properties, since inner-shell electrons provide information about the chemical environment. In this context, we here report a theoretical and experimental study of the carbon 1s core-level of ethanol in ethanol-water mixtures at different ethanol concentrations. Both X-ray photoelectron spectrum (XPS) and resonant Auger spectra have been recorded and the measurements were supported by *ab initio* calculations, where we fo-

cused on the differences between the signatures arising from the -CH<sub>3</sub> and -CH<sub>2</sub>OH carbons. In addition, we present the differences regarding the chemical shifts from the bulk and the surface of the sample. The C1s intensities establish a connection between the vapor composition of binary liquid mixtures and the liquid molecular surface in general.

Our results not only characterize the carbon shifts for the bulk and the surface environment but also show how this quantity depends on the ethanol concentration[1]. Also, it was observed an interesting inversion of the signal broadening regarding the two carbons, when compared to the gas phase[2], in the XPS spectrum. The calculations supporting the measurements were conducted combining molecular dynamics and quantum chemical calculations based on both DFT and RASPT2 level of theory.

### References

- [1] T. Löytynoja et al., 2014 J. Phys. Chem. B **118** 46
- [2] M. Abu samha et al., 2005 Phys. Rev. Letters **95** 103002

---

\*E-mail: [lucascor@unicamp.br](mailto:lucascor@unicamp.br)

## Observation of the hyperfine transition in hydrogen-like $^{208}\text{Bi}^{82+}$

R Sánchez<sup>1\*</sup>, M Horst<sup>2,3</sup>, Z Anelkovic<sup>1</sup>, C Brandau<sup>1</sup>, R J Chen<sup>1</sup>, D Freire Fernández<sup>4</sup>, Ch Geppert<sup>5</sup>, J Glorius<sup>1</sup>, V Hannen<sup>6</sup>, R Hess<sup>1</sup>, P Imgram<sup>2</sup>, S Klammes<sup>1</sup>, K König<sup>2</sup>, G Leckenby<sup>7</sup>, S Litvinov<sup>1</sup>, Y Litvinov<sup>1</sup>, B Lorentz<sup>1</sup>, J Meisner<sup>8</sup>, K Mohr<sup>2,3</sup>, P Müller<sup>2</sup>, W Nörtershäuser<sup>2,3</sup>, S Passon<sup>8</sup>, T Ratajczyk<sup>2</sup>, S Rausch<sup>2,3</sup>, J Rossbach<sup>1</sup>, S Sanjari<sup>1</sup>, R S Sidhu<sup>1,9</sup>, F Sommer<sup>2</sup>, U Spillmann<sup>1</sup>, M Steck<sup>1</sup>, T Stöhlker<sup>1,10,11</sup>, K Ueberholz<sup>6</sup>, C Weinheimer<sup>6</sup> and D Winters<sup>1</sup>.

<sup>1</sup>GSI Helmholtzzentrum für Schwerionenforschung GmbH, Darmstadt, 64291, Germany

<sup>2</sup>Institut für Kernphysik, Technische Universität, Darmstadt, 64289, Germany

<sup>3</sup>Helmholtz Forschungsakademie Hessen für FAIR, Darmstadt, 64289, Germany

<sup>4</sup>Max-Planck-Institut für Kernphysik, Heidelberg, 69117, Germany

<sup>5</sup>Institut für Kernchemie, Johannes-Gutenberg-Universität, Mainz, 55128, Germany

<sup>6</sup>Institut für Kernphysik, Westfälische Wilhelms-Universität, Münster, 48149, Germany

<sup>7</sup>TRIUMF, Vancouver BC, V6T 2A3, Canada

<sup>8</sup>Physikalisch-Technische Bundesanstalt, Braunschweig, 38116, Germany

<sup>9</sup>School of Physics and Astronomy, The University of Edinburgh, Edinburgh EH9 3FD, United Kingdom

<sup>10</sup>Helmholtz-Institut, Jena, 07743, Germany

<sup>11</sup>Institut für Optik und Quantenelektronik, Friedrich-Schiller-Universität, Jena, 07743, Germany

**Synopsis** The hyperfine line of the accelerator-produced isotope hydrogen-like  $^{208}\text{Bi}^{82+}$  has been observed for the very first time ever by direct laser spectroscopy. This is the first step towards the determination of the so-called specific difference in  $^{208}\text{Bi}$ , which can give new insights of bound-state strong-field QED.

Early this century the so-called specific difference between the ground state hyperfine splittings in hydrogen- and lithium-like ions was proposed as a tool to test bound-state QED in the strongest electromagnetic fields presently available in the laboratory [1]. Surprisingly, our measurements of these transitions on  $^{209}\text{Bi}$  by laser spectroscopy at GSI-ESR [2, 3] in the last decade revealed a deviation of the specific difference by  $7\sigma$  from the latest theoretical prediction [4]. This large discrepancy between experiment and theory – also known as the hyperfine puzzle [5] – was, however, resolved by a new measurement of the nuclear magnetic moment in  $^{209}\text{Bi}$  [6].

In this contribution we report on our experiment carried out at the GSI Helmholtz Center for Heavy Ion Research in spring last year. Here we succeeded to produce and separate a sufficient amount of  $^{208}\text{Bi}^{82+}$ , about  $10^5$  ions, to observe for the first time a laser resonance signal of an accelerator-produced isotope in a storage ring. Our preliminary results on this hyperfine transition show a good agreement with rest-frame value predicted in [7]. The experimental observation of this hyperfine line is an important step towards the determination of the specific differ-

\*E-mail: [r.sanchez@gsi.de](mailto:r.sanchez@gsi.de)

ence of  $^{208}\text{Bi}$ , which can provide one of the most significant tests of strong-field bound-state QED in the magnetic sector.

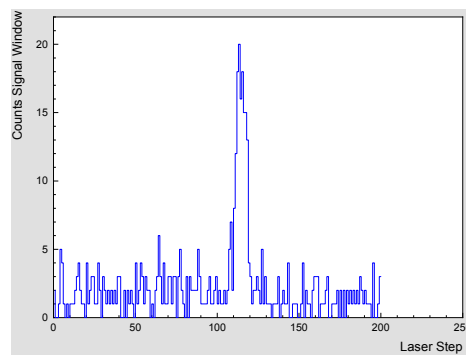


**Figure 1.** First resonance in  $^{208}\text{Bi}^{82+}$  recorded with about  $4 \times 10^5$  ions.

### References

- [1] Shabaev V M *et al.* 2001 *Phys. Rev. Lett.* **86** 3959.
- [2] Lochmann M *et al.* 2014 *Phys. Rev. A* **90** 030501.
- [3] Ullmann J *et al.* 2017 *Nat. Commun.* **8** 15484.
- [4] Volotka A V *et al.* 2012 *Phys. Rev. Lett.* **108** 073001.
- [5] Karr J P 2017 *Nat. Phys.* **13** 533.
- [6] Skripnikov L V *et al.* 2018 *Phys. Rev. Lett.* **120** 093001.
- [7] Schmidt S *et al.* 2018 *Phys. Lett. B* **779** 324.

## Hyperfine-induced transition in highly charged Ne-like ions studied with the cryogenic electrostatic ion storage ring RICE

N Kimura<sup>1\*</sup>, S Harayama<sup>1,2</sup>, K C Chartkunchand<sup>1</sup>, S Kuma<sup>1</sup>, Y Nakano<sup>3</sup>, and T Azuma<sup>1</sup>

<sup>1</sup>Atomic, Molecular and Optical Physics Lab., RIKEN, Saitama, 351-0198, Japan

<sup>2</sup>Department of Physics, Saitama University, Saitama, 338-8570, Japan

<sup>3</sup>Department of Physics, Rikkyo University, Tokyo, 171-8501, Japan

**Synopsis** We present lifetime measurements of the metastable  $2p^5 3s \ ^3P_0$  state of Ne-like  $^{35}\text{Cl}^{7+}$  and  $^{37}\text{Cl}^{7+}$ , which predominantly decays to the  $2p^6 \ ^1S_0$  ground state through a hyperfine-induced transition, utilizing the RIKEN cryogenic electrostatic ion storage ring (RICE).

Hyperfine-induced transitions in atoms and ions, mainly originating from magnetic interactions between the nucleus and electrons (hyperfine interactions), are one of the fundamental atomic processes which play an important role in a variety of research fields, e.g., atomic clocks, X-ray lasers, and astrophysical plasmas. While their transition rates have also been used for verification of theoretical calculations of hyperfine interactions, several experimental rates deviate significantly from the theoretical predictions, triggering further developments of atomic structure calculations [1].

Highly charged Ne-like ions possess a hyperfine-induced transition  $2p^5 3s \ ^3P_0 \rightarrow 2p^6 \ ^1S_0$ , whose decay is relatively fast, as shown in Fig.1(a). Its transition rate sensitive to hyperfine interactions can be a good benchmark for theoretical calculations. However, it is generally difficult to measure since the magnetic-field-induced transition rate is also fast, obscuring the contribution from hyperfine-mixing to the decay process from the metastable  $^3P_0$  state.

Here, we report the first experimental study for the hyperfine-induced transitions of highly charged Ne-like ions using the RIKEN cryogenic electrostatic ion storage ring (RICE) [2]. The RICE serves as an ideal experimental environment for transition rate measurements. The highly isolated vacuum condition ( $\sim 10^{-10}$  Pa) enables us to store objective ions for sufficiently long times ( $\sim 1$  s). The use of the electrostatic device also eliminates magnetic-mixing contributions to the decay of the metastable state. As shown in Fig. 1 (b), we successfully observed the difference in the decay profiles of  $^{35}\text{Cl}^{7+}$  and  $^{37}\text{Cl}^{7+}$ , leading to experimental verification of theoretical calculations of hyperfine interactions.

\* E-mail: [naoki.kimura@riken.jp](mailto:naoki.kimura@riken.jp)

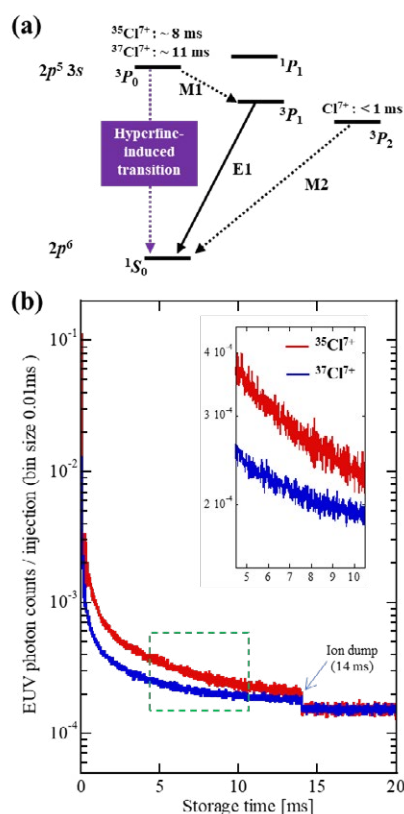


**Figure 1.** (a) Schematic energy diagram with decay channels for the metastable states of the Ne-like ion. (b) Decay profiles of the EUV photon counts during ion storage. The inset shows a magnified view of the decay profile of the area annotated by the dashed square.

### References

- [1] Schippers S *et al.* 2007 *Phys. Rev. Lett.* **98** [033001](#)
- [2] Nakano Y *et al.* 2017 *Rev. Sci. Instrum.* **88** [033110](#)



## Precise determinations of the energy of the $4s^24p\ ^2P_{3/2}-^2P_{1/2}$ transition and the lifetime of the $4s^24p\ ^2P_{3/2}$ level in Ga-like $\text{Mo}^{11+}$

J Liu<sup>1</sup>, Y Wang<sup>1</sup>, J Bao<sup>1</sup>, Y Li<sup>1</sup>, Y Zou<sup>1,2</sup>, L Huang<sup>1,2</sup> and K Yao<sup>1,2\*</sup>

<sup>1</sup>Shanghai EBIT laboratory, and Key Laboratory of Nuclear Physics and Ion-Beam Application (MOE), Institute of Modern Physics, Fudan University, Shanghai 200433, China

<sup>2</sup>Department of Nuclear Science and Technology, Fudan University, Shanghai 200433, China

**Synopsis** We have measured the wavelength of  $4s^24p\ ^2P_{3/2}-^2P_{1/2}$  transition with a precision of a few ppm and the radiative lifetime of  $4s^24p\ ^2P_{3/2}$  metastable level with an accuracy below 0.3% in Ga-like  $\text{Mo}^{11+}$  at an electron beam ion trap. The measured lifetime shows a discrepancy with the theoretical predictions including the electron anomalous magnetic moment correction.

Precise measurements of atomic transition energies and rates are of great interests. Since some forbidden transitions have been proposed as candidates for the ultraprecise optical clocks and may serve as sensitive probes to quantum electrodynamics (QED) effects [1, 2].

Recently, Yu *et al.* [2] have proposed that the  $4s^24p\ ^2P_{3/2}-^2P_{1/2}$  transition in Ga-like  $\text{Mo}^{11+}$  ions are suitable for the ultraprecise optical clocks. To ascertain the feasibility of the transition of interests, some crucial properties are impressive to be investigated, such as the transition energies, lifetimes and quality factors. Utilizing the internal calibration method shown in figure 1(a), the wavelength of the  $4s^24p\ ^2P_{3/2}-^2P_{1/2}$  transition in Ga-like  $\text{Mo}^{11+}$  was determined to 351.3092(24) (nm, vacuum) [3], reaching a precision level of few ppm.

Additionally, precise measurement of the  $4s^24p\ ^2P_{3/2}$  lifetime could be used to test the theoretical models involving the electron anomalous magnetic moment (EAMM) correction. By monitoring the temporal decay of the fluorescence shown in figure 1(b) from the  $4s^24p\ ^2P_{3/2}-^2P_{1/2}$  transition at EBIT, the lifetime of the  $4s^24p\ ^2P_{3/2}$  level was determined with an accuracy level below 0.3%. Comparing with theory, it agrees well with the results without the EAMM correction, while the EAMM correction make it diverge

from our result.

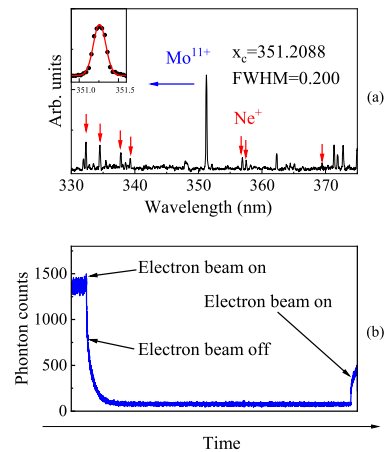


**Figure 1.** (a) Spectrum observed with Mo and Ne injected simultaneously. The  $\text{Ne}^+$  lines are marked with red arrows, while the  $\text{Mo}^{11+}$  line is marked with blue arrow. (b) Typical single-lifetime decay curve of the the  $4s^24p\ ^2P_{3/2}$  level in  $\text{Mo}^{11+}$ .

### References

- [1] A. Lapierre *et al.* 2006 *Phys. Rev. Lett.* **95** 183001
- [2] Y. Yu *et al.* 2019 *Phys. Rev. A* **94** 062502
- [3] Y. Li *et al.* 2021 *J. Phys. B: At. Mol. Opt. Phys.* **54** 235001

\*E-mail: [Keyao@fudan.edu.cn](mailto:Keyao@fudan.edu.cn)



## Precision Measurements of the ${}^2P_{1/2}$ - ${}^2P_{3/2}$ fine-structure splitting in B-like $S^{11+}$ and $Cl^{12+}$ at SH-HtscEBIT

X Liu<sup>1,2</sup>, X P Zhou<sup>2</sup>, W Q Wen<sup>2†</sup>, Q F Lu<sup>1</sup>, C L Yan<sup>1</sup>, J Xiao<sup>1\*</sup>, A V Volotka<sup>3</sup>, Y. S. Kozhedub<sup>4</sup>, M. Y. Kaygorodov<sup>4</sup>, and X Ma<sup>2</sup>

<sup>1</sup>Shanghai EBIT Laboratory, Institute of Modern Physics, Fudan University, Shanghai 200433, China

<sup>2</sup>Institute of Modern Physics, Chinese Academy of Sciences, 730000, Lanzhou, China

<sup>3</sup>School of Physics and Engineering, ITMO University, 197101 St. Petersburg, Russia

<sup>4</sup>Department of Physics, St. Petersburg State University, 199034 St. Petersburg, Russia

**Synopsis** Precision measurements of the electric dipole-forbidden transition between the  ${}^2P_{3/2}$  and  ${}^2P_{1/2}$  fine structure levels of boron-like ions  $S^{11+}$  and  $Cl^{12+}$  have been performed at Shanghai High-Temperature Superconducting electron beam ion trap (SH-HtscEBIT). The M1 transition wavelengths were determined to be 760.9635(29) nm and 574.1539(26) nm (in air) for  $S^{11+}$  and  $Cl^{12+}$ , respectively. As compared to the previously observed results, the accuracy of current experimental results are improved by more than ten times and 200 times for  $S^{11+}$  and  $Cl^{12+}$ , respectively.

Precision measurements of the fine structure transition energy of boron-like ions are considered important not only to investigate the fundamental physics [1], including QED effects, electron correlation effects, relativistic effects and atomic nuclear effects, but also to provide key atomic data for astrophysics [2]. Additionally, the M1 transition of the boron-like ions are considered for highly charged ion optical clocks [3].

We present the experimental results as well as the theoretical calculation of the electric dipole-forbidden transition  ${}^2P_{3/2} - {}^2P_{1/2}$  in boron-like  $S^{11+}$  and  $Cl^{12+}$  ions. The experiments were performed by using a high-resolution Czerny-Turner spectrometer at the SH-HtscEBIT [4]. Emission lines from  $S^{11+}$  and  $Cl^{12+}$  ions are shown in Figure 1 (a) and (b). The observed peaks belong to the  ${}^2P_{3/2} - {}^2P_{1/2}$  transition of B-like  $S^{11+}$  and  $Cl^{12+}$  ions are indicated. All random uncertainties including line position errors and standard deviation of wavelength calibration function have been calculated as a “root sum of squares,” whereas systematic calibration errors and uncertainties from calibration lines have been added linearly. The final transition wavelengths of  $S^{11+}$  and  $Cl^{12+}$  are determined as 760.9635(29) nm and 574.1539(26) nm (in air), respectively. Additionally, the M1 transition energies in  $S^{11+}$  and  $Cl^{12+}$  were evaluated within the ab initio QED framework to compare with the experimental data. The present experimental results agree with the theoretical calculations and provide a possibility to test QED effects and correlation effects with

high accuracy in few-electron highly charged ions. The details can be found in Ref. [5]

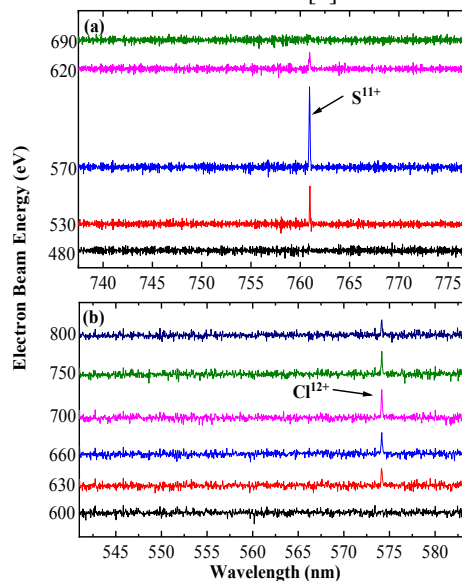


**Figure 1** Emission spectra of B-like ions. (a) for  $S^{11+}$  in the range of 737–777 nm and (b) for  $Cl^{12+}$  in the range of 541–584 nm. The nominal electron beam energies are labeled in the vertical axis respectively for each ion with different colors.

### References

- [1] I. Draganić *et al.* 2003 *Phys. Rev. Lett.* **91** 183001
- [2] G. Y. Liang *et al.* 2012 *A&A.* **547** A87
- [3] V. Yudin *et al.* 2014 *Phys. Rev. Lett.* **113** 233003
- [4] Q. Lu *et al.* 2020 *Phys. Rev. A* **102** 042817
- [5] X. Liu *et al.* 2021 *Phys. Rev. A* **104** 062804

\* E-mail: [xiao\\_jun@fudan.edu.cn](mailto:xiao_jun@fudan.edu.cn)

† E-mail: [wenweiqiang@impcas.ac.cn](mailto:wenweiqiang@impcas.ac.cn)

### EUV spectra of Ge<sup>4+</sup> - Ge<sup>13+</sup> ions in laser-produced plasmas

Y H Wu, H Y Li, S Q He, H D Lu, S Q Cao, M G Su and C Z Dong\*

Key Laboratory of Atomic and Molecular Physics & Functional Material of Gansu Province, College of Physics and Electronic Engineering, Northwest Normal University, Lanzhou 730070, People's Republic of China

**Synopsis** This work reports an experimental and theoretical investigation about EUV spectra of highly-charged germanium ions in laser-produced plasmas. Using the spatio-temporally resolved emission spectroscopy, the emission spectra has been recorded at 30 ns time delay and 0.2 mm distance from target and was found to be dominated by a great number of lines from 3d-nf, np and 3p-3d, 4s,4d transition arrays, which have been identified by comparison with the aid of Hartree-Fock with configuration interaction calculations.

Energy levels and transitions of highly-charged ions have always been of great interest in atomic physics, plasma and fusion physics, and astrophysics. In particular, narrowband radiation in the extreme ultraviolet (EUV) region from highly-charged ions with middle- and high-Z elements have had applications in EUV lithography [1] and radiation metrology [2].

Spectra of laser-produced germanium (Ge) plasmas have been acquired for the 8–16.5 nm wavelength range using spatio-temporally resolved emission spectroscopy. The characteristic features of experimental spectra are dominated by a broad quasi-continuous background and four intense broad bands. These derive from 3d-np,nf and 3p-3d,4s,4d transitions of Ge<sup>4+</sup>-Ge<sup>13+</sup> ions, according to Hartree-Fock calculations that evaluated configuration interaction effects. Figure 1 shows the energy level structures connected with the 3p and 3d excitations.

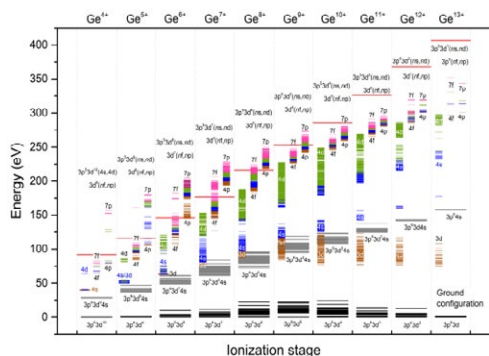


Figure 1. Energy level diagram of Ge<sup>4+</sup>-Ge<sup>13+</sup> ions.

To explain the origin of experimental spectrum, Figure 2 shows the comparison between experimental and theoretical contributions of

individual ion from Ge<sup>4+</sup> to Ge<sup>13+</sup>, which calculated based on the assumption of a normalized Boltzmann distribution among excited states and a steady-state collisional-radiative model. Several strong narrow-band of 3d-4p,4f transitions from Ge<sup>7+</sup> to Ge<sup>10+</sup> ion have been found at 9.02 nm, 9.98 nm, 11.45 nm and 13.09 nm, which have a good agreement with experimental features.

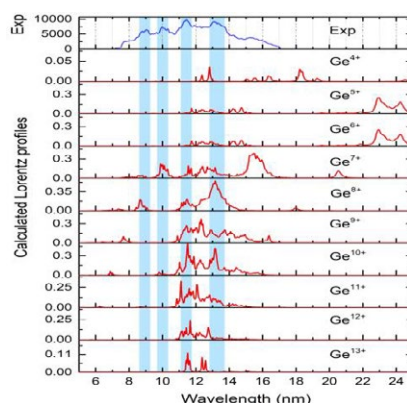


Figure 2. Comparison between experimental and individual theoretical contributions of Ge<sup>4+</sup> up to Ge<sup>13+</sup> ions.

These results will provide data for energy-level structures of highly-charged ions of middle- and high-Z elements and their radiative characteristics in plasmas.

#### References

- [1] Yoshida K et al. 2014 *Applied Physics Express* 7 086202
- [2] Fiedorowicz H et al. 2005 *J. Alloys Compounds* 401 99

\* E-mail: dongcz@nwnu.edu.cn

## Ultra-high precision laser spectroscopy of anti-hydrogen

J Nauta<sup>1</sup>\* on behalf of the ALPHA collaboration

<sup>1</sup>Department of Physics, Faculty of Science and Engineering, Swansea University, Swansea, SA2 8PP, Wales, UK

**Synopsis** To study fundamental symmetries between matter and antimatter, we aim to improve the precision of 1S-2S frequency measurement in antihydrogen, exploiting recent advances in antihydrogen accumulation and laser cooling. Therefore, we have implemented an active hydrogen maser and a Cs fountain clock as a local realization of the SI second. This will advance our frequency determination capability towards a fractional uncertainty as low as  $10^{-15}$ .

One of the big open questions in modern-day physics is the discrepancy between the matter-antimatter imbalance that is observed in the universe, and the balance required by the theoretical foundations that underpin the Standard Model. Hydrogen plays a fundamental role in the development of our understanding of quantum physics, which requires hydrogen to have the same energy levels as its antimatter counterpart, the antihydrogen atom. The 1S-2S transition in hydrogen has been measured to a fractional uncertainty of  $4.2 \cdot 10^{-15}$  [1], while our previous measurement in antihydrogen yields a relative precision of  $2 \cdot 10^{-12}$  [2]. Very recent advances have demonstrated that antihydrogen can now be accumulated and directly laser cooled [3]. Here, recent results and progress to improve the metrology capability of our laser system that will enable more accurate frequency determinations.

The Antihydrogen Laser Physics Apparatus (ALPHA) collaboration at CERN traps slow antiprotons in a Penning trap and combines the antiproton plasma with positrons to form antihydrogen. Antiatoms with a kinetic energy of less than 0.54 K are magnetically trapped and illuminated with a cavity-enhanced laser beam of 243 nm, exciting the forbidden 1S-2S transition. Absorption of a third photon leads to ionization and subsequent detection of the annihilating antiproton by a silicon vertex detector.

The optical frequency of the 243 nm laser system is counted via a frequency comb, which was previously referenced by a GPS-disciplined quartz oscillator. To improve on this, we recently implemented an active hydrogen maser, which is compared to other masers in national metrology labs via GNSS common-view fre-

quency transfer. To correct the maser independently of long-baseline links and obtain a local realization of the SI second, we are currently implementing a Cs fountain clock, which has been built at NPL [4]. The maser alone already led to an improvement of our frequency determination capability by an order of magnitude, while the implementation of the Cs fountain and fiber pathlength stabilization will enable fractional frequency uncertainties of  $10^{-15}$  or better.

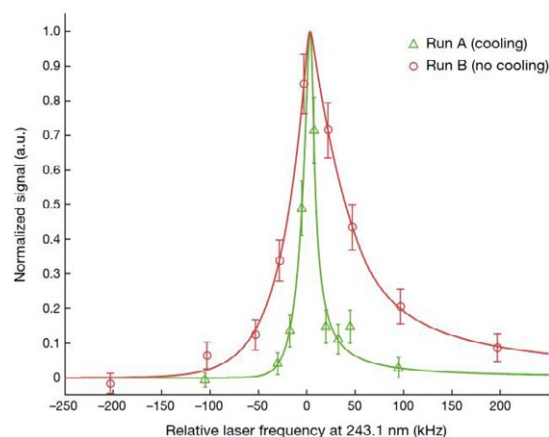


**Figure 1.** Demonstration of the effect of laser cooling on the linewidth of the 1S-2S transition in antihydrogen. [3]

### References

- [1] Parthey C G et al. 2011 *Phys. Rev. Lett.* [107 203001](#)
- [2] Ahmadi M B et al. 2018 *Nature* [557 71](#)
- [3] Baker C J et al. 2021 *Nature* [592 35](#)
- [4] Hendricks R J 2019 *IEEE Trans. Ultrason.* [66 624](#)

\* E-mail: [janko.nauta@cern.ch](mailto:janko.nauta@cern.ch)

## Development of microwave system for a high-precision Lamb shift spectroscopy of antihydrogen atoms

T A Tanaka<sup>1\*</sup>, P Blumer<sup>2</sup>, G Janka<sup>2</sup>, B Ohayon<sup>2</sup>, C Regenfus<sup>2</sup>, M Sato<sup>1</sup>, K S Tanaka<sup>1</sup>  
P Crivelli<sup>2</sup>, and N Kuroda<sup>1†</sup>, on behalf of the GBAR collaboration

<sup>1</sup>Institute of Physics, The University of Tokyo, Komaba, Meguro-ku, 153-8902 Tokyo, Japan

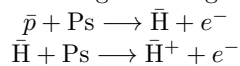
<sup>2</sup>Institute for Particle Physics, ETH Zürich, 8092 Zürich, Switzerland

**Synopsis** An Apparatus for Lamb shift spectroscopy on antihydrogen have been developed to determine the antiproton charge radius. A high-precision measurement using two microwave transmission lines is planned.

Measurements on the charge radius of proton have been actively carried out[1] since a 4% smaller value was reported in 2010 by a laser spectroscopy on muonic hydrogen[2], known as proton charge radius puzzle. On the other hand, the antiproton charge radius has never been experimentally investigated.

We aim to measure the antiproton charge radius by a high-precision Lamb shift spectroscopy on antihydrogen ( $\bar{\text{H}}$ ) atoms[3][4] produced in the GBAR beam line at CERN AD/ELENA.

The objective of the GBAR experiment[5] is to observe the gravitational free-fall of  $\bar{\text{H}}$  atoms by photodetachment of anti-ions ( $\bar{\text{H}}^+$ ) produced in the successive charge exchange reactions:



Around 10% of the  $\bar{\text{H}}$  atoms will be produced in the  $2S$  state for an incoming antiproton energy of 6 keV[6], hence utilized for Lamb shift spectroscopy.

We developed two microwave transmission lines, HyperFine State Selector (HFSS) and MicroWave Scanner (MWS) as shown in Fig. 1, for a high-precision spectroscopy[7].

HFSS depopulates  $2S(F = 1)$  hyperfine states beforehand to reduce the background and at the same time narrow and simplify the overall line-shape to be fitted. We optimized the structure of HFSS to resonate with the transition frequencies of these unwanted states in order to efficiently filter them out.

MWS is then used to obtain Lamb shift spectrum mainly of  $2S(F = 0)$  state. Since microwave frequency is swept here for several hun-

dreds MHz, we designed MWS which realizes flat power transmission.

Thus, developed microwave transmission lines will be installed at the GBAR beam line, and a measurement is planned in 2023 to confirm the existence of  $2S$  state  $\bar{\text{H}}$  atoms by detecting their Lyman- $\alpha$  photons. This will be followed by our first spectroscopy aiming at 1 % precision, and further attempts to improve the precision to the level of deriving the charge radius.

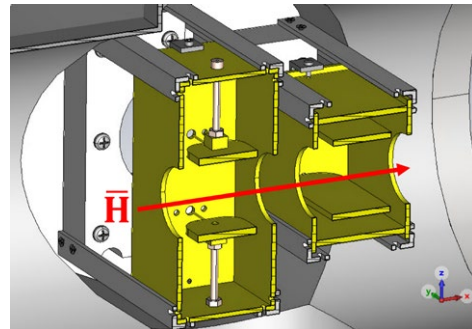


**Figure 1.** HFSS on the left and MWS on the right, with a red arrow indicating the trajectory of  $\bar{\text{H}}$ .

### References

- [1] H. Gao and M. Vanderhaeghen, *RMP*, **94**, 015002 (2022).
- [2] R. Pohl, et al., *Nature* **466**, 213-216 (2010).
- [3] P. Crivelli et al., *Phys. Rev. D*, **94**, 052008 (2016).
- [4] N. Kuroda et al., *JP Conf. Ser.*, **875**, 022054 (2017).
- [5] P. Perez et al., *Hyperfine Interact.*, **233**, 21 (2015).
- [6] C. M. Rawlins, A. S. Kadyrov, A. T. Stelbovics, and I. Bray, *Phys. Rev. A*, **93**, 012709 (2016).
- [7] S. R. Lundeen and F. M. Pipkin., *Metrologia*, **22**, 9-54 (1986).

\*E-mail: [takumi05@radphys4.c.u-tokyo.ac.jp](mailto:takumi05@radphys4.c.u-tokyo.ac.jp)

†E-mail: [kuroda@phys.c.u-tokyo.ac.jp](mailto:kuroda@phys.c.u-tokyo.ac.jp)

## Radiative lifetimes in atomic negative ions

J Karls<sup>1\*</sup>, D Leimbach<sup>1</sup>, M K Kristiansson<sup>2</sup>, N D Gibson<sup>3</sup>, H T Schmidt<sup>2</sup>, C W Walter<sup>3</sup>  
and D Hanstorp<sup>1</sup>

<sup>1</sup>Department of physics, University of Gothenburg, Gothenburg, SE-412 96, Sweden

<sup>2</sup>Department of physics, Stockholm university, AlbaNova, Stockholm, SE-106 91, Sweden

<sup>3</sup>Department of Physics and Astronomy, Denison University, Ohio, 43023, USA

**Synopsis** Radiative lifetimes of metastable states in several atomic negative ions have been investigated at the Double ElectroStatic Ion Ring ExpERiment (DESIREE) facility. The ions are stored in the cryogenic storage ring for several seconds or minutes and selective photodetachment is used to measure the population of the excited state over time and the decay rate is extracted. Radiative lifetimes for ions such as Rh<sup>-</sup>, W<sup>-</sup>, Bi<sup>-</sup> and several others have been mapped out.

The first new scientific output from the Double ElectroStatic Ion Ring ExpERiment (DESIREE) in Stockholm was a measurement of the lifetime of the metastable  $^2P_{1/2}^o$  level in  $^{32}\text{S}^-$  [1]. Subsequently, lifetimes of excited states in several atomic negative ions have been measured.

Since transitions between bound states in atomic negative ions are predominantly forbidden, lifetimes of excited states in negative ions are often very long. This means the lifetimes can only be investigated if the ions can be stored for a longer period of time, for example at a storage ring facility such as DESIREE [2].

Negative ions are produced in a sputtering ion source which yields very high populations in excited states. When the ions are injected into the storage ring, the lifetimes are measured using the selective laser photodetachment spectroscopy technique, where photons are used to photodetach only excited states in the ions. The laser beam intersects with the ion beam in a crossed beam or collinear geometry and the neutral residuals are detected. The lifetime is extracted from the measured population of the excited state as a function of the time after injection.

These experimental results can be used to benchmark theoretical methods beyond the independent particle model, since such models break down in the case of negative ions. In addition to this, the selective photodetachment method makes it possible to completely deplete the excited states in negative ions. This is useful for precision measurements of electron affinities, recently demonstrated in the case of O<sup>-</sup> at DESIREE [3]. Further, this method exhibits potential for mutual neutralization measurements,

\*E-mail: [julia.karls@physics.gu.se](mailto:julia.karls@physics.gu.se)

where a well-defined quantum state is desired.

So far, we have studied e.g. Ir<sup>-</sup> [4], Bi<sup>-</sup> [5], Rh<sup>-</sup>, Sb<sup>-</sup>, W<sup>-</sup> and Ge<sup>-</sup>. One ion studied recently is  $^{75}\text{As}^-$ , where two excited states were observed. The preliminary results indicate a  $^3P_1$  state with a lifetime of 44(2) s shown in figure 1.

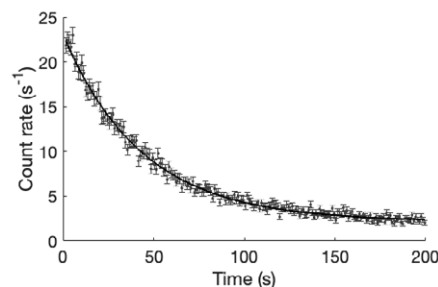


**Figure 1.** Photodetachment signal for the excited state  $^3P_1$  in  $\text{As}^-$  as a function of time after injection. An exponential fit yields a lifetime of 44(2) s.

The goal is to map out the lifetimes in all atomic negative ions and I will in this work present the experimental method and give a brief overview of the results to date.

### References

- [1] Bäckström E *et al* 2015 *Phys. Rev. Lett.* **114** 143003
- [2] Schmidt H T *et al* 2013 *Rev. Sci. Instrum.* **84**, 055115
- [3] Kristiansson, M K *et al* 2022 *Nat. Commun.* **13**, 5906
- [4] Kristiansson, M K *et al* 2022 *Phys. Rev. A* **103**, 062806
- [5] Kristiansson, M K *et al* 2022 *Phys. Rev. A* **105**, L010801



## Determination of the $2s^22p^5 \rightarrow 2s2p^6$ transition energy in fluorine-like nickel utilizing a low-lying dielectronic resonance

S X Wang<sup>1,2</sup>, Z K Huang<sup>3</sup>, W Q Wen<sup>3</sup>, H B Wang<sup>3</sup>, S Schippers<sup>1</sup>, Z W Wu<sup>4</sup>, Y S Kozhedub<sup>5</sup>, M Y Kaygorodov<sup>5</sup>, A V Volotka<sup>6</sup>, K Wang<sup>7</sup>, X Ma<sup>3†</sup> and L F Zhu<sup>2\*</sup> for the DR collaboration @ HIRFL

<sup>1</sup> I. Physikalisches Institut Justus-Liebig-Universität Gießen and HFHF Campus Gießen, Gießen, 35392, Germany

<sup>2</sup> Department of Modern Physics, University of Science and Technology of China, Hefei, 230026, China

<sup>3</sup> Institute of Modern Physics, Chinese Academy of Sciences, Lanzhou, 730000, China

<sup>4</sup> College of Physics and Electronic Engineering, Northwest Normal University, Lanzhou, 730070, China

<sup>5</sup> Department of Physics, St. Petersburg State University, Universitetskaya 7/9, 199034, St. Petersburg, Russia

<sup>6</sup> School of Physics and Engineering, ITMO University, Kronverkskiy prospekt 49, 197101, St. Petersburg, Russia

<sup>7</sup> The College of Physics Science and Technology, Hebei University, Baoding 071002, China

**Synopsis** We determined the  $2s^22p^5 \ ^2P_{3/2} \rightarrow 2s2p^6 \ ^2S_{1/2}$  transition energy in fluorine-like nickel by combining the experimental low-lying ( $2s2p^6[{}^2S_{1/2}]6s$ )<sub>*J=1*</sub> dielectronic resonance and the theoretical binding energy of the 6s electron in the resonance state.

The electron-ion recombination spectrum of fluorine-like nickel ion (Ni<sup>19+</sup>) has been measured at the heavy-ion storage ring HIRFL-CSRm [1]. The measured DR resonances are identified by comparing the experimental data with relativistic calculations utilizing the flexible atomic code (FAC). The experimental determination of the collision energy for the first resonance via the ( $2s2p^6[{}^2S_{1/2}]6s$ )<sub>*J=1*</sub> intermediate state at 86 meV reaches an uncertainty as low as  $\pm 4$  meV [2].

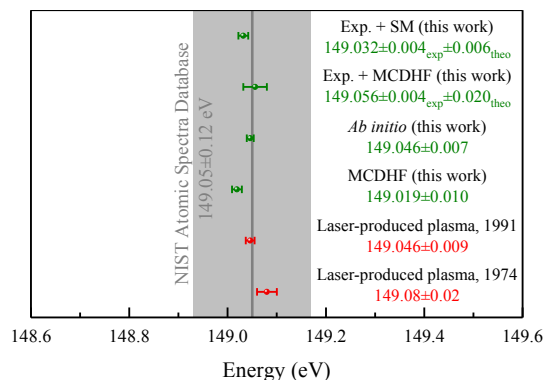


**Figure 1.** Comparison of the present experimental and theoretical transition energies with previous plasma observations and the NIST recommended data [3].

By employing the Multi-Configuration Dirac-Hartree-Fock (MCDHF) approach and stabilization method (SM), the binding energies of the 6s electron in the ( $2s2p^6[{}^2S_{1/2}]6s$ )<sub>*J=1*</sub> state are calculated, and yielding the following values of  $149.056(4)_{\text{exp}}(20)_{\text{theo}}$  eV and  $149.032(4)_{\text{exp}}(6)_{\text{theo}}$

eV, respectively, for the  $2s^22p^5 \ ^2P_{3/2} \rightarrow 2s2p^6 \ ^2S_{1/2}$  transition energy in fluorine-like nickel ion. Figure 1 displays a comparison of the present experimental and theoretical transition energies with previous plasma observations and the NIST recommended data. In addition, *ab initio* theoretical calculations with two different starting potentials, reveal that second-order QED contributes by about -0.03 eV to the total transition energy, and can, thus, be assessed by the present precision DR spectroscopic measurement. Table 1 presents the calculated individual contributions to the  $2s^22p^5 \ ^2P_{3/2} \rightarrow 2s2p^6 \ ^2S_{1/2}$  transition energy in fluorine-like nickel.

**Table 1.** Individual contributions to the  $2s^22p^5 \ ^2P_{3/2} \rightarrow 2s2p^6 \ ^2S_{1/2}$  transition energy in fluorine-like nickel (in eV).

Contribution	Core-Hartree	Kohn-Sham
Dirac	123.911	128.743
Correlation (1)	27.190	22.723
Correlation (2)	-1.536	-1.972
Correlation (3)	0.032(2)	0.102(2)
QED (1)	-0.506	-0.510
QED (2)	-0.033(6)	-0.028(6)
Recoil	-0.012(3)	-0.012(3)
Total	149.046(7)	149.046(7)

### References

- [1] S X Wang *et al.*, A&A [627 A171](#) (2019)
- [2] S X Wang *et al.*, Phys. Rev. A [106 042808](#) (2022)
- [3] Kramida, A., Ralchenko, Yu., Reader, J., and NIST ASD Team (2022). NIST Atomic Spectra Database (ver. 5.10).

\* E-mail: [lfzhu@ustc.edu.cn](mailto:lfzhu@ustc.edu.cn) † E-mail: [x.ma@impcas.ac.cn](mailto:x.ma@impcas.ac.cn)



## Breit effect on radiative transition rates of highly charged heavy ions

Zhimin Hu<sup>1\*</sup>

<sup>1</sup>Key Laboratory of Radiation Physics and Technology of Ministry of Education, Institute of Nuclear Science and Technology, Sichuan University, Chengdu 610064, China

**Synopsis** We present a giant contribution of the retardation effect in an electron-electron interaction via observing strong electric-dipole-allowed radiative transition rates. The relative transition rates are obtained for two dominant radiative transitions from the  $1s^2s^22p_{1/2}2p_{3/2}$  inner-shell excited state of boronlike tungsten and bismuth ions to  $1s^22s^22p_{1/2}$  and  $1s^22s^22p_{3/2}$ , and it was found that the transition rate ratio between the two transitions is affected by the retardation effect up to more than 100%.

The relativistic and quantum electrodynamics effects in electron-electron interaction can be described by the Breit interaction. In contrast to the minor contribution to atomic structure, it has been found that the Breit interaction can have a significant contribution to collision processes of highly charged heavy ions with electrons. The unexpectedly large or even dominant contribution in the electronic collisions is attributed to that the Breit term plays an important role in the electron-electron interaction operator.

On the other hand, the Breit interaction can hardly be expected to affect radiative transition

probabilities since it has no contribution to the operator for the radiative transition and only a small contribution to the transition frequency and the wavefunctions. In stark contrast to the previous studies, we predicted an unprecedentedly giant modification by the Breit interaction for electric dipole allowed transitions from the strongly correlated  $1s2s^22p^2$  inner shell excited state of B-like heavy ions, and it has been experimentally demonstrated with the electron beam ion traps in Shanghai and Tokyo. We elucidate the underlying mechanism is due to the drastic change in the wavefunctions of the  $1s2s^22p^2$  state resulting from the relativistic electron correlation effect appeared as a Breit-interaction-induced avoided crossing.

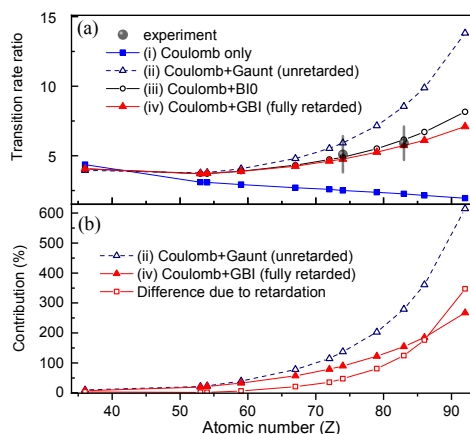


**Figure 1.** The Breit effect in the radiative transition of the excited state of B-like ions

### References

- [1] Zhimin Hu\* *et al.* 2022 *Phys. Rev. A* **105** L030801
- [2] Zhihao Yang, ..., Zhimin Hu\*. 2022 *Opt. Express* **30** 25326
- [3] Zhencen He, ..., Zhimin Hu\* *et al.* 2022 *J. Quant. Spectrosc. Radiat. Transf.* **288** 108276
- [4] Zhencen He, ..., Zhimin Hu\* *et al.* 2022 *Phys. Rev. A* **105** 022818
- [5] Junwen Gao, ..., Zhimin Hu\* *et al.* 2021 *Phys. Rev. A* **104** 032826
- [6] Zhihao Yang, ..., Zhimin Hu\*. 2021 *Phys. Rev. A* **104** 022809
- [7] Li Zhou, ..., Zhimin Hu\*. 2023 *J. Quant. Spectrosc. Radiat. Transf.* **297** 108469

\*E-mail: [huzhimin@scu.edu.cn](mailto:huzhimin@scu.edu.cn)

## The QED correction of the transition energy of $\text{Ne}^{7+}$ and $\text{Ca}^{17+}$ ions

Bingbing Li<sup>1</sup>, Jun Jiang<sup>1\*</sup>, Lei Wu<sup>1</sup>, D.H Zhang<sup>1</sup>, L.Y Xie<sup>1</sup>, D.X Sun,<sup>1</sup> C.Z Dong<sup>1</sup>

<sup>1</sup>Key Laboratory of Atomic and Molecular Physics and Functional Materials of Gansu Province, College of Physics and Electronic Engineering, Northwest Normal University, Lanzhou 730070, China

**Synopsis** The  $2p_{1/2} \rightarrow 2s_{1/2}$  transition energy of  $\text{Ne}^{7+}$  and  $\text{Ca}^{17+}$  ions are calculated by combining GRASP2018 and QEDMOD packages. The contributions of quantum electrodynamics effects are investigated. The contribution of off-diagonal elements have significant influence in the transition  $2p_{1/2} \rightarrow 2s_{1/2}$  of  $\text{Ne}^{7+}$  and  $\text{Ca}^{17+}$ .

High-precision measurements of the energy levels for many-electron ions require accurate theoretical calculations including relativistic, electron correlation, Breit interaction (BI) and quantum electrodynamics (QED) effects as well as nuclear recoil correlation. The simplest many-electron ions are Li-like ions, which are of particular interest since their properties can be calculated with high accuracy and comparison with experiments provides stringent tests of the theory. Investigations of Li-like ions can also accurately test the bound-state QED of many-body systems.

**Table 1.** The  $2p_{1/2} \rightarrow 2s_{1/2}$  transition energy of  $\text{Ne}^{7+}$  and  $\text{Ca}^{17+}$  ions (in eV). The superscripts “G” and “M” represent the QED effects contribution of total results are calculated using GRASP2018 and QEDMOD, respectively.

		$\text{Ne}^{7+}$	$\text{Ca}^{17+}$
	CI	15.8896	35.9457
	BI	0.0187	0.2229
	recoil	-0.0042	-0.0103
GRASP	SE	-0.0148	-0.2052
	VP	0.0008	0.0143
MOD	SE	-0.0156	-0.2098
	VP	0.0007	0.0138
Total <sup>G</sup>		15.8901	35.9674
Total <sup>M</sup>		15.8892	35.9624
Expt.		15.8887(2) [3]	35.9625(25)[4]

The QED effects are separated into two parts, namely, self-energy (SE) and vacuum polarization (VP). In this work, we compared the calculation of SE and VP using Grasp2018 and QED-

MOD [1, 2]. In the current GRASP2018 package, SE corrections are obtained based on a screened hydrogenic approximation, which contains diagonal matrix elements only. In the QEDMOD method, the one-loop QED operator is replaced by model potential operator, which contains diagonal and nondiagonal matrix elements of the one-loop SE operator. Table 1 lists the  $2p_{1/2} \rightarrow 2s_{1/2}$  transition energy and the contributions of the BI, QED effects and nuclear recoil correction, along with a comparison with experimental results [3, 4]. The “Total” denotes the sum of these contributions, where the “Total<sup>G</sup>” represents the contribution of QED in these summations from the GRASP2018 calculation, and “Total<sup>M</sup>” represents the contribution of QED from the QEDMOD calculation. The accuracy of “Total<sup>M</sup>” results is about one order of magnitude higher than the “Total<sup>G</sup>” results. It indicates that the contribution of off-diagonal elements are very important in the transition  $2p_{1/2} \rightarrow 2s_{1/2}$  of  $\text{Ne}^{7+}$  and  $\text{Ca}^{17+}$ .

This work has been supported by the National key Research and Development Program of China under Grant No. 2022YF A1602500, the National Natural Science Foundation of China under Grant No. 12174316.

### References

- [1] V.M Shabaev *et al* 2015 *Computer Physics Communications* **189** 175-181
- [2] V.M Shabaev *et al* 2013 *Phys. Rev. A* **88** 012513
- [3] Bengt Edlén, 1983 *Physica Scripta* **28** 51
- [4] Martin *et al* 1985 *Journal of physical and chemical reference data* **14** 751

\*E-mail: [phyjiang@yeah.net](mailto:phyjiang@yeah.net)

## Recent progress of muon catalyzed fusion study:

### II. New muonic X-ray spectroscopy

Y Toyama<sup>1\*</sup>, T Azuma<sup>2</sup>, D A Bennett<sup>3</sup>, W B Doriese<sup>3</sup>, M S Durkin<sup>3</sup>, J W Fowler<sup>3</sup>,  
 J D Gard<sup>3</sup>, T Hashimoto<sup>4</sup>, R Hayakawa<sup>5</sup>, G C Hilton<sup>3</sup>, Y Ichinohe<sup>5</sup>, K Ishida<sup>2</sup>,  
 S Kanda<sup>6</sup>, N Kawamura<sup>6</sup>, Y Kino<sup>7</sup>, R Konishi<sup>7</sup>, Y Miyake<sup>6</sup>, K M Morgan<sup>3</sup>,  
 R Nakashima<sup>7</sup>, H Natori<sup>6</sup>, H Noda<sup>8</sup>, G C O'Neil<sup>3</sup>, S Okada<sup>1</sup>, T Okumura<sup>9</sup>, K Okutsu<sup>7</sup>,  
 C D Reintsema<sup>3</sup>, K Sasaki<sup>7</sup>, T Sato<sup>5</sup>, D R Schmidt<sup>3</sup>, K Shimomura<sup>6</sup>, P Strasser<sup>6</sup>,  
 D S Swetz<sup>3</sup>, T Takahashi<sup>10</sup>, M Tampo<sup>6</sup>, H Tatsuno<sup>9</sup>, J N Ullom<sup>3</sup>, I Umegaki<sup>6</sup>,  
 S Watanabe<sup>11</sup>, S Yamada<sup>5</sup>, T Yamashita<sup>7</sup>

<sup>1</sup>Chubu University, Kasugai 487-8501, Japan

<sup>2</sup>RIKEN, Wako 351-0198, Japan

<sup>3</sup>National Institute of Standards and Technology, Boulder, CO 80305, USA

<sup>4</sup>Japan Atomic Energy Agency (JAEA), Tokai 319-1184, Japan

<sup>5</sup>Rikkyo University, Tokyo 171-8501, Japan

<sup>6</sup>High Energy Accelerator Research Organization (KEK), Tsukuba 305-0801, Japan

<sup>7</sup>Tohoku University, Sendai 982-0826, Japan

<sup>8</sup>Osaka University, Toyonaka 560-0043, Japan

<sup>9</sup>Tokyo Metropolitan University, Tokyo 192-0397, Japan

<sup>10</sup>The University of Tokyo, Kashiwa 277-8583, Japan

<sup>11</sup>Japan Aerospace Exploration Agency (JAXA), Sagami-hara, Kanagawa 252-5210, Japan

**Synopsis** A series of high-resolution muonic atom/molecule X-ray spectroscopy experiments has been conducted using state-of-the-art X-ray detectors at J-PARC in recent years. Here, we will focus on the dissociative X-ray spectroscopy experiment from the resonant muon molecules, which play an important role in muon-catalyzed fusion, conducted in 2023 with a solid hydrogen target.

We have been promoting high resolution X-ray spectroscopy of muonic atoms and molecules at the J-PARC using a multi-element superconducting Transition Edge Sensor (TES) microcalorimeter spectrometer [1] since 2019. Among them, a resonant muonic molecule  $dd\mu^*$ , which is Feshbach resonance of  $\mu d$  atom and deuteron, is an interesting target for quantum few body system studies. This is because the latest few-body calculation has revealed that  $dd\mu^*$  plays an important role in the muon catalyzed fusion ( $\mu$ CF) cycle and its ro-vibrational states can be explored by a structure of an X-ray spectrum (1.7-2 keV) emitted when it dissociates [2]. However, the conventional silicon semiconductor detector, e.g. Silicon Drift Detector, with an energy resolution of  $\Delta E > 100$  eV (FWHM) is unable to separate  $dd\mu^*$  dissociate X-ray from  $d\mu$  atomic X-ray, and is also unable to discriminate the difference in the vibrational quantum

numbers of the resonant molecules. Therefore, TES, which can achieve ultra-high energy resolution  $\Delta E \sim 5$  eV (FWHM) at 2 keV, was used to measure the X-ray from  $dd\mu^*$ .

In March 2022, a pilot experiment using gaseous hydrogen and deuterium targets were performed, showing that a resolution of 5 eV (FWHM) can be achieved for 2 keV X-rays in a high intensity pulsed muon beam environment, while no signal was obtained from  $dd\mu^*$ . In February 2023, an experiment using a solid deuterium target was performed based on the theoretical prediction that the production of  $dd\mu^*$  would be significantly increased by using a higher density target. In this presentation, overview of these experiments at the J-PARC and the preliminary spectrum will be shown.

#### References

- [1] W.B. Doriese *et al.*, 2017 *Rev. Sci. Instrum.* **88** 053108
- [2] T. Yamashita *et al.*, 2022 *Sci Rep* **12** 6393

\*E-mail: [toyama@isc.chubu.ac.jp](mailto:toyama@isc.chubu.ac.jp)

## Photoelectron signature of dressed-atom stabilization in intense XUV field

E Olofsson<sup>1\*</sup>, J M Dahlström<sup>1†</sup>

<sup>1</sup>Department of Physics, Lund University, Box 118, SE-221 00 Lund, Sweden

**Synopsis** We study non-perturbative effects in multiphoton (1+1) ionization of He atoms using the resolvent operator technique. We show that a previously predicted stabilization effect (Beers and Armstrong 1975) should be present in the case of ionization via  $1s2p$  in He when using circularly polarized light, and that the effect can be inferred from the asymmetry of the Autler-Townes doublet in the photoelectron spectrum.

We consider non-perturbative resonant multiphoton ionization (1+1) from atoms, for parameters accessible to a free-electron laser [1]. This is studied using the resolvent operator technique, enabling the description of non-perturbative effects such as Rabi oscillations. In addition to ionization from the excited state, non-resonant contributions also have to be considered at intensities on the order of  $10^{13} - 10^{14}$  W/cm<sup>2</sup> [1, 2]. The interference of these pathways is responsible for the dressed-atom stabilization effect predicted by Beers and Armstrong [3].

The Rabi oscillations lead to an Autler-Townes (AT) doublet structure in the photoelectron spectrum [1, 4], that can be interpreted in terms of the dressed states of the atom. Using a model based on time-dependent perturbation theory, we showed that interference between the resonant and non-resonant pathways leads to a detuning-dependent asymmetry between the two components of the doublet [1]. The model was able to explain observations made at FERMI for the  $1s^2 - 1s4p$  resonance in He, and agreed with simulations performed using the time-dependent configuration interaction singles method [1].

Here we extend the model used in Ref. [1], by accounting for depletion and AC-Stark shifts in the two-level system through an effective Hamiltonian. This is used to study photoelectrons resulting from resonant ionization with linearly or circularly polarized light. We show how the stabilization effect predicted by Beers and Armstrong depends on the number of available ionization continua, and that only circular polarization allows for stabilization in the case of ionization via  $1s2p$  in He [2]. Our main result is that

a signature of stabilization should be present in the photoelectron spectrum, with the component of the AT doublet associated to the stabilized dressed state vanishing for certain laser parameters. At the point of stabilization the spectrum will therefore be nearly completely asymmetric, with regards to the components of the AT doublet, as illustrated in Fig. 1.

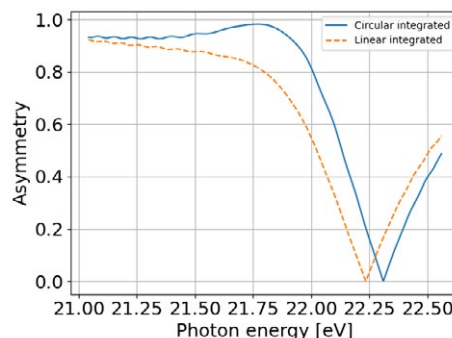


**Figure 1.** Asymmetry of the AT doublet for circular (full line) and linear polarization (dashed line) when the pulse duration is equal to 10 Rabi periods. When stabilization occurs the doublet becomes completely asymmetric (single peak) with asymmetry value close to one.

### References

- [1] Nandi S *et al.* 2022 *Nature* **608** 488
- [2] Olofsson E and Dahlström J M 2023 [arXiv:2305.07363](https://arxiv.org/abs/2305.07363)
- [3] Beers B L and Armstrong L 1975 *Phys. Rev. A* **12** 2447
- [4] Autler S H and Townes C H 1955 *Phys. Rev.* **100** 703

\*E-mail: [edvin.olofsson@matfys.lth.se](mailto:edvin.olofsson@matfys.lth.se)

†E-mail: [marcus.dahlstrom@matfys.lth.se](mailto:marcus.dahlstrom@matfys.lth.se)

## Laser-assisted reduction of graphene oxide coated on melamine sponge for advanced application in electromagnetic interference shielding

Yitbarek Fitwi<sup>1</sup>, Lee Hun<sup>1\*</sup>

<sup>1</sup>School of Electrical Engineering and Computer Science, Gwangju Institute of Science and Technology, Gwangju 61005, Republic of Korea

### Synopsis

Owing to their unique porous structure and excellent mechanical properties, i.e., lightweight, flexibility, compressibility, and breathability melamine foam (MF)-based electromagnetic interference (EMI) shielding materials are an excellent choice. Their 3D porous network structure transforms the EM energy into thermal energy through both conductive dissipation and multiple scattering and reflections, thereby, prevents secondary EMI pollution. Meanwhile, their lightweight and flexibility makes them favorable for practical application in aerospace and automobile industries.

For applications in EMI-shielding, MFs need to be modified with conductive materials, such as reduced graphene oxide (rGO). The state-of-art surface modifications of MF with rGO involves, coating GO on MF followed by reduction of GO to rGO hydrother-

mally in the presence of toxic and hazardous chemicals, like hydrazine. To avoid the use of such toxic chemicals, herein, we propose a facile and green laser-induced reduction process of GO coated on the surface of MF. First, GO was deposited on MF via simple dip coating. Next, the GO/MF composite was subjected to a femtosecond (fs) laser (780 nm wavelength; 70 fs pulse width; 50 MHz repetition rate) with a varied power range, 2 -18 mW.

The mechanism of reduction was studied via different analytical tools, i.e., SEM, XPS, and Raman spectroscopy. Results revealed that the laser-induced reduction of GO involves two pathways: (i) direct transformation from  $sp^3$  to  $sp^2$  carbon and (ii) cleavage and removal of oxygen functionalities. Performance evaluation of the EMI properties of the rGO/MF composite material is currently under investigation.

### References

- [1] D.L. Gong et al 2021 *J. Material Science & Technology*. 80 234-243.
- [2] R.M. Rudenko et al 2020 *Composites Science & Technology* 198 108284.

---

\* E-mail: lee2007@mju.ac.kr

# Quantification of Pressure-Enhanced Electron-Phonon Coupling in Bi<sub>2</sub>S<sub>3</sub> via Femtosecond Pump-Probe Spectroscopy

B Guan<sup>1</sup>, Y Chen<sup>1</sup>, R Wu<sup>1</sup>, H Liu<sup>1</sup>, Y Jiang<sup>1</sup>, J Dong<sup>2</sup>, Q Li<sup>1\*</sup> and M Jin<sup>1†</sup>,

<sup>1</sup>Institute of Atomic and Molecular Physics, Jilin University, Changchun, 130012, China

<sup>2</sup>State Key Laboratory of Superhard Materials, Jilin University, Changchun, 130012, China

**Synopsis** We demonstrate an efficient method for in-situ quantitative measurement of the electron-phonon coupling (EPC) constant  $\lambda$  of materials under hydrostatic pressure based on the high-pressure ultrafast spectroscopy system developed in recent years.

Theoretical studies have shown that when pressure increases the superconducting critical temperature  $T_c$ , it is often accompanied by the enhancement of the EPC [1], which means that the contribution of electron-phonon interactions to the Cooper pairing cannot be neglected. Therefore, in order to compare with the existing theoretical research and deepen the understanding of the mechanism of superconductivity under high pressure, it is particularly urgent to conduct in-situ quantitative measurements of the EPC in materials under extreme high pressure.

Here we investigated the ultrafast spectra and excited dynamics of few-layer Bi<sub>2</sub>S<sub>3</sub> by coupling a diamond anvil cell (DAC) with a home-built femtosecond broadband pump-probe system. The sample was excited with 400 nm pump pulse and probed by a supercontinuum (450 - 950 nm) after a sequential delay time under external pressure from 0 - 10 GPa.

The transient absorption signal of Bi<sub>2</sub>S<sub>3</sub> exhibited an obvious oscillation structure in the pressure measurement range. We performed global fitting on the transient absorption spectra, and subtracted the contribution of electron relaxation dynamics, thus obtained coherent phonon spectra at various pressures. The coherent phonon oscillation frequency  $\omega_0$  of Bi<sub>2</sub>S<sub>3</sub> was figured out via Fourier analysis, which red-shifted continuously as the pressure increased (pressure-induced phonon softening).

The EPC strength can be quantified by the modified Allen equation [2]:  $\lambda\langle\omega^2\rangle = \frac{2\pi}{3} \frac{k_B T_l}{\hbar\tau_{e-ph}}$ , where  $T_l = 300$  K is the lattice temperature, and  $\tau_{e-ph}$  is the electron-phonon relaxation time, which was obtained by global fitting (Fig. 1(a)). The EPC constant  $\lambda$  is estimated with the ex-

pression:  $\lambda\langle\omega^2\rangle = \lambda\omega_0^2$ , where  $\omega_0$  is the coherent phonon oscillation frequency. Our result is shown in Figure 1.

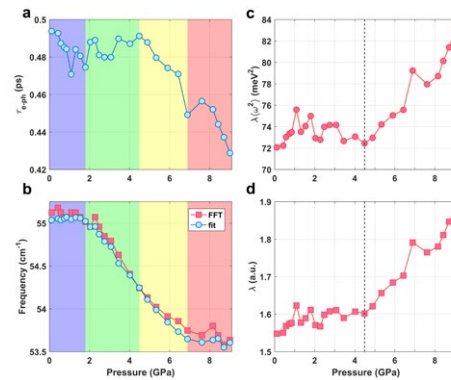


**Figure 1.** Pressure evolution of (a) the electron-phonon lifetime, (b) the oscillation frequency  $\omega_0$ , (c)  $\lambda\langle\omega^2\rangle$  and (d)  $\lambda$ .

As shown in Figure 1, with the pressure grows, both  $\lambda\langle\omega^2\rangle$  and  $\lambda$  increase, indicating evident enhancement of EPC. We believe a second-order isostructural transition occurs at 4.50 GPa (dashed line), after which  $\lambda\langle\omega^2\rangle$  and  $\lambda$  increase more significantly.

We acknowledge support from the National Key Research and Development Program (No. 2019YFA0307701), the National Natural Science Foundation of China (NSFC Nos. 11974138, 12204191).

## References

- [1] Zhang, L., et al., *Phys. Rev. B* **74**(18): 184519 (2006)
- [2] Gadermaier C., et al., *Phys. Rev. Lett.* **105**(25): 257001 (2010)

\*E-mail: liqy21@jlu.edu.cn

†E-mail: mxjin@jlu.edu.cn



## Fragmentation of pyrene molecules following double ionization by 70 eV electron impact

P J M van der Burgt<sup>1\*</sup> and M L Gradziel<sup>1</sup>

<sup>1</sup>Department of Experimental Physics, National University of Ireland Maynooth, Maynooth, Co. Kildare, Ireland

**Synopsis** We have performed coincidence mass spectrometry of fragmentation of pyrene molecules by 70 eV electron impact. Double ionization results in a number of prominent fragmentations producing two singly-ionized fragments. To maximize the fidelity of the final coincidence maps, a detailed model of the coincidence data acquisition was used to analyse the data, fully accounting for the effect of instrumental imperfections such as detector dead time, and for random coincidences. The first results will be presented at the conference.

Our earlier studies of electron impact on polycyclic aromatic hydrocarbons have focused on single ionization of anthracene and phenanthrene [1, 2], and on double ionization of anthracene [3]. Mass spectra for positive ions were recorded for electron energies from 0 to 100 eV in steps of 0.5 eV using a reflectron time-of-flight mass spectrometer. Ion yield curves and appearance energies of most of the fragment ions of anthracene and phenanthrene were determined. In these mass spectra clear evidence was observed for double ionization by electron impact at energies above 21 eV.

In this work we studied double ionization of pyrene employing coincident mass spectrometry, as previously done for anthracene [3]. A field programmable gate array (FPGA, National Instruments cRIO9075) was used for the timing of the pulsing of the electron gun and the ion extraction voltage, and for the recording of mass spectra on an event-by-event basis. LabVIEW code was developed for both the communication between the FPGA and a PC, running on the FPGA chassis, and the control of the experiment and the acquisition of the event-by-event data, running on the PC.

A detailed model of the coincidence data acquisition was used to process this raw event-by-event data, fully accounting for instrumental imperfections such as detector dead time, and for random coincidences. This model was implemented in C++ and enables us to reliably obtain the map of true coincidences.

We have improved the data acquisition by replacing the first ion extraction plate in the relectron mass spectrometer by a plate with a beveled edge to introduce a small amount of focusing and to enhance the collection of ions produced by double ionization. We have also reduced the effective detector deadtime by improving the pulse forming electronics.

We are in the process of measuring a coincidence matrix for double ionization of pyrene at 70 eV electron impact. First results will be presented at the conference. Preliminary results indicate that, similar to anthracene, fragmentations for which the total number of carbon atoms in both fragments is even are generally significantly stronger than fragmentations for which the total is odd.

### References

- [1] van der Burgt P J M, Dunne M, and Gradziel M L 2018 *Eur. Phys. J. D* **72**, 31
- [2] van der Burgt P J M, Dunne M, and Gradziel M L 2019 *J. Phys. Conf. Ser.* **1289**, 012008
- [3] van der Burgt P J M and Gradziel M L 2022 *Eur. Phys. J. D* **76**, 60

\* E-mail: [peter.vanderburgt@mu.ie](mailto:peter.vanderburgt@mu.ie)

## Reactive collisions of electrons with NS+ cation in interstellar media

Felix Iacob<sup>1\*</sup>, Zsolt Mezei<sup>2</sup>, Ioan F. Schneider<sup>3</sup> and Jonathan Tennyson<sup>4</sup>

<sup>1</sup>West University of Timisoara, Timisoara, Romania

<sup>2</sup>Institute for Nuclear Research (ATOMKI), Debrecen, Hungary

<sup>3</sup>LOMC, CNRS, Université Le Havre Normandie, Le Havre, France

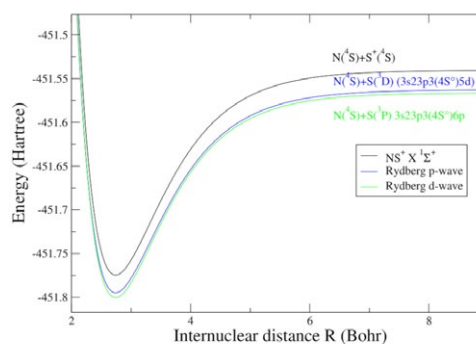
<sup>4</sup>Department of Physics and Astronomy, University College London, London, UK

**Synopsis** The intermediate states of the NS molecule are determined by the calculation of electrons scattering on the NS+ cation.

One of the challenges of astrochemistry is to study the mechanisms of formation and destruction of molecules and cations as well. The scattering of electrons on the cation is one of the common mechanisms that lead to its annihilation. Cold molecules in highly excited Rydberg states have been attracting a significant interest in recent years due to their interaction properties. An interesting feature of interaction properties is the realization of two-qubit gates in quantum computing. Another is Rydberg Matter (RM), a good candidate for Dark Matter (DM), and so on.

The purpose of this presentation is to provide the Rydberg potential interaction of mononitrogen monosulphide (NS) molecule and reliable data of dissociation limits. These data became of interest for molecular dynamics calculations after the recent discovery of this molecule in the interstellar medium [1]. The study is done according to the  $C_{2v}$  symmetry of the target and by the partial wave of the incoming electron, which is captured in a Rydberg state by the molecular cation forming a neutral. Part of the quantum chemistry calculation was performed using the

R-Matrix method in a previous paper [2]. The figure shows the  $X^1\Sigma^+$  ground state of NS+ of the ion, together with two highly excited states of the neutral in  $^2\Pi$  states symmetry. The state described by the blue potential comes from a p-wave and the green one comes from a d-wave incoming electron.



### References

- [1] Cernicharo J, et al. 2018 *ApJL* 853, L22.
- [2] F. Iacob et al, 2022 *Journal of Physics B: At. Molec. Optical Phys.* 55, 235202

\*E-mail: [felix.iacob@e-uvt.ro](mailto:felix.iacob@e-uvt.ro)

## H assisted Shape Resonance in Negative ion formation of Acetaldehyde

Surbhi Sinha<sup>1\*</sup>, Samata Gokhale, Vaibhav Prabhudesai<sup>1†</sup>, Y. Sajeew

<sup>1</sup> Tata Institute of Fundamental Research, Mumbai 400005 <sup>2</sup> Bhabha Atomic Research Center, Mumbai 400085

**Synopsis** We have studied the dissociation dynamics of acetaldehyde on attachment of low energy electrons and particularly looked at the  $H^-$  ion formation. We find two resonances in the formation of  $H^-$  at 6.5 eV and 9.2 eV. We have found that the negative ion formation at 6.5 eV is a Shape resonance stabilised by the H-atom at the neighbouring  $CH_3$  site, a novel case of stabilisation of anion resonance.

Low energy electrons interacting with molecules can form temporary bound states known as negative ion resonances (NIR). These resonances can decay either by autodetachment of the excess electron or, if they survive long enough, by dissociation of the molecule into a negative ion and one or more neutral fragments, a process called Dissociative Electron Attachment (DEA). In this study, we investigate DEA to acetaldehyde ( $CH_3CHO$ ). Previous studies have reported higher mass fragments  $CH_3^-$ ,  $O^-$ ,  $OH^-$ ,  $C_2H^-$ ,  $C_2HO^-$  and  $CH_3CO^-$  produced from resonances between 6 to 13 eV by Szymanska *et al.* [1]. However, they were unable to detect the lightest  $H^-$  ion. In our experiments, we observed  $H^-$  as the most abundant anionic product, showing two resonances at 6.5 eV and 9.2 eV. DEA resonances in organic molecules are site-specific depending on the functional groups present, as shown by Prabhudesai *et al.* [2]. To identify the origin of the  $H^-$  ions in the two resonances, we conducted DEA experiments on the deuterated sample of  $CH_3CDO$ . Our results show that the  $H^-$  ions at 6.5 eV originate purely from the aldehyde site ( $CHO$ ), while at 9.2 eV, they come from both the methyl site ( $CH_3$ ) and the aldehyde site. To gain further insights, we used the velocity slicing technique (VSI) to obtain momentum images of the  $H^-$  ions at the two energies. Interestingly, the momentum image shows a distinctive ring suggesting that the  $H^-$  ions at 6.5 eV arise from a two-body breakup. Our *ab initio* quantum chemical calculations indicate that the  $H^-$  ions at 6.5 eV originate from a shape resonance. Negative ion shape resonances are not commonly

known to survive for DEA at such high energy.

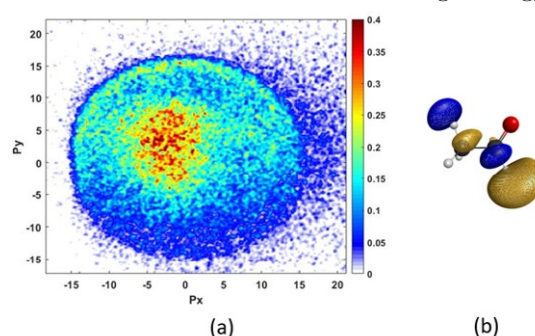


**Figure 1.** (a) Momentum image of  $H^-$  ion at 6.5 eV. The ring is suggestive of a two body break-up (b) Calculated electron density at 6.5 eV resonance. Shows anti-bonding nature in  $C-H$  bond at  $CHO$  site.

In acetaldehyde, this shape resonance is stabilized by the presence of an H-atom at the neighboring methyl site. We carried out the DEA study for tri-methyl acetaldehyde, where the H atoms are substituted by methyl groups, and here we noticed the 6.5 eV peak vanished. Our findings indicate a hydrogen atom stabilised anion resonance which has been seen for the first time. Such resonances may play an important role in electron interactions with biomolecules relevant to the fields of radiation biology and astrochemistry.

### References

- [1] Szymańska E *et al.* 2013 *Phys Chem Chem Phys* **15** 998-1005
- [2] Prabhudesai V S *et al.* 2005 *Phys. Rev. Lett.* **95**, 143202

\*E-mail: [surbhi.sinha@tifr.res.in](mailto:surbhi.sinha@tifr.res.in)

†E-mail: [vaibhav@tifr.res.in](mailto:vaibhav@tifr.res.in)

## L- and M-subshell ionization cross sections of heavy atoms

C. Montanari<sup>1</sup>, S. Segui<sup>2\*</sup>, D. Mitnik<sup>1</sup>, J.-M. Fernández-Varea<sup>3</sup>, M. Dingfelder<sup>4</sup>

<sup>1</sup> Instituto de Astronomía y Física del Espacio, CONICET – Univ. de Buenos Aires, C1428ZAA, Argentina

<sup>2</sup> Instituto de Física Enrique Gaviola, CONICET – FAMAF, Univ. Nacional de Córdoba, 5000, Argentina

<sup>3</sup> Facultat de Física, Universitat de Barcelona, E-08028 Barcelona, España

<sup>4</sup> Department of Physics, East Carolina University, Greenville, NC 27858, USA

**Synopsis** Inner-shell ionization finds many applications related to materials analysis. However, full theoretical calculations in heavy multielectronic atoms ( $Z \geq 75$ ) are scarce. In this contribution we present recent calculations for the case of protons and electrons in Au, Pb and Bi, for the L and M subshells.

Despite the long history of atomic collisions physics, different tasks remain to be completed, especially in the determination of ionization cross sections. From a theoretical point of view, the description of inner shells of multielectronic targets is far from the hypothesis of hydrogenic target with a single active electron in a central potential. Experimentally, the multiple bound shells and the many-decay paths to be considered, hamper the accurate assessment of the ionization cross sections from measured x-ray emission cross sections[1].

In this work we present a many-electron description to deal with inelastic processes at high impact velocities by means of the shellwise local plasma approximation (SLPA). This is a perturbative model within the dielectric formalism. The SLPA has been employed in total L-shell and M-shell calculations in the past [2], and recently for subshell calculations [3]. The only input data required by the theoretical SLPA are the binding energies and wave functions of the atomic subshells. These are implemented by fully relativistic solutions of the many-electron Dirac equation [4]. The obtained binding energies, including the spin-orbit splitting, agree within 5% with the experimental values. The present evaluation of the SLPA for separate subshells and the comparison with the available experimental data (see fig. 1) constitutes a detailed proof of its range of validity.

In addition, we perform calculations using a distorted wave Born approximation (DWBA) scheme [7]. This is an elaborate *ab initio* method to obtain ionization cross sections for inner atomic shells by the impact of electrons or other charged particles. DWBA has been com-

\*E-mail: [silvina.segui@mi.unc.edu.ar](mailto:silvina.segui@mi.unc.edu.ar)

pared with fully-relativistic plane-wave Born approximation (PWBA) to extend its validity and cover a wide range of projectile energies.

The present work also addresses the problem of relating the x-ray emission cross sections to ionization cross sections, by analysing the accuracy of the relaxation parameters involved in the conversion.

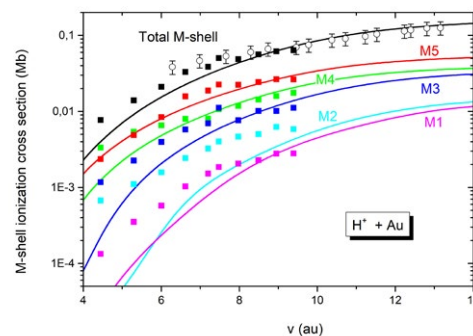


**Figure 1.** M-shell ionization cross section, including the  $M_i$  subshells. Curves: present theoretical results using the SLPA for proton impact. Symbols: Experimental data by Czarnota [5], solid-squares; and Ishi [6], hollow-circles.

### References

- [1] Carreras A *et al.* 2020 *Phys. Rev. A* **102**, 012817
- [2] Montanari C C *et al.* 2011 *Rad. Eff. Def. Solids* **166** 338
- [3] Oswal M *et al.* 2020 *Rad. Phys. Chem* **176** 108809
- [4] Bar-Shalom A *et al.* 2001 *J. Quant. Spect. Rad. Transf.* **71** 169
- [5] M Czarnota *et al.* 2009 *Phys. Rev. A* **79** 032710
- [6] K Ishi *et al.* 1975, *Phys. Rev. A* **11**, 119
- [7] Segui S *et al.* 2003 *Phys. Rev. A* **67**, 062710; Bote D and Salvat F 2008 *Phys. Rev. A* **77**, 042701

## Fine-structure energy levels, oscillator strengths and lifetimes in chromium

Vikas Tayal

Department of Physics, H.V.M. (Postgraduate) College, Raisi, Haridwar (Uttakhand) India  
Affiliation with Sri Dev Suman University, Uttakhand, India

**Synopsis** Energy levels, oscillator strengths, and transition probabilities for transitions among the fine-structure levels of the terms belonging to the  $(1s^2 2s^2 2p^6) 3s^2(^1S)$ ,  $3s3p(^1,^3P^o)$ ,  $3s3d(^1,^3D)$ ,  $3s4s(^1,^3S)$ ,  $3s4p(^1,^3P^o)$ ,  $3s4d(^1,^3D)$ ,  $3s4f(^1,^3F^o)$ ,  $3p^2(^1S, ^3P, ^1D)$ ,  $3p3d(^1,^3P^o, ^1,^3D^o, ^1,^3F^o)$ ,  $3p4s(^1,^3P^o)$ ,  $3p4p(^1,^3S, ^1,^3P, ^1,^3D)$ ,  $3p4d(^1,^3P^o, ^1,^3D^o, ^1,^3F^o)$ ,  $3p4f(^1,^3D, ^1,^3F, ^1,^3G)$  and  $3d^2(^1S, ^3P, ^1D, ^3F, ^1G)$  configurations of Mg-like Chromium are calculated using extensive configuration-interaction (CI) wave functions obtained with the CIV3 computer code of Hibbert. The relativistic effects in intermediate coupling are incorporated by means of the Breit-Pauli Hamiltonian. The energy splitting of 87 fine-structure levels, oscillator strengths and transition probabilities for electric-dipole-allowed and intercombination transitions and, also the lifetimes of fine-structure levels are presented and compared with available experimental and other theoretical results.

Emission lines due to allowed and intercombination transitions in multiply charged Si-like ions are observed in solar corona and laser produced plasma. The lines arise from intercombination transitions have been shown to be very useful, for instance, in understanding density fluctuations and elementary processes which occur in both interstellar and laboratory plasma. An accurate determination of transition energies, oscillator strengths and radiative decay rates for ions of Mg isoelectronic sequence are needed for a qualitative analysis of the spectra.

We have performed large scale CIV3 calculations of excitation energies from ground states for 87 fine-structure levels as well as of oscillator strengths and radiative decay rates for all electric-dipole-allowed and intercombination transitions among the fine-structure levels of the terms belonging to the  $(1s^2 2s^2 2p^6) 3s^2$ ,  $3s3p$ ,  $3s3d$ ,  $3s4s$ ,  $3s4p$ ,  $3s4d$ ,  $3s4f$ ,  $3p^2$ ,  $3p3d$ ,  $3p4s$ ,  $3p4p$ ,  $3p4d$ ,  $3p4f$  and of Mg-like Chromium, using very extensive configuration-interaction (CI) wave functions [1]. The important relativistic effects are incorporated through Breit-Pauli Hamiltonian [2]. Small adjustments to the diagonal elements of the Hamiltonian matrices have been made. These adjustments improve the accuracy of the mixing coefficients which depends in part on the accuracy of the eigenvalues. This is a justifiable [3] fine-tuning technique and is particularly useful for the calculation of intercombination lines [4].

Our adjusted excitation energies, including their ordering, are in excellent agreement (better than 0.5%) with the available experimental results [5]. In this calculation the mixing among several fine-structure levels is found to be very strong. These levels are identified by their dominant eigenvector [6]. From our transition probabilities, we have also calculated radiative lifetimes of the fine-structure levels. Our calculated data on oscillator strengths, radiative decay rates and the lifetimes are found to be in good agreement with the experimental and other theoretical results (wherever available). We predict new data for several levels where no other theoretical and/or experimental results are available.

### References

- [1] Hibbert A, 1975 *Comput. Phys. Commun.* **9** 141
- [2] Glass R and Hibbert A, 1978 *Comput. Phys. Commun.* **16** 19
- [3] McPeake D and Hibbert A, 2000 *J. Phys. B: At. Mol. & Opt. Phys.* **33** 2809
- [4] Hibbert A, 1979 *J. Phys. B: At. Mol. & Opt. Phys.* **12** L661
- [5] Shirai T, Nakai Y, Nakagaki T, Sugar J and Wiese W L, 1993 *J. Phys. Chem. Ref. Data* **22** 1306
- [6] Aggarwal K M, Tayal Vikas, Gupta G P and Keenan F P, 2007 *At. Data Nucl. Data Tables* **93** 615

E-mail: tayalvikas11@rediffmail.com



## Determination of ionic polarizability by nonsequential double ionization

H Kang<sup>1\*</sup>, M Wei<sup>2</sup>, Y Wang<sup>1</sup>, W Quan<sup>1</sup>, J Chen<sup>3</sup>, C Duan<sup>2</sup> and X Liu<sup>1</sup>

<sup>1</sup>State Key Laboratory of Magnetic Resonance and Atomic and Molecular Physics, Wuhan Institute of Physics and Mathematics, Innovation Academy for Precision Measurement Science and Technology, Chinese Academy of Sciences, Wuhan, 430071, China

<sup>2</sup>College of Physical Science and Technology, Central China Normal University, Wuhan, 430079, China

<sup>3</sup>Institute of Applied Physics and Computational Mathematics, P.O. Box 8009, Beijing, 100088, China

**Synopsis** We demonstrate theoretically the enhancement of recollision probability by the ionic polarization during nonsequential double ionization of Mg in circularly polarized intense light fields. A method to extract the ionic polarizability from the ratio of double to single ionization is proposed.

Nonsequential double ionization (NSDI) of atoms by intense laser fields has attracted tremendous attention, which could be understood nicely within the recollision model [1]. According to the recollision picture, NSDI probability will be significantly suppressed in circularly polarized (CP) light, because the additional transverse electric field steers the electron away from the core. However, the unexpected “knee” structure indicating of NSDI was observed in the ion yield curve for double ionization of Mg with CP light in [2]. There has been lots of interests from the community to understand this surprising phenomenon. On the other side, it has been shown that the laser-induced dipole potential will influence the photoelectron momentum distributions and the energy structure of the recolliding electrons for Mg [3,4]. However, whether and how the laser-induced dipole potential influences NSDI is unclear.

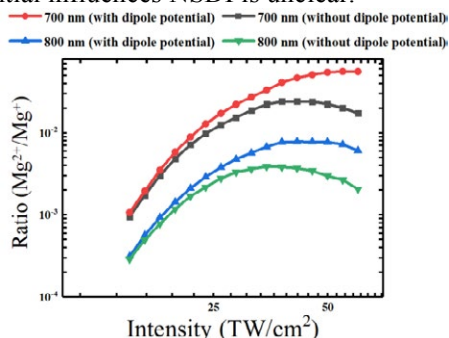


**Figure 1.** The ratio of  $\text{Mg}^{2+}/\text{Mg}^+$  versus laser intensity for 700 nm and 800 nm.

We here introduce a concise model to calculate the ratios of  $\text{Mg}^{2+}/\text{Mg}^+$  as functions of laser intensity with and without the dipole potential included in CP fields, as shown in Fig. 1.

\* E-mail: [kanghp@wipm.ac.cn](mailto:kanghp@wipm.ac.cn)

The NSDI ratios of 700 nm are significantly larger than the ones for 800 nm, which is because that the required initial transverse velocity to compensate the drift velocity resulting from the transverse electric field, is smaller for 700 nm. This leads to much higher tunnelling rate for return electrons, due to its exponential scale with the initial transverse velocity [5].

Furthermore, for each wavelength, the simulation without inclusion of the dipole potential becomes smaller and smaller than that considering the dipole potential with increasing intensity. This can be attributed to the laser-induced dipole forces attracting the recolliding electron along the transverse direction, resulting in larger NSDI yields.

Based on the analysis above, we propose a method allowing to extract the static polarizability of the  $\text{Mg}^+$  ion from the ratios of  $\text{Mg}^{2+}/\text{Mg}^+$ . By comparing the calculations with and without the dipole potential included for different intensities, we can obtain the value of the ionic static polarizability  $\alpha_i$  as the difference is due to the attraction by the dipole force, which strongly depends on  $\alpha_i$ . We determine the value of  $\alpha_i$  for the  $\text{Mg}^+$  ion as 32.64 a.u. (800 nm) or 34.49 a.u. (700 nm), which is very close to the theoretical value of 35.00 a.u.

### References

- [1] P. B. Corkum 1993 *Phys. Rev. Lett.* **71** 1994
- [2] G. D. Gillen *et al.* 2001 *Phys. Rev. A* **64** 043413
- [3] H. P. Kang *et al.* 2018 *J. Phys. B* **51** 105601
- [4] N. I. Shvetsov-Shilovski *et al.* 2012 *Phys. Rev. A* **85** 023428
- [5] M. Y. Wu *et al.* 2013 *Phys. Rev. A* **87** 013431



## Enhancement and Suppression of Nonsequential Double Ionization by Spatially Inhomogeneous Field

Xuan Luo<sup>1</sup>, Li Guang Jiao<sup>2,3\*</sup>, Aihua Liu<sup>1†</sup> and Xue-Shen Liu<sup>1‡</sup>

<sup>1</sup>Institute of Atomic and Molecular Physics, Jilin University, Changchun, 130012, China

<sup>2</sup>College of Physics, Jilin University, Changchun, 130012, China

<sup>3</sup>Helmholtz-Institut Jena, D-07743 Jena, Germany

**Synopsis** We theoretically investigated the nonsequential double ionization that driven by inhomogeneous field with single- or bowtie-shaped nanotip that being irradiated by ultrafast laser pulses. We find the interesting enhancement and suppression effects of the nonsequential double ionization of argon atom in the knee structure of double ionization yield. We analyzed and explained the enhancing and suppressing effects through simulations of classical ensembles.

The famous “knee” structure of double ionization yield over laser intensity is one of the most important characterization of nonsequential double ionization (NSDI) [1]. The NSDI can serve as an indicator for the intuitive electron-electron correlation of many-electron system. Over the past three decades, it has been explored by numerous investigators with all kinds of lasers. Recently the inhomogeneous fields generated by the gold nanotip has been applied to investigate the ultrafast phenomenon, such as the ionization and the high-harmonics generations [2,3].

Using the three-dimensional classical ensemble method, we theoretically studied the correlated electron dynamics of Ar atom within the laser field enhanced by a set of bowtie-nanotips. It is expected that we can observe enhancement of NSDI due to the field enhancement effect. However, as shown in Figure 1, we not only noticed the enhancement at lower laser intensity that well agrees with results of literature [3], but also observed the suppression of NSDI in the medium intensity laser field.

By analyzing the classical trajectories, energy distributions and momentum distributions of electrons, we found that the field enhancement of nanotips boost the single ionization at any intensity, but the energy and returning of first electron are essential key to the double ionization, especially in the case of NSDI. With variation in size, position and structures of nanotips,

the enhancement and suppression of NSDI are adjustable. More detail will be further discussed.

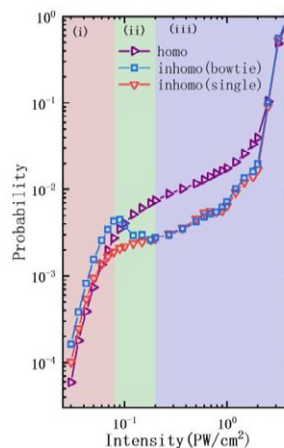


**Figure 1.** The double ionization probability of Ar as a function of laser intensity in homogeneous fields (purple triangles), inhomogeneous fields by a single tip (red triangles) and by bowtie tips (blue boxes). The different laser intensities are divided into three regions: (i) enhanced, (ii) suppressing and (iii) suppressed zones.

This work was supported by the National Key Research and Development Program of China (2022YFE0134200), the National Natural Science Foundation of China under Grant Numbers 12174147, 91850114 and 11774131.

### References

- [1] B Walker *et al.*, Phys. Rev. Lett. **73**, 1227 (1994).
- [2] S Kim *et al.*, Nature **453**, 757 (2008).
- [3] J Xu *et al.*, Opt. Express **30**, 15951 (2022).

\*E-mail: [lgjiao@jlu.edu.cn](mailto:lgjiao@jlu.edu.cn)

†E-mail: [aihualiu@jlu.edu.cn](mailto:aihualiu@jlu.edu.cn)

‡E-mail: [xslu@jlu.edu.cn](mailto:xslu@jlu.edu.cn)

## Internal collision double ionization of Ar driven by co-rotating two-color circularly polarized laser fields

Xuefeng Li<sup>1</sup>, Yue Qiao<sup>1</sup>, Jun Wang<sup>1</sup>, Fuming Guo<sup>1</sup> and Yujun Yang<sup>1\*</sup>

<sup>1</sup>Institute of Atomic and Molecular Physics, Jilin University, Changchun 130012, China

**Synopsis** The double ionization process of Ar in co-rotating two-color circularly polarized (CRTCCP) laser pulses is theoretically investigated with a three-dimensional classical ensemble model. It is found that, in addition to the generally considered nonsequential double ionization (NSDI) process, the double ionization mechanism also includes the internal collision double ionization (ICD) mechanism in sequential double ionization (SDI) process. The difference of these two ionization mechanisms are deeply studied.

The interaction of intense laser with atoms and molecules can produce non-sequential double ionization. The curve of divalent ion yield with laser intensity shows an obvious Knee structure [1]. NSDI originates from recollision to the parent ion after bound electron ionization, which can be explained by the three-step model [2]. Up to now, the research on the recollision process of NSDI has been quite in-depth, but there are relatively few studies on the ICD process. In the process, the electrons are far away from the nuclear region under the action of the light field and have the opportunity to scatter with electrons near the nucleus, and the recollision cannot result in the ionization of the atom due to the less energy obtained from the laser field.

The laser electric field is given by:

$$E(t) = E_{800}f(t)\left[\cos(\alpha t)\hat{x} + \sin(\alpha t)\hat{y}\right] + E_{400}f(t)\left[\cos(2\alpha t)\hat{x} + \sin(2\alpha t)\hat{y}\right]$$

where  $E_{800}$  and  $E_{400}$  are the electric field amplitudes for the 800-nm and 400-nm pulses. Here the period of the 800-nm pulse is defined as  $T$ , and  $f(t)$  is the envelope of the laser pulse which has a trapezoidal shape with  $2T$  turn on,  $6T$  at full strength, and  $2T$  turn off.

In Fig. 1(a), we present the statistical distribution of the electron position of the NSDI electron from the single ionization time to the double ionization time when the laser intensity is  $7 \times 10^{14}$  W/cm<sup>2</sup>. The statistical distribution of the electron position of the ICD electron from the beginning of the laser pulse to the single ionization time is shown in Fig. 1(b). For NSDI, the electron distribution range is relatively large, and the electrons are ionized and returned from a position far away from the nuclear region.

Compared with the recollision process of NSDI, the electron distribution range of ICD process is smaller, and the electrons are renucleated from the position closer to the nuclear region. Through further calculation, it is found that ICD accounts for 91% of SDI when the laser intensity is  $7 \times 10^{14}$  W/cm<sup>2</sup>.

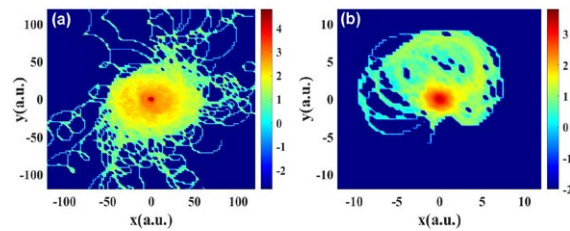


**Figure 1.** (a) The position distribution of the field plane between the single ionization time and the double ionization time of NSDI electrons; (b) The distribution of field plane position before ICD electron single ionization time

Therefore, we found that the NSDI and ICD processes can be clearly observed in the ionization process of Ar driven by the CRTCCP laser pulse, and the difference between the two mechanisms can be observed intuitively. It is found that the ionization mechanism of the system can be regulated by changing the driving laser parameters.

This work was supported by the National Natural Science Foundation of China under Grants No. 12074145.

### References

- [1] Walker B *et al.* 1994 Phys. Rev. Lett. 73 1227.
- [2] Corkum P B *et al.* 1993 Phys. Rev. Lett. 71 1994

\* E-mail: [yangyj@jlu.edu.cn](mailto:yangyj@jlu.edu.cn)

## Attosecond time-resolved photoemission dynamics in atoms and molecules

Xiaochun Gong\*, Kiyoshi Ueda, Jian Wu

State Key Laboratory of Precision Spectroscopy, East China Normal University, Shanghai, China

**Synopsis** Tailored strong laser fields opens unique opportunities for probing and controlling the electron and nuclear motions in the sub-cycle. Here we report our recent results on the attosecond control of electron and ion dynamics in atoms, molecules, and even in complex environments by employing electron-ion coincidence spectroscopy. Our newly developed atomic partial wave meter has been demonstrated to resolve the quantum interference black box in atomic photoionization.

Exposed to a strong laser field or an attosecond pulse train, a molecule may coherently absorb multiple photons to overcome the ionization threshold and break up. The abundant structures of the measured kinetic energy release (KER) spectrum of the nuclear fragments and photoelectrons allow us to understand the ultrafast electron and nuclear motion of molecules[1]. A shape resonance emerges during the light absorption in many molecules with a gigantic burst amplitude and a lifetime of hundreds of attoseconds. Recent advances in attosecond metrology revealed the attosecond lifetime of the shape resonance. For a heteronuclear molecule, the asymmetric initial state and landscape of the molecular potential would lead to an asymmetric shape resonance, whose effect, however, has not been characterized yet.

We experimentally constructed an attosecond coincidence interferometer by combing attosecond pulse trains. By developing employ an attosecond interferometer to investigate the molecular-frame photoionization time delay in the vicinity of the shape resonance of the NO molecule [2]. Driven by photons with energy ranging from 23.8 eV to 36.5 eV, a 150 attosecond difference in the time delay is observed between photoemission from the N/O end. Our quantum scattering theoretical simulations reproduce well our experimental findings and show that the observed shape resonance is created by the f-wave quasi-bound state. In the one-center approach, the asymmetric photoionization time delay between the N and O end is caused by the interference between the resonant and the nonresonant partial-wave channel. Additionally, we introduce a skew-polarization between the IR field and XUV-APT to realize the symmetry resolved photoemission time delays in rare gas atoms.

In the end, we will also introduce our recent development of the atomic partial wave meter and its demonstration in resolving the quantum interference black box in atomic photoionization time delays of neon and argon, where the degenerate intermediate states are generally invisible for experimental measurement.

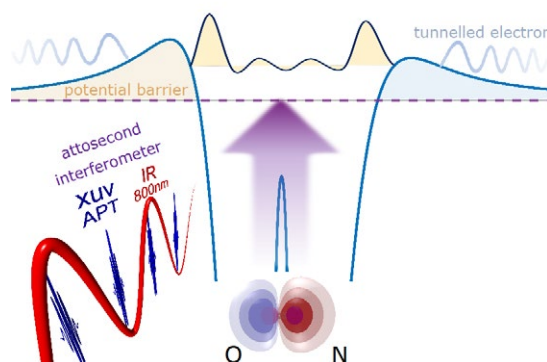


**Figure 1.** Schematic diagram of electron tunneling in molecular shape resonance

### References

- [1] Pan S et al 2021 *Phys. Rev. Lett.* 2021 126 063201.
- [5] Gong X et al 2022 *Phys. Rev. X* 2022 12 011002.
- [6] Jiang W et al 2022 *Nat. Commun.* 13 5205.
- [4] Qiang J et al 2022 *Phys. Rev. Lett.* 2022 128 243201.
- [2] Zhou L et al 2023 *Phys. Rev. Lett.* 130, 033201.
- [8] Chen F et al 2022 *Phys. Rev. Lett.* 2022 129 057402.
- [9] Chen F et al 2022 *Nano Lett.* 2022 22 2023.

\* E-mail: xcgong@lps.ecnu.edu.cn

## Spatially dependent laser assisted photoionization of He

R Della Picca<sup>1\*</sup>, J M Randazzo<sup>1</sup>, S D López<sup>2</sup>, M F Ciappina<sup>3</sup> and D. G. Arbó<sup>2</sup>

<sup>1</sup>Centro Atómico Bariloche (CNEA), CONICET and Instituto Balseiro (UNCuyo), Bariloche, 8400, Argentina

<sup>2</sup>Institute for Astronomy and Space Physics - IAFE (UBA-Conicet), Buenos Aires, C1428ZAA, Argentina

<sup>3</sup>Department of Physics, Guangdong Technion - Israel Institute of Technology, 241 Daxue Road, Shantou, Guangdong, 515063, China

**Synopsis** We present a theoretical study of atomic laser-assisted photoionization emission (LAPE) beyond the dipole approximation. By considering the non-relativistic non-dipole strong-field approximation, we analyze the different contributions to the photoelectron spectrum (PES).

When an extreme ultraviolet (XUV) pulse and an infrared (IR) laser field overlap in space and time with matter, the so-called laser-assisted photoionization emission (LAPE) processes take place. In the sideband regime, when the XUV pulse duration is longer than one IR optical cycle, the concurrent absorption of one XUV photon, together with the exchange of one or more additional photons from the IR laser field, leads to equally spaced “sideband” (SB) peaks in the energy-resolved photoelectron spectrum (PES).

Typically, the dipole approximation is considered provided (i) the IR laser is weak enough and (ii) laser wavelengths are short enough, i.e. magnetic effects can be neglected. Thus, the laser electric field is considered homogeneous. However, for long-wavelength high-intensity lasers, non-dipole effects start to play a role. Furthermore, the Lorentz force of the magnetic field gives rise to a momentum transfer of laser photons on the ejected electrons along the propagation direction.

In this work, in order to incorporate the first-order spatially inhomogeneous IR field, we study LAPE of He(1s) in a Strong Field Approximation (SFA) including non-dipole corrections [1]. Due to the periodicity properties, and in the same spirit of our previous work [2], we can rewrite the PES as a function of two principal contributions: the intra- and the intercycle factors. We present the modifications introduced in each factor by the non-dipole effects.

As an example, in Fig. 1 we present the intercycle factor as a function of the photoelectron energy and emission angle  $\theta$ , in the energy range comprising 10 sidebands. We show that the sideband energies under the dipole approximation

\*E-mail: [renata@cab.cnea.gov.ar](mailto:renata@cab.cnea.gov.ar)

do not depend on  $\theta$ . Contrarily, the inclusion of non-dipole effects produces a tilt on the sidebands. The vertical dashed lines indicate reference values corresponding to SB peaks for certain orders  $n$  within the dipole approximation. When the emission is opposite to the IR propagation ( $\cos\theta < 0$ ) the SBs are shifted towards higher energies. On the contrary, when  $\cos\theta > 0$ , the shift is in the direction of lower energies. This results in an emission asymmetry depending on whether the electron is emitted parallel or anti-parallel with respect to the propagation direction of the laser field [3].

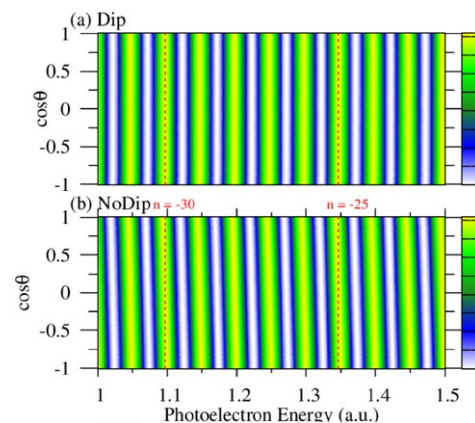


**Figure 1.** Intercycle factor showing the sidebands of PES: (a) dipole approximation and (b) non-dipole case.

### References

- [1] Joachain C *et al.* 2012 *Atoms in Intense Laser Fields*, Cambridge University Press.
- [2] Della Picca R *et al.* 2020 *Phys. Rev. A* **102** 043106
- [3] Della Picca R *et al.* 2023 to be submitted.

## Direct confirmation of 164-nm-wavelength superfluorescence from a dense sample of helium ions created using free-electron laser pulses

J R Harries<sup>1\*</sup>, H Iwayama<sup>2</sup>, A Iguchi<sup>3,4</sup>, and S Kuma<sup>3</sup>

<sup>1</sup>QST, SPring-8, Kouto 1-1-1, Sayo, Hyogo 679-5148, Japan,

<sup>2</sup>UVSOR/SOKENDAI, National Institutes of Natural Sciences, Okazaki, Aichi 444-8585, Japan.

<sup>3</sup>RIKEN, Wako, Saitama 351-0198, Japan, <sup>4</sup>Tokyo Metropolitan University, Hachioji, Tokyo 192-0397, Japan

**Synopsis** The emission of superfluorescence pulses at a wavelength of 164 nm from helium ions excited using a free-electron laser was studied in the time domain.

Superfluorescence is a phenomenon of great fundamental and practical interest, and its extension to short wavelengths is of potential relevance for the development of new analysis techniques. In previous work [1], we studied superfluorescence at extreme ultraviolet (EUV) wavelengths from helium ions by observation in the frequency domain and by investigating the spatial distribution of emission. Here we have attempted to directly characterise the pulses by detection in the time domain. Experimentally, we used intense pulses from the soft X-ray free-electron laser (FEL) beamline BL1 at SACLA to ionise and excite a dense (around  $2 \times 10^{23} \text{ m}^{-3}$ ) sample of helium gas. The photon energy was chosen to be resonant to  $3p$  (48.6 eV) or  $4p$  (51.2 eV) excitation of helium ions, and the pulse energy was sufficient that essentially all atoms along the path of the FEL beam were ionised and interacted with the radiation. Emitted radiation was dispersed using a grazing-incidence monochromator, and detected using a fast micro-channel plate detector with a rise time of less than 100 ps. Here the detector was positioned to select emission at a wavelength of 164 nm, and individual pulses were recorded using an oscilloscope.

Following excitation to the  $3p$  state, superfluorescence occurs on the  $3p$ - $2s$  transition at a wavelength of 164 nm. With excitation to the  $4p$  state, emission first occurs on the  $4p$ - $3s$  transition at a wavelength of 469 nm. With a sufficient number of excited ions, a superfluorescence cascade can then occur, with emission from the  $3s$  state to the  $2p$  state, also at a wavelength of 164 nm. There is no coherence between the  $3s$  state and  $2p$  state, so this emission is expected to occur as an independent emission, and separate time delays are expected for the upper (469 nm)

\*E-mail: [harries.james@qst.go.jp](mailto:harries.james@qst.go.jp)

and lower (164 nm) emissions. Shown in the figure are the distributions of detection times of 164 nm wavelength pulses for various number densities (labelled with the nozzle backing pressure). Scattered FEL light ('0.0 MPa') was also detected, and this provides a reference time. The distributions for 164-nm-emission following both  $3p$  and  $4p$  excitation show a time delay characteristic of superfluorescence, with in general longer delays for lower number densities. Compared to emission following  $3p$  excitation, emission following  $4p$  excitation occurs at later times due to it being the second step of a cascade emission. The emission at 469 nm was also detected using a fast photodiode (results not shown here).

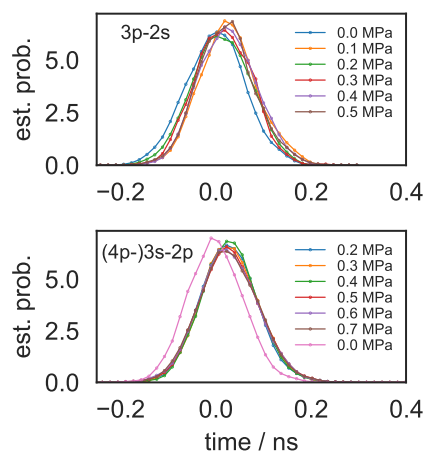


**Figure 1.** Distributions of pulse positions following  $3p$  (upper) and  $4p$  (lower) excitation for varying number densities.

### References

- [1] Harries J R *et al* 2018 *Phys. Rev. Lett.* **121** 263201



## Multiphoton ionization cross sections and photoelectron angular distributions of the helium atom

A Mihelič<sup>1\*</sup>, M Horvat<sup>2,3†</sup>

<sup>1</sup>Jožef Stefan Institute, Ljubljana, Slovenia

<sup>2</sup>Faculty of Mathematics and Physics, University of Ljubljana, Slovenia

<sup>3</sup>Lek, d.d., Ljubljana, Slovenia

**Synopsis** We present the results of our recent calculations of multiphoton ionization cross sections of helium and the corresponding asymmetry parameters of photoelectron angular distributions, which were obtained with our recently developed computational method. The method is based on an extraction of partial ionization amplitudes from the outgoing part of a scattering wave function, which is calculated by solving a system of driven, time-independent Schrödinger equations.

A direct solution of the time-dependent Schrödinger equation is often the preferred way of studying photoexcitation or photoionization. However, finding the solution may not always be feasible or desirable. In these cases, multiphoton ionization cross sections, or the corresponding amplitudes, may be used to calculate the probability for multiphoton ionization.

Theoretical description of multiphoton ionization is especially difficult when the number of photons absorbed exceeds the number of photons required to ionize the target (above threshold ionization, ATI) or when the continua involved in either the intermediate steps or the final step are resonant.

We have recently devised a method for the calculation of multiphoton ionization amplitudes and cross sections of few-electron atoms and molecules [1], which is an extension of our past

work [2]. The method is based on exterior complex scaling (ECS) and relies on a description of the outgoing part of the scattering wave function — calculated by solving a system of driven Schrödinger equations — in terms of a small number of Coulomb waves with fixed wave numbers. The method permits the calculations to be performed in simulation volumes of modest sizes, but avoids the difficulties connected to the damping of the driving terms in ATI calculations.

We present the results of the calculation of two-, three-, and four-photon ionization cross sections of the helium atom and the asymmetry parameters used to characterize the corresponding photoelectron angular distributions.

### References

- [1] Mihelič A, Horvat M 2021 *Phys. Rev. A* **103** 043108
- [2] Mihelič A 2018 *Phys. Rev. A* **98** 023409

---

\*E-mail: [andrej.mihelic@ijs.si](mailto:andrej.mihelic@ijs.si)

†E-mail: [martin.horvat@fmf.uni-lj.si](mailto:martin.horvat@fmf.uni-lj.si)



## Core-resonance line-shape analysis of atoms undergoing strong-field ionization

M Hartmann<sup>1</sup>, L Hutcheson<sup>2</sup>, G D Borisova<sup>1</sup>, P Birk<sup>1</sup>, S Hu<sup>1</sup>, A C Brown<sup>2</sup>, H W van der Hart<sup>2</sup>, C Ott<sup>1</sup> and T Pfeifer<sup>1</sup>

<sup>1</sup>Max-Planck-Institut für Kernphysik, Saupfercheckweg 1, 69117 Heidelberg, Germany

<sup>2</sup>Centre for Light-Matter Interaction, School of Mathematics and Physics, Queen's University Belfast, Belfast BT7 1NN, United Kingdom

**Synopsis** We investigate the build-up of absorption lines in xenon ions as a function of the near-infrared (NIR) pump intensity during strong-field ionization. We observe a half-cycle-periodic change in the line-shape asymmetry of the ionic  $4d - 5p$  resonances. In particular, we find the phase of the induced dipole emission is modified and the magnitude of this phase modulation decreases with increasing laser intensity. We discuss the influence of ground state depletion on interfering pathways involved in XUV-assisted strong-field ionization.

Attosecond transient absorption spectroscopy (ATAS) is well suited for the time-resolved investigation of strong-field ionization (SFI) since the all-optical approach probes the system while it is being ionised. Using XUV spectrometers with high spectral resolution, absorption lines can be investigated not only with respect to their energy and line/oscillator strength, but also their specific shape. The continuous transition from a symmetric Lorentzian to an asymmetric Fano line is the result of a change in the phase of the underlying dipole [1].

In this contribution, we perform a systematic analysis of the line shape of an ionic core-to-valence transition in xenon using ATAS at different NIR pump intensities [2]. We extract the dipole phase from the measured/simulated line-shape and identify an indirect ionization pathway. Strong-field ionization of neutral xenon from an XUV core-excited virtual state interferes with the direct pathway of valence-shell strong-field ionization. This interference leads to delay-dependent asymmetry changes of a xenon ion XUV absorption line shape. More specifically, we observe delay-dependent NIR-half-cycle oscillations of the line-shape asymmetry whose amplitude decreases with increasing NIR pump intensity. We attribute this effect to the depletion of the neutral ground state, and hence a weakening of the interfering virtual pathway, which is confirmed by calculating the remaining neutral Xe population [3].

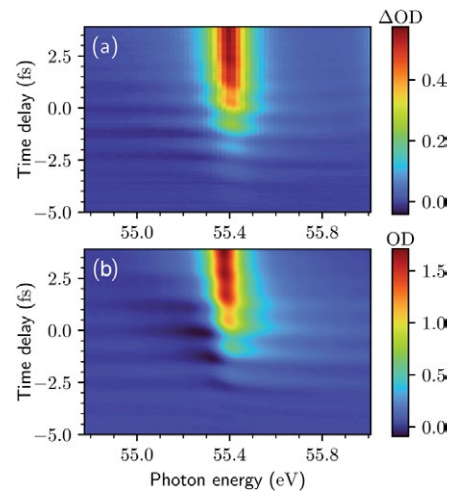


**Figure 1.** Attosecond transient absorption spectroscopy scan centered on the  $5p_{3/2}^{-1} \rightarrow 4d_{5/2}^{-1}$  transition in the time-delay overlap region at an NIR intensity of  $1.9 \pm 0.21 \times 10^{14} \text{ Wcm}^{-2}$ . (a) Measured and (b) simulated optical density, computed with the *ab initio* RMT approach. Delay of probe with respect to pump, pump centered at zero.

### References

- [1] C Ott *et al*, Science **340**, 716–20 (2013).
- [2] M Hartmann *et al*, J. Phys. B: At. Mol. Opt. Phys. **55**, 245601 (2022).
- [3] A C Brown *et al*, Comp. Phys. Commun. **250**, 107062 (2020).

## Carrier-envelope-phase and helicity control of electron vortices and spirals in photodetachment

M. M. Majczak<sup>1\*</sup>, F. Cajiao Vélez<sup>1</sup>, J. Z. Kamiński<sup>1</sup> and K. Krajewska<sup>1†</sup>

<sup>1</sup>Institute of Theoretical Physics, Faculty of Physics, University of Warsaw, Pasteura 5, 02-093 Warsaw, Poland

**Synopsis** We present an in-depth analysis of the formation of electron vortices and momentum spirals in photodetachment driven by either an isolated laser pulse or a pair of pulses with circular polarization.

Here we present the analysis of the formation of electron vortex structures (EVS) and momentum spirals in photodetachment of  $H^-$  ion and its dependence on carrier-envelope-phase (CEP) and helicity of the ultrashort, circularly polarized laser pulses driving the process. Momentum spirals manifest themselves, in the probability distribution of photoelectrons, as zones of large probability which follow concentric Fermat spirals with well-defined number of arms. However, other type of structures, known as electron vortices, can also be found in the momentum distribution of photoelectrons; they appear as continuous lines in the three-dimensional momentum space where the probability amplitude of photodetachment vanishes, and its phase changes from zero to integer multiples of  $2\pi$  around them [1]. Thus, EVS can be easily distinguished from momentum spirals as EVS carry quantized, non-vanishing orbital angular momentum (OAM). Both structures can be seen in probability amplitude distributions presented in **Figure 1**.

In this study we focus on how to control the location, orientation and formation of the aforementioned structures in photodetachment using CEP and helicity of a single laser pulse or two laser pulses driving the process. For single laser pulse scenario, it is shown that with changing the pulse CEP the probability amplitude distributions rotate around the polarization plane by exactly same angle. Also, it is demonstrated that helicity of that pulse decides about the direction of this rotation. Next, we study situa-

tion with two corotating laser pulses. We show that by manipulating CEP of both pulses we can observe creation and annihilation of vortex-antivortex pairs, where the latter results in formation of nodal surfaces. At last, we analyze the case of two counterrotating laser pulses. Here, we note that for laser pulse configuration with time reversal symmetry we can observe total annihilation of vortex structures and, as a consequence, formation of momentum spirals [2].

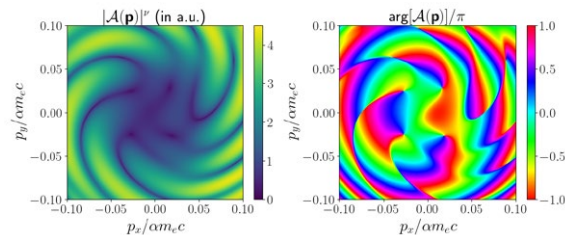


**Figure 1.** Momentum distributions of the absolute value  $|\mathcal{A}(p)|^\nu$  (left panel) and the phase  $\arg[\mathcal{A}(p)]/\pi$  (right panel) of the probability amplitude of photodetachment from  $H^-$  ion ( $\nu = 0.2$  for visual purposes). The numerical results are presented for driving pair of pulses in the counterrotating configuration. One can see the spiral branches and vortex-antivortex pairs.

### References

- [1] Geng L, Cajiao-Vélez F, Kamiński J Z, Peng L Y, and Krajewska K 2021 *Phys. Rev. A* **104**, 033111.
- [2] Majczak M M, Cajiao-Vélez F, Kamiński J Z and Krajewska K 2022 *Optics Express* Vol. **30**, Issue 24.

\*E-mail: [m.majczak@uw.edu.pl](mailto:m.majczak@uw.edu.pl)

†E-mail: [Katarzyna.Krajewska@fuw.edu.pl](mailto:Katarzyna.Krajewska@fuw.edu.pl)

## A time-dependent theory for RABBIT

M L Ocello<sup>1</sup>, S D López<sup>1</sup>, and D G Arbó<sup>1,2\*</sup>

<sup>1</sup>Instituto de Astronomía y Física del Espacio, IAFE (UBA- CONICET), Buenos Aires, Argentina

<sup>2</sup>Universidad de Buenos Aires, Facultad de Cs. Exactas y Naturales and Ciclo Básico Común, Buenos Aires, Argentina

**Synopsis** In this work, we present a time dependent analysis of phase delay in the RABBIT protocol by means of a semiclassical model. We show how phase delays arise from interfering electron trajectories in the time domain. We find very good agreement with the strong field approximation and numerical solutions to the Time Dependent Schrödinger Equation.

We study the reconstruction of attosecond harmonic beating by interference of two-photon transitions (RABBIT) technique for atomic ionization from a time-dependent viewpoint within the strong field approximation (SFA) [1]. In order to retrieve the phase shifts, we use RABBIT protocol, which can be thought of as a coherent combination of two laser assisted photo-emission processes (LAPE) in the perturbative regime for the driving field [2]. We find that phase delays stem from the interference of the classical trajectories starting with energies corresponding to different (odd) harmonics of the fundamental frequency of the driving field (forming the attosecond pulse train) and with the same final ATI (above-threshold ionization) or sideband energy. As expected, our semiclassical description arising from the saddle-point approximation (SPA) to the SFA reproduces the phase delays of the standard RABBIT protocol for a weak probe pulse but deviates significantly as its intensity increases. We compare our time-dependent semiclassical model with the numerical solution of the strong-field approximation and find a very good resemblance (see Fig. 1). In order to include the Wigner time delays due to the long-range atomic Coulomb Potential we compare our strong-field models with results by solving numerically the time-dependent Schrödinger equation.

In Figure 1 we show calculations of electron emission spectrum for varying phase delay between probe laser and the attosecond pulse train (pump). The probe has a frequency of 0.05 a.u. (911 nm) and maximum field strength of 0.004 a.u. ( $5.6 \times 10^{11}$  W/cm<sup>2</sup>) meanwhile the pump consist in the sum of 29<sup>th</sup> and 31<sup>st</sup> harmonics of the probe with maximum field strength of 0.05

a.u. ( $8.8 \times 10^{13}$  W/cm<sup>2</sup>). The ATI peaks are located at energies of 0.95 a.u. and 1.05 respectively. The sideband corresponding to absorption or emission of a single IR photon from the respective 29<sup>th</sup> and 31<sup>st</sup> harmonics has energy near 1 a.u.. It is easy to see that the modulation of the ATI and sideband are  $\pi$ -periodic, and SFA and SPA calculations show that the phase delay at the sideband is 0 or  $\pi$ , meanwhile for the ATI peaks, the phase delay correspond to  $\pi/2$  and  $3\pi/2$ .

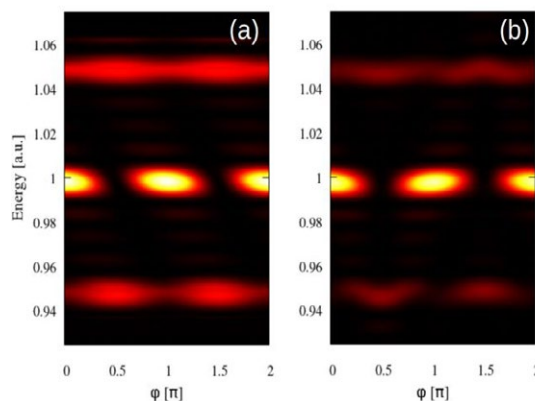


**Figure 1.** Density plot of the photoemission spectrum for electrons emitted in the forward direction as function of the phase delays, and electron energy, calculated with SPA (a) and SFA (b).

This work is supported by PICT 2020-01755, 2020-01434, and PICT-2017-2945 of ANPCyT (Argentina), PIP 2022-2024 11220210100468CO of Conicet (Argentina).

### References

- [1] Klünder K *et al* 2011 Phys. Rev. Lett. **106**, 143002
- [2] Gramajo A A *et al* 2018 J. Phys. B: At. Mol. Opt. Phys. **51** 055603

\* E-mail: [diego@iafe.uba.ar](mailto:diego@iafe.uba.ar)

## First-principles simulations of multielectron dynamics in strong laser pulses using the hardware-efficient ansatz on quantum computers

Y Orimo<sup>1\*</sup>, K L Ishikawa<sup>1</sup>, Y Kawashima<sup>2</sup>, T Gujarati<sup>2</sup>, T Sato<sup>1</sup>

<sup>1</sup>Graduate School of Engineering, The University of Tokyo, 7-3-1 Hongo, Bunkyo-ku, Tokyo 113-8656, Japan

<sup>2</sup>IBM Quantum, IBM Research Tokyo, Tokyo, 103-8510, Japan.

<sup>3</sup>IBM Quantum, IBM Research - Almaden, 650 Harry Road, San Jose, CA 95120, USA

**Synopsis** We present quantum and classical hybrid first-principles simulations using orbital-optimized hardware-efficient ansatz for multielectron dynamics in intense laser pulses. We have successfully simulated high harmonic generation from a helium atom in a one-dimensional system with the presented method.

Real-time first-principles simulations are an indispensable tool for investigating the electronic dynamics of matter under intense laser fields and ultrafast light pulses. Our previous research focused on developing first-principles simulations to solve multielectron dynamics in such laser fields[1]. However, the exponential growth of computational cost to simulate quantum many-body systems hinders the study of larger systems. Quantum computers, which have evolved rapidly in recent years, have the potential to make a breakthrough in this problem. Currently, noisy quantum computers without error correction are already available, and many applications to quantum chemical calculations have been reported. In this contribution, we further develop our first-principles methods for multielectron dynamics to enable hybrid simulations using classical and quantum computers and report simulations of high harmonic generation using the presented method.

A hybrid approach, in which quantum and classical computers cooperate, is needed to take full advantage of the noisy quantum computer. The time-dependent multiconfiguration wave function model [2] that we have intensively studied can be directly applied to the hybrid scheme. The multiconfiguration wave function model deals with multielectron systems by a superposition of multiple electronic configurations composed of time-dependent single-electron orbitals. In the hybrid scheme that is called the variational quantum simulation [3], we treat orbitals describing spatial dynamics of electrons on a classical computer, and configurations, which are represented by a parameterized quantum circuit, on a quantum computer. In this study, we have derived equations of motion of quantum circuit

parameters and orbitals for general quantum circuits. To achieve simulations on noisy quantum computers, we employ the hardware-efficient ansatz (HEA) [4], which is a relatively shallow circuit composed of device-friendly quantum gates, to describe the electronic configuration.

We demonstrate a quantum/classical hybrid simulation based on a quantum circuit emulator on a classical computer, where we simulate high harmonic generation from a helium atom in a one-dimensional system. Figure 1 shows high harmonic spectra, where we can see that the spectrum of HEA perfectly matches the full-CI result. This result indicates that HEA has sufficient expressive power and with a sufficient number of sampling, simulations comparable to full-CI are possible on a quantum computer.

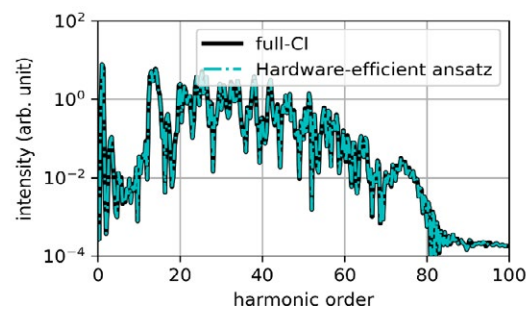


**Figure 1.** High harmonic spectra of a He atom in a one-dimensional system irradiated with a laser pulse with a peak intensity of  $4 \times 10^{14}$  W/cm<sup>2</sup> and 800 nm wavelength simulated using the hardware-efficient ansatz.

### References

- [1] Sato T, et al 2018 *J. Chem. Phys.* **148**, 051101
- [2] Ishikawa K L and Sato T 2015 *IEEE J. Sel. Top. Quantum Electron.* **21**, 1–16
- [3] Yuan X, et al 2019 *Quantum* **3**, 191
- [4] Kandala A, et al., 2017 *Nature* **549**, 242–246

\* E-mail: [ykormhk@atmo.t.u-tokyo.ac.jp](mailto:ykormhk@atmo.t.u-tokyo.ac.jp)

## Relativistic calculations of electron–parent ion entanglement using the KRAKEN protocol

C L M Petersson<sup>1\*</sup> and E Lindroth<sup>1</sup>

<sup>1</sup>Department of Physics, Stockholm University, AlbaNova University Center, SE-106 91 Stockholm, Sweden

**Synopsis** KRAKEN is a recently developed pump-probe method that aims to reconstruct the one-photon density operator. This is done by interferometric measurements of the two-photon electron distribution. The present communication uses the Relativistic Random Phase Approximation with Exchange (RRPAE) method to directly calculate the one-photon density operator and its KRAKEN reconstruction. This allows for a direct comparison, and for an evaluation of the quality of the approximations made in the KRAKEN protocol.

In most atomic systems, single ionisation-channel continua are the exception, rather than the norm. With multiple ionisation channels open, the purity  $\gamma$  of the state density operator can provide information on the electron–Parent Ion (PI) entanglement. Although this information may not be extracted using only an XUV pump, it can be obtained with the addition of a probe pulse. This is the principle behind pump-probe methods, which allow for extraction of time-dependent information through variation of the pump-probe delay.

One recently developed interferometric pump-probe method aimed at reconstructing the one-photon density operator  $\hat{\rho}_{XUV}$  is known as Kvanttillståndstomografi av AttosekundsElektroNvågpaket (KRAKEN) [1], which translates to quantum state tomography of attosecond electron wave packets. KRAKEN combines an XUV pump with a two-colour IR probe, allowing for interference measurements of the population at any two intermediate energies  $\varepsilon_1$  and  $\varepsilon_2$ . The retrieved information is assumed to be representative for the one-photon wave packet, allowing the density matrix elements  $\langle \varepsilon_1 | \hat{\rho}_{XUV} | \varepsilon_2 \rangle$  to be reconstructed. The ionisation paths from  $\text{Ar}(3p_j)$  are schematically shown in Figure 1, along with the magnitude of  $\hat{\rho}_{XUV}$ .

From the point of view of theory, both the one- and two-photon matrix elements can be directly obtained, without the need for any of the assumptions relied on in the KRAKEN protocol. Thus, both  $\hat{\rho}_{XUV}$  and its KRAKEN recon-

struction may be calculated—and compared—directly. The present work makes use of Relativistic Random Phase-Approximation with Exchange (RRPAE) [2] to simulate KRAKEN in argon, where the fine-structure splitting of the ground state results in separate ionisation channels. Both the  $\hat{\rho}_{XUV}$  and its KRAKEN reconstruction are calculated and compared to evaluate the assumptions present in the method.

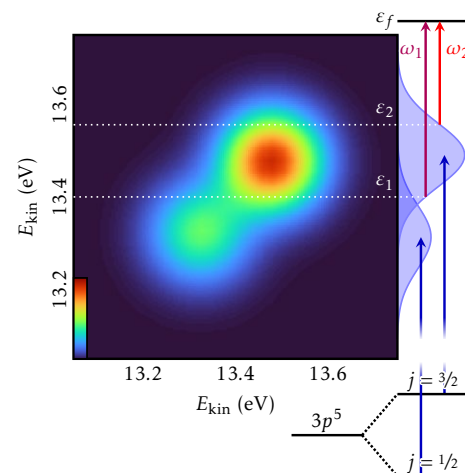


**Figure 1.** The magnitude of the calculated argon one-photon density operator  $\hat{\rho}_{XUV}$ . Two maxima are present, due to fine-structure splitting of the  $\text{Ar}^+ 3p^5$  ground state. The matrix elements  $\langle \varepsilon_1 | \hat{\rho}_{XUV} | \varepsilon_2 \rangle$  can be reconstructed from the beatings induced at a final energy  $\varepsilon_f$  by a two-colour IR-probe. The two-photon ionisation paths are shown to the right.

### References

- [1] Laurell H *et al.* *Phys. Rev. Research* **4** 033220
- [2] Vinbladh J *et al.* *atoms* **10**(3) 80

\*E-mail: [leon.petersson@fysik.su.se](mailto:leon.petersson@fysik.su.se)



## Estimating Rare Gas Spectra with a New Theoretical Model for Pump-Probe Spectroscopy

M Alarcón<sup>1\*</sup>, C H Greene<sup>1</sup>, J K Wood<sup>2</sup>, A Plunkett<sup>2</sup>, D Biswas<sup>2</sup>, and A Sandhu<sup>2</sup>

<sup>1</sup>Department of Physics and Astronomy, Purdue University, West Lafayette, IN, 47907, USA

<sup>2</sup>Department of Physics, University of Arizona, Tucson, Arizona 85721, USA

**Synopsis** This study presents a new theoretical model that uses multichannel quantum defect theory to add complexity to atomic states and improve the treatment of excitation, autoionization, and photonization. The authors demonstrate the effectiveness of this model by estimating the results of pump-probe spectroscopy experiments in neon and argon, showing that it can accurately predict the behavior of these systems. The success of the method is a good motivation to test it in future experiments.

Many successful models that describe pump-probe spectroscopy experiments rely on a simplistic view of the atomic structure. In this work, we present some recent results on the development of a theoretical model that aims to add the complexity of the atomic states by using the multichannel quantum defect theory (MQDT).

This model has the benefit of treating the excitation, autoionization, and photoionization to all channels on a more realistic basis depending on parameters that can, in principle, be calculated ab-initio or obtained directly from experimental data. We show two examples of uses of this model by providing estimates for the result of pump-probe spectroscopy experiments in neon and argon.

In the case of neon, we study a process similar to that of [1] where neon atoms are photoionized by double photon absorption after interacting with co-propagating pump and probe lasers. Here we study the dependence of the angular distribution of the photoelectrons on both the intensity and frequency of the probe and find the same change in geometry found in the experiment [?] due to the change in prevalence of the final ionized partial waves.

For argon, we study the quantum beats obtained in the photoionization spectrum following a two-probe photon absorption process (see [2] for another application of the formalism in the same system). We found, both experimentally and theoretically, that the quantum beats associated with ionization to each one of the spin-orbit split thresholds differ in phase by approximately

$\pi$  radians.

Currently, similar experiments are being constructed for neon to test the theoretical framework. We also want to investigate whether the rare gases share these observed spectral features.

This research is based upon work supported by the U.S. Department of Energy, Office of Science, Basic Energy Sciences, under Award No.DE-SC0010545

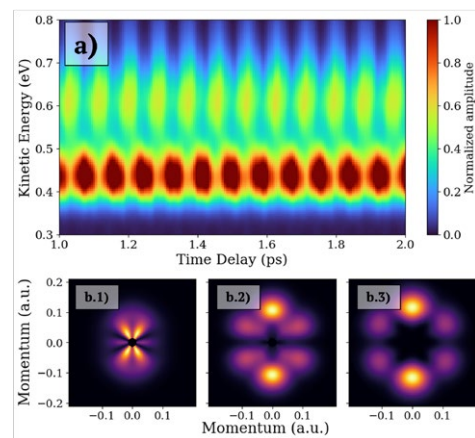


**Figure 1.** Panel (a) shows the theoretical spectrogram for the argon two-photon ionization. Panels (b) one through three shows the angular distribution of photoelectrons from neon for three different probe frequencies.

### References

- [1] Villeneuve, D. M., et al. 2017 *Science* 356(6343), 1150-1154
- [2] Plunkett, A., et al. 2022 *PRL* 128(8), 083001

\*E-mail: [malarco@purdue.edu](mailto:malarco@purdue.edu)



## Tracking Few-Femtosecond Auger Decay by Synchrotron Radiation

T Kaneyasu<sup>1,2\*</sup>, Y Hikosaka<sup>3</sup>, M. Fujimoto<sup>2,4</sup>, H. Iwayama<sup>2,5</sup> and M Katoh<sup>2,6</sup>

<sup>1</sup>SAGA Light Source, Tosu, 841-0005, Japan

<sup>2</sup>Institute for Molecular Science, Okazaki 444-8585, Japan

<sup>3</sup>Institute of Liberal Arts and Sciences, University of Toyama, Toyama 930-0194, Japan

<sup>4</sup>Synchrotron Radiation Research Center, Nagoya University, Nagoya, 464-8603, Japan

<sup>5</sup>Sokendai (The Graduate University for Advanced Studies), Okazaki 444-8585, Japan

<sup>6</sup>Hiroshima Synchrotron Radiation Center, Hiroshima University, Higashi-Hiroshima 739-0046, Japan

**Synopsis** We report the observation of quantum interference between electron wave packets launched from the 4d orbital of the Xe atom. Using pairs of light wave packets with attosecond-controlled spacing emitted from a synchrotron light source, we obtain time-domain interferogram for the inner-shell excitation. This approach enables us to track the few-femtosecond Auger decay by synchrotron radiation.

The sequential interaction of a pair of time separated pulses with an atomic or molecular system results in quantum interference between the resulting atomic/molecular wave packets. In this work, we use the recently disclosed ability of synchrotron light sources to perform wave packet interferometry experiments [1]. By using light wave packets with attosecond-controlled spacing, we observed the time-domain interferogram due to the interference between electron wave packets launched from the inner-shell 4d orbital of the Xe atom [2].

The experiment was carried using a tandem undulator setup in the UVSOR-III synchrotron. The electrons passing through the undulators emit pairs of 10-cycle light wave packets [3,4]. The peak photon energy was adjusted close to the energy of the  $4d_{5/2}^{-1}6p$  resonance. In order to monitor the population of the  $4d_{5/2}^{-1}6p$  excited state, we detected visible fluorescence photons of 460-nm-wavelength emitted from singly-charged ionic states.

Figure 1 shows the fluorescence yields measured as a function of time delay over a range from 0 to 21 fs. The time spectrum shows rapid oscillations, with a period of approximately 63 as. This can be understood as “time domain Ramsey fringes”, which arise from the quantum interference of electron wave packets launched at different times. Here the oscillation period corresponds to the transition frequency of the inner-shell excited state.

It is clear that the amplitude of the Ramsey fringes decreases with increasing time delay. This can be explained by considering the time

evolution of the first electron wave packet during the sequential interaction. Assuming a 6 fs lifetime for the  $4d_{5/2}^{-1}6p$  state, the time damped Ramsey fringe spectrum can be calculated as shown in Fig. 1(b). The good agreement between experiment and calculation confirms that the reduction in fringe amplitude does indeed arise from the excited state lifetime, lifetime, proving the time-domain access to femtosecond Auger decay processes using synchrotron light source.

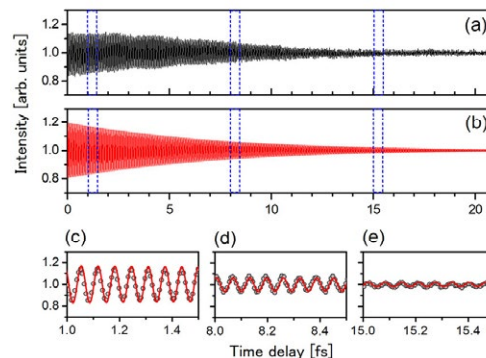


**Figure 1.** (a) Fluorescence yield measured as a function of time delay. (b) Calculated spectrum. (c)-(e) Comparison between the experimental and calculated spectra.

### References

- [1] Hikosaka Y *et al* 2019 *Nat. Commun.* **10** 4988
- [2] Kaneyasu T *et al* 2021 *Phys. Rev. Lett.* **126** 113202
- [3] Kaneyasu T *et al* 2022 *Sci. Rep.* **12** 9682
- [4] Fuji T *et al.*, 2023 *Optica* **126** 233401

\* E-mail: kaneyasu@saga-ls.jp

## Phase-resolved photoelectron-imaging of potassium atoms in two-color laser fields

Wankai Li, Yixuan Wang, Dongdong Zhang\* and Dajun Ding†

Institute of Atomic and Molecular Physics, Jilin University, Changchun 130012, China

Jilin Provincial Key Laboratory of Applied Atomic and Molecular Spectroscopy, Jilin University, Changchun 130012, China

**Synopsis** Combining with the velocity map imaging spectrometer (VMIs), the two-color phase-resolved photoelectron spectroscopy of potassium atoms are investigated. We experimentally extract continuum state electrons partial wave amplitude and phase. The electron-nucleus coulomb phase is analyzed with the help of the time-dependent Schrödinger equation (TDSE) calculation.

Outgoing photoelectrons ionized by laser fields carry the information of the interaction between electrons with parent nuclei [1, 2]. The amplitude of the continuum states wave function can be directly measured via photoelectron spectroscopy. Meanwhile, photoelectron angular distribution implicates the emission angle and phase information. Potassium atoms are easy to ionize in near infrared laser fields for their low ionization potentials [3]. Since there is only one  $s$  electron in the outermost shell, the single active electron approximation can describe the ionization process accurately. It is the benchmark objects of theoretical researches.

Combining with the VMIs the phase-resolved photoelectron imaging of potassium atoms is measured, we completely decouple continuum state electrons partial wave amplitude and phase. Two main ionization channels are found in potassium atoms. The angle-resolved photoelectron spectroscopy and the partial wave phase information of these two channels are obtained.

These phases can be associated with Wigner time-delay. Our experimental results agree well with the TDSE calculation, as shown in Figure 1. We show angle-resolved photoelectron imagings at the kinetic energy of 0.51 eV and its first order above-threshold ionization (ATI) channel. Due to the effect of the  $4s - 4p$  intermediate resonant state, we produce almost pure  $f$  electron partial wave. Relevant research work is still ongoing and we look forward to further theoretical support

to reveal the physical insights of the measured phases. Measuring continuum phase by interferometry method is an effective way to study the time issues in the ionization process.

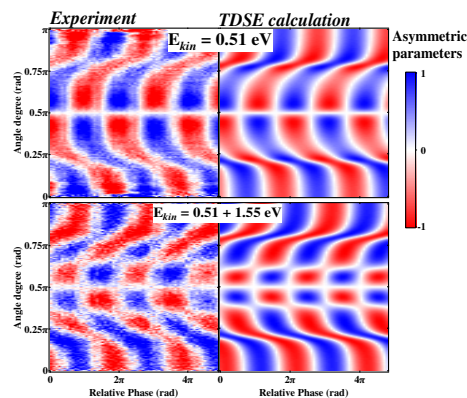


**Figure 1.** Two-color phase-resolved asymmetric parameters. The left figures are experimental results. The upper left is the two-color laser field phase-resolved photoelectron spectroscopy at 0.51 eV kinetic energy, and the lower left is the first order ATI. The right parts are the results from TDSE calculations. The color bar of experimental data are all adjusted to reduce background noise.

### References

- [1] Villeneuve *et al* 2017 *Science* **356** 6343
- [2] Wenhui Hu *et al* 2019 *Phys. Rev. A* **99** 011402
- [3] Wankai Li *et al* 2021 *Chin. Phys. Lett.* **38** 053202

\*E-mail: [dongdongzhang@jlu.edu.cn](mailto:dongdongzhang@jlu.edu.cn)

†E-mail: [dajund@jlu.edu.cn](mailto:dajund@jlu.edu.cn)

## Strong-field Effects on Time Delays in Correlated Ionization

W -C Jiang<sup>1\*</sup>, M -C Zhong<sup>1</sup>, Y -K Fang<sup>2</sup>, S Donsa<sup>3</sup>, I Březinová<sup>3</sup>, L -Y Peng<sup>2,†</sup> and J Burgdörfer<sup>3‡</sup>

<sup>1</sup>College of Physics and Energy, Shenzhen University, Shenzhen 518060, China

<sup>2</sup>State Key Laboratory for Mesoscopic Physics and Frontiers Science Center for Nano-optoelectronics, School of Physics, Peking University, 100871 Beijing, China

<sup>3</sup>Institute for Theoretical Physics, Vienna University of Technology, Wiedner Hauptstraße 8-10, A-1040 Vienna, Austria, EU

**Synopsis** Strong-field effects beyond the predictions of single-active-electron (SAE) models are identified in time delays of photoionization of helium by intense XUV pulses at photon energy 40 eV. Strong transient pulse-intensity and pulse-duration dependences are found when comparing the SAE and two-electron calculations. We interpret the strong-field effects as a consequence of the population dynamics of the two-electron wave packet during the interaction with the XUV pulse, including the initial-state depletion and the excitation of the remaining bound-state electron in  $\text{He}^+$ .

The ionization time delays in photoionization of helium are studied in the strong-field regime at an XUV photon energy of 40 eV, using our state-of-the-art numerical scheme of solving the full-dimensional time-dependent Schrödinger equation. The strong-field effects in ionization time delays can be interpreted as a consequence of the 2-electron wavepacket dynamics driven by the strong XUV pulse significantly modifying the time delay typically observed in the linear response regime. Consequently, the ionization time delay is sensitive to the intensity and duration of the XUV pulse. Such strong-field dynamics is generally beyond the prediction of the SAE theory. Even qualitative differences in pulse-intensity and pulse-duration dependence are found when comparing the SAE and two-electron results [1]. We present a theoretical framework for analyzing time delays in strong-field ionization observed by streaking or RABBIT processes in terms of the decomposition into a linear-response contribution into a linear-response contribution representing Eisenbud-Wigner-Smith (EWS) type delays  $\tau_{\text{EWS}}$  [2] and non-linear (NL) response corrections  $\tau_{\text{NL}}$  accounting for the transient non-linear response of the atomic system to be ion-

ized.

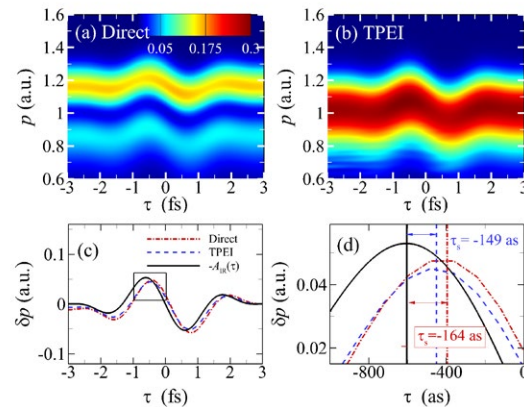


**Figure 1.** The streaking spectrogram for the one-photon direct (a) and the two-photon excitation ionization (TPEI) (b) channels along the polarization axis. The momentum shifts  $\delta p$  extracted from (a) and (b) are shown in (c) together with the IR (800 nm) streaking vector potential  $-A_{\text{IR}}(\tau)$ . The magnification of the black box in (c) is given in (d), where the streaking time delays of the direct channel ( $-164$  as) and the TPEI channel ( $-149$  as) are marked. The intensity and the FWHM duration of the Gaussian-shaped XUV pulse are  $I_X = 2.0 \times 10^{16}$  W/cm<sup>2</sup> corresponding to a Keldysh parameter  $\gamma = 2.6$  and  $T_X = 300$  as, respectively.

### References

- [1] W. Jiang, *et al.* in preparation
- [2] R. Pazourek, S. Nagele, and J. Burgdörfer 2015 *Rev. Mod. Phys.* **87** 765

\*E-mail: [jiang.wei.chao@szu.edu.cn](mailto:jiang.wei.chao@szu.edu.cn)

†E-mail: [liangyou.peng@pku.edu.cn](mailto:liangyou.peng@pku.edu.cn)

‡E-mail: [burg@concord.itp.tuwien.ac.at](mailto:burg@concord.itp.tuwien.ac.at)

## Experimental fingerprint of the electron's longitudinal momentum at the tunnel exit in strong field ionization

A Geyer<sup>1\*</sup>, D Trabert<sup>1</sup>, M Hofmann<sup>1</sup>, N Anders<sup>1</sup>, M S Schöffler<sup>1</sup>,  
L Ph H Schmidt<sup>1</sup>, T Jahnke<sup>2</sup>, M Kunitski<sup>1</sup>, R Dörner<sup>1</sup>, and S Eckart<sup>1†</sup>

<sup>1</sup>Institut für Kernphysik, Goethe-Universität, Max-von-Laue-Str. 1, 60438 Frankfurt am Main, Germany

<sup>2</sup>European XFEL, Holzkoppel 4, 22869 Schenefeld, Germany

**Synopsis** We present experimental data on the strong field tunnel ionization of argon in a counter-rotating two-color (CRTC) laser field. We find that the initial momentum component along the tunneling direction changes its sign comparing the rising and the falling edge of the CRTC field. If the initial momentum at the tunnel exit points towards the ion at the instant of tunneling, this manifests as an enhanced Coulomb interaction of the outgoing electron with its parent ion. Our conclusions are in accordance with predictions based on strong field approximation.

The strong field ionization of argon is experimentally investigated using a counter-rotating circularly polarized two-color (CRTC) field. The two-color field (central wavelengths of 390 nm and 780 nm) is generated in an interferometric two-color setup [1]. The intensity of the 780 nm [390 nm] pulse is  $8.5 \times 10^{13}$  W/cm<sup>2</sup> [ $5.6 \times 10^{13}$  W/cm<sup>2</sup>]. The three-dimensional electron momentum distribution is measured using cold target recoil ion momentum spectroscopy (COLTRIMS) [2].

We experimentally observe a qualitatively new feature in the electron momentum distribution. We find that this feature emerges because the component of the initial momentum at the tunnel exit that points towards or away from the residual ion modifies the Coulomb interaction of the electron with its parent ion after tunneling [4].

Fig. 1(a) shows the measured electron momentum distribution. Electrons that are born on the falling edge of the CRTC field (marked by a black circle) form a wing-like structure. We have performed a simulation using the non-adiabatic classical two-step (NACTS) model to reproduce the measured observables (see Fig. 1(b)) [3]. (c) [(d)] shows the initial momentum perpendicular [parallel] to the time-dependent laser electric field at the instant of tunneling as a function of the instant of tunneling  $t$ .

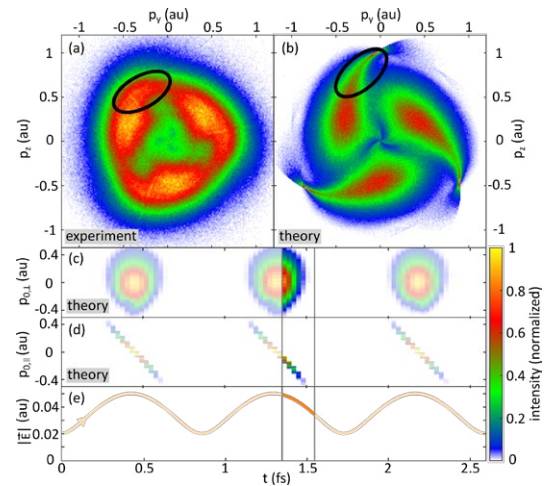


**Figure 1.** (a) Measured electron momentum distribution for the ionization by a CRTC field. (b) Simulated electron momentum distribution. (c) [(d)] Initial momenta perpendicular [parallel] to the time-dependent laser electric field at the instant of tunneling as a function of the electron's release time  $t$ . (e) Absolute laser electric field as a function of  $t$ . The events between the two gray lines in (c)-(e) belong to final momenta in the black circle in (a) and (b).

### References

- [1] Eckart S *et al* 2016 *Phys. Rev. Lett.* **117** 133202
- [2] Ullrich J *et al* 2003 *Rep. Prog. Phys.* **66** 1463
- [3] Trabert D *et al* 2021 *Phys. Rev. Lett.* **127** 273201
- [4] Geyer A *et al* 2022 *arXiv arXiv:2211.01791*

\*E-mail: [geyer@atom.uni-frankfurt.de](mailto:geyer@atom.uni-frankfurt.de)

†E-mail: [eckart@atom.uni-frankfurt.de](mailto:eckart@atom.uni-frankfurt.de)

## Orbital effects in laser tunneling ionization of Ar and H<sub>2</sub> studied by electron-ion coincidence momentum imaging

D. Ikeya,<sup>1</sup> H. Fujise,<sup>1</sup> S. Inaba,<sup>1</sup> M. Takahashi,<sup>1</sup> M. Yamamoto,<sup>1</sup> T. Nakamura,<sup>1</sup> Y. Nagao,<sup>1</sup>  
A. Matsuda,<sup>1</sup> M. Fushitani,<sup>1</sup> A Hishikawa<sup>1,2,\*</sup>

<sup>1</sup>Research Center for Materials Science, Nagoya University, Nagoya, 464-8602, Japan

<sup>2</sup>Graduate School of Science, Nagoya University, Nagoya, 464-8602, Japan

**Synopsis** Three-dimensional momentum distributions of tunnel-electrons produced from Ar and H<sub>2</sub> in circularly polarized intense laser fields (1035 nm, 35 fs,  $2 \times 10^{14}$  W/cm<sup>2</sup>) have been measured by electron–ion coincidence momentum imaging. Although ionization potentials are similar, significant differences are identified in the radius and the width of the photoelectron torus recorded in coincidence with the counterpart ions (Ar and H<sub>2</sub>). The differences are confirmed by theoretical calculations based on the strong-field approximation, showing that the orbital character of ionizing electrons is encoded in the momentum distribution of tunnel electrons.

Electrons produced by tunneling ionization carry properties of target atoms and molecules. The nascent momentum distribution can be experimentally measured by using circularly polarized laser fields, where the electron rescattering is suppressed because of the lateral shift of returning electrons. The momentum distribution perpendicular to the laser electric field, or the transverse momentum distribution (TMD), is preserved after the interaction with the laser fields.

Here we report measurements of photoelectron momentum distributions of H<sub>2</sub> having quasi *s*-orbital character (1*s*σ) and Ar (3*p*) in circularly polarized intense laser fields. Since the respective ionization potentials, (Ar) = 15.759 eV and (H<sub>2</sub>, adiabatic) = 15.426 eV are comparable, one can expect that the effect of the ionizing orbitals is more clearly elucidated in the difference of measured photoelectron torus, which will be useful to deepen the understanding of laser tunneling ionization towards the application to ultrafast spectroscopy.

For this purpose, we employ an electron–ion coincidence three-dimensional momentum imaging, where a static electric field is used to extract the electrons and ions from the target. To suppress the possible influence from experimental fluctuations, a gas mixture of Ar and H<sub>2</sub> is used. The electrons are recorded in coincidence with the counterpart ions, Ar and H<sub>2</sub>, to obtain the photoelectron momentum distribution from each species. The measured photoelectron momentum distributions show clear differences

between Ar and H<sub>2</sub>. It is shown that the SFA calculations can successfully explain the observed differences (Fig.1). On the other hand, some deviations from the experimental results are observed in the absolute values, suggesting further theoretical developments are necessary to fully understand the factors encoded in the momentum distribution of tunnel electrons.

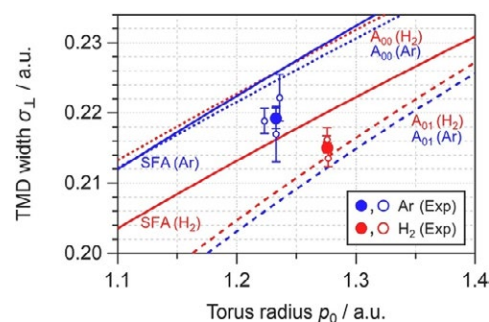


**Figure 1.** Width of transverse momentum distribution  $\sigma_{\perp}$  plotted against the torus radius  $p_0$  for Ar (blue) and H<sub>2</sub> (red) compared with the adiabatic ( $A_{00}$  and  $A_{01}$ ) and SFA calculations [2].

### References

- [1] L. Arissian, *et al.*, *Phys. Rev. Lett.* 105, 133002 (2010).
- [2] D. Ikeya, *et al.*, *J. Electron Spec. Rel. Phenomena* 267, 147280 (2023).

\* E-mail: hishi@chem.nagoya-u.ac.jp



## Coulomb focusing in attosecond angular streaking measurement of strong field tunneling ionization

X Li<sup>1</sup>, X Liu<sup>2</sup>, C Wang<sup>1\*</sup>, W Dong<sup>3</sup>, J Li<sup>3</sup>, S Zhou<sup>1</sup>, Y Yang<sup>1</sup>, X Song<sup>2†</sup>, W Yang<sup>2‡</sup> and D Ding<sup>1§</sup>

<sup>1</sup>Institute of Atomic and Molecular Physics, Jilin University, Changchun, 130012, China

<sup>2</sup>School of Science and Center for Theoretical Physics, Hainan University, Haikou, 570228, China

<sup>3</sup>Department of Physics, College of Science, Shantou University, Guangdong, 515063, China

**Synopsis** We reveal the critical role of the Coulomb focusing in the angular streaking measurement, which results that electrons emitted at different times can be focused to the same final momentum. Quantitative agreement of energy-dependent streaking angles in measurement and semiclassical simulation demonstrates the effect of sub-barrier Coulomb potential, which has an influence on the Coulomb focusing and leaves fingerprints on the measured angular offsets.

Angular streaking[1] is a sophisticated technique to study the electron tunneling dynamics with attosecond temporal resolution. In a recent angular streaking study on the nonadiabatic ionization of atomic hydrogen, a qualitative agreement is obtained about the trend of angular offsets versus energy when a strong-field approximation simulation is applied with nonadiabatic correction[2]. However, the underlying mechanism of the observed phenomena and especially, how it affects on the accuracy of attosecond angular streaking remain unclear.

Experimentally, we perform an energy-resolved angular streaking measurements on noble gas atoms with elliptically polarized laser pulses ( $\epsilon=0.79$ , 800 nm, 40 fs). It shows that the most probable emission angle increases with energy, similar to the hydrogen measurement[2]. Semiclassical simulations are performed by standard and improved Coulomb corrected strong-field approximation (CCSFA/ICCSFA) methods. Figure 1 shows that, comparing to the CCSFA, ICCSFA method that considers both long-range Coulomb effects in the continuum and under-barrier dynamics can obtain well-fitted offset angles with the results from experiment and numerical solutions of the time-dependent Schrödinger equation (TDSE).

It is demonstrated that the energy-dependent Coulomb focusing induces the observed trend. We found that electrons emitting at a broad span of position and time can be focused to the same final momentum via Coulomb interaction,

which shifts the observed angular streaking signal with maximum probability. Both experimental and ICCSFA data of distributions of transverse momentum further confirm that the Coulomb focusing still works in angular streaking method with close-to-circularly polarized laser pulse.

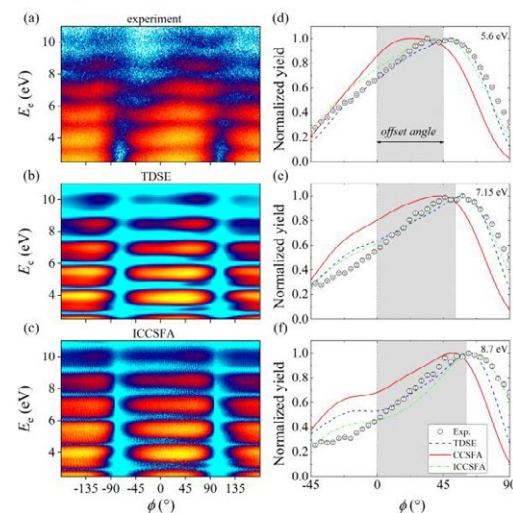


**Figure 1.** Energy-resolved photoelectron angular distributions and offsets from attosecond angular streaking measurement and simulations of xenon atom.

### References

- [1] Eckle P *et al.* 2008 *Science* **322**, 1525
- [2] Trabert D *et al.* 2021 *Phys. Rev. Lett.* **127** 273201

\* E-mail: [ccwang@jlu.edu.cn](mailto:ccwang@jlu.edu.cn)

† E-mail: [song\\_xiaohong@hainanu.edu.cn](mailto:song_xiaohong@hainanu.edu.cn)

‡ E-mail: [wfyang@hainanu.edu.cn](mailto:wfyang@hainanu.edu.cn)

§ E-mail: [dajund@jlu.edu.cn](mailto:dajund@jlu.edu.cn)



## Relativistic treatment of hole alignment due to autoionization processes and Cooper minima in noble gas atoms

R Tahouri\*, A Papoulia, F Zapata, S Carlström and J M Dahlström†

Department of Physics, Lund University, Lund, 22100, Sweden

**Synopsis** *Ab initio* relativistic simulations are used to study the distribution of ion holes with different magnetic quantum numbers in photoionized noble gases. Different spectral features are targeted by tuning the laser field frequency, reaching hole alignments with unprecedentedly high ratios.

The recent developments in attosecond physics allow us to study the temporal dynamics of photoelectrons as well as the corresponding ions in photoionization experiments [1]. In noble gases, the ion consists of different “holes” that are characterized by the properties of the missing electron. The alignment of the hole refers to the population ratio of different magnetic quantum numbers,  $m_j$ , with the same  $j$ , that are produced in the photoionization process [2]. In this work, we tune the laser field frequency to make use of particular spectral properties of the absorption cross section, like Fano profiles of autoionizing states, Cooper minima, and giant resonances, in order to control this alignment property. Since holes in noble gas atoms are coupled to the total angular momentum:  $j = \ell + s$ , a consistent treatment of relativistic effects should be employed. Here, we are using the recently proposed Relativistic Time-Dependent Configuration-Interaction Singles (RTDCIS) method [3].

The RTDCIS method can be used to study theoretical partial cross sections and photoelectron fluxes in noble gas atoms when interacting with ultra-fast pulses from free-electron laser (FEL) sources and attosecond pulses from high-order harmonic generation (HHG). This method, which is based on the Dirac-Fock spin-orbitals, accounts for electron correlation effects at the level of single excitations. Therefore, photoelectron and hole pairs can be simulated in a relativistic framework. Here, we focus on reduced ion channels, which correspond to unresolved photoelectrons, by summing incoherently (tracing out) the population of the outgoing electrons corresponding to a given hole state.

In previous studies, the photon energy was

\*E-mail: rezvan.tahouri@matfys.lth.se

†E-mail: marcus.dahlstrom@matfys.lth.se

tuned to autoionizing states [2]. Being spectrally narrow, hole alignment with such Fano resonances demands long XUV pulses (hundreds of fs) to achieve a high degree of alignment. Here, we consider the Cooper minimum of argon, which gives the possibility of employing shorter pulses (hundreds of as) to obtain a higher degree of alignment as can be seen in figure 1 where an alignment ratio of 23.6 is achieved. Thus, Fano resonances and Cooper minima present promising avenues to hole alignment studies for different pulses.

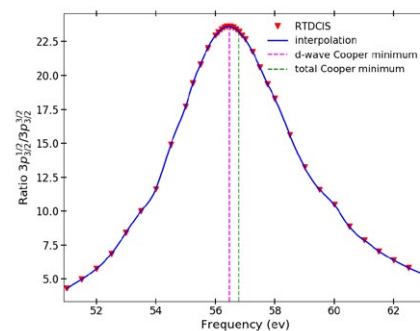


**Figure 1.** The ratio of ion populations with  $m_j = 1/2$  and  $3/2$ , for  $j = 3/2$ , in argon after interaction with a 300 as pulse. The central frequency (x-axis) is tuned over the Cooper minimum.

### References

- [1] Goulielmakis E *et al* 2010 *Nature* **466** 739-743
- [2] Heinrich-Josties E, Pabst S and Santra R 2014 *Phys. Rev. A*. **89** 043415
- [3] Zapata F, Vinbladh J, Ljungdahl A, Lindroth E and Dahlström J M 2022 *Phys. Rev. A*. **105** 012802

## Interferences due to Auger decay of a doubly excited atomic state

M Žitnik<sup>1,2\*</sup>, M Hrast<sup>1</sup>, A Mihelič<sup>1,2</sup>, K Bučar<sup>1,2</sup>, J Turnšek<sup>1,2</sup>, R Püttner<sup>3</sup>,  
G Goldsztejn<sup>4</sup>, T Marchenko<sup>4</sup>, R. Guillemin<sup>4</sup>, L Journal<sup>4</sup>, O Travnikova<sup>4</sup>, I Ismail<sup>4</sup>,  
M N Piancastelli<sup>4</sup>, M Simon<sup>4</sup>, D Céolin<sup>5</sup> and M Kavčič<sup>1,2</sup>

<sup>1</sup>Jožef Stefan Institute, Jamova cesta 39, SI-1000 Ljubljana, Slovenia

<sup>2</sup>Faculty of Mathematics and Physics, University of Ljubljana, Jadranska 31, SI-1000 Ljubljana, Slovenia

<sup>3</sup>Institut für Experimentalphysik, Freie Universität Berlin, Arnimallee 14, D-14195 Berlin-Dahlem, Germany

<sup>4</sup>Sorbonne Université, CNRS, Laboratoire de Chimie Physique-Matière et Rayonnement, LCPMR, F-75005 Paris Cedex 05, France

<sup>5</sup>Synchrotron SOLEIL, L'Orme des Merisiers, Saint Aubin, BP 48, F-91192 Gif-sur-Yvette Cedex, France

**Synopsis** Auger decay of doubly excited atomic resonances causes a non-trivial modulation of absorption spectrum above the core-hole ionization threshold because it interferes with both, the direct photoionization leading to the low-energy photoelectron continuum, and the shake-up Auger photoelectron recapture leading to the high-energy Auger electron continuum. The effects of both, the participator and spectator Auger coupling are clearly seen in our study of the isolated  $(1s3p)^{-1}4s^2\ ^1P$  atomic resonance in argon.

The modulation of absorption cross section in the region of doubly excited states is often considered a nuisance for a reliable EXAFS structural analysis which prefers to deal with a smooth core-hole continuum modulated by photoelectron scattering from neighboring atoms only. There are different approaches to remove/separate the resonant structure from the absorption spectra and some of them are relying on the spectral analysis of decay products. Namely, in both the radiative and the non-radiative channel, spectral features caused by decay of the core-hole continuum and of doubly excited states differ from each other. Moreover, while in the latter case the signal resonates and moves with a photon energy due to the Raman effect, the continuum part appears as a set of quasi constant spectral lines at more or less fixed energy positions. By analyzing the resonant inelastic x-ray scattering (RIXS) spectral maps, it was shown that resonant part of the spectrum can be separated from the continuum part [1]. However, the separation of the resonant structure in the x-ray emission channel does not mean that separation is achieved in the absorption too because the absorption signal summarizes the effect of *all* decay channels. By analyzing the resonant Auger spectral map, we show that the non-radiative decay introduces a non-negligible coupling between the resonant and the non-resonant component: the interferences were observed in both the participator and

\*E-mail: [matjaz.zitnik@ijs.si](mailto:matjaz.zitnik@ijs.si)

the spectator Auger decay channel of an isolated doubly excited state. The absorption cross section becomes inseparable to the resonant and the continuum part as soon as the two components interfere in at least one of the decay channels.

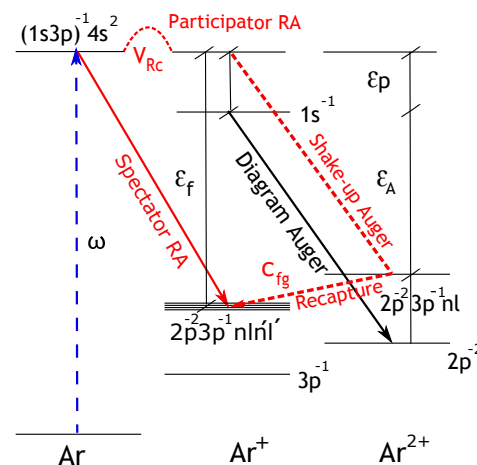


**Figure 1.** The scheme of nonradiative electronic transitions triggered by photoexcitation of  $(1s3p)^{-1}4s^2$  state in argon. The kinetic energies of the  $1s$  photoelectron and of the resonant and the non-resonant  $K-L_{23}^2$  electrons are denoted by  $\epsilon_p$ ,  $\epsilon_f$  and  $\epsilon_A$ , respectively.

### References

- [1] Kavčič M *et al.* 2009 *Phys. Rev. Lett.* **102** 143001

## Asymmetry parameters in single ionization of Ne by XUV pulse

J T Lei<sup>1,2</sup>, X Yu<sup>2,3</sup>, Z Y Liu<sup>1</sup>, J J Ding<sup>1\*</sup>, X Ma<sup>2,3</sup> and S F Zhang<sup>2,3†</sup>

<sup>1</sup>School of Nuclear Science and Technology, Lanzhou University, Lanzhou 730000, China

<sup>2</sup>Institute of Modern Physics, Chinese Academy of Sciences, Lanzhou 730000, China

<sup>3</sup>University of Chinese Academy of Sciences, Beijing 100049, China

**Synopsis** Fully differential cross-sections of single ionization of Ne atoms are studied by linearly polarized extreme ultraviolet (XUV) pulses in the energy range from 22.1 eV to 43.7 eV, using a reaction microscope. The  $\beta$  asymmetry parameters extracted from the angular distributions of Ne  $2p^6$  electrons are obtained. By comparing with different theoretical calculations, it is found that the contribution of the electron correlation effect in Ne  $2p^6$  single ionization is important, while the relativistic effect is relatively low in the whole incident energy range.

Photoionization is one of the fundamental processes in nature where detailed information about few-body dynamics can be extracted from ionization processes[1]. Differential cross sections such as photoelectron angular distribution (PAD) contain more detailed information of the atomic system. For different electronic states and strength of electron correlations, the PADs usually present profiles of different  $\beta$  asymmetry parameters[2] around the polarization direction, which can provide sensitive information on the electronic states.

In this work, PADs of Ne are studied in single ionization via ultrashort XUV pulses by a reaction microscope. For XUV photon energy ranging from 22.1 eV to 43.7 eV, the  $\beta$  asymmetry parameters are systematically studied with high accuracy, and comparison with different theoretical results are discussed.

Figure 1 illustrates the  $\beta$  parameters of Ne atoms as a function of incident photon energies from 22.1 to 43.7 eV. The observed  $\beta$  asymmetry parameter for  $2p$  photoelectron of Ne displays a monotonic variation with photon energy, and its curve shape is excellently reconstructed by the random-phase-approximation (RPA) calculation[3], while Dirac-Fock (D-F) theory is quite different from the experimental data. This indicates the influence of relativistic effect is small, but electron correlation is important in this process. It should be noted that, when the photon energy is below 23.5 eV, the results obtained by Hartree-Fock (H-F) and RPA

theory are very similar and in good agreement with the experimental data. That means the influence of electron correlation effect on the angular distribution for  $2p^6$  ionization is small, when the photon energy is below the first ionization threshold. With the incident photon energy increasing, the electron correlation effect becomes significant for PAD in this photoionization process.

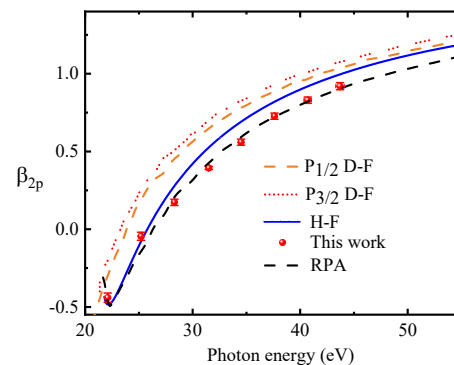


**Figure 1.**  $\beta$  asymmetry parameters for  $2p$  photoelectrons of Ne with different photon energies. The dash black line and blue solid line are the results from RPA and H-F calculation. The orange dash line and red dot line are D-F calculations for the  $P_{1/2}$  and  $P_{3/2}$  subshells.

### References

- [1] Goulielmakis E *et al* 2010 *Nature*. **466** 739
- [2] Manson S T *et al* 1982 *Rev. Mod. Phys.* **54** 389
- [3] Amusia M Ya *et al* 1972 *Phys. Lett. A* **40** 15

\*E-mail: dingjj@lzu.edu.cn

†E-mail: zhangshf@impcas.ac.cn

## K-shell photodetachment of carbon, oxygen, and silicon anions

S Schippers<sup>1\*</sup>, A Müller<sup>1</sup>, M Martins<sup>2</sup>, S Reinwardt<sup>2</sup>, F Trinter<sup>3,4</sup> and S Fritzsche<sup>5,6,7</sup>  
for the PIPE collaboration

<sup>1</sup>I. Physikalisches Institut, Justus-Liebig-Universität Gießen, Germany

<sup>2</sup>Institut für Experimentalphysik, Universität Hamburg, Germany

<sup>3</sup>Molecular Physics, Fritz-Haber-Institut der Max-Planck-Gesellschaft, Berlin, Germany

<sup>4</sup>Institut für Kernphysik, Goethe-Universität Frankfurt am Main, Germany

<sup>5</sup>Helmholtz-Institut Jena, Germany

<sup>6</sup>GSI Helmholtzzentrum für Schwerionenforschung, Darmstadt, Germany

<sup>7</sup>Institut für Theoretische Physik, Friedrich-Schiller-Universität Jena, Germany

**Synopsis** Using the PIPE end-station at PETRA III, we have measured cross sections for multiple photodetachment of  $C^-$ ,  $O^-$ , and  $Si^-$  in the photon-energy ranges 280–1000 eV, 525–1500 eV, and 1830–1900 eV, respectively. All cross sections exhibit near-threshold resonances and clear signatures of direct double detachment, i.e., the simultaneous removal of two electrons by one photon. For  $C^-$  and  $O^-$ , double  $K$ -shell hole creation is observed.

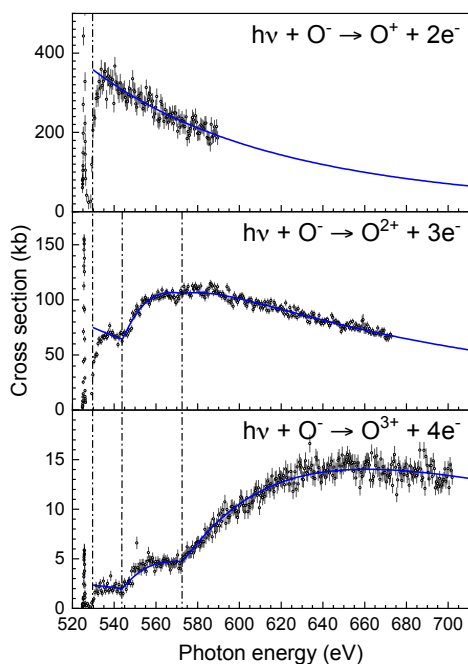


**Figure 1.** Experimental cross sections (symbols) for net double, triple, and fourfold photodetachment of  $O^-$  [2]. The vertical dash-dotted lines mark the thresholds for the direct single detachment of a  $1s$  electron and for direct  $1s + 2p$  and  $1s + 2s$  double detachment. The full lines result from fits of sums of semi-empirical cross-section formulae for these processes. For direct double detachment, the formula of Pattard [5] was used. The  $1s2s^22p^6$  below-threshold resonance at 525.6 eV [6] can be discerned in all measured cross sections.

\*E-mail: [stefan.schippers@physik.uni-giessen.de](mailto:stefan.schippers@physik.uni-giessen.de)

Employing the photon-ion merged-beams technique, we have measured cross sections  $\sigma_m$  for multiple ( $m$ -fold) photodetachment of  $C^-$  [1],  $O^-$  [2] (Fig. 1), and  $Si^-$  [3]. The experimental photon-energy ranges comprise the thresholds for direct detachment of one or two (for  $C^-$  and  $O^-$ )  $K$ -shell electrons. All cross sections exhibit near-threshold resonances that are associated with the excitation of a  $1s$  electron to either the  $2p$  or the  $3p$  subshell. For  $C^-$ , further resonances have been discovered at energies of up to 45 eV beyond the threshold for  $1s$  detachment. Several of the measured  $C^-$  and  $O^-$  cross sections contain sizeable contributions of the process of direct double detachment, i.e., the simultaneous removal of two electrons by one photon, as already observed earlier for  $F^-$  [4]. For  $C^-$  and  $O^-$ , the cross sections  $\sigma_5$  show signatures of double  $K$ -shell hole formation. Results of large-scale atomic-structure calculations, which treat the complex de-excitation cascades that set in after the initial creation of one or two inner-shell holes, agree surprisingly well with the experimental findings.

### References

- [1] Perry-Sassmannshausen A et al 2020 *Phys. Rev. Lett.* **124** 083203
- [2] Schippers S et al 2022 *Phys. Rev. A* **106** 013114
- [3] Perry-Sassmannshausen A et al 2021 *Phys. Rev. A* **104** 053107
- [4] Müller A et al 2018 *Phys. Rev. Lett.* **120** 133202
- [5] Pattard T 2002 *J. Phys. B* **35** L207
- [6] Schippers S et al 2016 *Phys. Rev. A* **94** 041401(R)

## Vibrationally resolved inner-shell photoexcitation of the molecular anion $C_2^-$

S Schippers<sup>1\*</sup>, P-M Hillenbrand<sup>1</sup>, A Perry-Sassmannshausen<sup>1</sup>, T Buhr<sup>1</sup>, S Fuchs<sup>1</sup>, S Reinwardt<sup>2</sup>, F Trinter<sup>3,4</sup>, A Müller<sup>1</sup> and M Martins<sup>2</sup>,

<sup>1</sup>I. Physikalisches Institut, Justus-Liebig-Universität Gießen, Germany

<sup>2</sup>Institut für Experimentalphysik, Universität Hamburg, Germany

<sup>3</sup>Institut für Kernphysik, Goethe-Universität Frankfurt am Main, Germany

<sup>4</sup>Molecular Physics, Fritz-Haber-Institut der Max-Planck-Gesellschaft, Berlin, Germany

**Synopsis** Carbon 1s core-hole excitation of the  $C_2^-$  anion has been experimentally studied at high resolution by employing the photon-ion merged-beams technique at a synchrotron light source. The experimental cross section for photo-double-detachment shows a pronounced vibrational structure associated with  $1\sigma_u \rightarrow 3\sigma_g$  and  $1\sigma_g \rightarrow 1\pi_u$  core excitations of the  $C_2^-$  ground level and the first excited level, respectively. A detailed Franck-Condon analysis provides the spectroscopic parameters of the associated core-excited levels.

Carbon 1s core-hole excitation of the dicarbon anion  $C_2^-$  has been experimentally studied at high resolution [1] by employing the photon-ion merged-beams technique as implemented at the PIPE end-station [2] at beamline P04 of the PETRA III synchrotron light source operated by DESY in Hamburg, Germany. As in our previous work with atomic  $C^-$  anions [3], we used a Cs-sputter ion source, here, for the production of a  $C_2^-$  ion beam. The experimental cross section for photo-double-detachment (PDD) of the  $^{12}C^{12}C^-$  anion shows a pronounced vibrational structure associated with  $1\sigma_u \rightarrow 3\sigma_g$  and  $1\sigma_g \rightarrow 1\pi_u$  core excitations of the  $X^2\Sigma_g$  ground level and of the  $A^2\Pi_u$  first excited level, respectively (Fig. 1).

A detailed Franck-Condon analysis, which involves the numerical calculation of the Franck-Condon factors between two displaced Morse potentials [4], reveals a strong contraction of the  $C_2^-$  anion by 0.2 Å upon this core photoexcitation. This is a much stronger contraction as observed for the isoelectronic  $N_2^+$  ion [5]. The associated change of the molecule's moment of inertia leads to a noticeable rotational broadening of the observed vibrational spectral features. This broadening is accounted for in the present analysis, which provides the spectroscopic parameters of the  $C_2^-$   $1\sigma_u^{-1}3\sigma_g^22\Sigma_u^+$  and  $1\sigma_g^{-1}3\sigma_g^22\Sigma_g^+$  core-excited levels. In principle, the present results should be useful for the identification of  $C_2^-$  anions in the interstellar medium and other cosmic objects.

\*E-mail: stefan.schippers@physik.uni-giessen.de

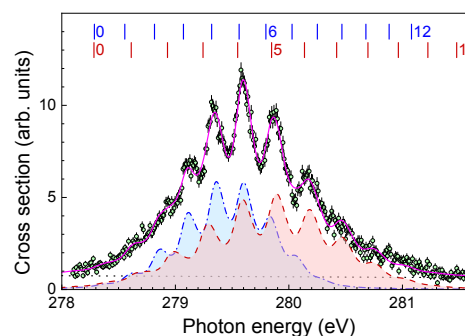


**Figure 1.** Experimental cross section for PDD of  $C_2^-$  (symbols) and Franck-Condon fit (pink full curve) [1]. The experimental photon-energy spread was 50 meV. The blue dashed-dotted and red dashed shaded curves represent contributions by the  $X^2\Sigma_g(v=0)$  ground level and the by the first excited  $A^2\Pi_u(v=0)$  metastable level, respectively. The vertical bars mark the energies of the respective core-excited vibrational levels. They are labeled with the associated vibrational quantum numbers  $v'$ . The dotted line represents the continuous cross section for direct ionization.

### References

- [1] Schippers S et al 2023 *ChemPhysChem* e202300061
- [2] Schippers S et al 2020 *X-ray Spectrom.* **49** 11
- [3] Perry-Sassmannshausen A et al 2020 *Phys. Rev. Lett.* **124** 083203
- [4] López V J C et al 2020 *Int. J. Quantum Chem.* **88** 280
- [5] Lindblad R et al 2020 *Phys. Rev. Lett.* **124** 203001

## Investigation of Interatomic Coulombic Decay after inner-shell ionization in heterogeneous rare gas clusters by multi-coincidence spectroscopy

C Küstner-Wetekam<sup>1\*</sup>, L Marder<sup>1</sup>, D Bloß<sup>1</sup>, N Kiefer<sup>1</sup>, U Hergenbahn<sup>2</sup>,  
A Ehresmann<sup>1</sup>, P Kolorenc<sup>3</sup> and A Hans<sup>1</sup>

<sup>1</sup>Institute of Physics and CINSaT, University of Kassel, Kassel, 34132, Germany

<sup>2</sup>Fritz-Haber-Institute of the Max-Planck Society, Berlin, 12489, Germany

<sup>3</sup>Institute of Theoretical Physics, Charles University, Prague, 18000, Czech Republic

**Synopsis** Auger spectroscopy is a frequently used method to investigate the decay of core-hole states in atoms. If the atom is placed in an environment, for example a weakly-bound cluster, its decay paths can change significantly and additional non-local decay mechanisms like interatomic Coulombic decay (ICD) become operable. Here, we investigate the cluster-site dependent behaviour of ICD when changing from homogeneous to heterogeneous rare gas clusters.

To understand the importance of non-local decay mechanisms in complex systems, it is necessary to study its dependence on different parameters in prototype systems like rare-gas clusters. The advantage of such artificial samples is that we can investigate some of their properties by varying the cluster conditions and thereby the composition in a controlled way.

The most prominent non-local decay channels such as interatomic Coulombic decay (ICD), electron-transfer mediated decay (ETMD) and radiative charge transfer (RCT) have been identified and characterized in a plethora of systems and excitation scenarios, e.g., from local Auger final states [1]. In the present work however, we study core-level ICD, which is a direct competitor to the local Auger decay and thereby allows us a direct comparison of local and non-local processes using multi-coincident electron spectroscopy [2].

Cluster-site sensitive measurements enable the study of the core-level ICD efficiency as a function of the number of nearest neighbors or – when changing from homogeneous to heterogeneous clusters – of the composition of the environment.

In the specific case of homogeneous Kr and heterogeneous ArKr clusters, we detect the *MNN* Auger and ICD electrons in coincidence with the Kr  $3d_{5/2}$  photoelectrons (see Fig. 1).

Comparison of both measurements after normalization to the Auger electron signal intensity shows a significant increase in ICD efficiency and an energy shift to lower kinetic energies for the heterogeneous clusters.

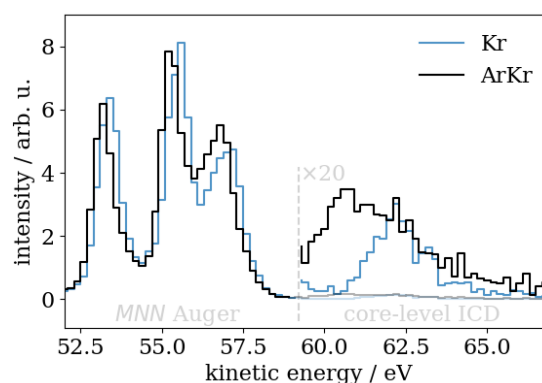


**Figure 1.** Electron spectra resulting from *MNN* Auger decay and competing core-level ICD of Kr (blue) and ArKr (black) clusters measured in coincidence with  $3d_{5/2}$  photoelectrons.

Therefore, a change in the environment of the inner-shell ionized Kr atom – from pure krypton to argon and krypton neighbors – changed the subsequent decay path significantly.

### References

- [1] Jahnke T, Hergenbahn U, Winter B, et al. 2020 *Chem. Rev.* **120** 11295-11369
- [2] Hans A, Küstner-Wetekam C, Schmidt Ph, et al. 2020 *Phys. Rev. Research* **2** 012022(R)

\* E-mail: [c.kuestner-wetekam@uni-kassel.de](mailto:c.kuestner-wetekam@uni-kassel.de)



## DFT study of $d$ -electron photoionization of $x@C_{60}$ with $x = Cu^+, Cu, Cu^-, Zn$

D T Forbes, S Prabhakar, R De and H S Chakraborty<sup>†</sup>

Department of Natural Sciences, D L Hubbard Center for Innovation, Northwest Missouri State University, Maryville, Missouri 64468, USA

**Synopsis** Using density functional theory in spherical geometry based on a jellium description of  $C_{60}$  ion core, we compute photoionization parameters of endofullerene molecules comprised of neutral and ionic Cu and neutral Zn. Features of electronic many-body interactions are compared among the systems to probe the effect of nuclear screening on the outer  $d$  electron emissions.

Theoretical studies of the photoionization spectroscopy of  $C_{60}$  endofullerene compounds engaging closed-shell and near closed-shell atoms are aplenty. In these, the models that incorporate  $C_{60}$  electrons explicitly have accessed effects of many-electron correlations including collective and single-electron resonances. The current study finds that the similar levels of nuclear screening for different choices of guest atoms or ions can draw comparable influences of  $C_{60}$  on the photoionization of outer levels. To illustrate the effect, we consider the sub-valent  $d$ -electron photoemission for a choice of four molecules:  $Cu^+@C_{60}$ ,  $Cu@C_{60}$ ,  $Cu^-@C_{60}$ , and  $Zn@C_{60}$ .

The calculation is performed in the frame of linear-response time-dependent density functional theory (LR-TDDFT) with the dipole response of the system to the incoming radiation [1]. The Kohn-Sham equations of the delocalized valence electrons are solved to obtain the ground state structures, while the cage of sixty  $C^{4+}$  ions is jelliumized. The LB94 exchange-correlation functional [2] is employed for asymptotic accuracy of the ground and continuum states.

Figure 1 presents the outer ( $3d$ ) cross section for all the systems considered. Results for  $Cu@C_{60}$  and  $Cu^-@C_{60}$  are very similar with strong influence of  $C_{60}$  plasmon resonances at lower energies, while retaining the atomic character as energy increases. Even though  $Cu^-$  has an extra  $4s$  valence electron, the sub-valent  $3d$  shell experiences comparable nuclear screening for both systems. However, the cross sections for  $Cu^+@C_{60}$  and  $Zn@C_{60}$  are also found similar, while being dramatically different from the results of the former pair. This is likely due to the similar screening felt by the  $d$ -electrons

even after two  $4s$  electrons and a proton need be added to  $Cu^+@C_{60}$  to turn it into  $Zn@C_{60}$ . The cross sections of the other  $d$  level (not shown) exhibit similar qualitative trend [3].

With the advances in the synthesis of endofullerenes in gas phase, in solution or as films [4], possible photoelectron spectroscopic measurements may probe these results.

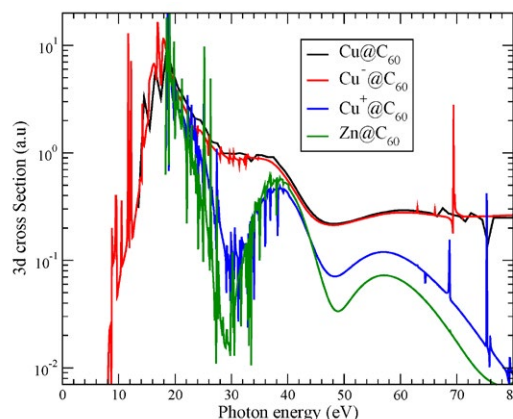


**Figure 1.** Cross sections for the outer  $d$  emission of four compounds as a function of the photon energy.

The research was supported by US-NSF PHY-2110318

### References

- [1] Choi J, Chang E H, Anstine D M, Madjet M E and Chakraborty H S 2017 *Phys. Rev. A*, **95** [023404](#)
- [2] Leeuwen R van and Baerends E J 1994, *Phys. Rev. A* **49**, [2421](#)
- [3] Forbes D T, Prabhakar S, De R and Chakraborty H S (*in preparation*)
- [4] Popov A 2017 *Nanostr. Sc. Tech. Ser.* [Springer](#)

<sup>†</sup> E-mail: [himadri@nwmissouri.edu](mailto:himadri@nwmissouri.edu)

## Photofragmentation of cyclo-dipeptides in the gas-phase and routes to the formation of peptide chains

Paola Bolognesi<sup>1\*</sup>, Darío Barreiro Lage<sup>2</sup>, Jacopo Charinelli<sup>1</sup>, Robert Richter<sup>3</sup>, Henning Zettergreen<sup>4</sup>, Mark Stockett<sup>4</sup>, Laura Carlini<sup>1</sup>, Sergio Diaz-Tendero<sup>2,5,6</sup>, Lorenzo Avaldi<sup>1</sup>

<sup>1</sup>CNR - Istituto di Struttura della Materia (CNR - ISM), Area della Ricerca di Roma 1, Monterotondo Scalo, Italy

<sup>2</sup>Departamento de Química, Módulo 13, Universidad Autónoma de Madrid, 28049 Madrid (Spain)

<sup>3</sup>Elettra, Sincrotrone Trieste S.C.p.A., Trieste, Italy

<sup>4</sup>Stockholm University, Stockholm, Sweden

<sup>4</sup>Condensed Matter Physics Center (IFIMAC), Universidad Autónoma de Madrid, 28049 Madrid (Spain)

<sup>5</sup>Institute for Advanced Research in Chemical Science (IAdChem), Universidad Autónoma de Madrid, 28049 Madrid (Spain).

**Synopsis** The photoionization and photofragmentation of three *cyclo*-dipeptides (c-Alanine-Alanine, c-Glycine-Alanine and c-Glycine-Glycine) have been studied by combining experiments and simulations.

In the early fifties<sup>1</sup> it was proven that organic compounds can be synthesized in abiotic processes from simple inorganic precursors. These findings explained the observation of the large variety of organic matter in meteorites and carbonaceous chondrites. Since then, many experiments and theoretical models have been devoted to understand the chemical evolution of biologically relevant compounds in astronomical objects and primitive Earth.

In this study experimental results and theoretical simulations/modelling have been combined to investigate the VUV ionization of three cyclo-dipeptides (c-Alanine-Alanine, c-Glycine-Alanine and c-Glycine-Glycine), and it has been theoretically proposed how these molecules have the potential to trigger diverse reactive mechanisms<sup>2,3</sup>.

In the experiments both the photoemission spectra and the electron-ion coincidence measurements were performed at the CIPO beamline of the Elettra synchrotron radiation facility, using a monochromatic photon beam of 60 eV.

Photoelectron spectra were estimated calculating ionisation potentials with the equation of motion coupled cluster method and the electron propagation theory within the OVGf propagator. A combination of molecular dynamics simulation and exploration of the potential energy surfaces have been used for the study of the fragmentation.

The molecular dynamics simulations have shown a large variety of sequential fragmentation mechanisms, initiated by the ring opening followed by the release of neutral CO or HNCO fragments. The studied dipeptides evolve under ionizing radiation generating different small aziridin moieties and ox-

azolidinones. According to the theoretical simulations, these two species may be key ingredients to produce peptide chains. The corresponding mechanisms have been computed and show that the reaction requires very low energy and may occur in environments with ionizing radiation of less than 14 eV. In particular, we found that the degradation of c-Alanine-Alanine after photoionization drives two relevant processes: (i) the reconstruction of the dipeptide itself through reactions between some of its decomposition products and (ii) the formation and elongation of a linear peptide, via isomerisation of the molecular parent ion into oxazolidinones structures.

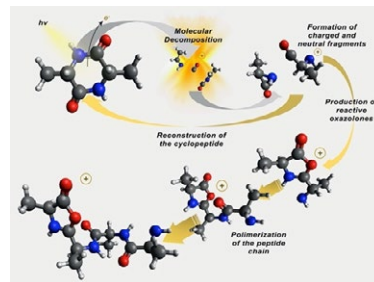


**Figure 1.** VUV radiolysis of cyclo-dipeptides results in a molecular decomposition with fragments that might lead to polymerization in peptide chains.

### References

- [1] S. L. Miller, 1953 *Science* **117** 528
- [2] D. Barreiro-Lage et al. 2021 *J. Chem.Phys. Lett.* **12** 7379
- [3] J. Chiarinelli et al. 2022 *Phys.Chem. Chem.Phys.* **24** 5855

\* E-mail: [paola.bolognesi@cnr.it](mailto:paola.bolognesi@cnr.it)

## Strong evidence for neighbor-induced recapture obtained by electron-photon-coincidence spectroscopy

N Kiefer<sup>1,\*</sup>, C Honisch<sup>1</sup>, C Küstner-Wetekam<sup>1</sup>, L Marder<sup>1</sup>, N Golchert<sup>1</sup>,  
A Ehresmann<sup>1</sup> and A Hans<sup>1</sup>

<sup>1</sup>Institute of Physics and CINSaT, University of Kassel, Kassel, 34132, Germany

**Synopsis** Spectroscopy on Auger electrons is a commonly used technique to investigate the decay of core-excited states in atoms and molecules. Atoms in a weakly-bound environment like van der Waals clusters can change their decay characteristics drastically, so that additional decay channels or scattering processes are enabled. Here, we report strong evidence to confirm that the neighbor induced recapture mechanism is present in argon clusters after  $2p$  ionization, by electron-photon-coincidence spectroscopy.

Irradiation of matter with soft X-rays can lead to highly excited core-hole states, which typically decay via autoionization processes like the well-known Auger decay.

The Auger decay most likely results in the complete transfer of the stored energy to a single emitted electron. In addition to the single Auger decay channel, decay cascades with emission of multiple electrons or radiative decays of excited Auger final states, are possible.

In weakly bound environments like van der Waals clusters, the Auger energies shift significantly due to polarization screening of the final states. Among others, competing processes to the local Auger or charge redistribution from Auger final states like radiative charge transfer (RCT) are enabled [1,2].

Lundwall et al. found evidence on a Bremsstrahlung-like process of photoelectrons with low kinetic energy caused by scattering with neighboring atoms resulting in a recapture of the initial photoelectron into a Rydberg state and subsequent Auger decay [3]. The process was described as neighbor-induced recapture (NIR) and appears to be a process of high probability in dense matter and photoelectrons with low kinetic energy.

In the present study we applied electron-photon-coincidence spectroscopy to observe the Bremsstrahlung-like photon in coincidence with the characteristic Auger electrons emitted after the recapturing process following  $2p$  photoionization in argon clusters.

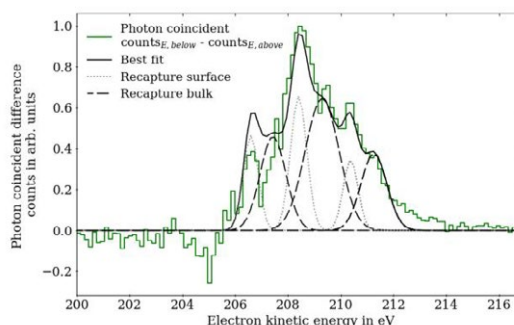


**Figure 1.** Signal assigned to NIR obtained as the difference (green line) in photon-coincident electron spectra at two exciting photon energies: 258 eV (within detector sensitivity) and 280 eV (above detector sensitivity). Dashed and dotted curves represent fitted individual states from surface and bulk according to Ref. [3].

The energy of the Bremsstrahlung-like photon disperses with the initial photoelectron kinetic energy. By altering the exciting-photon energy, the Bremsstrahlung-like photon was set to be either within the sensitivity range of the used photon detector (2-10 eV) or above. In Figure 1 we obtained the contribution assigned to NIR by the difference of photon-coincident electron spectra at two different exciting-photon energies.

### References

- [1] Hans A, Stumpf V, Holzapfel X, et al. 2018 *New J. Phys.* **20** 012001
- [2] Hans A, Küstner-Wetekam C, Schmidt P, et al. 2020 *Phys. Rev. Research.* **2** 012022
- [3] Lundwall M, Lindblad A, Öhrwall G, et al. 2008 *Phys. Rev. A* **78** 065201

\* E-mail: [nils.kiefer@uni-kassel.de](mailto:nils.kiefer@uni-kassel.de)

## Probing conical intersection dynamics in the dissociative photoionization of formaldehyde at FLASH

D V. Chicharro<sup>1</sup>, W Zhang<sup>1</sup>, H Lindenblatt<sup>1</sup>, F Trost<sup>1</sup>, P Recio<sup>2</sup>, A Zanchet<sup>3</sup>, R Y. Bello<sup>4</sup>, J G Vázquez<sup>4</sup>, U Fruehling<sup>5</sup>, M Braune<sup>5</sup>, S M Poullain<sup>2</sup>, L Bañares<sup>2</sup>, T Pfeifer<sup>1</sup>, R Moshhammer<sup>1</sup>

<sup>1</sup>Max-Planck-Institute für Kernphysik, Heidelberg, Germany; <sup>2</sup>Departamento de Química Física, Facultad de Ciencias Químicas, Universidad Complutense de Madrid, Madrid, Spain; <sup>3</sup>Instituto de Física Fundamental, Consejo Superior de Investigaciones Científicas, Madrid, Spain; <sup>4</sup>Departamento de Química, Universidad Autónoma de Madrid, Madrid, Spain; <sup>5</sup>Deutsches Elektronen-Synchrotron (DESY), Hamburg, Germany

**Synopsis** Pump-probe experiments have been performed to understand the role a conical intersection is playing on the dissociative photoionization of formaldehyde.

Conical intersections (CI) between electronic states often govern the photochemistry of molecules and radicals. Their role and characteristics have been largely studied before both theoretically and experimentally [1]. It has been proven that CI are crucial in different photochemical reactions such as electrocyclic ring-opening or cis-trans photoisomerization reactions [2,3] and more recently it has been observed how a CI can mediate producing a fast site-specific H-atom elimination in the photodissociation of ethyl radical [4].

Formaldehyde photoionization and photo-fragmentation has attracted considerable interest due to its role as a precursor of other organic and astrobiological molecules [5]. Its neutral fragmentation has been widely studied. However, the photoionization and dissociative photoionization have been less studied. Recently, theoretical calculations and experimental results suggest the presence of a conical intersection controlling the DPI mechanism between the  $X^2A'$  and  $B^2A'$  states. (see Figure 1) [6].

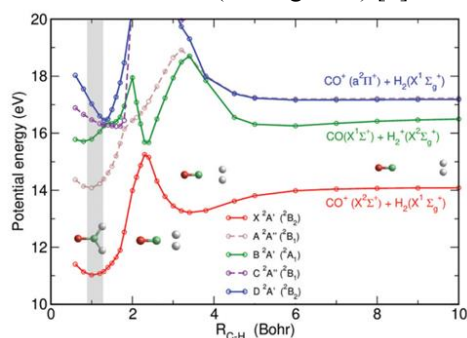


**Figure 1.** Potential energy curves of  $H_2CO$  leading to  $(H_2 + CO)^+$  as a function of  $R_{C-H_2}$ , from ref. 6.

\* E-mail: [david.chicharro@mpi-hd.mpg.de](mailto:david.chicharro@mpi-hd.mpg.de)

In order to understand if the DPI is controlled by a conical intersection, pump-probe schemes along with a reaction microscope have been used. The 3D-ion-electron momentum coincidence measurements, in combination with theoretical calculations will provide enough information to understand the underlying physics of this process.

### References

- [1] Domcke W, Yarkony DR, Köppel H. Conical Intersections: Theory, Computation and Experiment. vol. 17. WORLD SCIENTIFIC; 2011. <https://doi.org/10.1142/7803>.
- [2] Polli D, Altoè P, Weingart O, Spillane KM, Manzoni C, Brida D, et al. Conical intersection dynamics of the primary photoisomerization event in vision. *Nature* 2010;467:440–3. <https://doi.org/10.1038/nature09346>.
- [3] Levine B, Martinez T. Isomerization Through Conical Intersections. *Annu Rev Phys Chem* 2007;58:613–34. <https://doi.org/10.1146/annurev.physchem.57.032905.104612>.
- [4] Chicharro DV, Poullain SM, Zanchet A, Bouallagui A, García-Vela A, Senent ML, et al. Site-specific hydrogen-atom elimination in photoexcited ethyl radical. *Chem Sci* 2019;10:6494–502. <https://doi.org/10.1039/C9SC02140J>.
- [5] Blair SK, Magnani L, Brand J, Wouterloot JGA. Formaldehyde in the Far Outer Galaxy: Constraining the Outer Boundary of the Galactic Habitable Zone. *Astrobiology* 2008;8:59–73. <https://doi.org/10.1089/ast.2007.0171>.
- [6] Zanchet A, García GA, Nahon L, Bañares L, Marggi Poullain S. Signature of a conical intersection in the dissociative photoionization of formaldehyde. *Phys Chem Chem Phys* 2020;22:12886–93. <https://doi.org/10.1039/D0CP01267J>.

## Investigating the UV-Induced Dynamics of Methylated Cyclopentadiene with XUV Photoelectron Spectroscopy at FLASH

Zane Phelps<sup>1\*</sup>, Lisa Huang<sup>2</sup>, Tristan Fehl<sup>1</sup>, Dennis Meyer<sup>3</sup>, Fabiano Lever<sup>3</sup>, Stefan Duesterer<sup>3</sup>, Artem Rudenko<sup>1</sup>, Martin Centurion<sup>4</sup>, Adam Kirrander<sup>5</sup>, Peter M. Weber<sup>2</sup>, Markus Guehr<sup>3</sup>, Daniel Rolles<sup>1,5</sup>

<sup>1</sup>J.R. Macdonald Laboratory, Kansas State University, Manhattan, KS, USA

<sup>2</sup>Brown University, Providence, RI, USA

<sup>3</sup>Deutsches Elektronen Synchrotron DESY, Hamburg, Germany

<sup>4</sup>University of Nebraska, Lincoln, NE, USA

<sup>5</sup>Oxford University, Oxford, UK

<sup>6</sup>on behalf of the FLASH 11013355 collaboration

**Synopsis** We have applied time-resolved photoelectron spectroscopy (TRPES) using two UV-pump wavelengths (266 nm and 252 nm) along with a 30-eV XUV probe to study the ultrafast dynamics and possible ring conversion of methylated cyclopentadiene (CPD). Using an XUV pulse as the probe provides access to the molecular dynamics beyond the Frank-Condon region. Our preliminary analysis shows different de-excitation time-scales for tetramethyl-CPD and pentamethyl-CPD as well as a dependence on the excitation wavelength.

The motivation for this work is to understand the creation of highly strained three- and four-member rings from cyclopentadiene (CPD) and its methylated derivatives after UV excitation [1,4]. Previous time-resolved photoelectron spectroscopy (TRPES) experiments conducted on methylated cyclopentadienes, were limited to the dynamics in the Frank-Condon region due to the photon energy their UV probe pulses [2,3]. The 30-eV XUV probe photon energy used is energetically sufficient to ionize both the electronically excited states and the ground state (see schematic in Fig. 1).

The experiment was performed at the FLASH free-electron laser at DESY in Hamburg, Germany operated with 80 pulses per 10-Hz pulse train (i.e., 800 XUV pulses per second). 1,2,3,4,5-pentamethyl-cyclopentadiene (PMCPD) and 1,2,3,4-tetramethyl-1,3-cyclopentadiene (TMCPD) were excited at both 266nm (4.66 eV) and 252nm (4.92 eV) to investigate a possible dependence of the dynamics on the energy above the excited-state minimum.

We expect an excitation-wavelength dependence to arise in the delay moving from the 1B<sub>2</sub> to the 2A<sub>1</sub> state. Indeed, our preliminary results suggest that the higher excitation photon energy (4.92 eV) leads to a faster decay of the excited-state population in both PMCPD and TMCPD. We also observe slightly different deexcitation timescales for PMCPD and TMCPD.

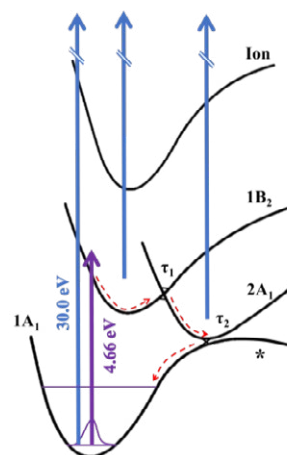


**Figure 1.** Time-resolved excitation and ionization scheme of cyclopentadienes. The 4.66 eV (266nm) pump pulse excites to the 1B<sub>2</sub> state. The ionization is achieved with a 30 eV XUV probe pulse. The conical intersections between the 1B<sub>2</sub> and the 2A<sub>1</sub> states is reached after a time delay  $\tau_1$ . The suggested dominant pathway back to the electronic ground state is via another conical intersection with an associated time constant  $\tau_2$ . Another pathway may lead to the creation of a highly strained metastable intermediate structure (\*), which was observed for CP but not (yet) for the methylated species.

### References

- [1] Fuß W et al. 2005 *Chem. Phys.* 316, 255-234
- [2] Rudakov F and Weber P 2010 *J. Phys. Chem. A.* 144, 4501-4506
- [3] Stollow A et al. 2010 *J. Phys. Chem. A.* 144, 4058-4064
- [4] Kuhlman T S et al. 2012 *Faraday Discuss.* 157, 193-212

\* E-mail: [zdphelps@phys.ksu.edu](mailto:zdphelps@phys.ksu.edu)



## Electron-rotation coupling in diatomics by intense UV pulses

Y R Liu<sup>1</sup>, V Kimberg<sup>2</sup>, Y Wu<sup>3,4</sup>, J G Wang<sup>3</sup>, O Vendrell<sup>5</sup> and S B Zhang<sup>1\*</sup>

<sup>1</sup>School of Physics and Information Technology, Shaanxi Normal University, Xi'an 710119, China

<sup>2</sup>Department of Chemistry, KTH Royal Institute of Technology, 10691 Stockholm, Sweden

<sup>3</sup>Institute of Applied Physics and Computational Mathematics, Beijing 100088, China

<sup>4</sup>Center for Applied Physics and Technology, Peking University, Beijing 100084, China

<sup>5</sup>Theoretical Chemistry, Institute of Physical Chemistry, Heidelberg University, 69120 Heidelberg, Germany

**Synopsis** The electronic angular momentum projected onto the diatomic axis, naturally couples with the angular momentum of the nuclei rotations. Such an electron-rotation coupling is safely neglected in weak-field regime, and rightly not included in the conventional model for pulse-molecule interactions. Our recent theoretical investigations improved the conventional pulse-molecule interaction model by including the electron-rotation coupling in the Hamiltonian, and revealed that such a coupling significantly affects the rotational motion of the system under electronic excitations by intense lasers. The importance of the electron-rotation coupling effect is presented through collecting the photodissociation dynamics as kinetic energy release spectra and angular distribution of photofragment. These theoretical results advance our in-depth understanding of intense pulse molecule interactions.

For diatomics, when the projection of the total electronic angular momentum onto molecular axis  $\Omega$  is not zero, the former is naturally coupled to the angular momentum of the rotation of the nuclear axis  $\mathbf{R}$ . This  $\mathbf{R}-\Omega$  coupling can be safely neglected in the weak-field regime owing to the large mass difference between the rotating nucleus and electrons and the small amount of angular momentum change experienced by the electrons.

However, under strong field excitation, the repeated Rabi cycling of the electronic transitions can affect the molecular rotational degrees of freedom, so that the  $\mathbf{R}-\Omega$  coupling must be taken into account for observables related directly to the rotational dynamics, such as molecular alignment and angular distribution of photofragments [1, 2]. We show that stronger probe pulse intensity and larger degrees of alignment increase the influence of the  $\mathbf{R}-\Omega$  coupling [3].

A UV pump-probe scheme is proposed to study the electron-rotation coupling effects, simulations of the rovibrational dynamics unravel clear fingerprints of the electron-rotation coupling effects that can be observed experimentally [4]. These theoretical results advance our in-depth understanding of intense pulse molecule interactions.

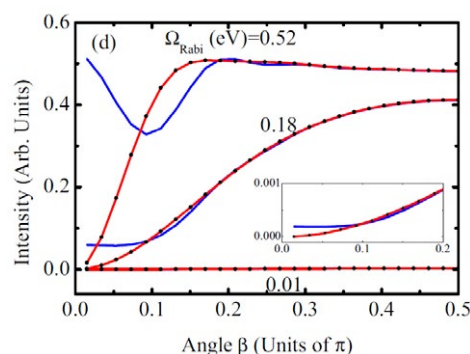


**Figure 1.** The angular distribution of photofragments of  ${}^1\Pi$  dissociative state excited from initial state  ${}^1\Sigma$ , by including (red-dot lines) and not including (blue lines) electron-rotation coupling by different intense pulses.

### References

- [1] Liu Y R, Wu Y, Wang J G, Vendrell O, Kimberg V and Zhang S B 2020 *Phys. Rev. A* **102** 033114
- [2] Liu Y R, Wu Y, Wang J G, Vendrell O, Kimberg V and Zhang S B 2020 *Phys. Rev. Res.* **2** 043348
- [3] Liu Y R, Kimberg V, Wu Y, Wang J G, Vendrell O and Zhang S B 2022 *Phys. Rev. Res.* **4** 013066
- [4] Liu Y R, Kimberg V, Wu Y, Wang J G, Vendrell O and Zhang S B 2021 *J. Phys. Chem. Lett.* **12** 5534

\*E-mail: [song-bin.zhang@snnu.edu.cn](mailto:song-bin.zhang@snnu.edu.cn)



## Initial-site characterization of hydrogen migration in ethanol

Travis Severt<sup>1</sup>, Eleanor Weckwerth<sup>2</sup>, B Kaderiya<sup>1</sup>, P Feizollah<sup>1</sup>, B Jochim<sup>1</sup>, K Borne<sup>1</sup>, F Ziaee<sup>1</sup>, Kanaka Raju P<sup>1</sup>, K D Carnes<sup>1</sup>, M Dantus<sup>3</sup>, D Rolles<sup>1</sup>, A Rudenko<sup>1</sup>, E Wells<sup>2\*</sup>, and I Ben-Itzhak<sup>1†</sup>

<sup>1</sup>J. R. Macdonald Laboratory, Physics Department, Kansas State University, Manhattan, Kansas 66506, USA

<sup>2</sup>Department of Physics, Augustana University, Sioux Falls, South Dakota 57108, USA

<sup>3</sup>Department of Chemistry, Michigan State University, East Lansing, Michigan 48824, USA

**Synopsis** We quantify the hydrogen migration contribution from each initial molecular site to the formation of hydrogen-rich fragments by using ion coincidence momentum-imaging measurements of a few deuterium-tagged isotopologues of ethanol. The resulting site-specific probabilities for the ion composition provide an important new benchmark for molecular dynamics calculations.

Hydrogen migration within polyatomic molecules has been studied in recent experiments and molecular dynamics calculations, e.g., [1, 2]. The objective of this work is to determine the likelihood of migration from each initial hydrogen site in ethanol. We present a method to experimentally distinguish the initial sites using several deuterium-tagged isotopologues, and we employ this method to determine comprehensive probabilities for the initial-site composition of hydrogen-rich photofragments of ethanol dications.

Ethanol,  $\text{CH}_3\text{CH}_2\text{OH}$ , has three non-equivalent hydrogen sites: the hydrogen in the hydroxyl group, the two  $\alpha$ -hydrogens attached to the central carbon, and the three  $\beta$ -hydrogens in the methyl group (depicted in the inset of Fig. 1). Ion coincidence momentum-imaging (COLTRIMS) measurements were conducted on seven isotopologues of ethanol, with the laser parameters monitored to ensure that conditions remained the same throughout the measurements. The yield in each breakup channel is used to define a fragmentation branching ratio, leading to an overdetermined system of equations relating each branching ratio to all possible initial-site combinations. A least-squares fitting procedure optimizes the site-specific probabilities to the measured data. In this manner, we measure the site-specific probabilities for two-body breakup of ethanol forming  $\text{H}_3^+$  (shown in Fig. 1),  $\text{H}_3\text{O}^+$ ,  $\text{H}_2\text{O}^+$ , and  $\text{CH}_4^+$ , as well as few-body breakup channels producing an  $\text{H}_3^+$  ion and one or two neutral hydrogen atoms.

\*E-mail: [eric.wells@augie.edu](mailto:eric.wells@augie.edu)

†E-mail: [ibi@phys.ksu.edu](mailto:ibi@phys.ksu.edu)

These measured site-specific probabilities provide benchmarks for calculations and answer outstanding questions about photofragmentation of ethanol dications, including establishing that the roaming  $\text{H}_\alpha\text{H}_\alpha$  moiety is 15 times more likely to abstract the hydroxyl proton than a methyl-group proton to form  $\text{H}_3^+$ , and indicating that hydrogen scrambling is important in  $\text{H}_2\text{O}^+$  formation. This technique extends to dynamical variables, demonstrated by the determination of the site-specific KER distribution of the  $\text{H}_3^+ + \text{C}_2\text{H}_3\text{O}^+$  channel. The extension to larger molecules is straightforward provided suitable isotopologues can be obtained.

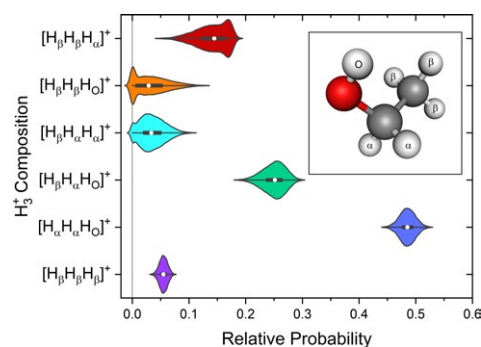


**Figure 1.** Relative probabilities for the two-body,  $\text{H}_3^+ + \text{C}_2\text{H}_3\text{O}^+$ , fragmentation channel. Inset: the ethanol molecule with labelled hydrogen sites.

### References

- [1] Ekanayake N *et al.* 2018 *Nat. Commun.* **9**, 5186
- [2] Kling N G *et al.* 2019 *Nat. Commun.* **10**, 2813

## Competition of photon and electron emission in the decay of doubly ionized ArKr clusters

L Marder<sup>1\*</sup>, C Küstner-Wetekam<sup>1</sup>, D Bloß<sup>1</sup>, N Kiefer<sup>1</sup>, A Ehresmann<sup>1</sup> and A Hans<sup>1</sup>

<sup>1</sup>Institute of Physics and CINSaT, University of Kassel, Kassel, 34132, Germany

**Synopsis** Non-local decay pathways are of high interest to gain a deeper understanding of relaxation mechanics in dense media. Results from multi-coincidence measurements on pure argon and heterogeneous argon-krypton clusters are presented, where we show the quenching of radiative decay from  $\text{Ar}^{2+}$  states. Since the typical decay path of such states, electron-transfer mediated decay (3), or ETMD(3), is energetically closed, we propose the existence of ETMD(4), an ionizing decay process involving four sites.

With the theoretical proposal and subsequent experimental verification of non-local decay mechanisms like the interatomic coulombic decay (ICD), significant progress has been made within the recent years towards an understanding of the role of an environment in possible relaxation pathways (see [1] and references therein). ICD and related phenomena have been discussed as possible causes for radiation damage in cells as they lead to the emission of slow electrons, which – unlike faster Auger electrons – are more likely to be mutagenic. Since the first validation of their occurrence, numerous additional more or less related processes have been discussed and successfully measured, one of them being the electron-transfer mediated decay (ETMD). In this process, an electron is transferred from a neutral site to an ionized neighbour, filling the vacancy. The difference in energy is then used to emit an electron either from the first site or a third one, where the process is then called ETMD(2) or ETMD(3), respectively, named after the number of participating sites.

We propose the existence of a further process of this family with the participation of a fourth site, hence named ETMD(4). In ETMD(4), two neutral sites simultaneously transfer an electron to a neighbouring site with two vacancies leading

to the emission of an electron at the fourth site (cf. Fig. 1).

Van-der-Waals bound rare-gas clusters represent prototype systems well-suited for the investigation of fundamental interatomic and intermolecular processes. We present our state-of-the-art experiment [2] on pure argon and heterogeneous argon-krypton clusters where both electrons and photons were detected in coincidence, which allows for investigation of multi-particle decay pathways after ionization with synchrotron radiation. The results indicate that the addition of krypton to initially pure argon clusters partially quenches radiative decay by the opening of the faster ionizing ETMD(4) relaxation pathway.

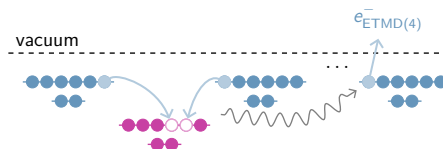


**Figure 1.** The ETMD(4) process in heterogeneous clusters with two different rare-gas species.

### References

- [1] Jahnke T *et al.* 2020 *Chem. Rev.* **120**, 20, 11295
- [2] Hans A *et al.* 2019 *Rev. Sci. Instrum.* **90** 093104

\*E-mail: [lutz.marder@uni-kassel.de](mailto:lutz.marder@uni-kassel.de)

## Isotope labelling as a tool for atto-chemistry

M Vacher<sup>1</sup>\*, A Boyer<sup>2</sup>, V Lorient<sup>2</sup>, F Lépine<sup>2</sup> and S Nandi<sup>2</sup>†

<sup>1</sup>Nantes Université, CNRS, CEISAM UMR 6230, F-44300 Nantes, France

<sup>2</sup>Univ de Lyon, Univ Claude Bernard Lyon 1, CNRS, Institut Lumière Matière, F-69622 Villeurbanne, France

**Synopsis** Following ionization by an ultrashort (attosecond to few-femtosecond), extreme ultraviolet (XUV) pulse, a molecule is often promoted to several highly excited cationic states. The subsequent relaxation process is quite complex, involving various nuclear and electronic degrees of freedom. Here, we show that isotopic substitution can be an efficient tool to disentangle the various relaxation pathways. We have tested the method for ethylene that lead to the identification of the most relevant nuclear co-ordinate and the electronic state responsible for nuclear as well as non-adiabatic dynamics in the XUV-ionized species.

The experimental realization of high-order harmonic generation (HHG) based sources, producing coherent photons in the extreme ultraviolet (XUV;  $h\nu = 10 - 120$  eV) domain, has enabled to simultaneously ionize and excite several cationic states in a complex molecule, leading to the development of atto-chemistry [1, 2]. There, probing the out-of-equilibrium electron and nuclear dynamics in molecules induced by attosecond to few-femtosecond XUV pulses are of great interests. However, following ionization by a broadband XUV pulse, several cationic states in the molecule can be excited, making the subsequent relaxation dynamics difficult to probe using traditional spectroscopic tools. Here, we show that by comparing the experimental isotope effects in the two isotopologues of a molecule with that from theoretical calculations, one can identify the most relevant nuclear co-ordinate and the electronic state that governs the XUV-induced relaxation processes.

We have used photons from an XUV attosecond pulse train (APT) produced via HHG in Krypton atoms, to ionize and excite the ethylene ( $C_2H_4$ ) molecule and its deuterated counterpart ( $C_2D_4$ ), wherein the subsequent relaxation dynamics were probed using a near-infrared (NIR) pulse. The resulting ionic fragments were collected as a function of the pump-probe delay using a velocity map imaging spectrometer.

We have found that the relaxation timescales in  $C_2H_4$  can be 40% faster compared to  $C_2D_4$ , which are supported by advanced non-adiabatic dynamics calculations. As shown in Fig. 1(a), the time-scales extracted from the two-color signal associated with  $H^+$  and  $D^+$  fragments dif-

fer from each other by  $7 \pm 2$  fs. It matches quantitatively with the theoretical isotope effect observed in case of C-H and C-D dissociation timescales for the cationic state  $Ex_2$  ( $B^2A_g$ ) (see Fig. 1(b)), allowing us to identify the electronic state ( $Ex_2$ ) along with the nuclear co-ordinate (C-H bond-length) responsible for the relaxation process. For other cationic states, the agreement between theory and experiment is only qualitative (Fig. 1(c)-(d)). Our results highlight the relevance of isotope substitution in few-femtosecond dynamics in polyatomic molecules [3].

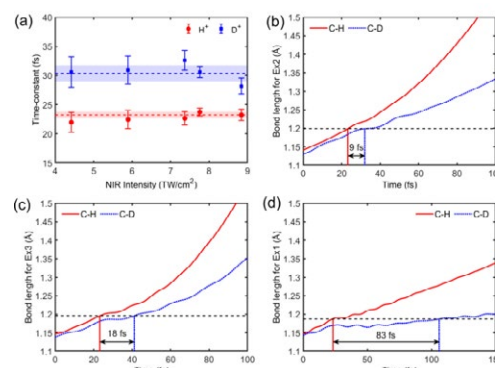


**Figure 1.** (a) Experimental and (b)-(d) theoretical isotope effects in  $C_2H_4$  and  $C_2D_4$ , following ionization by XUV attosecond pulse trains (reproduced from [3]).

### References

- [1] Nisoli M et al. 2017 *Chem. Rev.* **117** 10760
- [2] Merritt I C D et al. 2021 *J. Phys. Chem. Lett.* **12** 8404
- [3] Vacher M et al. 2022 *J. Phys. Chem. A* **126** 5692

\* E-mail: [morgane.vacher@univ-nantes.fr](mailto:morgane.vacher@univ-nantes.fr)

† E-mail: [saikat.nandi@univ-lyon1.fr](mailto:saikat.nandi@univ-lyon1.fr)

## Time-resolved imaging of an elusive molecular reaction: hydrogen roaming in acetonitrile

A C LaForge<sup>1\*</sup>, D Mishra<sup>1\*</sup>, L G Gorman<sup>1</sup>, S Díaz-Tendero<sup>2</sup>, F Martín<sup>2</sup> and N Berrah<sup>1</sup>

<sup>1</sup>Department of Physics, University of Connecticut, Storrs, Connecticut, 06269, USA

<sup>2</sup>Departamento de Química, Modulo 13, Universidad Autonoma de Madrid, Madrid, 28049, Spain

**Synopsis** Molecular dissociation triggered by photoabsorption is a fundamental process, which typically follows well-understood trajectories. In some cases, the dissociating fragment can remain weakly-bound and "roam" around the remaining molecule, which can lead to secondary interactions and even the formation of new molecules. The random nature of this type of roaming reaction makes it extremely difficult to capture the underlying dynamics. We present a time-resolved method to image roaming neutral fragments using coincident Coulomb explosion imaging combined with state-of-the-art theoretical simulations.

Roaming reactions have garnered significant interest in recent years since they defy the conventional reactions that follow minimum energy pathways. Instead, such reactions involve flat regions of the potential energy surface where molecular fragments remain weakly bound and participate in long-range interactions mediated by relatively weak forces. Furthermore, due to the neutral character of the roaming fragments, they follow a rather indeterminate trajectory, thus complicating their identification and systematic study.

Here, we will present a time-resolved study of the formation of  $D_3^+$  ions from the roaming of  $D_2$  neutrals in deuterated acetonitrile [1]. Using intense, femtosecond IR radiation combined with coincident Coulomb explosion imaging, we can directly reconstruct the momentum of the roaming  $D_2$ , thereby gaining an unambiguous, experimental signature of roaming as well as a kinematically complete picture of the underlying molecular dynamics. With the aid of quantum chemistry calculations, we can fully determine how this unique dissociative process occurs. To demonstrate our work, Fig. 1 shows the Newton diagram for the channel  $D^+ + D_2$  neutral +  $C_2N^+$ , where the momentum vector of  $C_2N^+$  is fixed along the x-axis, while those of  $D^+$  and the reconstructed  $D_2$  are plotted on the top and bottom halves, respectively. In comparison to the ionic fragments, the momentum of the neutral  $D_2$  appears quite different having a broad distribution with no clear angular dependence. This demonstrates the elusive nature of the neutral roamer, which makes tracking this process dif-

ficult. In general, our novel technique gives us a more straightforward means to observe 'invisible' neutral fragments which can allow us to gain a better understanding of the underlying molecular dynamics in roaming reactions.

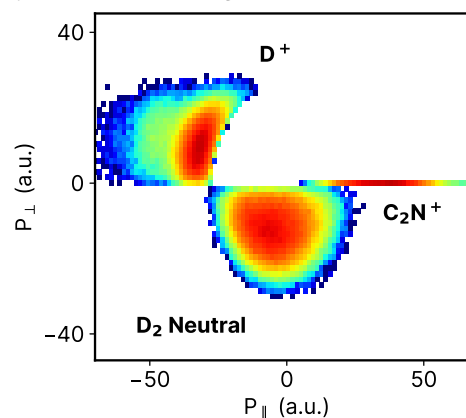


**Figure 1.** Newton diagram for the channel  $D^+ + D_2$  neutral +  $C_2N^+$  integrated over the first 200 fs of pump-probe delay. The momentum vector of  $C_2N^+$  lies along the x-axis while those of  $D^+$  and  $D_2$  neutral are plotted in the top and bottom halves, respectively.

The experimental work was funded by the National Science Foundation under award No. 1700551. The theory was supported by the MICINN (Spanish Ministry of Science and Innovation) projects PID2019-105458RB-I00 and PID2019-110091GB-I00.

### References

- [1] LaForge *et al.* 2023 *submitted to PNAS*  
<https://doi.org/10.48550/arXiv.2112.08508>

## Valence photo double ionization of CH<sub>3</sub>OD: Insights into Molecular Dynamics and Electron Correlation

S. Kumar<sup>1\*</sup>, M. Shaikh<sup>1</sup>, W. Iskandar<sup>1</sup>, R. Thurston<sup>1</sup>, M. A. Fareed<sup>1</sup>, D. Call<sup>2</sup>, R. Enoki<sup>2</sup>, C. Bagdia<sup>3</sup>, N. Iwamoto<sup>3</sup>, T. Severt<sup>3</sup>, J. B. Williams<sup>2</sup>, I. Ben-Itzhak<sup>3</sup>, D. S. Slaughter<sup>1</sup>, and Th. Weber<sup>1</sup>

<sup>1</sup>Chemical Sciences Division, Lawrence Berkeley National Laboratory, Berkeley, CA-94720, USA

<sup>2</sup>Department of Physics, University of Nevada, Reno, NV-89557, USA

<sup>3</sup>J. R. Macdonald Laboratory, Department of Physics, Kansas State University, Manhattan, KS-66506, USA

**Synopsis** The valence photo double ionization (vPDI) of CH<sub>3</sub>OD with one VUV photon provides valuable insights into the ionization mechanisms that remove two electrons and lead to a variety of 2- and 3-body dissociation channels of the molecular dication. Applying reaction microscopy, dissociation dynamics involving hydrogen migration is investigated.

Deuterated methanol (CH<sub>3</sub>OD) is a simple hydrocarbon molecule containing the methyl functional group, which is known for ultrafast dynamics such as, e.g., rapid proton migration and hydrogen elimination as well as CH<sub>3</sub> umbrella excitation. Methanol is also the simplest alcohol, and it, therefore, has fundamental importance in understanding solvation and the reactivity of the hydroxyl functional group. The vPDI of CH<sub>3</sub>OD with one 54 eV XUV photon ejects two electrons and can create an unstable dication, leading to a multitude of 2- and 3-body dissociation channels.

We conducted kinematically complete measurements at the Advanced Light Source synchrotron ring applying reaction microscopy, a.k.a. “COLTRIMS”, imaging the 3D-momenta of two electrons and two recoiling ions in coincidence; for 3-body breakup producing an additional single neutral fragment, the 3D-momentum of the latter was deduced from momentum conservation. While the 3-body reaction channels are dominated by direct vPDI, we observe remarkable contributions from autoionization, which is even stronger in some of the 2-body channels (e.g., see Fig. 1). Furthermore, electron-ion coincidence momentum imaging allows us to investigate the potential role of hydrogen migration in the 2-body dissociation channels producing H<sup>+</sup>, D<sup>+</sup>, HD<sup>+</sup>, and H<sub>2</sub>D<sup>+</sup>.

The 2-body dissociation channels are excellent candidates to track Rutherford scattering (of the outgoing electrons) in the angular distribution of the autoionizing electron, in the molecular

body-fixed frame of reference. Such diffraction patterns enabled us to estimate the internuclear distance when the autoionization took place with respect to the photoionization, and, hence, help to deduce the decay time [1].

We further investigate the coupled electronic and nuclear dynamics in intramolecular rearrangement. Detailed dynamics for 2- and 3-body reaction channels will be presented.

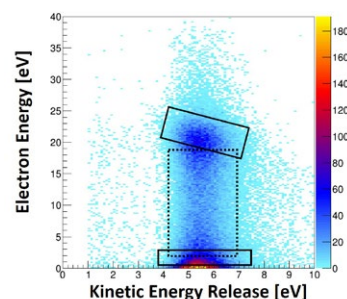


**Figure 1.** The photo double ionization yield (linear scale) of the CHO<sup>+</sup> and DH<sub>2</sub><sup>+</sup> channel as a function of electron energy and the kinetic energy release of the ionic fragments revealing contribution from autoionization (black boxes) and direct vPDI (dashed box).

**Acknowledgements:** This research is supported by Department of Energy under Contract No. DE-AC02-05CH11231 (LBNL) and No. DE-FG02-86ER13491 (KSU) as well as the National Sciences Foundation under Award No. NSF-1807017 and NSF-2208017 (UNR).

### References

- [1] Sann H. *et. al.*, 2011, *Phys. Rev. Lett.* **106** (13), 133001.

\*E-mail: [Skumar2@lbl.gov](mailto:Skumar2@lbl.gov)



## An ultrafast stopwatch to clock and manipulate molecular dynamics

S Pan and J Wu\*

State Key Laboratory of Precision Spectroscopy, East China Normal University, Shanghai, 200241, China

**Synopsis** Light-molecule interactions play a crucial role in photochemistry, at the heart of which is the breaking and formation of chemical bonds. Our ultrafast stopwatch scheme aims to clock the stretching of chemical bonds, explore fundamental physical mechanisms, and further manipulate light-induced molecular dynamics.

For molecules exposed in strong laser fields, valence electrons absorb photons and escape from the ionic potential, while the remaining cation interacts with the strong field and dissociates as nuclear fragments. In this respect, if we construct an ultrafast strong laser pulse characterized by time-dependent polarizations, the time information of ejected electrons and nuclear fragments can be recorded experimentally, and full-dimensional molecular dynamics are explored in principle.

In this presentation, we propose the scheme of an ultrafast stopwatch by constructing a polarization-skewed (PS) laser pulse and demonstrate its powerful applications in clocking and manipulating molecular dynamics in experiments. The PS laser pulses have unique characteristic of resolving ultrafast dynamics within neighboring optical cycles compared to linearly or circularly polarized ones.

First, we demonstrate a straightforward method on clocking the dissociative above-threshold double ionization of  $H_2$  [1], where two electrons and two protons are measured in coincidence. As illustrated in Fig. 1(a), the instants of the first and second ionization steps are encoded in the emission directions of two released electrons, forming an X-shaped momentum distribution. The time interval between the two ionization steps can be extracted from their crossing angle.

Second, we propose a universal approach to time the bond-stretching process during the strong-field dissociation of  $H_2$  from molecular-frame electron angular distributions [2]. The time-energy-resolved proton-electron coincidence measurements reveal the participation of high vibrational states beyond resonant one-photon or net-two-photon dissociation pathways [3].

Third, we discover the parallel and perpendicular multiphoton transitions in dissociative ionization of  $H_2$ . Our results demonstrate the ability of the waveform-shaped PS pulses to control reaction pathways through the manipulation of hybrid parallel and perpendicular transitions, as depicted in Fig. 1(b).

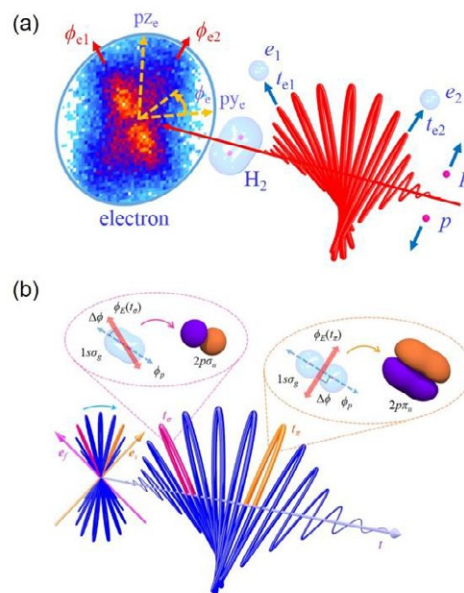


**Figure 1.** Schematic illustrations of the ultrafast stopwatch using a multicycle PS laser pulse to (a) clock the dissociative above-threshold double ionization and (b) manipulate parallel and perpendicular transitions and thus reaction pathways of  $H_2$  molecules.

### References

- [1] Pan S *et al* 2021 *Phys. Rev. Lett.* [126 063201](#)
- [2] Pan S *et al* 2022 *Ultrafast Sci.* [2022 9863548](#)
- [3] Ji Q *et al* 2019 *Phys. Rev. Lett.* [123 233202](#)
- [4] Pan S *et al* 2023 *Phys. Rev. Lett.* revised

\* E-mail: [jwu@phys.ecnu.edu.cn](mailto:jwu@phys.ecnu.edu.cn)



## Photoionization dynamics of cyano substituted PAHs in the Vacuum-Ultraviolet range

M Roy Chowdhury<sup>1\*</sup>, G A Garcia<sup>1</sup>, H Hrodmarsson<sup>2</sup>, J-C Loison<sup>3</sup> and L Nahon<sup>1†</sup>

<sup>1</sup>Synchrotron SOLEIL, L'Orme des Merisiers, Départementale 128, 91190 Saint Aubin, France

<sup>2</sup>Laboratory for Astrophysics, Leiden Observatory, Leiden University, NL-2300 RA Leiden, The Netherlands

<sup>3</sup>Université Bordeaux, CNRS, Bordeaux INP, ISM, UMR 5255, Talence F-33400, France

**Synopsis** Polycyclic aromatic hydrocarbons (PAHs) are strongly coupled to vacuum ultraviolet (VUV) radiation in the interstellar medium (ISM). The recent detection of the cyano substituted PAH in space with remarkably high abundance has escalated the need to perform laboratory investigations of these molecules interacting with VUV radiation along with shedding light on the photoelectric gas heating effect as PAHs play a dominant role to the gas heating of the ISM.

PAHs are a class of molecular species that have been postulated to be present abundantly in the ISM for a long time constituting a major source of carbon and playing critical roles in the physical and chemical conditions of astrophysical environments. The aromatic infrared emission bands (AIBs) in the 3-20  $\mu\text{m}$  range are the signatures of the existence of PAHs in the interstellar and circumstellar environments. The individual detection of PAHs is hindered by the absence of permanent electric dipole moments but recent searches focused on substituted PAHs have identified the presence of two cyanonaphthalene isomers [1]. The two nitrile group functionalized PAHs, i.e., 1- and 2-cyanonaphthalenes ( $\text{C}_{10}\text{H}_7\text{CN}$ ) might have been formed via barrierless reaction between the PAH and the CN radical with the release of a H atom, since CN is present ubiquitously in astrophysical media. In the interstellar and circumstellar media, PAHs are exposed to VUV radiation. The PAHs absorb the VUV radiation and relax via ionization and photodissociation processes in competition with radiative cooling (including IR emission). Ionization leads to gas heating [2] by thermalization of emitted electrons whereas photodissociation accounts for the chemical evolution of the PAHs giving rise to the production of small molecules and radicals.

In the present work, we study the VUV photodynamics of the two isomers of cyanonaphthalenes, especially in terms of photoionization and cation fragmentation processes. The exper-

imental investigations are carried out on the permanent molecular beam endstation SAPHIRS which is situated on one of the branches of the DESIRS undulator based VUV beamline at the SOLEIL Synchrotron facility, France. The molecular beam chamber is coupled to a double imaging photoelectron-photoion coincidence ( $i^2\text{PEPICO}$ ) spectrometer, DELICIOUS 3 [3]. We have obtained the high resolution threshold photoelectron spectrum (TPES) over an extended binding energy range which is further compared with *ab initio* calculations showing an overall good agreement between the predicted and observed bands. Outer valence Green's function calculations are used to assign the molecular orbitals observed in the TPES. Further, the cation state-selected fragmentation pattern over a wide photon energy range is obtained which when compared with the unsubstituted PAH unravels the effect of photostability of cyano-substituted PAHs. The present measurements can also be used to estimate the contribution of PAHs to the gas heating of the ISM since the experimentally obtained kinetic energy distributions of the photoelectrons as a function of photon energy can be employed to model the photoelectric heating for any incoming photon flux spectral distribution.

### References

- [1] McGuire B A *et. al.* 2021 *Science* **371** 1265
- [2] Berné O *et. al.* 2022 *A&A* **667** A159
- [3] Garcia G A *et. al.* 2013 *Rev. Sci. Inst.* **84** 053112

\* E-mail: [madhusree.roy-chowdhury@synchrotron-soleil.fr](mailto:madhusree.roy-chowdhury@synchrotron-soleil.fr)

† E-mail: [laurent.nahon@synchrotron-soleil.fr](mailto:laurent.nahon@synchrotron-soleil.fr)

## High Dose-Rate MeV Electron Beam from a Tightly-Focused Femtosecond IR Laser in Ambient Air: A Radiation Safety Issue

S Vallières<sup>1,2,\*</sup>, J Powell<sup>1</sup>, T Connell<sup>3</sup>, M Evans<sup>3</sup>, M Lytova<sup>1</sup>, S Fourmaux<sup>1</sup>, S Payeur<sup>1</sup>, P Lassonde<sup>1</sup>, F Fillion-Gourdeau<sup>1,4</sup>, S MacLean<sup>1,2,4</sup> and F Légaré<sup>1</sup>

<sup>1</sup>INRS-EMT, 1650 blvd. Lionel-Boulet, Varennes, QC, J3X 1P7, Canada

<sup>2</sup>Institute for Quantum Computing, 200 University Ave W., Waterloo, ON, N2L 3G1, Canada

<sup>3</sup>Medical Physics Unit, McGill University Health Center, 1001 blvd. Décarie, Montréal, QC, H4A 3J1, Canada

<sup>4</sup>Infinite Potential Laboratories, 485 Wes Graham Way, Waterloo, ON, N2L 0A7, Canada

**Synopsis** We present a straightforward method to generate MeV-ranged, high dose-rate (9 Gy/min) electrons in ambient air by tightly focusing a mJ-class femtosecond laser. We demonstrate that relativistic intensities are achievable in ambient air through intensity clamping suppression. Three-dimensional PIC simulations confirm the acceleration mechanism and match the measured electron energy. We discuss the scalability of this method with the continuing development of high average power mJ-class lasers. This technique also provides a promising approach for FLASH radiation therapy.

We report on the generation of a high dose-rate ionizing radiation source from the tight focusing in ambient air of a mJ-class femtosecond laser. Typically, focusing a femtosecond laser at ambient pressure will cause significant wavefront distortion due to nonlinear propagation effects. However, we have found that the combination of long wavelength, ultrashort pulse duration and extremely tight focusing minimizes the nonlinear effects and allows us to achieve relativistic intensities up to  $10^{19}$  W/cm<sup>2</sup> at atmospheric pressure. PIC simulations in 3D indicate we create a near-critical density plasma which provides a high conversion efficiency from the laser to the electrons.

The experiment [1] was performed at the ALLS laser facility (Varennes, Québec) which provided the 12 fs, 2.8 mJ, IR ( $\lambda_0 = 1.8 \mu\text{m}$ ) beamline running at 100 Hz. The focusing optic, shown on Figure 1, is a 1" on-axis parabola with NA  $\approx 1$ . Two types of radiation dose detectors were used with each measurement integrating over one minute at distances up to 6 m from the source.

Figure 1 shows the measured dose as a function of distance from the source, showing an inverse-square law behavior. The particle beam consists mostly of highly-directional ( $\approx 15^\circ$  divergence) electrons with energies up to 1 MeV, along with a more isotropic X-ray emission of photons in the tens to hundreds of keV. The measured dose rate, up to 9 Gy/min at 0.1 m away

\*E-mail: [simon.vallieres@inrs.ca](mailto:simon.vallieres@inrs.ca)

from the interaction zone, is nearly  $4\times$  higher than the typical dose rates used in conventional radiation therapy. For an exposed researcher positioned at 1 m from the source, the delivered dose exceeds the annual dose limit [2] in seconds to minutes and warrants the implementation of proper radiation protection following the ALARA principle.

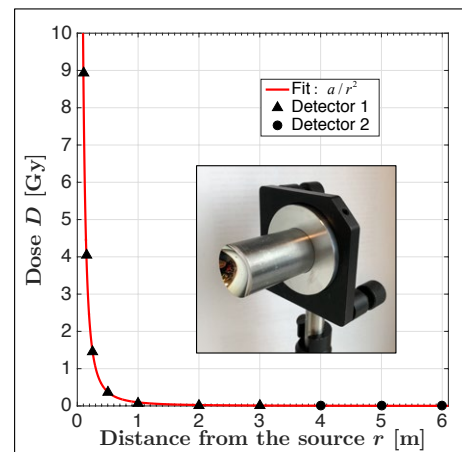


**Figure 1.** Dose per minute as a function of distance from the source, with the tight focusing parabola.

### References

- [1] Vallières S, Powell J *et al.* 2022 *arXiv*, DOI:10.48550/arXiv.2207.05773
- [2] Nuclear Safety and Control Act, Canadian Nuclear Safety Commission

## Femtosecond laser assisted chemical ionization mass spectrometry

T Cao<sup>1</sup>, S Liu<sup>1</sup>, Q Xu<sup>1\*</sup>, K Hu<sup>1</sup>, Z Li<sup>1</sup>, K Chen<sup>1</sup>, T Guo<sup>2</sup>, P Cheng<sup>2</sup> and J Peng<sup>1</sup>

<sup>1</sup>School of Optical and Electronic Information, Huazhong University of Science and Technology, Wuhan, 430074, China

<sup>2</sup>School of Environmental and Chemical Engineering, Shanghai University, Shanghai, 200444, China

**Synopsis** We propose a novel ion source for gas phase analytical mass spectrometry, which combines the both advantages of chemical ionization (CI) and femtosecond laser ionization (fsLI). A theoretical model is developed and proof-of-concept experiments are implemented.

Among the various analytical techniques, mass spectrometry (MS) is widely regarded as the most sensitive and broadly used one. Its applications range from ultrafast dynamics of single-molecule to the high-throughput analysis of proteins. With the continuous development of mass analyzers and detectors, ionization methods become the bottleneck of modern MS techniques. In order to preserve the integrity of molecular ions, femtosecond laser ionization (fsLI) [1] and proton transfer reaction (PTR) [2] are often employed, but the detection limits for both are clamped at hundred ppq (parts of quadrillion) level. Herein, by combining these two ion methods, we can promote sensitivity by two orders of magnitude.

The basic picture of femtosecond laser assisted chemical ionization (fsLACI) can be understood and modeled in three steps as illustrated in Figure 1. Similar to conventional CI experimental setups, low concentrations of analytes and higher concentrations of reagent molecules are mixed in atmospheric pressure background gas and continuously flow into the gas chamber next to the mass analyzer interface. In the first step, fsLI is utilized to generate high density of primary ions where the ion density can reach space-charge saturation [3]. Such a high concentration of reagent ions will continue to chemically ionize the analytes during their propagation to mass analyzer, which can be interpreted as expanding the tiny ionization volume of the solely fsLI.

We built a simple theoretical model to predict the signal yield of fsLACI, assuming that the CI process does not occur during the diffusion of the primary ions. The model could be further simplified if the condition for concentrations of

reagents and analytes differ significantly are met. All parameters used in the model can be obtained through consulting database and by fitting experimental data. The calculations indicate that more than two orders of magnitude of signal yield can be achieved by fsLACI compared to that of fsLI with moderate intensity laser pulses and conventional experimental conditions, which means ppq-level detection limits can be acquired if a cutting-edge TOF mass analyzer is employed.

We have also performed a set of experiments to verify the model, in which the analyte of 86 ppb cyclohexene and 1000 ppm of acetone reagent are employed. A reasonable space-charge saturation density and average reaction time are obtained from the fitting of experimental results. The ratio of the total fsLACI signal to the total fsLI signal exceeds 100 at different temperatures and pressures, confirming the previous predictions.

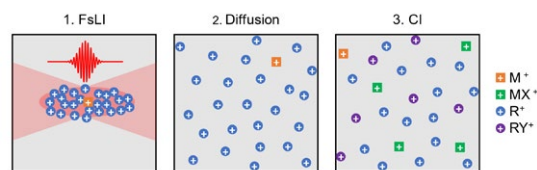


**Figure 1.** Illustration of the simplified fsLACI model.

### References

- [1] Peng J *et al* 2012 *Anal. Chem.* **84** 5633
- [2] Hansel A *et al* 1995 *Int. J. Mass Spectrom. Ion Process.* **149** 609
- [3] Lapsley A C 1953 *Rev. Sci. Instrum.* **24** 602

\*E-mail: [xuqi85@hust.edu.cn](mailto:xuqi85@hust.edu.cn)

## VUV photoelectron spectroscopy of vibrationally-excited CO<sub>2</sub> molecules

M Hoshino<sup>1\*</sup>, A Yodo<sup>1</sup>, N Hishiyama<sup>1</sup>, T Odagiri<sup>1</sup>, and J Adachi<sup>2</sup>

<sup>1</sup> Department of Physics, Sophia University, Tokyo 102-8554, Japan

<sup>2</sup> KEK, Photon Factory, Ibaraki 305-0801, Japan

**Synopsis** VUV photoelectron spectra have been measured for the vibrationally excited CO<sub>2</sub> molecules produced by the resistive heating technique in the photon energy range of 18 – 42 eV. The contributions from the vibrationally-excited CO<sub>2</sub> at the initial state were clearly observed for the  $1\pi_g^{-1}X^2\Pi_g$ ,  $1\pi_u^{-1}A^2\Pi_u$  and  $4\sigma_g^{-1}C^2\Sigma_g$  ionic states in the present photoelectron spectra.

Carbon dioxide (CO<sub>2</sub>) molecules are very important from an astrophysical point of view. CO<sub>2</sub> constitutes about 95% of Venus's atmosphere, the average surface temperature of which is ~460 °C. At such temperatures, CO<sub>2</sub> molecules are partially vibrationally-excited and those molecular vibrations must be taken into account for proper atmospheric modeling [1]. From a scientific perspective, since the vibrational wave function of the vibrationally-excited molecule has a larger spatial extent than that of the vibrational-ground state, spectroscopic study of vibrationally-excited molecules is a technique to probe different regions of potential energy surfaces compared to the analogous ground state measurement, based on the Frank-Condon principle. Indeed, those effects were clearly observed in our previous x-ray photoelectron spectra of the vibrationally-excited N<sub>2</sub>O [2]. In the present study, we report the photoelectron spectra of the vibrationally-excited CO<sub>2</sub> in the photon energy region of 18 – 42 eV. In addition, the vibrational branching ratio was extracted for the  $C^2\Sigma_g$  state and compared with the previous ones at room temperature [3,4]. The measurements were performed using the 3-m normal incidence vacuum monochromator at the BL-20A, Photon Factory. A 2400 lines/mm grating was used to achieve a resolution of 7.5 meV (FWHM) at 21 eV with slit widths of 150 μm. The photoelectrons were analyzed with a hemi-spherical electron energy analyzer (Scienta Omicron, R4000). The overall resolution of the photoelectron spectrum was ~12 meV at 21 eV. CO<sub>2</sub> was introduced into the interaction region through a newly built-in gas heating source. From the photoelectron spectra measured at room temperature and at high temperature (~450 °C), the contributions from the vibrationally-excited molecules at the initial states were extracted based on the Boltzmann distributions.

Figure 1 shows typical vibrationally-resolved photoelectron spectra for the  $C^2\Sigma_g$  state at 30 °C and 450

°C, that were normalized to the main peaks of the (000). A temperature effect between room and high temperatures was clearly observed for the bending vibration (010), whereas the noticeable differences were not so clear for the other vibrational excitations in Fig. 1. Excitation of a single quantum of the bending motion (010) becomes allowed due to the intra-channel coupling between the continuum electron and the vibrational motion associated with bending [3,4] that is sensitive to the molecular geometry. Therefore, the single quantum excitation from (010) excited by heating to the (020) excited state could strongly contribute in the photoelectron spectra shown in Fig. 1(b).

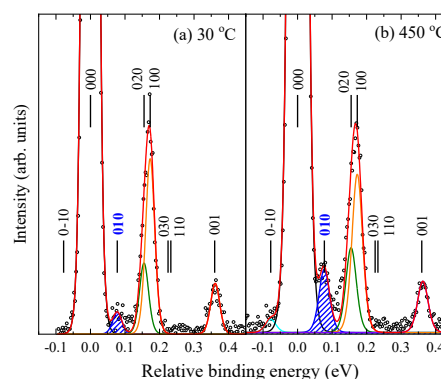


Fig. 1. Typical vibrationally resolved-photoelectron spectra of the CO<sub>2</sub> ( $C^2\Sigma_g$ ) ionic state recorded at 30 eV and at (a) 30 °C and (b) 450 °C.

### References

- [1] Tanaka T et al., Phys. Rev. Lett. **95**, 203002 (2005).
- [2] Hoshino M et al., J. Phys. B **51**, 065402 (2018).
- [3] Rathbone G. J et al., J. Chem. Phys. **114**, 8240 (2001).
- [4] Rathbone G. J et al., J. Chem. Phys. **120**, 612 (2004).

\* E-mail: masami-h@sophia.ac.jp

## Imaging the nuclear wavepacket dynamics of multiply charged Ar<sub>2</sub> using a two-color laser field

A Sen\*, M J J Vrakking and A Rouzée

Max Born Institute for Nonlinear Optics and Short Pulse Spectroscopy, Berlin, Germany

**Synopsis** The nuclear wavepacket dynamics resulting from the ionization of noble-gas dimers by intense, 800 nm laser pulses is investigated by time-resolved photoion spectroscopy using a time-delayed, tunable mid-infrared laser pulse.

Nuclear wavepacket dynamics plays an important role in various ultrafast chemical processes, like chemical bond breaking/formation, structural rearrangement, inter-atomic relaxation processes, etc. Ultrashort laser pulses serve as an important tool to temporally resolve such dynamics using pump-probe spectroscopic techniques[1, 2]. As rare gas dimers are weakly bound and have longer vibrational time periods compared to other diatomic molecular systems, they are particularly well-suited to investigate ultrafast nuclear wavepacket dynamics. In addition, the equilibrium distance of noble-gas dimers is larger in the neutral than in the ionic dimer. Hence, the dimer ions start to contract after photoionization of the neutral dimer.

In earlier two-color pump-probe studies performed in Ar<sub>2</sub> [3, 4], a depletion of the dissociative ionization channel was observed. This “frustrated dissociation effect” was attributed to the laser-induced coupling between two electronic states I(1/2)<sub>u</sub> and II(1/2)<sub>g</sub> of the dimer ions. In our study, we investigate the wavelength dependence of the photoionization dynamics of

Ar<sub>2</sub> dimers by a two-color laser field. A first near-IR pulse (~800 nm) was used to ionize the Ar<sub>2</sub> dimers and a second, time-delayed, tunable mid-IR pulse probe the resulting dynamics in the ionic dimers that were formed by monitoring the time-dependent Ar<sup>+</sup> kinetic energy distribution. The wavelength of the probe pulse was varied systematically from ~ 1.6–2.1 μm to control the laser-induced coupling between the I(1/2)<sub>u</sub> and II(1/2)<sub>g</sub> states, which is known to dissociative ionization channel. As a main result, we observed a broadening of the depletion region in the dissociative ionization channel with the increasing wavelength. This behavior reflects the propagation dynamics of the nuclear wavepacket in the laser-coupled potential energy surfaces, which can be fully resolved in our study.

### References

- [1] M. Kremer *et.al Physical Review Letters* **103** 213003
- [2] D. Ray *et.al Physical Review Letters* **103** 223201
- [3] J. Wu *et.al Physical Review Letters* **110** 033005
- [4] M. Magrakvelidze *et.al Physical Review A* **88** 013413

---

\*E-mail: [arnab.sen@mbi-berlin.de](mailto:arnab.sen@mbi-berlin.de)

## Carrier envelope phase sensitivity of photoelectron circular dichroism

V Hanus<sup>1,2\*</sup>, S Kangaparambil<sup>1</sup>, M Richter<sup>3,4</sup>, L Haßfurth<sup>3,4</sup>, M Dorner-Kirchner<sup>1</sup>, G G Paulus<sup>5</sup>, X Xie<sup>1,6</sup>, A Baltuška<sup>1</sup>, S Gräfe<sup>3,4</sup> and M Kitzler-Zeiler<sup>1†</sup>

<sup>1</sup>Photonics Institute, TU Wien, 1040 Vienna, Austria

<sup>2</sup>Institute for Solid State Physics and Optics, Wigner RCP, 1121 Budapest, Hungary

<sup>3</sup>Inst. of Phys. Chem. and Abbe Ctr. of Photonics, Friedrich Schiller University, 07743 Jena, Germany

<sup>4</sup>Fraunhofer Institute for Applied Optics and Precision Engineering, 07745 Jena, Germany

<sup>5</sup>Institute for Optics and Quantum Electronics, Friedrich Schiller University, 07743 Jena, Germany

<sup>6</sup>SwissFEL, Paul Scherrer Institute, 5232 Villigen, Switzerland

**Synopsis** We report on a combined experimental and numerical study of photoelectron circular dichroism (PECD) induced by intense few-cycle laser pulses, using methyloxirane as the molecular example. By comparison to simulations, we attribute the origin of the observed CEP-dependence of PECD to the CEP-induced modulation of ionization from different areas of the wave functions of three dominant orbitals.

The interaction of circularly polarized light and chiral molecules leads to forward-backward asymmetry: photoelectron circular dichroism (PECD) [1]. Strong-field ionization with ultra-short intense laser pulses is a particularly advantageous ionization regime since there the electron emission timing is linked to the laser field oscillations, which opens up the possibility to control and image molecular processes using the carrier-envelope phase (CEP) as a parameter.

The sensitivity of PECD to the sub-cycle variations of electron emission introduced by the CEP of few-cycle pulses has so far been neglected. As PECD in strong laser fields arises during the early stages of the electron emission process, one can expect non-negligible influence of CEP on PECD [2].

In this paper, using coincidence imaging and the methyloxirane molecule as the example, we show for the first time, to our knowledge, a dependence of the PECD strength on the CEP, see Fig.1(a). We show that both electrons emitted during a specific ionization-fragmentation reaction starting from the doubly charged molecular cation carry a CEP-dependent chirality.

Extracting the molecular breakup axis from our coincidence data we show the importance of the molecular orientation relative to the laser field's polarization plane. By comparison to the results of simulations we trace back the mechanism that determines the PECD strength during double ionization.

We propose the following mechanism: As the CEP is a laboratory-frame-defined quantity, it sets a preferential direction for the first ionization step, selecting a molecular orientation. The instant of the second ionization step is then linked to the first one by the CEP and the molecular-orbital-defined ionization probability, see Fig.1(b,c). As the observed PECD is determined by the chirality of the contributing molecular orbitals it is, thus, sensitive to the CEP.

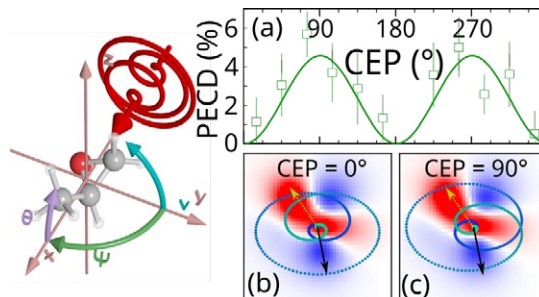


**Figure 1.** The PECD of methyloxirane molecules fragmenting along the laser propagation direction (left) shows a strong modulation by the CEP (a) due to the CEP-dependence of the ionization probability from different areas of specific orbitals (b,c).

### References

- [1] Beaulieu S et al. (2016) *New J. Phys.* **18**, 102002
- [2] Hanus V et al. (2023) *Phys. Chem. Chem. Phys.* **25**, 4656–4666

\* E-mail: [hanus.vaclav@wigner.hu](mailto:hanus.vaclav@wigner.hu)

† E-mail: [markus.zeiler@tuwien.ac.at](mailto:markus.zeiler@tuwien.ac.at)



## Capturing electron-driven molecular chirality

Vincent Wanie<sup>1\*</sup>, Etienne Bloch<sup>2</sup>, Erik P. Månsson<sup>1</sup>, Lorenzo Colaizzi<sup>1,3</sup>,  
 Krishna Saraswathula<sup>3</sup>, Sergey Ryabchuk<sup>3,4</sup>, Andrea Trabattoni<sup>1,5</sup>, Valérie Blanchet<sup>2</sup>,  
 Nadia Ben Amor<sup>6</sup>, Marie-Catherine Heitz<sup>6</sup>, Yann Mairesse<sup>2</sup>, Bernard Pons<sup>2</sup>, Francesca Calegari<sup>1,3,4</sup>

<sup>1</sup>Center for Free-Electron Laser Science, Deutsches Elektronen-Synchrotron DESY, Hamburg, 22607, Germany

<sup>2</sup>Université de Bordeaux - CNRS - CEA, CELIA, Talence, F-33405, France

<sup>3</sup>Physics Department, Universität Hamburg, Hamburg, 22761, Germany

<sup>4</sup>The Hamburg Centre for Ultrafast Imaging, Universität Hamburg, Hamburg, 22761, Germany

<sup>5</sup>Institute of Quantum Optics, Leibniz Universität Hannover, Welfengarten 1, 30167 Hannover, Germany

<sup>6</sup>CNRS, UPS, LCPQ (Laboratoire de Chimie et Physique Quantiques), FeRMI, Toulouse, F-31062, France

**Synopsis** Coherent electronic motion driven by UV-excited Rydberg states of methyl-lactate molecules leads to  $\sim 14$  fs oscillations of the molecular chiral properties. This is recorded in real-time using time-resolved photoelectron circular dichroism.

Photoionization of randomly oriented chiral molecules by circularly polarized radiation leads to an asymmetric photoelectron angular distribution with respect to the light propagation axis. This forward/backward asymmetry is known as PhotoElectron Circular Dichroism (PECD). Time-resolved (TR)-PECD has recently emerged as a powerful technique to track in real-time ultrafast molecular dynamics in gas-phase chiral molecules, such as internal conversion [1], photoemission delays [2] and photodissociation [3]. Here, we report our most recent work devoted to the investigation of electron-driven charge migration in *neutral* chiral molecules via TR-PECD and its applications to manipulate the outcome of photochemical and photophysical processes.

We used a new light source delivering few-femtosecond UV pulses [4] in order to photoexcite below the ionization threshold and trigger electronic dynamics in the Rydberg states of chiral methyl-lactate. TR-PECD allows us to image electronic coherences driving charge migration and disclose their impact on the molecular chiral response, allowing for an ultrafast chiroptical switching effect where the amplitude and direction of the photoelectron current generated by PECD can be controlled on a sub-10 fs timescale (Fig. 1). The results provide important perspectives to exploit charge-directed reactivity for controlling the chiral properties of matter at the molecular scale [5].

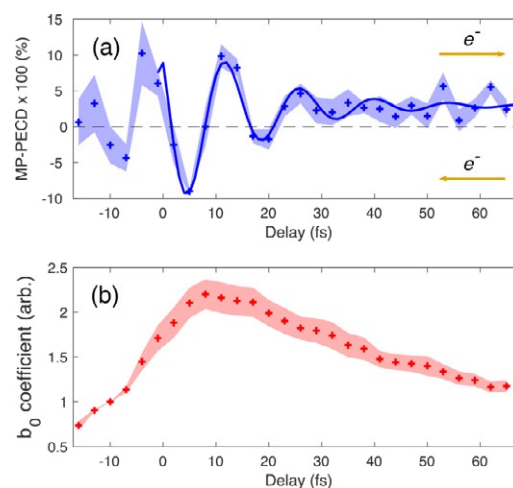


**Figure 1.** (a) Temporal evolution of the multiphoton (MP)-PECD describing the excess of electrons emitted backward (negative values) and forward (positive values) for photoelectrons with kinetic energies between 25 and 100 meV. (b) Corresponding  $b_0$  coefficient describing the total photoelectron yield. The blue solid line serves to guide the eye and the standard errors of the mean over 5 measurements are shown by the shaded areas. The background-free MP-PECD (a) allows us to identify a rapid modulation which is barely visible in (b).

### References

- [1] Blanchet V *et al.*, 2021 *PCCP* **23** 25612
- [2] Beaulieu *et al.*, 2017 *Science* **358** 1288
- [3] Svoboda *et al.*, 2021 *Sci. Adv.* **8** eabq2811
- [4] Galli. *et al.*, 2019 *Opt. Lett.* **44** 1308
- [5] Wanie V *et al.*, 2023 *arXiv:2301.02002*

\* E-mail: [vincent.wanie@desy.de](mailto:vincent.wanie@desy.de)

## Time-resolved Imaging of CH<sub>4</sub> Fragmentation in Strong Laser Fields

W Zhang<sup>1\*</sup>, David V. Chicharro<sup>1</sup>, T Pfeifer<sup>1</sup> and R Moshhammer<sup>1\*</sup>

<sup>1</sup>Max-Planck-Institut für Kernphysik, Heidelberg, 69117, Germany

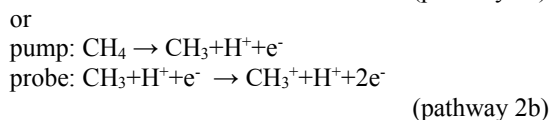
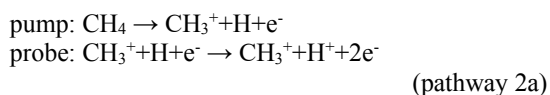
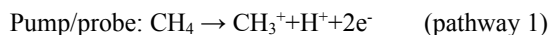
**Synopsis** This study investigates the time-resolved fragmentation of methane in few-cycle strong laser pulses using a combination of pulse shaping techniques and a Reaction Microscope. The results shed light on the dynamics of the dissociation pathways and symmetry variation in methane molecules.

Pulse shaping is widely used in various fields to generate adjustable laser pulses in terms of amplitude, polarization, relative phases, and time delays [1]. In strong laser fields, such flexibility enables better study of ionization and dissociation processes in atoms and molecules. When combined with a Reaction Microscope, which allows for coincidental reconstruction of the momentum of different fragmentation pieces, it provides opportunities to investigate molecular dynamics.

This work employs a dual-layer liquid crystal spatial light modulator [2] to compress light pulses and control the time delay between pump and probe pulses within the range of -50 fs to 1 ps.

Upon photoionization, the originally symmetric structure of methane's regular tetrahedral geometry is distorted due to the Jahn-Teller effect [3]. Depending on the charge localization of the dissociating CH<sub>4</sub><sup>+</sup> molecule, various dissociation pathways exhibit distinct angular distributions.

In pump-probe experiments, multiple pathways can result in the same fragments. In the channel detecting coincident CH<sub>3</sub><sup>+</sup> and H<sup>+</sup>, two pathways are involved: time-independent single-pulse interaction (pathway 1) and time-dependent sequential dissociation (pathways 2a and 2b), as depicted in Figure 1:



\* E-mail: [weiyu.zhang@mpi-hd.mpg.de](mailto:weiyu.zhang@mpi-hd.mpg.de)

\* E-mail: [r.moshhammer@mpi-hd.mpg.de](mailto:r.moshhammer@mpi-hd.mpg.de)

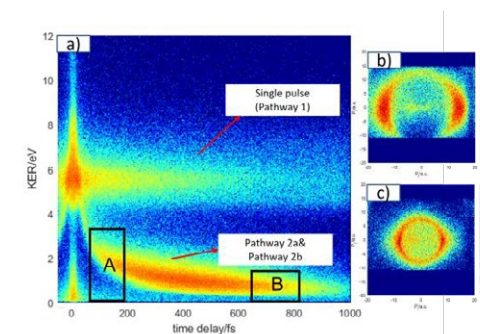


**Figure 1.** a) KER release of CH<sub>3</sub><sup>+</sup>+H<sup>+</sup> dissociation with time delay. b), c) Momentum Distribution of H<sup>+</sup> at different time delay ranges A and B, respectively.

As the pulse delay increases, the yield rate of H<sup>+</sup> is enhanced, and there is an observable change in the ratio of the two delayed ionization pathways. This change is visible in the shift from longitudinal to transverse events in the angular distribution (Fig. 1b and Fig. 1c), which exhibits different angular distributions that reflect the charge localization of the dissociating CH<sub>4</sub><sup>+</sup> molecule.

Furthermore, the dissociation channels of CH<sub>2</sub><sup>+</sup>+H<sub>2</sub><sup>+</sup> and CH<sup>+</sup>+H<sup>+</sup>+H<sup>+</sup> also show structural dynamics with respect to time delay. These rich structures provide us with opportunities to study the dynamics in methane molecules in greater depth.

### References

- [1] T Brixner and G Gerber 2001 *Opt. Lett.* **26** 557-559
- [2] Stefanie Kerbstadt, 2016, MA thesis. Universität Oldenburg
- [3] Ohta Y, Ohta K. Interconversion behavior of the C-H bond in the CH<sub>4</sub><sup>+</sup> radical cation: ab initio molecular dynamics study. *J Comput Chem.* 2004 Nov 30;25(15):1910-9 [doi: 10.1002/jcc.20134](https://doi.org/10.1002/jcc.20134).

## Camphor: Dynamics post C 1s ionisation and interaction with shaped laser pulses

S Sen<sup>1</sup>, A Sinha<sup>1</sup>, H Venugopal<sup>1</sup>, S Mandal<sup>2</sup>, A Sen<sup>2</sup>, R Gopal<sup>3</sup>, L B Ltaief<sup>4</sup>, S Turchini<sup>5</sup>, D Catone<sup>5</sup>, N Zema<sup>5</sup>, M Coreno<sup>6,7</sup>, R Richter<sup>6</sup>, M Mudrich<sup>4,8</sup>, SR Krishnan<sup>8</sup>, and V Sharma<sup>1\*</sup>

<sup>1</sup>Indian Institute of Technology Hyderabad, Kandi, 502285, India

<sup>2</sup>Indian Institute of Science Education and Research, Pune, 411008, India

<sup>3</sup>Tata Institute of Fundamental Research, Hyderabad, 500046, India

<sup>4</sup>Aarhus University, 8000 Aarhus C, Denmark

<sup>5</sup>Istituto di Struttura della Materia - CNR (ISM-CNR), Area di Ricerca di Tor Vergata via del Fosso del Cavaliere, 100, Rome, 00133, Italy

<sup>6</sup>Elettra-Sincrotrone Trieste, Basovizza, 34149, Italy

<sup>7</sup>Consiglio Nazionale delle Ricerche - Istituto di Struttura della Materia, Trieste, 34149, Italy

<sup>8</sup>QuCenDiEM - group and Department of Physics, Indian Institute of Technology - Madras, Chennai, 600036, India

**Synopsis** Ionisation and fragmentation dynamics of a prototype chiral molecule camphor is probed; 1) For doubly charged molecular ion following C 1s Auger decay, using velocity map imaging photoelectron-photoion-photoion coincidence (VMI-PEPIPICO) spectrometer and complementary molecular dynamics simulations. 2) Femtosecond laser pulses carrying orbital angular momentum and a mass spectrometer.

The behaviour of a molecule post interaction with radiation is significantly complex. Adding chirality makes it further intricate. However, exploring such processes is essential to comprehend these bifacial processes, involving properties of both the molecule and the radiation.

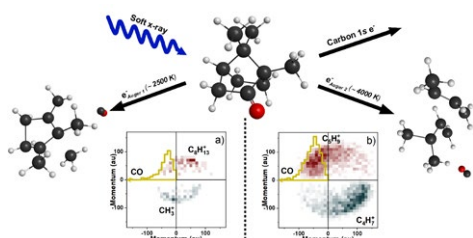


**Figure 1.** Schematic of the dissociation pathways,  $\text{CH}_3^+ + \text{C}_8\text{H}_{13}^+ + \text{CO}$  &  $\text{C}_4\text{H}_7^+ + \text{C}_5\text{H}_9^+ + \text{CO}$ . Molecular internal energy replicated as the bath temperature. (a & b) Experimental Newton diagrams.

C 1s ionised camphor excites the molecule to its doubly charged state following Auger decay. We studied the dissociation dynamics that follow, using a VMI-PEPIPICO spectrometer to record the 3-D momenta of the ionic fragments, complemented by molecular dynamics simula-

tion [1]. The internal energy of the molecular ion affects the dynamics causing fragmentation via various pathways. Two of the experimental pathways were correlated to the simulations and the angular distributions of the fragments match well. Unique signatures of the internal energy of the molecular ion were observed in the experimental kinetic energies of the neutral CO, emitted in the first step of the fragmentation pathways.

Additionally, chiral molecules are biologically relevant and the enantiomers are known to interact differently with biological systems. Chiral enantiomers can be probed via chiral probes like circularly polarised light. Recently, their interaction with light carrying orbital angular momentum is probed and similar behaviour is observed [2]. In our current experiment, we investigated the effect of orbital angular momentum (carried by femtosecond laser pulses) on the ionisation and fragmentation dynamics of the chiral system camphor, using a mass spectrometer.

### References

- [1] Sen S et al. 2022 *Phys. Chem. Chem. Phys.* **24** 2944
- [2] Bégin JL et al. 2022 *PREPRINT (Version 1)*

\*E-mail: [vsharma@phy.iith.ac.in](mailto:vsharma@phy.iith.ac.in)

## Dissociative Photoionization of EUV Lithography Photoresist Models

F Holzmeier<sup>1\*</sup>, M Gentile<sup>1</sup>, M Gerlach<sup>2</sup>, R Richter<sup>3</sup>, M van Setten<sup>1</sup>, J S Petersen<sup>1</sup>, P van der Heide<sup>1</sup>

<sup>1</sup>IMEC, Leuven, 3001, Belgium

<sup>2</sup>Institute of Physical and Theoretical Chemistry, University of Würzburg, Würzburg, 97074, Germany

<sup>3</sup>Elettra Sincrotrone Trieste, Basovizza, 34149, Italy

**Synopsis** Photoelectron photoion coincidence experiments employing 92 eV synchrotron radiation yield deep insights into the reaction mechanism of photoresist model molecules relevant in EUV lithography.

Extreme ultraviolet (EUV) lithography has recently been adopted in high-volume manufacturing of integrated circuits since the wavelength of 13.5 nm (92 eV) theoretically enables to print sub-10 nm features on wafers. In an EUV scanner, exposure of a photosensitive material with EUV light triggers a solubility switch, which produces three-dimensional feature after development. However, stochastic print failures are often decreasing the efficiency in the manufacturing process. The origin of these defects is not definitively clear since little is known about the chemical mechanism in photoresist materials, which are often composite blends, induced by the interaction with ionizing EUV light and governed by electron radiation chemistry.

In order to gain deep insights into the ionization process in EUV lithography, the dissociative photoionization of several prototype molecules for photoresists was studied employing 92 eV synchrotron radiation and photoelectron photoion coincidence detection at the GasPhase beamline of Elettra Sincrotrone Trieste. *Tert*-butyl methacrylate is a monomer unit that is found in commonly used environmentally stable chemically-amplified photoresists (ESCAP) [1]. The PEPICO experiments revealed that 92 eV radiation leads to numerous fragmentation channels, of which one directly deprotects the ester group in a McLafferty rearrangement. In ESCAP thin films this deprotection is responsible for the solubility switch enabling printing. By modifications of the electronic structure it might become possible to design resists in which this channel for dissociative photoionization is enhanced and competing ones suppressed and develop more efficient resist formulations.

Next to organic chemically amplified photoresists, resist platforms containing metal atoms with a high absorption at 92 eV (e.g. tin-oxo cages [2]) have become popular in EUV lithography. The dissociative photoionization of *n*-butyl tin oxo hydroxo, a precursor for tin-oxo resists [3] was therefore investigated as well and the main fragmentation channels identified and assigned to the electronic states in the cation.

Furthermore, complementary experiments on thin films employing IR spectroscopy and measuring the desorption of fragments upon EUV exposure were conducted. These set of experiments enable novel insights into the chemistry of EUV photoresists, which contribute to develop new resists with a higher performance.

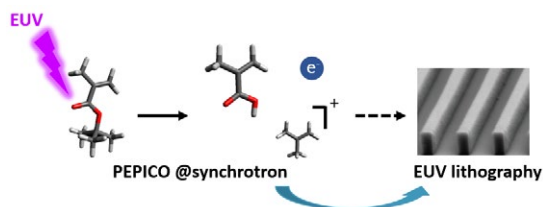


**Figure 1.** Dissociative photoionization of *tert*-butyl methacrylate contributes to the solubility switch wanted for EUV lithography.

### References

- [1] Ito H *et al* 1994 *J. Photopolym. Sci. Technol.* **7** 433-448
- [2] Cardineau B *et al* 2014 *Microelectron. Eng.* **127** 44-50
- [3] Frederick R *et al* 2019 *Microelectron. Eng.* **205** 26-31

\* E-mail: [fabian.holzmeier@imec.be](mailto:fabian.holzmeier@imec.be)

## Accurate molecular *ab initio* calculations in support of strong-field attosecond physics experiments

G. Visentin<sup>1,2\*</sup>, B. Ying<sup>3</sup>, G.G. Paulus<sup>3</sup> and S. Fritzsche<sup>1,2,3</sup>

<sup>1</sup> Helmholtz-Institut Jena, Jena, 07743, Germany

<sup>2</sup> GSI Helmholtzzentrum für Schwerionenforschung, Darmstadt, 64291, Germany

<sup>3</sup> Friedrich-Schiller -Universität Jena, Jena, 07743, Germany

**Synopsis** An accurate *ab initio* molecular approach is proposed to model the potential energy curves of  $\text{Ar}_2^+$  in the electronic ground and low-lying excited states across a wide interatomic distance range. The approach is targeted at the support and validation of strong-field physics experiments investigating the attosecond dynamics of diatomic molecules and ions. The theoretical curves reasonably agree with the experimental and theoretical reference data, thus providing a valuable support to the experiments in the investigation of the attosecond dynamics of dissociating diatomics.

Experimental techniques exploiting strong-field-processes allow for investigating the attosecond dynamics of molecules, such as their fragmentation into atoms [1]. Such experiments consist of a first step, where the molecule is ionized, followed by its fragmentation. There, two competing mechanism may occur, i.e., dissociation by recollision with the ejected electron [2] or dissociation of the molecular ion [1]. Evaluation of these two mechanisms is a crucial step in the experimental understanding of the dissociation dynamics of the molecule.

In this framework, accurate *ab initio* calculations of the potential energy curves (PECs) of the molecular ions may provide a valuable tool in support of the experiment. In this abstract, an accurate relativistic *ab initio* molecular approach is proposed to model the PECs of  $\text{Ar}_2^+$  in the electronic ground and lowest-lying excited states across a wide interatomic distance range up to the molecular dissociation limit.

The approach, based on the relativistic Fock-Space Coupled Cluster (FS-CC) level of theory,

yields PECs which are in good agreement with both the experimental results and the available theoretical literature and substantially supports the experimental interpretation and investigation of the possible dissociation pathways of the molecular ion.

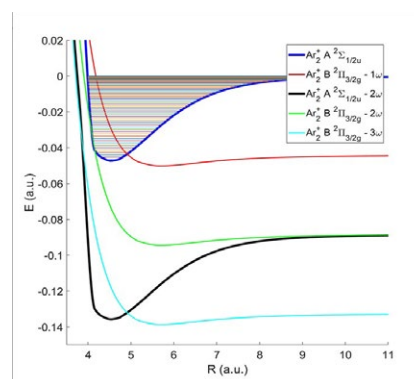


**Figure 1.** PECs of the electronic ground and the lowest-lying even-parity excited states of  $\text{Ar}_2^+$  in the Floquet representation.

### References

- [1] Rathje T., Sayler A.M., Zeng S., Wustelt P., Figger H., Esry B.D. and Paulus, G.G., 2013 *Phys. Rev. Lett.* **111** 093002.
- [2] Niikura H., Legaré F., Hasbani R., Bondrauk A.B., Ivanov M.Y., Villeneuve D.M. and Corkum P.B., 2002 *Nature* **417** 917-922.

\* E-mail: [g.visentin@hi-jena.gsi.de](mailto:g.visentin@hi-jena.gsi.de)



## Effect of the Breit interaction on the angular distribution of Auger electrons following electron-impact excitation of Be-like ions

Z W Wu<sup>1,2,3\*</sup>, Y Li<sup>1</sup>, Z Q Tian<sup>1</sup>, C Z Dong<sup>1</sup> and S Fritzsche<sup>2,3,4</sup>

<sup>1</sup>Key Laboratory of Atomic and Molecular Physics & Functional Materials of Gansu Province, College of Physics and Electronic Engineering, Northwest Normal University, Lanzhou 730070, P.R. China

<sup>2</sup>Helmholtz-Institut Jena, Fröbelstieg 3, D-07743 Jena, Germany

<sup>3</sup>GSI Helmholtzzentrum für Schwerionenforschung GmbH, Planckstrasse 1, D-64291 Darmstadt, Germany

<sup>4</sup>Theoretisch-Physikalisches Institut, Friedrich-Schiller-Universität Jena, D-07743 Jena, Germany

**Synopsis** Angular distribution of Auger electrons following  $1s \rightarrow 2p$  electron-impact excitation of Be-like ions was studied using the multi-configurational Dirac-Fock method and the relativistic distorted-wave theory. Special attention was paid to the effect of the Breit interaction on the angular distribution. It was found that for low- $Z$  ions the Breit interaction hardly contributes to the angular distribution, whereas its contribution becomes fairly different for medium- and high- $Z$  ions.

Electron-impact excitation of atoms or ions is one of fundamental atomic processes in astrophysical and laboratory plasmas. Chen and Reed studied the relativistic effect on the angular distribution of Auger electrons following electron-impact excitation of Be-like ions [1]. However, as a main part of the relativistic effect, the Breit interaction was not considered.

In the present work, we followed the work of Chen and Reed [1] and studied the angular distribution of Auger electrons following electron-impact excitation  $1s^2 2s^2 J=0 \rightarrow 1s 2s^2 2p_{1/2} J=1$  of Be-like  $Mg^{8+}$ ,  $Fe^{22+}$ ,  $Mo^{38+}$ ,  $Nd^{56+}$ ,  $Au^{75+}$ , and  $U^{88+}$  ions by using the multi-configurational Dirac-Fock method and the relativistic distorted-wave theory. Special attention was paid to the effect of the Breit interaction on the angular distribution of the emitted Auger electrons. It was found that for low- $Z$  ions such as  $Mg^{8+}$  ions the Breit interaction hardly contributes to the angular distribution of the Auger electrons, whereas for medium- and high- $Z$  Be-like ions the Breit interaction makes the angular distribution less anisotropic, which becomes first more prominent with increasing atomic number and, then, less and less as it increases further [2].

Fig. 1 shows the angular distribution of the Auger electrons for these Be-like ions at impact electron energy of 3.0 times their respective excitation thresholds. NB and B shows the results without and with the Breit interaction included, respectively. It is found that for high- $Z$  ions with atomic number larger than around 70 the effect of the Breit interaction on the angular distribution

\*E-mail: zhongwen.wu@nwnu.edu.cn

is nearly dependent of the atomic number, which is rather different from the case for the photon angular distribution associated with the same autoionizing level following the identical electron-impact excitation of Be-like ions [3].

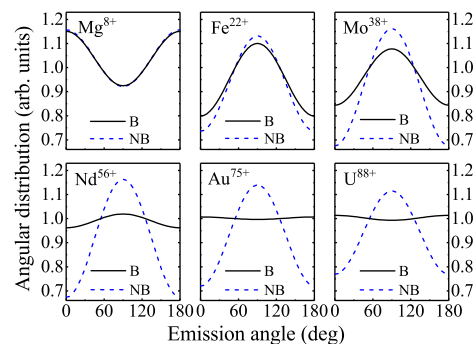


**Figure 1.** Angular distribution of the Auger electrons emitted from the nonradiative decay  $1s 2s^2 2p_{1/2} J=1 \rightarrow 1s^2 2s J=1/2$  of six Be-like ions for the impact electron energy of 3.0 times their respective excitation thresholds. Results are presented for both the NB (blue dashed lines) and B (black solid lines) cases.

This work was funded by the National Natural Science Foundation of China under Grants No. 12174315 and No. 11804280.

### References

- [1] Chen M H and Reed K J 1994 *Phys. Rev. A* **50** 2279
- [2] Wu Z W *et al* 2022 *Phys. Rev. A* **105** 032809
- [3] Wu Z W *et al* 2020 *Phys. Rev. A* **101** 022701



## Linear polarization and angular distribution of the Lyman- $\alpha_1$ line following electron-impact excitation of H-like ions

Z W Wu<sup>1,2,3\*</sup>, Z M He<sup>1</sup>, Z Q Tian<sup>1</sup>, C Z Dong<sup>1</sup> and S Fritzsche<sup>2,3,4</sup>

<sup>1</sup>Key Laboratory of Atomic and Molecular Physics & Functional Materials of Gansu Province, College of Physics and Electronic Engineering, Northwest Normal University, Lanzhou 730070, P.R. China

<sup>2</sup>Helmholtz-Institut Jena, Fröbelstieg 3, D-07743 Jena, Germany

<sup>3</sup>GSI Helmholtzzentrum für Schwerionenforschung GmbH, Planckstrasse 1, D-64291 Darmstadt, Germany

<sup>4</sup>Theoretisch-Physikalisches Institut, Friedrich-Schiller-Universität Jena, D-07743 Jena, Germany

**Synopsis** Linear polarization and angular distribution of highly charged H-like ions were studied using the multi-configurational Dirac-Fock method and the relativistic distorted-wave theory. A good agreement was obtained when compared with the theoretical results of Bostock *et al.* In particular, the effect of the Breit interaction on both the linear polarization and angular distribution of H-like ions was discussed in detail.

Over the past decades, angular and polarization behaviors of characteristic (x-ray) lines following electron-impact excitation of atoms and ions have been attracting much attention. In the light of the work of Reed *et al.* [1], we studied the effect of the Breit interaction on linear polarization and angular distribution of the Lyman- $\alpha_1$  line following electron-impact excitation of H-like ions using the multi-configurational Dirac-Fock method and relativistic distorted-wave theory [2].

for H-like  $\text{Ti}^{21+}$ ,  $\text{Mo}^{41+}$ ,  $\text{Ba}^{55+}$ , and  $\text{Au}^{78+}$  ions. It was found that for the Lyman- $\alpha_1$  polarization the present results with only the Coulomb interaction included are different from those of Reed *et al.* [1], whereas they agree well with the results obtained from the relativistic convergent close-coupling method [3]. Moreover, it was found that for medium- and high- $Z$  ions the Breit interaction contributes significantly to both the linear polarization and angular distribution, as shown in Fig. 1 and Fig. 2, which becomes more prominent with increasing atomic number and impact electron energy. To be more detailed, the Breit interaction changes even qualitatively its polarization and angular behaviors at high impact energies, say, 5.0 times the excitation thresholds.

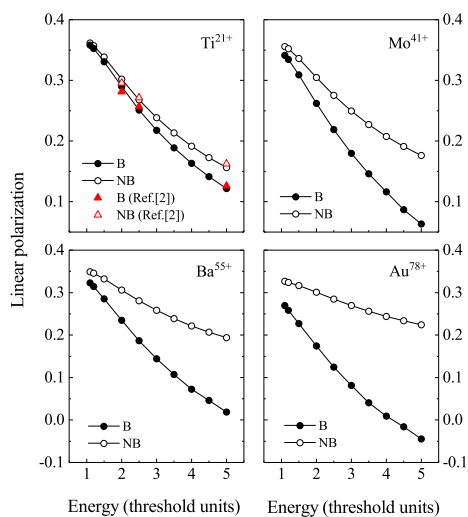


**Figure 1.** Linear polarization of the Lyman- $\alpha_1$  line of  $\text{Ti}^{21+}$ ,  $\text{Mo}^{41+}$ ,  $\text{Ba}^{55+}$ , and  $\text{Au}^{78+}$  ions as a function of impact energy in units of their respective excitation thresholds. NB and B denote the results without and with the Breit interaction included, respectively.

As an example, calculations were performed

\*E-mail: [zhongwen.wu@nwnu.edu.cn](mailto:zhongwen.wu@nwnu.edu.cn)

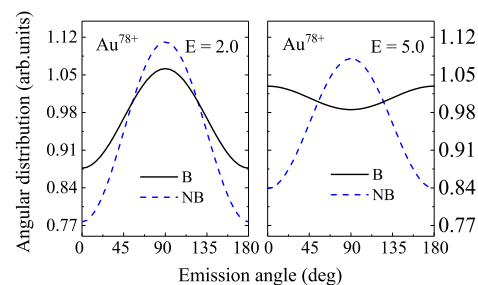


**Figure 2.** Angular distribution of  $\text{Au}^{78+}$  ions for both the NB and B cases. Results are presented for impact energies of 2.0 and 5.0 times the thresholds.

### References

- [1] K J Reed *et al* 1993 *Phys. Rev. A* **48** 3644
- [2] Z W Wu *et al* 2022 *Phys. Rev. A* **105** 062813
- [3] C J Bostock *et al* 2010 *Can. J. Phys.* **89** 503

## Classical description of the ionization of carbon by electron impact

N Bachi<sup>1\*</sup>, S Otranto<sup>1†</sup> and K Tókési<sup>2‡</sup>

<sup>1</sup>Instituto de Física del Sur (IFISUR), Departamento de Física, Universidad Nacional del Sur (UNS), CONICET, Av. L. N. Alem 1253, Bahía Blanca B8000CPB, Argentina

<sup>2</sup>Institute for Nuclear Research, 4026 Debrecen Bem tér 18/c, H-4026 Debrecen, Hungary

**Synopsis** A theoretical description of the ionization process in collisions between electrons and carbon atoms is presented using the classical trajectory Monte Carlo method. At impact energies greater than about 100 eV, the present methodology is in very good agreement with the reported experimental data. In contrast, the ionization cross section is overestimated at lower impact energies. We show that this behavior can be related to the formation of a transient system of two bound electrons and introduce a dynamical strategy that compensates the effect.

In this work, we calculate the total ionization cross sections of carbon atoms by 10 to 1000 eV electron impact using a three-body classical trajectory Monte Carlo (CTMC) method. The present calculations are restricted to the L-shell due to the large difference in the ionization potentials of the K-shell electrons, whose ionization cross sections are negligible in the energy range explored. Results obtained by means of the simple addition rule of the C(2s) and C(2p) orbitals are shown in Figure 1 and compared to the experimental data of Brook *et al* [1], and to the theoretical predictions of the generalized oscillator strength formulation of the Born approximation [2], the time-dependent close coupling (TDCC), the R-matrix-with-pseudo-states (RMPS), the time-independent distorted wave method (TIDW) and the B-spline R-matrix-with-pseudostates (BSR) [3, 4]. Good agreement is obtained with the data at impact energies greater than about 100 eV. In contrast, electron emission as the threshold region is approached seems to be overestimated.

A closer inspection of the classical dynamics at low impact energies reveals the formation of a transient double bound electron system [5]. It is well known that classical two-electron systems are unstable and their resulting dynamics are not expected to be accurately reproduced. In a first approach to the problem, we analyze the results obtained by switching-off the e-e interaction during the transient double bound state. Results are

included in Figure 1 and clearly evidence an improvement with respect to the standard CTMC description at the time they highlight the need of further studies.

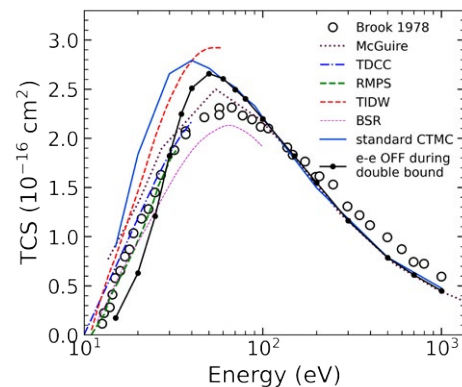


**Figure 1.** Total ionization cross section as a function of the impact energy for electron-carbon collisions. Expt. data from Ref. [1]. Theories as stated in the text.

### References

- [1] Brook E, Harrison M F A and Smith A C H 1978 *J. Phys. B: Atom. Mol. Phys.* **11** 3115
- [2] McGuire E J 1971 *Phys. Rev. A* **3** 267
- [3] Abdel-Naby S A, Ballance, C P, Lee T G, Loch S D and Pindzola M S 2013 *Phys. Rev. A* **87** 022708
- [4] Wang Y, Zatsarinny O and Bartschat K 2013 *Phys. Rev. A* **87** 012704
- [5] Bachi N, Otranto S and Tókési K 2023 *Atoms* **11** 16

\*E-mail: [nicolas.bachi@uns.edu.ar](mailto:nicolas.bachi@uns.edu.ar)

†E-mail: [sotranto@uns.edu.ar](mailto:sotranto@uns.edu.ar)

‡E-mail: [tokesi@atomki.hu](mailto:tokesi@atomki.hu)

## Impact Parameter and Kinematic Information for Differential Ionization of Argon by 1 keV Positrons and Electrons

K Tókesi<sup>1,\*</sup> and R D DuBois<sup>2</sup>

<sup>1</sup>Institute for Nuclear Research (ATOMKI), Debrecen, 4026, Hungary  
<sup>2</sup>Missouri University of Science and Technology, Rolla, MO, 65409, USA

**Synopsis** CTMC calculations for ionization of Ar(3p) by 1 keV positrons show that for positron impact the projectile is predominantly scattered away from the central core and the target electron is primarily ejected toward the core. Also, the “away” interactions occur at a smaller impact parameter than the “toward” interactions.

It is well known that the reversal of directions of the Coulomb field for positron and electron impact ionization produces trajectory changes for the projectile. This results in a larger impact parameter for positron impact with respect to that for electron impact. In addition, post-collision effects between the post-collision particles introduce additional trajectory effects. In order to test various theoretical models for ionization, comparisons on the differential level are used. For electron impact, a large amount of experimental information, ranging from singly to fully differential, is available whereas for positron impact, relatively few differential studies have been performed. Also, unlike the case for heavy ion impact where impact parameter information can be obtained, post-collision effects effectively prohibit such studies for lepton impact.

However, the Classical Trajectory Monte Carlo method allows us to investigate such kinematic effects and also to obtain information as a function of impact parameter. As an initial study, such information for ionization of argon 3p electrons by 1 keV positrons and electrons is presented. Similar to that used by Sparrow and Olson [1], the argon atom was modeled as a single 3p electron and a central core potential and interactions between all particle pairs are taken into account. Unlike previous studies, the present study also provides information about the impact parameter and the scattering and ejection directions, not just the angles but also whether the directions are “positive” or “negative”, i.e., toward, or away from the central core.

Figure 1 shows angular distributions for the scattered and ejected particles for 1 keV positron impact. The solid curves are the “normal”

singly differential cross sections, i.e., for all interactions, whereas the dashed and open circle curves are for interactions restricted to scattering toward and away from the central core. As seen, rather than being scattered symmetrically with respect to their initial direction, positrons predominantly are scattered away from the central core. This results in the target electron primarily being ejected toward the central core. As seen, the relative probability for these kinematics varies with observation angle. Not shown is impact parameter information. The bP(b) curves differ, with scattering away (towards) being centered at ~0.8 (~1.8) a.u. As a final note, for electron impact the preferred scattering and emission directions are reversed from those shown.

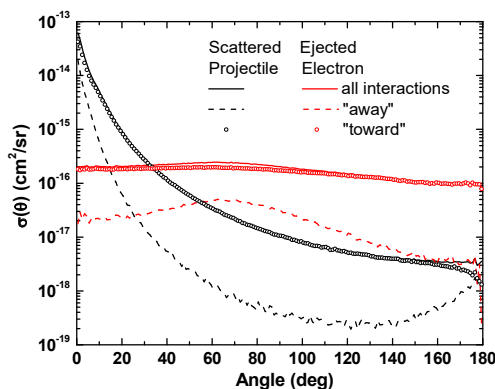


**Figure 1.** SDCS  $s(q)$  for 1 keV  $e^+-\text{Ar}(3p)$  ionization. See text for explanation of curves.

### References

- [1] Sparrow R A and Olson R E 1994 *J Phys. B: At. Mol. Opt. Phys.* **27** 2647

\* E-mail: [tokesi@atomki.hu](mailto:tokesi@atomki.hu)

## Convergent close-coupling calculations of positron scattering from carbon

N A Mori\*, L H Scarlett, I Bray, and D V Fursa

Department of Physics and Astronomy, Curtin University, Perth, Western Australia 6102, Australia

**Synopsis** Calculations of positron scattering from atomic carbon have been conducted using the single-centre convergent close-coupling method. A complex model potential has also been used to address the limitations of this approach. Important cross sections and quantities have been calculated for incident energies ranging from threshold to 5000 eV. Excellent agreement has been found at high energies with other theory and electron experiment. At low energies and for ionisation processes, different theoretical methods are in disagreement.

In recent years, there has been increasing demand for accurate cross-section data for positron scattering on atoms. This is partly due to the use of positrons in the biomedical industry, particularly in positron emission tomography (PET) scans and positron therapy. To calculate accurate cross sections for the complex biomolecules present in these applications, current approaches such as independent atom modelling (IAM) or Monte-Carlo methods require accurate cross-section data for the independent atoms which compose them. One such atom is carbon, which constitutes approximately 18% of the human body and is a major component in important biomolecules such as DNA.

The single-centre convergent close-coupling (CCC) method has been extended to obtain structure models and calculate positron scattering cross sections for atoms containing any number of active electrons, with or without an inert core. We have utilised the MULT program developed by Zatsarinny [1] and the multiconfigurational Hartree Fock (MCHF) code developed by Fischer [2]. A complex model potential calculation has also been employed to address drawbacks in the single-centre approach. With this technique, we can estimate cross sections at energies between the positronium-formation and ionisation thresholds, and explicitly calculate the positronium-formation and direct ionisation cross sections.

Using this approach, we generated an accurate target structure model for the carbon atom and calculated excitation, total ionisation, positronium-formation, direct ionisation,

and stopping power cross sections for positron scattering on carbon atoms for energies from threshold to 5000 eV. We also present energy levels, oscillator strengths, the scattering length, the hidden Ramsauer-Townsend minimum, the energy of the positron-carbon virtual state, and the mean excitation energy.

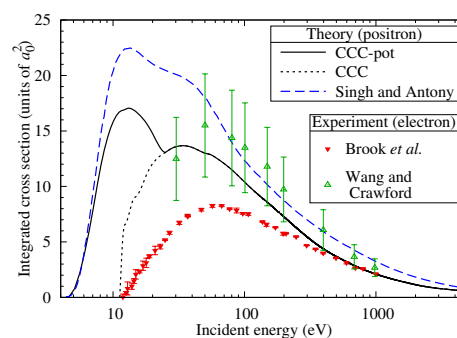


**Figure 1.** Total ionisation of carbon by positron impact. Theoretical results include the present CCC-pot and CCC calculations, and the spherical complex optical potential (SCOP) calculations of Singh and Antony [3]. Electron experiments are from Brook *et al.* [4] and Wang and Crawford [5].

### References

- [1] O. Zatsarinny 2006 *Comp. Phys. Commun.* **174** 273
- [2] C. F. Fischer 1991 *Comp. Phys. Commun.* **64** 369
- [3] S. Singh and B. Antony 2017 *Europhys. Lett.* **119** 50006
- [4] E. Brook, M. F. A. Harrison, and A. C. H. Smith 1978 *J. Phys. B: Atom. Mol. Phys.* **11** 3115
- [5] K. I. Wang and C. K. Crawford 1971 Tech. Rep. (MIT, Technical Report)

\*E-mail: [nicolas.mori@postgrad.curtin.edu.au](mailto:nicolas.mori@postgrad.curtin.edu.au)

## Low-energy elastic scattering of positron by helium

X.-J. Li<sup>1,2</sup>, M.-S. Wu<sup>3\*</sup>, J. Jiang<sup>1†</sup>, J.-Y. Zhang<sup>2‡</sup>, Z.-C. Yan<sup>4,2</sup> and K. Varga<sup>5</sup>

<sup>1</sup>College of Physics and Electronic Engineering, Northwest Normal University, Lanzhou 730070, China

<sup>2</sup>Innovation Academy for Precision Measurement Science and Technology, CAS, Wuhan 430071, China

<sup>3</sup>School of Science, Hainan University, Haikou 570228, China

<sup>4</sup>Department of Physics, University of New Brunswick, Fredericton, New Brunswick, Canada E3B 5A3

<sup>5</sup>Department of Physics and Astronomy, Vanderbilt University, Nashville, Tennessee 37235, USA

**Synopsis** The  $s$ -,  $p$ -, and  $d$ -wave elastic scattering of positron by helium is studied with the scattering energy below 11.1 eV using the confined variational method (CVM) [1]. In general, the calculated value of the annihilation rate parameter  $Z_{\text{eff}}$  is not as accurate as the corresponding phase shift. Therefore, comparing  $Z_{\text{eff}}$  determined by different theoretical methods, and comparing with accurate experimental values is an important test of the theoretical methods. The following table and figure show a comparison of some theoretical results obtained from the present CVM, the many-Body method (MBM) [2], the Kohn variational method (KVM) [3, 4], the polarized-orbital theory [5], and the semi-empirical model [6].

**Table 1.** Phase shifts of  $s$ -,  $p$ -, and  $d$ -waves in radians for positron scattering by helium.  $a[b]=a \times 10^b$ .

$k$ (a.u)	CVM	MBM [2]	KVM [3, 4]
$s$ -wave			
0.0	-0.477	-0.435	-0.48
0.04	1.664[-2]	1.514[-2]	
0.06	2.314[-2]	2.109[-2]	
0.08	2.855[-2]	2.606[-2]	
0.1	3.289[-2]	3.005[-2]	3.5(1)[-2]
0.3	3.033[-2]	2.760[-2]	3.0(1)[-2]
0.5	-2.084[-2]	-2.074[-2]	-2.1(1)[-2]
0.7	-8.853[-2]	-8.564[-2]	-8.9(1)[-2]
0.9	-1.583[-1]	-1.519[-1]	-1.57(1)[-1]
$p$ -wave			
0.1	2.648[-4]	2.403[-3]	3(1)[-3]
0.3	1.922[-3]	1.778[-2]	1.9(1)[-2]
0.5	4.027[-2]	3.795[-2]	4.1(1)[-2]
0.7	5.299[-2]	5.340[-2]	5.6(1)[-2]
0.9	5.965[-2]	6.034[-2]	6.1(1)[-2]
$d$ -wave			
0.1	4.209[-2]	3.788[-4]	1.4[-3]
0.3	3.769[-2]	3.396[-3]	4(1)[-3]
0.5	1.049[-2]	9.585[-3]	1.1(1)[-2]
0.7	2.012[-2]	1.868[-2]	2.1(1)[-2]
0.9	3.041[-1]	2.972[-2]	3.2(1)[-2]

In the table, the  $k = 0.0$  entry lists the scattering lengths, where our CVM value is in good agreement with the KVM value [3, 4].

\*E-mail: [mswu@hainanu.edu.cn](mailto:mswu@hainanu.edu.cn)

†E-mail: [phyjiang@yeah.net](mailto:phyjiang@yeah.net)

‡E-mail: [jy Zhang@apm.ac.cn](mailto:jy Zhang@apm.ac.cn)

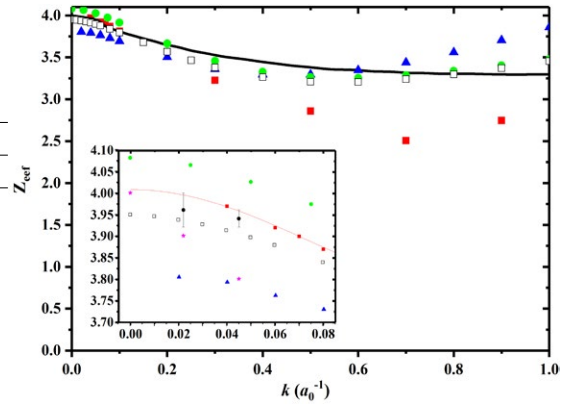


**Figure 1.** Energy dependence of  $Z_{\text{eff}}$  and a comparison among various theoretical methods. Red solid squares: CVM; red solid line: effective-range theory fitting; blue triangles: MBM [2]; pink stars: KVM [3, 4]; green circles: polarized-orbital theory [5]; black square: semi-empirical model [6]; black solid circles: experiment [7].

This work was supported by National Natural Science Foundation of China under Grant No. 11934014 and No. 12174399. Z.-C.Y. was supported by NSERC of Canada.

### References

- [1] Mitroy J., *et al.* 2008 *Phys. Rev. Lett.* **78** 123201.
- [2] Green D. G., *et al.* 2014 *Phys. Rev. A* **90** 032712.
- [3] Van Reeth P., *et al.* 1999 *J. Phys. B* **32** 3651.
- [4] Campeanu R. I., *et al.* 1977 *J. Phys. B* **10** L153.
- [5] McEachran R. P., *et al.* 1978 *J. Phys. B* **11** 951.
- [6] Mitroy J., *et al.* 2002 *J. Phys. B* **35** R81.
- [7] Coleman P., *et al.* 1975 *J. Phys. B* **8** 1734.

## Laser-assisted positron-H scattering in reduced quantum model

Xiao Hu Ji<sup>1</sup>, Li Guang Jiao<sup>1,2\*</sup>, and Aihua Liu<sup>3†</sup>

<sup>1</sup>College of Physics, Jilin University, Changchun 130012, People's Republic of China

<sup>2</sup>Helmholtz-Institut Jena, D-07743 Jena, Germany

<sup>3</sup>Institute of Atomic and Molecular Physics, Jilin University, Changchun 130012, People's Republic of China

**Synopsis** Laser-assisted collision of positron from hydrogen atom in a reduced-dimensional model is investigated by solving the time-dependent Schrödinger equation. The populations in the target excitation and positronium (Ps) formation channels are obtained utilizing the projection method. The Ps formation population at low incident energies is enhanced considerably with increasing the laser field intensity.

Laser-assisted atomic collision processes have attracted considerable interest in recent years due to the fast development of ultrashort and intense laser fields providing us a unique tool to manipulate the scattering dynamics. The laser-assisted positron-atom scattering, although has not been achieved experimentally at present, opens the opportunity to control and enhance the positronium (Ps) formation probability for future use. The recent work of Liu *et al.* [1] based on the classical trajectory Monte Carlo approach with a Heisenberg potential has demonstrated that the laser field would significantly modulate the Ps formation process in the positron-H scattering, even at low field intensities. A fully quantum mechanical treatment of this problem is necessary to tackle the interplay between scattering mechanism and laser interactions.

We employ a reduced quantum model proposed by Larkin *et al.* [2] to investigate the Ps formation in laser-assisted positron-H scattering. Both the target H atom and ejected Ps atom are modeled by soft-Coulomb potentials. The laser field has five optical cycles and a wavelength of 800 nm. The system scattering wave function is obtained by numerically solving the time-dependent Schrödinger equation. In Fig. 1, we present the final populations of the Ps formation in the ground state as a function of positron incident energy in the field intensities of 0,  $5 \times 10^{12}$ ,  $3 \times 10^{13}$ , and  $5 \times 10^{13}$  W/cm<sup>2</sup>. The dots and lines refer to the state-projection and mask-function methods, respectively, and they show good agreement with each other except at very small incident energies.

The final population of Ps atom is strongly

\*E-mail: [lgjiao@jlu.edu.cn](mailto:lgjiao@jlu.edu.cn)

†E-mail: [aihualiu@jlu.edu.cn](mailto:aihualiu@jlu.edu.cn)

modulated by the laser field. For the field-free case, the yield of Ps reaches a maximum at an energy of about 0.7. With increasing the field intensity, the channel opening threshold decreases and the maximum position is shifted to a smaller energy. This is because as the laser intensity increases, both the electron and positron are more likely to absorb photons from the laser field and then eject from the target ion. Our results suggest that the yield of Ps formation at low incident energies can be significantly increased by exposing a laser field with suitable intensity. More details of results will be reported.

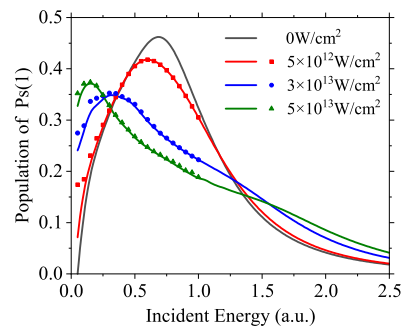


**Figure 1.** Population of Ps formation in the ground state as a function of positron incident energy. Solid lines with black, red, blue, and green colors represent field intensities of 0,  $5 \times 10^{12}$ ,  $3 \times 10^{13}$ , and  $5 \times 10^{13}$  W/cm<sup>2</sup>, respectively.

### References

- [1] S. Liu, D. Ye, and J. Liu, *Phys. Rev. A* **101**, 052704 (2020).
- [2] J. M. Larkin, J. H. Eberly, D. G. Lappas, and R. Grobe, *Phys. Rev. A* **57**, 2572 (1998).



## Low-energy total cross-sections of positronium scattering from the inert atoms

D M Newson\*, S J Brawley, R Kadokura, A Loreti, M Shipman, G Laricchia†

UCL Department of Physics and Astronomy, Gower Street, London WC1E 6BT, UK

Previous experimental determinations [1] of the positronium total scattering cross-section in combination with theoretical studies [2] have revealed the electron-like scattering of positronium at intermediate energies, persisting even in the vicinity of delicate quantum structures [3, 4, 5, 6]. Below the positronium break-up threshold energy a variety of *ab initio* [7, 8, 9] and model potential [10, 11] theoretical approaches have been brought to bear, as highlighted for the case of helium in figure 1. Brawley *et al.* [17] performed the first total cross-section measurements in the elastic region for argon and xenon, finding trends in stark contrast to theoretical works [18] but not dissimilar to that of an electron of equal velocity.

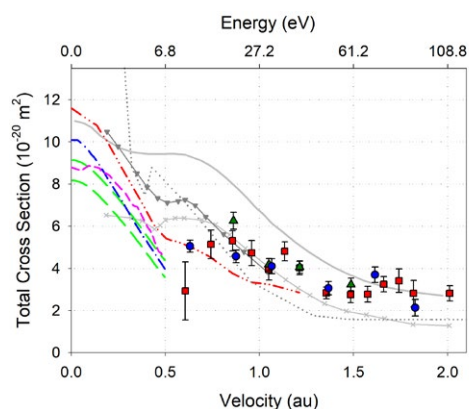


**Figure 1.** Experimental determinations of the positronium total scattering cross-section for helium: squares [12]; up triangles [13]; circles [1]. Also shown are theoretical studies as lines: dotted [14]; line and triangles [15]; double-dot dashed [7]; line and crosses [16]; short dashed [8]; solid [10]; upper and lower long dashed [11]; dot-dashed [9].

Now, experimental determinations of the total scattering cross-section of positronium collid-

ing with helium, neon and krypton have been extended to energies below the positronium break-up threshold. The results are presented and discussed in the context of available theoretical studies [7, 8, 9, 10, 11] and the previous experimental work [1, 17]. Insights into the basic interaction between positronium and atomic targets, suggested by the trends in the total cross-sections, are also considered.

EPSRC (UK) is thanked for financial support (EP/P009395/1, EP/R513143/1).

### References

- [1] Brawley S J *et al.* 2010 *Science* **330** 789
- [2] Fabrikant I I and Gribakin G F 2014 *Phys. Rev. Lett.* **112** 243201
- [3] Brawley S J *et al.* 2010 *Phys. Rev. Lett.* **105** 263401
- [4] Shipman M *et al.* 2017 *Phys. Rev. A* **95** 032704
- [5] Wilde R S and Fabrikant I I 2018 *Phys. Rev. A* **97** 052708
- [6] Wilde R S *et al.* 2021 *Phys. Rev. A* **104** 012810
- [7] Blackwood J E *et al.* 1999 *Phys. Rev. A* **60** 4454
- [8] Walters H R J *et al.* 2004 *Nucl. Instrum. Methods Phys. Res. B* **221** 149
- [9] Swann A R *et al.* 2021 [arXiv:2105.06749v1](https://arxiv.org/abs/2105.06749v1)
- [10] Wilde R S and Fabrikant I I 2018 *Phys. Rev. A* **98** 042703
- [11] Swann A R and Gribakin G F 2018 *Phys. Rev. A* **97** 012706
- [12] Garner A J *et al.* 1996 *J. Phys. B: At. Mol. Opt. Phys.* **29** 5961
- [13] Garner A J *et al.* 2000 *J. Phys. B: At. Mol. Opt. Phys.* **33** 1149
- [14] McAlinden M T *et al.* 1996 *Can. J. Phys.* **74** 434
- [15] Sarkar N K, Chaudhury P and Ghosh A S 1999 *J. Phys. B: At. Mol. Opt. Phys.* **32** 1657
- [16] Basu A *et al.* 2001 *Phys. Rev. A* **63** 052503
- [17] Brawley S J *et al.* 2015 *Phys. Rev. Lett.* **115** 223201
- [18] Blackwood J E *et al.* 2002 *J. Phys. B: At. Mol. Opt. Phys.* **35** 2661

\*E-mail: [ucapdne@ucl.ac.uk](mailto:ucapdne@ucl.ac.uk)

†E-mail: [g.laricchia@ucl.ac.uk](mailto:g.laricchia@ucl.ac.uk)

## Collective effects in positronium formation from rare gas atoms

P -A Hervieux<sup>1†</sup>, A Andoche<sup>1</sup>, K L ev eque<sup>1</sup>, and H S Chakraborty<sup>2</sup>

<sup>1</sup> Universit e de Strasbourg, CNRS, Institut de Physique et Chimie des Mat eriaux de Strasbourg, 67000 Strasbourg, France

<sup>2</sup> Department of Natural Sciences, D L Hubbard Center for Innovation, Northwest Missouri State University, Maryville, Missouri 64468, USA

**Synopsis** Using a density functional theoretical method to describe the many-electron correlation, we investigate the positronium formation from rare gas atoms. We are specifically interested to probe the effects of atomic giant collective resonance states on the Ps formation process.

Following the impact of positrons with matter the formation of an exotic electron-positron bound pair, positronium (Ps), is an important process in nature. This channel accounts for as large as half of the positron scattering cross section from simple atoms and molecules. Other than probing the structure and reaction mechanisms of matter, the Ps formation is a unique pathway to the electron-positron annihilation process. However, the role of innershell single-electron or collective many-electron excitation resonances in the continuum of captured electrons to affect the Ps formation is not known.

In this work, we study the Ps formation by the impact of fast positrons on rare gas atoms. To do so, we use the Coulomb Born approximation (CBA) method which is well adapted to describe this process [1, 2]. In this framework, the main objective of our study is to examine if the Ps formation process on electron shells containing several electrons (for example, there are ten electrons in the *d*-shell of Xe) is influenced by collective effects, i.e. by the correlated response of atomic electrons to the presence of the incident positron. Indeed, it is well known that the photoionization of the *4d* shell of Xe presents collective many-electron effects [3]. Figure 1 compares the measured [4] Xe *4d* giant shape resonance in photoionization with calculations [5] by one of us employing the time-dependent density functional theory (TDDFT).

It is therefore legitimate to look for such an effect in the formation of Ps from, say, Xe. To model this correlated electronic response, we have developed an original method based on the TDDFT technique.

<sup>†</sup> E-mail: [paul-antoine.hervieux@ipcms.unistra.fr](mailto:paul-antoine.hervieux@ipcms.unistra.fr)

The results will be presented in the conference. The success of the study will open efforts to explore resonant Ps formation including the plasmon resonance.

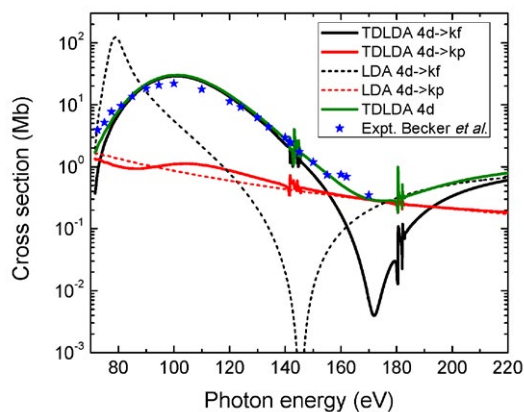


**Figure 1.** DFT and TDDFT photoionization dipole channel cross sections of Xe *4d*. The local density approximation (LDA) variant of the method is used. The TDLDA *4d* total cross section is compared with measurements [4] showing the giant resonance feature. The figure is reproduced from Ref. [5].

Supported by US-NSF PHY-2110318.

### References

- [1] Hervieux P -A, Chakraborty A R, and Chakraborty H S, 2017 *Phys. Rev. A* **95** 020701(R)
- [2] Hervieux P -A et al, 2006 *J. Phys. B* **39**, 409
- [3] Zhong S et al., 2020 *Nat Commun* **11**, 5042
- [4] Becker U et al., 1989 *Phys. Rev. A* **39** 3902
- [5] Magrakvelidze M, Madjet M E, and Chakraborty H S, 2016 *Phys. Rev. A* **94** 013429

## Calculation and Wigner law analysis of scattering cross sections for collisions of antihydrogen atom with excited positronium

T Yamashita<sup>1,2\*</sup>, Y Kino<sup>2</sup>, E Hiyama<sup>3,4</sup>, S Jonsell<sup>5</sup>, and P Froelich<sup>6</sup>

<sup>1</sup>Institute for Excellence in Higher Education, Tohoku University, Sendai, 980-8576, Japan

<sup>2</sup>Department of Chemistry, Tohoku University, Sendai, 980-8578, Japan

<sup>3</sup>Department of Physics, Tohoku University, Sendai, 980-8578, Japan

<sup>4</sup>Nishina Center, RIKEN, Wako, 351-0198, Japan

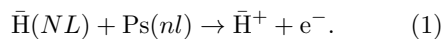
<sup>5</sup>Department of Physics, Stockholm University, Stockholm, SE-10691, Sweden

<sup>6</sup>Department of Chemistry, Uppsala University, Uppsala, Box 518 751-20, Sweden

**Synopsis** We present a 4-body calculation of the antihydrogen-positronium scattering cross sections near the antihydrogen positive ions ( $\bar{H}^+$ ) production threshold energy. Inelastic scattering cross sections including positronium excitation, deexcitation, and the polarization processes are reported together with the  $\bar{H}^+$  production cross sections. The cross section behaviour near the threshold energy is analysed in the context of the Wigner law and its modification due to the dispersion potential.

Antihydrogen atom ( $\bar{H}$ ) is a bound state of an antiproton ( $\bar{p}$ ) and a positron ( $e^+$ ). Energy levels of the  $\bar{H}$  have been measured for the purpose of testing the CPT symmetry [1] through comparison with the energy levels of ordinary hydrogen. Since the  $\bar{H}$  is electrically neutral, it can be used to test the matter-antimatter gravity, or the weak equivalence principle (WEP) of general relativity. Production of ultracold antihydrogen atoms is of importance for these experiments.

In contrast to the conventional  $\bar{H}$  production scheme using three-body recombination in a mixture of positron cloud and antiproton cloud, the  $\bar{H}$  production by antiproton injection into an excited positronium ( $\text{Ps} = e^+e^-$ ) target is under consideration at the AEgIS [2] and GBAR [3] experiments at CERN. The GBAR experiment will further utilize an antihydrogen positive ion ( $\bar{H}^+ = \bar{H}e^+e^+$ ) which is produced by a positron transfer from Ps to the  $\bar{H}$ :



The  $\bar{H}^+$  will be sympathetically cooled with matter cations and subsequently photoionized.

The four-body reaction between  $\bar{H}(NL)$  and  $\text{Ps}(nl)$  involves many theoretical challenges. The reaction is a rearrangement process in which the particle configurations change drastically before/after the collision. A number of inelastic scattering channels open above the  $\bar{H}^+ + e^-$  threshold energy; in particular,  $\bar{H}(N \geq 2) + \text{Ps}(nl)$  collision has infinite number of open chan-

\*E-mail: [tyamashita@tohoku.ac.jp](mailto:tyamashita@tohoku.ac.jp)

nels.

In this work, we report our recent calculation of  $\bar{H}(1s) + \text{Ps}(n \leq 3)$  collisions near the  $\bar{H}^+ + e^-$  threshold energy [4, 5]. Since in this energy range the number of open channels is finite and the scattering process can be treated rigorously. We include all possible inelastic processes: Ps excitation, Ps deexcitation, and Ps polarization where only the angular momentum of Ps changes without kinetic energy change.

We have calculated S-matrix elements for all allowed scattering processes, namely both in forward and reversed direction, without assumption of the detailed balance. Based on a partial-wave expansion, the scattering cross-sections are obtained for the total angular momenta  $J = 0 - 6$ . The numerical accuracy of the calculation is checked using the criterion of the unitarity and symmetry of the S-matrix. It is shown that the all inelastic reaction cross sections (including the polarization processes) satisfy the Wigner law [6], whereas the elastic scattering cross sections require modification because of the presence of dispersion potential.

### References

- [1] Ahmadi M P *et al.* 2017 *Nature* **541** 506
- [2] Amsler C *et al.* 2021 *Commun. Phys.* **4** 19
- [3] Perez P and Sacquin Y 2012 *Class. Quantum Grav.* **29** 184008
- [4] Yamashita T *et al.* 2021 *New J. Phys.* **23** 012001
- [5] Yamashita T *et al.* 2022 *Phys. Rev. A* **105** 052812
- [6] Wigner E P 1948 *Phys. Rev.* **73** 1002

## Electron impact excitation of Na-like $\text{Ar}^{7+}$ , $\text{Kr}^{25+}$ and $\text{Xe}^{43+}$

A K Sahoo<sup>1\*</sup>, S Rathi<sup>1</sup> and L Sharma<sup>1†</sup>

<sup>1</sup>Indian Institute of Technology Roorkee, Roorkee, 247667, India

**Synopsis** We carried out a detailed study on the electron impact excitation of highly charged Na-like inert gas ions of argon, krypton and xenon with the relativistic distorted wave approximation including the Breit in the evaluation of the scattering amplitude.

Highly charged ions (HCIs), particularly inert gas ions, play a crucial role in plasma physics as edge plasma coolant, the semiconductor industry for EUV lithography [1] and space aviation for electric propulsion ion thrusters [2]. However, these data for inert gas ions are either limited or not available. Therefore, We have implemented a relativistic perturbative approach, the relativistic distorted wave (RDW) theory, to study the electron impact excitation of Na-like  $\text{Ar}^{7+}$ ,  $\text{Kr}^{25+}$  and  $\text{Xe}^{43+}$  ions.

In the RDW calculations, first, the atomic bound state wavefunctions of  $\text{Ar}^{7+}$ ,  $\text{Kr}^{25+}$  and  $\text{Xe}^{43+}$  are obtained using the multiconfiguration Dirac-Fock approach with relativistic configuration interaction and leading quantum electrodynamic corrections. To establish the accuracy of these obtained bound state wavefunctions, we have bench-marked the level energies and transition rates in our recent work [3] using GRASP2018 [4]. Further, these atomic wavefunctions are used to obtain the relativistic distorted waves to describe the projectile and scattered electrons.

Other packages like FAC [5] also implement RDW theory to study the electron impact excitation processes. FAC is limited to providing integrated cross sections (ICSs) and not differential cross sections (DCSs). However, for modelling the atomic and molecular physics of injected impurities in fusion devices differential cross sections are also required [6]. We can directly obtain DCSs from our RDW program. Also, for highly charged ions, effect of the Breit interaction on scattering parameters is also found to be significant, particularly on the degree of linear polarization of emitted photons. FAC considers only the Coulomb interaction in the RDW calculations and does not include the Breit inter-

action. Therefore, we have recently developed our RDW code to implement Breit interaction in evaluating the scattering amplitude. For illustration, Fig. 1 shows electron impact excitation cross section of  $\text{Kr}^{25+}$  and  $\text{Xe}^{43+}$  for  $3s\ ^2S_{1/2}$  to  $3p\ ^2P_{1/2}$  and  $3s\ ^2S_{1/2}$  to  $3p\ ^2P_{3/2}$  transition in the incident electron energy range 200–5000 eV.

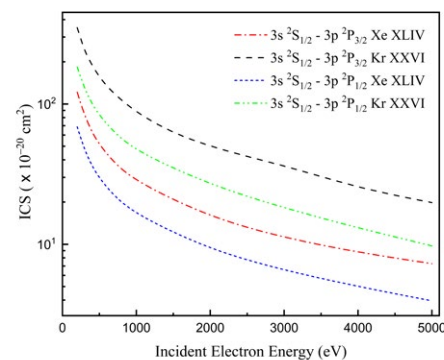


**Figure 1.** ICS results for excitation from  $3s\ ^2S_{1/2}$  to  $3p\ ^2P_{1/2}$  and  $3s\ ^2S_{1/2}$  to  $3p\ ^2P_{3/2}$  for 200 – 5000 eV incident electron energy.

This work is supported by IAEA, Vienna under the IAEA Research Contract No. 26504.

### References

- [1] Abramove IS *et al* 2018 *Phys. Rev. Appl.* **10** 034065
- [2] Beattie JR and Matossian JN 1990 *Rev. Sci. Instruments* **61** 348
- [3] Rathi S and Sharma L 2022 *Atoms* **10** 131
- [4] Fischer CF *et al* 2019 *Computer Physics Communications* **237** 184
- [5] Gu MF 2008 *Canadian Journal of Physics* **86** 675
- [6] Summary Report of a Consultancy Meeting in preparation of a Coordinated Research Project on Atomic Data for Injected Impurities in *Fusion Plasma*. Online [Accessed on 5-Mar-2023]

\*E-mail: [aloka.s@ph.iitr.ac.in](mailto:aloka.s@ph.iitr.ac.in)

†E-mail: [lalita.sharma@ph.iitr.ac.in](mailto:lalita.sharma@ph.iitr.ac.in)

## Electron impact excitation of Ar-like Kr XIX

A K Sahoo<sup>1</sup>, N Ghosh<sup>1</sup> and L Sharma<sup>1\*</sup>

<sup>1</sup>Indian Institute of Technology Roorkee, Roorkee, 247667, India

**Synopsis** We have implemented the multiconfiguration Dirac-Hartree-Fock method to study the energy levels and oscillator strength for the transitions between the levels [Ne]3s<sup>2</sup>3p<sup>6</sup>, [Ne]3s3p<sup>6</sup>3d, [Ne]3s<sup>2</sup>3p<sup>4</sup>3d<sup>2</sup> and [Ne]3s<sup>2</sup>3p<sup>5</sup>3d of Ar-like Kr (Kr XIX). Further, the electron impact excitation cross sections are obtained for transitions among these levels using relativistic distorted wave (RDW) theory.

The studies on energy levels, transition parameters and electron impact processes of highly charged ions of inert gases are crucial because of their application in fusion plasma applications. The success of plasma modeling relies heavily on the accuracy of these parameters. In the literature, limited studies are available on the atomic structure calculations of Kr XIX, while its electron impact excitation cross sections are hardly available in the literature. In this work, we have obtained the atomic energy levels of 150 levels from the configuration [Ne]3s<sup>2</sup>3p<sup>6</sup>, [Ne]3s3p<sup>6</sup>3d, [Ne]3s<sup>2</sup>3p<sup>4</sup>3d<sup>2</sup> and [Ne]3s<sup>2</sup>3p<sup>5</sup>3d and the weighted oscillator strengths and transition rates for the transitions among the above-mentioned configurations. We used the multiconfiguration Dirac-Hartree Fock (MCDHF) approach implemented in GRASP2018 [1] and also included the Breit Interaction and leading order QED corrections.

The atomic wavefunctions are obtained in the restricted active set approach. The single- and double-excitations are considered from the multireference (MR) set = {3s<sup>2</sup>3p<sup>6</sup>, 3s3p<sup>6</sup>3d, 3s<sup>2</sup>3p<sup>4</sup>3d<sup>2</sup>, 3s<sup>2</sup>3p<sup>5</sup>3d} to the active space AS1 = {4s, 4p, 4d, 4f}, AS2 = AS1 + {5s, 5p, 5d, 5f, 5g}, AS3 = AS2 + {6s, 6p, 6d, 6f, 6g} and AS4 = AS3 + {7s, 7p, 7d, 7f, 7g}. The convergence is achieved between the AS3 and AS4 results.

Due to the lack of measurements to compare the atomic structure results, another set of calculations is carried out with the many-body perturbation theory (MBPT) using the FAC [2]. To establish the accuracy of our calculated atomic wave functions, we have compared the weighted oscillator strengths for E1 transitions obtained from the MCDHF and MBPT methods as shown

in Figure (1) before proceeding with the electron impact excitation calculations using the RDW theory.

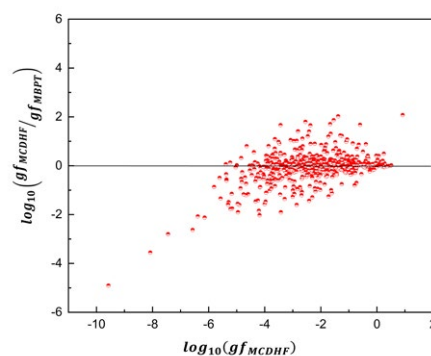


**Figure 1.** Comparison of the line strength results from MCDHF and MBPT methods for E1 transitions.

The MCDHF atomic wave functions are further used to calculate the electron impact excitation cross sections with our recently developed RDW code. The scattered and projectile electrons are assumed to be under the influence of the distortion potential that is taken as spherically symmetric static potential in the initial and final states of the ion. Further, our RDW code provides the flexibility to include the exchange and polarization effects as well as Breit interaction in the cross section calculations.

This work is supported by IAEA, Vienna under the IAEA Research Contract No. 26504.

### References

- [1] Fischer CF *et al* 2019 *Computer Physics Communications* **237** 184
- [2] Gu MF 2008 *Canadian Journal of Physics* **86** 675

\*E-mail: [lalita.sharma@ph.iitr.ac.in](mailto:lalita.sharma@ph.iitr.ac.in)



## Ionization cross section and plasma density effects

D Benredjem<sup>1\*</sup>, J.-C. Pain<sup>2,3†</sup>

<sup>1</sup>Université Paris-Saclay, CNRS, Laboratoire Aimé Cotton, rue Aimé Cotton, Orsay, 91405, France

<sup>2</sup>CEA, DAM, DIF, F-91297 Arpajon, France

<sup>3</sup>Université Paris-Saclay, CEA, Laboratoire Matière en Conditions Extrêmes, 91680 Bruyères-le-Châtel Cedex, France

**Synopsis** We propose an analytical expression of the electron-impact ionization cross section, involving a small set of adjustable parameters which are determined by fitting experimental data. The new formulation is well-suited to account for the plasma density effect known as Ionization Potential Depression. In the present work, we focus on C, N, O and Al ions.

The knowledge of the radiative properties in dense and hot plasmas requires accurate cross sections of the processes involving an ion and free electrons. In this work, we concentrate on the electron impact ionization (EII). As the modeling of such media involves large sets of radiative transitions (up to millions), the number of collisional radiative equations to be solved is huge. To handle such a system, one needs compact and accurate formulas for collisional cross sections in order to describe the population dynamics.

To study the ionization by free-electron impacts, we propose the following cross section formula:

$$\sigma(E) = A \frac{\ln(E/E_i)}{E/E_i} \times \sum_{l=0}^N \frac{B_l}{(E/E_i)^l},$$

where  $A$  and  $B_l$  are adjustable parameters,  $E$  the incident electron energy and  $E_i$  the ionization energy. The parameters are determined by a fit of measured or calculated cross sections. In the second case, we rely on codes such as FAC [1] or HULLAC [2]. The resulting cross section may then be used to obtain analytical expressions of the EII rate coefficient.

Plasma density effects [3], in particular the so-called Ionization Potential Depression (IPD), can modify the cross-section values as well as the energy threshold. An experiment at the Linac Coherent Light Source facility [4] reported, for aluminum ions, IPDs between 44 and 53 % of the ionization energies of the isolated ions. At such densities ( $\simeq 2.7 \text{ g/cm}^3$ ) the IPD affects significantly the cross sections.

\*E-mail: [djamel.benredjem@universite-paris-saclay.fr](mailto:djamel.benredjem@universite-paris-saclay.fr)

†E-mail: [jean-christophe.pain@cea.fr](mailto:jean-christophe.pain@cea.fr)

We present the EII cross sections of Be-like CNO ions (see Figure 1, nitrogen case). The adjustable parameters are determined by fitting experimental data [5]. The above formula then allows us

- to provide cross sections outside the experimental electron-energy range,
- to calculate analytically the rates and
- to account for the continuum lowering.

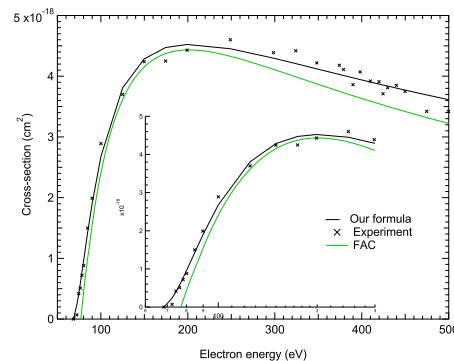


**Figure 1.** Be-like N as a function of the incident-electron energy. Experiment: [5], FAC: calculations with FAC code.

### References

- [1] Gu M F 2008 *Can. J. Phys.* **86** 675
- [2] Bar-Shalom A, Klapisch M and Oreg J 2001 *J. Quant. Spectrosc. Radiat. Transfer* **71** 109
- [3] Belkhiri M, Fontes C J and Poirier M 2015 *Phys. Rev. A* **92** 032501
- [4] Ciricosta O et al 2016 *Nat. Commun.* **7** 11713
- [5] Fogle M et al 2008 *Astrophys. J. Supp. Ser.* **175** 543



## $M\beta$ photon self-attenuation across the $M_5$ edge for elements with $70 \leq Z \leq 80$

S Segui<sup>1\*</sup>, S Limandri<sup>1</sup>, M Torres Deluigi<sup>2</sup>, C Montanari<sup>3</sup>, D Mitnik<sup>3</sup>, A Carreras<sup>1</sup>,  
G Castellano<sup>1</sup>, and J Trincavelli<sup>1</sup>

<sup>1</sup>Instituto de Física Enrique Gaviola, CONICET – FAMAF, Univ. Nacional de Córdoba, 5000, Argentina

<sup>2</sup>Instituto de Química de San Luis, CONICET – Univ. Nacional de San Luis, D5700HHW, Argentina

<sup>3</sup>Instituto de Astronomía y Física del Espacio, CONICET – Univ. de Buenos Aires, C1428ZAA, Argentina

**Synopsis** Significant inconsistencies arising in the description of electron-induced x-ray emission for  $70 < Z < 78$  suggest that tabulations of mass attenuation coefficients and binding energies from the literature should be updated. Experimental and theoretical approaches are combined to propose new values for these parameters.

X-ray attenuation in matter is involved in many areas ranging from radiation therapies to materials characterization by means of spectroscopical techniques. For elements with atomic number  $Z$  in the range  $70 < Z < 78$ , the literature reports that the  $M\beta$  emission energy ( $M_4N_6$  decay) slightly exceeds the  $M_5$  binding energy  $E_{M_5}$  [1], which implies a strong self-absorption of these characteristic x-rays when traversing the sample path towards the detector.

In a recent study [2], the description of the  $M\beta$  self-absorption in pure Re and Os targets has shown to depend critically on the  $E_{M_5}$  value, as well as on the mass absorption coefficient ( $\mu$ ) jump ratio across this edge. With this motivation, in the present work WDS pure spectra induced by 20 keV electrons have been acquired in an SEM to survey the bremsstrahlung absorption around the  $M_5$  edge. Figure 1 shows a Re spectrum along with two fitting curves using  $\mu$  values given in ref. [3] and considering different choices for  $E_{M_5}$ . Clearly, the predicted background contribution is not suitable when using the value reported in ref. [1]. A better spectral fitting is attained when the  $M_5$  edge is shifted around 26 eV towards higher energies.

Fully relativistic calculations implemented by using the HULLAC suite [4] have been performed for solving the many-electron Dirac equation, to provide an estimate for the configuration energy associated with  $M_5$  one-vacancy states. The obtained results are in good agreement with the experimental determination of  $E_{M_5}$  values.

On the other hand, experimental and simulated values of the  $M\beta/M\alpha$  intensity ratio, strongly dependent on  $\mu$ , show important dis-

\*E-mail: [silvina.segui@mi.unc.edu.ar](mailto:silvina.segui@mi.unc.edu.ar)

crepancies, evidencing an anomalous behavior. For instance, the experimental ratio from an EDS spectrum for Os bombarded with 28 keV electrons is 0.50, whereas the corresponding ratio obtained with Monte Carlo [5] under the same conditions is 0.28. A similar disagreement has been observed for other elements in the  $Z$  range considered. Since the database used by the simulation code involves  $E_{M_5}$  and  $\mu$  values, established in the literature, the observed discrepancy suggests that both magnitudes should be revised.

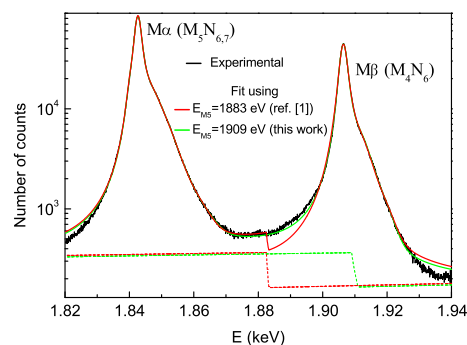


**Figure 1.** WDS X-ray spectrum for Re. Background contribution is shown with dashed lines.

### References

- [1] Bearden J 1967 *Rev. Mod. Phys.* **39** 78; Bearden J and Burr A 1967 *Rev. Mod. Phys.* **39** 125
- [2] Aguilar A *et al.* 2023 *J. Anal. At. Spectrom.* **38** 751
- [3] Chantler C 2000 *J. Phys. Chem. Ref. Data* **29** 597
- [4] Bar-Shalom A *et al.* 2001 *J. Quant. Spect. Rad. Transf.* **71** 169
- [5] Salvat F *et al.* *PENELOPE 2011 - A code system for Monte Carlo simulation of electron and photon transport.* Paris: OECD/NEA Data Bank

## Indirect ionization of the $\text{Mo}^{14+}$ ion in EBIT

C Q Wu<sup>1</sup>, X B Ding<sup>1,2\*</sup>, D H Zhang<sup>1,2</sup>, K Yao<sup>3,4</sup>, Y Yang<sup>3,4</sup>, Y Q Fu<sup>3,4</sup> and C Z Dong<sup>1,2</sup>

<sup>1</sup>Key Laboratory of Atomic and Molecular Physics Functional Materials of Gansu Province, College of Physics and Electronic Engineering, Northwest Normal University, Lanzhou 730070, China.

<sup>2</sup>Gansu International Scientific and Technological Cooperation Base of Laser Plasma Spectroscopy, Lanzhou 730070, China.

<sup>3</sup>Institute of Modern Physics, Department of Nuclear Science and Technology, Fudan University, Shanghai. 200433, China

<sup>4</sup>Key Laboratory of Nuclear Physics and Ion-Beam Application (MOE), Fudan University, Shanghai 200433, China.

**Synopsis** The spectra of the  $\text{Mo}^{15+}$  ions were observed experimentally at shanghai EBIT with electron beam energy lower than its first ionization energies. The energy level, cross section and radiation transition rates of  $\text{Mo}^{14+}$  and  $\text{Mo}^{15+}$  ions are calculated by using the configuration interaction method (RCI) based on FAC package. An appropriate collisional-radiative model is constructed to reveal the significant contribution from the indirect ionization of the metastable state of  $\text{Mo}^{14+}$  ion.

The long-lived metastable states have significant impact on the kinetic processes of astrophysics and laboratory plasma[1]. Not only are these long-lived metastable levels essential for an accurate comprehension of atomic structure and multipole decay processes, but they also make a significant contribution to the analysis of the spectrum, charge state distribution, and charge equilibrium of various plasmas.[2, 3].

Recently, we observed the M1 transition between the fine structure levels of the  $\text{Mo}^{15+}$  ion ground state  $3p^63d^9$  ( $^2D_{5/2}$ - $^2D_{3/2}$ ) in Shanghai-EBIT at lower electron beam energy ( $E_e=380$  eV), which lower than the ionization energy (IP=544.0 eV) of  $\text{Mo}^{14+}$  ion.

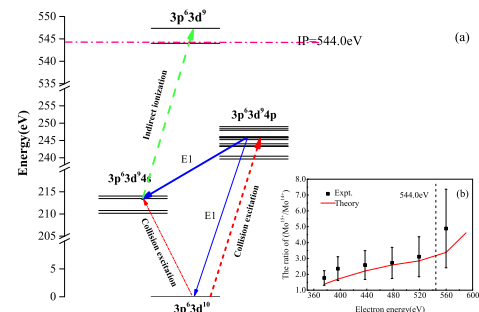
In this work, the energy levels, collision excitation and ionization cross sections as well as transition rates of  $\text{Mo}^{14+}$  and  $\text{Mo}^{15+}$  ions have been calculated using RCI method. The indirect ionization from the metastable state was included to show the significant contribution to the charge state distribution.

Fig.1 (a) shows the energy level structure with possible ionization, excitation, and decay channels of  $\text{Mo}^{14+}$  and  $\text{Mo}^{15+}$  ions. According to the calculation, the ground state of  $\text{Mo}^{14+}$  ions is collisional excited to the  $3d^94p$   $^1P_1$  state by electron, which then undergoes E1 decay to the metastable state  $3d^94s$   $^3D_1$ . Further, the  $^3D_1$  state was collisional ionized by the electron to produce the  $\text{Mo}^{15+}$  ions.

The charge state ratio of  $\text{Mo}^{15+}$  and  $\text{Mo}^{14+}$

\*E-mail: dingxb@nwnu.edu.cn

ions was also observed in the experiment. By considering various atomic processes of the above excitation and ionization channels, an appropriate CRM was constructed to analyze the dependence of the ratio of these two ions on the incident electron energy. Good agreement between the experiment and the theoretical results was obtained, as shown in Fig.1 (b).



**Figure 1.** (a) Energy level of  $\text{Mo}^{14+}$  and  $\text{Mo}^{15+}$  ion; (b) the ratio of the charge state distribution of  $\text{Mo}^{14+}$  and  $\text{Mo}^{15+}$  ions.

This work supported by the National Key R&D Program of China (2022YFA1602500) and the National Nature Science Foundation of China (12274352).

### References

- [1] Aušra Kyniene et al. 2019 *A&A*. **A14** 624
- [2] Q.Lu et al. 2019 *Phys.Rev.A* **99** 042510
- [3] B.Tu et al. 2017 *Phys.Rev.A* **96** 032705

## Theoretical investigation of KLL dielectronic-recombination processes of highly charged Cu ions

J. H. Deng<sup>1</sup>, S. B. Niu<sup>1</sup>, W. L. He<sup>1</sup>, Y. L. Ma<sup>1</sup>, L. Y. Xie<sup>1\*</sup>, and C. Z. Dong<sup>1</sup>

<sup>1</sup> Key Laboratory of Atomic and Molecular Physics and Functional Materials of Gansu Province, College of Physics and Electronic Engineering, Northwest Normal University, Lanzhou 730070, People's Republic of China

**Synopsis** The resonance energies, strengths and cross sections, as well as the degree of X-ray emissions associated with KLL dielectronic recombination processes of  $\text{Cu}^{28+}$ - $\text{Cu}^{24+}$  ions were calculated using the FAC code. The theoretical results of differential cross sections are in good agreement with EBIT measurements.

Dielectronic recombination (DR), which widely exists in high-temperature laboratory and astrophysical plasmas, plays an important role in determining the charge state distribution of highly charged ions and plasma radiation spectrum[1]. DR also provides resolved satellite lines that can be used for plasma temperature and density diagnostics. Exact knowledge of DR process is utilized to understand astrophysical observations and the atomic dynamics process.

Many experimental and theoretical researches focused on electron-ions recombination process of highly charged Cu ions[2-3]. For example, Zhang *et al.*[2] studied experimentally the KLn DR process of He-like Cu ions, cross sections of the DR experiments for He-like Cu ions are given. Gao *et al.*[3] calculated DR cross sections of  $\text{Cu}^{27+}$ - $\text{Cu}^{24+}$  ions and fitted the theoretical results to the EBIT experimental data, the distribution of  $\text{Cu}^{27+}$ - $\text{Cu}^{24+}$  ions in EBIT are obtained.

In this work, the KLL DR process of H-like to B-like Cu ions ( $\text{Cu}^{28+}$ - $\text{Cu}^{24+}$ ) are investigated. The resonance energies, strengths and cross sections are systematically calculated employing the relativistic FAC[4]. The degree of linear polarization of dielectronic satellite are calculated by using the density matrix formular[5]. The influence of Breit interactions on polarization properties of dielectronic satellite lines is studied. The calculated KLL DR spectra of Cu ions are compared with the EBIT experimental measurements[3], that shows an excellent agreement with the experimental results.

The work was supported by the National Key Research and Development Program of China (Grant Nos: 2022YFA1602500), the Natural Science Foundation of China (Grant Nos: 12064041, 11874051, 12104373), funds for Innovative Fundamental Research Group Project of Gansu Province (20JR5RA541)

\* E-mail: xiely@nwnu.edu.cn

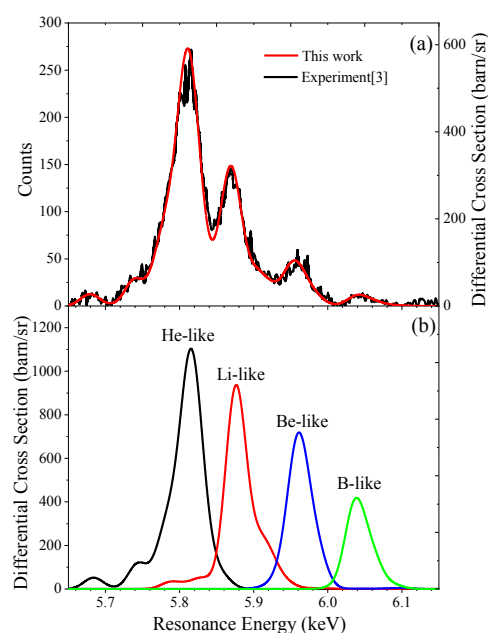


**Figure 1.** (a) The calculated KLL DR differential cross sections of  $\text{Cu}^{27+}$ - $\text{Cu}^{24+}$  ions in the ground states compared to the EBIT experimental measurements[3]. The characteristics of the He-, Li-, Be-, and B-like Cu ions in the spectrum are marked. The relative charge-state balance determined through the fitting process is He:Li:Be:B=52%:33%:14%:6%. (b) Theoretical differential cross sections of individual He-like to B-like Cu ions are displayed. The theoretical results are convolved with a Gaussian of FWHM 30 eV.

### References

- [1] M. E. Foord, S. H. Glenzer, et al. 2000 *Phys. Rev. Lett.* **85** 992
- [2] Zhang X M, Guo P L, et al. 2003 *Chin. Phys. Lett.* **20** 657
- [3] Y. H. Gao, X. M. Zhang, et al. 2008 *Chin. Phys. Lett.* **25** 930
- [4] M. F. Gu, *Can. J. Phys.* 2008 **86** 675
- [5] C. Shah, P. Amaro, et al. 2018 *APJS.* **234** 27

## Laser-assisted radiative attachment in short laser pulses

Deeksha Kanti<sup>1</sup>, J Z Kamiński<sup>1</sup>, Liang-You Peng<sup>2,3,4</sup> and K Krajewska<sup>1</sup>

<sup>1</sup>Institute of Theoretical Physics, Faculty of Physics, University of Warsaw, Pasteura 5, 02-093 Warsaw, Poland

<sup>2</sup>State Key Laboratory for Mesoscopic Physics and Frontiers Science Center for Nano-optoelectronics, School of Physics, Peking University, Beijing 100871, China

<sup>3</sup>Beijing Academy of Quantum Information Sciences, Beijing 100193, China

<sup>4</sup>Collaborative Innovation Center of Extreme Optics, Shanxi University, Taiyuan 030006, China

**Synopsis** We develop a comprehensive theoretical approach to treat laser-assisted radiative attachment (LARA) that accounts for the field-free and the field-modified processes. We observe coherent enhancement of the generated radiation spectra when the LARA occurs in the presence of a pulse train. By performing the time-frequency analysis of the LARA spectra, the temporal reconstruction of the accompanying laser field is possible.

Ability to generate intense and coherent light with controllable properties is one of the most inspiring achievements of recent years. Arguably, laser-assisted radiative attachment (LARA) lies at the heart of the development of nonlinear optics and laser technology. In light of this still ongoing progress, we analyze an electron-atom attachment accompanied by either an isolated laser pulse or a pulse train.

We formulate a comprehensive theoretical approach to describe LARA, which explicitly accounts for contributions from the field-free and the field-modified processes [1]. Moreover, in contrast to previous studies [2, 3], our theory prevents the appearance of unphysical oscillations in the LARA spectrum originating from the Gibbs effect [4, 5]. When accompanied by a train of identical pulses, we observe a coherent enhancement of the LARA energy spectra. This makes it possible to synthesize the LARA radiation into

short pulses. Another aspect of our investigations relates to temporal reconstruction of the accompanying laser field, which is based on the time-frequency analysis of the LARA radiation. As we argue, the method can be used for metrology of both isolated pulses and pulse trains; thus, proving its great versatility.

### References

- [1] Kanti D, Kamiński J Z, Peng L Y, and Krajewska K 2021 *Phys. Rev. A* **104** 033112
- [2] Bivona S, Burlon R, Ferrante G and Leone C 2006 *Opt. Express* **14** 3715
- [3] Bivona S, Burlon R, and Leone C 2007 *Laser Phys. Lett.* **4** 44
- [4] Jerri A J 1998 *The Gibbs Phenomenon in Fourier Analysis, Splines and Wavelet Approximations* (Springer, Dordrecht)
- [5] Duistermaat J J and Kolk J A C 2010 *Distributions - Theory and Applications* (Springer, New York)

## Positron annihilation spectra and binding energies for heterocyclic molecules

E Arthur-Baidoo\*, J R Danielson†, D R Witteman, S Ghosh, and C M Surko

Physics Department, University of California San Diego, La Jolla, CA 92093, USA

**Synopsis** Experimental measurements of positron annihilation rates and positron-molecule binding energies are reported for several heterocyclic molecules. Comparisons with other ring molecules will also be presented.

Studies have shown that positron-molecule annihilation below the positronium formation threshold often occurs via vibrational Feshbach resonances (VFRs) leading to enhanced annihilation rates [1]. The presence of VFRs yields a direct measure of the positron-molecule binding energy. To date, positron binding energies have been reported for several ring molecules and their derivatives, including benzene and its deuterated forms, using a high-resolution trap-based beam [2].

An in-depth understanding of low-energy positrons interactions with biological systems provides significant knowledge for diverse applications in medicine. For example, heterocyclic molecules are known for their role in medicinal chemistry and pharmaceutical products [3]. One example is pyridine ( $C_5H_5N$ ) - the simplest azine, where a single C-H group in benzene has been replaced by a nitrogen [4]. In this work, we report new measurements of positron annihilation spectra and binding energies for pyridine and other heterocyclic molecules using a trap-based positron beam with a total energy spread of <40 meV [5].

Figure 1 shows the annihilation spectrum of pyridine as a function of the mean parallel energy of the positron beam. The spectrum shows resonant features with the most prominent peaks in the range of 0.15 - 0.25 eV, associated with the high-energy dipole-allowed (DA) C-H stretch vibrational modes.

The resonant energies ( $\epsilon_r$ ) are downshifted from the vibrational mode frequencies ( $\hbar\omega$ ) by the binding energy,  $\epsilon_r = \hbar\omega - \epsilon_b$ . For pyridine, the measured binding energy  $\epsilon_b = 186$  meV, (cf. Figure 1). The observed  $\epsilon_b$  values are compared with those for benzene and recent measurements

for other heterocyclic molecules.

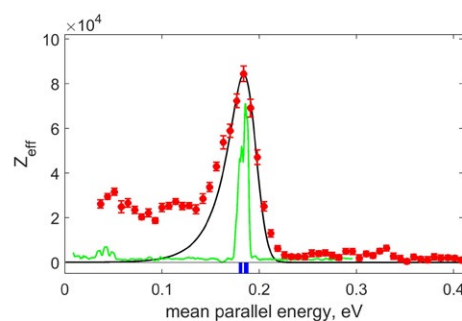


**Figure 1.** The positron annihilation spectrum of pyridine (solid red circles) as function of the mean parallel energy of the positron beam. The black curve is the VFR fit to the high-energy C-H modes. The green line is the downshifted infrared spectrum, and the vertical blue lines shows the locations of the downshifted DA modes.

The spectra of other heterocyclic molecules, including furan and cyclooctatetraene, will also be presented. The dependence of  $\epsilon_b$  on molecular properties, such as number of  $\pi$ -bonds, polarizability, and dipole moment, and open questions will be discussed.

This work is supported by the U. S. NSF, grant PHY-2010699.

### References

- [1] G. F. Gribakin, et al., 2010, *Rev. Mod. Phys.* **82**, 2557.
- [2] S. Ghosh, et al., 2022, *Phys. Rev. Lett.* **129**, 123401.
- [3] E. Kabir, and M. Uzzaman, 2022 *Results Chem.* **4**, 100606.
- [4] D. Stevens, et al., 2018, *J. Chem. Phys.* **148**, 144308.
- [5] M. R. Natisin, et al., 2016, *Phys. Plasmas* **23**, 023505.

\*E-mail: [earthurbaidoo@ucsd.edu](mailto:earthurbaidoo@ucsd.edu)

†E-mail: [jrdanielson@ucsd.edu](mailto:jrdanielson@ucsd.edu)

## Measurements of positron and electron scattering from biomolecules

D. Stevens<sup>1</sup>, Z. Cheong<sup>1</sup>, T. J. Babij<sup>1</sup>, J. Machacek<sup>1</sup> and J. P. Sullivan<sup>1\*</sup>

<sup>1</sup>Positron Research Group, Research School of Physics, Australian National University, Canberra ACT 2601, AUSTRALIA

**Synopsis** Using a Surko trap and beam system, measurements have been made of both positron and electron scattering for a range of targets, including biomolecules. This data is important for benchmarking theoretical calculations, which require a number of approximations to make the problem tractable. Absolute data from the experiment provides a stringent test for theoretical models, and can highlight areas that need improvement. Ultimately, the goal is to provide comprehensive data sets that can be used in advanced modelling of charged particle tracks and damage within living systems.

Since being developed in the 1990s, Surko traps have been used for a wide range of experiments in positron physics, ranging from scattering and annihilation experiments to antihydrogen production [1]. The techniques developed for measuring scattering using the magnetised beam are especially powerful, as they allow for the measurement of a wide range of quantitative cross sections, with relatively small absolute errors [2].

The technique relies on the emission of positrons from a <sup>22</sup>Na source, which emits via beta decay. Moderation of the positrons typically takes place using a solid rare gas moderator, resulting in a low energy beam that can be then trapped and cooled in a combined electric and magnetic field, relying on a buffer gas of N<sub>2</sub> and CF<sub>4</sub>. This produces a beam with an energy spread of 40 meV or better, which is suitable for low energy scattering measurements [3]. The moderation process also liberates a large number of secondary electrons, which can also be used as a primary source of charged particles for the trap system. Simply inverting the potentials used produces a comparable electron beam, allowing the same high precision measurements of electron and positron cross sections.

Our experimental program has taken advantage of this ability to measure scattering from biologically relevant molecules and compare to the latest theories. An example of one such comparison is shown in figure 1, for positron scattering from pyrazine at 3eV. Despite it being a relatively symmetric target, with no permanent dipole, there are large differences

between the theoretical calculations, and experiment does not agree well with any of them.

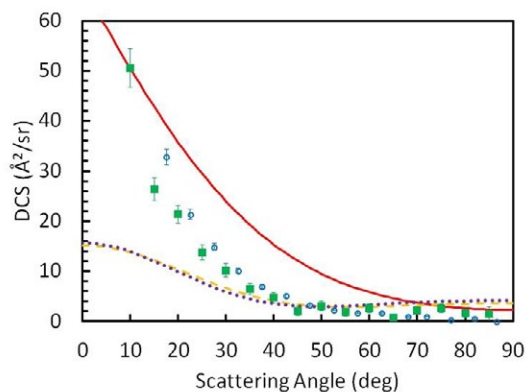


**Figure 1.** Electron scattering from pyrazine at an incident energy of 3eV [4]. Experimental data is compared to theoretical calculations, as well as a previous experiment. There are key points of disagreement between experiment and theory, even at this low energy.

This poster will present an overview of recent work in this area, along with a discussion of potential issues that lead to disagreement, along with plans for future work.

### References

- [1] J. R. Danielson et al., 2015 *Rev. Mod. Phys.* **87**, 247
- [2] J. P. Sullivan et al., 2002 *Phys. Rev. A* **66**, 042708
- [3] J. P. Sullivan et al., 2008 *Rev. Sci. Instr.* **79**, 113105
- [4] D. Edwards et al., 2021 *Phys. Rev. A* **104**, 042807

\* E-mail: [james.sullivan@anu.edu.au](mailto:james.sullivan@anu.edu.au)



## Quantum Monte Carlo study on positron binding to atomic anion dimers

S. Ito<sup>1</sup>, D. Yoshida<sup>2,1</sup>, Y. Kita<sup>1</sup>, T Shimazaki<sup>1</sup>, and M. Tachikawa<sup>1\*</sup>

<sup>1</sup>Graduate School of NanoBioScience, Yokohama City University, Yokohama 236-0027, Japan

<sup>2</sup>Nishina Center for Accelerator-Based Science, RIKEN, Wako 351-0198, Japan

**Synopsis** We have studied the positron ( $e^+$ ) interaction with unstable homonuclear anion dimer ( $X^-$ )<sub>2</sub> to form the positronic bound state of  $[X^-; e^+; X^-]$  ( $X = \text{H}$  and  $\text{Li}$ ) using the multi-component quantum Monte Carlo method. For the  $[\text{H}^-; e^+; \text{H}^-]$  system, we confirmed that the bound state is formed by the intermediate positron structure, called the “positronic covalent bonding”. Meanwhile, for  $[\text{Li}^-; e^+; \text{Li}^-]$ , we obtained that the bound state should have a different positronic bound state at the short internuclear distance. We resolved these different stabilities with the “positronium (complex between  $e^+$  and  $e^-$ ) binding abilities” of systems.

A Positron, which is the antimatter counterpart of the electron, exhibits rich and fascinating exotic matter chemistry with various atoms, molecules, and complexes. Recently, it was found that the positronic complex with ( $\text{H}^-$ )<sub>2</sub> can form the stable bound state concerning  $\text{H}^- + \text{PsH}$  by a positron intermediate bonding [1]. This bonding situation, which resembles the well-defined single covalent bond, was qualified as “positronic covalent bonding”. On the other hand, a similar binding mechanism may be possible for anion dimers of other one-valent (alkali) species such as lithium. In this study, we have investigated the stabilities of  $[X^-; e^+; X^-]$  homonuclear systems with  $X = \text{H}$  and  $\text{Li}$  using the quantum Monte Carlo method combined with the multi-component molecular orbital calculations.

Figure 1 shows the calculation results of potential energy curves (PECs) for  $[\text{Li}^-; e^+; \text{Li}^-]$  against the internuclear separation by the Hartree-Fock (HF), configuration interaction (CI), and fixed-node diffusion Monte Carlo (FN-DMC) methods. The results show that the system has a single energy minimum in all the PECs and its internuclear distance is drastically shortened by improving the accuracy of interparticle correlation effects. According to characteristics of the electron and positron densities, the energy minimum structure at the HF level appears like a positronic covalent bonding, whereas the compact structure predicted at the FN-DMC level may have strongly delocalized

characters of both one excess electron and a positron.

By evaluating PECs of both lower energy decays into  $\text{Ps} + \text{Li}_2^-$  and  $\text{Ps}^- + \text{Li}_2$ , we confirmed that the  $[\text{Li}^-; e^+; \text{Li}^-]$  system is locally stable with respect to these both thresholds. The analytical results suggest that the dominant structure is depicted as  $\text{Ps}$  binding to  $\text{Li}_2^-$  anion, which is different from the  $[\text{H}^-; e^+; \text{H}^-]$  case that has a locally stable structure at the long internuclear distance and an asymptotic dissociation into  $\text{H}^- + \text{PsH}$  on the PEC [1-3]. We will discuss the different stabilities between these substitutions with one-valent atoms in detail.

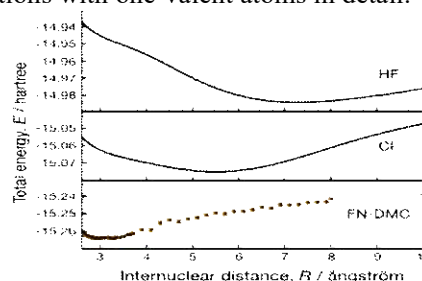


**Figure 1.** PECs against the internuclear separation for  $[\text{Li}^-; e^+; \text{Li}^-]$ .

### References

- [1] J. Charry, M. T. do N. Varela, and A. Reyes, *Angew. Chem. Int. Ed.* **57**, 8859 (2018).
- [2] S. Ito, D. Yoshida, Y. Kita, and M. Tachikawa, *J. Chem. Phys.* **157**, 224 (2020).
- [3] D. Bressanini, *J. Chem. Phys.* **154**, 224306 (2021).

\* E-mail: tachi@yokohama-cu.ac.jp

## Low-energy positronium scattering from O<sub>2</sub>

D M Newson<sup>1</sup>, R Kadokura<sup>1</sup>, H Allen<sup>1</sup>, S E Fayer<sup>1</sup>, S J Brawley<sup>1</sup>, M Shipman<sup>1</sup>, G Laricchia<sup>1</sup>, R S Wilde<sup>2</sup>, I I Fabrikant<sup>3\*</sup> and L Sarkadi<sup>4</sup>

<sup>1</sup>UCL Department of Physics and Astronomy, Gower Street, London, WC1E 6BT, UK

<sup>2</sup>Department of Natural Sciences, Oregon Institute of Technology, Klamath Falls, Oregon 97601, USA

<sup>3</sup>Department of Physics and Astronomy, University of Nebraska, Lincoln, Nebraska 68588, USA

<sup>4</sup>ATOMKI, Institute for Nuclear Research, H-4026 Debrecen, Bem ter 18/c, Hungary

**Synopsis** Cross sections for Ps-O<sub>2</sub> collisions have been measured and calculated using a quantal free-electron-gas model and classical-trajectory Monte Carlo method. Comparisons are made with earlier calculations and discussed in terms of both experimental and theoretical uncertainties.

The total cross section of Ps scattering from a wide variety of atoms and molecules has been observed to be similar to that of equivalent electrons [1], even in the vicinity of delicate quantum mechanical effects, such as resonances in CO<sub>2</sub> and N<sub>2</sub> [2, 3]. However, the similarity has been predicted usually to disappear in the low-energy region, although the size of this region depends on the target. In the present study [4], measurements of the Ps-O<sub>2</sub> total scattering cross-section have been extended to below the Ps break-up threshold to investigate possible deviations from electron-like behaviour [1] and explore the recent prediction of resonant peaks at approximately 2 eV and 4 eV [5]. Theoretical results were obtained by employing the free-electron-gas (FEG) model for electron exchange and correlations in Ps collisions with neutral targets [6].

Figure 1 compares experimental total Ps-O<sub>2</sub> cross sections with the sum of the cross sections for elastic scattering and Ps break-up, the dominant inelastic channel, calculated in Ref. [5] using the FEG model and the binary encounter (BE) approximation, respectively. The FEG approach has been also refined by including the contribution of higher partial waves and, in addition, the interference term correction to the correlation energy. The experimental results are seen to be broadly consistent with the trend of the underlying (non-resonant) theoretical cross-section, although systematically smaller below 30 eV. Discrepancies are discussed in terms of both experimental and theoretical uncertainties.

Ps break-up and O<sub>2</sub><sup>-</sup> formation cross-sections have also been calculated by the classical tra-

jectory Monte Carlo (CTMC) method. The obtained results exceed the BE cross-sections by a factor 2-3 above 10 eV. This is consistent with those for the CTMC cross-sections for Ps break-up by He. Thus it may be concluded that the present disagreement between BE and CTMC reflects quantum effects in  $e^-$ -O<sub>2</sub> and  $e^+$ -O<sub>2</sub> scattering.

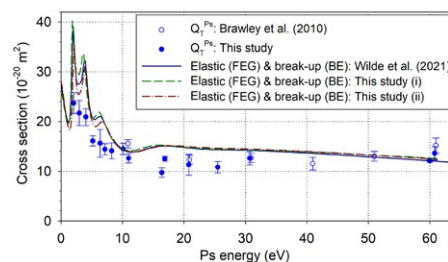


**Figure 1.** Experimental Ps-O<sub>2</sub> total cross-sections [4] alongside the sum of the theoretical elastic scattering (FEG) and break-up (BE) cross-sections as presented by Wilde et al. [5] and with the present improvement as described in the text.

### References

- [1] Brawley S J *et al.* 2010 *Science* **330** 789
- [2] Brawley S J, Williams A I, Shipman M, and Laricchia G 2010 *Phys. Rev. Lett.* **105** 263401
- [3] Wilde R S and Fabrikant I I 2018 *Phys. Rev. A* **97** 052708
- [4] Newson D M *et al.* 2023 *Phys. Rev. A* **107** 022809
- [5] Wilde R S, Ambalampitiya H B and Fabrikant I I 2021 *Phys. Rev. A* **104** 012810
- [6] Fabrikant I I and Wilde R S 2018 *Phys. Rev. A* **97** 052707

\*E-mail: ifabrikant@unl.edu

## Production of $O_2^+$ following the double ionization of $CO_2$

A B Monteiro-Carvalho<sup>1\*</sup>, L Sigaud<sup>1†</sup> and E C Montenegro<sup>2</sup>

<sup>1</sup>Instituto de Física, Universidade Federal Fluminense, Niterói, 24210-346, Brazil

<sup>2</sup>Instituto de Física, Universidade Federal do Rio de Janeiro, Rio de Janeiro, 21941-909, Brazil

**Synopsis** Although  $CO_2$  ionization and fragmentation have been the object of many studies, so far the production of  $O_2^+$  had not been reported. In this work, absolute cross sections for the production of  $O_2^+$  following ionization of  $CO_2$  by electron impact is reported for the first time. We guarantee that the  $O_2^+$  is produced by the  $CO_2$  fragmentation by measuring its kinetic energy distribution with the DETOF technique.

The removal of one or more electrons from molecules opens up a myriad of post-collisional pathways for the system, either through stabilization or fragmentation. Furthermore, when a molecule is ionized, it is usually taken, along the Franck-Condon region, to an excited vibrational state of the new electronic configuration. This creates the possibility for new bonds to be formed between nuclei that were not originally bound to one another in the parent molecule. One such example is the well-known pathways leading to the formation of (vibrationally excited)  $H_2$  in the fragmentation of the water molecule [1].

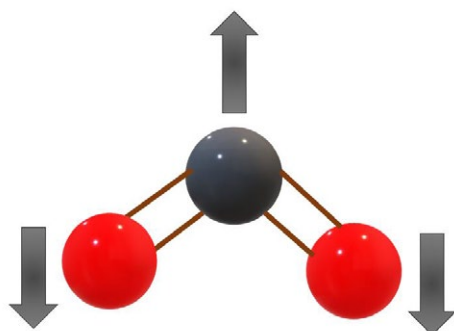


**Figure 1.** Illustration of the bending vibrational mode of the  $CO_2$  molecule that leads, after the removal of two electrons, to the  $C^+ + O_2^+$  fragments formation. Black and red represent the carbon and oxygen nuclei, respectively.

On the other hand, such a pathway has never been reported for carbon dioxide so far [2,3]. Differently from water, where the hydrogen nuclei stand at a  $\sim 104^\circ$  angle with respect to the oxygen nucleus in the fundamental state of the molecule, carbon dioxide presents a linear structure. Nevertheless, there are well-known vibrational states of the molecule [4], including stretching and bending modes (see figure 1). In addition,

the removal of more than one electron from a molecule has been shown to produce strong geometrical rearrangements in more complex compounds such as benzene [5], making it reasonable to expect that it can lead to moieties containing elements not originally bound.

The breakup of the  $CO_2$  following ionization was studied by means of a pulsed electron gun in the 30 to 800 eV energy range, a gas cell with monitored pressure and a time-of-flight mass spectrometer. Along with all other known ionic fragments coming from  $CO_2$  ionization [2,3], we report here the observation of the  $O_2^+$  ion. The DETOF technique, which allows one to determine the kinetic energy distributions presents for each produced fragment [5], was employed to ascertain that the detected  $O_2^+$  did not come from air contamination – if its parent molecule were  $O_2$ , then the resulting ion would have a Maxwell-Boltzmann thermal distribution, since it wouldn't have come from fragmentation and therefore would not acquire velocity, which happens in the breakup process. That was not the case here – the observed  $O_2^+$  has a kinetic energy distribution centered at 1.4 eV for all measured impact energies above 40 eV.

### References

- [1] Chang Y, An F, Chen Z *et al.* 2021 *Nature Comm.* **12** 6303
- [2] Tian Cechan and Vidal C R 1998 *J. Chem. Phys.* **108** 927
- [3] McConkey J W, Malone C P, Johnson P V, Winstead C, McKoy V and Kanik I 2008 *Phys. Rep.* **466** 1
- [4] Armenise I and Kustova E 2018 *J. Phys. Chem. A* **122** 8709
- [5] Sigaud L, Wolff W and Montenegro E C 2022 *Phys. Rev. A* **105** 032816

\* E-mail: [anabeatrizcarvalho@id.uff.br](mailto:anabeatrizcarvalho@id.uff.br)

† E-mail: [lsigaud@id.uff.br](mailto:lsigaud@id.uff.br)

## Observation of ultrafast proton and energy transfer in hydrated pyrrole dimers induced by electron impact

J Zhou, S Jia, X Xue, X Hao, Q Zeng, X. Ren \*

MOE Key Laboratory for Nonequilibrium Synthesis and Modulation of Condensed Matter, School of Physics, Xi'an Jiaotong University, Xi'an 710049, China

**Synopsis** Primary processes in hydrogen-bonded networks triggered by electronic ionization play a fundamental role in radiation chemistry and biology. The intermolecular proton and energy transfer processes of hydrated pyrrole dimers can potentially be initiated via a number of competing relaxation channels. By determining the fragmentation ions coincident momentum spectroscopy and the *ab initio* molecular dynamics (AIMD) simulations, the underlying ionization and subsequent fragmentation mechanisms are expected to be revealed.

The radiolysis of hydrated biomolecules is of great importance to a range of chemical and biological processes. The biomolecules can be excited or even ionized when they are exposed to ionizing radiation and the excited molecules are often unstable tending to dissociate. The presence of weakly bound neighbors, such as water, may substantially reduce the probability for fragmentation of the initially ionized molecules, which can manifest as a protective effect in biomatter. However, the mechanisms of electronic relaxation in hydrated molecules remain, to a large extent, unexplored due to the complex hydrogen bonding networks in these systems.

Recently, we studied the double ionization and fragmentation dynamics of hydrated pyrrole dimer by electron-impact ionization (200 eV). The experiments were performed using a reaction microscope [1], where the two resulting cations from the double ionization of H<sub>2</sub>O-C<sub>4</sub>H<sub>5</sub>N dimer are detected in coincidence and their three-dimensional momentum vectors are determined. The heterocyclic aromatic molecule pyrrole is selected as the prototype since it is an important building block of large biological molecules. The electron-initiated processes were recognized as crucial for understanding an essential part of fundamental science from planetary atmospheres to biological radiation damage.

In the experiment, the sequential ionization (SI), intermolecular Coulombic decay (ICD),

and electron transfer-mediated decay (ETMD) will lead to the dissociation channel H<sub>2</sub>O<sup>+</sup>+C<sub>4</sub>H<sub>5</sub>N<sup>+</sup>. For SI, the projectile electron successively kicks out one outer-valence electron from H<sub>2</sub>O and C<sub>4</sub>H<sub>5</sub>N. The ICD can be initiated with the removal of a carbon 2s (C2s) or an oxygen 2s (O2s) inner-valence electron. Afterward, an electron from the outer-valence shell of C<sub>4</sub>H<sub>5</sub>N<sup>+</sup> or H<sub>2</sub>O<sup>+</sup> fills the inner-valence vacancy, and the energy released ionizes the neighboring molecule [2]. The C2s<sup>-1</sup> and O2s<sup>-1</sup> state can also decay through the ETMD, where an electron from the neighboring molecule fills the initial vacancy causing the emission of another electron of the initial ionized unit [3]. While the localized double ionization of the complexes may cause the intermolecular proton transfer from the initial ionized unit to the neutral neighbor forming, e.g. the H<sub>3</sub>O<sup>+</sup>+C<sub>4</sub>H<sub>4</sub>N<sup>+</sup> or HO<sup>+</sup>+C<sub>4</sub>H<sub>6</sub>N<sup>+</sup> channels.

The competition between these local and nonlocal decay mechanisms, as well as the follow-up ultrafast dynamics is expected to be revealed by our further experiments and *ab initio* molecular dynamics calculations. Details about these results will be presented at the conference.

### References

- [1] X Ren et al. 2016 *Nat. Commun.* **7** 11093.
- [2] L Cederbaum et al. 2022 *Phys. Rev. Lett.* **79** 4778.
- [3] J Zobeley et al. 2001 *J. Chem. Phys.* **115** 5076.

\* E-mail: renxueguang@xjtu.edu.cn

## Development of atomic momentum spectroscopy of polyatomic molecules

S Kanaya<sup>1\*</sup>, Y Onitsuka<sup>1</sup>, N Watanabe<sup>1</sup>, H Kono<sup>2</sup>, and M Takahashi<sup>1†</sup>

<sup>1</sup> Institute of Multidisciplinary Research for Advanced Materials, Tohoku University, Sendai 980-8577, Japan

<sup>2</sup> Department of Chemistry, Graduate school of Science, Tohoku University, Sendai 980-8578, Japan

**Synopsis** We have developed atomic momentum spectroscopy (AMS) of polyatomic molecules. Experimentally, electron-atom Compton profiles due to the intramolecular motions of each atom with different masses have been obtained for the CH<sub>4</sub> molecule. Theoretically, a quantum chemistry-based AMS theory for polyatomic molecules has been formulated, which is accurate enough to help AMS experiments in design, data analysis and interpretation. We show AMS can now be used as a molecular spectroscopy technique not only for diatomic molecules but also for polyatomic molecules.

Intramolecular atomic motion has long been attracting a great deal of interest, as it often governs the reactivity and functionality of the molecule in question. In order to have an experimental technique to directly observe such intramolecular atomic motions, atomic momentum spectroscopy (AMS) measurements were proposed in 2001 [1]. Indeed, the proposal has recently been embodied by a series of attempts, involving developments of a multi-channel apparatus [2], a quantum chemistry-based AMS theory for diatomic molecules [3] and a data-analysis protocol to disentangle the experimental response of the intramolecular atomic motion from other related effects [3-5], and clarification of the large momentum transfer limit to use the feature of electron-atom Compton scattering [4]. Nevertheless, one may recognize AMS as a molecular spectroscopy under development. This is because AMS application is restricted only to diatomic molecules. The reason behind this situation is the lack of AMS theory for polyatomic molecules.

Under the above-mentioned circumstances, we have developed a quantum chemistry-based AMS theory for polyatomic molecules. Its validity has been tested and confirmed by comparison with AMS experiments on the CH<sub>4</sub> molecule, conducted at a scattering angle of 135° and at an incident electron energy of 2.0 keV.

As an example of the results, an experimental electron energy loss (EEL) spectrum of CH<sub>4</sub> is presented in Figure 1, in which two bands appear at around 0.3 and 3.7 eV. The former band is assigned to the C atom and the latter is to the H atom. Also included in this figure is a calculated EEL spectrum, generated by

using the AMS theory for polyatomic molecules. It is evident that the theoretical spectrum reproduces well the experimental one, demonstrating the validity and reliability of the theory. Furthermore, the agreement between experiment and theory in relative intensity of the C- and H-atom bands indicates another ability of AMS to perform elemental composition analysis of a polyatomic molecule. In the talk, we will discuss details of the present work and the possibility of AMS application to solid surfaces.

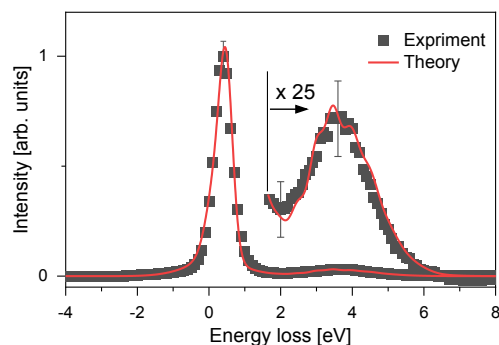


**Figure 1.** Comparison of experimental and theoretical electron energy loss spectra of CH<sub>4</sub>.

### References

- [1] Vos M, 2001 *Phys. Rev. A* **65** 012703
- [2] Yamazaki M, Hosono M, Tang Y, and Takahashi M 2017 *Rev. Sci. Instrum.* **88** 063103
- [3] Tachibana Y, Onitsuka Y, Kono H and Takahashi M, 2022 *Phys. Rev. A* **105** 052813
- [4] Onitsuka Y, Tachibana Y and Takahashi M, 2022 *Phys. Chem. Chem. Phys.* **24** 19716
- [5] Tachibana Y, Onitsuka Y, Kanaya S, Kono H and Takahashi M, 2023 *Phys. Chem. Chem. Phys.* **25** 6653

\* E-mail: [satoru.kanaya.r1@dc.tohoku.ac.jp](mailto:satoru.kanaya.r1@dc.tohoku.ac.jp)

† E-mail: [masahiko@tohoku.ac.jp](mailto:masahiko@tohoku.ac.jp)



## Development of a new molecular spectroscopy technique: mapping atomic motions and elemental composition analysis of a molecule

Y Onitsuka<sup>1\*</sup>, Y Tachibana<sup>1</sup>, S Kanaya<sup>1</sup>, H Kono<sup>2</sup>, and M Takahashi<sup>1†</sup>

<sup>1</sup> Institute of Multidisciplinary Research for Advanced Materials, Tohoku University, Sendai 980-8577, Japan

<sup>2</sup> Department of Chemistry, Graduate school of Science, Tohoku University, Sendai 980-8578, Japan

**Synopsis** It is known that an electron-atom Compton scattering experiment, often called atomic momentum spectroscopy (AMS), has the two potential abilities: one is to map intramolecular atomic motion, and another is to perform elemental composition analysis. In order to promote molecular science with AMS, we have recently embodied the two abilities by an AMS study on HD, based on our earlier work. Experimental momentum distributions of the H and D atoms in HD are shown to be identical with each other both in shape and intensity, as well as with quantum chemistry-based calculations.

Understanding of intramolecular atomic motions is one of essential approaches in molecular science. Laser vibrational spectroscopy, which has widely been employed, measures accurate frequencies of molecular vibration, but not the atomic motion itself. In order to have an experimental technique to directly observe such intramolecular atomic motions, electron-atom Compton scattering experiments or atomic momentum spectroscopy (AMS) were proposed in 2001 [1]. The AMS cross section is related to the momentum distribution  $\rho_j(P_j)$  of a scattering atom  $j$ , with the mass  $M_j$ , the momentum  $P_j$ , and the nuclear charge  $Z_j$ , in a target molecule as:

$$\frac{d^2\sigma}{d\Omega dE} \propto \sum_j Z_j^2 \int_{-\infty}^{+\infty} dP_j \rho_j(P_j) \delta\left(E_{\text{loss}} - \frac{q^2}{2M_j} - \frac{\mathbf{P}_j \cdot \mathbf{q}}{M_j}\right),$$

where  $E_{\text{loss}}$  and  $q$  denote the electron energy loss and the momentum transfer, respectively. AMS is thus expected to have two potential abilities: one is to map intramolecular atomic motion, and another is to perform elemental composition analysis. Based on our earlier attempts [2-4] such as development of a quantum chemistry-based AMS theory for diatomic molecules [3], we have recently embodied both the two abilities through the present work on HD [5].

The experiment on HD was conducted at a scattering angle of 135° and at incident electron energy of 2.0 keV using our AMS apparatus [2]. Briefly, electron backscattering occurred where the incident electron beam collided with a HD molecule in a gas beam. The energy loss was measured. Intramolecular momentum distributions of the H and D atoms were extracted from

the measured energy loss spectrum by using our data-analysis protocol [3].

Figure 1 shows an example of the results, which is the measured intramolecular momentum distributions of the H and D atoms in HD. They are indistinguishable from each other both in shape and in intensity. Furthermore, it is seen that they are in a good agreement with quantum chemistry-based calculations. These observations demonstrate that the two abilities of AMS have certainly been embodied.

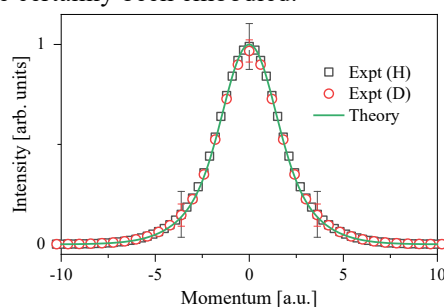


**Figure 1.** Comparison of momentum distributions of the H and D atoms in HD between experiment and quantum chemistry-based calculations.

### References

- [1] Vos M 2001 *Phys. Rev. A* **65** 012703
- [2] Yamazaki M, Hosono M, Tang Y, and Takahashi M 2017 *Rev. Sci. Instrum.* **88** 063103
- [3] Tachibana Y, Onitsuka Y, Kono H and Takahashi M, 2022 *Phys. Rev. A* **105** 052813
- [4] Onitsuka Y, Tachibana Y and Takahashi M, 2022 *Phys. Chem. Chem. Phys.* **24** 19716
- [5] Tachibana Y, Onitsuka Y, Kanaya S, Kono H and Takahashi M, 2023 *Phys. Chem. Chem. Phys.* **25** 6653

\* E-mail: [yuuki.onitsuka.e8@tohoku.ac.jp](mailto:yuuki.onitsuka.e8@tohoku.ac.jp)

† E-mail: [masahiko.takahashi.c4@tohoku.ac.jp](mailto:masahiko.takahashi.c4@tohoku.ac.jp)



## Velocity slice imaging probed for kinematically complete measurements of dissociative electron attachment to OCS molecule

N Kundu<sup>1</sup>, V Kumar<sup>1</sup> and D Nandi<sup>1,2\*</sup>

<sup>1</sup>Indian Institute of Science Education and Research Kolkata, Mohanpur, 741246, India

<sup>2</sup>Center for Atomic, Molecular and Optical Sciences and Technologies, Joint initiative of IIT Tirupati and IISER Tirupati, Tirupati, 517619, India

**Synopsis** Kinematically complete measurements of dissociative electron attachment (DEA) to gas-phase carbonyl sulfide (OCS) have been probed using well-established velocity slice imaging technique. The formation of both S<sup>-</sup> & O<sup>-</sup> are observed and S<sup>-</sup> being the dominant channel. Three well-resolved DEA resonances are observed for the formation of S<sup>-</sup>. Kinetic energy and angular distribution of S<sup>-</sup> ions at each resonances provide detailed dynamics involved in the DEA process.

The dissociative electron attachment (DEA) process is attributed fundamental importance in recent times, ranging from DNA damage to molecular cluster formation. We experimentally probe the dynamics for the formation of negative ion(s) arising from DEA to OCS molecule using velocity map imaging (VMI) spectrometer and obtained interesting results. Carbonyl sulfide (OCS) is most abundant sulfur-containing gaseous linear triatomic OCS molecule, observed in Venusian atmosphere, volcanic plumes, archean atmosphere, Orion hot core and dense molecular clouds beyond the solar system. It primarily acts as a coupling catalyst for the production of peptides from amino acids, promoting the molecule to an astrobiological significance.

Using time-of-flight (ToF) mass spectroscopy, Iga *et al.* [1] studied DEA resonances for S<sup>-</sup>/OCS and obtained the resonances at 1.4, 4.7, 7.0 and 10.2 eV incident electron energies. They also reported <sup>2</sup>Δ shape resonance for both the 4.7 and 10.2 eV resonances and proposed a rovibronic structure for high-speed S<sup>-</sup> anionic fragments at 7.0 eV resonance. Abouaf *et al.* [2] reported a fine structure in the DEA cross-section of S<sup>-</sup>/OCS at 1.4 eV resonance. Applying VMI with time-gated parallel slicing to S<sup>-</sup>/OCS, Li *et al.* [3] outlined three different dissociating kinetic energy bands. For the detailed systematic analysis of kinetic energy and angular distribution of the fragment S<sup>-</sup> ions, we employed conical time-gated velocity slice imaging

technique and obtained kinematically complete molecular dynamic informations.

We probed all the resonances above 4 eV and observed three distinct kinetic energy bands with distinct angular distributions. A vibronic intensity borrowing is observed in DEA for the first time for the formation of S<sup>-</sup> from OCS as evident from the figure 1. This observations can be explained using the theory of Condon approximated Herzberg-Teller vibronic coupling. The angular distribution analysis reveals the partial correlation among three-point group symmetries, possibly due to violation of axial recoil approximation during TNI's bending dissociation.

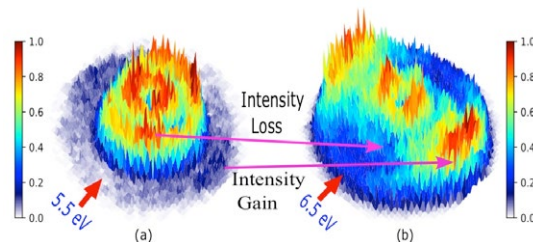


**Figure 1.** The velocity slice images of S<sup>-</sup>/OCS taken at (a) 5.5 eV and (b) 6.5 eV resonances, respectively. Red arrow shows the direction of electron beam.

### References

- [1] Iga I *et al.* 1996 *Int. J. Mass. Spec. Ion Proc.* **155** 99
- [2] Abouaf R and Fiquet-Fayard F 1976 *J. Phys. B* **9** L323
- [3] Li M *et al.* 2016 *Int. J. Mass. Spec.* **404** 20

\* E-mail: [dhananjay@iiserkol.ac.in](mailto:dhananjay@iiserkol.ac.in)

## Fragmentation dynamics of $\text{BrCN}^{q+}$ ( $q = 2-6$ ) induced by 1-keV electron impact

Wenchao Zhao, Enliang Wang\*, Lei Chen, Xu Shan† and Xiangjun Chen

Department of Modern Physics, University of Science and Technology of China, Hefei 230026, China

**Synopsis** We report the fragmentation dynamics of  $\text{BrCN}$  molecule induced by 1-keV electron impact. Six two-body and eleven three-body dissociation channels were identified. The concerted and sequential fragmentation mechanisms for three-body dissociation channels were investigated.

Fragmentation dynamics of multiply charged polyatomic molecules have captured continuous interest in the past decades[1-4]. It was found that the chemical bonds of highly charged polyatomic molecules break through nonsequential or sequential processes. The identification and elucidation of the fragmentation processes of polyatomic molecules are important for the understanding of multibody quantum correlation dynamics. One of major tasks in this field is to identify the dissociation process and to understand its mechanism.

In this work, the fragmentation dynamics of the  $\text{BrCN}^{q+}$  ( $q = 2-6$ ) induced by 1-keV electrons were studied by employing an ion momentum imaging spectrometer. Six two-body and eleven three-body fragmentation channels were identified and analyzed. The corresponding kinetic energy release (KER) distributions were obtained and compared with the predictions by the Coulomb explosion model. By means of the Dalitz plot, Newton diagram, and native frame method, we have studied the fragmentation mechanisms for three-body fragmentation channels. The sequential fragmentation processes were observed in the following channels:  $\text{BrCN}^{3+} \rightarrow \text{N}^+ + \text{BrC}^{2+} \rightarrow \text{Br}^+ + \text{C}^+ + \text{N}^+$ , and  $\text{BrCN}^{p+} \rightarrow \text{Br}^{l+} + \text{CN}^{2+} \rightarrow \text{Br}^{l+} + \text{C}^+ + \text{N}^+$  ( $p = l + 2$  and  $l = 1-3$ ). The KER for the intermediate dications, i.e.  $\text{BrC}^{2+}$  and  $\text{CN}^{2+}$  from the sequential mechanism, were determined and the electronic states of the intermediate molecular ion  $\text{CN}^{2+}$  were discussed. For the channels leading to higher charge states of the light elements, only the concerted fragmentation mechanism was observed. For the concerted fragmentation

of all the three-body fragmentation channels, the experimental KERs are lower than the predictions by the Coulomb explosion model. The reason may be ascribed to the ultrafast dissociation and electron transfer at the very beginning of the dissociation which results in a prolonged internuclear distance compared to the equilibrium geometry.

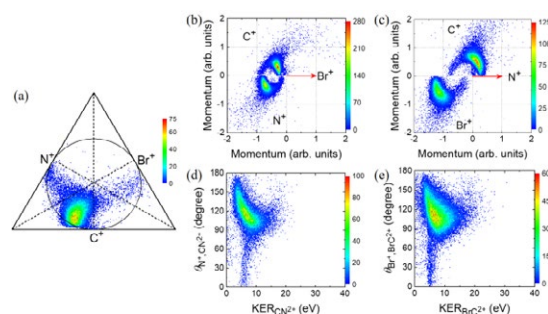


**Figure 1.** Experimental results for channel  $\text{Br}^+ + \text{C}^+ + \text{N}^+$ . (a) Dalitz plot, (b) and (c) Newton diagrams with  $\text{Br}^+$  and  $\text{N}^+$  as references, respectively. (d) Native frame plot assuming sequential breakup of  $\text{BrCN}^{3+}$  with  $\text{CN}^{2+}$  as the molecular intermediate. (e) Native frame plot assuming sequential breakup of  $\text{BrCN}^{3+}$  with  $\text{BrC}^{2+}$  as the molecular intermediate.

### References

- [1] Neumann *et al.*, Phys Rev Lett, **104**, 103201 (2010).
- [2] Wu *et al.*, Phys Rev Lett, **110**, 103601 (2013).
- [3] Wang *et al.*, Phys Rev A, **91**, 052711 (2015).
- [4] Shen *et al.*, J Chem Phys, **145**, 234303 (2016).

\* E-mail: [elwang@ustc.edu.cn](mailto:elwang@ustc.edu.cn)

† E-mail: [xshan@ustc.edu.cn](mailto:xshan@ustc.edu.cn)

## Elastic scattering and rotational excitation of H<sub>2</sub> by electron impact: Convergent close-coupling calculations

L H Scarlett<sup>1\*</sup>, U S Rehill<sup>1</sup>, M C Zammit<sup>2</sup>, N A Mori<sup>1</sup>, I Bray<sup>1</sup>, and D V Fursa<sup>1</sup>

<sup>1</sup>Department of Physics and Astronomy, Curtin University, Perth, Western Australia 6102, Australia

<sup>2</sup>Theoretical Division, Los Alamos National Laboratory, Los Alamos, New Mexico 87545, USA

**Synopsis** We apply the adiabatic-nuclei molecular convergent close-coupling (MCCC) method to the calculation of elastic scattering and rotational excitation of H<sub>2</sub> by 0.01–20 eV electrons. Integral cross sections are presented for all rotational transitions with  $|\Delta N| \leq 2$  and  $N_i = 0-31$  within the  $v = 0$  vibrational level, and differential cross sections for a selection of transitions.

The problem of low-energy electron-impact rotational excitation of H<sub>2</sub> has been studied in great detail over the last 60 years, due to its importance in low-temperature hydrogen plasmas and gasses. Below 10 eV, rotational excitation comprises up to 20% of the total cross section, and below the  $v = 0 \rightarrow 1$  threshold ( $\approx 0.5$  eV) it is the dominant contribution to electron energy loss. Accurate cross sections for the rotational transitions of H<sub>2</sub> are vital for modelling the emission spectra of astrophysical clouds, or for constructing collisional-radiative (CR) models of fusion-relevant plasmas. Up to 0.5 eV, the  $N = 0 \rightarrow 2$  and  $1 \rightarrow 3$  rotational excitation cross sections are well-known, with good agreement between the results of electron swarm experiments, which are reproduced by several calculations. At higher energies, however, the situation is less ideal, with substantial disagreement between various measurements and calculations.

The theoretical techniques applied to this problem in the past have utilised a variety of approximations to the treatment of coupling between rovibrational levels, from the adiabatic-nuclei (AN) approximation in which the coupling is neglected, to the most accurate rovibrational close-coupling approach. However, the common factor in all previous studies is the use of model potentials in place of coupling to the closed electronically-inelastic channels. The various choices of potential can lead to differences in the calculated cross sections far more significant than the errors introduced by the AN approximation, particularly since the greatest discrepancies are at energies more than 10 times the threshold energy, where the AN approximation is accurate. What is missing from the literature are theoretical studies of low-energy rotational excitation in which the coupling to closed electronic channels is accounted for rigorously. Within the AN approximation this is feasible provided one can solve

\*E-mail: [liam.scarlett@protonmail.com](mailto:liam.scarlett@protonmail.com)

the electronic scattering problem accurately. Here we apply the molecular convergent close-coupling (MCCC) method, which in recent years has been shown to completely solve the electronic scattering problem for H<sub>2</sub> [1]. The results presented here are available online [2].

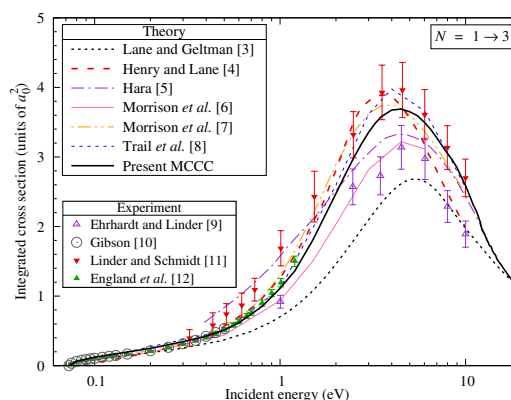


**Figure 1.** Integrated cross section for the  $N = 1 \rightarrow 3$  transition. Comparison is made with the available calculations [3, 5, 4, 6, 7, 8] and measurements [9, 10, 11, 12].

### References

- [1] Zammit *et al.* 2016 *Phys. Rev. Lett* **116** 233201
- [2] [mccc-db.org](http://mccc-db.org)
- [3] Lane N F and Geltman S 1967 *Phys. Rev.* **160** 53
- [4] Henry R J W and Lane N F 1969 *Phys. Rev.* **183** 221
- [5] Hara S 1969 *J. Phys. Soc. Japan* **27** 1592
- [6] Morrison M A *et al.* 1984 *Phys. Rev. A* **29** 2518
- [7] Morrison M A *et al.* 1987 *Aust. J. Phys.* **40** 239
- [8] Trail W K *et al.* 1990 *Phys. Rev. A* **41** 4868
- [9] Ehrhardt H and Linder F 1968 *Phys. Rev. Lett.* **21** 419
- [10] Gibson D K 1970 *Aust. J. Phys.* **23** 683
- [11] Linder F and Schmidt H 1971 *Zeitschrift für Naturforschung* **26** 1603
- [12] England J P *et al.* 1988 *Aust. J. Phys.* **41** 573

## Resonances in electron scattering from SO<sub>2</sub>

P Bingham and J D Gorfinkiel \*

School of Physical Sciences, Faculty of STEM, The Open University, Milton Keynes, UK

**Synopsis** We investigated resonance formation in electron scattering from SO<sub>2</sub> to address the discrepancy among dissociative electron attachment experiments and with prior theoretical calculations regarding the symmetry of the resonances involved in anion production at  $\sim 7.5$  eV.

SO<sub>2</sub> is an important air pollutant that causes acid rain; it is also present in the interstellar medium. Low energy electron scattering from SO<sub>2</sub> has been studied both experimentally and theoretically for almost 40 years. In particular, a number of experimental works have investigated dissociative electron attachment (DEA), with recent emphasis on determining the symmetry of the resonances that initiate the process [1, 2]. Interestingly, these VSI studies disagree on the symmetry of the resonances involved in the production of anions at  $\sim 7.5$  eV: while it is clear that more than one resonance is involved, one attributes them B<sub>1</sub> and B<sub>2</sub> symmetry [1], whereas another indicates the resonances are of A<sub>1</sub> and B<sub>2</sub> symmetry [2].

Theoretical studies of resonance formation at the equilibrium geometry are inconsistent with one another and shed little light on the DEA process. An earlier R-matrix study [3] identified B<sub>2</sub> and A<sub>2</sub> resonances that could lead to DEA at 7.5 eV, while more recent works either looked at shape resonances only or identified a single A<sub>2</sub> resonance that could contribute to DEA at that energy.

We have performed high-quality R-matrix scattering calculations for SO<sub>2</sub> in its ground state equilibrium geometry using the UKRmol+ suite [4]. The calculations were at the close-coupling level and included up to 300 target states to accurately describe the correlation-polarization effects. CASSCF orbitals generated using a DZP basis set were used to describe the target and partial waves up to  $l = 5$  were included in the continuum description. Inclusion of different numbers of excited states was tested: even with the latter number no convergence of the resonance positions and widths was achieved.

We have identified 6 resonances in this system (see Table 1): the lowest energy one is of A<sub>1</sub> sym-

\*E-mail: [j.gorfinkiel@open.ac.uk](mailto:j.gorfinkiel@open.ac.uk)

metry, identified by experiment as the symmetry of the resonance linked to DEA around 4.5 eV. Two resonances, of B<sub>2</sub> and A<sub>2</sub> symmetry, appear below 7.5 eV, and could therefore contribute to the DEA at 7.5 eV. A resonance of B<sub>1</sub> symmetry appears at 7.62 eV for our largest calculation, somewhat above the peak of the DEA signal, but possibly accessible for DEA at non-equilibrium geometries. The next resonance is of A<sub>1</sub> symmetry and appears at almost 8 eV in our largest calculations, with a B<sub>2</sub> resonance at 8.33 eV. It seems less likely that either of these resonances can directly contribute to DEA around 7.5 eV.

Preliminary analysis of our results indicates that both experimental symmetry assignments are possible and that an additional resonance of A<sub>2</sub> symmetry might also be involved in DEA at  $\sim 7.5$  eV. Further work is needed to resolve the uncertainty.

**Table 1.** Resonance positions and widths for our 300 target states close-coupling R-matrix calculation.

Resonance	E (eV)	width (eV)
1A <sub>1</sub>	3.06	0.068
1B <sub>2</sub>	4.12	5e-6
1A <sub>2</sub>	4.42	0.067
1B <sub>1</sub>	7.62	0.168
2A <sub>1</sub>	7.96	0.093
2B <sub>2</sub>	8.33	0.061

### References

- [1] Gope, K., Prabhudesai, V., Mason, N. & Krishnakumar, E. 2017 *J. Chem. Phys.* **147** 054304
- [2] Jana, I. and Nandi, D. 2018 *Phys. Rev.* **A97** 042706
- [3] Gupta, M. and Baluja, K. 2016 *Phys. Rev. A* **73** 042702
- [4] Mašín, Z., Benda, J., Gorfinkiel, J., Harvey, A. & Tennyson, J. 2020 *Computer Phys. Commun.* **249** 107092

## Comparison of electron induced reactions of $(\text{CH}_3)\text{AuP}(\text{CH}_3)_3$ under single collision conditions and its deposition composition in UHV FEBID.

A Kamali<sup>1</sup>, E Bilgiliyoy<sup>2</sup>, A Wolfram<sup>2</sup>, T Gentner<sup>3</sup>, G Ballmann<sup>3</sup>, S Harder<sup>3</sup>, H Marbach<sup>2,4</sup>, and O Ingólfsson<sup>1,\*</sup>

<sup>1</sup>Science Institute and Department of Chemistry, University of Iceland, Dunhagi 3, 107 Reykjavik, Iceland

<sup>2</sup>Physikalische Chemie II, Friedrich-Alexander Universität Erlangen-Nürnberg, 91058 Erlangen, Germany

<sup>3</sup>Inorganic and Organometallic Chemistry, Universität Erlangen-Nürnberg, 91058 Erlangen, Germany

<sup>4</sup>Carl Zeiss SMT GmbH, 64380 Roßdorf, Germany

**Synopsis** Ultra high vacuum deposition and dissociative ionization experiments on the potential focused electron beam induced deposition precursor  $(\text{CH}_3)\text{AuP}(\text{CH}_3)_3$ .

Based on their optical and electronic properties, gold nanostructures have high potential in a variety of applications in the field of sensor technology and beyond. [1] However, for this potential to fully unfold, precise fabrication of integrated, free standing 3D nanostructures is critical. While current lithographic and deposition methods are mainly layer by layer approaches, focused electron beam induced deposition (FEBID) is tailored for 3D printing of free-standing nanostructures of as good as any shape on smooth as well as uneven surfaces. [2] In FEBID of metallic structures, an organometallic precursor in gaseous form is introduced close to a substrate surface in vacuum under concomitant exposure to a tightly focused, high-energy electron beam. The precursor decomposes through interaction with the primary electrons of the beam as well as scattered and secondary electrons unavoidable in the interaction of ionizing irradiation with condensed matter. Ideally the pure metal is left on the surface, while ligands are pumped away. The lateral dimensions of the deposits are controlled by moving the relative position of the beam and vertical growth through variation in the dwell time. Currently the main challenges in FEBID are impurities in the deposits, resulting from incomplete decomposition of the precursors. Thus, it is important to understand the underlying electron induced decomposition mechanisms and how these are reflected in the resulting FEBID deposits and how these may eventually be used to achieve more complete dissociation and better composition control of deposits.

In the current study we approach this by combining FEBID experiments under UHV with the

potential gold precursor  $(\text{CH}_3)\text{AuP}(\text{CH}_3)_3$ , with studies on dissociative ionization of the same precursor. [3] Appearance energies are determined for individual DI channel and quantum chemical calculations are used to aid the assignment of the neutral counterparts in these fragmentation reactions. The FEBID deposits are analyzed with respect to their morphology and composition and compared to what would be expected from the unaltered dissociation processes as they are observed in the gas phase. Comparison is also made with a previous high-vacuum (HV) FEBID study of the same precursor [4], where co-deposition of components from the background gas are expected to play a role. In DI we find the average ligand loss to be that of 2 carbon and 0.8 phosphor per incident. This is in good agreement with the carbon content of the UHV deposits. However, in the UHV deposition experiments, a close to quantitative phosphor loss is observed leading to as good as phosphor free deposits. The HV deposits, on the other hand, show significant phosphor content.

The current results are discussed in context to the differences and similarities observed in the UHV and HV experiments and in context to the possible role of electron induced secondary reactions and oxidizing background gases in the HV deposition.

### References

- [1] Zhang Y et al. 2014 *Materials*, 7(7), 5169-5201
- [2] Utke I et al. 2008 *J. Vac. Sci. Technol. B* 2, 4
- [3] Kamali A et al. 2022 *Nanomaterials* 12(15)
- [4] Van Dorp W 1985 *Langmuir*, 2014. 30: p. 12097-12105

\* E-mail: [odduring@hi.is](mailto:odduring@hi.is)



# Dynamics of Dissociative Electron Attachment to Acetylacetone

Surbhi Sinha<sup>1\*</sup>, Vaibhav Prabhudesai<sup>1†</sup>

<sup>1</sup> Tata Institute of Fundamental Research, Mumbai 400005

**Synopsis** We have studied the dissociation dynamics of acetylacetone (AcAc) on attachment of low energy electrons and identified the negative ion fragments formed and their respective resonances. We also compare the dissociative electron attachment (DEA) mechanism to photodissociation of AcAc and comment on the similarities in the two processes. We have used Velocity Slice Imaging technique to obtain momentum images of the two major fragments H<sup>-</sup> and OH<sup>-</sup>.

Low energy electrons (0-15 eV), when interacting with molecules, can form a negative ion resonance state (NIR). This NIR state can decay by autodetachment of the excess electron, or if it survives long enough, the molecule can undergo dissociation into a negative ion and one or more neutral fragments. The latter process is called DEA. We have studied DEA to acetylacetone (AcAc) molecule in the gas phase. AcAc is an interesting organic molecule that exists in two tautomeric forms, keto and enol. In the gas phase, most molecules stay in the enolic form. This leads to the presence of multiple functional groups in the molecule, like alkene, polyene, carbonyl and enol. We have studied the dissociation dynamics of this molecule and recorded the negative ion fragments formed by varying the electron energy. The major negative ion fragments observed are H<sup>-</sup> and OH<sup>-</sup>, followed by O<sup>-</sup>, CH<sub>3</sub><sup>-</sup> and higher masses of 41 & 43, which we assign to be HCCO<sup>-</sup> & H<sub>2</sub>CCOH<sup>-</sup> respectively, and 57 & 59, which we assign to be CH<sub>2</sub>COCH<sub>3</sub><sup>-</sup> & CH<sub>3</sub>CHOCH<sub>3</sub><sup>-</sup>, respectively. All the ions are observed to have a resonance near 8.5 eV.

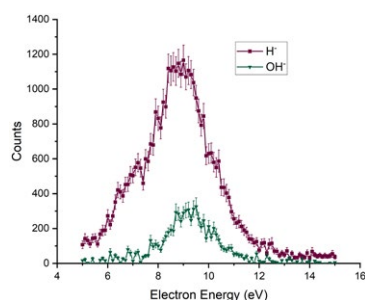


**Figure 1.** Excitation function of H<sup>-</sup> and OH<sup>-</sup> ion with varying electron energy.

This has two interesting implications. Firstly,

\*E-mail: [surbhi9630@gmail.com](mailto:surbhi9630@gmail.com)

†E-mail: [vaibhav@tifr.res.in](mailto:vaibhav@tifr.res.in)

based on functional group site selectivity [2], H<sup>-</sup> from the enolic site should peak around 6.5 eV, and that from the alkyl site should peak around 8.5 eV. Even though ground state AcAc is in the enolic form, we see no 6.5 eV peak. Secondly, 8.5 eV is very close to the photodissociation energy of AcAc, as recently studied by Antonov et al. [1]. Also, the DEA fragments at this energy are similar to photodissociation products. This suggests that the parent state for NIR in DEA is close to the excited dissociating state. We have compared the absolute cross-section of the formation of H<sup>-</sup>, OH<sup>-</sup>, and O<sup>-</sup> with acetone [3] and acetaldehyde.

**Table 1.** Absolute cross-sections of respective anions for Acetaldehyde, Acetylacetone and Acetone (in 10<sup>-18</sup> cm<sup>2</sup>).

	Acetaldehyde	Acetylacetone	Acetone
H <sup>-</sup>	0.28 (8.9 eV)	1.01 (8.5 eV)	0.25 (8.4 eV)
O <sup>-</sup>	0.11 (10 eV)	0.02 (9 eV)	0.04 (8.8 eV)
OH <sup>-</sup>	0.07 (10 eV)	0.23 (9 eV)	0.01 (7.8 eV)

We have also taken momentum images of H<sup>-</sup> and OH<sup>-</sup> ions at 8.5 eV. The images show low kinetic energy release for both of these fragments which suggests that the dissociation is a multi-body fragmentation process.

## References

- [1] Ivan Antonov et al. 2019 *J. Phys. Chem. A* **123** 5472
- [2] Vaibhav S. Prabhudesai et al. 2005 *Phys. Rev. Lett.* **95** 143202
- [3] Vaibhav S. Prabhudesai et al. 2014 *J. Chem. Phys.* **141** 164320



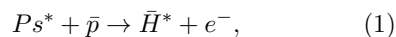
## AEgIS: Synthesis of mid-heavy antiprotonic atoms at CERN

A Linek\*, on behalf of the AEgIS collaboration

Institute of Physics, Faculty of Physics, Astronomy and Informatics, Nicolaus Copernicus University in Toruń, Grudziądzka 5, PL-87-100 Toruń, Poland

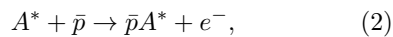
**Synopsis** AEgIS has successfully produced antihydrogen atoms and achieved remarkable performance in trapping antiprotons. The experiment is also exploring the formation and study of antiprotonic atoms. In this contribution, it is going to be presented the scheme for their formation and the status of the project.

At CERN's Antiproton Decelerator complex, the Antimatter Experiment: Gravity, Interferometry, Spectroscopy (AEgIS) strives to measure the influence of gravity on a pulsed horizontal beam of cold antihydrogen atoms [1], testing the Weak Equivalence Principle. The successful production of excited antihydrogen  $\bar{H}$  through a charge exchange reaction [2],



has been demonstrated by AEgIS. This involved using laser-excited positronium atoms  $Ps^*$  and cold antiprotons  $\bar{p}$  trapped in a Penning-Malmberg trap [3].

The developed scheme and the apparatus can be adapted to also produce medium-heavy antiprotonic atoms [4]. In such atomic systems, one of the electrons is substituted with an antiproton, i.e. a particle of the same charge but nearly 1836 times heavier. In the past, the studies of antiprotonic atoms were mostly focused on room-temperature antiprotonic hydrogen and antiprotonic helium, which were obtained by collisions of antiprotons with gaseous hydrogen and liquid helium in a non-vacuum environment [5, 6, 7]. The AEgIS solution to produce mid-heavy antiprotonic atoms  $\bar{p}A^*$  is based on the resonant charge exchange reaction,

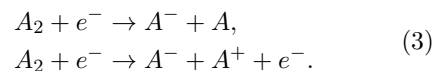


where a slow neutral atom in high Rydberg state,  $A^*$ , collides with a cold antiproton  $\bar{p}$ .

Both cold neutral atoms and antiprotons can be achieved with the Malmberg-Penning trap used for antihydrogen production. The mid-heavy anions will be co-trapped with antiprotons, cooled down, and then photonneutralized and ex-

cited to a high Rydberg state using multiple different laser pulses.

The production of the assemble of mid-heavy anions  $A^-$  is a challenging task. A proper scheme was developed at National Laboratory FAMO at Nicolaus Copernicus University in Toruń in Poland. It is based on the electron dissociative attachment, enhanced with the shape resonance effects. Two types of processes, which include a reaction between homonuclear halogen molecule  $A_2$  with an electron, are expected:



For the purpose of the AEgIS research, an iodine anion source is developed.

Integration of the built iodine anion source with the existing AEgIS apparatus will enable the formation of iodine antiprotonic atoms with an antiproton in a very high Rydberg state. The expected lifetime of the excited antiprotonic iodine atom is expected to be of tens of nanoseconds. The relaxation of the antiproton in the system causes the Auger emission of the electrons and the emission of photons in the X-ray spectrum. Eventually, these processes will result in obtaining an atomic system where only the iodine nucleus and the antiproton persist. This enables unique studies of the nucleus structure.

### References

- [1] M. Doser et al. 2012 *Class. Quantum Grav.* **29** 184009
- [2] D. Krasnický et al. 2016 *Phys. Rev. A* **94** 022714
- [3] C. Amsler et al. 2021 *Commun. Phys.* **4** 19
- [4] G. Kornakov et al. 2022 *arXiv* **2209.02596**
- [5] C. J. Batty 1989 *Rep. Prog. Phys.* **52** 1165
- [6] T. Yamazaki et al 2002 *Phys. Rep.* **87** 093401
- [7] M. Doser 2022 *Prog. Part. Nucl. Phys.* **125** 103964

\*E-mail: [a.linek@doktorant.umk.pl](mailto:a.linek@doktorant.umk.pl)

## Nonradiative electron capture in collisions of fast $\text{Xe}^{54+}$ with Kr and Xe

B. Yang<sup>1,2</sup>, D. Yu<sup>1,2</sup>\*, X. Cai<sup>1,2</sup>, C. Shao<sup>1,2</sup>, M. Zhang<sup>1,2</sup>, Y. Xue<sup>1,2</sup>, W. Wang<sup>1,2</sup>,  
J. Liu<sup>1</sup>, Z. Song<sup>1,2</sup>, Y. Wu<sup>1</sup>, R. Lu<sup>1</sup> and F. Ruan<sup>1</sup>

<sup>1</sup>Institute of Modern Physics, Chinese Academy of Sciences, Lanzhou, 730000, People's Republic of China

<sup>2</sup>University of Chinese Academy of Sciences, Beijing, 100049, People's Republic of China

**Synopsis** X rays emitted from the down-charged projectile ions produced by nonradiative electron capture in collisions of 95, 146, and 197 MeV/u  $\text{Xe}^{54+}$  projectiles with krypton or xenon gaseous targets were measured. The alignment of the projectile  $2p_{3/2}$  state and the relative population of its magnetic substates were deduced from the observed angular distribution of the Lyman- $\alpha_1$  transition of the  $\text{Xe}^{53+}$  ions. Moreover, the population of excited projectile states involving single and double electron capture were investigated.

In collisions of fast highly charged ions with atoms, the nonradiative electron capture (NRC) is one of the fundamental processes [1]. In NRC, a bound electron of the target atom is captured into a bound state of the projectile with the energy and momentum being shared between the target and the projectile [1]. NRC often competes with the radiative electron capture (REC) mechanism, in which energy and momentum conservations are fulfilled by emission of a photon [2]. NRC becomes more important than REC with decreasing projectile energy and increasing target atomic number. Electron capture are important for predictions of state-charge distributions and the lifetime of stored ion beams when operation of heavy-ion accelerator and cooling storage rings, as well as research in plasma physics and astrophysics [1, 2].

In the present work, we measured x rays emitted from  $\text{Xe}^{53+}$  and  $\text{Xe}^{52+}$  produced by NRC in single collisions of 95-197 MeV/u  $\text{Xe}^{54+}$  ions with Kr or Xe atoms at observation angles of 35°, 60°, 90°, 120°, and 145°. Our experiments were carried out at the internal jet target of the HIRFL-CSR [3].

Figure 1 shows the energy-dependence of the alignment parameter of the  $\text{Xe}^{53+}(2p_{3/2})$  state for  $\text{Xe}^{54+} + \text{Kr}$  collisions. A significant negative value of the alignment parameter at 95 MeV/u represents that NRC into the  $m_j = \pm 1/2$  magnetic substates of the  $2p_{3/2}$  state is about two times more probable than to the  $m_j = \pm 3/2$  ones, and the Lyman- $\alpha_1$  radiation is strongly linearly polarized. As the projectile energy increases, the corresponding population ratio steadily decreases and the population of the magnetic sublevels follows a statistical distribution at 197 MeV/u [4, 5]. The calculation of the alignment parameter of the REC process exhibits a rather weak dependence on the projectile energy for comparison. Moreover, the energy and target atomic

number dependences of the population of excited projectile states involving single and double electron capture were investigated by means of the intensity ratios of the corresponding transitions [6].

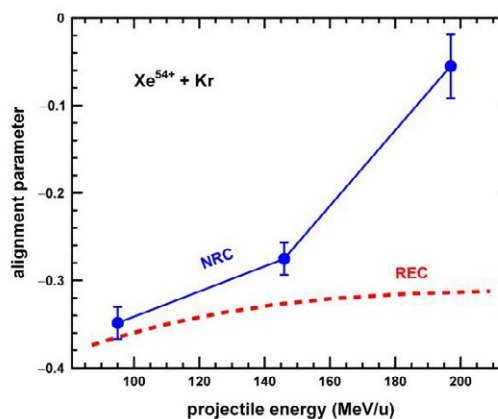


**Figure 1.** The experimentally determined alignment parameters of the  $2p_{3/2}$  state of  $\text{Xe}^{53+}$  ions following the NRC mechanism, as well as the theoretical results of the corresponding REC process for comparison.

We thank the crew of the accelerator department for their operation of HIRFL-CSR. This work is supported by the HIRFL research program No. HIR2021PY003 and “Young Scholars in Western China” of Chinese Academy of Sciences.

### References

- [1] Eichler J and Meyerhof W E 1995 *Relativistic Atomic Collisions*
- [2] Eichler J and Stöhlker Th 2007 *Phys Rep* **439** 1
- [3] Xia J W *et al* 2002 *Nucl Instrum Methods Phys Res A* **488** 11
- [4] Yang B *et al* 2020 *Phys Rev A* **102** 042803
- [5] Yang B *et al* 2023 *J Phys B* **56** 055203
- [6] Yang B *et al* 2021 *Phys Rev A* **104** 032815

\* E-mail: [d.yu@impcas.ac.cn](mailto:d.yu@impcas.ac.cn)

## An improved short-range description for CDW-EIS model with dressed projectiles

N J Esponda<sup>1\*</sup>, M A Quinto<sup>1</sup>, R D Rivarola<sup>1,2</sup> and J M Monti<sup>1,2</sup>

<sup>1</sup>Instituto de Física Rosario (CONICET-UNR), Rosario, 2000, Argentina

<sup>2</sup>Laboratorio de Colisiones Atómicas, Rosario, 2000, Argentina

**Synopsis** It has already accounted in the bibliography that the CDW-EIS model fails to account some anti-screening effects which arise when dealing with dressed projectiles. In fact, the transition amplitude related with short-range electronic interactions is responsible of these phenomena. Also, it is the asymptotic nature of the eikonal approximation which makes it an unsuitable approach to calculate such particular transition amplitude when dressed projectiles are involved. In this work we propose to replace the initial channel eikonal phase with the hydrogenic continuum distortion factor.

Among the Continuum Distorted Wave (CDW) theories, the Eikonal State (CDW-EIS) approximation has proven to be a successful model to study the single ionization of atoms and molecules in collisions with bare projectiles at intermediate to high impact energies [1]. However, with dressed projectiles CDW-EIS models have failed to reproduce some anti-screening effects such as the well known zero-degree binary-encounter emission (BEE) enhancement with increasing number of electrons [2, 3].

The interaction between the active electron and the electron cloud of the projectile may be treated as a short-range potential. As shown in [3], within CDW-EIS model the corresponding transition amplitude involves an asymptotic approximation for the projectile distortion which its limit may not be fulfilled. Therefore, in this work we propose to replace, in the short-range transition amplitude, the initial channel eikonal-phase projectile distortion with an hydrogenic continuum wavefunction. In other words, we calculate the mentioned amplitude as in the usual CDW theory. Since the term involving the perturbation remains the same as CDW-EIS, the inclusion of CDW divergences [4] is avoided. Let us call this modified model as CDW-EIS *hybrid*.

As seen in the figure, the CDW-EIS *hybrid* calculation does reproduce the BEE enhancement in collisions between boron ions and the hydrogen molecule, such as well as the CDW theory. Further results and details will be presented during the conference.

\*E-mail: [esponda@ifir-conicet.gov.ar](mailto:esponda@ifir-conicet.gov.ar)

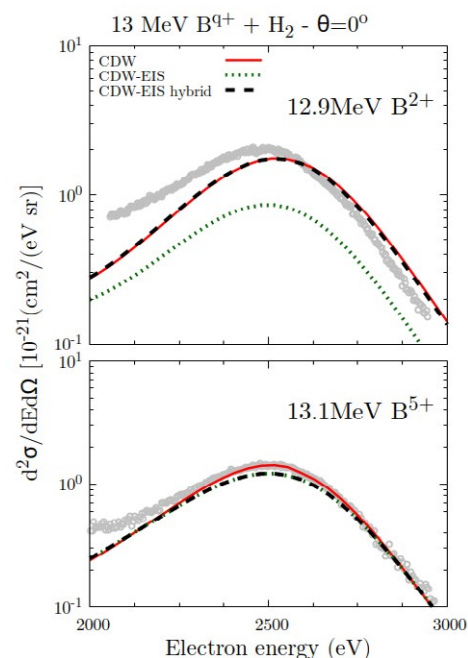


**Figure 1.** Binary encounter electron emission at  $0^\circ$  from collisions between bare and dressed boron projectiles impinging over a  $H_2$  target at 13 MeV. Dots are measurements from [3].

### References

- [1] Rivarola R D, Fojón O A *et al.* 2023 *Springer Handbook of Atomic, Molecular and Optical Physics* pp. 813-828
- [2] Monti J M, Rivarola R D and Fainstein P D 2011 *J. Phys. B* **11** 17
- [3] Esponda N J, Nanos S *et al.* 2023 *Atoms* **11** 17
- [4] Monti J M, Quinto M A and Rivarola R D 2021 *Atoms* **9** 3

## Target atomic number dependence of the electron capture and excitation process for the relativistic hydrogen-like Cs ions

C J Shao<sup>1,2</sup>, H Q Zhang<sup>3,\*</sup>, B Yang<sup>1,2</sup>, D Y Yu<sup>1,2</sup>, Z Y Song<sup>1,2</sup>, P F Li<sup>3</sup>, H Yuan<sup>3</sup>, Z D Cheng<sup>3</sup>, S Ha<sup>3</sup>, H W Zhang<sup>3</sup>, Y S Kozhedub<sup>4</sup>, W Wang<sup>1,2</sup>, M W Zhang<sup>1,2</sup>, J L Liu<sup>1,2</sup>, Y L Xue<sup>1,2</sup>, C L Wan<sup>3</sup>, Y Cui<sup>3</sup>, K Yao<sup>5,6</sup>, Z H Yang<sup>1,2</sup>, X H Cai<sup>1,2</sup>, R Schuch<sup>7</sup> and X M Chen<sup>3</sup>

<sup>1</sup>Institute of Modern Physics, Chinese Academy of Sciences, Lanzhou 730000, China

<sup>2</sup>University of Chinese Academy of Sciences, Beijing 100049, China

<sup>3</sup>School of Nuclear Science and Technology, Lanzhou University, Lanzhou, 730000, China

<sup>4</sup>Department of Physics, St. Petersburg State University, St. Petersburg 198504, Russia

<sup>5</sup>Institute of Modern Physics, Fudan University, Shanghai, 200433, China

<sup>6</sup>Key Laboratory of Nuclear Physics and Ion-Beam Application (MOE), Fudan University, Shanghai, 200433, China

<sup>7</sup>Physics Department, Stockholm University, S-10691, Stockholm, Sweden

**Synopsis** X-ray spectra from the 66.3-MeV/ $\mu$  caesium ion in single collision with nitrogen, argon, krypton and xenon gas targets are measured. The radiations from the projectile excited states  $Cs^{53+*}(1s2p)$  and  $Cs^{54+*}(2p)$  due to capture and excitation processes are identified and analyzed. From the relative intensities of the  $K\alpha$  and  $L\alpha$  lines, the single electron capture cross sections for various targets are determined. The obtained results are compared with that calculated with the relativistic eikonal approximation.

Nonradiative electron capture (NRC) is one of the fundamental processes in collisions of highly charged ions with atoms [1]. Due to the availability of the facility for the experiments, these studies are limited and most studied collision systems are the highly charged ions with light targets where the reasonable agreements have been reached between the theories and experiments [2, 3]. Concerning highly charged middle-velocity projectiles and heavy targets, the studies are rather less [4] and the NRC process in this region needs more investigations.

In present work target atomic number dependence of the NRC process for hydrogen-like Cs ions is studied at the HIRFL-CSR. The  $Cs^{54+}$  ions with an energy of 66.3 MeV/u were stored in CSR to interact with nitrogen, argon, krypton and xenon target, respectively. The x rays emitted from the projectiles were detected by an High Purity Germanium (HPGe) detector mounted at 35° observation angle with respect to the ion beam direction. The radiations from the projectile excited states  $Cs^{53+*}(1s2p)$  and  $Cs^{54+*}(2p)$  due to capture and excitation processes are identified and analyzed. By theoretically evaluating the well studied excitation processes including the cascading processes [5, 6], the theoretical excitation cross sections for our

collision systems are obtained and the experimental capture cross sections are then obtained by combining with the experimental radiation intensity ratio from the transitions  $Cs^{53+*}(1s2p-1s^2)$  to  $Cs^{54+*}(2p-1s)$ . The extracted capture cross sections are compared with that calculated with the relativistic eikonal approximation [1]. The overall agreement has been reached but the obvious deviation has been also found. The possible explanations of the deviations will be discussed.

The work was partially supported by the National Key R&D Program of China under Grant No. 2022YFA1602501 and the National Natural Science Foundation of China under Grants Nos. U1332206.

### References

- [1] Eichler J 1990 *Phys. Rep.* **193**, 165
- [2] Stöhlker Th et al., *Phys. Rev. A* 1998 **58**, 2043
- [3] Kröger F M et al., 2020 *Phys. Rev. A* **102**, 042825
- [4] Yang B et al., 2021 *Phys. Rev. A* **104**, 032815
- [5] Gumberidze A et al., 2010 *Phys. Rev. A* **82**, 052712
- [6] Ramírez C A and Rivarola R D 1995 *Phys. Rev. A* **52**, 4972

\* E-mail: [zhanghq@lzu.edu.cn](mailto:zhanghq@lzu.edu.cn)

## State-selective single-electron capture in 1 keV/u $\text{Ar}^{2+}$ -Ar collisions

S C Cui<sup>1,2</sup>, D D Xing<sup>1,2</sup>, X L Zhu<sup>2,3\*</sup>, M G Su<sup>1†</sup>, Y B Fu<sup>1</sup>, S F Zhang<sup>2,3</sup>, X Ma<sup>2,3</sup>

<sup>1</sup>Key Laboratory of Atomic and Molecular Physics Functional Material of Gansu Province, College of Physics and Electronic Engineering, Northwest Normal University, Lanzhou 730070, China

<sup>2</sup>Institute of Modern Physics, Chinese Academy of Sciences, Lanzhou 730000, China

<sup>3</sup>University of Chinese Academy of Sciences, Beijing 100049, China

**Synopsis** State-selective single electron capture in collisions of  $\text{Ar}^{2+}$  ions with Ar at a collision energy of 1 keV/u was studied by COLTRIMS. The dominant channel is the projectile captures one electron into 3p simultaneously a 3s electron excited to 3p state and the target keeps in its ground state or the projectile captures a 3s electron of target into 3p state. The process that scattered ions and recoil ions keep in  $\text{Ar}^+(3s^23p^5)$  state has an obvious contribution. The excitation process that scattered and target ions stay in  $\text{Ar}^+(3s3p^6)$  state has a minor contribution.

The state-selective cross-section and angle-differential cross-section of collisions between multi-charged ions and atoms are of great significance to basic scattering theory, and have a wide range of practical applications in astrophysics, plasma, and charged ion-induced biological radiation effects. Research on heavy targets is relatively scarce both theoretically and experimentally[1], mainly because heavy targets have more electrons and therefore many collision reaction channels, posing great challenges to both theory and experiment.

The experiment performed at IMP EBIS-A facility combined with a COLTRIMS[2]. Figure 1 show the two-dimensional momentum density distributions of  $\text{Ar}^+$  recoil ion for the 1 keV/u  $\text{Ar}^{2+}$ -Ar single electron capture process. Three vertical distributions were observed, indicated as A, B, and C in Figure 1. The related reaction processes are as follows:

A:  $\text{Ar}^{2+}(3s^23p^4)+\text{Ar}\rightarrow\text{Ar}^+(3s^23p^5)+\text{Ar}^+(3s^23p^5)$ ,  
 B:  $\text{Ar}^{2+}(3s^23p^4)+\text{Ar}\rightarrow\text{Ar}^+(3s3p^6)+\text{Ar}^+(3s^23p^5)$ ,  
 C:  $\text{Ar}^{2+}(3s^23p^4)+\text{Ar}\rightarrow\text{Ar}^+(3s3p^6)+\text{Ar}^+(3s3p^6)$ .

For a symmetric collision system, like in the energy gain spectroscopy, it is not distinguishable whether scattered projectile or the target ion is in the excited state in our experiment for reaction B (because the energy change is the same). Comparing with previous studies [3, 4] about 500 eV impact energy, reaction channel C is observed in our experiment. Moreover, the angular differential cross sections distributions can be obtained from the Figure 1 projected to the

\*E-mail: zhuxiaolong@impcas.ac.cn

†E-mail: sumg@nwnu.edu.cn

vertical axis.

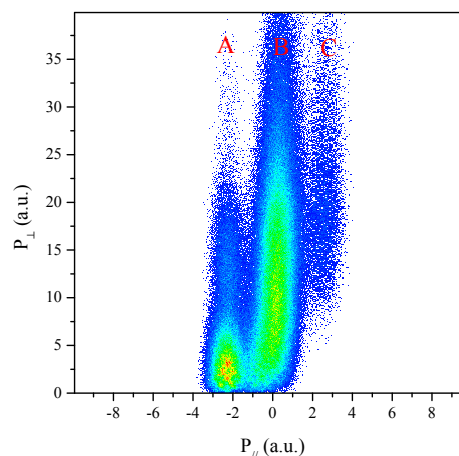


**Figure 1.** Two-dimensional momentum density plot for the 1 keV/u  $\text{Ar}^{2+}$ -Ar single electron capture process.

This work is supported by NSFC of China(11974358, 11934004) and Chinese Academy of Sciences Strategic Leading Science and Technology Project (XDB34020000).

### References

- [1] Zhang H L *et al* 2001 *Phys. Rev. A.* **64** 012715
- [2] Zhu X L *et al* 2019 *Nucl. Instrum. Methods Phys. Res., Sect. B* **460** 224
- [3] Huber B A *et al* 1980 *J. Phys. B: Atom. Mol. Phys.* **13** 809
- [4] Kamber E Y *et al* 1982 *J. Phys. B: Atom. Mol. Phys.* **15** 2051



## State-selective single electron capture in 9 keV N<sup>+</sup>-He collisions

D Xing<sup>1,2</sup>, S C Cui<sup>1,2</sup>, X L Zhu<sup>2,3\*</sup>, D H Zhang<sup>1†</sup>, S F Zhang<sup>2,3‡</sup>, X Ma<sup>2,3</sup>

<sup>1</sup>Key Laboratory of Atomic and Molecular Physics Functional Material of Gansu Province, College of Physics and Electronic Engineering, Northwest Normal University, Lanzhou 730070, China

<sup>2</sup>Institute of Modern Physics, Chinese Academy of Sciences, Lanzhou 730000, China

<sup>3</sup>University of Chinese Academy of Sciences, Beijing 100049, China

**Synopsis** The state-selective single-electron capture processes in collisions of N<sup>+</sup> ions with He at an impact energy of 9 keV have been studied experimentally by means of a cold-target recoil-ion momentum spectroscopy. The captured electron populated into the N(1s<sup>2</sup>2s<sup>2</sup>2p<sup>3</sup>) states is dominant for both the ground-state projectile N<sup>+</sup>(1s<sup>2</sup>2s<sup>2</sup>2p<sup>2</sup> <sup>3</sup>P) and the metastable-state projectile N<sup>+</sup>(1s<sup>2</sup>2s2p<sup>3</sup> <sup>5</sup>S).

Electron capture has been investigated experimentally and theoretically not only for interest in developing fundamental scattering theory, but also for its important role in various applications such as astrophysics or plasma physics. The cross-section of the electron capture process at low-energy collision is known to be dependent on the impact and internal energy of the projectile [1]. The previous studies focus on the total cross sections of electron capture processes from experimental side for low energy N<sup>+</sup>-He collisions [1, 2]. However, state-selective and angle dependent cross sections are still scarce [3].

The experimental work performed at IMP EBIS-A facility combined with a cold-target recoil-ion momentum spectroscopy [4] for the single electron capture in N<sup>+</sup>-He collisions at an impact energy of 9 keV. The longitudinal and transverse momentum of recoil ions were obtained. The different final states populations can be identified from the measured longitudinal momentum spectrum. Figure 1 shows the longitudinal momentum spectrum for single electron capture processes in N<sup>+</sup>-He collisions at an energy of 9 keV. The three peaks were observed from figure 1. Peak A corresponds to the metastable state projectile captures one electron from helium into 2s state. Peak B corresponds to the ground state projectile captures one electron from helium into 2p states. Peak C corresponds to the ground state projectile capture one electron from helium into nl (n≥3) states. The present results agree well with previous work [3]. Also the angular differential cross sections for different fi-

nal states were obtained. For the peak A, the oscillation structure in angular differential cross sections was observed, which may be from the Fraunhofer diffraction of projectile matter wave [5].

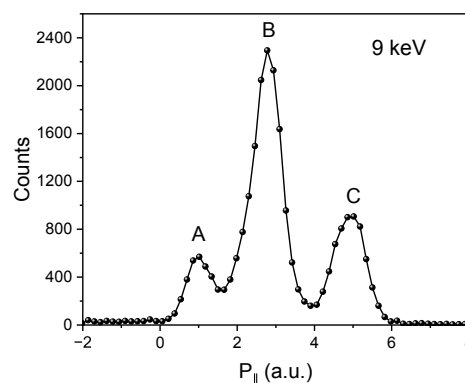


**Figure 1.** Measured longitudinal momentum spectrum of recoil in N<sup>+</sup>+He collisions for single electron capture processes at impact energy of 9 keV.

This work is supported by NSFC of China(11974358, 11934004) and Chinese Academy of Sciences Strategic Leading Science and Technology Project (XDB34020000).

### References

- [1] Kusakabe T *et al* 1990 *J. Phys. Soc. Jpn.* **59** 1987
- [2] Moran T F *et al* 1979 *J. Chem. Phys.* **70** 1467
- [3] Kimura M *et al* 1995 *Phys. Rev. A* **51** 2063
- [4] Zhu X L *et al* 2019 *Nucl. Instrum. Methods Phys. Res., Sect. B* **460** 224
- [5] Wang Q *et al* 2011 *J. Phys. B: At. Mol. Opt. Phys.* **45** 025202

\*E-mail: zhuxiaolong@impcas.ac.cn

†E-mail: zhangdh@nwnu.edu.cn

‡E-mail: zhangshf@impcas.ac.cn



## Fully Differential Study of Non-PCI Higher-Order Contributions to Ionization of Helium by Proton Impact

S. Majumdar<sup>1</sup>, S. Bastola<sup>1</sup>, R. Lomsadze<sup>2</sup>, A. Hasan<sup>3</sup>, and M. Schulz<sup>1</sup>

<sup>1</sup>Missouri University of Science and Technology, Rolla, MO 65409, USA

<sup>2</sup>Tbilisi State University, Tbilisi, 0179, Georgia

<sup>3</sup>University of United Arab Emirates, Al-Ain, UAE

**Synopsis** Fully differential ionization cross sections were measured for  $p + \text{He}$  collisions far from the matching velocity

We have measured fully momentum analyzed scattered projectiles and recoil-ions in coincidence for 75 keV  $p + \text{He}$  collisions. From the data we extracted fully differential cross sections (FDCS) for electrons ejected into the scattering plane as a function of the polar emission angle  $\theta_e$ . The electron energy and the momentum transfer  $q$  from the projectile to the target atom were fixed at various values.

Earlier, we reported several studies of FDCS for electron energies corresponding to electron speeds close to the projectile speed (velocity matching) [e.g. 1,2]. In this regime, higher-order contributions are known to be dominated by the post-collision interaction (PCI). In this process, the projectile interacts with the active electron at least twice. In the first interaction, enough energy is transferred to the electron to lift it to the continuum. In the second interaction, the projectile and the ejected electron focus each other towards the initial beam axis. In the data we found two signatures of PCI: a) the so-called binary peak was shifted in the forward direction relative to  $q$  and b) a pronounced peak structure in the initial projectile beam direction (forward peak) was observed.

The motivation for this project was to study higher-order effects other than PCI, those involving an interaction between the projectile and the target nucleus (PT interaction). We aimed at suppressing PCI contributions by selecting electron energies of 1 and 75.4 eV, which are far from the velocity-matching.

For 1 eV we found that one of the PCI signatures, the forward peak, was completely absent in the FDCS. In contrast, at 75.4 eV the forward peak

was significantly reduced compared to the velocity-matching regime, but a significant residue remained. On the other hand, the forward shift of the binary peak at 1 eV was as prominent as in the velocity-matching regime and even more pronounced than at 75.4 eV. However, earlier we pointed out that not every forward shift is indicative of PCI, but rather it can be caused by the PT interaction [3].

Fig.1 shows the shift of the binary peak as a function of the projectile energy loss  $\varepsilon$  (electron energy plus ionization potential). The data reveal two separate regimes, one at very small  $\varepsilon$  and one in the velocity-matching regime and at large  $\varepsilon$ . We

interpret these regions as being caused by PCI (velocity-matching) and higher-order effects involving the PT interaction

(small  $\varepsilon$ ), respectively. We thus conclude that at 1 eV the data are dominated by non-PCI higher-order contributions and by PCI at 75.4 eV.

This work was supported by NSF.

[1] M. Dhital et al., PRA **100**, 032707 (2019)

[2] M. Dhital et al., PRA **102**, 032818 (2020)

[3] M. Schulz et al., PRA **88**, 022704 (2013)

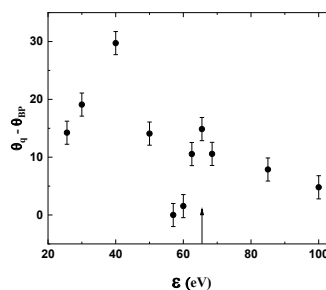


Figure 1 Forward shift of the binary peak as a function of energy loss

E-mail: [schulz@mst.edu](mailto:schulz@mst.edu)

## Energy and angular distributions of electrons produced in intermediate-energy proton-helium collisions

K. H. Spicer<sup>1\*</sup>, C. T. Plowman<sup>1</sup>, Sh. U. Alladustov<sup>1</sup>, I. B. Abdurakhmanov<sup>2</sup>, I. Bray<sup>1</sup> and A. S. Kadyrov<sup>1</sup>

<sup>1</sup>Curtin University, GPO Box U1987, Perth, WA 6845, Australia

<sup>2</sup>Pawsey Supercomputing Centre, 1 Bryce Ave, Kensington, WA 6151, Australia

**Synopsis** The wave-packet convergent close-coupling approach is applied to differential ionization in proton-helium collisions. The approach employs a correlated two-electron description of the helium atom. Also used is a method that reduces the target to an effectively single-electron system. The doubly differential cross section as a function of the energy and angle of the emitted electron is calculated for incident proton energies in the intermediate range. Results from the two methods practically coincide and are in excellent agreement with experimental data.

Modelling ionization in ion-atom collisions is a challenging problem since electrons may be emitted into either the continuum of the target or the projectile, requiring two-center effects to be accounted for. Here, we investigate single ionization of helium atoms by protons using the wave-packet convergent close-coupling (WP-CCC) approach. This method uses a correlated two-electron wave function to describe the helium target and discretizes the continuum using wave-packet pseudostates. We also apply an alternative, simpler approach that reduces the target to an effective single-electron (E1E) system. The doubly differential cross section (DDCS) is calculated in the intermediate energy (50–300 keV) region. Previously, we have calculated integrated [1] and all three types of singly differential [2] cross section, and the results displayed excellent agreement with respective experimental measurements. This work represents the first study of the DDCS for ionization in a nonperturbative manner.

In Fig. 1, a sample of the calculated DDCS is shown at an incident-proton energy of 150 keV. Results from both the E1E and two-electron WP-CCC methods agree very well with experimental data. At an ejection angle of 10°, the low-energy peak followed by wider ridge is perfectly captured by the present two-center calculations. However, at this ejection angle, both slightly overestimate the binary-encounter peak. At the three larger ejection angles shown, perfect agreement between the experiment and WP-CCC data is seen which is particularly notable due to the dif-

\*E-mail: [kate.bain@postgrad.curtin.edu.au](mailto:kate.bain@postgrad.curtin.edu.au)

ficulty in describing perpendicular and backward ejection. No other theoretical calculations are available for comparison at this collision energy.

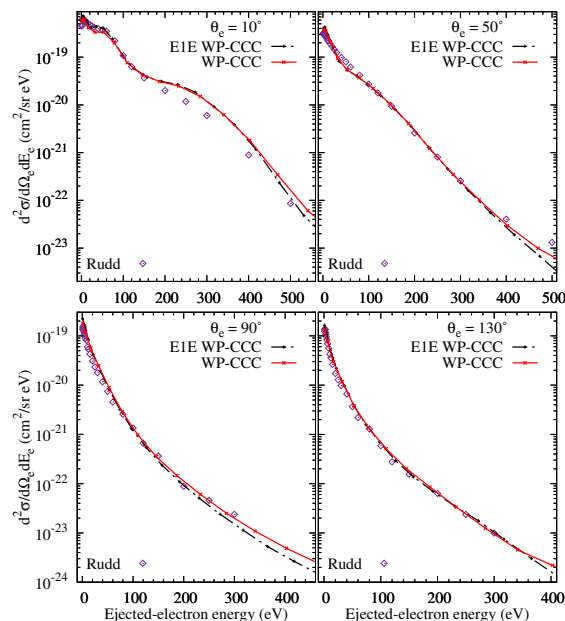


**Figure 1.** DDCS for 150 keV protons as a function of ejected-electron energy at ejection angles of 10, 50, 90, and 130°. Experimental data are by Rudd and Jorgensen [3]. The lines with points represent the present WP-CCC calculations.

### References

- [1] Alladustov *et al.* 2019 *Phys. Rev. A* **93** 012502
- [2] Spicer *et al.* 2021 *Phys. Rev. A* **104** 052815
- [3] Rudd and Jorgensen 1963 *Phys. Rev.* **131** 666

## Single ionization of helium by protons in the parabolic quasi-Sturmians approach

S A Zaytsev<sup>1</sup>, D S Zaytseva<sup>1</sup>, A S Zaytsev<sup>1</sup>, L. U. Ancarani<sup>2\*</sup>,  
K. A. Kouzakov<sup>3</sup> and Yu V Popov<sup>3</sup>

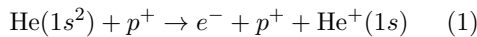
<sup>1</sup>Pacific National University, Khabarovsk 680035, Russia

<sup>2</sup>Université de Lorraine, CNRS, LPCT, 57000 Metz, France

<sup>3</sup>Lomonosov Moscow State University, Moscow 119991, Russia

**Synopsis** The parabolic quasi-Sturmian approach recently introduced for calculating ion-atom ionizing collisions is applied here to single ionization of helium induced by intermediate-energy proton impact. In this energy regime, the fully differential ionization cross sections (FDCS) are assumed to be more sensitive to the details of the interactions in this four-body system.

Understanding the dynamics of breakup processes of few-body Coulomb systems is paramount not only for its fundamental interest but also for numerous practical applications. We are interested here in the ionization process



yielding three unbound particles system  $(e^-, \text{He}^+, p^+) = (1, 2, 3)$  in the final state.

It follows from the property of the Green's function operator  $\hat{G}^{(+)}(E)$  for the final channel three-body Hamiltonian  $\hat{H}$  that the transition amplitude calculation can be cast in the form of a driven equation with outgoing boundary conditions. We expand the solution in terms of basis functions that we called *convoluted* quasi-Sturmians (CQS) [1]: they are constructed as a convolution of two suited one-particle parabolic quasi-Sturmians (QS), corresponding to the non-interacting hydrogen-like systems  $(p^+, \text{He}^+)$  and  $(e^-, \text{He}^+)$ . It turns out that the transition amplitude is then expressed as a sum of products of basis amplitudes associated to the asymptotic behavior of CQS. In our approach the proton-electron interaction  $\hat{U}$  is treated as a perturbation and is approximated by a truncated Sturmian basis-set expansion.

In [1] we have applied the proposed method to study ionization with high-energy incident protons. The obtained FDCS were in reasonable agreement with experimental data and with other theoretical results. In the present work, we focus on a lower incident energy regime (see fig. 1). For all transverse momentum transfers, except for  $\eta = 1.38$ , the calculated FDCS change

\*E-mail: [ugo.ancarani@univ-lorraine.fr](mailto:ugo.ancarani@univ-lorraine.fr)

insignificantly when the Coulomb interaction  $\hat{U}$  is taken into account.

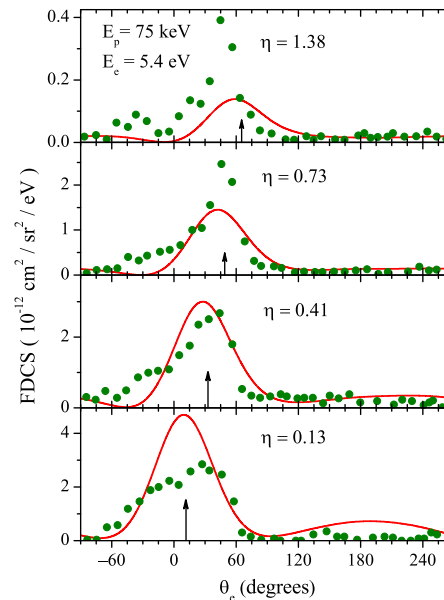


**Figure 1.** Our calculated FDCSs (line) are compared to experimental data [2] for single ionization of helium by 75 keV protons in the collision plane, for different transverse momenta  $\eta$ . The ejected electron ( $E_e = 5.4$  eV) is in the scattering plane.

### References

- [1] Zaytsev A S, Zaytseva D S, Zaytsev S A, Ancarani L U, Kouzakov K A 2022 *Phys. Rev. A* **105** 062818
- [2] Schulz M, Hasan A, Maydanyuk N V, Foster M, Tooke B and Madison D H 2006 *Phys. Rev. A* **73** 062704

## A 22-pole RF ion trap experimental setup to study the ion-neutral and ion-photon interactions relevant to astrophysical environments.

R Chacko<sup>1,2</sup>, N R Behera<sup>1</sup>, S Dutta<sup>1</sup>, S Barik<sup>1</sup>, and G Aravind<sup>1\*</sup>

<sup>1</sup>Department of Physics, Indian Institute of Technology Madras, Chennai 600036, India

<sup>2</sup>Department of Particle Physics and Astrophysics, Weizmann Institute of Science, Rehovot 7610001, Israel

**Synopsis** An experimental setup comprising a 22-pole radiofrequency ion trap is developed and tested for laboratory astrophysical studies. The collisional lifetime of  $SF_6^-$  is measured using the setup.

More than 250 molecules have been detected in the interstellar medium (ISM) and circumstellar envelopes. ISM is very non-homogeneous as it varies in density and temperature and is believed to be the birthplace of stars. Knowledge about ISM chemistry is pivotal in making models of astrochemical networks that could lead to the formation of biomolecules, which might be the building blocks of life [1]. In this context, it is vital to study the chemical reactions involving ions, neutrals, and photons that determine the ISM dynamics and understand their chemical kinetics and the lifetime of the short-lived ISM ions. Multipole ion traps with a facility to operate at very low temperatures are one of the most useful experimental techniques in laboratory astrophysics for such studies [2, 3]. We have built a 22-pole radiofrequency ion-trap experimental setup in this direction.

The setup incorporates an ion source, an ion beam bender for perpendicular extraction of ions, a quadrupole mass spectrometer (QMS-I) to choose the ion of interest, a 22-pole RF ion trap mounted on a liquid nitrogen-based coldhead, a second quadrupole mass spectrometer (QMS-II) to mass analyze the unloaded ions from the trap, a quadrupole bender, and a channeltron detector. Figure 1 shows the schematic of the setup. Incorporating the ion-beam bender and the quadrupole bender allows the shining of a laser in the axial direction, providing maximum

overlap between the trapped ions and the photons. Ion-optics elements are included wherever required for guiding and steering the ion beam. A plasma sputter ion source coupled to a piezoelectric valve is employed. Both positive and negative ions can be produced with this source. A pulsed plasma discharge ion source and an electron impact ion source are also made and tested.

We have produced positive and negative ions using  $SF_6$  gas.  $SF_5^+$  and  $SF_6^-$  are successfully trapped and the trapping efficiency is investigated. The collisional life time of  $SF_6^-$  is measured. The details of the experimental setup and initial results from the trap will be presented at the conference.

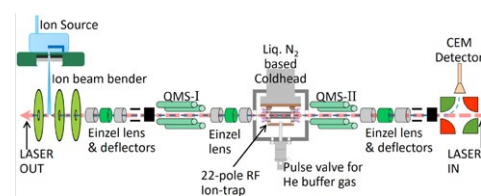


Figure 1. Schematic of 22-pole RF ion trap setup.

### References

- [1] Ian W. M. Smith 2011 *Annu. Rev. Astron. Astrophys.* **49** 29-66
- [2] Dieter Gerlich 1995 *Phys. Scr.* **1995** 256
- [3] Roland Wester 2009 *J. Phys. B: At. Mol. Opt. Phys.* **42** 154001

\*E-mail: [garavind@iitm.ac.in](mailto:garavind@iitm.ac.in)

## Upcoming atomic physics studies of ion-ion collisions

M. Jolly<sup>1,6\*</sup>, E. Lamour<sup>1</sup>, A. Méry<sup>2</sup>, A. Bräuning-Demian<sup>3</sup>, A. Dubois<sup>6</sup>, J-Y. Chesnel<sup>2</sup>, A. Gumberidze<sup>3</sup>, C. Hahn<sup>4</sup>, M. Lestinsky<sup>3</sup>, S. Macé<sup>1</sup>, C. Prigent<sup>1</sup>, JM. Ramillon<sup>2</sup>, J. Rangama<sup>2</sup>, P. Rousseau<sup>2</sup>, U. Spillmann<sup>3</sup>, S. Steydli<sup>1</sup>, Th. Stöhlker<sup>3,4,5</sup>, M. Trassinelli<sup>1</sup> and D. Vernhet<sup>1</sup>

<sup>1</sup>Institut des Nanosciences de Paris, Sorbonne Université, CNRS UMR 7588, Paris, 75005, France

<sup>2</sup>CIMAP, CEA/CNRS/ENSICAEN/Université de Caen Normandie, Caen, 14050, France

<sup>3</sup>GSI Helmholtzzentrum für Schwerionenforschung, Darmstadt, 64291, Germany

<sup>4</sup>Friedrich-Schiller-Universität Jena, Jena, 07743, Germany

<sup>5</sup>Helmholtz-Institut Jena, Jena, 07743, Germany

<sup>6</sup>Laboratoire de Chimie Physique-Matière et Rayonnement, Sorbonne Université, CNRS UMR 7614, Paris, 75005, France

**Synopsis** The importance of electronic processes in many research domains such as plasma physics, fusion research or hadrontherapy is widely recognized. Despite the availability of charge exchange cross section data [1], there is a lack of experimental data on the population of atomic levels following these processes for mid and high Z symmetric ion-ion collisions at low energy and more generally in the so-called intermediate velocity domain.

We present the current status of our experimental and theoretical developments for the study of electronic processes in multicharged ion-ion collisions. Theoretically, the project concerns the coupled channel description of electronic processes within the framework of the semi-classical approximation: the target and projectile ions relative motion is described classically while electron dynamic is treated by solving non-perturbatively the time dependent Schrödinger equation [2]. So far, the related code allows to model systems and processes with up to 4 active electrons. Our experimental approach involves not only measuring the charge state distribution after the collision, but also performing coincidence measurements using X-rays emitted by the collision partners during the collision. This will give us crucial information on the population of atomic levels of the collision products. For this purpose we develop a mobile platform that delivers keV/u ion beams, consisting of an ECR ion source connected to its beamline followed by three home-made devices. Upstream the collision zone, we use an omega-shaped system [3] to purify the charge state of the incoming ion beam. A collision chamber under UHV conditions is placed next and followed by an electrostatic ion spectrometer designed to separate the collision products from the primary beam. For the coincidence measurements, a silicon X-

ray spectrometer will be placed at the collision chamber. To perform keV/u-keV/u ion-ion collisions, this platform will be connected to another ECR ion source and its beamline, SIMPA (Source d'Ions Multichargés de PARIS). The experiments are expected to start in September 2023.

In November 2021 we tested the ion spectrometer at the ARIBE beamline (GANIL, Caen). All along the beamline, primary ions may collide with residual gas leading to electron capture and production of secondary beams of lower charge states. The ion spectrometer placed at the end of the beamline separates those beams which are then detected by a time-position sensitive detector. We identified three main background contributions [4] that we aim to reduce, and we modified the ion spectrometer accordingly. As a next step, MeV/u-keV/u ion-ion collisions will be also investigated experimentally by connecting the aforementioned platform to the CRYRING@ESR storage ring (GSI, Darmstadt) to reach the unexplored intermediate velocity domain. Coincidence detection will be made between two ion detectors for this study.

### References

- [1] Bräuning, H et al 2005 J. Phys. B, 38 2311
- [2] Gao, J.W et al, Phys. Rev. A 97, 052709 (2018)
- [3] Schury, D et al, RSI 90 083306 (2019)
- [4] Jolly, M et al. Atoms, 10, 146 (2022).

\*E-mail: [jolly@insp.jussieu.fr](mailto:jolly@insp.jussieu.fr)

## Three-particle one-dimensional model for ionization collisions: A simple laboratory to test perturbative approximations

T Guarda<sup>1,2\*</sup>, V D Rodríguez<sup>3†</sup> and R O Barrachina<sup>1,2‡</sup>

<sup>1</sup>Bariloche Atomic Centre, Comisión Nacional de Energía Atómica, 8400 Bariloche, Río Negro Argentina

<sup>2</sup>Balseiro Institute, 8400 Bariloche, Río Negro Argentina

<sup>3</sup>Universidad de Buenos Aires, FCEyN, Departamento de Física-IFIBA CONICET. Buenos Aires. Argentina.

**Synopsis** Here we present a simple 1D model to test both new and known ion-atom collision theories for ionization processes. A short-range exactly-solvable potential for the target and electron-projectile interactions is considered. The ionization spectra  $dP/dv$ , differential in the electron velocity  $v$ , is calculated by means of the numerical solution of the time-dependent Schrödinger equation (TDSE), and compared with perturbative approximations.

We use a 1D collision model for an ion impacting an atom composed of an electron initially bounded to a heavy nucleus. It is well known that even this simple 1D three-body problem requires, at best, the numerical solution of the time-dependent Schrödinger equation (TDSE). Some time ago, a similar model made it possible to successfully study the reliability of the Eikonal-Impulse theory to deal with excitation [1] and capture [2] processes.

In this work we have replaced the square-well model employed in [1] and [2] by the exactly-solvable Modified Pöschl-Teller potential [3]:

$$V(x) = -\frac{\lambda(\lambda+1)}{2a^2 \cosh(x/a)^2}. \quad (1)$$

Atomic units (a.u.) are used throughout this communication.

As a first and representative example, we have calculated the ionization spectra for a projectile velocity  $v_P = 3$  a.u., using the well-known Born approximation and a C2 theory, where the final electron continuum state is distorted by its interactions with the projectile and the target nucleus. In the figure we have chosen the parameters  $a$  and  $\lambda$  in such a way that both ions have two bound states with energies  $-2.0$  and  $-0.5$ , and a zero-energy resonant state.

One of the most striking features of the C2 calculation depicted in the figure is the presence

of an “electron capture to the continuum” (ECC) cusp when the velocities of the electron and the projectile coincide. This cusp is produced by a zero-energy resonance effect, as it was first experimentally observed in 1989 [4, 5].

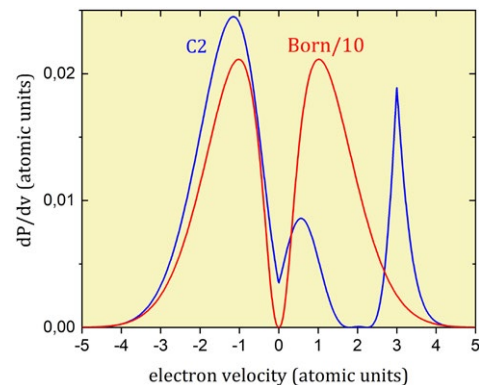


**Figure 1.** Cross section differential in the electron velocity  $v$  for the ionization of a 1D atom by an ion with velocity  $v_P = 3$  a.u. The Born approximation has been divided by a factor 10. See the text for more details.

### References

- [1] Rodríguez V D et al. 1991 *Phys. Scr.* **43** 52
- [2] Gravielle et al 1991 *Phys. Scr.* **43** 57
- [3] Pöschl G and Teller E 1933 *Z. Phys.* **83** 143
- [4] Sarkadi et al. 1989 *Phys. Rev. Lett.*, **62** 527
- [5] Báder A et al. 1997 *Phys. Rev. A*, **55** R14

\*E-mail: [tamaraguarda@ceea.gov.ar](mailto:tamaraguarda@ceea.gov.ar)

†E-mail: [vladimir@df.uba.ar](mailto:vladimir@df.uba.ar)

‡E-mail: [barra@cab.ceea.gov.ar](mailto:barra@cab.ceea.gov.ar)



## Dissociation pathways of methane dication

J Rajput<sup>1\*</sup>, Diksha Garg<sup>1</sup>, A. Cassimi<sup>2</sup>, A. Méry<sup>2</sup>, X. Flécharde<sup>3</sup>, J. Rangama<sup>2</sup>, C. P. Safvan<sup>4</sup>

<sup>1</sup>Department of Physics and Astrophysics, University of Delhi, Delhi 110007, INDIA.

<sup>2</sup>CIMAP, CEA-CNRS-ENSICAEN-UNICAEN, Normandie Université, F-14050 Caen Cedex 04, France.

<sup>3</sup>Université de Caen Normandie, ENSICAEN, CNRS/IN2P3, LPC Caen UMR6534, F-14000 Caen, France

<sup>4</sup>Inter-University Accelerator Centre, New Delhi 110067, INDIA

**Synopsis** The two-body and three-body fragmentation of methane dication has been studied using the technique of cold target recoil ion momentum spectroscopy. For the two-body breakup, the kinetic energy release distribution shows three different pathways, of which two are explained but the third, which appears only with particle impact excitation, remains unexplained. For the three-body breakup, it is shown that this process predominantly proceeds through a two step sequential mechanism.

The methane molecule is the smallest hydrocarbon with a three-dimensional structure and thus provide a test bench for both experimental and theoretical methods. The dication of methane,  $\text{CH}_4^{2+}$ , formed upon a Frank-Condon transition from the ground electronic state of neutral methane has a tetrahedral geometry with  $T_d$  symmetry. On the other hand, the minimum energy equilibrium structure of methane dication is predicted to have planar geometry. Because of these different geometries of neutral methane and its dication, the dissociation of methane dication is expected to involve significant structural changes. We have addressed the two-body and three-body dissociation of methane dication  $[\text{CH}_4]^{2+}$  using the technique of cold target recoil ion momentum spectroscopy (COLTRIMS) in an ion-molecule collision experiment.

For two body dissociation of methane dication, fragment pairs ( $\text{H}^+$ ,  $\text{CH}_3^+$ ) and ( $\text{H}_2^+$ ,  $\text{CH}_2^+$ ) are observed. For breakup into ( $\text{H}^+$ ,  $\text{CH}_3^+$ ), results on four different data sets will be presented [1]. We observe three distinct dissociation pathways (I,II,III) for each data set with mean kinetic energy releases (KER) of around 4.7 eV, 5.8 eV and 7.9 eV, respectively (see figure 1). Of the three observed pathways, pathway II has been observed and its origin is explained in earlier reports. We have proposed an explanation for observation of pathway III using existing *ab-initio* calculations on electronic states of methane dication but the pathway I still remains unexplained [1]. We have also estimated the relative branching ratios for the three pathways, and a strong correlation with the specific nature of the

\*E-mail: [jrajput.du@gmail.com](mailto:jrajput.du@gmail.com)

ion-molecule interaction is noted. A discussion on the electronic states leading to these different pathways will be presented.

For three body dissociation of methane dication the fragment sets ( $\text{H}$ ,  $\text{H}^+$ ,  $\text{CH}_2^+$ ) and ( $\text{H}$ ,  $\text{H}_2^+$ ,  $\text{CH}^+$ ) are studied. Our analysis shows that these three-body fragmentation channels are populated predominantly by a two-step sequential process. The first step of the process results in formation of molecular intermediates  $\text{CH}_3^+$  or  $\text{CH}_2^+$  with high internal energy content and these subsequently stabilize by emission of an H-atom. The statistics for fragment set ( $\text{H}$ ,  $\text{H}^+$ ,  $\text{CH}_2^+$ ) are of the same order as those for fragment set ( $\text{H}^+$ ,  $\text{CH}_3^+$ ). Contrast to this, the statistics for fragment set ( $\text{H}$ ,  $\text{H}_2^+$ ,  $\text{CH}^+$ ) is a very small fraction of the statistics for the set ( $\text{H}_2^+$ ,  $\text{CH}_2^+$ ).

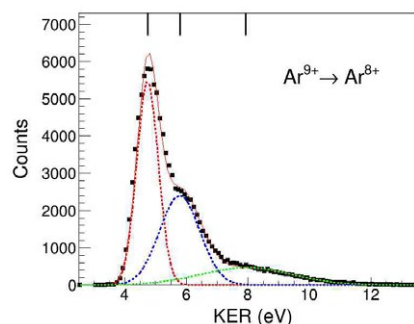


**Figure 1.** A typical fit for the KER distribution for the process,  $\text{CH}_4^{2+} \rightarrow \text{H}^+ + \text{CH}_3^+$ . The squares correspond to experimental data.

### References

- [1] J Rajput *et al.* 2022 *J. Chem. Phys.* **156** 054301

## Fragmentation upon collision-induced activation of cysteine–water cluster cations

L Tiefenthaler<sup>1</sup>, P Scheier<sup>1</sup>, E Erdmann<sup>2</sup>, N F Aguirre<sup>3</sup>, S Díaz-Tendero<sup>4</sup>, T F M Luxford<sup>5</sup> and J Kočíšek<sup>5</sup>\*

<sup>1</sup>Institute for Ion Physics and Applied Physics, University of Innsbruck, Austria

<sup>2</sup>Faculty of Applied Physics and Mathematics, Gdansk University of Technology, Poland

<sup>3</sup>Theoretical Division, LANL, Los Alamos National Laboratory, USA

<sup>4</sup>Departamento de Química, Universidad Autónoma de Madrid, Spain

<sup>5</sup>Heyrovsky Institute of Physical Chemistry, The Czech Academy of Sciences, Czechia

**Synopsis** Cysteine–water cluster cations have been prepared by assembly inside He droplets and subsequently analyzed by means of tandem mass spectrometry using collision-induced dissociation (CID). Quantum chemical calculations based on the Density Functional Theory as well as Monte Carlo approach provided theoretical support of the experimental findings. The energy redistribution within the clusters upon collision activation is investigated. A comparison between ergodic and non-ergodic processes is discussed.

Cysteine (C<sub>3</sub>H<sub>7</sub>NO<sub>2</sub>S), one of the nonessential amino acids, plays a key role in many important biological processes. Benchmark experimental data for the clusters of cysteine and water are relevant from the point of view of radiation biology of peptides. In this work, cysteine–water cluster cations in the canonical form Cys(H<sub>2</sub>O)<sub>3,6</sub><sup>+</sup> and protonated Cys(H<sub>2</sub>O)<sub>3,6</sub>H<sup>+</sup> have been prepared by assembly inside He droplets and subsequently analyzed by means of tandem mass spectrometry using CID. Complementary theoretical simulations allowed us to study energy redistribution in the cysteine–water system.

The theoretical approach applied in this work [1] follows our previous strategy [2, 3], which relies on the analysis of energetic structure and time propagation as well as entropy maximization for elucidation of the initial energy redistribution process. Firstly, the geometries of cysteine–water clusters were optimized at the M06-2X/6-31++G(d,p) level of theory. Secondly, for systems with three water molecules ab initio molecular dynamics simulations were carried out. To treat fragmentation dynamics of large clusters, such as Cys(H<sub>2</sub>O)<sub>6</sub><sup>+</sup>, a less computationally expensive method than ADMP is required. Therefore, the Microcanonical Metropolis Monte Carlo method, in its recent implementation in the M<sub>3</sub>C code [4], was applied for the first time to obtain the fragmentation branching ratios for such complex molecular clusters.

\*E-mail: [jaroslav.kocisek@jh-inst.cas.cz](mailto:jaroslav.kocisek@jh-inst.cas.cz)

The comparison of the experimentally measured appearance energies with dissociation energies for water loss channels obtained with the DFT calculations indicate that clusters do not fragment exclusively by sequential emission of single water molecules, but rather by the release of small water clusters. Through the fitting procedure of the M<sub>3</sub>C-obtained data with experimental relative ion yields we can comment on the energy partitioning after collisional activation. We find that only some of the collision energy redistributes via the ergodic process, while the rest is transferred into a non-ergodic channel leading to the loss of a single water molecule from the cluster. We conclude that modelling of collision-induced activation of weakly bound clusters requires the consideration of the possible non-ergodic processes.

### References

- [1] Tiefenthaler L, Scheier P, Erdmann E, Aguirre N F, Díaz-Tendero S, Luxford, T F M and Kočíšek J 2023 *Phys. Chem. Chem. Phys.* **25** 5361–5371
- [2] Erdmann E, Labuda M, Aguirre N F, Díaz-Tendero S and Alcamí M 2018 *The Journal of Physical Chemistry A* **122** 4153–4166
- [3] Erdmann E, Aguirre N F, Indraji S, Chiarinelli J, Domaracka A, Rousseau P, Huber B A, Bolognesi P, Richter R, Avaldi L, Díaz-Tendero S, Alcamí M and Labuda M 2021 *Phys. Chem. Chem. Phys.* **23** 1859–1867
- [4] Aguirre N F, Díaz-Tendero S, Hervieux P-A, Alcamí M and Martín F 2017 *Journal of Chemical Theory and Computation* **13** 992–1009

## Swift heavy ion irradiation of water, carbon monoxide, and methanol mixture in the solid phase

Ana L. F. de Barros<sup>1</sup>, C. Mejía<sup>2</sup>, A. Domaracka<sup>3</sup>, P. Boduch<sup>3</sup>, C. P. da Costa<sup>3</sup>, H. Rothard<sup>3</sup>, and E. F. da Silveira<sup>4</sup>

<sup>1</sup>Department of Physics - CEFET/RJ, Av. Maracanã 229, Rio de Janeiro, 20271-110, Brazil

<sup>2</sup>Facultad de Ciencias Químicas, Universidad de Cuenca, Av. 12 de Abril y Loja, 010168, Cuenca, Ecuador

<sup>3</sup>CIMAP-CIRIL-Ganil, Boulevard Henri Becquerel, CS 65133 14076, Cedex 5 Caen, France

<sup>4</sup>Department of Physics, PUC/Rio, Rua Marquês de São Vicente 225, 22451-900, Rio de Janeiro, RJ, Brazil

Swift heavy ions were employed to irradiate a sample composed of water, carbon monoxide, and methanol at cryogenic temperature. The chemical evolution of the sample film during irradiation was studied by infrared spectroscopy. Synthesized compounds were identified in the infrared spectra of irradiated samples. The destruction and formation cross-sections were determined from the column density evolution of precursors (water, carbon monoxide, ammonia, and methanol) and the synthesized molecules.

A significant amount of ice in the coldest regions of the Universe consists mainly of a combination of simple molecules such as water (H<sub>2</sub>O), carbon monoxide (CO), ammonia (NH<sub>3</sub>), and methanol (CH<sub>3</sub>OH). Mixture of such compounds form an ice layer covering the grains in the coldest regions of the interstellar medium. This frozen matter is constantly exposed to ionizing radiation from cosmic ray particles, which trigger chemical and physical modifications in the ice on astrophysical time scales. We replicated the astrophysical temperature and irradiation conditions to unravel the evolution of the sample during swift heavy ions irradiation.

The mixtures of molecules H<sub>2</sub>O:CO:CH<sub>3</sub>OH in the percentages of 73:24:3, 67:30:4, and 55:41:4 was condensed at 15 K and kept constant during the experiments. The samples were exposed to a 40 MeV <sup>58</sup>Ni<sup>11+</sup> ion beam with a constant flux of 10<sup>9</sup> ions.cm<sup>-2</sup>.s<sup>-1</sup>. These experiments were performed at the heavy ion accelerator facility GANIL (Grand Accélérateur National d'Ions Lourds) in Caen-France.

Irradiation-induced modifications were measured using the mid-infrared spectroscopy technique. Several spectra were recorded during irradiation as a function of projectile fluence, and the degradation in precursors revealed a number of new infrared bands corresponding to synthesized molecules. The identified molecules are CO<sub>2</sub>, HCO, HCOOH, CH<sub>4</sub>, H<sub>2</sub>CO and H<sub>2</sub>O<sub>2</sub>[2]. The chemical changes of the three samples were compared, showing similar behavior after irradiation. The evolution of the precursor's column

densities is shown in **Fig.1**, which is essential for understanding how molecules are modified in astrophysical ice.

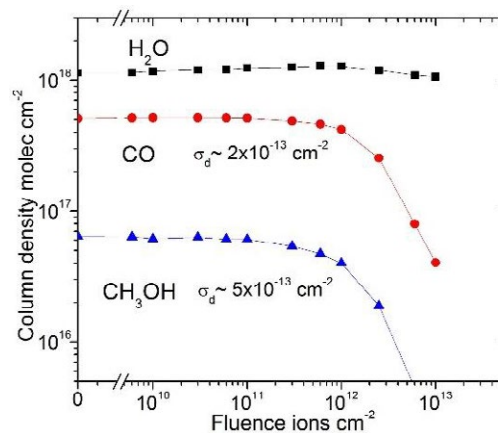


**Figure 1.** Degradation of precursors on fluence for H<sub>2</sub>O:CO:CH<sub>3</sub>OH (67:30:4) percentages. The relation of the destruction cross-sections of CO and CH<sub>3</sub>OH was 2.5. The initial sample thickness was around 1 μm.

### References

- [1] Mejía, C., de Barros, A. L. F., Rothard, H., Boduch, P., & da Silveira, E. F., 2022, MNRAS, **514**(3), 3789-3801.
- [2] de Barros, A. L. F., Mejía, C., Seperuelo Duarte, E., Domaracka, A., Boduch, P., Rothard, H., & da Silveira, E. F., 2022, MNRAS, **511**(2), 2491-2504.

\* E-mail: [ana.barros@cefet-rj.br](mailto:ana.barros@cefet-rj.br)

## Probing the fragmentation pathways of an Argon dimer in slow ion-dimer collisions

M. A. K. A. Siddiki\*, L. C. Tribedi, and D. Misra†

Department of Nuclear and Atomic Physics, Tata Institute of Fundamental Research, Mumbai-400 005, India

**Synopsis** A comparative study of Ar monomer and dimer cations are presented for different capture-associated channels with 2.5 keV/u  $O^{2+}$  projectile beam. The various interatomic relaxation channels are discussed for the  $Ar^+ + Ar^+$  fragmentation channel. In the  $Ar^{2+} + Ar^+$  fragmentation channel, orientation effects have been discussed for the dominant capture mechanism.

The study of multiple electron transfer collisions with atoms/molecules/clusters has raised more fundamental questions due to the involvement of various capture mechanisms. To understand the environment's effect on fragmentation, van der Waal dimers are the perfect candidate where two centers are separated by a few Angstroms (Å). In these weakly bound systems, the interatomic relaxation processes are known as interatomic Coulombic decay (ICD) [1,2], and radiative charge transfer (RCT) [3] has been studied.

The experiment was performed in the electron cyclotron resonance-based ion accelerator (ECRIA) [4] facility at TIFR, Mumbai, using the in-house cold target recoil ion momentum spectroscopy (COLTRIMS) setup [5]. The 2.5 keV/u  $O^{2+}$  projectile beam interacts perpendicularly with a supersonic Ar jet. The recoil ions were measured in coincidence with the final charge-changing projectiles.

We have conducted a comparative study between the monomer cations ( $Ar^{2+}$  and  $Ar^{3+}$ ) and dimer fragmentation channels ( $Ar^+ + Ar^+$  and  $Ar^{2+} + Ar^+$ ) for various capture-associated processes. For this slow  $O^{2+}$ - $Ar_2$  collision system, the near-resonant double electron capture (DC) is the dominant process. The kinetic energy release distributions (KERDs) are used as a gate to separate various relaxation mechanisms. For the  $Ar^{2+} + Ar^+$  fragmentation channel, the double capture and single ionization (DC +SI) is the dominating process. The angular distribution for this channel shows a maximum of around 50 and 130 degrees with

respect to the projectile beam axis. The orientation effect has been explained with the corresponding impact parameters [6].

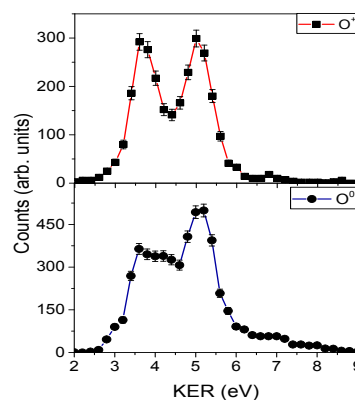


**Figure 1.** The KERDs for the  $Ar^+ + Ar^+$  fragmentation pathways in coincidence with different capture mechanisms. Coincidence with  $O^+$  projectiles, transfer ionization (TI), and transfer excitation (TE) are possible capture channels where neutral O only represents the DC.

### References

- [1] Cederbaum *et al.* *Physical review letters* [79,4778](#).
- [2] Jahnke *et al.* *Physical review letters*, [93,163401](#).
- [3] Matsumoto *et al.* *Physical review letters*, [105,263202](#).
- [4] Agnihotri *et al.* *Physica Scripta* [2011,014038](#).
- [5] Siddiki *et al.* *Review of Scientific Instruments* [2022,93,113313](#).
- [6] Siddiki *et al.* *Atoms*. 2023, [11,34](#).

\* E-mail: [md.siddiki@tifr.res.in](mailto:md.siddiki@tifr.res.in)

† E-mail: [d.misra@tifr.res.in](mailto:d.misra@tifr.res.in)

## Single-electron capture and ionisation in $\text{He}^{2+}\text{-H}_2$ collisions

A M Kotian\*, C T Plowman, I Bray, and A S Kadyrov

Curtin University, GPO Box U1987, Perth, WA 6845, Australia

**Synopsis** The two-centre wave-packet convergent close-coupling approach is used to model  $\text{He}^{2+}$  collisions with molecular hydrogen over the projectile energy range from 1 keV/u to 2 MeV/u. The hydrogen molecule is represented as an effective one-electron target. A sufficiently large basis is used to ensure that all of the calculated cross sections have converged to within 1%.

Theoretical studies of ion-molecule collisions have been scarce because of the difficult challenges it presents compared to modelling ion-atom collisions. We use the two-centre wave-packet convergent close-coupling (WP-CCC) approach to model single-electron capture and ionisation processes in  $\text{He}^{2+}\text{-H}_2$  collisions by treating the molecular target as a spherically symmetric single-electron system. For the total single-electron capture cross section, our results are in good agreement with the experimental measurements at energies above 100 keV/u. However, near the peak of the cross section, they overestimate the experimental data. Partial  $nl$ -resolved electron-capture cross sections have also been calculated, where  $n$  and  $l$  denote the final state principal and angular momentum quantum numbers, respectively.

The WP-CCC calculations for the total non-dissociative single-electron ionisation cross section are plotted in Fig. 1 alongside experimental measurements and other theoretical calculations. The present results are in good agreement with the measurements of Shah and Gilbody [1] and Shah *et al.* [2] at the low energies and high energies but are larger at the intermediate energies. Shah and Gilbody [1] and Shah *et al.* [2] also made separate measurements for the dissociative ionisation cross section and the results show that the contribution of dissociative ionisation towards the total ionisation cross section is negligible at high energies, but at low energies the contribution becomes significant. The present approach does not take into account possible dissociation. This explains why our results

underestimate the measurements by Puckett *et al.* [3] and Rudd *et al.* [4] at energies below 100 keV/u, as they measured the total single-electron ionisation cross section, which sums the dissociative and non-dissociative ionisation (NDI) cross sections.

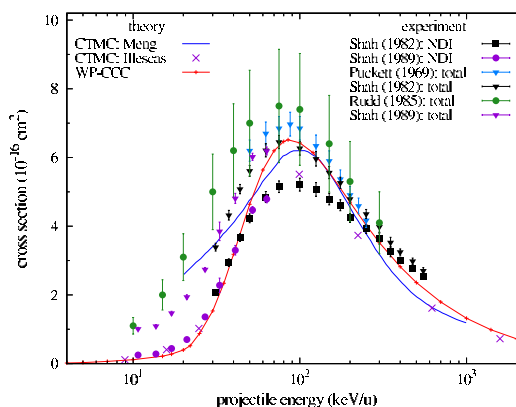


**Figure 1.** The total cross section for non-dissociative single-electron ionisation in  $\text{He}^{2+}\text{-H}_2$  collisions as a function of the projectile energy. Also included are the classical trajectory Monte Carlo calculations [5, 6] and the experimental measurements [1–4].

### References

- [1] Shah M B and Gilbody H B 1982 *J. Phys. B* **15** 3441
- [2] Shah M B *et al* 1989 *J. Phys. B* **22** 3983
- [3] Puckett L J *et al* 1969 *Phys. Rev.* **178** 271
- [4] Rudd M E *et al* 1985 *Phys. Rev. A* **32** 2128
- [5] Meng L *et al* 1989 *Phys. Rev. A* **40** 3637
- [6] Illescas C and Riera A 1999 *Phys. Rev. A* **60** 4546

\*E-mail: [akshit.kotian@postgrad.curtin.edu.au](mailto:akshit.kotian@postgrad.curtin.edu.au)

## Differential ionisation in proton collisions with molecular hydrogen

C T Plowman<sup>1\*</sup>, I B Abdurakhmanov<sup>2</sup>, I Bray<sup>1</sup>, and A S Kadyrov<sup>1</sup>

<sup>1</sup> Curtin University, GPO Box U1987, Perth, WA 6845, Australia

<sup>2</sup>Pawsey Supercomputing Centre, 1 Bryce Ave, Kensington, WA 6151, Australia

**Synopsis** Description of experimental data on energy and angular distributions of electrons produced in intermediate-energy proton collisions with H<sub>2</sub> has remained a long-standing problem. We have developed a coupled-channel method that provides the first accurate solution to this problem. Calculations of the doubly differential cross section for ionisation as a function of the energy and angle of the ejected electron demonstrate excellent agreement with experimental data.

Accurately calculating differential cross sections for ionisation in p + H<sub>2</sub> collisions in the intermediate-energy region presents a significant challenge. Experimental data for the doubly differential cross section (DDCS) for ionisation as a function of both energy and angle of the ejected electron has been available for many decades. However, theoretical results, currently available for selected electron energies and angles, show inconsistent agreement with the data.

We have applied the wave-packet convergent close-coupling (WP-CCC) method to this problem by treating the molecular target effectively as a one-electron system. The approach expands the total scattering wave function in terms of both target and projectile-centred basis states. Substituting this expansion into the Schrödinger equation for the scattering system leads to a set of coupled differential equations for the unknown expansion coefficients. The latter are then used to calculate the differential cross sections. The two-centre expansion allows us to determine direct ionisation and electron capture into the continuum of the projectile. Both components contribute significantly to the ionisation process at intermediate energies.

Results for projectile energies from 20 to 300 keV demonstrate excellent agreement with experimental data over a wide range of electron energies and emission angles leading to significant improvement over previously available calculations. Figure 1 shows the DDCS as a function of energy and angle of the ejected electron in p + H<sub>2</sub> collisions at 300 keV [1]. The present results consistently agree with the experimental data over the wide range of energy and emission angles shown in the figure.

\*E-mail: [corey.plowman@postgrad.curtin.edu.au](mailto:corey.plowman@postgrad.curtin.edu.au)

The WP-CCC approach to differential ionisation is the first theoretical method capable of accurately describing the DDCS across the entire kinematic regime of the emitted electron in p+H<sub>2</sub> collisions, which currently available perturbative methods are unable to accurately reproduce.

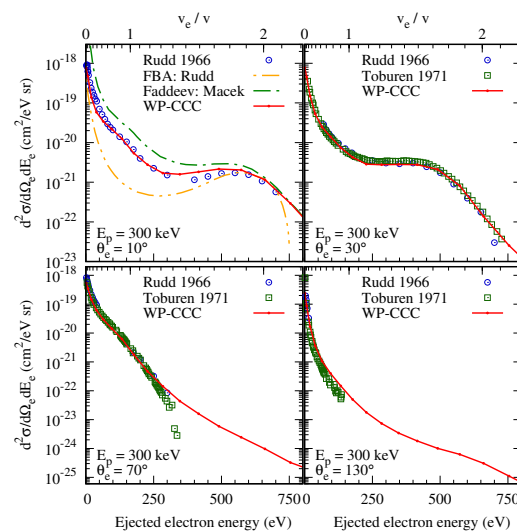


**Figure 1.** DDCS for ionisation as a function of energy and angle of the ejected electron in 300 keV proton collisions with H<sub>2</sub>. Experimental data are by Rudd *et al.* [2] and Toburen *et al.* [3]. The first Born approximation (FBA) results by Rudd *et al.* [2], and Faddeev calculations by Macek [4], available at the 10 deg emission angle, are also shown.

### References

- [1] Plowman C T *et al.* 2023 *Phys. Rev. A* (in production)
- [2] Rudd M E *et al.* 1966 *Phys. Rev.* **151** 20
- [3] Toburen L H *et al.* 1972 *Phys. Rev. A* **5** 247
- [4] Macek J 1970 *Phys. Rev. A* **1** 235



## Role of different electron capture mechanisms in fragmentation of $\text{CO}_2^{3+}$ ions into $\text{O}^+ + \text{C}^+ + \text{O}^+$

K Kumar <sup>\*</sup>, M A K A Siddiki, J Mukherjee and D Misra <sup>†</sup>

Department of Nuclear and Atomic Physics, Tata Institute of Fundamental Research, Mumbai, 400005, India

**Synopsis** In this abstract we will discuss about the fragmentation of  $\text{CO}_2^{3+}$  into  $\text{O}^+ + \text{C}^+ + \text{O}^+$  produced by electron capture upon collision between Ar beams of three different charges and different velocities and supersonically cooled  $\text{CO}_2$  molecules.

$\text{CO}_2$  being a linear triatomic system has attracted a lot of attraction from the point of view of fundamental physics involved. Three body fragmentation of  $\text{CO}_2^{3+}$  into  $\text{O}^+ + \text{C}^+ + \text{O}^+$  has been studied extensively by ion collision [1], Intense femtosecond laser induced ionization [2] and electron impact induced ionization [3], to name a few. Different pathways of fragmentation, i.e. sequential, where two C-O bonds break in a sequential manner, and concerted, in which both bonds break simultaneously, have been reported in the literature.

In present work, we studied roles of different electron capture mechanisms to produce  $\text{CO}_2^{3+}$  ion upon impact by 62 keV  $\text{Ar}^{3+}$ , 240 keV  $\text{Ar}^{6+}$  and 240 keV  $\text{Ar}^{8+}$  projectiles. These beams were produced by 14.5 GHz ECR ion source and supersonically cooled  $\text{CO}_2$  molecules were crossed inside COLTRIMS setup. Post collision projectile ions hit the MCP which gave the start signal for the data acquisition. The projectile MCP is used to construct post interaction charge altered projectile image which we used to separate different capture positions.

In Figure (1) we have plotted the vertical projection of projectile image for different KER ranges. We saw interesting variation across different beams. For  $\text{Ar}^{3+}$ , as we go towards higher KER, the contribution of second capture starts decreasing and that of third capture increases, i.e. pure triple capture (PTC) strengthens and single ionization double capture (SIDC) weakens as we go towards higher KER.

A similar variation was observed in case of  $\text{Ar}^{6+}$ . While in case of high KER, for  $\text{Ar}^{3+}$  PTC became dominant channel, but in case of  $\text{Ar}^{6+}$  although contribution of PTC becomes stronger but SIDC still prevails. In case of  $\text{Ar}^{8+}$ , We did not observe any contribution from PTC, and as we go towards high-

er KER, autoionizing triple capture (ATC) becomes stronger than triple capture with projectile double autoionization (TCDPAI).

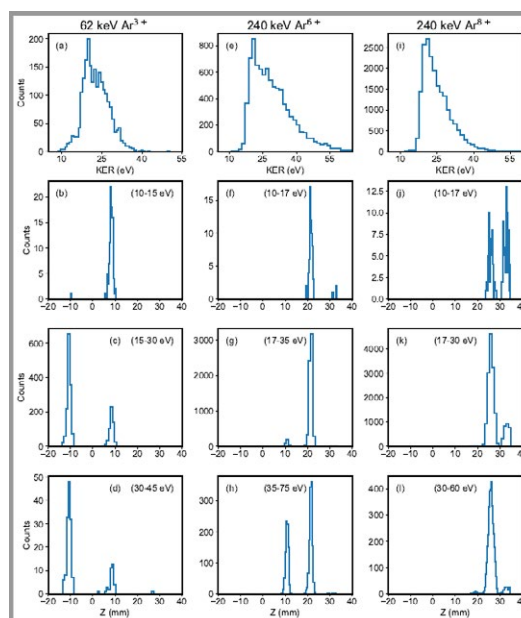


**Figure 1.** Histograms showing projectile vertical projection of the post collision charge altered projectile image for different kinetic energy release (KER) ranges.

### References

- [1] Neumann N et al. 2010 *Phys. Rev. Lett.* **104**, 103201
- [2] Bocharova I et al. 2011 *Phys. Rev. Lett.* **107**, 063201
- [3] Wang E et al. 2015 *Phys. Rev. A* **91**, 052711

<sup>\*</sup> E-mail: [kamalkg2451@gmail.com](mailto:kamalkg2451@gmail.com)

<sup>†</sup> E-mail: [dmisra@tifr.res.in](mailto:dmisra@tifr.res.in)

## Giant quadrupole plasmon resonance in C<sub>60</sub> in high perturbation collisions

L C Tribedi<sup>1</sup>\*, S Kasthurirangan<sup>1,3</sup>, and E Suraud<sup>2</sup>

<sup>1</sup> Tata Institute of Fundamental Research, Colaba, Mumbai – 400005, India.

<sup>2</sup> Laboratoire de Physique Theorique, Universite de Toulouse, F-31062 Toulouse Cedex, France.

<sup>3</sup> University of Mumbai, Santacruz, Mumbai – 400098, India.

**Synopsis** Strong Coulomb perturbation caused by fast highly charged ions has been used to probe the quadrupole plasmon excitation in C<sub>60</sub> fullerene. The C<sub>60</sub> electron-emission spectrum reveals a double-peak structure due to the decay of the giant plasmon resonance, which is identified as arising from the dipole and quadrupole modes of the plasmon through state-of-the-art TDDFT calculations. Furthermore, the electron angular distribution clearly shows a double-well-type distribution which is well reproduced by a model combining the plasmon excitations with long-range postcollisional Coulomb interaction.

The collective plasmon excitation mode known as the GPR (giant plasmon resonance), where the entire delocalised valence-electron cloud of C<sub>60</sub> oscillates collectively about the ionic shell, has been well-studied using photo-excitation, electron-impact and ion-impact excitation [1-3]. A direct observation of the dipole mode of the GPR has been reported earlier by using F<sup>9+</sup> ions (q=9, v~12.7 a.u) [3]. We have now measured the double differential cross section (DDCS) at even higher perturbation (q/v) i.e. in collisions with 91 MeV Si<sup>12+</sup> ions (q=12, v~11.4 a.u). The DDCS spectrum at low energy indicates a quadrupole plasmon resonance (GQPR) in addition to the dipole plasmon (GDPR).

plasmon resonance, using state-of-the-art time-dependent density functional theory (TDDFT) calculations at the level of the time-dependent local density approximation, augmented with average-density self-interaction correction (TDLDA-ADSIC), coupled to a classical description of the projectile ions via pseudopotentials [6]. Fig.1 shows the single-differential cross-section (SDCS) obtained by integrating the DDCS over all angles. The theoretically calculated plasmon contributions are seen to show excellent agreement with the data.

The dipole and quadrupole modes are also independently identified using the evolution of the plasmon-electron angular distributions with ejected electron energy, which shows clear signatures of the dipole and quadrupole plasmon modes. The inset to fig. 1 shows the angular distribution of DDCS at electron energy of 7 eV. The angular distribution is fitted with a Legendre polynomial fitting function, which includes both dipole and quadrupole terms. This is the first such explicit unambiguous experimental demonstration of the quadrupole excitation in atomic system[6].

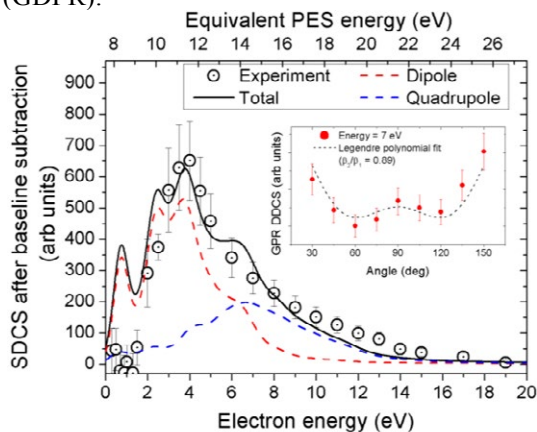


**Figure 1.** SDCS data and comparison with TDDFT calculations; inset: DDCS angular distribution [6]

We have unambiguously identified the dipole and quadrupole modes of the C<sub>60</sub> giant

### References

- [1] Hertel I V et al. 1992 *PRL* **68**, 784
- [2] Bolognesi P et al. 2012 *EPJD* **66**, 254
- [3] Kelkar A H et al. 2015 *PRA* **92**, 052708
- [4] Misra D et al. 2009 *NIM B* **267**, 157
- [5] Gao C-Z et al. 2017 *PRA* **95**, 033427
- [6] Kasthurirangan S et al. 2022 *PRA* **106**, 012820

\* E-mail: [lokesh@tifr.res.in](mailto:lokesh@tifr.res.in)

## Lifetime measurement of collision-induced delayed fragmentation from singly charged intermediate ions

T Nakao<sup>1\*</sup>, R Takasu<sup>1</sup>, S Li<sup>1</sup>, H Tsuchida<sup>1,2</sup>, M Saito<sup>1,2</sup> and T Majima<sup>1†</sup>

<sup>1</sup>Department of Nuclear Engineering, Kyoto University, Kyoto 615-8540, Japan

<sup>2</sup>Quantum Science and Engineering Center, Kyoto University, Uji 611-0011, Japan

**Synopsis** Delayed fragmentation is a characteristic process in the dissociation of polyatomic molecules. We performed a systematic study on the delayed fragmentation of gas-phase nucleobase molecules induced by fast ion collisions. We observed several delayed fragmentation channels for five nucleobase molecules. Additionally, we demonstrated a new method of evaluating the lifetimes of collision-induced delayed fragmentation from singly charged intermediate ions.

Delayed fragmentation has been reported for many molecules. Delayed fragmentation provides rich information about weak bonds in thermal dissociation. Additionally, various dissociation pathways, including sequential fragmentation through singly and doubly charged intermediate ions, can be analyzed. Collision-induced delayed fragmentation from gas-phase nucleobase molecules has been reported for adenine [1,2] but has not been studied for other nucleobases. Moreover, the dissociation lifetimes have not been analyzed owing to technical difficulties. In this study, we compared the delayed fragmentation pathways of the five nucleobase molecules in fast ion collisions to reveal the characteristic features of the fragmentation processes of each nucleobase molecules. Additionally, we determined the lifetimes of some delayed fragmentation channels using a new methodology that compensate for the low detection efficiency of the neutral fragments.

The experiments were performed using pulsed beams of 0.5-MeV  $H^+$  and 0.6–4.0-MeV  $C^{q+}$  ( $q = 1-3$ ) from a 1.7-MV Cockroft–Walton-type tandem accelerator. Gas-phase targets of adenine, guanine, cytosine, thymine, and uracil were prepared by heating each powder. The fragments were analyzed by a time-of-flight (TOF) mass spectrometer with a microchannel plate (MCP) detector and recorded in list mode. Notably, delayed fragmentation from singly charged intermediate ions was observed through the coincidence detection of a positive ion and a neutral fragment that were accelerated before dissociation. Fragmentation pathways were determined by comparing the experimental results with

calculated TOFs for the correlated fragments. To evaluate the lifetime, we estimated the absolute detection efficiency of the MCP detector for neutral fragments by analyzing the data obtained at two extraction voltages.

Figure 1(a) shows a part of the TOF correlation map of the first and second detected fragments from adenine. The long diagonal tails correspond to the delayed fragmentation from singly charged intermediate ions. Delayed fragmentation channels exhibit different features depending on the existence of an O atom. Delayed loss of neutral HCN was mainly observed for adenine, whereas delayed loss of neutral CO or CHNO was the major channels for the other nucleobase molecules. We obtained the decay curves for HCN loss processes from  $C_5H_5N_5^+$  and  $C_4H_4N_4^+$ , as shown in Fig. 1(b). The lifetimes were evaluated to be of microsecond order.

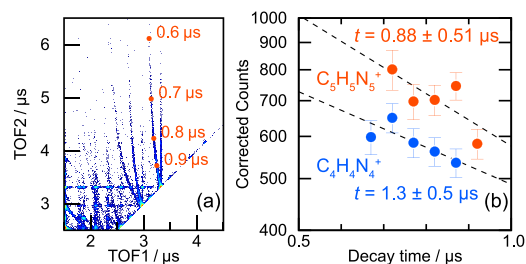


**Figure 1.** (a) TOF correlation map of the two fragments generated from adenine. (b) Decay curves for HCN loss processes from  $C_5H_5N_5^+$  and  $C_4H_4N_4^+$ .

### References

- [1] Moretto-Capelle *et al.*, *J. Chem. Phys.* **127**, 234311 (2007).
- [2] Martin *et al.*, *Phys. Rev. A* **77**, 062513 (2008).

\* E-mail: nakao.tomohiko.65w@st.kyoto-u.ac.jp

† E-mail: majima@nucleng.kyoto-u.ac.jp

## Ion molecule reaction dynamics of the radical anion $O^-$ with deuterated methane $CD_4$ and methyl iodide $CH_3I$

A Ayasli<sup>1\*</sup>, T Michaelsen<sup>1</sup>, A Khan<sup>2</sup>, T Gstir<sup>1</sup>, F Zappa<sup>1</sup> and R Wester<sup>1</sup>

<sup>1</sup>Institut für Ionenphysik und Angewandte Physik, Universität Innsbruck, 6020 Innsbruck, Austria

<sup>2</sup>Department of Physics, Indian Institute of Science Education and Research, Bhopal, India

**Synopsis** We present angle and energy dependent differential cross sections for reactive scattering of  $O^-$  with  $CD_4$  and  $CH_3I$ . We discuss different atomistic mechanisms leading to ionic products observed in these systems.

Our group studies ion-molecule reactions using a crossed-beam setup [1] with kinematically complete velocity map imaging (VMI). This has proven to be a powerful tool to obtain experimental insight into molecular reaction dynamics of ion-molecule reactions. Using the VMI technique, we obtain energy and angle dependent differential cross sections which can be used to identify atomistic reaction mechanisms during reactive collisions.

We present results on reactive scattering of the radical anion  $O^-$  with deuterated methane,  $CD_4$ , in the energy range of 0.2 to 1.5 eV relative collision energy. This reaction produces  $OD^-$  as the ionic product through deuteron transfer. At the lowest collision energy, we observe that the reaction is mainly facilitated through two different mechanisms. The predominant mechanism is direct rebound scattering, which hints towards an incident  $O^-$  approaching the  $CD_4$  molecule along one of the C-D bonds to abstract the deuterium. Further, we find evidence that, at that energy,  $O^-$  forms a long-lived complex with  $CD_4$  before dissociating into  $OD^-$  and  $CD_3$ .

At higher collision energies, complex formation is strongly suppressed in favor of more direct reaction dynamics. We observe products at high angular deflection, which is indicative of  $O^-$  hitting one of three off-axis deuterium atoms for the reaction to occur. Figure 1 summarizes the different visible mechanisms at the highest observed collision energy.

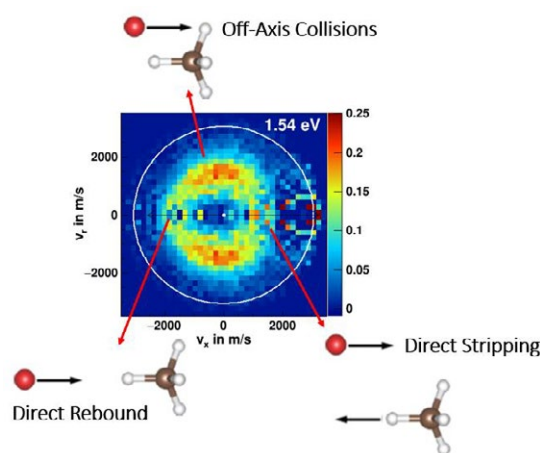


**Figure 1.** Differential cross section of  $OD^-$  for the reaction  $O^- + CD_4 \rightarrow OD^- + CD_3$  at a relative collision energy of 1.5 eV. Different atomistic fingerprints leading to  $OD^-$  are summarized in the figure.

We will compare the obtained differential scattering cross sections with reactive scattering experiments done by Carpenter and Farrar [2] on the  $O^- + CH_4$  system.

Additionally, we present results [3] on reactive scattering of  $O^-$  on methyl iodide  $CH_3I$ . Here, we discuss energy dependent differential cross-sections and branching ratios of four observed, competing reactions pathways.

### References

- [1] Wester R 2014 Phys. Chem. Chem. Phys. **16** 396
- [2] Carpenter M and Farrar J 1997 J. Chem. Phys. **106** 5951
- [3] Khan A et al 2022 J. Phys. Chem. A **126** 50

\* E-mail: [atilay.ayasli@uibk.ac.at](mailto:atilay.ayasli@uibk.ac.at)

## Survival of Interstellar Carbon Knockout Fragments

N Florin<sup>1\*</sup>, M Gatchell<sup>1,2</sup>, J Ameixa<sup>2,3,4</sup>, M Ji<sup>1</sup>, M H Stockett<sup>1</sup>, A Simonsson<sup>1</sup>, S Indrajith<sup>1</sup>, P Reinhed<sup>1</sup>, S Rosén<sup>1</sup>, H Cederquist<sup>1</sup>, H T Schmidt<sup>1</sup> and H Zettergren<sup>1</sup>

<sup>1</sup>Department of Physics, Stockholm University, SE-106 91, Stockholm, Sweden

<sup>2</sup>Institut für Ionenphysik und Angewandte Physik, Universität Innsbruck, Technikerstr. 25, A-6020 Innsbruck, Austria

<sup>3</sup>Atomic and Molecular Collisions Laboratory, CEFITEC, Department of Physics, Universidade NOVA de Lisboa, 2829-516 Caparica, Portugal

<sup>4</sup>Institute of Chemistry, University of Potsdam, Karl-Liebknecht-Str. 24-25, 14476 Potsdam-Golm, Germany

**Synopsis** We have performed experimental and theoretical studies of knockout processes with carbonaceous molecules, and draw conclusions about the lifetimes of their decay products and their possible survival in astrophysical environments.

The presence of polycyclic aromatic hydrocarbons (PAHs) in the interstellar medium was proposed in the 1980's [1][2] and later confirmed in 2021 [3][4][5][6]. Fullerenes, another family of carbon-based molecules, were experimentally observed [7] and later also discovered in space [8]. To gain better understanding of the formation and survival of these molecules in astrophysical environments, we have studied their collisions with single energetic atoms, leading to different knockout processes.

Spontaneous loss of a single carbon atom is an energetically unfavoured decay channel for PAHs and fullerenes. In contrast, when bombarded with atoms or ions, single atom knockout occurs at a significant rate for center of mass collision energies in the 100 eV range [9]. We have studied such knockout events on short (picosecond) timescales theoretically using the LAMMPS molecular dynamics software, and experimentally on timescales of up to minutes using an ion storage ring. The experimentally determined stability of the decay products of these carbon-based structures had previously been limited to studies on microsecond timescales [9][10][11][12]. In experiments at the DESIREE (Double Electro-Static Ion Ring ExpERiment) facility, however, we have now been able to monitor their survival on extended timescales, through colliding PAHs

and fullerenes of various energies with stationary He atoms and then store the knockout fragments in a cryogenic environment mimicking interstellar conditions. We find that a portion of the knockout fragments dissociate spontaneously on timescales of tens of milliseconds, but that a significant fraction are cold enough to remain intact for the entire duration of the measurements (minute timescales). This leads us to conclude that they will survive indefinitely[13].

### References

- [1] Leger A and Puget J L 1984 *Astron. Astrophys.* **137** L5
- [2] Allamandola L J *et al.* 1895 *Astrophys. J. Lett.* **290** L25.
- [3] Cernicharo J *et al.* 2021 *Astron. Astrophys.* **649** L15.
- [4] McGuire B A, Loomis R A, Burkhardt A M *et al.* 2021 *Science* **371** 1265
- [5] Burkhardt A M *et al.* 2021 *ApJL* **913** L18
- [6] Sita M L *et al.* 2022 *ApJL* **938** L12
- [7] Kroto H W *et al.* 1985 *Nature* **318** 162
- [8] Cami J *et al.* 2010 *Science* **329** 5996
- [9] Gatchell M and Zettergren H 2016 *Journal of Physics B* **49** 162001
- [10] Stockett M H *et al.* 2018 *Carbon* **139** 906
- [11] Stockett M H *et al.* 2014 *Phys. Rev. A* **89** 03271
- [12] Stockett M H *et al.* 2015 *J. Phys. Chem. Lett.* **22** 4504
- [13] Gatchell M *et al.* 2021 *Nature Communications* **12** 6646

\*E-mail: [naemi.florin@fysik.su.se](mailto:naemi.florin@fysik.su.se)



## Cold molecular dynamics and chemical reactions of H<sub>2</sub> (D<sub>2</sub>) in strong laser fields

L Zhou<sup>1</sup>, J Qiang<sup>1</sup>, H Ni<sup>1</sup>, Z Jiang<sup>1</sup>, W Jiang<sup>1</sup>, W Zhang<sup>1</sup>, P Lu<sup>1</sup>, K Lin<sup>2</sup>, H Stapelfeldt<sup>3</sup> and J Wu<sup>1\*</sup>

<sup>1</sup> State Key Laboratory of Precision Spectroscopy, East China Normal University, Shanghai 200241, China

<sup>2</sup> Institut für Kernphysik, Goethe-Universität Frankfurt am Main, Frankfurt am Main 60438, Germany

<sup>3</sup>Department of Chemistry, Aarhus University, Langelandsgade 140, 8000 Aarhus C, Denmark

**Synopsis** Rotational dynamics of D<sub>2</sub> molecules inside helium nanodroplets is investigated. The observations show that the D<sub>2</sub> molecules inside helium nanodroplets essentially rotate as free D<sub>2</sub> molecules. In addition, helium droplets provides the opportunity to capture two D<sub>2</sub> molecules, where D<sub>3</sub><sup>+</sup> is detected implying the presence of the reaction of (D<sub>2</sub>-D<sub>2</sub>)<sup>+</sup> → D<sub>3</sub><sup>+</sup>+D. We further time and control D<sub>3</sub><sup>+</sup> formation from bimolecular reaction in a D<sub>2</sub>-D<sub>2</sub> dimer in gas phase.

Helium (<sup>4</sup>He) nanodroplets with an extremely cold environment at 0.37 K and a broad transparent spectral range are ideal nanoreactors for light-induced physical and chemical reactions of the embedded atoms and molecules. The in-droplet molecules can rotate freely, manifesting the superfluidity of helium nanodroplets on a microscopic level. By using a non-resonant fs pulse to create rotational wave packets in D<sub>2</sub> molecules embedded in helium nanodroplets and measuring the rotational dynamics through timed strong-field ionization, we find the observed rotational dynamics is essentially the same as that of isolated gas-phase D<sub>2</sub> molecules [1].

As compared to the nuclear motion, the electron acts much faster and thus serves as an ultrafast probe of the condensed environment. More recently, we investigated the above-threshold multiphoton dissociative ionization of H<sub>2</sub> embedded in superfluid He nanodroplets driven by ultraviolet femtosecond laser pulses. We found that the surrounding He atoms enhance the dissociation of in-droplet H<sub>2</sub><sup>+</sup> from lower vibrational states as compared to that of isolated gas-phase molecules [2].

Cold molecular beams permit the formation of unstable molecular dimers, e.g. H<sub>2</sub>-H<sub>2</sub> dimers, achieved by precooling the molecules before its expansion into vacuum. We investigate the ultrafast formation dynamics of D<sub>3</sub><sup>+</sup> from a bimolecular reaction of a gas-phase D<sub>2</sub>-D<sub>2</sub> dimer driven by ultrashort laser pulses (Fig. 1a). The formation time varies for different reaction pathways (Fig. 1b). As compared to the fast double ionization pathway, the slow single ionization pathway takes about 139 fs

(Fig. 1c). By performing the molecular dynamics simulation, we track the reaction dynamics in time (Fig. 1d). Furthermore, we achieved control over the formation dynamics of D<sub>3</sub><sup>+</sup> ion by manipulating its emission direction using a tailored two-color laser field with unprecedented precision. More details can be found in Ref. [3].

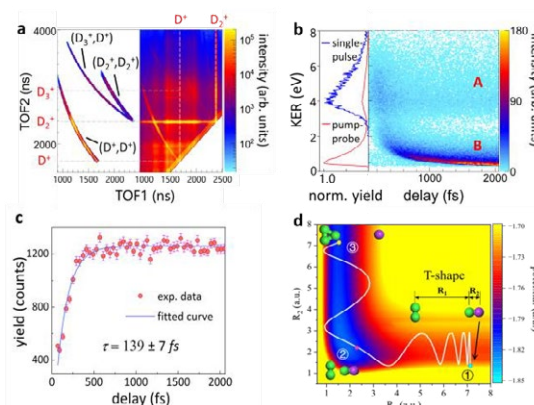


**Figure 1.** a, Measured photoion-photoion coincidence spectrum. b, Measured time-dependent kinetic energy release spectrum. c, Yield of D<sub>3</sub><sup>+</sup> as a function of pump-probe time delay. d, Nuclear dynamics evolving along the white curve to form D<sub>3</sub><sup>+</sup>.

### References

- [1] Qiang J, Zhou L *et al* 2022 *Phys. Rev. Lett.* **128**, 243201
- [2] Zhou L *et al* 2023 *Phys. Rev. Lett.* **130**, 033201
- [3] Zhou L *et al* 2023 *Nat. Chem.* (accepted, DOI:[10.21203/rs.3.rs-1951970/v1](https://doi.org/10.21203/rs.3.rs-1951970/v1))

\* Email: [jwu@phy.ecnu.edu.cn](mailto:jwu@phy.ecnu.edu.cn)



## Collective electron dynamics in large ultracold atomic ensembles

Mario Großmann<sup>1,2,3</sup>, Julian Fiedler<sup>1,2,3</sup>, Jette Heyer<sup>1,2,3</sup>, Amir Khan<sup>2</sup>,  
Markus Drescher<sup>1,2,3,\*</sup>, Klaus Sengstock<sup>1,2,3</sup>, Philipp Wessels-Staarmann<sup>1,2,3</sup>, and Juliette Simonet<sup>1,2,3</sup>

<sup>1</sup>The Hamburg Centre for Ultrafast Imaging (CUI), 22761 Hamburg, Germany

<sup>2</sup>Center for Optical Quantum Technologies, 22761 Hamburg, Germany

<sup>3</sup>Department of Physics, University of Hamburg, 22761 Hamburg, Germany

**Synopsis** Femtosecond photoionization of a <sup>87</sup>Rb Bose-Einstein Condensate creates a large number of interacting electrons and ions. The evolving collective dynamics leads to ultrafast cooling on picosecond to nanosecond time scales. Excitation below the ionization threshold may still create an ultracold plasma owing to collisional ionization of Rydberg states.

Post-collisional effects following atomic photoionization have traditionally been studied for the case of a single isolated electron in the direct vicinity of its mother-ion [1]. Creating dense clouds of ultracold atoms now opens up a regime where collective many-particle dynamics of a few thousand electrons and ions can be explored in all detail.

We prepare a  $\mu\text{m}$ -sized Bose-Einstein condensate (BEC) of  $\sim 10^4$  <sup>87</sup>Rb atoms at a typical density of  $10^{14}/\text{cm}^3$ . Upon illumination with a 200 fs light pulse half of the ensemble will be 2-photon ionized [2], thus initially forming a strongly-coupled plasma at ion temperatures below 40 mK. The much faster electrons transfer most of their initial temperature of a few thousand Kelvin to the ionic component within a few ps. The ion cloud forms a dynamical trap - its thermal expansion leads to further cooling on a slower time scale until after  $\sim 500$  ns an electron temperature of about 10 K is reached. Finally, field ionization liberates the trapped electrons which are detected with a transversal momentum corresponding to merely a few meV kinetic energy [3]. The observed 2-3 orders of magnitude electron cooling in the coupled ionic/electronic system is reproduced with a plasma simulation, that grants us insight into non-equilibrium dynamics on picosecond time scales.

The initial temperature and cooling rate are determined by the electrons' excess energy which is tuned via the laser wavelength. This directly impacts the neutrality of the plasma: High excess energies yield a highly charged

plasma with rapid electron cooling whereas low excess energies support a neutral plasma with strongly increased lifetimes.

Excitation below the 2-photon ionization threshold yields a population of discrete states. Owing to the comparably large spectral bandwidth of the femtosecond light pulse a prohibited population of Rydberg states within a radius of typically a few  $\mu\text{m}$  due to Rydberg blockade, usually observed upon excitation with narrow-band cw-radiation, is avoided here.

High-order, i.e. loosely bound Rydberg states with large orbits are prone to ionization by collisions with nearby electrons/ions. Consequently, also below-threshold excitation can lead to a partial ionization. The fraction of stable Rydberg states is observed to increase with decreasing main quantum number but the detailed evolution for the BEC appears to differ from a thermal gas.

This work is supported by the Cluster of Excellence 'Advanced Imaging of Matter' of the Deutsche Forschungsgemeinschaft (DFG) EXC 2056 project ID 390715994 and the Cluster of Excellence 'The Hamburg Centre for Ultrafast Imaging' of the Deutsche Forschungsgemeinschaft (DFG) EXC 1074 project ID 194651731.

### References

- [1] Schütte B et al 2012 *Phys. Rev. Lett.* **108** [253003](#)
- [2] Wessels P et al. 2018 *Commun. Phys.* **1** [32](#)
- [3] Kroker T et al. 2021 *Nat. Commun.* **12** [596](#)

\* E-mail: [markus.drescher@uni-hamburg.de](mailto:markus.drescher@uni-hamburg.de)

## Magneto-optical trap reaction microscope for cold strontium atoms

Shushu Ruan<sup>1,2</sup>, Xinglong Yu<sup>1,2</sup>, Zhenjie Shen<sup>1</sup>, Xincheng Wang<sup>3</sup>, Matthias Weidemüller<sup>4</sup>, Bing Zhu<sup>5\*</sup> and Yuhai Jiang<sup>1,2,3 †</sup>

<sup>1</sup>Shanghai Advanced Research Institute, Chinese Academy of Sciences, Shanghai 201204, China

<sup>2</sup>University of Chinese Academy of Sciences, Beijing 100049, China

<sup>3</sup>Center for Transformative Science and School of Physical Science and Technology, Shanghai Tech University, Shanghai 201210, China

<sup>4</sup>Physikalisches Institut, Universität Heidelberg, Im Neuenheimer Feld 226, 69120 Heidelberg, Germany

<sup>5</sup>HSBC Holdings Plc., Guangzhou 510510, China

**Synopsis** A magneto-optical trap reaction microscope (MOTReMi) for cold strontium atoms is reported. With the femtosecond laser pulses, for the first time we are allowed to observe the single and double ionization of cold strontium atoms in the ground state and the excited state. Coincident 3D momentum distributions of electrons and recoil ions present amazing dynamic information, where momentum resolutions of 0.05 a.u. and 0.2 a.u. for electrons and ions can be achieved.

Experiments about the excitation and ionization of atoms involving two valence electrons like strontium atoms in strong laser field are meaningful in probing wave packet evolution and electron-correlated dynamics. The Sr-MOTReMi utilized to cool and to trap the hot strontium atoms for extremely high momentum resolution is powerful tool for this scientific goal in the UV regime. This technique was reported here, analogy to that for rubidium [1, 2].

The schematic diagram of Sr-MOTReMi is shown in Figure.1(b). The hot atoms generated from the Sr oven are pre-cooled and trapped as a atomic cloud in the center of 2D MOT chamber by two orthogonal pairs of retroreflected 461nm laser beams and an auxiliary Zeeman slower. A pushing beam pushes the cloud to form a cold atomic beam which propagates into the science chamber. The atomic beam are further cooled by another three pairs of retroreflected cooling beams to generate 3D MOT target or molasses target in the center of science chamber, where the cold atoms are ionized by laser pulse. The charged fragments are collected by two position-sensitive detectors in  $4\pi$  solid angle. The three-dimensional momentum of each particle is reconstructed from the time-of-flight (TOF) and the position hit on the detectors.

The momentum resolution is characterised in single ionization of molasses target impacted with a 800nm pulsed laser. The coincident imaging of  $\text{Sr}^+$  and  $e^-$  in terms of momentum in the

TOF direction is shown in Figure.1(c). Under this circumstance, the momentum resolutions of ion and electron are better than 0.2 a.u. and 0.05 a.u.. With the femtosecond laser pulses, for the first time we observe the single and double ionization of cold strontium atoms in the ground state and the excited state. Coincident 3D momentum distributions of electrons and recoil ions present rich dynamic information, which will be presented later.

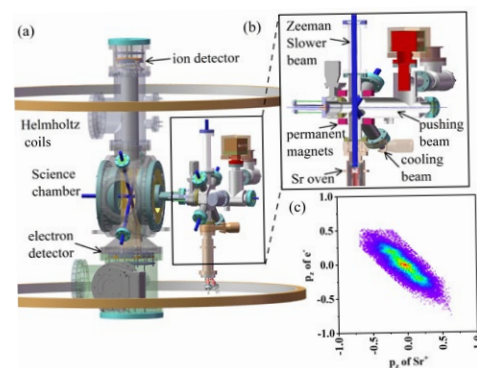


**Figure 1.** (a)the schematic diagram of Sr-MOTReMi. (b)the cutaway view of 2D MOT chamber. (c)the coincident momentum of  $\text{Sr}^+$  and  $e^-$ .

### References

- [1] Renyuan Li et al. 2019 *J. Instrum.* **14** P02022
- [2] Junyang Yuan et al. 2020 *Phys. Rev. A* **102** 043112

\*E-mail: [bing1.zhu@hsbc.com](mailto:bing1.zhu@hsbc.com)

†E-mail: [jiangyh3@shanghaitech.edu.cn](mailto:jiangyh3@shanghaitech.edu.cn)

## Microwave spectroscopy of high- $n$ low- $\ell$ $^{84}\text{Sr}$ Rydberg states in a cold gas<sup>†</sup>

R A Brienza<sup>1\*</sup>, Y Lu<sup>1</sup>, C Wang<sup>1</sup>, S K Kanungo<sup>1</sup>, T C Killian<sup>1</sup>, F B Dunning<sup>1</sup>, S Yoshida<sup>2</sup>, and J Burgdörfer<sup>2</sup>

<sup>1</sup>Department of Physics and Astronomy, Rice University, Houston, Texas 77005-1892, USA

<sup>2</sup>Institute for Theoretical Physics, Vienna University of Technology, Vienna, Austria, EU

**Synopsis** Microwave spectroscopy is used to accurately measure the transition frequencies, i.e., energy level separations, between  $^{84}\text{Sr}$   $n^1S_0$ ,  $n^1P_1$ ,  $n^1D_2$ , and  $n^1F_3$  levels for  $50 \leq n \leq 70$ . The results are being used to generate updated sets of self-consistent Rydberg-Ritz parameters for the corresponding quantum defects that enable energy level separations to be predicted with much greater precision than when using earlier parameter sets.

Atoms in high-Rydberg states are of increasing importance in cold-atom studies with applications in quantum computing, simulation, sensing, and optics. These applications exploit their strong tunable atom-atom interactions and optical non-linearities. Strontium is particularly attractive for such studies because of the availability of bosonic isotopes with no fine structure, and singlet states that possess particularly simple level structures.

Rydberg term values can be determined from their quantum defects, typically described using Rydberg-Ritz expressions of the form

$$\delta = \delta_0 + \frac{\delta_2}{(n - \delta_0)^2} + \frac{\delta_4}{(n - \delta_0)^4} \quad (1)$$

where  $\delta_0$ ,  $\delta_2$ , and  $\delta_4$  are constants. Values for these parameters have been published by earlier workers [1]. However, measurements involving microwave-coupled singlet states revealed that transition frequencies predicted using these parameters could be in error by up to  $\sim 80$  MHz (see Table 1). A detailed high-resolution,  $\pm 10$  kHz, spectroscopic study of energy-level separations between a variety of  $n^1S_0$ ,  $n^1P_1$ ,  $n^1D_2$ , and  $n^1F_3$  states with  $50 \leq n \leq 70$  was therefore initiated, taking care to minimize the effects of both AC and DC Stark shifts. These results are being used, in conjunction with earlier published term energies and quantum defects, to generate an updated self-consistent set of Rydberg-Ritz

parameters that can predict the measured transition frequencies to within an accuracy of 30 kHz.

Although the parameters are being optimized for the present range of  $n$ , they should also provide improved term energies and transition frequencies over a much broader  $n$  range, critical input when designing quantum simulation experiments that involve many coupled Rydberg levels such as, for example, in studies involving Rydberg-atom synthetic dimensions [2], where accidental single- or multi-photon resonances could induce spurious couplings.

**Table 1.** Differences,  $\Delta f$ , between the predicted and measured frequencies for the selected transitions indicated.

transition	$\Delta f$ (MHz)
$5s55s \ ^1S_0 \rightarrow 5s55p \ ^1P_1$	87.5
$5s60s \ ^1S_0 \rightarrow 5s60p \ ^1P_1$	67.6
$5s55s \ ^1S_0 \rightarrow 5s55d \ ^1D_2$	54.4
$5s60s \ ^1S_0 \rightarrow 5s60d \ ^1D_2$	43.5
$5s65d \ ^1D_2 \rightarrow 5s62f \ ^1F_3$	41.8
$5s70d \ ^1D_2 \rightarrow 5s67f \ ^1F_3$	33.3

<sup>†</sup>Research supported by NSF and FWF (Austria)

### References

- [1] Vaillant CL *et al.* 2012 *J. Phys. B: Atomic Molecular and Optical Physics* **45** 135004
- [2] Kanungo SK *et al.* 2022 *Nat. Commun.* **13** 972

\*E-mail: [rab13@rice.edu](mailto:rab13@rice.edu)

## Cold collisions of atomic and molecular hydrogen with astrochemically relevant anions.

C Lochmann\*, S Purushu-Melath, M Nötzold, R Wild, F A Gianturco and R Wester

Institut für Ionenphysik und Angewandte Physik, Universität Innsbruck, 6020 Innsbruck, Austria

**Synopsis** We present temperature dependent reaction rates of the astrochemically relevant anions  $\text{CN}^-$  and  $\text{C}_3\text{N}^-$  with atomic hydrogen and of  $\text{C}_2^-$  with molecular hydrogen in the temperature range between 6 K and 295 K.

To date six negatively charged ions have been identified in the interstellar medium (ISM). All six anions are carbon containing species of the form  $\text{C}_n\text{N}^-$  with  $n = 1, 3, 5$  and  $\text{C}_n\text{H}^-$  with  $n = 4, 6, 8$ . The discoveries of these anions opened up the need to understand their involvement in the chemical networks of the ISM.

Previously, we already performed absolute crosssection [1, 2] as well as threshold photodetachment studies on  $\text{CN}^-$  and  $\text{C}_3\text{N}^-$  at cryogenic temperatures, which provided accurate electron affinities [3, 4]. Furthermore, we performed vibrational pre-dissociation spectroscopy on  $\text{CN}^-(\text{H}_2/\text{D}_2)$  in regions between  $400\text{ cm}^{-1}$  and  $3100\text{ cm}^{-1}$ , which provided the first detailed vibrational spectra for these two complexes [5]. In order to understand the chemical relevance of these ions, it is also important to study their interaction with the most abundant reactive partners in the cold interstellar environments. Especially ion-neutral reactions are vital, as the long range interactions lead to significantly larger reaction rates.

Here, we present temperature dependent reaction rates of  $\text{CN}^-$  and  $\text{C}_3\text{N}^-$  with atomic hydrogen. Both reactions are associative recombination reactions which lead to the neutral species HCN and  $\text{HC}_3\text{N}$  plus a continuum electron, respectively. These reactions were previously studied at room temperature [6]. However, as the temperature of the environments in which these ions are found is usually below 100 K, we set out

to measure the rate as a function of temperature from room temperature down to 6 K. Additionally, we also measured the three-body reaction of  $\text{C}_2^-$  with molecular hydrogen.  $\text{C}_2^-$  is proposed to exist in the ISM due to the abundance of its neutral counterpart and high electron affinity. So far, however, it remains elusive.

All experiments were carried out in a 16-pole radio-frequency ion trap, mounted on a liquid helium cryostat which allows cooling down to 6 K. By buffer-gas cooling with helium the ions thermalize to the buffer-gas temperature which allows for temperature dependent measurements.

We find, that in the case of  $\text{CN}^-$  plus H the reaction rate experiences a significant reduction in the rate between 150 K and 250 K, while in the same region  $\text{C}_3\text{N}^-$  plus H stays constant. Below 50 K both rates seem to increase toward the Langevin limit.

In the case of  $\text{C}_2^-$  reacting with  $\text{H}_2$  we find that a pure three-body reaction takes place, which leads to the anionic product  $\text{C}_2\text{H}^-$ . A comparison to variational transition state theoretical calculations provides the understanding of the reactive pathway of this ternary reaction.

### References

- [1] Best T *et al.* 2011 *ApJ* **742** 63
- [2] Kumar S S *et al.* 2013 *ApJ* **776** 25
- [3] Simpson M *et al.* 2020 *J. Chem. Phys.* **153** 184309
- [4] Simpson M *et al.* 2021 *Phys. Rev. Lett.* **127** 043001
- [5] Dahlmann F *et al.* 2022 *Mol. Phys.* **120** 2085204
- [6] Yang Z *et al.* 2011 *ApJ* **739** 19

\*E-mail: [Christine.Lochmann@uibk.ac.at](mailto:Christine.Lochmann@uibk.ac.at)

## Theoretical Studies of Mutual Neutralization

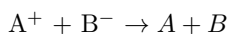
A E Orel<sup>1\*</sup> and Å Larson<sup>2†</sup>

<sup>1</sup>Department of Chemical Engineering, University of California, Davis, California 95616, USA

<sup>2</sup>Department of Physics, Stockholm University, SE-106 91 Stockholm, Sweden

**Synopsis** Total and differential cross sections for mutual neutralization in collisions of  $\text{Li}^+$  and  $\text{O}^-$  and  $\text{Na}^+$  and  $\text{O}^-$  are calculated *ab initio* and fully quantum mechanically. The potential energy curves and non-adiabatic couplings of the electronic states of LiO and NaO are studied as a function of basis set size. The nuclear dynamics are studied using a strict diabatic representation of the states. Atomic final state distributions are investigated and compared to available experimental data.

Mutual neutralization, the process:



is, in general, driven by non-adiabatic couplings arising from avoided crossings between ionic and covalent states occurring at large internuclear distances. Usually, highly excited electronic states are involved. For an *ab initio* description of the reaction, the potential energy curves of the ionic and covalent states of the reaction complex have to be computed as well as the corresponding non-adiabatic coupling elements.

**Table 1.** Energies (in eV) and crossing distances (in Bohr) of states involved in mutual neutralization. Energies are relative to the separated ground state atoms.

State	Energy	$R_x$	Ion-Pair
$\text{Li}^* + \text{O}$	1.84	13.01	3.93
$\text{Li} + \text{O}^*$	1.97	13.85	
$\text{Na}^* + \text{O}$	2.1	17.24	3.678
$\text{Na} + \text{O}^*$	1.97	15.46	

The systems LiO and NaO are particularly interesting due to the energetics. In both cases, channels leading to excited oxygen and ground state Li (or Na) or ground state oxygen and excited state Li (or Na) are open. The crossings between these excited neutral states and the ion-pair channel are at similar internuclear distances as shown in Table I. The process leading to  $\text{Li}^*$  (or  $\text{Na}^*$ ) requires a one-electron transition from the oxygen anion. The process leading to  $\text{O}^*$  requires a two-electron rearrangement. In other systems, the first process dominates. Recent experiments [1] on the NaO system indicate that

the  $\text{Na}^*$  channel dominates.

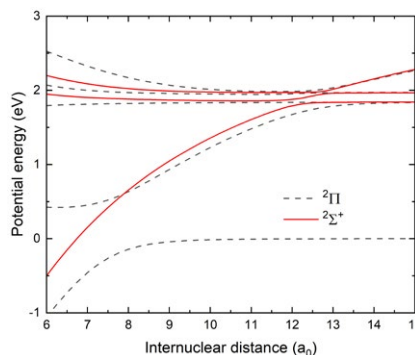


**Figure 1.** The potential energy curves for the LiO system.

We have carried out multi-reference configuration interactions quantum chemistry calculations on these systems to compute the potential energy curves (for example see Figure 1) and non-adiabatic couplings between the states. The data from these calculations is used as input for the scattering calculation where the coupled Schrödinger equation is solved numerically for fixed angular momentum,  $l$ . We will present total and differential cross sections and final state distributions and compare to the available experimental data [2, 3, 4].

### References

- [1] Douchain A Systematic study of mutual neutralization reactions between atomic species using the merged beam method and an asymptotic model [PhD] Louvain-La-Neuve 2022
- [2] Moseley, J T, Aberth W and Peterson J R 1972 J. Geophys. Res. **77** 255
- [3] Peart B and Foster S J 1987 J. Phys. B **20** L691
- [4] Hayton D A and Peart B 1995 J. Phys. B **28** L279

\*E-mail: [aeorel@ucdavis.edu](mailto:aeorel@ucdavis.edu)

†E-mail: [aasal@fysik.su.se](mailto:aasal@fysik.su.se)

## Theoretical studies of reactive scattering processes involving the $\text{H}_2$ reaction complex

J Hörnquist<sup>1\*</sup>, P Hedvall<sup>1</sup> Å Larson<sup>1</sup> and A E Orel<sup>2</sup>

<sup>1</sup>Department of Physics, Stockholm University, AlbaNova University Center, SE-106 91 Stockholm, Sweden

<sup>2</sup>Department of Chemical Engineering, University of California, Davis, California 95616, USA

**Synopsis** We study mutual neutralization of  $\text{H}^+ + \text{H}^-$  *ab initio* and fully quantum mechanically including effects which have not previously been considered such as rotational couplings and autoionization from electronic resonant states. A quasidiabatic model is developed to investigate the role of autoionization and higher excited states. This model can also be used to study a variety of other processes and is here applied in a study of associative ionization in collisions of  $\text{H}^+ + \text{H}^-$  and  $\text{H}(1s) + \text{H}(ns)$ .

The mutual neutralization process  $\text{H}^+ + \text{H}^- \rightarrow \text{H}(1s) + \text{H}(n)$ , where  $n$  is the principal quantum number, is important for understanding  $\text{H}_2$  formation in the early universe [1]. Here, this process is studied *ab initio* and fully quantum mechanically and the total and differential cross sections as well as the branching ratios are calculated. These calculations include effects which have not previously been considered, such as rotational couplings that couple  $^1\Sigma_{g/u}^+$  states to  $^1\Pi_{g/u}$  states, excited states correlating with the  $n \geq 4$  asymptotic limits and autoionization from electronic resonant states. We use accurate *ab initio* potential curves and couplings to describe the lower electronic states while a quasidiabatic model is developed to include the lowest electronic resonant state in each relevant symmetry as well as an arbitrary number of Rydberg states. With this model, we investigate the importance of higher excited states and the role of autoionization. While the inclusion of rotational couplings is found to be important, the effect of autoionization and higher excited states is shown to be small for this particular system [2].

Since the model includes couplings between bound electronic states as well as electronic resonant states and couplings to the ionization continuum, it can also be used to study other processes such as double charge transfer, dissociative recombination, resonant ion-pair formation and

associative ionization. We also present the results of a study of the associative ionization processes  $\text{H}^+ + \text{H}^- \rightarrow \text{H}_2^+ + e^-$  and  $\text{H}(1s) + \text{H}(ns) \rightarrow \text{H}_2^+ + e^-$ . For these processes we investigate the importance of non-local effects by including a non-local complex potential.

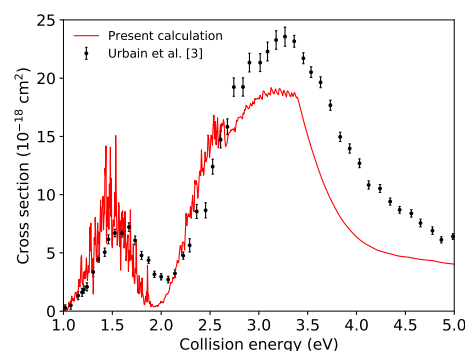


**Figure 1.** Calculated  $\text{H}(1s) + \text{H}(2s)$  associative ionization cross section compared with the measurement of Ref. [3].

### References

- [1] Glover S C, Savin D W and Jappsen A K 2006 *ApJ* **640** 553
- [2] Hörnquist J, Hedvall P, Larson Å and Orel A E 2023 *Phys. Rev. A* **106** 062821
- [3] X Urbain, A Cornet, F Brouillard and A Giusti-Suzor 1991 *Phys. Rev. Lett.* **66** 1685

\*E-mail: [johan.hornquist@fysik.su.se](mailto:johan.hornquist@fysik.su.se)



## Mutual neutralization of ${}^1,2\text{H}^-$ with $\text{Li}^+$ , $\text{O}^+$ , $\text{N}^+$ and $\text{C}^+$ at DESIREE

A F Schmidt-May<sup>1\*</sup>, G Eklund<sup>1</sup>, S Rosén<sup>1</sup>, M C Ji<sup>1</sup>, J Grumer<sup>2</sup>, P S Barklem<sup>2</sup>,  
H Cederquist<sup>1</sup>, H Zettergren<sup>1</sup>, and H T Schmidt<sup>1†</sup>

<sup>1</sup> Stockholm University, Stockholm, 114 19, Sweden

<sup>2</sup> Uppsala University, Uppsala, 752 36, Sweden

### Synopsis

We present mutual neutralization studies of  ${}^1,2\text{H}^-$  with  $\text{Li}^+$ ,  $\text{O}^+$ ,  $\text{N}^+$  and  $\text{C}^+$  at DESIREE. The systems are of astrophysical interest and the collisions take place at sub-electronvolt energies which are typical collision energies in cool stellar photospheres, such as the Sun. For  $\text{Li}^+$ , we find a strong isotope effect on the branching fraction into  $\text{Li}(3s)$ , which constitutes one of the first observations of its kind. We compare our results to theoretical predictions with varying degree of agreement.

Stellar photospheres commonly deviate from thermal equilibrium and inelastic processes influence the population distribution. The impact of collisions with the most abundant element hydrogen on the abundance analysis was studied in detail in the cases of Li, Na and Mg [1, 2, 3, 4]. Charge-transfer reactions such as mutual neutralization, and its reverse process ion-pair production, were found to have a significant influence on the abundance. Cross sections employed in non-LTE modelling are commonly estimated and reliable cross sections are highly sought after. Barklem introduced an asymptotic model based on linear combinations of atomic orbitals (LCAO) for the molecular structure and combined it with a multi-channel Landau-Zener model for the dynamics with the idea of being more widely applicable than full quantum methods [5]. Experimental results on the branching fractions such as ours serve as an important benchmark for these calculations. Specifically when studying hydrogen, the large mass ratio between hydrogen and the collision partner poses a technical challenge and hydrogen is often replaced by deuterium in the experiments. With our measurement of the MN of  $\text{Li}^+ + {}^1,2\text{H}$ , we offer one of the first experimental observations of an isotope effect on the product distribution. The obtained kinetic-energy distributions are displayed in Fig. 1 and show the significant decrease of the  $\text{Li}(3s)$  product when deuterium

replaces hydrogen. Additionally, we present preliminary results on  ${}^1\text{H}^- + \text{C}^+$ ,  $\text{N}^+$  and  $\text{O}^+$  and compare the experimentally obtained product distributions to the predictions by LCAO.

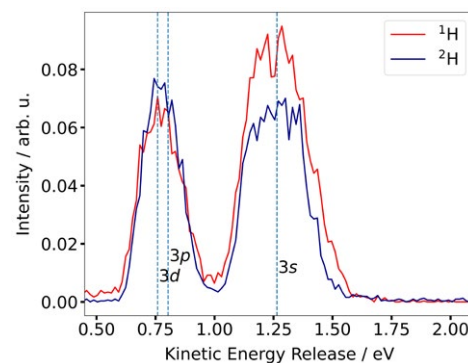


**Figure 1.** The obtained kinetic-energy-release distributions of MN between  ${}^7\text{Li}^+$  and  ${}^1\text{H}^-$  in red and  ${}^2\text{H}^-$  in blue. The deuterium data are from a previous study at DESIREE [6]. Both distributions are normalized to the counts in the unresolved  $3p$ - $3d$  peak.

### References

- [1] Barklem P S *et al* 2003 *A&A* **409** L1
- [2] Lind K *et al* 2009, *A&A* **503** 541
- [3] Barklem P S *et al* 2021 *Astrophys. J.* **908** 245
- [4] Osorio, Y *et al* 2015 *A&A* **579** A53
- [5] Barklem, P S 2016 *Phys. Rev. A* **93** 042705
- [6] Eklund G *et al* 2020, *Phys. Rev. A* **102** 012823

\*E-mail: [alice.schmidt-may@fysik.su.se](mailto:alice.schmidt-may@fysik.su.se)

†E-mail: [schmidt@fysik.su.se](mailto:schmidt@fysik.su.se)

## Mutual neutralization in collision of $\text{Na}^+$ with $\text{O}^-$ and $\text{S}^-$

A Aerts<sup>1</sup>, A. Dochain<sup>2,3</sup>, J Liévin<sup>1</sup>, X Urbain<sup>2\*</sup> and N Vaeck<sup>1†</sup>

<sup>1</sup>Université Libre de Bruxelles, SQUARES (Spectroscopy, QUantum chemistry and Atmospheric RE mote Sensing), 1050 Brussels, Belgium

<sup>2</sup>Université catholique de Louvain, Institute of Condensed Matter and Nanosciences, 1348 Louvain-la-Neuve, Belgium

<sup>3</sup>Stockholm University, Department of Physics, 106 91 Stockholm, Sweden

**Synopsis** Merged-beams measurements of the mutual neutralization of  $\text{Na}^+$  with  $\text{O}^-$  and  $\text{S}^-$  have revealed an important contribution of excited O and S. The potential energy curves for the ground and first excited states of NaO and NaS have been computed at the complete active space self-consistent field (CASSCF) and configuration interaction (CI) level. The charge transfer cross sections are computed for both systems using the multichannel Landau-Zener approach and compared with a full quantum wave packet propagation method.

Mutual neutralization of a cation and an anion has attracted much attention in the recent years due to the detection of anionic species in several astrophysical environments [1], and the rapid progress made in the techniques of investigation. We have performed partial cross section measurements of the  $\text{Na}^+ + \text{O}^-$  and  $\text{Na}^+ + \text{S}^-$  mutual neutralization reactions (MN) using our single-pass merged beam setup as described by Launoy *et al.* [2]. The simultaneous measurement of the position and time of arrival of the Na and O/S products enables the determination of the kinetic energy release, leading to unambiguous determination of the excited state of the products. Both reactions reveal the contribution of the  $\text{X}^* + \text{Na}(3s)$  channel (minor with  $\text{X}=\text{O}$ , major with  $\text{X}=\text{S}$ ). In order to rationalize this finding, a fully *ab initio* treatment of the NaO and NaS molecular systems is in order.

The potential energy curves for the ground and four excited  $^2\Pi$  states and for the three lowest  $^2\Sigma^+$  states of NaO have been computed at the complete active space self-consistent field (CASSCF) and configuration interaction (CI) level using an AV5Z basis set as implemented in

the MOLPRO quantum chemistry package. In the asymptotic region, the  $^2\Pi$  and  $^2\Sigma^+$  states dissociate into the following channels ordered by increasing energy:  $2p^6 3s^2 S$  of Na and  $2p^4 3P$  of O,  $2p^6 3s^2 S$  of Na and  $2p^4 1D$  of O,  $2p^6 3p^2 P^o$  of Na and  $2p^4 3P$  of O and the ionic channel  $2p^6 1S$  of  $\text{Na}^+$  and  $2p^5 2P^o$  of  $\text{O}^-$ .

The non-adiabatic radial coupling elements  $F_{mm'} = \langle \Phi_m | \delta_R | \Phi_{m'} \rangle$  are calculated using finite difference. The equation

$$\delta_R D(R) + F(R) \cdot D(R) = 0,$$

where  $D(R)$  is the adiabatic-to-diabatic transformation matrix, was solved by continuity. A similar approach has been used to describe the NaS molecular system. The charge transfer cross sections are computed for both systems using the multichannel Landau-Zener approach and compared with a full quantum wave packet propagation method.

### References

- [1] ] Millar T J, Walsh C, and Field T A 2017 *Chem. Rev.* **117** 1765
- [2] Launoy T, Loreau J, Dochain A, Liévin J, Vaeck N, and Urbain X 2019 *Astrophys. J.* **883** 85

\*E-mail: [xavier.urbain@uclouvain.be](mailto:xavier.urbain@uclouvain.be)

†E-mail: [nathalie.vaeck@ulb.be](mailto:nathalie.vaeck@ulb.be)

## Charge transfer in Sodium Iodide collisions

P Hedvall<sup>1\*</sup>, M Odelius and Å Larson<sup>1†</sup>

<sup>1</sup>Department of Physics, Stockholm University, Albanova University Center, S-106 91 Stockholm, Sweden

### Synopsis

The charge transfer collision reactions  $\text{Na} + \text{I} \leftrightarrow \text{Na}^+ + \text{I}^-$  are studied from an *ab initio* approach and the total and differential cross sections are calculated for the reactions. The *ab initio* results are compared to measured total and differential cross sections, and the reactions are furthermore studied using a semi-classical treatment and with a semi-empirical spin-orbit coupling model.

Sodium Iodide (NaI) has over the years served as a prototype system in the studies of non-adiabatic dynamics. Most notably, due to the pioneering experimental work of Zewail and co-workers [1]. Here, the charge transfer collision reactions  $\text{Na} + \text{I} \leftrightarrow \text{Na}^+ + \text{I}^-$  (mutual neutralization and ion-pair formation) are studied from an *ab initio* approach and the total and differential cross sections are calculated for the reactions. This involves electronic structure calculations on NaI to obtain adiabatic potential energy curves, non-adiabatic and spin-orbit couplings followed by nuclear dynamics, treated fully quantum mechanically in a strict diabatic representation. A single avoided crossing at  $13.22 a_0$  dominates the reaction and the total cross section is well captured by the semi-classical Landau-Zener model. Compared to measured ion-pair formation cross section [2], the calculated cross section is about a factor two smaller. The overall shape of the calculated differential cross section is in reasonable agreement with measured ion-pair formation differential cross section [3], as can be seen in Fig. 1. However, the measured total and differential cross sections are both well captured when treating the Landau-Zener coupling as an empirical parameter of 0.05 eV and doing full quantum mechanical cross section calculations including rotational coupling. A semi-empirical spin-orbit coupling model is also investigated, making use of the empirical (or calculated) spin-orbit coupling of the separated atoms, giving satisfactory estimation of the effects of spin-orbit interaction for

the reactions.

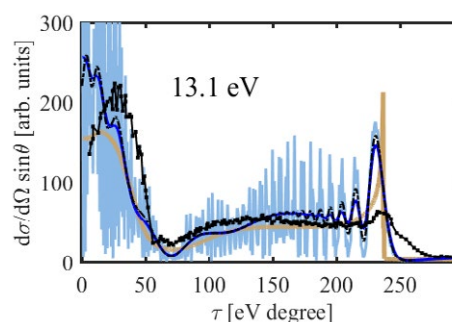


**Figure 1.** Differential cross section for the reaction  $\text{Na} + \text{I} \rightarrow \text{Na}^+ + \text{I}^-$  at collision energy 13.1 eV. The quantum differential cross section (excluding rotational coupling) is displayed with light blue curve, and a smoothed curve of the quantum results is displayed by blue solid lines. The classical differential cross section is displayed with orange solid line and the quantum differential cross section including rotational coupling (smoothed) is displayed with dotted black line. The measured differential cross section of Delvigne *et al.* [3] is displayed with black solid lines. The differential cross section is multiplied with  $\sin \theta$  and plotted against  $\tau = \theta E$ , where  $E$  is the collision energy.

### References

- [1] Rose T S, Rosker M J and Zewail A H 1988 J. Chem. Phys. **88** 6672
- [2] Moutinho A M, Aten J A and Los J 1971 Physica **53** 471-492
- [3] Delvigne G A L and Los J 1973 Physica **67** 166-196

\*E-mail: [patrik.hedvall@fysik.su.se](mailto:patrik.hedvall@fysik.su.se)

†E-mail: [aasal@fysik.su.se](mailto:aasal@fysik.su.se)

## Molecular-rotation-induced splitting of the binary ridge in the velocity map of sub-eV H<sup>+</sup> (D<sup>+</sup>) ions ejected from H<sub>2</sub> (D<sub>2</sub>) molecules by ion impact

Z Juhász<sup>1\*</sup>, S T S Kovács<sup>1</sup>, V Vizcaíno<sup>2</sup>, P Herczku<sup>1</sup>, S Demes<sup>1</sup>, R Rácz<sup>1</sup>, B Sulik<sup>1</sup>, S Biri<sup>1</sup>, N Sens<sup>2</sup>, D V Mifsud<sup>3,1</sup>, G Lakatos<sup>1,4</sup>, K. K. Rahul<sup>1</sup> and J-Y Chesnel<sup>2</sup>

<sup>1</sup> Institute for Nuclear Research (Atomki), Debrecen, H-4026, Hungary

<sup>2</sup> CIMAP, UMR 6252 CEA-CNRS-ENSICAEN-UNICAEN, Normandie Université, 14000 Caen, France

<sup>3</sup> University of Kent, Canterbury CT2 7NH, United Kingdom

<sup>4</sup> University of Debrecen, H-4032, Debrecen, Hungary

**Synopsis** We study H<sup>+</sup> (D<sup>+</sup>) fragment emission in collisions of keV-energy O<sup>q+</sup> ions with H<sub>2</sub> (D<sub>2</sub>) molecules using a field-free time-of-flight technique developed to detect sub-eV fragments. We have found that, in the velocity map, the binary ridge due to direct H<sup>+</sup> (D<sup>+</sup>) knockout is split arising from the rotational motion of the target molecule. By the split, different rotational levels from  $J=1$  to  $J=3$  could be identified. For higher projectile charge states, higher- $J$  contributions have been observed. The fragmentation yields have been found to be affected by isotope and target coherence effects.

In studies of ion-induced molecular fragmentation, the challenging measurement of the velocity distribution of fragments emitted below 1-eV kinetic energy is rarely achieved, although most fragments have an energy below this value. We study H<sup>+</sup> (D<sup>+</sup>) fragment emission in collisions of 5- to 20-keV O<sup>q+</sup> ions ( $q=1, 2, 4$ ) with H<sub>2</sub> (D<sub>2</sub>) molecules using a field-free time-of-flight technique developed specifically to detect sub-eV fragments [1].

We have found that, in the velocity map, the binary ridge due to direct H<sup>+</sup> knockout by O<sup>+</sup> is split into two parts arising from the rotational motion of the H<sub>2</sub> molecule in its  $J=1$  rotational state (Fig. 1a). Being directly proportional with the rotational velocity, the split is half as large for D<sub>2</sub> isotopologues (Fig. 1b).

The asymmetry in the intensity of the left- and right-shifted binary ridges is due to the imbalance of the two rotational directions, which is indicative of rotational transitions prior to the collision. For multiply-charged projectiles, more effective rotational excitations result in the appearance of binary ridges for  $J=2$  and  $J=3$  rotational levels, too.

We have observed strong isotopic effects in terms of cross sections in the produced fragments. Moreover, target coherence effects have been demonstrated by changing the distance of the effusive nozzle to the collision center,

which affects the coherence length of the molecules according to van Cittert–Zernike theorem.

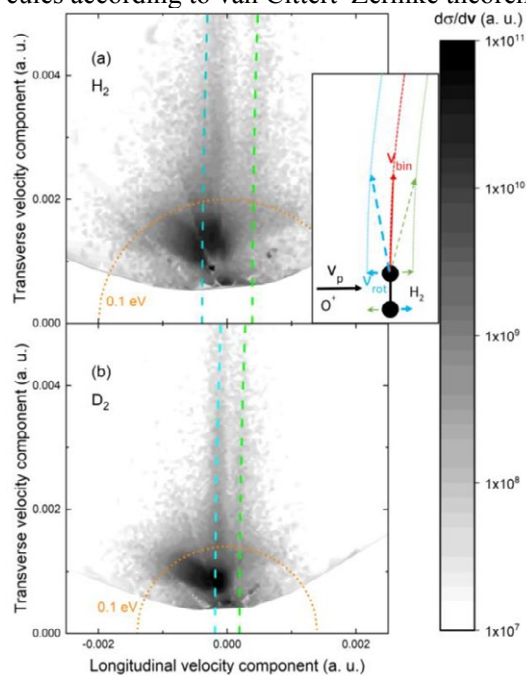


**Figure 1.** Velocity distributions of (a) H<sup>+</sup> and (b) D<sup>+</sup> ions respectively arising from H<sub>2</sub> or D<sub>2</sub> molecules in collision with 10-keV O<sup>+</sup> ions [1]. The ridges for the direct binary knock-out process are marked by segmented lines.

### References

- [1] Juhász Z, Kovács S T S, Vizcaíno V. et al. 2023 *Phys. Rev. A* **107** L010801

\* E-mail: [zjuhasz@atomki.hu](mailto:zjuhasz@atomki.hu)

## Two-photon optical shielding of collisions between ultracold polar molecules

Charbel Karam<sup>1</sup>, Mara Meyer zum Alten Borgloh<sup>3</sup>, Romain Vexiau<sup>1</sup>, Maxence Lepers<sup>2</sup>, Silke Ospelkaus<sup>3</sup>,  
Nadia Bouloufa-Maafa<sup>1\*</sup>, Leon Karpa<sup>3</sup>, and Olivier Dulieu<sup>1</sup>

<sup>1</sup>Université Paris-Saclay, CNRS, Laboratoire Aimé Cotton, Orsay 91400, France

<sup>2</sup>Laboratoire interdisciplinaire Carnot de Bourgogne, Cedex F-21075 Dijon, France

<sup>3</sup>Institut für Quantenoptik, Leibniz Universität Hannover, 30167 Hannover, Germany

**Synopsis** We propose a method to engineer repulsive long-range interactions between ultracold ground-state molecules using optical fields, thus preventing short-range collisional losses. It maps the microwave coupling recently used for collisional shielding onto a two-photon transition, and takes advantage of optical control techniques. In contrast to one-photon optical shielding [5], this scheme avoids heating of the molecular gas due to photon scattering. The proposed protocol, exemplified for  $^{23}\text{Na}^{39}\text{K}$ , should be applicable to a large class of polar diatomic molecules.

The growing availability of quantum gases of ultracold polar molecules in several labs revealed a very peculiar situation in the context of few-body physics: at ultracold energies, two such molecules in their absolute ground level collide with a universal collisional rate, even if they have no inelastic or reactive energetically allowed channels, so that they leave the molecular trap with a short characteristic time. Instead of attempting to fully describe this four-body system, with the aim of identifying the exact cause of the universal loss rate, one can design protocols where molecules would simply not reach short distances in the course of their collision. Several options have been proposed and experimentally demonstrated, based on the modification of the long-range interaction (LRI) between molecules using static electric fields [1] or microwave (mw) fields [2-4], in order to "shield" their collisions.

In a previous work [5] we proposed an alternative way to engineer LRIs using a laser with a frequency blue detuned from the one of a suitable molecular rovibronic transition. Such a one-photon optical shielding (1-OS), inspired from previous works on cold atoms, results in the laser-induced coupling of the attractive collisional entrance channel to a repulsive one, thus preventing the molecules from reaching short distances, and from creating a sticky complex. One limitation of the 1-OS could be the heating of the molecular

quantum gas due to the continuous scattering of off-resonant photons of the 1-OS laser.

In this work we propose a two-photon optical shielding (2-OS) scheme, aiming at overcoming the above limitation, while mapping the case of the microwave shielding [2-4]. Such a scheme combines the best features of the 1-OS (no restriction for the field polarization, convenient laser power, tunability, geometrical versatility, broad compatibility) and mw shielding (no spontaneous emission or photon scattering). The scheme relies on coupling three molecular states  $|g_1\rangle$ ,  $|q\rangle$  and  $|g_2\rangle$  where  $|g_1\rangle$  is the entrance channel and  $|q\rangle$  and  $|g_2\rangle$  are well chosen states of the collisional complex via a two-photon transition from  $|g_1\rangle$  to  $|g_2\rangle$ . In the dressed state picture, this maps the mw shielding scheme onto an effective optical coupling of the dressed states.

The proposed protocol, exemplified for  $^{23}\text{Na}^{39}\text{K}$ , should be applicable to a large class of polar diatomic molecules.

### References

- [1] G. Quémener and J.L. Bohn, Phys. Rev. A 81, 022702 (2010).
- [2] L. Lassablière and G. Quémener, Phys. Rev. Lett. 121, 163402 (2018).
- [3] T. Karman and J. M. Hutson, Phys. Rev. Lett. 121, 163401 (2018).
- [4] A. Schindewolf, et al., Nature 607, 677 (2022).
- [5] T. Xie, et al., Phys. Rev. Lett. 125, 153202 (2020).

\* E-mail: [nadia.bouloufa@u-psud.fr](mailto:nadia.bouloufa@u-psud.fr)

## Emergent s-wave dimers near a p-wave Feshbach resonance in a strongly confined Fermi gas

K G S Xie<sup>1\*</sup>, K G Jackson<sup>1</sup>, C J Dale<sup>1</sup>, J Maki<sup>2</sup>, S Zhang<sup>3</sup>, and J H Thywissen<sup>1†</sup>

<sup>1</sup>Department of Physics and CQIQC, University of Toronto, Toronto, M5S 1A7, Canada

<sup>2</sup>Pitaevskii BEC Center and CNR-INO, Università di Trento, Trento, via Calepina 14-38122, Italy

<sup>3</sup>Department of Physics and HKU-UCAS Joint Institute for Theoretical and Computational Physics at Hong Kong University, The University of Hong Kong, Hong Kong, China

**Synopsis** We present emergent s-wave interactions in a quasi-two-dimensional (quasi-2D) system of <sup>40</sup>K near a p-wave Feshbach resonance with orbital degrees of freedom. The emergent exchange symmetry is enabled by excited-band population in the strongly confined direction. We characterize the scattering channels by measuring dimer binding energies and “contact” parameters with radio-frequency (rf) methods.

Ultracold atomic gases are highly tunable platforms for exploring low-dimensional physics, but are often prepared in motional ground states, neglecting orbital dynamics. We demonstrate that scattering channels activated with orbital degrees of freedom provide new routes for exploring few- and many-body phenomena.

Here, we prepare orbitally excited systems of spin-polarized fermionic potassium (<sup>40</sup>K) near a p-wave Feshbach resonance. An optical lattice generates a strongly confined quasi-2D regime. Orbital degrees of freedom are activated by manipulating atomic populations of the excited band of the confinement lattice. While ground-band interactions possess p-wave character, collisions between ground- and excited-band atoms allow emergent s-wave behavior to appear [1].

Interactions are enhanced near the confinement-induced resonance associated with each scattering channel. We characterize the resonances by measuring quasi-2D dimer binding energies with rf association. Emergent s-wave dimers appear when orbital bands hybridize with the p-wave dimer in the corresponding confinement direction, and we demonstrate this by performing measurements in two confinement geometries. The results are compared to a quasi-2D scattering model that include band excitations.

In a second set of measurements, we study the strengths of resonantly enhanced interactions for each quasi-2D dimer by measuring spin-flip rates from rf spectroscopy as a function of magnetic field and confinement strength with and with-

out activated orbital degrees of freedom. The resulting atom-atom correlations are interpreted through a set of universal relations, revealing the contact parameters [2, 3]. These studies extend the paradigm previously established in quasi-one-dimensional confinement [1] and provide a comprehensive framework for engineering exotic interactions with orbital dynamics in low-dimensional systems.

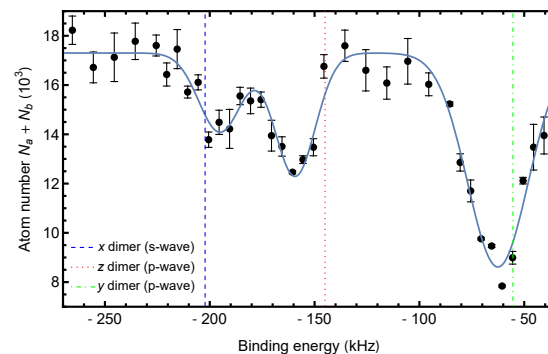


**Figure 1.** Typical dimer association loss measurement for an optical lattice along the  $x$  direction with activated orbital degrees of freedom. Blue dashed, red dotted, and green dot-dashed lines indicate predicted dimer energies and are labelled by the short-range 3D p-wave dimer direction and scattering channel.

### References

- [1] Jackson K G *et al* 2023 *Phys. Rev. X* (in press)
- [2] Tan S 2008 *Ann. of Phys.* **323** 12
- [3] Luciuk C *et al* 2016 *Nat. Phys.* **12** 6

\*E-mail: [kgs.xie@utoronto.ca](mailto:kgs.xie@utoronto.ca)

†E-mail: [jht@physics.utoronto.ca](mailto:jht@physics.utoronto.ca)



## Resonant processes and their impact in many-body dynamics

R Côté<sup>1\*</sup>

<sup>1</sup>Department of Physics, University of Massachusetts Boston,  
100 William T. Morrissey Blvd, Boston, MA 02125, USA

**Synopsis** We discuss a general process, resonant exchange, that occurs in several atomic and molecular systems. We show that a simple approximation accounts for the exchange cross section over wide range of collision energy.

Resonant exchange is a general process playing a key role in many-body dynamics and transport phenomena, such as spin, charge, or excitation diffusion. The underlying process is described by the resonant exchange cross section  $\sigma_{\text{exc}}$ . A prime example is the diffusion of an ion  $A^+$  in its parent neutral gas  $A$ . In fact, the charge actually behaves as a hole (h) at ultralow temperatures, hopping from atom to atom instead of staying on its heavy center (the ion) [?]. We have predicted a faster diffusion coefficient for the hole ( $D_h$ ) than if the charge was diffusing via collision ( $D_{\text{coll}}$ ).

In this work, we show that the exchange symmetry for identical (homonuclear) atom-ion system leads to special outcomes for ion transport in ultracold experiments. We compute the two body charge hopping probabilities and rates, which are used to model charge hopping in the dynamics of an ultracold  ${}^6/7\text{Li}^+$  ion immersed within an ultracold gas of  ${}^6/7\text{Li}$  atoms at micro-Kelvin temperatures [?]. We show that the charge hopping and collisional diffusion compete, giving unique results leading to charge trapping in regions of high atomic density gradient, leading to a region of “negative” diffusion.

As mentioned above, the dynamics is dictated by  $\sigma_{\text{exc}}$ . In previous work [?], we showed that the locking of  $s$ -wave phase shifts could be used to explain the behavior of  $\sigma_{\text{exc}}$  at ultracold temperatures. Moreover, we found an unexpected

consequence of phase-shift locking; namely, the behavior of the resonant-exchange cross section over a broad range of energies is largely dictated by  $s$ -wave scattering, whose influence extends high above the  $s$ -wave Wigner regime. We now generalize our treatment to higher energies and derive an analytical expression for the resonant-exchange cross section which accounts not only for the locking of phase shifts, but also for their gradual unlocking as the energy increases. We find good agreement between the computed (fully quantal) cross section and our newly obtained result, which we illustrate for resonant charge-transfer in ion-atom collisions (see Fig.1 for  ${}^{174}\text{Yb}$ ).

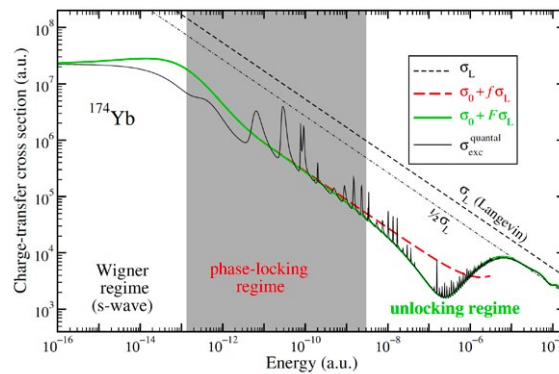


**Figure 1.** Exchange cross section.

### References

- [1] R. Côté, PRL **85**, 5316 (2000).
- [2] N. Joshi, M. Niranjana, A. Pandey, O. Dulieu, R. Côté., S.A. Rangwala PRA **105**, 063311 (2022).
- [3] R. Côté and I. Simbotin, PRL **121**, 173401 (2018).

\*E-mail: [robin.cote@umb.edu](mailto:robin.cote@umb.edu)

## Dynamical instabilities and macroscopic quantum self-trapping in a rotating Bose-Einstein condensate

D Kamp<sup>1\*</sup> and D O'Dell<sup>1†</sup>

<sup>1</sup> Department of Physics and Astronomy, McMaster University, ON L8S 4L8 Hamilton, Canada

**Synopsis** We theoretically investigate the occurrence of macroscopic self-trapping and quantum catastrophes in the vicinity of an instability for a two-mode Bose-Einstein condensate in a rotating toroidal trap.

We consider a dilute gas of bosons in a slowly rotating toroidal trap [1], focusing on the two-mode regime consisting of a non-rotating mode and a rotating mode corresponding to a single vortex. This system undergoes a symmetry breaking transition as the ratio of interactions to 'disorder potential' is varied and chooses one of the two modes spontaneously, an example of macroscopic quantum self-trapping.

We also compare an enhanced mean-field theory which uses the truncated Wigner approximation comprising multiple classical trajectories with a fully quantum many-body description. Following a sudden quench, we find quasi-periodic dynamics where the condensates oscillate between the modes and identify cusp-shaped structures [2] in the wavefunction as quantum versions of elementary catastrophes.

Analyzing elementary excitations around the BEC using Bogoliubov theory [3], regions of energetic instabilities with negative excitation frequencies are found, as well as dynamical instabilities, where excitations have complex

frequencies [4]. For the latter, amplitudes grow or decay exponentially [5]. Those complex eigenvalues suggest that the Bogoliubov Hamiltonian is non-Hermitian.

Instabilities can occur at bifurcations where the classical field theory provided by the Gross-Pitaevskii equation predicts that two or more solutions appear or disappear [2]. We make connections to the description of bifurcations using catastrophe theory but modified to include field quantization.

### References

- [1] Baharian S and Baym G 2013 *Phys. Rev. A* 87 013619
- [2] Mumford J, Kirkby W, and O'Dell D 2017 *J. Phys. B - AT MOL OPT* 50 044005
- [3] Fetter A 1972 *Ann. Phys.* 70 67
- [4] Machholm M, Pethick C, and Smith H 2003 *Phys. Rev. A* 67 053613
- [5] Wu B and Niu Q 2003 *New J. Phys.* 5 104

---

\*E-mail: [kampd@mcmaster.ca](mailto:kampd@mcmaster.ca)

†E-mail: [dodell@mcmaster.ca](mailto:dodell@mcmaster.ca)

## Observation of Sequential Tunneling in Driven Optical Lattices

XX Ma<sup>1</sup>, XY Tong<sup>1</sup>, NC Zhang<sup>1</sup>, X Zhang<sup>2†</sup>, KK Huang<sup>1</sup>, XH Lu<sup>1\*</sup>

<sup>1</sup> School of Physics, Zhejiang University, Hangzhou 310027, China

<sup>2</sup> Institute of Advanced Technology, Zhejiang University, Hangzhou 310027, China

**Synopsis** Atomic wave packets collapse in optical lattice potentials due to the decoherence is investigated with Alkali-metal atomic gases <sup>87</sup>Rb. This situation is referred to as sequential tunneling, which differs from the coherent tunneling. This sequential tunneling process of <sup>87</sup>Rb in one-dimensional vertical amplitude modulated optical lattice is observed experimentally for the first time.

In recent years, coherent delocalization of atomic wave packets in driven lattice potentials has been realized in <sup>88</sup>Sr ensemble [1]. This isotope of strontium atom has no nuclear spin so that in the ground state it is a scalar particle which is virtually insensitive to stray magnetic fields, and its extremely small scattering length ( $a=-2a_0$ ) results in reduced decoherence due to cold collisions [2]. Compared to the <sup>88</sup>Sr with small scattering length, Alkali-metal atomic gases <sup>87</sup>Rb with larger scattering length results in raised decoherence in experiments measuring gravity based on Bloch oscillations. This dephasing process occurs at a given constant rate  $L$  for all of the lattice sites, after a certain time it is likely that the extended wave packet collapses into one single site. This situation is referred to as sequential tunneling, which differs from the coherent tunneling [3]. However, to date sequential tunneling has not been investigated experimentally in driven optical lattices.

The ultracold atoms of <sup>87</sup>Rb in an optical lattice are trapped in a shallow potential, for instance in our experimental setup the potential barrier  $U_0$  is just about a few  $\mu$ K deep. When the modulation frequency has a slight detune from the Bloch frequency, we can measure the size of a thermal cloud instead of the extent atomic wave packets to observe the sequential tunneling. Assuming that there is no decoherence in the experiment, i.e.  $L = 0$  and other experimental conditions remain unchanged, the resonance spectrum profile is  $|\text{sinc}(x)|$  modulation represented by the blue line in Fig. 1. The red line is a fit to the experimental data indicated by the black square, which tends to have Gaussian distribution, where the dephasing rate

$L = 0.3$ . In experiment, the modulation time is set as 70ms.

The resonance spectrum profile of sequential tunneling differs noticeably from the Bessel function of coherent tunneling. In our work, this sequential tunneling process of rubidium ultracold atomic gas in one-dimensional vertical amplitude modulated optical lattice raised from decoherence can be observed experimentally.

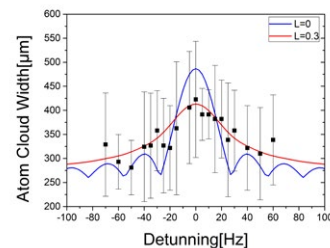


**Figure 1.** Spectrum recorded by modulation experimental results of the lattice depth at the Bloch frequency for 70ms with a modulation depth of 80% in <sup>87</sup>Rb ensemble. The red line is a fit of experimental data (black square) with a function differ from the  $|\text{sinc}(x)|$  (blue line).

This work is supported by National Natural Science Foundation of China under Grants No. 11474254 and 11804298, by National Key Research and Development Program of China under Grants No. 2017YFA0304202 and by Fundamental Research Funds for the Central Universities under Grants No. 2017QN81005.

### References

- [1] Ivanov V V *et al* 2008 *Phys. Rev. Lett.* **100** 043602
- [2] Mickelson P G *et al* 2005 *Phys. Rev. Lett.* **95** 223002
- [3] Wacker A *et al* 1998 *Phys. Rev. Lett.* **217** 80.

\* E-mail: [xhlu@zju.edu.cn](mailto:xhlu@zju.edu.cn)

† E-mail: [xianzhang@zju.edu.cn](mailto:xianzhang@zju.edu.cn)

## Two-Dimensional Turbulence in dipolar Bose-Einstein condensate

S Sabari<sup>1</sup>, R Kishor Kumar<sup>2</sup> and L Tomio<sup>1\*</sup>

<sup>1</sup>Instituto de Física Teórica, Universidade Estadual Paulista, 01140-070 São Paulo, SP, Brazil

<sup>2</sup>Department of Physics, Centre for Quantum Science, and Dodd-Walls Centre for Photonic and Quantum Technologies, University of Otago, Dunedin 9054, New Zealand.

**Synopsis** We investigate the emission of vortex dipoles and turbulent flow in perturbed dipolar Bose-Einstein condensates using the quasi-two-dimensional mean-field Gross-Pitaevskii (GP) model. We explore the range of dipolar interaction strengths and evaluate the regime in which turbulent behaviors can be observed.

The remarkable observations of Bose-Einstein condensates (BECs) for dipolar atomic systems, as <sup>52</sup>Cr, <sup>164</sup>Dy, and <sup>168</sup>Er, have opened a wholly new exciting branch within cold-atom investigations. Due to the long-range nature and anisotropic character of the dipole-dipole interaction (DDI), the dipolar BEC possesses many distinct features and new phenomena including superfluid, super-solid states. Vortices are non-linear physical entities that arise due to the excitation of BECs, being associated with superfluidity. As a signature of quantum turbulence, vortex tangles caused by an oscillatory perturbation were observed experimentally in Ref. [1]. Recently, the observation of vortex-dipoles in dipolar quantum gases was reported [2]. Introducing a periodic oscillating potential in atomic dipolar BECs helps to analyze the intrinsic nucleation of topological defects and synergy dynamics of vortices and rarefaction pulses [3].

In our study, we investigate the emission of vortex and antivortex pairs in dipolar BECs produced by circularly moving blue detuned laser, simulated by a moving Gaussian obstacle. The range of dipolar interaction strengths and velocity of the obstacle were analyzed for different types of vortex emissions, including regular and cluster dipole emissions. The continuous injection of dipoles makes the condensate turbulent, which can be confirmed by calculating the incompressible kinetic energy spectrum which goes as  $k^{-5/3}$  in agreement with the Kolmogorov classical law associated with turbulence. So, to understand the process of vortex injection, we analyze the decomposed compressible and incompressible kinetic energy parts. This study may impact the experimental investigations of vortex and antivortex pairs in dipolar condensates, as

\*E-mail: lauro.tomio@unesp.br (Presenting Author)

considering the dipole orientations.

Through numerical simulations using the corresponding dipolar GP formalism under periodic moving perturbation, we investigate the nucleation and dynamics of vortex-antivortex pairs. A sample result of this dynamics is provided in Fig. 1, where it was shown the nucleation of vortices in a dBEC during the movement of a non-breathing penetrable Gaussian obstacle, considering two different frequencies, as explained in the caption. In our investigation, in which turbulent regimes are also explored, we provide phase diagrams for the critical velocities of the obstacle, which can be useful for experimental realizations.

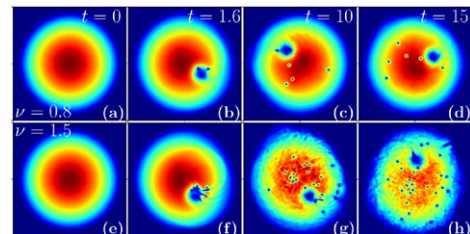


**Figure 1.** Vortex nucleations by Gaussian obstacle. In the upper row ( $\nu = 0.8$ ), they arrive as vortex dipoles. In the bottom row ( $\nu = 1.5$ ), emerge as clusters. Corresponding animations are in [4].

*Acknowledgment:* Work partially supported by FAPESP (Brazil).

### References

- [1] Henn E A L *et al* 2009 *Phys. Rev. Lett.* **103** 045301
- [2] Klaus L *et al* 2022 *Nat. Phys.* **18** 1453
- [3] Sabari S and Kumar K R 2018 *Eur. Phys.J. D* **72** 48
- [4] <https://youtu.be/XQ3AzDBX5xY>

## Electronic $K$ x rays emitted from muonic atoms: an application of density functional theory

X M Tong<sup>1\*</sup>, D Kato<sup>2,3</sup>, T Okumura<sup>4,5</sup>, S Okada<sup>4,6</sup>, T Azuma<sup>4</sup>

<sup>1</sup>Center for Computational Sciences, University of Tsukuba, Tsukuba, 305-8577, Japan

<sup>2</sup>National Institute for Fusion Science (NIFS), Toki, 509-5292, Japan

<sup>3</sup>Interdisciplinary Graduate School of Engineering Sciences, Kyushu University, Kasuga, 816-8580, Japan

<sup>4</sup>Atomic, Molecular and Optical Physics Laboratory, RIKEN, Wako 351-0198, Japan

<sup>5</sup>Department of Chemistry, Tokyo Metropolitan University, Hachioji, Tokyo 192-0397, Japan

<sup>6</sup>Center for Muon Science and Technology, Chubu University, Kasugai, Aichi 487-8501, Japan

**Synopsis** We develop a method of the relativistic density functional theory (DFT) with self-interaction correction to evaluate the electronic  $K$  x rays emitted from muonic atoms. Compared with the results of non-relativistic DFT, we found that the relativistic effect is significant (about 100 eV) even for middle  $Z$  atoms, like Cu. The screening effects, from inner-shell to outer-shell, and conduction band, are also discussed. The present work provides all the transition lines of muonic atoms, which can be used to narrow down the possible transitions by comparing them with the measurements.

Muonic atoms are atoms with an electron replaced by a negatively charged muon and have been studied extensively. A muon is about 200 times heavier than an electron, so it moves closer to the nucleus; muonic atoms thus connect atomic physics and nuclear physics. When a muon is captured to a highly excited state by an atom, the muonic atom can emit two kinds of x rays. One is called a muonic x ray due to transitions between two muon states. The other is called an electronic x ray due to transitions between two electron states. X rays emitted from muonic atoms encode information about the muon state and electron configuration of exotic atoms. Such information can be decoded by comparing the measured x-ray energies with the calculated ones.

Recently, a measurement of electronic  $K_{\alpha}$  x rays from muonic Fe atomic ions was reported [1]. These measured  $K_{\alpha}$  x rays are emitted from different muon states and ionic Fe states. The number of possible transitions is about a quarter million without considering the energy level splitting for the same electron configuration and different angular momentum couplings. If we consider all the atomic energy levels, the number could reach ten million or more. This stimulates us to develop a simple, fast theoretical approach yet with reasonable accuracy to estimate the energy structures of muon atoms.

We performed a simulation based on the relativistic DFT [2] and the results are shown in

\*E-mail: [tong.xiaomin.ga@u.tsukuba.ac.jp](mailto:tong.xiaomin.ga@u.tsukuba.ac.jp)

Fig. 1 for  $\mu\text{Cu}$  atomic ions.

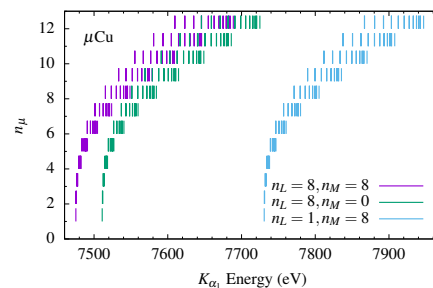


**Figure 1.**  $K_{\alpha_1}$  energies of  $\mu\text{Cu}$  as a function of muonic states  $(n_{\mu}, j_{\mu})$  with different numbers of  $M, L$ -shell electrons calculated by the relativistic local density approximation method.

We also studied the relativistic effect by comparing the relativistic and non-relativistic results and found that the relativistic effect is significant (about 100 eV) even for middle  $Z$  atoms, like Cu. The screening effects, from inner-shell to outer-shell, and conduction band, are also discussed. The present work provides all the transition lines of muonic atoms, which can be used to narrow down the possible transitions by comparing them with the measurements.

### References

- [1] Okumura T, *et. al.*, 2021 *Phys. Rev. Lett.* **127** 053001
- [2] Tong XM, *et. al.*, 2023 *Phys. Rev. A* **107** 012804

## High precision theory for the Rydberg states of helium up to $n = 24$ : test of a $7\sigma$ discrepancy with experiment

G W F Drake<sup>\*</sup>, A T Bondy<sup>†</sup>, E Ene<sup>‡</sup>, E M R Petrimoulx<sup>§</sup>, and L A Sati<sup>¶</sup>

Department of Physics, University of Windsor, Windsor, N9B 3P4 Canada

**Synopsis** Methods for performing high precision variational calculations for the Rydberg P-states of helium are extended up to  $n = 24$  in order to compare with a recent experiment by Clausen *et al.* to test a  $7\sigma$  discrepancy between theory and experiment for the  $1s2s\ ^3S_1$  metastable state. The results are in excellent agreement with experiment, thereby confirming the  $7\sigma$  discrepancy. Relativistic and QED corrections up to order  $m\alpha^5$  are included.

The primary motivation for the present work is to investigate a  $7\sigma$  discrepancy between theory and experiment for the ionization energy of the low-lying metastable  $1s2s\ ^3S_1$  state of helium [1]. In order to provide an independent experimental check of the discrepancy, Clausen *et al.* [2] have performed measurements for the Rydberg P-states of helium from  $n = 24$  to  $n = 100$  and extrapolated to  $n = \infty$  in order to find the absolute ionization energy. To provide a direct theoretical comparison, the present work reports an extension of high precision variational calculations for the high-lying Rydberg states of helium far beyond the previous limit of principal quantum number  $n = 10$  [3] up to  $n = 24$ . The method of calculation uses triple basis sets in Hylleraas coordinates [4]. With the inclusion of relativistic and QED corrections, the results provide a direct theoretical test against the Clausen measurement at  $n = 24$ . Since the theoretical uncertainty due to higher-order QED corrections and nuclear size effects decrease in proportion to  $1/n^3$ , they become a negligibly small  $\pm 1$  kHz at  $n = 24$ . An experimental value at  $n = 24$  can be obtained both from a quantum defect fit to the data up to  $n = 100$  [2], and also directly from the observed  $1s2s\ ^1S_0 - 1s2p\ ^1P_1$  transition frequency. The quantum defect fit has the Rydberg-Ritz form

$$E_n = E_1(2\ ^1S_0) - \frac{R_{\text{He}}}{n^{*2}}$$

where  $n^* = n - \delta(n)$  is the effective principal quantum number and

$$\delta(n) = \delta_0 + \frac{\delta_2}{(n - \delta)^2} + \frac{\delta_4}{(n - \delta)^4} + \dots$$

containing only even powers. As shown Table 1, the results are in excellent agreement, thereby confirming the  $7\sigma$  discrepancy between theory and experiment for the  $1s2s\ ^3S_1$  state of helium. The experimental ionization energy is 1152 842 742.640(32) MHz and the theoretical one is 1152 842 742.231(52) MHz for a difference of 0.409(61) MHz [2].

**Table 1.** Comparison of theory and experiment for the  $1s24p\ ^1P_1$  ionization energy  $^4\text{He}$

Source	Value (MHz)
Theory	5704 980.350(1)
Expt., from QD fit	5704 980.312(95)
Expt., from $\nu(2\ ^1S-24\ ^1P)$	5704 980.352(40)*

\* Gloria Clausen, private communication.

### References

- [1] Patkos V, Yerokhin V A and Pachucki K 2021 *Phys. Rev. A* **103** 042809
- [2] Clausen G *et al.* 2021 *Phys. Rev. Lett.* **127** 093001
- [3] Drake G W F and Yan Z-C 1992 *Phys. Rev. A* **46**, 2378
- [4] Drake G W F, Cassar M M and Nistor R A (2002) *Phys. Rev. A* **65** 054501

\*E-mail: [gdrake@uwindsor.ca](mailto:gdrake@uwindsor.ca)

†E-mail: [bondy11u@uwindsor.ca](mailto:bondy11u@uwindsor.ca)

‡E-mail: [enee@uwindsor.ca](mailto:enee@uwindsor.ca)

§E-mail: [petrimoe@uwindsor.ca](mailto:petrimoe@uwindsor.ca)

¶E-mail: [satil@uwindsor.ca](mailto:satil@uwindsor.ca)



## Theoretical study on radii of neutral atoms and singly charged negative ions

Mingmin Luo, Guangxin Min, Guannan Guo, Xuemei Zhang<sup>1</sup>

Institute of Modern Physics, Fudan University, Shanghai 200433, China  
Applied Ion Beam Physics Laboratory, Fudan University, Key Laboratory of the Ministry of Education, China

**Synopsis** Systematic theoretical calculations of the ground state of atomic radii and singly charged negative ionic radii for elements with  $1 \leq Z \leq 118$  have been performed in a multi-configuration Dirac–Hartree–Fock method including all relativistic effects. Three radii of atoms and singly charged negative ions are computed in this work. They are the radii of the maximum radial charge density of every subshell, the total mean radius and total mean spherical radius based on the total charge density. Results are compared with the radii of the maximum radial charge density calculated by Waber et al. and the experimental ionic radii from Shannon. This work is the first systematic study of singly charged negative ionic radii for all elements in the periodic table (if the corresponding singly charged negative ion exists).

The atomic and ionic radii are an important physical property of every element in periodic table, revealing the periodic variation law of elements. The radii are also crucial in predicting bond lengths, coordination numbers (CNs) and crystal structures.

In this work, using the general relativistic atomic structure package developed in 2000 (GRASP 2K), we have calculated three radii of atoms and singly charged negative ions. [1] They are the radius of the maximum radial

the total charge density. This is the first systematic study on the singly charged negative ionic radii for all the elements of the periodic table.

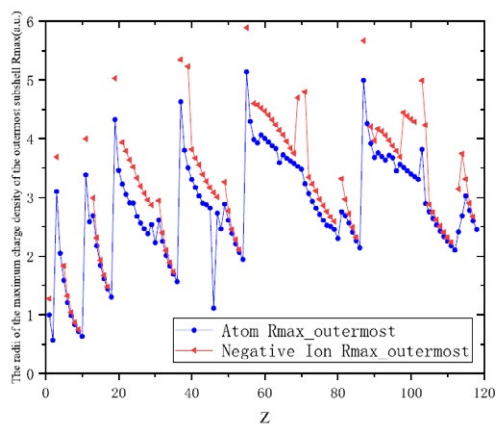


**Figure 1.** The atomic radii and singly charged negative ionic radii of maximum charge density in the outermost subshell of elements with  $1 \leq Z \leq 118$ .

charge density of every subshell, the total mean radius and total mean spherical radius based on

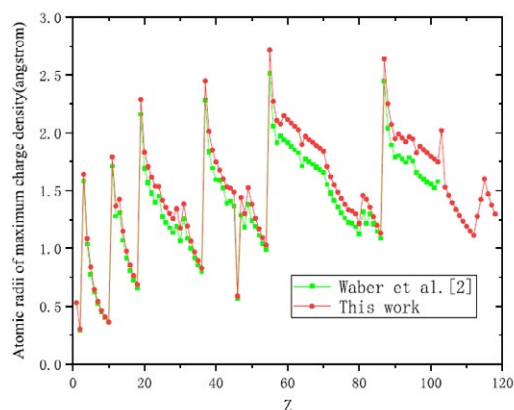


**Figure 2.** Comparison of the radii of the maximum charge density in the outermost subshell of elements obtained in this work and the calculation results of Waber et al..

### References

- [1] M. Luo *et al* 2021 *Atomic Data and Nuclear Data Tables* 138 101392

<sup>1</sup>E-mail: [zhangxm@fudan.edu.cn](mailto:zhangxm@fudan.edu.cn)

## The planetary states of the Sr atom

M Génévriez<sup>1\*</sup>, and U Eichmann<sup>2†</sup>

<sup>1</sup>Institute of Condensed Matter and Nanosciences, Université catholique de Louvain, Louvain-la-Neuve, Belgium

<sup>2</sup>Max-Born-Institute, Berlin, Germany

**Synopsis** The dynamics of two electrons in highly excited (planetary) states offer a fascinating perspective on the quantum three-body problem. We report ongoing theoretical and experimental investigations in the Sr atom that aim at characterizing the two-electron motion and studying its evolution with the strength of correlations, going from the independent-electron picture to correlated planetary dynamics caused by the concerted action of all three Coulomb interactions.

Because the quantum numbers of high lying doubly excited states can be controlled in a precise manner, the motion of two highly excited electrons in the field of the nucleus can be studied in great detail. By fine-tuning electron correlations, the fascinating transition from independent-electron dynamics to a strongly correlated behavior is investigated both in the time and frequency domains [1]. In the laboratory, multiphoton isolated-core excitation of alkaline-earth atoms has permitted unprecedented control over the two electrons. Calculations relying on multichannel quantum defect theory [2] proved essential to study the complex experimental spectra recorded for asymmetric excitation, i.e., when the approximate principal quantum numbers of the two electrons are very different ( $n \gg N$ ). The recent development of configuration interaction with exterior complex scaling has allowed to treat accurately the increased extent of electron correlations when the core is further excited, which opened the possibility to describe higher lying doubly excited states and offered a remarkable view of correlated electron dynamics [3].

We have undertaken a systematic experimental and theoretical exploration of the high lying doubly excited of Sr. The strength and spatial extent of electron correlations, is controlled by the degree of excitation of the core electron ( $N$ ) and the principal- and orbital-angular-momentum quantum numbers ( $n, l$ ) in which the Rydberg electron is first prepared. Near the  $N = 5$  ionization threshold and for  $n \sim 20$  and  $l \sim 12$ , long-range electron correlations lead to a breakdown of the independent-electron picture,

visible in the spectra through the excitation of entire Rydberg series that are not coupled to the initial state by independent-electron electric-dipole selection rules. Theoretical calculations and modelling reveal that the excitation of these Rydberg series is in fact driven by their coupling to a *single* optically active state [4]. Among these series, an electric-*quadrupole* isolated-core excitation is also observed for the first time.

For higher core excitations near the  $\text{Sr}^+(7d)$  and  $\text{Sr}^+(8p)$  ionization thresholds, the inner electron is strongly polarized by the electric field of the slow outer electron. Depending on the sign of the core polarizability, the two electrons describe a planetary-type motion where they orbit the nucleus either on the same side ( $\langle \theta_{12} \rangle \sim 0^\circ$ ) or on opposite sides ( $\langle \theta_{12} \rangle \sim 180^\circ$ ), as revealed by the electronic densities calculated with CI-ECS [3]. The investigation of yet higher core excitation, and therefore yet stronger electron correlations, is under way to further our understanding of the transition of three-body quantum dynamics from the independent-particles case to the strongly correlated regime.

### References

- [1] Eichmann U, Lange V and Sandner W 1990 *Phys. Rev. Lett.* **64** 274 ; Pisharody S N and Jones R R 2004 *Science* **303** 813 ; Camus P *et al.* 1989 *Phys. Rev. Lett.* **62** 2365
- [2] Aymar M, Greene C H and Luc-Koenig E 1996 *Rev. Mod. Phys.* **68** 1015
- [3] Génévriez M, Rosen C and Eichmann U 2021 *Phys. Rev. A* **104** 012812
- [4] Génévriez M and Eichmann U 2023 *Phys. Rev. A* **107** 012817

\*E-mail: [matthieu.genevriez@uclouvain.be](mailto:matthieu.genevriez@uclouvain.be)

†E-mail: [eichmann@mbi-berlin.de](mailto:eichmann@mbi-berlin.de)

## Table-top setup for independent phase and timing control of XUV pulse pairs

Sarang D Ganeshamandiram<sup>1</sup>, Ronak N Shah<sup>1\*</sup>, Fabian Richter<sup>1</sup>, Ianina Kosse<sup>1</sup>, Jahanzeb Muhammad<sup>1</sup>, Lukas Bruder<sup>1†</sup>, Frank Stienkemeier<sup>1</sup> and Giuseppe Sansone<sup>1</sup>

<sup>1</sup>Physikalisches Institut, Albert-Ludwigs Universitaet Freiburg, Freiburg, 79104, Germany

**Synopsis** High Harmonic generation (HHG) are routinely used to generate attosecond laser pulses in the extreme ultraviolet (XUV) regime in several laboratories worldwide. Albeit material limitation to modulate the phase of XUV laser pulses, we modulate the phase of the infrared pulse (IR) which is then coherently transferred to the XUV pulses in the HHG. An interferometric setup to modulate the phase of the IR pulses in each interferometer arm thus gives us complete phase and timing control between XUV pulse pairs.

Independent phase and timing control of a sequence of ultrashort laser pulses forms the basis of wave packet interferometry (WPI) [1]. Modulation of the phase of the IR/visible laser using the acousto-optic (AO) effect, provides a precise control over the phase of laser pulses [1,2]. Phase modulation of XUV radiation from the generating ultraviolet light has been shown in a lab-based HHG setup (up to ~14 eV) and seeded free electron lasers [3,4]. Further scaling in a lab-based HHG setup (>14 eV), is limited by the peak intensity and acceptance aperture in AO crystals [5].

In this work, we are developing a setup for the phase control of a pair of XUV pulses generated by HHG up to 30eV. Combining the photoelectron/photoion signal generated by photoionization using the attosecond XUV pulses with a lock-in detection improves the detection sensitivity. These developments open new perspectives for wave packet interferometry and phase modulated spectroscopy in the XUV spectral regime in a table-top lab setup.

### References

- [1] Tekavec P. F., et. al., 2006, J. Chem. Phys. [125, 194303](#)
- [2] Dazzler™, 2018, [Fastlite](#)
- [3] Wituschek A., et. al., 2020 New J. Phys. [22, 092001](#)
- [4] Wituschek A., et. al., Nature Communications 2020 [11, 883](#)
- [5] Technical paper, Understanding AOMs and EOMs, 2022, [G&H Group](#)

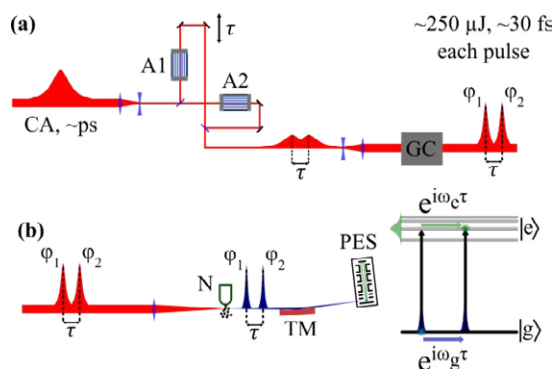


**Figure 1. (a, b)** Experimental setup to independently control the phase ( $\phi_1$  and  $\phi_2$ ) and timing ( $\tau$ ) of a pair of infrared laser pulses used to generate XUV harmonic radiation up to 30 eV for wave packet interferometry. CA: chirped and amplified laser pulses, A1, A2: Acousto-optic modulator to modulate the phase, GC: grating compressor, N: Nozzle, TM: Toroidal mirror, PES: Photoelectron spectrometer

\* E-mail: [ronak.shah@physik.uni-freiburg.de](mailto:ronak.shah@physik.uni-freiburg.de)

† E-mail: [lukas.bruder@physik.uni-freiburg.de](mailto:lukas.bruder@physik.uni-freiburg.de)

## Intensity variation of N<sub>2</sub> and CO in the presence of two-color ultrafast pulses.

Madhusudhan P<sup>1\*</sup>, and Rajesh Kumar Kushawaha<sup>1†</sup>

<sup>1</sup>Physical Research Laboratory(PRL), Ahmedabad, Gujarat, 380009, India

**Synopsis:** This research focuses on studying the behaviors of nitrogen (N<sub>2</sub>) and carbon monoxide (CO) molecules under the influence of two-color ultrafast laser fields. By varying the intensity of the laser fields at a fixed relative phase, the ionization and dissociation pathways of N<sub>2</sub> and CO are analyzed, shedding light on their respective dynamics. This research provides valuable insights into the behavior of N<sub>2</sub> and CO in two-color laser fields, contributing to our understanding of fundamental processes and potential applications in areas such as laser-induced molecular alignment and control of chemical reactions.

Ultrafast laser pulses offer unique opportunities for investigating the interaction between light and matter at the molecular level, enabling control over electronic dynamics and exploration of novel phenomena<sup>1</sup>. The study of two-color ultrafast laser fields has gained significant attention due to its ability to manipulate and control the behavior of matter at the molecular level. One of the key advantages of two-color laser fields is the ability to tailor the excitation pathways of molecules. By adjusting the relative phase, intensity, polarization and time delay between the two laser pulses (schematic shown in Figure 1.), it is possible to selectively excite specific molecular states, control the direction of electron motion, and even induce coherent quantum interference effects. This level of control enables the manipulation of chemical reactions, the generation of high-order harmonics, and the exploration of attosecond dynamics.

Nitrogen (N<sub>2</sub>) and carbon monoxide (CO) exhibit a striking similarity in their ionization energies despite their distinct molecular structures. The primary objective of this work is to investigate the similarities between the homonuclear diatomic system, N<sub>2</sub> and heteronuclear diatomic system, CO under the influence of two-color ultrafast laser fields (OTC and PTC) and gain valuable insights into their respective behaviors. The effect of relative phase has previously been studied and has been identified as a strong candidate for quantum control<sup>2</sup>. Here, by varying the intensity of the laser fields, the response of N<sub>2</sub> and CO molecules is analyzed, focusing on ionization and dissociation pathways. Experimental measurements are complemented by semi-classical electron trajectory

simulations to provide a comprehensive understanding of the underlying dynamics.

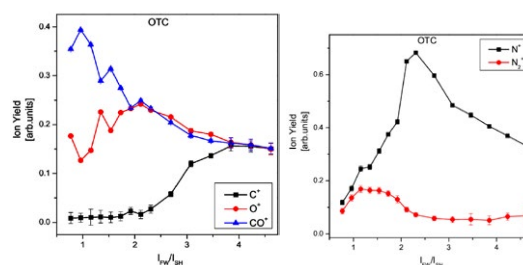


**Figure 1.** Ion yield of parents and fragments of CO[left] and N<sub>2</sub>[right] as a function of intensity ratio (800nm/400nm) of OTC fields at a fixed relative phase.

By combining two laser beams with different wavelengths, we could harness the unique properties of each wavelength to induce specific electronic and vibrational excitations in target molecules. This approach provides enhanced control over the molecular dynamics and opens up new avenues for exploring fundamental processes and phenomena.

### References

- [1] Zhang, L., Xie, X., Roither, S., Kartashov, D., Wang, Y., Wang, C., Schöffler, M., Shafir, D., Corkum, P.B., Baltuška, A. and Ivanov, I., 2014. *Physical Review A*, 90(6), p.061401.
- [2] Madhusudhan, P., Das, R., Bhardwaj, P., KM, M.S., Nimma, V., Soumyashree, S. and Kushawaha, R.K., 2022. *Journal of Physics B: Atomic, Molecular and Optical Physics*, 55(23), p.234001.

\* E-mail: madhusudhanp@prl.res.in

† E-mail: kushawaha@prl.res.in

## Ultrafast Imaging of Molecular Chirality with Photoelectron Vortices

X B Planas<sup>1</sup>, A F Ordóñez<sup>1</sup>, M Lewenstein<sup>1,2</sup>, and A S Maxwell<sup>1,3\*</sup>

<sup>1</sup>ICFO-Institut de Ciències Fòtoniques, The Barcelona Institute of Science and Technology, 08860 Castelldefels (Barcelona), Spain. <sup>2</sup>ICREA, Pg. Lluís Companys 23, 08010 Barcelona, Spain.

<sup>3</sup>Department of Physics and Astronomy, Aarhus University, DK-8000 Aarhus C, Denmark.

**Synopsis** We propose a highly enantio-sensitive effect exploiting helicity in twisted photoelectrons ionized from a chiral target, dubbed photoelectron vortex dichroism (PEVD) [1]. We show that strong-field ionization of a chiral target with a few-cycle linearly polarized 800 nm laser pulse yields photoelectron vortices, whose chirality reveals that of the target. PEVD opens novel opportunities for chiral imaging based on recollision phenomena.

Chirality plays a pivotal role in biological systems, and distinguishing between molecular enantiomers is a crucial task. The most sensitive methods are those that directly use the electric-dipole interaction, such as in photoelectron circular dichroism (PECD) [2]. Recent progress in electron optics has allowed the production and measurement of vortex states carrying orbital angular momentum (OAM) [3]. The inherent helical structure of vortex states, makes them a direct probe of chirality [4]. Yet, the potential of photoelectrons carrying OAM as an enantio-sensitive probe, particularly for linearly polarized fields, is underdeveloped. Thus, using basic properties for the photoelectron OAM in strong-field ionization [5], we reveal the connection between molecular chirality and photoelectron OAM [1].

We demonstrate, ‘Photoelectron Vortex Dichroism’ (PEVD), through strong-field ionization of a simple chiral target with *linearly* polarized light, resulting in photoelectron vortices that encode the molecular chirality. Solving the time-dependent Schrödinger equation and projecting onto electron vortex states, we demonstrate that the OAM-resolved momentum distribution is highly asymmetric, see Figure 1. This asymmetry is dependent on the chiral enantiomer as well as the sign of the OAM. The asymmetry is quantified using the normalized difference, denoted  $\text{PEVD}_v^{\pm}$  (see Figure 1), which approaches the maximum value of 200%.

The asymmetry results from the transfer of chirality from the bound orbital to the photoelectron vortex wave packet. A direct corollary of this is that chiral molecules are a natural source of electron vortices, without any special require-

\*E-mail: [andrew.maxwell@phys.au.dk](mailto:andrew.maxwell@phys.au.dk)

ment on the spin angular momentum of the photon or on the net OAM of the initial state. PEVD relies only on a single beam of linearly polarized light, which allows for recollision, enabling processes such as laser-induced electron diffraction and paves the way for investigating electronic OAM in recollision-based ultrafast chiral imaging.

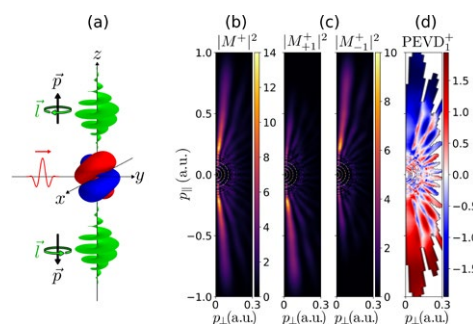


**Figure 1.** (a) Depiction of PEVD. (b) Photoelectron spectrum from strong-field ionization with a 2-cycle pulse,  $I = 10^{14}$  W/cm<sup>2</sup>, and  $\lambda = 800$  nm. (c) OAM-resolved photoelectron spectra for OAM  $l_v = \pm 1$ . (d) Normalized difference between enantiomers. Taken from [1].

### References

- [1] XB Planas et al., Phys. Rev. Lett. 129, 233201 (2022).
- [2] MHM Janssen et al, Phys. Chem. Chem. Phys. **16**, 856 (2013)
- [3] KY Bliokh et al, Phys. Rep. **690**, 1 (2017)
- [4] A Asenjo-Garcia et al, Phys. Rev. Lett. **113**, 066102 (2014)
- [5] AS Maxwell, et al, Faraday Discuss. **228**, 394 (2021) and Y Kang, et al, Eur. Phys. J. D **75**, 199 (2021)



## Ionization dynamics of $CO_2$ in intense XUV and strong IR pump/probe at REMI end station FLASH2

Atia-Tul-Noor<sup>1\*</sup>, S Kumar<sup>1</sup>, H Lindenblatt<sup>2</sup>, B Manschwetus<sup>1</sup>, C Passow<sup>1</sup>, C Papadopoulou<sup>1</sup>, F Trost<sup>2</sup>, M Braune<sup>1</sup>, S Meister<sup>2</sup>, N Schrimel<sup>1</sup>, F Kuschewski<sup>1</sup>, S Schulz<sup>1</sup>, S Düsterer<sup>1</sup>, B Erk<sup>1,2</sup>, and R Moshhammer<sup>2</sup>

<sup>1</sup> Deutsches Elektronen-Synchrotron DESY Hamburg, 22607, Germany,

<sup>2</sup>Max-Planck-Institute for Nuclear Physics, Heidelberg, Germany.

**Synopsis** The ionization and fragmentation dynamics of singly and doubly charged carbon dioxide molecules is studied using multi-coincidence ion-imaging technique in a pump-probe experiment. The time dependent of the low and high kinetic energy release of dissociation and Coulomb explosion dynamics are investigated.

The advent of free-electron lasers (FEL) capable of producing intense and short pulses has enabled new time-resolved studies into photo dynamics. Combining XUV and near infrared (NIR) optical pulses in a pump-probe experiment has opened new ways to get insight into photo induced process and their evolution. However in this case high temporal resolution is a persistent challenge, as it is limited by both ultrashort pulses of pump and probe as well as their synchronisation. Here we present the results of a most recent developments in the temporal resolution of the Ultrashort XUV-NIR pulses at the beamline FL26 REMI end station at FLASH2 with a resolution of order of less than 50fs (FWHM). The experiment was carried out using a cold-target recoil ion momentum spectroscopy (COLTRIMS) reaction microscope [1, 2] at the beamline FL26, FLASH2 at DESY in Hamburg. The laser assisted x-ray photo ionization in Xe atoms is used to quantify the temporal resolution of a pump probe experiment as well as  $CO_2$  molecules ionisation and fragmentation is studied.

In the presented experiment, dissociative single and double ionization of  $CO_2$  molecules is investigated. The molecules are ionised by 90eV photons from FEL beam and time delayed near infrared pulses are used to probe the dynamics. The time dependent yield of doubly charged parent and low energy  $CO^+$  ion from disso-

ciative ionization gives signatures of transient cationic states by the absorption of XUV. The time-dependent energy distribution of ionic fragments measured by reaction microscope exhibit rapid changes associated with the dissociative and Coulomb explosion dynamics.

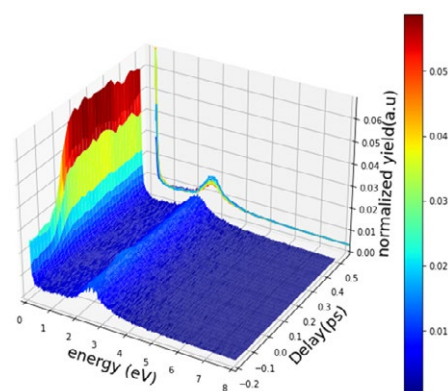


**Figure 1.** The low and high energy yield of  $CO^+$  ion as a function of XUV and NIR delay.

### References

- [1] Schmid G, Schnorr K, Augustin S, Meister S, Lindenblatt H, Trost F, Liu Y, Braune M, Treusch R, Schröter CD, Pfeifer T. *J. Synchrotron Rad.* 2019 May 1;26(3):854-67.
- [2] Meister S, Lindenblatt H, Trost F, Schnorr K, Augustin S, Braune M, Treusch R, Pfeifer T, Moshhammer R. *Applied Sciences.* 10(8) 2953

\*E-mail: [atia.tul.noor@desy.de](mailto:atia.tul.noor@desy.de)



# Geometry dependence of photoionization asymmetry parameter of CH<sub>3</sub>I

P Modak\*, and L Greenman†

J. R. Macdonald Laboratory  
Department of Physics, Kansas State University, Manhattan, KS 66502, USA

**Synopsis** The UKRmol+ suite is used to study geometry dependent photoionization asymmetry parameter ( $\beta$ ) for methyl iodide (CH<sub>3</sub>I) over the photon energy range from its ionization threshold to 50 eV. Only the ground state of CH<sub>3</sub>I neutral and ground & first excited states of its ionic counterpart (CH<sub>3</sub>I<sup>+</sup>) are included in the present work.

With the advancement of ultrashort laser pulses ionization and dissociation dynamics in CH<sub>3</sub>I have been investigated by several groups, viz., Forbes et al.[1], Cheng et al. [2], Allum et al. [3], Amini et al. [4], Sánchez et al. [5] These studies suggest photoionization of CH<sub>3</sub>I producing CH<sub>3</sub>I<sup>+</sup> ion in the ground (X<sup>2</sup>E<sub>3/2,1/2</sub>) and <sup>2</sup>A<sub>1</sub> and <sup>2</sup>E excited states led to dissociation of the C-I bond and produce CH<sub>3</sub><sup>+</sup> ion and I atom. The present study aims to understand the evolution of the photoionization asymmetry parameter ( $\beta$ ) into the C-I bond dissociation pathway for CH<sub>3</sub>I<sup>+</sup>.

We employed the R-matrix theory implemented in the UK Rmol+ [6] suite, which treats the photoionization problem as electron scattering from a cation and then uses time-reversal symmetry to obtain the  $\beta$  parameter. The target (CH<sub>3</sub>I<sup>+</sup>) orbitals were prepared within the complete active space-self-consistent field (CAS-SCF) approximation. We used the ground state geometry of CH<sub>3</sub>I and atomic natural orbital (ANO) basis to construct the target orbitals. Here, we considered ground, X<sup>2</sup>E (*core*,(a<sub>1</sub>'5s<sub>1</sub>)<sup>4</sup>e<sup>4</sup> $\sigma$ <sup>2</sup>5 $\pi$ <sub>1</sub><sup>3</sup>) and first excited, <sup>2</sup>A<sub>1</sub> (*core*,(a<sub>1</sub>'5s<sub>1</sub>)<sup>4</sup>e<sup>4</sup> $\sigma$ <sup>1</sup>5 $\pi$ <sub>1</sub><sup>4</sup>) states of CH<sub>3</sub>I<sup>+</sup> ion without spin-orbit coupling. The continuum states were generated employing both Gaussian and  $\beta$ -spline basis functions, i.e., using a hybrid model. Finally, we used the complete active space-configuration interaction (CAS-CI) method to represent the e<sup>-</sup>+CH<sub>3</sub>I<sup>+</sup> scattering problem under R-matrix theory.

Figure 1 shows the total  $\beta$  parameter associ-

\*E-mail: [paresh@phys.ksu.edu](mailto:paresh@phys.ksu.edu)

†E-mail: [lgreenman@phys.ksu.edu](mailto:lgreenman@phys.ksu.edu)

ated with X<sup>2</sup>E and <sup>2</sup>A<sub>1</sub> states of CH<sub>3</sub>I<sup>+</sup>.

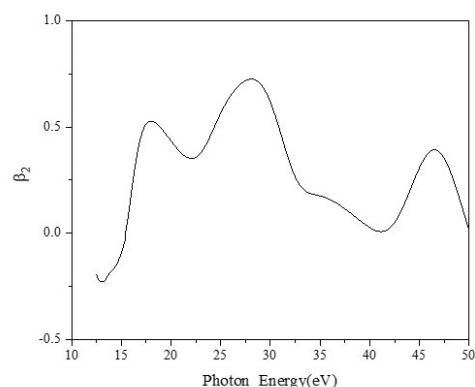


Figure 2: Photoionization asymmetry parameter ( $\beta$ ) for CH<sub>3</sub>I in ground state geometry.

We observed three prominent and one shallow resonance like structure in  $\beta$  around 17.5 eV, 27.6 eV, 46 eV, and 36 eV respectively. The structures in  $\beta$  arise due to interference among different angular momentum terms. Further details of the calculation and some prior results will be presented at the conference.

## References

- [1] Ruairidh Forbes and Felix Allum *et al* 2020 *J. Phys. B* **53** 224001
- [2] Yu-Chen Cheng and Bart Oostervijk *et al* 2021 *J. Phys. B* **54** 014001
- [3] Felix Allum and Michael Burt *et al* 2018 *J. Chem. Phys.* **149** 204313
- [4] Kasra Amini and Evgeny Savelyev *Struct.Dyn.* **5** 014301
- [5] Marta L Murillo-Sánchez and Geert Reitsma 2021 *New J Phys.* **23** 073023
- [6] Zdeněk Mašín and Jakub Benda 2020 *Comput. Phys. Commu.* **249** 107092

## Molecular ion time-dependent rotational relaxation dynamics probed by photoelectron in an ion trap

Abhishek Shahi<sup>1,2</sup>, Deepak Sharma<sup>1</sup>, Sunil Kumar<sup>1,3</sup>, Saurabh Mishra<sup>1</sup>, Igor Rahinov<sup>4</sup>, Oded Heber<sup>1,\*</sup> and Daniel Zajfman<sup>1</sup>

<sup>1</sup>Department of particle Physics and Astrophysics Weizmann Institute of Science, Rehovot, 76100, Israel

<sup>2</sup>School of sciences Woxsen University, Kamkole, Hyderabad, Telangana, 502345 India.

<sup>3</sup>Saha Institute of Nuclear Physics, 1/AF, Bidhannagar, Kolkata 700064, India

<sup>4</sup>Department of Natural Sciences, The Open University of Israel, 4310701 Ra'anana, Israel

**Synopsis** The internal dynamics of rotational transition in hot OH<sup>-</sup> anion were measured as a function of time and compared to Boltzmann distribution as well as to full dynamics master equation transition model for  $J < 50$  in a room temperature environment. although for a non-equilibrium system, the temperature is not a suitable parameter, the actual internal energy distribution dynamics during the observed time (0-3s) are proximate to the Boltzmann distribution.

Hot gaseous ions are common in many systems ranging from chemical reactions, plasma, and atmospheric science to interstellar medium. A fundamental difficulty is understanding the way such a system's internal dynamics evolve as a function of time in nonequilibrium conditions with the environment. For a practical example, such a nonequilibrium condition in molecules is expected in the diffused interstellar medium.

We are reporting on a new experiment incorporating a hot molecular ion source that produces hot OH<sup>-</sup> anions, an Electrostatic Ion Beam Trap (EIBT) and an electron spectrometer (VMI). This experiment can follow internal molecular dynamics as a function of trapping time in the EIBT using a coincidence between particle detectors, the VMI spectrometer, and lasers [1].

The rotational distribution of hot OH<sup>-</sup> molecules distribution ( $J < 50$ ) is measured as a function of time in a room-temperature environment. It was found that the Boltzmann distribution only reasonably describes the system (temperature), and a full-dynamic model using master equations is better in the first second after production. However, although the temperature is not a suitable parameter, the actual internal energy distribution dynamics behavior

during the observed time (0-3s) is proximate to the Boltzmann distribution. The contribution of the black body radiation to the internal dynamics starts to be influential on time longer than 1 second in our experiment[2].

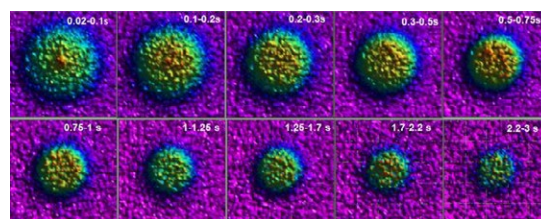


**Figure 1.** VMI time-dependent images of photoelectron distribution. The wider image at the beginning indicates a broad rotational distribution which continuously narrows down in the later images during the 3-second trapping time.

### References

- [1] K. Saha et al. 2017 Review of Scientific Instruments **88** 053101
- [2] A. Shahi et al. 2022 Scientific Reports **12** 22518

\* E-mail: [oded.heber@weizmann.ac.il](mailto:oded.heber@weizmann.ac.il)

## Cusp-electron production in collisions of open-shell $O^{6+}(1s2s)$ ions with He

S. Nanos<sup>1,2</sup>, N.J. Esponda<sup>3</sup>, P.-M. Hillenbrand<sup>4,5</sup>, A. Biniskos<sup>1</sup>, A. Laoutaris<sup>6,2</sup>, M.A. Quinto<sup>3</sup>, N. Petridis<sup>5</sup>, E. Menz<sup>5,7,8</sup>, T.J.M. Zouros<sup>6</sup>, Th. Stöhlker<sup>5,7,8</sup>, R.D. Rivarola<sup>3,9</sup>, J.M. Monti<sup>3,9</sup> and E.P. Benis<sup>1</sup>

<sup>1</sup>Department of Physics, University of Ioannina, GR-45110 Ioannina, Greece

<sup>2</sup>Tandem Accelerator Laboratory, INPP, NCSR "Demokritos", GR-15310 Ag. Paraskevi, Greece

<sup>3</sup>Instituto de Física Rosario (CONICET-UNR), Bv 27 de Febrero 210 bis, 2000 Rosario, Argentina

<sup>4</sup>I. Physikalisches Institut, Justus-Liebig-Universität, 35392 Giessen, Germany

<sup>5</sup>GSI Helmholtzzentrum für Schwerionenforschung, 64291 Darmstadt, Germany

<sup>6</sup>Department of Physics, University of Crete, GR-70013 Heraklion, Greece

<sup>7</sup>Institut für Optik und Quantenelektronik, Friedrich-Schiller-Universität, 07743 Jena, Germany

<sup>8</sup>Helmholtz-Institut Jena, 07743 Jena, Germany

<sup>9</sup>Laboratorio de Colisiones Atómicas, FCEIA, IFIR, Universidad Nacional de Rosario, Avenida Pellegrini 250, Rosario 2000, Argentina

**Synopsis** We report on a combined experimental and theoretical study of cusp electrons emitted at zero degrees in 24-MeV collisions of open-shell  $O^{6+}(1s2s)$  projectiles with He targets. Theoretical cusp DDCS results, obtained within the CDW-EIS framework, are compared to the measurements, showing an overall good agreement. Details on the contributions of the ECC and ELC processes from the different ion cores are discussed.

Fast ion-atom collisions involving unpaired electrons have proven to be a powerful tool for studying subtle dynamic aspects of fundamental processes. In this report, we present a combined theoretical and experimental investigation on the processes of electron capture to the continuum (ECC) and electron loss to the continuum (ELC), for fast ion-atom collisions involving open-shell projectiles. Specifically, we studied the sharp cusp peak of the electrons emitted at zero degrees with respect to the projectile velocity, bearing the signatures of ECC and ELC, in collisions of 24-MeV pre-excited  $O^{6+}(1s2s)$  ions with He gas targets.

The experimental cusp DDCS electron spectra were obtained by applying our double measurement technique, involving a measurement with a mixed-state  $O^{6+}(1s^2, 1s2s)$  and a measurement with a ground state  $O^{6+}(1s^2)$  beam [1]. The measurements were conducted using an electrostatic single-stage hemispherical deflector spectrograph operating at the NCSR "Demokritos" 5.5 MV tandem accelerator laboratory [2]. The theoretical DDCS calculations were obtained within the continuum distorted-wave eikonal initial-state (CDW-EIS) framework [3]. A direct comparison between the DDCS of the CDW-EIS results and the measurements are

presented in figure 1, showing an overall good agreement [4]. Details on the contributions of the ECC and ELC processes from the different orbitals of the ion cores are discussed.

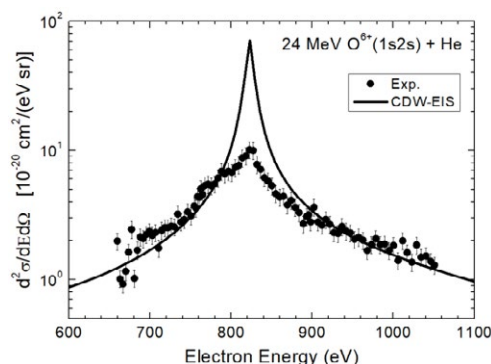


**Figure 1.** Theoretical and experimental DDCS of cusp electrons for collisions of 24-MeV open-shell  $O^{6+}(1s2s)$  ions with He gas targets.

### References

- [1] E.P. Benis et al., *Atoms* **6**, 66 (2018)
- [2] S. Harissopulos et al., *Eur. Phys. J. Plus* **136**, 617 (2021)
- [3] N.J. Esponda et al., *Phys. Rev. A* **105**, 032817 (2022)
- [4] S. Nanos et al., *Phys. Rev. A*, accepted (2023)

\* E-mail: [s.nanos@uoi.gr](mailto:s.nanos@uoi.gr)

## Suppression of three-body loss near a $p$ -wave Feshbach resonance in a quasi-1D ultracold fermionic system

K Nagase<sup>1\*</sup>, Z Xu<sup>1</sup>, N Takahashi<sup>2</sup> and T Mukaiyama<sup>1</sup>

<sup>1</sup>Department of Physics, Tokyo Institute of Technology, Meguro, 152-8551, Japan

<sup>2</sup>Graduate School of Engineering Science, Osaka University, Toyonaka, 560-8531, Japan

The  $p$ -wave three-body relaxation in ultracold fermionic atoms has inhibited realization of the  $p$ -wave superfluid, which is one of the holy grails in the field of ultracold atoms. Although it has been predicted that one dimensional confinement suppresses the three-body relaxation, experimental confirmation is still underway by several groups [1]. Here, we study the three-body relaxation loss and determine the loss coefficient  $L_3$  of spin-polarized  ${}^6\text{Li}$  atoms in quasi-1D near a  $p$ -wave Feshbach resonance. We find that  $L_3$  in quasi-1D is more than one order of magnitude suppressed compared to 3D.

Ultracold atom systems have contributed to elucidating the physical properties of superfluidity with two-body interactions, because of controllability of interatomic interactions using Feshbach resonances. In contrast to  $s$ -wave BCS-BEC crossover, in which the phase diagram of  $s$ -wave superfluidity throughout all scattering length regime has been fully clarified [2], physical properties of superfluidity with non-zero angular momentum interactions, such as  $p$ -wave interactions, are yet to be understood.

Three-body relaxation loss, which is naturally suppressed in  $s$ -wave fermionic systems, however, inhibits realization of superfluidity in  $p$ -wave fermionic systems. The three-body relaxation loss occurs as a result of vibrational relaxation; weakly-bound molecules (Feshbach molecules) turn to deeply-bound molecules due to collisions with unpaired atoms, in which the energy difference of the two molecular states converts to kinetic energy that kicks out both the deeply-bound molecules and unpaired atoms from the trap. The relaxation rate is highly affected by the wavefunction overlap between the molecular states before and after the relaxation, and the existence of the centrifugal barrier in a  $p$ -wave interaction enhances this unwanted relaxation. Recently, a wise theoretical proposal was made that the wavefunction of weakly-bound molecules can be stretched in 1D confinement due to the absence of the centrifugal barrier. Thus, the three-body relaxation loss is expected to be suppressed in a 1D system [3].

In this work, we study the three-body relaxation loss of spin-polarized  ${}^6\text{Li}$  atoms in the lowest hyperfine state confined in a quasi-1D optical trap near a

$p$ -wave Feshbach resonance located at 159 G. Figure 1, which is our main result, shows the extracted loss coefficient in both 1D (trap depth of  $20 E_R$ , where  $E_R$  is the recoil energy) and 3D at various magnetic field. The temperature for this measurement is kept nearly constant, to guarantee suppression of the loss rate is attributed to only the difference of dimensionality, but not to temperature difference. We observe a 37-fold suppression at this condition of confinement strength. Aiming for a full understanding of the underlying physics of the three-body loss suppression by the 1D confinement, we further study how  $L_3$  depends on the temperature of the atoms  $T$  and the confinement strength  $V_L$ . We observe a  $L_3 \propto T^2 V_L^{-4}$  dependence, which indicates further suppression of three-body loss at lower temperature and higher confinement strength. This may realize  $p$ -wave superfluidity in ultracold atom systems.

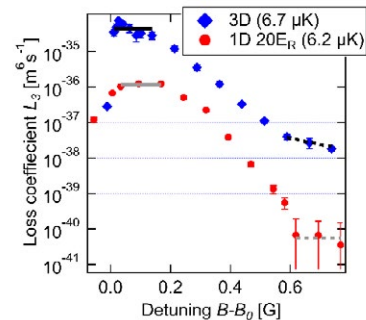


**Figure 1.** The three-body loss coefficient  $L_3$  for 3D(blue) and 1D(red) vs. detuning of magnetic field  $B - B_0$ .

### References

- [1] Y. Chang, *et al.* Phys. Rev. Lett., 125, 263402(2020).
- [2] C. Regal, *et al.* Phys. Rev. Lett., 92, 040403(2004).
- [3] L. Zhou, *et al.* Phys. Rev. A, Phys. Rev. A 96, 030701 (2017).

\* E-mail: nagase.k.ae@m.titech.ac.jp

## Precise measurement of the electron affinity of C<sub>60</sub>

J E Navarro Navarrete<sup>1,\*</sup>, P Martini<sup>1,†</sup>, M Kristiansson<sup>1</sup>, S Indrajith<sup>1</sup>, M. Björkhage<sup>1</sup>, S Rosén<sup>1</sup>, A Simonsson<sup>1</sup>, P Reinhed<sup>1</sup>, J D Alexander<sup>1</sup>, M Gatchell<sup>1</sup>, H Cederquist<sup>1</sup>, H T Schmidt<sup>1</sup>, H Zettergren<sup>1</sup>.

<sup>1</sup>Stockholm University (SU), Department of Physics, AlbaNova University Center, 10691 Stockholm, Sweden

**Synopsis** The electron affinity of the C<sub>60</sub> molecule has been measured in an cryogenic electrostatic ion storage ring by using laser photodetachment threshold spectroscopy (LPTS). This measurement is in agreement with photoelectron spectroscopy (PES) measurements but not with previous reported LPTS measurements done in room-temperature storage rings.

The electron affinity (EA) of the C<sub>60</sub> molecule has been a matter of disagreement in the literature [1-4]. The most precise values reported from Laser Photodetachment Threshold Spectroscopy (LPTS) experiments are 2.666(1) eV [2] and 2.664(5) eV [3] for anions stored in room temperature ion storage rings. In contrast, the most precise Photoelectron Spectroscopy (PES) experiments has reported a value of 2.6835(6) eV [4] for anions cooled in a cryogenic controlled ion trap. The reason for this large discrepancy has been attributed to uncertainties related to spectrometer calibrations in the PES experiments [3], and elevated temperatures in the storage ring experiments such that hot band contributions cannot be neglected when determining the electron detachment energy using LPTS [4].

By conducting LPTS experiments at the Double Electrostatic Storage Ion Ring Experiment (DESIREE), we were able to determine the threshold energy with sufficient precision to distinguish the two previous results. The cryogenic operation of DESIREE, which gives a background pressure of 10<sup>3</sup> He/cm<sup>3</sup> (at 13 K) [5], allows the C<sub>60</sub><sup>-</sup> ions to cool down on time scales ranging up to 200 s. The threshold energy corresponding to the EA was determined by monitoring how the hot band contributions to the photodetachment cross section becomes less important as the anions cool when they are stored, while the signal from the actual EA threshold remains constant. The EA is measured to 2.684(2) eV, in agreement with the PES experiments [4,6,7] but not with the previous LPTS experiments (see Fig. 1). This supports the interpretation in Ref 4, i.e. that hot band

contributions are the reason for the disagreement between the PES and LPTS experiments.

In follow-up experiments, we aim to use a depletion laser technique, based on the experiments of the hitherto most precise EA measurement of any atomic species [8], to eliminate the contribution from long-lived excited states and improve the measurement of the EA of C<sub>60</sub> with unprecedented precision.

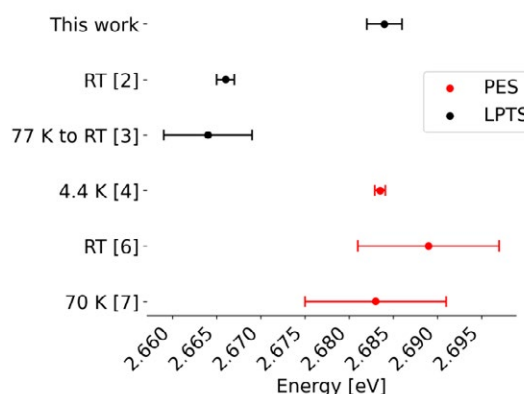


**Figure 1.** Comparison of the present result with earlier measurements of the electron affinity of C<sub>60</sub> (RT – room temperature).

### References

- [1] Smalley R *et al.* 1991 *Chem. Phys. Lett.* **182** 5
- [2] Brink C *et al.* 1995, *Chem. Phys. Lett.* **233** 52
- [3] Stöckel K and Andersen J U 2013. *J. Chem. Phys.* **139** 164304
- [4] Huang *et al.* 2014 *J. Chem. Phys.* **140** 224315
- [5] Schmidt H.T. *et al.* *Rev. Sci. Instrum.* **84** 055115
- [6] Wang X B *et al.* 1999 *J. Chem. Phys.* **110** 8217
- [7] Wang X B *et al.* 2005 *J. Chem. Phys.* **123** 051106
- [8] Kristiansson M *et al.* 2022 *Nat. Comm* **13** 5906

\* E-mail: [jose.navarrete@fysik.su.se](mailto:jose.navarrete@fysik.su.se)

† E-mail: [paul.martini@fysik.su.se](mailto:paul.martini@fysik.su.se)



## X-ray spectra of highly-charged Nd in an EBIT plasma: line identifications and effect of metastable states on ionization balance

A Hosier<sup>1,2\*</sup>, J N Tan<sup>3†</sup>, T Burke<sup>1</sup>, Dipti<sup>2</sup>, G O'Neil<sup>4</sup>, E Takacs<sup>1,2</sup>, Yu Ralchenko<sup>3</sup>

<sup>1</sup>Department of Physics and Astronomy, Clemson University, Clemson, SC 29634-0978

<sup>2</sup>Associate, National Institute of Standards and Technology, Gaithersburg, MD 20899

<sup>3</sup>National Institute of Standards and Technology, Gaithersburg, MD 20899

<sup>4</sup>National Institute of Standards and Technology, Boulder, CO 80305

**Synopsis** The NIST Electron Beam Ion Trap generated Co-like and Ni-like ions of Nd below the Ni-like ionization potential. X-ray spectra were collected with the NIST Transition-Edge Sensor microcalorimeter. Population dynamics of metastable levels were investigated after line identification with collisional-radiative code NOMAD.

Several dozens of spectral lines due to electric-dipole and higher-order transitions, including a forbidden magnetic-octupole (M3) transition, were measured and identified in spectra of highly charged Nd produced at the electron beam ion trap (EBIT) of the National Institute of Standards and Technology (NIST). The typical beam energy was about 2 keV and intensified in a magnetic field of about 2 T. The EBIT x-ray spectra were recorded with the NIST Transition-Edge Sensor (TES) microcalorimeter [1] over the photon energy range of 500 eV to 8000 eV with the energy resolution of around 4 eV. Metallic samples fluoresced with an external X-ray source were used for calibration. The strongest observed transitions were the resonance transitions  $3d^{10}-3d^9nf$  and  $3d^9-3d^8n'f$  in Ni-like and Co-like ions, respectively. It was found that Co-like lines were present in the spectra in spite of the electron beam energy being kept below the ground state ionization potential of the Ni-like ion,  $I(\text{Nd}^{32+}) \approx 2134$  eV [2]. The populations of Nd levels in the EBIT plasma and the ensuing spectra were calculated with the collisional-radiative code NOMAD [3] using atomic data generated with the Flexible Atomic Code (FAC)

[4]. The population dynamics of metastable levels were investigated to explain the presence of Co-like spectral lines in the observed spectra.

### References

- [1] Szypryt, P., G. C. O'Neil, E. Takacs, J. N. Tan, S. W. Buechele, A. S. Naing, D. A. Bennett, et al. "A Transition-Edge Sensor-Based x-Ray Spectrometer for the Study of Highly Charged Ions at the National Institute of Standards and Technology Electron Beam Ion Trap." *Review of Scientific Instruments* 90, no. 12 (December 1, 2019): 123107.
- [2] Kramida, A., Yu. Ralchenko, J. Reader, and NIST ASD Team (2022). NIST Atomic Spectra Database (ver. 5.10), [Online]. Available: <https://physics.nist.gov/asd> [2023, June 1]. National Institute of Standards and Technology, Gaithersburg, MD. DOI: <https://doi.org/10.18434/T4W30F>
- [3] Ralchenko, Yu. V., and Y. Maron. "Accelerated Recombination Due to Resonant Deexcitation of Metastable States." *Journal of Quantitative Spectroscopy and Radiative Transfer* 71, no. 2-6 (October 2001): 609-21.
- [4] Gu, M. F. "The Flexible Atomic Code." *Canadian Journal of Physics* 86, no. 5 (May 1, 2008): 675-89.

\*E-mail: [ahosier@clemson.edu](mailto:ahosier@clemson.edu)

†E-mail: [joseph.tan@nist.gov](mailto:joseph.tan@nist.gov)



## CollisionDB: An online repository of plasma collisional data sets

C Hill<sup>1\*</sup>, M Haničinec and K Heinola<sup>1</sup>

<sup>1</sup>Atomic and Molecular Data Unit, Department of Nuclear Sciences and Applications, International Atomic Energy Agency, Vienna A-1400, Austria

**Synopsis** CollisionDB is a database of plasma collisional process data sets curated by the International Atomic Energy Agency (IAEA). A comprehensive data model, browser-based search interface and Application Programming Interface (API) have been developed and a Python library (PyCollisionDB) released to allow cross sections and rate coefficients to be downloaded, compared and transformed.

Fundamental data on the collisional processes between electrons, ions, atoms and molecules, mainly in the form of either cross sections or rate coefficients, is essential for the modelling of plasmas for scientific and engineering applications. Despite the large amount of such data reported in the literature each year, very little of it is routinely stored in convenient, searchable online databases. Furthermore, there is no generally-agreed standard for the metadata essential to the proper description of such data sets.

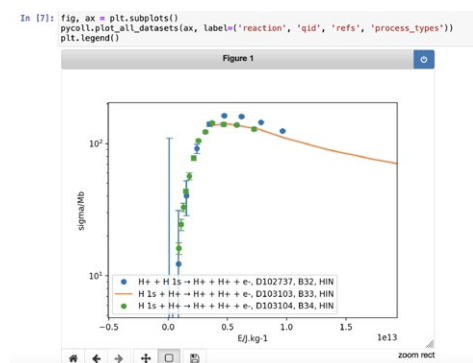


**Figure 1.** A comparison of data sets visualized using the PyCollisionDB library.

This presentation introduces a database, CollisionDB [1, 2], which has been built around an open set of standards for the concise description of atomic and molecular species, states and collisional processes [3, 4]. Data can be queried by publication DOI, author name, “reactant” and “product” species, process type and method (“experiment”, “theory”); data sets (with attached metadata in JSON format) can be visualized in the browser and downloaded in a com-

pressed archive. Fit functions and uncertainties are supported.

The CollisionDB database also exposes an API which can be queried programmatically from modelling codes or interactively using the PyCollisionDB Python library [5], which allows the easy filtering, aggregation, transformation and visualization (Figure 1) of data.

Data sets described in the peer-reviewed literature may be provided to the CollisionDB maintainers in a concise, text-based format and are timestamped and permanently attached to metadata at the time they are imported into the database. BibTeX output of the references associated with data sets can also be provided through the online interface.

As of June 2023, there are 122 352 data sets available in CollisionDB, with a focus on the processes relevant to plasmas in magnetically confined fusion reactors. The consistent data format employed by the database facilitates its use in modelling codes and by machine learning algorithms.

### References

- [1] Hill C, Dipti and M. Haničinec 2023, *Phys. Scr.*, submitted
- [2] <https://amdis.iaea.org/db/collisiondb/>
- [3] Hill C 2022 PyValem, GitHub repository; <https://github.com/xnx/pyvalem>
- [4] Hill C, et al. 2022 “Classification of Processes in Plasma Physics”, Version 2.4; IAEA Publication, <https://amdis.iaea.org/media/miscellaneous-publications/plasma-processes-classification-v2.4.pdf>
- [5] Hill C 2022 PyCollisionDB, GitHub repository, <https://github.com/xnx/pycollisiondb>

\*E-mail: [ch.hill@iaea.org](mailto:ch.hill@iaea.org)

## Characterization of the longitudinal gas density profile in the microfluidic gas cell

J Turnšek<sup>1,2\*</sup>, K Bučar<sup>1,2</sup>, M Žitnik<sup>1,2†</sup>, M Coreno<sup>3,4</sup>, A G Ciriolo<sup>5</sup> and R Martinez Vazquez<sup>6</sup>

<sup>1</sup>J. Stefan Institute, Jamova 39, SI-1000 Ljubljana, Slovenia

<sup>2</sup>Faculty of Mathematics and Physics, University of Ljubljana, Jadranska 31, SI-1000 Ljubljana, Slovenia

<sup>3</sup>Eletra-Sincrotrone Trieste, Strada Statale 14-km 163.5, I-34149, Basovizza Trieste, Italy

<sup>4</sup>Consiglio Nazionale delle Ricerche–Istituto di Struttura della Materia, LD2 unit, 34149, Trieste, Italy

<sup>5</sup>Department of Physics, Politecnico di Milano, Piazza Leonardo da Vinci, 32, 20133 Milano, Italy

<sup>6</sup>CNR Istituto di Fotonica e Nanotecnologie, Piazza Leonardo da Vinci, 32, 20133 Milano, Italy

**Synopsis** We determined the longitudinal pressure profile of a microfluidic glass cell by measuring VIS fluorescence from helium gas after resonant excitation of the  $3^1P$  state with synchrotron light. A numerical simulation of the absorption-emission process in the high pressure environment was performed to identify the pressure profile which explains the observed fluorescence profile and VUV absorption in the resonance region.

Due to strong absorption of VUV light, experiments on gases are usually performed without using any entrance windows, relying on injection of gas into the vacuum environment.[1, 2] However, in such cases the target density remains below 1 mbar and drops to the  $10^{-4}$  to  $10^{-2}$  mbar range in typical gas phase experiments. It is challenging to form an open-end gas target with a well-controlled and localized spatial gas density distribution with pressure maximum as high as 100 mbar.

We employed an open ended glass device to trap Helium gas up to pressures of 86 mbar. The open ended construction allowed the unimpeded passing of light, while limiting the flux of escaping gas. The device also allowed us to measure the resulting fluorescence of Helium along the length of the device, which we compared to the calculated profile.

Helium gas was resonantly excited with 23.1 eV light to the  $1s3p^1P$  level. Using a VIS spectrometer,  $1s3d^1D \rightarrow 1s2p^1P$  and  $1s3p^1P \rightarrow 1s2s^1S$  fluorescent channels were observed at 501.57 nm and 667.82 nm respectively. Their total fluorescent yield was observed with respect to the longitudinal coordinate, and with respect to the backing pressure.

The absorption was modeled by solving the Beer-Lambert law, for which the absorption line shape had to be thoroughly considered. For this, a simple approach, based on the Anderson Thalmann lineshape theory was employed.[3] Radia-

tion trapping and collisional state transfer effects were also considered in the model.

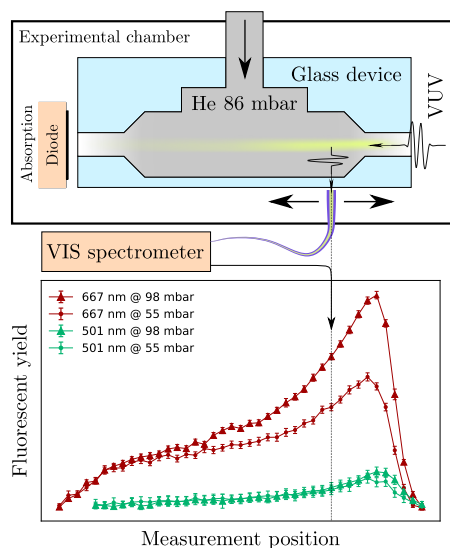


**Figure 1.** Experimental setup with the longitudinal glass microfluidic cell (above) and measured longitudinal distribution of emitted VIS intensity for different settings of the driving pressure (below).

### References

- [1] Marr G V 1987 [Handbook on Synchrotron Radiation](#)
- [2] M Žitnik et al 2003 *J. Phys. B: At. Mol. Opt. Phys.* **36** 4175
- [3] Margenau H and Lewis M 1959 *Rev. Mod. Phys.* **31** 569

\*E-mail: [janez.turnsek@ijs.si](mailto:janez.turnsek@ijs.si)

†E-mail: [matjaz.zitnik@ijs.si](mailto:matjaz.zitnik@ijs.si)

## Laser cooling experiments at the CSRe: explanation for the observed wide deceleration range on a coasting ion beam by a cw laser

D Y Chen<sup>1</sup>, H B Wang<sup>1</sup>, W Q Wen<sup>1</sup>, Y J Yuan<sup>1</sup>, D Winters<sup>2</sup>, S Klammes<sup>2,3</sup>, Th Walther<sup>3,4</sup>,  
U Schramm<sup>5,6</sup>, M Bussmann<sup>5,7</sup>, X Ma<sup>1†</sup> and Laser Cooling Collaboration

<sup>1</sup> Institute of Modern Physics, Chinese Academy of Sciences, Lanzhou, 730000, China

<sup>2</sup> GSI Helmholtzzentrum für Schwerionenforschung GmbH, Darmstadt, 64291, Germany

<sup>3</sup> Institut für Angewandte Physik, Technische Universität Darmstadt, Darmstadt, 64289, Germany

<sup>4</sup> Helmholtz Forschungsakademie Hessen für FAIR, Darmstadt, Darmstadt, 64289, Germany

<sup>5</sup> Helmholtz-Zentrum Dresden-Rossendorf, Dresden, 01328, Germany

<sup>6</sup> Technische Universität Dresden, Dresden, 01069, Germany

<sup>7</sup> Center for Advanced Systems Understanding, Görlitz, 02826, Germany

**Synopsis** A significant deceleration effect on a coasting ion beam by a cw laser was observed in the laser cooling experiment at the CSRe in Lanzhou, China. By taking into account the transverse betatron oscillation of the ion beam and angular misalignment of the laser beam, this observation is explained for the first time with simulations.

Laser cooling of Li-like  $O^{5+}$  ion beams with an relativistic energy of 275.7 MeV/u was achieved for the first time at the storage ring CSRe in Lanzhou, China[1]. A significant deceleration effect, two orders of magnitude beyond the calculated value, on a coasting ion beam by a cw laser was observed in the experiment. Simulations reveal that the deceleration range of the typically narrow cw laser force is highly enlarged by taking into account the betatron oscillation of the ions with large emittance and the angular misalignment of the laser direction. Fig. 1 shows the simulated ion distribution, Schottky-noise spectrum, and transverse envelope of

coasting ion beam after interaction with an anti-collinear laser. Transverse betatron oscillation enables more ions to be resonant with the laser, which leads to an increasingly broader deceleration range. For detailed simulations and discussions, please refer to the published paper[2]. The present work is crucial for forthcoming laser cooling and precision laser spectroscopy experiments and simulations on heavy highly charged ions at the CSRe and the future facility HIAF.

### References

[1] W Q Wen *et al* to be submitted.

[2] D Y Chen *et al* 2023 *Nucl. Instrum. Methods A* **1047** 167852.

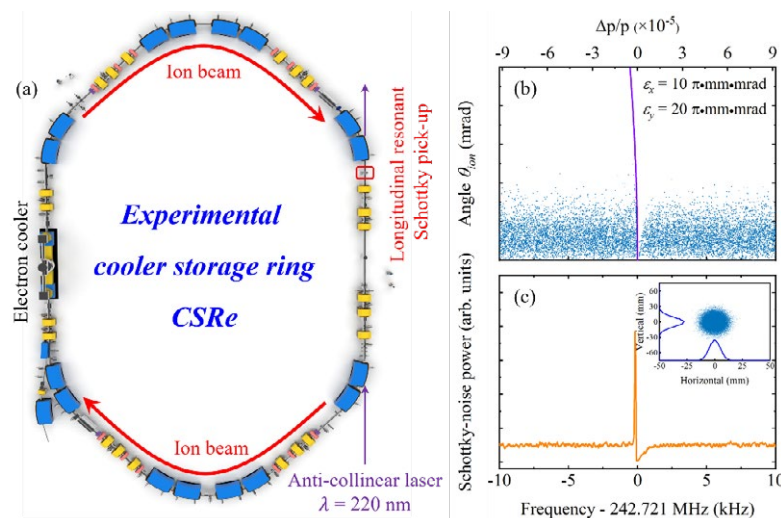


**Figure 1.** (a) Schematic view of the laser cooling experiment with the  $^{16}O^{5+}$  ion beam at the storage ring CSRe. (b) Ion distribution and (c) Schottky-noise spectrum of coasting ion beam after interaction with an anti-collinear cw laser, and the inset shows the transverse envelope of the ion beam.

<sup>†</sup> E-mail: [x.ma@impcas.ac.cn](mailto:x.ma@impcas.ac.cn)

## Quantum Holography in Above Threshold Ionization

S D López<sup>1</sup> and D G Arbó<sup>1,2 †</sup>

<sup>1</sup>Institute for Astronomy and Space Physics IAFE (CONICET-UBA), C1428ZAA, Buenos Aires, Argentina

<sup>2</sup>Universidad de Buenos Aires, Facultad de Cs. Exactas y Naturales and Ciclo Básico Común, Buenos Aires, Argentina

**Synopsis** We present a theoretical analysis of interferences in the photoelectron spectra using a numerical solution of the time dependent Schrödinger equation (TDSE) and the semiclassical two-step model (SCTS). Some structures can be interpreted as holograms, i.e. the interference pattern between the direct (reference) and the rescattered (signal beam) electrons. In this way, the information of the interaction is encoded in the interference pattern between the reference and the signal. We analyze the ionization of atomic hydrogen to characterize the role that the long-range Coulomb interaction plays in the holographic structure.

When an intense short laser pulse interacts with an atom ionizing it, the photoelectron spectra present several structures that can be understood as double slit interferences in the time domain, namely intra- and inter-cycle interferences formed by electrons that emerge from the atom and follow directly to detector [1]. Another type of structures requires the interaction of the ejected electron with the parent core. In a classical picture, rescattering trajectories return to the parent ion driven by the laser field and rescatters off to the detector. Holographic structures can be explained only when long-range Coulomb interactions take place and can be interpreted as holograms, i.e. the interference pattern between the direct (reference) and the rescattered (signal beam) electrons [2].

We use the semiclassical two-step model of Shvetsov-Shilovski *et al* [3] to elucidate the nature of the holographic structure. Three different types of trajectories are characterized during the ionization process by a single cycle pulse with three different types of interferences. We show that the holographic interference arises from the ionization yield only during the first half cycle of the pulse, whereas the coherent superposition of electron trajectories during the first half cycle and the second half cycle gives rise to two other kinds of intracycle interference. Although the picture of interference of a reference beam and a signal beam is adequate, we show that our results for the formation of the holographic pattern agree with the glory rescattering theory of Xia *et al* [4,5]. We show in Fig. 1 photoelectron distributions as a function of parallel  $k_z$  and perpendicular  $k_\perp$  momentum to polarization axis calculated with the semi-

classical two step model (SCTS) model (a) and the numerical solution of the time dependent Schrödinger equation (TDSE) (b). We observe interference patterns resembling a dispersion of an electron wave packet from a potential centered in the origin in both calculations.

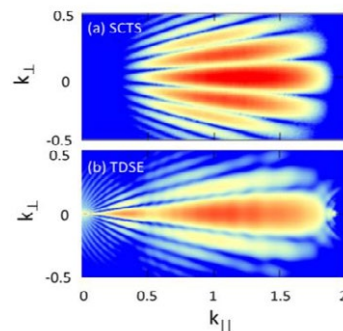


**Figure 1.** Momentum distribution after interaction of a near-infrared ( $\lambda = 800$  nm) one-cycle laser pulse with H. (a) SCTS, (b) TDSE.  $I = 10^{14}$  W/cm<sup>2</sup>.

This work is supported by PICT 2020-01755, 2020-01434, and PICT-2017-2945 of ANPCyT (Argentina), PIP 2022-2024 11220210100468CO of Conicet (Argentina).

### References

- [1] Arbó D G *et al* 2010 *Phys. Rev. A* **82**, 043426; *ibid* **81**, 021403.
- [2] Huismans Y *et al* 2011, *Science* **331**, 61
- [3] Shvetsov-Shilovski N *et al* 2016, *Phys. Rev. A* **94**, 013415
- [4] López S D *et al* 2019 *Phys. Rev. A* **100**, 023419
- [5] López S D *et al* 2019 *Eur. Phys. Jour. D* **73**, 28

<sup>†</sup> E-mail: [diego@iafe.uba.ar](mailto:diego@iafe.uba.ar)

## First principles simulation of high harmonic generation using quantum computer

H Gi<sup>1\*</sup>, Y Orimo<sup>1</sup>, K L Ishikawa<sup>1</sup>, Y Kawashima<sup>2</sup>, T Gujarati<sup>3</sup>, T Sato<sup>1†</sup>

<sup>1</sup> Graduate School of Engineering, The University of Tokyo, 7-3-1 Hongo, Bunkyo-ku, Tokyo 113-8656, Japan

<sup>2</sup> IBM Quantum, IBM Research Tokyo, Tokyo, 103-8510, Japan

<sup>3</sup> IBM Quantum, IBM Research - Almaden, 650 Harry Road, San Jose, CA 95120, USA

**Synopsis** We calculated the high harmonic generation from a one-dimensional Helium atom model under a high-intensity laser using the quantum computer `ibm_kawasaki`.

Atto second science and strong-field physics are being actively studied to precisely observe and control material on an electronic scale. High harmonic generation (HHG) from atoms and molecules irradiated by a strong laser field is one of the most important high-field phenomena.

Recently, quantum chemistry and physics on quantum computers have been attracting more and more attention [1]. Since our laboratory has been developing first-principles simulation methods for molecules under high-intensity laser fields, we have been exploring the application of quantum computers. Many types of research have been conducted on the time-independent Schrödinger equation and the time-dependent Schrödinger equation (TDSE). Using quantum computers, calculations that take exponential time on classical computers are expected to take polynomial time on quantum computers. In this study, we used the quantum computer `ibm_kawasaki` to simulate a one-dimensional model of a Helium atom under a high-intensity laser field.

To solve TDSE for multi-electron systems, time-dependent wavefunction theory expresses the wavefunction of molecules as a superposition of Slater determinants and solves it by evolving the expansion coefficients and orbital functions in time [2]. The classical method, the multi-configuration time-dependent Hartree-Fock (MCTDHF) method, which includes all electron configurations, can rigorously incorporate electron correlations. However, the computational cost increases exponentially with the number of electrons in both classical and quantum computers. This study used the time-dependent optimized unitary coupled-cluster (TD-OUCC) method on a quantum computer, which takes an

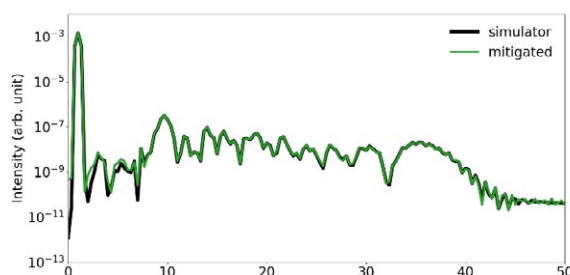


**Fig. 1.** High harmonic generation spectrum from one-dimensional helium model exposed to a laser field with an intensity of  $2 \times 10^{14}$  W/cm<sup>2</sup> and a wavelength of 800 nm. Comparison of the results of a quantum circuit simulator (simulator), and `ibm_kawasaki` with readout error mitigation (mitigated).

exponential cost on classical computers but polynomial time on quantum computers. We calculated the expectation value of the dipole acceleration of electrons and Fourier transform the dipole acceleration to calculate the high harmonic spectrum when irradiated by a three-cycle linearly polarized pulse for a 1D Helium model.

From the results in Fig. 1., we can observe the plateau and cut-off both of which are characteristic of HHG. The result from the quantum computer which is processed with read-out error mitigation almost matched the result of the noiseless simulator in the dynamic range of  $10^{-3}$  to  $10^{-11}$  orders.

### References

- [1] McArdle S, Endo S, Aspuru-Guzik A, Benjamin SC, Yuan X, *Rev. Mod. Phys.* **92** 015003
- [2] Ishikawa K L, Sato T, 2015 *IEEE J Quantum Electron* **21** 1

\*E-mail: [gi-hiroki139@g.ecc.u-tokyo.ac.jp](mailto:gi-hiroki139@g.ecc.u-tokyo.ac.jp)

†E-mail: [sato@atto.t.u-tokyo.ac.jp](mailto:sato@atto.t.u-tokyo.ac.jp)



# Impact of nondipole corrections on photoelectron rescattering off atomic targets in intense midinfrared laser pulses

R Kahvedžić<sup>1,2,\*</sup>, S Gräfe<sup>1,2,3†</sup>

<sup>1</sup>Institute of Physical Chemistry, Friedrich Schiller University Jena, Jena, 07743, Germany

<sup>2</sup>Max Planck School of Photonics, Jena, 07745, Germany

<sup>3</sup>Fraunhofer Institute for Applied Optics and Precision Engineering, Jena, 07745, Germany

**Synopsis** The influence of nondipole corrections on rescattering of photoelectrons emitted in the above-threshold ionization process by intense, midinfrared laser pulses is theoretically analyzed by applying the strong-field approximation with leading-order nondipole corrections.

Above-threshold ionization (ATI) of atomic targets in intense light fields is a highly non-perturbative process which may result in photoelectrons with energies exceeding the photon energy by several orders of magnitude. [1] Theoretical descriptions of ATI in the wavelength regime suitable for a typical table-top experiment ( $\simeq 800$  nm) usually rely on the dipole approximation, where one neglects the spatial dependence of the field and considers the interaction with a purely time-dependent electric field in the polarization plane. As the wavelength of the intense field increases toward the infrared regime, motion of the electron along the propagation direction of the field becomes more pronounced, nondipole effects become observable and the dipole approximation breaks down.[2]

Employing the strong-field approximation (SFA) with leading-order nondipole corrections [2, 3, 4], which is suitable for the theoretical description of strong-field ionization in the nonrelativistic midinfrared regime, we compute the photoelectron spectra and analyze the impact of nondipole corrections on rescattered photoelectrons. Our theoretical consideration demonstrates that the longitudinal momentum component (along the field propagation direction) of the electron exhibits a quadratic dependence on the transverse momentum component (in the polarization plane) in the low-energy region of the spectrum where the direct electrons, i.e. the electrons not experiencing rescattering, give the largest contribution ( $-2$  a.u.  $\lesssim p_{\perp} \lesssim 2$  a.u. in Figure 1). Rescattering with the parent ion leads to additional exchange of momentum, dramati-

cally changing this dependence, as can be seen in Figure 1 for  $p_{\perp} \lesssim -2$  a.u. and  $p_{\perp} \gtrsim 2$  a.u.. Moreover, in the vicinity of zero transverse momentum, we observe a counter-intuitive momentum shift opposite to the propagation direction of the field. Applying the saddle-point approximation, we further investigate how nondipole corrections influence different ionization pathways, their interference pattern and how this reflects on the above mentioned features.

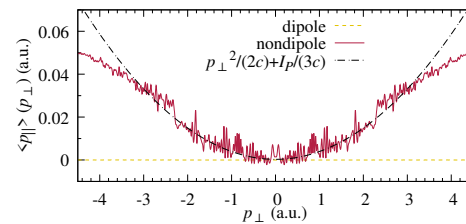


**Figure 1.** Partial average of the longitudinal momentum component  $\langle p_{\parallel} \rangle(p_{\perp})$  as a function of the perpendicular momentum component  $p_{\perp}$  of photoelectrons emitted from  $F^{-}$ , computed for a linearly polarized long field characterized by wavelength  $\lambda = 4 \mu\text{m}$  and peak intensity  $I = 1.8 \times 10^{13} \text{ W/cm}^2$ . [2]

## References

- [1] Milošević D B et al 2006 *J. Phys. B: At. Mol. Opt. Phys.* **39**, R203
- [2] Kahvedžić R and Gräfe S 2022 *Phys. Rev. A* **105**, 063102
- [3] Kahvedžić R and Gräfe S 2022 *Phys. Rev. A* **106**, 043122
- [4] Kahvedžić R, Habibović D, Becker W, Gräfe S and Milošević D B 2023 *Ann. Phys.(Berlin)* **2200616**

\*E-mail: [resad.kahvedzic@uni-jena.de](mailto:resad.kahvedzic@uni-jena.de)

†E-mail: [s.graefe@uni-jena.de](mailto:s.graefe@uni-jena.de)



## Attosecond-resolved Non-dipole Electron Dynamics

Jintai Liang,<sup>1</sup> Meng Han,<sup>2,\*</sup> Yijie Liao,<sup>1</sup> Jia-bao Ji,<sup>2</sup> Leung Chung Sum,<sup>2</sup> Wei-Chao Jiang,<sup>3</sup> Kiyoshi Ueda,<sup>2,4</sup> Yueming Zhou,<sup>1,†</sup> Peixiang Lu,<sup>1</sup>, Hans Jakob Wörner<sup>2</sup>

<sup>1</sup>School of Physics, Huazhong University of Science and Technology, Wuhan 430074, China

<sup>2</sup>Laboratorium für Physikalische Chemie, ETH Zürich, Zürich, 8093, Switzerland

<sup>3</sup>College of Physics and Optoelectronic Engineering, Shenzhen University, Shenzhen 518060, China

<sup>4</sup>Department of Chemistry, Tohoku University, Sendai, 980-8578, Japan

**Synopsis** The advanced attosecond technology has enabled the measurement of the ultrafast electron dynamics in atom/molecule photoionization with unprecedented temporal resolution. However, only the electric dipole transition dynamics has been accessed. The non-dipole dynamics is not touched yet, mainly because the non-dipole effects are typically orders of magnitude smaller than that of the dipole contribution. We demonstrated a self-reference attosecond photoelectron interferometry to resolve the attosecond non-dipole dynamics, with which subcycle electron motion along the light propagation direction in a range of 15 picometers driven by the magnetic component of a near-infrared laser field is successfully tracked. Furthermore, we measured a time delay of about 15 attoseconds between the electric dipole and quadrupole transitions in photoionization of helium. Our work opens a research direction of attosecond non-dipole physics.

In atomic photoionization within dipole approximation, the photoelectron momentum distribution are exactly asymmetric along the laser propagation direction. The breakdown of the dipole approximation lead to the tiny asymmetry of the photoelectron momentum distribution along the laser propagation direction. Though this effect has been experimentally observed in a broad range of light spectrum, all of the reports are limited to the static measurement. With the RABBIT technique, we reported the first study on the attosecond non-dipole electron dynamics in atomic photoionization. Different from previous studies with the RABBIT technique, in our study we analyzed the forward-backward asymmetry along the laser propagation direction as a function of the time delay between the XUV attosecond pulse train and the IR field in the RABBIT scheme. Figure 1 compares the time-delay dependence of the forward-backward asymmetry with that of the photoelectron yield. It reveals a tiny phase shift between this two oscillations, which indicates a time delay of about  $15 \pm 10$  as between the electric dipole and quadrupole transitions in helium photoionization.

Moreover, we observed the effect of the magnetic component of the IR field in the RABBIT experiment. This effect exhibits as the different energies of the photoelectrons emitted

into the forward and backward directions. The measured result agrees well with the theoretical prediction based on non-dipole strong-field approximation. Different from previous experiment in multiphoton ionization where it is shown that the backward electron possesses the larger energy, our measurement shows that the energy difference depends on the ionization time. Our measurement definitely reveals the picometer motion of the photoelectron driving by the magnetic-component of the IR field.

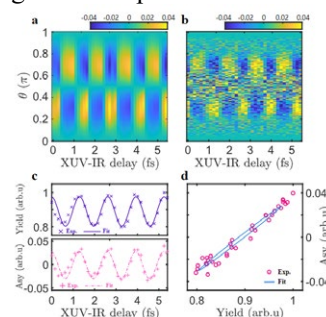


**Figure 1.** The asymmetry of the photoelectron yield as a function of the time delay. A is the TDSE result and the others are the experimental data.

### References

- [1] K. Klunder et al., Phys. Rev. Lett. 106, 143002 (2011).
- [2] K. Lin, et al., Sci. Adv. 8, eabn7386 (2022)

\* E-mail: [corresponding.menhan@ethz.ch](mailto:corresponding.menhan@ethz.ch);

† E-mail: [corresponding.zhouymhust@hust.edu.cn](mailto:corresponding.zhouymhust@hust.edu.cn)

## Multi-photon double ionization of helium by ultrashort XUV pulses: probing the role of electron correlations

W -C Jiang<sup>1,2\*</sup>, M Ederer<sup>2,3</sup>, S Donsa<sup>2</sup>, J Feist<sup>4</sup>, I Březinová<sup>2</sup> and J Burgdörfer<sup>2</sup>

<sup>1</sup>College of Physics and Energy, Shenzhen University, Shenzhen 518060, China

<sup>2</sup>Institute for Theoretical Physics, Vienna University of Technology, Wiedner Hauptstraße 8-10, A-1040 Vienna, Austria, EU

<sup>3</sup>University Service Centre for Transmission Electron Microscopy, Vienna University of Technology, Wiedner Hauptstraße 8-10, A-1040 Vienna, Austria, EU

<sup>4</sup>Departamento de Física Teórica de la Materia Condensada and Condensed Matter Physics Center (IFIMAC), Universidad Autónoma de Madrid, 28049 Madrid, Spain, EU

**Synopsis** Multi-photon double ionization of helium by up to 5 XUV photons is investigated by numerically solving the time-dependent Schrödinger equation (TDSE) for helium in its full dimensionality. We identify a new pathway to double ionization (DI) involving correlated excitation-ionization as intermediate step which can provide a contribution to the total DI yield comparable to the conventional direct sequential double ionization. We find that the ejection mode where the energy is equal and the electrons are emitted in the same direction can be dominant in higher-order multi-photon double ionization.

Most of the existing studies on multi-photon double ionization (MPDI) of atoms in the XUV regime are restricted to the low-order processes of 1-photon double ionization (1PDI) and 2-photon double ionization (2PDI). Only recently, experimental investigations of higher order processes have become available [1]. We have systematically investigated double ionization by ultrashort XUV pulses by varying the number of absorbed photons (up to 5) and the pulse duration from about 100 attoseconds to 20 femtoseconds by solving the TDSE in its full dimensionality, using a wave-splitting method to make the numerical calculations at long pulse durations feasible [2].

We have explored the interplay between sequential and non-sequential double ionization for different photon orders and have identified alternative pathways towards double ionization. Most importantly, we find that a path involving a multi-photon two-electron excitation-ionization step followed by a one- or multi-photon ionization of excited He<sup>+</sup> competes with the direct non-resonant sequential ionization via the ground state of He<sup>+</sup>. Electron correlation effects are shown to be of importance also for sequential processes. This applies also to the two-electron continuum where side-by-side emission with equal energy sharing becomes possible in the sequential

regime for long pulses due to Coulomb repulsion. For ultrashort pulses in the attosecond regime MPDI becomes strongly non-sequential with correlation effects in the time domain even in the spectrally sequential regime.

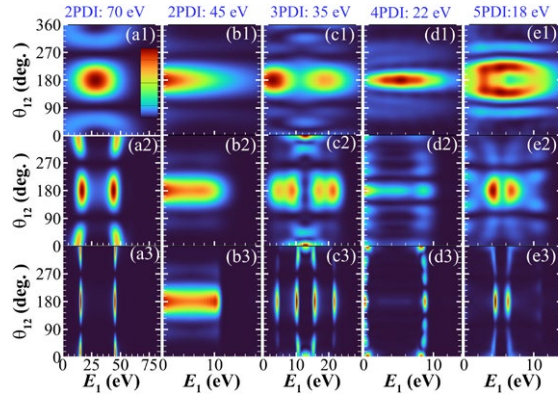


**Figure 1.** The angle-resolved energy spectra  $P(E_1, \theta_{12})$  at  $\theta_1 = 0$ . Results of three pulse durations of 5 (the first row), 20 (the second row), and 100 (the third row) cycles are shown.

### References

- [1] A. Hishikawa, *et al.* 2011 *Phys. Rev. Lett.* **107** 243003
- [2] W. Jiang, *et al.* *Phys. Rev. A* submitted

\*E-mail: [jiang.wei.chao@szu.edu.cn](mailto:jiang.wei.chao@szu.edu.cn)

## Precise control of intracycle interference with a phase-stabilized polarization-gated laser pulse

Y L Wang\*, R P Sun, X Y Lai, H P Kang, W Quan, and X J Liu†

State Key Laboratory of Magnetic Resonance and Atomic and Molecular Physics, Wuhan Institute of Physics and Mathematics, Innovation Academy for Precision Measurement Science and Technology, Chinese Academy of Sciences, Wuhan 430071, China

**Synopsis** We use a polarization-gated (PG) pulse to precisely control the interferences between electron wave packets (EWPs) released at different times within one optical cycle. Our work shows that, with this specific PG control scheme, it becomes possible to create a highly distinct interference pattern composed of well-separated structures produced by different types of intracycle interferences in the measured photoelectron momentum distributions (PMDs).

Interference lies at the heart of quantum mechanics. In recent years, a versatile scenario of the double-slit interference effect has been identified via strong-field ionization [1]. Therein an atom or a molecule is tunnel ionized in an intense femtosecond laser field and the EWPs created at different times with the same final momentum will interfere with each other, generating rich interference features in the final PMDs. In particular, intracycle interference originated from EWPs emitted within one laser cycle has attracted much attention recently since it could provide deep insight into the attosecond electronic dynamics during the tunneling ionization process. However, it is always buried in a wealth of other more prominent structures, e.g., intercycle interference and PH structures.

In our work, we employ a PG pulse consisting of two counterrotating circularly polarized and carrier-envelope phase (CEP) stabilized few-cycle laser pulses, to demonstrate experimentally subcycle precise control of the intracycle interferences [2, 3]. The key of the scheme is the strong dependence of the attosecond electron wave-packet dynamics on the subcycle shape of the electric field of the PG pulse, which can be well controlled by the time delay and CEP of the combining few-cycle pulses. Our work shows that the PG laser field can effectively suppress the intercycle interference and the forward-rescattering PH structures and create a highly distinct interference pattern that is composed of well-separated structures caused by different types of intracycle interferences in the PMD. Quantum

trajectory Monte Carlo (QTMC) simulations reproduce well the experimental findings and uncover the physical mechanism behind this subcycle control of EWPs with a PG pulse. Our work will boost the PG technique as a powerful and universal tool to steer attosecond electron dynamics with high precision.

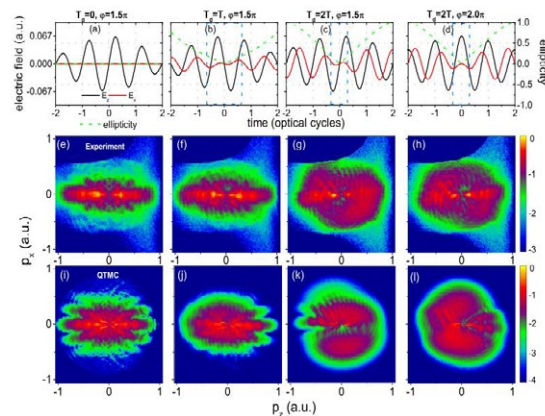


**Figure 1.** (a)–(d) Electric-field components in the  $z$  and  $x$  directions and the ellipticity of the PG pulses for different time delay and CEP. (e)–(h) Measured PMDs of Ar ionized in the PG pulse with the same laser parameters as in (a)–(d), respectively. (i)–(l) Corresponding QTMC-simulated PMDs.

### References

- [1] F Lindner, et al., 2005 *Phys. Rev. Lett.* **95** [040401](#)
- [2] Y L Wang, et al., 2018 *Phys. Rev. A* **98** [043422](#)
- [3] R P Sun, et al., 2022 *Phys. Rev. A* **105** [L021103](#)

\* E-mail: [ylwang@wipm.ac.cn](mailto:ylwang@wipm.ac.cn)

† E-mail: [xjliu@wipm.ac.cn](mailto:xjliu@wipm.ac.cn)

## Twisted attosecond pulse trains driven by amplitude-polarization pulses

E G Neyra<sup>1</sup>, D Biasseti<sup>1</sup>, F Videla<sup>1</sup>, L Rebón<sup>2</sup> and M Ciappina<sup>4\*</sup>

<sup>1</sup>Centro de Investigaciones Ópticas (CICBA-CONICET-UNLP), La Plata, Argentina

<sup>2</sup>Instituto de Física de La Plata, CONICET - UNLP, La Plata, Argentina

<sup>3</sup>Department of Physics, Guangdong Technion - Israel Institute of Technology, 241 Daxue Road, Shantou, Guangdong, 515063, China

**Synopsis** We propose here a novel method to generate a twisted attosecond pulse train (APT). We demonstrate that, by using an IR pulse with amplitude polarization, it is possible to obtain a twisted APT with a well-defined linear polarization. We show how this can be achieved through quantum mechanical simulations and signal processing tools, providing a high degree of control over the polarized-sculpted XUV sources.

Attosecond pulses are keys to capturing and tracking dynamical processes in the atomic world. These have been generated through the high-order harmonics (HHG) process, where an IR photon is upconverted into an XUV one. However, there is still much to be learned about the underlying physics behind the APT generation processes and how to manipulate these ultrashort coherent sources in real time. In fact, the ability to control the XUV coherent radiation is highly challenging, because, in general, there are no simple physical devices designed for that wavelength range, and therefore, the control of the different properties of the coherent XUV radiation generated via HHG should come from the manipulation of the IR driving pulse.

In this work, we introduce a straightforward procedure to generate an APT in which each of the attosecond pulses has a well-defined linear polarization, but different between them. This goal is achieved through the manipulation of the IR driving pulse, whose electric field  $\mathbf{E}(t)$  is *amplitude-polarized* (AP). Experimentally, the AP polarization scheme was presented and synthesized in Ref. [1]. In our contribution, we analyze the interaction between IR-AP pulses and a prototypical atomic target, both in the multi- and few-cycle regimes. The full temporal 3D-representation of the twisted APT can be seen in Fig. 1, where we have also included the laser electric field of the AP pulse. From this figure, the temporal evolution of each attosecond pulse polarization in the train and how it rotates is clearly observed by following the temporal evo-

\*E-mail: [marcelo.ciappina@gtiit.edu.cn](mailto:marcelo.ciappina@gtiit.edu.cn)

lution of the AP pulse.

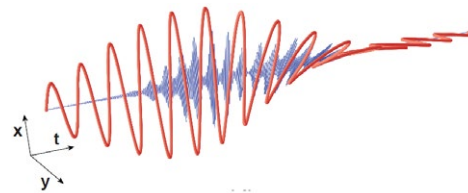


**Figure 1.** A 3D-representation of the twisted APT (blue solid line) and the laser electric field of the AP pulse (red solid line).

The concrete possibility to manipulate the polarization angle between the attosecond pulses in an APT would bring attosecond-based spectroscopy techniques to another, more advanced, level. Beyond photoelectron spectroscopy, this twisted APT can be useful to (i) study or drive highly anisotropic systems where there are preferential directions, such as molecular systems, low-dimensional crystalline structures, etc. and (ii) characterize multidimensional laser fields in the time domain utilizing the well-known streaking technique, amongst others. Our approach presents clear advantages compared to other isolated attosecond pulse generation techniques [2]: the possibility to work with multi-cycle pulses, and the fact that the synthesis of the AP is achieved with a single color field without the need for an involved interferometric setup [3].

### References

- [1] Karras G, *et al.* 2015 *Phys. Rev. Lett.* **114**, 103001.
- [2] Chini M, Zhao K and Chang Z 2014 *Nat. Photon.* **8**, 178.
- [3] Neyra E *et al.* 2023 submitted.

## Tailoring the spectral phase of attosecond pulse trains generated by intense femtosecond two-color fields

T A Olsson, S Burrows, S Jain, J Davis, S Chumley, W Medlin, and G M Laurent\*

Department of Physics, Auburn University, 380 Duncan Drive, Auburn, AL 36849, USA

**Synopsis** The spectral phases of attosecond pulse trains (APTs) generated by intense, two-color, femtosecond fields ( $\omega + 2\omega$ ) via the high harmonic generation (HHG) process are investigated within the Strong Field Approximation (SFA). We show that the spectral phases exhibit high tunability for an intensity ratio between the two colors of the driving field in the range of 0.1 to 5%. By varying both the phase and the intensity ratio between the two colors, we show that the spectral phases can be manipulated in order to produce either one or two attosecond pulses per optical cycle of the driving field.

The development of attosecond light sources based on the high-harmonic generation process has offered new possibilities to probe dynamics in matter down to the natural timescale of electron motion. So far, attosecond measurements have been generally performed through the generation of an electron wavepacket by absorption of the attosecond pulse. The dynamics under scrutiny can then be unravelled from the attributes of the electron wavepacket assuming that the spectral components of the attosecond pulse encoded in the measurement are known.

The spectral characteristics of APTs generated by an one-color driving field have been reported extensively in the literature. In particular, it is well known that the frequency-dependence of the spectral phase (namely the attochirp) limits the achievable level of synchronization of the frequencies making up the pulse [1]. On the contrary, studies on the spectral phases of APTs generated by a multi-color field have been sparse, despite the potential such APTs could have for attosecond experiments [2].

In this work, we show that the spectral phases of APTs generated by intense two-color femtosecond fields ( $\omega + 2\omega$ ) can be tuned by varying both the intensity ratio and the phase between the two components of the driving field. The spectral phases have been computed within the Strong Field Approximation theory, which has proved to be successful at qualitatively reproducing the characteristics of the HHG radia-

tion generated with single- and multi-color fields. As shown in Fig. 1, we found that the spectral phases exhibit high tunability for an intensity ratio between the two colors of the driving field in the range of 0.1 to 5%. In particular, we show that the spectral phases can be manipulated in order to produce either one or two attosecond pulses per optical cycle of the driving field [3].

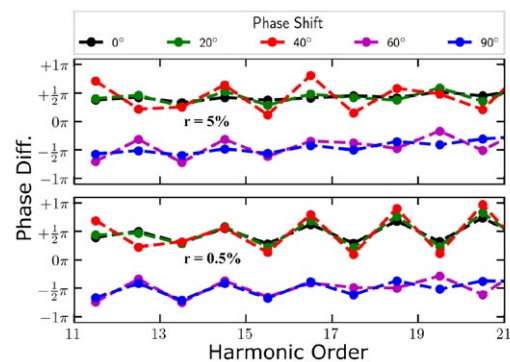


**Figure 1.** Calculated relative phase between consecutive odd and even harmonics for various intensity ratios  $r$  and relative phases  $\phi$  between the  $2\omega$  and  $\omega$  components of the two-color driving field.

### References

- [1] Maitresse Y *et al* 2003 *Science* **302** 1540
- [2] Mitra S *et al* 2020 *Journal of Physics B* **53** 134004
- [3] Unzicker B *et al* 2021 *New Journal of Physics* **23** 013019

\*E-mail: [glaurent@auburn.edu](mailto:glaurent@auburn.edu)



## Study of the effect of higher-order dispersions on photoionisation induced by ultrafast laser pulses

I Márton<sup>1\*</sup> and L Sarkadi<sup>2</sup>

<sup>1</sup>MTA Atomki Lendület Quantum Correlations Research Group, Institute for Nuclear Research, (ATOMKI), Debrecen, H-4001, Hungary

<sup>2</sup>Institute for Nuclear Research, (ATOMKI), Debrecen, H-4001, Hungary

**Synopsis** We studied the effect of higher-order dispersion on ultrafast photoionisation with Classical Trajectory Monte Carlo (CTMC) method. We found that the pulses with negative second- third- or fourth- order dispersion results in higher ionisation yield and electron energies compared to pulses shaped with positive dispersion values. We have also investigated how the Carrier Envelope Phase (CEP) dependence of the ionisation is influenced by dispersion. We found that the left-right asymmetry is more pronounced for pulses shaped with positive Group Delay Dispersion (GDD).

We investigated the effect of higher-order dispersion on ultrafast photoionisation with Classical Trajectory Monte Carlo (CTMC) method for hydrogen and krypton atoms [1]. In our calculations we used linearly polarised ultrashort 7 fs laser pulses,  $6.5 \times 10^{14} \text{W/cm}^2$  intensity, and a central wavelength of 800 nm. Our results show that electrons with the highest kinetic energies are obtained with transform limited (TL) pulses. The shaping of the pulses with negative second- third- or fourth- order dispersion results in higher ionisation yield and electron energies compared to pulses shaped with positive dispersion values. This phenomenon can be quantitatively characterised by the asymmetry parameter defined as

$$A(D) = \frac{N(D) - N(-D)}{N(D) + N(-D)} \quad (1)$$

where  $N(D)$  is the number of photoelectrons at a given value of dispersion. We have also investigated how the Carrier Envelope Phase (CEP) dependence of the ionisation is influenced by dispersion. We calculated the left-right asymmetry defined as

$$A(E, \varphi_{CEP}) = \frac{N^+(E, \varphi_{CEP}) - N^-(E, \varphi_{CEP})}{N^+(E, \varphi_{CEP}) + N^-(E, \varphi_{CEP})} \quad (2)$$

where  $N^+$  and  $N^-$  mean the number of electrons

having positive and negative momentum along the polarization axis respectively. We carried out the calculations for sodium atoms employing pulses of 4.5 fs, 800 nm central wavelength, and  $4 \times 10^{12} \text{W/cm}^2$  intensity. We found that the left-right asymmetry is more pronounced for pulses shaped with positive Group Delay Dispersion (GDD).

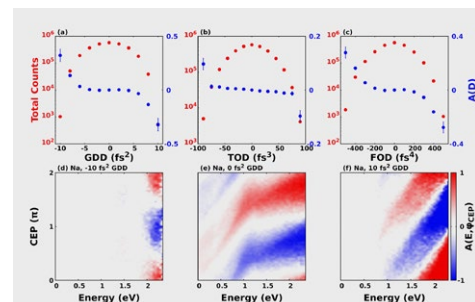


**Figure 1.** Number of electron counts and asymmetry parameters for hydrogen calculated with different GDD (a), TOD (b) and FOD (c). Calculated maps of the asymmetry defined by Eq. (2) for Na at  $4 \times 10^{12} \text{W/cm}^2$  intensity with different values of GDD (d)-(f).

### References

- [1] Márton I and Sarkadi L 2022 *Scientific Reports* **12** 13841

\*E-mail: [marton.istvan@atomki.hu](mailto:marton.istvan@atomki.hu)



## Carrier-phase envelope control of nondipole effects in ionization

J Derlikiewicz\*, M C Suster†, J Z Kaminski and K Krajewska

Institute of Theoretical Physics, Faculty of Physics, University of Warsaw, Pasteura 5, 02-093 Warsaw, Poland

**Synopsis** We show that for high-frequency attosecond laser pulses, the direction of radiation pressure exerted on electrons bound in atoms does not have to coincide with the direction of pulse propagation and can be significantly changed by the carrier-envelope phase. This crucially affects the nondipole signatures observed in photoelectron momentum distributions.

Ultrashort laser pulses can be used to study and to effectively manipulate processes involving atomic or molecular targets. Strategies for controlling photoprocesses involve various laser field parameters which can be precisely adjusted; one of them being the carrier-envelope phase (CEP). In this context, the CEP control of nondipole effects observed in photoionization becomes of particular interest [1, 2, 3, 4].

In our theoretical investigations, we focus on the influence of CEP of a driving attosecond pulse on nondipole features revealed in ionization. In particular, we demonstrate that such process can be spatially controlled. More precisely, the nondipole interference structures in the momentum distributions of ionized electrons can be rotated by adjusting the CEP of a driving pulse. The maximum rotation that we were able to achieve was close to  $\pi/2$ , oriented ei-

ther clockwise or counterclockwise. Our results were obtained using a new theoretical framework for simulating strong-field laser-matter interactions beyond the dipole approximation. While the method itself is applicable for both low- and high-frequency fields, the aforementioned nondipole effects are predicted theoretically for high-frequency pulses [4]. Thus, it should be possible to verify them experimentally using pulses generated, for instance, in the European XFEL facility.

### References

- [1] Chirilă C C *et al.* 2002 *Phys. Rev. A* **66**, 063411
- [2] Førre M *et al.* 2006 *Phys. Rev. Lett.* **97**, 043601
- [3] Daněk J *et al.* 2018 *J. Phys. B: At. Mol. Opt. Phys.* **51**, 114001
- [4] Suster M C *et al.* 2022 [arXiv:2211.15126](https://arxiv.org/abs/2211.15126) (submitted to *Phys. Rev. A*)

---

\*E-mail: [Julia.Derlikiewicz@fuw.edu.pl](mailto:Julia.Derlikiewicz@fuw.edu.pl)

†E-mail: [Mihai.Suster@fuw.edu.pl](mailto:Mihai.Suster@fuw.edu.pl)

## Spin-polarized electron vortices generated in single-photon ionization of atoms

Yibo Hu, Qiangfei Ma, and Kunlong Liu\*

School of Physics, Huazhong University of Science and Technology, Wuhan 430074, China

**Synopsis** We theoretically investigate a scheme to produce spin-polarized electrons based on the vortex interference of the photoelectrons in single-photon ionization of rare gas atom krypton. The results show that, the vortex-shaped photoelectron momentum distributions for the ionization channels of  $J=1/2$  and  $J=3/2$ , as well as those associated with the initial  $p_+$  and  $p_-$  orbitals, can be well dislocated in the momentum space, leading to the spin polarization exceeding 50% at certain momenta.

Early in 1960s, Fano theoretically proposed that in single-photon ionization of Cs atom in a circularly polarized light, spin polarization of the photoelectrons can be achieved in the vicinity of the Cooper minima [1]. A physically different way to produce spin-polarized photoelectrons is the nonadiabatic tunnel ionization of atoms, as proposed by Barth and Smirnova in 2013 [2]. In 2018, two research groups independently demonstrated that the above-threshold ionization (ATI) spectra for the ionization channels to the ionic states  $J=1/2$  and  $J=3/2$  of xenon can be well separated in ultraviolet ( $\sim 400$  nm) laser pulses, resulting in the maximum of the spin polarization exceeding 50% [3,4].

As the ATI peaks are essentially the interference structure originating from the photoelectron ejected at each optical cycle, it would be appealing to seek for a more flexible way to steer the photoelectron interference in momentum space and achieve the controllable spin polarization. In this work [5], we turn to the scheme based on the electron vortices, which appear to be a vortex-shaped interference pattern in the photoelectron momentum distribution (PMD) for the photoionization by two time-delayed counter-rotating circularly polarized laser pulses.

We show that the way to produce electron vortices in single-photon ionization is also a powerful approach for manipulating spin-polarized photoelectrons. The underlying mechanism of our scheme relies on the phase difference between the wave functions of the  $p_{\pm}$  electrons. We demonstrate that, as the phase information is encoded in the vortex-shaped momentum distribution, the photoelectrons from the  $p_{\pm}$  orbitals can be separated in the momentum space by wave packet interference. More importantly, the spectra for the ionization

channels to the ionic states  $J=1/2$  and  $J=3/2$  are also well separated in the electron vortices. It ultimately leads to the spin polarization exceeding 50% (see Fig. 1). Furthermore, our numerical results show that by adjusting the time delay, the wavelength, or the relative phase of two time-delayed laser pulses, the kinetic energy as well as the ejection angle of the spin-polarized electrons can be flexibly controlled.

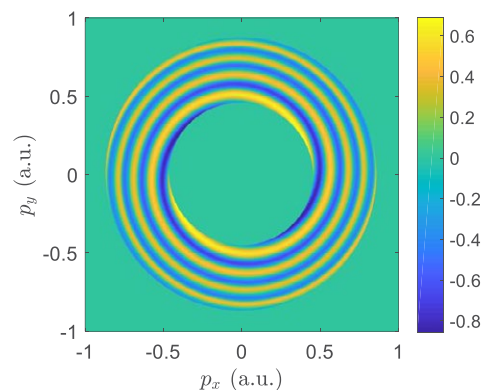


Figure 1. The momentum-resolved spin polarization of the photoelectrons generated by two time-delayed counter-rotating circularly polarized laser pulses.

### References

- [1] U. Fano, Phys. Rev. **178**, 131 (1969).
- [2] I. Barth and O. Smirnova, Phys. Rev. A **88**, 013401 (2013)
- [3] M.-M. Liu, et al, Phys. Rev. Lett. **120**, 043201 (2018).
- [4] D. Trabert, et al, Phys. Rev. Lett. **120**, 043202 (2018).
- [5] Y. Hu, et al, Phys. Rev. A, *accepted* (Mar 2023).

\*E-mail: [liukunlong@hust.edu.cn](mailto:liukunlong@hust.edu.cn)

## Measuring the photoelectron angular distribution after nonlinear interaction of two photons with two active electrons in helium

M Straub<sup>1</sup>, T Ding<sup>1</sup>, M Rebholz<sup>1</sup>, G D Borisova<sup>1</sup>, A Magunia<sup>1</sup>, H Lindenblatt<sup>1</sup>, S Meister<sup>1</sup>, F Trost<sup>1</sup>, Y Wang<sup>2</sup>, S Palutke<sup>3</sup>, M Braune<sup>3</sup>, S Düsterer<sup>3</sup>, R Treusch<sup>3</sup>, C H Greene<sup>2</sup>, R Moshhammer<sup>1</sup>, T Pfeifer<sup>1</sup> and C Ott<sup>1\*</sup>

<sup>1</sup>Max-Planck-Institut für Kernphysik, Heidelberg, 69117, Germany

<sup>2</sup>Department of Physics and Astronomy, Purdue University, West Lafayette, Indiana 47907, USA

<sup>3</sup>Deutsches Elektronen Synchrotron DESY, Hamburg, 22607, Germany

**Synopsis** We report about a fundamental process of nonlinear light-matter interaction in AMO physics: the interaction of two photons with two electrons through the angular-differential measurement of two-photon single ionization of helium after the excitation of a doubly excited state. This is enabled by combining the detection of photoionization events in the reaction microscope at Beamline FL26 at the FLASH Free-Electron-Laser (FEL) with the shot-by-shot measurement of the FEL spectral intensity distribution.

We introduce a new experimental methodology for the fully differential measurement of ionizing interactions of few photons with few electrons, and including the specificity to narrow-band resonantly excited states. The experiment is performed in the reaction microscope at Beamline FL26 at FLASH, which enables the coincident detection of all charged fragments after XUV (multi-)photon-ionization at high repetition rates. We have augmented this apparatus with a home-built high-resolution XUV photon spectrometer to measure the FEL spectral intensity distribution on a shot-by-shot basis. In the experiment (Fig. 1a) we employ linearly polarized FEL pulses at  $\sim 30$  eV to resonantly excite the  $2p^2\ ^1D^e$  doubly excited state at 59.9 eV in helium after the nonlinear absorption of two photons. The spectral resolution is improved to below 0.1 eV by selecting and sorting individual FEL pulses with respect to the peak position of their stochastic SASE spectra (Fig. 1b), thus performing a virtual narrow-band photon-energy sweep. As a result, (Figs. 1c&d) the resonant two-photon transition could be isolated and the photoelectron angular distribution was measured [1] and compared to theory [2]. A close comparison with theory further reveals the weak interference contribution of the FEL 2<sup>nd</sup> harmonic. This opens up new possibilities for  $\omega$ - $2\omega$  coherent control with SASE FEL pulses, and, with this new methodology in general, for multi-modal coincidence spectroscopy of few-body quantum dynamics involving electrons, ions and photons.

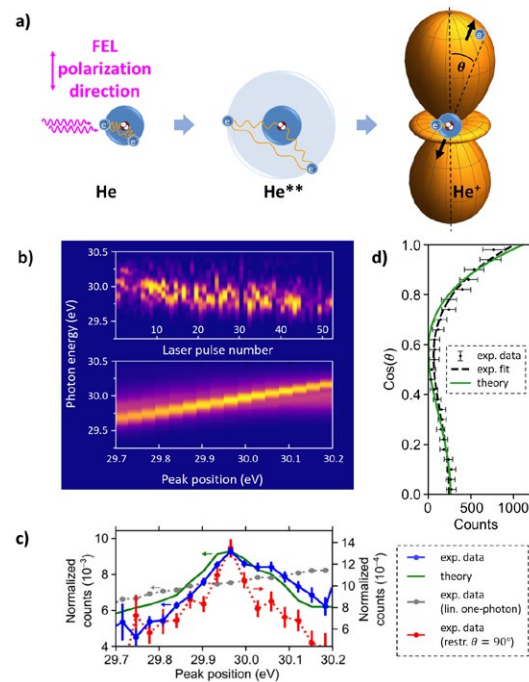


**Figure 1.** a) Schematic of two-photon single ionization of helium via a doubly excited state. The shot-by-shot detection and sorting of FEL spectra (b) isolates the resonant  $^1D^e$  two-electron state (c) for the angle-resolved measurement (d) of photoionization events.

### References

- [1] Straub M, Ding T, Rebholz M et al. 2022 *Phys. Rev. Lett.* **129** 183204
- [2] Wang Y and Greene C H 2021 *Phys. Rev. A* **103** 033103

\* E-mail: [christian.ott@mpi-hd.mpg.de](mailto:christian.ott@mpi-hd.mpg.de)

## Multi-sideband interference structures observed via high-order photon-induced continuum-continuum transitions in helium

D Bharti<sup>1\*</sup>, H Srinivas<sup>1</sup>, F Shobeiry<sup>1</sup>, R Moshhammer<sup>1</sup>, T Pfeifer<sup>1</sup>, K R Hamilton<sup>2</sup>,  
A T Bondy<sup>3,4</sup>, S Saha<sup>4</sup>, K Bartschat<sup>4†</sup> and A Harth<sup>5</sup>

<sup>1</sup>Max-Planck-Institute for Nuclear Physics, D-69117 Heidelberg, Germany

<sup>2</sup>Department of Physics, University of Colorado Denver, Denver, Colorado 80204, USA

<sup>3</sup>Department of Physics, University of Windsor, Windsor, Ontario N9B 3P4, Canada

<sup>4</sup>Department of Physics and Astronomy, Drake University, Des Moines, Iowa 50311, USA

<sup>5</sup>Department of Optics and Mechatronics, Hochschule Aalen, D-73430 Aalen, Germany

**Synopsis** We report a joint experimental and theoretical study of a three-sideband (3-SB) modification of the RABBIT scheme, with special emphasis on the angle-dependence of the RABBIT phase in the three sidebands.

Continuing our recent work on argon [1], we report a joint experimental and theoretical study of a three-sideband (3-SB) modification of the “reconstruction of the attosecond beating by interference of two-photon transitions” (RABBIT) setup [2–4]. The 3-SB arrangement makes it possible to investigate phases resulting from interference between transitions of different orders in the continuum, independent of a chirp in the harmonics, by comparing the RABBIT phases extracted from specific SB groups formed by two adjacent harmonics [5, 6].

While experimentally more challenging than argon, using a helium target has the advantage of a well-defined orbital angular momentum after the  $1s \rightarrow \epsilon p$  step induced by the high-order harmonic radiation. Furthermore, predictions from the single-active-electron (SAE) approximation are expected to be of similar quality as those from much more sophisticated approaches such as the multi-electron R-matrix with time dependence method (RMT) [7].

Figure 1 shows angular-dependent RABBIT phases extracted for the first 3-SB group in helium. The sidebands were produced by combining a 50 fs (FWHM), 1030 nm IR pulse with peak intensity of  $\approx 3 \times 10^{11}$  W/cm<sup>2</sup> and high-order harmonics generated from the frequency-doubled 1030 nm fundamental beam in another arm.

Comparing the experimental data with SAE predictions shows qualitative agreement, but significant discrepancies remain in the details. Of particular interest is the lowest sideband  $S_l$ , which exhibits a very different behavior from  $S_c$

and  $S_h$ . We are currently investigating potential reasons for the similarities and differences between experiment and theory, as well as the angular dependence of the individual sidebands. Our findings, including the intensity dependence of the results, will be presented at the conference.

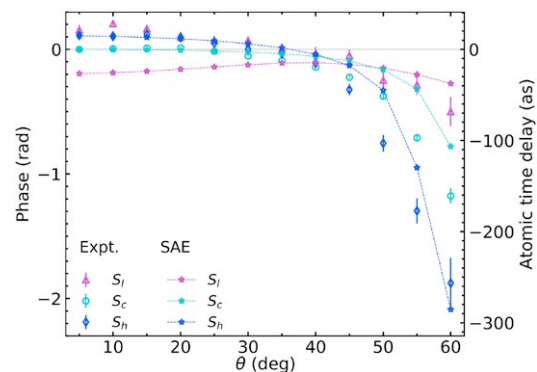


**Figure 1.** Angular-dependent 3-SB RABBIT phases in helium. The experimental data for the low ( $S_l$ ), center ( $S_c$ ), and high ( $S_h$ ) sidebands are compared with SAE predictions.

Work supported by the DFG under HA 8399/2-1 and IMPRS-QD, NSERC, and the NSF under OAC-1834740, PHY-2110023, and ACCESS-090031.

### References

- [1] Bharti D *et al* 2023 *Phys. Rev. A* **107** 022801
- [2] Paul P *et al* 2001 *Science* **292** 1689
- [3] Muller H *et al* 2002 *Appl. Phys. B* **74** S17
- [4] Dahlström J *et al* 2013 *Chem. Phys.* **414** 53
- [5] Harth A *et al* 2019 *Phys. Rev. A* **99** 023410
- [6] Bharti D *et al* 2021 *Phys. Rev. A* **103** 022834
- [7] Brown A C *et al* 2020 *Comp. Phys. Comm.* **250** 107062

\*E-mail: [divya.bharti@mpi-hd.mpg.de](mailto:divya.bharti@mpi-hd.mpg.de)

†E-mail: [klaus.bartschat@drake.edu](mailto:klaus.bartschat@drake.edu)

## Extended RPAE method for cross sections and delays

A Ljungdahl<sup>1</sup>, J Vinbladh<sup>1</sup>, CLM Petersson<sup>1</sup>, S Saha<sup>1</sup>, J Sörngård<sup>1</sup>, and E Lindroth<sup>1\*</sup>

<sup>1</sup>Department of Physics, Stockholm University, AlbaNova University Center, SE-106 91 Stockholm, Sweden

**Synopsis** We present an extended RPAE-type method for photoionization cross sections and delays. It is based on matrix equations, and includes classes of correlations effects beyond traditional RPAE.

Attosecond techniques have provided new tools to study photoionization processes. The phase information, and the insight into the temporal dynamics it gives, complements cross-section measurements nicely. With increasing capabilities to combine high temporal *and* spectral resolution [1, 2, 3], a range of many-body effects such as resonances and shake-up processes can be revisited to gain a deeper understanding.

It is through inference between two-(or several) photon paths that phase information can be extracted. The random phase approximation with exchange (RPAE), originally developed to describe photoionization, can be extended to describe also this situation [4, 5], where the photoelectron absorbs or emits a photon when it is already in the continuum. The treatment of such continuum-continuum transitions calls for special care. Still it is possible to perform full two-photon RPAE[6].

RPAE is known to produce good overall-cross-sections, while still being rather cheap. But, it lacks two-hole-two-particle correlation, preventing inclusion of shake-up satellites, and limiting the accuracy of ionization thresholds and resonances. For resonances not only positions, but also widths and cross section profiles can be affected. Traditionally the RPAE-equations are solved iteratively, and the presence of resonances then often leads to convergence problems.

To improve the description of resonances, and to add two-hole two-particle correlation, we have developed a matrix formulation of RPAE, both non-relativistically and relativistically, which can be solved by diagonalization, or through a linear-solve approach, with no convergence problems close to thresholds or in the vicinity of resonances. We have further added selected two-hole-two-particle contributions which gives significantly improved results for resonances. The matrix formulation can also be used to include

\*E-mail: [Eva.Lindroth@fysik.su.se](mailto:Eva.Lindroth@fysik.su.se)

the interaction with additional photons, and thereby improve the treatment of the new sets of resonances which then become reachable.

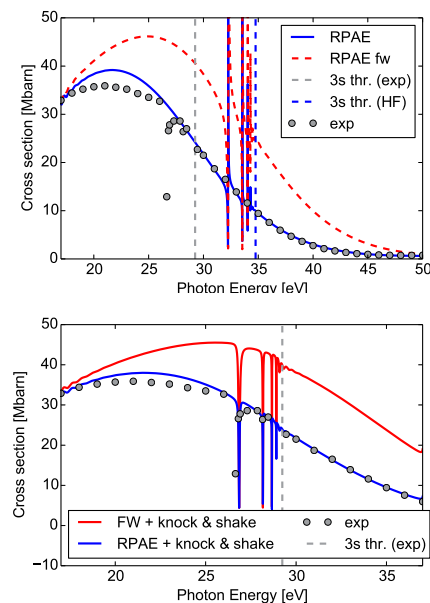


**Figure 1.** Photoionization from argon in the vicinity of the 3s-threshold. Upper panel: RPAE typically performs better than just the forward class of effects (also called CI-singles), but fails here with threshold positions and resonance properties. Lower panel: The addition of selected two-hole two-particle contributions improves this significantly.

### References

- [1] Isinger M, *et al* (2017) *Science*, **358** 893
- [2] Alexandridi C *et al* (2021) *Phys. Rev. Research*, **3** L012012
- [3] Zhong S *et al* (2020) *Nat. Comm.*, **11** 5042
- [4] Dahlström J M and Lindroth E (2014) *J. Phys. B*, **47**, 124012
- [5] Vinbladh J, Dahlström J M, and Lindroth E (2022) *Atoms* **10** 80
- [6] Vinbladh J, Dahlström J M, and Lindroth E (2019) *Phys. Rev. A* **100** 043424



## Disentangling interferences in the photoelectron momentum distribution from strong-field ionization

T Wang<sup>1\*</sup>, Z Dube<sup>1</sup>, Y Mi<sup>1</sup>, G Vampa<sup>1</sup>, D M Villeneuve<sup>1</sup>, P B Corkum<sup>1</sup>, Xiaojun Liu<sup>2</sup>, and A. Staudte<sup>1†</sup>

<sup>1</sup>Joint Attosecond Science Laboratory, NRC & University of Ottawa, 100 Sussex Drive, Ottawa, Canada

<sup>2</sup>State Key Laboratory of Magnetic Resonance and Atomic and Molecular Physics, Wuhan Institute of Physics and Mathematics, Innovation Academy for Precision Measurement Science and Technology, Chinese Academy of Sciences, Wuhan 430071, China

**Synopsis** Using the semiclassical two-step model for strong-field ionization, we theoretically investigate sub-cycle interference structures in the photoelectron momentum distribution. Specifically, we focus on the low-momentum fanlike interference structure and demonstrate that this interference structure is particularly sensitive to the ion potential and thereby offers another path to probe ultrafast electronic structure dynamics.

In multiphoton ionization of atoms and molecules by intense multicycle laser pulses the photoelectron wave packets created at each crest of the optical wave interfere with each other, giving rise to a wealth of structures in the observable photoelectron momentum distributions [1–6]. Whereas some of these interferences arise directly from the symmetry of the optical wave driving the electron current, others inherently rely on the scattering in the parent ion's potential. These scattering interferences have a particular potential for revealing electronic structure and dynamics.

We developed a semiclassical two-step model to resolve the subcycle interference of photoelectron wave packets by using a quarter-cycle interference scheme [7]. Fig.1(a, b) shows the photoelectron momentum distribution from a complete laser pulse, while Fig.1(c-h) show the interference structures from different quarter-cycle combinations. Particularly, we focus on the fanlike interference structure in the low-momentum region of the photoelectron distribution which is shown in Fig.1(b). The disentanglement of this interference structure is accomplished by considering its temporal structure and the Coulomb potential effect from the ion separately. We show that this structure originates in the interference between scattered and unscattered electron wave packets from different direct quarter cycles within a single optical cycle. Furthermore, our analysis reveals that the parent ion's influence on the scattered photoelectron is greatest only a short time after tunneling ionization and well before the moment of closest approach. We believe that this specific

structure can resolve ion dynamics on the sub-optical-cycle time scale.

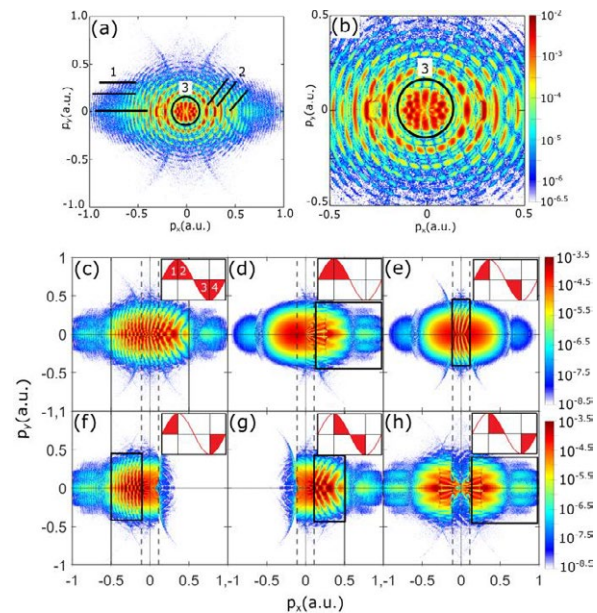


**Figure 1.** Photoelectron momentum distributions. (a): ionization within a complete pulse. (b): Magnification of (a). (c-h): ionization within different quarter-cycle combinations.

### References

- [1] R. Gopal et al 2009 *Phys.Rev. Lett.* **103**, 053001
- [2] D.G. Arbol et al 2010 *Phys.Rev. A* **81**, 021403(R)
- [3] X.-B. Bian et al 2011 *Phys.Rev. A* **84**, 043420
- [4] A. S. Maxwell et al 2017 *Phys.Rev. A* **96**, 023420
- [5] N. Shilovski et al 2018 *Phys.Rev. A* **97**, 013411
- [6] Y. Huisman et al 2011 *Science* **331**, 61
- [7] T. Wang et al 2022, *Phys.Rev. A* **106**, 013106

\* E-mail: [twang110@uottawa.ca](mailto:twang110@uottawa.ca), † E-mail: [andre.staudte@nrc.ca](mailto:andre.staudte@nrc.ca)



## Energy variation of double $K$ -shell photoionization of Ne

T W Gorczyca<sup>1\*</sup>, S T Manson<sup>2</sup>, S H Southworth<sup>3</sup>, S Li<sup>3</sup>, D Kouliantanos<sup>3</sup>, G Doumy<sup>3</sup>, L Young<sup>3,4</sup>, D A Walko<sup>5</sup>, R Püttner<sup>6</sup>, D Céolin<sup>7</sup>, R Guillemin<sup>7,8</sup>, I Ismail<sup>7,8</sup>, O Travnikova<sup>7,8</sup>, M N Piancastelli<sup>7,8</sup>, M Simon<sup>7,8</sup>

<sup>1</sup>Department of Physics, Western Michigan University, Kalamazoo, Michigan 49008, USA

<sup>2</sup>Department of Physics and Astronomy, Georgia State University, Atlanta, Georgia 30303, USA

<sup>3</sup>Chemical Sciences and Engineering Division, Argonne National Laboratory, Lemont, Illinois 60439, USA

<sup>4</sup>The James Franck Institute and Department of Physics, The University of Chicago, Chicago, Illinois 60637, USA

<sup>5</sup>Advanced Photon Source, Argonne National Laboratory, Lemont, Illinois 60439, USA

<sup>6</sup>Fachbereich Physik, Freie Universität Berlin, Arnimallee 14, D-14195 Berlin, Germany

<sup>7</sup>Synchrotron SOLEIL, l'Orme des Merisiers, Saint-Aubin, BP 48, 91192 Gif-sur-Yvette, France

<sup>8</sup>Sorbonne Université, CNRS, Laboratoire de Chimie Physique-Matière et Rayonnement, LCPMR, F-75005 Paris, France

**Synopsis** The ratio of double to single  $K$ -shell ionization of Ne is studied theoretically and experimentally over a broad x-ray energy range. Fairly good agreement is found and a scaling model of the ratio with  $Z$  is demonstrated.

We report on an experimental and theoretical study of double  $K$ -shell photoionization of Ne over the 2.3-8.5 keV x-ray energy range. The ratio of double-to-single  $K$ -shell photoionization cross sections was determined experimentally by measuring the relative rates of the  $KK - KL_{2,3}L_{2,3}$  ( $^2D$ ) Auger hypersatellite and the  $K - L_{2,3}L_{2,3}$  ( $^1D$ ) diagram Auger transitions [1]. By scaling the hypersatellite/diagram Auger-electron ratios to  $KK/K$  cross-section ratios, comparison was made with theoretical cross-section ratios of He-like  $\text{Ne}^{8+}$  determined by the R-matrix with pseudostates (RMPS) method [2, 3]. The experimental Ne and theoretical  $\text{Ne}^{8+}$  cross section ratios show similar variations with energy, but the experimental ratios systematically exceed the calculated ratios and also show a lower threshold energy for the double  $K$ -shell photoionization onset compared to the computed  $\text{Ne}^{8+}$  threshold. The discrepancy is attributed to effects of  $L$ -shell electrons not included in the He-like  $\text{Ne}^{8+}$  calculations. Quantified scaling with nuclear charge  $Z$  along the He-like isoelectronic sequence indicates that the measured 10-electron  $Z = 10$  double  $K$ -shell photoionization cross section behaves like the computed He-like  $Z = 8.9$  cross section, suggesting an effective nuclear screening parameter of  $s_L = 1.1$  by the additional eight outer  $L$ -shell electrons. The work at ANL and GSU was supported by the US De-

\*E-mail: [gorczyca@wmich.edu](mailto:gorczyca@wmich.edu)

partment of Energy, Office of Science, Basic Energy Sciences, Chemical Sciences, Geosciences, and Biosciences Division. The work at WMU was supported in part by NASA.

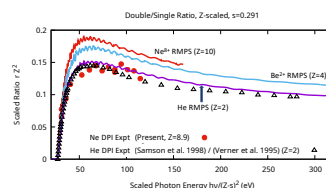


**Figure 1.** Scaled double-to-single  $K$ -shell photoionization cross-section ratios for He and He-like  $\text{Be}^{2+}$  and  $\text{Ne}^{8+}$ , compared to earlier He experiments ( $Z = 2$ , double cross section divided by single  $1s$  Hartree-Slater results) and present Ne experimental ratios ( $Z = 8.9$ ). The effective  $1s - 1s$  mutual  $K$ -shell screening parameter of  $s = 0.291$  was used rather than the variational calculated result of  $s = 0.3125$

### References

- [1] Southworth S H, Li S, Kouliantanos D, Doumy G, Young L, Walko D A, Püttner R, Céolin D, Guillemin R, Ismail I, Travnikova O, Piancastelli M N, Simon M, Manson S T and Gorczyca T W 2023 *Phys. Rev. A* **107** 023110.
- [2] Gorczyca T W and Badnell N R 1997 *J. Phys. B* **30** 3897.
- [3] Burke P G 2011 *R-matrix Theory of Atomic Collisions* (Springer, New York, 2011).

## *R*-matrix with time dependence theory for double photoionization of general atoms

G S J Armstrong<sup>1</sup>, M Plummer<sup>2\*</sup>, A C Brown<sup>1†</sup>, and H W van der Hart<sup>1‡</sup>

<sup>1</sup>Centre for Light-Matter Interaction, Queen's University Belfast, Belfast BT7 1NN, Northern Ireland

<sup>2</sup>Scientific Computing Department, STFC Daresbury Laboratory, Sci-tech Daresbury, Cheshire WA4 4AD, UK

**Synopsis** We present an extension of the *R*-matrix with time dependence method to treat photoionization of up to two electron in general atoms.

The *R*-matrix with time dependence (RMT) approach solves the time-dependent Schrödinger equation for multielectron atoms and molecules interacting with laser pulses. The associated suite of codes now describe the atomic and molecular response to arbitrarily-polarized laser pulses, as well as semi-relativistic atomic dynamics [1, 2].

This work presents the latest developments in the *R*-matrix method, namely the extension of the codes to treat double ionization processes. Building on previous investigations of one- and two-photon double ionization of helium [3, 4], we extend the method to treat general atoms.

The method incorporates the traditional *R*-matrix partitioning of configuration space into a multielectron inner region, where all electrons are considered bound, and an outer region, where one electron is considered detached from the parent ion. To treat double ionization, we add a two-electron outer region, into which two electrons may escape. In this region, a set of coupled two-dimensional radial equations must be solved. These equations describe the interactions between the two outer electrons and the laser field, as well as their Coulomb repulsion. To treat general atomic systems, the method also describes the interaction of the residual dication with the laser field.

The time-dependent Schrödinger equation for the two outer electrons is solved using a two-dimensional finite-difference radial grid. A Taylor series time propagation scheme is used to propagate the wavefunction in all regions.

As an initial proof of principle investigation, we have performed calculations for single-photon

double ionization of helium. Figure 1 shows the ratio of double to single ionization yields calculated using RMT compared to those of an earlier *R*-matrix approach [5]. The RMT results are in reasonable agreement with the literature values.

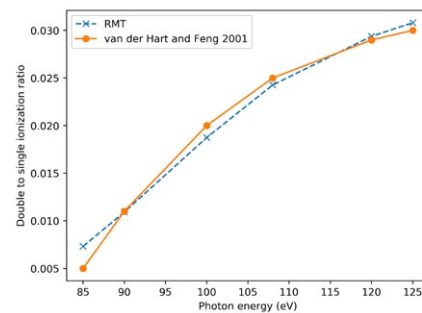


**Figure 1.** Photon-energy dependent double to single ionization ratios for He calculated using RMT compared to those obtained in previous B-spline *R*-matrix calculations [5].

Future code development will enable the calculation of a variety of differential observables, as well as the interfacing of RMT with *R*-matrix inner codes for double ionization of general atoms, with a view to investigating double ionization of noble gas atoms.

### References

- [1] Moore L R et al. 2011 *J. Mod. Opt.* **58** 1132
- [2] Brown A C et al. 2020 *Computer Physics Communications* **250** 107062
- [3] van der Hart H W 2014 *Phys. Rev. A* **89** 053407
- [4] Wragg J, Parker J S and van der Hart H W 2015 *Phys. Rev. A* **92** 022504
- [5] van der Hart H W and Feng L 2001 *J. Phys. B: At. Mol. Opt. Phys.* **34** L601

\*E-mail: [martin.plummer@stfc.ac.uk](mailto:martin.plummer@stfc.ac.uk)

†E-mail: [andrew.brown@qub.ac.uk](mailto:andrew.brown@qub.ac.uk)

‡E-mail: [h.vanderhart@qub.ac.uk](mailto:h.vanderhart@qub.ac.uk)

## Angular Distributions of Attosecond Time Delay in the Photoionization of $ns$ Subshells of Atomic Systems: Relativistic and Nondipole Effects

R. Hosseini<sup>1\*</sup>, P C Deshmukh<sup>2,3#</sup>, S. T. Manson<sup>1§</sup>

<sup>1</sup>Department of Physics and Astronomy, Georgia State University, Atlanta, GA 30030, USA

<sup>2</sup>Department of Physics, Dayanada Sagar University, Bengaluru 560114, India

<sup>3</sup>Department of Physics and CAMOST, Indian Institute of Technology Tirupati, Tirupati 517506, India

**Synopsis** Relativistic and nondipole effects are shown to introduce significant angular dependence into the photoionization time delay of atomic  $ns$  subshells, particularly around Cooper minima. Theoretical results are presented for the outer  $ns$  subshells of the noble gases with calculations performed for dipole and quadrupole channels using the relativistic-random-phase approximation.

The dynamics of atomic electrons on their natural time scale can be probed by Eisenberg-Wigner-Smith (EWS) time delay studies [1] in photoionization [2]. The time delay for a given photoionizing transition generally has an angular dependence [3,4]. However, for atomic  $ns$  states, the time delay is isotropic at the level of nonrelativistic calculations which constitute most of the extant theoretical work [2].

In the nonrelativistic dipole approximation, the time delay for atomic  $ns$ -states does not depend upon angle; inclusion of relativistic effects of spin-flip transitions and nondipole (quadrupole) effects renders the time-delay angle-dependent. Since the amplitude for the dominant dipole photoionization channel (without spin-flip) vanishes at certain angles as a result of angular momentum geometry, quadrupole and spin-flip transitions dominate; specifically, where the dipole amplitude vanishes, the time delay is a combination of spin-flip dipole and quadrupole photoionization time delay, and the attosecond dynamics of these channels can be investigated. Relativistic expressions have been derived showing where quadrupole and/or spin-flip channels determine the time delay. Relativistic random phase approximation (RRPA) [5] calculations for the angular dependence of time delay of  $ns$ -subshells of noble gas atoms for the angular distribution of time delay including both dipole and quadrupole channels have been studied. Of particular interest is the situation in the vicinity of Cooper minima [6] where the no-spin-flip dipole amplitude goes through a minimum as seen in Fig. 1 for Ar 3s photoionization at 38 eV near the Cooper minimum. The

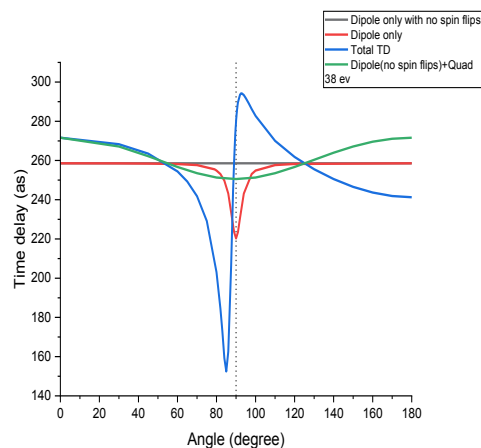


**Figure 1.** Ar 3s time delay near the cooper minimum at a photoelectron energy of 38 eV at various levels of approximation as indicated.

The work of STM was supported by the US Department of Energy, Office of Science, Basic Energy Sciences under Award Number DE-FG02-03ER15428.

### References

- [1] Wigner E P 1955 *Phys. Rev.* **98** 145
- [2] Pazourek R, Nagwele S and Burgdorfer J 2015 *Rev. Mod. Phys.* **87** 765
- [3] Wätzel J et al, 2015 *J. Phys. B* **48** 025602
- [4] Mandal A et al 2017 *Phys. Rev. A* **96** 053407
- [5] Johnson W R and Lin C D 1979 *Phys. Rev. A* **20** 964
- [6] Cooper J W 1962 *Phys. Rev.* **128** 681

\* E-mail: [rkhademhosseini@student.gsu.edu](mailto:rkhademhosseini@student.gsu.edu)

# E-mail: [pcd@iittp.ac.in](mailto:pcd@iittp.ac.in)

§ E-mail: [smanson@gsu.edu](mailto:smanson@gsu.edu)

## Singlet/triplet branching ratios in core-valence double photoionization of neon

T Odagiri<sup>1\*</sup>, Y Sugawara<sup>1</sup>, T Kaneyasu<sup>2</sup>, J Adachi<sup>3</sup>,  
H Tanaka<sup>2</sup>, I H Suzuki<sup>1,3</sup>, S Suzuki<sup>1</sup> and Y Hikosaka<sup>4</sup>

<sup>1</sup>Dept. of Materials and Life Sciences, Sophia University, Tokyo, 102-8554, Japan

<sup>2</sup>SAGA-LS, Tosu, 841-0005, Japan

<sup>3</sup>Photon Factory, Institute of Materials Structure Science, KEK, Tsukuba, 305-0801, Japan

<sup>4</sup>Institute of Liberal Arts and Sciences, Toyama University, Toyama, 930-0194, Japan

**Synopsis** Dynamics of core-valence double photoionization of Ne are studied with their final doubly-charged states being resolved by a multi-electron coincidence technique. Singlet/triplet branching ratios change with incident photon energy, suggesting spin dependence of the knock-out mechanism.

Double ionization of atoms due to absorption of a single photon is a process in which electron correlation plays significant roles. While two mechanisms, shake-off (SO) and knock-out (KO), are known for the double photoionization (DPI) of atoms [1], dynamics of them has not yet been fully understood. In this study, we investigate distribution of the final states,  $^1,^3S$  and  $^1,^3P$ , of  $Ne^{2+}$  in the  $1s^{-1}2s^{-1}$  and  $1s^{-1}2p^{-1}$  core-valence DPI of Ne by using the multi-electron coincidence method for the purpose of revealing the DPI dynamics. The ratios of the singlet/triplet states and probabilities of the DPI processes to form each final state have been obtained.

The experiments were carried out at the undulator beamline BL-2B of Photon Factory, KEK. The synchrotron ring was operated with the hybrid-fill mode whose bunch structure has a train of low-current bunches in one half of the ring and an isolated high-current bunch at the middle of another half. The pulse selector #3 [2] was used to obtain light pulse with a repetition rate of 229 kHz. The electrons emitted by absorption of the soft X-ray were collected by an inhomogeneous magnetic field generated by a permanent magnet and a solenoid coil. They were energy analyzed by a 2.5-m long time-of-flight tube and detected in coincidence [3]. The measurements were done for the photon energy range of about 200 eV above the threshold of the DPI processes in Ne.

Figure 1 shows the ratios of the cross sections to form the  $^1,^3S$  and  $^1,^3P$  states of  $Ne^{2+}$  in the DPI as a function of the incident photon energy. The vertical bars represent the thresh-

olds for the DPIs to different final states. Both ratios in figure 1 change relatively largely near the thresholds. Since the SO mechanism seems to contribute at high photon energies and the ratios through the SO mechanism are expected to be constant against energy [4], it is concluded that the KO mechanism is important near the threshold region. The variations in the singlet/triplet ratios suggest a significance of the spin-dependence on the KO mechanism.

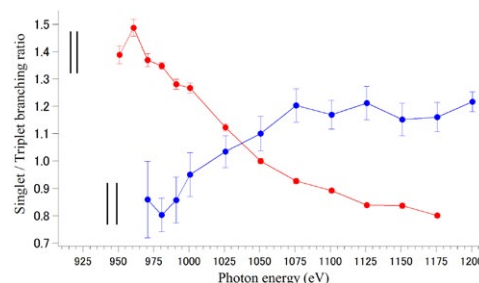


**Figure 1.** Branching ratios of the singlet to triplet final  $Ne^{2+}$  states,  ${}^1S/{}^3S$  (blue) and  ${}^1P/{}^3P$  (red), in the  $1s^{-1}2s^{-1}$  and  $1s^{-1}2p^{-1}$  core-valence DPIs.

### References

- [1] Schneider T and Rost J M 2003 *Phys. Rev. A* **67** 062704
- [2] Adachi J *et. al.* 2020 *J. Phys. ;Conf. Ser.* **1412** 152092
- [3] Hikosaka Y *et. al.* 2021 *Phys. Rev. A* **103** 043119
- [4] Ågren H *et. al.* 1978 *J. Electron Spectrosc. Relat. Phenom.* **14** 27

\*E-mail: [odagiri.t@sophia.ac.jp](mailto:odagiri.t@sophia.ac.jp)

# Photoionization of a Quantum Grating formed by a Single Atom

S F Zhang<sup>1,2\*</sup>, B Najjari<sup>1</sup> and X Ma<sup>1,2†</sup>

<sup>1</sup>Institute of Modern Physics, Chinese Academy of Sciences, Lanzhou 730000, China

<sup>2</sup>University of Chinese Academy of Sciences, Beijing 100049, China

**Synopsis** When an atom passes through a macroscopic diffraction grating its wave function acquires a regular space structure and its collision by another particle can be thought of as scattering, of the latter, on a grating composed of a single atom (hereafter termed as “quantum-grating”). Photoionization of such a ‘quantum grating’ unveils interference features and in particular a striking difference in the photoelectron and recoil ion spectra which no longer ‘mirroring’ each other as in the case of photoionization of atoms or molecules. We show that complete information about the macroscopic diffraction grating is directly contained in the recoil ion spectra while only partly exhibited in the spectra of the electron.

In collision physics, processes involving a molecular target compared to an atom can unveil different features due to the nature of their corresponding electronic wave functions. For instance, in the ionization processes, the electron is emitted from the multi-sites of the molecule and the coherent contributions of the corresponding indistinguishable pathways lead to interference phenomena. However, research works performed in this field dealt exclusively with ionization of atomic targets including molecules and clusters. Yet, none of these studies have considered the breakup of an atom passed through a diffraction grating induced in collision with charged particles nor by absorption of photons.

Because of the uncontrolled exchanged momentum between the atom and the diffraction grating, the wave function of such an atom will acquire a wave-packet property due to the uncertainty principle. When such an atom is taken to interact with a charged particle, or a photon, the result can be viewed as scattering of the latter on an object which can be thought as a diffraction grating and will be referred to as ‘quantum grating’. Like its macroscopic analogous this quantum grating (QG) possesses a periodic spacial structure, which consists of stronger and weaker interacting parts in space corresponding to respectively larger and smaller values of the atomic probability density but constructed only from a single atom. This can be viewed as ‘splitting’ the atom into a set of identical atomic ‘copies’ at equidistant separation from each other. Such an

atomic QG qualitatively differs from a molecular object where the ‘multi-site’ structure of the electron wavefunction is due to the presence of ‘real’ nuclei [1].

As an illustration Figure 1 represents fully differential crossections of photoelectron (upper panel) and the corresponding recoil (lower panel) spectra in momentum space for photoionization of a **He** atom moving initially with momentum  $P_i = 800 \pm 80$  a.u. passed through a diffraction grating with  $N_0 = 7$  slits.

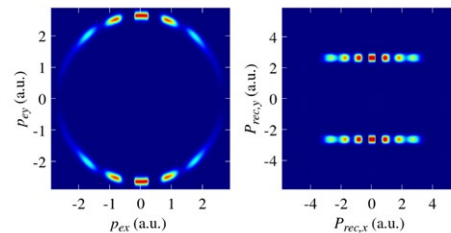


**Figure 1.** Photoelectron spectra ( $d\sigma/d^3\mathbf{p}_e d\mathbf{P}_{rec,x}$ ) and the recoil spectra ( $d\sigma/d^3\mathbf{P}_{rec} dp_{e,x}$ ) of a **He** atom moving initially with momentum  $P_i = 800 \pm 80$  a.u. passed through a diffraction grating with  $N_0 = 7$  slits, along the  $x$ -direction, whose dimensions  $a = d/2 = 100$   $\mu\text{m}$

## References

- [1] Zhang, S. F.; Najjari, B. and Ma, X. Photoionization of a quantum grating formed by a single atom 2021 *Journal of Physics B: Atomic, Molecular and Optical Physics* **54** 15LT01

\*E-mail: [zhangshf@impcas.ac.cn](mailto:zhangshf@impcas.ac.cn)

†E-mail: [x.ma@impcas.ac.cn](mailto:x.ma@impcas.ac.cn)



## Recurrent fluorescence rates of tetracene cations $C_{18}H_{12}^+$ measured at two electrostatic Storage Rings: DESIREE and Mini-Ring.

J Bernard<sup>1\*</sup>, MC Ji<sup>2</sup>, S Indrajith<sup>2</sup>, M H Stockett<sup>2</sup>, J E Navarro Navarrete<sup>2</sup>, N Kono<sup>2</sup>, H Cederquist<sup>2</sup>, S Martin<sup>2</sup>, H T Schmidt<sup>2</sup>, and H Zettergren<sup>2</sup>

<sup>1</sup>Institut Lumière Matière (iLM), UMR5306 Université Lyon 1-CNRS, Université de Lyon 69622 Villeurbanne, France

<sup>2</sup>Department of Physics, Stockholm University, Roslagstullsbacken 21, SE-106 91, Stockholm, Sweden

**Synopsis** Very high recurrent fluorescence rates have been measured for internally hot tetracene cations  $C_{18}H_{12}^+$  using photodissociation technique at two electrostatic storage rings, Mini-Ring (small dimension and room temperature) and DESIREE (larger dimension and cryogenic) in order to explore an extended internal energy range.

The survival of Polycyclic Aromatic Hydrocarbons (PAHs) in the interstellar medium (ISM) depends upon the absorption of UV radiation emitted from nearby stars and the competition between the two main relaxation processes occurring after UV-photon absorption: unimolecular dissociation and radiative cooling. Investigating this competition in conditions that are relevant for the ISM, i.e., high isolation (very dilute gas phase), low temperatures (below 30 K), and long observation times, is of great importance in order to provide the astrophysics community with accurate dissociation and radiative cooling rates. It has been shown in the past decade that Recurrent Fluorescence (RF) contributes efficiently to the cooling of several PAH cations and should be included in astrophysical models as the minimum size of observable PAHs in the ISM may strongly depend on this process[1, 2]. In the present study, we have used plasma ion sources to heat and ionize tetracene molecules in order to store 'hot' tetracene cations in two electrostatic ion storage rings (ESRs), DESIREE (a facility at Stockholm University, Sweden, operated at 13 K, and with a circumference of 8.6 m) and Mini-Ring (ESR in Lyon, France, operated at room temperature, and with a circumference of 0.71 m). Due to the smaller revolution period of tetracene cations in Mini-Ring (about 6 $\mu$ s), it is dedicated to studying the cooling dynamics of the hotter ions that decay fast, whereas DESIREE is better suited to investigate the colder ions on longer time scales up to several hundred of milliseconds due to its cryogenic environment and extremely low back-

ground gas pressure ( $< 10^{-14}$  mbar).

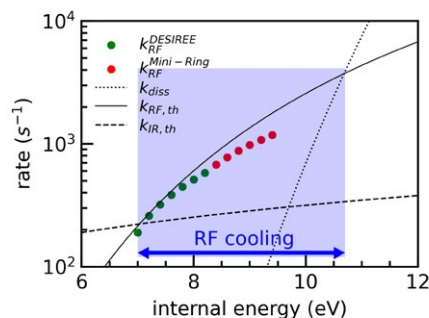


**Figure 1.** Measured RF rates (green dots: DESIREE; red dots: Mini-Ring). Theoretical RF (solid line), infrared emission cooling (dashed line), and dissociation (dotted line) are displayed to highlight the relative importance of these processes as a function of internal energy.

In the accessible internal-energy range to both storage rings (7-9.2 eV), we have measured that RF cooling rates vary from about 200 to 1200  $s^{-1}$ , which is much higher than the dissociation and infrared emission cooling rates. As illustrated in Fig. 1, RF cooling is expected to be the dominant relaxation process in the 7-10.7 eV range. Thus, if tetracene cations were to be found in some regions of the ISM, the majority of these species should survive after UV photon absorption in this energy range.

### References

- [1] Martin S et al. 2013 *Phys. Rev. Lett.* **110** 063003
- [2] Stockett M H et al. 2023 *Nat. Commun.* **14** 395

\*E-mail: [jerome.bernard@univ-lyon1.fr](mailto:jerome.bernard@univ-lyon1.fr)



## Resonant intercluster Coulombic decay in the photoionization of $\text{Na}_{20}$ confined inside $\text{C}_{240}$

R Shaik<sup>1</sup>, K Prajapat<sup>1</sup>, H R Varma<sup>1\*</sup>, H S Chakraborty<sup>2†</sup>

<sup>1</sup>School of Physical Sciences, IIT Mandi, Himachal Pradesh, 175075, India

<sup>2</sup>Department of Natural Sciences, D L Hubbard Center for Innovation, Northwest Missouri State University, Maryville, Missouri 64468, USA

**Synopsis** The photoionization dynamics of an endohedral system, such as  $\text{Na}_{20}@\text{C}_{240}$ , provides a great opportunity to study electron correlation effects. The present work shows the decay of Auger resonances in  $\text{C}_{240}$  through the ionization continuum of  $\text{Na}_{20}$ . A systematic study of these intercluster Coulombic decays (ICDs) is carried out here.

The synthesis of giant fullerenes capable of enclosing clusters and nanocrystals has made it possible to study interesting features, such as, the resonant intercluster Coulombic decay (RICD) [1], when a cluster is doped inside the fullerene. We report photoionization (PI) calculations of  $\text{Na}_{20}$  inside the giant fullerene  $\text{C}_{240}$  ( $\text{Na}_{20}@\text{C}_{240}$ ) to study properties based on the ICD exchange of dynamical coherent or incoherent responses between the two systems. A recent work of ours has shown a remarkable feature where the  $\text{C}_{240}$  giant plasmon decays through the  $\text{Na}_{20}$  continuum [2].

We employed jellium-based density functional theory (DFT) to calculate the ground state of  $\text{Na}_{20}@\text{C}_{240}$ . The dynamical response of the system to the incoming photon is calculated using a linear-response time-dependent DFT (LR-TDDFT). The method includes local density approximation to the exchange-correlation functional, artificially eliminating the self-interaction for each orbital making the ground state potential orbital specific [2]. In the LR-TDDFT scheme, the PI cross section is calculated as

$$\sigma_{PI}(\omega) = \sum_{nl} 2(2l+1) \left| \langle kl' | \delta V(\vec{r}', \omega) | nl \rangle \right|^2$$

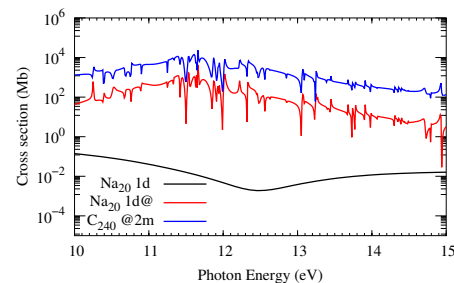
where  $\delta V$  is the complex self-consistent field induced potential that includes both the dipole interaction ( $z$ ) and important electron correlation terms. Here,  $nl$  denotes the occupied ionizing state and  $kl'$  are dipole-selected continuum states.

Figure 1 shows the pristine  $\text{Na}_{20}$  1d PI cross

\*E-mail: [hari@iitmandi.ac.in](mailto:hari@iitmandi.ac.in)

†E-mail: [himadri@nwmissouri.edu](mailto:himadri@nwmissouri.edu)

section free from any resonant structure. The minimum appears in the curve is a part of diffractive oscillations [3]. On the other hand, the 1d@ cross section, when  $\text{Na}_{20}$  is confined, shows evidence of RICD characteristic features resulting from the decay of  $\text{C}_{240}$  @ $nl$  vacancies through  $\text{Na}_{20}$  continua. Detailed comparisons between  $\text{Na}_{20}@\text{C}_{240}$  with that of isolated  $\text{Na}_{20}$  and  $\text{C}_{240}$  are carried out to investigate these ICD resonances which will be presented in the conference. The study may motivate new frontiers of RICD research in loosely bound clusters.



**Figure 1.** LR-TDDFT photoionization cross sections of free  $\text{Na}_{20}$  1d compared with the results for @2m of doped  $\text{C}_{240}$  and 1d@ of dopant  $\text{Na}_{20}$  in  $\text{Na}_{20}@\text{C}_{240}$ .

Funding support: US-NSF Grant No. PHY-2110318 (HSC) and SERB-CRG Grant No. CRG/2022/002309, India (HRV).

### References

- [1] Jahnke T et al. 2020 *Chem. Rev.* **120** 11295.
- [2] Shaik R et al. 2022 *arXiv:2212.01487* and references therein.
- [3] Shaik R et al. 2021 *J. Phys. B* **54** 125101.

## Efficient indirect interatomic Coulombic decay induced by photoelectron impact excitation in large pure He nanodroplets

L. Ben Ltaief<sup>1\*</sup>, K. Sishodia<sup>2</sup>, S. Mandal<sup>3</sup>, S. De<sup>2</sup>, S. R. Krishnan<sup>2</sup>, C. Medina<sup>4</sup>, N. Pal<sup>5</sup>, R. Richter<sup>5</sup>, T. Fennel<sup>6</sup> and M. Mudrich<sup>1†</sup>

<sup>1</sup>Department of Physics and Astronomy, Aarhus University, 8000 Aarhus C, Denmark

<sup>2</sup>Institute of Technology, Madras, Chennai 600036, India

<sup>3</sup>Indian Institute of Science Education and Research, Pune 411008, India

<sup>4</sup>Institute of Physics, University of Freiburg, 79104 Freiburg, Germany

<sup>5</sup>Elettra-Sincrotrone Trieste, 34149 Basovizza, Trieste, Italy

<sup>6</sup>Institute for Physics, University of Rostock, 18051 Rostock, Germany

**Synopsis** Ionization of matter by energetic radiation generally causes complex secondary reactions which are hard to decipher. Using high-resolution electron spectroscopy, we report here on observation of an indirect interatomic ionization secondary process—Interatomic Coulombic Decay (ICD)—in large He droplets irradiated with one single XUV photon of energy  $h\nu \geq 44.4$  eV. We find that this ICD becomes the dominant process of electron emission in nearly the entire XUV range in droplets with radius  $\geq 40$  nm. It likely plays an important role in other dense systems as well, including biological matter.

Weakly-bound systems are ubiquitous in nature, especially in biology, where hydrogen-bonded complexes are essential building blocks of living tissue. There, decay processes mediated by energy or charge transfer such as interatomic Coulombic decay (ICD) can efficiently occur [1]. These processes are not only of fundamental interest but of paramount importance for the understanding of radiation damage and have even been considered as a versatile tool for its control in radiotherapy [2]. Here, we report a study on a novel indirect ICD induced by electron scattering and trapping in superfluid helium droplets by employing high-resolution electron spectroscopy. This novel ICD has a working principle that makes its existence also likely in other condensed phase systems; i.e. liquid water. It is mainly based on the formation of two excited He atoms as a result of the absorption of a single XUV photon of energy  $h\nu \geq 44.4$  eV. While the first excited atom is formed just via impact excitation driven by the primary photoelectron, the second excited atom is a result of the friction-induced slowdown of the electron through electron-atom collisions. The eventual re-capture of the electron by the original residual ion forms the second excited atom. The correlated decay—ICD—of the pair of excited atoms produces a very unusual and characteristic ICD electron signal (See Fig. 1). It even becomes the dominant decay channel of electron emission in droplet with radius  $\geq 40$  nm. Our study presents systematic data recorded for different

droplet sizes and  $h\nu$ 's at different synchrotron facilities using two detection techniques—velocity map imaging spectrometer and hemispherical electron analyser. The experimental data are additionally supported by sophisticated molecular dynamics Monte Carlo simulations.

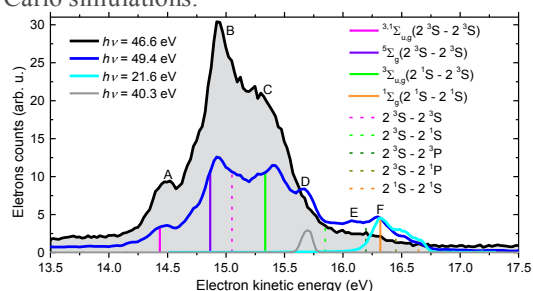


Figure 1. High-resolution ICD electron spectra of He droplets recorded for different  $h\nu$ 's. The dashed and solid lines indicate expected electron energies for ICD involving two He\* atoms and metastable dimer of two He\* atoms. The cyan line is a reference spectrum of He droplet measured at  $h\nu = 21.6$  eV. The gray line is a He photoline recorded at  $h\nu = 40.3$  eV used for calibration purpose.

### References

- [1] Cederbaum L. S, Zobel J and Tarantelli F 1997 *Phys. Rev. Lett.* **79** 4778
- [2] Sanche L 2016 *Rad. Phys. Chem.* **128** 36

\* E-mail: [ltaief@phys.au.dk](mailto:ltaief@phys.au.dk)

† E-mail: [mudrich@phys.au.dk](mailto:mudrich@phys.au.dk)

## The primary steps of ion solvation in helium nanodroplets

S H Albrechtsen<sup>1</sup>, J K Christensen<sup>2</sup>, C A Schouder<sup>3</sup>, A V Muñoz<sup>2</sup>, M Barranco<sup>4,5</sup>, M Pi<sup>4,5</sup>, and H Stapelfeldt<sup>2\*</sup>

<sup>1</sup>Department of Physics and Astronomy, Aarhus University, Ny Munkegade 120, DK-8000 Aarhus C, Denmark

<sup>2</sup>Department of Chemistry, Aarhus University, Langelandsgade 140, DK-8000 Aarhus C, Denmark

<sup>3</sup>LIDYL, CNRS, CEA, Université Paris-Saclay, 91191 Gif-sur-Yvette, France

<sup>4</sup>Departament FQA, Facultat de Física, Universitat de Barcelona, Av. Diagonal 645, 08028 Barcelona, Spain

<sup>5</sup>Institute of Nanoscience and Nanotechnology (IN2UB), Universitat de Barcelona, Barcelona, Spain

**Synopsis** The solvation dynamics of alkali cations in liquid helium are studied in a femtosecond pump-probe experiment. This allows us to measure the distribution of the number of helium atoms in the alkali cation solvation complex in the primary steps of the ion solvation. We find that He attaches to Na<sup>+</sup> at a constant rate of 1.5 atoms per ps. for the first 8 He atoms, which agrees well with time-dependent DFT simulations. Li<sup>+</sup> is experimentally found to attract He atoms at a rate of 1.9 atoms per ps.

Recently, we have obtained experimental results on the solvation dynamics of a single alkali cation in liquid helium, measured with atomic resolution and with femtosecond time resolution.

A single Na or Li atom sitting in its equilibrium position on the surface of a He nanodroplet is ionized by a 50 fs laser pulse. Thereby, an alkali ion, Ak<sup>+</sup>, is effectively introduced instantly to the liquid helium solvent from the gas phase. Hereafter, the Ak<sup>+</sup> ion will gradually pick up helium atoms to form a solvation complex, Ak<sup>+</sup>He<sub>n</sub>. After a time delay, a Xe atom, residing in the interior of the droplet, is ionized by a 50 fs probe pulse. The Xe<sup>+</sup> ion created pushes the Ak<sup>+</sup>He<sub>n</sub> complex away from the droplet, due to the internal Coulomb repulsion. The combination of a Velocity Map Imaging (VMI) spectrometer and a TPX3CAM detector records both the mass and velocity of all Ak<sup>+</sup>He<sub>n</sub> complexes.

By repeating this measurement for a large number of time delays, we measure the time dynamics of the number of He atoms attached to the Ak<sup>+</sup> ion, and find that these attach at a constant rate for the first few atoms. Specifically,

Na<sup>+</sup> binds the first 8 He atoms at a constant rate of 1.5 atom per ps, while Li<sup>+</sup> binds the first 5 He atoms at a rate of 1.9 atom per ps. The case of Na<sup>+</sup> solvation was simulated by time-dependent DFT simulations. The simulation gave an attachment rate of 1.2 He atoms per ps, in good agreement with the measured results.

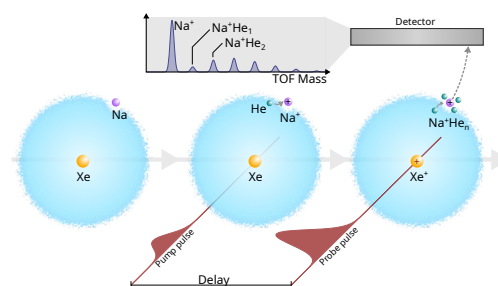


**Figure 1.** Schematic figure showing the principle of the experiment. Solvation of the Na cation is started by the pump pulse, and the solvation complex is ejected when the probe pulse ionizes the Xe atom in the interior. Thereby, the time dynamics of the number of He atoms attached to the Na<sup>+</sup> ion can be measured.

\*E-mail: [henriks@chem.au.dk](mailto:henriks@chem.au.dk)

## Carrier-envelope-phase measurement of sub-cycle UV pulses using angular photofragment distributions

X X Dong<sup>1,7</sup>, Y R Liu<sup>1,7</sup>, V Kimberg<sup>2,3</sup>, O Vendrell<sup>4</sup>, Y Wu<sup>5,6</sup>, J G Wang<sup>5</sup>, J Chen<sup>5,6</sup>, and S B Zhang<sup>1\*</sup>

<sup>1</sup>School of Physics and Information Technology, Shaanxi Normal University, Xi'an 710119, China

<sup>2</sup>Theoretical Chemistry and Biology, Royal Institute of Technology, Stockholm 10691, Sweden

<sup>3</sup>International Research Center of Spectroscopy and Quantum Chemistry, Siberian Federal University – IRC SQC, 660041 Krasnoyarsk, Russia

<sup>4</sup>Theoretical Chemistry, Institute of Physical Chemistry, Heidelberg University, 69120 Heidelberg, Germany

<sup>5</sup>Institute of Applied Physics and Computational Mathematics, Beijing 100088, China

<sup>6</sup>HEDPS, Center for Applied Physics and Technology, Peking University, Beijing 100084, China

<sup>7</sup>Equally contributed

**Synopsis** Carrier-envelope-phase (CEP) of the sub-cycle pulses are playing an increasingly important role in many different studies. Here we investigate photodissociation of a diatomic molecule from its ground-rovibrational state in a linearly polarized weak sub-cycle UV pulse with a controlled CEP. The angular distribution of photofragments shows an asymmetric profile, which can be identified as a way to imprint CEP. We unveil that such an effect stems from the temporal neighboring rotational excitation by molecular permanent dipole interaction through the joint contributions between counter-rotating and rotating terms. Our results pave ways for understanding and manipulating electron, nuclear and their joint dynamics with variation of CEP of attosecond pulses.

Carrier-envelope-phase (CEP) of sub-cycle ultraviolet (UV) pulse strongly influences the dynamics of quantum systems, but its characterization is not accessible experimentally. In this work we consider diatomic LiF molecule as a showcase probed from its ground rovibronic state to valence excited dissociative states by linearly polarized sub-cycle attosecond UV pulses with various CEP. Figure 1 illustrates the excitation scheme and shows involved potential energy curves of LiF.

As it is illustrated in Fig. 1d–g the angular distribution of photofragments shows an asymmetric profile deviating from the well-known  $\cos^2$ – or  $\sin^2$ –like ones, which can be identified as a way to imprint CEP. With the help of a model based on perturbation theory, we unveil that such an effect stems from the temporal neighboring rotational excitation by molecular permanent dipole interaction through the joint contributions between counter-rotating and rotating terms. This in turn, opens different pathways in photodissociation dynamics [1].

In the present study we have shown that CEP of the attosecond pulse can be used as a fine tuner for manipulation of the temporal excita-

tion and the followed dynamics. The present results can be further extended and applied for investigations of ultrafast dynamics in atoms and molecules, when electron excitation and ionization, as well as nuclear dynamics and coupled electron-nuclear dynamics can be effectively controlled by CEP of sub-cycle attosecond UV and XUV pulses.

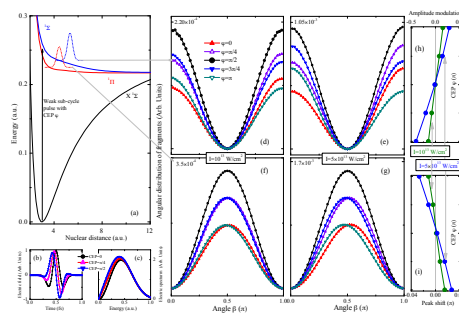


**Figure 1.** Carrier-envelope-phase dependent angular distribution of photofragments.

### References

- [1] Dong X X and Liu Y R and Kimberg V and Vendrell O and Wu Y and Wang J G and Chen J and Zhang S B 2022 *Commun. Phys.* **5** 181

\*E-mail: [song-bin.zhang@snnu.edu.cn](mailto:song-bin.zhang@snnu.edu.cn)

## Chiral Molecular Frame Photoelectron Angular Distributions in achiral formic acid

D. Tsitsonis<sup>1\*</sup>, F. Trinter<sup>1,2</sup>, T. Jahnke<sup>1</sup>, R. Dörner<sup>1</sup> and M. S. Schöffler<sup>1†</sup>

<sup>1</sup>Institut für Kernphysik, Goethe University, Frankfurt Max-von-Laue Str. 1, 60438, Germany

<sup>2</sup>Fritz Haber Institute, Max Planck Society, Berlin Faradayweg 4-6, 14195, Germany

**Synopsis** Molecular Frame Photoelectron Angular Distributions were determined for C(1s) photoionization of formic acid (HCOOH). Signals of chirality of the molecule in different excited states were examined.

The investigation of chiral molecules has gained much of great interest in recent years. Fundamental questions as well as applications such as determination of the configuration are a keystone to stereochemistry. Chiral molecules exist in either one of two enantiomers, which are mirror images of each other. When interacting with another chiral probe, such as circularly polarized light, the reaction of a certain enantiomer is different than the other. Well known is here the so-called Photoelectron Circular Dichroism (PECD), which is the difference of the amount of emitted electrons upon photoionization with left and right handed circularly polarized light. Compared to regular Circular Dichroism, PECD is much stronger as it works already in the dipole regime. However with a few percent it is still a weak effect. The signal strength can be increased by partly fixing the molecule in space [1, 2, 3].

Fixing the molecule completely in space, e. g. measuring the Molecular Frame Photoelectron Angular Distribution (MFPAD) [4], has proven to show strongest PECD-effects, up to 100 % [5]. It allows for the investigation of chiral systems and the extraction of information about the molecular geometry and its constituents. Here we report on formic acid (HCOOH), which is achiral in its ground state. Experiments using short laser pulses already showed that formic acid might turn into a chiral molecule by a bending motion [6]. Here we are targeting the photoelectron with a kinetic energy of 15 eV from C(1s) photoionization.

In order to investigate the ionization and following fragmentation of formic acid we utilize the COLTRIMS technology [7, 8]. Liquid for-

mic acid is evaporated and expands with its vapor pressure through a 200  $\mu\text{m}$  nozzle, forming a free super sonic gas jet, which is then skimmed twice. A homogeneous electric field projects the electrons and ions onto position and time sensitive detectors, with the ion-detector having a high-efficiency funnel micro channel plates [9]. Upon removal of the C(1s) photoelectron with 15 eV kinetic energy, the molecule undergoes multiple Auger decays, resulting in the production of various charge states and ionic and neutral fragments. The handedness of the incoming light was swapped every two hours.

Here we report on the observed nuclear dynamics of formic acid, which clearly showed in the fragmentation pattern chiral structures. Surprisingly this non-planar geometry is already be observable in the molecular frame angular distributions of the photoelectron, which is basically the messenger from the instant of ionization.

### References

- [1] M. Tia et al. J. 2017 *Phys. Chem. Lett.* [8 2780](#)
- [2] G. Nalin et al. 2021 *Phys. Chem. Chem. Phys.* [23 17248](#)
- [3] K. Fehre et al. 2022 *Phys. Chem. Chem. Phys.* [24 13597](#)
- [4] K. Fehre et al. 2022 *Phys. Chem. Chem. Phys.* [24 26458](#)
- [5] K. Fehre et al. 2021 *Phys. Rev. Lett.* [127 103201](#)
- [6] K. Fehre et al. 2019 *Sci. Adv.* [5 3](#)
- [7] R. Dörner et al. 2000 *Phys. Rep.* [330 95](#)
- [8] J. Ullrich et al. 2003 *Rep. Prog. Phys.* [66 1463](#)
- [9] K. Fehre et al. 2018 *Rev. Sci. Instrum.* [89 045112](#)

\* E-mail: [dtsitson@atom.uni-frankfurt.de](mailto:dtsitson@atom.uni-frankfurt.de)

† E-mail: [schoeffler@atom.uni-frankfurt.de](mailto:schoeffler@atom.uni-frankfurt.de)

## Ultrafast imaging of molecular chirality via low-order nonlinear interactions

J Vogwell<sup>1</sup>, L Rego<sup>1</sup>, O Smirnova<sup>2,3</sup> and D Ayuso<sup>1,2\*</sup>

<sup>1</sup>Department of Physics, Imperial College London, SW7 2AZ London, United Kingdom

<sup>2</sup>Max-Born-Institut, Max-Born-Str. 2A, 12489 Berlin, Germany

<sup>3</sup>Technische Universität Berlin, 10623 Berlin, Germany

**Synopsis** We introduce an ultrafast and all-optical method for efficient chiral recognition based on chiral sum-frequency generation (SFG) spectroscopy. In chiral SFG, two non-collinear incident beams with frequencies  $\omega_1 \neq \omega_2$  drive an optical response in a chiral medium at the sum-frequency  $\omega_1 + \omega_2$ . In contrast to traditional SFG implementations, we can encode the medium's handedness in the *intensity* of the SFG signal, rather than in its *phase*, without the need of adding a local oscillator, and enabling full control over the enantio-sensitive response.

Chiral molecules exist in pairs of mirror-reflected versions: the left and right enantiomers, which behave identically unless they interact with another chiral object. Opposite enantiomers can behave very differently, e.g. in biochemical contexts, making chiral discrimination vital.

Traditional chiral spectroscopy relies on the *spatial* helix of circularly polarised light, but its pitch is orders-of-magnitude larger than the molecule, which leads to tiny sensitivity (<0.1%). To overcome this limitation, one can shape light's *local* polarization in *time* to drive chiral effects via electric-dipole interactions in the strong-field regime [1-3] (100% enantio-sensitivity). Here we bring this giant sensitivity to the *perturbative* regime, by combining third harmonic generation (THG) with sum-frequency generation (SFG).

SFG [4] uses two incident lasers with frequencies  $\omega_1 \neq \omega_2$ , wave vectors  $\mathbf{k}_1$  and  $\mathbf{k}_2$ , and polarisation  $\hat{\mathbf{e}}_1$  and  $\hat{\mathbf{e}}_2$ , which drive a second-order response with frequency  $\omega_3 = \omega_1 + \omega_2$  and polarisation  $\hat{\mathbf{e}}_3 = \hat{\mathbf{e}}_1 \times \hat{\mathbf{e}}_2$ , leading to light emission with  $\mathbf{k}_3 = \mathbf{k}_1 + \mathbf{k}_2$ . SFG exclusive of chiral media, and driven by purely electric-dipole interactions. However, the intensity of SFG is not enantio-sensitive, the molecular handedness remains hidden in the *phase* of the signal [4].

Here we show how, by making the driving field *locally* chiral, we can achieve full control over the *intensity* of SFG in randomly oriented chiral molecules. Our setup (Fig. 1a) leads to emission of SFG and THG radiation in the same direction (Fig. 1b), so they can efficiently interfere. By controlling the two-colour phase delay in the second beam (Fig. 1a), we control the field's chirality, and thus the enantio-sensitive

interference. As a result, we can maximise emission of light at 266nm in one enantiomer while fully quenching it in its mirror twin (Fig. 1c).

Imaging molecular chirality on ultrafast time scales via low-order nonlinear processes, which requires gentle laser intensities, creates exciting opportunities for efficient chiral recognition in the liquid phase, the natural medium of biological molecules, or in amorphous chiral solids.

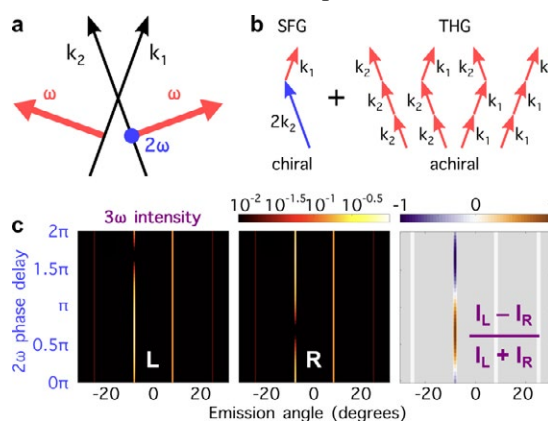


**Figure 1.** **a**, Non-collinear setup combining linearly polarised  $\omega$  and  $2\omega$  colours. **b**, Multiphoton diagrams of momentum conservation in chiral SFG (left) and achiral THG (right). The induced polarisation associated with SFG has the same amplitude and opposite phase in opposite enantiomers,  $\mathbf{P}_{\text{SFG}}^L = -\mathbf{P}_{\text{SFG}}^R$ , whereas  $\mathbf{P}_{\text{THG}}^L = \mathbf{P}_{\text{THG}}^R$ . **c**, Intensity emitted from left/right propylene oxide at frequency  $3\omega$  (266nm). TDDFT results;  $\omega = 0.057\text{au}$ . (800nm), opening angle  $25^\circ$ ,  $I_\omega = 3 \cdot 10^{12} \text{Wcm}^{-2}$ ,  $I_{2\omega} = 7 \cdot 10^{11} \text{Wcm}^{-2}$ ,  $T = 7\text{fs}$ .

- [1] Ayuso et al, *Nat Photon* **13**, 866 (2019)
- [2] Ayuso et al, *Nat Commun* **12**, 3951 (2021)
- [3] Ayuso et al, *Optica* **8**, 1243 (2021)
- [4] Fischer and Hache, *Chirality* **17**, 421 (2005)

\* E-mail: [d.ayuso@imperial.ac.uk](mailto:d.ayuso@imperial.ac.uk)



## Revealing the wave-function-dependent zeptosecond birth time delay in molecular photoionization

X.Y. Lai<sup>1</sup>\*, S.P. Xu<sup>1</sup>, S.G. Yu<sup>1</sup>, M.W. Shi<sup>1</sup>, Y.L. Wang<sup>1</sup>, W. Quan<sup>1</sup>, and X.J. Liu<sup>1</sup>

<sup>1</sup>Wuhan Institute of Physics and Mathematics, Innovation Academy for Precision Measurement Science and Technology, Chinese Academy of Sciences, Wuhan 430071, China

**Synopsis** We study the photoionization of molecule  $H_2^+$  in an XUV pulse by numerically solving the time-dependent Schrödinger equation simulation and focus on a zeptosecond birth time delay of a photoelectron from the different cores. We propose a simple and robust method to extract accurately the zeptosecond birth time delay with double-slit interference minima. Based on this extraction method, our results show that the birth time delay is strongly affected by the initial bound-electron wave function due to the deviation of the electron emission position from the central core.

When a molecule interacts with a strong laser field, the electron wave packets may be emitted from the different cores, forming a double-slit interference pattern in the photoelectron momentum distributions. Usually, these electron wave packets are assumed to be launched simultaneously. But, due to the travel of the photon across the molecules, there is a very small birth time delay between the electron emission, leading to an angular shift of the double-slit interference pattern in the forward direction with respect to the photon propagation. This scheme has been demonstrated by studying the ionization of the hydrogen molecule under a circularly polarized laser field with a photon energy of 800 eV and the angular shift of the double-slit interference pattern in the forward direction is clearly observed in the photoelectron momentum spectra [1]. It is worthy noting that the electron wave packets under the strong laser field are assumed to be emitted from the central position of each core. However, the emission positions might deviate from the central positions of the cores, because the bound-electron wave function is usually not completely concentrated at the center of the core, but has a spatial distribution. Thus, how the emission positions are affected by the initial electron wave distribution and whether the birth time delay is changed accordingly are still open questions.

In this work, we theoretically investigate the photoionization of the simplest prototype

molecule, i.e.,  $H_2^+$  and address the relevance of the zeptosecond birth time delay with the initial electron wave functions [2]. By considering the propagation of the photon across the molecule in the time-dependent Schrödinger equation simulation [3], we well reproduce the double-slit interference pattern in the photoelectron momentum spectra with a clear angular shift induced by the birth time delay. Furthermore, we propose and demonstrate a robust method to extract accurately the birth time delay, which is based on the double-slit interference minima and has its advantage of being free from the influence of the photoionization cross section of the constituent atoms inside the molecule. With this simple and robust method, we reveal that the emission position depends strongly on the initial bound-electron wave function. Accordingly, this will give rise to a significant dependence of the birth time delay on the initial wave function. Furthermore, in order to explain this intriguing effect, an experimental scheme based on the inner-shell ionization of a diatomic molecule is proposed. Our study sheds more light on the zeptosecond birth time delay in molecular photoionization.

### References

- [1] Grundmann S *et al.*, 2020 *Science* [370 339](#)
- [2] Lai X Y *et al.*, 2021 *Phys. Rev. A* [104 043105](#)
- [3] Picón A *et al.*, 2010 *New J. Phys.* [12 083053](#)

\* E-mail: xylai@wipm.ac.cn

## Time-Resolved Images of Intramolecular Charge Transfer in Organic Molecules

F Fernández-Villoria<sup>1,2\*</sup>, J González-Vázquez<sup>2</sup>, A Palacios<sup>2</sup>, and F Martín<sup>1,2</sup>

<sup>1</sup>Instituto Madrileño de Estudios Avanzados en Nanociencia, Madrid, 28049, Spain

<sup>2</sup>Departamento de Química, Universidad Autónoma de Madrid, Madrid, 28049, Spain

**Synopsis** In this work we simulate the ultrafast charge dynamics taking place in the first part of a UV-pump XUV-probe scheme to study the charge transfer process in organic molecules in real time.

Ever since the first models of organic solar cells were proposed more than 40 years ago [1], the search for new materials with the ability to produce a charge separation, necessary for photovoltaic applications, has kept drawing the scientific community's attention. Organic photovoltaic devices usually achieve charge photo-generation by using charge transfer complexes, which act as an intermediate step between exciton dissociation and charge extraction [2].

In order to capture the real time evolution at the early stages of such electronic process, a sub-femtosecond time-resolution is required. Therefore, in this work we propose the use of a pump-probe scheme employing ultrafast laser sources to track the charge transfer process using as target a typical donor-acceptor molecule in the gas phase. In particular, we investigate and compare the ultrafast dynamics following the excitation of para-nitroaniline (PNA) and meta-nitroaniline (MNA). The molecules will be excited using a few-fs UV laser pulse. The ensuing electron-nuclear dynamics will be later probed by a time-delayed attosecond XUV pulse which will ionize the molecule. The time-varying ionization yields are expected to capture the complex dynamics triggered in the excited molecule.

As a first step to describe this process we present the simulation of the initial UV excitation and the subsequent coupled electron-nuclear dynamics. These dynamics are described by means of a surface-hopping method, i.e. within

a semi-classical picture. In short, the time-dependent wave function is retrieved at each time step, computing the electronic structure on-the-fly by means of a quantum mechanical description, while the nuclear dynamics follows the classical equations of motion.

Combining this approach with wavefunction analysis we are able to follow the real time evolution of the electronic charge in the different regions of the studied systems (Figure 1), which allows for a better understanding of the charge-transfer process.

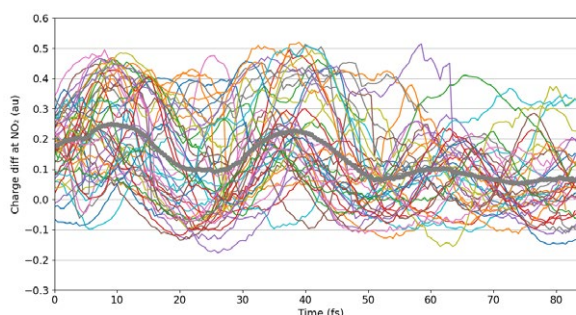


**Figure 1.** Temporal evolution of the electronic charge excess around the NO<sub>2</sub> radical in the different trajectories (thin lines) and their average (thick dotted line) for the PNA molecule.

### References

- [1] Chamberlain G A 1983 *Solar cells* **8** 47
- [2] Deibel C, Strobel T and Dyakonov V 2010 *Advanced materials* **22** 4097

\*E-mail: [francisco.fernandez@imdea.org](mailto:francisco.fernandez@imdea.org)

## Theory of molecular photoionization time delays

A J Suñer-Rubio<sup>1</sup> \*, R Y Bello<sup>1,2</sup>, C Lemell<sup>3</sup>, J Burgdörfer<sup>3</sup>, A Palacios<sup>1,4</sup> and F Martín<sup>1,5,6</sup>

<sup>1</sup> Departamento de Química, Módulo 13, Universidad Autónoma de Madrid (UAM), 28049 Madrid, Spain

<sup>2</sup> Departamento de Química Física, Módulo 13, UAM, 28049 Madrid, Spain

<sup>3</sup> Institute for Theoretical Physics, TU Wien, Wiedner Hauptstr. 8-10/E136 1040 Wien, Austria

<sup>4</sup> Institute of Advanced Research in Chemical Sciences (IAdChem), UAM, 28049 Madrid, Spain

<sup>5</sup> Instituto Madrileño de Estudios Avanzados IMDEA Nanociencia, Cantoblanco, 28049 Madrid, Spain

<sup>6</sup> Condensed Matter Physics Center (IFIMAC), UAM, 28049 Madrid, Spain

**Synopsis** We theoretically investigate the time delay in molecular photoemission using both (numerically) exact quantum calculations as well as semi-classical methods applied to the  $H_2^+$  molecule.

The time-resolved observation of electronic motion has become possible with the advent of the first attosecond pulses (1 as =  $10^{-18}$  s) [1,2]. It is thus nowadays possible to obtain real-time images of the formation and breaking of chemical bonds or to quantify the electron dynamics upon excitation or ionization processes [3,4].

Photoionization has been shown to be not instantaneous but time-shifted relative to the arrival of the crest of the ionizing pulse. The time shift between the arrival and the formation of the outgoing electron wavepacket is identified as the photoionization time delay. The most successful experimental strategies to extract these photoionization time delays in atoms are the attosecond electron streaking [4-6] and the RABBITT technique [2,7].

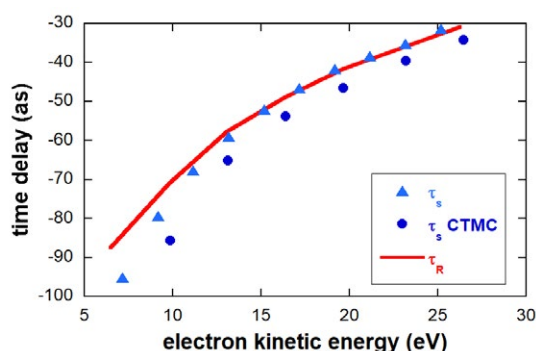


**Figure 1.** Streaking (symbols) and RABBITT (solid line) time delays for  $H_2^+$  as a function of the asymptotic kinetic energy of the photoelectrons. We compare CTMC results with data from full quantum simulations.

Both techniques use a pump-probe scheme, combining attosecond pulses with IR fields, to characterize the electronic wave packet, accessing the ultrafast dynamical information. The former uses a single pulse as a pump, while the latter uses a train of pulses.

The theoretical description and interpretation of photoionization time delays for molecules [8-10] in the non-Born-Oppenheimer regime is still a wide-open question. As a benchmark system we consider the simplest molecule, the hydrogen molecular ion  $H_2^+$ . We perform for the first time full-dimensional quantum simulations accounting for the coupling between electronic and nuclear degrees of freedom during the photoionization and Coulomb explosion processes. Comparison with (semi-)classical trajectory Monte-Carlo simulations (CTMC [11]) allows to disentangle distinct classical and quantum contributions to the resulting streaking time delay.

### References

- [1] Hentschel M et al. 2001 *Nature* **414** 509
- [2] Paul P M et al. 2001 *Science* **292** 1689
- [3] Krausz F and Ivanov M 2009 *Rev. Mod. Phys.* **81** 163
- [4] Nisoli N et al. 2017 *Chem. Rev.* **117** 10760
- [5] Constant N et al. 1997 *Phys. Rev. A* **56** 3870
- [6] Itatani J et al. 2002 *Phys. Rev. Lett.* **88** 173903
- [7] Muller H G 2002 *Appl. Phys. B* **74** s17
- [8] Pazourek R et al. 2015 *Rev. Mod. Phys.* **87** 765
- [9] Baykusheva D and Wörner H J 2017 *J. Chem. Phys.* **146** 124306
- [10] Nandi S et al. 2020 *Sci. Adv.* **6** eaba7762
- [11] Shvetsov-Shilovski N et al. 2016 *Phys. Rev. A* **94** 013415

\* E-mail: [adrian.sunner@uam.es](mailto:adrian.sunner@uam.es)

## Ultrafast competition between $H_2^+$ and $H_3^+$ formation via a $H_2$ roaming mechanism

K Gope<sup>1,2\*</sup>, I Luzon<sup>2</sup>, D Bittner<sup>2</sup>, E Livshits<sup>3</sup>, R Baer<sup>3</sup>, and D Strasser<sup>2†</sup>

<sup>1</sup>Physikalisch-Technische Bundesanstalt, Braunschweig, 38116, Germany

<sup>2</sup>Hebrew University of Jerusalem, Jerusalem, 91904, Israel

<sup>3</sup>Fritz Haber Research Center for Molecular Dynamics, The Hebrew University of Jerusalem, Jerusalem 91904, Israel

**Synopsis** We present a combined experimental and theoretical investigation of the roaming mechanism of neutral  $H_2$  dynamics, which are initiated by double-ionization of isolated organic molecules. This mechanism has a central role in formation of the ubiquitously observed  $H_3^+$  production after ionization of organic molecules. Our studies of the methanol dication system have identified an ultrafast competition between proton-transfer and long-range electron-transfer processes that determine whether the roaming mechanism of neutral  $H_2$  results in formation of  $H_3^+$  or  $H_2^+$  fragments, respectively.

The dynamics of multiply ionized isolated molecules play a significant role in many environments like interstellar medium, planetary chemistry, manmade plasma, and experimental studies with ionizing radiation. Therefore, developing a simple and general tool for probing dynamical structural rearrangement in the course of chemical reactions is the holy grail of ultrafast science. We have developed new ways of utilizing table-top HHG sources for production of ultrafast EUV pulses towards investigation of complex molecular dynamics using time and position resolved 3-dimensional coincidence imaging techniques. Utilizing these techniques, we have demonstrated a multifaceted agreement between ab initio theoretical predictions and experimental measurements in Coulomb explosion induced two- and three-body breakup processes in methanol.<sup>1</sup> This work led to the identification of new mechanisms, including direct nonadiabatic Coulomb explosion responsible for CO bond-breaking, a long-range "inverse harpooning" dominating the production of  $H_2^+ + HCOH^+$ ,<sup>2</sup> a transient proton migration. It leads to surprising energy partitioning in three-body fragmentation and other complex dynamics forming exotic products such as tri-hydrogen ( $H_3^+$ ). We have settled the dispute arising from previous conflicting findings on the formation timescale of  $H_3^+$ , which is  $\sim 70$  fs (see Fig 1a).<sup>3</sup> We have developed new tools for directly comparing time independent simulated results with pump-probe experimental results for modelling the complex molecular

dynamics. These tools allowed us an unprecedented peek into the ultrafast competition

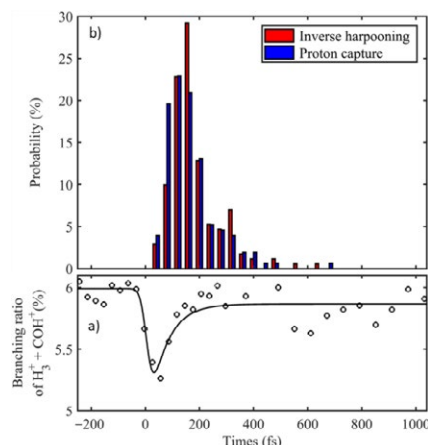


**Figure 1.** (a) The experimentally measured  $H_3^+ + COH^+$  branching ratio by a time-delayed near-IR probe pulse following an ultrafast EUV pump pulse that initiates double ionization of methanol. (b) The Comparing simulated inverse harpoon and proton capture times.<sup>2</sup>

between proton-transfer and by the roaming of neutral  $H_2$  leading to the formation of  $H_3^+$  or  $H_2^+$  fragments, respectively, as shown in Fig 1b.<sup>2</sup>

### References

- [1] Luzon *et al.* 2019 *J. Phys. Chem. Lett.*, **10**, 1361
- [2] Livshits *et al.* 2020 *Communications Chemistry*, **3**, 49
- [3] Gope *et al.* 2022 *Science Advances*, **8**, eabq8084

\* E-mail: [krishnendu.gope@ptb.de](mailto:krishnendu.gope@ptb.de)

† E-mail: [strasser@huji.ac.il](mailto:strasser@huji.ac.il)

## Ionization Dynamics in H<sub>2</sub> by Interference of One- and Two-Photon Pathways employing VUV FEL Pulses

F Holzmeier<sup>1,2,3\*</sup>, A Gonzalez-Castillo<sup>4,5</sup>, T Baumann<sup>6</sup>, C Callegari<sup>8</sup>, M Di Fraia<sup>8</sup>, M Lucchini<sup>3,9</sup>, M Meyer<sup>6</sup>, O Plekan<sup>8</sup>, K C Prince<sup>8</sup>, E Roussel<sup>7</sup>, R Wagner<sup>6</sup>, A Palacios<sup>4</sup>, F Martín<sup>4,5</sup>, and D Dowek<sup>1</sup>

<sup>1</sup>Université Paris-Saclay, CNRS, Institut des Sciences Moléculaires d'Orsay, Orsay, 91405, France

<sup>2</sup>imec, Leuven, 3001, Belgium

<sup>3</sup>Dipartimento di Fisica, Politecnico di Milano, Milan, 20133, Italy

<sup>4</sup>Departamento de Química, Universidad Autónoma de Madrid, Madrid, 28049, Spain

<sup>5</sup>Instituto Madrileño de Estudios Avanzados (IMDEA) en Nanociencia, Madrid, 28049, Spain

<sup>6</sup>European XFEL, Schenefeld, 22869, Germany

<sup>7</sup>Université Lille, CNRS, UMR 8523, PhLAM-Physique des Lasers Atomes et Molécules, Lille, 59000, France

<sup>8</sup>Elettra-Sincrotrone Trieste, Basovizza, 34149, Italy

<sup>9</sup>Institute for Photonics and Nanotechnologies, IFN-CNR, Milano, 20133, Italy

**Synopsis** The unique properties of the FERMI free-electron laser providing two-color longitudinally coherent vacuum ultraviolet pulses enabled us to study ionization dynamics in H<sub>2</sub>. Strong anisotropies are observed in the photoelectron angular distribution allowing to explore the interplay between electron and nuclear motions in the multiphoton path.

The investigation of time-resolved photoionization dynamics usually relies on pump/probe experiments using attosecond light sources. The unique capabilities of the FERMI free-electron laser (FEL) to provide two-color  $\omega/2\omega$  femtosecond (fs) pulses with full longitudinal coherence and a precise control of their relative phase [1] offers an alternative pathway to access ionization dynamics. This study demonstrates such a coherent control scheme for a molecule. Short (50 fs), tunable, bright, linearly polarized and fully coherent vacuum ultraviolet pulses (VUV) at 24.2 eV ( $2\omega$ ) and 12.1 eV ( $\omega$ ) with a defined phase relation were delivered by the FERMI FEL. The latter photon energy leads to resonantly enhanced two-photon ionization of H<sub>2</sub>(X<sup>1</sup> $\Sigma_g^+$ ) selecting a single vibrational level in the H<sub>2</sub>(B<sup>1</sup> $\Sigma_u^+$ ) intermediate state [2], in this case  $v=6$ . This scheme enabled creation of a molecular interferometer [3] in H<sub>2</sub> molecules by controlling the phase between the resonantly enhanced  $\omega+2\omega$  two-photon pathway and the  $2\omega$  single-photon process populating the same cationic final state in H<sub>2</sub><sup>+</sup> (X<sup>2</sup> $\Sigma_g^+$ ,  $v^+$ ), where the nuclear motion in the cationic state adds another degree of freedom in molecules compared to atomic targets. Since the one-photon and the two-photon processes lead to electron partial waves with *ungerade* and *gerade* symmetry, respectively, an asymmetry in the photoelectron

velocity map image is observed along the axis of polarization. This anisotropy characterized by the  $\beta_1$  and  $\beta_3$  asymmetry parameters varies as a function of both the relative phase of the  $\omega$  and  $2\omega$  fields, and the electron energy signature of the vibrational level in the H<sub>2</sub><sup>+</sup>(X) final state. The electron energy dependence of the phase of these oscillations reflects ultrafast ionization dynamics. The interpretation of the experimental findings is supported by full-dimensional time-dependent state-of-the-art simulations employing perturbation theory for fully oriented molecules.

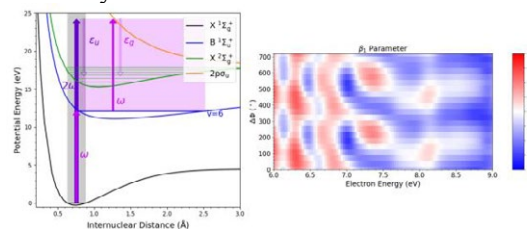


**Figure 1.** Ionization pathways (left) and 2D map of the  $\beta_1$  asymmetry parameter as a function of the  $\omega$ - $2\omega$  relative phase and electron energy (right).

### References

- [1] Prince K C *et al.* 2016 *Nat. Photon.* **10** 176
- [2] Holzmeier F *et al.* 2018 *Phys. Rev. Lett.* **121** 103002
- [3] Palacios A *et al.* 2014 *PNAS* **111** 3973-3978

\* E-mail: [fabian.holzmeier@imec.be](mailto:fabian.holzmeier@imec.be)



## Chiral photoelectron angular distributions from ionization of achiral atomic and molecular species

A Pier<sup>1,\*</sup>, K Fehre<sup>1</sup>, S Grundmann<sup>1,†</sup>, I Vela-Perez<sup>1</sup>, N Strenger<sup>1</sup>, M Kircher<sup>1</sup>, D Tsitsonis<sup>1</sup>,  
J B Williams<sup>2</sup>, A Senftleben<sup>3</sup>, T Baumert<sup>3</sup>, M S Schöffler<sup>1</sup>, P V Demekhin<sup>3</sup>, F Trinter<sup>4,5</sup>, T Jahnke<sup>1</sup>  
and R Dörner<sup>1</sup>

<sup>1</sup>Institut für Kernphysik, Goethe-Universität, 60438 Frankfurt, Germany

<sup>2</sup>Department of Physics, University of Nevada, Reno, Nevada 89557, USA

<sup>3</sup>Institut für Physik und CINSaT, Universität Kassel, 34132 Kassel, Germany

<sup>4</sup>Photon Science, Deutsches Elektronen-Synchrotron (DESY), 22607 Hamburg, Germany

<sup>5</sup>Molecular Physics, Fritz-Haber-Institut der Max-Planck-Gesellschaft, Faradayweg 4-6, 14195 Berlin, Germany

**Synopsis** We show that the combination of two achiral components—an atomic or molecular target plus a circularly polarized photon—can yield chirally structured photoelectron angular distributions.

Chiral molecules display a chirally structured photoelectron angular distribution upon photoionization. However, the concept of chirality can be applied to any three-dimensional object. We investigated if achiral atomic or molecular species can also display a chiral photoelectron angular distribution (PAD) under certain geometric configurations

We used the P04 beamline at PETRA III (DESY) and applied a reaction microscope to investigate carbon K-shell photoionization of CO followed by Auger decay at 310 eV photon energy and the one-photon double ionization of He at 255 eV and 800 eV.

We found that for photoionization of CO, the angular distribution of carbon K-shell photoelectrons is chiral when the molecular axis is neither perpendicular nor (anti)parallel to the light propagation axis [see Fig. 1 d) and e)]. In photo-double-ionization of He, the distribution of one electron is chiral if the other electron is oriented like the molecular axis in the former case and if the electrons are distinguishable by their energy. In both scenarios, the circularly polarized photon defines a plane with a sense of rotation and an additional axis is defined by the CO molecule or one electron.

We showed that in order to produce such a chirally structured electron angular distribution, an unambiguous coordinate frame of well-defined handedness is necessary but not sufficient and that additional electron-electron interaction or scattering processes are needed to create the chiral angular distribution.

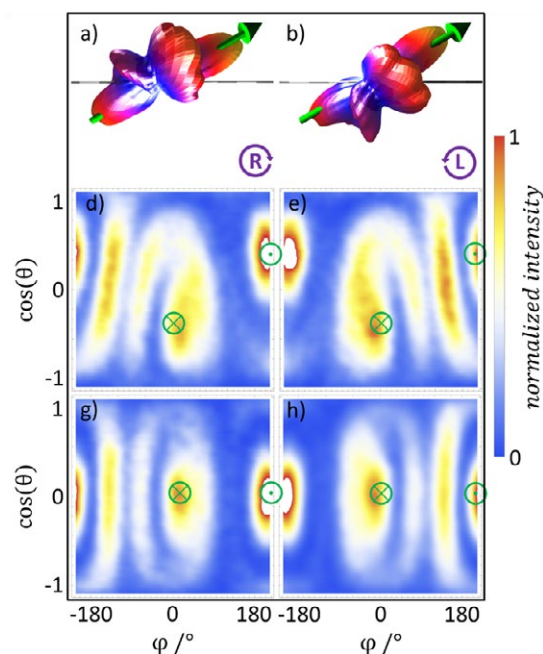


**Figure 1.** Measured photoelectron angular distributions of the carbon K-shell electron emission of CO, obtained from circularly polarized light at 310 eV. The panels on the left [right] correspond to right-handed [left-handed] circularly polarized light.

### References

- [1] Pier A *et al* 2020 *Phys. Rev. Research.* **2** 033209

\* E-mail: [pier@atom.uni-frankfurt.de](mailto:pier@atom.uni-frankfurt.de)

† E-mail: [grundmann@atom.uni-frankfurt.de](mailto:grundmann@atom.uni-frankfurt.de)



## The Big, the Small & the Shoulder: Controlling OCS post-Ionization Dynamics

T Endo<sup>1,2</sup>, K M Ziems<sup>3</sup>, M Richter<sup>3</sup>, A Hishikawa<sup>4</sup>, S Gräfe<sup>3</sup>, F Légaré<sup>1\*</sup> and H Ibrahim<sup>1\*</sup>

<sup>1</sup>Advanced Laser Light Source (ALLS) at Institut national de la recherche scientifique, Varennes, Canada

<sup>2</sup>Kansai Photon Science Institute, National Institutes for Quantum Science & Technology, Kyoto, Japan

<sup>3</sup>Inst. of Phys. Chem. & Abbe Center of Photonics, F. Schiller U. & M Planck School of Photonics, Jena, Germany

<sup>4</sup>Chemistry Dept., Graduate School of Science & Research Center for Materials Science, Nagoya U., Aichi, Japan

**Synopsis** Using phase-locked two-color laser fields, we demonstrate control of the fragment ejection direction and selective bond scission in the heavy polar molecule OCS. Detected with Coulomb explosion imaging (CEI) we analyse different break-up channels with different dynamics in a major channel, a minor one and a shoulder peak. In addition to the expected direct ionization effects from these asymmetric laser fields, we also see important post-ionization contributions, which are usually not visible in heavy polar molecules.

Photo-chemical reactions can be coherently controlled in various ways. Simple pulse shaping techniques using asymmetric electric field such as carrier-envelope-phase (CEP) stabilized few-cycle pulses or phase-locked two-color laser fields have been employed to investigate the underlying mechanisms of such reaction control.

The importance of post-ionization interactions, e.g. population transfer or potential deformation in the cation to control the fragment ejection direction has been discussed for many *non-polar molecules* such as H<sub>2</sub>, C<sub>2</sub>H<sub>2</sub>, and CO<sub>2</sub>. On the contrary, the fragment ejection direction in asymmetric laser fields of *polar molecules* has been exclusively explained by the anisotropy of the tunneling ionization rate, which is determined by the shape of the ionizing molecular orbital (usually the highest occupied molecular orbital) and the molecule's permanent dipole moment rather than by post-ionization interactions. Here, we investigated the break-up processes of the prototypical polar molecule OCS in phase-locked two-color intense laser fields and identified post-ionization interaction effects [1].

To obtain these asymmetric fields, a fundamental beam is superimposed with its second harmonic while controlling the relative phase between both of them.

Dissociation into the two break-up channels of the dication, OCS<sup>2+</sup> → O<sup>+</sup>+CS<sup>+</sup> (minor channel) and OC<sup>+</sup>+S<sup>+</sup> (major channel) was studied and controlled. The branching ratio of the breaking of the C–O and C–S bonds followed a pronounced 2π-oscillation, depending on the relative phase of the two-color laser fields.

The fragment ejection direction of the main peak of both break-up channels reflects the anisotropy of the tunneling ionization rate, following a 2π-periodicity, as well.

Besides the main peak, the major channel also shows a shoulder peak that was not previously observed. These two dissociation pathways in the C–S bond breaking channel show different phase dependencies of the fragment ejection direction, which are assigned to post-ionization dynamics. These observations, resulting from the excitation with asymmetric two-color intense laser fields, supported by state-of-the-art theoretical simulations, reveal the importance of post-ionization population transfer in addition to tunneling ionization in the molecular fragmentation processes, even for heavy polar molecules.

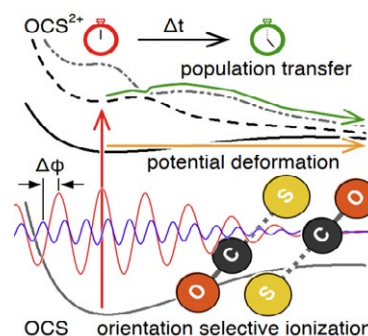


Figure 1. Scheme of post-ionization dynamics in OCS.

### References

- [1] T. Endo, et al., *Front. Chem.* [10:859750](https://doi.org/10.859750) (2022).

\* E-mail: [heide.ibrahim@inrs.ca](mailto:heide.ibrahim@inrs.ca)

† E-mail: [francois.legare@inrs.ca](mailto:francois.legare@inrs.ca)

## Exploration of VUV photodissociation of aniline as a source of astronomically important HC<sub>2</sub>N

S. Muthuamirthambal<sup>1</sup>, S. Arun<sup>1</sup>, K. Ramanathan<sup>1</sup>, R. Richter<sup>2</sup>, N. Pal<sup>2</sup>, P. Bolognesi<sup>3</sup>, L. Avaldi<sup>3</sup>, M. V. Vinitha<sup>1</sup>, C. S. Jureddy<sup>1</sup> and U. Kadhane<sup>1\*</sup>

<sup>1</sup>Indian Institute of Space Science and Technology, Thiruvananthapuram 695547, Kerala, India.

<sup>2</sup>Elettra-Sincrotrone Trieste, Strada Statale 14 - km 163,5 in AREA Science Park, Basovizza, TS 34149, Italy.

<sup>3</sup>CNR-Istituto di Struttura della Materia, Area della Ricerca di Roma 1, Monterotondo, Roma 00015, Italy.

**Synopsis** An investigation of the astronomically significant radical molecule HCCN as a fragment molecule of aniline under VUV photodissociation. Using DFT calculations, the possible pathways for the fragment neutral have been explored and validated in comparison to the experimental results.

In TMC-1, where stars are expected to form, the discovery of cyanobenzene and the subsequent identification of small cyclic compounds raise the possibility that aromaticity is a feature of many of these dark molecular clouds and the PANHs may be linked to smaller molecules via an association mechanism [1]. Aniline is the structural core of many proteins and nucleobases. An in-depth analysis of aniline will improve our comprehension of the formation mechanism of larger PANHs. One of the aniline's fragments is HCCN, a neutral molecule with astronomical significance, especially in the atmosphere of Titan.

The photoelectron photoion coincidence experiment was done using the VMI setup in the gas-phase beam line at Elettra, synchrotron facility. The photoelectrons were recorded and the kinetic energy of the electrons were extracted using MEVELER algorithm.

Despite the modest intensity of the mass 39 loss channel, the possible fragment neutral of this channel needs to be validate further. The fragment neutral corresponding to mass 39 loss could be a C<sub>3</sub>H<sub>3</sub>, HCCN or HNCC. Given that masses 39 and 54, respectively, correspond to cyclopropenyl (C<sub>3</sub>H<sub>3</sub>) and cyanoethyl (C<sub>3</sub>H<sub>4</sub>N) radicals, it seems improbable that the ion and fragment are both radicals. The HNCC and HCCN are two other possible fragment molecules.

To comprehend the associated neutral molecule of this channel, the potential energy surface for this channel has been calculated. After several attempt there was no reachable pathway for C<sub>3</sub>H<sub>3</sub> loss. The energy required for

losing HNCC neutral from the aniline cation is  $\approx 15.3eV$  which is well above the observed onset energy of the mass 39 loss channel. The other possible fragment neutral could be only HCCN. The Fig1. shows the potential energy surface diagram of the HCCN loss channel.

Compare with the other primary channel stationary states in their PES, HCCN loss happens via ring expansion than ring contraction. The HCCN bond from the last intermediate state could be a direct cleavage with no reverse activation barrier. The bond cleavage of HCCN from the intermediate structure is not seen in the relaxed coordinate scan. Since the internal energy of the ion is above this final step in real case the bond cleavage can be happened resulting the fragment loss.

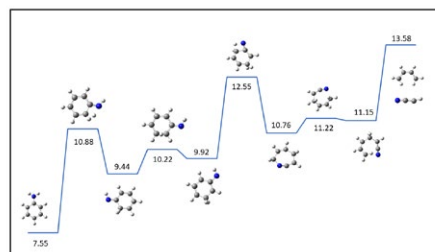


**Figure 1.** Potential energy surface of the HCCN fragmentation channel.

### References

- [1] R. Siebenmorgen and F. Heymann "Polycyclic aromatic hydrocarbons in protoplanetary disks: emission and x-ray destruction" *Astronomy Astrophysics* (2012)

\*E-mail: [rkumesh@gmail.com](mailto:rkumesh@gmail.com)

## Differentiating Molecular Structures using Laser-induced Coulomb Explosion Imaging

Huynh Van Sa Lam<sup>1</sup>, Anbu Selvam Venkatachalam<sup>1</sup>, Surjendu Bhattacharyya<sup>1</sup>, Keyu Chen<sup>1</sup>, Vinod Kumarappan<sup>1</sup>, Artem Rudenko<sup>1</sup>, Daniel Rolles<sup>1\*</sup>

<sup>1</sup>James R. Macdonald Laboratory, Kansas State University, Manhattan, KS 66506, USA

**Synopsis** We show that laser-induced Coulomb explosion imaging can serve as a robust method for differentiating molecular structures and holds great promise for following structural changes, such as ring opening, with atomic resolution in pump-probe experiments.

Coulomb explosion imaging (CEI) with XFELs has recently been demonstrated as a powerful method for obtaining detailed structural information of gas-phase planar ring molecules with eleven atoms [1]. This opens up the possibility of using time-resolved CEI to directly image structural changes of intermediate-size molecules during photochemical reactions, such as ring-opening processes, with atomic resolution. However, distinguishing different products in a time-resolved measurement remains challenging.

In this work, we investigate the potential of this method in the context of CEI using a tabletop laser. We study the static CEI patterns of planar and nonplanar molecules that resemble the structures of ring-closed, open-chain, and ring-chain products formed in UV-induced ring-opening reactions [2]. As shown in Fig. 1, each molecule fragments into a well-localized and distinctive pattern in 3D momentum space, allowing the differentiation of these structures. These patterns provide direct information about molecular structure and can be qualitatively reproduced using a simple classical Coulomb explosion simulation model.

Our findings suggest that laser-induced CEI can serve as a robust method for differentiating molecular structures. Furthermore, the technique holds great promise for following structural changes at the individual atom level in pump-probe experiments, such as ring-opening reactions.

This work is supported by the Chemical Sciences, Geosciences, and Biosciences Division, Office of Basic Energy Sciences, Office of Science, U.S. Department of Energy, Grants DE-FG02-86ER13491 and DE-SC0020276 (SB), and by the National Science Foundation Grant PHYS-1753324 (ASV).

\*E-mail: [rolles@phys.ksu.edu](mailto:rolles@phys.ksu.edu)

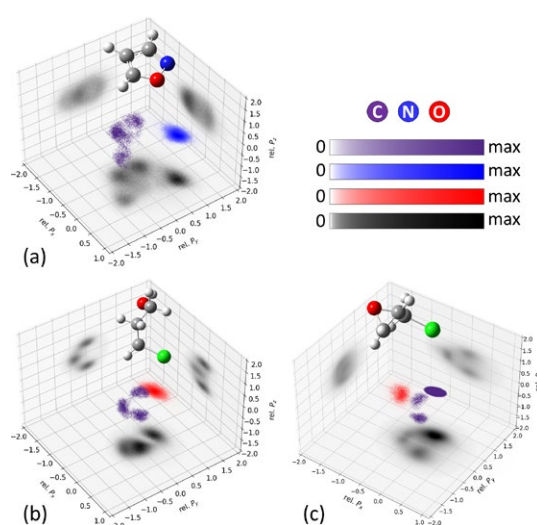


**Figure 1.** 3D scatter plots showing the normalized measured momenta of individual atoms in (a) isoxazole, (b) 3-chloro-1-propanol, and (c) epichlorohydrin from the 4-body (a) ( $C^+$ ,  $C^+$ ,  $N^+$ ,  $O^+$ ), and (b-c) ( $C^+$ ,  $C^+$ ,  $O^+$ ,  $Cl^+$ ) channels. The position of each data point is determined by its normalized momentum, while its color corresponds to the surrounding density. In (a), the recoil frame is rotated and rescaled such that the momentum of  $O^+$  is set as the unit vector along the  $x$ -axis (so-called  $x$ -reference ion), and the momentum of  $N^+$  is in the  $xy$  plane (referred to as  $xy$ -reference ion). Momenta of other ions are plotted in this frame of coordinates. The  $x$ - and  $xy$ -reference ions are  $Cl^+$  and  $O^+$  in (b), and  $Cl^+$  and the first  $C^+$  in (c). The  $x$ -reference ion is not plotted in any panels. We also do not plot the  $xy$ -reference ion in the  $p_z p_x$  and  $p_z p_y$  projections; they are simply a high-intensity line along  $p_z = 0$ .

### References

- [1] Boll, R. *et al.* (2022) *Nat. Phys.* **12**(9) 795-800.
- [2] Pathak, S. *et al.* (2020) *Nat. Chem.* **18**(4) 423-428.

## Fully differential double photoionization of linear molecules beyond $H_2$

F L Yip<sup>1\*</sup>, R R Lucchese<sup>2</sup>, T N Rescigno<sup>2</sup>, and C W McCurdy<sup>2,3</sup>

<sup>1</sup>Dept. of Sciences and Mathematics, California State University-Maritime Academy, Vallejo, CA 94590 USA

<sup>2</sup>Chemical Sciences Division, Lawrence Berkeley National Laboratory, Berkeley, CA 94720 USA

<sup>3</sup>Department of Chemistry, University of California, Davis, Davis, CA 95616 USA

**Synopsis** Double photoionization results are calculated at the most detailed level for molecular targets beyond  $H_2$ , with  $Li_2$  being analogous to the former and  $LiH$  being a heteronuclear diatomic target with core electrons.

Molecular double photoionization in the body frame reveals a richness of information about the nature of electron correlation, and to date has been fully explored by theory and experiment for only the simplest molecular target,  $H_2$ , a purely two-electron system that subsequently Coulomb explodes when doubly ionized. We report on extension of computational methods [1] to calculate the angular- and energy-differential cross sections for single photon double ionization of linear molecules with core electrons, doubly ionizing the valence electrons in the presence of core electrons. Double photoionization of  $Li_2$  represents a fully differential theoretical study of double ionization from a many-electron molecule analogous to molecular hydrogen; in addition to being possessing core electrons whose interactions influence the outgoing valence electrons, the symmetry of the overall initial and final states parallel those for the same process in  $H_2$ , thus permitting a direct comparison of the body-frame angular distributions that result from double ionization from these two molecular targets. In the case of  $LiH$  we find a heteronuclear molecular target with core electrons. We present a theoretical framework for accurately accounting for the presence of core electrons and how the influence of (in the case of molecular  $Li_2$ , for example) the closed-shell core molecular orbitals  $(1\sigma_g)^2$  and  $(1\sigma_u)^2$ , are accounted for in the double ionization process where the photon removes the valence  $(2\sigma_g)^2$  electrons. For both  $Li_2$  and  $LiH$ , the method builds on previous theoretical foundations for single photoionization from molecular targets [2]. We also examine the nature of initial state correlation in a natural orbital expansion [3], revealing the impact of the electron correlation in the initial state. The advance of *ab*

*initio* methods described here to molecules with more than two electrons represents an important and necessary step towards being able to describe even the simplest many-electron molecular double photoionization event.

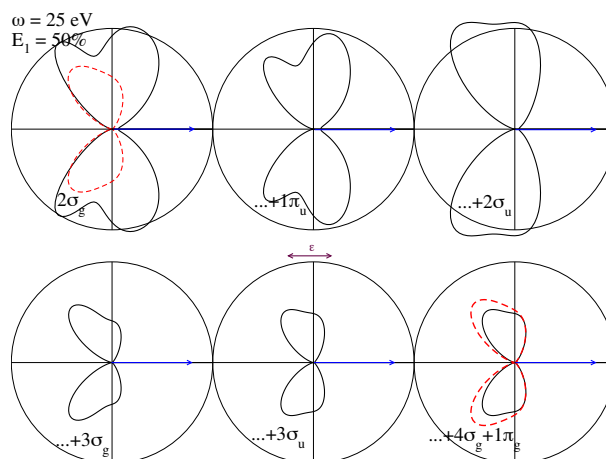


**Figure 1.** Triple differential cross section (TDCS) results of  $Li_2$  at 25 eV photon energy for equal energy sharing with the molecular axis parallel to the photon polarization (horizontal) with the fixed electron at  $\theta_1 = 0^\circ$ . In each panel, the indicated natural orbital(s) are subsequently added to those of the previous, building up the correlation terms of the initial state. The dashed red curve is the fully converged TDCS result.

### References

- [1] Vanroose W, Horner D A, Martín F, Rescigno, T N and McCurdy, C W *Phys. Rev. A* **74** 052702
- [2] Yip F L, McCurdy C W, and Rescigno, T N *Phys. Rev. A* **90** 063421
- [3] Bello, R Y, Yip F L, Rescigno, T N, Lucchese R R, and McCurdy C W *Phys. Rev. A* **99** 013403

\*E-mail: [fyip@csu.edu](mailto:fyip@csu.edu)

## First principle approach to the simulation of attosecond XUV pump XUV probe spectra for small organic molecules

G Grell<sup>1\*</sup>, J González-Vázquez<sup>2</sup>, P Decleva<sup>3</sup>, A Palacios<sup>2</sup> and F Martín<sup>1,2,4†</sup>

<sup>1</sup>IMDEA Nanoscience Institute, Madrid, 28049, Spain

<sup>2</sup>Departamento de Química, Universidad Autónoma de Madrid, Madrid, 28049, Spain

<sup>3</sup>Istituto Officina dei Materiali (CNR-IOM), 34149 Basovizza - Trieste, Italy

<sup>4</sup>Condensed Matter Physics Center (IFIMAC), Universidad Autónoma de Madrid, Madrid, 28049, Spain

**Synopsis** We present a first-principles approach to simulate attosecond pump-probe spectra of the ultrafast charge migration dynamics in small organic molecules using all-attosecond pulses in the XUV to soft X-Ray energy regime. Therein, the pump-ionization which creates the coherent superposition of states, the ensuing coupled electron-nuclear dynamics, and the interaction with the probe pulse, i.e., ionization or absorption, are modeled explicitly to obtain the respective transient spectra.

Tunable sub-fs soft X-Ray (SXR) pulses are now available at the LCLS X-Ray free electron laser (XFEL) at intensities that exceed those of current SXR high harmonic generation (HHG) sources by many orders of magnitude [1]. This overcomes the intensity related limitation of HHG-based attosecond XUV pump-probe experiments to using sub-fs XUV or SXR pulses as either the pump or the probe field. The first realizations of nonlinear X-Ray spectroscopic experiments employing sub-fs SXR pulses for driving and interrogating the attosecond electron-nuclear dynamics in molecules are currently undertaken.

To decipher the measured traces of intricate dynamics high level theoretical modeling of the final observable would be desirable. However, accurate simulations of the individual steps, i.e., (i) the ionization by the sub-fs SXR pump, (ii) the ensuing coupled electron-nuclear dynamics, and (iii) the interaction with the sub-fs SXR probe are extremely challenging tasks on their own. Their combination limits the computationally tractable system size severely, in particular, if the transient photoionization spectrum is sought after, which requires probe ionization calculations as well. We present a protocol that bal-

ances computational cost and accuracy to allow complete, (i)-(iii), simulations of sub-fs pump-probe spectra in the XUV to SXR photon energy range for small organic molecules. Therein, we describe the bound molecular states with the CASPT2 method and use the static exchange B-spline DFT approach to model the outgoing electrons wave functions. The coupled electron-nuclear dynamics after the pump is modeled with the trajectory surface hopping method, where an ensemble of trajectories, representing the nuclear zero-point energy of the system, is launched in each state populated by the pump [2]. To decipher the dynamics from multiple perspectives, we evaluate three different spectroscopic observables, i.e., the transient absorption, valence photoionization, and core photoionization spectra, respectively.

Further, various simplifications to our protocol will be scrutinized, such as neglecting the motion of the nuclei and disregarding continuum states for the probe ionization, i.e., the sudden approximation.

### References

- [1] Duris J et al. 2020 *Nat. Phot.* **14** 30
- [2] Delgado J et al. 2021 *Faraday Discuss.* **228** 349

\*E-mail: [gilbert.grell@imdea.org](mailto:gilbert.grell@imdea.org)

†E-mail: [fernando.martin@uam.es](mailto:fernando.martin@uam.es)



## Sub-cycle resolved tunnel ionization of chiral molecules

M Hofmann<sup>1\*</sup>, A Geyer<sup>1</sup>, D Trabert<sup>1</sup>, N Anders<sup>1</sup>, J Kruse<sup>1</sup>, J Rist<sup>1</sup>, L Ph H Schmidt<sup>1</sup>,  
T Jahnke<sup>2</sup>, M Kunitski<sup>1</sup>, M S Schöffler<sup>1</sup>, S Eckart<sup>1</sup>, and R Dörner<sup>1†</sup>

<sup>1</sup>Institut für Kernphysik, Goethe-Universität, Max-von-Laue-Str. 1, 60438 Frankfurt am Main, Germany

<sup>2</sup>European XFEL, Holzkoppel 4, 22869 Schenefeld, Germany

**Synopsis** We report on the strong field ionization of S- and R-propyleneoxide in circularly polarized two-color laser fields (395 nm & 790 nm). We find that the relative helicity of the two single color laser fields affects the photoelectron circular dichroism (PECD). Further, we observe that the PECD is modulated as a function of the sub-cycle release time of the electron. This modulation is in line with our simulations and reveals the interplay of the chiral initial momenta after tunneling and the subsequent propagation in the Coulomb potential of the parent ion.

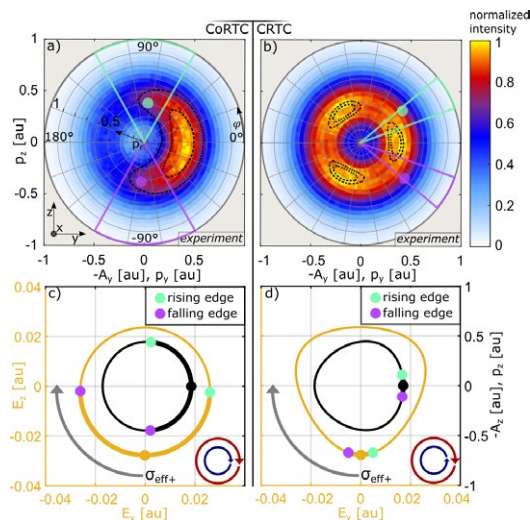


**Figure 1.** a) [b)] Measured electron momentum distribution  $p_{\text{final}}$  in the polarization plane ( $p_y p_z$ ) for the CoRTC [CRTC] two-color field. (c) [(d)] Lissajous curves of the used CoRTC [CRTC] two-color field  $E(t)$  and the corresponding negative vector potential  $-A(t)$ .

Strong field ionization of chiral molecules is known to show photoelectron circular dichroism. It is a long standing controversy, if this chiral signature results from the chiral structure of the orbital from which the electron is tunneling, or if it is generated during the light driven propagation of the electron in the chiral potential of the molecular ion after tunneling. We report on an experiment which supports the first explanation. We use co-rotating (CoRTC) and counter-rotating (CRTC) circularly polarized two-color

laser field to vary the effective angular frequency and the strength of the laser electric field on a sub-cycle time scale (Fig. 1) [1, 2]. The three-dimensional electron momenta of propyleneoxide (electron detected with the parent ion without molecular breakup) have been measured in coincidence with ions using cold-target recoil-ion momentum spectroscopy (COLTRIMS) [3]. We report on two findings: First, the PECD depends on the effective angular frequency. Second, the angle-resolved PECD differs comparing electrons that are born on the rising and the falling edge of the laser field. In both cases, the radial momentum ( $p_r$ )-dependent sign change of the PECD is apparent, which is characteristic in the strong field regime [4] and was already attributed to chiral propensity rules [5, 6]. We use a simplified SFA+CTS [7] model to show that these chiral initial states, in combination with a classical propagation of the electron after tunneling in an achiral Coulomb potential, are sufficient to describe all the effects mentioned above. This suggests that chiral initial conditions are causal for the observed asymmetries.

### References

- [1] Eckart S et al. 2018 *Phys. Rev. Lett.* **16** 121
- [2] Eckart S et al. 2018 *Nat. Phys.* **14** 701
- [3] Jagutzki O et al. 2002 *IEEE Tr. on N. Sc.* **5** 49
- [4] Fehre K et al. 2019 *Phy. Rev. Res.* **1** 3
- [5] Ordonez A and Smirnova O 2022 *Phys. Chem. Chem. Phys.* **9** 24
- [6] Artemyev A et al. 2022 *J. Chem. Phys.* **3** 156
- [7] Geyer A et al. 2023 *arXiv* 2211.01791

\*E-mail: [hofmann@atom.uni-frankfurt.de](mailto:hofmann@atom.uni-frankfurt.de)

†E-mail: [doerner@atom.uni-frankfurt.de](mailto:doerner@atom.uni-frankfurt.de)



## UV-induced ring-opening dynamics investigated by time-resolved Coulomb explosion imaging

K Chen<sup>1\*</sup>, S Bhattacharyya<sup>1</sup>, A S Venkatachalam<sup>1</sup>, H V S Lam<sup>1</sup>, K Borne<sup>1</sup>, S Usenko<sup>2</sup>, B Senfftleben<sup>2</sup>, D Rivas<sup>2</sup>, T Mullins<sup>2</sup>, T Baumann<sup>2</sup>, B Erk<sup>3</sup>, A Röhrig<sup>2</sup>, P Schmidt<sup>2</sup>, S Sasikumar<sup>2</sup>, S Dold<sup>2</sup>, T Mazza<sup>2</sup>, M Meyer<sup>2</sup>, B F E Curchod<sup>4</sup>, M N R Ashfold<sup>4</sup>, F Allum<sup>5</sup>, A Green<sup>5</sup>, E Warne<sup>6</sup>, J McManus<sup>6</sup>, M Burt<sup>6</sup>, M Brouard<sup>6</sup>, R J G Forbes<sup>5</sup>, J P F Nunes<sup>7</sup>, M Centurion<sup>7</sup>, P M Weber<sup>8</sup>, A Rouzee<sup>9</sup>, R M P Tanyag<sup>10</sup>, H Stapelfeldt<sup>10</sup>, K Lin<sup>11</sup>, R Ingle<sup>12</sup>, E Wang<sup>1</sup>, F Trinter<sup>3</sup>, T Jahnke<sup>2</sup>, R Boll<sup>2</sup>, D Rolles<sup>1</sup> and A Rudenko<sup>1</sup>

<sup>1</sup>J.R. Macdonald Laboratory, Department of Physics, Kansas State University, Manhattan, KS 66502, USA; <sup>2</sup>European XFEL, 22869 Schenefeld, Germany; <sup>3</sup>Deutsches Elektronen Synchrotron (DESY), 22607 Hamburg, Germany; <sup>4</sup>School of Chemistry, University of Bristol, Bristol BS8 1QU, UK; <sup>5</sup>SLAC National Accelerator Laboratory, Menlo Park, CA 94025, USA; <sup>6</sup>Department of Chemistry, University of Oxford, Oxford OX1 3TA, UK; <sup>7</sup>Department of Physics and Astronomy, University of Nebraska-Lincoln, Lincoln, NE 68588, USA; <sup>8</sup>Department of Chemistry, Brown University, Providence, RI 02912, USA; <sup>9</sup>Max Born Institute, 12489 Berlin, Germany; <sup>10</sup>Aarhus University, 8000 Aarhus, Denmark; <sup>11</sup>University of Frankfurt, 60323 Frankfurt, Germany; <sup>12</sup>University College London, London WC1E 6BT, UK.

**Synopsis** We present the results of experiments that employ Coulomb explosion imaging with intense, femtosecond X-ray and near-infrared laser pulses to investigate the UV-induced ring-opening dynamics in a prototypical heterocyclic molecule, thiophenone.

Ultrafast ring-opening reactions driven by ultraviolet (UV) light play an important role in many chemical and biological processes. Thiophenone (C<sub>4</sub>H<sub>4</sub>OS) has been recently used as a model heterocyclic molecule for studying these reactions with time-resolved photoelectron spectroscopy (TRPES) [1] and ultrafast electron diffraction (UED) [2]. However, the TRPES approach provides only indirect structural information, whereas UED is yet to reach sub-100 fs temporal resolution required to directly image the ring-opening process.

Here, we present results of experiments that utilize Coulomb explosion (CE) by intense, femtosecond X-ray and near-infrared (NIR) laser pulses to map the ring-opening dynamics of thiophenone. Specifically, we excite the molecule to the S<sub>2</sub> electronically excited state using a UV pump pulse at 266 nm, which results in C-S bond extension, ring opening and ultrafast nonradiative decay via two conical intersections back to the electronic ground state, where different families of photoproducts are formed [1,2]. We probe the evolving molecular structure using multiple ionization and CE by X-ray or NIR probe pulses at various time delays and detecting four or more ionic fragments in coincidence [3]. Comparing the results with CE simulations, we find signatures of the ring opening in the delay-dependent angle between

the O<sup>+</sup> and S<sup>+</sup> momenta, and in molecular-frame proton emission patterns (see Fig. 1). While the data for the X-ray probe (above sulphur *Is* edge) manifest much higher signal to background ratio, the results obtained with the NIR probe reveal the dynamics unfolding on sub-100 fs time scale.

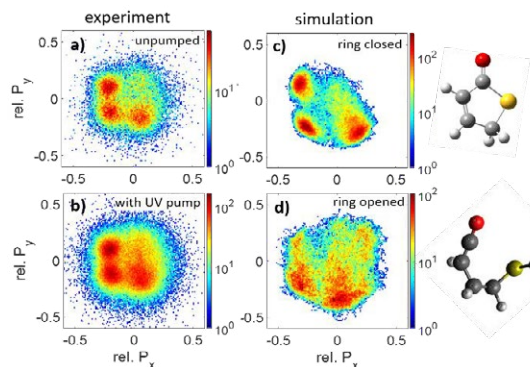


**Figure 1.** (a,b) Molecular-frame momentum distribution of protons from thiophenone after CE by intense 2.7 keV X-ray pulses. The data are shown for H<sup>+</sup> ions detected in coincidence with C<sup>+</sup>, O<sup>+</sup> and S<sup>+</sup>, where the S<sup>+</sup> momentum defines the +x direction, and (S<sup>+</sup>, O<sup>+</sup>) momenta define the molecular plane. (a) no pump (X-ray only data); (b) UV pump 500 ps before the X-ray probe. (c,d) CE simulations for ring-closed (c) and ring-opened (d) thiophenone.

### References

- [1] Pathak S et al. 2020 *Nature Chem.* **12**, 795-800
- [2] Nunes J P F et al. 2023, *submitted*
- [3] Boll R et al. 2022 *Nature Phys.* **18**, 423-428

\* E-mail: [keyu@phys.ksu.edu](mailto:keyu@phys.ksu.edu)

## Resonant Double-Core Excitation of N<sub>2</sub>

E Pelimanni<sup>1\*</sup>, A Fouda<sup>1</sup>, P Ho<sup>1</sup>, T Baumann<sup>2</sup>, A De Fanis<sup>2</sup>, S Dold<sup>2</sup>, I Ismail<sup>3</sup>, D Koulentianos<sup>4</sup>, T Mazza<sup>2</sup>, M Meyer<sup>2</sup>, M N Piancastelli<sup>3</sup>, R Püttner<sup>5</sup>, D Rivas<sup>2</sup>, B Senfftleben<sup>2</sup>, M Simon<sup>3</sup>, L Young<sup>1,6</sup>, and G Doumy<sup>1†</sup>

<sup>1</sup>Chemical Sciences and Engineering Division, Argonne National Laboratory, Lemont, IL 60439, USA

<sup>2</sup>European XFEL, Holzkoppel 4, 22869 Schenefeld, Germany

<sup>3</sup>Sorbonne Université, CNRS, Laboratoire de Chimie Physique-Matière et Rayonnement, LCPMR, F-75005 Paris, France

<sup>4</sup>Center for Free-Electron Laser Science, Deutsches Elektronen-Synchrotron DESY, Notkestraße 85, 22607 Hamburg, Germany & Department of Physics, Universität Hamburg, Luruper Chaussee 149, 22761 Hamburg, Germany

<sup>5</sup>Fachbereich Physik, Freie Universität Berlin, Arnimallee 14, D-14195 Berlin, Germany

<sup>6</sup>The James Franck Institute and Department of Physics, The University of Chicago, Chicago, IL 60637, USA

**Synopsis** We report on the experimental observation of a *resonant double-core excitation* process in the diatomic molecule N<sub>2</sub>, where a single few fs broad bandwidth XFEL pulse excites two 1s $\sigma_{g,u}$  core level electrons to the same unoccupied 1 $\pi_g^*$  molecular orbital and forms an exotic  $K^{-1}K^{-1}V^2$ -type neutral double core hole state.

In recent theoretical work by Fouda *et al.* [1], it was proposed that a single few fs soft X-ray Free Electron Laser (XFEL) pulse should be able to induce a so-called *resonant double-core excitation* process, where *two* core level electrons are sequentially promoted to the same unoccupied molecular orbital. Herein, with results obtained at the SQS instrument of the European XFEL, we report on the experimental observation of this process in N<sub>2</sub>. While the well-known first N<sub>2</sub> +  $h\nu \rightarrow$  N<sub>2</sub>(1s $\sigma_u^{-1}$ 1 $\pi_g^{*1}$ ) resonance lies at  $\sim$ 401 eV, the second N<sub>2</sub>(1s $\sigma_u^{-1}$ 1 $\pi_g^{*1}$ ) +  $h\nu \rightarrow$  N<sub>2</sub>(1s $\sigma_u^{-1}$ 1s $\sigma_g^{-1}$ 1 $\pi_g^{*2}$ ) step is red-shifted by  $\sim$ 1.5 eV. Applying  $\sim$ 15 fs pulses with a bandwidth of  $\sim$ 3.5 eV FWHM, both resonances could be simultaneously covered in a single pulse. Comparing low (Fig. 1 a) and high intensity (Fig. 1 b) X-rays, de-excitation from these double core hole (DCH) states was monitored with electron time of flight spectroscopy, while scanning the photon energy. The kinetic energies of the signature single- (DCH-SP) and double participator (DCH-PP) channels, and their red-shifted absorption maximum, are in good agreement with our electronic structure calculations (Fig. 1 c). Such multi-core excitation schemes should be general in small molecules and larger systems, enabling high cross section and state se-

lective resonant X-ray pump/probe schemes and the production of exotic neutral multi-core hole states which are inaccessible at weak fields.

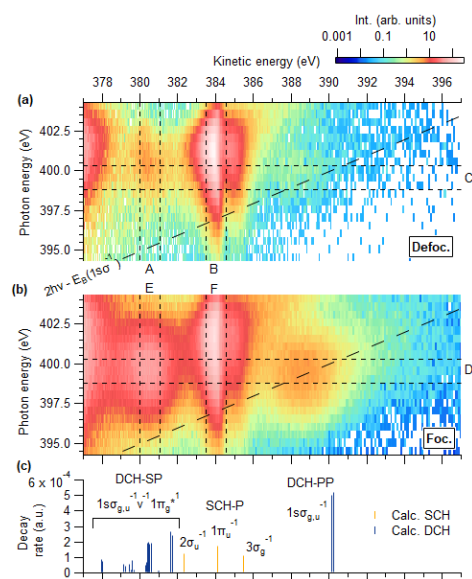


**Figure 1.** (a): Low X-ray intensity. (b): High X-ray intensity. (c): Calculated results.

### References

- [1] Fouda A *et al.* 2022 *Mol. Phys.* <https://doi.org/10.1080/00268976.2022.2133749>

\*E-mail: [epelimanni@anl.gov](mailto:epelimanni@anl.gov)

†E-mail: [gdoumy@anl.gov](mailto:gdoumy@anl.gov)

## Metrology of Attosecond Soft X-ray Pulses at European XFEL

Markus Ilchen<sup>1\*</sup>, Sadia Bari<sup>1,2</sup>, Thomas M. Baumann<sup>3</sup>, Rebecca Boll<sup>3</sup>, Markus Braune<sup>1</sup>, Francesca Calegari<sup>1</sup>, Alberto De Fanis<sup>3</sup>, Kristina Dingel<sup>4</sup>, Stefan Düsterer<sup>1</sup>, Felix Egun<sup>5</sup>, Arno Ehresmann<sup>4</sup>, Benjamin Erk<sup>1</sup>, Lars Funke<sup>6</sup>, Andreas Galler<sup>3</sup>, Gianluca Geloni<sup>3</sup>, Gesa Goetzke<sup>1</sup>, Tais Gorkhover<sup>7</sup>, Jan Grünert<sup>3</sup>, Patrik Grychtol<sup>3</sup>, Marc Guetg<sup>3</sup>, Andreas Hans<sup>4</sup>, Arne Held<sup>6</sup>, Ruda Hindrikson<sup>4</sup>, Moritz Hoesch<sup>1</sup>, Till Jahnke<sup>3,8</sup>, Reinhard Kienberger<sup>9</sup>, Stephan Kuschel<sup>7</sup>, Joakim Laksman<sup>3</sup>, Mats Larsson<sup>10</sup>, Jia Liu<sup>3</sup>, Jon Marangos<sup>5</sup>, Lutz Marder<sup>4</sup>, David Meier<sup>11</sup>, Michael Meyer<sup>3</sup>, Najmeh Mirian<sup>3</sup>, Jacobo Montaña<sup>3</sup>, Terence Mullins<sup>3</sup>, Valerija Music<sup>1,3,4</sup>, Christian Ott<sup>12</sup>, Thorsten Otto<sup>4</sup>, Yevheniy Ovcharenko<sup>3</sup>, Christopher Passow<sup>1</sup>, Thomas Pfeifer<sup>12</sup>, Nils Rennhack<sup>3</sup>, Daniel Rivas<sup>3</sup>, Daniel Rolles<sup>13</sup>, Artem Rudenko<sup>13</sup>, Patrick Rupprecht<sup>12</sup>, Sara Savio<sup>1,6</sup>, Albert Schletter<sup>9</sup>, Frank Scholz<sup>1</sup>, Jörn Seltmann<sup>1</sup>, Svitozar Serkez<sup>3</sup>, Philipp Schmidt<sup>3</sup>, Evgeny Schneidmiller<sup>1</sup>, Bernhard Sick<sup>4</sup>, Richard D. Thomas<sup>10</sup>, Kai Tiedtke<sup>1</sup>, Sergey Usenko<sup>3</sup>, Jens Viehhaus<sup>11</sup>, Peter Walter<sup>14</sup>, Vincent Wanie<sup>1</sup>, Niclas Wieland<sup>6</sup>, Lasse Wülfing<sup>8</sup>, Mikhail Yurkov<sup>1</sup>, Vitali Zhaunerchyk<sup>15</sup>, and Wolfram Helml<sup>6†</sup>

<sup>1</sup>Deutsches Elektronen-Synchrotron DESY, Germany

<sup>2</sup>University of Groningen, The Netherlands

<sup>3</sup>European XFEL, Schenefeld, Germany

<sup>4</sup>University of Kassel, Germany

<sup>5</sup>Imperial College London, United Kingdom

<sup>6</sup>Technical University of Dortmund, Germany

<sup>7</sup>University of Hamburg, Germany

<sup>8</sup>University of Frankfurt, Germany

<sup>9</sup>Technical University of Munich, Germany

<sup>10</sup>University of Stockholm, Sweden

<sup>11</sup>Helmholtz-Zentrum Berlin für Materialien und Energie, Germany

<sup>12</sup>Max-Planck Institut für Kernphysik, Heidelberg, Germany

<sup>13</sup>Kansas State University, Manhattan, USA

<sup>14</sup>SLAC National Accelerator Laboratory, Menlo Park, USA

<sup>15</sup>University of Gothenburg, Sweden

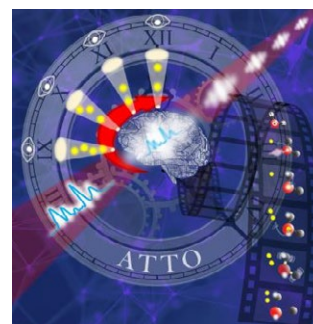
**Synopsis** Site-specifically exploring electron dynamics on time scales of fundamental processes like the Auger-Meitner decay and charge migration in molecular systems has recently been enabled by sub-femtosecond X-ray pulses of free-electron lasers. They uniquely allow for an efficient exploration of these hitherto inaccessible phenomena directly in time. Strategies to tackle their challenging metrology as well as first results from the recent atto-campaign at European XFEL will be presented.

How do electron dynamics evolve on their natural time scale between attoseconds and femtoseconds? How do they translate into and couple with chemical phenomena? How does this interplay of physics and chemistry ‘look’ like in real time and from element-specific observer sites?

Several answers to these questions can be obtained with ultrabright sub-femtosecond X-ray free-electron laser (XFEL) pulses which are at the cutting edge of today’s technological capabilities [1,2]. The European XFEL is the first high-repetition rate (X)FEL in the world that has very recently entered the attosecond regime as confirmed and directly measured in the time domain via angular streaking of photoelectrons from the neon core shell using 1 keV photons. The results of this first atto-campaign will be presented in the light of different machine operation modes and the imminently resulting scientific perspectives. An overview of instrumentation upgrades and machine advances at European

XFEL and DESY will complement the presentation. Scientific highlights for short-wavelength attosecond pulses in synergy with the versatile and rapidly evolving portfolio of FELs, e.g., in terms of polarization control, will be outlined.

**Figure 1.** Attosecond angular streaking analyzed via machine-learning techniques retrieves the full time-energy structure of XFEL pulses, thus enabling new perspectives on a novel storyline in molecular movies, i.e., electron dynamics [3].



### References

- [1] Hartmann N et al. 2018 *Nat. Photon.* **12** 215
- [2] Duris J et al. 2020 *Nat. Photon.* **14** 30
- [3] Dingel K et al. 2022 *Sci.Rep.* **12** 17809

\* E-mail: [markus.ilchen@desy.de](mailto:markus.ilchen@desy.de)

† E-mail: [wolfram.helml@tu-dortmund.de](mailto:wolfram.helml@tu-dortmund.de)

## XUV-induced dynamics in complex molecular ions in the gas phase

R Brédy<sup>1\*</sup>, A Boyer<sup>1</sup>, M Hervé<sup>1</sup>, I Compagnon<sup>1</sup> and F Lépine<sup>1</sup>

<sup>1</sup>Univ Lyon, Université Claude Bernard Lyon 1, CNRS, Institut Lumière Matière, F-69622, Villeurbanne, France

**Synopsis** We present experiments performed with extreme ultraviolet (XUV) high harmonic generation source to photoexcite large molecular ions produced by electrospray ionisation source. Light induced dissociative ionization and proton migration are observed in model systems. Following the XUV photoionization of large protonated molecules we measured ultrafast dynamics of few tens of femtoseconds. These ultrafast dynamics studies on large molecular ions offer new perspectives in attosecond science.

Intrinsic properties and dynamics of isolated systems such as molecules can be investigated on timescales ranging from picoseconds down to attoseconds by combining gas phase experiments with ultrafast technologies. Due to the high degree of sophistication required for such experiments, the dynamics of ultrafast processes induced by attosecond pulse light have been studied mostly on atomic or small neutral model systems. New questions were addressed from these experiments as well as from theoretical investigations, for example, on hole migration or on the role of electron correlation after excitation to highly excited electronic states of such systems [1, 2, 3].

However, in natural environment a majority of molecules carry a charge which has a strong influence on their electronic structure and global properties. While results on static properties of molecular ions, such as proteins, have been extensively reported for a broad range of electromagnetic radiations (from IR up to X-ray) to our knowledge none of these experiments have been able to measure realtime ultrafast processes involved in high energy photon excitation [4]. With ionization and/or excitation of molecular ions by high photon energy, new fundamental questions arise as for instance the dynamics of the native charge and its interaction with the charge created by photoionization.

In this context, we have developed a new experimental setup devoted to the study of ultrafast dynamics in complex and large mass-selected molecular ions. It combines an ultrashort tabletop XUV source based on high harmonic generation coupled to an electrospray ionization source

and "on-the fly" mass spectrometry. We observe light induced dissociative ionization and proton migration in model systems such as reserpine, insulin and cytochrome c [4]. Ultrafast dynamics of few tens of femtoseconds following the XUV photoionization of large protonated molecules have been observed [5, 6].

These first results on XUV-induced ultrafast dynamics in large molecular ions offer perspectives for applications in attochemistry [7] and challenge for theory interpretation.

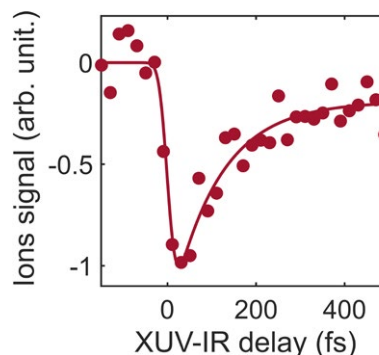


**Figure 1.** Time-dependent signal of fragment  $m/z$  414 from XUV photoionization of protonated reserpine.

### References

- [1] Nisoli M *et al.* 2017 *Chem. Rev.* **117** 10760-10825
- [2] Calegari F *et al.* 2014 *Science* **346** 336-339
- [3] Hervé M *et al.* 2021 *Nat. Phys.* **17** 327-331
- [4] Hervé M *et al.* 2022 *Sci. Rep.* **12** 13191
- [5] Boyer A 2022 *PhD Thesis, Univ Lyon, France*
- [6] *To be submitted*
- [7] Hervé M *et al.* 2022 *Adv. Phys.-X* **7** 212328

\*E-mail: [richard.bredy@univ-lyon1.fr](mailto:richard.bredy@univ-lyon1.fr)

## Mass spectrometry at the limits of biological objects: viruses, bacteria and amyloid fibers

S Maclot<sup>1\*</sup>, R Antoine<sup>1†</sup> and P Dugourd<sup>1</sup>

<sup>1</sup>Institut Lumiere Matiere UMR 5306, Université Claude Bernard Lyon 1, CNRS, Univ Lyon, F-69100 Villeurbanne, France

**Synopsis** This project aims to develop both an analytical chemistry approach to characterize bioparticles by charge detection mass spectrometry, and to push the limits of photo-fragmentation induced by laser irradiation on intact viruses or other bioparticles (bacteria or amyloid fibers) to develop new structural characterization tools.

Bioparticles consisting of self-organized biomolecular assemblies are ubiquitous in nature. Viruses are a good example of this and are the most abundant and robust biological entities on Earth.

New electrostatic traps (Benner trap) based on charged detection mass spectrometry (CDMS) have recently been set up to carry out fragmentation experiments on selected ions with masses up to several GigaDalton [1]. One of this setup has been developed in the SpectroBio group of iLM at University of Lyon 1 - FR, allow coupling with a laser and performing infrared multiphoton dissociation, monitoring fragmentation and determining the activation energy of unimolecular dissociation of bioparticles and whole DNAs [2, 3, 4].

A large part of this project will be to develop both an analytical chemistry approach to characterize bioparticles by mass spectrometry, and to push the limits of photo-fragmentation induced by laser irradiation on intact viruses or other bioparticles (bacteria or amyloid fibers) to develop new structural characterization tools.

This project is part of the FET-OPEN **ARIADNE VIBE** (Airborne Ion Analysis with Dissociation and Non-destructive Evaluation of Viruses and Bacteria – Grant agreement 964553)

funded by Europe on the characterization of viruses and bacteria using CDMS technique.

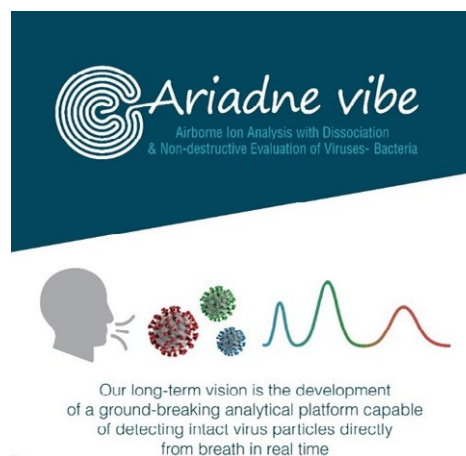


Figure 1. ARIADNE VIBE project.

### References

- [1] T Doussineau et al. *Rapid Commun. Mass Spectrom.* **25** 617 (2011)
- [2] R. Antoine et al. *Phys. Rev. A* **87** 013435 (2013)
- [3] T. Doussineau et al. *J. Phys. Chem. Lett.* **3** 2141 (2012)
- [4] T. Doussineau et al. *J. Am. Soc. Mass Spectrom.* **26** 7 (2015)

\*E-mail: [sylvain.maclot@univ-lyon1.fr](mailto:sylvain.maclot@univ-lyon1.fr)

†E-mail: [rodolphe.antoine@univ-lyon1.fr](mailto:rodolphe.antoine@univ-lyon1.fr)



## Observation of $H_3^+$ formation from molecular hydrogen dimers

Y Mi<sup>1\*</sup>, E Wang<sup>2,3</sup>, Z Dube<sup>1</sup>, T Wang<sup>1</sup>, A Yu Naumov<sup>1</sup>, D M Villeneuve<sup>1</sup>, P B Corkum<sup>1</sup> and A Staudte<sup>1</sup>

<sup>1</sup>Joint Attosecond Science Laboratory, National Research Council and University of Ottawa, 100 Sussex Drive, Ottawa K1A 0R6, Canada

<sup>2</sup>Hefei National Research Center for Physical Sciences at the Microscale and Department of Modern Physics, University of Science and Technology of China, Hefei 230026, China

<sup>3</sup>Max Planck Institut für Kernphysik, Saupfercheckweg, 1, 69117 Heidelberg, Germany

**Synopsis** We experimentally demonstrate that the trihydrogen cation ( $H_3^+$ ) can be produced via single photoionization of the molecular hydrogen dimer ( $H_2-H_2$ ). Using near-infrared, femtosecond laser pulses and coincidence momentum imaging, we find that the dominant channel after single ionization of the dimer is the ejection of a hydrogen atom, resulting in the formation of an  $H_3^+$  cation. The formation mechanism is supported and reproduced by an ab-initio molecular dynamics simulation.

$H_3^+$  (trihydrogen cation) is one of the most important molecular ions in the universe, as it plays a critical role in a variety of astrophysical processes [1]. It is primarily produced in the interstellar medium through the ion-molecule reaction between  $H_2$  and  $H_2^+$  following ionization of  $H_2$  by cosmic rays. However, this pathway alone cannot explain the  $H_3^+$  abundance in molecular clouds [2].

In this study, we investigated the formation of the deuterated version of  $H_3^+$ ,  $D_3^+$ , using both experimental and computational methods. We prepared  $D_2$  dimers in a cold molecular beam through supersonic expansion of  $D_2$  gas into a high-vacuum chamber using a 10- $\mu\text{m}$  nozzle and skimmer. We used a cold-target recoil-ion momentum spectroscopy (COLTRIMS) reaction microscope to measure the time-of-flight (TOF) and photoion-photoion coincidence (PiPiCo) spectra.

In Figure 1A, the primary peak corresponds to  $D_2^+$  resulting from the single ionization of  $D_2$  molecules in the gas jet. Multiple peaks centered around 1590 ns in the spectrum represent  $D^+$  ions ejected during  $D_2^+$  dissociation. Additionally, a broad peak with a mass-to-charge ratio of 6 was observed at around 2750 ns, providing the first evidence of  $D_3^+$  production from  $D_2-D_2$ .

The PiPiCo spectrum, displayed in Fig. 2B, exhibits correlations of  $D_2^+ + D_2^+$  and  $D^+ + D_3^+$ , in addition to the  $D^+ + D^+$  correlation that indicates Coulomb explosion of  $D_2$  molecules. These two channels originate from the double

ionization and subsequent break-up of  $D_2$  dimers, confirming the pathway of  $D_3^+$  formation.

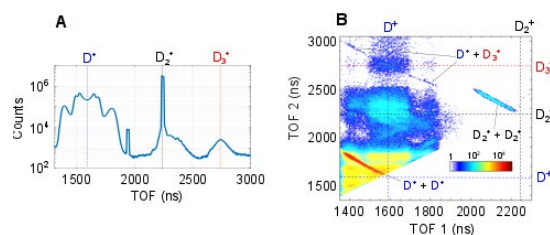


**Figure 1.** (A) Measured time-of-flight (TOF) spectrum of the photoions. (B) Measured photoion-photoion coincidence (PiPiCo) spectrum

To further support this finding, we calculated the potential energy surface of the  $D_2-D_2$  dimer [2] and discovered that  $D_2-D_2^+$  was an unstable molecular ion that dissociated into  $D_3^+$  and  $D$  after removing one electron from the dimer. Additionally, we conducted an ab-initio molecular dynamics simulation to extract temporal information on the  $D_3^+$  formation. The simulation involved 1000 trajectories, with 892 of them resulting in  $D_3^+$  formation. This result agrees with the experimental conclusion that single photoionization of  $D_2-D_2$  dimer is an effective mechanism for  $D_3^+$  formation.

### References

- [1] Geballe, T. R. and Oka, T. *Science* **312**, 1610-1612 (2006).
- [2] Mi, Y *et al.*, *Nat. Chem.* (accepted)

\* E-mail: [yumi@uottawa.ca](mailto:yumi@uottawa.ca)



## Coincidence Measurements of Photodouble Ionization of Thiophene

N L Wong<sup>1\*</sup>, J Howard<sup>1</sup>, E Sokell<sup>1</sup>, P Bolognesi<sup>2</sup> and L Avaldi<sup>2</sup>

<sup>1</sup>School of Physics, Science Centre North, University College Dublin, Belfield Dublin 4, Ireland

<sup>2</sup>CNR-Istituto di Struttura della Materia, Area della Ricerca di Roma 1, 00015 Monterotondo Scalo, Italy

**Synopsis** New photodouble ionization (PDI) triple differential cross sections (TDCS) of thiophene have been measured under equal energy sharing conditions ( $KE_1=KE_2=10$  eV). A method to compare the TDCS for benzene and thiophene at 10 and 20 eV equal energy sharing conditions is discussed.

Photodouble ionization (PDI) arises from electron-electron correlation and proceeds via either a direct “knock-out” process or a resonant mechanism involving either a neutral or singly ionized state [1]. The interpretation of PDI in aromatic hydrocarbons and aromatic heterocyclic molecules, like benzene ( $C_6H_6$ ) and thiophene ( $C_4H_4S$ ) [2], have suggested mechanisms beyond direct “knock-out” may exist. Our team has measured the triple differential cross section (TDCS) of benzene and thiophene to investigate the PDI mechanisms in detail.

TDCS models have yielded electron correlation and kinematic information for atomic cases [1,3], but these models have not yet been extended to more complicated molecules. Presented here are the measured PDI TDCS for thiophene and a path to a simple model to describe the data and enable comparisons, until a more complete theoretical model exists.

The experiment was done at the GasPhase beamline at the Elettra Synchrotron, with freeze-pump-thawed samples. 9 hemispherical analyzers were mounted  $30^\circ$  apart, with 3 on a stationary frame and 6 on a rotatable frame. Bolognesi et al. have described the data acquisition and processing details [3]. Figure 1 is the TDCS of thiophene for electrons coincident with ones at the  $60^\circ$  fixed analyzer.  $0^\circ$  is the polarization vector of the linearly polarized synchrotron light. The TDCS was taken at 10 eV equal energy sharing conditions and displays lobes in the half plane opposite the fixed analyzer, including back-to-back emission. For the simplest model of He at equal energy sharing, back-to-back emission is forbidden [1], but it has been observed in unequal energy sharing for He [3] and in less common residual noble gas ions [4]. Implementation of a back-to-back emission model to describe the data is ongoing.

The present equal energy sharing measurements and previous ones of thiophene at 20 eV and benzene at 10 and 20 eV will be compared to lend insight into electron correlation differences in these molecules and into the non-direct “knock-out” PDI contributions observed for symmetric hydrocarbons [2].

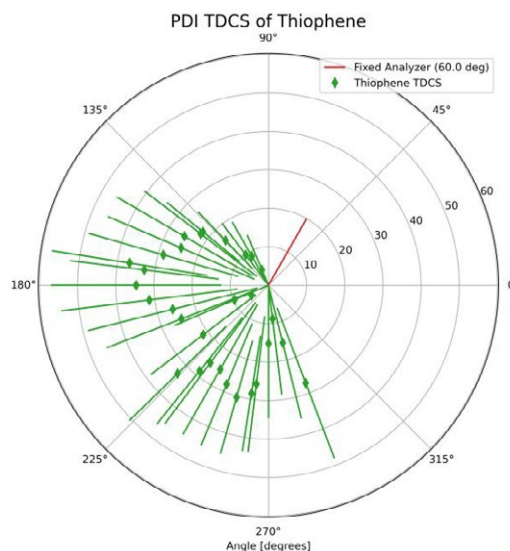


**Figure 1.** PDI (46.5 eV) TDCS of thiophene (3 point smoothed) under equal energy sharing conditions (green diamonds) and the fixed analyzer angle (solid red line).

### References

- [1] Avaldi L and Huetz A 2005 *J. Phys. B: At. Mol. Opt. Phys.* **38** S861
- [2] Wehlitz R 2016 *J. Phys. B: At. Mol. Opt. Phys.* **49** 222004
- [3] Bolognesi P et al 2004 *J. of Electron Spectrosc. Relat. Phenom.* **141** 105
- [4] Mazeau J et al 1997 *J. Phys. B: At. Mol. Opt. Phys.* **30** L293

\* E-mail: [nicholas.wong1@ucdconnect.ie](mailto:nicholas.wong1@ucdconnect.ie)

## On the role of isomerisation in the photo dissociation of PANHs : A casestudy with methyl amidogen abstraction

S. Arun<sup>1\*</sup>, K. Ramanathan<sup>1</sup>, S. Muthuamirthambal<sup>1</sup>, R. Richter<sup>2</sup>, N. Pal<sup>2</sup>, J. Chiarinelli<sup>3</sup>, P. Bolognesi<sup>3</sup>, L. Avaldi<sup>3</sup>, M. V. Vinitha<sup>1</sup>, C. S. Jureddy<sup>1</sup>, and U. Kadhane<sup>1†</sup>

<sup>1</sup>Indian Institute of Space Science and Technology, Thiruvananthapuram 695547, Kerala, India.

<sup>2</sup>Elettra-Sincrotrone Trieste, Strada Statale 14 - km 163,5 in AREA Science Park, Basovizza, TS 34149, Italy.

<sup>3</sup>CNR-Istituto di Struttura della Materia, Area della Ricerca di Roma 1, Monterotondo, Roma 00015, Italy.

**Synopsis** Results of velocity map imaging experiments using synchrotron light source with 3-methyl-quinoline and 2 naphthylamine is presented. An astronomically important molecule, ie the methyl amidogen radical loss in case of the monocation and ion in case of the dication loss is identified as the dominant fragmentation channel in both molecules using Ion-neutral and Ion-Ion coincidence maps and photo-electron-photo-ion coincidence curves. Experimental signatures highly indicative of common isomerisation mechanisms preceding dissociation is also discussed using the methyl amidogen loss channel.

The role of polycyclic aromatic hydrocarbons (PAH) and their nitrogenated counterparts (PANH) in shaping the molecular evolution of the universe can hardly be overstated [1]. Furthermore, the first direct detection of two of these molecules in the Taurus molecular cloud [2] recently, which in itself is a dynamically evolving environment, only reinforces the importance of understanding the response of these molecules to the harsh radiation conditions prevalent in space.

With this in the background, a series of velocity map imaging experiments were performed at the Elettra-Sincrotrone Trieste on the gas-phase beamline with 2-naphthylamine and 3-methyl quinoline. Photon energies of 21 eV to 48 eV was used to record the photo electron photo ion spectra, so that the decay dynamics of both the mono-cation and the di-cation was captured. Along with this, kinetic energy release distributions (KERD) and ion-ion coincidence maps were obtained.

For both molecules in both charge states, the loss of methyl amidogen (HCNH) was found to be the dominant channel by far. In case of the monocation, this reflects as a peak at  $m/z = 115$  amu. The loss of an intact HCNH was assigned to be the channel responsible for the peak, rather than sequential losses of HCN and hydrogen on the basis of a detailed analysis into the binding energy curves using a unique procedure. Further-

more this was reaffirmed using the ion-neutral traces found on the ion-ion coincidence maps, which was confirmed using complimentary ion-optic simulations. In case of the dication, the loss of the  $\text{HCNH}^+$  ion manifested as the most dominant island with a metastable tail in the two dimensional time of flight correlation spectra.

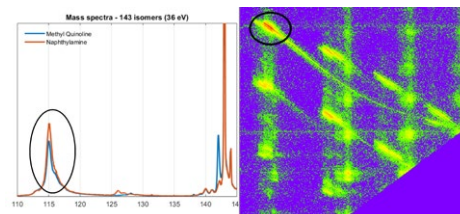


**Figure 1.** HCNH loss (circled) in the mass spectra and 2D ToF correlation spectra of 2-naphthylamine and 3-methyl quinoline.

Furthermore, a comparison of the binding energy curves and KERD of the two molecules reveal remarkable similarities in their decay dynamics. These experimental signatures collectively hint towards a role of a common isomerisation mechanism that underlines the fragmentation of the two molecules.

### References

- [1] Tielens, A. G. G. M. 2013 *Rev. Mod. Phys.* **85** 1021
- [2] McGuire, B. A et.al. 2021 *Science* **371** 1265

\*E-mail: [arun.sc18b149@ug.iist.ac.in](mailto:arun.sc18b149@ug.iist.ac.in)

†E-mail: [umesk@iist.ac.in](mailto:umesk@iist.ac.in)

## Diatomic molecular vibrations in a strong infrared laser field: an analytic treatment of the laser-dressed Morse potential

Sz Hack<sup>1,2\*</sup>, S Varró<sup>1,3</sup>, G Paragi<sup>2,4,5</sup>, P Földi<sup>1,2</sup>, I F Barna<sup>3</sup>, and A Czirják<sup>1,2</sup>

<sup>1</sup> ELI ALPS, ELI-HU Non-Profit Ltd., Szeged, H-6728, Hungary

<sup>2</sup> Department of Theoretical Physics, University of Szeged, H-6720 Szeged, Hungary

<sup>3</sup> Wigner Research Centre for Physics, H-1121 Budapest, Hungary

<sup>4</sup> Institute of Physics, University of Pécs, H-7624 Pécs, Hungary

<sup>5</sup> Department of Medical Chemistry, University of Szeged, H-6720 Szeged, Hungary

**Synopsis** A general mathematical procedure to treat a Morse potential in the presence of a strong harmonic excitation is presented. Permanent and field-induced dipole moments and their gradients are included in the interaction term of the molecular Hamiltonian. Analytic formulae for the bond-length change and for the shifted energy eigenvalues of the Morse potential are derived by using the Kramers-Henneberger frame. Our results are applied to the important cases of H<sub>2</sub> and LiH, driven by a near- or mid-infrared laser field in the 10<sup>13</sup> W/cm<sup>2</sup> intensity range.

Diatomic molecules driven by strong laser pulses show a rich variety of fundamentally important processes, depending on how the laser pulse parameters are related to the diatomic's properties. Although the theoretical framework for molecules interacting with laser fields is well established, analytic methods are rare and approximate in the strong-field domain, while most of the numerical methods have heavily increasing cost for infrared (IR) wavelength [1, 2].

In this contribution we present a general mathematical method to treat a Morse potential in the presence of a strong IR excitation. The dipole moment function in the Hamiltonian includes the permanent and the field-induced terms and their gradients, which is verified by density-functional theory calculation. Therefore, our model can be applied both to heteronuclear and to homonuclear diatomic molecules and to certain (e.g. alkali metal) atomic dimers. As a possible use we apply our procedure to H<sub>2</sub> and LiH and we show how an IR laser field in the intensity range of 10<sup>13</sup> W/cm<sup>2</sup> noticeably shifts the vibrational levels (see figure 1) and the equilibrium internuclear distance of the molecules. According to our results, the dipole gradient and the polarizability gradient are the essential molecular parameters in these effects. We give the exact analytic vibrational levels and bond-length change of a diatomic molecule utilizing the Kramers-Henneberger frame which are valid in a wide wavelength range [3].

\*E-mail: [szabolcs.hack@eli-alps.hu](mailto:szabolcs.hack@eli-alps.hu)

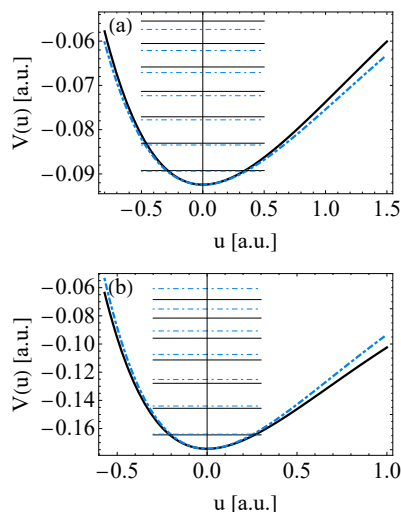


**Figure 1.** The field-free and the laser-dressed Morse potential of LiH (a) and H<sub>2</sub> (b) plotted by black solid curve and blue dash-dotted curve, respectively. The horizontal lines with corresponding styles mark the first seven energy levels of the corresponding Morse potential. The parameters of the laser field are  $I_0 = 2.8 \cdot 10^{13}$  W/cm<sup>2</sup> and  $\lambda = 1500$  nm.

### References

- [1] Palacios A, Sanz-Vicario J L and Martín F 2015 *J. Phys. B* **48** 242001
- [2] Molnár B, Földi P, Benedict M G and Bartha F 2003 *EPL* **61** 445–451
- [3] Varró S, Hack Sz, Paragi G, Földi P, Barna I F and Czirják A 2023 (*submitted*) [arXiv: 2303.04858](https://arxiv.org/abs/2303.04858)

## Fragmentation of methanol molecules after valence photoexcitation studied by negative-ion positive-ion coincidence spectroscopy

H Sa'adeh<sup>1,2\*</sup>, A Kivimäki<sup>2,3</sup>, C Stråhlman<sup>4</sup>, K C Prince<sup>5</sup>, and R D Thomas<sup>6</sup>

<sup>1</sup>Department of Physics, The University of Jordan, Amman 11942, Jordan

<sup>2</sup>MAX IV Laboratory, Lund University, Lund 22100, Sweden

<sup>3</sup>Nano and Molecular Systems Research Unit, University of Oulu, Oulu 90014, Finland

<sup>4</sup>Malmö University, Malmö 20506, Sweden

<sup>5</sup>Elettra Sincrotrone Trieste, Area Science Park, Basovizza, Trieste, Italy

<sup>6</sup>Department of Physics, Stockholm University, Stockholm 106 91, Sweden

**Synopsis** Ionic fragmentation of methanol upon valence photoexcitation has been studied using time-of-flight (TOF) mass spectrometry and negative-ion positive-ion coincidence (NIPICO) spectroscopy. The NIPICO spectra were utilized to determine the appearance energies and yields of different ion pair channels.

One of the main advantages of using negative-ion positive-ion coincidence (NIPICO) spectroscopy is the ability to determine ion-pair appearance energies, rather than just the appearance energy of the negative ion, as it is the case in conventional negative ion spectroscopy. This enhances the understanding of the fragmentation dynamics. In this work, we report results on ionic fragmentation upon valence photoexcitation of the simplest aliphatic alcohol, methanol ( $\text{CH}_3\text{OH}$ ,  $m = 32$  u). Methanol is an interesting organic compound; it is an interstellar molecule, a clean energy resource, and the chemical building block for hundreds of everyday products. It also serves as a good candidate for photodissociation studies due to its simple structure.

NIPICO spectra at C 1s and O 1s resonances were previously measured for methanol [1]. To our knowledge, there have been no reports on formation of negative ions in photon-excited methanol molecules in the valence region, which we report in this contribution.

Measurements were performed at the gas-phase end station (GPES) of the FinEstBeAMS beamline [2] in MAX IV Laboratory, Lund, Sweden, using the NIPICO setup where two time-of-flight (TOF) spectrometers are mounted opposite one another: One of these is for positive ions, and the other for negative ions and electrons. We have measured NIPICO spectra at several selected ranges of photon energy in the VUV region, by collecting coincidence signals at each photon energy for one hour. The obtained NIPICO spectra (e.g., Figure 1) revealed the following fragmentation channels (i.e., ani-

on/cation pairs):  $\text{H}/\text{H}^+$  (after 18.8 eV excitation),  $\text{OH}/\text{CH}_3^+$ ,  $\text{H}/\text{CHO}^+$ ,  $\text{H}/\text{CH}_2\text{O}^+$ , and  $\text{H}/\text{CH}_3\text{O}^+$ .

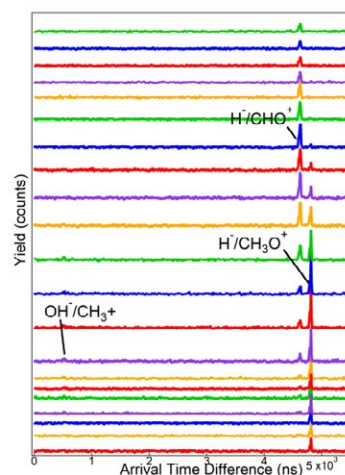


**Figure 1.** NIPICO spectra of methanol, measured at photon energies 13.0-16.4 eV (from bottom to top). [3]

### Acknowledgements

HS acknowledges a 3-month SESAME-MAX IV Exchange Scholarship awarded by the Swedish Institute, Stockholm, Sweden, and the one-year sabbatical leave (2022-2023) granted by the University of Jordan, Amman, Jordan.

### References

- [1] Kivimäki A *et al* 2018 *J. Phys. Chem. A* **122** 224
- [2] Kooser K *et al* 2020 *J. Synchrotron Radiat.* **27** 1080
- [3] Sa'adeh H *et al* In preparation.

\* E-mail: [Hanan.Saadeh@ju.edu.jo](mailto:Hanan.Saadeh@ju.edu.jo)

## Unexpected enhanced terahertz radiation in two-foci cascading plasmas

Jing Jing Zhao<sup>1,2</sup>, Yizhu Zhang<sup>3\*</sup>, Yanjun Gao<sup>1,2</sup>, Meng Li<sup>4</sup>, and Yuhai Jiang<sup>1,4†</sup>

<sup>1</sup>Shanghai Advanced Research Institute, Chinese Academy of Sciences, Shanghai, 201210, China

<sup>2</sup>University of Chinese Academy of Sciences, Beijing, 100049, China

<sup>3</sup>Center for Terahertz Waves and School of Precision Instrument and Optoelectronics Engineering, Tianjin University, Tianjin, 300072, China

<sup>4</sup>Center for Transformative Science and School of Physical Science and Technology, Shanghai Tech University, Shanghai, 201210, China

**Synopsis** We found that, when the foci of two-color beams are noticeably separated along the propagation axis resulting in cascading plasmas, the THz conversion efficiency is surged by one order of magnitude and the bandwidth is stretched by more than two times, achieving  $10^{-3}$  conversion efficiency and  $>100$  THz bandwidth under the condition of 800/400 nm,  $\sim 35$  fs driving lasers. With the help of the pulse propagation equation and photocurrent model, the observations can be partially understood by the compromise between THz generation and absorption due to the spatial redistribution of laser energy in cascading plasmas.

The temporal and spatial mixing of strong fundamental frequency ( $\omega$ ) and second harmonic ( $2\omega$ ) laser fields in a gas-phase medium can produce an ultrashort terahertz (THz) pulse [1]. The bright broadband THz radiation has applications in broadband spectroscopy, atomic and molecular ultrafast imaging, etc [2].

beams are, respectively, focused by two identical lenses with 10 cm focus length. (b) THz bandwidth versus  $d$  between two-color plasmas.

We found, when the two-color plasmas are concentrically separated along the propagation axis into cascading plasmas, the characteristics of THz radiation is significantly improved. Therefore, we introduce a new control knob, the distance between the two-color foci, to considerably increase the yield and bandwidth of THz emission. The experimental schematics is shown in Fig. 1(a).

The THz spectral features  $I_{\text{THz}}$  at  $I_{\omega} = 870 \mu\text{J}$ ,  $I_{2\omega} = 460 \mu\text{J}$  are measured with Fourier transform spectroscopy, as shown in Fig. 1(b). The spectral measurement shows that, when varying  $d$  between two-color plasmas, the THz bandwidth is significantly broadened above 100 THz. And the THz conversion efficiency is surged by one order of magnitude.

In conclusion, we introduce a new control knob, the distance between the two-color cascading plasmas, to promote THz radiation in the two-color scheme. With the distance appropriately optimized, the THz conversion efficiency reaches  $\sim 10^{-3}$  and the bandwidth can be broadened to  $>100$  THz with an 800 nm, 35 fs laser pulse [3].

### References

- [1] Cook, D.J et al 2000 *Opt. Lett.* **25** 1210-1212
- [2] Tonouchi M 2007 *Nature Photon* **1**. 97-105
- [3] Yizhu Zhang et al 2022 *Opt. Lett.* **47** 3816

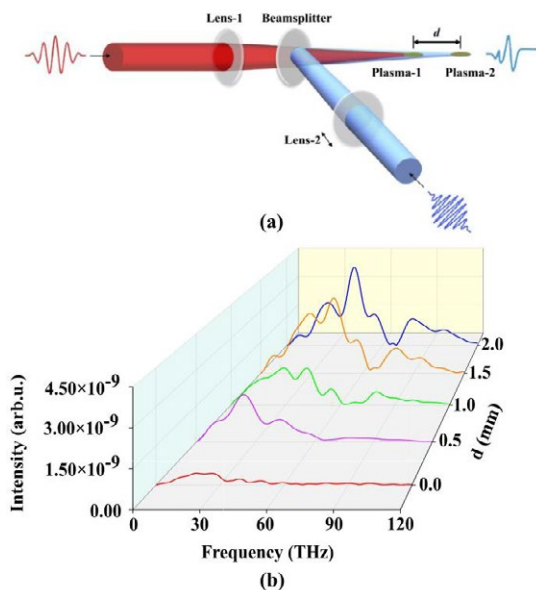


**Figure 1.** (a) Experimental schematics of ultra-broadband THz amplification. The  $\omega$  and  $2\omega$

\* E-mail: [zhangyizhu@tju.edu.cn](mailto:zhangyizhu@tju.edu.cn)

† E-mail: [jiangyh3@shanghaitech.edu.cn](mailto:jiangyh3@shanghaitech.edu.cn)



## Realtime tracking of ultrafast dynamics in liquid water

G Giovannetti<sup>1\*</sup>, S Ryabchuk<sup>2,3</sup>, A bin Wahid<sup>1</sup>, H Y Chen<sup>4</sup>, E P Maansson<sup>1</sup>, A Trabattoni<sup>1,5</sup>, V Wanie<sup>1</sup>, H Marroux<sup>6</sup>, M Chergui<sup>4</sup> and F Calegari<sup>1,2,3</sup>

<sup>1</sup>Center for Free-Electron Laser Science, Deutsches Elektronen-Synchrotron DESY, Notkestr. 85, 22607 Hamburg, Germany

<sup>2</sup>Physics Department, University of Hamburg, Luruper Chaussee 149, 22761 Hamburg, Germany

<sup>3</sup>The Hamburg Centre for Ultrafast Imaging, Universität Hamburg, 22761 Hamburg, Germany

<sup>4</sup>Ecole Polytechnique Fédérale de Lausanne, Rte Cantonale, 1015 Lausanne, Switzerland

<sup>5</sup>Institute of Quantum Optics, Leibniz Universität Hannover, Welfengarten 1, 30167 Hannover, Germany

<sup>6</sup>Laboratoire Interactions, Dynamiques et Lasers, CEA-Saclay, 91191 Gif-sur-Yvette, France

**Synopsis** The ultrafast vibrational dynamics of liquid water, initiated via Impulsive Stimulated Raman Scattering (ISRS) by a sub-4 fs NIR pump pulse in the ground state of the molecule, is revealed with unprecedented time resolution via transient absorption of sub-2 fs UV pulses. The coherent signal is dominated by the O-H stretching mode and decays in 25 fs, revealing an extremely fast dephasing of this mode.

Understanding the properties of aqueous solutions is a key first step in determining the effects of the liquid environment on the chemical reactions occurring in biological systems, for this reason vibrational relaxation and therefore energy dissipation in liquid water have been intensely investigated [1, 2].

Pump-probe spectroscopy is a powerful technique allowing the realtime investigation of the combined electronic and vibrational dynamics occurring in photoexcited water. So far, pump-probe measurements performed in liquid water have been limited to a time resolution of a few tens of femtoseconds [3].

Here, we present a time-resolved investigation of the vibrational dynamics initiated in liquid water by a sub-4 fs near-infrared (NIR) pump pulse. The rapid evolution of the vibrational wave packet, created by impulsive stimulated Raman excitation in the ground state of the molecule, is then probed with unprecedented time resolution by monitoring the transient absorption using sub-2 fs UV probe pulses [4]. In our experiment, the NIR pump and UV probe pulses are focused on a thin liquid jet operating in vacuum. The transmitted UV probe pulse is recorded as a function of the pump-probe delay.

A preliminary analysis of our data shows an oscillatory transient signal with a period of 10 fs and a decay time of 25 fs. These values match the ones expected for the O-H stretching mode in the ground

electronic state of liquid bulk water [5], here measured for the first time in the time domain. The large bandwidth of our UV pulses allows to probe the dynamics in different spectral regions. In particular, the blue and red sides of the transient absorption exhibit out-of-phase oscillations between positive and negative values.

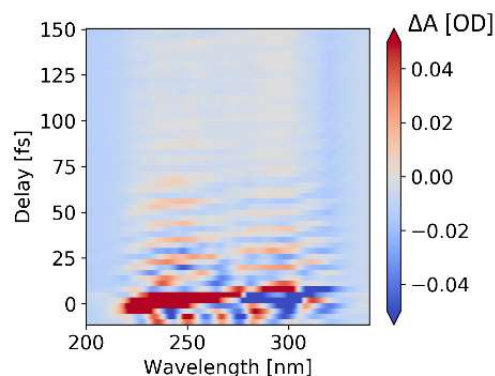


**Figure 1.** Colormap of the measured transient absorption signal as a function of the UV probe wavelength and the pump-probe time delay.

Further theoretical insights will allow us to assign specific contributions from the ground, excited and ionized states.

### References

- [1] Nagata Y 2015 *Phys. Rev. X* 5 021002
- [2] Yun CC 2020 *Nat Commun* 11 5977
- [3] Lindner J 2006 *Chem. Phys. Lett.* 421 4-6 329-333
- [4] Galli M 2019 *Opt. Lett.* 44 1308-1311
- [5] Liu J J. *Chem. Phys.* 2011 135 244503

\* E-mail: [gaia.giovannetti@cfel.de](mailto:gaia.giovannetti@cfel.de)



## Enhanced cutoff energies in strong-field photoelectron emission of plasmonic nanoparticles

E. Saydanzad<sup>1\*</sup>, J. A. Powell<sup>1,2</sup>, A. Rudenko<sup>1</sup>, and U. Thumm<sup>1†</sup>

<sup>1</sup>Department of Physics, Kansas State University, Manhattan, Kansas 66506, USA

<sup>2</sup> INRS, Énergie, Matériaux et Télécommunications, 1650 Bld. Lionel Boulet, Varennes, Québec, J3X1S2, Canada

**Synopsis** We measured and modeled strong-field photoelectron (PE) emission from metal nanoparticles (NPs), scrutinizing the interplay of the incident and induced plasmonic electric fields, PE interactions with residual positive charges, Coulomb repulsion between PEs, and PE rescattering and recombination. Compared to well-understood cutoff energies for strong-field photoemission from gaseous atomic targets, our measured and simulated PE spectra reveal a dramatic increase of two orders of magnitude with a higher contribution from direct PE emission, due to the presence of strong PE Coulomb repulsion.

We measured [1] and numerically simulated [2] velocity-map-image (VMI) PE spectra by exposing prototypical spherical gold NPs to intense short laser pulses in the infrared spectral regime. We examine the sensitivity of VMI spectra and cutoff energies to competing elementary interactions (incident and induced plasmonic electric field interactions, PE interactions with residual positive charges, and Coulomb repulsion between PEs) for direct and rescattered photoemission pathways.

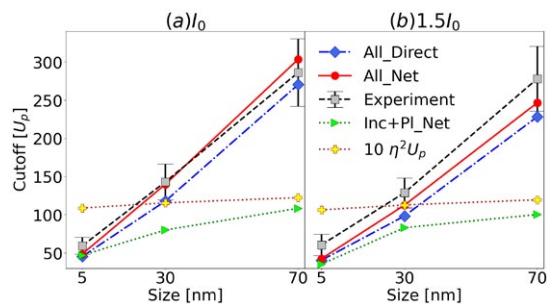


**Figure 1.** Comparison of simulated and experimental photoelectron cutoff energies scaled by the incident-laser ponderomotive energy  $U_p(I_0)$  for 5, 30, and 70 nm diameter gold nanospheres and laser peak intensities of (a)  $I_0 = 8.0 \times 10^{12} \text{ W/cm}^2$  and (b)  $1.5 I_0$ .

Figure 1 display calculated cutoff energies including all the interactions for, respectively, direct (denoted as 'All\_Direct') and net (denoted

as 'All\_Net', i.e., direct and rescattered) photoemission. Overall, our most comprehensive 'All\_Net' numerical simulations agree in trend and - either within or close to the experimental error bars - with our measured data [2]. Simulations only including incident- and plasmonic-field interactions are denoted as 'Inc+Pl\_Net'. Yellow 'plus' markers show gas-phase atomic cutoff energies,  $10 U_p$ , scaled by the plasmonic intensity enhancement  $\eta^2$ .

Our findings reveal that the cutoff energy is dramatically increased by two orders of magnitude, compared to well-understood rescattering PE cutoff energies for strong-field photoemission from gaseous atomic targets. Additionally, our results indicate a significantly higher contribution from direct photoemission, with direct PEs reaching up to 93% of the rescattered electron cutoff energy, compared to only 20% for gaseous atoms. These findings suggest a novel approach for developing compact tunable tabletop electron sources.

*This work was supported by the National Science Foundation and the AFO-SR program of Department of Defense.*

### References

- [1] E. Saydanzad *et al.* 2023 submitted to *Nanophotonics*
- [2] E. Saydanzad, J. Li, and U. Thumm 2022 *Phys. Rev. A* **106**, 033103
- [3] J. A. Powell *et al.* 2022 *ACS Photonics* **9**, 3515

\*E-mail: [e.saydanzad@phys.ksu.edu](mailto:e.saydanzad@phys.ksu.edu)

†E-mail: [thumm@phys.ksu.edu](mailto:thumm@phys.ksu.edu)

## Nonadiabatic Tunneling of Photoelectrons Induced by Few-Cycle Near-Fields

B Lovász<sup>1</sup>, V Hanus<sup>1</sup>, P Sándor<sup>1</sup>, G Z Kiss<sup>1</sup>, B Bánhegyi<sup>1</sup>, Z Pápa<sup>1,2</sup>, J Budai<sup>2</sup>, C Priet<sup>3</sup>, J R Krenn<sup>3</sup>, and P Dombi<sup>1,2\*</sup>

<sup>1</sup>Institute for Solid State Physics and Optics, Wigner RCP, 1121 Budapest, Hungary

<sup>2</sup>ELI-ALPS Research Institute, ELI-HU Nonprofit Kft., Szeged, 6720, Hungary

<sup>3</sup>Institute of Physics, Universität of Graz, Graz, 8010, Austria

**Synopsis** Nonadiabatic tunneling of photoelectrons in the near-field of gold nanostructures is demonstrated, occurring in the transition region between the multiphoton emission [MPE] and tunneling emission [TE] regimes. Measured kinetic energy spectra at higher laser intensities indicates strong-field electron acceleration and recollision, characteristic for the TE regime. At the same time constant scaling of the photoelectron current with the intensity has been measured, a trait of the MPE regime. The Keldysh value for the transition yields  $\gamma \approx 2$ , which is in good agreement with numerical calculations.

Our work demonstrates nonadiabatic tunneling of photoelectrons in the vicinity of nanostructures with a characteristic size of around 100 nm. In particular, we use 7 fs laser pulses at 80 MHz from a Ti:sapphire femtosecond laser oscillator to excite localized surface plasmons on different gold nanoparticles. We determine the enhancement by measuring the kinetic energy spectrum of the electrons that are photoemitted from the surface of the nanoparticle as a function of incident laser intensity [1,2]. From the shape of the energy spectra, and the retrieved field enhancement values, we are able to follow the transition between two regimes: the first is characterized by multiphoton emission, while in the second (at higher intensities), tunneling emission of the electrons through the potential barrier distorted by the laser field is more pronounced.

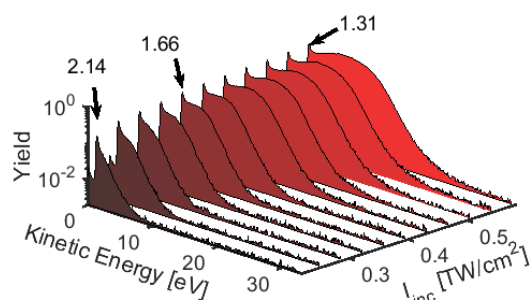


**Figure 1.** Measured photoemission spectra for different incident laser intensities, the local Keldysh parameter values are indicated with arrows for some of the spectra.

There have been studies of these two emission regimes for select systems, but little is known about the transition region between them, the so-called non-adiabatic tunneling. For low laser intensities photoelectron spectra consist of a peak at low kinetic energies which exponentially decays for enhanced energies. Upon increasing the intensity, the spectra develops a characteristic plateau region (Figure 1.). The plateau contains electrons accelerated in the laser field and rescattered from the surface of the nanoparticles, a phenomenon that is switched on by increasing the intensity. This plateau, characteristic for the TE regime, is present in the measurements alongside with the constant nonlinearity of the photocurrent, the latter a trait of the MPE regime. These mixed photoemission features imply, that the measurements are taking place in the transition region for the highest intensities. Determining the field enhancement enables us to pinpoint the transition intensity and calculate the corresponding adiabaticity (Keldysh) parameter. The transition occurs around  $\gamma \approx 2$  [3]. This value is in good agreement with the results acquired by the numerical solution of the Schrödinger equation and other numerical calculations [4].

### References

- [1] Rác P et al. 2017 *Nano Lett.* **17** 1181–1186
- [2] Budai J et al. 2018 *Nanoscale* **10** 16261–16267
- [3] Lovász B et al. 2022 *Nano Lett.* **22** 2303–2308
- [4] Xiaolei H et al. 2016 *Opt. Express* **24**, 25250–25257

\* E-mail: [dombi.peter@wigner.hu](mailto:dombi.peter@wigner.hu)

# Photoionization of H Debye plasmas in strong field approximation

Yu Gang Yang<sup>1</sup>, Li Guang Jiao<sup>1,2\*</sup>, and Aihua Liu<sup>3†</sup>

<sup>1</sup>College of Physics, Jilin University, Changchun 130012, People's Republic of China

<sup>2</sup>Helmholtz-Institut Jena, D-07743 Jena, Germany

<sup>3</sup>Institute of Atomic and Molecular Physics, Jilin University, Changchun 130012, People's Republic of China

**Synopsis** The second-order strong field approximation is employed to calculate the above-threshold ionization of hydrogen atoms embedded in weakly-coupled plasmas under intense laser pulses. The photoelectron energy spectra are compared with accurate predictions obtained by numerically solving the time-dependent Schrödinger equation. The plasma screening effects on photoelectron energy spectra and momentum distributions are analyzed.

Investigation of the plasma screening effects on fundamental atomic processes has attracted considerable interest in atomic and optical physics, astrophysics, inertial confinement fusion, and laser-induced plasma physics. In weakly-coupled plasmas, the interaction between charged particles is modeled by the Debye-Hückel (DH) potential  $V(r) = -\frac{Z_1 Z_2 e^2}{r} e^{-\lambda r}$ , where the plasma screening parameter reads  $\lambda = \sqrt{4\pi e^2 n_e / k_B T_e}$  which depends upon the temperature and electron density of the plasmas.

The strong field approximation (SFA) has been widely employed to simulate the non-linear phenomena of atoms and molecules exposed in intense laser fields, e.g., the above-threshold ionization (ATI) and high-order harmonic generation. The second-order SFA (SFA2), which accounts for the rescattering of the returning electron with the target ion, has been shown to successfully reproduce the high-energy portion of the photoelectron energy spectra and momentum distributions [1]. In this work, we apply the SFA2 method to investigate the ATI spectra of hydrogen atom in weakly-coupled plasmas where the screening effects on both the target atom and electrostatic interaction are taken into account, while the effect on photoelectron is omitted due to the short-range character of the DH potential.

Figure 1 displays the ATI energy spectra of H atom embedded in DH plasmas ( $\lambda = 0.1$ ) under a five-cycle laser pulse with the wavelength of 800 nm and peak intensity of  $1.0 \times 10^{14}$  W/cm<sup>2</sup>. The ground state of H atom was expressed in terms of Slater-type orbitals with the eigenenergy being 0.407 a.u. The TDSE numerical calculations

are also included in Fig. 1 for comparison, and it can be seen that the SFA2 method reproduces fairly well the TDSE results in both the low- and high-energy region of the energy spectra, while slightly underestimates the ionization probability at intermediate energies. The screening effect of plasma environments on the photoelectron momentum distributions will be reported elsewhere.

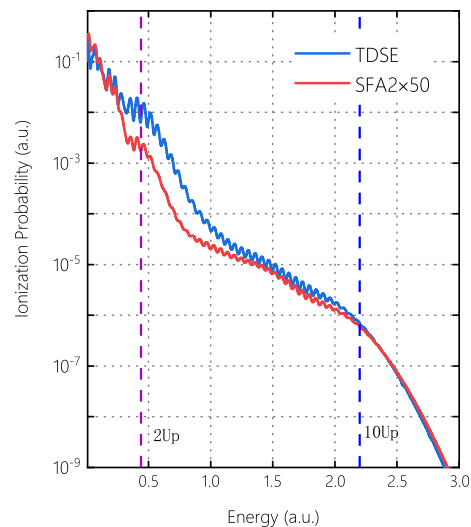


**Figure 1.** Photoelectron energy spectra of H atom in DH plasmas ( $\lambda = 0.1$ ) by a five-cycle laser pulse with the wavelength of 800 nm and peak intensity of  $1.0 \times 10^{14}$  W/cm<sup>2</sup>.

## References

- [1] Z. Chen, T. Morishita, A.-T. Le, and C. D. Lin 2007 *Phys. Rev. A* **76** 043402

\*E-mail: [lgjiao@jlu.edu.cn](mailto:lgjiao@jlu.edu.cn)

†E-mail: [aihualiu@jlu.edu.cn](mailto:aihualiu@jlu.edu.cn)

## Shake-up and shake-off satellites as probe of ultrafast charge delocalization in liquid water

F Trinter<sup>1,2\*</sup>, B Winter<sup>1</sup> and S Thürmer<sup>3</sup>

<sup>1</sup>Molecular Physics, Fritz-Haber-Institut der Max-Planck-Gesellschaft, 14195 Berlin, Germany

<sup>2</sup>Institut für Kernphysik, Goethe-Universität, 60438 Frankfurt am Main, Germany

<sup>3</sup>Department of Chemistry, Graduate School of Science, Kyoto University, Kitashirakawa-Oiwakecho, Sakyo-Ku, Kyoto 606-8502, Japan

**Synopsis** Employing synchrotron radiation and liquid-jet photoelectron spectroscopy, we study shake-up and shake-off satellites as probe of ultrafast charge delocalization in liquid water.

Probing decays of molecular systems after core ionization, either via Auger electrons from non-radiative decay or via photons in the radiative decay channel, gives insight into nuclear dynamics as well as charge and energy transfers on the timescale of the core-hole lifetime. In particular, Auger studies on liquid water have revealed ultrafast proton dynamics in liquid water, driven via hydrogen bonding [1]. It is well known that core ionization with sufficient energy can be accompanied by the additional promotion of a valence electron into an unoccupied orbital or into the continuum, termed shake-up and shake-off, respectively. The former produces an excited, doubly ionized state, while the latter yields a triply ionized species. While these processes and the resulting spectral satellite structures have been studied intensively since the 1970s, so far, they remain unexplored in the liquid phase. Furthermore, due to the increased computational complexity, the energetics of shake-up processes have been described far less. In the case of the water molecule, early studies on the shake-off satellites exist both for via X-ray [2] and Auger emission [3], but shake-up processes have been only considered in the direct photoemission channel (e.g., [4]). Studying shake-up and shake-off satellites in liquid water promises to give new insight into ultrafast charge- and energy-transfer processes during these alternative decay pathways. For example, electrons residing in the lowest unoccupied orbital (LUMO) are known to have a high probability of delocalizing into the liquid. Also, a triply charged species may have the ability to drive bond elongation and proton transfers much more strongly. Here, it is beneficial to explore both X-ray and Auger emission channels, as the

latter channel involves a change in charge state of the remaining ion and is much more sensitive to the different energetics of the shake-up and shake-off processes. Here, we systematically study shake-up satellites in gaseous and liquid water for the first time, and show that satellite states can be used to identify novel charge-transfer channels in the liquid phase. Our results will give new insight into the mechanism of proton-transfer dynamics in liquid water.

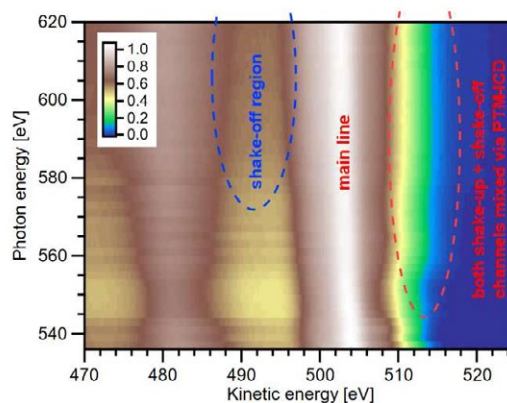


**Figure 1.** Liquid-water Auger emission spectra measured while scanning the photon energy above ionization; spectra are normalized to the K-1b<sub>1</sub>1b<sub>1</sub> Auger line. An increase in intensity at kinetic energies specific to shake-up (above main line) and shake-off (below main line) satellites is observed.

### References

- [1] Thürmer S et al. 2013 *Nat. Chem.* **5** 590
- [2] Rubensson J-E et al. 1985 *J. Chem. Phys.* **82** 4486
- [3] Siegbahn H et al. 1975 *Chem. Phys. Lett.* **35** 330
- [4] Sankari R et al. 2006 *Chem. Phys. Lett.* **422** 51

\* E-mail: [trinter@fhi-berlin.mpg.de](mailto:trinter@fhi-berlin.mpg.de)

## High-order harmonic generation and confinement in artificial atoms

H N Gopalakrishna<sup>1,2</sup>, R Baruah<sup>3,1</sup>, C Hünecke<sup>1</sup>, V Korolev<sup>1</sup>, M Thümmeler<sup>1</sup>, A Croy<sup>1</sup>, U Peschel<sup>1</sup>,  
S Gräfe<sup>1,4</sup>, M Wächtler<sup>3,1,5</sup>, and D Kartashov<sup>1\*</sup>

<sup>1</sup>Friedrich-Schiller University Jena, Max-Wien-Platz 1, 07743 Jena, Germany

<sup>2</sup>Helmholtz-Institut Jena, Helmholtzweg 4, 07743 Jena, Germany

<sup>3</sup>Leibniz Institute of Photonic Technology, Albert-Einstein-Straße 9 07745 Jena, Germany

<sup>4</sup>Fraunhofer Institute for Applied Optics and Precision Engineering, Albert-Einstein-Str.7, 07745 Jena, Germany

<sup>5</sup>Department of Chemistry and Research Center OPTIMAS, Technical University Kaiserslautern, Erwin-Schrödinger-Straße 52, 67663 Kaiserslautern, Germany

**Synopsis** We report on the results of experimental and numerical investigations of high-order harmonic generation in semiconductor quantum dots for different laser intensity, wavelength and polarization and various dot diameters. We show that spatial confinement of electron motion leads to off-wall scattering, chaotization of motion and suppression of interband harmonics.

In this contribution we report on results of systematic experimental-theoretical investigation of high-order harmonic generation (HHG) in nanoscale crystalline solids, resembling strong spatial confinement of electron motion.

HHG spectra were measured in transmission from micron thickness layers of CdSe quantum dots (QD), deposited on a sapphire substrate and illuminated by 100 fs mid-IR pulses at 3.7  $\mu\text{m}$  and 4.7  $\mu\text{m}$  wavelengths, as a function of dot's size, laser intensity and ellipticity of the laser polarization. As a reference, 140 nm thick bulk polycrystalline CdSe film was used. The results of HHG spectra measurements at the 4.74  $\mu\text{m}$  wavelength and 1.2 TW/cm<sup>2</sup> intensity are shown in Fig.1. In summary, our main experimental results are: a) we observe abrupt suppression of above bandgap harmonics when the dot size is reduced below 3 nm, whereas below bandgap harmonics remain largely unaffected; b) the power index in the dependence of harmonic's yield on the laser intensity gradually increases with reduction in the dot size but its value is weakly dependent on harmonic's order; c) the bulk and QD's of all sizes show a very similar dependence of the harmonic yield on the laser polarization ellipticity.

We conducted detail numerical simulations of HHG in QDs using various theoretical methods such as density functional calculations, real-time real-space time-dependent density functional calculations, time-dependent Schrödinger equation and classical trajectory analysis with Monte Carlo simulations. Our analysis suggests

that, in contrast to [1], the main mechanism of HHG suppression is electron scattering off the dot's wall when the dot's size is smaller than the oscillatory radius. The scattering results in a substantial reduction of acquired ponderomotive energy and chaotization of motion, leading to a loss of coherence and suppression of Corkum mechanism of harmonic generation.

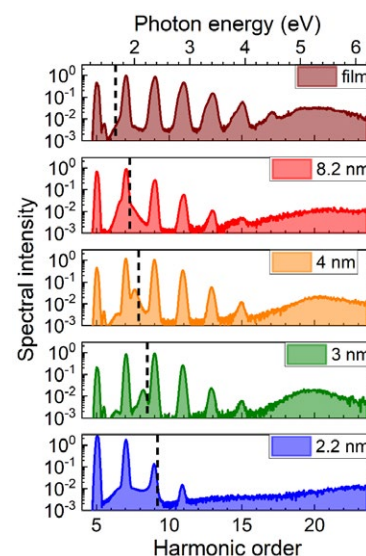


**Figure 1.** Size dependent HHG spectra from the bulk CdSe film and QD's of different size. The dashed line marks the bandgap energy.

### References

- [1] Nakagawa K et al. 2022 *Nature Phys.* [18 874](#)

\* E-mail: [daniil.kartashov@uni-jena.de](mailto:daniil.kartashov@uni-jena.de)



# Studying the Optical Properties of 1-decanol for Ultrashort Pulse Generation

N Drouillard<sup>1\*</sup>, and TJ Hammond<sup>1</sup>

<sup>1</sup>ACMElab, University of Windsor, Windsor, N9B 3P4, Canada

**Synopsis** We study 1-decanol as an alternative nonlinear optical medium to commonly used liquids such as CS<sub>2</sub> due to its comparatively low toxicity and measure a comparable nonlinear index. To inform our calculation of the nonlinear index, we make the first reported measurement of the dispersion and index of refraction of 1-decanol. At high intensities, we observe stable supercontinuum generation, suggesting that with its high nonlinearity and low dispersion, 1-decanol is a promising liquid for ultrashort pulse generation.

Liquids offer several advantages as nonlinear optical media, namely their high-density, high nonlinearity, and resistance to damage. Commonly used liquids for nonlinear optics include CS<sub>2</sub> and other highly toxic chemicals. In search of liquids with lower toxicities, we turned to organic alcohols and found that 1-decanol is a suitable candidate due to its high boiling point. We previously reported spectral broadening in 1-decanol[1] and sought to further study this liquid as an optical medium. We use the z-scan technique to measure the transmittance of 1-decanol through a focus and find that it has a nonlinear index of  $n_2 = 2.47 \times 10^{-20} m^2/W$  at  $I_0 = 0$ .

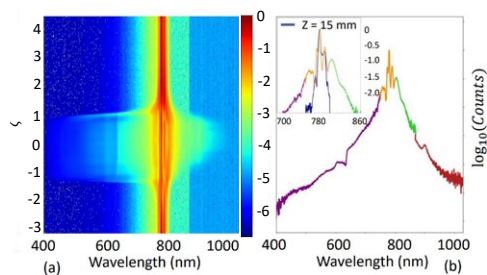


**Figure 1.** (a) As the 1-decanol passes through the focus ( $\zeta = 0$ ), the spectrum rapidly broadens.  $\zeta = z/z_0$  where  $z$  is the axial position and  $z_0$  is the Rayleigh range. (b) A lineout of the spectrum at the focus. Insert: comparing lineout at low intensity.

Furthermore, we use  $n_2(I)$  to calculate  $n_4 = 7.16 \times 10^{-35} m^4/W^2$ , which we find makes a significant contribution to the overall nonlinearity

of the liquid at high intensities, such as above  $2.8 \times 10^{15} W/m^2$ , where the nonlinearity exceeds that of CS<sub>2</sub>. We observe a filament that leads to supercontinuum generation near the focus, as shown in Fig. 1(a). The supercontinuum contains frequencies across more than an octave, from approximately 400 nm to 950 nm, as shown in Fig. 1(b).

In order to obtain the values of  $n_2$  and  $n_4$ , we perform a nonlinear least squares fit to the z-scan data, which requires the index of refraction across the bandwidth of interest. To this end, we develop a modified method for spectrally resolved white-light interferometry (SRWLI)[2] using a Mach-Zehnder interferometer to generate a series of interferograms. To our knowledge, this is the first reported measurement of the dispersion and index of refraction of 1-decanol.

In summary, we expect our method of SRWLI to prove useful for characterizing new materials. We also expect that given its high nonlinearity and long-term stability, 1-decanol will be beneficial for creating broadband ultrashort pulses, and that its relatively low dispersion will allow for good phase control. Finally, 1-decanol offers the benefits of liquid media for nonlinear optics while maintaining a relatively low toxicity when compared to commonly used liquids such as CS<sub>2</sub>.

## References

- [1] Stephen J, Arachchige CJ and Hammond TJ 2022 *J. Phys. B: At. Mol. Opt. Phys.* **55**
- [2] Drouillard N and Hammond TJ *Opt. Express* **30** 22

\*E-mail: [droui116@uwindsor.ca](mailto:droui116@uwindsor.ca)



## Supercontinuum amplification for nonlinear optics

N Drouillard<sup>1</sup>, S Ghosh<sup>2</sup>, and TJ Hammond<sup>1\*</sup>

<sup>1</sup>Dept of Physics, University of Windsor, Windsor ON Canada

<sup>2</sup>Manipal Institute of Technology, Manipal, Karnataka, India

**Synopsis** We amplify a supercontinuum seed spanning nearly an octave of bandwidth through a Kerr-based parametric amplifier. The amplification process maintains the spatial and temporal profile of the seed. We demonstrate third harmonic generation from sapphire from the infrared beam, implying good spatial coherence and near transform-limited amplified pulses.

Kerr instability amplification (KIA) uses the third-order nonlinearity of a material for parametric amplification [1]. We have previously demonstrated high gain in both the visible and infrared portions of the spectrum [2]. Here, we demonstrate the feasibility of amplifying a supercontinuum spectrum spanning nearly an octave.

We split the output of a 1 mJ 100 fs Ti:Sapphire laser to produce a supercontinuum seed in 5 mm sapphire plate. We combine this supercontinuum with the pump in a 0.5 mm thick MgO crystal at 5.5 degrees. When the seed and pump are spatially and temporally overlapped, we see amplification up to 1000x.

As shown in Fig. 1(a), we scan the delay of the pump with respect to the seed during the amplification process. The amplified spectrum is pump-delay dependent due to the chirp of the supercontinuum.

In Fig. 1(b), we compare the total amplified supercontinuum spectrum, which spans nearly an octave from 500 to 1000 nm, to KIA theory, showing good spectral agreement. Seed-pump mode overlap limits the experimental amplification factor.

In Fig. 1(c), we isolate the infrared portion of the amplified pulse and focus it ( $f=75$  mm) onto a piece of 0.5 mm thick sapphire. By scanning the seed-pump delay, we show that we are able to directly generate the third harmonic. The pulse duration is nearly transform limited to reach the sufficient intensities for third harmonic generation.

We will discuss optimizing the amplification, parameters that can tune the amplified bandwidth, and future uses of these amplified supercontinuum pulses.

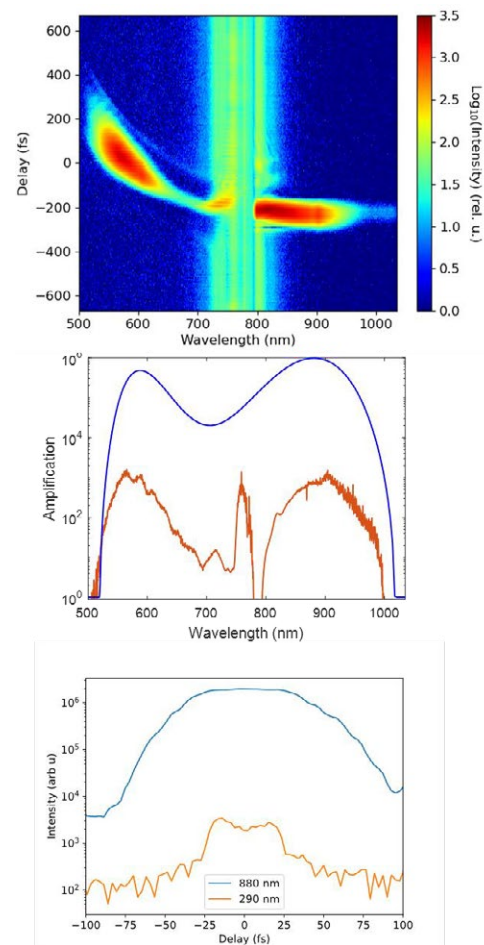


**Figure 1.** (a) Delay scan showing amplification. (b) KIA theory (blue) compared to experiment (red). (c) Generation of 3<sup>rd</sup> harmonic directly from IR portion.

### References

- [1] Nesrallah M, *et al*, "Theory of Kerr instability amplification," *Optica*, **5** 271-278 (2018)
- [2] Arachchige CJ *et al*, *Opt. Lett.* **46** 5521-5524 (2021)

\* E-mail: [thammond@uwindsor.ca](mailto:thammond@uwindsor.ca)

## Application of LIBS spectral data fusion in quantitative analysis of *Astragalus*

P Zhao<sup>1</sup>, W W Han<sup>1</sup>, D X Sun<sup>1</sup>, G D Zhang<sup>1</sup>, M G Su<sup>1\*</sup>

<sup>1</sup>Key Laboratory of Atomic and Molecular Physics and Functional Material of Gansu Province. College of Physics and Electronic Engineering, Northwest Normal University, Lanzhou, 730070, China

**Synopsis** A data fusion method based on spectral intensity and Hog Feature is proposed to improve the accuracy and precision of laser-induced breakdown spectroscopy (LIBS) quantitative analysis. Based on this, the feasibility of miniaturization of the spectrometer is being studied. The Chinese medicinal herb *Astragalus* was taken as the research object, and the detection performance of LTB and Avantes spectrometers was analyzed and compared. For eight groups of *Astragalus* standard samples containing heavy metals Cu and Pb, select the characteristic bands of 324.63-324.95 nm, 327.25-327.69 nm, 405.46-406.10 nm, establish spectral images, and then perform data fusion, quantitative analysis after combining with partial least squares regression (PLSR). Comparing the quantitative results before and after data fusion, the corresponding figures of merit were superior to the fusion.

In recent years, laser-induced breakdown spectroscopy (LIBS) technology has been widely used and rapidly developed in the identification and quantitative analysis of material components [1]. With the further miniaturization of the instrument, quantitative analysis performance is one of the main factors to be considered.

*Astragalus* in Minxian County was selected and configured into eight groups of standard samples containing heavy metals Cu and Pb. The traditional LIBS detection device was used for measurement. The plasma signal was collected by two-way light receiving system and coupled to LTB (LTB, aryelle 200) and Avantes (AvaSpec-Mini2048CL) spectrometers to obtain the corresponding spectral data. Select the characteristic bands of 324.63-324.95 nm, 327.25-327.69 nm, 405.46-406.10 nm to establish Cu and Pb spectral images, HOG features are extracted and fused with spectral intensity, quantitative analysis after combining with partial least squares regression (PLSR).

Comparing the quantitative results before and after data fusion, the corresponding figures of merit were superior to the fusion, as shown in Figure 1, before data fusion, the figures of merit of the PLSR quantitative model for Cu element of *Astragalus* Samples  $S_{pu}$ ,  $RMSECV$ ,  $R_{CV}^2$ ,  $[LOD_{min}, LOD_{max}]$  [2],  $RMSEP$ ,  $R_p^2$  followed by 0.9457, 35.05 ppm, 0.98, [17.15, 31.37 ppm], 32.71 ppm, 0.98, after data fusion, the corresponding results were 0.9879, 11.11ppm, 0.99, [6.67, 9.98ppm], 10.41ppm, 0.99. The

results of heavy metal Pb also showed the same trend. At the same time, the results show that the miniaturization of the spectrometer is feasible.

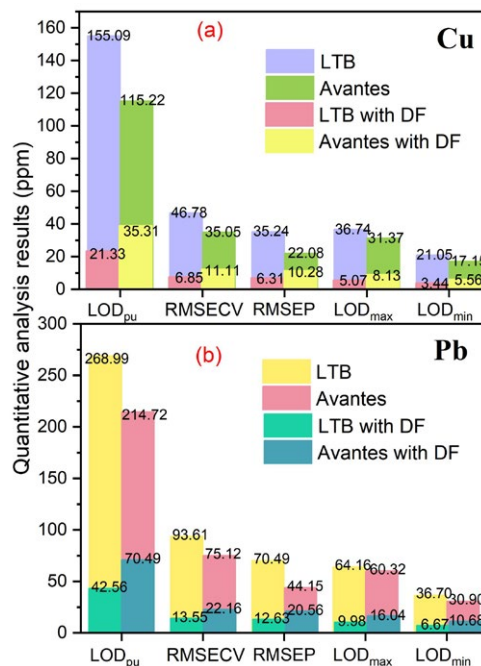


**Figure 1.** Comparison of PLSR quantitative analysis figures of merit of the two spectrometers: (a) doped with heavy metal Cu, (b) doped with heavy metal Pb.

### References

- [1] Brunnbauer L *et al* 2023 *TrAC* [159 116859](#).
- [2] Allegrini F *et al* 2014 *Anal Chem* [86 7858](#).

\* E-mail: [sumg@nwnu.edu.cn](mailto:sumg@nwnu.edu.cn)

## Experimental and theoretical study on the extreme ultraviolet radiation behavior of laser-produced Al-Sn alloy plasmas

M G Su\*, H Y Li and Y B Fu†

Key Laboratory of Atomic and Molecular Physics & Functional Material of Gansu Province, College of Physics and Electronic Engineering, Northwest Normal University, Lanzhou 730070, People's Republic of China

**Synopsis** In this paper, a time-resolved laser-produced plasma emission spectrum technology is used to measure the extreme ultraviolet spectra of pure Sn and aluminum-tin alloy plasmas with atomic percentages of 5:95, 50:50 and 95:5, respectively. For understanding the radiation contribution of ions of different element, a normalized Boltzmann distribution among the excited states and a steady-state collisional-radiative model were assumed for the spectral simulations, and used to estimate the electron temperature and density in these plasmas.

Laser-produced plasmas (LPPs) have been an attractive research topic because of their potential use as pulsed short wavelength light sources such as extreme ultraviolet (EUV) lithography and EUV metrology. In order to reduce the opacity and out-of-band composite radiation, some research on tin mixtures is carried out with the mixture of tin and low-Z materials [1].

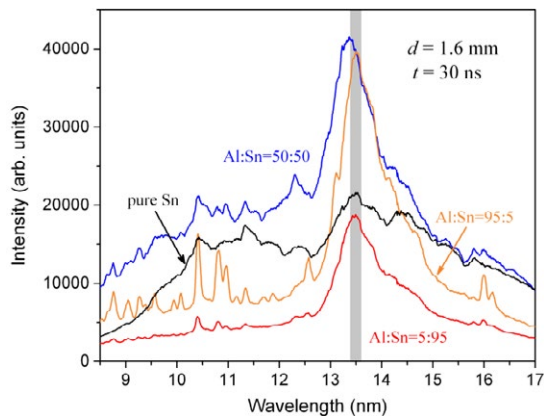


**Figure 1.** Comparison of EUV spectra of three different proportion Al-Sn targets and pure tin target.

To understand the radiation contribution of different element ions, a series of spectral measurements of laser-produced plasmas of pure tin and aluminum-tin alloy plasmas with atomic percentages of 5:95, 50:50 and 95:5 were carried out in vacuum, respectively. Figure 1 shows the measured results at a 1.6 mm distance from target and 30 ns time delay. It

can be seen that with the decrease of Sn concentration, the discrete spectral characteristics of highly charged Al ions are gradually prominent, the broadband spectral characteristics from Sn ions are also gradually enhanced, and the plasma opacity is significantly reduced.

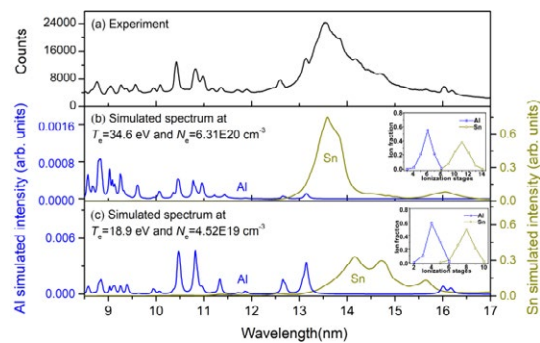


**Figure 2.** Comparison between experimental and simulated spectral Profiles.

In order to explain the contribution of different ions to the spectral profile, Figure 2 represents the simulated EUV spectra of laser-produced plasma with Al-Sn atomic ratio of 50:50, and compares the theoretical spectrum and experimental characteristics of the two states, and identifies the ionization state and their fractions.

### References

- [1] Bakshi V 2006 *SPIE-International Society for Optical Engineering*

\* E-mail: [sung@nwnu.edu.cn](mailto:sung@nwnu.edu.cn)

† E-mail: [fuyb@nwnu.edu.cn](mailto:fuyb@nwnu.edu.cn)

## Analysis of 4p-5s spectral characteristics in laser-produced Ag plasmas in the EUV region

M J Li<sup>1</sup>, M G Su<sup>1\*</sup> and C Z Dong<sup>1†</sup>

<sup>1</sup>Key Laboratory of Atomic and Molecular Physics & Functional Material of Gansu Province, College of Physics and Electronic Engineering, Northwest Normal University, Lanzhou 730070, People's Republic of China

**Synopsis** Experimental and theoretical analyses are reported for the spatiotemporal evolution of extreme ultraviolet spectra in laser-produced silver (Ag) plasmas. The time-resolved spectra were acquired 1.5 mm from the target surface. The 4p excitations of  $\text{Ag}^{7+}$ – $\text{Ag}^{13+}$  ions were calculated via Hartree-Fock configuration-interaction theory. The spectral line distributions of transitions in the dominant 4p-5s transition arrays and their variations with the degree of ionization were analyzed.

The electronic structures and emissions of atoms and lower-ionization ions in the fifth row of the periodic table have been essential for experimental and theoretical studies [1,2]. Specifically, silver (Ag) has been important for x-ray lasers, material science, and celestial and fusion plasmas.

In this work, a series of emission spectra over the range 8.5–13.5 nm were acquired to characterize the time evolution of the laser-produced Ag plasma created with a laser power density of  $5.2 \times 10^{10}$  W/cm<sup>2</sup>. Figure 1 shows the comparison between experimental spectrum at a 1.5 mm from the target surface and a 30-ns time delay and simulated spectra at 25-eV electron temperature and  $1 \times 10^{19}$  cm<sup>-3</sup> electron density. The inserted column chart shows the ion fractions for the range  $\text{Ag}^{8+}$ – $\text{Ag}^{13+}$ . Good agreement was obtained when the dominant fractions were  $\text{Ag}^{10+}$ ,  $\text{Ag}^{11+}$ , and  $\text{Ag}^{12+}$ , with values of approximately 21.4%, 49%, and 27%, respectively.

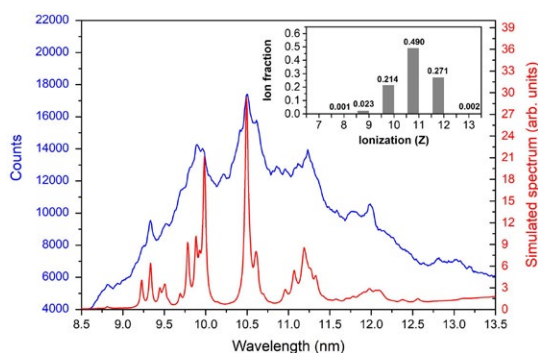


**Figure 1.** Comparison between experimental and simulated spectra at 25-eV electron temperature.

\* E-mail: [sumg@nwnu.edu.cn](mailto:sumg@nwnu.edu.cn)

† E-mail: [dongcz@nwnu.edu.cn](mailto:dongcz@nwnu.edu.cn)

Figure 2 shows spectral distributions of 4p-5s transitions of highly-charged Ag ions. The spectral distribution of the 4p-5s transition array occurs at shorter wavelengths with increased degree of ionization. The large number of spectral lines for  $\text{Ag}^{7+}$ – $\text{Ag}^{9+}$  are very close, and some Gaussian peak fits are wide.

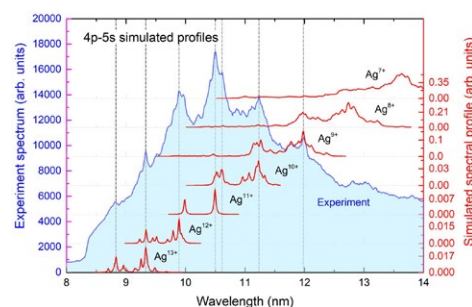


**Figure 2.** Comparison of simulated and experimental spectral profiles of Ag ions for a Boltzmann distribution at a 25-eV electron temperature.

The energy-level population contribution of the normalized Boltzmann distribution and the effect of autoionization broadening were very important for the spectral simulations concerned with differences between Gaussian and resonance emission profiles, especially for  $\text{Ag}^{9+}$  and  $\text{Ag}^{10+}$ .

### References

- [1] Ishikawa T, Kawakami H and Mori H 1997 *Nuclear Instruments and Methods in Physics Research Section B: Beam Interactions with Materials and Atoms* 121 437
- [2] Müller M, Schmidt M and Zimmermann P 1986 *Europhys Lett* 2 359

## Commissioning of a new energy-scan system for electron-impact ionization experiments and first results for $\text{La}^{1+}$

B M Döhring<sup>1,2\*</sup>, A Borovik Jr<sup>1</sup>, F Gocht<sup>1</sup>, K Huber<sup>1</sup>, A Müller<sup>1</sup> and S Schippers<sup>1,2</sup>

<sup>1</sup>I. Physikalisches Institut, Justus-Liebig-Universität Gießen, Germany

<sup>2</sup>Helmholtz Forschungsakademie Hessen für FAIR (HFHF), Campus Giessen, Germany

**Synopsis** We report on the design and the commissioning of a fast electron-energy-scan system for the 3.5-keV high-power electron gun at the Giessen electron-ion crossed-beams setup. This energy-scan system synchronously switches all electrode voltages on the millisecond time-scale. It permits the investigation of resonance structures in electron-impact ionization (EII) cross sections in small electron-energy steps. First experimental results were obtained for EII of  $\text{La}^{1+}$  ions. Such cross sections are of interest, e.g., for the modeling of kilonovae.

Electron-impact ionization (EII) of ions is fundamental atomic collision process that governs the charge balance in plasmas. Experimental measurements of the corresponding cross sections on an absolute scale are indispensable for testing the theoretical approaches that provide most of the data required for applications such as magnetically confined fusion, light sources for EUV lithography, or astrophysical plasmas. A prominent example are kilonovae, i.e., the afterglows of neutron-star merger events where the heavy elements in the Universe are forged. Modelling of kilonova light-curves aims at determining the abundances of the thus created heavy elements [1]. Here, we report on new cross section measurements for single, double, and triple ionization of  $\text{La}^{1+}$  ions by electron impact. For energies up to 1000 eV, these agree with previously measured data [2] and, in addition, extend the experimental energy range by a factor of 2.

For these measurements, we have employed our high-intensity electron gun, which provides electron currents of up to 1 A at energies of up to 3.5 keV [3]. In particular, we have mapped out the resonance structures in the EII cross sections by employing a fast scanning of the electron energies, which requires the computer-controlled synchronous switching of all electrode voltages on a millisecond time scale. Based on our experience with an older 1-keV electron gun [4], we have recently implemented such a system also for the 3.5-keV electron gun. The new scanning system makes use of 18-bit DACs and a special control unit, which provide voltage accuracy in the mV range. Figure 1 presents the first results

that were obtained with the new scanning system.

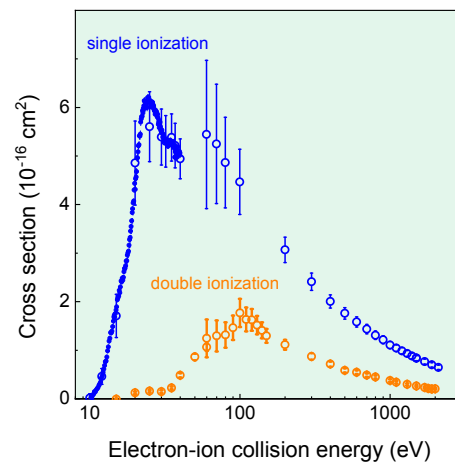


**Figure 1.** Experimental cross section for single and double EII of  $\text{La}^{1+}$  ions [5]. Large open symbols represent absolute cross sections. The associated error bars comprise statistical and systematic uncertainties. As compared to previous measurements [2] the experimental energy range has been extended by a factor of 2. Small full symbols represent energy-scan results which were scaled to the absolute data points.

### References

- [1] Watson D et al 2019 *Nature* **574** 497
- [2] Müller A et al 1989 *Phys. Rev. A* **40** 3584
- [3] Ebinger B et al 2017 *Nucl. Instrum. Meth. B* **408** 317
- [4] Müller A et al 1989 *Phys. Rev. Lett.* **61** 70
- [5] Döhring B M et al 2023 *to be published*

\*E-mail: [Michel.Doehring@physik.uni-giessen.de](mailto:Michel.Doehring@physik.uni-giessen.de)



## High-resolution dielectronic recombination of $\text{Pb}^{78+}$ ions at the ultra-cold electron cooler of the CRYRING@ESR storage ring

S Fuchs<sup>1,2</sup>, Z Anelkovic<sup>3</sup>, D Banaš<sup>4</sup>, A Borovik Jr<sup>1</sup>, C Brandau<sup>1,3</sup>, M Fogle<sup>5</sup>, S Fritzsche<sup>3,6,7</sup>, Z Harman<sup>8</sup>, F Herfurth<sup>3</sup>, C Kozhuharov<sup>3</sup>, C Krantz<sup>3</sup>, M Lestinsky<sup>3</sup>, E Lindroth<sup>9</sup>, X Ma<sup>10</sup>, E B Menz<sup>3,4</sup>, A Müller<sup>1</sup>, R Schuch<sup>9</sup>, U Spillmann<sup>3</sup>, A Surzhykov<sup>11,12</sup>, M Steck<sup>3</sup>, M Trassinelli<sup>13</sup>, G Vorobyev<sup>3</sup>, S X Wang<sup>1,2</sup>, T Stöhlker<sup>3,6,7</sup>, Y Zhang<sup>14</sup>, and S Schippers<sup>1,2\*</sup>, for the SPARC Collaboration

<sup>1</sup>JLU Gießen, <sup>2</sup>HFHF, <sup>3</sup>GSI, <sup>4</sup>JKU Kielce, <sup>5</sup>Auburn University, <sup>6</sup>HI Jena, <sup>7</sup>FSU Jena, <sup>8</sup>MPIK <sup>9</sup>Stockholm University, <sup>10</sup>IMP Lanzhou, <sup>11</sup>TU Braunschweig, <sup>12</sup>PTB, <sup>13</sup>UMPC Paris, <sup>14</sup>Xian Jiantong University,

**Synopsis** Dielectronic recombination (DR) of highly-charged Be-like  $\text{Pb}^{78+}$  ions was measured at the low-energy heavy-ion storage ring CRYRING@ESR operated by GSI/FAIR in Darmstadt, Germany. The highly charged ions were injected from the GSI chain of accelerators and merged with the electron beam of the ultra-cold electron cooler. The  $1s^2 2s 2p 19\ell$  and  $1s^2 2s 2p 20\ell$  groups of DR resonances were scanned with high resolving power. In combination with atomic theory, the results testify the establishment of high-resolution electron-ion collision spectroscopy of slow highly-charged ions at CRYRING@ESR.

Electron-ion collision spectroscopy is a very successful approach for studying the properties of highly charged ions [1, 2], in particular if low-energy dielectronic recombination (DR) resonances are scrutinized. The heavy-ion storage ring CRYRING@ESR of the international FAIR facility in Darmstadt, Germany, is particularly attractive for DR studies, since it is equipped with an electron cooler that provides an ultra-cold electron beam promising highest experimental resolving power and precision. Due to its versatility and the high experimental precision DR spectroscopy plays an important role in the physics program of the SPARC collaboration as is outlined, e.g., in the CRYRING@ESR Physics Book [3].

Here, we report on the results from the first DR experiment with highly-charged ions which were injected into CRYRING@ESR from the full chain of GSI accelerators consisting of the linear accelerator UNILAC, the heavy-ion synchrotron SIS18, and the high-energy storage ring ESR.  $\text{Pb}^{78+}$  ions were produced by stripping at an energy of about 12 GeV and injected into ESR, where they were cooled and decelerated to an energy of 11 MeV/u. Finally, up to  $5 \times 10^6$  ions per cycle were injected into the CRYRING where the beam lifetime was about 30 s, mainly limited by collisions with residual gas particles.

DR spectra were measured in the 0–40 eV

\*E-mail: [stefan.schippers@physik.uni-giessen.de](mailto:stefan.schippers@physik.uni-giessen.de)

collision-energy range where  $2s2p(^3P_1)19\ell$  and  $2s2p(^3P_1)20\ell$  resonances occur that are associated with  $2s^2(^1S_0) \rightarrow 2s2p(^3P_1)$  excitations of the Be-like ion core. The measured relative peak positions and peak strengths agree well with theoretical calculations that employed the methodology described, e.g., in Ref. [4]. From the comparison between experiment and theory we infer the longitudinal and transverse electron beam temperatures  $k_B T_{\parallel} \approx 0.08$  meV and  $k_B T_{\perp} \approx 3$  meV, which are in accord with the expectations. This preliminary result of our experiment already clearly demonstrates that CRYRING@ESR is indeed excellently suited for high-resolution electron-ion collision spectroscopy of very highly charged ions, which makes it a world-unique facility for the investigations of the above mentioned physics cases. More detailed results will be presented on the poster.

This research was supported by the ErUM-FSP T05 “APPA” [5] (BMBF grant nos. 05P19RGFA1 and 05P21RGFA1).

### References

- [1] Schippers S 2015 *Nucl. Instrum. Methods Phys. Res. B* **350** 61
- [2] Brandau C *et al* 2015 *Phys. Scr.* **T166** 014022
- [3] Lestinsky M *et al* 2016 *Eur. Phys. J. ST* **225** 797
- [4] Harman Z *et al.* 2019 *Phys. Rev. A* **99** 012506
- [5] <http://fsp-appa.fair-center.eu>



## Continuous injection of metallic elements into an electron-beam ion trap using an electron-beam evaporator

N Kimura<sup>1</sup>\*, G Kiyama<sup>2</sup>, D Ito<sup>2</sup> and N Nakamura<sup>2</sup>

<sup>1</sup>Atomic, Molecular and Optical Physics Lab., RIKEN, Saitama, 351-0198, Japan

<sup>2</sup>Institute for Laser Science, The University of Electro-Communications, Tokyo 182-8585, Japan

**Synopsis** We demonstrate a versatile injection method of metallic elements into an electron-beam ion trap using an electron-beam evaporator which provides a continuous neutral-atom-beam. The proof-of-principle experiment for this method has been done by employing highly charged niobium and tungsten ions.

Spectroscopic study of highly charged ions (HCIs) using an electron-beam ion trap (EBIT) is one of the sophisticated approaches for studying atomic physics with relativistic and quantum electrodynamics theory. In particular, systematic studies of emission spectra in an isoelectronic sequence provide rich information for understanding the atomic structures. For such experiments, an injection method of metallic elements into an EBIT is necessary, and various schemes using a variety of techniques, e.g., a metal vapor vacuum arc ion source, an aluminosilicate ion emitter, a Knudsen cell, high-vapor-pressure complex molecules for gas-phase injection, and pulsed laser ablation, have been demonstrated [1-3]. However, each of these methods has various restrictions, for example, the temperature limits of the equipment. Namely, the development of the injection methods is one of the important research topics in the basic technology for EBITs.

Here, we demonstrate a continuous injection scheme of neutral metallic atoms into an EBIT. Figure 1 (a) shows a schematic setup for the present method. The continuous electron-beam impact realizes local evaporation in the metal target and supplies the metal vapor to an EBIT. In the present demonstration, we succeeded in observing visible emission spectra of Nb<sup>9+-11+</sup> and W<sup>12+-14+</sup> ions in the compact electron beam ion trap (CoBIT) [4]. Both niobium and tungsten are metallic elements with extremely low vapor pressure, which require heating over 2000 degrees for their evaporation, even in an ultra-high vacuum environment. Figure 1 (b) compares the emission spectra of tungsten ions injected by the present method and a gas injector using a compound W(CO)<sub>6</sub> powder. The present method suppresses the decrease in ion charge

states due to charge exchange reactions and has a good response to stopping the injection.

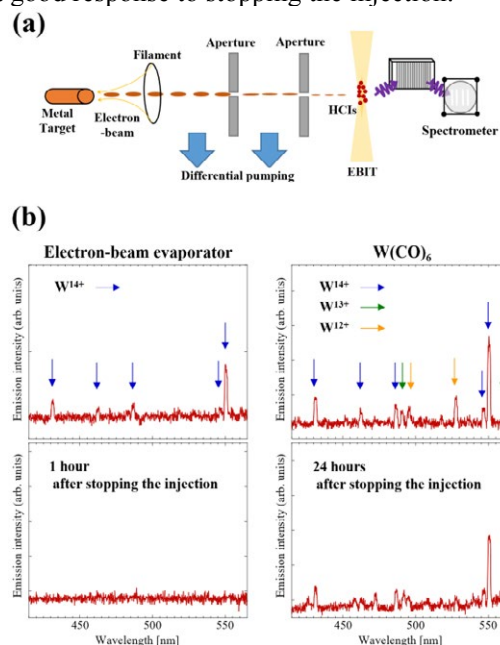


**Figure 1.** (a) Schematic overview of the present metal injection setup. (b) Comparison of emission spectra of tungsten HCIs which were generated by the present injection method(left) and a gas injector using a compound W(CO)<sub>6</sub> powder(right). The below spectra were measured after the injections were stopped. All spectra were measured by the same electron beam condition.

### References

- [1] Nakamura N *et al.* 2000 *Rev. Sci. Instrum.* **71** 684
- [2] Yamada C *et al.* 2006 *Rev. Sci. Instrum.* **77** 066110
- [3] Niles A M *et al.* 2006 *Rev. Sci. Instrum.* **77** 10F104
- [4] Nakamura N *et al.* 2008 *Rev. Sci. Instrum.* **79** 063104

\* E-mail: [naoki.kimura@riken.jp](mailto:naoki.kimura@riken.jp)

## Recombination processes in He-like oxygen ions measured at CRYRING@ESR electron cooler

W. Biela-Nowaczyk<sup>1,2\*</sup>, P. Amaro<sup>3</sup>, C. Brandau<sup>1,4</sup>, S. Fuchs<sup>4,5</sup>, F. Grilo<sup>3</sup>, M. Lestinsky<sup>1</sup>, E. B. Menz<sup>1,6,7</sup>, S. Schippers<sup>4,5</sup>, T. Stöhlker<sup>1,6,7</sup>, A. Warczak<sup>2</sup>

<sup>1</sup> GSI Helmholtzzentrum für Schwerionenforschung, Darmstadt, 64291, Germany

<sup>2</sup> Institute of Physics, Jagiellonian University, Cracow, 31-007, Poland

<sup>3</sup> Laboratory of Instrumentation, Biomedical Engineering and Radiation Physics (LIBPhys-UNL), NOVA School of Science and Technology, NOVA University Lisbon, Caparica, 2829-516, Portugal

<sup>4</sup> Justus-Liebig-Universität, Gießen, 35392, Germany

<sup>5</sup> Helmholtz Forschungsakademie Hassen für FAIR (HFHF), Campus Gießen, 35392, Germany

<sup>6</sup> Helmholtz Institute, Jena, 07743, Germany

<sup>7</sup> Friedrich-Schiller-Universität, Jena, 07743, Germany

**Synopsis** A program for DR experiments was started at CRYRING@ESR. One of the first species studied was  $O^{6+}$ . The stored ion beam was collinearly merged with the ultra-cold electron beam of the cooler, leading to electron-ion interactions. The resonant condition for dielectronic capture was achieved by detuning the electron energy. The recombination channel was identified by observing  $O^{5+}$  ions with a downstream particle detector. The preliminary results of the experiment will be shown.

Electron-ion recombination is a fundamental atomic process occurring in plasmas. Accurate experimental recombination cross-sections are particularly important for astrophysical models. Among the recombination processes the dielectronic recombination (DR) process especially affects the dynamics of astrophysical objects [1]. DR is a two-step process. The first step, called dielectronic capture, is essentially the time reversal of the Auger process. This way, an excited state is produced. To complete the DR process a radiative deexcitation takes place in a second step.

A program for DR experiments was started at the low-energy storage ring CRYRING@ESR. In order to provide the experimental data for both high- and low-temperature plasmas, DR has been investigated for the  $\Delta n=1$  and  $\Delta n=0$  transitions, respectively. The data presented in Figure 1 was collected for K-Ln ( $n=L, M, N, \dots$ ) DR of He-like oxygen ions. Oxygen is one of the most abundant elements in the universe and, therefore, is of particular importance [1, 2]. DR spectra were measured by applying collision spectroscopy of ions merged in a cold electron beam [3]. He-like oxygen ions were passing through an ultra-cold electron beam hundreds of thousands times per second. This beam was essentially a target, and as a signature for recombination,  $O^{5+}$

ions were detected. The resonant condition was achieved by changing the relative electron-ion energy. This high-precision spectroscopy method has been successfully used before [3]. It is of special importance within the research program of the SPARC Collaboration [4].

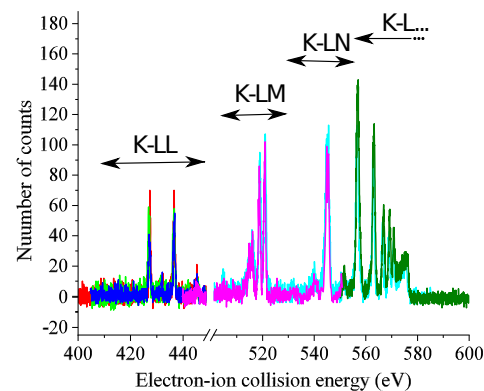


**Figure 1.** Preliminary results of measured DR resonances of  $O^{6+}$  ions at CRYRING@ESR electron cooler.

### References

- [1] Burgess A 1964 *Astron. J.* **139** 776
- [2] Schippers S 2012 *J. Phys.: Conf. Ser.* **388** 012010
- [3] Brandau C et al 2015 *Phys. Scr.* **T166** 014022
- [4] Lestinsky M et al 2016 *Eur. Phys. J. ST* **255** 797

\*E-mail: [w.biela-nowaczyk@gsi.de](mailto:w.biela-nowaczyk@gsi.de)

## Plasma screening effects on dielectronic satellites

N R Badnell\* and K Benedek

Department of Physics, University of Strathclyde, Glasgow, G4 0NG, UK

### Synopsis

We have incorporated a non-uniform ion-sphere model potential to describe the plasma screening of ions in dense plasmas into the general atomic code AUTOSTRUCTURE. We provide illustrative results of its effect on autoionization rates and dielectronic satellite line emissivities which are important plasma temperature and density diagnostics in both laboratory and astrophysical plasmas.

He-like dielectronic satellite lines [1] have been recognized as important plasma temperature and density diagnostics ever since their first observation in the solar corona [2]. Their astrophysical importance today continues through the upcoming XRISM mission whose microcalorimeter detector will give unprecedented resolution in the X-ray region [3].

Laboratory plasmas are equally important. The high core temperature to be achieved in the ITER magnetic fusion device means that the charge-exchange diagnostics used in smaller cooler devices are less applicable and dielectronic satellites will need to be utilized again [4]. Laser-produced plasmas and indirect drive inertial confinement also make important use of dielectronic satellite diagnostics [5].

At densities  $\gtrsim 10^{21} \text{ cm}^{-3}$  plasma ions can no longer be treated as isolated with a Coulomb potential extending to infinity. Plasma electrons neutralize the ions at an increasingly small distance from the nucleus. Uniform ion-sphere model potentials have been used extensively in the past. But these do not reflect the non-uniform nature of the bound and free-electron distributions. A self-consistent treatment using the Kohn-Sham equations [6] is apparently necessary.

However, recently Li et al. [7] proposed a standalone analytic plasma screening potential which reproduces the self-consistent use of non-uniform electron distributions, including the non-Maxwellian distribution found at extremely high densities where a lattice-like structure appears.

We have incorporated the non-uniform ion-

\*E-mail: [badnell@phys.strath.ac.uk](mailto:badnell@phys.strath.ac.uk)

†A PEC is just a partial dielectronic recombination rate coefficient resolved by photon energy/wavelength.

sphere potential of Li et al. [7] into the general atomic code AUTOSTRUCTURE [8]. We have carried-out a preliminary study of its effect on both autoionization rates and photon emissivity coefficients (PECs)<sup>†</sup> for He-like Oxygen dielectronic satellite lines using a fixed population model.

Autoionization rates are much more sensitive to plasma screening effects than radiative rates due to the presence of a continuum wavefunction. We find that even some of the strongest PECs change by 20% and more at densities  $> 10^{20} \text{ cm}^{-3}$  and that differences between the use of uniform and non-uniform ion-sphere potentials become noticeable by  $> 5 \times 10^{21} \text{ cm}^{-3}$ . By  $10^{22} \text{ cm}^{-3}$  the difference between the use of Maxwellian and Fermi-Dirac free-electron distributions becomes increasingly apparent.

Future work will combine such data with population modelling to make direct comparison with measurements of PECs in dense plasmas.

This work was supported by STFC UK.

### References

- [1] Dubau J and Volonté S 1980 *Rep.Prog.Phys* **43** 199
- [2] Gabriel A H and Jordan C 1969 *Nature* **221** 947
- [3] XRISM Team 2022
- [4] Piel A 2010 In *Plasma Physics* (Springer Berlin, Heidelberg)
- [5] Bhattacharyya S, Saha J K and Mukherjee T K 2015 *Phys.Rev.A* **91** 042515
- [6] Kohn W and Sham L J 1965 *Phys.Rev.* **140** A1133
- [7] Li X, Rosmej B, Lisitsa V S and Astapenko V A 2019 *Physics of Plasmas* **26** 033301
- [8] Badnell N R 2011 *Comput.Phys.Comm* **182** 1528 <http://amdpp.phys.strath.ac.uk/autos>

## The effect of electron correlation on trielectronic recombination rate coefficients for Be-like argon

Chunyu Zhang<sup>1\*</sup>, Chongyang Chen<sup>2</sup> and Nigel Badnell<sup>1</sup>

<sup>1</sup>Department of Physics, University of Strathclyde, Glasgow G4 0NG, UK

<sup>2</sup>Shanghai EBIT Lab, Key Laboratory of Nuclear Physics and Ion-beam Application, Institute of Modern Physics, Department of Nuclear Science and Technology, Fudan University, Shanghai 200433, China

The merged-beam rate coefficients of dielectronic and trielectronic recombinations (DR and TR) within  $\Delta N = 0$  channels for Be-like Ar<sup>14+</sup> were measured by Huang *et al.* [Astrophys. J. Supp. Ser. 235, 2 (2018)] with the cooler storage ring at Lanzhou, China. Meanwhile, theoretical data were also calculated with AUTOSTRUCTURE (AS) code for comparison with the measured resonance spectrum. However, the AS calculations in most cases significantly underestimated TR resonance strengths. In the present work, we find that the electron correlation be-

tween DR and TR resonance states with different captured electron principal quantum numbers  $n$  can lead to an obvious enhancement in TR resonance strengths, which is cross-validated via the relativistic distorted-wave (RDW) approximation implemented in the Flexible Atomic Code (FAC) and the semi-relativistic distorted-wave (SRDW) approximation implemented in the AS code. Previous theoretical calculations for this system, however, did not include this form of electron correlation.

---

\*E-mail: [chunyu.zhang@strath.ac.uk](mailto:chunyu.zhang@strath.ac.uk)

# Theoretical study on Dielectronic recombination process and X-ray line polarization of B-like Ar ion

S B Niu<sup>1</sup>, L Y Xie<sup>1\*</sup>, J H Deng<sup>1</sup>, W L He<sup>1</sup>, Y L Ma<sup>1</sup>, and C Z Dong<sup>1</sup>

<sup>1</sup>Key Laboratory of Atomic and Molecular Physics and Functional Materials of Gansu Province, College of Physics and Electronic Engineering, Northwest Normal University, Lanzhou 730070, China

**Synopsis** The K-shell DR strength and cross sections for B-like Ar ions are calculated using the flexible code based on the relativistic configuration interaction method with Breit and QED corrections. And the degree of linear polarization of dielectronic satellite lines, and polarization-dependent DR satellite line spectra are calculated using density matrix formalism.

Dielectronic recombination (DR) is a prominent resonant recombination process in collisions of electrons with highly charged ions that plays a vital role in determining the equilibrium conditions of hot collisional plasmas[1]. DR cross section at the resonance energy is often orders of magnitude larger than that of competing recombination processes. It strongly affects both the charge-state distribution, energy level populations, and the x-ray line emissions of plasmas. Accurate knowledge of DR cross sections, rate coefficients, and likewise of the polarization of the x-ray lines, are needed for modeling of astrophysical and fusion plasmas[2].

In this work, we studied the K-shell DR processes of B-like Ar ions using the flexible code (FAC)[3] based on the relativistic configuration interaction (RCI) method with Breit and QED corrections. The detailed resonance energies, the state-state resolved DR strength, cross sections, and rate coefficients were systematically calculated under the isolated resonance approximation. Simultaneously, the degree of linear polarization of dielectronic satellite lines, and polarization-dependent DR satellite line spectra are calculated using density matrix formalism[4]. In the calculations, the high-order trielectronic recombination (TR) and quadruelectronic recombination (QR) processes are also incorporated, that show strong effects on DR satellite line spectra of B-like Ar ions.

The work was supported by the National Key Research and Development Program of China (Grant Nos: 2022YFA1602500), the Natural Science Foundation of China (Grant Nos: 12064041, 11874051, 12104373), and funds for Innovative Fundamental Research Group Project of Gansu

\*E-mail: [xiely@nwnu.edu.cn](mailto:xiely@nwnu.edu.cn)

Province (20JR5RA541).

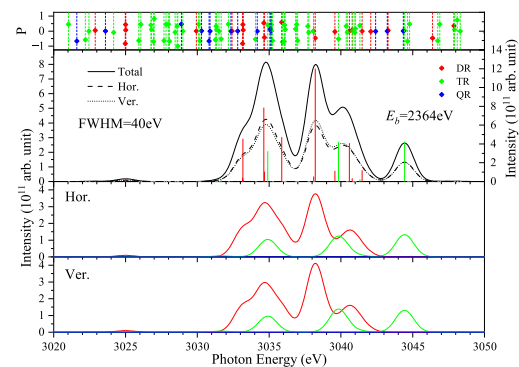


**Figure 1.** The theoretical polarization-dependent spectrum from incident electron energy of 2364eV of B-like Ar ions. The solid black line represents the total intensity of the dielectronic satellite line, while the black dotted and short line represent the intensity associated with the vertical and horizontal polarization states, respectively. The contributions of different polarization mechanisms are also shown, with the red, green, and blue lines representing the contributions of DR, TR, and QR processes, respectively. In the top panel, the position (short vertical bar) and degree of polarization (diamond) of each individual dielectronic satellite line are displayed.

## References

- [1] Inal M K and Dubau J 1987 *J. Phys. B: At. Mol. Opt. Phys.* **20** 4221
- [2] Gall A C, Dipti, Buechele S W et al 2020 *J. Phys. B: At. Mol. Opt. Phys.* **53** 145004
- [3] Gu M F, Dipti, Buechele S W et al 2020 *Can. J. Phys.* **86** 675
- [4] Shah C, Amaro P, Steinbiugge R et al 2018 *APJS*. **234** 27



## Measurement of Dielectronic Recombination of $\text{Ne}^{2+}$ at CRYRING@ESR

E B Menz<sup>1,2,3\*</sup>, M Lestinsky<sup>1†</sup>, S Fuchs<sup>4,5</sup>, W Biela-Nowaczyk<sup>1,6</sup>, A Borovik Jr.<sup>2,4</sup>, C Brandau<sup>1,4</sup>, C Krantz<sup>1</sup>, G Vorobyev<sup>1</sup>, B Arndt<sup>1</sup>, A Gumberidze<sup>1</sup>, P-M Hillenbrand<sup>1,4</sup>, T Morgenroth<sup>1,2,3</sup>, R S Sidhu<sup>1,7</sup>, S Schippers<sup>4,5</sup> and T Stöhlker<sup>1,2,3</sup>

<sup>1</sup>GSI Helmholtzzentrum für Schwerionenforschung, Darmstadt, 64291, Germany

<sup>2</sup>Helmholtz Institute Jena, 07743, Germany

<sup>3</sup>Friedrich Schiller University Jena, 07743, Germany

<sup>4</sup>I. Physikalisches Institut, Justus-Liebig University Giessen, 35390, Germany

<sup>5</sup>Helmholtz Forschungsakademie Hessen für FAIR, Campus Giessen, 35392, Germany

<sup>6</sup>Institute of Physics, Jagiellonian University, Cracow, 31-007, Poland

<sup>7</sup>School of Physics and Astronomy, The University of Edinburgh, Edinburgh, EH9 3FD, United Kingdom

**Synopsis** A measurement of dielectronic recombination (DR) of astrophysically relevant  $\text{Ne}^{2+}$  was performed at the electron cooler of the CRYRING@ESR storage ring at GSI.

Modelling plasmas is key to astrophysical research since the majority of the luminous matter in the universe is in a plasma state. Thus, accurate ionisation and recombination rates for a wide range of plasma temperatures are needed, including low-temperature environments like planetary nebulae, where the charge state distribution (CSD) is largely determined by photoionisation with light from the UV-bright, hot white dwarf in the centre of the nebula. In an optically thin, dilute plasma, electron-ion recombination competes with ionisation and drives the CSD to lower charge states. Resonant electron capture through dielectronic recombination (DR) is particularly important. DR is a recombination process whereby an electron is captured from the continuum while a second bound electron is excited, resulting in a doubly-excited state of the recombined ion which is vulnerable to auto-ionisation but can also relax via photon emission. Previous experiments have found notable discrepancies to theoretical rates for low transition energies around 1 eV, meaning that experimental data from storage rings are important for the validation of underlying rate equation networks in astrophysical modelling [1].

The CRYRING@ESR ion storage ring is a unique facility for the investigation of electron-ion recombination providing absolute cross-sections from high-precision spectroscopy [2]. The experiments were conducted at the electron cooler which provides an ultra-cold elec-

tron beam in a merged-beam configuration giving access to extremely low relative energies between the recombination partners [3]. The electron cooler section has been equipped with a new setup for DR measurements including a control system that allows for precise ramping of the electron beam energy and two particles detectors to observe recombined ions with different  $q/m$  ratios.

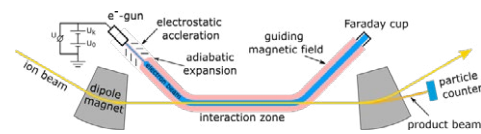


**Figure 1.** Schematic of the DR measurement setup at the CRYRING@ESR electron cooler.

This setup was used to measure DR of  $\text{Ne}^{2+}$  which will be presented in this contribution. Neon is one of the most abundant elements in the universe and has low-energy DR resonances associated with  $2s \rightarrow 2p$  transitions which have never been measured. We present data on the  $\text{Ne}^{2+}$  measurement, which we hope to be the first in a series of DR measurements on ion species abundant in low-temperature astrophysical plasma.

### References

- [1] Netzer H 2004 *Astrophys. J.* **604**, 551
- [2] Lestinsky M et al 2016 *Eur. Phys. J. Spec. Top* **225**, 797
- [3] Schippers S et al 2015 *Nucl. Instrum. Methods* **350**, 61-65

\*E-mail: [e.menz@hi-jena.gsi.de](mailto:e.menz@hi-jena.gsi.de)

†E-mail: [m.lestinsky@gsi.de](mailto:m.lestinsky@gsi.de)

## Theoretical investigation of dielectronic satellite spectra of $\text{Au}^{69+}$ - $\text{Au}^{65+}$ ions

W L He, L Y Xie\*, S B Niu, J L Rui, Y L Ma and C Z Dong†

Key Laboratory of Atomic and Molecular Physics and Functional Materials of Gansu Province, College of Physics and Electronic Engineering, Northwest Normal University, Lanzhou 730070, People's Republic of China

**Synopsis** The  $L$ -shell dielectronic recombination associated with  $2s / 2p \rightarrow 3l$  ( $\Delta n = 1$ ) excitations of Ne-like to Si-like gold ions are systematically studied using the flexible atomic code based on the relativistic configuration interaction method with considering Breit and QED corrections. The theoretical dielectronic satellite spectra is obtained.

Dielectronic recombination (DR) is a resonant electron-ion recombination process of known importance in astrophysical and fusion plasmas. It usually dominates the recombination rate of the plasma and thus the charge state balance, energy-level populations, as well as the radiative spectrum of hot plasmas [1-2]. In the indirect laser drive of inertial confinement fusion (ICF), gold is used as a work material of particular interest in a hohlraum. Hence accurate DR cross sections, rate coefficients and the degree of linear polarizations of the x-ray dielectronic satellite lines of highly ionized gold ions are needed for modeling astrophysical and fusion plasmas [3].

In this work, The  $L$ -shell DR process of highly charged Ne- to Si-like gold ( $\text{Au}^{69+}$ - $\text{Au}^{65+}$ ) ions in the ground state are investigated. The detailed resonance energies, the state-state resolved DR strength, cross sections were systematically calculated for  $\Delta n = 1$  ( $2s / 2p \rightarrow 3l$ ) transitions using the flexible atomic code (FAC) [4] based on the relativistic configuration interaction method. In the calculation of wave functions and energy levels, the contributions from electron correlations, quantum electrodynamics (QED), and Breit interaction are well considered. Furthermore, the degree of linear polarizations of dielectronic satellite lines produced by dominant LMM, LMN DR processes are calculated using density matrix formalism [5]. Fig.1 shows our calculated DR satellite spectra convoluted with a resolution function of the linewidth of  $0.02 \text{ \AA}$  (FWHM) Gaussian distribution for  $\text{Au}^{69+}$ - $\text{Au}^{65+}$  ions. The distribution of the

dominant dielectronic satellite lines is in x-ray regions with wavelength of  $0.7$ - $1.5 \text{ \AA}$ .

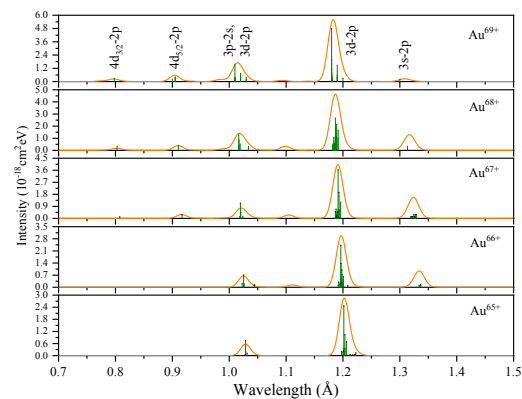


**Figure 1.** The calculated DR satellite spectra (solid line) of  $\text{Au}^{69+}$ - $\text{Au}^{65+}$  ions by convolving the dielectronic satellite line strengths (vertical bars) with a  $0.02$ - $\text{\AA}$ -wide Gaussian line profile in the interval of  $0.7$ - $1.5 \text{ \AA}$ .

The work was supported by the National Key Research and Development Program of China (Grant No: 2022YFA1602500), the Natural Science Foundation of China (Grant Nos: 12064041, 11874051, 12104373), funds for Innovative Fundamental Research Group Project of Gansu Province (20JR5RA541).

### References

- [1] Hahn Y 1997 *Rep. Prog. Phys.* **60** 691
- [2] Xie L Y et al 2022 *Phys. Rev. A.* **105** 012823
- [3] Lindl J 1995 *Phys. Plasmas.* **2** 3933
- [4] Gu M F 2008 *Can. J. Phys.* **86** 675
- [5] Shah C P et al 2018 *Astrophys. J. Suppl. Ser.* **234** 27

\* E-mail: [xiely@nwnu.edu.cn](mailto:xiely@nwnu.edu.cn)

† E-mail: [dongcz@nwnu.edu.cn](mailto:dongcz@nwnu.edu.cn)

# Electron Scattering Cross Sections for Neutral and Doubly-Charged Tin

H Umer<sup>1\*</sup>, Yu Ralchenko<sup>2</sup>, I Bray<sup>1</sup> and D V Fursa<sup>1</sup>

<sup>1</sup>Department of Physics and Astronomy, Curtin University, Perth WA, 6102, Australia

<sup>2</sup>National Institute of Standards and Technology, Gaithersburg MD, 20899, USA

**Synopsis** A cross section dataset has been calculated for electron scattering from the ground and first four excited states of neutral tin using the Relativistic Convergent Close-Coupling method. Integrated cross sections have been produced over a projectile energy range of 0.1 eV to 1000 eV for all major processes. Maxwellian rate coefficients with analytical fits are available for electron temperatures ranging from 0.5 eV to 200 eV. Cross sections for electron collisions with Sn<sup>2+</sup> have also been produced for various transitions.

With recent developments in the fields of fusion research and nano-lithography, collision datasets for tin are becoming increasingly important. Plasma-facing components in tokamak fusion reactors such as ITER experience large amounts of erosion due to bombardment from the plasma [1]. This damage from erosion is especially an issue for the divertor region of such fusion reactors [2]. To combat this, liquid metal designs for the divertor are currently in development for the European DEMO reactor which promises major improvements over the current tungsten mono-block design adopted in ITER. The primary candidate material for this new design is tin. Extreme-ultraviolet (EUV) lithography is an advanced microchip manufacturing technique which uses a tin plasma to generate the 13.5 nm light [3]. However, the details on how this light is produced in the plasma are not well understood. Ongoing research in both fusion and EUV requires reliable electron collision datasets for tin and its ions.

The Relativistic Convergent Close-Coupling method (RCCC) [4] has been applied to calculate integrated cross sections for elastic scattering, various excitations, total scattering (TCS), total-inelastic scattering (inel-TCS), and single-ionisation of the ground and first four excited states of neutral tin. State-resolved cross sections have been produced for excitations to all states in the  $5p^2$ ,  $5p6s$ ,  $5p5d$  and  $5p6p$  manifolds. Previous studies for tin have not been as extensive and used first-order approximations which are accurate only at high projectile energies. This is the first study in which accurate re-

\*E-mail: [haadi.umer@postgrad.curtin.edu.au](mailto:haadi.umer@postgrad.curtin.edu.au)

sults have been produced for all transitions studied over the entire projectile energy range from 0.1 eV to 1000 eV. Rate coefficients with fits to a simple formula have been included for use in modelling applications.

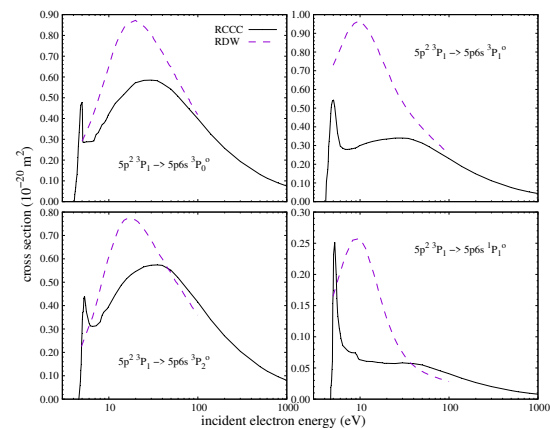


**Figure 1.** Comparison between RCCC and Relativistic Distorted Wave (RDW) [5] for excitations from  $5p^2 \ ^3P_1$  to the  $5p6s$  manifold in neutral tin.

Similarly, various cross sections for e-Sn<sup>2+</sup> have also been calculated.

## References

- [1] Foster A *et al* 2007 *Journal of Nuclear Materials* **363** 152
- [2] Rindt P *et al* 2021 *Fusion Engineering and Design* **173** 112812
- [3] O'Sullivan G *et al* 2015 *J Phys B: At. Mol. Opt. Phys.* **48** 144025
- [4] Fursa D V and Bray I 2008 *Phys. Rev. Lett.* **100** 113201
- [5] Sharma L *et al* 2017 *Eur. Phys. J. D* **71** 121

## Electron impact ionization of atoms and molecules: an improved BBK model

M Attia<sup>1\*</sup>, T Khatir<sup>1,2</sup>, S Houamer<sup>1</sup> and K Bechane<sup>1</sup>

<sup>1</sup> LPQSD, Department of Physics, Faculty of Sciences, University Sétif1, Sétif 19000, Algeria

<sup>2</sup> CRNA, 02, Boulevard Frantz Fanon, B.P. 399 Alger RP, Algeria

**Synopsis** Triple differential cross sections (TDCSs) are calculated using a new model to study the dynamics of electron impact ionization of atoms and molecules. The model is in fact an improved BBK description where the two outgoing electrons are both described by a Coulomb wave with variable charges  $Z(r)$  instead of an effective constant charge. Calculations are carried out for coplanar asymmetric kinematics, and the results are compared with those from available experiments.

In the present work we introduce an improved theoretical approach to describe the  $(e,2e)$  reaction for atoms and molecules, it is in fact an extension of our earlier studies which provided rather good agreement between experiment and theory [1]. The present theoretical description is a fully quantum mechanical approach, it is actually a kind of BBK model in which the ejected and the scattered electrons are both represented by Coulomb waves with variable charge  $Z(r)$  instead of an effective charge ( $Z=1$  for  $(e,2e)$ ). The ejected electron sees a charge  $Z_e = N$  at the center of the target and  $Z_e = 1$  asymptotically. For the scattered electron we have to emphasize an important detail since we consider here asymmetric coplanar kinematics, where the scattered electron is faster than the ejected electron. At the center of the target the scattered electron sees a charge  $Z_s = N$ , while asymptotically two features should be considered: first, the scattered electron can asymptotically see a charge  $Z_s = 1$  like the ejected one; the model is then called BBK2CWZ1. On the other hand, as the scattered electron is faster, he could also feel that the ejected electron is part of the ionic target and sees an asymptotic charge  $Z_s = 0$ , the model is then called BBK2CWZ0. As an illustration, we investigate in figure 1 the ionization of argon 3p [2]. It is observed that the best description is exhibited by BBK2CWZ1 and BBK2CWZ0 models which provide results rather close to the data in almost parts of the TDCS. The BBK model in contrast appears unable to reproduce most of the data since no structure of the TDCS is visible beyond an ejected angle of around  $90^\circ$ . This should be attributed to the fact that the kinematics represented here correspond to a large momentum transfer ( $K=1.27$  au) involving a large recoil momentum

absorbed by the target. As a result, the interaction with the target, especially that of the outgoing electrons, with the residual ion is important. The modeling of the process in the recoil region therefore represents a challenge for the theory. In this case BBK turns out to be unable at all to describe the process in the recoil region.

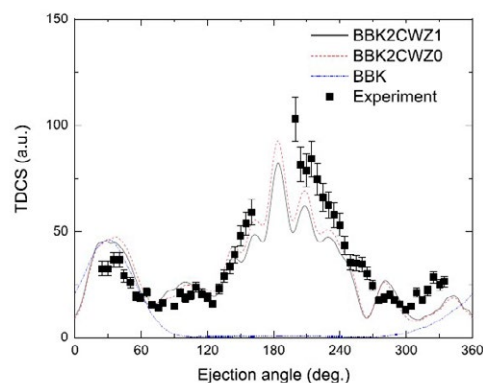


**Figure 1.** TDCS, in  $10^{-4}$  au, for the ionization of argon 3p with  $\theta_a = 3^\circ$ ,  $E_a = 500$ ,  $E_b = 205$  eV [3]. The theoretical results have been normalized to BBK2CWZ1 at the maximum of the binary peak. The data have been normalized for the best visual agreement with theory.

### References

- [1] Khatir T, Houamer S and Dal Cappello C 2019 J. Phys. B **52** 245201
- [2] Attia M, Houamer S, Khatir T, Bechane K and Dal Cappello C 2023 J. Phys. B . **56** 075201
- [3] Catoire F et al 2006 J. Phys. B **39** 2827

\* E-mail: [attia.maroua19@gmail.com](mailto:attia.maroua19@gmail.com)

## Laser-assisted ionization of atomic hydrogen by the impact of an twisted electron beam

Neha<sup>1\*</sup>, N Dhankhar<sup>1†</sup> and R Choubisa<sup>1‡</sup>

<sup>1</sup> Department of Physics, BITS Pilani, Pilani Campus Vidya Vihar, Pilani - 333031

**Synopsis** We compute the Triple Differential Cross Section (TDCS) for Laser-assisted (e,2e) processes on atoms to investigate the effects of Laser parameters, intrinsic angular momentum, and the opening angle ( $\theta_p$ ) of the twisted electron beam. We observed that these parameters have a significant impact on the angular profile of TDCS.

Since the first experimental measurement of (e,2e) process by Ehrhardt et al. [1], there have been extensive theoretical and experimental studies on (e,2e) processes on different atoms, molecules, and solid targets. In the last decade, the study of the influence of the laser field on the dynamics of (e,2e) collisions by a plane wave on different atomic targets also has been done [2] [3]. In recent times, there have been few studies of (e,2e) and (e,3e) processes on atoms and molecules using twisted electron beam [4]. To the best of our knowledge, no study has been conducted on Laser-assisted (LA) twisted electron beam impact ionization processes. We can get more information when we study the ionization of atoms and molecules by the impact of the twisted electron beam in the presence of a laser field. The Laser-assisted TEB ionization processes represent new degrees of freedom like laser frequency, field strength, orbital angular momentum, and apex angle of the twisted electron beam. In this communication, we present the results of our calculations for (e,2e) process on atomic targets to elucidate the effects of OAM and the apex angle of the twisted electron beam in the presence of a laser field on the coincidence differential cross sections. The formalism is de-

veloped within the first Born approximation using the plane wave and the twisted wave for the incident electron beam. The interaction of the laser field with the unbound electrons is treated in a nonperturbative way by the use of Volkov waves. We have used the Coulomb wave function for the ejected electron moving in the combined field of the residual ion and the laser. Our study on the Laser-assisted (e,2e) process showed that TDCS significantly depends on OAM no.  $m$  and the apex angle ( $\theta_p$ ) of the twisted electron beam. At the conference, we will present our detailed results for LA (e,2e) processes.

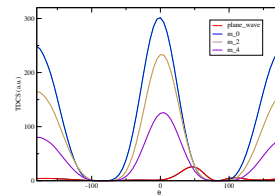


**Figure 1.** TDCS as a function of ejected electron angle  $\theta_e$  for H atom in coplanar asymmetric geometry. Incident energy ( $E_i$ ) = 500eV, ejected electron ( $E_e$ ) = 20eV, scattering angle ( $\theta_s$ ) = 100mr, opening angle ( $\theta_p$ ) = 100mr, Laser frequency  $\omega$  = 1.17eV, no. of transfer photons ( $l$ ) = 1, Laser field strength ( $\epsilon_p$ ) =  $6 * 10^9 V/m$ .

### References

- [1] Ehrhardt et al. 1969 PhysRevLett.22.89 **22** 89
- [2] Joachain et al. 1988 PhysRevLett.61.165 **61** 165
- [3] Ajana et al. 2014 Journal of Phys B: At. Mol. Opt. Phys. **47** 17
- [4] Nikita Dhankhar et al 2022 J. Phys. B: At. Mol. Opt. Phys. 55 165202 **55** 165202

\*E-mail: [p20210062@pilani.bits-pilani.ac.in](mailto:p20210062@pilani.bits-pilani.ac.in)

†E-mail: [mndhankhar.92@gmail.com](mailto:mndhankhar.92@gmail.com)

‡E-mail: [rchoubisa@pilani.bits](mailto:rchoubisa@pilani.bits)



## Helical structures of alignment angle function in the electron-atom collision studies

M Piwiński<sup>1\*</sup> and Ł Kłosowski<sup>1</sup>

<sup>1</sup>Institute of Physics, Faculty of Physics, Astronomy and Informatics, Nicolaus Copernicus University in Toruń,  
Grudziądzka 5, 87-100 Toruń, Poland

**Synopsis** The Electron Impact Coherence Parameters (EICP) describing the inelastic electron-atom collision process were widely analysed in both energy and scattering angle domains. Our Zn and Cd EICP experimental data found narrow structures predicted by theories. Such local structures can be used to precisely compare and verify obtained theoretical results with experimental data.

The Electron Impact Coherence Parameters are widely used for a precise description of the inelastic electron-atom collision process [1]. Such experimental data can be obtained using electron-photon coincidence [2] or superelastic technique [3]. Due to typically long-lasting measurements, the database of EICP values is very limited. Such experimental studies have been realized so far for calcium [4], barium [5], magnesium [6], ytterbium [7], helium [8, 9], zinc [10, 11] and cadmium [12]. However, in most cases, the lack of systematic data for a wide range of collision energy makes it impossible to form general conclusions on EICP dependence on energy and scattering angle. Our systematic studies on cadmium [13] and zinc [14] enabled us to observe some characteristic behaviour of the EICP functions. In particular, it concerns the helical structure of the alignment angle parameter. Due to its very narrow character, this structure can be used to compare and verify theoretical models with experimental results.

Moreover, this issue is a scarce physical phenomenon where one of the scattering channels is completely closed. It is manifested by reaching the maximum parameter value determining total angular momentum transfer  $L_{\perp}$ , and zeroing the shape parameter  $P_L$ .

Nowadays, there is no analytical method for predictions of the experimental conditions for which such structures can be observed. Thus identifying them in the EICP data brings us to a deeper understanding of the collision process. Such structures were found in our zinc and

cadmium data. However, it was also possible to identify them in the existing EICP data for magnesium [15], calcium [3], strontium [16] and barium [17].

### References

- [1] Andersen N. *et al.* 1988, *Phys. Rep.* **165**, no. 1-2, 1
- [2] Piwiński M. *et al.* 2013 *Eur. Phys. J. Special Topics* **222**, no. 9, 2273
- [3] Knight-Percival A. *et al.* 2011 *J. Phys. B: At. Mol. Opt. Phys.* **44**, 105203
- [4] Dyl D. *et al.* 1999 *J. Phys. B: At. Mol. Opt. Phys.* **32**, no. 3, 837
- [5] Johnson P. V. *et al.* 2005 *J. Phys. B: At. Mol. Opt. Phys.* **38**, 2793
- [6] Pursehouse J. *et al.* 2018 *Phys. Rev. A* **98**, 022702
- [7] Hein J. D. *et al.* 2011 *J. Phys. B: At. Mol. Opt. Phys.* **44**, 075201
- [8] Kłosowski Ł. *et al.* 2007 *Meas. Sci. Tech.* **18**, 3801
- [9] Kłosowski Ł. *et al.* 2009 *Phys. Rev. A* **80**, no. 6, 062709,
- [10] Piwiński M. *et al.* 2012 *Phys. Rev. A* **86**, no. 5, 052706
- [11] Piwiński M. *et al.* 2015 *Phys. Rev. A* **91**, no. 6, 062704
- [12] Piwiński M. *et al.* 2002 *J. Phys. B: At. Mol. Opt. Phys.* **35**, no. 18, 3821
- [13] Piwiński M. *et al.* 2006 *J. Phys. B: At. Mol. Opt. Phys.* **39**, no. 8, 1945
- [14] Piwiński M. *et al.* 2018 *J. Phys. B: At. Mol. Opt. Phys.* **51**, no. 8, 085002
- [15] Fursa D.V. *et al.* 2001 *Phys. Rev. A* **63**, 032708
- [16] Beyer H.J. *et al.* 1994 *Z. Phys. D* **30**, 91
- [17] Fursa D.V. *et al.* 1999 *Phys. Rev. A* **59**, 282

\* E-mail: Mariusz.Piwiński@fizyka.umk.pl

## A binary (e, 2e) study on Ne at incident electron energies up to 4 keV: Asymptotic behavior of the (e, 2e) cross section to its high energy limits

I Nakajima<sup>1</sup>, M Yamazaki<sup>1\*</sup>, Yu Popov<sup>2,3</sup>, S Houamer<sup>4</sup> and M Takahashi<sup>1†</sup>

<sup>1</sup> Institute of Multidisciplinary Research for Advanced Materials, Tohoku University, Sendai, 980-8577, Japan

<sup>2</sup> Skobeltsyn Institute of Nuclear Physics, Lomonosov Moscow State University, Moscow, 119991, Russia

<sup>3</sup> BLTP, Joint Institute of Nuclear Research, Dubna, Moscow Region 141980, Russia

<sup>4</sup> LPQSD, Department of Physics, Faculty of Science, University Sétif-1, 19000 Setif, Algeria

**Synopsis** We have examined the range of the validity of the distorted-wave Born approximation (DWBA) and the plane-wave impulse approximation (PWIA) by comparisons with the ratio of binary (e, 2e) cross sections measured for the Ne 2s and 2p orbitals. It is found that while the DWBA reproduces well the experiment over an incident electron energy ( $E_0$ ) range up to 4.0 keV, the agreement between the PWIA and experiment is lower at lower  $E_0$ . This observation indicates that not only effect of the difference in electron density distribution but also that in potential the target electron sees when ionizing are clearly probed in terms of the cross section ratio.

Binary (e, 2e) spectroscopy, also known as electron momentum spectroscopy (EMS), is an experimental technique to look at individual electron orbitals in momentum space [1,2]. The key to directly relate the (e, 2e) cross section to momentum distribution of the ionized electron orbital is the plane-wave impulse approximation (PWIA). The knowledge about the range of the validity of the PWIA is therefore of vital importance for promoting molecular science with EMS. We have thus conducted binary (e, 2e) experiments on the Ne 2s and 2p orbitals at several incident electron energies ( $E_0$ ) up to 4.0 keV. The momentum and  $E_0$  dependence of the cross sections of the two orbitals were analyzed in both shape and relative intensity to make the present study a rigorous test for the PWIA.

Figure 1 plots the relative intensity of the 2s orbital to the 2p orbital as a function of  $E_0$ . Here, since the relative intensity is maintained in the experiment, the experimental intensity of the 2p orbital is normalized to associated distorted-wave Born approximation (DWBA) and PWIA calculations respectively, while spectroscopic factor ( $S_f$ ) or pole strength is considered. It is seen that the DWBA is always very close to the  $S_f$  value of 0.869 for the 2s orbital predicted by molecular orbital theory [3]. This means that the DWBA reproduces well the experiment over the  $E_0$  range covered. On the other hand, although the PWIA is far from the  $S_f$  value at  $E_0 = 1.2$  keV, it approaches the value with the increase in  $E_0$ . In the contribution, we show that these

observations originate from the difference in potential that the target electron sees when ionizing as well as the difference in electron density distribution between the two orbitals. The target goal of the present study is to develop a modified PWIA theory that relates the experimental responses to spatial distributions of molecular orbitals in the most quantitative way.

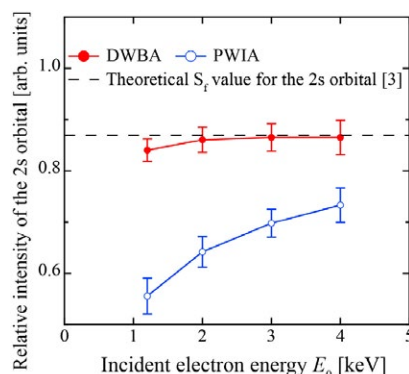


Figure 1. Relative intensity of the (e, 2e) cross sections of the Ne 2s orbital to the 2p orbital.

### References

- [1] Weigold E and McCarthy I E 1999 *Electron Momentum Spectroscopy* (New York: Kluwer Academic/Plenum)
- [2] Takahashi M 2009 *Bull. Chem. Soc. Jpn.* **82** 751
- [3] Fronzoni G and Decleva P 1997 *Chem. Phys.* **220** 15

\* Present address: School of Science, Tokyo Tech.

† E-mail: [masahiko.takahashi.c4@tohoku.ac.jp](mailto:masahiko.takahashi.c4@tohoku.ac.jp)

## Low to intermediate energy (e,2e) measurements from Krypton in the perpendicular plane

J P Rogers<sup>1\*</sup>, and A J Murray<sup>1†</sup>

<sup>1</sup>Photon Science Institute, Dept. of Physics and Astronomy, University of Manchester, Manchester, M13 9PL, UK

**Synopsis** New experimental results for (e,2e) measurements from Kr in the perpendicular plane are presented from 2 eV to 120 eV above the ionization potential. The results are compared to data from other noble gases, as well as to published calculations in this energy regime. A trend in the evolution of the Argon cross-section with energy that disagrees with theory is likewise observed in Krypton in the same energy range.

(e,2e) measurements provide a sensitive test of different models of the ionization process. The collision results in scattered and ejected electrons that can emerge from the interaction over  $4\pi$  steradians, their correlation having different probabilities that depend on their momenta and energy. The probability of ionization is determined experimentally by measuring a differential cross-section  $\sigma$  that depends on the incident momentum  $\mathbf{k}_0$  and the outgoing electron momenta  $\mathbf{k}_1$  and  $\mathbf{k}_2$ .

In the work presented here, the outgoing electrons are detected in the perpendicular plane orthogonal to  $\mathbf{k}_0$  and are selected to have equal energies. The incident electron beam is produced by an unselected energy gun and the outgoing electrons are detected in coincidence using two hemispherical analysers. The incident beam ranges in energy from 2 eV to 120 eV above the ionization potential (IP) of Krypton (14 eV).

New data obtained for this target are then compared to measurements from previous experiments [1] and to calculations using different models as published in [3]. The results are also compared to data from Argon in the same energy regime that found disagreement with the calculations [2]. An example of these results is shown in Figure 1 at an incident energy of 50 eV above the IP for both targets. The calculations are a distorted wave Born approximation (DWBA), a plane wave approximation (PWA) and a DWBA calculation that includes post collisional interactions (PCI) (DWBA +  $N_{ee}$ ). The DWBA calculation without PCI is seen to agree with experiment for Krypton but not with the data for

Argon under the same kinematic conditions.

A full set of results will be presented for both targets, allowing the data to be compared over a wide range of energies in this kinematic regime.

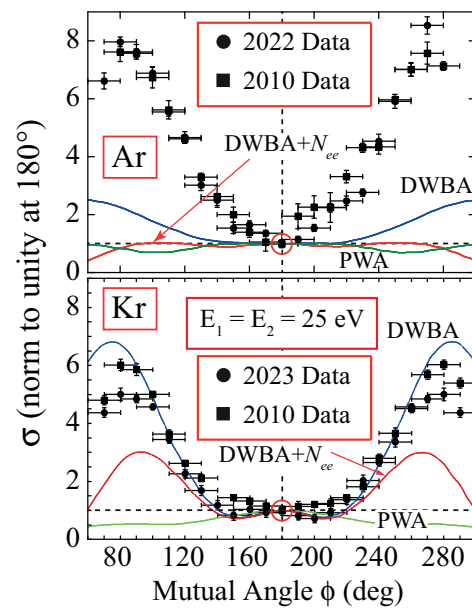


**Figure 1.** Results from Argon and Krypton 50 eV above the IP compared to calculations from [3].

### References

- [1] Nixon K L and Murray A J and Kaiser C 2010 *J. Phys. B: At., Mol. Opt. Phys.* **43** 085202
- [2] Patel M and Murray A J 2022 *Phys. Rev. A* **105** 042815
- [3] Miller F K and Walters H R J and Whelan C T 2015 *Phys. Rev. A* **91** 012706

\*E-mail: [joshua.rogers@manchester.ac.uk](mailto:joshua.rogers@manchester.ac.uk)

†E-mail: [andrew.murray@manchester.ac.uk](mailto:andrew.murray@manchester.ac.uk)

## FEBID of $[(\text{CH}_3)_2\text{AuCl}]_2$ and its fragmentation through low energy electron interaction under single collision conditions.

E Bilgilisoy<sup>1</sup>, A Kamali<sup>2</sup>, A Wolfram<sup>1</sup>, T Gentner<sup>3</sup>, G Ballmann<sup>3</sup>, S Harder<sup>3</sup>, H Marbach<sup>1,4</sup>, and O Ingólfsson<sup>2,\*</sup>

<sup>1</sup>Physikalische Chemie II, Friedrich-Alexander Universität Erlangen-Nürnberg, 91058 Erlangen, Germany

<sup>2</sup>Science Institute and Department of Chemistry, University of Iceland, Dunhagi 3, 107 Reykjavik, Iceland

<sup>3</sup>Inorganic and Organometallic Chemistry, Universität Erlangen-Nürnberg, 91058 Erlangen, Germany

<sup>4</sup>Carl Zeiss SMT GmbH, 64380 Roßdorf, Germany

**Synopsis** Combined study of UHV FEBID of  $[(\text{CH}_3)_2\text{AuCl}]_2$  and its fragmentation by dissociative electron attachment and dissociative ionization in the gas phase under single collision conditions.

Based on the optoelectronic properties of gold nanoparticles, these have found applications in a wide range of medical imaging, diagnostics, and therapy. [1] These gold nanoparticles are generally of a shape and size distributions and several physical and chemical methods have been established for their fabrication. [2] However, methods to fabricate well defined 3D nanostructures to be integrated into electronic devices are less advanced. Focused electron beam induced deposition (FEBID) [3] is one such method, ideally suited for 3D printing of free-standing nanostructures of as good as any shape on any surface topography.

In FEBID a precursor gas is introduced close to a substrate surface under vacuum conditions. These are physisorbed on the surface and are decomposed under a tightly focused high-energy electron beam. The volatile fragments are pumped away while the non-volatile build the deposit, and lateral control is achieved by moving the beam and vertical control by variation of the dwell time. For metallic nanostructures, the precursor molecules are generally organometallics and in the ideal case all ligands are cleaved of and pumped away, leaving a pure metal deposit. Currently, however, incomplete decomposition of the precursor molecules and thus ligand contamination in the deposits remains the main challenge in FEBID. Consequently, significant effort has been given in the last decade to design precursor molecules that enable high purity deposits. This is not a simple task as inelastically scattered and secondary electrons, produced through interaction of the primary beam with the substrate and the forming deposits, play a significant role in the fragmentation process. Hence, the electrons respon-

sible for the decomposition have a wide energy distribution and may cause dissociation by as different processes as dissociative electron attachment (DEA), dissociative ionization (DI), and neutral and dipolar dissociation through electron excitation (ND and DD, respectively). [4] It is thus important to understand the underlying processes and their extent, and how these influence the deposits, to eventually be able to design high performance precursors.

Here we take a step in this direction and study the morphology and composition of deposits created from  $[(\text{CH}_3)_2\text{AuCl}]_2$  as precursor in FEBID under UHV conditions. The compound is also studied with respect to its fragmentation through DEA and DI in the gas phase under single collision conditions and the appearance energies are determined for individual channels. These are compared to quantum chemical threshold calculations for the  $m/z$  ratios observed to aid the assignment of ions and the neutral counterparts formed in these processes. Comparison is also made with a previous high-vacuum (HV) FEBID [5] of the same precursor, where co-deposition of components from the background gas are expected to play a role.

### References

- [1] Dykman LA and Khlebtsov NG 2011 *Acta Naturae*. 3(2), 34–55.
- [2] Zhang Y et al. 2014 *Materials*, 7(7), 5169–5201
- [3] Utke I et al. 2008 *J. Vac. Sci. Technol.* B 2, 4
- [4] Ingólfsson O 2019 *Low-Energy Electrons Fundamentals and Applications*, Jenny Stanford Publishing, New York.
- [5] Van Dorp W 1985 *Langmuir*, 2014. 30(40): p. 12097-12105

\* E-mail: [odduring@hi.is](mailto:odduring@hi.is)

## Triple ionization and fragmentation of benzene trimers following ultrafast intermolecular Coulombic decay

J Zhou<sup>1</sup>, X Yu<sup>2</sup>, S Luo<sup>2</sup>, X Xue<sup>1</sup>, S Jia<sup>1</sup>, X Zhang<sup>2</sup>, Y Zhao<sup>1</sup>, X Hao<sup>1</sup>, L He<sup>2</sup>, C Wang<sup>2</sup>, D Ding<sup>2\*</sup>, X. Ren<sup>1†</sup>

<sup>1</sup>School of Physics, Xi'an Jiaotong University, Xi'an 710049, China

<sup>2</sup>Institute of Atomic and Molecular Physics, Jilin University, Changchun 130012, China

**Synopsis** Intermolecular interactions that involve aromatic rings are ubiquitous in biochemistry and play a crucial role in determining the properties of various organic materials. Here, we study the triple ionization and fragmentation mechanisms of benzene trimers upon electron-collision ionization. Using the triple-coincidence ion momentum spectroscopy, accompanied by ab-initio calculations and further supported by strong-field laser experiments, the fragmentation dynamics of benzene trimers are revealed in detail.

The noncovalent  $\pi$ - $\pi$  interaction between aromatic molecules has been associated with cooperative phenomena such as protein folding, DNA base stacking, self-assembly, crystal synthesis, and so on. However, our knowledge of the structures and dynamics of high-order aromatic clusters remains incomplete due to the increased difficulty in isolating artificial model systems.

In this work, we study the ionization and subsequent reaction dynamics of benzene trimer initiated by electron impact (260 eV). The experiments were performed using a multiparticle imaging spectrometer (reaction microscope), where the resulting cations are measured in coincidence and their three-dimensional momentum vectors are determined [1]. In our experiment, the  $C_6H_6^+ \cdot C_6H_6^+ \cdot C_6H_6^+$  trications are primarily produced via two channels, i.e., (i) The double sequential ionization plus intermolecular Coulombic decay (dSI+ICD), where one outer-valence and one inner-valence vacancy are created separately at two molecules of the trimer and the following ICD process causes the ionization of the third benzene molecule (Fig. 1a); (ii) The double intermolecular Coulombic decay (dICD), which is initiated by electron-collision with the removal of a deep-lying carbon 2s (C2s) inner-valence electron. Afterward, an electron from the outer-valence shell of  $C_6H_6^+$  fills the  $C2s^{-1}$  vacancy, and the energy released ionizes the neighboring two molecules (Fig. 1b).

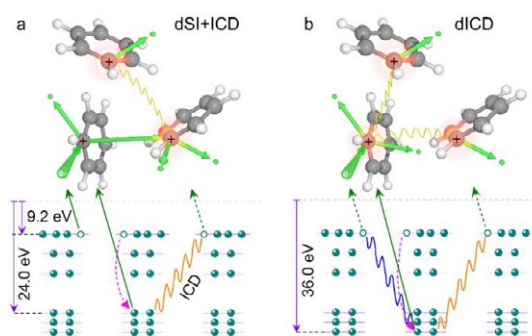


**Figure 1.** (a) Schematic of electron-impact induced double sequential ionization plus ICD (dSI+ICD) and (b) double ICD (dICD) processes.

Our further strong-field laser experiments show that electron-collision-induced dSI+ICD and dICD processes can take place in the fs regime. The nuclear dynamics during the ultrafast timescale are nearly frozen, which allows us to reconstruct the structure of the benzene trimer by Coulomb explosion imaging. These results indicate that the cyclic structure is the main conformer of benzene trimers in the gas jet. Due to the prevalence of aromatic trimers in proteins and DNA [2], and the crucial role of secondary electrons in radiation effects in biological tissues [3], the present findings could have important implications for biomolecular imaging and also a better understanding of radiation biology at the molecular level. Details will be presented at the conference.

### References

- [1] J Zhou et al. 2022 *Nat. Commun.* **13** 5335.
- [2] S Sathiyashivan et al. 2015 *RSC Adv* **5** 74705.
- [3] M Huels et al. 2003 *JACS* **125** 4467.

\* E-mail: dajund@jlu.edu.cn

† E-mail: renxueguang@xjtu.edu.cn



## Computed total and partial cross sections for direct electron and positron impact ionisation

V Graves<sup>1\*</sup>,

<sup>1</sup>School of Physical Sciences, The Open University, Walton Hall, Milton Keynes, UK

**Synopsis** RAPID-CS is a software tool for computing total and partial ionisation cross sections. In particular, this tool requires no experimental input but maintains a reasonable accuracy with experimental results. Here, electron and positron impact ionisation is compared for a range of molecules against experimental data.

Understanding ionisation events has applications in a variety of areas, including, plasma physics, space sciences, health sciences and environmental sciences. For these applications, accurate measurements for a range of molecules are required.

There are many methods for computing total ionisation cross sections that don't require experimental data. For example, the (e-)BEB[1] cross section was initially developed for electron impact ionisation and only uses orbital constants that can be easily determined from an HF calculation. Various modifications of the BEB cross section have been investigated in order to describe positron impact ionisation as well.

Partial cross sections can be determined by taking a total cross section and multiplying it by a fragment-specific branching ratio. From an ionisation event, the target molecule can dissociate into different fragments. The probability that the target molecule will dissociate into a specific fragment is the branching ratio.

Here, we outline the new software tool called RAPID-CS; Relative and Absolute Partial Ionisation and Dissociation - Cross Sections. This tool can be used to compute fragmentation branching ratios of ionisation and dissociative ionisation events using a simple dissociation threshold law[2]. The functionality then extends to providing total cross sections which can be combined with the branch ratios to generate partial cross sections.

Electron and positron impact ionisation are investigated for a range of molecules and compared to experimental data when possible. The aim is to produce a full solution for ionisation problems which requires no experimental input

and has high accuracy. Figure 1 displays e-BEB total and computed partial electron impact ionisation cross sections of H<sub>2</sub>O compared to experimental data[3]. It can be seen that the total cross section is in reasonably good agreement with the experiment. The same can be said for the partial cross sections. The only exception is OH<sup>+</sup> which is slightly underestimated by the theory.

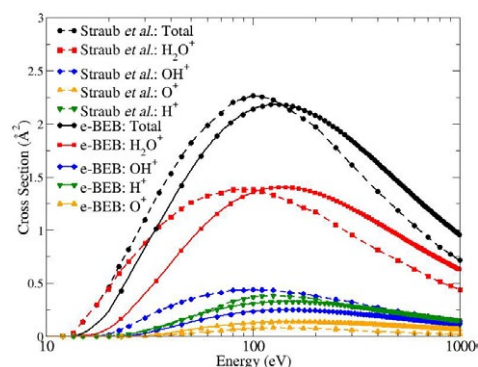


**Figure 1.** Total and partial electron impact ionisation cross sections of H<sub>2</sub>O. Experimental data recommended by Straub *et al.*[3]; dashed lines, e-BEB; solid lines. Black circles; total cross section, red squares; H<sub>2</sub>O<sup>+</sup> partials, blue diamonds; OH<sup>+</sup> partials, yellow up-triangles; O<sup>+</sup> and green down-triangles; H<sup>+</sup> partials.

### References

- [1] Kim Y K, Weinberger N M, Ali M A, and Rudd M E 1997 *J. Chem. Phys.* **106** 1026-1033
- [2] Huber S E, Mauracher A, Süß D, Sukuba J, Borodin D, and Probst M 2019 *J. Chem. Phys.* **150** 024306
- [3] Straub H C, Lindsay B G, Smith K A, and Stebbings R F 1998 *J. Chem. Phys.* **108** 109-116

\*E-mail: [vhg7@open.ac.uk](mailto:vhg7@open.ac.uk)

## Convergent close-coupling calculations of electrons scattering on $\text{HeH}^+$

L H Scarlett<sup>1\*</sup>, M C Zammit<sup>2</sup>, I Bray<sup>1</sup>, B I Schneider<sup>3</sup>, and D V Fursa<sup>1</sup>

<sup>1</sup>Department of Physics and Astronomy, Curtin University, Perth, Western Australia 6102, Australia

<sup>2</sup>Theoretical Division, Los Alamos National Laboratory, Los Alamos, New Mexico 87545, USA

<sup>3</sup>National Institute of Standards and Technology, Gaithersburg, Maryland 20899-8422, USA

**Synopsis** We use the molecular convergent close-coupling (MCCC) method to perform calculations of 10–1000 eV electron scattering on the ground state of  $\text{HeH}^+$ . Cross sections are presented for excitation of the first 18 excited electronic states, as well as ionisation. We also present cross sections for  $\text{He}^+$  and  $\text{H}^+$  production following dissociative excitation and ionisation.

The helium hydride molecular ion  $\text{HeH}^+$  is comprised of the two most universally abundant elements, hydrogen and helium. Along with the hydrogen molecule,  $\text{HeH}^+$  is expected to form in the cooler edge and divertor regions of fusion reactors, where it is well-known that electron collisions with molecular species play an important role in governing the plasma dynamics. It was also the first molecule to form in the early stages of the universe, and is thought to be present in significant quantities in helium-rich stars, nebulae, and molecular clouds. Collisional reactions with the early forming molecules such as  $\text{HeH}^+$  would have had a significant effect on the gravitational collapse of interstellar clouds during the formation of the first stars.

Understanding the important influence of electron collisions with molecules in plasmas requires accurate cross-section data for many reactions over a broad range of collision energies. Here we apply the molecular convergent close-coupling (MCCC) method to study electronic excitation and ionisation from the ground (electronic and vibrational) state of  $\text{HeH}^+$ .

Previous calculations for this collision system have been almost exclusively limited to low-energy rovibrational excitation, and the only available measurements are for helium ion production following electron-impact dissociation of  $\text{HeH}^+$ . In this poster, we present cross sections for ionisation, and excitation of the first 18 excited electronic states, which we use to estimate the  $\text{He}^+$  production cross section for comparison with the experiment.

Figure 1 presents MCCC cross sections [1] for dissociative excitation and ionisation of  $\text{HeH}^+$  leading to  $\text{He}^+$  fragments. Comparison is made with measurements from Lecointre *et al.* [3] and Strömholm *et al.* [4], and the complex Kohn calculations of Orel & Rescigno [2]. The MCCC DE calculations agree with

the measurements of Strömholm *et al.* [4] at low energies, and are in reasonable agreement with Lecointre *et al.* [3] for ionisation. However, the MCCC total  $\text{He}^+$  production cross section is 30% larger than measurements at the cross section peak around 100 eV incident energy. With only one set of measurements and no other calculations in this energy region the source of the discrepancy is not clear, and further experimental and theoretical work would be desirable to help clarify the situation.

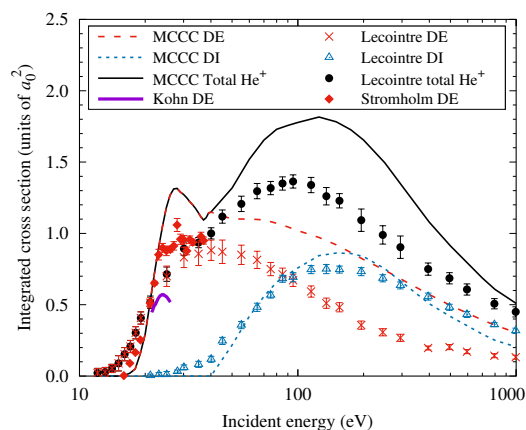


**Figure 1.** Cross sections for production of  $\text{He}^+$  from electron-impact dissociative excitation (DE) and ionisation (DI) of  $\text{HeH}^+$ . Comparison is made between the MCCC calculations, the complex Kohn calculations of Orel & Rescigno [2], and the measurements of Lecointre *et al.* [3] and Strömholm *et al.* [4].

### References

- [1] Scarlett L H *et al.* 2022 *Phys. Rev. A* **106** 042818
- [2] Orel A E and Rescigno T N 1991 *Phys. Rev. A* **44** 4328
- [3] Lecointre J *et al.* 2014 *J. Phys. B* **47** 015203
- [4] Strömholm C *et al.* 1996 *Phys. Rev. A* **54** 3086

\*E-mail: [liam.scarlett@protonmail.com](mailto:liam.scarlett@protonmail.com)

## Probing electron projectile coherence with twisted electron collisions

A L Harris \*

Physics Department, Illinois State University, Normal, IL 61790, USA

**Synopsis** We present theoretical triple differential cross sections (TDCSs) for electron-impact ionization and show that Laguerre-Gauss (LG) and Bessel projectiles can be used to study coherence effects. We show that a localized projectile alters the shape and magnitude of the TDCSs and that interference structures present for delocalized projectiles are not present for projectiles with small coherence length. Projectiles with large coherence lengths yield cross sections that more closely resemble their plane wave counterparts.

In traditional charged particle scattering theory, the projectile is usually assumed to have an infinite coherence length. However, recent studies with heavy-ion projectiles have shown that the projectile's transverse coherence length cannot be ignored, even when the projectile-target interaction is within the perturbative regime [1,2]. This discovery has spurred many investigations into projectile coherence, all of which involved heavy-ion projectiles.

For electron projectiles, it is more challenging to study coherence effects because of the larger deBroglie wavelengths. However, the recent experimental demonstration of sculpted electron wave packets opens the door to studying projectile coherence effects in electron-impact collisions. We report here theoretical triple differential cross sections (TDCSs) for electron-impact ionization of helium and  $H_2^+$  using Bessel and Laguerre-Gauss projectiles [3].

Unlike their plane wave counterparts, these sculpted electron wave packets are transversely localized and can carry quantized orbital angular momentum. By altering the opening angle, order, and beam waist of the sculpted electron wave packet, the projectile's transverse coherence can be controlled.

Figure 1 (left) shows the transverse electron densities for Bessel projectiles with  $l = 0$  at different opening angles  $\alpha$ . Figure 1 (right) shows the TDCSs for ionization of  $H_2^+$  with an on-center Bessel projectile ( $l = 0$ ) as a function of  $\alpha$  and ejected electron angle ( $\theta_e$ ). TDCSs were calculated within the Born approximation.

For small opening angles, the projectile is most similar to a delocalized plane wave and the TDCSs show clear interference structures

corresponding to ionization from both nuclear centers. As the opening angle increases, the projectile coherence length decreases and the interference structures are not present in the TDCSs.

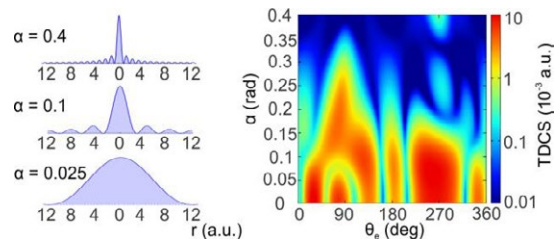


**Figure 1.** Left - transverse density of a Bessel projectile for  $l = 0$  and opening angle  $\alpha$  (rad). Right - TDCSs for ionization of  $H_2^+$  by a 1 keV Bessel projectile with scattering angle 100 mrad and ionized electron energy 100 eV.

Our results demonstrate that the coherence length of the projectile can be controlled through the electron vortex parameters and that twisted wave packets can be used to study projectile coherence effects in electron-impact ionization collisions.

### References

- [1] Egodapitiya K N, Sharma S, Hasan A, Laforge A C, Madison D H, Moshhammer R and Schulz M 2011 *Phys. Rev. Lett.* **106** 153202
- [2] Jarai-Szabo F and Nagy L 2015 *Eur. Phys. J. D* **69** 4
- [3] Harris A L 2023 "Projectile coherence effects in twisted electron ionization of helium" under review 28 Feb 2023

We gratefully acknowledge the support of the National Science Foundation under Grant No. PHY-1912093.

\* E-mail: [alharri@ilstu.edu](mailto:alharri@ilstu.edu)

## Valence-shell electronic excitations of nitrogen dioxide studied by fast electron scattering

Qiang Sun<sup>1</sup>, Shu-Xing Wang<sup>1\*</sup> and Lin-Fan Zhu<sup>1†</sup>

<sup>1</sup> Department of Modern Physics, University of Science and Technology of China, Hefei, Anhui 230026, China

**Synopsis** Based on a fast electron energy loss spectrometer and the relative flow technique, the absolute generalized oscillator strengths (GOSs) of the valence-shell excitations of NO<sub>2</sub> at different momentum transfers were determined at a high resolution (70 meV), and the momentum transfer dependence behavior of the valence-shell excitations of NO<sub>2</sub> has been studied.

NO<sub>2</sub> is one of the most important pollutants in the atmosphere, which is difficult to remove chemically. Meanwhile, NO<sub>2</sub> has a non-negligible indirect impact on the greenhouse effect, although it isn't a greenhouse gas itself. More seriously, NO<sub>2</sub> is an important intermediate product involving in the cyclic catalytic decomposition of atmosphere ozone, thus posing a threat to the ozone shield [1]. In addition, NO<sub>2</sub> has attracted the attention of many theorists for its open shell structure. Therefore, accurate molecular data including oscillator strengths and cross sections of the valence-shell excitations of NO<sub>2</sub> are vital for monitoring its evolution in the atmosphere and theoretical research.

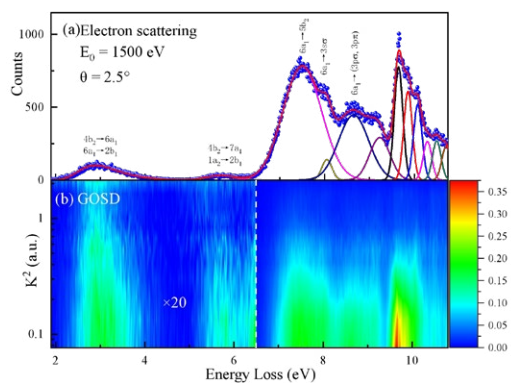


**Figure 1.** (a) Typical electron energy loss spectrum of the valence-shell excitations of NO<sub>2</sub> at the scattering angle of 2.5°. The solid lines are the fitted curves. (b) A 2D map of the GOSDs of NO<sub>2</sub> vs. the energy loss and squared momentum transfer.

A typical electron energy loss spectrum and the generalized oscillator strength densities (GOSDs) of the valence-shell excitations of NO<sub>2</sub> are shown in

\* E-mail: [wangshuxing@ustc.edu.cn](mailto:wangshuxing@ustc.edu.cn)

† E-mail: [lfzhu@ustc.edu.cn](mailto:lfzhu@ustc.edu.cn)

Figs. 1(a) and (b), with the corresponding excited states assigned [2]. The difficulty with handling its dimer N<sub>2</sub>O<sub>4</sub> was overcome by low gas pressures based on the cross-beam technique [3]. The corresponding GOSs are shown in Fig. 2, along with their fitted curves, which can be extrapolated and integrated to obtain their optical oscillator strengths (OOSs) and integral cross sections (ICSSs). It is obvious that the GOSs displayed in Fig. 2 show typical profiles as dipole-allowed transitions.

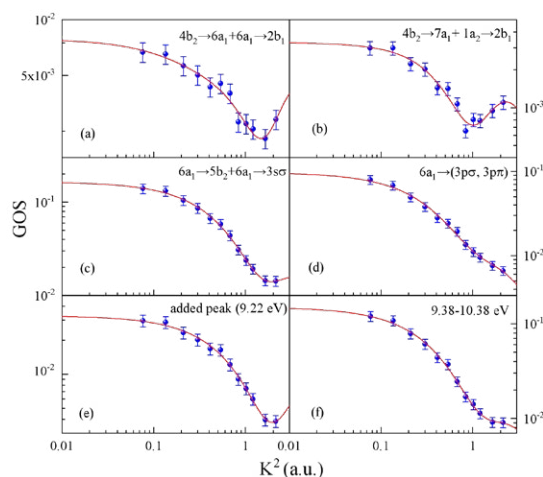


**Figure 2.** The GOSs of the valence-shell excitations of NO<sub>2</sub>.

### References

- [1] S. Elliott and F.S. Rowland, *J. Chem. Educ.* 64, 387
- [2] J.W. Au and C.E. Brion, *Chem. Phys.* 218, 109.
- [3] A. M. Bass et al., *J. Res. Nat. Bur. Stand., Sect. A*, 80, 143.

## Theoretical electronic excitation cross sections of CCl<sub>4</sub>

N Watanabe<sup>1\*</sup> and M Takahashi<sup>1</sup>

<sup>1</sup> Institute of Multidisciplinary Research for Advanced Materials, Tohoku University, Sendai 980-8577, Japan

**Synopsis** We report a theoretical study of valence shell excitation in CCl<sub>4</sub> by electron impact. Generalized oscillator strengths are calculated for the molecule at the EOM-CCSD level. It is found that excitations to  $\sigma^*$  antibonding orbitals play dominant roles below the excitation energy of  $\sim 9$  eV. Furthermore, the calculations reveal that the asymmetric stretching vibration significantly affects the valence excitations at small momentum transfer, indicating that vibrational effects have a considerable influence on Cl formation in the photolysis of CCl<sub>4</sub>.

The decomposition of carbon tetrachloride by ultraviolet (UV) and vacuum UV absorption leads to the formation of Cl atoms, which play a key role in ozone destruction in the stratosphere. Since the Cl formation processes involve valence shell excitations in the molecule, the excited electronic states and excitation cross sections have been the subject of many experimental studies. On the other hand, ab-initio calculations on excited states are extremely scarce for CCl<sub>4</sub>. In the absence of reliable theoretical studies, most of the spectral features observed have been assigned to excitations to Rydberg levels by means of semi-empirical procedures that rely on term values estimated using quantum defect theory. However, the validity of the methods is questionable for transitions to valence and valence-Rydberg-mixed states. Indeed, no clear assignments have been made for several transition bands, indicating that excited electronic structure of CCl<sub>4</sub> is not well understood, despite its importance.

Electron energy loss spectroscopy (EELS) provides a powerful tool to elucidate the origin of spectral features. The electron scattering cross section is proportional to the generalized oscillator strength (GOS), whose momentum-transfer dependence reflects the character of the excited state; thereby, comparison with reliable theoretical calculations offers an opportunity to make unambiguous assignments of transition bands. In this study, we have performed theoretical calculations of the GOS profiles of CCl<sub>4</sub> at the highly accurate EOM-CCSD level to get a detailed understanding of the valence shell excitations in the molecule [1]. For elucidating the influence of nuclear dynamics on the excitation cross sections, effects of molecular vibration have been included. Based on a comparison

with recent experimental data [2], several reassignments of spectral features have been made.

Figure 1 shows a comparison between the theoretical and experimental GOS profiles of the transition band at the electron energy loss of 8.6 eV. No clear assignment has been made so far for this band. The EOM-CCSD calculation predicts the appearance of the  $3\ ^1T_1$  ( $2t_1 \rightarrow 4s$ ) and  $2\ ^1E$  ( $2t_1 \rightarrow 8t_2\ \sigma^*$ ,  $2e \rightarrow 7a_1\ \sigma^*$ ) transitions around 8.6 eV. However, when assuming the nuclei fixed at the equilibrium positions, the theoretical result (equilibrium geometry calculation) significantly underestimates the experiment at small momentum transfer ( $K$ ). On the other hand, the calculation including vibrational effects shows an excellent agreement with the experimental data. It indicates that the 8.6 eV band can unambiguously be attributed to the  $3\ ^1T_1$  and  $2\ ^1E$  transitions and also that the molecular vibration plays a crucial role in the electronic excitations.

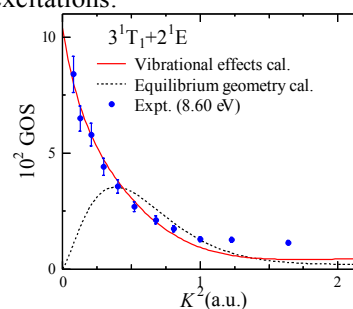


**Figure 1.** Comparison between theoretical and experimental GOS profiles of the  $\{3\ ^1T_1 + 2\ ^1E\}$  band of CCl<sub>4</sub>.

### References

- [1] Watanabe N and Takahashi M 2023 *J. Phys. Chem. A* **127** 1866
- [2] Wang L-H *et al* 2022 *J. Phys. Chem. A* **126** 453.

\* E-mail: [noboru.watanabe.e2@tohoku.ac.jp](mailto:noboru.watanabe.e2@tohoku.ac.jp)



## Absolute Electron Impact Ionization Cross Sections of Carbon Dioxide

Weizhe Huang, Xu Shan\* and Xiangjun Chen†

Hefei National Research Centre for Physical Sciences at the Microscale and Department of Modern Physics, University of Science and Technology of China, Hefei, Anhui, 230026, China

**Synopsis** We report the absolute partial and total ionization cross sections of carbon dioxide measured by electron impact experiment in the electron energy range from 350 eV up to 8000 eV.

Carbon dioxide (CO<sub>2</sub>) is one of the fundamental constituents of the planetary atmosphere. In particular, it is the most abundant molecule in the atmospheres of Venus and Mars. Precipitation of solar wind and magnetosheath electrons provides an important energy source to the Martian upper atmosphere (the dominant energy source on the nightside). Electron impact ionization and dissociation of CO<sub>2</sub> is regarded as a dominant source of neutral atoms and charged particles in the ionosphere and thermosphere of Mars [1-3]. Accurate and reliable electron impact ionization cross sections in a wide energy range are demanded, as the important input parameters in the established numerical simulation models including thermosphere and ionosphere model, global plasma model, electron transport model, etc.[4] However, most of the available ionization cross sections are limited in the electron energy range from threshold to 1000 eV or less [5-8], while the data for higher energies are especially scarce.

In this work, we report the absolute electron impact ionization cross sections of CO<sub>2</sub> measured by an ion imaging mass spectrometer [9,10] in the impact energy range from 350 eV to 8000 eV. The spectrometer incorporates a pulsed electron beam and a pulsed ion extraction system as well as a relative flow technique for determining absolute cross sections. Two kinds of high purity gases, CO<sub>2</sub> and Ar, are mixed homogeneously with a fixed molecule number ratio (1:1) controlled by flowmeters. The partial ionization cross sections (PICSSs) of ionic products (CO<sub>2</sub><sup>+</sup>, CO<sup>+</sup>, C<sup>+</sup>, O<sup>+</sup>, CO<sub>2</sub><sup>2+</sup>, C<sup>2+</sup>, O<sup>2+</sup>) and two dissociative channels (CO<sub>2</sub><sup>2+</sup> → O<sup>+</sup> + CO<sup>+</sup> and CO<sub>2</sub><sup>3+</sup> → C<sup>+</sup> + O<sup>+</sup> + O<sup>+</sup>) are obtained, as well as the total ionization cross sections (TICSSs). As a representative data, Figure 1 presents the absolute TICSS of CO<sub>2</sub> molecule. The present result showed a good agreement with the

previous works at the impact energy below 1000 eV, and supplemented the data at higher energies. More results and discussion will be presented in the poster.

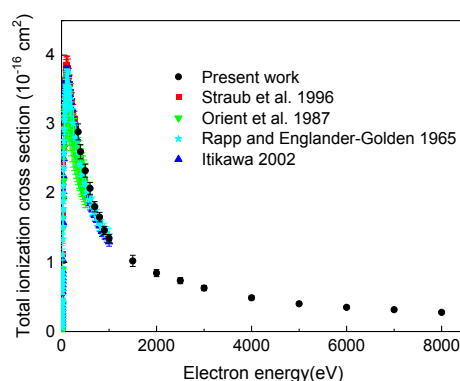


**Figure 1.** Absolute total electron impact ionization cross section of CO<sub>2</sub>.

### References

- [1] McElroy M B and McConnell J C, 1971 *J. Geophys. Res.*, **76** 6674.
- [2] Jane L. Fox, 2004 *J. Geophys. Res. Space Phys.*, **109**, A08306.
- [3] Girazian Z, Mahaffy P, Lillis R J et al, 2017 *Geophys. Res. Lett.*, **44** 11248.
- [4] Lillis R J and Fang X, 2015 *J. Geophys. Res. Planets*, **120** 1332.
- [5] Straub H C, Lindsay B G, Smith K A et al., 1996 *J. Chem. Phys.* **105** 4015.
- [6] Orient O J and Strivastava S K, 1987 *J. Phys. B: Atom. Mol. Phys.* **20** 3923.
- [7] Rapp D and Englander-Golden P, 1965 *J. Chem. Phys.* **43** 1464.
- [8] Itikawa Y, 2002 *J. Phys. Chem. Ref. Data*, **31** 749.
- [9] Wang E L, Shan X, Shi Y F et al., 2013 *Rev. Sci. Instrum.* **84** 123110
- [10] Chen L, Shan X, Wang E L et al, 2019 *Phys. Rev. A* **100** 062707

\* E-mail: xshan@ustc.edu.cn

† E-mail: xjun@ustc.edu.cn

## R-matrix calculation of electron collisions with interhalogen compounds

J Singh<sup>1\*</sup>, and J Tennyson<sup>2</sup>

<sup>1</sup>Department of Physics, Keshav Mahavidyalaya, University of Delhi, Delhi-110034, India.

<sup>2</sup>Department of Physics and Astronomy, University College London, Gower st., London WC1E 6BT, UK.

**Synopsis** Interhalogen compounds plays a crucial role in the earth's atmosphere. The R-matrix method is used in present calculations which are performed using Quantemol Electron Collisions (QEC) expert system integrated with MOLPRO package. The results (potential energy curves and cross sections) computed for ICl molecule in different scattering models. Two resonances are also observed. The resonance parameters are important in the study of electron attachment followed by dissociation of ICl molecule into fragments.

The study of interhalogen compounds is of importance due to their role in ozone layer depletion [1]. This work is motivated by the need of theoretical data to support the experimental studies on ICl in the field of atmospheric research [2].

The R-matrix method [3, 4] used to perform calculation in different scattering models with support of MOLPRO [5] package which provides molecular orbitals energies. The present calculations are performed using the Quantemol Electron Collisions (QEC) expert system [6]. QEC runs the UKRmol+ suites of codes [7] and integrated with MOLPRO package.

Elastic and excitation cross sections are computed. The excited states are included upto 10 eV. Differential cross section are calculated as a function energy and scattering angle for a 2-state CC model. Electron impact ionization cross section are shown in figure 1.

Two resonances are observed and given in table 1. The fragments of ICl molecule both have a positive electron affinity which means either anion can be formed as result of dissociation via appropriate resonances formed by electron attachment. These process are important for plasma modeling and atmospheric research. An estimate of dissociate electron attachment cross section and rate coefficients are also computed in present study.

The theoretical understanding of electronic-excitation of the ICl molecule in plasma modeling involved in aerospace engineering may be achieved by these scattering calculations.

\*E-mail: [jasmeet.singh@keshav.du.ac.in](mailto:jasmeet.singh@keshav.du.ac.in)

**Table 1.** ICl resonance parameters for close coupling model at bond length 2.4 Å.

Symmetry	Position (eV)	Width (eV)
$2\Sigma^+$	4.40	0.154
$2\Pi$	3.98	0.008

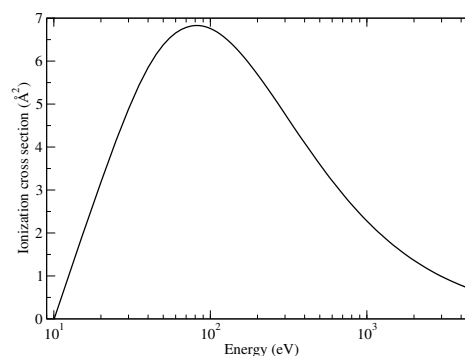


**Figure 1.** Electron-impact ionization cross sections for ICl.

### References

- [1] Tham Y J et al 2021 *Proceedings of the National Academy of Science* **118** e2009951118
- [2] Wiens J P et al 2016 *Phys. Rev. A* **93** 032706
- [3] Burke P G 2011 *R-matrix Theory of Atomic Collisions: Application to Atomic, Molecular and Optical Processes*
- [4] Tennyson J 2010 *Physics Reports* **491** 29-76
- [5] Werner H J et al, Version 2009.1 <http://www.molpro.net>
- [6] Cooper B et al 2019 *Atoms* **7** 97
- [7] Masin Z et al 2020 *Comp. Phys. Comm.* **249** 107092

## Comparison of Theoretical Methods to Calculate Electron-Impact Ionization Cross-Sections of Benzene Derivatives

A Krishnadas<sup>1\*</sup>, N Sinha<sup>2</sup>, H J Lüdde<sup>3</sup>, T Kirchner<sup>1†</sup> and B Antony<sup>4</sup>

<sup>1</sup>Department of Physics and Astronomy, York University, Toronto, Ontario, Canada, M3J 1P3

<sup>2</sup>Division of Plasma Convergence Research, Korea Institute of Fusion Energy, Gunsan, 54004, Republic of Korea

<sup>3</sup>Center for Scientific Computing, Goethe-Universität, D-60438 Frankfurt, Germany

<sup>4</sup>Atomic and Molecular Physics Lab, Department of Physics, IIT(ISM) Dhanbad Jharkhand, India

**Synopsis:** Calculations of the electron-impact ionization cross-section of various benzene derivatives are reported over a wide energy range. A comparison of theoretical models, viz. Multi-Scattering Spherical Complex Optical Potential, Complex Scattering Potential-ionization contribution, Pixel Counting Method, and the Binary Encounter Bethe model are carried out. It is demonstrated that all model results are in reasonable agreement with each other. Comparison is also made with other theoretical data where available.

This work reports various theoretical methods to calculate electron-impact ionization cross-sections ( $Q_{ion}$ ) for pyrene, anthracene, benzoyl chloride, benzophenone, and phthalonitrile from threshold to 5000 eV. The molecules are chosen based on their relevance and application in basic science and industries. The methods used are Multi Scattering Spherical Complex Optical Potential and Complex Scattering Potential-Ionization Contribution (MSCOP + CSP-ic) [1], Pixel Counting Method (PCM) [2] and Binary Encounter Bethe (BEB) [3].

One approach this work uses is extracting  $Q_{ion}$  from the inelastic scattering cross-section  $Q_{inel}$  using CSP-ic, a ratio method. First,  $Q_{inel}$  is calculated using MSCOP [1]. The second method we look at is the PCM to modify the results of MSCOP and CSP-ic. PCM [2] was introduced for ion collisions, breaking up superimposed atomic cross-section areas into pixels and counting those visible from the incident ions to account for geometric overlap effects. BEB [3] is the third method used to calculate  $Q_{ion}$ . BEB considers the binding energy and the kinetic energy of the orbitals of the target, which contribute to ionization. The structure data are calculated using GAUSSIAN 16 [4].

There are two ways of applying PCM: the first is referred to as MSCOP +CSP-ic +PCM. In this model, PCM is applied on  $Q_{ion}$  obtained from CSP-ic. Alternatively, in MSCOP+PCM+CSP-ic, PCM is used on  $Q_{inel}$  obtained from MSCOP, and then CSP-ic is used to extract  $Q_{ion}$ . Finally, the results from all the methods are compared. Figure 1 shows the total ionization cross-section of anthracene as an example.

\* E-mail: [anirudhk@yorku.ca](mailto:anirudhk@yorku.ca)

† E-mail: [tomk@yorku.ca](mailto:tomk@yorku.ca)

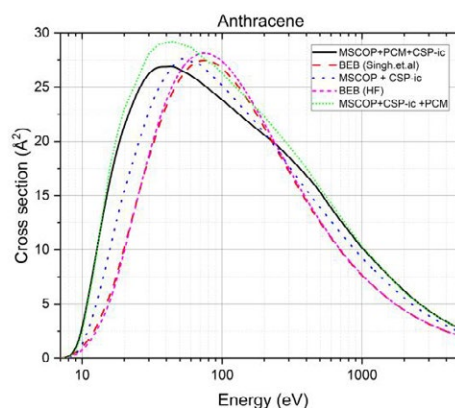


**Figure 1.** Total cross section for electron-impact ionization of anthracene. Solid black line: present MSCOP+PCM+CSP-ic. Dashed red line: Singh and Antony [5]. Dotted blue line: present MSCOP+ CSP-ic. Short dashed magenta line: present BEB result calculated at Hartree Fock level. Short dotted green line: present MSCOP+CSP-ic+PCM.

The present work is considered a starting point for using PCM, which was introduced for ion collisions to do electron collision studies. MSCOP, CSP-ic, and BEB are well-established methods for electron collisions and, with the introduction of PCM, eliminate the uncertainty of molecular grouping in MSCOP. The results of all four methods give similar results for  $Q_{ion}$  within a range of 5%.

### References

- [1] Sinha N 2019 *J. Phys. B* **52**, 145202
- [2] Lüdde H J 2016 *Eur. Phys. J. D* **70**
- [3] Kim Y K 1994 *Phys. Rev. A* **50**, 3954
- [4] Frisch M J *Gaussian 16*, Revision C.01.
- [5] Singh S 2020 *J. Phys. Chem. A* **124**, 7088

## Electron impact ionization cross sections of tyrosine

Suriyaprasanth S<sup>1\*</sup>, Dhanoj Gupta<sup>2†</sup>

<sup>1,2</sup> Department of Physics, School of Advanced Sciences, Vellore Institute of Technology, Vellore - 632014, India.

**Synopsis** We study of the total electron impact ionization cross sections and partial total electron impact ionization cross section of tyrosine, an important biological molecule, a precursor of many other amino acid which are very crucial for maintaining normal physiological function in a living organism.

Study of electron impact ionization cross sections of bio-molecules are important to various fields of science and technology and are difficult to study experimentally due to the size and nature of the target. When an electron impinges on a biological matter, the primary electron produces free radicals, which produces secondary electron by detaching an electron in order to stabilize themselves which is responsible for causing ailments to the living organism by breaking the DNA strands and leading to mutation of DNA [1]. Tyrosine is one of the important amino acid present in our body. At low electron impact energies, dissociative electron attachment (DEA)/electrons capture processes becomes important that leads to the various fragmentation of molecules. At higher energies processes such as ionization and excitation dominates. Recently the fragmentation pattern of tyrosine was experimentally investigated at low energies leading to different fragmentation products through various dissociation pathways [3]. The fragmentation pattern of the target depends on the structure, bond length, dihedral angle, symmetry, type of molecular groups present in the target. Here we present the total electron impact ionization cross sections (TICS) and partial electron impact ionization cross sections (PICS) of the various fragments as seen in the experimental work of [3] using the Binary Encounter Bethe Model (BEB) [2]. Apart from calculation of TICS and PICS of tyrosine we have also studied the DEA process using Quantum Chemical Mass Spectrometry (QCxMS) method [4] to val-

idate with the experimental results. In figure 1, we have presented the TICS calculated using the BEB model. The detailed study about PICS and DEA will be presented in the conference.

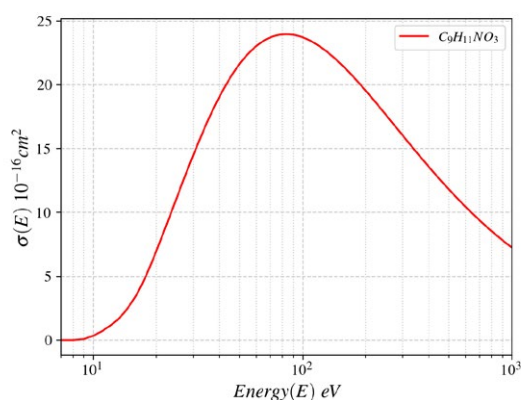


**Figure 1.** The TICS calculated using BEB model for tyrosine ( $C_9H_{11}NO_3$ ) molecule at the range of 10 eV – 5 keV.

### References

- [1] Kumar, A. et al(2019).*Int. J. Mol. Sci.* **20(16)**, 3998.
- [2] Guerra, M. et. al. (2012). *Int J Mass Spectrom*, **313**, 1-7.
- [3] Tamulienė, J et. al. (2023). *Eur. Phys. J. D* **77(1)**, 13 and references within.
- [4] Koopman, J, et. al. (2022) *J. Am. Soc. Mass Spectrom*, 2022, **33(12)** 2226-2242.
- [5] Zhang, P et. al. (2019) *Scientific reports*,**9(1)**, 6453.

\*E-mail: [s.suriyaprasanth@gmail.com](mailto:s.suriyaprasanth@gmail.com)

†E-mail: [dhanoj.gupta@vit.ac.in](mailto:dhanoj.gupta@vit.ac.in)

†Corresponding author

## Electron-electron-ion coincidence studies for electron impact ionization of small water clusters

K. Hossen<sup>1,2</sup>, S. Jia<sup>3</sup>, J. Zhou<sup>3</sup>, X. Xue<sup>3</sup>, X. Ren<sup>3</sup> and A. Dorn<sup>1,\*</sup>

<sup>1</sup>Max Planck Institute for Nuclear Physics, Heidelberg, 69117, Germany

<sup>2</sup>Patuakhali Science and Technology University, Patuakhali, 8602, Bangladesh

<sup>3</sup>MOE Key Laboratory for Nonequilibrium Synthesis and Modulation of Condensed Matter, School of Physics, Xi'an Jiaotong University, Xi'an, 710049, People's Republic of China

**Synopsis** The ionization and fragmentation of small water clusters induced by low energy electron-impact ( $E_0 = 80$  eV) is investigated. We find that excited electronic states (vacancies below the HOMO) of the cluster ions preferentially decay by the evaporation of all neutral water molecules ending up in the  $\text{H}_3\text{O}^+$  channel.

Experimentally we use a multi-particle coincidence spectrometer (reaction microscope) where all three charged final state particles, two outgoing electrons and the fragment ion, are detected. Small water clusters  $(\text{H}_2\text{O})_n$  ( $n < 10$ ) are produced in a supersonic helium gas jet seeded with water vapour.

In the TOF mass spectra non-protonated  $(\text{H}_2\text{O})_2^+$  and protonated  $(\text{H}_2\text{O})_n\text{H}^+$ , ( $n = 2 - 5$ ) cluster ions are identified. The formation of these species is studied using ion kinetic energy distributions and ionized electron binding energy (BE) spectra as they are shown in Figure 1. Three major BE peaks corresponding to the ionization of the  $1b_1$ ,  $3a_1$  and  $1b_2$  valence orbitals are obtained. The relative intensities are strongly varying for the different ion channels. For the larger cluster ions the  $3a_1$  and  $1b_2$  lines are comparatively weak while these and the inner valence  $2a_1$  intensity are strong for the  $\text{H}_3\text{O}^+$  channel. This indicates that for water clusters the electronic excitation energy of these vacancies is converted to inter-molecular vibration followed by evaporation of neutral water molecules. This is in accordance with wave packet propagation studies by Suárez et al. [1] for the excited ionized monomer. These show that the initial wave packet produced, e.g., by  $1b_2$  ionization propagates via a conical intersection and Renner-Teller coupling down to the vibrationally excited electronic ground state. While for the monomer this results in a characteristic fragment ion branching ratio, for clusters we observe emission of neutrals.

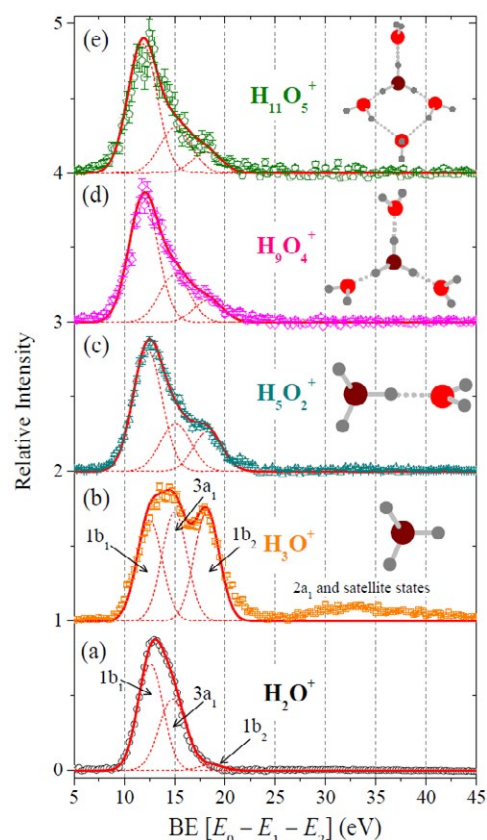


**Figure 1.** (a) The binding energy (BE) spectrum for ionization of water monomers  $\text{H}_2\text{O} \rightarrow \text{H}_2\text{O}^+$ . (b-e) The BE spectra for the labeled outer and inner-valence orbitals leading to the different protonated cluster ions. The insets show the structures of the cluster ions.

### References

- [1] J. Suárez, L. Méndez and I. Rabadán, Phys. Chem. Lett. 6, 72 (2015).

\* E-mail: [A.Dorn@mpi-k.de](mailto:A.Dorn@mpi-k.de)



## Cross sections for ionization of liquid water by electron impact

M L de Sanctis<sup>1\*</sup>, M-F Politis<sup>2</sup>, R Vuilleumier<sup>3</sup>, C Stia<sup>1</sup> and O Fojón<sup>1†</sup>

<sup>1</sup>Instituto de Física Rosario (IFIR, CONICET-UNR), Bvd. 27 de febrero 210 bis, Rosario, 2000, Argentina

<sup>2</sup>Laboratoire Analyse et Modélisation pour la Biologie et l'Environnement, Bv. Mitterrand, 91025 Evry, France

<sup>3</sup>École Normale Supérieure, Dépt. de Chimie, UPMC, 24, rue Lhomond, 75005 Paris, France.

**Synopsis** We study the ionization of water molecules in liquid phase by impact of energetic electrons. We present angle integrated cross sections averaged over all orientations of the water molecule as a function of the ejection energy for several incident energies. As no experiments for the liquid phase are available, we compare our predictions with results for water vapor and other theories.

Ionization of water molecules is a basic reaction of importance in many domains such as plasma physics, fusion experiments, astrophysics, and in radiobiology. In particular, this reaction is of great relevance to understand the mechanisms of energy deposition in living matter by ionizing radiations.

We present total and differential cross sections for the ionization of liquid water by energetic electrons, obtained through a first-order model [1]. Asymmetric conditions and a coplanar geometry are considered, while exchange is not taken into account. The condensed phase is described in a realistic way by a methodology based on Wannier's orbitals [2]. We present integrated cross sections at several impact energies. We compare our results for the liquid phase with the available experiments for vapor [3,4], as well as with other first-order models

[5,6]. Angle integrated cross sections averaged over all orientations of the molecule (AICS) as a function of the ejection energy are analyzed. At 500 eV, these AICS are greater than those reported for the gas phase. However, as the incident energy increases, this scenario is reversed. This could be attributed to the screening of the liquid medium [7] and the dipole character of the reaction.

### References

- [1] de Sanctis ML et al, *J. Phys. B* **45** (2012) 045206, *J. Phys. B* **48** (2015) 0155201
- [2] Hunt P et al, *Chem. Phys. Lett.* **376** (2003) 68
- [3] Bolorizadeh MA et al, *Phys. Rev. A* **33** (1985) 882
- [4] Opal CB et al, *Atomic Data* **4** (1972) 209
- [5] Houamer S et al, *J. E. S. and R. P.* **161** (2007) 38
- [6] Champion C et al, *J. Chem. Phys.* **117** (2002) 197
- [7] Joshipura KN et al, *J. Phys. C.S.* **80** (2007) 012008

\* E-mail: [mldesanc@ifir-conicet.gov.ar](mailto:mldesanc@ifir-conicet.gov.ar)

† E-mail: [fojon@ifir-conicet.gov.ar](mailto:fojon@ifir-conicet.gov.ar)

## Novel results for the electron-impact recombination and excitation of molecular cations: the role of the core-excited bound resonances

J Zs Mezei<sup>1,2\*</sup>, A Orbán<sup>1</sup>, J Boffelli<sup>2</sup>, F Gauchet<sup>2</sup>, R Hassaine<sup>2</sup>, N Pop<sup>3</sup>, F Iacob<sup>4</sup>  
M. Ayouz<sup>5</sup>, V. Kokoouline<sup>6</sup>, J. Tennyson<sup>7</sup> and I F Schneider<sup>2,8</sup>

<sup>1</sup>Institute for Nuclear Research (ATOMKI), Debrecen, 4001, Hungary

<sup>2</sup>LOMC, CNRS-University Le Havre Normandie, Le Havre, 76600, France

<sup>3</sup>Politehnica University Timișoara, Timișoara, 300006, Romania

<sup>4</sup>West University of Timișoara, Timișoara, 300223, Romania

<sup>5</sup>LGPM, CNRS-CentraleSupélec, Université Paris-Saclay, 91190 Gif-sur-Yvette, France

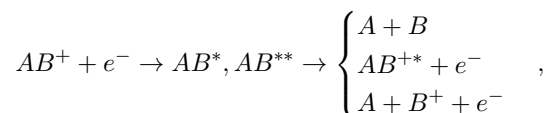
<sup>6</sup>Department of Physics, University of Central Florida, 32816 Orlando, Florida, United States of America

<sup>7</sup>Department of Physics and Astronomy, University College London, WC1E 6BT London, UK

<sup>8</sup>LAC CNRS-University Paris-Saclay, Orsay, 91400, France

**Synopsis** The major role of the core-excited bound resonances in the reactive collisions of electrons with molecular cations will be illustrated in the case of diatomic and polyatomic targets recently studied.

Electron impact recombination, (ro-) vibrational-, electronic- and dissociative excitation of molecular cations:



are in the heart of the molecular reactivity in the cold ionized media [1], being major charged particles destruction reactions and producing often atomic species in metastable states, inaccessible through optical excitations. They involve super-excited molecular states undergoing predissociation and autoionization, having thus strong resonant character. Consequently, they are subject to beyond-Born-Oppenheimer approximation within the quasi-adiabatic representation of molecular states. In addition, they require sophisticated methods for describing the dynamics, and involve the superposition of many continua and infinite series of Rydberg states.

The methods based on the Multichannel Quantum Defect Theory (MQDT) [1, 2] are the most suitable approaches for these processes, capable to account the strong mixing between ionization and dissociative channels, open - direct mechanism - and closed - indirect mechanism, via capture into prominent Rydberg resonances correlating to the ground and excited ionic states, and the rotational effects.

Whereas some of these features, characteriz-

ing the extreme (very low and very high) energies of the incident electron will be outlined in a progress report at this meeting [3], I will focus on the low and intermediate energy range, where core-excited bound resonances are prominent, for SH<sup>+</sup> [4], N<sub>2</sub><sup>+</sup> [5], NS<sup>+</sup> [6], etc., comparisons with other existing theoretical and experimental results being displayed.

Advancement in the theoretical treatment - as the inclusion of new dissociative pathways for noble gas hydrides, the effect of the energy-dependence of the quantum defect on vibronic interactions for the benchmark cation H<sub>2</sub><sup>+</sup>, the isotopic effects for diatomic and polyatomic systems like H<sub>2</sub><sup>+</sup> [7], N<sub>2</sub>H<sup>+</sup> [8], C<sub>2</sub>H<sup>+</sup>, etc. - will also be presented.

Research supported by the Normandy region, CNRS-PCMI, ANR-MONA and NKFIH-OTKA.

### References

- [1] Schneider IF, Dulieu O, Robert J, eds., *EPJ Web of Conferences* **84** (2015).
- [2] Mezei JZs *et al*, *ACS Earth and Space Chem* **3** 2276 (2019).
- [3] Schneider IF *et al*, progress report at IC-PEAC2023.
- [4] Boffelli J *et al*, submitted to *MNRAS* (2023).
- [5] Abdoulanziz A *et al*, *J. Appl. Phys.* **129** 052202 (2021).
- [6] Iacob F *et al*, *J. Phys. B: At. Mol. Opt. Phys.* **55** 235202 (2022).
- [7] Epée Epée MD *et al*, *MNRAS* **512** 424 (2022).
- [8] Mezei JZs *et al*, submitted to *EPJST* (2023).

\*E-mail: [mezei.zsolt@atomki.hu](mailto:mezei.zsolt@atomki.hu)

## Dissociative recombination of $\text{ArH}^+$ at the Cryogenic Storage Ring

Á Kálosi<sup>1,2\*</sup>, M Grieser<sup>2</sup>, L W Isberner<sup>3,2</sup>, D Paul<sup>1,2</sup>,  
D W Savin<sup>1</sup>, S Schippers<sup>3</sup>, V C Schmidt<sup>2</sup>, A Wolf<sup>2</sup> and O Novotný<sup>2</sup>

<sup>1</sup>Columbia Astrophysics Laboratory, Columbia University, New York, 10027 New York, USA

<sup>2</sup>Max-Planck-Institut für Kernphysik, 69117 Heidelberg, Germany

<sup>3</sup>I. Physikalisches Institut, Justus-Liebig-Universität Gießen, 35392 Gießen, Germany

### Synopsis

We have carried out experimental studies for dissociative recombination (DR) of rotationally cold  $\text{ArH}^+$  molecules with free electrons at the Cryogenic Storage Ring (CSR) in Heidelberg, Germany. The low temperature DR rate coefficient for the electronic, vibrational, and rotational ground state of  $\text{ArH}^+$  is important for astrochemical models of diffuse clouds, where observed abundances of  $\text{ArH}^+$  are used to infer the cosmic ray ionization rate.

The cosmic ray ionization rate is an influential parameter of diffuse interstellar cloud models.  $\text{ArH}^+$  formation is closely linked to the cosmic ray ionization rate via ionization of atomic Ar. The resulting  $\text{Ar}^+$  can undergo hydrogen abstraction with  $\text{H}_2$  to form  $\text{ArH}^+$ , which, in turn, can be destroyed by reactions with electrons through dissociative recombination (DR), with neutrals through proton transfer, or by ultraviolet photodissociation. A steady-state chemical model of this network enables one to estimate the cosmic ray ionization rate from the observed  $\text{ArH}^+$  abundances. But such models require reliable rate coefficients that account for internal excitations of the reactants. A previous room-temperature storage ring experiment placed an upper limit on the DR rate coefficient for diffuse-cloud conditions [1]. Theoretical calculations have so far predicted a negligible rate coefficient at those conditions [2].

This contribution presents merged-beams experiments for  $\text{ArH}^+$  interacting with free electrons produced in a low-energy electron cooler, which enables electron-ion collision studies at translational temperatures as low as  $\sim 10$  K. For this, we have stored fast  $\text{ArH}^+$  ion beams in the cryogenic environment of CSR. Previous studies showed that infra-red active diatomic hydrides relax to their lowest rotational states within minutes of storage inside CSR [3]. The DR rate coefficient for  $\text{ArH}^+$  at low energies is expected to be several orders of magnitude smaller than the typical rate coefficient of other molecules. In the present experiment, we took special care with purifying the stored ion beam from potential iso-

\*E-mail: [abel.kalosi@hotmail.com](mailto:abel.kalosi@hotmail.com)

baric contaminants before recording DR spectra as a function of center-of-mass collision energy.

In Figure 1, we compare our preliminary results with a theoretical calculation [2] in the collision energy range from 1 to 7 eV. In the poster, we will present our preliminary results for the full DR spectrum, particularly at the low energies relevant for diffuse clouds.

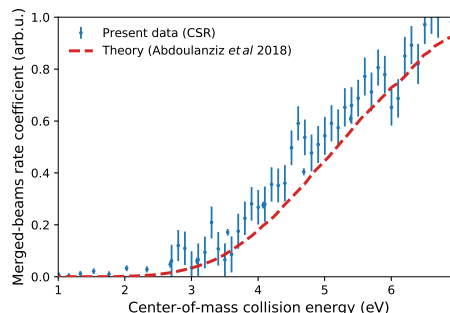


**Figure 1.** Merged-beams rate coefficients plotted as a function of center-of-mass collision energy. The preliminary dataset (CSR) is compared to a previous theoretical calculation [2]. The absolute scale of the experimental data is not yet fully determined.

This project is supported, in part, by the NASA Astrophysics Research and Analysis program under grant 80NSSC19K0969 and by the Max Planck Society.

### References

- [1] Mitchell J B A *et al* 2005 *J. Phys. B: At. Mol. Opt. Phys.* **38** L175–L181
- [2] Abdoulanziz A *et al* 2018 *MNRAS* **479** 2415–2420
- [3] O'Connor A P *et al* 2016 *Phys. Rev. Lett.* **116** 113002

## AMOS Gateway: A Portal for Research and Education in Atomic, Molecular, and Optical Science

K R Hamilton<sup>1\*</sup>, K Bartschat<sup>2</sup>, I Bray<sup>3</sup>, A C Brown<sup>4</sup>, N Douguet<sup>5</sup>, C F Fischer<sup>6</sup>,  
J G Vasquez<sup>7</sup>, J D Gorfinkiel<sup>8</sup>, R Lucchese<sup>9</sup>, F Martin<sup>7</sup>, S Pamidighantam<sup>10</sup>,  
B I Schneider<sup>6</sup>, and A Scrinzi<sup>11</sup>

<sup>1</sup>Department of Physics, University of Colorado Denver, Denver, Colorado 80204, USA

<sup>2</sup>Department of Physics and Astronomy, Drake University, Des Moines, Iowa 50311, USA

<sup>3</sup>Department of Physics and Astronomy, Curtin University, Perth 6102, Western Australia

<sup>4</sup>School of Mathematics and Physics, Queens University, Belfast, Belfast BT7 1NN, UK

<sup>5</sup>Department of Physics, Kennesaw State University, Kennesaw, GA 30144, USA

<sup>6</sup>National Institute of Standards and Technology, Gaithersburg, MD 20899, USA

<sup>7</sup>Universidad Autónoma de Madrid, 28049 Madrid, Spain

<sup>8</sup>The Open University, Milton Keynes, MK7 6AA, UK

<sup>9</sup>Lawrence Berkeley National Laboratory, Berkeley, CA 94720, USA

<sup>10</sup>Department of Chemistry, Indiana University, Bloomington, IN 47405, USA

<sup>11</sup>Faculty of Physics, Ludwig-Maximilians-Universität, 80539 München, Germany

**Synopsis** We report on recent developments of our efforts to provide the atomic, molecular, and optical science community with a portal, where practitioners can access a synergistic, full-scope platform for computational Atomic, Molecular, and Optical Science (AMOS).

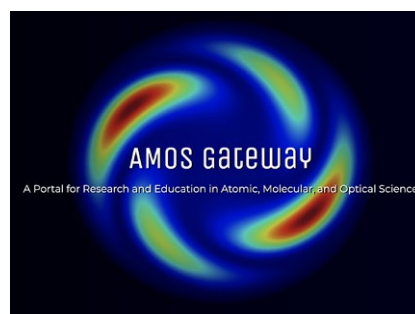
A challenge facing the Atomic, Molecular, and Optical Science (AMOS) community is the lack of a coordinated approach to using and sharing the computational tools and data that have grown organically in the theoretical community. The overarching goal of this project is to create a comprehensive cyberinfrastructure (CI), through which AMO scientists can access resources for computational AMOS via the AMOS gateway [1].

The prototype gateway currently hosts seven state-of-the-art software suites with applications including the computation of electron collision and photoionization cross sections, as well as the control of atomic and molecular systems by laser-atom/molecule interactions. It has 350 registered users to date. The gateway is powered by an advanced CI to enable a flexible and easy-to-use platform for the broad AMOS community, as well as researchers and educators who are not computational AMOS scientists [2,3].

The applications are directly accessed on the gateway, where they have been compiled on several NSF-supported compute systems. Users can access and modify input files for their own purposes and submit them for execution using an ACCESS AMOS Gateway account.

\*E-mail: [kathryn.r.hamilton@ucdenver.edu](mailto:kathryn.r.hamilton@ucdenver.edu)

In addition, the gateway serves as an excellent vehicle to educate students in computational AMOS via hands-on calculations, and as a hub for material created by the developers for teaching, workshops, and conferences. We will report on the current status of the gateway, demonstrate its use, and show results of some recent calculations using the gateway.



### References

- [1] <https://amosgateway.org>
- [2] Schneider B I *et al* 2020 *PEARC '20: Practice and Experience in Advanced Research Computing Atomic and Molecular Scattering Applications in an Apache Airavata Science Gateway*
- [3] Schneider B I *et al* 2022 *NIST Blog AMO for All: How Online Portals Are Democratizing the Field of Atomic, Molecular and Optical Physics*

## Two- and three-body dissociations of C<sub>3</sub>H<sub>6</sub> isomer dications investigated by 4 keV/u Ar<sup>8+</sup> impact

D L Guo<sup>1,2\*</sup>, K Z Lin<sup>3,1</sup>, X L Zhu<sup>1,2</sup>, R T Zhang<sup>1,2</sup>, Y Gao<sup>1,2</sup>, D M Zhao<sup>1,2</sup>, X B Zhu<sup>1,2</sup>, S F Zhang<sup>1,2</sup> and X Ma<sup>1,2†</sup>

<sup>1</sup>Institute of Modern Physics, Chinese Academy of Sciences, Lanzhou 730000, China

<sup>2</sup>University of Chinese Academy of Sciences, Beijing 100049, China

<sup>3</sup>Department of Modern Physics, University of Science and Technology of China, Hefei, Anhui 230026

**Synopsis** The fragmentation dynamics of two isomers of C<sub>3</sub>H<sub>6</sub> induced by 4 keV/u Ar<sup>8+</sup> are investigated employing a reaction microscope. The attention is mainly addressed to the four two-body fragmentation channels which were completely detected, and two abundant three-body fragmentation channels with only one neutral H elimination. The individual fragmentation dynamics of these processes and the isomer effects are discussed.

The study of the fragmentation process of hydrocarbons is of great importance in many fields, such as astrophysics, fusion plasmas physics and radiation physics. In addition to the application importance, from a pure physical point of view, the study of the fragmentation of hydrocarbons with different molecular structures gives access to the basic fragmentation dynamics.

In this work, the fragmentation dynamics of C<sub>3</sub>H<sub>6</sub> isomers, cyclopropane (*c*-C<sub>3</sub>H<sub>6</sub>) and propene (*l*-C<sub>3</sub>H<sub>6</sub>), induced by 4 keV/u Ar<sup>8+</sup> are investigated using the reaction microscope [1]. Four two-body and the main multi-body dissociation channels have been identified from the 2D TOF correlation spectra (Figure 1). The isomer manifestation of fragmentation mechanisms is investigated in the four completely detected two-body channels and two three-body dissociation channels involving one H elimination.

For the two-body dissociation of C<sub>3</sub>H<sub>6</sub><sup>2+</sup>, the CH<sub>3</sub><sup>+</sup> + C<sub>2</sub>H<sub>3</sub><sup>+</sup> channel is the most populated for both isomers. For *l*-C<sub>3</sub>H<sub>6</sub>, the channels CH<sub>3</sub><sup>+</sup> + C<sub>2</sub>H<sub>3</sub><sup>+</sup> and CH<sub>2</sub><sup>+</sup> + C<sub>2</sub>H<sub>4</sub><sup>+</sup> are more likely created through a direct process via the CC single or double bond cleavage, which may qualitatively explain the much higher yield of the former channel. The higher average value of the KER distribution for CH<sub>2</sub><sup>+</sup> + C<sub>2</sub>H<sub>4</sub><sup>+</sup> as compared to CH<sub>3</sub><sup>+</sup> + C<sub>2</sub>H<sub>3</sub><sup>+</sup> could be attributed to the shorter length of the CC double bond as compared to the CC single bond. Interestingly, the ratios of the count of the channel CH<sub>2</sub><sup>+</sup> + C<sub>2</sub>H<sub>4</sub><sup>+</sup> to that of the channel CH<sub>3</sub><sup>+</sup> + C<sub>2</sub>H<sub>3</sub><sup>+</sup> present remarkable differences for the two molecules, indicating a manifesta-

tion of the isomer effects. Contrasting to the dominant CC bond breaking channels, the two CH bond breaking channels producing H<sub>3</sub><sup>+</sup> or H<sub>2</sub><sup>+</sup> make only small contributions for both *l*-C<sub>3</sub>H<sub>6</sub><sup>2+</sup> and *c*-C<sub>3</sub>H<sub>6</sub><sup>2+</sup> dications.

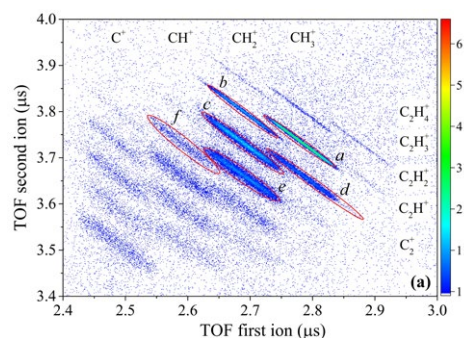


**Figure 1.** The TOF correlation spectrum of *c*-C<sub>3</sub>H<sub>6</sub> zoomed to get a clear view of the CC bond breaking channels.

For the three-body dissociation channels with one neutral H elimination, a sequential dissociation mechanism with single H-evaporation followed by charge separation, was found to be the most probable pathway for both dimers. Obvious isomer effects are revealed as well in the comparison of the yields of the two channels for the two isomers. It is worth noting that for *c*-C<sub>3</sub>H<sub>6</sub>, the observation of the CH<sub>3</sub><sup>+</sup> or H<sub>3</sub><sup>+</sup> formation channels provides direct evidence of the proton migration among the carbon skeleton before dissociation.

### References

- [1] Guo D *et al.* 2022 *J. Chem. Phys.* **157** 154309

\*E-mail: guodalong@impcas.ac.cn

†E-mail: x.ma@impcas.ac.cn



## Ionization of oxygen in collisions with 2.5-MeV/u Si<sup>12+</sup> ions

S K Maurya<sup>1</sup>, D Chakraborty<sup>1</sup>, A Bhogale<sup>1</sup>, C Bagdia<sup>1</sup>, L Gulyás<sup>2</sup>, and L C Tribedi<sup>1\*</sup>

<sup>1</sup>Tata Institute of Fundamental Research, Homi Bhabha Road, Colaba, Mumbai, 400005, India

<sup>2</sup>Institute of Nuclear Research of the Hungarian Academy of Sciences (ATOMKI), H-4001 Debrecen, Hungary

**Synopsis** Ionization of O<sub>2</sub> in collisions with 2.5-MeV/u Si<sup>12+</sup> ions is studied. The double differential cross section (DDCS) is measured using the electron spectroscopy technique. The values of DDCS are compared with the state-of-the-art continuum distorted wave–eikonal initial state (CDW-EIS) model. The DDCS ratio (O<sub>2</sub>/2O) has been investigated to study the Young type interference and a signature of interference oscillation is observed for extreme forward and backward angles. The interference oscillations are fitted well by the Cohen-Fano model. The forward-backward angular asymmetry is also determined.

Electron emission from atoms and molecules upon impact with external perturbations gives a detailed insight into the dynamics of the interactions. The cross sections in collisions of ions with atoms play an important role in various applications, such as, ion-matter interaction, astrophysics, radiation damage, plasma physics, etc. The collision of ions with diatomic molecules has attracted the special attention after the prediction of the Young type interference effect by Cohen and Fano [1] for photoionization. Thereafter, there are several studies on the investigation of the interference effect in case of diatomic molecules [2-3]. Ilchen *et al* showed the interference pattern with photoionization [4]. The interference oscillations have also been observed using electron impact ionization of O<sub>2</sub> [5]. Nandi *et al* also studied the interference effect in collisions of 3.5-MeV/u and 4.25-MeV/u bare C-ions with O<sub>2</sub>, with perturbation strength  $S(q/v) \sim 0.51$  a.u. and 0.46 a.u., respectively [6, 7].

In the present work, experiment is performed with 2.5-MeV/u Si<sup>12+</sup> ions ( $S \sim 1.19$  a.u) where we have studied the ionization of O<sub>2</sub> molecules. The DDCS, single differential cross section (SDCS), and total cross section (TCS) are measured and compared with the CDW-EIS models. The DDCS ratio (O<sub>2</sub>/2O) is also determined, which shows a clear interference oscillation. The ratios are fitted with the Cohen-Fano

model, which matches well with the data. The CDW-EIS model using MO model also shows an oscillation. However, the model prediction does not reproduce the phase of the oscillations. The earlier investigations on oxygen ion induced ionization of O<sub>2</sub> molecule revealed no primary oscillation but secondary oscillation only after dividing the DDCS ratio by a suitable straight line [8]. In this respect the present investigation which reveals a clear primary oscillation by using a much higher charge state of the projectile will provide new insight in the study of interference.

### References

- [1] Cohen H D and Fano U 1996 *Phys. Rev.* **150** [30](#)
- [2] Stolterfoht N *et al.* 2001 *Phys. Rev. Lett.* **87** [023201](#)
- [3] Tanis J A, Hossain S, Sulik B, and Stolterfoht N 2005 *Phys. Rev. Lett.* **95** [079301](#)
- [4] Ilchen *et al.* 2014 *Phys. Rev. Lett.* **112** [023001](#)
- [5] Chowdhury M R and Tribedi L C 2017 *J. Phys. B: At. Mol. Opt. Phys.* **50** [155201](#)
- [6] Nandi S *et al.* 2012 *Phys. Rev. A* **85** [062705](#)
- [7] Nandi S *et al.* 2013 *Phys. Scr.* **T156** [014038](#)
- [8] Winkworth M *et al.* 2009 *Nucl. Instrum. Meth. Phys. Res. B* **267** [373](#)

\* E-mail: [lokesh@tifr.res.in](mailto:lokesh@tifr.res.in)

# Classical-trajectory Monte Carlo calculations for ionizing proton–ammonia-molecule collisions: the role of multiple ionization

A Jorge<sup>1\*</sup>, M Horbatsch<sup>2†</sup> and T Kirchner<sup>2‡</sup>

<sup>1</sup>Departamento de Química, Universidad Autónoma de Madrid, Cantoblanco, E-28049 Madrid, Spain

<sup>2</sup>Department of Physics and Astronomy, York University, Toronto, Ontario, Canada M3J 1P3

**Synopsis** A mean-field model to describe electron dynamics at the  $\hbar = 0$  level is used to calculate differential and total cross sections for electron emission in proton–ammonia-molecule collisions. The role of multiple ionization processes is studied.

Collisions of protons with small molecules continue to be an active field of research. In recent work, we introduced a mean-field model to describe electron transfer and ionization processes in collisions involving water molecules at the  $\hbar = 0$  level, and implemented it using the classical-trajectory Monte Carlo (CTMC) method [1, 2]. This model is applied to the proton–ammonia-molecule (p-NH<sub>3</sub>) system for which differential and total cross sections for electron emission have been measured [3, 4]. The molecular structure and geometry are taken into account in terms of a multi-center model potential designed to yield single-electron energy eigenvalues which are in close agreement with results of self-consistent field calculations. To compare with the available experimental data, we extract both differential and total cross sections for electron emission from the time-evolved trajectories and use the independent electron model (IEM) to distinguish between processes involving different electron multiplicities  $q$ .

We find significant contributions to net ionization from multiplicities  $q > 1$ . For differential electron emission there are no experimental data available to scrutinize our  $q$ -specific IEM results. In the case of total ionization, recent coincident measurements by Wolff *et al.* [4] indicate much weaker  $q > 1$  contributions than our calculations, as shown in Fig. 1. However, these data are based on the counting of charged fragments, and incomplete detection and the possible misidentification of events complicate the comparison with our calculations. In particular, the experimental results for  $q = 3$  included in the figure are associated

solely with H<sup>+</sup> + N<sup>2+</sup> coincidences.

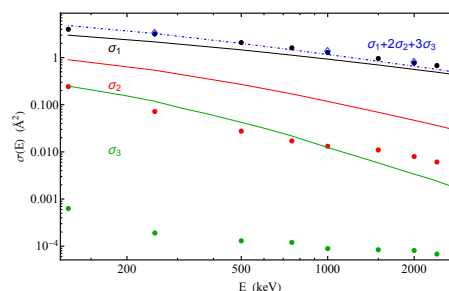


**Figure 1.** Total cross sections for p-NH<sub>3</sub> collisions. Dash-dotted line: CTMC approximate net ionization result,  $\sum_{q=1}^3 q\sigma_q^{\text{ion}}$ . Open diamonds: net ionization cross sections from [3]. Solid lines from top to bottom: CTMC results for  $\sigma_q^{\text{ion}}$  with  $q = 1, 2, 3$ . Dots: experimental values for  $\sigma_q^{\text{ion}}$  from fragmentation yields [4].

A detailed account of our calculations as well as comparisons with the differential net electron emission measurements of Ref. [3] and total  $q$ -specific ionization results obtained from independent-atom-model calculations [5] will be presented at the conference.

## References

- [1] Jorge A, Horbatsch M, Illescas C and Kirchner T 2019 *Phys. Rev. A* **99** 062701
- [2] Jorge A, Horbatsch M and Kirchner T 2020 *Phys. Rev. A* **102** 012808
- [3] Lynch D J, Toburen L H and Wilson W E 1976 *J. Chem. Phys.* **64** 2616
- [4] Wolff W, Luna H, Montenegro E C and Rodrigues Junior L C 2020 *Phys. Rev. A* **102** 052821
- [5] Lüdde H J, Horbatsch M and Kirchner T 2022 *Phys. Rev. A* **106** 022813

\*E-mail: [albamaria.jorge@gmail.com](mailto:albamaria.jorge@gmail.com)

†E-mail: [marko@yorku.ca](mailto:marko@yorku.ca)

‡E-mail: [tomk@yorku.ca](mailto:tomk@yorku.ca)

## Alpha particle transport modeling in a biological environment with *TILDA-V*

A Larouze<sup>1\*</sup>, M E Alcocer-Avila<sup>2</sup>, N Esponda<sup>3</sup>, M A Quinto<sup>3</sup>, J M Monti<sup>3</sup>, R D Rivarola<sup>3</sup>, E Hindie<sup>4,5</sup>  
and C Champion<sup>1†</sup>

<sup>1</sup>Centre Lasers Intenses et Applications, Université de Bordeaux, Talence, 33405, France

<sup>2</sup>Institut de Physique des 2 infinis de Lyon, Université Claude Bernard Lyon 1, Lyon, 69000, France

<sup>3</sup>Instituto de Fisica Rosario, CONICET – Universidad Nacional de Rosario, Rosario, 2000, Argentina

<sup>4</sup>Service de médecine nucléaire, CHU de Bordeaux, Université de Bordeaux, Talence, 33400, France

<sup>5</sup>Institut universitaire de France, Paris, 75231, France

**Synopsis** In this study, we report improvements of the homemade code *TILDA-V* for simulating the slowing-down of  $\alpha$ -particles in water. Especially, new cross sections implemented for ionization, electron capture and electron loss using CDW-EIS model are detailed. The original purpose of this code is to evaluate therapeutic potential of  $\alpha$ -particle emitters. Therefore, results for several  $\alpha$ -particle emitters are presented in terms of S-values.

Radiotherapy is nowadays one of the main methods for treating cancer, along with chemotherapy and surgery. In the current work, we focus on internal vectorized radiotherapy that consists in coupling a radionuclide to biological molecule vector able to target tumour cells. Describing the properties of such a radio-element thus becomes challenging in medical physics research.

Through Monte Carlo numerical simulations, it may be possible to describe the radiation-induced energy deposits in biological samples. However, in order to correctly simulate particle transport in a given medium, Monte Carlo track structure codes require access to large databases of differential and total cross sections to describe the various interactions induced by the particles in the biological medium irradiated.

In this context, we here details all the models we developed and implemented into our *TILDA-V* code [1] to describe the transport of helium particles in water. For modeling the elastic scattering, we first used a quantum-mechanical approach to describe the interaction potential between the biological samples and the charged particles, that is finally implemented into a classical description of the elastic scattering process. For describing the  $\text{He}^{q+}$ -induced ionization, electron capture and electron loss, we developed a CDW-EIS prior model using two corrections recently developed. Figure 1 depicts the total ionization cross sections of  $\text{He}^{2+}$  projectiles on water vapor.

Finally, we computed S-values for various  $\alpha$ -emitters. Table 1 shows results for  $^{225}\text{Ac}$ . Comparisons with existing data [2,3] exhibited a good agreement.

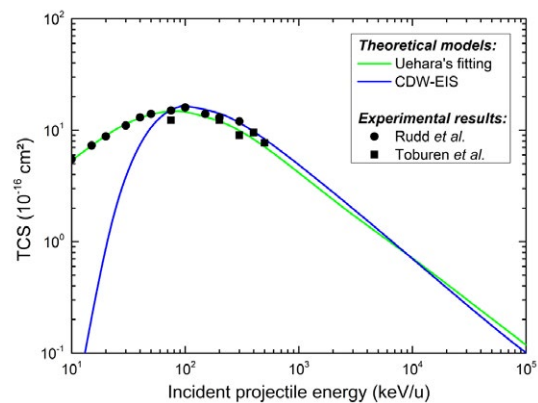


**Figure 1.** Total ionization cross sections of water vapor impacted by  $\text{He}^{2+}$  projectiles.

**Table 1.** S-values for  $^{225}\text{Ac}$  ( $\text{Gy}\cdot\text{Bq}^{-1}\cdot\text{s}^{-1}$ ).

	$S(N \leftarrow \text{CS})$	$S(N \leftarrow N)$
Alone	$2.38 \times 10^{-2}$	$9.23 \times 10^{-2}$
Series	$8.47 \times 10^{-2}$	$3.21 \times 10^{-1}$

### References

- [1] Quinto M A *et al.* 2017 *Eur. Phys. J. D* [71 130](#)
- [2] Vaziri B *et al.* 2014 *J. Nucl. Med.* [55 1557](#)
- [3] Lee D *et al.* 2018 *Radiat. Res.* [190 236](#)

\* E-mail: alexandre.larouze@u-bordeaux.fr

† E-mail: christophe.champion@u-bordeaux.fr

## Fragmentation Dynamics of a Carbon Dioxide Dication Produced by Ion Impact

H. Yuan<sup>1,3</sup>, S. Xu<sup>1,2\*</sup>, E. Wang<sup>3</sup>, Jiawei Xu<sup>1,2,5</sup>, Y. Gao<sup>1,3</sup>, X. L. Zhu<sup>1,2</sup>, D. L. Guo<sup>1,2</sup>, B. Ma<sup>6</sup>, D. Zhao<sup>1</sup>, S. F. Zhang<sup>1,2</sup>, S. Yan<sup>1,2</sup>, R. T. Zhang<sup>1,2</sup>, Y. Gao<sup>1,2</sup>, Z. F. Xu<sup>2</sup> and X. Ma<sup>1,2</sup>

<sup>1</sup>Institute of Modern Physics, Chinese Academy of Sciences, Lanzhou 730070, China

<sup>2</sup>School of Nuclear Science and Technology, University of Chinese Academy of Sciences, Beijing 100049, China

<sup>3</sup>School of Physics, Xi'an Jiaotong University, Xi'an 710049, China

<sup>4</sup>Hefei National Laboratory for Physical Sciences at the Microscale and Department of Modern Physics, University of Science and Technology of China, Hefei, Anhui 230026, China

<sup>5</sup>Advanced Energy Science and Technology, Guangdong Laboratory, Huizhou 516000, China

<sup>6</sup>School of Physics, Sichuan University, Chengdu, Sichuan 610064, China

**Synopsis** We present the investigation of the three-body fragmentation dynamics of  $\text{CO}_2^{2+}$  to  $\text{C}^+ + \text{O}^+ + \text{O}$  initiated by 1-keV/u  $\text{Ar}^{2+}$  impact. Besides the concerted and sequential fragmentation pathways, a novel isomerization pathway with transitory formation of  $\text{O}_2^+$  is identified. The fragmentation mechanisms identified in the present work may contribute to the  $\text{O}^+$  or  $\text{O}$  escaping from the Martian atmosphere.

The three-body fragmentation of  $\text{CO}_2^{2+}$  to  $\text{C}^+ + \text{O}^+ + \text{O}$  induced by 1 keV/u  $\text{Ar}^{2+}$  impact is investigated employing the Reaction microscope. The momentum vectors of  $\text{C}^+$  and  $\text{O}^+$  are measured directly, while the momentum vector of the neutral  $\text{O}$  is reconstructed according to momentum balance with  $\text{C}^+$  and  $\text{O}^+$ . With the help of the KEs and momentum vectors relationships among the three fragments, three different dissociation mechanisms are clearly identified. Another possible dissociation pathway, i.e., the sequential dissociation pathway with deferred charge separation, is not observed in our measurement. This is supported by the potential energy calculation.

After unambiguous identification of the three decay paths, we evaluate the branching ratios of them. The concerted fragmentation with two CO bonds breaking simultaneously is dominant (61.7%), which contains contributions from different molecular structures, i.e., both linear and bending structures. While the sequential pathway with  $\text{CO}^+$  as the intermediate also makes a significant contribution (36.6%). Also, a novel isomerization pathway with transitory formation of  $\text{O}_2^+$  is identified. This mechanism makes a minor contribution of 1.7%.

The KE distributions of three fragments for different pathways are obtained in our measurement. It was found that most of the measured  $\text{O}^+$  KE is higher than the escape energy of oxygen in the Martian atmosphere of 1.9 eV. Thus

the mechanisms identified in the present study can contribute to the escape of  $\text{O}^+$  from Martian atmosphere. Meanwhile, the two sequential fragmentation pathways may also contribute to escape of neutral  $\text{O}$ .

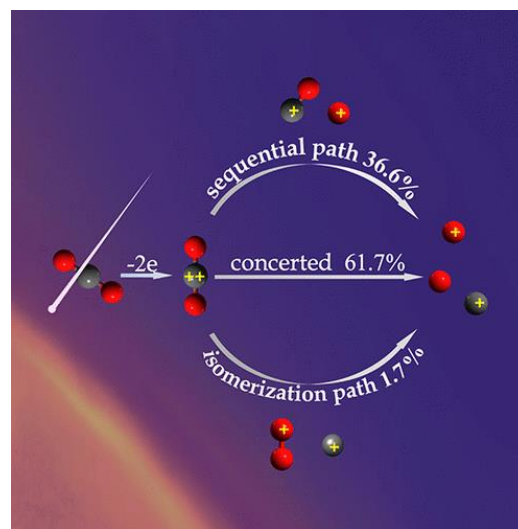


**Figure 1.** The different fragmentation pathways and their branching ratios of  $\text{CO}_2^{2+}$  to  $\text{C}^+ + \text{O}^+ + \text{O}$  channel.

### References

- [1] H. Yuan, S. Xu, E. Wang *et al.* 2022 *J. Phys. Chem. Lett.* **13**, 7594.

\* E-mail: [s.xu@impcas.ac.cn](mailto:s.xu@impcas.ac.cn)

## Gas-phase collision studies as a tool to investigate molecular mechanisms underlying radiation damage

W. Li<sup>1</sup>, O. Kavatsyuk<sup>2</sup>, W. Douma<sup>1</sup>, X. Wang<sup>1</sup>, R. Hoekstra<sup>1</sup>, D. Mayer<sup>3</sup>, M. S. Robinson<sup>3</sup>, M. Gühr<sup>3</sup>, M. Lalande<sup>4</sup>, M. Abdelmouleh<sup>4</sup>, M. Ryszka<sup>4</sup>, J. C. Pouilly<sup>4</sup>, T. Schlathölter<sup>1,2,\*</sup>

<sup>1</sup>University of Groningen, Zernike Institute for Advanced Materials, 9747 AG Groningen, Netherlands

<sup>2</sup>University of Groningen, University College Groningen, 9718 BG Groningen, Netherlands

<sup>3</sup>Universität Potsdam, Institut für Physik und Astronomie, 14476 Potsdam, Germany

<sup>4</sup>CIMAP UMR 6252 (CEA/CNRS/ENSICAEN/Université de Caen Normandie), Boulevard Becquerel, 14070 Caen Cedex 5, France

The creation of inner-shell vacancies by ionization or excitation is one of the first steps in many types of biological radiation damage. Protons and heavy ions at Bragg-peak energies but also therapeutic X-ray photons and electrons have the potential to create inner shell vacancies in DNA. In light elements 1s holes predominantly decay by Auger processes and in biological systems the interaction of Auger electrons with e.g. DNA play an important role in the evolution of radiation tracks.

The decay of inner-shell vacancies in DNA can be investigated in great detail in gas-phase studies. We have studied the interaction of soft X-rays and MeV ions at Bragg peak energies with gas-phase deprotonated DNA. We have brought [dTGGGGT-2H]<sup>2-</sup> anions into the gas-phase by means of electrospray ionization. The mass-selected oligonucleotides were then stored in a radiofrequency ion trap. The trapped ions were exposed to monochromatic soft X-rays from the U492/PGM1 beamline of the BESSY II synchrotron (Helmholtz Zentrum Berlin, Germany) or to MeV C<sup>4+</sup> ions from the IRRSUD beamline at GANIL (Caen, France). Interaction products were then analyzed using time-of-flight mass spectrometry,

The dominating decay mechanism of the X-ray induced inner shell vacancy was found to be Auger decay with detachment of at least three electrons, leading to charge reversal of the anionic precursor and the formation of positively charged photofragment ions. The same process is observed in heavy ion (12 MeV C<sup>4+</sup>) collisions with [dTGGGGT-2H]<sup>2-</sup> where inner shell vacancies are generated as well, but with smaller probability.

\* E-mail: [t.a.schlatholter@rug.nl](mailto:t.a.schlatholter@rug.nl)

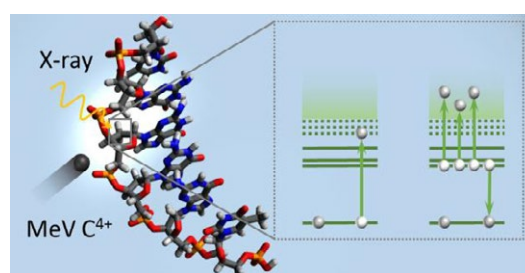


**Figure 1.** Multi-electron Auger processes in DNA (from [1]).

Auger decay of inner-shell vacancies in DNA that is not followed by single high-energy Auger electron emission but instead by removal of three or more low energy electrons has profound implications for DNA damage and damage modelling. Lower electron energies imply shorter mean free path and therefore more localized damage. Our findings therefore imply that secondary electron-induced DNA damage will be much more localized around the initial K-shell vacancy. The fragmentation channels triggered by triple electron detachment Auger decay are predominantly related to protonated guanine base loss and even loss of protonated guanine dimers is tentatively observed. The fragmentation is not a consequence of the initial K-shell vacancy but purely due to multiple detachment of valence electrons, as a very similar positive ion fragmentation pattern is observed in femtosecond laser-induced dissociation experiments.

### References

- [1] W. Li, O. Kavatsyuk, W. Douma, X. Wang, R. Hoekstra, D. Mayer, M. Robinson, M. Gühr, M. Lalande, M. Abdelmouleh, M. Ryszka, J. Christophe Pouilly, T. Schlathölter, 2021 *Chemical Science* **12** 13177



## Characterization of collision-induced dissociation of deprotonated dAMP in an ion funnel

Uma Namangalam<sup>1\*</sup>, Salvi M<sup>1</sup>, Hemanth Dinesan<sup>1,2</sup>, and S Sunil Kumar<sup>1,†</sup>

<sup>1</sup>Department of Physics and Center for Atomic, Molecular, and Optical Sciences and Technologies (CAMOST), Indian Institute of Science Education and Research (IISER) Tirupati, Tirupati, India

<sup>2</sup>(Present address) Laboratoire de Physique des Lasers CNRS in the Université Paris 13, FRANCE

**Synopsis** We study the collision-induced dissociation (CID) of deprotonated 2'-deoxyadenosine 5'-monophosphate experimentally under two different scenarios and analyze the results with the help of numerical simulations.

Studying the structure and spectra of biomolecules in their natural environment is a challenging undertaking due to their complex structures and large mass. The significant involvement of charged biomolecules and their response to environments are observed in various interdisciplinary fields that incorporate biology. Studying a sample can provide insights into a specific aspect of a larger system, making it easier to understand. One could consider deprotonated deoxy-adenosine monophosphate (d-dAMP) as a representative building block of DNA, as it is a nucleotide that plays a foundational role in the formation of the larger DNA molecule. This biomolecule exhibits unique spectral characteristics and a distinctive response to electromagnetic radiation [1, 2]. The scientific literature contains numerous studies that have probed dissociation mechanisms of d-dAMP by collisions [3, 4] and photoabsorption [1, 2].

Our study is mainly focused on exploring the fragmentation of d-dAMP in an ion funnel, an electrodynamic device typically employed in electrospray-based high-resolution mass spectrometers, for focusing and guiding ions at relatively low vacuum conditions (0.1-10 mbar). In an ion funnel, the combined effect of radiofrequency (RF), and electrostatic fields, together with the gas flow efficiently transport ions from atmospheric pressure into a high-vacuum system. In this work, we investigate the energy-dependent fragmentation of biomolecules within the ion funnel in two ways: 1) by varying the DC gradient between the ion funnel electrodes, and 2) by changing the

potential difference between ion-transfer capillary and the ion funnel. These measurements are carried out at different combinations of frequency and amplitude of RF potential applied on the ion funnel electrodes. The major objective of the study is to gain an understanding of various experimental parameters that determine the fragmentation of ions inside an ion funnel and hence to choose an optimized setting that minimizes the fragmentation of parent ions while maintaining the best possible transmission efficiency of the system.

We use SIMION to calculate electric fields and particle trajectories, while COMSOL is employed to include fluid dynamics to study the flow patterns and turbulence affecting biomolecule fragmentation.

By combining the simulations from these two software packages, we gain a better understanding of how different factors such as electric fields and fluid dynamics influence the fragmentation of biomolecules.

### References

1. Sunil Kumar, S., et al., *J. Phys. Chem. A* (2011): 10383–90
2. Nielsen, et al., *Physical Review Letters* (2003), 048302.
3. Ho, et al., *Int. J. Mass Spectrom and ion processes* (1997): 433–45
4. Rodgers, et al., *Int. J. Mass Spectrom and ion processes* (1994): 121–49.

\*E-mail: [umann@students.iisertirupati.ac.in](mailto:umann@students.iisertirupati.ac.in)

† E-mail: [sunil@iisertirupati.ac.in](mailto:sunil@iisertirupati.ac.in)

## Temperature of $H_3^+$ produced in the $H_2 + H_2^+$ reaction

M Astigarreta<sup>1\*</sup>, L Sigaud<sup>1†</sup> and E C Montenegro<sup>2</sup>

<sup>1</sup>Universidade Federal Fluminense, Niterói, 24210-346, Brasil

<sup>2</sup>Universidade Federal do Rio de Janeiro, Rio de Janeiro, 21941-909, Brasil

**Synopsis** In this work we investigate the ion-molecule collision leading to the formation of  $H_3^+$  ion starting from the ionization of the hydrogen gas by electron impact with energy of 100 eV and applying the DETOF technique. A new methodology within the well-established DETOF technique allowed us to obtain the kinetic energy distribution for the charged product of secondary  $H_2^+ + H_2$  reaction. New results are shown concerning the  $H_3^+$  formation kinetic energy which until this day has not been directly obtained and yet is of extreme importance for the understanding of chemical and physical processes taking place in interstellar media.

Besides its essential role in the production of ingredients for the existence of life, the presence of  $H_3^+$  molecules in the interstellar medium and gas giants' atmosphere is also an indicative of the astrophysical and astrochemical phenomena taking place in these environments [1]. That said, not only its interaction with the surrounding environment must be investigated to comprehend such phenomena but also the mechanisms through which these molecules were created.

Some questions concerning  $H_3^+$  and its properties remain unanswered until this day such as the kinetic energy released in its production in the reaction  $H_2 + H_2^+ \rightarrow H_3^+ + H$ .

Here we propose a methodology which provides the kinetic energy distribution of  $H_3^+$  ions. This methodology is based on the delayed extraction time of flight (DETOF) mass spectrometry technique [2], where a 100 eV pulsed electron beam is used to ionize the hydrogen gas and a pulsed electrostatic field is responsible for the ions collection.

The DETOF technique consists in obtaining the kinetic energy distributions of the ions produced in a collision by means of a controlled variation of the delay time between the ionization and extraction of ions. During this time interval a chemical reaction between the produced  $H_2^+$  and the remaining  $H_2$  may lead to the formation of  $H_3^+$ . In this case, both  $H_2^+$  and  $H_3^+$  behave as Maxwell-Boltzmann distributions [3], with temperature being the only free parameter. There-

fore, we can assign to each ion a different temperature with which they were produced, corresponding to their formation energy.

Preliminary results show that the kinetic energy of the  $H_3^+$  ion can be fitted by a Maxwell-Boltzmann distribution approximately 30K hotter than the one for  $H_2^+$ , which is at room temperature. This shift in the  $H_3^+$  kinetic energy should be independent from the initial gas temperature.

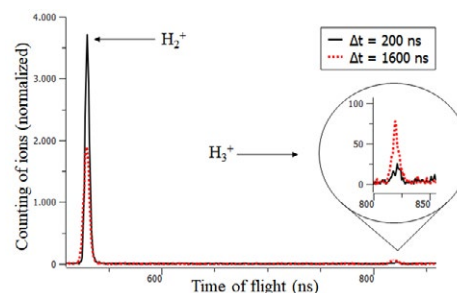


**Figure 1.** Time of flight spectra for different delay times ( $\Delta t$ ). One can see, in the zoomed region, the increase of  $H_3^+$  in the interaction region within the gas cell with the increase of  $\Delta t$ , concomitantly with the decrease of  $H_2^+$ .

### References

- [1] Oka T 2006 *Proc. Natl. Acad. Sci.* **103** 33
- [2] Sigaud L, de Jesus V L B, Ferreira N and Montenegro E C 2016 *Rev. Sci. Instrum.* **87** 083112
- [3] Gerlich D 1989 *J. Chem. Phys.* **90** 127

\*E-mail: moastigarreta@id.uff.br

†E-mail: lsigaud@id.uff.br

## Exploring Three Body Fragmentation of Acetylene Trication

Jatin Yadav<sup>1\*</sup>, C.P. Safvan<sup>2</sup> Pragma Bhatt<sup>2</sup>, Pooja Kumari<sup>1</sup>, Jasmeet Singh<sup>3</sup> and Jyoti Rajput<sup>1</sup>

<sup>1</sup>Department of Physics and Astrophysics, University of Delhi, Delhi 110007, INDIA

<sup>2</sup>Inter-University Accelerator Center, Aruna Asaf Ali Marg, New Delhi 110067, INDIA

<sup>3</sup>Department of Physics, Keshav Mahavidyalaya, University of Delhi, Delhi 110034, INDIA

**Synopsis** Three body fragmentation of triply charged acetylene ( $[\text{C}_2\text{H}_2]^{3+}$ ) into ( $\text{H}^+$ ,  $\text{C}^+$ ,  $\text{CH}^+$ ) and ( $\text{H}^+$ ,  $\text{H}^+$ ,  $\text{C}_2^+$ ) fragments is studied and different modes of breakup are identified and compared. Hydrogen migration in triply charged acetylene has been observed. Formation of  $[\text{C}_2\text{H}]^{2+}$  intermediate molecular ion is observed in sequential breakup of  $[\text{C}_2\text{H}_2]^{3+}$ . *Ab-initio* calculations are performed for  $[\text{C}_2\text{H}]^{2+}$  molecular ion and the experimental observations are discussed in light of these calculations.

We report on the three body fragmentation of  $[\text{C}_2\text{H}_2]^{3+}$  into ( $\text{H}^+$ ,  $\text{C}^+$ ,  $\text{CH}^+$ ) and ( $\text{H}^+$ ,  $\text{H}^+$ ,  $\text{C}_2^+$ ) fragments formed in interaction of neutral acetylene with a slow highly charged ion ( $\text{Xe}^{9+}$  having a velocity of  $\approx 0.5$  a.u.). The experiment was performed at the Low Energy Ion Beam Facility (LEIBF) of Inter-University Accelerator Centre (IUAC), New Delhi, INDIA. The momenta of the set of three fragments were measured in coincidence using the technique of Recoil Ion Momentum Spectroscopy (RIMS).

The breakup of  $[\text{C}_2\text{H}_2]^{3+}$  into ( $\text{H}^+$ ,  $\text{C}^+$ ,  $\text{CH}^+$ ) is analysed using the method of “native frames” [1]. This method allowed us to conclude that breakup into this set of fragments proceed in three ways: concerted breakup in acetylene configuration, concerted breakup in vinylidene configuration and a sequential breakup via  $[\text{C}_2\text{H}]^{2+}$  intermediate molecular ion. By collecting partial data which belongs primarily to concerted breakup events, a Newton diagram is plotted to study angular correlation between momentum vectors and is shown in figure 1.

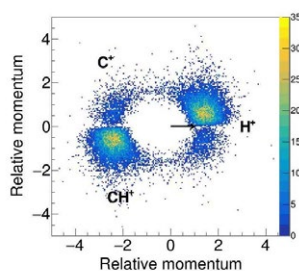


Figure 1. Newton diagram for breakup of  $[\text{C}_2\text{H}_2]^{3+}$  into ( $\text{H}^+$ ,  $\text{C}^+$ ,  $\text{CH}^+$ ).

From this diagram, concerted breakup from acetylene and vinylidene configuration can be clearly seen. The Newton diagram for the remaining data shows a semi-circular arc like feature and is a signature of the sequential breakup via  $[\text{C}_2\text{H}]^{2+}$  intermediate molecular ion [2].

The *ab-initio* calculations of the potential energy surface (PES) for the lowest electronic state of  $[\text{C}_2\text{H}]^{2+}$  are performed. This PES shows two dissociation pathways, one along the C–C stretch coordinate and another along the C–H stretch coordinate with potential barriers of  $\approx 0.6$  eV and  $\approx 2.7$  eV respectively. This indicates that it is easier for this electronic state to dissociate via the C–C stretch by tunnelling. The measured KER for the unimolecular breakup of  $[\text{C}_2\text{H}]^{2+}$  along the C–C stretch is in good agreement with the *ab-initio* calculations indicating that the lowest electronic state of  $[\text{C}_2\text{H}]^{2+}$  is populated in our experiment.

For the breakup of  $[\text{C}_2\text{H}_2]^{3+}$  into ( $\text{H}^+$ ,  $\text{H}^+$ ,  $\text{C}_2^+$ ), only concerted mode of breakup is observed [3] through the asymmetric and symmetric stretch of the C–H coordinate of the  $[\text{C}_2\text{H}_2]^{3+}$  molecular ion.

JY acknowledges the Council for Scientific and Industrial Research (CSIR), INDIA, for providing financial support. JR and CPS acknowledge the Department of Science and Technology, Government of INDIA, for financial assistance (Grant No. CRG/2018/001165).

### References

- [1] J Rajput *et. al.* 2018 *Phys. Rev. Lett.* **120**, 103001
- [2] J Yadav, C P Safvan, P Bhatt, P Kumari, A Kumar and J Rajput 2022 *J. Chem. Phys.* (Comm.) **156** 141101
- [3] J Yadav, C P Safvan, P Bhatt, P Kumari, J Singh and J Rajput 2023 *J. Chem. Phys.* **158** 074302

\* E-mail: [jatinyadav222@gmail.com](mailto:jatinyadav222@gmail.com)

## Formation and elongation of polyglycine via unimolecular reactions in the gas phase

M. Farizon<sup>1\*</sup>, H. Lissillour<sup>1</sup>, L. Parrado Ospina<sup>1</sup>, D. Comte<sup>1,4</sup>, L. Lavy<sup>1</sup>, P. Bertier<sup>1</sup>, P. Calabria<sup>1</sup>, R. Fillol<sup>1</sup>, F. Calvo<sup>2</sup>, I. Daniel<sup>3</sup>, B. Farizon<sup>1</sup>, T. D. Märk<sup>4</sup>

<sup>1</sup> Université Lyon 1, CNRS/IN2P3, UMR 5822, Institut de Physique des 2 Infinis de Lyon, F 69622 Villeurbanne, France

<sup>2</sup> Université Grenoble Alpes, CNRS LIPHY-38000 Grenoble, France

<sup>3</sup> Université Lyon 1, Ens Lyon, CNRS, UMR 5276, LGL-TPE, F 69342, Lyon, France

<sup>4</sup> Institut für Ionenphysik und Angewandte Physik, Leopold Franzens Universität 6020 Innsbruck, Austria

**Synopsis** Peptide chain formation in abiotic conditions is one of the keys of origin of life chemistry. A laboratory astrochemistry experiment (DIAM@IP2I<sub>Lyon</sub>) provides evidence for the formation of polyglycine peptides in the absence of water or substrate.

Peptide chains of amino acids play a crucial role in the emergence of living organisms. Unlike their synthesis by living systems or under industrial conditions, understanding the growth of peptide chains under abiotic conditions is an important question, especially considering the increasing amount of complex molecules detected in various astrophysical environments [1]. Recently, we found that the growth of peptide chains can occur under gas-phase conditions via a dehydration reaction in a protonated molecular amino acid dimer ion [2]. The proton not only induces dipeptide formation but also contributes to further elongating the peptide chain. Combining experimental measurements and quantum chemistry calculations, we show that polymerization reactions leading to the peptide of glycine (diglycine) takes place after excitation of a protonated glycine dimer in a single high velocity collision, and we provide evidence for the further growth of the peptide chain. The formation of a protonated mixed dimer consisting of a diglycine and a glycine molecule is dominant and its further excitation can lead to the formation of the tripeptide. The various relaxation pathways of the excited protonated dimers and the unimolecular reaction dynamics are investigated by velocity map imaging of the water molecules eliminated in the polymerization reactions (Figure 1).

Peptide chain growth is thus demonstrated to occur via a unimolecular gas-phase reaction in an excited cluster ion without extra substrate such as dust or ice. The proton facilitates the dehydration reaction in a pure molecular dimer and chaperones the further growth of the peptide-chain via further dehydration reactions in mixed dimer and cluster ions. These results obtained with glycine, the most abundant amino acid detected in extraterrestrial objects, show that the detected intradimer dehydration reaction could be a conceivable abiotic pathway towards the possible existence of peptide chains in Space.

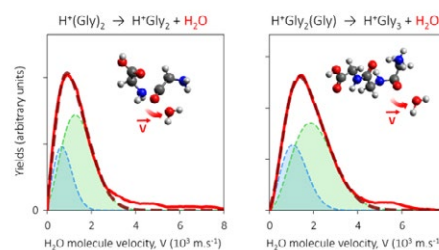


**Figure 1:** Measured velocity distributions (red solid lines) of water molecules eliminated from pure or mixed protonated glycine dimer after single collisions.

### References

- [1] – Pearce B.; Pudritz R. E.; Semenov D. A.; Henning T. K., *Proc. Natl. Acad. Sci. U.S.A.* 2017, 114, 11327–11332.  
 [2] – Comte D., Lavy L., Bertier P., Calvo F., Daniel I., Farizon B., Farizon M., Märk T. D. *J. Phys. Chem. A* 2023, 127, 3, 775–780.

\* E-mail: m.farizon@ip2i.in2p3.fr

## Dissociation dynamics in Tetrachloromethane molecule induced by ion impact

Nirmallya Das<sup>1</sup>, Sankar De<sup>2</sup>, Pragya Bhatt<sup>3</sup>, C. P. Safvan<sup>3</sup> and Abhijit Majumdar<sup>1</sup>

<sup>1</sup>Department of Physics, Indian Institute of Engineering Science and Technology, Howrah-711103, India.

<sup>2</sup>Saha Institute of Nuclear Physics, HBNI, 1/AF, Bidhannagar, Kolkata 700064, India.

<sup>3</sup>Inter-University Accelerator Centre, Aruna Asaf Ali Marg, New Delhi 110067, India.

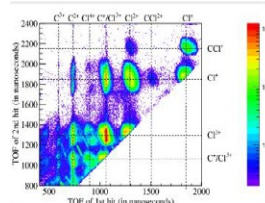
**Synopsis** The ion impact multiple ionization and subsequent dissociation of CCl<sub>4</sub> is studied using a beam of Ar<sup>7+</sup> ion having the energy of about 1 MeV in a linear time-of-flight mass spectrometer. The complete, as well as incomplete Coulomb explosion pathways are identified and studied. Possible modes of fragmentation pathways, i.e., concerted and/or sequential, for all the identified channels are studied using Newton diagrams, Dalitz plots, and kinetic energy distributions. The nature of the fragmentation process is further investigated with simulated Dalitz plots and Newton diagrams using the simple classical mechanical model.

The ion impact multiple ionization and subsequent dissociation of CCl<sub>4</sub> is studied using a beam of Ar<sup>7+</sup> ion having energy of about 1 MeV in a linear time of flight mass spectrometer coupled with a position sensitive detector [1]. Our objective is to identify the possible modes of fragmentation pathway for all the identified channels with the help of kinetic energy release and momentum distributions of fragmented ions.

Tetrachloromethane (CCl<sub>4</sub>) is found in the natural environment and has been identified to be a long-lived green-house gas which is responsible for ozone depletion in both the troposphere and the stratosphere. It has widespread industrial applications like reactive etching gas for silicon wafers in semiconductor microchip industries as well as cleaning surfaces by chemical vapour deposition. The dissociative ionization of tetrachloromethane have been explored in intense linearly polarized laser field of picosecond and attosecond [2] time scale. The properties such as fragmentation pattern, angular distribution of ionic fragments like Cl<sup>+</sup> arising from it, were studied and compared with the 70 eV electron induced fragmentation

The complete as well as incomplete Coulomb explosion pathways for CCl<sub>4</sub><sup>2+</sup> and CCl<sub>4</sub><sup>3+</sup> ions are identified and studied. The kinetic energy release distributions (KERD) of channels, kinetic energies and momentum distributions of fragmented ions as well as neutrals are also calculated.

**Figure 1.** Coincidence plot of CCl<sub>4</sub> molecule due to the impact of about 1 MeV Ar<sup>7+</sup> beam. The TOF of 1<sup>st</sup> and 2<sup>nd</sup> hit is plotted along X- and Y-axis respectively in nanosecond time scale.



Possible modes of fragmentation pathway i.e. concerted and/or sequential for all the identified channels are studied using Newton diagram, Dalitz plot and kinetic energy distribution. The dynamical information and fragmentation pathways were analysed with Dalitz plot and Newton diagram for the three-body dissociation channel. A sequential mode of fragmentation for an incomplete 3-body dissociation channel has been identified. The nature of the fragmentation process is further investigated with simulated Dalitz plots and Newton diagram using simple classical mechanical model.

### References

- [1] N. Das, S. De, P. Bhatt, C. P. Safvan, and A. Majumdar, *J. Chem. Phys.* **158**, 084307 (2023).
- [2] V. R. Bhardwaj, F. A. Rajgara, K. Vijayalakshmi, V. Kumarapan, D. Mathur, and A. K. Sinha, *Phys. Rev. A* **58**, 3849 (1998).



## Effect of vanadium implantation on the structure of glassy carbon

O.S. Odutemowo<sup>1</sup>, T. Fodor<sup>2</sup>, K. Tórkési<sup>2\*</sup> and J.B. Malherbe<sup>1</sup>

<sup>1</sup>Physics Department, University of Pretoria, Hatfield 0028, Pretoria, South Africa

<sup>2</sup>Institute for Nuclear Research (ATOMKI), Debrecen 4026, Hungary

**Synopsis** We present investigation of the structural effects of Vanadium ions implantation on glassy carbon. The glassy carbon was implanted with 15 keV ions to a fluence ranging from  $1 \times 10^{12}$  ions/cm<sup>2</sup> to  $1 \times 10^{15}$  ions/cm<sup>2</sup> at room temperature. The structural changes due to the different implantation fluences were then monitored using visible-Raman spectroscopy and the structural damage (amorphization) was simulated with SRIM. We found that amorphisation was noticeable at ion fluences  $10^{14}$ /cm<sup>2</sup> and above.

All countries have radioactive waste, which has to be stored until its radioactivity has decayed to safe levels. The waste ranges from low level waste to high level waste. The aim of the recent studies is to find a new material for the storage of high level radioactive nuclear waste to prevent leakage of the radioactive waste from the container thereby contaminating the environment. It seems to be that the vanadium implanted glassy carbon is one of the good candidates for this purpose.

Along this line, in this work, the structural effects of vanadium ion implantation on glassy carbon were investigated. The carbon substrates were implanted with 15 keV vanadium ions to a fluence ranging from  $1 \times 10^{12}$  to  $1 \times 10^{15}$  V<sup>+</sup>/cm<sup>2</sup> at room temperature. The implantation was shown to be successful with XPS, with most of the vanadium present in its metallic (unoxidized) form. SRIM simulations showed that the damage introduced with low V<sup>+</sup> implantation fluence ( $\leq 10^{13}$  cm<sup>-2</sup>) ranged from 0.001 – 0.014 dpa, well below the 0.2 dpa required to amorphise glassy carbon, while predicting 0.2 and 1.1 dpa for the  $10^{14}$  and  $10^{15}$  cm<sup>-2</sup> levels, respectively.

Raman spectroscopy was used to monitor the structural changes in the samples as a result of the implantation. The Raman spectrum of the pristine glassy carbon sample shows the characteristic D and G peaks at 1350 cm<sup>-1</sup> and 1588 cm<sup>-1</sup>. Raman spectra of samples implanted at  $1 \times 10^{12}$ ,  $5 \times 10^{12}$  and  $1 \times 10^{13}$  V<sup>+</sup>/cm<sup>2</sup> show that the glassy carbon structure remains unchanged when compared to that of the pristine glassy carbon, indicating that the low fluence implantation of vanadium indeed does not result in the

radiation damage of the glassy carbon structure. High fluence implantation at  $10^{14}$  and  $10^{15}$  V<sup>+</sup>/cm<sup>2</sup> resulted in a slight change of the Raman spectrum: The D and G peaks merged into each other and became wider suggesting that the samples became amorphised after implanting at these high fluences, in agreement with the simulations.

### Acknowledgements

The work was supported by the bilateral relationships between South Africa and Hungary in science and technology (S&T) under the project number 2019-2.1.11-TET-202000123. The XPS measurements were supported by the projects TKP2021-NKTA-42 and 2019-2.1.7-ERA-NET-2021-00021 financed by the National Research, Development and Innovation Fund of the Ministry for Innovation and Technology, Hungary.

### References

- [1] US Nuclear regulatory commission, *Radioactive waste: Production, storage, disposal*, NRC, Washington, DC, United States of America, 2002.
- [2] H.O. Pierson 1993 *Handbook of carbon, graphite, diamond and fullerenes*, Noyes Publ., Park Ridge NJ.
- [3] J.B. Malherbe, O.S. Odutemowo, E.G. Njoroge, T.T. Hlatshwayo and C.C. Theron 2018 *Vacuum* **149** 19-22.
- [4] P.J.F. Harris and S.C. Tsang 1997 *Philos. Mag. A Phys. Condens. Matter, Struct. Defects Mech. Prop.* **76** 667–677

\* E-mail: [tokesi@atomki.hu](mailto:tokesi@atomki.hu)

## Collisions between solar wind ions and the lunar surface

J Brötznner<sup>1</sup>, H Biber<sup>1</sup>, N. Jäggi<sup>2</sup>, P. S. Szabo<sup>3</sup>, C. Cupak<sup>1</sup>, A. Galli<sup>2</sup>, P. Wurz<sup>2</sup>, and F. Aumayr<sup>1\*</sup>

<sup>1</sup>Institute of Applied Physics, TU Wien, Vienna, 1040, Austria

<sup>2</sup>Physics Institute, University of Bern, Bern, 3012, Switzerland

<sup>3</sup>Space Sciences Laboratory, University of California, 94720 Berkeley, USA

**Synopsis** This study investigates the erosion of the lunar surface caused by solar wind ions through the process of sputtering. The sputtering yield and angular distribution of sputtered particles were measured for two types of lunar samples - regolith pellets and thin films grown using Pulsed Laser Deposition. The findings of the study, along with simulation approaches, will help to model the creation of the Moon's exosphere.

The surface of our Moon is constantly bombarded by solar wind ions, a steady stream of mainly protons and alpha particles, which liberate material through sputtering [1] (fig. 1). This material contributes to the formation of the lunar exosphere. To properly model exosphere creation, it is necessary to understand sputtering and experimentally assess physical quantities such as the sputtering yield and the angular distribution of sputtered particles.

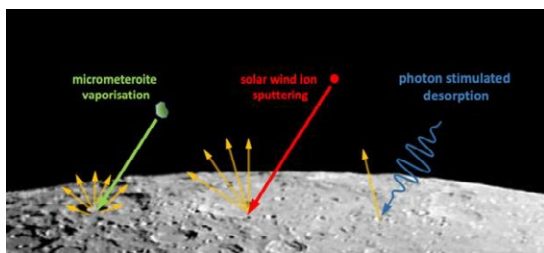


**Figure 1.** Interaction processes leading to surface erosion of airless planetary bodies such as the Moon and release of refractory and volatile species into the exosphere.

To achieve this, we have studied the erosion of two types of samples prepared from lunar soil obtained during the Apollo 16 mission in 1972. The lunar soil material was either pressed into pellets [2], or used to grow thin films of typically 100 nm thickness onto quartz resonators through Pulsed Laser Deposition (PLD).

As projectiles, typical ions present in the solar wind (hydrogen, helium) were applied with specific impact energies of 1 keV/amu, corresponding to the solar wind velocity of around 440 km/s.

The thin PLD films were used in a sensitive Quartz Crystal Microbalance (QCM) setup to directly measure the mass depletion of the

sample layer caused by ion sputtering as a change in the resonance frequency of the QCM. This methodology was successfully tested and perfected on Lunar and Mercury analog materials before [3, 4].

For the pellet samples, pressed from lunar soil material, another QCM was installed to collect the sputtered particles. This setup allows to determine the angular distribution of the emitted particle flux by collecting sputtered material at varying polar angles [5]. Such differential sputter yield measurements indirectly provide access to the total sputtering yield of pellet targets relative to the thin film targets.

Differences between thin film and pressed pellet samples could be attributed to different surface roughness. For this purpose simulations with the codes SPRAY [6] and SDTrimSP-3D [7, 8] were conducted, which yielded very good agreement. We will present our experimental findings for both types of samples along with simulation approaches.

This work was funded by the Austrian FWF Proj. No. I4101-N36 as well as the Swiss SNF 200021L\_182771/1.

### References

- [1] Wurz P et al 2022 Space Sci. Rev. [218 10](#)
- [2] Jäggi N et al 2021 Icarus [365 114492](#)
- [3] Szabo P S et al 2020 Astrophys. J. [891 100](#)
- [4] Szabo P S et al 2020 J. Geophys. Res.: Planets [125 e2020JE006583](#)
- [5] Biber H et al 2022 Planet. Sci. J. [3 271](#)
- [6] Cupak C et al 2021 Appl. Surf. Sci. [570 151204](#)
- [7] von Toussaint U et al. 2017 Phys. Scr. [T170 014056](#)
- [8] Szabo P S et al 2022 Nucl. Instr. Meth. B [522 47](#)

\* E-mail: [friedrich.aumayr@tuwien.ac.at](mailto:friedrich.aumayr@tuwien.ac.at)

## Can the ion charge state be observed while travelling within a solid?

R A Wilhelm<sup>1\*</sup>, A Niggas<sup>1</sup>, and F Aumayr<sup>1</sup>

<sup>1</sup>TU Wien, Institute of Applied Physics, Vienna, 1040, Austria, EU

**Synopsis** We present experimental work on the transmission of slow highly charged ions through free-standing layers of single, double and triple layer graphene. By varying the ion velocity and the layer thickness independently, we can conclude, that the interaction time between ion and solid alone determines the charge exchange.

In contrast to electrons or photons which have a fixed charge of -1 or 0, respectively, the charge of an ion is a dynamic quantity which can change once in close contact to a solid. The capture or release of an electron from an ion is typically associated with a change of internal energy. For slow ions prepared in high charge states the total amount of internal (i.e., potential energy) can amount to several 10 keV in typical experiments. Upon neutralisation of the ion, this energy is released to a solid target surface and can drive a plethora of different processes ranging from photon and electron emission to nanoscale material modification with interesting applications for defect engineering of thin films [1].

An ion impact on a solid lasts only several 10 fs from the initial contact to the full stop of the ion. The majority of the charge exchange itself is even much faster and occurs on the order of 1 fs. As such, there exists no direct time-resolved experiment to measure the ion charge state within a material. Still, it is important to know the charge state, because it also determines the stopping (i.e., slowing down process) of the ion and is therefore a fundamental quantity of all ion-solid interaction processes. Since charge exchange involves both the dynamics of the ion-perturbed electron density in the solid as well as the atomic physics of charge redistribution (and de-excitation) within the ion (and the solid target), no *ab-initio* simulation methods exist to describe the complex ion charge exchange fully. Recently there has been progress in using time-dependent density functional theory coupled to molecular dynamics in the Ehrenfest dynamics scheme to describe charge state effects on the stopping and simulate the charge evolution inside solids [2].

Here we present experimental work on ion

\*E-mail: [wilhelm@iap.tuwien.ac.at](mailto:wilhelm@iap.tuwien.ac.at)

interaction with and transmission through free-standing two-dimensional materials with layer thicknesses ranging from 1 to 3 atomic layers [3]. We use slow heavy ions in high initial charge states, i.e., far from charge equilibrium in a solid, and this allows us to determine the charge exchange upon ion transmission. We can vary the interaction time of the ion with the material by two independent methods: (i) changing the initial ion velocity and (ii) changing the layer number (thickness) of the material and find that the charge state within the material decays exponentially with time. The exponential decay constant (converted to velocity instead of time directly) is shown in Fig. 1. Therefore, the part of the ion trajectory in close contact with the target atoms dominates the overall charge dynamics with little influence of above-surface (front and back) charge transport to our measured charge exchange.

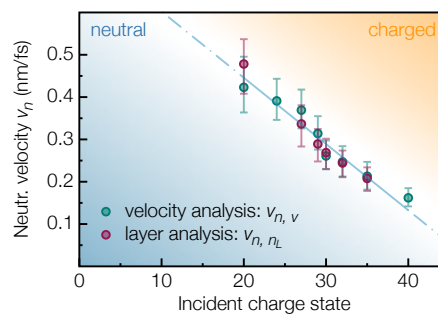


**Figure 1.** Phase diagram of charge state evolution for highly charged Xe ions in carbon material [3].

### References

- [1] Wilhelm R A 2023 *Surf. Sci. Rep.* **7** 100577
- [2] Ojanperä A and Krasheninnikov A V 2014 *Phys. Rev. B* **89** 035120
- [3] Niggas A *et al.* 2021 *Commun. Phys.* **4** 180

## Study of charge state distribution for Si projectile with carbon target

D.K. Swami<sup>1,3\*</sup>, Sarvesh Kumar<sup>2</sup>, S. Ojha<sup>1</sup> and R.K. Karn<sup>3</sup>

<sup>1</sup>Inter University Accelerator Centre, New Delhi-110067

<sup>2</sup>Chemical Sciences Division, Lawrence Berkeley National Laboratory, Berkeley, California 94720, United States

<sup>3</sup>Jam. Co-operative College, Kolhan University, Chaibasa, Jharkhand

**Synopsis** The charge state distribution of Si projectiles with initial charge states of 4, 5, 6, 7, 8, 9, and 10+ after passing through a 10  $\mu\text{g}/\text{cm}^2$  carbon foil has been studied in the energy range of 1.78-3.93 MeV/u. The relevant parameters of the charge state distribution, such as mean charge state, distribution width, and asymmetric parameter, have also been determined and compared with the Fermi gas model and ETACHA4 predictions.

The study focused on the charge state distribution of Si projectiles with initial charge states ranging from 4 to 10+ and energies between 1.78 and 3.93 MeV/u after passing through a carbon foil with a thickness of 10  $\mu\text{g}/\text{cm}^2$ . The aim of the study was to determine the relevant parameters of the charge state distribution such as mean charge state, distribution width, and asymmetric parameter, and compare them with the predictions of the Fermi gas model[1] and ETACHA4[2].

The results of the study showed a significant difference between the experimental results and the theoretical calculations, with the theoretical calculations overestimating the experimental results. This overestimation was attributed to the non-radiative electron capture taking place at the exit surface in the influence of wake and dynamic screening effect.

Charge state fractions are important parameters that are used in various applications[4], such as detecting superheavy ions and solving problems in laboratory and astrophysical plasma. Therefore, studies like this are important for understanding the behavior of charged particles in matter and improving the accuracy of theoretical models.

This study concludes that the non radiative electron capture at the exit surface of the target is very important and it needs to be included in the theoretical calculations.

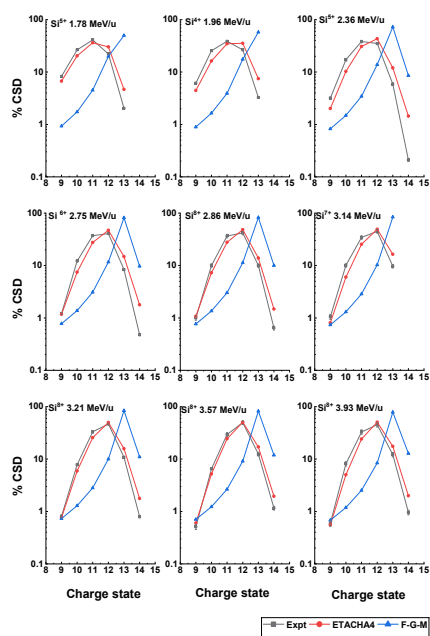


Fig. 2. Charge state fraction (%) (CSF) versus Charge state ( $q$ ): Comparison between experimental, ETACHA4 and F-G-M charge state distribution for  $^{28}\text{Si}$  on C for various beam energies. Due to small values, errors are embedded in symbol itself.

### References

- [1] Brandit W., Laubert R., and Mourino M. 1973 *Phys. Rev. Lett.* **30** 358
- [2] Lamour E. et. al. 2015 *Phys. Rev. A* **92** 4270

\* E-mail: [swami@iuac.res.in](mailto:swami@iuac.res.in)

## Fast heavy-ion-induced anion–molecule reactions on the droplet surface

T Majima<sup>1\*</sup>, Y Mizunami<sup>1</sup>, T Takemura<sup>1</sup>, T Teramoto<sup>2</sup>, H Tsuchida,<sup>1,3</sup> and M Saito<sup>1,3</sup>

<sup>1</sup>Department of Nuclear Engineering, Kyoto University, Kyoto 615-8540, Japan

<sup>2</sup>Institute for Radiation Sciences, Osaka University, Toyonaka 560-0043, Japan

<sup>3</sup>Quantum Science and Engineering Center, Kyoto University, Uji 611-0011, Japan

**Synopsis** We performed a mass spectrometric study of secondary ions emitted from microdroplet surfaces by using MeV-energy heavy ions. We found that a wider variety of negative ions than positive ions were formed. We propose that the primary formation mechanism of complex negative ions is rapid association reactions of anion fragments and neutral fragments. This study provides new insights into the importance of anion–molecule reactions among fragments as the mechanism that generates complex molecular species in fast heavy-ion-induced reactions in condensed matter.

MeV-energy heavy ions deposit a large amount of energy into molecules along their trajectories in condensed matter via ionization and electronic excitation. Various fragment ions and radicals can be produced at high densities. As a result, complex molecules are expected to be produced in secondary reactions among the fragments. Secondary ions emitted from surfaces after fast heavy-ion impacts are powerful probes for obtaining molecular-level understanding of physicochemical reactions in heavy-ion tracks. Recently, we developed a coincidence measurement system for mass spectrometry on liquid surfaces—using microdroplet targets under high vacuum—to investigate complex ion–molecule reactions induced by heavy-ion irradiation [1,2]. In this study, we observed positive and negative secondary ions from droplet surfaces; such as ethanol [1,2], methanol [3], and water–methanol mixtures. In addition, we compared the results of methanol (CH<sub>3</sub>OH) with deuterated methanol (CH<sub>3</sub>OD) to identify the hydrogen elimination site of the intermediates that are involved in the reactions.

Microdroplets were generated by ultrasonic atomization under 1-atm Ar and then transported to the collision chamber with a differential pumping system. The droplets were irradiated with 2-MeV C<sup>2+</sup> and 4-MeV C<sup>3+</sup> beams from a 2-MV Pelletron accelerator. Positive and negative secondary ions were separately analyzed by time-of-flight (TOF) mass spectrometry using a coincidence technique in which forward-scattered ions were detected with a Si semiconductor detector. Correlations between the TOF and the energy of forward-scattered ions were recorded for each event in list mode [2].

Figure 1 compares the TOF mass spectra of CH<sub>3</sub>OH with CH<sub>3</sub>OD droplets in the range of  $m/z < 80$ . We observed a variety of reaction product ions; i.e., C<sub>2</sub>H<sub>*i*</sub><sup>−</sup> ( $i = 0, 1$ ), C<sub>2</sub>H<sub>*i*</sub>O<sup>−</sup> ( $i = 0, 1, 3, 5$ ), and C<sub>2</sub>H<sub>*i*</sub>O<sub>2</sub><sup>−</sup> ( $i = 3, 5$ ). Comparing the peak shift due to deuterium substitution, we propose that the primary formation mechanism is association reactions of anion and neutral fragments, such as CH<sub>3</sub>O<sup>−</sup> + CO → C<sub>2</sub>H<sub>3</sub>O<sub>2</sub><sup>−</sup>. Quantum chemical calculations confirm that these reactions can proceed without energy barriers. This study proposes the importance of rapid anion–molecule reactions among fragments in fast heavy-ion-induced reactions.

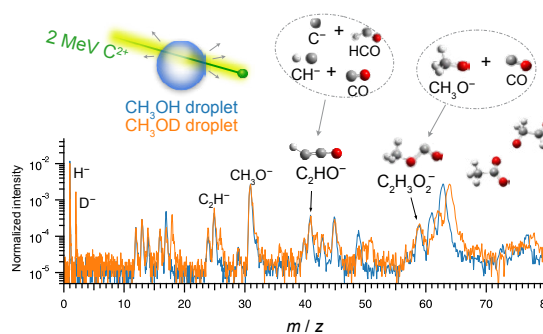


**Figure 1.** TOF mass spectra of the negative secondary ions from CH<sub>3</sub>OH (blue line) and CH<sub>3</sub>OD (orange line) droplets.

### References

- [1] Kitajima K et al. 2018 *Nucl. Instrum. Methods. Phys. Res., Sect. B* **424** 10
- [2] Majima T et al. 2020 *J. Chem. Phys.* **153** 224201
- [3] Majima T et al. 2022 *J. Phys. Chem. A* **126** 8988

\* E-mail: [majima@nucleng.kyoto-u.ac.jp](mailto:majima@nucleng.kyoto-u.ac.jp)



## Amorphous and crystalline pyridine ices irradiated by MeV ions

C A P da Costa<sup>1\*</sup>, A Bychkova<sup>1</sup>, P Boduch<sup>1</sup>, A L F de Barros<sup>2</sup>, I Bouchard de La Poterie<sup>1</sup>,  
Z Kaňuchová<sup>3</sup>, H Rothard<sup>1</sup> and A Domaracka<sup>1</sup>

<sup>1</sup>Centre de Recherche sur les Ions, les Matériaux et la Photonique (CEA/CNRS/ENSICAEN/Université de Caen- Normandie/Normandie Université),UMR 6252,CIMAP – CIRIL – GANIL, Caen, 14076, France

<sup>2</sup>Departamento de Física, Centro Federal de Educação Tecnológica Celso Suckow da Fonseca, Rio de Janeiro, 20271-110, Brazil.

<sup>3</sup> Astronomical Institute of the Slovak Academy of Science, Tatranska Lomnica, 059 60, Slovak Republic.

**Synopsis** The radioresistance of pyridine was probed under MeV ion beams irradiation by investigating the dependence of radiolysis and structural modifications on projectile stopping power, sample temperature and crystalline state.

Pyridine (C<sub>5</sub>H<sub>5</sub>N) is an important complex organic molecule (COM). It is heterocyclic and appears in compounds such as vitamins and pharmaceuticals [1]. Although pyridine has not yet been directly observed in space, Parker et al. (2015)[2] have revealed a potential pathway to a facile pyridine synthesis in the gas phase via the reaction of the cyano vinyl (C<sub>2</sub>H<sub>2</sub>CN) radical with vinyl cyanide (C<sub>2</sub>H<sub>3</sub>CN) in high temperature environments simulating conditions in carbon-rich circumstellar envelopes.

Pyridine ices, in amorphous and crystalline phases, have been irradiated with 396 MeV Ar<sup>17+</sup> and 61 MeV Kr<sup>15+</sup> at 10, 15 and 130 K in the SME and IRRSUD beam lines of the GANIL heavy ion accelerator facility. Infrared spectroscopy was employed to follow the structural and chemical evolution of the samples as a function of projectile fluence. The apparent destruction cross sections,  $\sigma_d^{ap}$ , which includes the dissociation effects of radiolysis and also ejection of particles by sputtering, were measured for all samples. The local doses needed to complete amorphization of the crystalline samples were calculated as well, see Fig. 1.

Pyridine ices that were initially crystalline present apparent destruction cross sections approximately four times higher than amorphous ones. However, after amorphization is completed, originally crystalline samples have the same  $\sigma_d^{ap}$  as ices that were initially amorphous. Targets irradiated at 130 K are more radioresistant than the ones at 10 K, they have smaller destruction cross sections  $\sigma_d^{ap}$ .

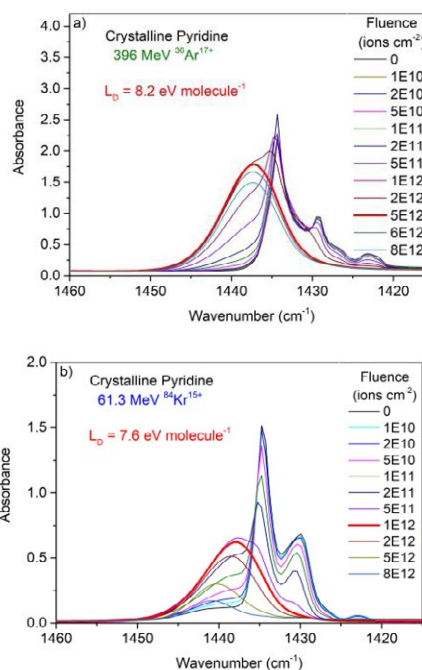


**Figure 1.** Evolution of infrared spectra of crystalline pyridine with projectile fluence of (a) 396 MeV Ar<sup>17+</sup> and (b) 61.3 MeV Kr<sup>15+</sup> ion beams irradiated at 15 K. Thicker red curves indicate the transition fluence value to complete amorphization. Obtained local doses are 8.2 and 7.6 eV/molecule, respectively.

### References

- [1] E. F. Scriven, & R. Murugan, 2000, Kirk Othmer Encyclopedia of Chemical Technology.  
[2] D. S. Parker, R. I. Kaiser, O. Kostko, et al. 2015, Physical Chemistry Chemical Physics, 17, 32000.

\* E-mail: [cintia-apc@hotmail.com](mailto:cintia-apc@hotmail.com)

## Spin-dependent metastable He ( $2^3S$ ) atom scattering from $\text{Fe}_3\text{O}_4(100)$ surfaces

H Maruyama<sup>1,2\*</sup>, M Kurahashi<sup>2</sup>, K Asakawa<sup>1</sup> and A Hatakeyama<sup>1†</sup>

<sup>1</sup> Department of Applied Physics, Tokyo University of Agriculture and Technology, 2-24-16 Naka-cho, Koganei, Tokyo 184-8588, Japan

<sup>2</sup> National Institute for Materials Science, 1-2-1 Sengen, Tsukuba, Ibaraki 305-0047, Japan

**Synopsis** We measured the spin states of metastable helium ( $\text{He}^*$ ) scattered from  $\text{Fe}_3\text{O}_4(100)$  surfaces. The experiments showed that the spin orientation of  $\text{He}^*$  was mostly preserved during scattering and the survival probability of  $\text{He}^*$  depended on its spin orientation with respect to the surface spin. These findings imply that  $\text{He}^*$  atoms scattered from  $\text{Fe}_3\text{O}_4(100)$  will become spin-polarized.

Spin polarized gaseous atoms have many research applications such as atomic magnetometers, probes of the surface electronic states, neutron spin filters and magnetic resonance imaging (MRI) of the lung. The spin-polarized gases are often used in containers. Although spin depolarization due to collisions with container walls is detrimental to the applications, the collisions with spin-polarized solid surfaces would be able to produce polarized gases. Previous studies have indicated that the survival probability of metastable helium ( $\text{He}^*$ ) in the  $2^3S_1$  state during scattering from ferromagnetic surfaces depends on the electron spin of  $\text{He}^*$  [1]. The spin dependent survival probabilities would lead to the production of a spin polarized  $\text{He}^*$  gas by scattering on ferromagnetic surfaces. However, the spin states of surviving  $\text{He}^*$  have not been clarified and should be verified experimentally.

In this study, we measured the spin states of  $\text{He}^*$  scattered from surfaces to explore the possibilities of the production of spin polarized  $\text{He}^*$  gas [2]. We irradiated a spin polarized  $\text{He}^*$  beam to a surface and measured the spin states of scattered  $\text{He}^*$ . The surfaces investigated included clean  $\text{Fe}_3\text{O}_4(100)$ , hydrogen (H)-terminated  $\text{Fe}_3\text{O}_4(100)$ , benzene adsorbed on H-terminated  $\text{Fe}_3\text{O}_4(100)$ , and Cu(100).  $\text{Fe}_3\text{O}_4$  is predicted to be a half-metal with a spin polarization of  $-100\%$  at the Fermi level in the bulk. Spin polarization at the Fermi level for  $\text{Fe}_3\text{O}_4$  surfaces is much lower than that for bulk, but it is known that the half metallicity recovers with H-termination for the  $\text{Fe}_3\text{O}_4(100)$  surface.

Figure 1 shows the ratio of the intensity of the scattered  $\text{He}^*$  with its spin states changed to that with its spin states preserved. This ratio roughly represents the spin-flopping probability.

$R_P$  ( $R_A$ ) corresponds to the spin-flop scattering where the incident  $\text{He}^*$  spin is parallel (antiparallel) to the majority spin of  $\text{Fe}_3\text{O}_4$ . The figure shows that the initial spin states were mostly preserved, and spin-flop scattering of  $\text{He}^*$  only occurred with small probabilities up to approximately 0.1. We also found that the  $\text{He}^*$  survival probability was higher when the  $\text{He}^*$  spins and the majority spin of clean  $\text{Fe}_3\text{O}_4(100)$  and H-terminated  $\text{Fe}_3\text{O}_4(100)$  were parallel. From these findings, we concluded that a non-polarized  $\text{He}^*$  gas will be spin-polarized after collision with clean  $\text{Fe}_3\text{O}_4(100)$  and H-terminated  $\text{Fe}_3\text{O}_4(100)$  surfaces. We are currently investigating the polarized  $\text{He}^*$  gas production by surface scattering.

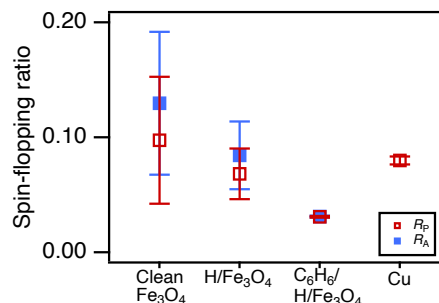


**Figure 1.** Spin-flopping ratios of scattered  $\text{He}^*$  intensities for clean  $\text{Fe}_3\text{O}_4(100)$ , H-terminated  $\text{Fe}_3\text{O}_4(100)$ , multilayered benzene on H-terminated  $\text{Fe}_3\text{O}_4(100)$ , and Cu(100).

### References

- [1] Kurahashi M, Suzuki T, Ju X, and Yamauchi Y, *Phys. Rev. Lett.* 91, 26 (2003)
- [2] Maruyama H, Kurahashi M, Asakawa K, and Hatakeyama A, *Phys. Rev. A* 107, 022811 (2023)

\* E-mail: [h-maruyama@st.go.tuat.ac.jp](mailto:h-maruyama@st.go.tuat.ac.jp)

† E-mail: [hatakeya@cc.tuat.ac.jp](mailto:hatakeya@cc.tuat.ac.jp)

## Progress on observation of radiative double-electron capture (RDEC) with $F^{9,8+}$ on graphene

D S La Mantia<sup>1\*</sup>, K Bhatt<sup>2</sup>, S Dutta<sup>2</sup>, T D Ulrich<sup>2</sup>, U Abesekera<sup>2</sup>, M J Hall<sup>2</sup>, H Weeraratne<sup>2</sup>, J A Tanis<sup>2</sup>, and A Kayani<sup>2</sup>,

<sup>1</sup>National Institute of Standards & Technology, Sensor Science Division, Gaithersburg, MD 20899 U.S.A.

<sup>2</sup>Western Michigan University, Department of Physics, Kalamazoo, MI 49008 U.S.A.

**Synopsis** New evidence for radiative double-electron capture is presented for highly-charged ions colliding with single-layer graphene. Preliminary results for 2.11 MeV/u (40 MeV)  $F^{9+}$  and  $F^{8+}$  have recently been reported [1]. Additional data has since been collected, and progress on those results will be shown and compared with previous RDEC studies for thin-foil carbon targets ( $\sim 100\times$  thicker) and gas ( $N_2$  and Ne) targets, as well as the available theoretical predictions. The similarities and differences will be discussed.

Radiative double-electron capture (RDEC) is a fundamental collision process wherein two bound electrons are captured from a target to bound states in a projectile with the simultaneous emission of a single photon [2]. RDEC can be considered the ion-atom analog of double photoionization due to a single photon. Current progress on observation of RDEC for 2.11 MeV/u  $F^{9,8+}$  (40 MeV) ion projectiles striking a single-layer graphene target are presented.

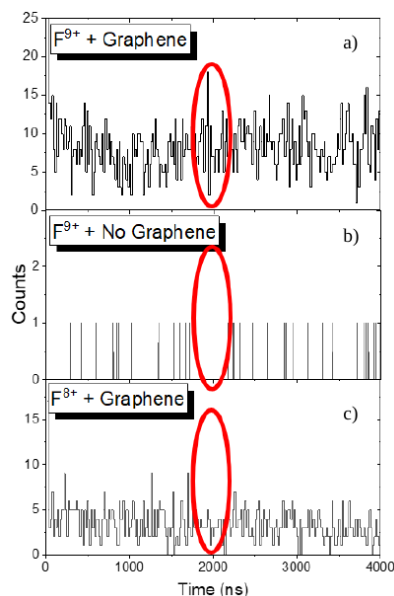
This work was performed using the tandem Van de Graaff facility at Western Michigan University. The  $F^{9,8+}$  ion beams were directed towards a  $\sim 0.35$  nm thick graphene sample mounted on a 200 nm thick silicon nitride grid with  $\sim 6400$  holes of 2  $\mu\text{m}$  diameter on a 200  $\mu\text{m}$  thick silicon substrate (purchased commercially). A Si(Li) x-ray detector at  $90^\circ$  to the beamline collected emitted photons. The charge-changed beam components were then collected by separate silicon surface-barrier detectors. Event-mode data collection assigned coincidences between x rays and charge-changed particle events.

Fig. 1 shows the preliminary x-ray gated particle spectra from Ref. [1] for (a)  $F^{9+}$  on graphene ( $\sim 7\text{--}8$  counts), (b)  $F^{9+}$  with no graphene target (no counts, as expected), and (c)  $F^{8+}$  on graphene (possibly a single count). The counts collected correspond to a preliminary total cross section of 11 b for  $F^{9+}$ , a value well in line with earlier values found for the carbon target [3], and larger by a factor of about four than for the gas targets [4]. Since that reporting, additional data has been collected and is currently being analyzed. Those data will be presented and com-

\*E-mail: david.lamantia@nist.gov

pared to the previous results, as well as the best available theory.

<sup>†</sup>Supported in part by NSF Grant 1707467.



**Figure 1.** Sorted doubly charge-changed particle spectra associated with RDEC energy photons: 2.11 MeV/u a)  $F^{9+}$  on graphene; b)  $F^{9+}$  with no target (null run); and c)  $F^{8+}$  on graphene [1].

### References

- [1] La Mantia D S *et al* 2023 *Atoms* **11**, 6
- [2] Miraglia J and Gravielle M. S. 1987 *ICPEAC XV: Book of Abstracts* p. 517 Brighton, U.K.
- [3] La Mantia D S *et al* 2020 *Phys. Rev. A* **102** 060801(R)
- [4] La Mantia D S *et al* 2020 *Phys. Rev. Lett.* **124** 133401

## A versatile 3D transmission setup for ion-solid interaction studies using keV ion energies at Uppsala University

R Holeňák<sup>1\*</sup>, S Lohmann<sup>1,2</sup>, E Ntemou<sup>1</sup> and D Primetzhofer<sup>1</sup>

<sup>1</sup>Department of Physics and Astronomy, Uppsala University, Uppsala, 75120, Sweden

<sup>2</sup>Institute of Ion Beam Physics and Materials Research, HZDR, Dresden, 01328, Germany

**Synopsis** The capability of our highly configurable scattering setup at Uppsala University is presented with a focus on the trajectory dependence of ion-solid interaction in the keV energy regime.

The renewed and broadened interest in the medium energy ion scattering (MEIS) technique with increasing focus on single crystalline targets and 2D materials, combined with much better technology for high-speed, position-sensitive detectors with improved lateral resolution, motivated the development of time-of-flight MEIS systems (TOF-MEIS) at Uppsala University, Sweden [1]. The highly configurable character of our setup makes it a powerful experimental research tool with particular focus on *in-situ* studies as well as for studying ion-solid interactions in several dimensions with the possibility to employ coincidence measurements.

The velocity of keV ions as projectiles being comparable to the one of electrons in the target valence and conduction bands renders the interactions highly dynamic and strongly trajectory dependent [2]. Several charge exchange processes including Auger neutralization and collision-induced reionization as well as electron promotion due to creation of molecular orbitals lead to an oscillatory alternation of the projectile charge and directly affect the specific energy loss. Ion transmission through self-supporting crystalline targets was shown to be an excellent model system to study the trajectory dependence of the ion-solid interactions.

Understanding energy deposition and electronic excitation by energetic charged particles in matter is imperative for prediction of ion-induced materials modification, as in semiconductor doping or extreme environments like e.g. fusion devices. Such understanding also forms the basis for analytical tools based on ion beams and can yield a well-defined test scenario for theoretical models, which aim to predict equilibrium [DFT] and non-equilibrium conditions [TD-DFT] in solids.

In this contribution, we showcase a set of experiments revealing the broad applicability of our instrumentation for studying ion-solid interaction:

- Analysis of primary ions transmitted through thin self-supporting foils allows for mapping of intensity and different energy loss moments [3,4].
- A deflection unit allows for studying the equilibrium charge distributions of the transmitted projectiles [5].
- Other energy transfer channels i.e. electron and photon emission can be addressed in coincidence detection with the transmitted projectiles [6,7].
- By employing heavier projectiles, recoils can be detected with high sensitivity for light elements and surface structure [8].
- TOF approach allows for studying ion-induced surface sputtering and desorption [9].

The most recent upgrade to the system comprises of a versatile *in-situ* preparation chamber. This extension enables extended control over target quality and allows for *in-situ* material modifications, also enabling more complex systems to be investigated.

### References

- [1] Sortica M A et al. 2020 *NIMB* **463** 16-20
- [2] Lohmann S et al. 2020 *PRL* **124** 096601
- [3] Holeňák R et al. 2020 *Ultramicroscopy* **217**
- [4] Lohmann S et al. 2023 *PRB* **107** 085110
- [5] Holeňák R et al. 2021 *Vacuum* **185** 109988
- [6] Lohmann S et al. 2020 *NIMB* **479** 217-221
- [7] Lohmann S et al. 2018 *NIMB* **417** 75-80
- [8] Holeňák R et al. 2022 *Vacuum* **204** 111343
- [9] Lohmann S et al. 2018 *NIMB* **423** 22-26

\* E-mail: [radek.holenak@physics.uu.se](mailto:radek.holenak@physics.uu.se)

## Characterization of a double torsion pendulum for detecting torque exerted by the spins of gaseous atoms

R Yasuda<sup>1\*</sup> and A Hatakeyama<sup>1†</sup>

<sup>1</sup>Tokyo University of Agriculture and Technology, Tokyo, 184-8588, Japan

**Synopsis** We characterized a double torsion pendulum system by measurement of photon-spin-induced torque using forced oscillation caused by polarization modulation of light incident on a suspended object. Through simple passive isolation of the suspended object from external vibration noise, the achieved torque sensitivity was  $2 \times 10^{-17}$  N m in a measurement time of  $10^4$  s, which reached the thermal noise limit. The observed spin-induced torque exerted on the light-absorbing optics was consistent with the angular momentum transfer of  $\hbar$  per photon.

The torsion pendulum or torsion balance is one of the most sensitive force detectors in modern physics and engineering. Various torsion pendulums have been used in the measurements of weak forces, such as gravitational constant measurements and Coulomb's constant measurements. Einstein and de Haas[1], and Beth[2] used torsion pendulums to detect small torques on macroscopic objects exerted by quantum spin flip. We can understand these results in term of angular momentum conservation of quantum (atomic or photonic) spins and classical angular momentum, or spin transfer from atoms or photons to a macroscopic object.

The final goal of our research[3] is to extend quantum-to-classical spin-transfer research to gas-solid interfaces. Gaseous atoms can easily be spin-polarized with circularly polarized light; the technique is called optical pumping. Spin-polarized gaseous atoms are used in many precise measurements such as frequency and magnetic field measurements. However, it is known that the polarized gas loses its spins when the gaseous atoms collide with solid surfaces. This phenomenon is called spin relaxation. In the viewpoint of angular momentum conservation, the spin relaxation can be regarded as spin transfer from gaseous atoms to solid.

In this study[4], we report that characterization of our torsion pendulum (Fig. 1) based on Beth's experiment for observing the torque induced by spin transfer from gaseous atoms. Our strategy is four-fold: 1) using a double torsion pendulum for isolating external vibration noise, 2) forced oscillation induced periodically at resonance frequency by switching external torque, 3) operating the pendulum in vacuum ( $\sim 10^{-5}$  Pa) for avoiding damping by friction with air, and 4) applying torque with photon spins for evalua-

tion of the detecting torque. We confirmed that the pendulum properly detected the torque induced by photon spins; the observed spin-induced torque exerted on the light-absorbing optics was consistent with the angular momentum transfer of  $\hbar$  per photon. The torque uncertainty of the pendulum was  $2 \times 10^{-17}$  N m in a measurement time of  $10^4$  s, almost reaching thermal noise limit.

Using the double torsion pendulum characterized in this study, we will observe the rotation induced by spin transfer from gaseous atoms to solid through atom-surface collisions.

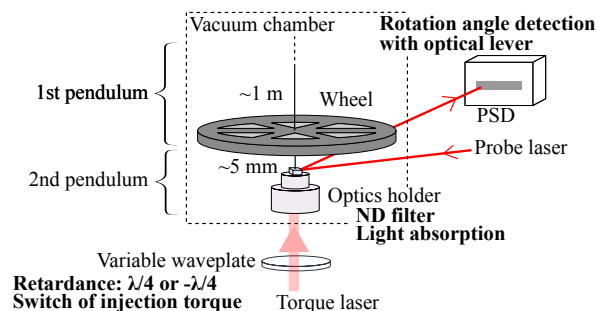


**Figure 1.** Apparatus. The wheel is hung in the 1st pendulum and the optical holder is hung in the 2nd pendulum. PSD: position-sensitive detector. The variable waveplate periodically switches the retardance between  $+\lambda/4$  and  $-\lambda/4$ , and the applied torque periodically switches between  $+\hbar$  and  $-\hbar$  per photon ( $\hbar$ : Dirac's constant).

### References

- [1] A. Einstein and W. J. de Haas, Proc. K. Ned. Akad. Wet. **18**, 696 (1915).
- [2] R. A. Beth, Phys. Rev. **50**, 115 (1936).
- [3] A. Hatakeyama, RY *et al.*, AIP advances **9**, 075002 (2019).
- [4] RY and A. Hatakeyama, Review of Scientific Instruments **92**, 105108 (2021).

\* E-mail: r-yasuda@st.go.tuat.ac.jp

† E-mail: hatakeya@cc.tuat.ac.jp



## Detecting sample surface magnetism with highly charged ions

P Dergham<sup>1\*</sup>, E Lamour<sup>1</sup>, S Macé<sup>1</sup>, C Prigent<sup>1</sup>, S Steydl<sup>1</sup>, D Vernhet<sup>1</sup>, M Trassinelli<sup>1†</sup>

<sup>1</sup> Institut des NanoSciences de Paris, UMR 7588 CNRS– Sorbonne Université, Paris, 75005, France

**Synopsis** Surface magnetism detected by x-ray spectroscopy of highly charged ions colliding a magnetically ordered sample is presented for the first time. Hollow atom spectra change their characteristics as a function of the sample temperature close to its ferro-paramagnetic phase transition showing a dependency on the spin orientation of the capture electron.

At sub-MeV energies, ion–surface collisions are characterized by multiple capture of electrons from the sample surface to the projectile ions. Subsequently, the atom de-excites by Auger and radiative processes. In cases of surfaces presenting a ferromagnetic phase, the electron spin alignment is expected to favor the population of ion excited states with a large value of  $S$ . When capture occurs above the surface [1], involved processes are exclusively sensitive to the first atomic layers of the sample. The imprint of the surface magnetic order influences the characteristic spin quantum number  $S$  of the excited levels occupied by the captured electrons.  $S$  is partially conserved during some of the de-excitation processes and the measurement of characteristic radiation allows in principle to obtain information on the magnetic order of the sample surface. The ability to detect the presence of a ferromagnetic ordered phase in ion–surface interaction has been demonstrated in the past using Auger spectroscopy [2] and polarized Auger spectroscopy [3]. This observation has been however questioned [4] due to a possible contamination of the samples inducing a dependency of the work function with the sample temperature. To overcome the difficulties of Auger spectra and to provide more quantitative results, we probe the surface magnetism via x-ray spectroscopy. The very first and preliminary results are presented in the case of the interaction between a 170 keV  $\text{Ar}^{17+}$  ion beam with a nickel (110) monocrystal at different temperatures, which has a ferro-paramagnetic phase transition at 354°C. The spectra are recorded with a state-of-the-art silicon-drift detector and present a clear dependency with the sample temperature. The characteristics  $n=2 \rightarrow 1$  unresolved transitions show a shift to lower energies for higher temperatures (see figure), indicating a larger electron population of the  $n=2$

level. This is expected from the reduction of the Pauli exclusion effect in the  $n=2$  level, i.e., a reduced Pauli shielding [5], due to the loss of spin alignment of the captured electrons caused by the change of magnetic phase (from a ferro- at low temperature to a paramagnetic phase at higher temperature).

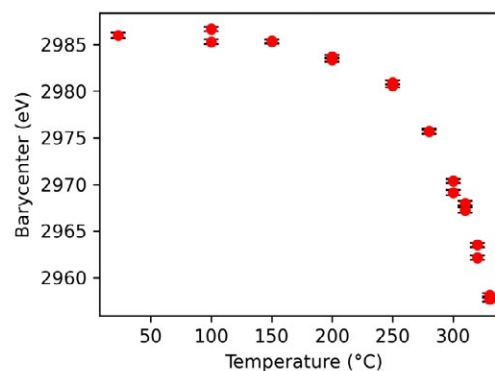


**Figure 1.** Shift of the unresolved  $n=2 \rightarrow 1$  transitions of  $\text{Ar}^{17+}$  ion beam interacting with a nickel sample at different temperatures. The indicated temperatures correspond to the sample holder and not to the sample.

The authors acknowledge the support of the French Agence Nationale de la Recherche (ANR) under reference ANR-20-CE91-0007.

### References

- [1] Winter H and Aumayr F 1999 *J. Phys. B* **32** R39
- [2] Unipan M, Robin A, Morgenstern R, and Hoekstra R 2006 *Phys. Rev. Lett.* **96** 177601
- [3] Pfandzelter R, Bernhard T, and Winter H 2001 *Phys. Rev. Lett.* **86** 4152-4155
- [4] Busch M, Wethekam S, and Winter H 2008 *Phys. Rev. A* **78** 010901
- [5] Madesis I, Laoutaris A, Zouros T J M, Benis E P, Gao J W, and Dubois A 2020 *Phys. Rev. Lett.* **124** 113401

\* E-mail: [perla.dergham@insp.jussieu.fr](mailto:perla.dergham@insp.jussieu.fr)

† E-mail: [martino.trassinelli@insp.jussieu.fr](mailto:martino.trassinelli@insp.jussieu.fr)

## Clocking ultrafast relaxation of Rydberg hollow atoms at surfaces by x-rays

Ł Jabłoński, D Banaś, P Jagodziński, A Kubala-Kukuś, D Sobota,  
I Stabrawa, K Szary and M Pajek\*

Institute of Physics, Jan Kochanowski University, 25-406 Kielce, Poland

**Synopsis** Ultrafast relaxation of Rydberg hollow atoms ( $n \sim 30$ ), formed in collisions of slow highly charged  $\text{Xe}^{q+}$  ions ( $q \sim 30$ ) with Be surface, was studied by observing the x-ray emission. The measured spectra of Paschen series, dominated by fast ( $nf \rightarrow 3d$ ) electric dipole x-ray transitions, exhibit a cut-off at high  $n_{\text{cut}} \sim 20$  indicating a domination of faster interatomic Coulombic decay (ICD) process for higher  $n$ -states. Using the measured fluorescence yields we demonstrate that relaxation of RHA proceeds in a femtosecond time scale.

In slow collisions of highly charged ions  $\text{Xe}^{q+}$  ions ( $q \gg 1$ ) with surfaces the highly excited Rydberg ( $n \approx q$ ) hollow atoms (RHA) are formed [1]. Their rapid relaxation to the ground state in solids was a subject of intense debates in last years. In particular, in the experiments with monoatomic layers [2,3] it was demonstrated that relaxation of RHA proceeds in a femtosecond time scale [2] and it was proposed [3] that ICD process [4] is responsible for a successive deexcitation of RHA, but only between the highest Rydberg states. Consequently, further relaxation of RHA down to ground state needs more investigations.

In the present experiment we have studied x-ray emission from collisions of slow, highly charged  $\text{Xe}^{q+}$  ions ( $q=23-36$ ) with metallic Be foil in order to access more details on relaxation of RHA in solids. The pulsed beams of  $\text{Xe}^{q+}$  ions were produced in the EBIS facility and the dominating M-X-rays ( $nf \rightarrow 3d$ ) emitted in radiative relaxation of highly excited Xe were measured by a Si drift detector.

The measured x-ray spectra, which were interpreted in terms of the MCDF calculations, clearly demonstrate, despite of the radiative and Auger deexcitation, the importance of more exotic two-electron relaxation processes in RHA, namely, the internal dielectronic excitation (IDE) [5], the interatomic Coulombic decay (ICD) and the two-electron-one photon (TEOP) transitions. By interpreting the x-ray spectra measured for different charge states, relative contributions of discussed processes were extracted and the decay rates were estimated using known decay rates of radiative transitions as “internal clock”. In particular, by observing a cut-off of x-ray emission in the measured

Paschen series at  $n_{\text{cut}} \approx 23$  for  $\text{Xe}^{35+}$  ions, it was demonstrated *experimentally* that ICD plays dominating role in early stage ( $n > n_{\text{cut}}$ ) of nonradiative relaxation of RHA in solids. Further ( $n < n_{\text{cut}}$ ) fast deexcitation of hollow atoms by Auger and IDE processes, as estimated from the measured x-ray fluorescence yields, makes the full relaxation to the ground state an ultrafast process with estimated lifetime of about 1.8 femtosecond.

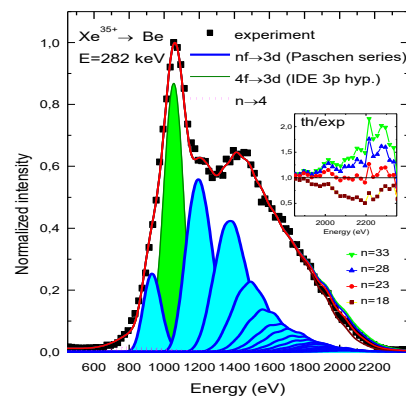


**Figure 1.** Measured spectrum of M-x-ray  $nf \rightarrow 3d$  transitions (Paschen series) in collisions of  $\text{Xe}^{35+}$  ions with Be. Contributions of IDE (3p-hypersatellite) and ICD cut-off for  $n_{\text{cut}} \approx 23$  are shown in the figure.

### References

- [1] Briand J P et al. 1990 *Phys. Rev. Lett.* **65** 159
- [2] Gruber E et al. 2016 *Nature Comm.* **7** 13948
- [3] Wilhelm R A et al. 2017 *Phys. Rev. Lett.* **119** 103401
- [4] Cederbaum et al. L S 1997 *Phys. Rev. Lett.* **79** 4778
- [5] Schuch R et al. 1993 *Phys. Rev. Lett.* **70** 1073

\* E-mail: [pajek@ujk.edu.pl](mailto:pajek@ujk.edu.pl)

## Nanostructures formed on a gold crystal surface by the impact of slow highly charged xenon ions

A Foks<sup>1</sup>, D Banaś<sup>1\*</sup>, I Stabrawa<sup>1</sup>, K Szary<sup>1</sup>, A Kubala-Kukuś<sup>1</sup>, P Jagodziński<sup>1</sup>, Ł Jabłoński<sup>1</sup>, M Pajek<sup>1</sup>, D Sobota<sup>1</sup>, R Stachura<sup>1</sup>, M D Majkić<sup>2</sup>, N N Nedeljković<sup>3</sup>

<sup>1</sup>Institute of Physics, Jan Kochanowski University, 25-406 Kielce, Poland <sup>2</sup>Faculty of Technical Sciences, University of Priština in Kosovska Mitrovica, Knjaza Miloša 7, 38220 Kosovska Mitrovica, Serbia <sup>3</sup>Faculty of Physics, University of Belgrade, P.O. Box 368, 11001 Belgrade, Serbia

**Synopsis** In this work, we studied the process of energy deposition and formation of nanostructures on the surface of gold crystal as a result of irradiation with slow (in the range of hundreds of keV) highly charged xenon ions (HCI). Using the STM technique, we observed various modifications on the irradiated surface resulting from the interaction of the single HCI, mostly in the form of craters with various closely lying adatom structures.

Fundamental understanding how materials respond to deposition of highly charged ion (HCI) energy is important for defect engineering, ion beam processing, ion beam analysis and modification, tokamak plasma-wall interaction, and many other applications. It is now well known, that the interaction of slow HCI with solids transfers its kinetic and potential energy to the electrons and atoms of the solid and can lead to the formation of various surface nanostructures [1]. However, the understanding of the processes of deposition/dissipation of internally coupled energy in electronic and atomic subsystems, in particular in materials with high density of free electrons (e.g. metals), is still incomplete [2].

Recently, using micro-staircase model, based on the quantum two-state vector model of the ionic Rydberg states population, we showed how the process of energy deposition occurs during the impact of highly charged xenon ions with gold nanolayers [3]. According to the model, the formation of the nanostructures in such interactions, is governed by the processes of the ionic neutralization in front of the surface and the kinetic energy loss inside the solid. The interplay of these two types of processes in the surface structure creation is described by the critical velocity.

In this work, we studied the process of nanostructure formation during the interaction of xenon ions with the surface of Au (111) crystal. The experiment was performed on the high purity single crystal, with the face centered cubic (FCC) structure produced by Czochralski method. The sample was irradiated by highly charged Xe<sup>q+</sup> ions (q=20-40) at the Kielce EBIS

\*E-mail: [d.banas@ujk.edu.pl](mailto:d.banas@ujk.edu.pl)

facility (Jan Kochanowski University, Kielce, Poland). The surfaces were imaged using scanning tunneling microscope SPM Aarhus 150 (SPECS & University of Aarhus). Various modifications on the irradiated surface resulting from the interaction of a single xenon ion were observed (see e.g. in Fig. 1), mostly in the form of craters surrounded by different adatoms structures, including hillocks made of amorphous gold, a consequence of the high cooling rate of the ion-metal interaction zone. The results are presently interpreted based on micro-staircase model [4].

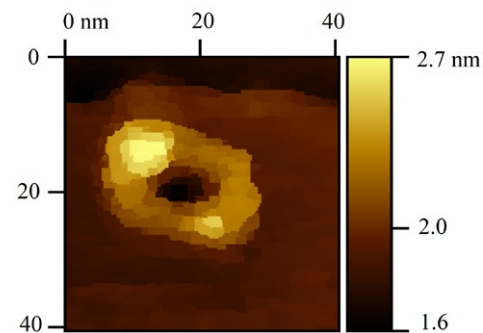


**Figure 1.** STM image of a nanostructure on the surface of a Au(111) crystal formed as a result of a single HCI impact.

### References

- [1] Aumayr F *et al* 2011 *J. Phys.: Condens. Matter* **23** 393001
- [2] Zhang Y and Weber W J 2020 *Appl. Phys. Rev.* **7** 041307
- [3] Stabrawa I *et al* 2023 *Vacuum* **210** 111860
- [4] Nedeljković N N and Majkić M D 2023 *Eur. Phys. J. D* **77** 3

## Effect of the accelerator-related materials preparation on the ion stimulated desorption yield

S Steydli<sup>†</sup>, R Levallois<sup>2</sup>, M Bender<sup>3</sup>, S Bilgen<sup>4</sup>, G Sattonnay<sup>4</sup>, A Lévy<sup>1</sup>, C Stodel<sup>2</sup>, C Prigent<sup>1</sup>, M Trassinelli<sup>1</sup>, V Velthaus<sup>3</sup> and E Lamour<sup>1\*</sup>

<sup>1</sup> Institut des Nanosciences de Paris, Sorbonne Université, CNRS UMR 7588, Paris, 75005, France

<sup>2</sup> GANIL, Grand Accélérateur d'Ions Lourds, Caen, 14076, France

<sup>3</sup> GSI Helmholtzzentrum für Schwerionenforschung, Darmstadt, 64291, Germany

<sup>4</sup> IJCLab, Université Paris Sud, CNRS, Orsay, 91405, France

**Synopsis** Heavy ion-induced gas desorption is an important problem for accelerators that intend to provide beams with very high intensities. Cu, W and stainless steel samples having undergone different surface treatments have been irradiated by a few MeV/u Ca ion beams so as to measure their desorption yield. Mitigation of such a quantity is a crucial aspect for accelerator developments.

Ion-stimulated desorption (ISD) is one of the processes that may drastically limit the vacuum conditions in accelerators or colliders affecting the ion beam transmission and lifetime [1-3]. This limitation is even more worrying with the avenue of high-intensity accelerators [4] such as SPIRAL2/GANIL and FAIR/GSI. Ion beams can impact the walls of the beam pipe and/or various diagnostic or selection devices. This leads to a pressure rise which, in turn, increases the probability of interaction with the released gas reducing the intensity of the beam of interest. Mitigation of the ISD yield, i.e., the number of released gas by incident ion, is then crucial. Its value depends on the ion energy, charge and mass as well as on the material, its pretreatment procedure and its history (material maintained under vacuum and/or exposed to air).

The main materials used for the construction of accelerator beamlines are copper, stainless steel and tungsten. Samples submitting to different treatments (chemical, lapping, annealing treatments) have been irradiated at the UNILAC accelerator of GSI. We will present results obtained with 4.8 MeV/u Ca<sup>10+</sup> or Ca<sup>19+</sup> ions. Beams impacting at normal incidence or at 45° are defocused on the sample to have an area of 8×7 mm<sup>2</sup> homogeneously illuminated. Applied ion fluxes are around 10<sup>10</sup> ions/s. Short (a few min) and long (up to 10h) irradiation have also been performed to better understand the dynamic vacuum. The ISD yields are evaluated from the pressure rise with respect to the base pressure (~10<sup>-9</sup> mbar) inside the vacuum chamber

during the irradiation, the pumping speed extracted from Molflow simulations and the ion flux. The influence of the sample treatment has been examined. For instance, Figure 1 shows the annealing effect (320°C during 2h) on samples stored at air after the annealing procedure.

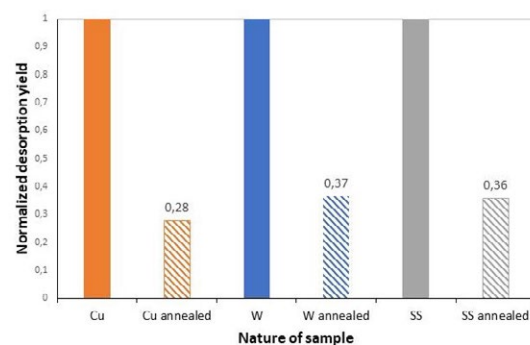


**Figure 1.** Normalized ISD yields of Cu, W and stainless steel samples without and with annealing irradiated by Ca<sup>19+</sup> ions.

Additional results will be presented: the charge state effect on the ISD yield and the most relevant released gas composition through partial pressure measurements.

### References

- [1] E Mahner 2009 *PRST* **11** 104801
- [2] Z Q Dong *et al* 2017 *NIMA* **870** 73–78
- [3] E Hedlund *et al* 2009 *NIMA* **599** 1–8
- [4] M Bender *et al* 2015 *J of Phys* **599** 012039

\* E-mail: [emily.lamour@sorbonne-universite.fr](mailto:emily.lamour@sorbonne-universite.fr)

<sup>†</sup> E-mail: [sebastien.steydli@sorbonne-universite.fr](mailto:sebastien.steydli@sorbonne-universite.fr)

## Irradiation of Oxygen-Bearing Ices on Top of Elemental Sulphur Layers: Implications for Astrophysical Sulphur Chemistry

DV Mifsud<sup>1,2\*</sup>, P Herczku<sup>2</sup>, O Auriacombe<sup>3</sup>, STS Kovács<sup>2</sup>, B Sulik<sup>2</sup>, Z Juhász<sup>2,†</sup>, R Rácz<sup>2</sup>, G Lakatos<sup>2,4</sup>, KK Rahul<sup>2</sup>, S Biri<sup>2</sup>, I Vajda<sup>2</sup>, I Rajta<sup>2</sup>, RW McCullough<sup>5</sup>, S Ioppolo<sup>6,7</sup>, NJ Mason<sup>1,2</sup>, Z Kaňuchová<sup>8</sup>

<sup>1</sup>Centre for Astrophysics and Planetary Science, University of Kent, Canterbury, United Kingdom

<sup>2</sup>Institute for Nuclear Research (Atomki), Debrecen, Hungary.

<sup>3</sup>Department of Microtechnology and Nanoscience, Chalmers University of Technology, Göteborg, Sweden

<sup>4</sup>Institute of Chemistry, University of Debrecen, Debrecen, Hungary

<sup>5</sup>Department of Physics and Astronomy, Queen's University Belfast, Belfast, United Kingdom

<sup>6</sup>Department of Physics and Astronomy, Aarhus University, Aarhus, Denmark

<sup>7</sup>School of Electronic Engineering and Computer Science, Queen Mary University of London, United Kingdom

<sup>8</sup>Astronomical Institute, Slovak Academy of Sciences, Tatranská Lomnica, Slovakia

**Synopsis** The routes towards the solid-phase formation of simple sulphur-bearing molecules in space remain poorly understood. Radiation processing in astrophysical environments has often been invoked to explain astrochemical reactions. Therefore, in this study, we have investigated the 1 MeV He<sup>+</sup> irradiation of a series of pure oxygen-bearing ices (O<sub>2</sub>, CO, CO<sub>2</sub>, CH<sub>3</sub>OH, and H<sub>2</sub>O) on top of layers of elemental sulphur at different temperatures. Our results indicate that sulphur volatilization as a result of irradiation is possible, and that a number of simple sulphur-bearing molecules can be formed.

The solid-phase chemistry of sulphur in interstellar and outer Solar System environments remains poorly understood [1]. Although a number of simple sulphur-bearing molecules (e.g., SO<sub>2</sub>, H<sub>2</sub>S) are known to exist on, for instance, the surfaces of the Galilean moons of Jupiter, the routes towards their formation are largely unknown. The radiation environments in astrophysical settings mediated by galactic cosmic rays, stellar winds, and magnetospheric plasmas has led to the suggestion that radiation chemistry may play a key role in the production and destruction of molecules in space.

One aspect of solid-phase sulphur radiation chemistry that has been largely overlooked is the role played by elemental sulphur. This is perhaps unexpected, given the fact that allotropes of sulphur are expected to be widespread in interstellar icy grain mantles and on the surfaces of outer Solar System moons [2,3]. To this end, we made use of the ICA set-up at Atomki [4,5] to carry out the 1 MeV He<sup>+</sup> irradiation of a series of pure oxygen-bearing ices on top of elemental sulphur layers.

**O<sub>2</sub> Ice on Sulphur.** The irradiation at 20 K resulted in the formation of SO<sub>2</sub> ice, along with larger quantities of O<sub>3</sub>.

**CO Ice on Sulphur.** The irradiation at 20 K resulted in the formation of various oxocarbon

molecules, similar to the irradiation of pure CO ice. CS<sub>2</sub> was also noted to form as a product.

**CH<sub>3</sub>OH Ice on Sulphur.** The irradiation at 25 K was qualitatively very similar to that of the irradiation of CH<sub>3</sub>OH in the absence of sulphur, although a small quantity of CS<sub>2</sub> was also observed to form.

**CO<sub>2</sub> Ice on Sulphur.** The irradiation at 20 K resulted in the formation of CO, CO<sub>3</sub>, and O<sub>3</sub>; along with some SO<sub>2</sub> and CS<sub>2</sub>. At 70 K, the abundances of SO<sub>2</sub> and CS<sub>2</sub> produced were amplified, and OCS was also noted to form.

**H<sub>2</sub>O Ice on Sulphur.** The irradiation at 20 K did not yield any sulphur-bearing products. A small amount of hydrated H<sub>2</sub>SO<sub>4</sub> was produced when the irradiation was repeated at 70 K.

Our results demonstrate that the irradiation of oxygen-bearing ices on top of sulphur allows for sulphur volatilization and could contribute to the formation of simple sulphur-bearing molecules in space.

### References

- [1] Mifsud *et al.* (2021) *Space Sci. Rev.* **217**, 14.
- [2] Carlson (2009) *Europa*, University of Arizona Press (Tucson, USA).
- [3] Cazaux *et al.* (2022), *A&A* **657**, A100.
- [4] Herczku *et al.* (2021), *RSI* **92**, 084501.
- [5] Mifsud *et al.* (2021), *EPJD* **75**, 182.

\* E-mail: [mifsud.duncan@atomki.hu](mailto:mifsud.duncan@atomki.hu)

† Presenting author



## Investigation of the evolution of defect in Si ion implanted GaN after UHPA by means of RBS/channeling and HR-XRD methods

K. D. Pałowska<sup>1\*</sup>, I. Sankowska<sup>1</sup>, P. Jóźwik<sup>2</sup>, K. Sierakowski<sup>3</sup>, A. Taube<sup>1</sup>, P. Prystawko<sup>3</sup>,  
M. Boćkowi<sup>3</sup>, A. Szerling<sup>1</sup> and I. Grzegory<sup>3</sup>

<sup>1</sup>Lukasiewicz Research Network – Institute of Microelectronics and Photonics, Warsaw, 02-668, Poland

<sup>2</sup>National Centre for Nuclear Research, Otwock, 05-400, Poland

<sup>3</sup>Institute of High Pressure Physics, Polish Academy of Sciences, Warsaw, 01-142, Poland

**Synopsis** In the present work the results of investigation of the evolution of defect in Si ion implanted GaN after ultra high pressure annealing by means of RBS/channeling and HR-XRD methods will be presented.

The detailed understanding of defects formation and transformation in GaN after ion implantation and subsequent activation annealing is of great interest for the development of novel semiconductor devices. The complexity of processes involved in defects buildup causes many issues which still must be clarified. One of the challenges to overcome is decomposition of GaN surface at temperatures over 800°C at normal pressure. To solve this problem an ultra high pressure annealing method (UHPA)[1] was developed at IHPP PAS with allows to activate implanted species at high temperature and high pressure without surface degradation.

In the experiment, three sets of GaN samples that differed in the total dose of Si implanted ions ( $3 \times 10^{14}$  at/cm<sup>2</sup>,  $1 \times 10^{15}$  at/cm<sup>2</sup> and  $3 \times 10^{15}$  at/cm<sup>2</sup>) were prepared. After implantation each set of the samples were annealed using UHPA method at temperatures of 1200°C, 1300°C and 1400°C under 1 GPa pressure. Then the as-implanted and annealed samples were characterized using RBS/channeling with 1.7 MeV <sup>4</sup>He ions beam and HR-XRD methods.

The experimental RBS/channeling spectra showed that the highest concentration of point defects and dislocation defects occurred for the  $3 \times 10^{15}$  at/cm<sup>2</sup> dose. For samples annealed at temperatures of 1200°C and 1300°C a similar concentration of defects of both types were observed. The highest level of the crystal lattice reconstruction was noticed for sample annealed at highest annealing temperature of 1400°C.

The RBS/channeling damage distributions were evaluated using the McChasy Monte Carlo simulation code assuming that the randomly displaced lattice atoms and linear defects of the dislocation type were taken under calculations.

The measured  $2\theta/\omega$  diffraction curves of as-implanted structures showed that the degradation of the crystal quality of the structure is directly proportional to the amount of the Si implantation dose – is the greatest  $3 \times 10^{15}$  at/cm<sup>2</sup> for and the smallest for  $3 \times 10^{14}$  at/cm<sup>2</sup>. Regardless of the size of the dose, it was observed that thermal annealing caused partial or almost full (but not completely) reconstruction of GaN crystal lattice. The greatest improvement was noticed for 1400°C annealing temperature. The shape of experimental diffraction curves was reproduced in a simulation taking into account depth-dependent the strain distribution. The results obtained for both used characterisation methods are complementary.

This work was partially supported by the National Centre for Research and Development under Agreement nr TECHMATSTRATEG-III/0003/2019 for project "Complete vertically integrated technological chain for vertical GaN-on-GaN power electronics: from GaN substrate to Intelligent Energy Bank" and the Polish National Science Center; grant OPUS UMO-2019/33/B/ST5/02756.

### References

- [1] Sierakowski, K et al. 2020 *Electronics* **9**, 1380.

\* E-mail: [karolina.palowska@imif.lukasiewicz.gov.pl](mailto:karolina.palowska@imif.lukasiewicz.gov.pl)

## Emission of x rays in collisions of xenon ions with metal surfaces

Y P Guo<sup>1,2\*</sup> Z W Wu<sup>3</sup> Z Y Song<sup>2</sup> Q M Xu<sup>2</sup> and Z H Yang<sup>2</sup>

<sup>1</sup> College of Astronautics, Nanjing University of Aeronautics and Astronautics, Nanjing 210016, P. R. China

<sup>2</sup> Institute of Modern Physics, Chinese Academy of Sciences, Lanzhou 730000, P.R. China

<sup>3</sup> Key Laboratory of Atomic and Molecular Physics & Functional Materials of Gansu Province, College of Physics and Electronic Engineering, Northwest Normal University, Lanzhou 730070, P.R. China

**Synopsis** This work reports x-ray spectra emitted in collisions of 1500~3500-keV projectile Xe<sup>q+</sup> (q=12-29) ions with medium-Z Fe, Ni, and Cu targets as well as higher-Z Ta targets. The lines from the collisions with higher-Z targets are mainly composed of characteristic x rays of target atoms, while those from the collisions with medium-Z targets consist mainly of characteristic x rays of projectile ions and broad molecular-orbital x rays. The origins of all these lines are analyzed in detail within the framework of the transient quasi-molecular states.

Ion-solid surface collisions have been studied both theoretically and experimentally for many decades [1-2]. These studies have been employed to help understand fundamental processes in atomic and molecular physics. Moreover, the corresponding research data are also very important a series of application fields ranging from studies of radiation effects on biological systems to astrophysical observations [3-4].

In the present experiment, X rays radiated in the collisions of 1500~3500-keV Xe<sup>q+</sup> (q=12-29) ions with Fe, Ni, Cu, and Ta targets are detected. The experiment was performed at the 320 kV High Voltage Platform of the Institute of Modern Physics, Chinese Academy of Sciences. Xe<sup>q+</sup> (q=12-29) ions utilized in the experiment are provided by the high-charge-state all-permanent-magnet Electron Cyclotron Resonance Ion Source [5]. Surface-polished metal targets with a purity of 99.99%, a thickness of 50 μm, and a size of 20×21 mm<sup>2</sup>, are employed. The pressure of the target chamber is maintained at 2×10<sup>-8</sup> mbar. X rays radiated are counted by a Si(Li) detector with an energy resolution of 165 eV at 5.9 keV and an energy detection range of 1-60 keV. Typical x-ray spectra are shown in Figs. 1 and 2.

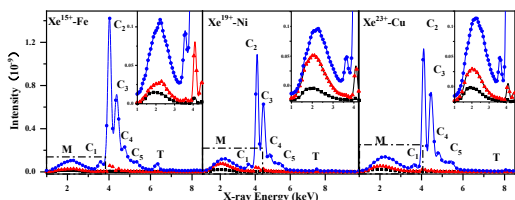


**Figure 1.** Typical x-ray spectra from collisions of Xe<sup>29+</sup> ions with Fe, Ni, and Cu targets.

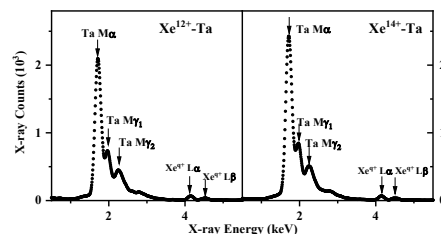


**Figure 2.** Typical x-ray spectra from the collisions of Xe<sup>q+</sup> ions with a Ta target.

From Figs. 1 and 2, one can see that during these collisions, two different phenomena are observed simultaneously. Specifically, only characteristic lines are observed from the collisions with higher-Z targets (Nb, Mo, and Ta), while characteristic x rays and MO x rays (non-characteristic lines) are simultaneously observed from the collisions with medium-Z targets (Fe, Ni, and Cu). The origin of these x-ray lines (i.e., the production of the inner-shell vacancies) is interpreted by means of the electron promotion model within the MO framework.

The full paper is chemical physics Vol. 562 (2022) 111628.

### References

- [1] Mantia D S La, Kumara P N S and Tanis J A 2020 Nucl. Instr. Meth. B **475 8**
- [2] Lapicki G and Lichten W 1985 Phys. Rev. A **31 1354**
- [3] Lyons D, Cumbee R S and Stancil P C 2017 Astrophys. J., Suppl. **Ser. 232 27**
- [4] Cumbee R S, Mullen P D, Lyons D, et al 2018 Astrophysical J. **852 7**
- [5] Sun L T, Li J Y, Zhang X Z, et al 2007 High Energy Phys. Nucl. Phys. **31 55**

\* E-mail: [guoyipan@nuaa.edu.cn](mailto:guoyipan@nuaa.edu.cn)

## Neutron spectra in nuclear hybrid reactors

J. Garcia Gallardo<sup>1,†</sup>, N. Gimenez<sup>1</sup> and J. L. Gervasoni<sup>1,2,\*</sup>

<sup>1</sup>Comisión Nacional de Energía Atómica (CNEA), 8400 Bariloche, Argentina

<sup>2</sup>Consejo Nacional de Investigaciones Científicas y Técnicas (CoNICET), 8400 Bariloche, Argentina

**Synopsis** In this work we analyze an example of Fast Fusion-Fission Hybrid Reactor (FFHR) fuelled with 8%-enriched Uranium and D-T in order to analyse its neutron spectra. Our simulations show that in the region of fissile shells, this reactor has a fast spectra as required to burn minor actinides. In the Tritium Breeder Blanket region (TBB), these spectra are shifted towards lower energies, which is even more notably in the Tungsten-made reflecting shell.

The Hybrid Fusion-Fission Reactors (FFHR) are arrangements formed by a nuclear-fusion device and a subcritical-fission-set (See Figure 1). The function of the fusion device is to provide neutrons to drive the subcritical assembly which then, uses those neutrons to generate energy. These parts are arranged concentrically forming a three-layer system to optimize the use of neutrons.

Nevertheless, achieving a reasonable neutron yield, in order to drive an FFHR, is difficult with current fusion devices, which is why the use of so-called multiplier cascades has been proposed [1]. These cascades consist of concentric shells where the fissile material is placed, separated by a very large empty space. The dimensions, shape, and fuel of the shells and the size of the empty space between them, determine the multiplying capacity of the system. A distinctive feature of the hybrid reactor is that, since it is actually made up of two reactors, it requires two different fuels: in addition to the fissile material, the use of Deuterium and Tritium is required (D-T). Deuterium is a reasonably readily available gas, but Tritium, given the complications involved in storage and transportation, is preferred to be generated on-site. For this reason, an hybrid reactor while using fusion technology, will need to be fitted with a Tritium Generating Shell (TGS). This shell is usually made of a Lithium compound, which generates

Tritium by means of the  ${}^6\text{Li}(n,t){}^4\text{He}$  and  ${}^7\text{Li}(n,n){}^4\text{He}$  channels. Figure 1 shows a model of FFHR following these principles, where two shells of 8% enriched Uranium are placed as fuel, a Lithium silicate is used as TGS, and a Tungsten layer plays the role of reflector and shielding. This arrangement was simulated using MCNP5 to find the spectra of the whole system [2].

The spectra obtained show that the neutron spectra are quite similar to that ones expected in conventional fast reactors, and therefore, compatible with actinide burn.

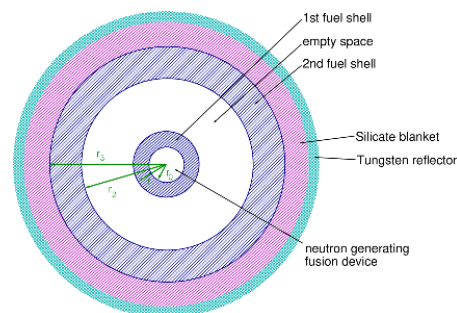


**Figure 1:** scheme of an FFHR

### References

- [1] A. Clause, L. Soto, C. Friedli and L. Altamirano. *Annals Of Nuclear Energy*, 78, (2015). pp10-14.
- [2] J. A. Garcia Gallardo, M. A. N. Giménez, J. L. Gervasoni, *Annals of Nuclear Energy*. Vol.147, (2020), 107739.

\* E-mail: gervason@cab.cnea.gov.ar

† E-mail: garcia.gallardo@gmail.com

## Modeling and computation of atomic cascades

S Fritzsche<sup>1,2,3\*</sup>, P Palmeri<sup>4</sup> and S Schippers<sup>5,6</sup>

<sup>1</sup>Helmholtz-Institut Jena, Germany

<sup>2</sup>GSI Helmholtzzentrum für Schwerionenforschung, Darmstadt, Germany

<sup>3</sup>Institut für Theoretische Physik, Friedrich-Schiller-Universität Jena, Germany

<sup>4</sup>Physique Atomique et Astrophysique, Université de Mons-UMONS, Belgium

<sup>5</sup>I. Physikalisches Institut, Justus-Liebig-Universität Gießen, Germany

<sup>6</sup>Helmholtz Research Academy Hesse for FAIR (HFHF), Campus Gießen, Germany

**Synopsis** Atomic cascades are ubiquitous in nature and have therefore been explored within very different scenarios, from precision measurements to the modeling of astrophysical spectra, and up to the radiation damage in biological matter. We here suggest a classification of atomic cascades and demonstrate how they can be modeled within the framework of the Jena Atomic Calculator.

If atoms or ions are initially excited into the continuum of the next higher charge state (or even beyond), they usually stabilize via various decay processes towards different ground configurations. Experimentally, this stabilization then results into different spectra (or distributions) of ions, electrons, or photons that need to be understood with regard to their relative intensities, time scales, or even for the coincidence of different events. Such atomic cascades typically include ions in three or more subsequent charge states [cf. Figure 1], and which are connected to each other by the (quantum) amplitudes of processes, such as (auto-) ionization or photon emission. Apart from such decay processes, one often also needs to account for the initial excitation and, hence, to distinguish between different cascade schemes, including the photoexcitation and ionization, electron-impact excitation, a (stepwise) decay, or between various electron-capture cascades.

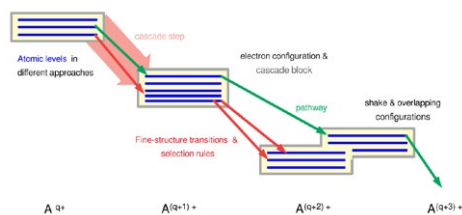


**Figure 1.** Important building blocks of all cascade computations.

In practice, such (atomic) cascades may exhibit an enormous complexity, even if just the dominant decay pathes are taken into account.

\*E-mail: [s.fritzsche@gsi.de](mailto:s.fritzsche@gsi.de)

This complexity arises first of all from the large number of different decay paths. To systematically model such cascades, we make use of JAC, the Jena Atomic Calculator [2], that supports the calculation of different atomic shell structures and processes. To model the excitation and subsequent decay of atoms and ions, we have classified and implemented a number of atomic cascade schemes within the framework of JAC. Moreover, this implementation is based on a clear distinction between (so-called) cascade computations, to first generate all of the necessary transition data, and subsequent simulations in order to properly combine these data and compare them with experiment. Moreover, a hierarchy of (cascade) approaches is considered for keeping the computation overall feasible. These approaches mainly refer to the representation of the level structures and, thus, help to understand the role of atomic interactions and inter-electronic correlations upon the observed spectra.

Examples from recent work demonstrate the use of this implementation for modeling the decay of 4s ionized xenon [3] and for providing data for the astrophysical spectra [4, 5], as well as at various places elsewhere.

### References

- [1] Fritzsche S, Palmeri P and Schippers S 2021 *Symmetry* **13** 520
- [2] Fritzsche S 2019 *Comp. Phys. Commun.* **240** 1
- [3] Hikosaka Y and Fritzsche S 2022 *Phys. Chem. Chem. Phys.* **24** 17535
- [4] Beerwerth R et al 2019 *Astrophys. J.* **887** 189
- [5] Schippers S et al 2021 *Astrophys. J.* **908** 52

## Separation of the inner and outer electrons for two-electron atoms near the critical bound limit

Li Guang Jiao<sup>1,2,3\*</sup>, Yew Kam Ho<sup>4</sup>, Stephan Fritzsche<sup>2,3†</sup>

<sup>1</sup>College of Physics, Jilin University, Changchun 130012, People's Republic of China

<sup>2</sup>Helmholtz-Institut Jena, D-07743 Jena, Germany

<sup>3</sup>GSI Helmholtzzentrum für Schwerionenforschung GmbH, D-64291 Darmstadt, Germany

<sup>4</sup>Institute of Atomic and Molecular Sciences, Academia Sinica, Taipei 10617, Taiwan

**Synopsis** The inner and outer electron radial density distributions for hydrogen negative ions in  $2p^2\ ^3P^e$  state are investigated near the critical nuclear charge. We show that when the system approaches the critical bound-continuum limit, by slightly decreasing the nuclear charge, the inner electron behaves stably like a  $2p$  electron, while the outer electron dominates the critical stability and asymptotic behavior of the two-electron system.

The critical stability and asymptotic behavior of the two-electron atom near the bound-continuum limit is one of the most intriguing phenomena in quantum few-body systems due to its connection with the Efimov physics, Borromean binding, quantum phase shift, and symmetry breaking. The  $2p^2\ ^3P^e$  state is considered as the second bound state of  $H^-$  ion and its critical nuclear charge ( $Z_c = 0.99478\dots$ ), below which the bound state transforms into a shape resonance, has been determined with high accuracy [1]. In the present work, we separate the radial density distributions of the inner  $\rho(r_<)$  and outer  $\rho(r_>)$  electrons and investigate the variation of them along with decreasing the nuclear charge.

The system wave function is expanded in terms of the explicitly-correlated Hylleraas configuration-interaction (HyCI) basis set [2] and the inner and outer electron density distributions are calculated by  $\rho(r_<) = 2 \int_{r_<}^{\infty} dr_2 \rho_2(r_<, r_2)$  and  $\rho(r_>) = 2 \int_0^{r_>} dr_2 \rho_2(r_>, r_2)$ , respectively, where  $\rho_2(r_1, r_2)$  is the two-electron radial density distribution. Our results for the two-electron atom in the  $2p^2\ ^3P^e$  state at  $Z_c$  are shown in the inset of Fig. 1, where they strictly obey the rule  $\rho(r_<) + \rho(r_>) = 2\rho(r)$ .

The inner electron behaves like a hydrogenic  $2p$  electron, and the outer electron is distributed in a region far from the nucleus, with the maximum density being four times smaller than the inner electron. However, by slightly decreasing the nuclear charge from 1 to  $Z_c$ , i.e., when the ionization energy of the two-electron system becomes zero, the inner electron density does

not change significantly, while the variation of the outer electron density is nearly ten times larger than that for the inner electron [3]. This phenomenon indicates that the critical stability and asymptotic behavior of the two-electron atom near corresponding bound-continuum limit is dominated by the outer electron.

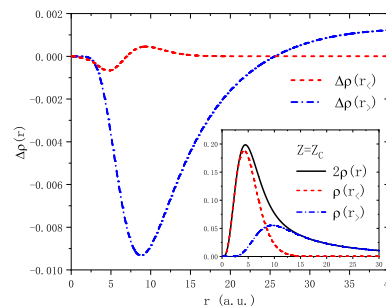


**Figure 1.** Variation of the density distributions for the inner and outer electrons of the two-electron atom in the  $2p^2\ ^3P^e$  state by decreasing the nuclear charge from 1 to  $Z_c$ . Inset shows the magnitudes of the inner, outer, and total electron radial densities.

### References

- [1] Z. C. Yan and Y. K. Ho, *arXiv*: [1506.06487v1](https://arxiv.org/abs/1506.06487v1) (2015).
- [2] L. G. Jiao, L. R. Zan, L. Zhu, Y. Z. Zhang and Y. K. Ho, *Phys. Rev. A* **100**, [022509](https://doi.org/10.1103/PhysRevA.100.022509) (2019).
- [3] R. Y. Zheng, L. G. Jiao, A. Liu, J. Ma, and H. E. Montgomery Jr., Y. K. Ho and S. Fritzsche, *J. Phys. B*, to be published (2023).

\*E-mail: [lgjiao@jlu.edu.cn](mailto:lgjiao@jlu.edu.cn)

†E-mail: [s.fritzsche@gsi.de](mailto:s.fritzsche@gsi.de)



## A community platform for just atomic computations

S Fritzsche<sup>1,2,3</sup>

<sup>1</sup>GSI Helmholtzzentrum für Schwerionenforschung, Darmstadt, Germany

<sup>2</sup>Helmholtz-Institut Jena, Jena, Germany

<sup>3</sup>Institut für Theoretische Physik, Friedrich-Schiller-Universität Jena, Germany

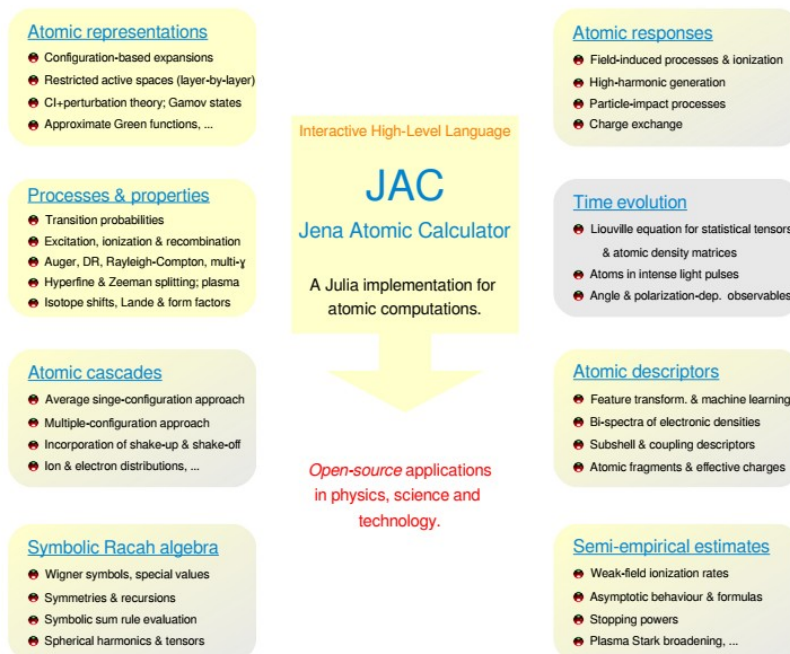
**Synopsis** JAC, the Jena Atomic Calculator, has been developed to support the calculation of atomic structures, processes and cascades. This toolbox aims for providing a general and easy-to-use toolbox for the atomic physics community, including an interface that is equally accessible for code developers as well as scientists working in experiment or theory.

Electronic structure calculations of atoms and ions have a long tradition in physics with applications in basic research and spectroscopy. With the Jena Atomic Calculator (JAC), I here present a new implementation of a (relativistic) electronic structure code for the computation of atomic amplitudes, properties as well as a large number of excitation and decay processes for open-shell atoms and ions across the periodic table. JAC [1] is based on Julia, a new programming language for scientific computing, and provides an easy-to-use but powerful platform to extent atomic theory towards new applications.

A primary guiding philosophy in designing JAC was to develop a general and easy-to-use toolbox for the atomic physics community, including an interface that is equally accessible for working spectroscopists, theoreticians and code developers. In addition, I also wish to provide a modern code design, a reasonable detailed documentation of the code and features for integrated testing [2].

### References

- [1] Fritzsche S 2019 *Comp. Phys. Commun.* 240 1  
<https://github.com/OpenJAC/JAC.jl>  
 [2] Fritzsche S 2022 User Guide & Compendium to JAC (unpublished)



\* E-mail: s.fritzsche@gsi.de

## The ARTEMIS experiment: Towards high precision g-factor measurements on highly charged ions

B Reich<sup>1,2\*</sup>, A Krishnan<sup>1,3†</sup>, K Anjum<sup>1,4</sup>, P Baus<sup>3</sup>, G Birkl<sup>3</sup>, Kanika<sup>1,2</sup>, J Klimes<sup>1,2</sup>, W Quint<sup>1,2</sup> and M Vogel<sup>1,2</sup>

<sup>1</sup>GSI Helmholtz Centre for Heavy Ion Research, Darmstadt, 64291, Germany

<sup>2</sup>University of Heidelberg, Heidelberg, 69120, Germany

<sup>3</sup>Technical University of Darmstadt, Darmstadt, 64289, Germany

<sup>4</sup>University of Jena, Jena, 07743, Germany

**Synopsis** The ARTEMIS experiment at the HITRAP facility at GSI focuses on precision measurements of electron magnetic moments in highly charged ions as a benchmark of QED in extreme fields. The resistively cooled ions are detected using non-destructive techniques followed by laser-microwave double-resonance spectroscopy within an asymmetric Penning trap setup.

The ARTEMIS experiment [1] aims to measure the magnetic moment or g-factor of a bound electron in heavy, highly charged ions (HCI) at the  $10^{-9}$  level by performing laser-microwave double-resonance spectroscopy. The desired goal is testing QED in extreme fields by studying higher-order Zeeman [2] effects providing different outlooks to the theory of QED for an atomic nucleus.

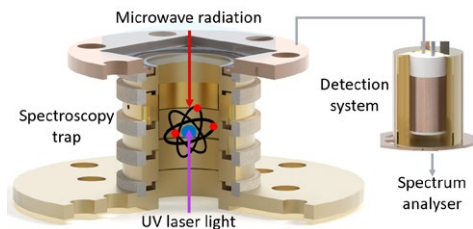


**Figure 1.** Schematic picture of the laser-microwave double-resonance spectroscopy at the ARTEMIS experiment

The heart of the high-precision experiment ARTEMIS is the asymmetric Penning trap stack inside the 7T superconducting magnet. It consists of two connected Penning traps: the creation trap (CT) and the spectroscopy trap (ST). The CT is a mechanically compensated trap with open endcaps and equipped with a field emission point. It can create HCI in-situ with the help of a gas inlet system. The ST is of a dedicated half-open [3] design and electrically compensated. For harmonicity and optical access, one of the endcaps of the ST is replaced by an

\*E-mail: [bi.reich@gsi.de](mailto:bi.reich@gsi.de)

†E-mail: [a.krishnan@gsi.de](mailto:a.krishnan@gsi.de)

electrically conducting and optically transparent Indium Tin Oxide window.

The non-destructive electronic detectors within ARTEMIS detect and cool [4] the ions inside the traps. The cleaning of the ion cloud is done by using the Stored Waveform Inverse Fourier Transform (SWIFT) technique and can be applied on the CT as well as on the ST.

To test and develop the experimental setup and methods a test ion needed to be chosen, which has a Zeeman splitting in the laser accessible domain as well as suitable ionisation potentials for the in-situ creation. Therefore  $^{40}\text{Ar}^{13+}$  was chosen while  $^{209}\text{Bi}^{82+}$  will be taken for future measurements.

The current laser system for spectroscopy consists of two external cavity diode lasers, while the Zeeman splitting is probed using tunable microwave radiation.

On the way of connecting ARTEMIS to the HITRAP facility at GSI a new cryogenic fast-opening shutter (CFS) has been designed and implemented giving periodic access for ions and laser light, while keeping the ambient conditions inside the trap stable. The CFS can be controlled remotely and has an opening and closing cycle of less than 100 ms keeping the vacuum within the trap at  $10^{-16}$  mbar.

### References

- [1] Quint W et al. 2008 *Phys. Rev. A* **78** 032517
- [2] Lindenfels D et al. 2013 *Phys. Rev. A* **87** 023412
- [3] Lindenfels D et al. 2014 *Hyp. Int.* **227** 197-207
- [4] Ebrahimi M S et al. 2018 *Phys. Rev. A* **98** 023423

## Lifetimes of excited states of the lanthanum negative ion

C W Walter<sup>1\*</sup>, N D Gibson<sup>1</sup>, F E Vassallo<sup>1</sup>, J Karls<sup>2</sup>, D Leimbach<sup>2</sup>, D Hanstorp<sup>2</sup>, J E Navarro Navarrete<sup>3</sup>, M K Kristiansson<sup>3</sup>, M Björkhage<sup>3</sup>, R D Thomas<sup>3</sup>, H Zettergren<sup>3</sup>, and H T Schmidt<sup>3</sup>

<sup>1</sup>Department of Physics and Astronomy, Denison University, Granville, OH, 43023, USA

<sup>2</sup>Department of Physics, University of Gothenburg, Gothenburg 41296, Sweden

<sup>3</sup>Department of Physics, Stockholm University, Stockholm 10691, Sweden

**Synopsis** The lifetimes of low-lying bound excited states of the lanthanum negative ion have been measured at the DESIREE facility at Stockholm University. State-selective photodetachment was used to monitor the populations of ground and excited La<sup>-</sup> ions over hundreds of seconds in the cryogenic electrostatic ion-beam storage ring. The measured lifetimes test theoretical predictions and provide insights into the potential of La<sup>-</sup> for laser cooling applications, which has not yet been achieved for atomic negative ions.

Negative ions are interesting both for their importance in a variety of physical processes and for the fundamental insights they can provide into electron correlations. Because the extra electron in negative ions is not bound to the neutral core by a net Coulomb force, their stability depends crucially on electron interactions.

The shallow potential well in an atomic negative ion can typically support only a single bound state configuration. To date, electric dipole (E1) allowed transitions between bound states have been observed in only four atomic negative ions. Among these, the negative ion of lanthanum is particularly intriguing because of its large number of bound states of both even- and odd-parity [1,2]. The E1 transition between the La<sup>-</sup> <sup>3</sup>F<sub>2</sub><sup>e</sup> ground state and <sup>3</sup>D<sub>1</sub><sup>o</sup> excited state has been proposed as a promising candidate for laser cooling due to its relative strength and nearly closed channel cycle [1-3]. A potential complication for laser cooling of La<sup>-</sup> is predicted small leakage from the closed cycle due to decay branching of <sup>3</sup>D<sub>1</sub><sup>o</sup> to long-lived excited fine structure levels that may require re-pumping [3].

In the present work, the lifetimes of low-lying bound excited states of La<sup>-</sup> were measured at the DESIREE facility at Stockholm University [4]. Ions were injected into the cryogenic electrostatic ion-beam ring, and the populations of different states were monitored over storage times up to 800 s using selective photodetachment. A cw laser at 2800 nm (443 meV) was used to detach ions from the excited fine structure state <sup>3</sup>F<sub>4</sub><sup>e</sup> and weaker bound levels. A pulsed OPO was used either at 2230 nm (556 meV) to detach from the lowest excited state <sup>3</sup>F<sub>3</sub><sup>e</sup> or at 1550 nm (800 meV) to detach all ions including the ground state <sup>3</sup>F<sub>2</sub><sup>e</sup>. The observed photodetached neutral

atom signals as functions of storage time were fit with exponentials to extract the radiative decay lifetimes of the excited states.

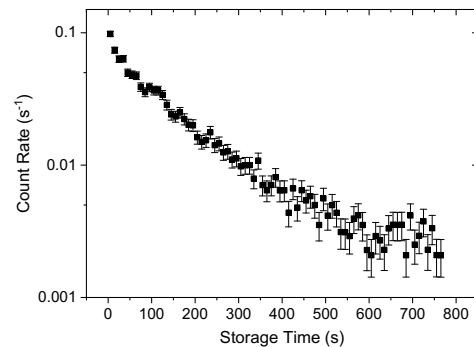


Figure 1. Measured photodetachment signal from La<sup>-</sup> showing decay of three distinct ion populations in the storage ring: <sup>3</sup>F<sub>4</sub><sup>e</sup> ( $t < 50$  s), <sup>3</sup>F<sub>3</sub><sup>e</sup> ( $50 < t < 400$  s), and <sup>3</sup>F<sub>2</sub><sup>e</sup> ground state ( $t > 500$  s).

The measured lifetimes for the predominantly magnetic dipole decay of the excited fine structure levels will be compared to previous theoretical predictions of the lifetimes of ~130 s [1,3]. These results give further insights into the structure and dynamics of La<sup>-</sup> that will help assess its feasibility for laser cooling applications.

### References

- [1] O'Malley S M and Beck D R 2010 *Phys. Rev. A Phys. Rev. A* **81**, 032503
- [2] Walter C W, Gibson N D, Matyas D J *et al.* 2014 *Phys. Rev. Lett.* **113**, 063001
- [3] Jordan E, Cerchiari G, Fritzsche S, Kellerbauer A 2015 *Phys. Rev. Lett.* **115**, 113001
- [4] Thomas R D, Schmidt H T, Andler G *et al.* 2011 *Rev. Sci. Instrum.* **82**, 065112

\* E-mail: [walter@denison.edu](mailto:walter@denison.edu)

## Toward a new type of gas phase spectroscopy for complex organic ions

S. Knaffo<sup>1\*</sup>, M.L. Rappaport<sup>1</sup>, H. Kreckel<sup>2</sup>, K. Blaum<sup>2</sup>, A. Wolf<sup>2</sup>, Th. Henning<sup>3</sup>,  
Y. Toker<sup>4</sup>, S.Sunil Kumar<sup>5</sup>, O. Heber<sup>1</sup>, D. Zajfman<sup>1</sup>

<sup>1</sup>Department of Particle Physics, Weizmann Institute of Science, Rehovot 76100, Israel

<sup>2</sup>Max-Planck-Institut für Kernphysik, Saupferchweg 1, 69117 Heidelberg, Germany

<sup>3</sup>Max-Planck-Institut für Astronomie, Königstuhl 17, 69117 Heidelberg, Germany

<sup>4</sup>Department of Physics and Institute of Nanotechnology and Advanced Materials, Bar-Ilan University, 529002 Ramat-Gan, Israel

<sup>5</sup>Department of Physics and Center for Atomic, Molecular, and Optical Sciences and Technologies, IISER Tirupati, Tirupati 517507, Andhra Pradesh, India

**Synopsis** One of the most sensitive spectroscopic methods in existence is Laser-Induced-Fluorescence (LIF), with applications ranging from environmental studies to genomic sequencing. Current limitations arise from the fact that larger molecular ions often do not exhibit electronic fluorescence, but re-distribute and emit the absorbed energy through vibrational transitions in the mid-infrared. We intend to exploit this mid-infrared emission - and thus extend the principle of LIF toward more complex molecules - using a cryogenic ion trap combined with an ultra-sensitive mid-infrared detection scheme.

More than 270 molecules have been detected in interstellar space to date, and modern telescopes continue to add entries to the catalog of identified species at a steady pace [1]. In recent years the detection of complex organic molecules (COMs) with clear pre-biotic relevance has picked up in pace, with important implications for open questions such as the possible delivery of organic material to Earth and the origin of life. However, there is currently no established technique to obtain gas phase spectra of large molecular ions.

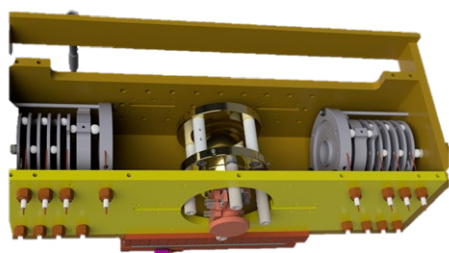


**Figure 1.** The CEBIT with BIB detectors modification

We propose to develop a novel spectroscopy technique that is based on laser excitation of electronic transitions in complex molecules, followed by internal re-distribution of the energy among vibrational states and finally the emission of mid-infrared photons [2]. We intend to detect these photons using a sensitive mid-infrared detector. To this end we will combine an existing cryogenic electrostatic ion trap with a mid-infrared detector module based on blocked-impurity-band (BIB) arsenic-doped silicon diodes. The ion trap and the detector have been developed and tested separately. Here, we present the challenges and goals to combine these two techniques in the laboratory and the current design stage of the experiment.

### References

- [1] Brett A. McGuire 2022, *Astrophys. J. Suppl.* **295** 30
- [2] L. J. Allamandola, A. G. G. M. Tielens, M and J. R. Barker 1989, *Astrophys. J. Suppl.* **71** 733

\*E-mail: [stav.knaffo@Weizmann.ac.il](mailto:stav.knaffo@Weizmann.ac.il)

## Precision X-Ray Spectroscopy of He-like Uranium employing Metallic Magnetic Calorimeter Detectors

Ph Pfäfflein<sup>1,2,3</sup>, S Allgeier<sup>4</sup>, Z Andelkovic<sup>2</sup>, S Bernitt<sup>1,2,3</sup>, A Borovik<sup>5</sup>, L Duval<sup>6,7</sup>, A Fleischmann<sup>4</sup>, O Forstner<sup>1,2,3</sup>, M Friedrich<sup>4</sup>, J Glorius<sup>2</sup>, A Gumberidze<sup>2</sup>, Ch Hahn<sup>1,2</sup>, F Herfurth<sup>2</sup>, D Hengstler<sup>4</sup>, M O Herdrich<sup>1,3</sup>, P-M Hillenbrand<sup>5</sup>, A Kalinin<sup>2</sup>, M Kiffer<sup>1,3</sup>, F M Kröger<sup>1,2,3</sup>, M Kubullek<sup>3</sup>, P Kuntz<sup>4</sup>, M Lestinsky<sup>2</sup>, B Löher<sup>2</sup>, E B Menz<sup>1,2,3</sup>, T Over<sup>1,3</sup>, N Petridis<sup>2</sup>, S Ringleb<sup>1,3</sup>, R S Sidhu<sup>2,8</sup>, U Spillmann<sup>2</sup>, S Trotsenko<sup>1,2</sup>, A Warczak<sup>9</sup>, G Weber<sup>1,2</sup>, B Zhu<sup>1,2,3</sup>, C Enss<sup>4</sup>, and Th Stöhlker<sup>1,2,3</sup>

<sup>1</sup>Helmholtz Institute Jena, Jena, 07743, Germany

<sup>2</sup>GSI Helmholtzzentrum für Schwerionenforschung, Darmstadt, 64291, Germany

<sup>3</sup>Institute of Optics and Quantum Electronics, Friedrich Schiller University Jena, Jena, 07743, Germany

<sup>4</sup>Kirchhoff Institute for Physics, Heidelberg University, Heidelberg, 69210, Germany

<sup>5</sup>I. Physikalisches Institut, Justus Liebig University Giessen, Giessen, 35392, Germany

<sup>6</sup>Laboratoire Kastler Brossel, Sorbonne Université, CNRS, ENS-PSL Research University, Collège de France, Paris, 75005, France

<sup>7</sup>Institut des NanoSciences de Paris, CNRS, Sorbonne Université, 75005, Paris, France

<sup>8</sup>School of Physics and Astronomy, University of Edinburgh, EH9 3FD Edinburgh, United Kingdom

<sup>9</sup>Marian Smoluchowski Institute of Physics, Jagiellonian University in Kraków, Kraków, 30-348, Poland

**Synopsis** In a recent experiment, two metallic magnetic calorimeters have been applied for X-ray spectroscopy of helium-like Uranium at CRYRING@ESR at GSI, Darmstadt. The ground state transitions were recorded with a resolution of better than 90 eV at transition energies of around 100 keV. This allowed to resolve the substructure of the  $K\alpha_1$  and  $K\alpha_2$  lines for the first time, leading to a substantial improvement in the determination of the transition energies compared to previous studies.

Helium-like ions are the simplest atomic multi-body systems. Their study along the isoelectronic sequence provides a unique testing ground for the interplay of the effects of electron-electron correlation, relativity and quantum electrodynamics. However, for ground-state transitions in ions with nuclear charge  $Z > 54$ , where photon energies of up to 100 keV are reached, there is currently no data available with sufficient resolution and accuracy to challenge state-of-the-art theory [1]. In this context, the recent development of metallic magnetic calorimeter (MMC) detectors is of particular importance. Their high spectral resolution of a few tens of eV FWHM at 100 keV incident photon energy, in combination with a broad spectral acceptance down to a few keV, will enable new types of precision X-ray experiments [2, 3].

First X-ray spectroscopy studies at the electron cooler of the low-energy storage ring CRYRING@ESR at GSI, Darmstadt have recently been performed for highly-charged ions [4, 5]. We report on the second campaign, where

MMC detectors have been used to study X-ray emission associated with the formation of excited helium-like uranium ( $U^{90+}$ ) as a result of radiative recombination between stored  $U^{91+}$  ions and cooler electrons. The achieved spectral resolution of better than 90 eV at X-ray energies close to 100 keV enabled us to resolve the substructure of the  $K\alpha_1$  and  $K\alpha_2$  lines. In contrast to former experiments [6, 7], this enables a direct comparison with theoretical predictions for the individual ground-state transitions in He-like uranium without any further assumptions.

### References

- [1] P Indelicato 2019 J. Phys. B: At. Mol. Opt. Phys. **52** 232001
- [2] D Hengstler et al 2015 Phys. Scr. **2015** 014054
- [3] S Kraft-Bermuth et al. 2018 Atoms **2018** 59
- [4] B Zhu et al. 2022 Phys. Rev. A **105** 052804
- [5] Ph Pfäfflein et al. 2022 Phys. Scr. **97** 114005
- [6] J P Briand et al. 1990 Phys. Rev. Lett. **65** 2761
- [7] A Gumberidze et al. 2004 Phys. Rev. Lett. **92** 203004



## Design and Underlying Concepts of a Python Based Quantum Package for High Precision Atomic Structure Calculations

Vipul Badhan<sup>1\*</sup>, Bindiya Arora<sup>1,2</sup> and Bijaya K. Sahoo<sup>3</sup>

<sup>1</sup>Department of Physics, Guru Nanak Dev University, Punjab, India

<sup>2</sup>Perimeter Institute for Theoretical Physics, Waterloo, Canada

<sup>3</sup>Physical Research Laboratory, Ahmedabad, Gujarat, India

### Synopsis

The focus of our work is the development of a Python program that uses the Dirac-Hartree-Fock[1] method to solve the mean-field wave equation for monovalent atomic systems with various basis sets. Specifically, we will write a Dirac-Hartree-Fock code in Python using the matrix method for solving the eigenvalue problem. We intend to implement the basis function method with a focus on maintaining kinetic balances between the large and the small components of the basis sets. Additionally, we will utilize the frozen core approximation to calculate relativistic wave functions, which will enable the use of the coupled cluster method for more precise calculations as needed.

In the atomic physics community, various basis sets and kinetic balances are in use such as Gaussian Type Orbitals(GTOs)[2], Slater Type Orbitals(STOs)[3] and BSplines[4] either without any balance or by imposing Kinetic Balance, Dual Kinetic Balance, etc. Each research group claims superiority in their results based on the quality of the basis sets and methods they employ. However, the scientific community has not yet fully investigated the extent of the differences in results arising from the use of various basis sets. An option to use various basis sets and different kinetic balances within the package for calculating atomic properties will be provided in the program in order to compare the results using different basis sets and to propose a better basis set.

The role of the basis sets for calculating various atomic properties such as electric dipole moments, dipole and quadrupole polarizabilities, lifetimes, hyperfine constants, black body friction forces and parity non-conserving amplitudes[5] with a precision better than the previously available results will be investigated to get a fundamental insight of atomic systems. A module to use B-splines as a basis set to produce relativistic higher excited Rydberg states of the systems will be part of the complete package.

An option to calculate non-relativistic results using the Numerov Method will also be given. Properties such as oscillator strengths, lifetimes (with contribution from finite temper-

ature), dipole, quadrupole and hyperpolarizabilities, black body friction forces, etc will be included. More properties will be added as and when required. To ensure more accurate calculations of atomic properties, a bridge between FORTRAN and Python will be created, allowing the coupled-cluster method written in FORTRAN to be called.

The proposed objective is to offer a comprehensive package with an easily accessible interface using Python as the programming language. This will enable a large number of users, even those with minimal knowledge of programming environments, to utilize it.

### References

- [1] Atomic Many-Body Theory by Ingvar Lindgren, John Morrison, Springer Series in Chemical Physics.
- [2] W. J. Hehre and J. A. Pople. "Self-Consistent Molecular Orbital Methods. XIII. An Extended Gaussian-Type Basis for Boron". In: The Journal of Chemical Physics 56.8 (1972), pp. 4233–4234.
- [3] E. Van Lenthe and E. J. Baerends. "Optimized Slater-Type Basis Sets for the Elements". In: J. Comput. Chem. 24.9 (2003), pp. 1142–1156.
- [4] W. R. Johnson, S. A. Blundell, and J. Sapirstein. "Finite basis sets for the Dirac equation constructed from B splines". In: Phys. Rev. A 37 (2 Jan. 1988), pp. 307–315.
- [5] C. S. Wood et al. "Measurement of Parity Non-conservation and an Anapole Moment in Cesium". In: Science 275.5307 (1997), pp. 1759–1763.

\*E-mail: [vipulbadhan269@gmail.com](mailto:vipulbadhan269@gmail.com)

## The spectrum of the vacuum as a primary reference for radiometry

S Lemieux<sup>1\*</sup>

<sup>1</sup>Joint Attosecond Science Laboratory, National Research Council of Canada and University of Ottawa, Ottawa, Ontario K1A 0R6, Canada

<sup>2</sup>INRS-EMT, 1650 Blvd. Lionel-Boulet, Varennes, Québec J3X 1P7, Canada

**Synopsis** Vacuum fluctuations trigger spontaneous processes. The rate of photon pair emission, like in spontaneous parametric down-conversion, crucially depends on the amplitude of those fluctuations. Therefore, the specific functional dependence of vacuum fluctuations on frequency can be used as a reference for radiometry. Here, we experimentally demonstrate that parametric down-conversion can be utilized to measure the instrument response function and quantum efficiency of a spectrometer over a broad spectral range, without requiring any reference detector or source of light.

The discovery of Planck's law of radiation helped lead to the development of quantum mechanics. This law, which is a function of temperature and radiation frequency only, was crucial for the accurate description of the black body, a perfect absorber at thermal equilibrium. For the last century, the black body has been used by most metrology institutes as the primary source of light for radiometry. Here, we introduce a primary radiometric standard that exploits the quantum properties of vacuum-seeded nonlinear optical processes.

The quantum-mechanical fluctuations of the electromagnetic vacuum exhibit a specific functional dependence on frequency. Those vacuum fluctuations act as a seed for the spontaneous emission of photons. At the same time, the emission rate crucially depends on the amplitude of those fluctuations. In this work, we use the spectrum of vacuum fluctuations to trigger spontaneous processes. In particular, our method relies on parametric down-conversion (PDC), a nonlinear optical process based on three-wave mixing with only one input field. Since we can relate the output of phase-matched PDC to the spectrum of the vacuum, PDC qualifies as a reference for the calibration of radiometric instruments, such as spectroradiometers [2, 3, 4]. In particular, we deduce the spectral response of a spectrometer using spontaneous PDC—this is a relative calibration. In the strong-coupling regime of PDC, spontaneous emission stimulates the emission of more photons in a nonlinear manner, leading to a distortion of the frequency spectrum. Since there

is a one-to-one correspondence between the number of downconverted photons and the spectral shape of high-gain PDC, we possess all the necessary knowledge to deduce the spectral quantum efficiency of the spectrometer—this is an absolute calibration. In the experiment, we pump a nonlinear crystal with a pulsed laser and acquire a large number of spectra corresponding to different phase-matching conditions over a broad spectral range. We deduce the response function by comparing our results with the reference spectrum for phase-matched spontaneous PDC. In the second step of our calibration procedure, we establish the quantum efficiency of the measurement apparatus from the shape of high-gain PDC spectra, based on our previous measurement of the response function. We obtain a value of  $\eta = 0.42 \pm 0.04$  at the wavelength 710 nm, whereas we expected a value of  $0.38 \pm 0.07$ , estimated from the losses of each optical components.

In summary, we demonstrated that the amplitude of vacuum fluctuations and its nonlinear amplification can serve as a primary radiation standard, and we used this insight to completely characterize a spectrometer.

### References

- [1] Klyshko D 1977 *Sov. J. Quantum Electron.* **7** 591
- [2] Kitaeva G and Penin A N and Fadeev V V and Yanait Y A 1979 *Soviet Physics Doklady* **24** 564
- [3] Migdall A and Datla R and Sergienko A and Orszak J S and Shih Y H 1998 *Appl. Opt.* **37**16 3455

\*E-mail: [samzlemieux@gmail.com](mailto:samzlemieux@gmail.com)

## New methods for implementing photon addition with postselection and swift electrons

H Jeng<sup>1,2,3\*</sup>, J-W Henke<sup>1,2</sup>, G Arend<sup>1,2</sup>, A Feist<sup>1,2</sup>, C Ropers<sup>1,2†</sup>

<sup>1</sup>Max Planck Institute for Multidisciplinary Sciences, D-37077 Göttingen, Germany

<sup>2</sup>4th Physical Institute, University of Göttingen, D-37077 Göttingen, Germany

<sup>3</sup>Research School of Physics, Australian National University, Canberra, 2600, Australia

**Synopsis** Photon addition is an invaluable tool for quantum optics. We demonstrate several applications for quantum information, and we investigate a unique implementation that uses quantized energy transfer between swift electrons and light.

Adding single quanta to a beam of light—colloquially known as photon addition—is interesting because it can be used to generate quantum states of light that are otherwise difficult to obtain. Despite much research since the first experimental demonstration [1], implementations of photon addition by optical means remains challenging, leaving many of its potential applications unexplored.

Using a novel optical and data-processing technique [2], we developed several applications of photon addition for quantum information. Our investigations reveal: (i) Adding photons to coherent states leads to strong cubic phase shifts (Fig. 1), which is an essential resource for universal continuous-variable quantum computation. (ii) Adding photons to two-mode-squeezed-vacuum states results in non-Gaussian quantum correlations that are associated with greater secret-key generation rates (when the simplifying assumption of Gaussian extremality is not made). (iii) Adding photons to thermal states leads to a counter-intuitive transformation of the average number of photons, demonstrating, in a simple and direct manner, that photons do not follow the rules of classical statistics.

While we were researching into these applications, we became aware of the possibility of implementing photon addition using a wildly different physical system. It has been shown that coherent, quantized energy transfer can take place between swift electrons and optical near-fields inside a transmission electron microscope [3], thus by measuring the kinetic energy and selecting only electrons associated with a certain energy-change, one ought to be able to add a specific

number of photons to the optical field.

We investigated theoretically the quantum-optical effects that could arise in this system, with key findings as follows: (i) Weak coherent optical driving results in a small amount of quantum squeezing, and (ii) strong thermal driving leads, once more, to the counter-intuitive change of the average number of photons, except now the effect can be tested with a far greater number of added photons. Experiments are underway to detect these effects.

The numerous applications of photon addition in quantum information combined with the unique properties of swift electrons opens up research into a new class of quantum technologies.

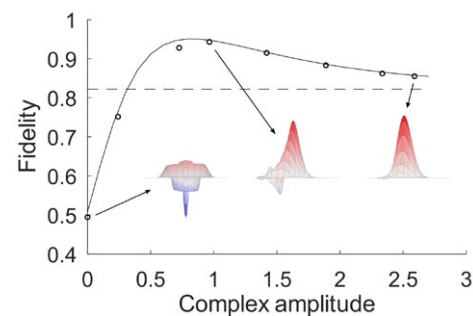


**Figure 1.** Adding photons to coherent states lead to cubic phase shifts.

### References

- [1] Zavatta A, Viciani S, and Bellini M 2004 *Science* **306** 660
- [2] Chrzanowski H, Walk N, Assad S M, Janousek J, Hosseini S, Ralph T C, Symul T, Lam P K 2014 *Nature Photonics* **8** 333
- [3] Feist A, Echterkamp K E, Schauss J, Yalunin S V, Schaefer S, and Ropers C 2015 *Nature* **521** 200

\*E-mail: [hao.jeng@mpinat.mpg.de](mailto:hao.jeng@mpinat.mpg.de)

†E-mail: [cropers@gwdg.de](mailto:cropers@gwdg.de)

## Fast-ion induced electron emission from nano-structured gold: applications as a radiosensitizer for cancer cell killing in hadron therapy

J L Shinpaugh<sup>1</sup>\*, W L Hawkins<sup>2</sup>, N Libby<sup>1</sup>, T K Gaddis<sup>1</sup>,  
E C Maertz<sup>1</sup>, N Carlson<sup>1</sup>, C Boyd<sup>1</sup>, and M Dingfelder<sup>1</sup>

<sup>1</sup>Department of Physics, East Carolina University, Greenville, North Carolina, 27858, USA

<sup>2</sup>Gardner-Webb University, Boiling Springs, North Carolina, 28017, USA

**Synopsis** Recent results are presented for tumor cell killing for *in-vitro* irradiation by protons of malignant prostate and breast cells treated with gold nano-particles in an energy range approaching the Bragg peak (maximum energy deposition). To explore the modeling of the energy deposition of fast ions in biologic materials, we are expanding current track structure simulation models to include ion-induced secondary electron production from metallic surfaces and nano-structures. To assist with these models, we have measured electron emission from hydrated and nano-structured gold surfaces.

Nano-structured materials are widely being studied as radiosensitizers to increase the efficacy of radiation therapy in the treatment of cancer. While many such studies have been conducted for traditional high-energy photon radiation therapy, fewer studies exist for hadron (or ion-beam) therapy which is now rapidly expanding as a treatment modality.

Here we present recent results for enhanced cell killing for *in-vitro* irradiation by protons of malignant prostate and breast epithelial cells treated with gold nano-particles in an energy range approaching the Bragg peak, i.e., the end of the ion range with maximum energy deposition.

The experiments were conducted in the ion beam facility at East Carolina University using the recently upgraded cell irradiation beamline. A 3 MeV proton beam was extracted into air to irradiate the cells in custom microtiter plates. The irradiated cells were subsequently assayed to determine cell survival.

In addition, we are expanding current Monte Carlo track structure simulation models to include swift-ion-induced secondary electron production from gold surfaces. Furthermore, to explore the difference between electron emission from the bulk and from nano-structured surfaces, we have measured doubly differential electron emission yields from gold surfaces (foils), hydrated gold surfaces, and from gold nano-structures induced by fast proton and carbon ion impact. Shown in figure 1 are representative

spectra for electron emission induced by 2-MeV proton impact on a gold foil and 10-nm gold nano-particles, where enhanced low-energy electron emission is clearly observed. These data suggest the importance of the surface structure on low-energy electron emission, which may affect radiation damage from secondary electrons in the cellular environment and influence cell killing.

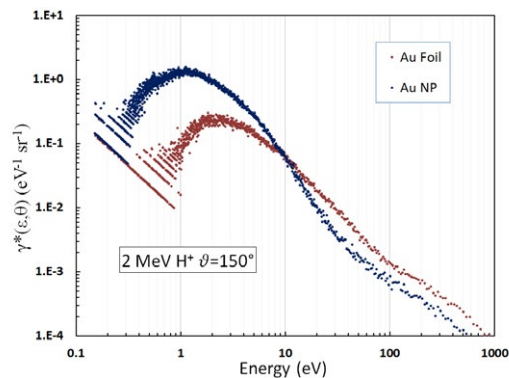


**Figure 1.** Relative doubly differential electron emission yields as function of emitted electron energy induced by 2-MeV protons incident on a 1- $\mu$ m-thick gold foil are compared to the emission spectrum from a gold grid coated with 10-nm gold nano-particles (NP). The yields were measured at an emission angle of 150 degrees with respect to the incident proton beam.

\* E-mail: [ShinpaughJ@ecu.edu](mailto:ShinpaughJ@ecu.edu)

## A numerical approach to the deexcitation of a hollow atom

M Werl<sup>1</sup>, A Niggas<sup>1\*</sup>, T. Koller<sup>1</sup>, P. Haidegger<sup>1</sup>,  
K Tőkési<sup>2</sup>, F Aumayr<sup>1</sup>, and R A Wilhelm<sup>1</sup>

<sup>1</sup>TU Wien, Institute of Applied Physics, Vienna, 1040, Austria

<sup>2</sup>Institute for Nuclear Research (ATOMKI), Debrecen, 4026, Hungary

**Synopsis** We present a numerical approach that allows us to study the deexcitation of a hollow atom based on solving rate equations for non-radiative and radiative decay in a Monte-Carlo approach. Calculated emission spectra of electrons and photons are compared with recent literature results.

In addition to their kinetic energy ions also possess a potential energy, i.e., the binding energies of all missing electrons. For highly charged ions (HCIs) in charge states  $q > 30$  this potential energy can reach several tens of keV. When such an HCI approaches a solid surface, it interacts with the material's electronic system and target electrons resonantly populate high  $n$ -shells of the projectile, where  $n \sim q$  [1]: a neutral but still highly excited atom – a hollow atom – is created.

If propagating freely in vacuum this hollow atom deexcites via radiative and non-radiative (Auger) channels. We present a computational approach that allows us to study this deexcitation: a hollow atom is formed via resonant electron transfer close to a solid surface and the subsequent decay is modelled via solving rate equations for both deexcitation channels in a Monte-Carlo fashion. As an input we have to provide decay rates that depend on the atomic number  $Z$  as well as initial  $n_i$  and final shells  $n_f$ , respectively.

For radiative decay, there exists a variety of experimental data [3] of hydrogen-like ions that we used to find a multi-variable fit function for the decay rate  $\Gamma_{\text{rad}} = \Gamma_{\text{rad}}(Z, n_i, n_f)$ . Experimental data for decay rate as well as calculated values using our fit are given for various  $\Delta n = n_i - n_f$  in Figure 1.

On the other hand, for non-radiative decay, i.e., Auger processes, literature data for high  $n$ -shells is scarce. Therefore, we use the flexible atomic code (FAC) [4] to calculate  $\Gamma_{\text{Auger}}$  for a large number of parameters  $Z, n_i$ , and  $n_f$  in order

to find another fit  $\Gamma_{\text{Auger}} = \Gamma_{\text{Auger}}(Z, n_i, n_f)$ .

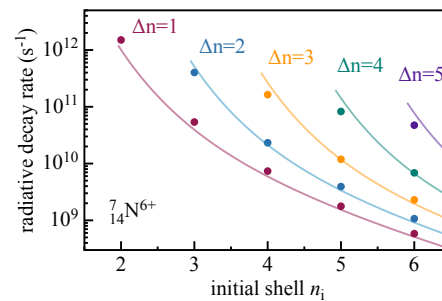


**Figure 1.** Experimental decay rates [3] for the deexcitation of hollow nitrogen atoms in dependence of the initial shell  $n_i$  for five different  $\Delta n$ . In continuous lines the results from the fit used for our calculation are added.

As output of our calculations we then obtain not only a life time of the hollow atom, but also emission spectra of secondary electrons and photons, respectively. Preliminary results show strong  $K_\alpha$  lines for the latter, as well as a spectrum of low-energy ( $< 50$  eV) electrons. In this contribution we will present not only an overview of the method, but also a comparison of calculated emission spectra with literature data as presented, e.g., in [5, 6].

### References

- [1] Burgdörfer J *et al.* 1991 *Phys Rev A* **44** 9
- [2] Tőkési K *et al.* 2001 *Phys Rev A* **64** 042902
- [3] NIST Atomic Spectra Database (2022-01-05)
- [4] Gu M F 2008 *Can J Phys* **86** 675
- [5] Niggas A *et al.* 2022 *Phys Rev Lett* **129** 086802
- [6] Schwestka J *et al.* 2018 *NIMB* **422** 63

\*E-mail: [niggas@iap.tuwien.ac.at](mailto:niggas@iap.tuwien.ac.at)



## Stopping power of heavy ions under channeling condition

R Holeňák<sup>1\*</sup>, S Lohmann<sup>1,2</sup>, E Ntemou<sup>1</sup> and D Primetzhofer<sup>1</sup>

<sup>1</sup>Department of Physics and Astronomy, Uppsala University, Uppsala, 75120, Sweden

<sup>2</sup>Institute of Ion Beam Physics and Materials Research, HZDR, Dresden, 01328, Germany

**Synopsis** We present experimental work providing evidence on the mechanisms underlying the observed trajectory dependence of inelastic energy deposition by heavy ions in the keV energy regime.

We present experimental results on the inelastic energy loss of a wide range of ions in the 4-300 keV energy regime in single crystalline matrices. The comparable velocity of ions and electrons in the target's valence and conduction bands renders the underlying interaction highly dynamic and strongly trajectory-dependent. Ion transmission experiments through self-supporting crystalline silicon targets provide an excellent model system to study the trajectory-dependence due to its simple geometry, which allows for an exclusive choice of projectile trajectories [1].

The stopping power of all ions except protons is found to be highly reduced under channeling conditions compared to random incidence [1,2]. However, a reduction in electron-hole pair excitation alone cannot explain the disparity of the electronic excitations in different geometries since the core-shell electrons are no longer accessible. While an influence of different electron densities is expected, the observed dependence of the differences on the atomic number of the ion indicates that additional energy loss processes are involved. We explain our observation by several charge exchange processes, such as electron promotion due to the creation of molecular orbitals occurring in close collisions of ions with target atoms only accessible in random geometry. Additional to direct losses in the electron promotion, these events result in trajectory-dependent mean charge states that heavily affect the energy loss.

The evidence for the altered charge state distribution developed along different trajectories is investigated by discrimination of transmitted projectiles based on their charge state. Considerably larger fractions of higher charge states are emerging from random geometry, while the channeled projectiles tend to remain more neutral.

Furthermore, the large energy-loss events in the promotion events leave a signature in the shape of the energy distribution of transmitted projectiles in the form of energy loss straggling. For projectiles heavier than protons and helium, the velocity scaling of the straggling in random geometry suggests a minimum and increase towards lower projectile velocities [4].

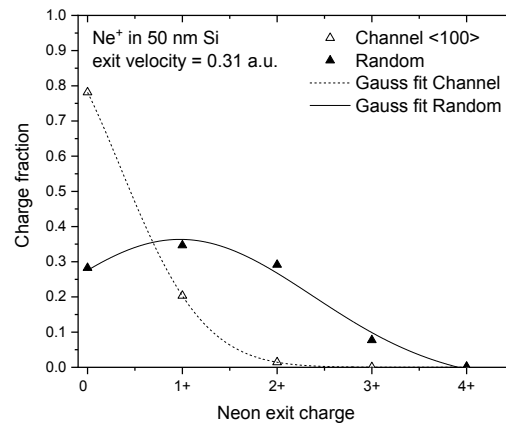


**Figure 1.** Charge fraction distributions of Neon projectiles at exit velocity 0.31 a.u. after transmission through 50 nm Si crystal.

Ongoing development of our understanding forms the basis for analytical tools based on ion beams, irradiation damage, sputtering and other industrial methods. Above that, the channeling condition being to a large extent not affected by the complex charge exchange processes can yield a well-defined test scenario for theoretical models on ion-electron dynamics, which aim to predict equilibrium [DFT] and non-equilibrium conditions [TD-DFT] in solids [3].

### References

- [1] Holeňák R et al. 2020 *Ultramicroscopy* **217**
- [2] Lohmann S et al. 2020 *PRL* **124** 096601
- [3] Lohmann S et al. 2020 *PRA* **102** 062803
- [4] Lohmann S et al. 2023 *PRB* **107** 085110

\* E-mail: [radek.holenak@physics.uu.se](mailto:radek.holenak@physics.uu.se)

## Generating Ultrafast MeV Electrons with a mJ-class Laser

J Powell<sup>1\*</sup>, S Vallières<sup>1,2</sup>, S Payeur<sup>1</sup>, S Fourmaux<sup>1</sup>, S Jolly<sup>3</sup>, F Fillion-Gourdeau<sup>4</sup>, H Ibrahim<sup>1</sup>,  
S MacLean<sup>1,2,3</sup> and F Légaré<sup>1</sup>

<sup>1</sup>INRS, Énergie, Matériaux et Télécommunications, Varennes, Québec, J3X 1S2, Canada

<sup>2</sup>Institute of Quantum Computing, University of Waterloo, Waterloo, Ontario, N2L 3G1, Canada

<sup>3</sup>Service OPERA-Photonique, Université Libre de Bruxelles (ULB), Brussels, Belgium

<sup>4</sup>Infinite Potential Laboratories, Waterloo, Ontario, N2L 0A9, Canada

**Synopsis** We present experimental results detailing our ability to generate an ultrafast beam of relativistic electrons by direct laser acceleration. Electrons with energies greater than 1 MeV were measured after tightly focusing a radially polarized, mJ-class, femtosecond laser in a low-density gas. A clear dependence on ionization dynamics is revealed by varying the laser intensity and gas species, agreeing with simulation. This tabletop source of high-energy electrons is ideal for applications such as ultrafast electron diffraction.

Laser-based tabletop sources of electrons are an active research area that promises to provide a compact alternative to conventional sources. Plasma-mediated techniques such as laser wakefield acceleration are increasingly common but typically require large lasers and complex vacuum systems. In contrast, direct laser acceleration utilizes the electric field of the laser to generate the high energy electrons and can produce ultrashort electron bunches due to the ultrafast nature of the interaction.

In this work, we demonstrate our ability to accelerate electrons to relativistic energies by employing a radially polarized laser mode to produce a large longitudinal electric field through the tight focusing of a mJ-class femtosecond IR laser [1,2]. The Advanced Light Laser Source (ALLS) facility in Varennes, Québec provided up to 3.5 mJ of pulse energy with a central wavelength at 1.8  $\mu\text{m}$  and a pulse duration of 12 fs. An on-axis parabola ( $\text{NA} \approx 1$ ) generated an estimated focal intensity greater than  $10^{18}$  W/cm<sup>2</sup>, capable of large accelerating fields and inner shell ionization of the gas (O<sub>2</sub>, Ar or Kr).

Figure 1 illustrates the electron energy distribution measured when using krypton gas, giving a mean electron energy over 500 keV and a cutoff energy of greater than 1.3 MeV. We observed the final electron energy to be dependent on the laser intensity and gas type, with significant deviations seen at high intensity between the gases. Simulation reveals a complex interplay between the ionization dynamics of the different gases and the injection of the pho-

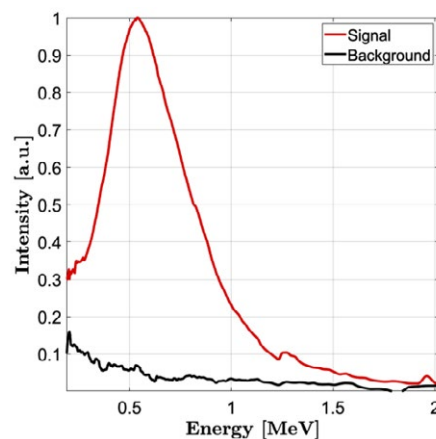


**Figure 1.** Electron energy distribution from krypton (mean = 560 keV, cutoff = 1.3 MeV). A radially polarized ( $\lambda = 1.8 \mu\text{m}$ , 12 fs, 3.5 mJ) laser was focused with an on-axis parabola of  $\text{NA} \approx 1$  into a  $\sim 100\text{mTorr}$  backfilled chamber of gas.

toelectrons into the laser field. At high intensities, inner shell electrons from krypton are optimally injected into the peak of the laser field. In the same conditions, electrons from oxygen are injected earlier and thus experience smaller acceleration fields and attain lower energies.

We have demonstrated a viable tabletop method to generate relativistic electron beams using direct laser acceleration with only a few mJ of pulse energy, ideal for applications such as ultrafast electron diffraction.

### References

- [1] Varin *et al.*, *Appl. Sci.* **3**, 70-93 (2013).
- [2] Powell *et al.*, CLEO Technical Digest, paper FF1A.1 (2021).

\* E-mail: [jeffrey.powell@inrs.ca](mailto:jeffrey.powell@inrs.ca)

## Selective field ionization of Rydberg atoms in a room-temperature vapor

D S La Mantia<sup>1\*</sup>, A P Rotunno<sup>2</sup>, N Prajapati<sup>2</sup>, M Simons<sup>2</sup>, C L Holloway<sup>2</sup>, E B Norrgard<sup>1</sup>, and S P Eckel<sup>1</sup>

<sup>1</sup>National Institute of Standards & Technology, Sensor Science Division, Gaithersburg, MD 20899 U.S.A.

<sup>2</sup>National Institute of Standards & Technology, RF Technology Division, Boulder, CO 80305 U.S.A.

**Synopsis** A novel system has been developed in an attempt to perform selective field ionization of Rydberg atoms in a room-temperature vapor. This technique has previously been demonstrated in ultra-high vacuum environments for state population readout using electron-multiplication devices. Here, we discuss detection of field-ionized Rydberg atoms in a vapor cell near 300 K without the aid of in-vacuum electronic multiplication.

Sensing of electromagnetic radiation is a principal facet of modern physics. A ubiquitous source of incoherent radiation is blackbody radiation (BBR): electromagnetic radiation emitted by a body in thermal equilibrium with its surroundings. It then follows that BBR characterization is a logical way to accurately assess the temperature of a distant entity. A thermal radiation detector integrating an invariable quantum system represents the next technological leap in radiation thermometry while being directly traceable to the new International System of Units (SI). Rydberg atoms are highly polarizable, and are therefore a natural sensor of electric fields such as BBR. Efforts are underway to use Rydberg atoms as calibration-free, SI-traceable thermal radiation sensors, thereby characterizing reference blackbodies at the 100 ppm level [1] and greatly reducing the calibration uncertainty for classical thermal radiation sensors.

Selective field ionization of Rydberg atoms [2, 3] is the measurement technique to be employed; a schematic of that process is shown in Fig. 1. The Rb atoms are pumped to Rydberg states via a two-photon process using counter-propagating lasers: the 780 nm laser drives the  $5S_{1/2} \rightarrow 5P_{3/2}$  transition and the 480 nm laser drives the final  $5P_{3/2} \rightarrow nS_{1/2}$  transition. The atoms then evolve for a variable amount of time in the BBR field absent the lasers, where they populate neighboring  $P$  states (or photoionize, much smaller probability). An electric field is applied between plates in the vapor cell and ramped as high as 2 kV/cm to selectively ionize Rydberg levels as the field intensity increases. The ions

\*E-mail: [david.lamantia@nist.gov](mailto:david.lamantia@nist.gov)

are then collected on a cathode.

A custom Rb vapor cell has been designed and constructed, with great care taken to minimize stray fields and capacitances. The cell has demonstrated direct ion readout (without the ramping field), as well as ionization due to an applied field. Efforts towards selective field ionization are underway. The results and progress will be discussed and compared to literature, where applicable. †Supported in part by DARPA.

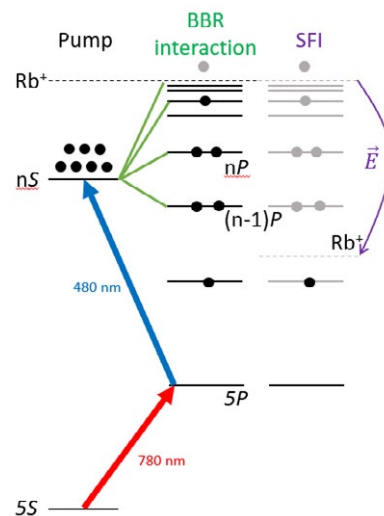


**Figure 1.** Schematic of selective field ionization of Rydberg Rb following BBR interaction.

### References

- [1] E. B. Norrgard, *et al.*, *New Journal of Physics* **23**, 033037 (2021).
- [2] T. F. Gallagher, *et al.*, *Phys. Rev. A* **16**, 1098 (1977).
- [3] E. J. Galvez, *et al.*, *Phys. Rev. A* **51**, 4010 (1995).

## Momentum of Light in an Atom

J Hainge<sup>1\*</sup> and D H J O'Dell<sup>1†</sup>

<sup>1</sup> Department of Physics and Astronomy, McMaster University, Hamilton, L8S 4K1, Canada

**Synopsis** We consider the possibility of measuring the momentum of light within a medium consisting of a single atom via their interaction time, in the hopes of contributing to the discussion surrounding the Abraham-Minkowski controversy.

The Abraham-Minkowski “controversy” is a debate in physics which began over a century ago, stemming from an ambiguity in defining the momentum of light within a medium. One such formulation is attributed to Minkowski [1], while the other is credited to Abraham [2, 3]. Simple physical arguments lead to a prediction that the momentum of light should either increase or decrease by a factor of the refractive index (compared to its value in the vacuum) upon entering a medium; the first result is in line with Minkowski’s prediction, while the latter agrees with Abraham.

Experimental attempts to discriminate between the two theories often support one over the other at first glance, but upon deeper consideration cannot refute one or the other [4]. While a

resolution to the alleged paradox has been proposed [5], some physicists remain unconvinced, as evidenced by continued publication on the subject.

We theoretically investigate the possibility of measuring the interaction time between an electrically polarizable atom and a light pulse in order to discriminate between the two hypothesized momentum-transfer scenarios.

### References

- [1] Minkowski H 1910 *Math. Ann.* **68** 472
- [2] Abraham M 1909 *Rend. Circ. Mat. Palermo* **28** 1
- [3] Abraham M 1910 *Rend. Circ. Mat. Palermo* **30** 33
- [4] Pfeifer N C *et al.* 2007 *Rev. Mod. Phys.* **79** 1197
- [5] Barnett S M 2010 *Phys. Rev. Lett.* **104** 070401

---

\*E-mail: [haingej@mcmaster.ca](mailto:haingej@mcmaster.ca)

†E-mail: [dodell@mcmaster.ca](mailto:dodell@mcmaster.ca)

## Photoelectron holography: an interplay between difference interference mechanisms.

S. Borbély<sup>1\*</sup>, A. Tóth<sup>2</sup> and L. Nagy<sup>1</sup>

<sup>1</sup>Faculty of Physics, Babeş-Bolyai University, str. Kogălniceanu 1, 400084 Cluj, Romania

<sup>2</sup>ELI-ALPS, ELI-HU Nonprofit Ltd., Dugonics tér 13, H-6720 Szeged, Hungary

**Synopsis** Photoelectron holograms are observed in the momentum distribution of continuum electrons created during the interaction of atomic systems with ultrashort laser pulses. They are the result of interference between different electronic pathways. Here these interference mechanisms are investigated based on *ab initio* calculations.

During the interaction of ultrashort laser pulses with atoms and molecules the electronic wave packets following different spatial and temporal paths interfere leading to the formation of photoelectron holograms [1, 2]. In our previous investigations [3, 4] we have studied the photoelectron hologram induced by few-cycle time-symmetric laser pulse with sine-square envelope. Due to the particular shape of those laser pulses, in the observed hologram the dominant component was attributed to the spatial interference (wavepackets emitted at the same time moment but following different paths), while the component attributed to the temporal interference (wavepackets emitted at different time moments of the laser pulse) was barely visible.

In the present study we performed *ab initio* calculations for the ionization of the hydrogen atom in interaction with few-cycle flat-top laser pulses, each half-cycle having the same amplitude. The parameters of the driving laser field are chosen in such way, that the intensity of the continuum wave packets created by the different half-cycles of the driving field are similar. By doing so, we have ensured that both the spatial and temporal interference patterns are visible

and their coherent superposition can be studied. The formation of the spatial and temporal interference patterns, and their coherent superposition were investigated in details using the wavefunction splitting technique [3].

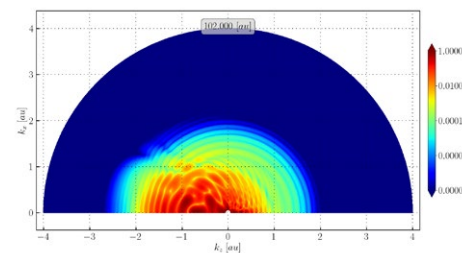


**Figure 1.** The photoelectron hologram obtained for the hydrogen atom interacting with a two-cycle flat-top laser pulse with  $E_0 = 0.08$  a.u. amplitude and  $\omega_0 = 0.125$  a.u. carrier-wave frequency.

### References

- [1] X.B. Bian et. al 2011 *Phys. Rev. A* **84** 043420.
- [2] Y. Huismans et al. 2011 *Science* **331** 61.
- [3] S Borbély, A Tóth, D.G. Arbó, K Tókési, L Nagy 2019 *Phys. Rev. A* **99** 013413.
- [4] G. Zs. Kiss, S. Borbély, A. Tóth, L. Nagy 2020 *Eur. Phys. J. D* **74** 1.

\*E-mail: [sandor.borbely@ubbcluj.ro](mailto:sandor.borbely@ubbcluj.ro)



## Soft x-ray spectroscopy on non-linear interaction of x-rays with matter at the Small Quantum Systems instrument of European XFEL

T.M. Baumann<sup>1\*</sup>, M. Agåker<sup>2</sup>, H. Ågren<sup>2</sup>, O. Björneholm<sup>2</sup>, R. Boll<sup>1</sup>, J. Bozek<sup>3</sup>, S. Cardoch<sup>2</sup>, S. Coriani<sup>4</sup>, L. Cornetta<sup>2</sup>, A. De Fanis<sup>1</sup>, E. De Santis<sup>2</sup>, S. Dold<sup>1</sup>, G. Doumy<sup>5</sup>, U. Eichmann<sup>6</sup>, X. Gong<sup>7</sup>, J. Gråsjö<sup>2</sup>, I. Ismail<sup>9</sup>, L. Kjellsson<sup>10</sup>, K. Li<sup>11</sup>, E. Lindroth<sup>12</sup>, T. Mazza<sup>1</sup>, J. Montaña<sup>1</sup>, T. Mullins<sup>1</sup>, H. Ni<sup>7</sup>, J. Nordgren<sup>2</sup>, C. Ott<sup>13</sup>, Y. Ovcharenko<sup>1</sup>, M. Patanen<sup>14</sup>, T. Pfeifer<sup>13</sup>, M.N. Piancastelli<sup>9</sup>, R. Püttner<sup>15</sup>, N. Rennhack<sup>1</sup>, N. Rohringer<sup>16</sup>, C. Sánchez-Hanke<sup>8</sup>, C. Sâthe<sup>10</sup>, P. Schmidt<sup>1</sup>, B. Senfftleben<sup>1</sup>, M. Simon<sup>9</sup>, J.C. Söderström<sup>2</sup>, S.-K. Son<sup>16</sup>, S. Southworth<sup>5</sup>, N. Timneanu<sup>2</sup>, M. Togawa<sup>1</sup>, K. Ueda<sup>17</sup>, S. Usenko<sup>1</sup>, H.J. Wörner<sup>18</sup>, W. Xu<sup>19</sup>, Z. Yin<sup>17</sup>, L. Young<sup>5</sup>, M. Meyer<sup>1</sup>, and J.-E. Rubensson<sup>2†</sup>

<sup>1</sup>European XFEL, Schenefeld, Germany

<sup>2</sup>Uppsala University, Uppsala, Sweden

<sup>3</sup>Synchrotron Soleil, Gif-sur-Yvette Cedex, France

<sup>4</sup>Technical University of Denmark, Lyngby, Denmark

<sup>5</sup>Argonne National Laboratory, Lemont, USA

<sup>6</sup>Max-Born-Institut, Berlin, Germany

<sup>7</sup>East China Normal University, Shanghai, China

<sup>8</sup>Diamond Light Source, Chilton, United Kingdom

<sup>9</sup>Sorbonne University, Paris, France

<sup>10</sup>Max IV Laboratory, Lund University, Lund, Sweden

<sup>11</sup>University of Chicago, Chicago, USA

<sup>12</sup>Stockholm University, Stockholm, Sweden

<sup>13</sup>Max-Planck-Institut für Kernphysik, Heidelberg, Germany

<sup>14</sup>University of Oulu, Oulu, Finland

<sup>15</sup>Freie Universität Berlin, Berlin, Germany

<sup>16</sup>Deutsches Elektronen-Synchrotron, Hamburg, Germany

<sup>17</sup>Tohoku University, Sendai, Japan

<sup>18</sup>ETH Zürich, Zürich, Switzerland

<sup>19</sup>ShanghaiTech University, SHINE, Shanghai, China

**Synopsis** We present first results obtained with a newly developed 1D-imaging spectrometer at the Small Quantum Systems Instrument of European XFEL. Its high-resolution soft x-ray fluorescence spectra provide a novel insight into multiphoton ionization processes during the interaction of intense x-ray radiation with Ne and Xe atoms.

Matter irradiated by intense and short x-ray free-electron laser (XFEL) pulses undergoes rapid multiphoton ionization reaching very high charge states on a femtosecond timescale. The intricate dynamic interplay between sequential ionization, autoionization and resonant excitation is challenging state-of-the-art ionization dynamics calculations [1, 2, 3]. Such fundamental interactions are studied at the Small Quantum Systems (SQS) instrument at the SASE3 soft x-ray undulator branch of European XFEL.

Recently, a novel 1D-imaging grating spectrometer was taken into operation at SQS, which covers the spectral range from 150 eV to 1200 eV. A pair of Wolter-mirrors images the source in one dimension. This allows for measuring spectra with a spatial coordinate dependence along the FEL propagation (see Fig.1). The observed sample is injected into a gas cell at pressures up to 1 bar.

We present results of the first measurement campaign studying fluorescence emission after the interaction of FEL pulses with neon and xenon atoms near ambient pressure. We ob-

served emission from high charge states, up to Ne<sup>9+</sup>, multiple excited states e.g., in Ne<sup>8+</sup> and forbidden decays, allowing to identify the dominant ionization and decay pathways by comparison to theory. Furthermore, the influence of electron collisions at such high sample densities was investigated.

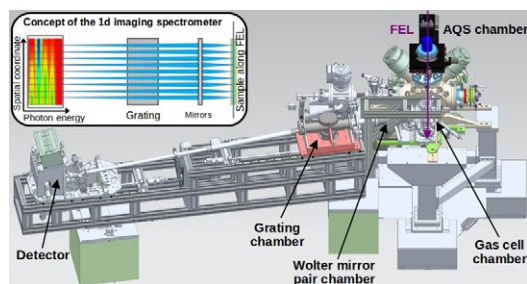


**Figure 1.** Conceptual drawing and CAD model of the 1D-imaging spectrometer at SQS.

### References

- [1] B. Rudek *et al.*, 2012, *Nat. Photon.* **6**, 858
- [2] A. Rörig, *et al.*, 2023, [arXiv:2303.07942](https://arxiv.org/abs/2303.07942)
- [3] S.-K. Son, *et al.*, 2011, *Phys.Rev.A* **83**, 033402

\* E-mail: [thomas.baumann@xfel.eu](mailto:thomas.baumann@xfel.eu)

† E-mail: [jan-erik.rubensson@physics.uu.se](mailto:jan-erik.rubensson@physics.uu.se)

## Fano-ADC(2,2) method for multi-electron decay processes

P Koloreň<sup>1\*</sup>

<sup>1</sup>Charles University, Faculty of Mathematics and Physics, Institute of Theoretical Physics  
V Holešovičkách 2, Prague, 180 00, Czech Republic

### Synopsis

Two-electron relaxation processes following inner-shell ionization of matter, such as the Auger-Meitner effect, play an essential role in radiation damage. Recent experiments suggest that even higher-order processes involving multi-electron transitions can reach surprisingly high intensities. These hitherto little investigated mechanisms thus might also affect the response of matter to radiation. However, their *ab initio* theoretical investigation is challenging. We will demonstrate the performance of the recently developed Fano-ADC(2,2) method on several examples of three-electron decay processes in atoms.

Two-electron relaxation processes following inner-shell ionization of matter play an essential role in biological damage inflicted by radiation. Relevant mechanisms comprise acceleration of photodissociation or production of slow electrons and reactive secondary products. Recent experiments suggest that even higher-order relaxation processes involving multi-electron transitions can reach surprisingly high intensities, both in molecules and in weakly bound clusters [1,2]. Their theoretical description is thus of utmost importance.

Among the fundamental characteristics of a metastable state belongs decay width, which is directly related to its lifetime. The Fano-ADC method [3] is one of the most successful approaches to *ab initio* computation of intra- and inter-atomic electronic decay widths. It is based on the Fano theory of resonances and algebraic diagrammatic construction (ADC) in the intermediate state (IS) representation [4] for the description of the many-electron wave function. However, implementations based on the extended second-order ADC scheme [ADC(2)x] comprise only  $1h$  and  $2h1p$  excitation classes and cannot be used to study processes with two electrons in continuum. Furthermore, the  $2h1p$ -like states (shake-up ionization satellites) are seriously under-correlated compared to the  $1h$ -like main ionic states, which can affect the accuracy of the calculated decay widths.

To remedy these issues, we have developed ADC(2,2) scheme [3]. It offers unprecedented consistency in the description of main and satel-

lite ionization states and is thus particularly valuable for studying the inner valence regions of molecules where the  $1h$  and  $2h1p$  characters of states are usually strongly mixed due to the so-called molecular orbital picture breakdown. Comprising also the  $3h2p$  excitation class, the resulting Fano-ADC(2,2) provides access to the second-order decay processes with two electrons in the continuum. In this contribution, we demonstrate its performance on several examples of multi-electron decay processes for which the common ADC(2)x scheme is inadequate.

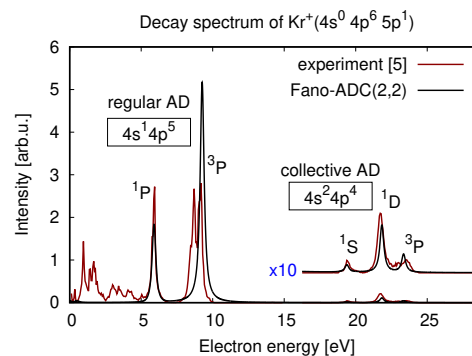


Figure 1.  $3e^-$  Auger decay spectrum in Kr.

### References

- [1] A H Roos *et al*, *Sci. Rep.* **8**, 16405 (2018).
- [2] A C LaForge *et al*, *Sci. Rep.* **4**, 3621 (2014).
- [3] P Koloreň and V Averbukh, *JCP* **152**, 214107 (2020).
- [4] F Mertins and J Schirmer, *PRA* **53**, 2140 (1996).
- [5] J H D Eland *et al* *New J. Phys.* **17**, 122001 (2015).

\*E-mail: [premysl.kolorenc@matfyz.cuni.cz](mailto:premysl.kolorenc@matfyz.cuni.cz)

## Nonadiabatic Strong Field Ionization of Atomic Hydrogen

D Trabert<sup>1\*</sup>, N Anders<sup>1</sup>, S Brennecke<sup>2</sup>, M S Schöffler<sup>1</sup>, T Jahnke<sup>1</sup>, L Ph H Schmidt<sup>1</sup>,  
M Kunitski<sup>1</sup>, M Lein<sup>2</sup>, R Dörner<sup>1</sup> and S Eckart<sup>1†</sup>

<sup>1</sup>Institut für Kernphysik, Goethe-Universität, Frankfurt, 60438, Germany

<sup>2</sup>Institut für Theoretische Physik, Leibniz Universität, Hannover, 30167, Germany

**Synopsis** In a recent publication [1], we have presented experimental data on the nonadiabatic strong field ionization of atomic hydrogen using elliptically polarized femtosecond laser pulses at a central wavelength of 390 nm. Our measured results are in agreement with a numerical solution of the time-dependent Schrödinger equation (TDSE). Experiment and TDSE show four above-threshold ionization peaks in the electron's energy spectrum. The most probable emission angle (also known as "attoclock offset angle" or "streaking angle") is determined for each energy peak individually.

In a pioneering experiment, Sainadh *et al* have applied the technique of angular streaking [2,3] to adiabatic tunnel ionization of atomic hydrogen using a driving laser field at a central wavelength of 770 nm [4].

Here, we present experimental data on a similar experiment but choose a driving field at a central wavelength of 390 nm and thus increased the nonadiabaticity of the ionization process significantly. Our results have been published in [1] recently. In short, we study the strong field ionization of atomic hydrogen using elliptically polarized femtosecond laser pulses at an ellipticity of  $\varepsilon=0.85$ , and a peak intensity of  $1.4 \times 10^{14}$  W/cm<sup>2</sup>.

A COLTRIMS reaction microscope was used to measure the three-dimensional momenta of electron and ion in coincidence. Figure 1(a) shows the electron momentum distribution projected onto the laser's polarization plane ( $p_x p_y$  plane). Figure 1(b) shows the corresponding result that is obtained from a numerical solution of the time-dependent Schrödinger equation (TDSE). Experiment and TDSE result are in agreement. This is underlined by Figure 1(c), which shows the corresponding electron energy distributions.

The "angular offset"  $\alpha_{\text{off}}$  (see Fig. 1(a),(b)) is found to increase with energy, a trend that is opposite to standard predictions based on Coulomb interaction with the ion. This increase of deflection angle can be explained by a nonadiabatic, classical two-step model (NACTS) that includes nonadiabatic corrections of the initial momentum distribution at the tunnel exit and nonadiabatic corrections of the tunnel exit position itself [5,6].

\* E-mail: [trabert@atom.uni-frankfurt.de](mailto:trabert@atom.uni-frankfurt.de)

† E-mail: [eckart@atom.uni-frankfurt.de](mailto:eckart@atom.uni-frankfurt.de)

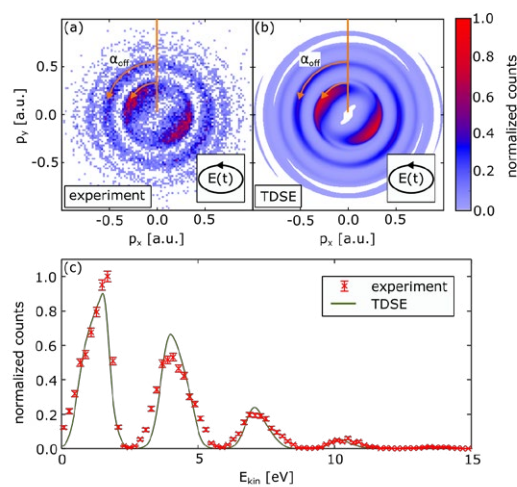


**Figure 1.** (a) Measured electron momentum distribution projected onto the laser's polarization plane for the ionization of atomic hydrogen by femtosecond laser pulses at a central wavelength of 390 nm, an ellipticity of  $\varepsilon = 0.85$ , and a peak intensity of  $1.4 \times 10^{14}$  W/cm<sup>2</sup>. The light's helicity and the orientation of the polarization ellipse are indicated by the inset in the lower right corner. (b) Focal-averaged numerical solution of the TDSE for the parameters that were used in (a).  $\alpha_{\text{off}}$  indicates the "angular offset" with respect to the minor axis of the ellipse of the laser electric field in (a) and (b). (c) shows a comparison of the electron energy distribution for the data shown in (a) and (b). The data is the same as in Ref. [1].

### References

- [1] Trabert D *et al* 2021 *Phys. Rev. Lett.* **127**, 273201
- [2] Smolarski M *et al* 2010 *Opt. Express* **18**, 17640
- [3] Eckle P *et al* 2008 *Science* **322**, 1525
- [4] Sainadh U *et al* 2019 *Nature* **568**, 75
- [5] Brennecke S *et al* 2020 *Phys. Rev. Lett.* **124**, 153202
- [6] Brennecke S *et al* 2021 *J. Phys. B* **54**, 164001

## Nondipole effects in strong-field ionization using few-cycle laser pulse

Danish Furekh Dar<sup>1,2,3\*</sup> and Stephan Fritzsche<sup>1,2,3</sup>

<sup>1</sup>Helmholtz-Institut Jena, Fröbelstieg 3, D-07743 Jena, Germany

<sup>2</sup>GSI Helmholtzzentrum für Schwerionenforschung GmbH, Planckstrasse 1, D-64291 Darmstadt, Germany

<sup>3</sup>Theoretisch-Physikalisches Institut, Friedrich-Schiller-Universität Jena, Max-Wien-Platz 1, D-07743 Jena, Germany

**Synopsis** The ionization of atoms and molecules under strong laser fields has been studied both theoretically, using the strong-field approximation (SFA), and experimentally. However, the SFA, derived for plane-wave beams, has limitations in predicting nondipole effects despite its effectiveness in explaining ionization processes. This work proposes an extended version of the SFA that can handle the intricate temporal structure of short laser pulses. This extension enables better prediction of peak shifts and provides greater control over the laser field in inducing above threshold ionization. Our findings indicate that the improved SFA shows better agreement with experimental investigations than previous theoretical studies.

The interaction of atoms and molecules with high-intensity laser fields is a topic of significant interest. The time-dependent Schrödinger equation (TDSE) is used to study the complex behavior of atoms in such laser fields. Numerical, classical, and semiclassical methods are used for solving the TDSE, but the strong-field approximation (SFA) is a particularly intuitive and widely used method enabling to solve TDSE analytically.

Recently [1], femtosecond pulsed lasers have been used to examine nondipole-induced peak shifts in the momentum of the photoelectron, which have garnered significant attention in the field. Traditionally, SFA has been applied to laser fields under the dipole approximation. However, with new research [2], SFA has been extended to encompass nondipole scenarios, which has demonstrated its broad applicability.

In this work, we present an extension of the SFA that considers the complex temporal structure of a few-cycle pulse, which allows for the prediction of peak shifts in above-threshold ionization processes. The results demonstrate that the NSFA is a valuable theoretical method for calculating the effects of strong electromagnetic fields on the behavior of electrons. In particular, the NSFA with extension to few-cycle limit is better suited for predicting the peak shifts observed in experimental investigations. Overall, this study highlights the potential of the NSFA

\*E-mail: [danish.dar@uni-jena.de](mailto:danish.dar@uni-jena.de)

for providing enhanced control over the characteristics of laser pulses and better understanding the behavior of atoms in high-intensity laser fields.

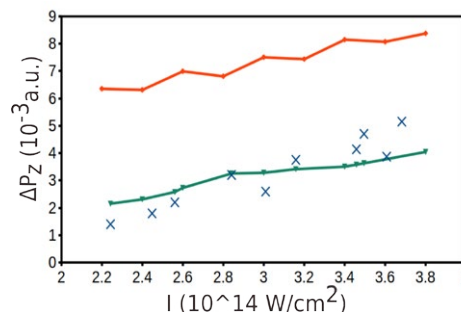


**Figure 1.** The peak shift  $\Delta P_z$  of the maxima in ATI spectra are plotted as a function of laser intensity  $I$  for a circularly polarized 800 nm, 15 fs laser pulse. The results of this work (green) are compared to previous experimental (blue crosses) [1] and theoretical work (orange) [2].

### References

- [1] C. T. L. Smeenk, L. Arissian, B. Zhou, A. Mysyrowicz, D. M. Villeneuve, A. Staudte, and P. B. Corkum. Partitioning of the linear photon momentum in multiphoton ionization. *Phys. Rev. Lett.*, 106:193002, May 2011.
- [2] Birger Böning, Willi Paufler, and Stephan Fritzsche. Nondipole strong-field approximation for spatially structured laser fields. *Phys. Rev. A*, 99:053404, May 2019.

# Nonsequential double ionization of Ne with elliptically polarized laser pulses

Fang Liu<sup>1,2\*</sup>, Zhangjin Chen<sup>3</sup> and Stephan Fritzsche<sup>1,2</sup>

<sup>1</sup>Helmholtz-Institut Jena, 07743 Jena, Germany

<sup>2</sup>Theoretisch-Physikalisches Institut, Friedrich-Schiller-Universität Jena, 07743 Jena, Germany

<sup>3</sup>Department of Physics, College of Science, Shantou University, 515063 Shantou, Guangdong, China

**Synopsis** Nonsequential double ionization. 2D ion momentum distribution. Elliptically polarized laser pulses. The improved quantitative re-scattering model (QRS) model. Theoretical simulation.

We show through simulation that the improved quantitative re-scattering model (QRS) [1] can successfully predict the nonsequential double ionization (NSDI) process by intense elliptically polarized laser pulses. Using the QRS model, we calculate the correlated two-electron and ion momentum distributions of NSDI in Ne exposed to intense elliptically polarized laser pulses with a wavelength of 788 nm at a peak intensity of  $5.0 \times 10^{14} \text{ W/cm}^2$ . We analyze the asymmetry in the doubly charged ion momentum spectra observed by H. Kang et al. [2] in going from linearly to elliptically polarized laser pulses.

In the present work, we have aimed to unveiling the mechanisms for the symmetry in the momentum distribution of ions for linear polarization and the collapse of the symmetry in the momentum distribution of ions for elliptical polarization. Our study reveals that the drift velocity along the minor axis when the ellipticity is nonzero is responsible for asymmetric distribution for elliptically polarization. The overall good agreement between our model results and the experimental measurements confirms the basic assumptions of the QRS model, namely that recollisions occur most probably after the  $E_z$  field zero crossing. This work provides guidelines for the study of NSDI with both linearly and elliptically polarized laser fields within the framework of the QRS model. Finally, it should be noted that without taking into account the RESI, the model fails to reproduce the ion momentum distributions in the range of  $|p_z| < 0.7$ . The agree-

ment with experiment could be improved if the contribution from RESI is considered.

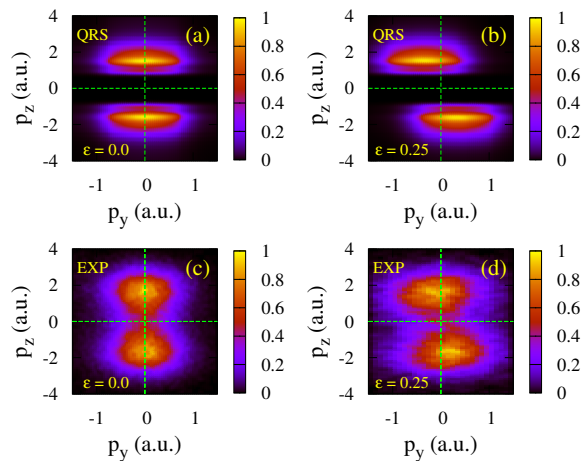


**Figure 1.** Comparison of the momentum distributions of the theoretical simulations (top row) and the experimental measurements (bottom row) for  $\text{Ne}^{2+}$  ions in the  $y$ - $z$  polarization plane of elliptically polarized laser pulses at a peak intensity of  $5.0 \times 10^{14} \text{ W/cm}^2$  with a wave length of 788 nm. The ellipticities are  $\epsilon = 0.0$  and  $0.25$ , respectively.

## References

- [1] Z. Chen, A.-T. Le, T. Morishita, and C. D. Lin 2009 *Phys. Rev. A* **79** 033409
- [2] H. Kang, K. Henrichs, M. Kunitski, Y. Wang, X. Hao, K. Fehre, A. Czasch, S. Eckart, L. Ph. H. Schmidt, M. Schöffler, T. Jahnke, X. Liu, and R. Dörner 2018 *Phys. Rev. Lett.* **120** 223204

\*E-mail: [fang.liu@uni-jena.de](mailto:fang.liu@uni-jena.de)



## Strong field phenomena with sculpted laser pulses

A L Harris\* and D Yaacoub

Physics Department, Illinois State University, Normal, IL 61790, USA

**Synopsis** We present numerical simulations of above threshold ionization and attosecond streaking of atoms using sculpted Airy laser pulses. Our results show that the third order spectral phase of the Airy pulse alters the timing of ionization and the dynamics of electron rescattering. These changes translate into shifts in the ATI energy plateaus and the intra- and intercycle interference peaks in the photoelectron momentum distributions.

In the last few decades, there have been countless experimental and theoretical studies of strong field phenomena that have shaped our understanding of laser-matter interactions. Despite these decades of study, strong field phenomena still have insights to share. In this work, we use temporally sculpted laser fields in the form of Airy pulses [1] to study strong field processes, including above threshold ionization (ATI) and attosecond streaking (AS).

To date, most studies using temporally sculpted pulses used two-color laser fields [2], consisting of the fundamental field and one of its harmonics. In this case, alteration of the relative phase between the two frequency components is used to shape the pulse envelope. Airy laser fields offer an alternative method of pulse shaping through manipulation of the third order spectral phase. Unlike traditional sin-squared or Gaussian wave forms, Airy pulses can have more complicated envelope functions with multiple peaks, and they exhibit self-acceleration, self-healing, and limited diffraction.

We present theoretical studies of ATI and AS using temporal Airy and Gaussian pulses [3] that are carefully chosen to have identical power spectra, but different spectral phases and temporal envelopes. We solved the time-dependent Schrödinger equation to calculate energy and momentum spectra and streaking spectrograms. The simple man's model was used to provide a qualitative understanding of the electron motion after ionization. Our results show that the spectral phase of the Airy pulse alters the timing of ionization and the dynamics of the rescattering process, which is reflected in changes to the energy and momentum spectra.

Figure 1 shows the ATI photoelectron energy spectra for neon using Airy and Gaussian laser pulses. The use of an Airy pulse shifts the

plateau cutoff energies to lower values due to a reduced pondermotive energy. The side lobes of the Airy pulse envelopes lead to additional electron release times, and therefore additional intercycle interference peaks are seen in Fig. 1.

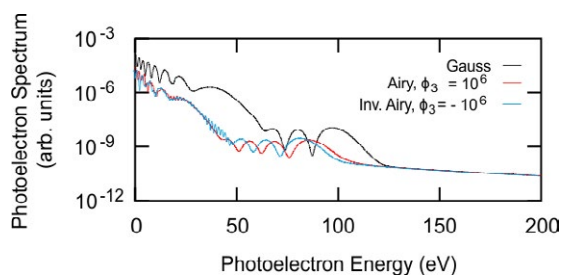


**Figure 1.** ATI photoelectron energy spectra for neon ( $I = 2.5 \times 10^{14}$  W/cm<sup>2</sup>,  $\lambda = 800$  nm,  $fwhm = 110$  a.u.).

The time difference between intracycle release times is also altered for Airy pulses, leading to changes in the intracycle interference. These changes are observed as shifts in the photoelectron momentum, which scale approximately linearly with the third order spectral phase of the Airy pulse.

### References

- [1] Siviloglou G A, Broky J, Dogariu A and Christodoulides D N 2007 *Phys. Rev. Lett.* **99** 213901
- [2] Muller H G, Bucksbaum P H, Schumacher D W and Zavriyev A 1990 *J. Phys. B: At. Mol. Opt. Phys.* **23** 2761
- [3] Harris A L 2023 *J. Phys. B: At. Mol. Opt. Phys.* <https://doi.org/10.1088/1361-6455/acc49e>

We gratefully acknowledge the support of the National Science Foundation under Grant No. PHY-2207209.

\* E-mail: [alharri@ilstu.edu](mailto:alharri@ilstu.edu)

## Optical tunnelling without a barrier?

A Weber<sup>1\*</sup>, and E Pisanty<sup>1</sup>

<sup>1</sup>Department of Physics, King's College London, London WC2R 2LS, United Kingdom

**Synopsis** We study tunnel ionization by a bichromatic strong-field driver in which the  $\omega$ -field is gradually replaced by the  $2\omega$ -field. We show that there is a tunnelling event contributing to the spectrum of ATI for which the electric field at the time of ionization is zero. This represents a purely nonadiabatic optical tunnelling ionization event which cannot be modelled within the semi-classical picture of optical tunnel ionization.

Tunnel ionization is a central phenomenon of strong-field physics involved in essentially all intense laser-matter interactions. Strong-field ionization in the tunnelling regime takes place as discrete events which the strong-field approximation describes via saddle points that give rise to the well-established formalism of quantum orbits.

In this work we consider the nonadiabatic above-threshold ionization of a 1D model atom by a bichromatic field. We pose the question of what happens to these ionization events (i.e., saddle points of the action) when we gradually replace a monochromatic beam with its second harmonic (Figs. 1(a) through (d)). Over this replacement, the number of ionization events per cycle of the fundamental changes from two to four. We therefore ask: Which ones are new? And, how did they get there?

The transition comprises two interesting features. Firstly, we identify configurations in which the saddle points describing ionization events coalesce in a caustic (triangle in Fig. 1(b)) and form a branch point. Here, continuous labelling of saddle points becomes impossible, the saddle point approximation breaks down and instead uniform approximations have to be employed.

More remarkably, we find that the new saddle points start contributing to the ionization yield long before the field changes sign (Fig. 1(c)). In other words, we present a tunnelling ionization event which occurs when the instantaneous electric field is zero, and hence at a time when there is no barrier. This results purely from a nonadiabatic picture of tunnelling, and presents a situation which cannot be modelled within the semi-classical picture of optical tunnel ionization.

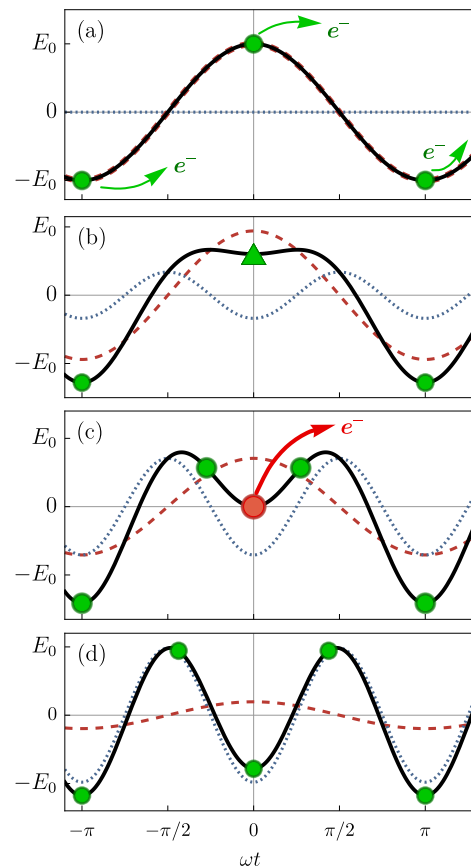


**Figure 1.** Total electric field formed by superposing a fundamental with its second harmonic. Green disks represent ionization events and the triangle marks the coalescence of solutions. The red disk in (c) shows a tunnelling ionization event when the electric field is zero and there is therefore no tunnelling barrier.

### References

- [1] Weber A and Pisanty E 2023 *in preparation*

\*E-mail: [anne.weber@kcl.ac.uk](mailto:anne.weber@kcl.ac.uk)

# Streaked angle-resolved shake-up photoemission from He

Hongyu Shi and Uwe Thumm

Department of Physics, Kansas State University, Manhattan, Kansas 66506, USA

**Synopsis** We calculated *ab initio* attosecond time-resolved spectra for streaked XUV photoemission (PE) from helium. For the  $n = 2$  shake-up channel, we find PE time-delays relative to direct [ $\text{He}^+ (n = 1)$ ] PE in agreement with the experimental and calculated results of Ref. [1]. In addition, we provide relative PE delays for  $n = 3$  shake-up. Within a multipole expansion and by comparing our *ab initio* results for angle-resolved spectra with a simplified single-active-electron calculation, we examine the contributions of the lowest multipole orders of the residual  $\text{He}^+(n = 2, 3)$  charge distributions on the PE delay.

To simulate the full streaking spectrum, we extended our FE-DVR [2] code for the *ab initio* calculation of single- and double photoionization of He to explore the effects of electronic correlation on attosecond time- and emission-angle-resolved spectra. Our IR-streaked XUV PE spectra and relative PE time delays between direct ionization ( $n = 1$ ) and shake-up ionization to the  $\text{He}^+ (n = 2)$  channel (i) agree with experimental and theoretical data in [1] and (ii) allow us to scrutinize the relevance of the residual excited  $\text{He}^+ (n = 2, 3)$  ion's transient induced dipole on the PE dynamics (Fig. 1).

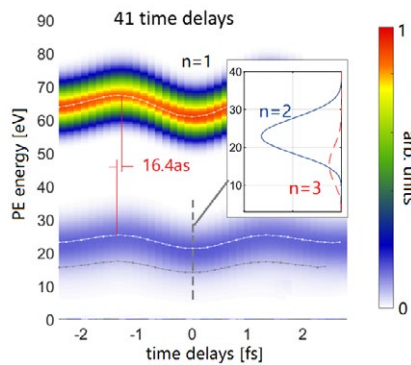


**Figure 1.** Single-90-eV-photon XUV PE spectrum of He, streaked by an 800 nm laser pulse, for direct and shake-up ionization. Inset: Line-out at zero delay.

The energy- and angle-resolved time delays in Fig. 2 show that the absolute streaking delays generally increase with photoelectron energy and decrease with the PE angle relative to the IR and XUV polarization direction.

To investigate the imprint of electric correlation in shake-up PE, we use a multipole analysis for the charge distribution of

$\text{He}^+$  in Fig. 3 [3]. We found the residual  $\text{He}^+ (n = 2, 3)$  charge distribution to oscillate with a period of 90 and 123 as respectively.

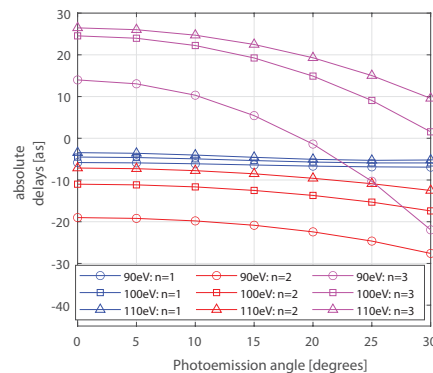


**Figure 2.** Angle- and energy-resolved absolute streaking delays for He for XUV photon energies of 90, 100, and 110 eV.

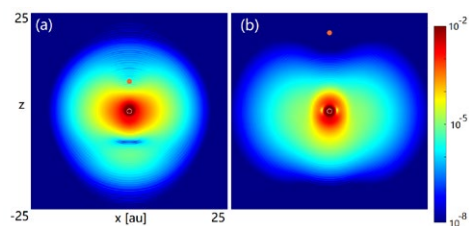


**Figure 3.**  $\text{He}^+$  charge distribution for (a) 136.6 as and (b) 360.4 as after ionization. The bright dot shows the most probable photoelectron position.

This work is supported by the US DoE and NSF.

## References

- [1] Ossiander M *et al.* 2017, *Nat. Phys.* **13**, 280
- [2] Liu A and Thumm U 2015, *Phys. Rev A* **91**, 043416
- [3] Shi H and Thumm U, to be published.

## Circular Dichroism in Multiphoton Ionization of Resonantly Excited Helium Ions near Channel Closing

R Wagner<sup>1,2</sup>, M Ilchen<sup>1,3,4</sup>, N Douguet<sup>5</sup>, C Callegari<sup>6</sup>, Z Delk<sup>5</sup>, M Di Fraia<sup>6</sup>, J Hofbrucker<sup>7</sup>, V Music<sup>1,3,4</sup>, O Plekan<sup>6</sup>, K C Prince<sup>6</sup>, D E Rivas<sup>1</sup>, P Schmidt<sup>1</sup>, A N Grum-Grzhimailo<sup>8</sup>, K Bartschat<sup>9</sup> and M Meyer<sup>1\*</sup>

<sup>1</sup>European XFEL, Holzkoppel 4, 22869 Schenefeld, Germany

<sup>2</sup>Department of Physics, Universität Hamburg, 22607 Hamburg, Germany

<sup>3</sup>Institut für Physik und CINSaT, Universität Kassel, 34132 Kassel, Germany

<sup>4</sup>Deutsches Elektronen-Synchrotron DESY, Notkestr. 85, 22607 Hamburg, Germany

<sup>5</sup>Department of Physics, Kennesaw State University, Marietta, Georgia 30060, USA

<sup>6</sup>Elettra-Sincrotrone Trieste S.C.p.A., 34149 Basovizza, Trieste, Italy

<sup>7</sup>Helmholtz-Institut Jena, Fröbelstieg 3, 07743 Jena, Germany

<sup>8</sup>Kirovogradskaya 40-2-216, 117534 Moscow, Russia

<sup>9</sup>Department of Physics and Astronomy, Drake University, Des Moines, Iowa 50311, USA

**Synopsis** We report a joint experimental and theoretical study of the intensity and wavelength dependence of the circular dichroism in multiphoton ionization of a resonantly excited state in ionized He atoms.

Investigations of the circular dichroism (CD) in photoionization of atoms and molecules reveal very detailed information about the underlying dynamics. For example, a strong intensity dependence of the CD in the multiphoton ionization of resonantly excited He ions was observed and explained by a polarization-dependent AC-Stark shift of the oriented He<sup>+</sup>(3p) resonance [1,2]. The present study confirms these earlier results and extends it to a much wider intensity range and to different wavelengths of the ionizing laser. It also reveals another important mechanism of resonance control via the optical laser, namely, Freeman resonances.

Combining circularly-polarized extreme ultraviolet (XUV) pulses from the free-electron laser FERMI and circularly-polarized near-infrared (NIR) pulses, the yields and angular distributions of photoelectrons generated by multiphoton ionization of excited He<sup>+</sup> ions, in the 3p ( $m=+1$ ) state, are examined. Using co- and counter-rotating NIR and XUV pulses, the CD of the multiphoton process was determined for different NIR intensities. A complex variation of the CD for the main line as well as the Above-Threshold-Ionization (ATI) channels is observed. The intensity-dependent shift of the ionization threshold causes channel closing. It is different for co- and counter-rotating pulses and hence opens new perspectives regarding coupling mechanisms and the fundamentals of CD.

The experimental results are compared with numerical predictions based on the solution of

the time-dependent Schrödinger equation to identify and interpret the pronounced variation of the experimentally observed CD. Figure 1 summarizes the results for the CD of the electron lines corresponding to multiphoton ionization (MPI) and the first and second ATI peaks.

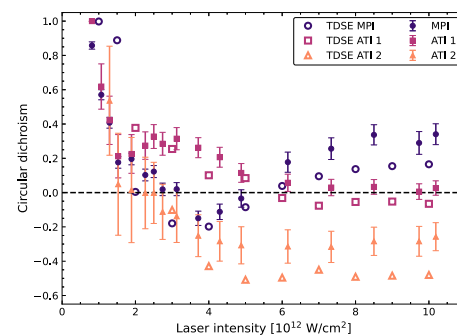


**Figure 1.** Experimental and theoretical CD values at different laser peak intensities for the MPI, ATI-1, and ATI-2 lines of the photoelectron spectrum. The solid symbols with error bars represent the experimental data; the TDSE predictions are displayed as open symbols.

Work supported by the Deutsche Forschungsgemeinschaft (DFG) through SFB-925–project 170620586 and the NSF under OAC-1834740, PHY-2012078, PHY-2110023, and ACCESS-090031.

### References

- [1] Ilchen M *et al* 2017 *Phys. Rev. Lett.* **118** 013002
- [2] Grum-Grzhimailo A N *et al* 2019 *Phys. Rev. A* **100** 033404

\* E-mail: [michael.meyer@xfel.eu](mailto:michael.meyer@xfel.eu)

## Quasi-chirp-free isolated attosecond pulse generation from atoms by optimized two near-infrared pulses and their second harmonic fields

J X Du<sup>1</sup>, G L Wang<sup>1\*</sup>, X Y Li<sup>2</sup> and X X Zhou<sup>1</sup>

<sup>1</sup>College of Physics and Electronic Engineering, Northwest Normal University, Lanzhou 730070, China

<sup>2</sup>College of Electrical Engineering, Northwest Minzu University, Lanzhou, 730030, China

**Synopsis** We theoretically demonstrate the possibility for generating the quasi-chirp-free isolated attosecond pulse (IAP) from neon atom driven by the optimized four-color laser field which are synthesized by two fundamental near-infrared lasers and their second-harmonic fields. We find that the high-order harmonics chirp is significantly reduced by using the optimized four-color laser pulse and the corresponding duration of IAP is shortened to 37 as which is almost the same as the fourier-transform-limited duration.

As everyone knows, there exists an inherent chirp in the attosecond pulse from the high-order harmonic. Therefore, the duration of the attosecond pulse generated by the various gating schemes is much longer than the duration of the fourier-transform-limited pulse. To shorten the attosecond pulse duration, there are many important methods proposed to compensate for harmonic chirp [1]. However, there is a certain degree of difficulty in the experimental implementation of the currently proposed method. Here we propose an efficient method for reducing the harmonic chirp in a single atom response by a combination of two near-infrared pulses and their second harmonic fields.

The form of the driven laser field with multi-color coherent synthesis can be written as

$$E(t) = \sum_{i=1}^n E_i f(t - \tau_i) \cos[\omega_i(t - \tau_i) + \varphi_i], \quad (1)$$

where  $E_i$  is the electric field amplitude,  $f(t)$  is the pulse envelope with the Gaussian shape,  $\omega_i$  is laser angular frequency,  $\tau_i$  is relative time delay, and  $\varphi_i$  is carrier envelope phase. In the optimization process, we take the total laser intensity of  $7 \times 10^{14} \text{W/cm}^2$ . The wavelengths of the laser are taken to be  $\lambda_1 = 800 \text{ nm}$  and  $\lambda_2 = 1200 \text{ nm}$  in the near-infrared, respectively, and the other two beam lasers are the second harmonic fields of the first and second color lasers. The duration of each laser is 16 fs. The high-order harmonics emissions are simulated by the strong field approximation model.

Figure 1 shows one of our main simulation results. It can be found that by applying second harmonic fields to the near-infrared laser fields

and optimizing the laser parameters, the emission properties of high-order harmonics from single-atom can be greatly improved, and the chirp-free harmonic emission can be realized within a certain energy range. As a result, the IAP with a pulse width up to 37 as is obtained which is almost same as the fourier-transform-limited duration of 36 as. After taking into account the macroscopic propagation effects, a IAP with pulse widths up to 41 as were obtained.

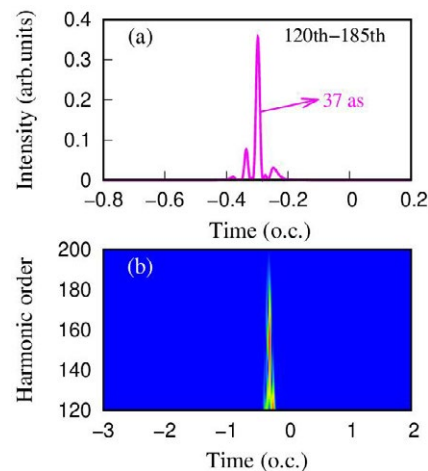


**Figure 1.** (a) The temporal profile of IAP synthesized from 120th-185th harmonics, driven by optimized the four-color field. (b) Time-frequency analysis of the harmonic spectra generated by optimized four-color field. o.c. is the optical cycle of 800 nm laser pulse.

Project supported by the National Natural Science Foundation of China under Grants No. 91850209 and No. 11964033.

### References

[1] Kazamias S *et al.* 2004 Phys. Rev. A [69 063416](#)

\* E-mail: [wanggl@nwnu.edu.cn](mailto:wanggl@nwnu.edu.cn)



## Complete reconstruction of an electron wavepacket generated by absorption of an attosecond pulse

J Vaughan<sup>1</sup>, S Mehmood<sup>2</sup>, C Cariker<sup>2</sup>, T Olsson<sup>1</sup>, S Jain<sup>1</sup>, S Burrows<sup>1</sup>, E Lindroth<sup>3</sup>, L Argenti<sup>2,4</sup>\*, and G M Laurent<sup>1</sup>†

<sup>1</sup> Department of Physics, Auburn University, 380 Duncan Drive, Auburn, AL 36849, USA

<sup>2</sup> Department of Physics, University of Central Florida, Orlando, Florida 32816, USA

<sup>3</sup> Department of Physics, Stockholm University, Stockholm SE-106 91, Sweden

<sup>4</sup> CREOL, University of Central Florida, Orlando, Florida 32816, USA

**Synopsis** In this work, we propose a novel interferometric scheme to measure time delays in photoionization. Our method is based on two angularly resolved RABBITT measurements performed sequentially with the same attosecond pulse train (APT) and two distinct probe field energies. We show that the time delays in the *bound-to-continuum* and *continuum-to-continuum* transitions can be retrieved from the experiment. Our method is supported by theoretical calculations demonstrating the feasibility of the retrieval procedure.

The recent development of XUV light sources with attosecond duration has opened up new avenues for experimentalists to probe electron dynamics in matter. So far, time-resolved measurements have been mostly achieved by using an attosecond pulse to trigger a given electronic process, and a phase-locked femtosecond field to probe its dynamics. The electron dynamics under scrutiny are thus unravelled by varying the time delay between the two pulses.

Several procedures have been proposed to extract the dynamics from such pump-probe measurements. The RABBITT technique [1] has proved to be particularly promising for accessing photoemission time delays. This measurement, however, probes three entangled unknowns, namely, the time delays in the *bound-to-continuum* and *continuum-to-continuum* transitions, as well as the spectral phase of the attosecond pulses. The retrieval of a given time delay, therefore, is impossible without some *a-priori* knowledge of the other two unknowns. To circumvent this issue, most RABBITT studies measure only the relative measurement between two distinct transitions [2, 3].

In this work, we propose a novel interferometric scheme to retrieve the time delays in the *bound-to-continuum* and *continuum-to-continuum* transitions from the same experiment. As shown in Fig. 1, our method is based on two angularly resolved RABBITT measurements performed sequentially with the same

\*E-mail: [Luca.Argenti@ucf.edu](mailto:Luca.Argenti@ucf.edu)

†E-mail: [glaurent@auburn.edu](mailto:glaurent@auburn.edu)

APT made of odd harmonics and two distinct probe fields (the fundamental field and its second harmonics). Within some approximations, we show that the time delays can be retrieved from the photoelectron angular distributions. Our method is supported by theoretical calculations demonstrating the feasibility of the retrieval procedure.

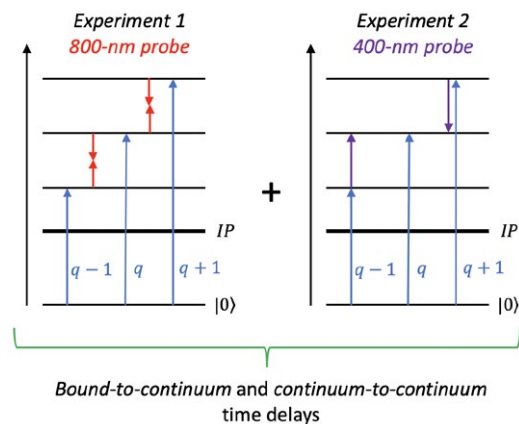


**Figure 1.** Schematic view of the experiment: two RABBITT traces taken sequentially with the same APT allows to reconstruct the *bound-to-continuum* and *continuum-to-continuum* time delays.

### References

- [1] Paul P M *et al* 2001 *Science* **292** 1689
- [2] Klünder K *et al* 2011 *New Journal of Physics* **106** 143002
- [3] Fuchs J *et al* 2020 *Optica* **7** 154

## Time-domain investigation of strong-field recollision to measure recombination time delay

D H Ko<sup>1,2\*</sup>, C Zhang<sup>3</sup>, G G Brown<sup>4</sup> and P B Corkum<sup>1,2†</sup>

<sup>1</sup>Joint Attosecond Science Laboratory, University of Ottawa, Ottawa, K1N 6N5, Canada

<sup>2</sup>Joint Attosecond Science Laboratory, National Research Council, Ottawa, K1A 0R6, Canada

<sup>3</sup>Beijing Institute of Technology, No. 5, South Street, Zhongguancun, Haidian District, Beijing, China

<sup>4</sup>Max Born Institute, Max Born Str. 2a, 12489 Berlin, Germany

**Synopsis** All-optical perturbative measurement of strong-field recollision process has been applied to demonstrate the investigation of time-delayed recombination phenomena while generating extreme ultraviolet (XUV) radiations. Consequently, we confirm that the *in situ* measurement by introducing a weak field to manipulate recollision trajectories can be utilized as an alternative way to study time-dependent dynamics of ultrafast multi-electron correlation in strong field physics.

Observing ultrafast dynamics in short time scale has been a great interest of attosecond communities. It was developed in attosecond regime since extremely short X-ray pulses were produced by high harmonic generation. Therefore, photoionization delays associated with different orbitals of neon and doubly excited states of helium were investigated by photoelectron streaking. These experiments called as *ex situ* measurements of ultrafast phenomena have been a standard attosecond metrology, taking place the generation and measurement of attosecond pulses separately.

Here, we demonstrate perturbative measurement of recombination time delays while generating XUV radiations in recollision process. By controlling the strong-field-driven electron-ion collision with a weak field, the group delay of the recollision electron wave packet is retrieved through the spectral modulation of attosecond pulses. It is *in situ* measurement of time delay as an alternative of the conventional attosecond measurements, utilizing the generated XUV photon as a detection source. This approach enables us to determine photorecombination delay of 150 as originated from Cooper minimum of argon [1]. It is clearly confirmed by a TD-DFT simulation with the experimental conditions. Recently, we develop a highly efficient way to *in situ* measurement by linking it with near-field imaging technique to characterize the attosecond pulse using a single spectral image [2]. We apply this all-optical single image measurement of an attosecond pulse to explore the xenon giant

resonance, verifying a large delay above the photon energy of 75 eV as presented in Figure 1. Our results advocate a new paradigm of attosecond science, observing ultrafast phenomena by modulating recollisional processes with a weak field under an intense laser field.

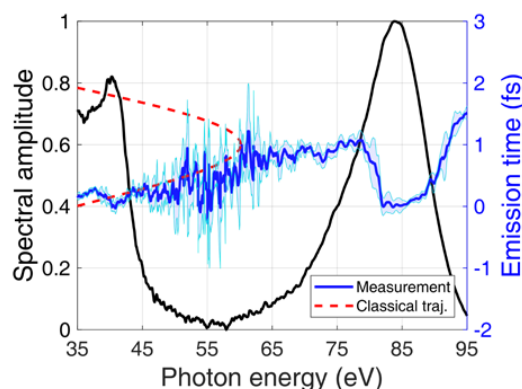


**Figure 1.** Spectral amplitude (black) and emission time (blue) of an attosecond pulse at the xenon giant resonance. The red-dashed-line indicates the classically calculated dispersion curve of an attosecond pulse due to different electron trajectories for each photon energy.

### References

- [1] Zhang C, Brown G G, Ko D H and Corkum P B 2021 arXiv:[2104.00844](https://arxiv.org/abs/2104.00844)
- [2] Ko D H, Brown G G, Zhang C and Corkum P B 2021 *Optica* **8** 1632-1637

\* E-mail: [donghyuk.ko@uottawa.ca](mailto:donghyuk.ko@uottawa.ca)

† E-mail: [pcorkum@uottawa.ca](mailto:pcorkum@uottawa.ca)

## Nondipole study of backward emission of electrons in ionization driven by high-frequency laser pulses

M C Suster\*, J Derlikiewicz, F Cajiao Vélez, J Z Kamiński, K Krajewska

Institute of Theoretical Physics, Faculty of Physics, University of Warsaw, Pasteura 5, 02-093 Warsaw, Poland

**Synopsis** Using a new numerical framework for treating light-matter interactions beyond the dipole approximation, we show that the backward emission in ionization driven by high-frequency laser pulses is an inherently quantum effect stemming from the "post-pulse" spreading of the electron wave packet combined with the Coulomb focusing effect.

The field of ultrafast lasers, i.e., devices capable of generating ultrashort pulses of light, is one of the fastest-growing branches of laser technology. Such sources of radiation have led to numerous scientific breakthroughs and enabled revolutionary discoveries and applications in medicine, telecommunication, and manufacturing, among others. Further development of advanced laser techniques for fundamental and applied research heavily relies on theoretical and numerical resources that provide necessary insight into the mechanisms governing complex light-matter interactions at multiple regimes of parameters.

Here, we propose a new method for numerically solving the time-dependent Schrödinger equation operating beyond the dipole approximation, i.e., accounting for nondipole effects without the use of any additional approximations, corrections, or unitary transformations [1]. It relies on a combination of the Suzuki-Trotter scheme combined with the split-step Fourier approach [2, 3]. With this new tool, we show that the ionization process is governed by two distinct mechanisms depending on whether it is driven by low- or high-frequency laser pulses. In the former case, the entire interaction of the electrons with the parent ion takes place in the presence of the laser field. Thus, as expected, the rescattering processes are predominant [4, 6, 5, 7]. In the latter, however, the rescattering processes are negligible, as the electron wave packet is forced out of the atom entirely at the very beginning of its

interaction with the laser pulse. The center of the wave packet closely follows the characteristic figure-eight trajectory stemming from the classical equations of motion. When the pulse is over, the electron wave packet starts to spread out and the portion of it that reaches the parent ion experiences Coulomb focusing. As a result, a rich interference structure in the photoelectron momentum distribution forms opposite to the direction of light propagation, and a significant portion of photoelectrons gets emitted in that direction. This demonstrates that the backward emission in ionization driven by high-frequency pulses is an inherently quantum effect. Furthermore, it contradicts the current status quo in which the presence of electrons opposite to the direction of pulse propagation is thought to be caused by a fully classical "in-pulse" trajectory modification [8].

### References

- [1] Suster M C *et al.* 2022 *arXiv* [arXiv:2211.15126](https://arxiv.org/abs/2211.15126) (submitted to *Phys. Rev. A*)
- [2] Muslu G M and Erbay H A 2005 *Math. Comput. Simul.* **67** 581-595
- [3] Hatano N and Suzuki M 2005 *Springer-Verlag LNP* **679** 37-68
- [4] Smeenk C T L *et al.* 2011 *Phys. Rev. Lett.* **106** 193002
- [5] Reiss H R 2014 *J. Phys. B: At. Mol. Opt. Phys.* **47** 204006
- [6] Ludwig A *et al.* 2014 *Phys. Rev. Lett.* **113** 243001
- [7] Cajiao Vélez F *et al.* 2018 *Phys. Rev. A* **97** 043421
- [8] Førré M *et al.* 2006 *Phys. Rev. Lett.* **97** 043601

---

\*E-mail: [mcsuster@fuw.edu.pl](mailto:mcsuster@fuw.edu.pl)

## A comparison study for high-order harmonic generation in helium

A T Bondy<sup>1,2</sup>, S Saha<sup>2</sup>, N Douguet<sup>3</sup>, K R Hamilton<sup>4</sup>, A C Brown<sup>5</sup>, and K Bartschat<sup>2\*</sup>

<sup>1</sup>Department of Physics, University of Windsor, Windsor, Ontario N9B 3P4, Canada

<sup>2</sup>Department of Physics and Astronomy, Drake University, Des Moines, Iowa 50311, USA

<sup>3</sup>Department of Physics, Kennesaw State University, Kennesaw, Georgia 30144, USA

<sup>4</sup>Department of Physics, University of Colorado Denver, Denver, Colorado 80204, USA

<sup>5</sup>Centre for Light-Matter Interactions, Queen's University Belfast, Belfast BT7 1NN, Northern Ireland

**Synopsis** We report calculations for high-order harmonic generation in helium and compare predictions from a single-active-electron model and several coupled-channel approaches. Given the sensitivity of the predictions to details of the models, we suggest that results for HHG spectra *always* be reported on an absolute scale.

High-order harmonic generation (HHG) is an important nonlinear process to generate extreme ultraviolet radiation by exposing an atom or molecule to intense long-wavelength infrared (IR) pulses and taking advantage of the radiation emitted when the active electron recollides with the target. HHG can *qualitatively* be understood in terms of the semiclassical “three-step model” model suggested by Corkum [1].

While the model has been extremely successful in predicting a cut-off frequency for the plateau in the HHG spectrum, which has been verified by many experiments as well as calculations using a variety of models, it does not provide any information regarding the conversion efficiency, essentially the area under the plateau. Even though this is a quantifiable observable (similar to the *absolute* cross section in photoionization or charged-particle collisions) and is also of great practical importance, experimentalists and theorists alike tend to only present the results of their measurements and calculations on a *relative* scale. A notable exception is the recent paper by Finger *et al.* [2] who advocated the publication of absolute numbers.

In the current work, we investigate the emission spectrum after a 6-cycle (3 ramp-on, 3 ramp-off) IR pulse with a central wavelength of 800 nm, peak intensity  $10^{14}$  W/cm<sup>2</sup>, and a sine-squared envelope of the electric field irradiates a helium atom. Specifically, we compare results from a single-active-electron (SAE) model with those obtained with the R-matrix with time-dependence (RMT) [3] method. In particular, we analyze the effects of the target description and the potential influence of channel coupling.

\*E-mail: [klaus.bartschat@drake.edu](mailto:klaus.bartschat@drake.edu)

Our preliminary results in Fig. 1 indicate that these effects are by no means negligible. The SAE and 1stHF predictions are close due to similar 1s orbitals being used, but convergence with the number of states in the close-coupling expansion has not yet been achieved.

We suggest that theoretical predictions for HHG spectra *always* be reported on absolute scales to better compare the various treatments.

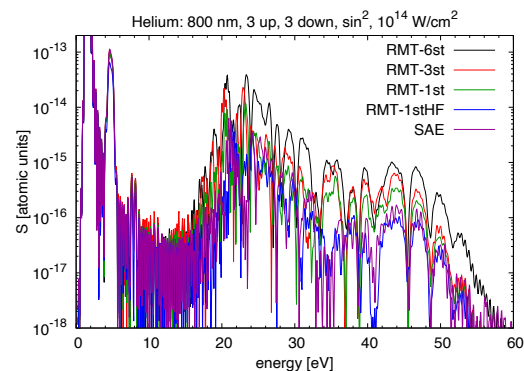


**Figure 1.** Emission spectrum obtained with SAE and RMT with only the He<sup>+</sup> ground state (1-st) but different 1s orbitals (ionic and Hartree-Fock of the He initial state), and added coupling to the  $n=2$  (3-st) and further the  $n=3$  (6-st) ionic states. The dominant fundamental is cut off to improve the readability of the other results.

Work supported by NSERC and the NSF under OAC-1834740, PHY-2012078, PHY-2110023, and ACCESS-090031.

### References

- [1] Corkum P B 1993 *Phys. Rev. Lett.* **71** 1994
- [2] Finger K *et al* 2022 *Phys. Rev. A* **106** 063113
- [3] Brown A C *et al* 2020 *Comp. Phys. Comm.* **250** 107062

## Analytical Guidelines to Choose the Right Pressure Profile for High-harmonic Generation in Gas Targets

B Major<sup>1,2\*</sup> and K Varjú<sup>1,2</sup>

<sup>1</sup> ELI ALPS, ELI-HU Non-Profit Ltd., Wolfgang Sandner utca 3., Szeged, 6728, Hungary

<sup>2</sup> Department of Optics and Quantum Electronics, University of Szeged, Dóm tér 9., Szeged, 6720, Hungary

**Synopsis** We extend the model proposed by Constant and co-workers [PRL 82, 1668 (1999)] to analyze phase matching of high-harmonic generation in gases; and introduce new guidelines to choose the right pressure profile for flux optimization.

In the past decades high-harmonic generation (HHG) in gases has become the main, table-top source of coherent extreme-ultraviolet (XUV) radiation, also giving the possibility to obtain attosecond pulses [1]. There is continuous work ongoing for optimization to achieve high photon flux with these sources [2]. In short, this can be achieved by optimizing phase matching. For HHG, a one-dimensional phase-matching model was proposed more than two decades ago [3], which provides rule-of-thumb guidelines to obtain optimal generation conditions, and is still followed nowadays [2]. This model simplifies macroscopic HHG to a situation where all relevant parameters are constant in the generation volume. Since this is generally not true, here we extend this model to deal with situations where these parameters vary linearly with propagation distance, still in an analytical form, providing further simply applicable laws for optimizing HHG in gases [4]. This model is also used to obtain guidelines on choosing an optimal pressure profile for the gas target [4].

As proposed by Constant et. al. using their one-dimensional model [3], to have at least half of the absorption-limited maximum of flux during high-harmonic generation, there are two conditions to fulfill: the coherence length ( $L_{\text{coh}}$ ) of the generated radiation has to be at least  $2\pi$  times the absorption length ( $L_{\text{abs}}$ ), and the medium length ( $L_{\text{med}}$ ) has to be at least three times the absorption length [3]. In a general, dimensionless form this can be expressed as  $R < 1$  and  $L > 1.5$ , where  $R = 2\pi L_{\text{abs}} / L_{\text{coh}}$  and  $L = 0.5 L_{\text{med}} / L_{\text{abs}}$  are dimensionless measures of coherence length and medium length.

It can be shown that the model is extendable, and it can be used when a gas density that changes linearly with propagation distance  $z$

(see Fig. 1). So we studied the effect of the pressure gradient at the end of the medium for different pressure profiles, like a trapezoidal. A general conclusion of the results, shown by the curves in Fig. 1, is that it is crucial to maintain a steep density gradient at the end of the medium to not lose the generated photons. Thanks to the dimensionless expressions [4], it can be shown that to have at least 4/5 of the XUV maintained, the gradient has to be shorter than 1/5 of the absorption length (see inset of Fig. 1).

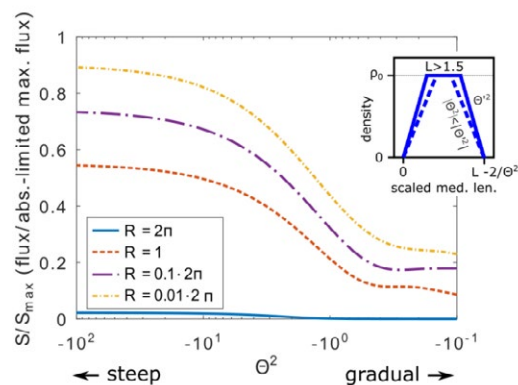


**Figure 1.** The effect of the medium-end gradient of gas density on the achievable XUV flux for a trapezoidal pressure profile (see inset) with different pressure gradients  $\theta^2 = \rho_1 / \rho_0^2$ , defined by  $\rho(z) = \rho_0 + \rho_1 \times z$ .

### References

- [1] Li J et al. 2020 *Nat. Commun.* **11** 2748
- [2] R Weissenbilder et al. 2022 *Nat. Rev. Phys.* **4** 713-722
- [3] E Constant et al. 1999 *Phys. Rev. Lett.* **82** 1668-1671
- [4] B Major and K Varjú 2021 *J. Phys. B: At. Mol. Opt. Phys.* **54** 224002

\* E-mail: [balazs.major@eli-alps.hu](mailto:balazs.major@eli-alps.hu)



## High-order harmonic generation of alkali metals in few-cycle laser pulses

C Y Lin\*

Department of Physics, Soochow University, Taipei, 111, Taiwan

**Synopsis** High-order harmonic generation of atoms in ultrashort laser pulses is one of the important approaches to producing ultrashort attosecond pulses. For few-cycle driving pulses, the carrier-envelope phase becomes a crucial factor for the control of laser-atom interactions. In the present work, we take alkali metals as target atoms to investigate the nonlinear process of high-order harmonic generation using a time-dependent theoretical method. The calculated results showing the influence of the carrier-envelope phase on electron dynamics in ionization processes are exhibited.

With the advances of laser technology, it has been feasible to shape and control intense laser pulses composed only of a few optical cycles. The rapid variation of electric field during one cycle in such pulses lead to the significant influence on electron dynamics. The temporal offset between the maximum of pulse envelope and of optical cycle, namely carrier-envelope phase, becomes a crucial factor for the control of laser-atom interactions [1]. As one of the most appealing processes in strong field physics, high-order harmonic generation has drawn much attention for its ability of producing isolated attosecond pulses. Considerable efforts have been devoted to investigate the role of carrier-envelope phase on high-order harmonic generation. Using ultrashort driving pulse, one can enhance the yield and cutoff energies of the high-order harmonic generation profoundly [2].

Owing to the features of one valence electron on the outer-most energy shell and lower binding energies as compared to rare gas atoms, we take alkali metals as target atoms to study the nonlinear process of high-order harmonic generation. A time-dependent scheme is adopted to investigate the ionization of alkali metals by various shapes of few-cycle laser pulses, which are controlled by the carrier-envelope phase. Short

iterative Lanczos method [3] and finite-element discrete variable representation [4] are utilized to characterize the temporal propagation and spatial discretization of atomic wavefunctions, respectively. Based on the single active electron approximation, alkali metals are modeled by a pseudo-potential accounting for the frozen inner electrons.

In this work, we explore the influence of laser carrier-envelope phase on ionization processes of alkali-metal atoms. Pulse duration dependence of the Ionization probability is illustrated. Airy peaks with uneven spacing in the high-order harmonic generation spectra are exhibited. The sensitivity of carrier-envelope phase on induced dipole moments and high-order harmonic spectra are demonstrated and discussed. Our results are useful for the manipulation of electron dynamics through the intense and short laser pulse.

### References

- [1] Baltuška, A., Udem, T., Uiberacker, M. et al. 2003 *Nature* **421** 611
- [2] Neyra, E., Videla, F., Ciappina, M. F. et al. 2018 *Phys. Rev. A* **98** 031403
- [3] Schneider, B. I., Gharibnejad, H. 2020 *Nat Rev Phys* **2** 89
- [4] Lin, C. Y., Ho, Y. K. 2011 *Phys. Rev. A* **84** 023407

---

\*E-mail: [cylin@gm.scu.edu.tw](mailto:cylin@gm.scu.edu.tw)

## Investigation of the spatial distribution of atomic high-order harmonic generation using the bohmian trajectories scheme

Susu Zhang<sup>1</sup>, Yue Qiao<sup>1</sup>, Jun Wang<sup>1</sup>, Fuming Guo<sup>1</sup> and Yujun Yang<sup>1\*</sup>

<sup>1</sup>Institute of Atomic and Molecular Physics, Jilin University, Changchun, 130012, China

**Synopsis** The interaction between matter and intense laser produces high-order harmonic radiation. The generation of the high-order harmonic can be understood as the ionized electrons return to the different spatial positions of the parent ions to produce coherent emission of high-energy photons. In order to explore the spatial distribution difference of different energy harmonics emitted on the atomic scale, the Bohmian trajectories scheme is applied.

High-order harmonic generation (HHG) can be observed when an intense laser interacts with atoms and molecules. The physical mechanism of HHG can be given by the semi-classical rescattering model [1]. However, this theory does not consider the effect of the spatial distribution of the ion wave packet on HHG. The Bohmian trajectories scheme not only contains all quantum information, but also retains the particle property of the electron wave packet. Therefore, this paper proposes to use the Bohmian trajectories scheme to study the HHG at different spatial positions.

By numerically solving the time-dependent Schrödinger equation (TDSE), the wave function of the system is obtained, and then the Bohmian trajectories (BTs) are calculated [2]. The time-dependent dipole moment of the system can be obtained by using the BTs information, and Bohmian particles (BPs) are distributed near the core region according to different weights  $|\psi(x, t_0)|^2$  at the initial time, so the spatial distribution of HHG can be calculated. In this work, a linear polarization field at 800 nm is used to irradiate the He atom.

In Fig. 1(a), we present the harmonic spectra calculated by numerically solving TDSE and the Bohmian trajectories scheme. The harmonic spectra calculated by these two methods are in good agreement. Figure 1(b) depicts the HHG at different spatial distributions calculated by the Bohmian trajectories scheme. On the whole, the harmonics generated by the BPs distributed near the nucleus are stronger. However, the spatial distribution of harmonic emission presents different behavior for different harmonic energy. At the 10th, the resonance structure of harmonic

emission appears, and the spatial distribution of harmonic emission is wider. The spatial distribution of harmonics in the platform region presents the tilted structure, which is considered to be the result of multiple coherent emissions of BPs. In the cutoff region, the harmonic distribution generated by the BPs at different spatial positions is continuous.

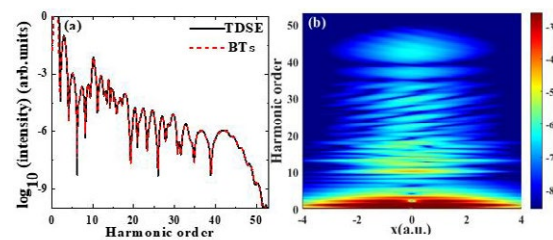


**Figure 1.** (a) Harmonic spectra calculated by numerical solution of TDSE and Bohmian trajectories scheme. (b) HHG at different spatial distributions calculated by the Bohmian trajectories scheme.

By using the Bohmian trajectories scheme, we can observe the spatial distribution difference of harmonic emission with different energy. Through further exploration, we are expected to use the spatial distribution effect of wave packets to give the harmonic emission mechanism of complex molecules and provide a more intuitive physical image.

This work was supported by the National Natural Science Foundation of China under Grants No. 12074145.

### References

- [1] Corkum P B *et al.* 1993 Phys. Rev. Lett. 71 1994.
- [2] Song Y *et al.* 2012 Phys. Rev. A 86 033424.

\* E-mail: [yangyj@jlu.edu.cn](mailto:yangyj@jlu.edu.cn)

## Photoionization of Rydberg atoms out of an optical dipole trap

K. L. Romans\*, B. P. Acharya, K. Foster, and D. Fischer†

Physics Department and LAMOR, Missouri University of Science & Technology, Rolla, MO 65409, USA

**Synopsis** The reaction-microscope (ReMi) [1] is an excellent tool for investigating ionization processes involving atomic Alkali targets when the ionizing laser is pulsed. However, when used in pump-probe schemes that rely on continuous wave probes vital information on the time of flight for each fragment is no longer known. This study reports on a method in which the ReMi method is extended in time and applied to ionization of  ${}^6\text{Li}$  atoms out of an optical dipole trap (ODT). These atoms are excited into Rydberg states and the resulting decay-dynamics and structure are examined.

Rydberg atoms are a well-suited platform for quantum information applications, because they can be cooled, trapped, and excited in optical dipole traps (ODTs), they have comparably long lifetimes, and they exhibit controllable long-range interactions. However, the interaction of the Rydberg atoms with the trapping laser field can result in photoionization and in a loss of the atoms. In this study we use a ReMi to investigate dynamics of Rydberg ionization in an ODT.

ReMi experiments rely typically on the use of pulsed lasers in order to characterize the time of flight (ToF) for each fragment, which – along with their positions on a detector – allow reconstructing their momenta [3]. In this current study, optically pumped  ${}^6\text{Li}$  atoms in prepared in an all-optical trap (AOT) [2] and are subjected to both a pulsed femtosecond and continuous wave (CW) ODT laser field. In the femtosecond pulse, atoms are excited to Rydberg states. With the addition of a CW field to create the ODT, these atoms can be ionized at any time between pulses and the ToF is no longer known. To extend the utility of the ReMi technique the total momentum of each ionization event (which is supposed to be close to zero due to momentum conservation) is minimized with respect to the ionization time of each electron. The derived times yielded from minimization are used to reconstruct the ToF spectra for the whole ensemble.

Once established, the time-resolved technique is applied to the system exploring both the time-independent structure of the momentum distributions as well as the time-dependent population dynamics of the system as it decays. Of particular interest, a circularly polarized fs-pulse is used

\*E-mail: [klnyc@mst.edu](mailto:klnyc@mst.edu)

†E-mail: [fischerda@mst.edu](mailto:fischerda@mst.edu)

exciting the system from either a 2S or 2P initial state into a superposition of Rydberg states while an ODT field constantly probes the system.

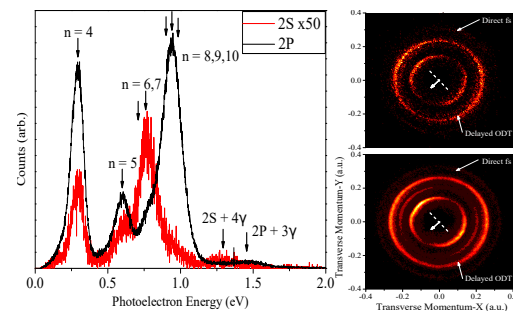


**Figure 1.** (Left) Photo-electron energy spectra for both 2S/2P initial states. Principle quantum numbers for dominate participating states are denoted as well as the direct multi-photon ionization peaks. (Right) Corresponding photo-electron transverse momentum spectra for both 2S (top) and 2P (bottom) states.

Apart of the practical relevance for quantum information technology, the photoionization of Rydberg atoms by optical radiation is particularly interesting, because it bears the potential to expose violations of the electric-dipole approximation, which is at the heart of essentially any perturbative atomic photoionization studies.

### References

- [1] R. Hubele, et al. *Review of Scientific Instruments* **86**, 033105 (2015)
- [2] S. Sharma, et al. *Phys. Rev. A* **97**, 043427 (2018)
- [3] D. Fischer, in *Ion-Atom Collisions*, edited by M. Schulz (De Gruyter, 2019) pp.103-156

## Photoionization of Atomic Sodium Near Threshold

C P Ballance<sup>1</sup>, T W Gorczyca<sup>2\*</sup>, N R Badnell<sup>3</sup>, S T Manson<sup>4</sup>, and D W Savin<sup>5</sup>

<sup>1</sup>School of Mathematics and Physics, Queen's University Belfast, Belfast, BT7 1NN, Northern Ireland, UK

<sup>2</sup>Department of Physics, Western Michigan University, Kalamazoo, Michigan 49008, USA

<sup>3</sup>Department of Physics, University of Strathclyde, Glasgow G4 0NG, UK

<sup>4</sup>Department of Physics and Astronomy, Georgia State University, Atlanta, Georgia 30303, USA

<sup>5</sup>Columbia Astrophysics Laboratory, Columbia University, New York, NY 10027

### Synopsis

R-matrix with pseudostates (RMPS) calculations are carried out for the low-energy photoionization of atomic sodium. Particular attention is paid to the Cooper minimum occurring just above threshold, and the spin-orbit splitting of minima, resulting in a non-zero total cross section.

Near-threshold photoionization of atomic Na has been of interest for basic physics. Theoretical studies have been carried out for the photoionization of Na for more than 70 years, beginning with the pioneering Hartree-Fock calculations of Seaton [1], where it was revealed that the minimum in the radial dipole matrix element occurred due to differing nodal structure of the absorbing electron and the photoelectron, as elucidated even earlier by Bates [2], and is now referred to as a Cooper Minimum [3]. This makes accurate computation of the near-threshold region problematic since the very small photoionization cross section in the region of the minimum is highly sensitive to the details of the wave functions. Experimentally, the early work of Hudson and Carter [4, 5] delineated the Cooper minimum, although the cross section at energies just above the minimum exhibits a strange feature. Here we theoretically quantify this Cooper minimum in detail and obtain reliable near-zero cross sections in the photon energy range just above threshold.

Of further interest, it was also pointed out by Seaton [1] that because of relativistic effects the zeros in the two continuum  $\epsilon p$  channels in the alkalis occur at different energies and as a result the minimum in the cross section does not reach zero. Cooper [3] subsequently analyzed the minima and showed that they were a ubiquitous general phenomenon in valence photoionization of atoms throughout the periodic table and not restricted to alkali spectra; for this reason, the minima are designated as Cooper minima.

\*E-mail: [gorczyca@wmich.edu](mailto:gorczyca@wmich.edu)

The work at GSU was supported in part by DOE, Office of Science. The work at U. Strathclyde was supported in part by UK STF. The work at WMU and Columbia University was supported in part by NASA.

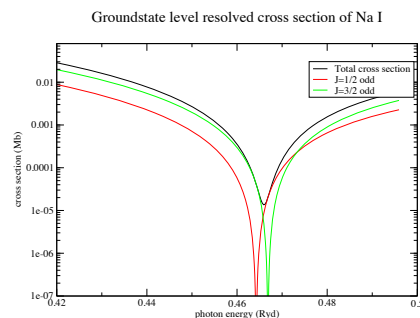


**Figure 1.** Na photoionization cross section in the vicinity of the Cooper minimum, showing the spin-orbit split  $j = 1/2$  and  $j = 3/2$  partial cross sections and the total cross section. The total cross section never reaches zero due to the energy shift between the two channels.

### References

- [1] Seaton M J 1951 *Proceedings of the Royal Society of London Series A* **208** 418
- [2] Bates D R 1946 *Mon. Not. Royal Astron. Soc.* **106** 432
- [3] Cooper J W 1962 *Phys. Rev.* **128** 681
- [4] Hudson R D and Carter V L 1967 *J. Opt. Soc. Am.* **57** 651
- [5] Hudson R D and Carter V L 1967 *J. Opt. Soc. Am.* **58** 227

## Probing Photoelectron Dynamics by Coulomb-distorted Terahertz Radiation

Ziyang Gan<sup>1,5</sup>, Kaixuan Zhang<sup>2</sup>, Yuan Gao<sup>1</sup>, Yizhu Zhang<sup>3</sup>, Tian-Min Yan<sup>1</sup>, and Yuhai Jiang<sup>4,1,5\*</sup>

<sup>1</sup>Shanghai Advanced Research Institute, Chinese Academy of Sciences, Shanghai 201210, China

<sup>2</sup>Zhejiang Provincial Key Laboratory of Ultra-Weak Magnetic-Field Space and Applied Technology, Hangzhou Innovation Institute, Beihang University, Hangzhou 310051, China

<sup>3</sup>Center for Terahertz waves and College of Precision Instrument and Optoelectronics Engineering, Key Laboratory of Opto-electronics Information and Technical Science, Ministry of Education, Tianjin University, Tianjin 300350, China

<sup>4</sup>ShanghaiTech University, Shanghai 201210, China

<sup>5</sup>University of Chinese Academy of Sciences, Beijing 100049, China

**Synopsis** We developed the Coulomb-corrected classical trajectory Monte Carlo (CTMC) method to intuitively establish the relation between the THz emission and the dynamics of photoelectron wave packet driven by both the external light and the Coulomb field. It provides a systematic method of all-optical detection for problems which are difficult to detect with photoelectrons, e.g., in material science, such as detecting lattice structure and the electron dynamics.

Radiation from terahertz wave (THz) to extreme ultraviolet (XUV) is an important means to understand and study the interactions between laser pulses and atoms or molecules in the strong field while containing a wealth of information about the structure and dynamics of the generating medium. The high-order harmonic generation (HHG) with the emission of high-energy photons provides a compact laboratory X-ray light source and delivers spatially and temporally coherent ultrashort pulses, paving the way toward attosecond sciences. In the contrast, the emission of the low-energy photons, known as the terahertz (THz) wave generation (TWG), is also observed when gas atomic mediums are ionized [1]. Recently, the TWG was considered within an all-optical measurement approach to determine the tunneling time of the emitting photoelectron wave packet [2], analogous to the implementation of attoclock with the measurement of photoelectron distributions.

According to Coulomb-corrected CTMC method, we present the evidence that strong field induced TWG can be significantly modulated by the Coulomb interaction, which affects the asymmetry of the propagating photoelectron wave packet, eventually influencing the THz emission. The mechanism indicates the effective potential of the parent core can be inferred by THz wave detection, providing an innovative all-optical scheme to

reconstruct the effective potential imposed onto the photoelectron and probe its wave packet dynamics.

The TWG is associated to the continuum-continuum transition, showing the long-term "smooth" motion that is normally far away from the parent core. Such long term motion, nevertheless, still contains critical information of the near-core potential due to its sensitive dependence on the initial stage when the Coulomb interaction is significant. Therefore, the TWG and HHG can play complementary roles in inferring information of systems despite of their distinct generation mechanisms.

In addition, present trajectory analysis of Coulomb-corrected CTMC method shows that the elastic scattering of parent core modifies the orientation of THz electric field by twisting the asymptotic momentum of electron trajectory, and the core recaptures the electron, which impedes the THz radiation. Further, the CTMC calculations predict that, the two-color mid-infrared field can effectively accelerate the electron rapidly away from the parent core to relieve the disturbance of Coulomb potential, and simultaneously create large transverse acceleration of trajectories, leading to the circularly-polarized THz radiation.

### References

- [1] H. Hamster *et al* 1993 *Phys. Rev. Lett.* 71,2725
- [2] I. Babushkin *et al* 2022 *Nat. Phys.* 1

\* E-mail: jiangyh3@shanghaitech.edu.cn



## Towards understanding the electronic structure of essential medicines: a photoemission study of aspirin, paracetamol, and ibuprofen in the gas phase

H Sa'adeh<sup>1,2\*</sup>, K C Prince<sup>2,3†</sup>, R Richter<sup>2</sup>, V Vasilyev<sup>4</sup>, D P Chong<sup>5</sup> and F Wang<sup>3</sup>

<sup>1</sup>Department of Physics, The University of Jordan, Amman 11942, Jordan

<sup>2</sup>Elettra Sincrotrone Trieste, Area Science Park, Basovizza, Trieste, Italy

<sup>3</sup>Department of Chemistry and Biotechnology, School of Science, Computing and Engineering Technologies, Swinburne University of Technology, Melbourne, Victoria 3122, Australia

<sup>4</sup>National Computational Infrastructure, Australian National University, Canberra, ACT 0200, Australia

<sup>5</sup>Department of Chemistry, University of British Columbia, Canada

**Synopsis** The electronic structures of aspirin, paracetamol, and ibuprofen have been studied by valence photoemission spectroscopy (PES) and core X-ray photoelectron spectroscopy (XPS) and interpreted with the aid of quantum chemical calculations. Although the three compounds share several motifs, their spectroscopic fingerprints indicate dissimilar electronic charge distributions, and therefore diverse chemical interactions.

We report results on three essential, commonly used medications: aspirin ( $C_9H_8O_4$ ), paracetamol ( $C_8H_9NO_2$ ), and ibuprofen ( $C_{13}H_{18}O_2$ ). Although they operate under physiological conditions, a first step in understanding their detailed electronic structure is investigation of the isolated molecules.

Valence band photoelectron spectra and theoretical calculations of the valence structures of paracetamol and ibuprofen were previously reported [1]. To our knowledge, there have been no reports of the valence photoelectron spectrum of aspirin, nor of the core photoelectron spectra of any of these three compounds.

We have measured valence band (VB) photoelectron spectrum of aspirin and the core level spectra of paracetamol, aspirin and ibuprofen (see, e.g., Figure 1). In addition, we have carried out quantum chemical calculations using the outer valence Green function (OVGF) model for the valence bands and core electron binding energy (CEBE) model for the core levels [2]. XPS probes the chemical state of the molecule because the binding energy shifts depend on the chemical environment of the atom that is ionized, while VB spectra provide complementary information about the valence states. The obtained spectra agree well with the present theoretical calculations, and aspirin and paracetamol are clearly related to their parent compounds, salicylic acid and 4-aminophenol, respectively. Although all three compounds contain a di-substituted benzene ring, the C 1s

spectra of the 6 carbon atoms are all different, indicating different local potentials, and hence underlining the diversity of these drugs.

Measurements were performed at the Gas-Phase (GAPH) Photoemission beamline of Elettra-Sincrotrone Trieste, Italy. Results and their interpretation in the light of our quantum chemical calculations will be presented.

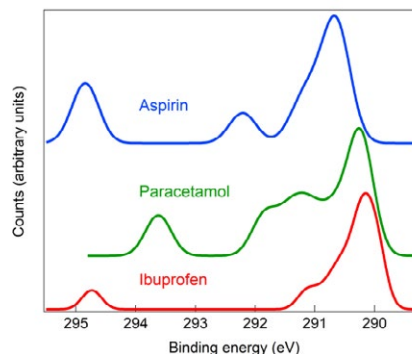


Figure 1. C 1s spectra of the investigated molecules [3].

### Acknowledgements

HS acknowledges the TRIL fellowship awarded by the ICTP, Trieste, Italy, and the one-year sabbatical leave (2022-2023) granted by the University of Jordan, Amman, Jordan.

### References

- [1] Novak I *et al* 2013 *Spectrochim. Acta A: Mol. Biomol. Spectrosc.* **112** 110
- [2] Chong D P 1996 *Canadian J. Chem.* **74** 1005
- [3] Sa'adeh H *et al* Under review.

\* E-mail: [Hanan.Saadeh@ju.edu.jo](mailto:Hanan.Saadeh@ju.edu.jo)

† E-mail: [Prince@elettra.eu](mailto:Prince@elettra.eu)

## Isomer effects and orbital features in the ellipticity dependence of high-order harmonics from C<sub>20</sub> isomers

Km Akanksha Dubey<sup>1,2</sup>, Oren Cohen<sup>3</sup> and Marcelo F. Ciappina<sup>1,2\*</sup>

<sup>1</sup>Physics Program, Guangdong Technion-Israel Institute of Technology, Shantou 515063, Guangdong, China

<sup>2</sup>Technion-Israel Institute of Technology, Haifa 32000, Israel

<sup>3</sup>Solid State Institute and Physics Department, Technion-Israel Institute of Technology, Haifa 3200003, Israel

**Synopsis** The generation of coherent extreme ultraviolet radiation (XUV) using high-order harmonic generation (HHG) is typically obstructed due to its low conversion efficiency. Thus, there exists a steady search for non-linear media able to enhance the HHG yield. Here, large-size quantum objects, for instance; nanomaterials and clusters, are the objects of interest. In our study, we choose the smallest fullerene and its isomers to study the ellipticity dependence and geometrical effects present in the HHG spectra. The impact of different orbital contributions on the HHG process is assessed.

In modern times, strong-field physics has emerged at a forefront of exciting research. The underlying electron dynamics in giant targets, as carbon clusters/fullerenes, still contain rich physics encoded in the many-body effect combined together with atom-like features [1–4]. Carbon clusters provide additional flexibility for the implementation of several morphological shapes. The enhancement in the HHG efficiency is attributed to their intrinsic characteristics, an increase in the concentration of emitters, an enhanced recombination cross section compared to those of atoms, and additional degrees of freedom. We present a theoretical study of HHG in C<sub>20</sub> and its isomers (Table 1), using a molecular version of the strong-field approximation (MSFA).

**Table 1.** Intrinsic features of cage, bowl, and ring isomers of C<sub>20</sub>. All values are in atomic units.

	radius	$I_p$ (HOMO),	$I_p$ (HOMO-1)
Cage	3.8688	0.2092	0.2700
Bowl	6.0586	0.2689	0.2689
Ring	7.7695	0.2212	0.2226

The initial molecular wavefunction is evaluated by employing GAMESS, within the framework of density functional theory (DFT) with B3LYP functional in a 6-311G basis set. As a test calculation, we primarily choose two atomic centers (labeled 1 & 2) out of the 20 carbon atoms in the various isomeric geometries. An electron ionized from one center and recombining to the same center gives rise to the so-called *direct harmonics* (DH). On the other hand, an electron ion-

\*E-mail: [marcelo.ciappina@gtiit.edu.cn](mailto:marcelo.ciappina@gtiit.edu.cn)

ized at one center and recombined at the second one generates the *transfer/exchange harmonics* (TH/EH) [1, 2]. In principle, the overall HHG yield will be a coherent contribution from all the atomic centers in both the direct and transfer harmonics modes. In our calculations, the driving laser pulse has a wavelength of 800 nm, a peak intensity of  $5 \times 10^{14}$  (W/cm<sup>2</sup>), and a time duration of 8 cycles ( $\approx 20$  fs).

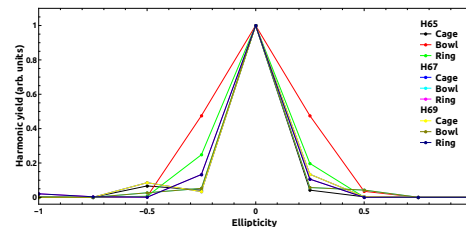


**Figure 1.** Ellipticity dependence of selected DH for different C<sub>20</sub> isomers.

Distinct geometrical features and the electronic structure of the C<sub>20</sub> are encoded in the HHG spectra; i.e. isomer effects show up. Therefore, by studying the behaviour of a particular harmonic as a function of the ellipticity (Fig. 1), we could pave the way toward a more complete understanding of the underlying electron dynamics in these complex targets.

### References

- [1] Ciappina M F, *et al.* 2007 *Phys. Rev. A* **76** 063406
- [2] Ciappina M F, *et al.* 2008 *Phys. Rev. A* **78** 063405
- [3] Ganeev R A, *et al.* 2010 *Phys. Rev. A* **82** 053831
- [4] Ganeev R A 2012 *J. Mod. Opt.* **59** 409–439

## Time-resolved resonant Auger scattering clocks distortion of a molecule

C Wang<sup>1</sup>, M M Gong<sup>1</sup>, Y J Cheng<sup>1</sup>, V Kimberg<sup>2</sup>, X J Liu<sup>3</sup>, O Vendrell<sup>4</sup>, K Ueda<sup>3,5</sup>, and S B Zhang<sup>1\*</sup>

<sup>1</sup>School of Physics and Information Technology, Shaanxi Normal University, Xi'an 710119, China

<sup>2</sup>Theoretical Chemistry and Biology, Royal Institute of Technology, Stockholm 10691, Sweden

<sup>3</sup>School Physical Science and Technology, ShanghaiTech University, Shanghai 201210, China

<sup>4</sup>Institute of Physical Chemistry, Heidelberg University, Heidelberg 69120, Germany

<sup>5</sup>Department of Chemistry, Tohoku University, Sendai 980-8578, Japan

**Synopsis** Resonant Auger scattering (RAS) provides information on the core-valence electronic transition that occurs during the femtosecond lifetime of the core-excited electronic state, impressing a rich fingerprint of the electronic structure and nuclear configuration at the time initiating RAS process. Here we suggest Using a femtosecond UV-pump and X-ray-probe, a strategy to resolve RAS of a highly distorted molecule in time is proposed. Varying the time delay, the RAS measurements imprint both their electronic structures and changing geometries. This strategy is showcased in H<sub>2</sub>O prepared in an O-H dissociative valence state, where molecular and fragment lines appear in RAS spectra as signatures of ultrafast dissociation. We analyze the specificity and information content about the molecular dynamics captured by the RAS spectra as a function of the time delay. Given the generality of this approach for a broad class of molecules, this work opens a new alternative pump-probe technique for mapping the core and valence dynamics with ultrashort X-ray probe pulses.

Using a femtosecond UV-pump and X-ray-probe, a strategy to resolve RAS of a highly distorted molecule in time is proposed. As illustrated in a H<sub>2</sub>O molecule, the UV pulse promotes the ground molecule into valence-excited dissociative state  $^1\tilde{A}(1b_1^{-1}4a_1^1)$ . The following nuclear evolution results in the stretching of the H<sub>2</sub>O molecule. RAS of a stretched H<sub>2</sub>O molecule can be triggered by a time-delayed femtosecond X-ray pulse, resonantly promoting an electron from a  $1a_1$  core orbital to the  $1b_1$  valence orbital and creating the core-excited state  $^1A'(1a_1^{-1}4a_1^1)$  [1].

We reveal that these time-dependent dynamical Auger spectra are directly related to different stretched geometries of the core-excited state or the positions of potential energy surfaces. And, when  $\bar{R}_{OH^2}$  is larger than 4.5 a.u. at  $\Delta t > 10$  fs, H<sub>2</sub>O could be well considered as combination of fragments OH<sup>1</sup> and H<sup>2</sup>. Meanwhile,  $\bar{R}_{OH^1}$  exhibits oscillations with a time-period of  $\sim 10$  fs, indicating the coherent vibrational dynamics [2] that revivals on the OH<sup>1</sup> fragment.

The present work paves a new avenue for clocking molecular distortion in the valence-excited state and mapping core-valence state dynamics in the clocked highly distorted geometry with respect to various nuclear coordinates, as well as the monitoring of coherence transfer for

\*E-mail: [song-bin.zhang@snnu.edu.cn](mailto:song-bin.zhang@snnu.edu.cn)

various molecules.

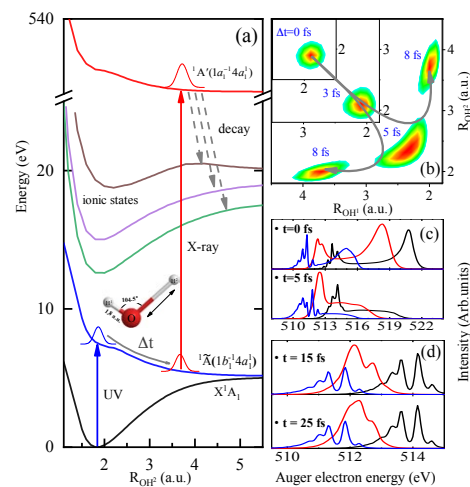


**Figure 1.** (a) Illustration under one-dimensional model. (b) Two-dimensional nuclear wave packet evolution on the dissociative state  $^1\tilde{A}(1b_1^{-1}4a_1^1)$  at different time-delays. (c) and (d) are RAS spectra with full PESs at different time-delays  $\Delta t$ .

### References

- [1] Wang C, Gong M M, Cheng Y J, Kimberg V, Liu X J, Vendrell O, Ueda K and Zhang S B Submitted.
- [2] Zhang S B and Rohringer N 2015 *Phys. Rev. A.* **92** 043420

## Ultrafast Dynamics in Donor-Acceptor Prototype Molecules by XUV-IR Attosecond Spectroscopy

F Fernández-Villoria<sup>1,2\*</sup>, F. Vismarra<sup>3,4</sup>, R. Borrego-Varillas<sup>3</sup>, Y. Wu<sup>3,4</sup>, D. Mocci<sup>3,4</sup>, L. Colaizzi<sup>3</sup>, M. Reduzzi<sup>3</sup>, F. Holzmeier<sup>5</sup>, L. Carlini<sup>6</sup>, P. Bolognesi<sup>6</sup>, R. Ritcher<sup>7</sup>, L. Avaldi<sup>6</sup>, J González-Vázquez<sup>2</sup>, A Palacios<sup>2</sup>, J. Santos<sup>1,8</sup>, M. Lucchini<sup>3,4</sup>, L. Bañares<sup>1,9</sup>, N. Martín<sup>1,8</sup>, F Martín<sup>1,2</sup> and M. Nisoli<sup>3,4</sup>

<sup>1</sup>Instituto Madrileño de Estudios Avanzados en Nanociencia, Cantoblanco, 28049, Spain

<sup>2</sup>Departamento de Química, Universidad Autónoma de Madrid, Cantoblanco, 28049, Spain

<sup>3</sup>Department of Physics, Politecnico di Milano, Milano, 20133 Italy

<sup>4</sup>IFN-CNR, Milano, 20133 Italy

<sup>5</sup>mec, Leuven, 3001, Belgium

<sup>6</sup>Istituto di Struttura della Materia-CNR (ISM-CNR), Roma, Italy

<sup>7</sup>Sincrotrone Trieste, Area Science Park, Basovizza, Trieste, Italy

<sup>8</sup>Departamento de Química Orgánica I, Universidad Complutense de Madrid, Madrid, 28040, Spain

<sup>9</sup>Departamento de Química Física, Universidad Complutense de Madrid, Madrid, 28040, Spain

**Synopsis** In this work we study both theoretically and experimentally the ultrafast dynamics following photoionization in small donor-acceptor molecules.

Electron transfer and charge transfer processes lay at the core of photovoltaic applications. In order to fully understand these processes real-time tracking of the coupled electron-nuclear dynamics, which take place on the few-femtosecond time scales is needed [1]. In this work we study both theoretically and experimentally the ultrafast dynamics triggered by photoionization in nitroanilines, the simplest donor-acceptor system. We focus on three different molecules with different donor radicals: 4-nitroaniline, 3-nitroaniline and N,N-Dimethyl-4-nitroaniline.

Experimentally a pump-probe scheme is applied to track the coupled electron-nuclear dynamics. Initially the molecules are ionized using an XUV pulse producing a cationic state which is probed by a second intense IR pulse. Information about the produced molecular fragments and their kinetic energy distribution is measured using mass spectrometry in order to gain insight on the above-mentioned dynamics. The most interesting behavior was observed for the NO<sup>+</sup> fragments which displayed an ultrafast transient signal with a formation time of the order of 10 fs and a decay between 20 and 30 fs. For a better understanding of the induced dynamics complementary PEPICO experiments were also carried

out allowing to assign these dynamics to precise fragmentation pathways, mediated by Coulomb explosion [2].

In order to rationalize the mechanisms giving rise to this kind of behavior, theoretical simulations using semi-classical trajectories with the surface hopping method and a multi reference approach for the electronic structure calculations were carried out. Our results suggest that the origin of the transient signal is due to a combination of two factors: first the differences in the potential energy surface of the molecular cation and the dication where the fragmentation takes place and second the rapid spreading of the cationic wave-packet produced during the initial ionization.

In summary, the combined experimental and theoretical approach allowed us to disentangle the complex dynamics following photoexcitation in nitroanilines and shed new light onto the role of ultrafast wave-packet spreading in the internal relaxation of prototype donor-acceptor systems.

### References

- [1] Nisoli M, et al. 2017 *Chem. Reviews* **117** 16
- [2] Cooper L, Shpinkova G, Rennie E E, Holland D M P and Shaw D A 2001 *Int. J. Mass Spectrometry* **207** 3

\*E-mail: [francisco.fernandez@imdea.org](mailto:francisco.fernandez@imdea.org)

## Scaling laws for the cooling dynamic of catacondensed PAH cations

S Indrajith<sup>1\*</sup>, MC Ji<sup>1</sup>, J E Navarro Navarrete<sup>1</sup>, P Martini<sup>1</sup>, J Bernard<sup>2</sup>, S Martin<sup>2</sup>, M H Stockett<sup>1</sup>, M Gatchell<sup>1</sup>, H Cederquist<sup>1</sup>, H T Schmidt<sup>1</sup> and H Zettergren<sup>1</sup>

<sup>1</sup>Department of Physics, Stockholm University, SE-106 91, Stockholm, Sweden

<sup>2</sup>Institut Lumière Matière (iLM), UMR5306 Université Lyon 1-CNRS, Université de Lyon, 69622, Villeurbanne, France

**Synopsis** Our aim in this study is to establish scaling laws for the internal energy dependent dissociation and radiative cooling rates as functions of the size of polycyclic aromatic hydrocarbons (PAHs) and their nitrogen substituted species. This kind of scaling laws could be used for modelling their survival probabilities in space.

Polycyclic Aromatic Hydrocarbons (PAHs) are a class of organic molecules based on two or more fused hexagonal aromatic carbon rings with hydrogen atoms attached at their outer rims. They are found and formed in a wide variety of environments. In the case of extraterrestrial environments, PAHs are believed to be an important component in interstellar dust and gas and as such are responsible for infrared emission features that dominate the spectra of many galactic and extragalactic sources [1]. PAHs can be categorised as peri- or cata-condensed defined by the arrangement of those rings. Here, we choose to focus on catacondensed PAHs cations such as naphthalene (C<sub>10</sub>H<sub>8</sub>), anthracene (C<sub>14</sub>H<sub>10</sub>) and tetracene (C<sub>18</sub>H<sub>12</sub>) but also nitrogen substituted PAHs (PANHs) such as acridine (C<sub>13</sub>H<sub>9</sub>N) and phenazine (C<sub>12</sub>H<sub>8</sub>N<sub>2</sub>).

When exposed to high-energy photons, PAH molecules may be electronically excited; thus increasing their internal temperature considerably by rapidly redistributing the absorbed energy among all available vibrational states. On longer timescales, they can then relax, by either fragmenting or emitting photons. Emission of IR photons (vibrational de-excitations) is typically a very slow process occurring on timescales exceeding seconds, while Recurrent Fluorescence (RF) or so called Poincaré fluorescence have been shown to effectively stabilize internally hot PAHs on millisecond timescales [2, 3]. In the RF process, vibrational excitation is converted into electronic excitation (inverse internal conversion - IIC) followed by relaxation to the electronic ground state through photon emission.

For the catacondensed PAHs considered in the present study, the emitted photons are in

\*E-mail: [suvasthika.indrajith@fysik.su.se](mailto:suvasthika.indrajith@fysik.su.se)

the 1,5-2,5 eV range, which leads to an efficient cooling and a much higher survival probability than cooling via IR emission alone. Key ingredients determining the RF rate are the energy of the excited state being populated in IIC and the oscillator strength for the electronic transition. As these scale with the size of the catacondensed PAHs, we aim to find a simple scaling law for the RF rate by combining theoretical and experimental results from the literature and from novel studies carried out at electrostatic storage ring facilities in Lyon [4] and in Stockholm [5] by members of the present collaboration (see Fig.1). In a similar fashion, we aim to establish a scaling law for the dissociation rate. With these in hand, the survival probabilities for any catacondensed PAH may be determined as a function of internal energy and used in, e.g., astrophysical modelling.

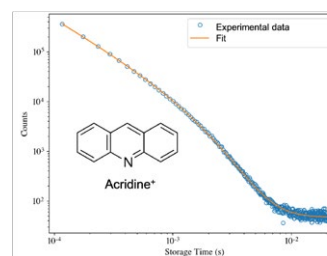


**Figure 1.** Spontaneous decay curve of acridine cations stored in DESIREE.

### References

- [1] Tielens 2008 *Ann. Rev. Astron. Astrophys.* **46** 289
- [2] Martin S et al. 2013 *Phys. Rev. Lett.* **110** 063003
- [3] Stockett et al. 2023 *Nat. Commun.* **14** 395
- [4] Bernard et al. 2019 *J. Chem. Phys.* **150** 054303
- [5] Bernard et al. 2023 *PCCP* accepted



## A new pulsed superfluid helium droplet machine for experiments at a free-electron laser beamline

J R Harries<sup>1\*</sup>, A Iguchi<sup>2,3</sup>, and S Kuma<sup>3†</sup>

<sup>1</sup>QST, SPring-8, Kouto 1-1-1, Sayo, Hyogo 679-5148, Japan

<sup>2</sup>RIKEN, Wako, Saitama 351-0198, Japan

<sup>3</sup>Tokyo Metropolitan University, Hachioji, Tokyo 192-0397, Japan

**Synopsis** We are developing new superfluid helium droplet machine producing a pulsed size-controlled beam tailored for imaging and spectroscopy experiments at a free-electron laser.

Superfluid helium droplets are ideally suited both for studying macroscopic quantum effects in isolated particles of nanometre to micrometre size, and as free-flying cryogenic media for studying encapsulated, cooled molecules and nanoparticles. X-ray free electron lasers (XFELs) are a versatile tool for studying both the droplets themselves using for example coherent X-ray diffraction imaging, and also for studying dynamics in encapsulated particles using for example pump-probe Coulomb explosion imaging.

Based on an existing design [1], we have developed a new portable droplet machine suited for use at an XFEL (or synchrotron) beamline.

Design considerations include: pulsed operation (using a Parker valve) for maximum versatility when using a pulsed lightsource, wide range of droplet size tunability, and modular design for integration with a range of downstream equipment.

The upper panel of the figure shows peak heights obtained by detecting mass-selected ions in a residual gas analyser, with the fragments created by electron-impact ionisation at a position 1.02 m from the pulsed nozzle, operating at a source pressure of 2.0 MPa and a repetition rate of 1 Hz.  $\text{He}_2^+$ ,  $\text{He}_3^+$ , and  $\text{He}_4^+$  fragments were detected. (A lower detector gain was used for  $\text{He}_2^+$  fragments so the intensities cannot be directly compared in this figure). The lower panel shows the time-of-flight spectra of detected  $\text{He}_3^+$  fragments. The increase in the yield of the larger fragments at temperatures below 10 K is indicative of the creation of very large droplets, and analysis is ongoing. The decrease at temperatures below 6 K is due to insufficient pumping of background helium. The nozzle assembly can be

\*E-mail: [harries.james@qst.go.jp](mailto:harries.james@qst.go.jp)

†E-mail: [susumu.kuma@riken.jp](mailto:susumu.kuma@riken.jp)

maintained at 3.8 K under 1 Hz operation.

We will present a detailed description of the apparatus, and hope to complete an analysis of the available droplet size distribution determined using a gas titration method.

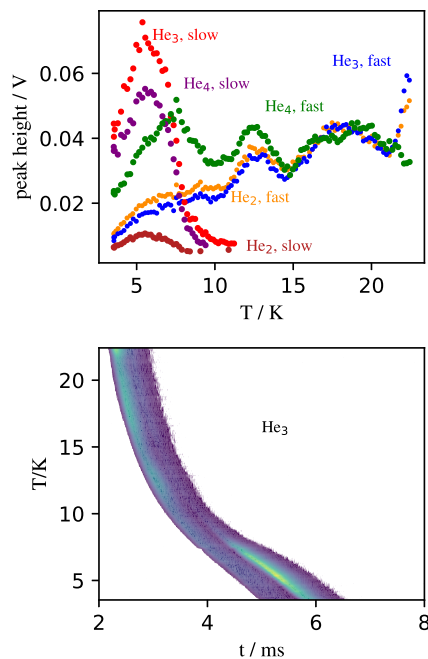


**Figure 1.** Peak heights of droplet fragments created by electron-impact ionisation as a function of nozzle assembly temperature (upper). Arrival times of  $\text{He}_3^+$  fragments (lower). The splitting into two components at lower temperatures can be seen.

### References

- [1] Kuma S and Azuma T 2017 *Cryogenics* **88** 76

## Ion-neutral coincidence experiments to characterize the photofragmentation of cyclo-dipeptides

Jacopo Charinelli<sup>1\*</sup>, Robert Richter<sup>2</sup>, Lorenzo Avaldi<sup>1</sup>, Paola Bolognesi<sup>1</sup>

<sup>1</sup>CNR - Istituto di Struttura della Materia (CNR - ISM), Area della Ricerca di Roma 1, Monterotondo Scalo, Italy

<sup>2</sup>Elettra, Sincrotrone Trieste S.C.p.A., Trieste, Italy

**Synopsis** In the photofragmentation of a cation at least one of the products is a neutral species, usually undetected in mass spectrometric studies. Here we show that a time of flight spectrometer can enable also the detection of the neutral moiety in coincidence with the charged partner. The technique is applied to the study of the VUV fragmentation of three *cyclo*-dipeptides (c-Alanine-Alanine, c-Glycine-Alanine and c-Glycine-Glycine).

Mass spectrometry in gas phase is a powerful technique to shed light on the molecular composition and the chemical-physics processes taking place in several environments from the deep space to the human body. The aim of the technique is to unveil the fragmentation paths resulting from the ionization of the target molecule. This is not a simple task because of the numerous undetected neutral moieties. Ion-neutral coincidence experiments are a powerful tool to provide information on all the actors of a metastable fragmentation, even when subsequent processes take place.

Ion-neutral coincidence experiments have been performed using a Wiley-McLaren TOF mass spectrometer and a rare gas discharge lamp as ionizing source<sup>1</sup>. The TOF spectrometer is operated in a continuous extraction mode, with DC electric fields in the extraction and acceleration regions. All photoelectrons released in the photoionisation are detected by an electron multiplier mounted behind the mesh of the repeller of the TOF spectrometer. The electron signal triggers a multihit TDC that measures the flight time of any charged/neutral particle that, impinging on the TOF detector, produces a signal.

In the two-body fragmentation of a cation, the parent ion ( $P_{ion}$ ) breaks into a daughter ion ( $D_{ion}$ ) and a neutral fragment ( $N_{frag}$ ). While ions can be handled by electric fields, neutrals cannot. Nevertheless, if they travel towards the TOF spectrometer and hit the detector with sufficient energy, they can be detected. In our set-up, with constant DC extraction fields, any ion begins its travel towards the TOF immediately at the time of its birth. Qualitatively, it is easy to visualize that when  $P_{ion}$  dissociates in a region where it is subject to an accelerating field then i) the flight time of  $D_{ion}$  with a smaller  $m/z$  will be shorter than the nominal flight time of  $P_{ion}$  while ii)  $N_{frag}$  travelling in a free flight at a constant speed may or may not reach the detector and be detected

after at a flight time longer than the nominal flight time of  $P_{ion}$ . The 'nominal flight time' corresponds to a prompt dissociation. Therefore a metastable dissociation produces a distribution of correlated partners ( $D_{ion}$ ,  $N_{frag}$ ) that can be measured in a coincidence experiment and encode the information on the position/time where the fragmentation occurred. As an example, the ion-neutral coincidence map for the fragmentation of the cyclo-alanine alanine (cAA) molecule<sup>1</sup> by VUV radiation is shown in Fig. 1. The sequence of successive fragmentations starting from the parent ion as well the existence of competing channels (for example  $99^+ \rightarrow 71^+$ ,  $58^+$  and  $44^+$ ) are clearly identified in the map.

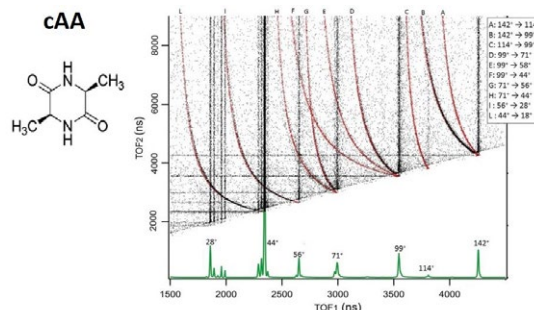


**Figure 1.** The mass spectrum (green) and 2D coincidence map obtained of the VUV photofragmentation of cAA molecule. The traces due to ion-neutral coincidences of metastable fragmentations are highlighted in red while the involved ionic moieties are reported in the inset.

### References

- [1] J. Chiarinelli et al. 2022 *Phys.Chem. Chem.Phys.* **24** 5855

\* E-mail: [jacopo.chiarinelli@ism.cnr.it](mailto:jacopo.chiarinelli@ism.cnr.it)

## Visualisation and laser-induced modification of a vibrational wave-packet revival in the excited $H_2$ molecule

G D Borisova<sup>1\*</sup>, P Barber Belda<sup>1</sup>, S Hu<sup>1</sup>, P Birk<sup>1</sup>, V Stooß<sup>1</sup>, M Hartmann<sup>1</sup>, D Fan<sup>1</sup>, R Moshhammer<sup>1</sup>, A Saenz<sup>2</sup>, C Ott<sup>1</sup> and T Pfeifer<sup>1†</sup>

<sup>1</sup>Max-Planck-Institut für Kernphysik, Saupfercheckweg 1, 69117 Heidelberg, Germany

<sup>2</sup>Institut für Physik, Humboldt-Universität zu Berlin, 12489 Berlin, Germany

**Synopsis** We use attosecond pulsed coherent extreme ultraviolet (XUV) light to spectrally resolve the vibrational bands of electronically singly excited states in molecular hydrogen. Selecting the vibronic resonances of only the  $D$  band, we reconstruct the time-dependent dipole response of the associated  $D$  vibrational wave packet and observe a signature of its revival. An additional interaction with a 5-fs near-infrared (NIR) pulse of adjustable intensity modifies the vibrational wave-packet revival, shifting it in time. We thus identify the NIR intensity as a knob to coherently control the nuclear dynamics in neutral  $H_2$  in an electronically excited state.

Extreme ultraviolet (XUV) light in the spectral range 13–17 eV drives multiple transitions between the ground state and excited vibronic states in the neutral hydrogen molecule, Fig.1(a). Applying spectral filtering to the rich absorption spectrum we select only the transitions to the electronically excited  $D^1\Pi_u 3p\pi$  state, Fig.1(b), and use the technique of real-time reconstruction of the dipole response [1] to obtain the time-dependent dipole of the  $D$  vibrational wave packet (WP), with the WP revival at 270 fs imprinted on it, Fig.1(c). A subsequent interaction with a 5-fs short near-infrared (NIR) pulse at a fixed time delay after the fast (attosecond-scale) XUV excitation modifies the excited vibrational wave packet and changes the revival signature in the reconstructed dipole, Fig.1(d). An experimental study of the intensity dependence of the WP revival and a supporting multi-level simulation solving the time-dependent Schrödinger equation show: the higher the NIR intensity, the earlier the revival time. In this general approach for wave-packet modification, transferable also to more complex molecules, the molecular ground state acts as the probe for the visualisation of the modified wave packet and only a pump and a control laser pulse are required, which makes the implemented experimental scheme non-destructive for the molecule [2].

### References

- [1] Stooß V *et al.* 2018 *Phys. Rev. Lett.* **121** 173005  
 [2] Borisova G D *et al.* 2023 [arXiv:2301.03908](https://arxiv.org/abs/2301.03908)

\*E-mail: [borisova@mpi-hd.mpg.de](mailto:borisova@mpi-hd.mpg.de)

†E-mail: [thomas.pfeifer@mpi-hd.mpg.de](mailto:thomas.pfeifer@mpi-hd.mpg.de)

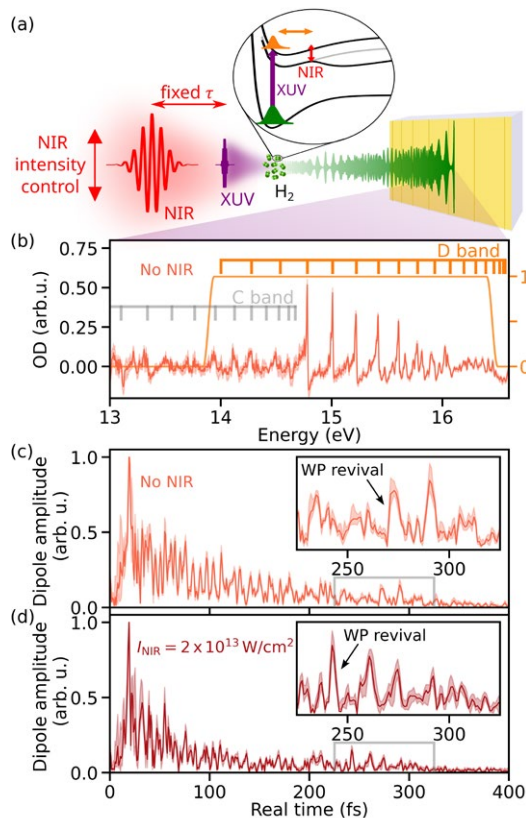


**Figure 1.** (a) Schematic of the experimental setup. (b) Optical density (OD) spectrum as measured after transmission through a 10 mbar 3 mm hydrogen sample. (c) and (d) Reconstructed time-dependent dipole amplitude of the  $D$ -state vibrational wave packet in an XUV-only configuration and for an NIR field with  $I_{\text{NIR}} \approx 2 \times 10^{13} \text{ W/cm}^2$ , respectively. The insets show the wave-packet revival region.

## Ultrafast temporal evolution of interatomic Coulombic decay in NeKr dimers

F Trinter<sup>1,2\*</sup>, T Miteva<sup>3</sup>, M Weller<sup>1,4</sup>, A Hartung<sup>1</sup>, M Richter<sup>1</sup>, J B Williams<sup>5</sup>, A Gatton<sup>4,6</sup>, B Gaire<sup>4</sup>, J Sartor<sup>6</sup>, A L Landers<sup>6</sup>, B Berry<sup>7</sup>, I Ben-Itzhak<sup>7</sup>, N Sisourat<sup>3</sup>, V Stumpf<sup>8</sup>, K Gokhberg<sup>8</sup>, R Dörner<sup>1</sup>, T Jahnke<sup>9</sup> and T Weber<sup>4</sup>

<sup>1</sup>Institut für Kernphysik, Goethe-Universität, 60438 Frankfurt am Main, Germany

<sup>2</sup>Molecular Physics, Fritz-Haber-Institut der Max-Planck-Gesellschaft, 14195 Berlin, Germany

<sup>3</sup>Laboratoire de Chimie Physique Matière et Rayonnement, UMR 7614, Sorbonne Université, CNRS, 75005 Paris, France

<sup>4</sup>Lawrence Berkeley National Laboratory, Chemical Sciences Division, Berkeley, California 94720, USA

<sup>5</sup>Department of Physics, University of Nevada, Reno, Nevada 89557, USA

<sup>6</sup>Department of Physics, Auburn University, Auburn, Alabama 36849, USA

<sup>7</sup>J. R. Macdonald Laboratory, Department of Physics, Kansas State University, Manhattan, Kansas 66506, USA

<sup>8</sup>Theoretische Chemie, Physikalisch-Chemisches Institut, Universität Heidelberg, 69120 Heidelberg, Germany

<sup>9</sup>European XFEL GmbH, 22869 Schenefeld, Germany

**Synopsis** Employing synchrotron radiation and COLTRIMS reaction microscopy, we investigate the ultrafast temporal evolution of interatomic Coulombic decay (ICD) in NeKr dimers. We show how ICD in NeKr evolves within the first 250 femtoseconds after photoionization. A time resolution of  $\sim 10$  fs is achieved, while changes in the internuclear distance as small as 0.3 Å are tracked.

We investigate interatomic Coulombic decay (ICD) in NeKr dimers after neon inner-valence photoionization using a synchrotron light source. We measure with high energy resolution the two singly charged ions of the Coulomb-exploding dimer dication and the photoelectron in coincidence. By carefully tracing the post-collision interaction between the photoelectron and the emitted ICD electron we are able to probe the temporal evolution of the state as it decays. Although the ionizing light pulses are 80 picoseconds long, we determine the lifetime of the intermediate dimer cation state and visualize the contraction of the nuclear structure on the femtosecond time scale [1-3].

Figure 1 shows the mean internuclear distance  $R$  in the  $\text{Ne}^+ + \text{Kr}^+$  breakup of the  $(\text{NeKr})^{++}$  dimer cation in the ICD process as a function of the decay time. For every decay time the black curve shows the maximum of a Gaussian function that was used to fit the experimental  $R$  data. The blue curve shows the theoretical results. A contraction of the NeKr dimer from 3.76 Å to 3.51 Å is clearly visible in the experimental data. The error in the experimental  $R$  is estimated to be  $\pm 0.15$  Å, which is represented by the grey shaded area. For the employed photon energy of 48.68 eV, we were able to extract decay times down to 10 fs. The green dashed line at 3.75 Å shows the mean in-

ternuclear distance of the neutral NeKr dimer, computed from the ground-state wave packet density distribution.

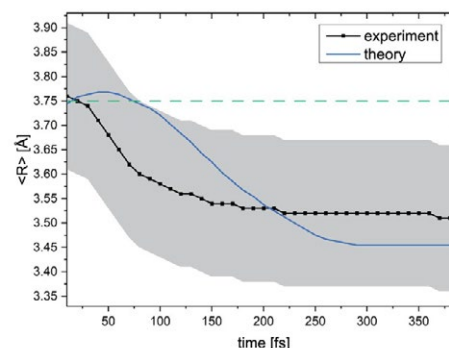


**Figure 1.** Mean internuclear distance  $R$  in the  $\text{Ne}^+ + \text{Kr}^+$  breakup of the  $(\text{NeKr})^{++}$  dimer cation in the ICD process as a function of the decay time.

### References

- [1] Trinter F et al. 2022 *Chem. Sci.* **13** 1789
- [2] Trinter F et al. 2013 *Phys. Rev. Lett.* **111** 093401
- [3] U. Fröhling et al. 2015 *J. Electron Spectrosc. Relat. Phenom.* **204** 237-244

\* E-mail: [trinter@atom.uni-frankfurt.de](mailto:trinter@atom.uni-frankfurt.de)

# Polarization-induced molecular photoionization delays and equivalence of RABITT and streaking dipole-laser coupling

J Benda<sup>1\*</sup> and Z Mašín<sup>1</sup>

<sup>1</sup>Institute of Theoretical Physics, Charles University, Prague 8, 180 00, Czech Republic

**Synopsis** We utilize the recently developed stationary molecular multi-photon theory to analyze the two-photon ionization amplitudes in RABITT experiments. We demonstrate that existence of dipole coupling between energetically close final states of the residual ion induces a new contribution to RABITT delay. Furthermore, we illustrate that dynamics of the initial state of a strongly polar molecule in the IR field gives rise to another delay in RABITT identical to dipole-laser coupling otherwise observable in attosecond streaking.

Photoionization delays provide an intriguing observable that delivers information about the photoionization event, sometimes with greater sensitivity than the photoionization cross sections. Direct measurement of these delays is experimentally inaccessible; however, several methods that employ absorption of further photons have been devised to overcome this limitation. These either make use of classical addition of momenta with the electromagnetic vector potential (attosecond streaking), or take advantage of subtle multi-pathway interference (reconstruction of attosecond beating by interference of two-photon transitions, RABITT). We show that the addition of the second (IR) field allows to study laser-induced electron correlation effects.

Theoretical analysis of above-threshold multi-photon ionization has been notoriously difficult and this process is typically solved either in fully time-dependent way or using asymptotic approximation. As a computationally very efficient alternative, a comprehensive time-independent molecular multi-photon theory [1] has been developed recently, which allows one to directly calculate multi-photon ionization amplitudes resolved in ion states and partial waves without the asymptotic approximation.

In this contribution we leverage the strength of the multi-photon method to discover an overlooked contribution to the RABITT sideband delay [2] that arises in the “ion-ion” transition during absorption of the probe IR photon. This delay is significant for residual cation states that are separated by energies comparable to the IR photon energy, and which have non-zero transi-

tion dipole.

Additionally, we analyze dynamics of the initial state of strongly polar molecules in the IR field, observing that the IR field dresses the initial state and gives rise to new emission/absorption pathways in RABITT on top of the standard XUV±IR pair [3]. Inclusion of these pathways results in appearance of the dipole-laser coupling delay known from attosecond streaking. Its effect is particularly strong in the molecular frame.

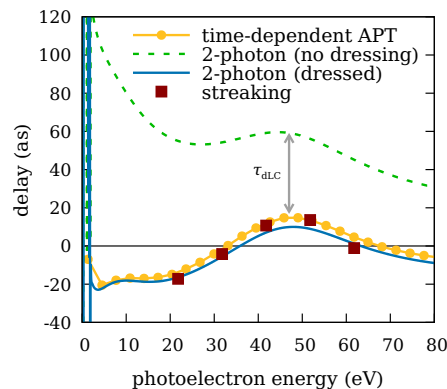


**Figure 1.** Calculated RABITT and streaking delays in LiH. Parallel configuration, emission from Li end, static exchange model, 780-nm IR field.

## References

- [1] Benda J and Mašín Z 2021 *Sci. Rep.* **11** 11686
- [2] Benda J, Mašín Z and Gorfinkiel J D 2022 *Phys. Rev. A* **105** 053101
- [3] Benda J and Mašín Z 2023 *ArXiv* 2209.06676

\*E-mail: [jakub.benda@matfyz.cuni.cz](mailto:jakub.benda@matfyz.cuni.cz)



## Photoionization and Resonance Formation in Formic Acid Monomer and Dimer

Julio C Ruivo<sup>1\*</sup>, Thomas Meltzer<sup>1</sup>, Alex G Harvey<sup>1</sup>, Jakub Benda<sup>1</sup> and Zdeněk Mašín<sup>1</sup>

<sup>1</sup>Institute of Theoretical Physics, Faculty of Mathematics and Physics, Charles University, V Holešovičkách 2, 180 00 Prague 8, Czech Republic

**Synopsis** We employed R-Matrix and multiple quantum chemistry methods to evaluate photoionization cross sections and infer shape resonance formation in the formic acid monomer and dimer molecules. We build a framework to study photoionization in molecular dimers with a well balanced description of target and continuum states which can be employed in further investigations of resonant states in nucleobase pairs.

The photophysics of nucleobases has been largely motivated by DNA damage induced by ultraviolet (UV) light. In particular, UV-induced long-lived charged-transfer (CT) states in stacked nucleobase pairs can decay by formation of mutant species [1]. Our work aims to study generation of CT states by electron impact and photoionization as alternative processes which have not been studied so far. We focus on formation of resonant states which are known to enhance elastic and inelastic collision processes and choose formic acid, a precursor of amino acids, as a simple model of nucleobases and a prototype target for the development of dimer scattering models.

However, modeling of continuum states of dimers poses serious computational difficulties owing to doubling of the number of electrons in the system compared to monomers. To make the calculations feasible requires development of efficient configuration-interaction approaches.

In this work we compare resonance formation in the formic acid monomer (FAM) and its dimer (FAD). We employed the R-Matrix method using the UKRmol+ suite [2] to calculate scattering and photoionization cross sections, as well as the time-delay matrix to study resonance formation.

FAM has two sites supporting hydrogen bonds, which supports a highly stable dimeric structure, therefore they are an ideal prototype to initiate studies of biomolecule pairs [3]. FAM photoionization cross section shows a  $\sigma^*$  resonance at about 7 eV above the first ionization threshold [4]. FAD photoionization cross section shows two shape resonances at 4 eV and 8 eV above the first ionization threshold, originating in the original monomer virtual  $\sigma^*$  orbital (figure 1) and weaker resonances at higher energies. We employed

different models to describe the molecular electronic states, such as Static-Exchange (SE), Polarization-Consistent Coupled Hartree-Fock (PC-CHF) [4], CASSCF and its variant with only single and double (SD) excitations and discuss their differences and computational affordability. This work introduces an efficient computational framework we developed to investigate temporary states in dimers. We also discuss our findings concerning the population of CT states in the dimer and the employment of this framework for nucleobase pairs.

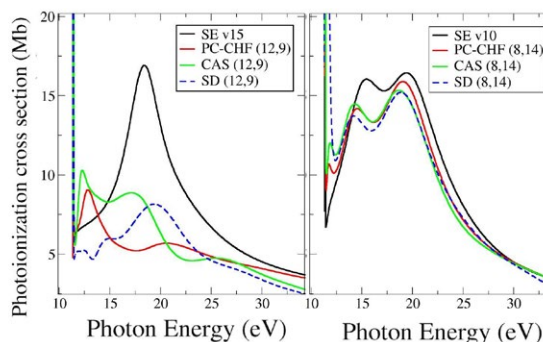


**Figure 1.** Partial photoionization cross section for the first cation state of FAM (left) and FAD (right) calculated using different models. The (n,p) labels refers to n electrons and p orbitals included in the active space.

### References

- [1] Barbatti M *et al* 2015 *Springer* **355** 1-32
- [2] Mašín Z *et al* 2020 *Comput. Phys. Commun.* **249** 107092
- [3] Tenorio B *et al* 2019 *J. Chem. Phys.* **150** 154308
- [4] Meltzer T and Mašín Z 2022 *J. Phys. B* **55** 035201

\* E-mail: [julio.ruivo@matfyz.cuni.cz](mailto:julio.ruivo@matfyz.cuni.cz)

## Angular distribution and energy spectra of photoelectrons from tetrahydrofuran illuminated by VUV photon source

I Márton<sup>1\*</sup>, L Ábrók<sup>1,2</sup>, D Nagy<sup>1,2</sup>, Á Kövér<sup>1</sup>, L Gulyás<sup>1</sup>, S Demes<sup>1</sup> and S Ricz<sup>1</sup>

<sup>1</sup>Institute for Nuclear Research, (ATOMKI), Debrecen, H-4001, Hungary

<sup>2</sup>Doctoral School of Physics, University of Debrecen, Debrecen, H-4032, Hungary

**Synopsis** Energy and angular distributions of photoelectrons from the valence shell of tetrahydrofuran (THF) ionized by a He(I) vacuum ultraviolet (VUV) photon source are measured. The experimental results are in good agreement with the theoretically calculated binding energies and cross sections of the molecular orbitals. The investigations show the role of dipole transition in the angular distributions of the photoelectrons.

The radiation damage of DNA molecule is actively studied as a result of the increasing importance of cancer therapy. To better understand the radiation damage in biological and other materials we need to study the photon, ion and electron interactions with atoms and molecules. One way to study the structure of the molecules is to measure the energy and angular distributions of the photoelectrons, the so called double differential cross section (DDCS) of the photoelectrons. For simulation of DNA-damages, i.e. on a level of cellular and subcellular scales, a detailed knowledge of the atomic and molecular properties of the target is needed. High energy- and angle-resolved photoelectron spectroscopy (HR-ARPES) together with a narrow bandwidth of He(I) vacuum ultraviolet (VUV) radiation is a sensitive method for investigating the dynamical aspect of the ionization processes such as electron correlation, multipole and channel interactions, etc. Tetrahydrofuran (THF,  $C_4H_8O$ ) is often used as a model molecule representing the deoxyribose group in DNA backbone. The valence electronic structure of THF molecules has been experimentally studied with the method of electron energy loss and low energy photoelectron spectroscopy with moderate energy resolution [1, 2, 3].

Employing the HR-ARPES technique we determined the DDCS spectra for the valence shell electrons of THF molecule. We are not aware of any former experimental investigation with such details in the literature. We measured the energy and angular distribution of photoelectrons (see Fig 1.) for determining the binding energies, the anisotropy (dipole and non-

dipole) parameters and the absolute ionization cross sections for valence electrons of the THF molecule. For our studies we applied HR-ARPES and VUV photons and compared our results with results performed by other groups. We have also performed numerical calculations to study the process. Ground state configurations were calculated using density functional theory, meanwhile the transitions were calculated with Fermi's golden rule.

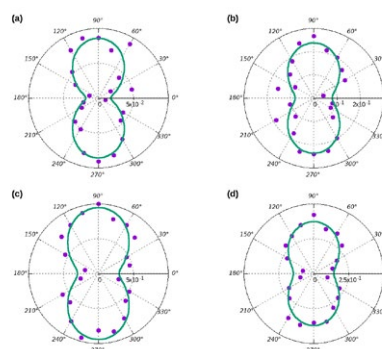


**Figure 1.** Angular distribution of photoelectrons corresponding to binding energies  $\sim 16.6$  eV (a);  $\sim 14.5$  eV (b);  $\sim 11.9$  eV (c) and  $\sim 9.7$  eV (d). Dots: present measurement. Lines: present calculation.

### References

- [1] Boudaïffa B, Cloutier P, Hunting D, Huels M A, and Sanche L 2000 *Science* **287** 1658
- [2] Shojaei S H R, Morini F, and Deleuze M S 2013 *The Journal of Physical Chemistry A* **117** 1918
- [3] Shojaei S H R, Vandenbussche J, Deleuze M S, and Bultinck P 2013 *The Journal of Physical Chemistry A* **117** 8388

\*E-mail: [marton.istvan@atomki.hu](mailto:marton.istvan@atomki.hu)

## Direct signatures of coherent bending vibrations observed using laser-induced Coulomb explosion imaging

Huynh Van Sa Lam<sup>1</sup>\*, Anbu Selvam Venkatachalam<sup>1</sup>, Sina Jacob<sup>2</sup>, Surjendu Bhattacharyya<sup>1</sup>, Keyu Chen<sup>1</sup>, Vinod Kumarappan<sup>1</sup>, Daniel Rolles<sup>1</sup>, Artem Rudenko<sup>1</sup>†

<sup>1</sup>James R. Macdonald Laboratory, Kansas State University, Manhattan, KS 66506, USA

<sup>2</sup>Goethe University Frankfurt, Frankfurt, Germany

**Synopsis** We use laser-induced Coulomb explosion imaging to directly map coherent bending vibrations in a laser-ionized small molecule with high temporal resolution.

Light-induced vibrational wave packets play a fundamental role in many types of molecular dynamics and have been studied extensively [1]. However, most studies using conventional mass spectrometry provide only indirect information on evolving molecular structures. In this work, we show that one can directly map coherent bending vibrations in a laser-ionized small molecule with excellent temporal resolution using Coulomb explosion imaging (CEI).

As depicted in Fig. 1, we use a strong 28-fs, 790-nm laser pulse to ionize SO<sub>2</sub> and induce vibrational wave packets in its cationic states (near 400 cm<sup>-1</sup>). Subsequently, a second NIR pulse of higher intensity is employed to further ionize and dissociate the molecules. The ionic products are detected in coincidence using a COLTRIMS apparatus. We focus on mapping the O-S-O bending vibrations and find that this motion influences many observables in the multi-dimensional coincidence data. We show that the bending-mode vibration can be observed directly in the delay-dependent kinetic energy spectra and angular distributions of high-charge-states channels. Our observations are supported by classical Coulomb explosion simulations.

Our work illustrates the direct sensitivity of CEI to the change in the spatial distribution of atoms, which can be utilized in more complex cases where multidimensional data is crucial to separate different dynamics. One such example is investigating coherent nuclear dynamics near intersections of potential energy surfaces, where the Born-Oppenheimer approximation fails and the couplings between vibrational and electronic degrees of freedom and/or different vibrational

modes govern molecular dynamics. Future work can study UV-induced excited-state dynamics of triatomic molecules, such as SO<sub>2</sub> [2] or CS<sub>2</sub> [3], where strong nonadiabatic couplings determine the transition between geometries and influence the vibration/dissociation dynamics.

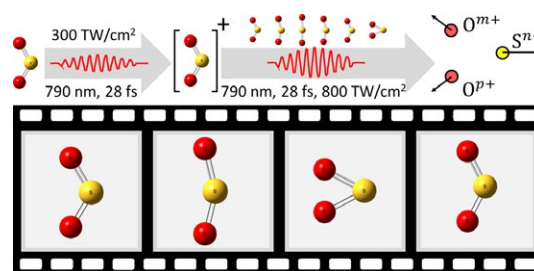


**Figure 1.** The first laser pulse ionizes SO<sub>2</sub> and induces vibrational wave packets in its cationic states. The second laser pulse further ionizes and dissociates the molecules. The ionic fragments are detected in coincidence, and their momenta are used to retrieve the molecular structures and produce a molecular movie of structural changes of the coherent bending-vibration wave packet.

This work is supported by the Chemical Sciences, Geosciences, and Biosciences Division, Office of Basic Energy Sciences, Office of Science, U.S. Department of Energy, Grants DE-FG02-86ER13491 and DE-SC0020276 (SB), and by the National Science Foundation Grant PHYS-1753324 (ASV).

### References

- [1] Ohmori, K., *Ann. Rev. Phys. Chem.* **60** 487-511 (2009).
- [2] Wilkinson, I. *et al.*, *J. Chem. Phys.* **140**(20) 204301 (2014).
- [3] Karashima, S., Suzuki, Y. I., Suzuki, T., *J. Phys. Chem. Lett.* **12**(15) 3755-3761 (2021).

\*E-mail: [huynhslam@phys.ksu.edu](mailto:huynhslam@phys.ksu.edu)

†E-mail: [rudenko@phys.ksu.edu](mailto:rudenko@phys.ksu.edu)

## Strong-field-driven dissociation dynamics in $\text{CO}_2^+$

Van-Hung Hoang and Uwe Thumm\*

J. R. Macdonald Laboratory, Department of Physics, Kansas State University, Manhattan, KS 66502, USA

**Synopsis:** We investigate strong-field XUV-IR pump-probe dissociative ionization of  $\text{CO}_2$  by solving the Schrödinger equation for the nuclear motion in full dimensionality on the lowest five coupled Oppenheimer (BO) potential-energy surfaces. Applying a multi-configurational self-consistent-field quantum-chemistry code to calculate *ab initio* non-BO, laser dipole, and spin-orbit couplings between adiabatic electronic states, we provide kinetic energy release (KER) spectra for the  $\text{O}(3\text{P}_g) + \text{CO}^+(X^2\Sigma^+)$  and  $\text{O}^+(^4\text{S}_u) + \text{CO}(X^1\Sigma_+)$  dissociation channels and their branching ratio. Our KER spectra identify the vibrational excitations of  $\text{CO}^+$  fragments along a dominant  $3\omega$  dissociation paths. Mediated by the nuclear dynamics near the conical intersection of the  $\text{CO}_2^+$   $\text{A}^2\Pi_u$  and  $\text{B}^2\Sigma_u^+$  states, we reproduce a core-hole oscillation period 115 fs, in good agreement with the experiment of Timmers *et al.* [1]. In addition, we find 62 fs oscillations in the  $\text{CO}^+$  fragmentation channel due to quantum beats between specific vibrational and electronic  $\text{CO}_2^+$  states.

We model the ionization of  $\text{CO}_2$  in the XUV pulse in Franck-Condon approximation and trace the nuclear motion in the excited residual molecular anion by numerically propagating the coupled-channel nuclear Schrödinger equation on the  $\text{A}^2\Pi_u$ ,  $\text{B}^2\Sigma_u^+$ ,  $\text{C}^2\Sigma_g^+$ ,  $\text{b}^4\Pi_u$  and  $\text{a}^4\Sigma_g^-$  BO surfaces of  $\text{CO}_2^+$ . The ionization process is assumed to only populate the  $\text{B}^2\Sigma_u^+$  vibrational ground state, due to its strongest FC overlap with the ground state of  $\text{CO}_2$ .

We employ a 45 fs,  $2 \times 10^{13}$  W/cm<sup>2</sup> Gaussian IR pulse and include the non-BO coupling between the  $\text{A}^2\Pi_u$  and  $\text{B}^2\Sigma_u^+$  states of  $\text{CO}_2^+$  that receive relevant population by ionizing ground state  $\text{CO}_2$  in the XUV pump pulse with 18 eV central photon energy. We include the  $\text{C}^2\Sigma_g^+$  state of  $\text{CO}_2^+$  since it is accessible by dipole coupling in the 1.58 eV IR probe pulse. From these excited states,  $\text{CO}_2^+$  can dissociate by spin-orbit coupling of the  $\text{C}^2\Sigma_g^+$  state into the  $\text{O}(^3\text{P}_g) + \text{CO}^+(X^2\Sigma^+)$  and  $\text{O}^+(^4\text{S}_u) + \text{CO}(X^1\Sigma_+)$  asymptotic channels of the  $\text{b}^4\Pi_u$  and  $\text{a}^4\Sigma_g^-$  states, respectively. We calculate potential energy surfaces and coupling matrix elements with the MCSCF package GAMESS [2].

Figure 1(a) shows the total  $\text{CO}^+$  yield as a function of the time delay between the XUV pump and IR probe pulses. Our  $\text{CO}^+$  KER spectra reveal that  $3\omega$  vibrational excitations from the  $\text{B}^2\Sigma_u^+$  to the  $\text{C}^2\Sigma_g^+$  state are most relevant for dissociation into the repulsive  $\text{b}^4\Pi_u$  and  $\text{a}^4\Sigma_g^-$  states. We reproduce a core-hole oscillation period of 115 fs between mediated by the

nuclear dynamics near the  $\text{A}^2\Pi_u$  and  $\text{B}^2\Sigma_u^+$  conical intersection in good agreement with the experiment [1] and assign this oscillation to quantum beats between  $\text{B}^2\Sigma_u^+(0,0,0)$  and  $\text{A}^2\Pi_u(1,0,2)$ , instead of  $\text{A}^2\Pi_u(3,1,1)$  in [1]. In addition, we find 62 fs oscillations in the  $\text{CO}^+$  fragmentation channel, due to beating  $\text{B}^2\Sigma_u^+(0,0,0)$  and  $\text{A}^2\Pi_u(5/6,0,0)$  states [Fig. 1(b)].

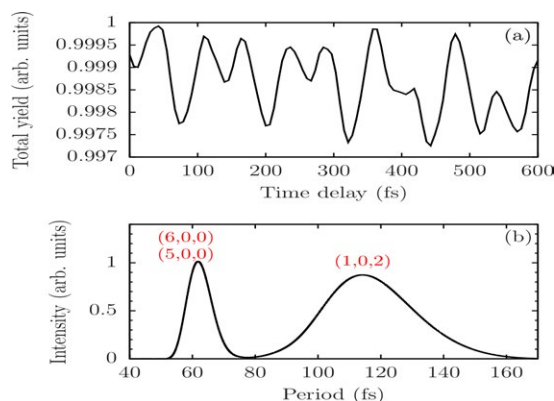


**Figure 1.** (a)  $\text{CO}^+$  yield versus time delay. (b) Fourier analysis of the  $\text{CO}^+$  ion yield.

This work was supported by the Chemical Sciences, Geosciences, and Biosciences Division, Office of Basic Energy Sciences, Office of Science, U.S. DOE under Award, DEFG02-86ER13491.

[1] H. Timmers *et al.*, Phys. Rev. Lett. **113**, 113003 (2014).

[2] G. M. J. Barca, *et al.*, J. Chem. Phys. **152**, 154102. (2020).

\* E-mail: thumm@phys.ksu.edu

## Ultrafast dynamics in tryptophan-based peptides controlled by micro-environment

R Brédy<sup>1</sup>\*, M Hervé<sup>1</sup>, A Boyer<sup>1</sup>, A R Allouche<sup>1</sup>, I Compagnon<sup>1</sup> and F Lépine<sup>1</sup>

<sup>1</sup>Univ Lyon, Université Claude Bernard Lyon 1, CNRS, Institut Lumière Matière, F-69622, Villeurbanne, France

**Synopsis** We present UV-IR pump-probe experiments on small tryptophan-based peptides ions with tailored micro-environment. Ultrafast charge transfer dynamics is observed revealing that control of the micro-environment at the atomic scale allowed us to tune the timescale of the  $\pi\pi^* - \pi\sigma^*$  dynamics by more than one order of magnitude. Combined with quantum chemistry calculations, we show that this effect is due to the tuning of the relative energy between the delocalized  $\pi\pi^*$  and localized  $\pi\sigma^*$  states, that is induced by the interaction with the adduct.

General process in UV excitation of molecules involves the excitation of a chromophore that carries a localized electronic excited state. Relaxation of such excited states can be complex and ultrafast pump-probe experiments in the gas-phase are used to unravel the subtle mechanisms at play such as ultrafast charge transfer, structural rearrangement and energy dissipation between the electronic and/or the nuclear degrees of freedom. The dynamics of these mechanisms can be strongly affected by a simple modification of the environment of the molecule that impacts its electronic structure.

Electrospray ionization source (ESI) technology allows to form and isolate complex fragile systems with micro-environment controlled at the atomic scale using adduct atoms. To investigate how modifications of the atomic environment of a biomolecular ion can influence its non-stationary properties we have combined UV-IR pump-probe experiments with ESI and mass spectrometry (MS) technologies. Charge transfer dynamics have been studied in three tryptophan-containing systems [1], the protonated tryptophan (Trp.H<sup>+</sup>), the sodiated tryptophan (Trp.Na<sup>+</sup>) and the sodiated alanyl-tryptophan (AlaTrp.Na<sup>+</sup>). These small peptides exhibit a  $\pi\pi^* - \pi\sigma^*$  coupling that plays an important role in photochemical properties [2]. The  $\pi\pi^*$  state corresponds to the excitation of typical

aromatic chromophores, and the  $\pi\sigma^*$  state has a  $\sigma$  character located on a specific X-H bond X being usually a heteroatom (N, O, or S). The measured ultrafast photo-induced  $\pi\pi^* - \pi\sigma^*$  dynamics reveal a striking increase of the timescale by more than one order of magnitude when changing the added adduct atom (Fig. 1). To rationalize this observation we proposed a simple model based on the localized and delocalized effects of the adduct on the electronic structure of the molecule [1]. These results show that the dynamics can be tuned by controlling the environment of the chromophore.

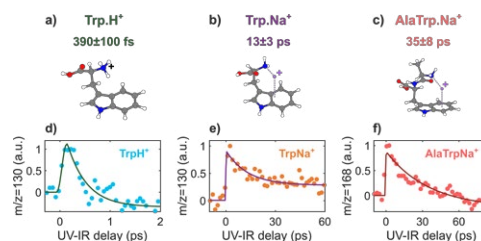


**Figure 1.** 267 nm-800 nm pump-probe experiment on charged peptides a) Trp.H<sup>+</sup>, b) Trp.Na<sup>+</sup> and c) AlaTrp.Na<sup>+</sup> with time-dependent ion signals for specific m/z fragments (d-e).

### References

- [1] Hervé M *et al.* 2021 *Commun. Chem.* **4** 124
- [2] Sobolewski ALG *et al.* 2002 *Phys. Chem. Chem. Phys.* **4** 1093-1100

\*E-mail: [richard.bredy@univ-lyon1.fr](mailto:richard.bredy@univ-lyon1.fr)



## Observation of the ions $\text{CH}_3^+$ , $\text{SH}^+$ , $\text{SH}_2^+$ and $\text{CH}_3\text{S}^+$ from thiophene and tetrathiothiophene by laser radiation at 532,355 and 266 nm

A Guerrero, I Álvarez, E Prieto, C Cisneros<sup>1</sup>

<sup>1</sup> Instituto de Ciencias Físicas. Universidad Nacional Autónoma de México. Cuernavaca  
62210, Morelos, México.

**Synopsis.** Experimental results of the interaction of high intensity laser radiation  $\lambda = 266, 355$  and  $532$  nm with thiophene(T) and tetrahydrothiophene (THT), that have been reported to be present in planetary atmospheres are presented. It is suggested that the presence of  $\text{CH}_3^+$  ( $m=15$ ),  $\text{SH}^+$  ( $m=33$ ),  $\text{SH}_2^+$  ( $m=34$ ) and  $\text{CH}_3\text{S}^+$  ( $m=47$ ) ions is due to molecular rearrangement and from proton transfer processes.

The reports of presence of T and THT in interstellar space and in planetary atmospheres [1,2] in addition to their use in various research areas makes them attractive for theoretical and experimental study. The interaction of these compounds with ultraviolet light leads to the formation of fragments that have been detected in interstellar space. In this work, possible fragmentation routes of T and THT are studied and suggested for the formation of some of the relevant fragments detected, when irradiated with intense fields of UV radiation from a pulsed Nd:YAG laser (frequency 30 Hz) and generated by ionization/dissociation induced by multiphoton absorption in a reflectron. The T and THT (Sigma Aldrich 99% purity) are introduced into the spectrometer through a pulsed valve/skimmer whose opening is coupled to the laser shots, ensuring the coincidence of the molecular beam and the laser in the interaction zone. The radiation of  $\lambda=532, 355$  and  $266$  nm coming from harmonics in an KDP crystal, is passed through a converging lens reaching powers  $\sim 10^9$  W/cm<sup>2</sup> at the focus. The intensity of the fragments produced are recorded by their time of flight and for different intensities of the laser beam. Mass spectra of Thiophene is shown in Figure A at  $\lambda=355$  nm.

It is observed that high intensities of  $\text{H}^+$ ,  $\text{C}^+$  and  $\text{S}^+$  indicate high fragmentation with absorption of two photons (8.33 eV). The formation of low molecular weight ions for high radiation values and of heavy ions for low radiation intensities is true for  $\lambda=532$  and  $266$  nm, but is reversed for  $355$  nm. The migration of H leading to  $\text{CH}_2^+$  and  $\text{C}_2\text{H}_3^+$  is shown indirectly. A migration of H towards S probably gives rise to the products  $\text{C}_3\text{H}_3^+$  and  $\text{HCS}^+$ . The  $\text{C}_3\text{H}_n^+$  and  $\text{C}_4\text{H}_n^+$  fragments stand out for the loss of

H ( $n=0,\dots,6$ ) The dependence of the ionic currents of the fragments with respect to the radiation intensity is manifested in the generation of the parent ion. The absence of the parent ion in the spectrum suggests a dissociation-ionization mechanism and the presence of  $\text{CH}_3^+$  and  $\text{CH}_3\text{S}^+$  reinforces the assumption of H migrations. Tetrahydrothiophene being a saturated structure analogous and aliphatic to thiophene, great similarities would be expected, but some of the differences in the intensities in the spectra must come from the fact that the THT uses a part of the absorbed energy in the breaking of the C-H bonds.

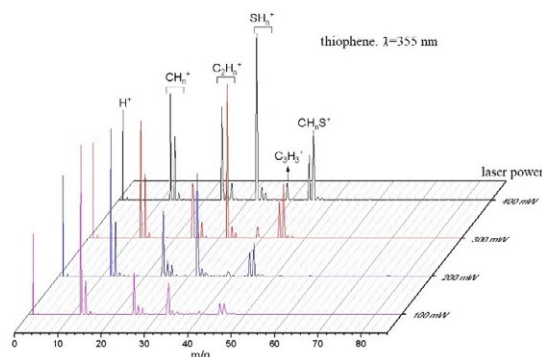


Fig.A Mass spectrum of thiophene at 355 nm and different laser power

Work supported by DGAPA-UNAM IN104423

### References

- [1] Jacob Heinza, Dirk-Schulze-Makuch. Thiophenes on Mars: Biotic or Abiotic Origin? *Astrobiology* 2020 Apr;20(4):552-561. doi: 10.1089/ast.2019.2139
- [2] Pietro Candori et al. Kinetic energy release in molecular dications fragmentation after vuv and euv ionization and escape from planetary atmospheres. *Planet. Space Sci.*, 99(149{157}): <http://dx.doi.org/10.1016/j.pss.2014.04.020>,

e-mail: alfonsog@icf.unam.mx

## Vibrational patterns in dissociative photoionization of $\text{H}_2$ and $\text{D}_2$ molecules by VUV + NIR absorption

S Burrows<sup>1</sup>, J Dvořák<sup>2\*</sup>, I Ben-Itzhak<sup>3</sup>, B Berry<sup>3</sup>, E Champenois<sup>2</sup>, R Dörner<sup>4</sup>, A Gatton<sup>2</sup>, W Iskandar<sup>2</sup>, K Larsen<sup>2</sup>, G Laurent<sup>1</sup>, R Lucchese<sup>2</sup>, D Metz<sup>4</sup>, T Rescigno<sup>2</sup>, H Sann<sup>4</sup>, T Severt<sup>3</sup>, N Shivaram<sup>2</sup>, D Slaughter<sup>2</sup>, M Weller<sup>4</sup>, J Williams<sup>5</sup>, C W McCurdy<sup>2</sup>, and T Weber<sup>2</sup>

<sup>1</sup>Department of Physics, Auburn University, Auburn, Alabama 36849, USA

<sup>2</sup>Chemical Sciences Division, Lawrence Berkeley National Laboratory, Berkeley, California 94720, USA

<sup>3</sup>J. R. Macdonald Laboratory, Physics Department, Kansas State University, Manhattan, Kansas 66506, USA

<sup>4</sup>Institut für Kernphysik, J. W. Goethe Universität, Max-von-Laue-Strasse 1, 60438 Frankfurt, Germany

<sup>5</sup>Department of Physics, University of Nevada Reno, Reno, Nevada 89557, USA

**Synopsis** We studied the dissociation of  $\text{H}_2$  and  $\text{D}_2$  after absorption of VUV and NIR photons. The vibrational patterns observed in the spectra are discussed using Chase's approximation.

We report the results of our joint experimental and theoretical study on the dissociation of  $\text{H}_2$  and  $\text{D}_2$  molecules induced by two-color photon absorption. First, the neutral molecules were ionized by vacuum-ultraviolet (VUV) radiation with energies of 17.9, 18.34, and 18.54 eV from the Advanced Light Source synchrotron. In the second step, the molecular ions  $\text{H}_2^+$  and  $\text{D}_2^+$  left in specific vibrational states were dissociated by a synchronized near-infrared (NIR) laser pulse with energy of 1.2 eV and duration of 12 ps. The time delay between the VUV and NIR pulses was controlled.

Using the COLTRIMS technique to measure the momenta of the photoelectrons and the  $\text{H}^+$  and  $\text{D}^+$  ions in coincidence, we obtained the molecular frame photoelectron angular distribution spectra, including their dependence on the orientation of the VUV and NIR polarizations.

In this contribution, we focus on the joint distributions of the nuclear kinetic energy release and photoelectron kinetic energy, which show peaks that correspond to the specific vibrational states of the  $\text{H}_2^+$  and  $\text{D}_2^+$  molecular ions. To explain why some of the peaks are missing, we employed Chase's approximation for both the photoionization and photodissociation steps. For the initial photoionization, we calculated the photoionization amplitudes for relevant internuclear distances using the multichannel configuration interaction method. The intensity of the ob-

served peaks is explained well by the theory, except for a few lowest-lying peaks, which are more pronounced in the experiment. After investigating the role of molecular rotations, we are currently considering the effects of the light-induced conical intersection [1].

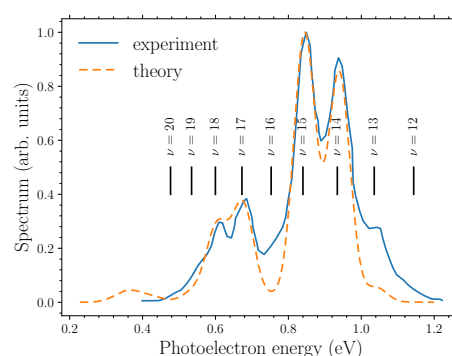


**Figure 1.** Vibrational pattern for two-color photodissociation of  $\text{D}_2$  with VUV and NIR energies of 18.54 and 1.2 eV.

We gratefully acknowledge the support provided by US DOE, Office of Science, Office of Basic Energy Sciences, Division of Chemical Sciences, Geosciences and Biosciences.

### References

- [1] Szidarovszky T, Halász G, Császár A, Cederbaum L, and Vibók Á 2018 *J. Phys. Chem. Lett.* **9** 2739

\*E-mail: [jdvorak2@lbl.gov](mailto:jdvorak2@lbl.gov)

## How does solvation affect molecular ultrafast dissociation?

D Vasconcelos<sup>1\*</sup>, O Björneholm<sup>1</sup>, G Öhrwall<sup>2</sup>, M Tchapyguine<sup>2</sup>, R Marinho<sup>3</sup>, and A Brito<sup>4</sup>

<sup>1</sup> Department of Physics and Astronomy, Uppsala University, Uppsala, SE-75120, Sweden

<sup>2</sup> MAX IV Laboratory, Lund University, SE-22100, Sweden

<sup>3</sup> Department of Physics, Universidade de Brasília, Brasília, 70297-400, Brazil

<sup>4</sup> Department of Physics, Universidade Estadual do Estado de São Paulo, Campinas, 13083-859, Uppsala, Brazil

**Synopsis** This present work reports on how solvation affects the ultra-fast dissociation (UFD) in chloroform. To study UFD for CHCl<sub>3</sub> in both gas phase and in ethanol solution, we have recorded resonant Auger spectra as function of photon energy around the Cl2p edge and found that UFD is suppressed in the solution.

X-ray-induced molecular fragmentation is an important process in radiation chemistry and radiation biology. One such phenomenon is molecular ultrafast dissociation (UFD), in which a core-excited molecule dissociates during the core-hole lifetime of a few femtoseconds.

UFD has been extensively studied for gas phase molecules via the core-hole Auger decay [1,2], which may occur anytime throughout the dissociation process. For the few cases where UFD has been studied in both gas phase and condensed phase, the effects go in opposite directions: Clustering has been seen to suppress UFD for bromomethane [2], whereas core-ionized water molecules have been shown to dissociate during the core-hole lifetime in the liquid but not in the gas phase [3]. Much of radiation chemistry and radiation biology occurs in solution, where solvation may affect UFD through various mechanisms, e.g. by changing the ground state electronic and geometric structure of the molecule, as well as by affecting the dissociation process via impeding the dissociative nuclear motion and/or via solute-solvent charge transfer.

Here we have aimed to investigate to how solvation affects UFD in chloroform.

The resonant Auger spectrum (RAS) was recorded as a function of photon energy around the Cl2p edge as shown in figure 1. In the case of the gas phase, the atomic states appear as narrow peaks, while broad features are associated with “non-dissociated” final states.

Although these characteristics in the liquid cannot be seen, we can see corresponding peaks at the resonance energy. The relative intensity of these peaks compared to the features from non-dissociative states is clearly lower than in the

gas phase, indicating a suppression of the dissociation in the condensed phase for chloroform. The detailed analysis is in progress, and we hope that the knowledge obtained from model systems such as this can be transferred to more complex systems of relevance to radiation chemistry and radiation biology.

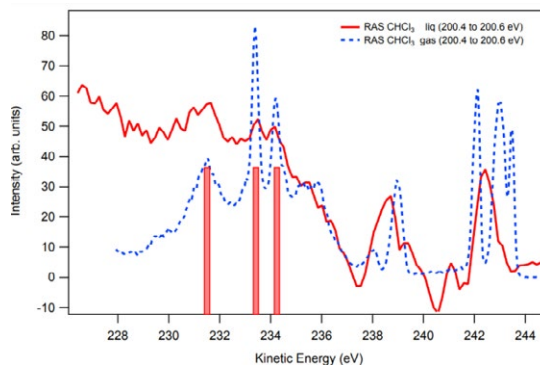


**Figure 1.** Chloroform RAS at 200.4 eV. Gas phase results are the dashed blue curve while liquid is represented by a solid red curve. Red bars indicating the resonances observed in gas phase.

### References

- [1] Thürmer S, Ončák M, Ottosson N, et al. 2013 *Nat Chem.* 5, [590](#)
- [2] P. Morin and C. Miron 2012, *J. Electron Spectrosc. Relat. Phenom.* 185, [259](#)
- [3] T. Rander, et al. 2014, *J. Chem. Phys.*, [141 224305](#)
- [4] Björneholm, M. Bäessler, et al. 2001, *Chem. Phys. Letts.* 2001, [1511 334151](#)

\* E-mail: [debora.nbv@physics.uu.se](mailto:debora.nbv@physics.uu.se)

## Impact of the XFEL shot-to-shot variation onto soft X-Ray pump-probe studies of attosecond charge migration in molecules

G Grell<sup>1\*</sup>, P Decleva<sup>2</sup>, A Palacios<sup>3</sup> and F Martín<sup>1,3,4†</sup>  
on behalf of the LCLS Attosecond Campaign Collaboration<sup>5</sup>

<sup>1</sup>IMDEA Nanoscience Institute, Madrid, 28049, Spain

<sup>2</sup>Istituto Officina dei Materiali (CNR-IOM), 34149 Basovizza - Trieste, Italy

<sup>3</sup>Departamento de Química, Universidad Autónoma de Madrid, Madrid, 28049, Spain

<sup>4</sup>Condensed Matter Physics Center (IFIMAC), Universidad Autónoma de Madrid, Madrid, 28049, Spain

<sup>5</sup><https://lcls.slac.stanford.edu/depts/amo/asc>

**Synopsis** The shot-to-shot variation inherent to SASE XFELs may hinder the study of charge migration, since each pulse leads to a different coherent superposition of states and ensuing dynamics. We show with first-principles simulations of the charge motion triggered in the para-aminophenol molecule by 260 eV sub-fs pulses generated at the LCLS that the shot-to-shot variation has a much weaker effect on the dynamics than the dephasing due to the initial nuclear wave function of the molecule.

Sub-fs soft X-Ray pulses are currently being produced at the LCLS X-Ray free electron laser (XFEL) with the recent implementation of the X-Ray laser-enhanced attosecond pulse generation method [1]. These pulses are many orders of magnitude more intense than their high harmonic generation counterparts, making it possible to conduct nonlinear X-Ray spectroscopies of attosecond electron dynamics. However, most XFELs build up their pulses from noise via self-amplified spontaneous emission, which introduces a stochastic shot-to-shot variation of the pulses' characteristics. This ultimately translates into different created superpositions of states and resulting charge dynamics for each so-generated pump pulse. Measuring transient spectra averaged over an ensemble of pump pulses may thus diminish the dynamical features. While one can exclude this effect by only considering data for a small fraction of similar pump pulses, such an approach requires considerably longer beamtimes, questioning its practical feasibility.

This contribution showcases our first-principles calculation results regarding the impact of the shot-to-shot variation within an ensemble of 100 sub-fs pump pulses at 260 eV, obtained from start-to-end simulations of the XFEL at the LCLS, onto pump-probe studies

of the charge migration dynamics in the prototypical para-aminophenol molecule ( $\text{NH}_2\text{-C}_6\text{H}_4\text{-OH}$ ). Therein, the static-exchange B-spline DFT method is used to explicitly model the molecular continuum states, while the bound states can be described independently with the CASPT2 method. Our results show that the shot-to-shot variation alone reduces the charge fluctuation amplitudes by no more than 35%. We found that this is much weaker than the effect of the initial nuclear wave function, which has been explicitly accounted for by averaging over an ensemble of geometries sampled from the ground-state nuclear Wigner distribution of the molecule. The so-introduced dephasing damps the charge dynamics within the first 3 fs following the pump pulse, such that the charge fluctuations reach at most 20% of their maximum amplitude beyond this point in time.

These results suggest that attosecond soft X-Ray spectroscopies at XFELs are not restricted by the inherent shot-to-shot variation and may be reliably used to investigate pristine charge dynamics at its early stages. We will demonstrate in addition how the shot-to-shot variation manifests in explicitly simulated pump-probe spectroscopic observables, completing the picture.

### References

- [1] Duris J et al. 2020 *Nat. Phot.* **14** 30

\*E-mail: [gilbert.grell@imdea.org](mailto:gilbert.grell@imdea.org)

†E-mail: [fernando.martin@uam.es](mailto:fernando.martin@uam.es)

## Formation of Breathing Ions via Coherent Shake-Up

J. Tarrant<sup>1\*</sup>, M. Khokhlova<sup>2,3</sup>, P. Kolorenč<sup>4</sup>, M. Ruberti<sup>1</sup>, and V. Averbukh<sup>1</sup>

<sup>1</sup>Blackett Laboratory, Imperial College London, London SW7 2AZ, United Kingdom

<sup>2</sup>Max Born Institute, Berlin 12489, Germany

<sup>3</sup>Department of Physics, King's College London, London WC2R 2LS, United Kingdom

<sup>4</sup>Charles University, Faculty of Mathematics and Physics, V Holešovičkách 2, 180 00 Prague, Czech Republic

**Synopsis** We show theoretically that a broad-band coherent XUV ionising pulse targeted at the shake-up region of the ionic spectrum of an atom produces a long-lived coherent superposition of ionic states characterised by the expansion and contraction in time of the electron cloud. This provides a first numerical demonstration of a phenomenon which we term 'breathing ions'.

When an inner-shell orbital of an atom or molecule is ionised, it is not possible to accurately describe the resulting ionic states in terms of a single configuration. Instead, in the region corresponding to ionisation of that orbital there is a series of states of partial one-hole character. These often take the form of a largely one-hole main state alongside many shake-up satellites of primarily two-hole one-particle character associated with ionisation of one electron and excitation of a second. We suggest that with a sufficiently broad ionising pulse, each of these states can be coupled to the same set of continuum orbitals, allowing the creation of a coherent superposition of these ionic states.

In this work, we seek to show that it is possible to create such a superposition by looking at the specific case of argon ionisation. We model the coherent population of the main and shake-up ionic states by a short pulse which spans the energy region from the argon  $3s^{-1}$  main state up to the double ionisation potential. We predict that this system will display oscillatory dynamics, with the electron cloud expanding and contracting in time - a behaviour which leads us to describe such systems as 'breathing ions'. Similarly to the related phenomenon of hole migration via the 'frustrated Auger' process in molecules [1], this can be interpreted as an Auger transition which is energy-forbidden, forcing the departing electron to return to the system. One crucial difference here, however, is that there is no loss of coherence due to nuclear motion, and we can therefore show that oscillations in this atomic system will be long-lived.

We use the time-dependent RCS b-spline

\*E-mail: [jt2615@ic.ac.uk](mailto:jt2615@ic.ac.uk)

algebraic diagrammatic construction (ADC) method [2, 3] at the ADC(2)x level for the calculation of the Hamiltonian and the time-propagation of the system. This *ab initio* numerical technique uses b-splines to describe both bound and continuum states of the system, allowing for an accurate description of ionisation dynamics. We additionally use the ADC(2,2) [4] technique used to further improve the accuracy of our description of the bound-like states of the ionic system.

We show by looking at the time variation of surfaces of constant electron density that the radius of the electron cloud does oscillate in time. We also quantify the magnitude of these oscillations by calculating the variation in time of the average radius of the distortion in the electron cloud after ionisation.

In a practical setup, this breathing behaviour could subsequently be measured via a delayed probe pulse, with the oscillations of the wavepacket reflected in the modulation of the double ionisation yield with the probe delay [5, 6].

### References

- [1] Barillot, T. *et al.* 2021 *Phys. Rev. X* **11** 031048
- [2] Ruberti, M., Averbukh, V and Decleva, P. 2014 *J. Chem. Phys.* **141** 164126
- [3] Ruberti, M. 2019 *J. Chem. Theory Comput.* **15** 63635
- [4] Kolorenč, P. and Averbukh, V. 2020 *J. Chem. Phys.* **152** 214107
- [5] Cooper, B., Kolorenč, P., Frasinski, L., Averbukh, V., and Marangos, J. 2014 *Faraday Discuss.* **171** 93
- [6] Ruberti, M., Decleva, P., and Averbukh, V. 2018 *J. Chem. Theory Comput.* **14** 104991



## Real-time first-principles simulations of molecules in intense laser fields using the erf-gau potential

Y Orimo<sup>1\*</sup>, T Sato<sup>1</sup>, K L Ishikawa<sup>1</sup>

<sup>1</sup>Graduate School of Engineering, The University of Tokyo, 7-3-1 Hongo, Bunkyo-ku, Tokyo 113-8656, Japan

**Synopsis** We propose the use of the *erfgau* potential that is smooth and has no singularity instead of the Coulomb potential of nuclei in real-time first-principles simulations of molecules in intense laser fields. We found that the potential is less demanding for spatial resolution and can reproduce correct results in simulations of high harmonic generation.

Electronic dynamics driven by intense laser pulses and ultrafast light pulses has attracted great research interest over a dozen years. To theoretically investigate such dynamics, we have developed real-time first-principles approaches based on the time-dependent multiconfiguration self-consistent field (TD-MCSCF) method [1], and we have implemented them for general molecules using the adaptive finite element method [2], whose complex but flexible discretization allows to treat a molecular Coulomb potential with complicated shape. In this study, to make molecular simulations easier, we propose the use of the *erfgau* potential [3] that is smooth and has no singularity instead of the Coulomb potential in first-principle simulations.

The *erfgau* potential approximates the Coulomb potential  $1/r$  by an error function and a Gaussian function,

$$\frac{1}{r} \rightarrow V(r) = c \exp(-\alpha r^2) + \frac{\operatorname{erf}(\mu r)}{r}.$$

The error function eliminates the singularity of  $1/r$  and render the potential smooth, thereby reducing the need for high spatial resolution. There are many ways to determine the parameters ( $c, \alpha, \mu$ ) in the *erfgau*. We follow the reference [4], where  $c$  and  $\alpha$  are defined as linear functions of  $\mu$  and  $\mu$  determines the degree of the approximation. As  $\mu$  increases, the *erfgau* potential more closely approximates the Coulomb potential. An alternative method that substitutes the potential with easily computable one is pseudo-potential. In comparison, the *erfgau* potential is considerably simpler in both theory and implementation, and can be generated at nearly zero cost.

Here, we demonstrate first-principles simulations with *erfgau* potentials by computing high harmonic generation of a hydrogen molecule. Figure 1 compares high harmonic spectra using the Coulomb potential and *erfgau* potentials with some parameters, and regardless of the parameter  $\mu$ , the results of *erfgau* potentials reproduce the correct result. This means that the *erfgau* potential that is originally designed for static states of hydrogen-like atoms is applicable to multielectron dynamics in molecules, and it would be helpful to achieve precise simulations of larger molecules with less computational costs.

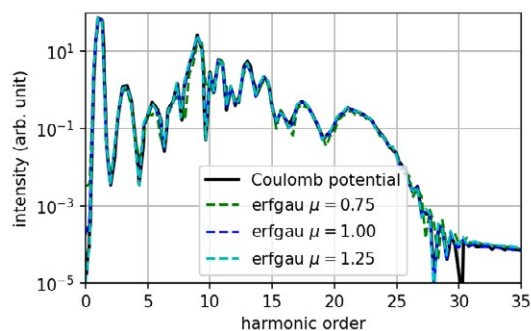


**Figure 1.** High harmonic spectra of a hydrogen molecule irradiated with a laser pulse with a peak intensity of  $1 \times 10^{14}$  W/cm<sup>2</sup>, 800 nm wavelength and 3 optical cycles.

### References

- [1] Ishikawa K L and Sato T 2015 *IEEE J. Sel. Top. Quantum Electron.* **21**, 1–16
- [2] Orimo Y, *et al.* *Can. J. Chem.* (Accepted)
- [3] Toulouse J, *et al.* 2004 *Phys. Rev. A* **70**, 062505
- [4] González-Espinoza C E, *et al.* 2016 *Theor. Chem. Acc.* **135**, 256

\* E-mail: [ykormhk@atto.t.u-tokyo.ac.jp](mailto:ykormhk@atto.t.u-tokyo.ac.jp)

## Absolute photodetachment cross-section of deprotonated indole using a 16-pole ion trap

Salvi M<sup>1</sup>, Uma N N, Abheek Roy, Hemanth Dinesan\* and S Sunil Kumar

Department of Physics, Indian Institute of Science Education and Research (IISER) Tirupati & Center for Atomic, Molecular, and Optical Sciences & Technologies, Tirupati 517507 Andhra Pradesh, India

\* Present address: CNRS Laboratoire de Physique del Laser(LPL), Universite Sobornne Paris Nord Villetaneuse, France

**Synopsis** Measurement of the absolute photodetachment cross-section of deprotonated indole with a newly built experimental station hosting a 16-pole radiofrequency ion trap.

Photodetachment is the process of electron detachment from atomic or molecular anions due to radiation. It is an excellent tool for investigating electron correlation effects, which are otherwise dominated by long-range interactions [1]. The accurate determination of the absolute photodetachment cross-section is crucial to ensure the success of the applications like radiation protection, controlled thermonuclear research plasma, and stellar atmosphere [2]. The quantity can provide insights into the stability against competing photodestruction and fluorescence pathways. Further, for molecules relevant to astronomy, this could lead to prediction of the molecule's existence in extraterrestrial environments.

Conventional experimental techniques for measuring photodetachment cross-sections provide only relative measurements. For the existing absolute cross-section values, the measurement is made with reference to an atomic/molecular species for which absolute cross-sections are available. This requires ensuring the same experimental conditions as the reference, which can result in large measurement uncertainties due to systematic errors. However, measuring the absolute photodetachment cross-section directly, without relying on normalization procedures, can provide highly accurate results and can be reliably used for further analysis.

A 16-pole radiofrequency ion trap-based experimental station is built and tested at Astrobiolab, IISER Tirupati, India [3]. Absolute photodetachment cross-section of deprotonated indole is measured. Indole is the chromophore in the amino acid tryptophan. The fluorescence of indole is most commonly utilized in spectroscopic studies of biological systems and has been used to probe protein folding/unfolding dynamics [4]. The electrospray ionization (ESI) technique is employed for the gas-phase generation of biomolecular ions. These ions are transported to the ion trap region maintained at a high

vacuum through an ion funnel, a quadrupole ion guide, and a quadrupole mass filter. The mass-selected ions are trapped and exposed to laser for spectroscopic studies. The present work is the first-ever experimental data recorded from the newly built experimental station focused on the photodetachment decay rate of deprotonated indole ions. The photodetachment decay rate acquired along the entire ion distribution within the ion trap can be used for the absolute photodetachment cross-section. The results from this experimental investigation together with computational data will provide a further understanding of molecular dynamics.

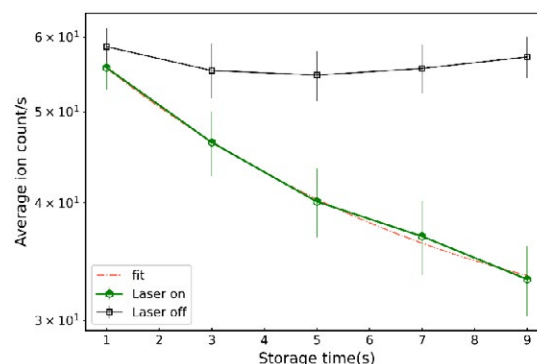


**Figure 1.** Photodetachment decay of deprotonated indole PD lifetime is calculated to be  $5.0 \pm 0.2$  s calculated from exponential fit using 405 nm diode laser at 34 mW power.

### References

- [1] Trippel, S., Mikosch, J., Berhane, R., Otto, R., Weidemüller, M. and Wester, R. PRL **97**, 193003 (2006).
- [2] Baghel, S. S., Gupta, S., Gangwar, R. K., & Srivastava, R. PSST, **30(5)**, 055010 (2021).
- [3] Rajeevan, G., Mohandas, S. and Kumar, S.S. Phys. Scr. **96**, 124001, (2021).
- [4] Nelson, D.J., Oliveira, A.M. and Lineberger, W.C.J. Chem. Phys. **148**, 064307 (2018).

<sup>1</sup> E-mail: [salvim@students.iisertirupati.ac.in](mailto:salvim@students.iisertirupati.ac.in)

## Late recollisions in dissociative strong-field ionization of $D_2$

S Hell<sup>1</sup>, and M Kübel<sup>1\*</sup>

<sup>1</sup>Institute of Optics and Quantum Electronics, University of Jena, 07743, Germany

**Synopsis** We present coincidence measurements of the dissociative ionization of  $D_2$  in intense 515 nm laser field, with a half-frequency perturbation. The measured phase-dependent photoelectron spectra, depend strongly on the  $D^+$  kinetic energy release (KER), and reveal the role of laser-driven recollisions. Our results indicate that, even at moderate  $D^+$  energy, bond breakage is facilitated by inelastic recollisions, which take place several optical cycles after ionization. This implies that molecular ion and photoelectron may remain intertwined and exchange energy over a significantly longer period than expected.

Recollisions are known to contribute to high-KER (i.e. several eV) ion emission from  $D_2$  [1]. Low-KER ion emission (i.e. up to few eV), however, is typically understood to result from single or multiphoton absorption from the field.

Here, we show experimentally that recollisions can contribute to dissociation of  $D_2^+$ , even at KER as low as 1 eV. The interesting implication is that the photoelectron and the molecular ion exchange energy long after ionization, because low ion energies imply long internuclear distances and the molecular ion requires several femtoseconds to stretch.

Our experiment uses a two-color technique based on a second harmonic field (515 nm, 40 fs, 90 TW/cm<sup>2</sup>) and a perturbative fundamental (1030 nm,  $\approx 0.01$  TW/cm<sup>2</sup>). The perturbation induces phase-dependent sidebands in the ATI spectrum, generated by the 515 nm light. Both, main ATI peaks and sidebands depended on the relative two-color phase, allowing us to use phase-of-the-phase spectroscopy [2]: the experimental data are Fourier-transformed with respect to the relative phase, and the oscillation amplitude ("relative-phase contrast",  $RCP$ ), and the oscillation phase (the "phase-of-the-phase",  $PP$ ) are plotted as a function of the electron momenta.

Experimental results are presented in Figure 1. While the PP map for  $D_2^+$  (Fig. 1(b)) shows various color patterns corresponding to direct electron emission, forward and backward scattering. In stark contrast, the PP map for  $D^+$  (Fig. 1(d)) shows only a single color pattern, which coincides with the one observed for backscattered electrons in (Fig. 1(b)) - though,

at substantially lower momenta. In addition, a narrower angular distribution is observed for  $D^+$ , again indicating reduced scattering momentum. The KER of  $D^+$  of 2 eV indicates an internuclear distance of  $R > 3$  a.u. at the time of inelastic recollision, which can be reached  $\approx 7$  fs after ionization. This implies that the inelastic collision takes place four optical cycles after ionization.

More generally, our results emphasize the correlation of photoelectron and parent ion in photoionization.

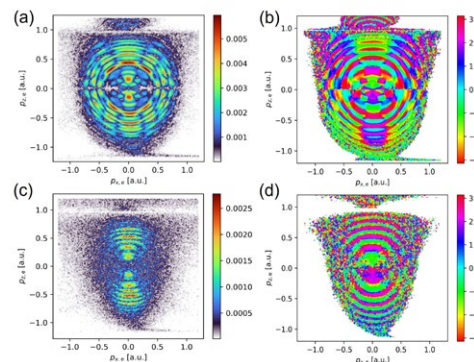


**Figure 1.** Phase-dependent ATI momentum distributions of electrons detected in coincidence with (a,b)  $D_2^+$ , (c,d)  $D^+$  ions ( $1.8 \text{ eV} < \text{KER} < 2.4 \text{ eV}$ ). Panels (a, c) show the relative-phase contrast (amplitude) and (b,d) show the phase-of-the-phase.

### References

- [1] Ibrahim, H., et al. *J. Phys. B At. Mol. Opt. Phys.* 51, 42002 (2018).
- [2] Skruszewicz, S. et al., *Phys. Rev. Lett.* 115, 1–6 (2015).
- [3] Hell, S., et al., *in preparation*

\*E-mail: [matthias.kuebel@uni-jena.de](mailto:matthias.kuebel@uni-jena.de)

## Time-dependent multicomponent optimized coupled-cluster method for nonadiabatic electro-nuclear dynamics

T Sato<sup>1,2,3\*</sup>, C Osaku<sup>1</sup>, Y Orimo<sup>1</sup>, and K. L. Ishikawa<sup>1,2,3</sup>

<sup>1</sup> Department of Nuclear Engineering and Management, School of Engineering, The University of Tokyo, Tokyo, 113-8656, Japan

<sup>2</sup> Photon Science Center, School of Engineering, The University of Tokyo, Tokyo, 113-8656, Japan

<sup>3</sup> Research Institute for Photon Science and Laser Technology, The University of Tokyo, Tokyo, 113-0033, Japan

**Synopsis** We report successful formulation and implementation of the time-dependent multicomponent optimized coupled-cluster (TD-MC-OCC) method for nonadiabatic electro-nuclear dynamics.

We have developed time-dependent multi-configuration self-consistent-field (TD-MCSCF) [1] and time-dependent optimized coupled-cluster (TD-OCC) [2] methods for simulating intense laser-driven electron dynamics. These methods are based on the configuration-interaction (CI) or coupled-cluster (CC) expansion of the total wave function using time-dependent orbitals for efficiently describing ionization dynamics. In particular, the size-extensivity of the TD-OCC method guarantees a uniformly accurate description of the multielectron dynamics independent of the number of electrons.

On the other hand, one needs to treat both electrons and nuclei in a molecule quantum mechanically to describe nonadiabatic molecular dynamics. Various methods have been developed to this end as summarized in a recent review [3], including the general TD-MCSCF method for electro-nuclear dynamics [4], which can treat an arbitrary multicomponent system consisting of different kinds and numbers of interacting fermions and bosons, based on the general CI expansion using time-dependent orbitals.

In this work, we formulate the time-dependent multicomponent optimized coupled-cluster (TD-MC-OCC) method for electro-nuclear dynamics. It uses the multicomponent CC expansion with time-dependent electronic and nuclear orbitals. The present method is size extensive, gauge invariant, and polynomial cost-scaling, achieving a uniformly accurate description of electro-nuclear dynamics inde-

pendent of the number of particles. Numerical applications of the method to intense-laser driven ionization/dissociation dynamics of molecules will be presented (Fig. 1).

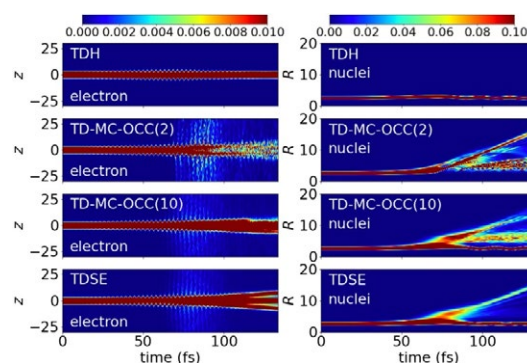


**Figure 1.** Contour plot of the time-dependent electronic (left) and nuclear (right) density of a one-dimensional hydrogen molecular ion model [4] exposed to a laser pulse with an intensity of  $2 \times 10^{14}$  W/cm<sup>2</sup>, a wavelength of 800 nm, and a duration of 50 optical cycles. Numerical results with time-dependent Hartree (top), TD-MC-OCC with two and 10 orbitals each for the electron and nuclei (middles), and numerically exact time-dependent Schrödinger equation (bottom).

### References

- [1] Ishikawa K L, Sato T 2015 *IEEE J. Sel. Top. Quantum Electron.* **21**, 8700916
- [2] Sato T *et al* 2018 *J. Chem. Phys.* **148** 051101
- [3] A. U. J. Lode *et al* 2020 *Rev. Mod. Phys.* **92** 011001
- [4] Anzaki R, Sato T, Ishikawa K L 2017 *Phys. Chem. Chem. Phys.* **19** 22008

\* E-mail: [sato@atto.t.u-tokyo.ac.jp](mailto:sato@atto.t.u-tokyo.ac.jp)

## Quantitative broadband coherent anti-Stokes Raman scattering microscopy based on a simple laser source

Z Li<sup>†</sup>, T Cao, K Chen, Q Xu and J Peng

School of Optical and Electronic Information, Huazhong University of Science and Technology, Wuhan, 430074, China

**Synopsis** A home-built robust, simple, and compact all polarization-maintaining fiber laser source for broadband coherent anti-Stokes Raman scattering signal generation is employed to image lipid distributions in murine brain tissue. Combining with the time resolved technique, a method is proposed to retrieve the information of nonlinear susceptibility and *in situ* light field from the spectrogram.

Coherent Raman scattering offers improved speed, resolution, and sensitivity compared to spontaneous Raman scattering, while still maintaining noninvasive and chemically sensitive nature. Broadband coherent anti-Stokes Raman scattering (BCARS), as a variant, employs ultrashort laser pulse pairs with broad bandwidth to coherently drive multiple electronic states, gaining rich spectral information in one single measurement.

In the present work, we show that a home-built all polarization-maintaining fiber laser source enables BCARS microscopy imaging of murine brain tissue. The two output branches of the laser deliver a broadband (exceeding  $4000\text{cm}^{-1}$ ) pulse to provide both pump and Stokes photons and a narrowband probe pulse to ensure fine spectral resolution, respectively [1]. After being colinearly aligned, the two beams are focused into a tissue sample, and the broadband CARS signal is collected by a spectrometer with a pixel dwell time of 50ms.  $2917\text{cm}^{-1}$  peak of the broadband signal, associated with lipid, is picked out at each point to build a pseudo-color image with a spatial resolution of  $2.5\mu\text{m}$ .

An algorithm has also been developed [2] to simultaneously retrieve the ultrashort laser pulses and the nonlinear susceptibility during the CARS process to do quantitative mapping. First, a spectrogram is attainable by introducing a time delay between the broad- and narrowband beam. The Hilbert transform and baseline detrending combining the successive deconvolution gives a retrieved susceptibility. Then, by tracing the signal maximum along time delay at all frequencies, the phase of broadband pump autocorrelation could be obtained, thus characterizing the whole field information. Finally, the time profile of the

probe pulse at a cross-section of Raman silent frequency combining measured spectrum enables phase retrieval through the GS algorithm. This method paves a way for further understanding of the interaction between photons and molecules *in situ*, e.g. local fields and nonlinearities in the LSP hotspots.

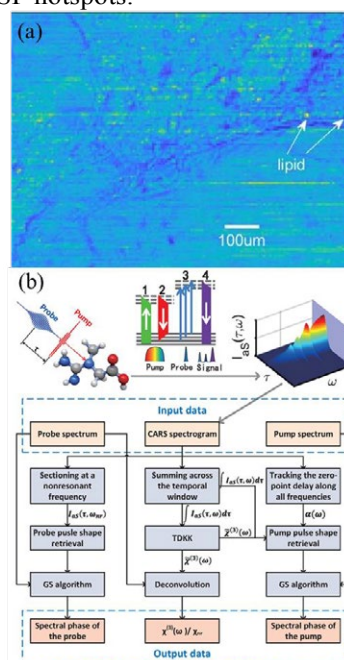


**Figure 1.** (a) Pseudo-color image of murine brain tissue section. (b) Flow diagram of the proposed method.

### References

- [1] Cao T, Yan J, Chen Y, et al. Applied Physics Letters, 2020, [117\(8\): 081103](#).
- [2] Cao T, Li Z, Yan J, et al. The Journal of Physical Chemistry Letters, 2021, [12\(2\): 925-930](#).

<sup>†</sup> E-mail: [lizhou20@hust.edu.cn](mailto:lizhou20@hust.edu.cn)



## Attosecond chronoscopy of the photoemission of a layered system

D Potamianos<sup>1</sup>, M Schnitzenbaumer<sup>1</sup>, C Lemell<sup>2</sup>, P. Scigalla<sup>1</sup>, F Libisch<sup>2</sup>, E Schock-Schmidtke<sup>1</sup>, M Haimerl<sup>1</sup>, M Schäffer<sup>1</sup>, J T Kühle<sup>1</sup>, J Riemensberger<sup>3</sup>, Y Cui<sup>4,5</sup>, U Kleinberg<sup>4,5</sup>, J Burgdörfer<sup>2</sup>, J V Barth<sup>1</sup>, P Feulner<sup>1</sup>, F Allegretti<sup>1</sup>, and R Kienberger<sup>1</sup> \*

<sup>1</sup> Physik Department, Technische Universität München, James-Frank-Str 1, 85748 Garching, Germany

<sup>2</sup> Inst. for Theoretical Physics, TU Wien, Wiedner Hauptstr. 8-10, 1040 Vienna, Austria.

<sup>3</sup> École Polytechnique Fédérale de Lausanne (EPFL), Laboratory of Photonics and Quantum Measurements (LPQM), Lausanne CH-1015, Switzerland

<sup>4</sup> Max-Planck Institut für Quantenoptik, Hans-Kopfermann-Str. 1, 85748 Garching, Germany

<sup>5</sup> Fakultät für Physik, Ludwig-Maximilians-Universität München, Am Coulombwall 1, 85748 Garching, Germany

**Synopsis** We report on the energy-dependence of the photoemission time delay from highly oriented pyrolytic graphite. Our experiments reveals an increase of the photoemission time delay when the final state energy of the excited electrons lies in the vicinity of the band gap.

Attosecond pump-probe experiments succeeded in directly measuring time delays between photoelectrons emitted from different initial states. For the gas phase, measurements with time resolution on the single attosecond scale was achieved [1]. Since the first attosecond chronoscopy on a solid surface [2], many aspects of ultrafast photoemission dynamics affecting the (apparent) emission time of photoelectrons have been investigated. Usually only time differences between groups of electrons are experimentally accessible. However, comparison between numerically exact simulations and experimental data has allowed to determine the absolute timing of processes involved in the emergence photoelectrons for atomic systems as well as solids [3,4].

In this work, we investigate final state effects on the apparent emission time of photoelectrons in a prototypical layered system, highly oriented pyrolytic graphite (HOPG), featuring an unusually wide band gap at about 90 eV above its Fermi level suggesting a slowed-down electron flux and an increased dwell time of the outgoing electrons. Dwell times are directly related to the density of states of the scattering structure [5] and represent an upper bound for the EWS delays.

In our experiment (Fig. 1) we find relative differences in dwell times for electrons from s- and p-type initial states of around 20 as (1 as =  $10^{-18}$ s) if the final-state energy lies near the

band gap of HOPG. Due to the strongly anisotropic dielectric properties of the material we are also able to isolate different contributions to the absolute emission delay as measured with the help of a monoatomically thin adlayer on the target. Accompanying simulations aid in the interpretation of the data.

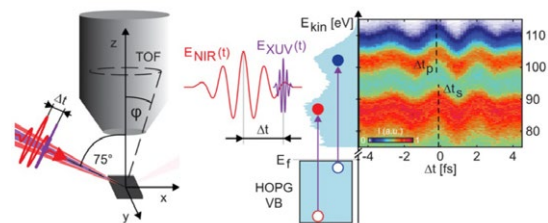


**Figure 1.** Experimental setup and typical streaking spectrogram of the photoemission from from s-type and p-type initial states of HOPG. Electrons are excited to a high lying region of the band structure by an ultrashort XUV pulse, the modulation of momentum imparted on the photoelectrons depends on their time of emission.

### References

- [1] Ossiander M et al. 2017 *Nature Physics* **13** 280
- [2] Cavalieri A L et al. 2007 *Nature* **449** 1029
- [3] Pazourek R et al. 2015 *Rev. Mod. Phys.* **87** 765
- [4] Ossiander M et al. 2018 *Nature* **561** 374
- [5] Iannaccone G 1995 *Phys. Rev. B* **51** 4727

\* E-mail: [reinhard.kienberger@tum.de](mailto:reinhard.kienberger@tum.de)

## Features of the grazing interaction of microfocal bremsstrahlung with the surface edge

V A Smolyanskiy \*, M M Rychkov and V V Kaplin

R&D Laboratory for Betatron Tomography of Large Objects, Tomsk Polytechnic University; Tomsk; 7, Savinyh street 634028 Tomsk; Russian Federation

**Synopsis** The results of studying the grazing interaction of microfocal bremsstrahlung with the edge surface of a plastic framework of the radiographic image quality standard Duplex IQI are presented. The results show that the edge contrast depends on the orientation of the edge surface and can be more complex than the two narrow bands of increased and decreased darkening on the X-ray radiographic pattern, which are determined by radiation refraction. The results were obtained using microfocal bremsstrahlung generated by grazing interaction of an internal electron beam of a B-18 betatron with an energy of 18 MeV with a surface of the Si target 50 or 8  $\mu\text{m}$  thick and 4 mm long along the electron beam. The results are compared with the results on edge contrast obtained using the microfocal bremsstrahlung of a 450-keV X-ray tube with a focus size of 400  $\mu\text{m}$ .

An experimental distribution of microfocal bremsstrahlung generated in the narrow silicon target of a betatron by electrons with an energy of 18 MeV and scattered by the side surface of the plastic plate of the Duplex IQI reference is presented. The observed pattern, consisting of two narrow bands of increased and decreased darkening along the image of the edge of the plate, can be explained in terms of a simple model of radiation refraction on the side surface. In this case, the effect of radiation refraction increases the contrast of the image of the plate, that is, the difference between the darkening on both sides of the plate edge. In addition, the image sharpness of the edge of the plate is high due to the small size of the radiation source and the small slope angle of the side surface relative to the radiation. The presented results show that the "edge" contrast can have a more complex form than two narrow bands of increased and decreased darkening on the image of the plate edge. At a larger inclination angle of the side surface with respect to the direction of radiation, two dark bands and a weak light band are seen in the images, and the sharpness of the plate edge image is lower than in the first case. This is due to the larger inclination angle of the lateral surface of the sample relative to the radiation direction, since the width of the edge blurring image is determined by the width of the enlarged projection of the lateral surface onto the plane perpendicular to the direction of radiation incident on this surface. The formation of two bands of increased darkening on the im

age of the edge of the sample cannot be explained within the framework of a simple model of radiation refraction on the side surface.

To elucidate the mechanism of the formation of such contrast, detailed studies of the orientational dependence of the "edge" image and its theoretical analysis are required.

A complex multiband "edge pattern" was found only for monochromatic X-ray radiation from a microfocal source (see, for example, [1]) due to the diffraction of radiation. In the case of polychromatic bremsstrahlung, as in the present work, such an effect is not obvious. Although, as was noted in [2], for a rather small source size, i.e., with a high spatial coherence of radiation, the condition of longitudinal coherence (monochromaticity) is automatically satisfied for all types of synchrotron sources with polychromatic radiation.

The presented results showed the high quality of radiation from a microfocal source based on a betatron with a narrow target inside. Such a microfocal source can also be used as a laboratory source for research, for example, in materials science or wave effects in X-ray and gamma-ray optics.

### References

- [1] M. El-Ghazaly, H. Backe, W. Lauth, G. Kube, P. Kunz, A. Sharafutdinov, and T. Weber, *Eur. Phys. J. A* 28, 197 (2006).
- [2] Y. Hwu, Wen-Li Tsai, A. Groso, G. Margaritondo, and Ho Je Jung, *J. Phys. D: Appl. Phys.* 35, R105 (2002).

\* E-mail: vsmol@tpu.ru

## Ultrafast THz Magnetic Field Generation Using Quantum Interference Control of Semiconductor Currents

Kamalesh Jana<sup>1\*</sup>, Yonghao Mi<sup>1</sup>, Søren H. Møller<sup>1</sup>, Shawn Sederberg<sup>2</sup> and, P. B. Corkum<sup>1</sup>

<sup>1</sup>Joint Attosecond Science Laboratory, University of Ottawa and National Research Council Canada, 25 Templeton Street, Ottawa, Ontario K1N 7N9 Canada

<sup>2</sup>School of Engineering Science, Simon Fraser University, 8888 University Drive, Burnaby, BC, V5A 1S6, Canada

**Synopsis:** Using femtosecond structured light pulses for two-color coherent control, we generate transient current structures in GaAs. Optically generated semiconductor currents are the sources of THz magnetic impulses. The potential applications of these ultrafast magnetic fields lie in spintronics, imaging and spectroscopy.

Driving ring currents with two-color femtosecond laser pulses provides a new way to generate spatially isolated, intense, ultrafast THz magnetic fields [1]. Two-color coherent control allows the amplitude and the direction of the current to be controlled by changing the relative phase between a fundamental beam and its second harmonic. Applying spatially structured pulses enables us to generate transient current structures which act as sources of spatially tailored ultrafast THz magnetic fields [2,3].

We use liquid crystal devices (q-plates or a SLM) to synthesize the spatially structured light pulses that are used to generate transient current structures in GaAs. We measure the spatial distribution of the excited currents using a single pixel current detector. These dynamic current elements act as an active metasurfaces that emit electromagnetic radiation in THz frequency range.

We measure the single-cycle THz pulses radiated from the ring current structure excited by bichromatic azimuthally vector pulses. Radiated THz is measured at far-field by electro-optic-sampling using a zinc telluride (ZnTe) crystal. We spatially characterize THz pulses by raster scanning the probe beam with a pinhole placed after ZnTe crystal. The space-time map of the measured THz (Fig. 1a) electric field clearly shows a doughnut-shaped structure. We derive spatiotemporal structure of the corresponding magnetic field (Fig. 1b) using Maxwell's equations.

In summary, we present the generation of THz bandwidth magnetic pulses by controlling

currents with two-color femtosecond laser pulses in GaAs. The two-color light pulses inject a transient ring current that radiates a single-cycle THz pulse, known as 'Flying Electromagnetic Doughnut'. The THz pulse has a strong longitudinal isolated magnetic field at the center. Space-time structure of the magnetic field is calculated from the spatiotemporal maps of the measured electric fields.

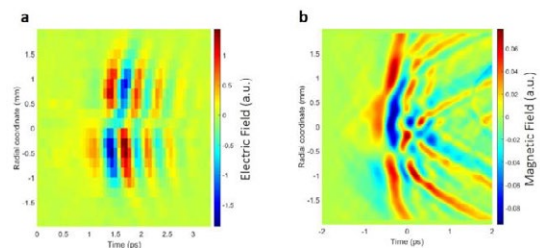


**Figure 1.** (a) Space-time structure of the  $\theta$ -component of the measured THz electric field. (b) Spatiotemporal map of the calculated longitudinal magnetic field.

Similarly, in gases it will be possible to drive large current density and hence, more intense THz magnetic pulses. All-optically generated very fast magnetic field pulses will be useful for time-resolved spectroscopy of magnetic properties of matters.

### References

- [1] S. Sederberg et al., "Tesla-scale terahertz magnetic impulses," *Phys. Rev. X* **10**, 011063 (2020).
- [2] S. Sederberg et al., "Vectorized optoelectronic control and metrology in a semiconductor," *Nature Photon.* **14**, 680-685 (2020).
- [3] K. Jana et al., "Reconfigurable optoelectronic circuits for magnetic fields," *Nat. Photonics* **15**, 622-626 (2021).

\* E-mail: [kjana@uottawa.ca](mailto:kjana@uottawa.ca)

## MsSpec-DFM (Dielectric function module): Towards a multiple scattering approach to plasmon description

A Mandal<sup>1,2\*</sup>, S Tricot<sup>2</sup>, R Choubisa<sup>1</sup> and D Sébilleau<sup>2†</sup>

<sup>1</sup>Department of Physics, Birla Institute of Technology and Science-Pilani, Pilani Campus, Pilani, Rajasthan, 333031, India

<sup>2</sup>Univ Rennes, CNRS, IPR (Institut de Physique de Rennes) - UMR 6251, F-35000 Rennes, France

**Synopsis** The Dielectric Function Module, or MsSpec-DFM module, is a novel independent module of the MsSpec software package. The calculation of model dielectric functions in homogeneous electron gas or Fermi liquids, one- or two-component plasmas, and classical liquids forms the basis of MsSpec-DFM. In many fields of physics, including radiation physics, material analysis, Auger-electron spectroscopy (AES), and X-ray photoelectron spectroscopy (XPS), the scattering of electrons by atoms, molecules, and objects plays a significant role. It will finally be possible to explain Photoemission Energy Loss Spectroscopy (PEELS), thanks to the addition of the current module to the MsSpec package. The goal of this spectroscopy is to monitor and study the plasmon peak, which is a type of imaging phenomenon that can be used to study the surface or bulk dielectric function. This information can be used to describe PEELS. In order to accurately model the dielectric function, it is necessary to perform a study on the plasmon peaks data.

Here, we introduce the MsSpec Dielectric Function module (MsSpec-DFM) [1], which is a new independent module of the MsSpec [2] program package which produces dielectric functions in an electron gas or a liquid, either on an independent or integrated into an overall environment. It offers a flexible method to calculate the fluctuation potential that is incorporated into the quasi-boson modeling of the plasmon field developed by Hedin, Fujikawa, and colleagues [3, 4] from the perspective that includes multiple scattering. In addition to standard models such as the plasmon pole and the random phase approximation, this module also provides more involved methods incorporating local field corrections, Boltzmann-Vlasov hydrodynamical methods, the relaxation-damped Mermin and the diffusion-damped Hu-O'Connell methods, as well as moment-based methods using either a Nevannlinna function or a memory function [5]. The potential of this module extends far beyond the specific issue of plasmon anchoring in the context

of multiple scattering. In fact, it offers a variety of techniques for computing dielectric functions in a variety of materials and can also be used to determine optical characteristics and the cross-section of particular spectroscopies (Electron Energy Loss Spectroscopy - EELS, X-ray inelastic scattering, Raman scattering, ...). Ultimately, through the use of form factors, the MsSpec-DFM module will be able to address a wide range of materials such as metals, semiconductors, including inversion layers, hetero-structures, superconductors, quantum wells, quantum wires, quantum dots, Dirac materials such as graphene, and liquids.

### References

- [1] Mandal A et al, 2022 *arXiv:2207.09924 [cond-mat.other]*
- [2] Sébilleau D et al, 2011 *Comp. Phys. Comm.* **182** 2567
- [3] Hedin L, Michiels J and Inglesfield J, 1998 *Phys. Rev. B* **58** 15565
- [4] Kazama M et al, 2014 *Phys. Rev. B* **89** 045110
- [5] Mandal A et al, 2022 *Phys. Rev. B* **105** 195424

\*E-mail: [p2016009@pilani.bits-pilani.ac.in](mailto:p2016009@pilani.bits-pilani.ac.in)

†E-mail: [didier.sebilleau@univ-rennes1.fr](mailto:didier.sebilleau@univ-rennes1.fr)

## Pressure-dependent Photoluminescence of 0D/2D Heterostructures

R Wu, B Guan, Y Jiang, H Liu, Q Li\*, and M Jin†

Institute of Atomic and Molecular Physics, Jilin University, Changchun, 130012, China

**Synopsis** Among the zero-dimensional/two-dimensional (0D/2D) heterostructures, materials composed of quantum dots (QDs) and transition metal dichalcogenide (TMDCs) crystals have attracted a lot of attention in extracting photogenerated electrons and holes. Here we experimentally demonstrated the interfacial charge behavior of CdSe/ZnS-MoS<sub>2</sub> 0D/2D heterostructures under hydrostatic pressure via photoluminescence (PL) measurements. We found that the formation of HS suppresses the quantum confinement effect, which leads to finer manipulation of photoelectric properties in promising devices based on nano-heterostructures.

In recent years, heterostructures (HS) based on 0D/2D materials such as QDs and TMDCs have become promising candidates for solar cells and photodetectors, because they not only enable strong light absorption but also promote the spatial segregation of photogenerated carriers. QDs are excellent materials with high quantum efficiency and seamless tunability of band gap, while TMDCs crystals have high carrier mobility. The researchers combined these two types of systems to form a new one using their respective strengths [1]. This is an emerging field for probing photoexcited carrier interactions in nano-heterostructures. In today's 0D/2D HS, their components interact via interfacial charge transfer (CT) and non-radiative energy transfer (ET). It is found that the interfacial charge behavior of 0D/2D HS can be varied under external stimuli such as charge doping, temperature, and pressure through the modification of coupling at the interface [1], which facilitates performance optimization of optoelectronic devices.

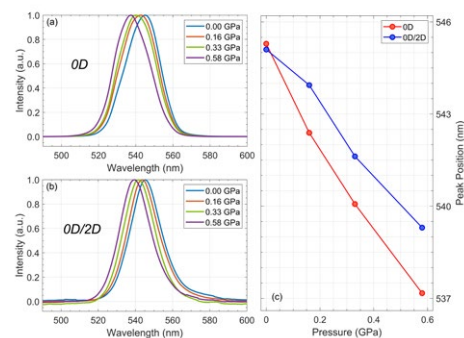
In the present study, we examined the pressure-induced manipulation of interfacial charge behavior of CdSe/ZnS-MoS<sub>2</sub> 0D/2D HS via PL measurements. Mechanical exfoliation was used to obtain few-layer MoS<sub>2</sub>, on which QDs were spin-coated. The sample was placed in a symmetric diamond anvil cell (DAC) device for in-situ high-pressure experiments. The PL spectra of QDs and HS were obtained under excitation with a 410 nm laser.

Figure 1 (a) and (b) show that the PL spectra of CdSe/ZnS QDs and HS undergoes an evident successive blue shift under pressure. Previous studies have shown that hydrostatic pressure

\*E-mail: liqy21@jlu.edu.cn

†E-mail: mxjin@jlu.edu.cn

leads to an enhancement of the quantum confinement effect in QDs and manifests as PL spectral shifts shown in Figure 1(a) [2]. As shown in Figure 1(c), the blue-shift of PL in HS slows down obviously compared with that in QDs. This spectral feature indicates that the formation of HS may relieve the pressure-enhanced quantum confinement effects in QDs via interfacial charge transfer.



**Figure 1.** Representative PL spectra of the (a) QDs on the substrate and (b) QDs/MoS<sub>2</sub> HS under various pressures. (c) The PL peak positions of CdSe/ZnS QDs (red dots) and HS (blue dots) as a function of pressure.

We acknowledge support from the National Key Research and Development Program (No. 2019YFA0307701), the National Natural Science Foundation of China (NSFC Nos. 11974138, 12204191).

### References

- [1] Boulesbaa, A., et al., *J. Am. Chem. Soc.* **138**(44): 14713-14719 (2016)
- [2] Shan, W., et al., *Appl. Phys. Lett.* **84**: 67 (2004)



## Electron excitation dynamics in silicon irradiated by femtosecond double pulses of different wavelength combination

Eiyu Gushiken<sup>\*</sup>, Mizuki Tani<sup>†</sup> and Kenichi L. Ishikawa<sup>‡</sup>

School of Engineering, The University of Tokyo, Tokyo, 113-8656, Japan

**Synopsis** We explore silicon's interaction with intense femtosecond double pulses of different wavelengths using the time-dependent density functional theory. Our results highlight efficient energy transfer with a short-wavelength first pulse and a long-wavelength second pulse. The key factor contributing to this effect is increased mean carrier energy rather than increased carrier numbers. The long-wavelength second pulse further excites conduction electrons, which have been efficiently generated by the high-photon-energy first pulse, while also exciting valence electrons in deeper energy bands.

Ultrashort intense laser interactions with solid-state materials have gained attention due to the fundamental interest in strong-field physics and attosecond science as well as their applications in high-quality laser ablation with minimal heat-affected zones. Efficient processing requires a high energy-absorption-to-incident-pulse-energy ratio. We have recently reported enhanced energy absorption through mixed irradiation of ultraviolet and infrared pulses [1]. In the present study, we theoretically examine how the energy absorption in silicon subject to femtosecond double pulses can be maximized by optimizing the wavelength combination.

We calculate the interaction between intense laser pulses and a Si unit cell based on the time-dependent density functional theory using the open-source program SALMON [2]. We consider a double pulse separated by 35 fs, each with a peak intensity of  $5 \times 10^{12}$  W/cm<sup>2</sup>, a pulse width of 10.8 fs, and a wavelength of 515 nm, 1030 nm, or 2060 nm. We evaluate absorbed energy as the work exerted by the laser electric field on the current density.

Figure 1 displays energy transfer for various wavelength combinations. Although the first pulse's energy absorption is nearly wavelength-independent (not shown), total energy absorption depends significantly on wavelength combinations. Energy deposition from the second pulse relies on both pulse wavelengths. Generally, efficient energy absorption results from combining a short-wavelength first pulse with a long-wavelength second pulse.

<sup>\*</sup>E-mail: [gushiken-eiyu20003@g.ecc.u-tokyo.ac.jp](mailto:gushiken-eiyu20003@g.ecc.u-tokyo.ac.jp)

<sup>†</sup>E-mail: [mzktani@atto.t.u-tokyo.ac.jp](mailto:mzktani@atto.t.u-tokyo.ac.jp)

<sup>‡</sup>E-mail: [ishiken@n.t.u-tokyo.ac.jp](mailto:ishiken@n.t.u-tokyo.ac.jp)

To understand the underlying mechanism, we decompose absorbed energy into the number of generated carriers and their mean energy absorption. The first pulse generates more carriers at shorter wavelengths, i.e., higher photon energies. However, the total (final) carrier generation remains largely unaffected by wavelength combinations, indicating that increased mean energy absorption is the key factor for high total energy absorption. Detailed band population analyses reveal that the long-wavelength second pulse further excites conduction electrons generated by the high-photon-energy first pulse while also exciting valence electrons in deeper energy bands.

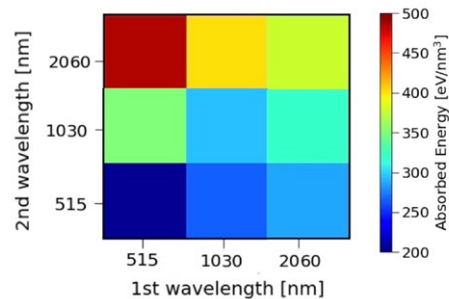


**Figure 1.** Energy transferred to silicon as a function of the first and second pulse wavelengths.

### References

- [1] Tani M, Sasaki K, Shinohara Y, and Ishikawa KL 2022 *Phys. Rev. B* **106** 195141
- [2] Noda M *et al.* 2019 *Comput. Phys. Commun.* **235** 356

## Visualization of ultrafast plasmon by nonlinear multi-photon photoemission electron microscopy

B Y Ji P Lang Y Xu X W Song and J Q Lin\*

School of Physics, Changchun University of Science and Technology, Changchun 130022, China

**Synopsis** we demonstrate subwavelength imaging of ultrafast plasmon and control of the near-field distribution in gold nanostructure through ultrafast nonlinear photoemission electron microscopy.

In recent years, ultrafast plasmon including femtosecond localized surface plasmon(LSP) and propagation surface plasmon(SPP), which can be realized by concentrating femtosecond laser pulses in a subwavelength structure, have been intensively explored[1–2], and it has potential in fabrication of the plasmonic chip with speed in the Peta–Hertz domain.[3] Also, manipulation of plasmonic field on ever smaller length and ever shorter time scale offers the ability to perform ultrafast optical near-field coherent control and nano-optical switching.[4–5] Coherent control of the near field in a nanostructure could be realized by selectively exciting the surface plasmon. The ability to engineer a plasmonic system providing a desired ultrafast response in a predetermined nanostructure is crucial, thus it is necessary to full disclose the distribution of ultrafast plasmon field and to manipulate the optical near field in a given nanoscale volume. Obviously, towards this direction a technique that is capable of imaging plasmons with nanometer resolution is imperative. Photoemission electron microscope (PEEM) assisted with nonlinear multiphoton emission process is an ideal tool to visualize ultrafast plasmons with ultrahigh spatial resolution.

In this presentation, we demonstrate sub-wavelength imaging of ultrafast plasmon and control of the near-field distribution in gold bow-tie as well as in Ag trench through ultrafast nonlinear photoemission electron microscopy. A series of images of local surface plasmon modes on different tips of the bowtie are obtained by the two-color photoemission electron microscopy, and accordingly a comprehensive disclose of the localized near-field distribution within a bow-tie nanostructure are realized [6]. The enhanced photoemission assist

ed by the opening of two-color quantum channel is found to be responsible for the underlying physics. On the other side, visualization of the propagation surface plasmon control on a flat surface with the trench structure at different femtosecond laser excitation wavelengths and polarization angles are given, and found that both the field distribution and propagation direction of SPP can be controlled by varying femtosecond laser parameters [7].

### References:

- [1]D.Brinks, M.Castro-Lopez, Hildner R and Hulst N F 2013 *Proc. Natl. Acad. Sci. USA*,110 18386,
- [2]Rewitz C, Keitzl T, Tuchscherer P, Huang J S, Razinslas G, Hecht B and Brixner T , 2012 *Nano Lett.* 12 45,
- [3][http://www.bacatec.de/en/gefoerderte\\_projekte.html](http://www.bacatec.de/en/gefoerderte_projekte.html)
- [4]Stockman M I, Sergey V F and David J B 2002 *Phys. Rev. Lett.* 88 067402,
- [5]Brixner T, de Abajo F G J, Schneider J and Pfeiffer W 2005 *Phys. Rev. Lett.* 95 093901,
- [6]Ji, B., Song, X., Tao, H., Hao, Z. & Lin, J., 2018 *New J. Phys.* 20 073031.
- [7]Yulu Qin, and Jingquan Lin, 2021 *Photonic Research.* 12 1326

\* E-mail: [linjingquan@cust.edu.cn](mailto:linjingquan@cust.edu.cn)

## Orbital perspective of high-harmonic generation in ReS<sub>2</sub>

A Galán<sup>1,2</sup>, C Bossaer<sup>1,2,\*</sup>, G Ernotte<sup>1</sup>, A Parks<sup>3</sup>, R Silva<sup>4</sup>, D Villeneuve<sup>1</sup>, A Staudte<sup>1</sup>, T Brabec<sup>3</sup>, A Luican-Mayer<sup>3</sup> and G Vampa

<sup>1</sup>Joint Attosecond Science Laboratory, National Research Council of Canada and University of Ottawa, Ottawa, ON K1A 0R6, Canada

<sup>2</sup>Max-Born-Institute, Berlin, D-12489, Germany

<sup>3</sup>Department of Physics, University of Ottawa, Ottawa, ON K1N 6N5, Canada

<sup>4</sup>Instituto de Ciencia de Materiales de Madrid (ICMM), Consejo Superior de Investigaciones Científicas (CSIC), 28049 Madrid, Spain

**Synopsis** A real-space theoretical framework is used to identify the atoms in the unit cell of an ReS<sub>2</sub> crystal that contribute to the emission of high-order harmonics. Our findings provide an unprecedented and intuitive atomic perspective on strong-field dynamics in crystals.

High-harmonic generation (HHG) in solids allows probing and controlling of electron dynamics in crystals on few femtosecond time-scales. The foundational concept underpinning attosecond physics, and HHG in gas-phase atoms and molecules in particular, is the energetic recollision of an electron ionized and accelerated by a strong laser field with the parent ion [1]. This dynamic real-space framework is instrumental to link the characteristics of the emitted harmonic radiation (amplitudes, phases and polarization) to sub-laser-cycle dynamics of atomic and molecular orbitals [2].

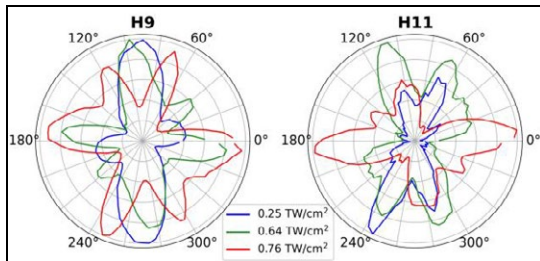


**Figure.** Measured orientation-dependent HHG from bulk ReS<sub>2</sub> for harmonics 9 and 11 for different laser intensities and polarizations  $\theta$ .

A real-space approach offers an intuitive framework compared to the reciprocal-space approach paramount in virtually all solid-state HHG investigations [3, 4]. In the spatial domain, recent advances in the real-space interpretation

of HHG in solids allows the imaging of field-free, static, potential of the valence electrons with picometer resolution [5]. The combination of such extreme spatial and temporal resolutions to measure/control strong-field dynamics in solids at the atomic scale is poised to unlock a new frontier of lightwave electronics.

Here, we report a strong intensity-dependent anisotropy in the HHG from ReS<sub>2</sub> that we attribute to angle-dependent interference of currents from the different atoms in the unit cell, that contribute to the emission of a particular harmonic order. Furthermore, we demonstrate how the laser parameters control the relative contribution of these atoms to the HHG.

Our findings provide an unprecedented atomic perspective on strong-field dynamics in crystals and suggest that crystals with a large number of atoms in the unit cell are not necessarily more efficient harmonic emitters than those with fewer atoms.

### References

- [1] Corkum, P 1993 *Phys. Rev. Lett.* **71** 1994
- [2] Levesque J *et al* 2007 *Phys. Rev. Lett.* **98** 183903
- [3] Vampa G *et al* 2014 *Physical Review Letters* **113** 73901
- [4] Ndabashimiye G *et al* 2016 *Nature* **534** 520
- [5] Lakhotia, H. *et al* 2020 *Nature* **583** 55

\* E-mail: [cboss007@uottawa.ca](mailto:cboss007@uottawa.ca)

## Characterizing high harmonics using frequency resolved optical switching

Saadat Mokhtari<sup>1,2</sup>, Mayank Kumar<sup>1</sup>, Tristan Guay<sup>1</sup>, Giulio Vampa<sup>†2</sup>, Francois Legare<sup>1†</sup>,

<sup>1</sup>Centre Énergie Matériaux Télécommunications, Institut National de La Recherche Scientifique, Varennes, Canada

<sup>2</sup>Joint Attosecond Science Laboratory, National Research Council of Canada and University of Ottawa, Ottawa, Canada

### Synopsis

Characterizing high harmonics in time domain is important because it reveals the physics of electron hole dephasing time or band structure changes the intensity of high harmonics is low and, therefore, they cannot be characterized by common pulse characterization based on nonlinear frequency conversion method like second-harmonic frequency-resolved optical gating, which depend nonlinearly on the signal to be measured. Herein, we are developing a new way to characterize high harmonics using frequency resolved optical switching.

High harmonics are generated when intense light interacts with a solid-state material. In fact, the recollision between the excited electron and its parent hole generates attosecond high harmonic pulses of the driving frequency of laser [1]. High harmonics include information about the quantum process at the atomic levels and the dynamics associated with high harmonic generation [2]. Characterization and understanding of high harmonics is crucial due to their possible applications.

High harmonics are not intense enough to be characterized with the methods based on nonlinear frequency conversion, such as second harmonic generation frequency-resolved optical gating (SHG-FROG).

In this study, we aim to characterize high harmonics using frequency-resolved optical switching (FROSt), a pulse characterizing method that is linear in the field to be measured and free of phase matching limitations. The method has been shown to work in the infrared range [4]. Here we extend the FROSt technique to visible and ultraviolet frequencies, thus opening the way for measuring solid-state high harmonics.

FROSt is based on pump-probe experiments, with the pump being strong enough to generate carriers or, in the other words, to induce a rapid transmissivity change for the probe (a “switch”). If the probe pulses are chirped, each frequency of the probe is absorbed a different time. Thus, measuring the time-dependent spectrum of the probe can retrieve the probe spectral amplitude and phase.

Firstly, we show that FROSt is also applicable in the visible range. Figure 1 shows the FROSt reconstruction result of a 35 fs pulse centered at 515 nm passing through a 5 mm CaF<sub>2</sub> window. As shown in Figure 1a, the full width at half maximum (FWHM) based on the FROSt reconstruction result is 45 fs, with the

blue and red curves representing the intensity and temporal phase reconstructed by the FROSt technique. The reconstruction result is compared with the theoretical result based on the following equation, where  $\sigma_{out}$  is the pulse duration when the initial pulse with a time duration of  $\sigma_{in}$  passes through a material with a thickness of  $d$ , and GVD is the group velocity dispersion of the window (CaF<sub>2</sub> in our case) at the driving frequency of  $\omega_0$ . In our case, GVD = 48.68 fs<sup>2</sup>/mm. Thus, the calculated pulse duration is 40 fs, confirming that the FROSt technique is working in the visible range. Figure 1b and 1c are experimental and reconstructed spectrogram in intensity, respectively.

$$\sigma_{out} = \sqrt{\sigma_{in}^2 + [dGVD(\omega_0)\frac{1}{2\sigma_{in}}]^2} \quad \text{eq. 1}$$

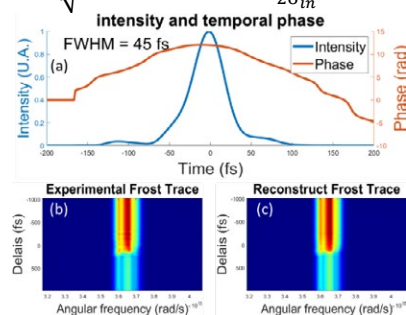


**Figure 1.** FROSt reconstruction result of a 35 fs pulse at 515 nm passing through 5mm CaF<sub>2</sub>. (a) Intensity (blue) and phase reconstructed (red). (b) Experimental spectrogram in intensity (c) Reconstructed spectrogram in intensity

### References

- [1] G. Vampa et al., (2015) *nature* **522** 462-464.
- [2] E. Frumker et al., (2009) *Optica* **34** 3026-3028.
- [3] C. Heide et al., (2022) *Optica* **9** 512– 516.
- [4] A. Leblanc et al., (2019) *Opt.Express* **27** 28998-29015.

<sup>†</sup> E-mail: [Francois.Legare@inrs.ca](mailto:Francois.Legare@inrs.ca)

<sup>†</sup> E-mail: [Giulio.Vampa@nrc-cnrc.gc.ca](mailto:Giulio.Vampa@nrc-cnrc.gc.ca)

## Tunable spectral shift of high-order harmonic generation in atoms by a plasmon-assisted shaping pulse

Yuan Wang<sup>1</sup>, Qingyi Li<sup>1</sup>, Zhou Chen<sup>1</sup>, Jun Wang<sup>1\*</sup>, Fuming Guo<sup>1</sup>, Yujun Yang<sup>1</sup>

<sup>1</sup>Institute of Atomic and Molecular Physics, Jilin University, Changchun 130012, China

**Synopsis** We have investigated the harmonic emission process of atoms under the action of a plasmon-assisted shaping pulse. In this case, the spectral shift that occurs in atomic HHG can be achieved easily. It is shown that the photon energy of the generated harmonics is controllable in the range of 0.2 eV. The shift of the frequency peak position is rooted in the asymmetry of the rising and falling edge of the laser pulse. Further we also found that by altering oscillation frequencies  $T$ , the bandwidth of the generated high-order harmonics is changed.

When an intense laser pulse interacts with atoms, high-order harmonic generation (HHG) can be observed. It is the most reliable pathway for producing coherent light source with spectra range from extreme ultraviolet (XUV) to soft x-ray. It deserves more attention that photon energy-tunable XUV radiation is very important in many fields such as ultrafast spectroscopy, XUV holography, etc.

By solving the time-dependent Schrödinger equation, we investigated the harmonic emission from a helium atom under the action of a plasmon-assisted shaping pulse. The driving laser electric field is shaped in frequency domain [1]. The phase function [2] is  $\varphi(\omega) = A \sin[(\omega_{ref} - \omega) * T + \phi]$ , where  $A$  describes the amplitude of the phase modulation function,  $T$  is the frequency of the sinusoidal oscillation, and  $\phi$  is phase offset. Spatial function [3] is  $E_S = y_0 + \sum_{i=1}^3 \alpha_i \exp(-\frac{x-x_0}{\beta_i})$ .

The variations of the harmonic intensity (40-45 orders) for various parameter values are given in Figure 1. It can be seen that the harmonic intensities of He atoms under different parameters  $T$  are significantly modified. The photon energy of the generated harmonics is modulated within the range of 0.2 eV. And by altering  $T$ , we can observe the alteration of the bandwidth of the generated high-order harmonics.

The spectrally shifted HHG from He atoms is attributed to the asymmetry of the rising and falling parts of the laser pulse. When  $T = 1400$ , the distance between the sub-pulses and the main pulse is small, and the first incident sub-pulse will interfere constructively with the main pulse. The overall pulse presents an asymmetrical distribution relative to the intermediate

moment. The rising part of the pulse will possess a higher intensity than the falling part, resulting in a large variation in the harmonic frequency. On the other hand, when  $T$  increases, the sub-pulse gradually moves away from the main pulse, the overall pulse tends to show symmetrical structure. Thus when  $T = 2000$ , the harmonic peak position hardly changes. In the meantime, we also note that the obtained harmonic spectral lines are a little wider. In order to make the individual harmonic shift more distinct, moderately thinner harmonics can be generated by decreasing the spectral width of the driving field [4].

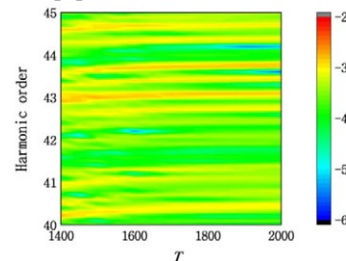


**Figure 1.** Variation of harmonic intensity for different values of oscillation frequencies  $T$ .

This work was supported by the National Key Research and Development Program of China (No. 2022YFE0134200), the National Natural Science Foundation of China under Grants No. 12074145.

### References

- [1] M. Wollenhaupt *et al* 2006 Phys. Rev. A **73** 063409.
- [2] Y Qiao *et al* 2022 Chin. Phys. B **31** 064214.
- [3] J Wang *et al* 2015 Phys. Rev. A **92** 033848.
- [4] LG Oldal *et al* 2020 Phys. Rev. A **102** 013504.

\* E-mail: [wangjun86@jlu.edu.cn](mailto:wangjun86@jlu.edu.cn)



## Far-ultraviolet (FUV) emission from laser-produced plasma of Al, Fe, Cu and Inconel

S. Tamaki<sup>1</sup>, H. Ohnishi<sup>1</sup>, Y. Shiina<sup>1,2</sup>, and Y. Nakano<sup>1,2,\*</sup>

<sup>1</sup>Department of Physics, Rikkyo University, Tokyo 171-8501, Japan

<sup>2</sup>Research Center for Measurement in Advanced Science (RCMAS), Rikkyo University, Tokyo 171-8501, Japan

**Synopsis** We studied the far-ultraviolet (FUV) emission from the laser-produced plasma in the prospect of possible applications as a light source. The FUV spectra were observed for Al, Fe, Cu, and Inconel alloy and analyzed using the NIST LIBS database. We also developed a parabolic mirror, which successfully collected the plasma radiation into a collimated beam with an intensity enhanced by 35 times.

Emission from laser-produced plasma is widely studied for laser-induced breakdown spectroscopy (LIBS) and use as a light source in a broad range of wavelengths from THz to X-rays. These light sources are commercially available in the near-infrared to ultraviolet (170 – 2100 nm) and the EUV (13.5 nm) for semiconductor lithography. However, application in the far-ultraviolet (FUV) has not yet been exploited.

In this work, we performed a spectroscopic analysis and plasma characterization of the laser-produced plasma of Al, Fe, Cu, and Inconel alloy (Ni/Cr/Fe) to explore their potential application in the far-ultraviolet (FUV) region. Using the 2<sup>nd</sup> harmonics of the Q-switched Nd:YAG laser at 532 nm, we produced the metal plasma and observed the FUV emission through a vacuum monochromator. Each target showed a characteristic spectral profile in the FUV region. In Figure 1, the solid line shows the plasma emission spectrum from the Al target. We estimated the plasma temperature to be 6.36 eV from the intensities of known transitions. The colored dashed lines are the simulation by the NIST LIBS database. The electron density was estimated to be  $2 \times 10^{21} \text{ cm}^{-3}$  for Al. The FUV intensity was increased proportionally to the 2.1th power of the laser pulse energy. On the other hand, the electron temperature and the overall spectral shape did not depend on the laser pulse energy from 100 to 550 mJ.

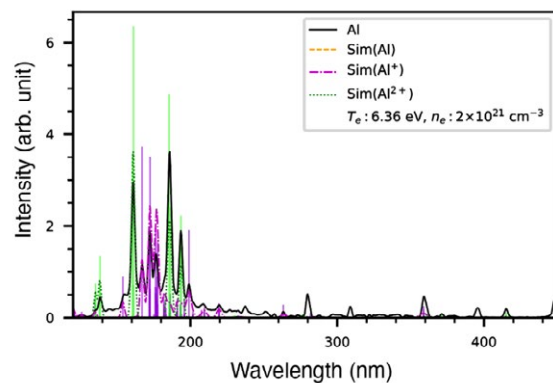


**Figure 1.** Observed spectrum (solid line) of the laser-produced Al plasma and the simulation (dashed lines) by the NIST LIBS database.

We also developed an off-axis parabolic mirror to collect and collimate the plasma emission. By setting the parabola focus on the position of the plasma, the FUV light was reflected into a collimated beam. As a result, the FUV intensity at the monochromator exit was enhanced by 35 times, making the FUV intensity up to  $10^7$  photon/pulse/1% bandwidth.

### References

- [1] H. Ohnishi *et al.*, submitted to J. Appl.Phys..

\* E-mail: [nakano@rikkyo.ac.jp](mailto:nakano@rikkyo.ac.jp)

## Recent progress of muon catalyzed fusion study: I. new kinetics model with muonic molecular resonances

T Yamashita<sup>1\*</sup>, Y Kino<sup>1</sup>, K Okutsu<sup>1</sup>, Y Toyama<sup>2</sup>, S Okada<sup>2</sup>, and M Sato<sup>2</sup>

<sup>1</sup>Tohoku University, Sendai, 980-8578, Japan

<sup>2</sup>Chubu University, Kasugai 487-8501, Japan

**Synopsis** We present a kinetics model of muon catalyzed fusion ( $\mu$ CF) cycle including muonic molecular resonances. Our model agrees with the previous experimental values of cycle rates in a wide range of target temperature and tritium concentrations. We also perform a precise three-body calculation to reveal the X-ray spectrum from the muonic molecular resonances. We overview the roles of these states in  $\mu$ CF.

A muonic molecule is a bound state of a muon ( $\mu$ ) and two hydrogen nuclei. Owing to the 207 times larger mass of  $\mu$  than the electron, the inter-nuclear distance shrinks by a factor of 100 from the corresponding ordinary hydrogen molecular ion  $H_2^+$ . The overlap of the nuclear wavefunctions results in a intra-molecular nuclear fusion in particular for the muonic molecules  $dd\mu$ ,  $dt\mu$ , and  $tt\mu$ . After the nuclear fusion reaction, the  $\mu$  becomes free from the nuclei, and repeats the molecular formation and the nuclear fusion. These processes are called muon catalyzed fusion ( $\mu$ CF) [1].

Recently, the  $\mu$ CF is revisited with new experimental techniques and renewed motivation. The improvement of the energy resolution of X-ray detectors allows us to reveal the dynamics of muon atomic processes [2] in more detail. It has been pointed out that the formation and decay of muonic molecular resonances (hereafter denoting  $dt\mu^*$  and so on) could play an important role in the  $\mu$ CF cycles to explain discrepancies between experimental observations and theoretical predictions [3]. However, no experimental observation has been reported for the muonic molecular resonances so far, and theoretical investigation into the muonic atom cascade processes [4] has been limited. Besides,  $\mu$ CF in high temperature compressed gas target is newly under consideration [5].

In this work we examine the model of  $\mu$ CF in  $D_2$ - $T_2$  target including the formation/decay of the muonic molecular resonance states,  $dd\mu^*$ ,  $dt\mu^*$ , and  $tt\mu^*$ , by solving a set of 19 rate-

equations. These molecules decay via non-radiative dissociation producing a high-energy ( $\sim 1$  keV) muonic atom or via radiative dissociation, e.g.

$$dd\mu^*(v, J) \rightarrow d\mu(1s) + d + \gamma, \quad (1)$$

where  $v, J$  denote vibrational and rotational quantum numbers. The X-ray spectra of  $dd\mu^*$ ,  $dt\mu^*$ , and  $tt\mu^*$  can be a signal to test the preset model, and are calculated by a precise three-body treatment using a complex coordinate rotation method.

Our model is found to reproduce the experimental  $\mu$ CF cycle rates over a wide range of tritium concentration conditions [5]. The proposed kinetics model predicts that the cycle rate increases as an increase of target temperature ( $\sim 1000$  K) and density. The roles of the muonic molecular resonances are summarized as follows: (i) change of isotopic muonic atom population, (ii) production of epi-thermal muonic atoms, and (iii) inducing fusion in-flight. We also point out that the X-ray intensity from the resonant muonic molecules would provide a positive signal for verification of the  $\mu$ CF kinetics.

### References

- [1] Froelich P 1992 *Adv. Phys.* **41** 405
- [2] Okumura T *et al.* 2021 *Phys. Rev. Lett.* **127** 053001
- [3] Froelich P and Wallenius J 1995 *Phys. Rev. Lett.* **75** 2108
- [4] Popov V P and Pomerantsev V N 2022 *Phys. Rev. A* **105** 042804
- [5] Yamashita T *et al.* 2022 *Sci. Rep.* **12** 6393

---

\*E-mail: [tyamashita@tohoku.ac.jp](mailto:tyamashita@tohoku.ac.jp)

## Recent progress of muon catalyzed fusion study:

### III. Alternative measurement of nuclear fusion reaction in muonic molecule

K Okutsu<sup>1</sup>, T Yamashita<sup>1</sup>, Y Kino<sup>1\*</sup>, R Nakashima<sup>1</sup>, R Konishi<sup>1</sup>, K Sasaki<sup>1</sup>, K Miyashita<sup>1</sup>, Y Toyama<sup>2</sup>, S Okada<sup>2</sup>, M Sato<sup>2</sup>, T Oka<sup>3</sup>, N Kawamura<sup>4</sup>, S Kanda<sup>4</sup>, K Shimomura<sup>4</sup>, P Strasser<sup>4</sup>, S Takeshita<sup>4</sup>, M Tampo<sup>4</sup>, S Doiuchi<sup>4</sup>, Y Nagatani<sup>4</sup>, H Natori<sup>4</sup>, S Nishimura<sup>4</sup>, A D Pant<sup>4</sup>, Y Miyake<sup>4</sup>, K Ishid<sup>5</sup>

<sup>1</sup>Tohoku University, Sendai 980–8578, Japan

<sup>2</sup>Chubu University, Kasugai 487–8501, Japan

<sup>3</sup>Japan Atomic Energy Agency (JAEA), Tokai 319–1195, Japan

<sup>4</sup>High Energy Accelerator Research Organization (KEK), Tokai, 319-1195, Japan

<sup>5</sup>RIKEN, Wako, Saitama 351-0198, Japan

**Synopsis** After a nuclear fusion reaction occurs in the muonic deuterium molecule  $dd\mu$ , the muon is liberated having a peak kinetic energy of 1.1 keV. Observation of the liberated muon can be an alternative measurement of nuclear fusion in the muonic molecule and  $\mu$ -<sup>3</sup>He sticking processes.

A muonic molecule ( $dd\mu$ ) consisting of a muon ( $\mu$ ) and two deuterons ( $d$ ) is regarded as an analogous system of  $D_2^+$  ( $= dde$ ), where the electron is replaced by  $\mu$ . Due to the small spatial size of the  $dd\mu$  molecule, a nuclear fusion reaction ( $dd\mu \rightarrow {}^3\text{He} + n + \mu + 3.27 \text{ MeV}$  or  $p + t + \mu + 4.03 \text{ MeV}$ , where  $n$ ,  $p$ , and  $t$  are a neutron, a proton, and a triton, respectively), occurs inside the muonic molecule. After the nuclear reaction the  $\mu$  can form another  $dd\mu$  molecule and cause the nuclear reaction again. The series of the reactions is called muon-catalyzed fusion ( $\mu\text{CF}$ ) [1,2]. Observations of the nuclear fusion reactions has been done by measuring the 2.45 MeV fusion  $n$  or 8 keV x-ray from the muonic <sup>3</sup>He atom (<sup>3</sup>He $\mu$ ) formed in the  $\mu$ -<sup>3</sup>He sticking reaction ( $dd\mu \rightarrow {}^3\text{He}\mu + n + 3.27 \text{ MeV}$ ). We have tried to perform another kind of measurement for the nuclear fusion reaction by detecting the released  $\mu$  just after the nuclear reaction. We call the released  $\mu$  as “recycling muon” because it continues the  $\mu\text{CF}$ . The recent state of the art calculation gives most dominant energy of 1.1 keV [3].

In order to detect the recycling  $\mu$ , we extracted the recycling  $\mu$  into the vacuum from the solid deuterium target where the  $\mu\text{CF}$  occurred. Since the range of the recycling  $\mu$  is a few  $\mu\text{m}$  in the target, we used the solid  $\text{H}_2/\text{D}_2$  target prepared for the x-ray spectroscopy for the muonic atoms with unstable nuclei [4]. The  $\text{H}_2/\text{D}_2$  target consisting of 1 mm thick of  $\text{H}_2$  layer doped with 0.1 % of  $\text{D}_2$  and 1  $\mu\text{m}$  thick of  $\text{D}_2$  layer faced to the vacuum. The injected  $\mu$  from the accelerator stopped in the  $\text{H}_2$  layer and formed a  $p\mu$  atom. Due to the energy difference between the  $p\mu$  and  $d\mu$  atoms,

the  $\mu$  transferred to the  $d\mu$  with kinetic energy of 43 eV. The elastic cross section of the  $d\mu + p$  at ca 1 eV is nearly zero because of the Ramsauer–Townsend effect, and the  $d\mu$  could go through the  $\text{H}_2$  layer and would stop at the thin  $\text{D}_2$  layer [5]. We accumulated the recycling  $\mu$  emitted to the vacuum by newly developed charged particle transformation system consisting of negatively charged wire and grounded cylinder [6]. The  $\mu$ 's were transferred to the low background area by the static electric field. Finally, the  $\mu$ 's were injected into thin Ag foil and distinguished from the scattered  $\mu$  beam by detecting characteristic x-ray of muonic Ag atom [7].

We have done feasibility studies at J-PARC/MLF and obtained x-ray spectra suggesting the recycling muon extraction. The measurement of the recycling  $\mu$  is expected to supply an important information to promote  $\mu\text{CF}$  process. Extraction of regenerative muons would advance the development of slow  $\mu$  source.

#### References

- [1] Nagamine K and Kamimura M 1998 *Adv. Nucl. Phys.* **24** 151
- [2] Yamashita T *et al.*, 2022 *Sci Rep* **12** 6393
- [3] Kmamimura M *et al.* 2023 *Phys. Rev. C* **107** 034607
- [4] Strasser P *et al.*, 2001 *Nucl. Instrum. Methods Phys. Res., Sect. A* **460** 451
- [5] Mulhauser F *et al.*, 2006 *Phys. Rev. A* **73** 034501
- [6] Nagatani Y *et al.*, 2020 *Japanese patent application* No. 2020-178286
- [7] Okutsu K *et al.*, 2021 *Fusion Eng. Des.* **170** 112712

\* E-mail: y.k@tohoku.ac.jp

## Triple-differential cross sections in three-dimensional kinematics for electron-impact-ionization dynamics of tetrahydrofuran at 250-eV projectile energy

X Xue<sup>1</sup>, D M Mootheril<sup>2</sup>, E Ali<sup>3,4</sup>, M Gong<sup>5</sup>, S Jia<sup>1</sup>, J Zhou<sup>1,2</sup>, E Wang<sup>5,2</sup>, J Li<sup>1</sup>, X Chen<sup>5</sup>, D Madison<sup>6,\*</sup>, A Dorn<sup>2</sup>, and X Ren<sup>1,2,†</sup>

<sup>1</sup>School of Physics, Xi'an Jiaotong University, Xi'an, 710049, China

<sup>2</sup>Max-Planck-Institut für Kernphysik, Heidelberg, 69117, Germany

<sup>3</sup>Department of Natural Sciences, D. L. Hubbard Center for Innovation, Northwest Missouri State University, Maryville, Missouri, 64468, USA

<sup>4</sup>Department of Physics, Faculty of Arts and Sciences-El Marj, University of Benghazi, El Marj, 9480, Libya

<sup>5</sup>Synergetic Innovation Center of Quantum Information and Quantum Physics,

University of Science and Technology of China, Hefei, Anhui, 230026, China

<sup>6</sup>Department of Physics, Missouri University of Science and Technology, Rolla, Missouri, 65409, USA

**Synopsis** We report a combined experimental and theoretical study of the ionization dynamics of tetrahydrofuran induced by 250 eV electron impact. The triple-differential cross sections for the single ionization of tetrahydrofuran are experimentally measured by a reaction microscope. The experimental data are compared with predictions from the molecular three-body distorted-wave (M3DW), the multicenter distorted-wave (MCDW) approaches, and the MCDW-WM method. There is an overall better agreement between the M3DW predictions and the experimental data than the MCDW calculations.

Electron-impact-ionization cross sections are relevant in many fields of sciences and technologies. From the simple atoms and molecules to larger systems including biomolecules, the triple-differential cross sections (TDCSs) provide information which can help to explore the few-body quantum dynamics, and to obtain electronic structure of the targets. There have been recent systematic investigations of the ionization dynamics of biomolecules, e.g., for tetrahydrofuran (THF, C<sub>4</sub>H<sub>8</sub>O), which can be regarded as a molecular analog of the deoxyribose sugar ring in the DNA backbone [1,2]. A number of theoretical models were developed to compare with the experimental TDCSs, where the different theories show larger discrepancies with experiment and also between each other [1]. It is difficult to reflect on the quality of the theoretical models since the experiments do not show a sufficient good statistical significance.

In the present work, we reported a comprehensive study of the electron-impact-ionization dynamics of THF for a projectile energy of 250 eV and a scattering angle of  $\theta_1 = -10^\circ$  [3]. Figure 1 presents the TDCSs in three orthogonal planes at  $\theta_1 = -10^\circ$  and  $E_2 = 10.0$  eV. Comparing the experimental data to the theoret-

ical results from the M3DW, MCDW, and MCDW-WM models, we see that the M3DW predictions are generally in good agreement with the experimental results, particularly regarding the angular dependence in the recoil region and the relative magnitude between binary and recoil lobes. The present experimental data substantially enhance the still very limited set of data currently available to thoroughly test theoretical methods for more accurately describing the electron track structures in bio-relevant systems.

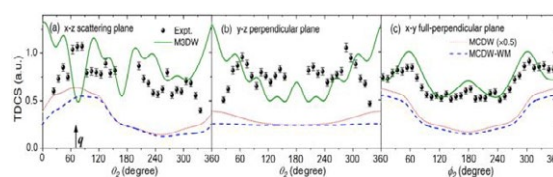


**Figure 1.** Experimental and theoretical TDCSs for the ionization of THF as a function of the ejected-electron emission angle at scattering angles  $\theta_1 = -10^\circ$  for ejected-electron energies  $E_2 = 10.0$  eV.

### References

- [1] E. Ali et al 2020 *J. Chem. Phys.* **152** 124303
- [2] J. Zhou et al 2021 *Phys. Rev. A* **104** 012817
- [3] X. Xue et al 2022 *Phys. Rev. A* **106** 042803

\*Deceased.

†E-mail: [renxueguang@xjtu.edu.cn](mailto:renxueguang@xjtu.edu.cn)

## Calculation of molecular ionization cross-sections using complex Gaussian representations of the continuum

A Ammar<sup>1,2</sup>, A Leclerc<sup>1\*</sup> and L U Ancarani<sup>1†</sup>

<sup>1</sup>Université de Lorraine, CNRS, LPCT, F-57000 Metz, France

<sup>2</sup>Present postal address: Université de Toulouse, CNRS, LCPQ, F-31062 Toulouse, France

**Synopsis** The theoretical study of molecular ionization processes requires an efficient description of the electronic continuum. Using complex Gaussian-type orbitals to represent the outgoing electron wavefunction, we obtained analytical, closed-form expressions for all the integrals involved in cross-section calculations. The proposed method is applied to the photoionization and electron-impact ionization of methane.

The theoretical description of molecular ionization processes requires accurate multicentric wavefunctions. Because of their very interesting mathematical properties, Gaussian basis sets are widely exploited for bound states calculations, while their use is far less developed in the context of fragmentation processes where continuum states play a leading role. In a series of recent papers [1-4], we have explored the possibility of representing continuum states with complex Gaussian-type orbitals (cGTO). While nodeless real GTOs (rGTO) usually fail in representing oscillating wavefunctions, their complex counterparts perform better and lead to sufficiently accurate representations (up to 30 a.u. using typically 30 cGTO) reliable enough for physical applications. Whether with rGTO or Slater representations of the molecular target, and within given approximations, the cGTO strategy allows us to derive closed form expressions for all the multicenter one-electron integrals involved in the calculations of photoionization or electron-impact ionization observables.

The method has been applied so far to the photoionization cross-section and asymmetry parameters of neon-like molecules (NH<sub>3</sub>, H<sub>2</sub>O and CH<sub>4</sub>) using monocentric approximations for the initial state of the target. Theoretical formulae and results will also be presented at the conference for the case of electron-impact ionization of CH<sub>4</sub>, using the kinematic parameters of two different experiments [5,6] (see figure 1).

We will also show that the monocentric approximation of the initial state can be dropped, exploiting again the mathematical advantages of cGTO.

\*E-mail: [arnaud.leclerc@univ-lorraine.fr](mailto:arnaud.leclerc@univ-lorraine.fr)

†E-mail: [ugo.ancarani@univ-lorraine.fr](mailto:ugo.ancarani@univ-lorraine.fr)

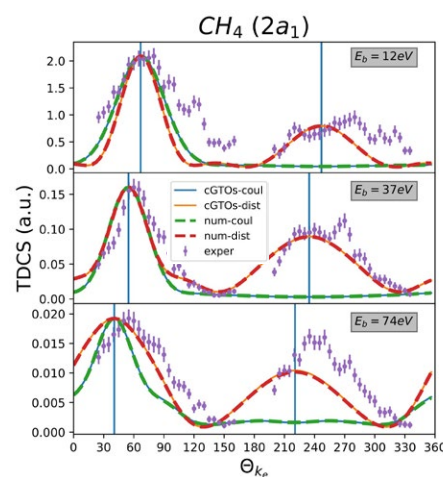


**Figure 1.** (e,2e) TDCS for the inner valence orbital ( $2a_1$ ) of CH<sub>4</sub>, as a function of ejection angle for the experimental kinematical parameters [5]. cGTO analytical calculations using either Coulomb or distorted waves for the ejected electron are compared with purely numerical results and with experimental points.

### References

- [1] Ammar A, Leclerc A and Ancarani U 2020 *J. Comput. Chem.* **41** 2365
- [2] Ammar A, Ancarani U and Leclerc A 2021 *J. Comput. Chem.* **42** 2294
- [3] Ammar A, Leclerc A and Ancarani U 2021 *Adv. Quantum Chem* **83** 287
- [4] Ammar A, Leclerc A and Ancarani U 2023 *Adv. Quantum Chem* in press
- [5] Lahmam-Bennani A *et al* 2009 *J. Phys. B: At. Mol. Opt.* **42** 165201
- [6] Ali E *et al* 2019 *J. Chem. Phys.* **150** 194302



## Many-body theory and calculations of $\gamma$ spectra for low-energy positron annihilation in polyatomic molecules

A R Swann<sup>1</sup>, S K Gregg<sup>1\*</sup>, J P Cassidy<sup>1</sup>, J Hofierka<sup>1</sup>, B Cunningham<sup>1</sup>, C M Rawlins<sup>1</sup>, C H Patterson<sup>2</sup>, and D G Green<sup>1†</sup>

<sup>1</sup>School of Mathematics and Physics, Queen's University Belfast, Belfast, BT7 1NN, Northern Ireland, United Kingdom

<sup>2</sup>School of Physics, Trinity College Dublin, Dublin, Ireland

**Synopsis** Many-body theory has been developed and applied to calculate Doppler-broadened  $\gamma$  spectra for positron annihilation in polyatomic molecules, implemented in the Gaussian-orbital EXCITON+ code.

The ability of positrons to annihilate with atomic and molecular electrons — forming two detectable  $\gamma$  rays whose Doppler-shifted energies are characteristic of the electronic structure — makes them unique probes of matter, and gives them important use in e.g., materials science (for ultrasensitive studies of surfaces, defects and porosity) [1, 2], medical imaging (positron emission tomography), and astrophysics (as a probe of the molecular composition of the galaxy) [3, 4].

Proper interpretation of the materials science experiments and development of the antimatter-based technologies requires fundamental understanding of positron interactions with molecules, and ideally predictive capability. Positron-molecule interactions are, however, characterised by strong many-body correlations [5, 6, 7, 8], e.g., polarisation of the electron cloud by the positron, screening of the positron by the electrons, and virtual-positronium formation. They significantly modify the scattering properties and enhance annihilation rates. They also make the description of positron-molecule interactions a challenging theoretical and computational problem. The extent of the challenge is highlighted by the fact that despite the important applications, and that there are long-standing positron-trap-based measurements of  $\gamma$  spectra for over 50 molecules [4], there has yet to be accurate calculations of positron-molecule  $\gamma$  spectra which take proper account of many-body correlations.

We have extended our recent many-body theory approach to positron binding [5] to enable the calculation of Doppler-broadened  $\gamma$  spectra for positron annihilation in polyatomic molecules,

including the effects of positron-molecule correlations. Our approach, which is implemented in our massively-parallelised Gaussian-orbital basis code EXCITON+, solves the Dyson equation involving the positron-molecule self energy calculated via the Bethe-Salpeter equations for the two-particle propagators.

We will present the computational implementation and recent calculations for various polyatomic molecules that bind the positron, including polyaromatic hydrocarbons recently discovered in the interstellar medium, DNA nucleobases, and small non-positron-binding molecules including H<sub>2</sub>, N<sub>2</sub> and CH<sub>4</sub> [9], quantifying the effects of the correlations and highlighting the individual contributions of molecular orbitals to the  $\gamma$ -spectra.

### References

- [1] Tuomisto F and Makkonen I, *Rev. Mod. Phys.* **85**, 1583 (2013).
- [2] Hugenschmidt C, *Surf. Sci. Rep.* **71**, 547 (2016).
- [3] Prantzos N, *et al.* *Rev. Mod. Phys.* **83**, 1001 (2011).
- [4] Iwata K, Greaves R G, and Surko C M, *Phys. Rev. A* **55**, 3586 (1997).
- [5] Hofierka J, Cunningham B, Rawlins C M, Patterson C H and Green D G, *Nature* **606**, 688–693 (2022).
- [6] Green D G and Gribakin G F, *Phys. Rev. Lett.* **114**, 093201 (2015).
- [7] Green D G *et al.*, *New J. Phys.* **14** 035021 (2012).
- [8] Green D G and Gribakin G F, *Phys. Rev. A* **95**, 036701 (2017).
- [9] Swann A R, Cassidy J P, Gregg S K, Hofierka J, Cunningham B J, Rawlins C M, Patterson C H and Green D G (in preparation).

\*E-mail: [sgregg07@qub.ac.uk](mailto:sgregg07@qub.ac.uk)

†E-mail: [d.green@qub.ac.uk](mailto:d.green@qub.ac.uk)

## Many-body theory calculations of positron binding to halogenated hydrocarbons

J P Cassidy<sup>1</sup>\*, J Hofierka<sup>1</sup>, B Cunningham<sup>1</sup>, C M Rawlins<sup>1</sup>, C H Patterson<sup>2</sup> and D G Green<sup>1</sup>†

<sup>1</sup>Queen's University Belfast, Belfast, BT7 1NN, Northern Ireland, United Kingdom

<sup>2</sup>School of Physics, Trinity College Dublin, Dublin, Dublin 2, Ireland

**Synopsis** We present *ab initio* many-body theory calculations of positron binding to chlorinated and fluorinated molecules, comparing with experiment and model-potential calculations where possible.

It is now well established that positrons can bind to a variety of polyatomic molecules [1], a process mainly facilitated via vibrational Feshbach resonances. Using trap-based beams, positron binding energy measurements have been made for around 90 molecules over the last two decades (see e.g., [1]). Here, we extend our *ab initio* many-body-theory approach [2] to study a variety of polyhalogenated molecules, including planar molecules where anisotropic effects are important [3]. In 2021, model calculations and measurements of positron binding to chlorinated hydrocarbons were performed by Swann and Gribakin *et al.* [4]. Their model calculations are in excellent agreement with experiment for many of the molecules they consider, however, their model assumes that the positron-molecule interactions are asymptotically isotropic, and fails to find agreement with experiment for planar molecules where the true interactions are highly anisotropic. Anisotropic interactions were accounted for in a DFT model approach [5], which saw improved agreement with experiment, but which relies on an adjustable parameter that differs for each molecule.

Applying our many-body-theory approach [2], we find very good agreement with experiment, especially so for those chlorinated molecules with 2 or less chlorine atoms. For molecules with 3 or more chlorine atoms, the molecules are typically weakly or non-polar, and the positron wave function is very diffuse, making an accurate calculation computationally difficult. Going further, we study the fluorinated counterparts of the chlorinated molecules, and show that these molecules generate a less attrac-

tive positron-molecule potential due to higher MO ionization energies and smaller density of occupied valence molecular orbitals. This results in severely weakened, or in most cases loss of, positron binding.

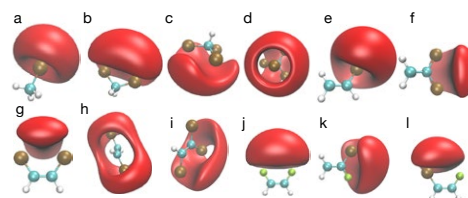


**Figure 1.** Positron Dyson wave functions at 80% of the wave function maximum for: a) chloromethane, b) dichloromethane, c) trichloromethane, d) tetrachloromethane (93% of max), e) vinyl chloride, f) vinylidene chloride, g) *cis*-1,2-dichloroethylene, h) *trans*-1,2-dichloroethylene (90% of max), i) trichloroethylene, j) *cis*-1,2-difluoroethylene, k) 1-chloro-1-fluoroethylene, l) (*Z*)-chlorofluoroethylene.

### References

- [1] Gribakin G F, Young J A and Surko C M 2010 *Rev. Mod. Phys.* **82** 2557
- [2] Hofierka J, Cunningham B, Rawlins C M, Patterson C H and Green D G 2022 *Nature* **606** 688
- [3] Cassidy J P, Hofierka J, Cunningham B, Rawlins C M, Patterson C H and Green D G [arXiv:2303.05359](https://arxiv.org/abs/2303.05359)
- [4] Swann A R, Gribakin G F, Danielson J R, Ghosh S, Natisin M R and Surko C M 2021 *Phys. Rev. A* **104** 012813
- [5] Suzuki H, Otomo T, Iida R, Sugiura Y, Takayanagi T and Tachikawa M 2020 *Phys. Rev. A* **102** 052830

\*E-mail: [jcassidy18@qub.ac.uk](mailto:jcassidy18@qub.ac.uk)

†E-mail: [d.green@qub.ac.uk](mailto:d.green@qub.ac.uk)

## Low-energy positron collisions with tetrachloroethylene ( $C_2Cl_4$ ) molecule

R O Lima<sup>1</sup>, A S Barbosa<sup>1\*</sup>, M H F Bettega<sup>1</sup>, S D Sanchez<sup>1</sup> and G M Moreira<sup>1†</sup>

<sup>1</sup>Departamento de Física, Universidade Federal do Paraná, Caixa Postal 19044, 81531-980 Curitiba, Paraná, Brazil

**Synopsis** We report integral (ICS) and differential (DCS) cross-sections for low-energy positron elastic collisions with tetrachloroethylene molecule. For this purpose, we employed Schwinger multichannel method in the static plus polarization approximation. To investigate the description of polarization effects, several calculations, with different polarization schemes, have been performed. We compared our results with experimental data available in the literature and our results agree qualitatively well with the most recent experimental data for the ethylene molecule.

In recent years, positrons have gained increasingly use in diverse applications, ranging from medicine to annihilation spectroscopy [1, 2]. For many of these applications, obtaining data of positron collisions is of fundamental importance. Hence, the interest in positron-molecule collisions has grown with the advance of experimental and theoretical methodologies [3].

Tetrachloroethylene is a simple polyatomic molecule and has already been studied on low-energy electron-molecule collision. Experimental realizations on positron collisions with this system indicated a positron-molecule bound state formation [4]. Therefore, theoretical study of positron collisions with tetrachloroethylene may bring new interesting data in comparison with electron-molecule collisions, once there is the change of sign of interaction potential and the absence of the exchange potential. To compute the cross sections of low-energy positron collisions with tetrachloroethylene, Schwinger Multichannel method (SMC) was employed with TZV ++ (2d,p) basis set, in the static plus polarization (SP) approximation. All valence orbitals were used as hole and scattering orbitals. The calculations with 47 MVOs (modified virtual orbitals) as particle orbitals will be labeled as SP-1 and the calculations with 72 MVOs will be labeled as SP-2.

We will present theoretical results of integral and s-wave elastic cross sections for energies ranging from  $10^{-6}$  to 10 eV. From fig-

ure 1, we could identify the Ramsauer-Townsend (RT) minimum in all calculations. Analyzing the scattering length (SL) data and eigenphase, we observed the existence of a positron-molecule bound state formation for DIF-3 calculation.

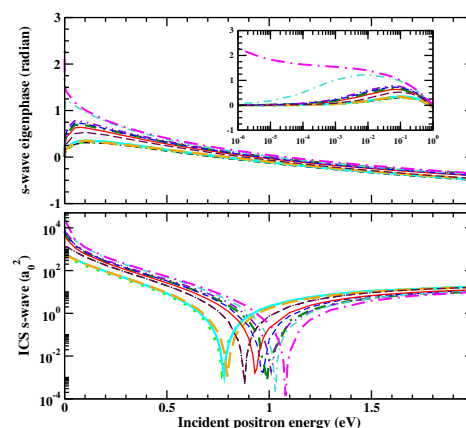


**Figure 1.** s-wave cross section (lower panel) and the corresponding eigenphase (top panel) obtained employing all polarization schemes. The insert presents the same data, in order to highlight their very low-energy behavior.

### References

- [1] Karwasz G P *et al* 2004 *J. Alloys Compd.* **382** 244
- [2] Visioni A *et al* 2011 *Surg. Clin. North Am.* **91** 249
- [3] Brunger *et al* 2017 *J. Phys. Chem. Ref. Data* **46**023102
- [4] Natisin M R *et al* 2017 *Phys. Rev. Lett.* **119** 113402

\*E-mail: [alessandra@fisica.ufpr.br](mailto:alessandra@fisica.ufpr.br)

†E-mail: [gmm08@fisica.ufpr.br](mailto:gmm08@fisica.ufpr.br)

## Electron and Positron impact ionisation of few biologically relevant molecules for coplanar and perpendicular plane emission of electrons

Alpana Pandey<sup>1\*</sup>, Ghanshyam Purohit<sup>1†</sup>

<sup>1</sup> Department of Physics, University College of Science, Mohanlal Sukhadia University, Udaipur, 313001, India

**Synopsis** One of the most effective theoretical techniques, the distorted-wave Born approximation (DWBA), has been expanded to calculate the projectile-impact ionisation of molecules. It enables the solution to three-body problems involving two outgoing electrons, which are used in the Schrödinger equation and represented by a spherically symmetric potential. These calculations determine the energy and momenta of all final-state particles, resulting in a triple-differential cross-section. We will be giving an overview of ionisation in the low to intermediate energy range for a few molecular targets.

The study of charged particle motion in the vicinity of a nucleus is one of the most significant collision processes in atomic and molecular physics. This study is useful not only in the fields of astrophysics, biology, and medicine but also in the development of various experimental and calculation methods. In the coincidence study, triple differential cross sections (TDCS) are obtained to provide detailed information about (e, 2e) collision processes, which have been of interest since Ehrhardt's pioneering work [1]. In recent years, many atomic and molecular targets like  $H_2$  [2],  $N_2$  [3],  $CH_4$  and  $H_2O$  have been the subject of extensive ionization cross-section studies. We will report electron and positron impact ionisation triple differential cross sections (TDCSs) of molecules like  $CO_2$ ,  $N_2$ ,  $H_2O$  and pyrimidine.

The ionization cross-sections will be obtained in the first Born approximation formalism which will be extended to the next higher order i.e. the second Born approximation using orientation averaged molecular orbital (OAMO) approximation. The post-collision interaction (PCI) is also included to treat the interaction between two outgoing particles. The obtained results will be compared with the recently available measurements and analysed in terms of binary and recoil peak positions and intensities in both coplanar and perpendicular plane geometrical conditions. In the present communication, we report the results of TDCS obtained for  $CO_2$  molecule. TDCSs have been calculated over the three valence orbitals  $1\pi_g$ ,  $1\pi_u$ ,  $3\sigma_u$  which are inter-normalized

across scattering angles at ejected electron energy 8eV and compared with the experimental results [4].

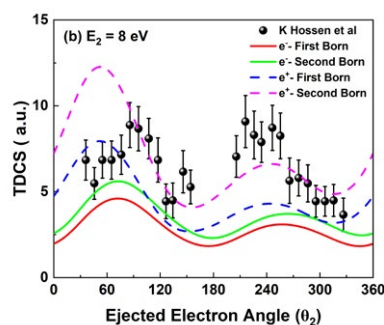


**Figure 1.** Scattering plane triple-differential cross sections for  $CO_2$  molecules and summed TDCS of  $1\pi_g$ ,  $1\pi_u$ ,  $3\sigma_u$  (a) Solid red line shows electron impact in first Born (b) Solid green line shows electron impact in second Born (c) Dashed blue line shows positron impact in first Born (d) Dashed pink line shows positron impact in second Born (e) solid circles with error bars show experimental summed TDCS [4].

### References

- [1] Ehrhardt H, Hesselbacher KH, Jung K, Willmann K 1972 *Journal of Physics B* **5(8)** 1559
- [2] Madison DH, Al-Hagan O 2010 *Journal of Atomic and Molecular Physics* **2010**
- [3] Pandey A, Purohit G 2022 *Atoms* **10(2)** 50
- [4] Hossen K, Ren X, Wang E, Gong M, Li X, Zhang SB, Chen X, Dorn A. 2021 *Journal of Physics B* **51(21)** 215201

\*E-mail: [phd22\\_alpana@mlsu.ac.in](mailto:phd22_alpana@mlsu.ac.in)

†E-mail: [ghanshyam.purohit@mlsu.ac.in](mailto:ghanshyam.purohit@mlsu.ac.in)

## Electronic excitation of benzene by electron impact: a theoretical and experimental investigation

A G Falkowski<sup>1</sup>, R F da Costa<sup>2</sup>, M A P Lima<sup>1</sup>, A De Avila Cadena<sup>3</sup>, R Pcoroba<sup>3</sup>, M A Khakoo<sup>3</sup> and F Kossoski<sup>4\*</sup>

<sup>1</sup>Instituto de Física Gleb Wataghin, Universidade Estadual de Campinas, Campinas, 13083-872, Brazil

<sup>2</sup>Centro de Ciências Naturais e Humanas, Universidade Federal do ABC, 09210-580, Brazil

<sup>3</sup>Physics Department, California State University, Fullerton CA 92831, USA

<sup>4</sup>LCPQ (UMR 5626), Université de Toulouse, CNRS, UPS, France

**Synopsis** New angle-differential measurements for electron impact of the first five electronic bands of benzene are reported at impact energies of 10, 12.5, 15, and 20 eV. They are compared with scattering calculations using the Schwinger multichannel method, for a varying number of coupled open channels (up to 437). The agreement between experiment and theory is improved when higher-lying Rydberg states are included in the calculations.

Modelling electronic excitation of molecules by the impact of electrons requires a series of different approximations. A specially relevant one concerns the truncation of target states included in the calculations. Measurements of differential excitation cross sections can provide a stringent test for this aspect of theoretical models.

The present contribution extends our joint experimental-theoretical investigation on elastic scattering from benzene [1] to the electronic excitation domain. Electron scattering calculations were performed with the Schwinger multichannel (SMC) method [2]. Three different scattering models were considered (B1, B2, and B3), which accounted for progressively more Rydberg states in the space of energetically allowed target states, totaling 117, 305, and 437 open channels, respectively. Further methodological details are the same as in Refs. [1, 3]. New angle-differential measurements for the first five electronic bands of benzene are reported as well.

As the complete set of results is extensive, we illustrate in Figure 1 a specific comparison: the differential cross sections for the excitation of band IV of benzene, at the electron impact energy of 15 eV. Increasing the number of higher-lying Rydberg states as open channels significantly improves the comparison between calculations with the present and previous [4] measurements, which in turn agree very well with each other.

Similar trends were observed for other bands and impact energies. Importantly, the computed

electronic excitation cross sections have indications of convergence with respect to inclusion of Rydberg states. However, discrepancies in the forward direction (see Figure 1) stress the need to improve the description of excitation mediated by the long range potential in the SMC method.

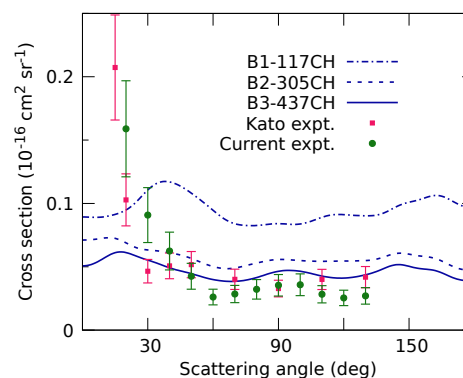


**Figure 1.** Differential cross sections for electron impact excitation of band IV of benzene, at 15 eV, according to SMC calculations with three levels of multichannel coupling, and compared to the present and previous [4] measurements.

### References

- [1] Cadena A de A *et al.* 2022, *Phys. Rev. A* **106** 062825
- [2] da Costa R F *et al.* 2015, *Eur. Phys. J. D* **69** 159
- [3] Falkowski A G *et al.* 2021, *Eur. Phys. J. D* **75** 310
- [4] Kato H *et al.* 2011, *J. Chem. Phys.* **134** 134308

\*E-mail: [fkossoski@irsamc.ups-tlse.fr](mailto:fkossoski@irsamc.ups-tlse.fr)



## Scaled Born approximation for electron impact excitations of N<sub>2</sub> molecule

J L S Lino

Assessoria e Orientação Estudantil-AOE, São José dos Campos, São Paulo, Brazil

**Synopsis** Replace this text with your synopsis. The synopsis should be 16 cm wide. Keep it concise at a maximum length of 600 characters including spaces. Use single-spaced lines with 10 pt Roman font.

We discuss recent investigations on the scaling plane wave Born cross sections for electron impact by N<sub>2</sub> molecule. The scaled Born approximation was originally proposed by Kim [1] and the expression of work is given by

$$\sigma_{\text{scaled}} = (f_{\text{acc}}/f_{\text{Born}}) [E_0/(E+B+E_{\text{exc}})] \cdot \sigma_{\text{Born}}$$

where  $E_0$  is the incident electron,  $B$  is the binding energy of the electron excited, and  $E$  the excitation energy of the target (the scaled Born is called BE $f$ -scaling). Although this type of scaling has been used in several studies, its success remains to be explored. We have proposed a simple modification where the  $(B+E_{\text{ex}})$  term now can be associated with the closure approximation used in the second Born approximation (SBA)[2]. This analogy between the  $(B+E_{\text{ex}})$  term and SBA suggests that the BE $f$ -scaling may be related to the polarizability of the target. The fact that when is adopted  $C < (B+E_{\text{ex}})$  a better agreement of cross sections with experimental data can be observed. The BE $f$ -scaling cross section depends on two independent approximations: (a) a first Born approximation (FBA), and (b) parameters as “ $B$ ” e  $E_{\text{ex}}$ .

We will test the BE $f$ -scaling modified for the electronic excitation of N<sub>2</sub> by electron impact. As observed in Fig.1, the BE $f$ -scaling modified is very encouraging when compared with experimental data[2].

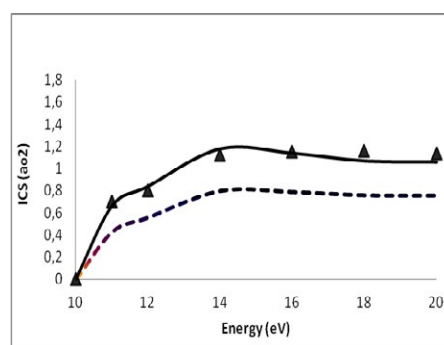


Fig.1: Integral cross sections (ICS) for electron-N<sub>2</sub>(a<sup>1</sup> $\pi_g$ ). Solid line, BE $f$ -scaling modified; dashed line, BE $f$ -scaling; black triangle, experimental data[2]

### References

- [1] Kim Y K 2007 *J. Chem. Phys.* 126 064305
- [2] Sullivan et al 2001 87 073201

E-mail: aulas.aoe@hotmail.com

## Electron Impact Induced Fragmentation of $\text{ND}_3^+$

M. O. A. El Ghazaly<sup>1,2,\*</sup>, J.J. Jureta<sup>1,3</sup>, O. Al-Hagan<sup>2</sup> and P. Defrance<sup>1</sup>

<sup>1</sup>IMCN, Catholic University of Louvain, Chemin du Cyclotron, 2, 1348 Louvain-la-Neuve, Belgium

<sup>2</sup>Department of Physics, King Khalid University, Guraiger 62529, Saudi Arabia

<sup>3</sup>Institute of Physics, University of Belgrade, Belgrade 11081, Serbia

Absolute cross sections for electron impact ionization and dissociative excitation or ionization of  $\text{ND}_3^+$  ions have been measured in a single-pass experiment using crossed-beams technique. In this experiment, the ionization product  $\text{ND}_3^{2+}$  along with different singly-charged dissociation products,  $\text{ND}^+$  and  $\text{ND}_2^+$  were collected separately. Excitation and ionization mechanisms are analyzed.

Molecular ions play a significant role in interstellar space, in atmospheres of planets and in planetary ionospheres, as well. Likewise, they are an important player in laboratory plasmas such as of combustion engines or in the divertor and edge regions of ITER-like fusion devices [1]. In either type of plasma, molecular ions undergo various excitation and ionization reactions, which, in turn, mostly lead to dissociation. In particular, nitrogenated ions are of significance in planetary aeronomy and in ion-chemistry of interstellar clouds. Electron-induced dissociative excitation (DE) or ionization (DI) of interstellar  $\text{NH}_3^+$  ammonia cation is a significant process in nitrogen-rich regions of space, likely on Pluto on Titan's upper atmosphere [2], in interstellar ices, molecular clouds and interstellar grains. These reactions likely occur in interstellar space, within the interaction of solar-wind with interstellar nitrogen-rich molecular clouds.

Electron-impact ionization and dissociation processes have been widely studied in the single-pass electron-ion experiment at the Catholic University of Louvain, Belgium, and the present investigation is a part of a series dedicated to nitrogenated molecular ions [3-5].  $\text{ND}_3^+$  ions are extracted from an ECR, being accelerated to 8 keV and mass purified, the ion beam crosses the electron beam at right angle. The electron energy is tunable from a few eV up to 2.5 keV. Fig. 1 shows the absolute cross section for electron impact ionization of  $\text{ND}_3^+$ . Cross-sections for various DE and DI channels were measured, as well. Detailed re-

sults for  $\text{D}_2^+$ ,  $\text{N}^+$ ,  $\text{N}^{2+}$ ,  $\text{ND}^+$  and  $\text{ND}_3^{2+}$  will be presented and discussed at the Conference.

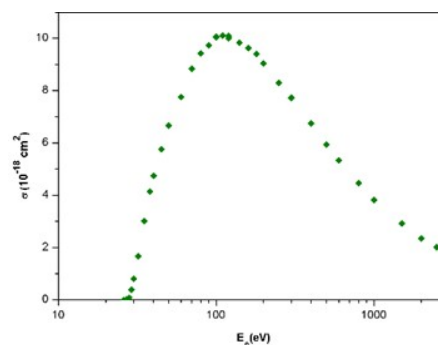


**Figure 1.** Absolute electron-impact ionization cross-section of  $\text{ND}_3^+$ .

### References

- [1] J Braams and H.-K. Chung, *J. Phys.: Conf. Ser.* 576 (2015) 011001
- [2] H. B., Niemann, S. K. Atreya, J. E. Demick *et al. JGR*, 115 (2010) E12006
- [3] M.O.A. El Ghazaly, J. B. Mitchell, J.J. Jureta and P. Defrance, *J. Phys. Chem. A* 118 (2014) 10020–10027
- [4] J. Lecointre, J.J. Jureta and P. Defrance, *J. Phys. B: At. Mol. Opt. Phys.* 43 (2010) 105202
- [5] E. M. Bahati, J.J. Jureta, D. S. Belie, H. Cherkani-Hassani, M. O. Abdellahi and P. Defrance. *J. Phys. B: At. Mol. Opt. Phys.* (2001) 34 2963

\* E-mail: mohamed.elghazaly@uclouvain.be

## Elucidating geometrical features of e-C<sub>60</sub> interaction from their elastic scattering spectra

R Aiswarya<sup>1</sup>, J. Jose<sup>1</sup>, R Shaik<sup>2</sup>, H R Varma<sup>\*2</sup>, and H S Chakraborty<sup>3</sup>

<sup>1</sup> Department of Physics, Indian Institute of Technology Patna, Bihar 801103, India

<sup>2</sup> School of Physical Sciences, Indian Institute of Technology Mandi, H P 175005, India

<sup>3</sup> Department of Natural Sciences, D L Hubbard Center for Innovation, Northwest Missouri State University, Maryville, Missouri 64468, USA

**Synopsis** The present study calculates the elastic scattering cross-section of e-C<sub>60</sub> collision and interprets the results in terms of geometrical features of C<sub>60</sub>. The fullerene molecule is considered as a spherical diffractor that induces structural attributes in the spectra.

From material synthesis point of view, C<sub>60</sub> offers a possibility to encapsulate atoms within the hollow cage to form stable systems, known as endohedral fullerenes. How the properties of the atom alter in such a confining ambience is of fundamental interest. From a technological point of view, fullerene systems have been proposed as building blocks of the quantum computer [1,2]. Furthermore, fullerene complexes carry potentials for applications in photovoltaic devices, high T<sub>c</sub> super conductivity etc. [3,4].

This study explores the elastic scattering of e-C<sub>60</sub> using Density Functional Theory (DFT) jointly with a partial wave approach. Additionally, an annular square well (ASW) potential is used as a model for C<sub>60</sub> to draw parallels between the sophisticated DFT and ASW results. Born approximation is employed to confirm the interpretation of the spectra.

One knows from measurements of elastic scattering that e-C<sub>60</sub> collision cross-sections bear diffraction-type minima and maxima. The current investigation finds effects of the C<sub>60</sub> geometry in calculated differential cross-sections (DCS). Results from the partial wave analysis, in conjunction with Born approximation, prove that C<sub>60</sub> acts as a diffractor in the scattering process. The work, thus, concludes that DCS bears signatures of the fullerene geometry that can be measured for target information.

A comparison between DCS from ASW result at a high impact energy (200 eV) and the corresponding analytical result *via* Born approximation with ASW potential is shown in figure 1. The reasonable agreement, as seen, prompted us to extend the analysis to look for features in DCS using born approximation in

the momentum transfer scale. A Fourier transform analysis sheds direct light on the connection between diffraction-type oscillations to the geometry of C<sub>60</sub>. These results motivated us to further explore the phenomenon in DCS obtained using the DFT model and also from experimental results with some success.

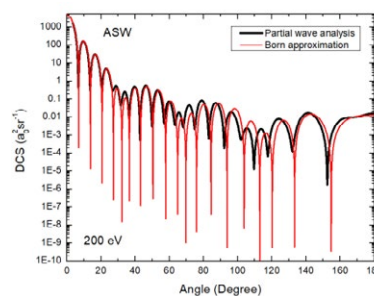


**Figure 1.** Comparison of DCS for e-C<sub>60</sub> elastic scattering calculated using ASW potential using partial wave analysis and Born approximation for 200 eV.

Funding supports: SERB Grant No.

CRG/2022/000191(JJ) and

CRG/2022/002309(HRV); US-NSF Grant No.

PHY-2110318(HSC).

### References

- [1] Yang W L, Xu Z Y, Wei H, Feng M, and Suter D 2010 *Phys. Rev. A* **81**, 32303
- [2] Ju C, Suter D and Du J, 2011 *Phys. Lett. A* **375**, 1441
- [3] Hedley G J, Ward A J, Alekseev A, Howells C T, Martins E R, Serrano L A, Cooke G, Ruseckas A, and Samuel I D W 2013 *Nat. Commun.* **4**, 2867
- [4] Zadik R H, Takabayashi Y, Klupp G, Colman R H, Ganin A Y, Potočník P, Jeglič P, Arčon D, Matus P, Kamarás K, Kasahara Y, Iwasa Y, Fitch A N, Ohishi Y, Garbarino G, Kato K, Rosseinsky M J, and Prassides K 2015 *Sci. Adv.* **1**, e1500059

\* E-mail: [hari@iitmandi.ac.in](mailto:hari@iitmandi.ac.in)

## Tracing the expansion of molecular plasma with electron collision

Guangqing Chen, Zonglin Yao, Xu Shan\* and Xiangjun Chen†

Department of modern physics, School of Physical Sciences, University of Science and Technology of China, Hefei, 230026, P. R. China

We report the creation of molecular plasma by photoionization of toluene which is detected by electron collision during the expansion. The preliminary results of binding energy spectrum of toluene after being irradiated by the laser are shown.

The expansion of a plasma is caused by the thermal pressure of electrons. How the electron temperature evolves is crucial for us to understand the dynamics of the plasma expansion [1]. Here, we report investigation on molecular plasma using a time-resolved (e, 2e) spectrometer [2], which is based on the electron impact ionization combined with pump-probe technique.

In the experiment, two-photon resonance enhanced ionization of toluene via  $S_1$  state by a 267 nm picosecond pump laser leads to the formation of a molecular plasma, which is probed by an 800 eV, 100 ns pulsed electron beam.

An ionization peak at 0 eV is observed in binding energy spectrum, which is attributed to the ionized electrons trapped in the Coulomb potential well of toluene ions. The evolution of the momentum distribution of the plasma electrons was observed and will be presented in detail at the forthcoming conference.

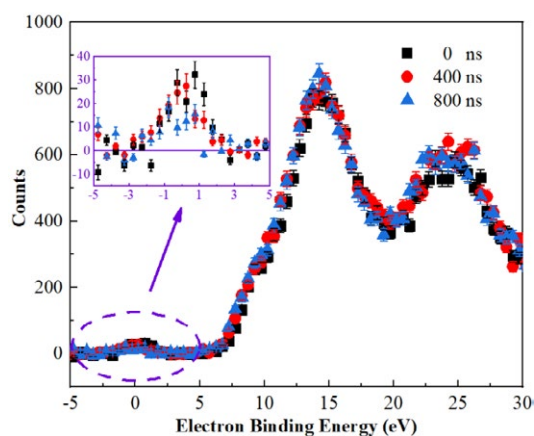


**Figure 1.** Binding energy spectrum of toluene after being irradiated by the pump laser at three time delays.

### References

- [1] T. C. Killian et al. 1999 Phys. Rev. Lett. **83**, 4776
- [2] Y. Tang et al. 2018 Rev. Sci. Instrum. **89**, 033101

\* E-mail: [xshan@ustc.edu.cn](mailto:xshan@ustc.edu.cn)

† E-mail: [xjun@ustc.edu.cn](mailto:xjun@ustc.edu.cn)

## Oscillator strengths and cross sections of the valence-shell excitations of HBr studied by fast electron impact

J H Zhu<sup>1</sup>, S X Wang<sup>1\*</sup> and L F Zhu<sup>1†</sup>

<sup>1</sup>Department of Modern Physics, University of Science and Technology of China, Hefei, Anhui 230026, China

**Synopsis** The oscillator strengths and integral cross sections of the valence-shell excitations of HBr have been determined by fast electron scattering with an incident electron energy of 1500 eV and an energy resolution of 80 meV. The present results show that the strong spin-orbital interaction results in the observation of some triplet states in the ( $\Lambda, S$ ) coupling and the constant generalized oscillator strength ratio of  $b^3\Pi_1$  and  $C^1\Pi(v=0)$ .

The excited states of HBr show a tendency to change from ( $\Lambda, S$ ) coupling to ( $\Omega, \omega$ ) coupling for their strong spin-orbital (SO) interaction[1]. Therefore, the cross sections and oscillator strengths of the valence-shell excitations of HBr are important for understanding this strong SO interaction.

In this work the generalized oscillator strengths (GOSs) of the valence-shell excitations of HBr have been measured by the fast electron scattering method, and the corresponding optical oscillator strengths (OOSs) are determined by extrapolating the GOSs to the limit of the zero squared momentum transfer, i.e.,  $K^2 \rightarrow 0$ .

Figs. 1(a)-(d) show the present GOSs and the fitted curves using the Lassettre formula for the  $a^3\Pi + A^1\Pi$ ,  $b^3\Pi$  and  $C^1\Pi(v=0, 1)$  excitations. It is obvious that both GOSs of the  $b^3\Pi$  and  $C^1\Pi(v=0)$  states show the same behavior of the dipole-allowed transition. Generally, the spin-exchange excitations are weak enough to be neglected for the typical ( $\Lambda, S$ ) coupling in the fast electron scattering. However, the strong SO interaction of HBr causes the mixture of the wavefunctions of  $b^3\Pi$  and  $C^1\Pi$ . So the wavefunction of the  $b^3\Pi$  state with the SO coupling consists of the pure triplet component of  $b^3\Pi$  and singlet component of  $C^1\Pi$  in the ( $\Lambda, S$ ) coupling without considering the SO interaction. The former component is strictly forbidden in the fast electron impart experiment due to the singlet nature of the ground state  $X^1\Sigma^+$ . The latter component is allowed and contributes to the intensity of the  $b^3\Pi$  state. As a result, the GOS ratio of the  $b^3\Pi$  to the  $C^1\Pi(v=0)$  should be a constant and

independent of the squared momentum transfer, which is demonstrated clearly in Fig. 1(e).

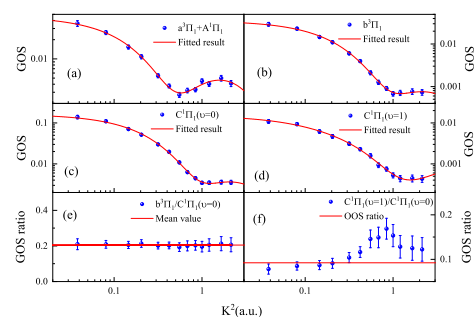


**Figure 1.** The present GOSs of (a)  $a^3\Pi_1 + A^1\Pi_1$ , (b)  $b^3\Pi_1$ , (c)  $C^1\Pi_1(v=0)$  and (d)  $C^1\Pi_1(v=1)$  and the experimental GOS ratios (e) between  $b^3\Pi_1$  and  $C^1\Pi_1(v=0)$  and (f) between  $C^1\Pi_1(v=1)$  and  $C^1\Pi_1(v=0)$  of HBr. The dots and solid lines are the experimental results and the fitted curves, respectively.

Another notable phenomenon is shown in Fig. 1(f) that the intensity ratio of  $C^1\Pi(v=1)$  to  $C^1\Pi(v=0)$  varies with the squared momentum transfer. However, according to the Franck-Condon approximation, the intensity ratio of the different vibrational states in the same electronic state should be a constant. The reason of the violation of the Franck-Condon approximation of  $C^1\Pi$  may be due to its interaction with the nearby states.

### References

- [1] Ginter M L and Tilford S G *J. Mol. Spectrosc.* **34** 206

\*E-mail: wangshuxing@ustc.edu.cn

†E-mail: lfzhu@ustc.edu.cn



## Effects and data of electron collisions on various molecules for medical applications

Y Park<sup>1\*</sup>, M Y Song<sup>1</sup>, M Dinger<sup>2</sup>, W Y Baek<sup>2</sup>

<sup>1</sup>Korea Institute of Fusion Energy, Gunsan-city, 54004, Republic of Korea

<sup>2</sup>Physikalisch-Technische Bundesanstalt, Braunschweig, 38116, Germany

**Synopsis** The experimental results on electron collision effects and data on molecules of interest required for anticancer treatment applications are presented here.

Low energy electrons (LEEs) are known to interact with DNA molecules and induce various forms of damage[1, 2]. In this work, we have experimentally investigated the possible mechanisms and the consequences of the DNA damage through electron collision on the DNA-metal ion adducts. The procedure of the experiment consists of two main parts: irradiating DNA films with 10 eV electrons and analyzing the resulting damage using gel electrophoresis and high performance liquid chromatography (HPLC). We find that LEE interactions with DNA can basically lead to single- and double-strand breaks. And in the case of DNA to which metal ions were bound, DNA damage was increased or suppressed compared to pure DNA. These results are interpreted to be related to the change in the sensitivity of incident electrons by the structure in which metal ions are bonded. Figure 1 illustrates the possible pathways of DNA damage induced by electron collisions. The basic mechanism of DNA damage caused by LEE collisions can be explained by the formation of transient negative ion state and subsequent dissociation process. When metal ions are bonded, the nitrogen atoms in the guanine base can coordinate with  $\text{Cu}^{2+}$  to form a complex with a square planar geometry. This interaction can lead to changes in the structure and stability of the DNA molecule. We have assumed that DNA damage will increase or decrease due to changes in the capturing probability of incident LEEs resulted from the structural change of the DNA molecule. This interpretation of mechanisms is controversial and requires theoretical verification.

In order to calculate a precise dose in radiation therapy, electron collision data for the molecules constituting the human body's are required. As the first step, the differential elastic

electron scattering cross sections (DCS) of ethanol were measured for scattering angles of  $30^\circ$  to  $150^\circ$  using the relative flow technique and  $\text{N}_2$  as the reference gas[3]. We briefly introduce measurement results and comparisons with other group results.

Our experimental results should provide new insights into the mechanisms and consequences of LEE interactions with DNA. These findings have potential implications for understanding the effects of radiation on living organisms and for developing new strategies for cancer therapy and radiation protection.

**Keywords:** Low energy electrons, DNA damage, transient negative ion, ethanol, differential cross section.

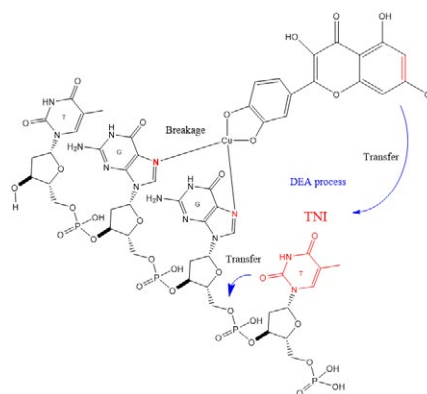


**Figure 1.** The possible pathways of DNA damage induced by low energy electron collision.

### References

- [1] Sanche L 2016 *Radiat. Phys. Chem.* **128** 36.
- [2] Gao Y, Zheng Y and Sanche L 2021 *Int. J. Mol. Sci.* **22** 7879.
- [3] Dinger M *et al.*, 2023 *Eur. Phys. J. D* in progress.

\* E-mail: parkys@kfe.re.kr

## Oscillator model applied to calculations of energy loss in anisotropic 2D materials

S Segui<sup>1\*</sup>, J L Gervasoni<sup>2,3</sup>, Z L Mišković<sup>4</sup> and N R Arista<sup>2,3</sup>

<sup>1</sup> Instituto de Física Enrique Gaviola (IFEG-CONICET), FAMAFC UNC, Córdoba, Argentina.

<sup>2</sup> Centro Atómico Bariloche (CNEA), 8400 S. C. de Bariloche, Argentina.

<sup>3</sup> Instituto Balseiro (CNEA - UNCuyo), 8400 S. C. de Bariloche, Argentina.

<sup>4</sup> University of Waterloo, Waterloo, Ontario, Canada N2L 3G1.

**Synopsis** We apply the oscillator model to study the energy loss processes of external charged particles interacting with a two-dimensional (2D) material characterized by an anisotropic conductivity tensor. We model the material as a monolayer of harmonic oscillators, with anisotropic modes for the in-plane electronic vibration. We consider parallel and perpendicular trajectories of the external particle, obtaining analytical expressions in terms of reduced variables. This allows us to analyze in detail the interaction and to adapt the model to the considered material using adequate values for the physical parameters involved.

Anisotropic 2D materials are of interest due to their multiple potential applications in nanoscale optoelectronics. In particular, the anisotropic optical response allows the propagation of the so-called hyperbolic plasmon-polaritons, of interest in waveguides, hyperlenses, focusing, etc. In these 2D materials, the anisotropy arises as a consequence of the atomic structure. Some examples are germanene, silicene, antimonene, and specially phosphorene, which stands out as a reference material.

In the present work we explore the properties of an anisotropic 2D material through its interaction with a beam of charged particles. To this end, we adapt the oscillator model developed previously [1, 2] representing the material as a planar array of anisotropic, non-interacting oscillators (the atomic electrons) harmonically bound to the nuclei. The characteristic frequencies of these oscillators are derived from the material's conductivity tensor. The anisotropy is introduced by allowing different frequencies  $\{\omega_x, \omega_y\}$  and effective masses  $\{m_x, m_y\}$  along the crystallographic directions  $\{x, y\}$ . The energy exchange takes place along the incident particle's trajectory, which is considered to be rectilinear, either parallel or perpendicular to the layer.

We obtain several useful analytical expressions for the energy loss as a function of the relevant parameters of the process. Figure 1 shows a polar representation of stopping power  $S$  for a particle traveling on a parallel trajectory as a function of its direction with respect to the crys-

\*E-mail: [silvina.segui@mi.unc.edu.ar](mailto:silvina.segui@mi.unc.edu.ar)

tallographic axes  $\{x, y\}$ , for a fixed velocity. Calculations were made for several values of impact parameter  $\bar{b}_0$  (distance from the trajectory to the material plane), and given fixed variables. The anisotropy of the material appears in the elongated shape of the curves, which stretch along the  $y$  or  $x$  axes depending on the value of  $\bar{b}_0$ .

This model gives a promising alternative to study 2D materials with their distinctive properties.

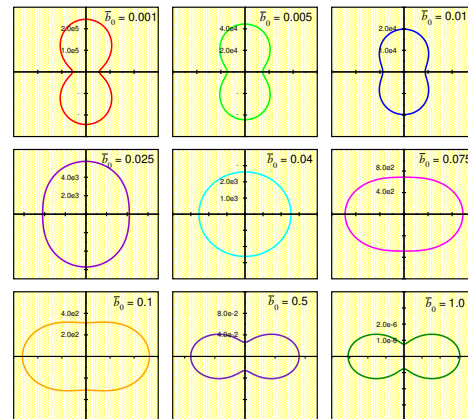


**Figure 1.** Polar representation of the reduced stopping power for parallel trajectory and different values of impact parameter  $\bar{b}_0$ .  $\beta = v/c = 0.1$ ,  $\omega_y/\omega_x = 1$ ,  $m_x = 0.2m_0$  and  $m_y = m_0$  (with  $m_0$  the electron mass).

### References

- [1] Segui S *et al* 2021 *Nucl. Inst. Meth. B* **490** 18
- [2] Segui S *et al* 2021 *J Appl Phys* **130** 114302

## Secondary electron emission & detection of low-energy charged particles impacting channel electron multipliers

D M Newson<sup>1\*</sup>, S J Brawley<sup>1</sup>, M Shipman<sup>1</sup>, R Kadokura<sup>1</sup>, T J Babij<sup>2</sup>, D Cooke<sup>1</sup>, D E Leslie<sup>1</sup>, G Laricchia<sup>1†</sup>

<sup>1</sup>UCL Department of Physics and Astronomy, Gower Street, London WC1E 6BT, United Kingdom

<sup>2</sup>Research School of Physics and Engineering, Australian National University, Canberra, ACT 2600, Australia

The detection efficiency of positrons and positronium is required to determine quantities involving the ratio of the count rates such as the positronium fragmentation cross-section [1] and absolute differential positronium-formation cross-section [2, 3]. Secondary electron emission underlies this specific detection process and is also relevant to a wide range of applications, such as particle accelerators [4], fusion apparatus [5], satellite systems [6] and extreme ultraviolet lithography [7].

Experimental determinations of the positron detection efficiency from channel electron multipliers are presented for impact energies between 0 – 1400 eV (figure 1). The energy-dependence is found to follow that of a log-normal indicating the statistical behaviour of the process [9]. The ratio of the positron and positronium detection efficiencies, as a function of the *positronium* impact energy, is extracted from the log-normal fit to the detection efficiency data, using an equivelocity relationship [1, 10]. Detection efficiencies for other projectiles are examined and shown to also have a log-normal energy-dependence.

With the aid of a Monte Carlo simulation of the positron beam impacting the major components of the experimental setup, specifically grids and the channel electron multiplier surface, the contributions of secondary electron emission from the grids is identified. The log-normal is applied to measured secondary electron emission coefficients for electron, positron and ion impact and is found to describe the energy-dependence well, offering a means of interpolating and, in some cases, extrapolating existing experimental

data [11].

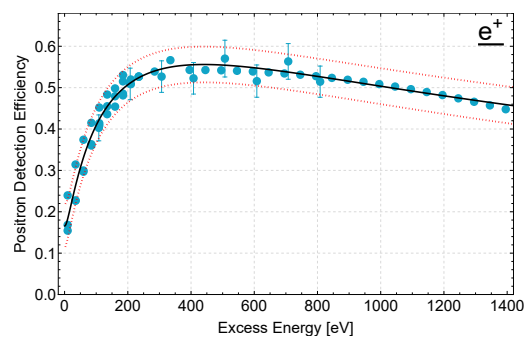


**Figure 1.** Experimental determinations of the positron detection efficiency [8] (symbols) alongside a four-parameter log-normal fit (solid line) and 95% confidence bands (dotted lines).

EPSRC (UK) is thanked for financial support (EP/P009395/1, EP/R513143/1).

### References

- [1] Armitage S *et al.* 2002 *Phys. Rev. Lett.* **89** 173402
- [2] Shipman M *et al.* 2015 *Phys. Rev. Lett.* **115** 033401
- [3] Fayer S E *et al.* 2019 *Phys. Rev. A* **100** 062709
- [4] Hartung *et al.* 2015 *Nucl. Instrum. Methods Phys. Res. A* **783** 95
- [5] Toliás P 2014 *Plasma Phys. Contr. F* **56** 123002
- [6] Lai S T 2011 *Princeton University Press* ISBN 9781400839094
- [7] Chen J *et al.* 2010 *Appl. Surf. Sci.* **257** 354
- [8] Newson D M *et al.* 2022 *JINST* **17** P11026
- [9] Laricchia G *et al.* 2010 *Sci. Rep.* **8** 15056
- [10] Newson D M 2022 PhD Thesis, UCL
- [11] Newson D M *et al.* 2023 *Nucl. Instrum. Methods Phys. Res. B* **536** 119

\*E-mail: [ucapdne@ucl.ac.uk](mailto:ucapdne@ucl.ac.uk)

†E-mail: [g.laricchia@ucl.ac.uk](mailto:g.laricchia@ucl.ac.uk)

## Determination of Electron Inelastic Mean Free Path and Stopping Power of Hafnium Dioxide

J.M. Gong<sup>1</sup>, K. Tórkési<sup>3</sup>, X. Liu<sup>1</sup>, B. Da<sup>4,5</sup>, H. Yoshikawa<sup>4</sup>, S. Tanuma<sup>5</sup> and Z.J. Ding<sup>\*,1,2</sup>

<sup>1</sup>Department of Physics, University of Science and Technology of China, Hefei, Anhui 230026, P.R. China

<sup>2</sup>Hefei National Laboratory for Physical Sciences at Microscale, University of Science and Technology of China, Hefei, Anhui 230026, P.R. China

<sup>3</sup>Institute for Nuclear Research (ATOMKI), Debrecen, Hungary

<sup>4</sup>Research and Services Division of Materials Data and Integrated System, National Institute for Materials Science, 1-1 Namiki, Tsukuba, Ibaraki 305-0044, Japan

<sup>5</sup>Research Center for Advanced Measurement and Characterization, National Institute for Materials Science, 1-2-1 Sengen, Tsukuba, Ibaraki 305-0047, Japan

**Synopsis** We present inelastic mean free path (IMFP) and stopping power data of the hafnium dioxide applying the relativistic dielectric response theory. Our calculations are based on the energy loss function of hafnium dioxide derived from reflection electron energy loss spectroscopy spectrum. We show that the bandgap has a significant influence on the IMFP and on the stopping power.

With the development of the semiconductor industry, HfO<sub>2</sub> has received much more attention as a representative high-*k* dielectric material which has low leakage current and good thermal stability. For example, due to excellent optical and thermal properties, HfO<sub>2</sub> has emerged as an ideal material for the improvement of absorption efficiency and thermal stability of solar energy. HfO<sub>2</sub> also plays a key role in optical coating materials field for its high transmittance in the ultraviolet to near-infrared band, and high laser damage threshold. Therefore, it is important to know the IMFP and stopping power of HfO<sub>2</sub> especially for the electron microscope analysis of this material. The inelastic mean free path (IMFP) and the stopping power are basic and very important physical quantities describing the transport properties of electrons in materials. For instance, it can help determine the thickness of HfO<sub>2</sub> film which is an important factor affecting the performance of HfO<sub>2</sub> as a semiconductor device or optical element in practical applications.

In this work we present highly accurate electron IMFP and stopping power data of the hafnium dioxide by applying the relativistic dielectric response theory [1]. Our calculations were based on the energy loss function (ELF) of hafnium dioxide derived from the reflection electron energy loss spectroscopy (REELS) spectra.

The probability of the energy loss is determined by the dielectric response function  $\epsilon(q, \omega)$  as a function of the frequency  $\omega$  and the wavenumber  $q$  of the electromagnetic disturbance. The full Penn algo-

rithm (FPA) [2] was used to expand the optical energy loss function,  $\text{Im}\{-1/\epsilon(\omega)\}$ , into the  $(q, \omega)$ -plane. Furthermore, we also applied the super-extended Mermin algorithm [3] to calculate the IMFP and stopping power for comparison with the results of the FPA model.

We have shown that the FPA and SMA results are almost identical at high electron kinetic energies above ~70 eV. However, they differ significantly below 70 eV. We have shown that the bandgap value has a significant influence on IMFP and stopping power data. Therefore, for compound semiconductors, the bandgap must be considered in order to obtain accurate IMFP and stopping power data for applications.

### Acknowledgements

This research was supported by the Education Ministry through "111 Project 2.0" (BP0719016), and by European Cost Actions CA18212 (MDgas). This work was also supported by the National Institute for Materials Science under the Support system for curiosity-driven research, JSPS KAKENHI Grant Number JP21K14656 and Grant for Basic Science Research Projects from The Sumitomo Foundation. The work was also support by the by the Bilateral relationships between China and Hungary in science and technology (S&T) under the project number 2021-1.2.4-TÉT-2021-00055.

### References

- [1] M. Gong et al., 2023 to be published in ATOMS
- [2] Penn, D.R., 1987 Phys. Rev. B, 35, 482-486.
- [3] Da, B.; Shinotsuka, H.; Yoshikawa, H.; Ding, Z. J.; Tanuma, 2014, S. Phys. Rev. Lett., 113, 063201.

\* E-mail: [zjding@ustc.edu.cn](mailto:zjding@ustc.edu.cn)

## Energy Loss Function of Samarium determined from the reflection electron energy loss spectroscopy spectra

T.F. Yang<sup>1</sup>, R.G. Zeng<sup>3</sup>, L.H. Yang<sup>1</sup>, A. Sulyok<sup>4</sup>, M. Menyhárd<sup>4</sup>, K. Tókesi<sup>5#</sup> and Z.J. Ding<sup>1,2\*</sup>

<sup>1</sup>Department of Physics, University of Science and Technology of China, Hefei, Anhui 230026, People's Republic of China

<sup>2</sup>Hefei National Research Center for Physical Sciences at the Microscale, University of Science and Technology of China, Hefei, Anhui 230026, People's Republic of China

<sup>3</sup>National Key Laboratory on Surface Physics and Chemistry, Institute of Materials, China Academy of Engineering Physics, P.O. Box 9071, Jianguyou, Sichuan 621907, People's Republic of China

<sup>4</sup>Research Institute for Technical Physics and Materials Science, Centre for Energy Research, ELKH, P.O. Box 49, H-1525 Budapest, Hungary

<sup>5</sup>Institute for Nuclear Research, ELKH, P.O. Box 51, Debrecen, Hungary

**Synopsis** We present a combined experimental and theoretical studies to obtain the high accuracy energy loss function (ELF) or the excitation spectrum and thereby the dielectric function, the refractive index and the extinction coefficient of samarium in the energy loss range between 3 eV and 200 eV. The accuracy of our result was justified by using the *f*- and *ps*-sum rules. We found that a bulk mode locates at 14.2 eV with the peak width ~6 eV and the corresponding broaden surface plasmon mode locates at energies of 5-11 eV.

Lanthanides have nowadays become of vital importance in advanced materials and technology. Applications in laser science, solar cells, fluorescent lamps and a new organic light-emitting diodes components, as well as luminescent probes are strongly related with their optical and/or electronic properties. Samarium and its compounds are among the most frequently used lanthanides in the investigations during the last years. But the precise excitation property, especially the plasmon structure of samarium is still not known. It is not surprising because all lanthanides are highly reactive elements and interact strongly with oxygen and hydrogen. So, experimentally it is really a challenging to obtain accurate results. The excitation properties are intrinsically embodied in the energy loss function (ELF),  $\text{Im}\{-1/\varepsilon(\omega)\}$ , which is clearly related with the frequency dependent complex dielectric function  $\varepsilon(\omega)$ . Da et al. [1] developed a reverse Monte Carlo (RMC) method for the derivation of the ELF and thereby the dielectric function and optical constants of solids in a much wider photon energy range than that of the usual optical measurements. The RMC method combines a Monte Carlo modelling of electron transportation for REELS spectrum simulation with a Markov chain Monte Carlo calculation of parameterized ELF.

Our RMC technique was used to obtain the electron energy loss features buried in the REELS spectra of

samarium [2]. The accuracy of the ELF was checked by applying the Thomas-Ritchie-Kuhn (*f*-sum rule) and the perfect-screening sum rules (*ps*-sum rule). We found that the *ps*- and *f*-sum rules with our ELF, imaginary part of the complex dielectric function  $\varepsilon_2$ , and extinction coefficient *k* fulfils very accurately and reach the nominal values with 0.2% and 2.5% accuracy, respectively. We were able to separate the contribution from the bulk and the surface excitations. We show the detailed excitation characteristic in the optical data in the energy range between 3 and 60 eV. We found a surface plasmon mode at 10.4 eV and the corresponding bulk mode 14.3 eV.

### Acknowledgements

This work was supported by the Fund of National Key Laboratory on Surface Physics and Chemistry (XKFZ202103), Chinese Education Ministry through "111 Project 2.0" (BP0719016). The work was also supported by the by the Bilateral relationships between China and Hungary in science and technology (S&T) under the project number 2021-1.2.4-TÉT-2021-00055. We thank Prof. H. M. Li and the supercomputing centre of USTC for the support of parallel computing.

### References

- [1] B. Da et al 2013 J. Appl. Phys. **113** 21430.  
[2] Yang T.F. et al., 2023 Scientific Reports | 13:3909

\* E-mail: [zjdjng@ustc.edu.cn](mailto:zjdjng@ustc.edu.cn)

# E-mail: [tokesi@atomki.hu](mailto:tokesi@atomki.hu)



## Focusing an electron beam by the self-arranged formation of a quadrupole-like electrostatic field inside a quartz capillary of square cross section

H Q Zhang<sup>1,\*</sup>, P F Li<sup>1,3</sup>, S Ha<sup>1</sup>, Y Z Pan<sup>1</sup>, Y Cui<sup>1</sup>, C L Wan<sup>1</sup>, Z H Yang<sup>4</sup>, D Lu<sup>5,†</sup>, R Schuch<sup>6</sup>, and X M Chen<sup>1</sup>

<sup>1</sup>School of Nuclear Science and Technology, Lanzhou University, 730000 Lanzhou, P. R. China.

<sup>3</sup>College of Nuclear Science and Technology, Harbin Engineering University, 150001 Harbin, P. R. China.

<sup>4</sup>Institute of Modern Physics, Chinese Academy of Sciences, 730000 Lanzhou, P. R. China.

<sup>5</sup>Department of Physics, University of Gothenburg, S-405 30 Gothenburg, Sweden.

<sup>6</sup>Physics Department, Stockholm University, S-106 91 Stockholm, Sweden.

**Synopsis** We find a peculiar beam focusing/shaping effect that a cross-like electron transmission profile is formed via a quartz capillary of square cross section. Simulations have revealed that it is due to that the negative charges tend to deposit around the corners of the square capillary, forming a unique quadrupole-like electrostatic field. This opens up new horizons of focusing/shaping charged particle beams through insulating micro- to macro-structures of special cross sections in various applications.

Great potential in the development of charged particle beam optics for the so-called guiding effect in the transmission of charged particle beams through insulating nanocapillaries, has been advocated [1-3]. The guiding mechanism is due to a sequential, self-arranged formation of charge patches along the inner capillary wall that produce repulsive electrostatic fields to deflect the incident charged particles and finally avoid their close collisions with the inner surfaces [4]. The studies concerning positive ions have reached a wide agreement of the above mentioned mechanisms. However, for negatively charged particles, i.e., electrons and negative ions, the charge deposition is complex and different from that of positive ions and there are still complexities and controversies concerning the transport mechanisms inside the capillaries [5, 6].

In this work, we have experimentally studied the transmission behavior of a 3 keV electron beam through a macroscopic quartz capillary of square cross section. For the first time, we find a peculiar beam focusing/shaping effect that the electron transmission profiles present a very neat cross shape during the charge-up process. It remains steady for over one hour under suitable conditions. Simulations have been performed also to understand the experimental observations. It is revealed that the negative charges tend to deposit around the corners of the square capillary, forming a unique quadrupole-like electrostatic field, which

focuses/shapes the electron beam towards a cross-like transmission profile. The view of the cross shaped structure as well as the potential distribution inside the capillary are shown in Fig. 1. This opens up new horizons of focusing/shaping charged particle beams through insulating micro- to macro-structures of special cross sections in various applications.

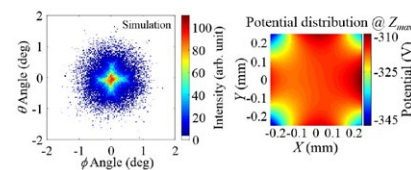


**Figure 1.** Simulated transmission profile (left) and the corresponding potential distribution inside the capillary (right).

### References

- [1] Stolterfoht N et al. 2002 *Phys. Rev. Lett.* **88** [133201](#)
- [2] Stolterfoht N and Yamazaki Y 2016 *Phys. Rep.* **629** [1](#)
- [3] Lemell C, Burgdörfer and Aumayr F 2013 *Prog. Surf. Sci.* **88** [237](#)
- [4] Skog P, Zhang H Q and Schuch R 2008 *Phys. Rev. Lett.* **101** [223202](#)
- [5] Schiessl K et al. 2009 *Phys. Rev. Lett.* **102** [163201](#)
- [6] Stolterfoht N and Tanis J A 2018 *Nucl. Instrum. Methods Phys. Res., Sect. B* **421** [32](#)

\* E-mail: [zhanghq@lzu.edu.cn](mailto:zhanghq@lzu.edu.cn)

† E-mail: [di.lu@physics.gu.se](mailto:di.lu@physics.gu.se)

## Wave-packet continuum discretisation approach to dressed carbon ion collisions with atomic hydrogen

N W Antonio<sup>1\*</sup>, C T Plowman<sup>1</sup>, I B Abdurakhmanov<sup>2</sup>, I Bray<sup>1</sup> and A S Kadyrov<sup>1</sup>

<sup>1</sup>Curtin University, GPO Box U1987, Perth, WA 6845, Australia

<sup>2</sup>Pawsey Supercomputing Centre, 1 Bryce Avenue, Kensington, Western Australia 6151, Australia

**Synopsis** The two-centre wave-packet convergent close-coupling method is extended to treat dressed ion collisions with atomic hydrogen. This is done by using an effective potential to approximate the interactions between the projectile ion core with the target proton and active electron, initially bound to the target. We apply this approach to study dressed carbon ion collisions with H. Calculations for the total electron-capture and ionisation cross sections are performed in the intermediate energy region, where coupling to the ionisation channels is important.

Collisions involving dressed ions is important for many applications such as fusion plasma modelling, analysing X-ray spectra from comets and modern cancer treatments such as hadron therapy. From a theoretical perspective, modelling collisions which involve more than two electrons in a completely *ab initio* manner is currently infeasible. Therefore, to overcome this limitation we employ an effective potential to treat the interactions with the multi-electron projectile ion in a spherically symmetric manner. This reduces the scattering problem of dressed ion collisions with atomic hydrogen to an effective three-body problem. We have incorporated this model potential into the two-centre wave-packet convergent close-coupling (WP-CCC) formalism and applied in the projectile energy range between 1 keV/u to 1 MeV/u, the energy range where electron capture, target excitation and ionisation are equally likely. Hence, all scattering channels should be strongly coupled. This new extension of the WP-CCC approach has been applied to study partially stripped carbon ion collisions with atomic hydrogen.

In Fig. 1 we show the projectile energy dependence of the total electron-capture (EC) cross section for  $C^{3+}$  collisions with  $H(1s)$ . For energies above 5 keV/u, we find excellent agreement with available measurements [1, 2]. At lower energies we note a discrepancy between our results and the experimental data [3, 4]. A possible reason for this is the two-electron processes that our

method does not take into account.

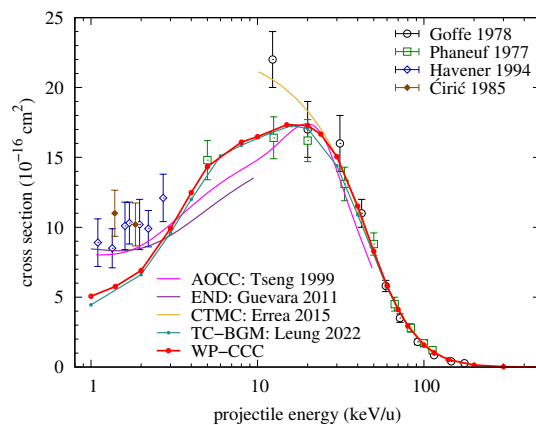


**Figure 1.** Total electron-capture cross section in  $C^{3+}$ - $H(1s)$  collisions. The present WP-CCC results are compared with experimental measurements [1, 2, 3, 4] and theoretical calculations [5, 6, 7, 8].

### References

- [1] Goffe T V *et al.* 1978 *J. Phys. B: At. Mol. Opt. Phys.* **12** 3763
- [2] Phaneuf R A *et al.* 1978 *Phys. Rev. A.* **17** 534
- [3] Havener C C *et al.* 1994 *Phys. Rev. A.* **51** 2982
- [4] Ćirić D *et al.* 1978 *J. Phys. B: At. Mol. Opt. Phys.* **18** 3629
- [5] Tseng H C and Lin C D 1999 *J. Phys. B: At. Mol. Opt. Phys.* **32** 5271
- [6] Guevara N L *et al.* 2011 *Phys. Rev. A.* **83** 052709
- [7] Errea L F *et al.* 2015 *J. Phys.: Conf. Ser.* **576** 012002
- [8] Leung A C K and Kirchner T 2022 *Atoms* **10** 11

\*E-mail: [nicholas.antonio@postgrad.curtin.edu.au](mailto:nicholas.antonio@postgrad.curtin.edu.au)

## Quantum vortices in the fully differential cross section for the ionization of atoms by the impact of protons and positrons

T. Guarda<sup>1,2\*</sup>, F. Navarrete<sup>3†</sup> and R O Barrachina<sup>1,2‡</sup>

<sup>1</sup>Bariloche Atomic Centre, Comisión Nacional de Energía Atómica, 8400 Bariloche, Río Negro Argentina

<sup>2</sup>Balseiro Institute, 8400 Bariloche, Río Negro Argentina

<sup>3</sup>Institute of Physics, University of Rostock, Germany

**Synopsis** We theoretically study the presence of quantum vortices in the ionization of atoms by impact of positrons and protons. We analyze the differences and similarities between both cases, and the possibilities of their experimental observation.

Since their experimental observation as isolated zeros in the differential cross section of the (e,2e) process in helium [1], quantum vortices have been studied with increasing detail and interest in different ionization processes [see, for example, [2] and references therein]. In this communication we perform a detailed theoretical analysis of the presence of vortices in the fully differential cross section (FDCS) for the ionization of atoms by impact of positrons and protons, paying particular attention to their similarities and differences.

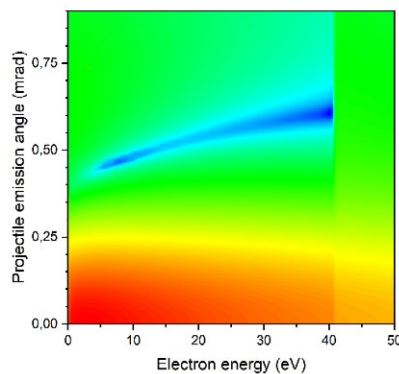


**Figure 1.** FDCS for Helium ionization by 75 keV protons, as a function of the electron energy  $E_e$  and projectile angle  $\theta_p$ . The electron is emitted in the forward direction. The "Electron Capture to the Continuum" (ECC) cusp at  $E_e \approx 41$  eV has been removed from the graph, leaving only its characteristic asymmetric structure. Two vortices at  $\theta_p \approx 0.46$  and  $0.60$  mrad are clearly visible. Note that this last zero produces a strong distortion of the ECC asymmetry.

\* E-mail: [tamaraguarda@cnea.gob.ar](mailto:tamaraguarda@cnea.gob.ar)

† E-mail: [francisco.navarrete@uni-rostock.de](mailto:francisco.navarrete@uni-rostock.de)

‡ E-mail: [barra@cab.cnea.gov.ar](mailto:barra@cab.cnea.gov.ar)

Figures 1 and 2 show typical results for this effect in both situations. In particular, we analyze how vortex points, lines and surfaces could be experimentally observed in a direct way; or their presence inferred through the distortion they produce on other structures, such as -for example- the electron capture to the continuum (ECC) cusp, the ionization kinematic threshold, the binary collision process, or the Thomas double scattering mechanism.

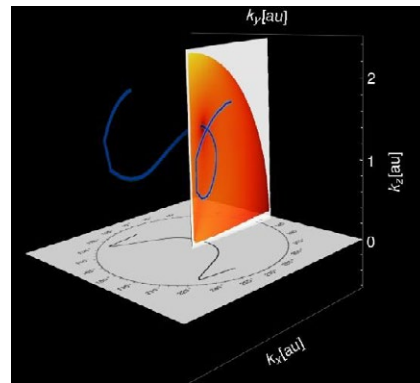


**Figure 2.** Vortex line in the FDCS for Hydrogen ionization by 100 eV positrons in the moment space of the emitted electron. The projectile is deflected at an angle of  $20^\circ$  in the xz plane from the initial z-direction. Instead of forming a closed structure, the vortex line starts and ends at the kinematic threshold.

### References

- [1] Murray A J and Read F H 1993 *Phys. Rev. A* **47** 3724
- [2] Navarrete F and Barrachina R O 2020 *J. Phys.: Conf. Ser.* **1412** 152014

## DIRECT DETERMINATION OF THE FULLY DIFFERENTIAL CROSS SECTION OF THE IONIZATION BY THE WAVE FUNCTION

Zorigt Gombosuren<sup>1\*</sup>, Khenmedekh Lochin<sup>2</sup>, Aldarmaa Chuluunbaatar<sup>3</sup>

<sup>1,2,3</sup>Department of Physics, Mongolian University of Science and Technology, Ulaanbaatar city, 14200, Mongolia

This work is focused on showing that the fully differential cross section of ionization during a collision of a proton and an antiproton with a hydrogen atom is directly expressed by the wave function in the coordinate representation.

One of the quantities measured experimentally in a result of atomic collisions with charged particles is the fully differential cross section (FDCS). We calculated the electron-wave function of the hydrogen atom as a time-dependent Schrödinger equation (TDSE) [1]. We used the Coulomb wave function's discrete variable representation (CWDVR) [2] method and impact parameter method [3].

The time-dependent probability density distribution of electron in terms of the wave function at a specific scattering angle is shown in the paper [4-7].

We converted the wave function in the Impact parameter representation to the momentum transfer representation by a two-dimensional Fourier transform. This wave function corresponds to the specific scattering angle of the projectile ion (Fig. 1a).

$$\Psi_{\vec{\eta}}(t, \vec{r}) = \frac{1}{2\pi} \int d\vec{b} e^{i\vec{\eta}\vec{b}} e^{i\delta(b)} \Psi_{\vec{b}}(t, \vec{r}) \quad (1)$$

Here  $\vec{\eta}$  is the transverse component of the projectile momentum transfer,  $t$ -is the time,  $\Psi_{\vec{b}}(t, \vec{r})$  the wave function denotes the correspond to  $b$ -is impact parameter,  $\delta(b)$  is the phase at which the nucleus of the hydrogen atoms interaction [8].

The electron probability density is written as follows:

$$\frac{d^3P(\eta)}{dVd\eta} = |\Psi_{\vec{\eta}}(t, \vec{r})|^2 \quad (2)$$

In this case, we write the differential of the volume in the spherical coordinate system.  $\varepsilon$  is a function dependent on  $r$  and we write the differential probability by transferring the variable as follows

$$\frac{d^3P(\eta)}{d\varepsilon d\Omega_e d\eta} = \frac{|\Psi_{\vec{\eta}}(t, \vec{r})|^2 r^2 dr}{d\varepsilon}. \quad (t \rightarrow \infty) \quad (3)$$

The FDCS is written as follows:

$$\frac{d^3\sigma}{d\varepsilon d\Omega_e d\Omega_p} = K_i K_f \frac{|\Psi_{\vec{\eta}}(t, \vec{r})|^2 r^2}{d\varepsilon/dr}. \quad (4)$$

Here, using the phase of the wave function, the relationship between coordinates and ejection energy  $\varepsilon$  is written as follows.

$$\varepsilon(\vec{r}, t) = -\frac{\partial}{\partial t} S(\vec{r}, t) \quad (5)$$

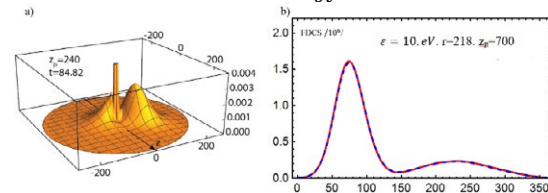


**Figure 1.** a) Distributions of ejected electrons in the scattering plane. b) FDCS solid line red is the traditional method, blue dash line is the present method (4).

The result of FDCS (4) calculated by the time-dependent wave function is in agreement with the value of the FDCS calculated by the transition amplitude (traditional method) fig1.b. This method has the disadvantage that it needs to be calculated over a large range of space and time compared to the traditional method, but the advantage is it does not use the continuum wave function. By the atom with multi electrons, the continuum wave function is not readily defined, making it difficult to calculate the FDCS. This problem can be avoided by using the new expression FDCS (4).

### References

- [1] G. Zorigt, L. Khenmedekh, Ch. Aldarmaa, IJMA-10(5), (2019) 19-23.
- [2] Peng. Liang-You and Starace. Anthony F, The journal of chemical physics 125, (2006) 154311.
- [3] M. McGovern, D. Assafrao, J. R. Mohallem, C. T. Whelan, and H. R. J. Walters, Phys. Rev. A 79, (2009) 042707.
- [4] J. Azuma, N. Toshima, K. Hino, and A. Igarashi, Phys. Rev. A 64, 062704 (2001).
- [5] Emil Y Sidky and C D Lin. J. Phys. B: At. Mol. Opt. Phys. 31 (1998) 2949–2960
- [6] J. C. Wells, D. R. Schultz, P. Gavras and M. S. Pindzola. Phys. Rev. A 54, (1996)
- [7] B. Pons. Phys. Rev. A 63, (2000) 0127
- [8] A. I. Bondarev, Y. S. Kozhedub, I. I. Tupitsyn, V. M. Shabaev, and G. Plunien. Phys. Rev. A 95, (2017) 052709

\* E-mail: [zorigt@must.edu.mn](mailto:zorigt@must.edu.mn)

## Quadrupole $l$ -changing collisions

N R Badnell\* and E Deliporanidou

Department of Physics, University of Strathclyde, Glasgow, G4 0NG, UK

**Synopsis** We have developed a simple analytic formula which well describes quadrupole  $l$ -changing collisions on comparison with numerical quantal Born calculations with the program AUTOSTRUCTURE. We find increasing disagreement however (for  $l \gtrsim n/2$ ) with the results of previous quantal calculations based-upon an analytic solution of the time-dependent Schrödinger equation.

There has been a resurgence in interest in  $l$ -changing collisions in recent years following the work of Vrinceanu & Flannery [1] who analytically solved the quantum mechanical (QM) time-dependent Schrödinger equation for a colliding heavy particle creating a weak electric field which lifts the Stark degeneracy in Rydberg atomic states.

The classic treatment of  $l$ -changing collisions by Pengelly & Seaton [2] is based-upon impact parameter theory and led to the provision of simple analytic expressions for cross sections and rate coefficients which have been used for decades by the astrophysics community to model the observed recombination spectra of H I and He II etc.

Comparison of these rate coefficients with the QM ones [3] showed that the simple expression of Pengelly & Seaton was not sufficiently accurate in extreme cases such as low temperatures and/or for non-degenerate transitions. A simple modification of the original Pengelly & Seaton formulae by Guzmán et al. [3] and Badnell et al. [4] handled these extreme cases.

The above discussion relates to dipole  $l$ -changing collisions. The contribution from quadrupole  $l$ -changing collisions was studied briefly by Guzmán et al. [3] and they found that dipole transitions dominated as expected but in some instances the effect of quadrupole transitions was noticed. High precision is required when modelling recombination spectra to constrain Dark Matter cosmologies.

The simple Pengelly & Seaton method [2] is only valid for dipole transitions. The QM method [1] is applicable to quadrupole (and higher multipole) transitions but is computationally demanding. A simplified semi-classical approach was developed [5] but we find that it can

\*E-mail: [badnell@phys.strath.ac.uk](mailto:badnell@phys.strath.ac.uk)

differ from the QM rate coefficients by up to  $\sim 40\%$ .

An alternative approach to heavy-particle quadrupole transitions has been pioneered by Burgess & Tully [6]. It is based-upon Born and impact parameter theory. They attempted to find a simple analytic expression for modelling purposes. Its final form still required some parameterization by specific Born calculations. Their approach was not specific to the energy-degenerate case of  $l$ -changing collisions.

We have developed a simple standalone analytic formula applicable to quadrupole  $l$ -changing collisions which can be written in terms of the quadrupole line strength in a fashion similar to the dipole formula of Pengelly & Seaton. It reproduces our exact Born rate coefficients (calculated with the program AUTOSTRUCTURE) to within a few percent except for extreme cases where the rates are very small.

Comparing our exact Born rate coefficients with those of the QM method of Vrinceanu & Flannery [1] we find good agreement (within 10%) at low- $l$  but an increasing divergence for  $l \gtrsim n/2$  which tends to a factor  $\sim n/2$  for  $l \approx n$ .

This work was supported by the STFC UK.

### References

- [1] Vrinceanu D and Flannery M R 2001 *Phys. Rev. A* **63** 032701
- [2] Pengelly R M and Seaton M J 1964 *MNRAS* **127** 165
- [3] Guzmán F, Badnell N R, Williams R J R, et al. 2017 *MNRAS* **464** 312
- [4] Badnell N R, Guzmán F, Brodie S, et al. 2021 *MNRAS* **507** 2922
- [5] Vrinceanu D, Onofrio R and Sadeghpour H R 2012 *ApJ* **747** 56
- [6] Burgess A and Tully J A 2005 *J. Phys. B* **38** 2629



## Towards determination of absolute cross sections for excitation of hydrogen-like uranium in collisions with neutral atoms

G. Weber<sup>1</sup>, A. Gumberidze<sup>2\*</sup>, D. B. Thorn<sup>3</sup>, A. Surzhykov<sup>4,5</sup>, C. J. Fontes<sup>6</sup>, M. O. Herdrich<sup>1</sup>, R. Märtin<sup>1</sup>, U. Spillmann<sup>2</sup>, S. Trotsenko<sup>2</sup>, N. Petridis<sup>2</sup>, and Th. Stöhlker<sup>1,2,7</sup>

<sup>1</sup>Helmholtz Institute Jena, Germany

<sup>2</sup>GSI Helmholtzzentrum für Schwerionenforschung, Darmstadt, Germany

<sup>3</sup>Lawrence Livermore National Laboratory, Livermore, CA, USA

<sup>4</sup>Physikalisch-Technische Bundesanstalt, Braunschweig, Germany

<sup>5</sup>Technische Universität Braunschweig, Germany

<sup>6</sup>Los Alamos National Laboratory, New Mexico, USA

<sup>7</sup>Friedrich-Schiller-Universität Jena, Germany

**Synopsis** In this work, a measurement of the K-shell excitation of hydrogen-like uranium ( $U^{91+}$ ) in relativistic collisions with hydrogen and nitrogen gas targets is presented. Particular emphasis is given to obtaining the absolute excitation cross sections by exploiting simultaneously observed Radiative Electron Capture (REC) process.

In relativistic collisions of hydrogen-like heavy ions, e.g. hydrogen-like uranium ( $U^{91+}$ ) with light gas atoms, one can experimentally access fundamental atomic processes of proton- and electron-impact excitation [1]. While these processes have been extensively studied for low- and mid-Z ions, e.g. at electron beam ions traps (EBIT) [2], at GSI we have in the recent years extended the studies into the high-Z regime [3-5]. In particular, in the previous studies for the heaviest hydrogen-like ion ( $U^{91+}$ ) we have experimentally accessed the electron-impact excitation (EIE) by looking at the intensity ratios of the  $Ly\alpha_1$  ( $2p_{3/2} - 1s_{1/2}$ ) and the  $Ly\alpha_2$  ( $2s_{1/2}, 2p_{1/2} - 1s_{1/2}$ ) lines for different targets and different beam energies [3]. Our experimental results agreed well with state-of-the-art relativistic calculations, emphasizing with importance of including the generalized Breit interaction (GBI) in the description of the EIE process [6,7].

In the current work, we aim to determine absolute excitation cross sections (K-L) by using simultaneously observed Radiative Electron Capture (REC) process as a reference, i.e. normalizing the observed Lyman radiation intensity to the intensity of the radiation emitted during the capture of target electrons into the K and L shell of projectile (K- and L-REC). In Fig. 1, we display the x-ray spectra observed in our measurement in (anti-) coincidence with charge-changed projectiles ( $U^{90+}$ ). In the coincident spectrum, the REC lines are clearly visible along with the characteristic  $K\alpha$  lines from helium-like uranium ( $U^{90+}$ ).

The spectrum in anticoincidence with the charge exchange shows the  $Ly\alpha$  lines due to (de-)excitation of the hydrogen-like uranium. A comparison of our experimental results with state-of-the-art theories will be presented as well.

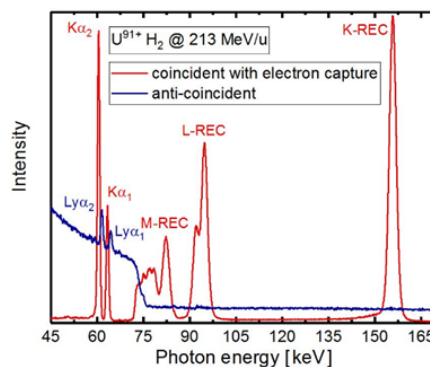


**Figure 1.** X-ray spectrum recorded by a Ge(i) detector located at  $120^\circ$  with respect to the ion beam axis.

### References

- [1] B. Najjari et al., Phys. Rev. A 85 052712 (2012)
- [2] D. L. Robbins et al., Phys. Rev. A 74, 022713 (2006).
- [3] A. Gumberidze et al., Phys. Rev. Lett. 110, 213201 (2013).
- [4] A. Gumberidze et al., J. Phys. B 48, 144006 (2015).
- [5] A. Gumberidze et al., Atoms 9, 20 (2021).
- [6] C. J. Bostock et al., Phys. Rev. A 80, 052708 (2009).
- [7] C. J. Fontes et al., Phys. Rev. A 49, 3704 (1994).

\* E-mail: [a.gumberidze@gsi.de](mailto:a.gumberidze@gsi.de)

## M X-ray Production Cross-Sections in $_{70}\text{Yb}$ Induced by Nitrogen Ions

Balwinder Singh<sup>1</sup>, Shehla<sup>2</sup>, Anil Kumar<sup>1</sup>, Deepak Swami<sup>3</sup>, Ajay Kumar<sup>4</sup> and Sanjiv Puri<sup>1\*</sup>

<sup>1</sup>Department of Physics, Punjabi University, Patiala-147002, Punjab, India

<sup>2</sup>Department of Physics, Govt. Mohindra College, Patiala-147002, Punjab, India

<sup>3</sup>Inter University Accelerator Centre, New Delhi, Delhi-110067, India

<sup>4</sup>Nuclear Physics Division, Bhabha Atomic Research Centre, Trombay, Mumbai-400 085, India

**Synopsis** The M X-ray production cross sections for  $_{70}\text{Yb}$  ( $\sim 30$  microgram/cm<sup>2</sup>), prepared on the backing of carbon ( $\sim 20$  microgram/cm<sup>2</sup>) by using vacuum evaporation technique at Inter University Accelerator Center (IUAC), New Delhi, India, induced by 1.75 MeV and 1.5 MeV nitrogen ion have been measured in the present work.

Accurate knowledge of the X-ray production (XRP) cross sections and relative intensities for different elements at various incident ion energies are important for ion-beam applications including material modification by ion-implantation and the quantitative elemental analysis of different types of samples employing proton induced X-ray emission (PIXE) technique. Besides, such data is useful for testing the theories governing the ion-atom collisions. The M X-ray production cross sections for  $_{70}\text{Yb}$  ( $\sim 30$  microgram/cm<sup>2</sup>), prepared on the backing of carbon ( $\sim 20$  microgram/cm<sup>2</sup>) by using vacuum evaporation technique at Inter University Accelerator Center (IUAC), New Delhi, India, induced by 1.75 MeV and 1.5 MeV nitrogen ion have been measured in the present work. The thickness of targets has been measured by RBS method at IUAC, New Delhi, In-

dia. To check the reliability of theoretical models, experimental values are compared with theoretical M XRP cross sections calculated using nitrogen ionization cross sections based on the ECUSAR and ECPSSR model [1], X-ray emission rates based on Dirac-Hartree-Slater (DHS) model [2], fluorescence yields and Coster-Kronig transition probabilities based on Dirac-Hartree-Slater (DHS) model [3].

### References

- [1] Z. Liu, S. Cipolla, *Comput. Phys. Commun.* 97, 315 (1996), 176, 157 (2007); 180, 1716 (2009); 182, 2439 (2011).
- [2] S. Puri, *At. Data Nucl. Data Tables* 93, 730(2007).
- [3] Y. Chauhan, S. Puri, *At. Data Nucl. Data Tables* 94, 38 (2008).

\* E-mail: [sanjivpurichd@yahoo.com](mailto:sanjivpurichd@yahoo.com)

## Interaction between highly charged ions near the Bohr velocity energy region and laser-produced plasmas

S Q Cao<sup>1\*</sup>, R Cheng<sup>2</sup>, M G Su<sup>1</sup>, L L Shi<sup>1,2</sup>, Z Wang<sup>1,2</sup>, Z X Zhou<sup>1,2</sup>, S Q He<sup>1</sup>, Y H Wu<sup>1</sup>, H D Lu<sup>1</sup>, Q Min<sup>1</sup>,  
D H Zhang<sup>1</sup>, C Z Dong<sup>1†</sup>

<sup>1</sup> Key Laboratory of Atomic and Molecular Physics and Functional Material of Gansu Province, College of Physics and Electronic Engineering, Northwest Normal University, Lanzhou 730070, China

<sup>2</sup>Institute of Modern Physics, Chinese Academy of Sciences, Lanzhou 73000, China

**Synopsis** An experimental setup was built for the research on interaction between ions near the Bohr velocity and laser-produced plasmas (LPP), based on the 320 kV experimental platform at the Institute of Modern Physics, Chinese Academy of Sciences. Using this setup, real-time diagnosis of LPP state and accurate measurement of ion charge state distribution and energy loss during the interaction between highly charged ions and LPP can be achieved. The high-accurated experimental data from this setup can be used to improve our understanding about the ions-plasma interaction process.

Interaction between highly charged ions and dense plasmas is one of the important physics problems in the fields of high-energy density physics and inertial confinement fusion. The related research is of great significance for energy transport in ion beam driven fusion reactions, rapid ignition of ion beams, and self-sustaining combustion of fusion targets, and so on.[1] In the Bohr velocity energy region, there are few related experiments, and there is a lack of understanding of the charge exchange mechanism and energy deposition laws in the interaction, which is due to the strong coupling between ions and plasma in this energy region, the non equilibrium behavior of charge states, and the multiple charge exchange process become prominent.

In this work, we have constructed an experimental setup for the research on interaction between ions near the Bohr velocity and hot dense laser-produced plasmas (LPP), based on the 320 kV experimental platform at the Institute of Modern Physics, Chinese Academy of Sciences. The state of LPP diagnosed by combining spectroscopy, transient imaging, and laser interference. The charge state and energy loss of the ion beam passing through the plasma are obtained by using a high energy ion measurement system.

In the experiment, a proton beam with hundred keV penetrated through the laser-induced Al plasma target, and the energy losses of protons, as show in figure1. The experimental results are so precise that some theoretical models can be benchmarked hopefully. In future, a sys-

tematic experiment can be carried out basen on this setup concerning the interaction between highly charged ions and dense plasmas near the Bohr velocity. The high-accurated experimental data can be used to improve our understanding about the ions-plasma interaction process.

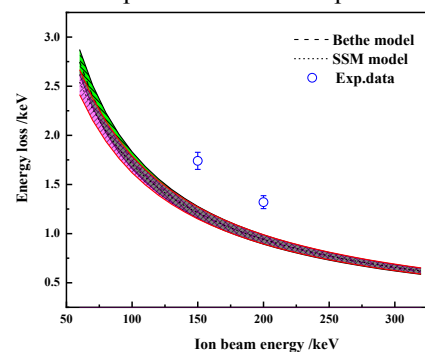


**Figure 1.** Comparison of the experimental energy losses of 150 keV and 200 keV protons in the Laser-induced plasma with the theoretical predictions from the Bethe and SSM models.

This work supported by the National Key R&D Program of China (2022YFA1602500), the National Natural Science Foundation of China (12204382,12064040) and the Science and Technology Project of Gansu Province (21JR7RA129)

### References

- [1] Cheng R, Zhang S, Shen G *et al* 2020 *SCIENTIA SINICA Physica, Mechanica & Astronomica* **50** 112011

\* E-mail: [caosq@nwnu.edu.cn](mailto:caosq@nwnu.edu.cn)

† E-mail: [dongcz@nwnu.edu.cn](mailto:dongcz@nwnu.edu.cn)

## Probing the formation of quasi-molecules in collisions of $\text{Kr}^{q+}$ -ion with Pb and Bi

C. V. Ahmad<sup>1,2</sup>, K. Chakraborty<sup>1,2</sup>, R. Gupta<sup>1,2</sup>, D. Swami<sup>3</sup> and P. Verma<sup>2\*</sup>

<sup>1</sup>Department of Physics and Astrophysics, University of Delhi, New Delhi, 110007, India

<sup>2</sup>Department of Physics, Kalindi College, University of Delhi, New Delhi, 110008, India

<sup>3</sup>Inter University Accelerator Centre, Aruna Asaf Ali Marg, New Delhi-110067, India

**Synopsis** X-Ray based investigations to explore the possibility of formation of quasi-molecules with united atomic numbers  $Z_{UA} = 118$  and  $119$  during the collision of 2–3.8 MeV  $\text{Kr}^{q+}$ -ions with Pb and Bi.

Superheavy systems, with atomic numbers greater than 100, are of interest considering the exotic attributes related to such systems. Some of these attributes like significant increase in the electron binding energies, enhanced spin–orbit splitting in the  $p$  orbitals and considerable shrinking of shell radius still remain widely unexplored. These superheavy atomic systems can be formed transiently during a quasiadiabatic heavy-ion–heavy-atom collision. Under adiabatic condition ( $Z_P/Z_T \approx 1$  and  $v_P/v_{Ts} \ll 1$ , where  $Z$  denotes the atomic number and  $v$  denotes the velocity with P as projectile, T as target and  $s = K, L, M, \dots$  shell) i.e., for very symmetric and low energy collisions, molecular orbitals (MO) are formed, and at very small inter atomic distance between the collision partners there is a probability of formation of transient quasi-molecules having atomic number equal to the sum of the atomic numbers of the collision partners ( $Z_{UA} = Z_P + Z_T$ ) [1]. Formation of such quasi-molecules can be explored by creating vacancies in the inner shells and studying their decay via X-Ray emission. Presently, the low energy ion beam accelerator equipped with a 10 GHz ECR-ion source at Inter University Accelerator Centre (IUAC), New Delhi, India has been used to accelerate  $\text{Kr}^{q+}$ -ions to energies of 2–3.8 MeV. The accelerated  $\text{Kr}^{q+}$ -ions were then bombarded on thin film targets of  $\text{Pb}_{82}$  and  $\text{Bi}_{83}$  (target thickness  $\sim 390 \mu\text{g}/\text{cm}^2$  for each target). X-Rays emitted from both the collision partners have been recorded with silicon drift detectors having a resolution of  $\sim 129 \text{ eV}$  @  $5.9 \text{ keV}$ . **Figure 1** shows the X-Ray spectrum of  $\text{Pb}_{82}$  due to the impact of 2, 3 and 3.8 MeV  $\text{Kr}^{q+}$ -ions. Energy shifts relative to the standard values [2] in X-

rays from both collision partners have been observed. The observation of enhanced target X-ray production and ionization cross-sections along with abnormal target to projectile intensity ratios compared to direct coulomb ionization models points to the formation of quasi-molecules [3].

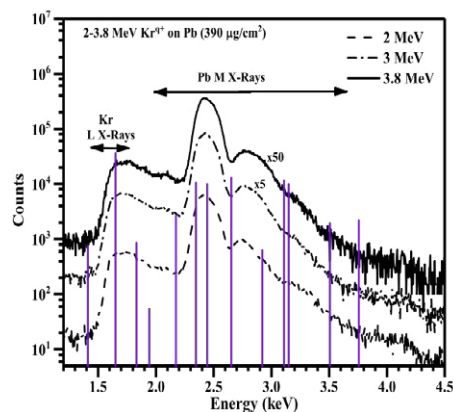


**Figure 1.** X-ray spectrum of  $\text{Pb}_{82}$  (target thickness =  $390 \mu\text{g}/\text{cm}^2$ ) due to the impact of 2, 3 and 3.8 MeV  $\text{Kr}^{q+}$ -ions, depicting the energy shifts relative to the standard values [2] (vertical lines on the energy axis).

Diabatic correlation diagrams have been drawn to examine and verify the origin of vacancy transfer mechanism during the collision for both  $\text{Kr}-Z_T$  ( $82 \leq Z_T \leq 83$ ) combinations. Further calculations are being carried out to decipher the coupling radii of the quasi-molecules formed.

### References

- [1] Anholt R 1985, Rev. Mod. Phys., **57**, 995.
- [2] J A Bearden 1967, Rev. Mod. Phys., **39** (1), 78.
- [3] C.V. Ahmad *et al* 2022, NIM B **531**, 9-23.

\* E-mail: [punitaverma@kalindi.du.ac.in](mailto:punitaverma@kalindi.du.ac.in)

## Efficiency enhancement of the dynamical capture of ion bunches by instantaneous ion-mode coupling

S. Ringleb<sup>1</sup> \*, M. Kiffer<sup>1</sup> †, S. Kumar<sup>2</sup>, M. Vogel<sup>3</sup>, W. Quint<sup>3,4</sup>, Th. Stöhlker<sup>1,3,5</sup>, G.G. Paulus<sup>1,5</sup>

<sup>1</sup> Institut für Optik und Quantenelektronik, Friedrich-Schiller-Universität, 07743 Jena, Germany

<sup>2</sup> Inter-University Accelerator Centre, 110067 New Delhi, India

<sup>3</sup> GSI Helmholtzzentrum für Schwerionenforschung GmbH, 64291 Darmstadt, Germany

<sup>4</sup> Physikalisches Institut, Ruprecht Karls-Universität Heidelberg, 69120 Heidelberg, Germany

<sup>5</sup> Helmholtz-Institut Jena, 07743 Jena, Germany

**Synopsis** We have set up an ion trap to prepare a well-defined ion target for laser-ion experiments at relativistic intensities. In the presented trap configuration, we are able to capture the ions directly into a harmonic potential. Here we will present the efficiency enhancement of the capture process using instantaneous ion-mode coupling.

Highly charged ions are an ideal candidate to investigate matter-light interactions and a Penning trap is a suitable device to store highly charged ions, particularly of several charge states represented by the reaction products and educts. [1, 2]. In particular, hydrogen-like and lithium-like systems provide a single active electron in a well-defined quantum state. For ions, such as  $O^{7+}$  or  $Ne^{7+}$ , the mean electric field intensity of the nucleus is of the order of  $10^{20} W/cm^2$ , which is in the range of high-intensity laser systems. This gives the opportunity to measure relativistic tunnel ionisation or high-harmonic generation in highly charged ions.

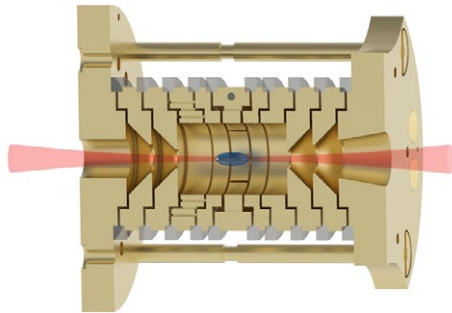


**Figure 1.** Sketch of the experiment. An ion cloud is compressed in the trap centre and irradiated with a high-intensity laser.

We will present the capabilities of the new designed HILITE (High-Intensity Laser Ion-Trap Experiment) Penning trap. HILITE provides a well-defined ion target for experiments with external laser facilities. The setup includes an ion

\*E-mail: [stefan.ringleb@uni-jena.de](mailto:stefan.ringleb@uni-jena.de)

†E-mail: [markus.kiffer@uni-jena.de](mailto:markus.kiffer@uni-jena.de)

source (EBIT) that creates bunches of arbitrary ion species. These bunches are transported by a beamline and captured dynamically into a harmonic Penning trap. Since many ions are captured with unstable trajectories leading to fast ion loss after capture, we have applied an instantaneous mode-coupling procedure in order to enhance the number of stored ions. With this procedure, we have increased the number of stored ions as well as the storage time significantly. We will show results of this high-efficient ion-bunch capture and the dependence on the capture or coupling parameters. We will also give an overview of the planned experiments and expected observations at the upcoming beamtime at the JETI200 laser facility in Jena.

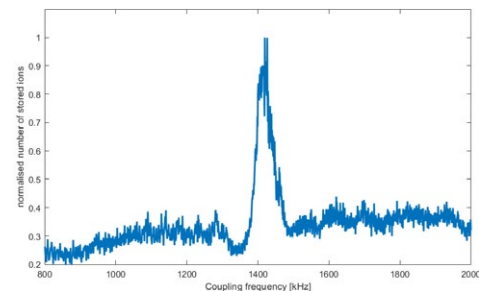


**Figure 2.** Number of stored ions depending on the coupling frequency.

### References

- [1] Vogel M, Quint W, Paulus G G and Stöhlker, Th *NIMB: Beam Interactions with Materials and Atoms* **285**
- [2] Ringleb S et al. *Physica Scripta* **97** 8



## Resonance-Enhanced Electron Capture in the Laser-Assisted Proton-Hydrogen Collision

Shan Gao<sup>1</sup>, Fengzheng Zhu<sup>2</sup>, Li Guang Jiao<sup>3,4\*</sup>, Aihua Liu<sup>1†</sup> and Uwe Thumm<sup>5‡</sup>

<sup>1</sup>Institute of Atomic and Molecular Physics, Jilin University, Changchun, 130012, China

<sup>2</sup>School of Mathematics and Physics, Hubei Polytechnic University, Huangshi, 435003, China

<sup>3</sup>College of Physics, Jilin University, Changchun, 130012, China

<sup>4</sup>Helmholtz-Institut Jena, D-07743 Jena, Germany

<sup>5</sup>Department of Physics, Kansas State University, Manhattan, Kansas 66506-2604, USA

**Synopsis** The resonance-enhanced electron capture in the laser-assisted proton-hydrogen collision is investigated by numerically solving the time-dependent Schrödinger equation. It is found that the electron capture probabilities can be greatly enhanced by the laser field with its frequency being coincident with the resonance energy between the ground and excited states of the target atom.

Electron capture and ionization processes in the ion-atom collisions play important roles in many physical and chemical processes. The proton-hydrogen collision provides the most simplest prototype to investigate the intricate scattering dynamics. In strong laser fields, the electronic dynamics leading to capture and ionization, and thus the final transfer and emission probabilities change dependent on the initial laser phase [1,2].

By numerically solving the time-dependent Schrödinger equation [3], we have investigated the resonance effect of the electron capture and ionization in the proton-hydrogen collisions with the assistance of circularly polarized laser fields. As shown in Fig. 1, by applying suitable laser parameters, we find a significant enhancement of the electron capture probability due to the one- or two-photon resonance between the target ground and excited states. The excited states have a larger electron capture cross section. The presence of laser field build a ‘bridge’ between ground and excited states of target hydrogen atom.

We further found a noticeable circular dichroism in the capture probability for lower laser frequencies ( $\omega < 0.1$  a.u.), and such circular dichroism effect diminishes or disappears for higher laser frequencies ( $\omega > 0.2$  a.u.), in accordance with the projected influence of resonant laser excitation (Fig. 1).

\*E-mail: [lgjiao@jlu.edu.cn](mailto:lgjiao@jlu.edu.cn),

†E-mail: [aihualiu@jlu.edu.cn](mailto:aihualiu@jlu.edu.cn),

‡E-mail: [thumm@phys.ksu.edu](mailto:thumm@phys.ksu.edu)

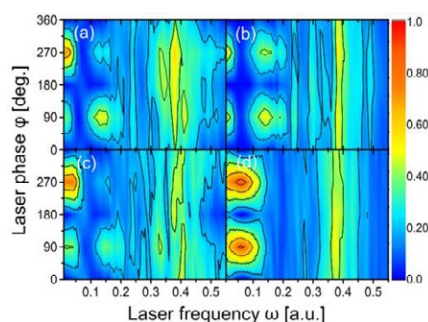


**Figure 1.** Colour-coded electron-capture probabilities as a function of the laser initial phase and frequency for impact parameters (a)  $b=0$ , (b)  $b=1$ , (c)  $b=2$  and (d)  $b=3$ , and for a proton incident energy of 1.21 keV. The laser peak intensity is  $5 \times 10^{13}$  W/cm<sup>2</sup>.

This work was supported by the National Key Research and Development Program of China (2022YFE0134200), the National Natural Science Foundation of China under Grant Numbers 12174147, 91850114 and 11774131, and the U.S. NSF and the Division of Chemical Sciences, Office of Basic Energy Sciences, Office of Energy Research, U.S. DoE.

### References

- [1] Niederhausen T, Feuerstein, B and Thumm U 2004 *Phys. Rev. A* **70**, 023408.
- [2] Niederhausen T and Thumm U 2006 *Phys. Rev. A* **73**, 041404(R).
- [3] Zhou S-P, Liu A-H, Liu F, Wang C-C and Ding D-J, *Chin. Phys. B*, 2019 **28**, 083101

## Development of electrospray ion source and setup for collision induced dissociation experiments of large molecules

K Kumar <sup>\*</sup>, M A Rehman and D Misra <sup>†</sup>

Department of Nuclear and Atomic Physics Tata Institute of Fundamental Research, Mumbai, 400005, India

**Synopsis** In this abstract we will discuss about the developmental work on bulding the experimental setup to study collision induced dissociation of biomolecular ions.

Interactions involving atoms, molecules and clusters are play important role in plasmas [1], astrochemistry, planetary atmosphere. Studies involving ions are important to understand how molecules are formed and destroyed in space and planetary atmosphere. Mass spectrometry is commonly used to study ion reactions to find out different masses which produce in collision induced fragmentations. Electrospray ion source mass spectrometry is one such method to produce ions of large molecules without breaking them.

We are setting up an electrospray ion source (EIS) and a test bench for conducting collision induced dissociation experiments of larger molecules, e.g., adenine, adenosine, adenosine monophosphate and others. Design of the setup is motivated by that of N. de Ruelle *et al.* [2].

The setup is in its primary phase. The EIS setup is followed by an ion funnel to focus them to the next stage where ions will be guided, bunched and stored for further experiments. We are conducting simulation-based analysis in this phase and therefore designing of the setup is in progress. One of the electrodes which is ion funnel, will be discussed in this abstract.

Figure (1) is the results of simulation of ion funnel which will be used to pass and focus the ions generated by the EIS source. The electrodes of the ion funnel will carry rf voltage of opposite parity applied to the alternate electrodes. The geometry of the funnel is such that the ions, while passing through, will be focussed, and guided to the subsequent chambers.

We are interested in ion transmission through the funnel, and our focus will be on achieving 100% transmission. The ion transmission simulations (performed in Simion 8.0) for different masses, as a

function of peak-to-peak rf voltage  $V_{pp}$  at a frequency of  $f=1.75$  MHz.

After the funnel, the subsequent sections will consist of octupole guide, octupole trap, ion optics, quadrupole deflector, ring electrode trap, cold head, acceleration and setup for collision experiments. Ring electrode trap consists of 30 ring shaped electrodes that will be used to cool and store the ions, which will be etracted towards the acceleration region where extraction of upto 50 kV be applied to accelerate them. Ions inside the ring electrode trap will be cooled by the cold head.

With this setup, we will study the electron-capture induced fragmentation of large molecules upon collision with other neutral gases.

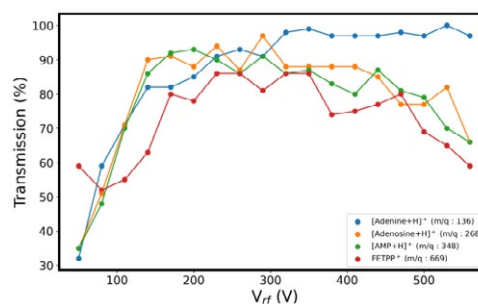


**Figure 1.** Ion transmission through Ion Funnel as a function of RF voltage applied to the Funnel electrode for a variety of ion having different  $m/q$  ratio. The ions studied are [Adenine+H]<sup>+</sup> ( $m/q=136$ ), FETPP<sup>+</sup> ( $m/q=669$ ), [AMP+H]<sup>+</sup> ( $m/q=348$ ) and [Adenosine+H]<sup>+</sup> ( $m/q=268$ ).

### References

- [1] Tandero C, et al., 2006 *Spectrochim. Acta, Part B* **61**, 4111
- [2] de Ruelle N et al. 2018 *Review of Scientific Instruments* **89**, 075102

<sup>\*</sup> E-mail: [kamalkg2451@gmail.com](mailto:kamalkg2451@gmail.com)

<sup>†</sup> E-mail: [dmisra@tifr.res.in](mailto:dmisra@tifr.res.in)

## Dissociation dynamics in Chloroform molecule induced by ion impact

Nirmallya Das<sup>1</sup>, Sankar De<sup>2</sup>, Pragya Bhatt<sup>3</sup>, C. P. Safvan<sup>3</sup> and Abhijit Majumdar<sup>1</sup>

<sup>1</sup>Department of Physics, Indian Institute of Engineering Science and Technology, Howrah-711103, India.

<sup>2</sup>Saha Institute of Nuclear Physics, HBNI, 1/AF, Bidhannagar, Kolkata 700064, India.

<sup>3</sup>Inter-University Accelerator Centre, Aruna Asaf Ali Marg, New Delhi 110067, India.

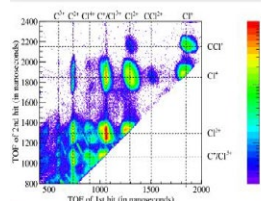
**Synopsis** The ion impact multiple ionization and subsequent dissociation of CCl<sub>4</sub> is studied using a beam of Ar<sup>7+</sup> ion having the energy of about 1 MeV in a linear time-of-flight mass spectrometer. The complete, as well as incomplete Coulomb explosion pathways are identified and studied. Possible modes of fragmentation pathways, i.e., concerted and/or sequential, for all the identified channels are studied using Newton diagrams, Dalitz plots, and kinetic energy distributions. The nature of the fragmentation process is further investigated with simulated Dalitz plots and Newton diagrams using the simple classical mechanical model.

The ion impact multiple ionization and subsequent dissociation of CCl<sub>4</sub> is studied using a beam of Ar<sup>7+</sup> ion having energy of about 1 MeV in a linear time of flight mass spectrometer coupled with a position sensitive detector [1]. Our objective is to identify the possible modes of fragmentation pathway for all the identified channels with the help of kinetic energy release and momentum distributions of fragmented ions.

Tetrachloromethane (CCl<sub>4</sub>) is found in the natural environment and has been identified to be a long-lived green-house gas which is responsible for ozone depletion in both the troposphere and the stratosphere. It has widespread industrial applications like reactive etching gas for silicon wafers in semiconductor microchip industries as well as cleaning surfaces by chemical vapour deposition. The dissociative ionization of tetrachloromethane have been explored in intense linearly polarized laser field of picosecond and attosecond [2] time scale. The properties such as fragmentation pattern, angular distribution of ionic fragments like Cl<sup>+</sup> arising from it, were studied and compared with the 70 eV electron induced fragmentation

The complete as well as incomplete Coulomb explosion pathways for CCl<sub>4</sub><sup>2+</sup> and CCl<sub>4</sub><sup>3+</sup> ions are identified and studied. The kinetic energy release distributions (KERD) of channels, kinetic energies and momentum distributions of fragmented ions as well as neutrals are also calculated.

**Figure 1.** Coincidence plot of CCl<sub>4</sub> molecule due to the impact of about 1 MeV Ar<sup>7+</sup> beam. The TOF of 1<sup>st</sup> and 2<sup>nd</sup> hit is plotted along X- and Y-axis respectively in nanosecond time scale.



Possible modes of fragmentation pathway i.e. concerted and/or sequential for all the identified channels are studied using Newton diagram, Dalitz plot and kinetic energy distribution. The dynamical information and fragmentation pathways were analysed with Dalitz plot and Newton diagram for the three-body dissociation channel. A sequential mode of fragmentation for an incomplete 3-body dissociation channel has been identified. The nature of the fragmentation process is further investigated with simulated Dalitz plots and Newton diagram using simple classical mechanical model.

### References

- [1] N. Das, S. De, P. Bhatt, C. P. Safvan, and A. Majumdar, *J. Chem. Phys.* **158**, 084307 (2023).
- [2] V. R. Bhardwaj, F. A. Rajgara, K. Vijayalakshmi, V. Kumarapan, D. Mathur, and A. K. Sinha, *Phys. Rev. A* **58**, 3849 (1998).

## Excitation processes in collisions of He<sup>+</sup> ions with N<sub>2</sub>, O<sub>2</sub> molecules

Malkhaz R Gochitashvili<sup>1</sup>, Ramaz A Lomsadze<sup>1</sup>, Roman Ya Kezerashvili<sup>2,3</sup> and Michael Schulz<sup>4</sup>

<sup>1</sup>Tbilisi State University, Tbilisi, 0179, Georgia

<sup>2</sup>Physics Department, New York City College of Technology, The City University of New York, Brooklyn, NY 11201, <sup>3</sup>The Graduate School and University Center, The City University of New York, NY 10016, United States of America,

<sup>4</sup>Missouri University of Science and Technology, Rolla, MO 65409, United States of America.

**Synopsis** Absolute cross sections for dissociative excitation processes of He<sup>+</sup> - O<sub>2</sub> and He<sup>+</sup> - N<sub>2</sub> pairs are determined. In the case of He<sup>+</sup> - O<sub>2</sub> pair the high-intensity oxygen ionic line has been observed. In the case of He<sup>+</sup> - N<sub>2</sub> pair the linear polarization of the helium atomic and nitrogen ionic lines have been measured. The experimental results are interpreted qualitatively in terms of quasidiatomic approximation.

In this work, for the He<sup>+</sup> - O<sub>2</sub> collision pair the absolute cross sections for dissociative excitation processes of oxygen atomic and ionic lines are determined. The high-intensity oxygen ionic line OII (83.4 nm) has been observed. In the case of He<sup>+</sup>-N<sub>2</sub>, the pair emission cross-section and the linear polarization of the atomic Hel lines ( $\lambda=388.9\text{nm}$ , transition  $3p\ ^3P_0 \rightarrow 2s\ ^3S$ ;  $\lambda=587.6\text{nm}$ , transition  $3d\ ^3D \rightarrow 2p\ ^3P$ ) and nitrogen ionic NII ( $\lambda=500.1\text{-}500.5\text{nm}$ , transition  $3d\ ^3F_0 \rightarrow 3p\ ^3D$ ) lines have been measured for a broad range of collision energies (1-10keV). A high degree of polarization  $P = -20\%$  was observed in the case of the helium line (fig.1). Such a great negative value of the degree of polarization indicates that  $m_L = \pm 1$  sublevels of the excited state  $3^3P$  of helium atom are preferably populated. An expression for the first Stoke's parameter has been derived on the basis of the general approach developed by Macek and Jaecks [1].

$$P = \frac{I_{//} - I_{\perp}}{I_{//} + I_{\perp}} = \frac{15(\sigma_0 - \sigma_1)}{41\sigma_0 + 67\sigma_1} \quad (1)$$

where  $I_{//}$  and  $I_{\perp}$  denote the measured intensities of radiation with the electric field vector parallel and perpendicular to the incident ion beam, respectively;  $\sigma_0$  and  $\sigma_1$  stand for the cross sections for a population of sublevels with  $m_L = 0$  and  $m_L = \pm 1$ , respectively. Considering that the experimentally observed value of  $P$  is  $-20\%$  one obtains from (1) that  $\sigma_1 / \sigma_0 \approx 15$ . Such a large

value of this ratio indicates that  $m_L = \pm 1$  sublevels of the excited helium atom are preferably populated.

The analysis of the experimental results indicates that the electron density formed in He\* during the collision is oriented perpendicularly with respect to the incident beam direction. A strong correlation is revealed between inelastic channels of the formation of excited helium and nitrogen particles. The experimental results are interpreted qualitatively in terms of quasidiatomic approximation.

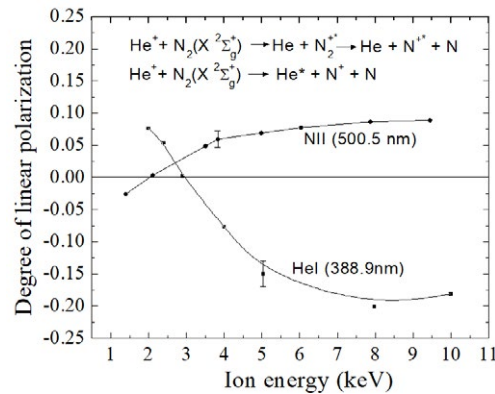


Figure 1. Energy dependence of degree of polarization.

### References

- [1] J. Macek, D. H. Jaecks Phys Rev A 4 2288, (1971)

\* E-mail: [malkhaz.gochitashvili@tsu.ge](mailto:malkhaz.gochitashvili@tsu.ge)

† E-mail: [schulz@mst.edu](mailto:schulz@mst.edu)

## Ionization of molecules by bare ions impact: dynamic effective charge in the residual-target continuum state

M.F. Rojas<sup>1\*</sup>, M.A. Quinto<sup>2†</sup>, N.J. Esponda<sup>2</sup>, R.D. Rivarola<sup>2</sup> and J.M. Monti<sup>2</sup>

<sup>1,2</sup>Instituto de Física Rosario (CONICET-UNR) and Facultad de Ciencias Exactas, Ingeniería y Agrimensura, Universidad Nacional de Rosario, 2000 Rosario, Argentina

**Synopsis** In order to improve the representation of the residual-target final state, a dynamic-depending charge defined by the emission angle and energy of the ionized electron is considered in the residual-target continuum state.

The CDW-EIS distorted wave model (Continuum Distorted Wave-Eikonal Initial State) was applied with success to calculate total and multiply differential cross sections for single ionization by bare projectile impact on several molecular targets like H<sub>2</sub>O, NH<sub>4</sub>, CH<sub>3</sub> and larger molecules like the DNA and RNA basis (see for example [1, 2]). However, it presents a systematic underestimation of the experimental data for double differential cross sections, calculated at large emission angles and high emission energies. With the purpose of reducing these underestimations, we approximate the non-Coulomb potential of the final continuum state to an effective Coulomb potential with a dynamic effective charge which depends on the emission angle and emission energy (DC-CDW-EIS).

To represent molecular orbitals the well-known CNDO approximation (Complete Neglected Differential Overlap) has been used, with each molecular orbital described as a linear combination of atomic orbitals.

The consideration of a dynamic charge results in a major improvement of the backward emission over the whole range of emission energies for many systems. In this work, we will show the function that represents the dynamic charge in the DC-CDW-EIS model and some results obtained for molecular targets compared with the conventional CDW-EIS model and CDW-EIS with numerical functions.

Further details about the calculations and the function defining the dynamic effective charge will be provided during the Conference.

\*E-mail: [rojas@ifir-conicet.gov.ar](mailto:rojas@ifir-conicet.gov.ar)

†E-mail: [quinto@ifir-conicet.gov.ar](mailto:quinto@ifir-conicet.gov.ar)

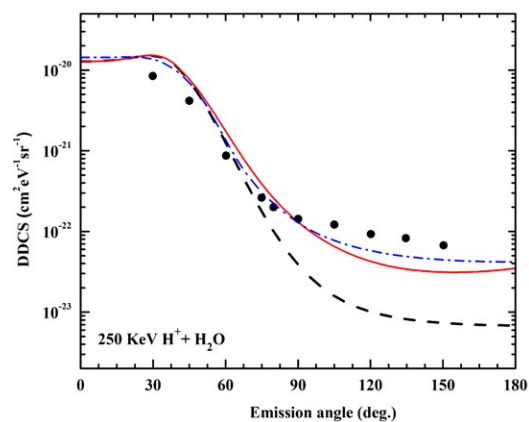


**Figure 1.** DDCS for single ionization of H<sub>2</sub>O by the impact of 250 keV/u H<sup>+</sup> for 320 eV electron energy and as a function of the electron angle. Theory: red line DC-CDW-EIS, dashed black line CDW-EIS, and dotted dashed blue line CDW-EIS with numerical functions. Experimental data: black points [3].

### References

- [1] C. Tachino, J. Monti, O. Fojón, C. Champion, and R. Rivarola, *J. Phys. B: At. Mol. Opt. Phys.* **47** 035203
- [2] Anuvab Mandal, Chandan Bagdia, Madhusree Roy Chowdhury, Shamik Bhattacharjee, Deepankar Misra, Juan M. Monti, Roberto D. Rivarola, and Lokesh C. Tribedi. (2020) *Phys. Rev. A*, **101** 062708
- [3] Abhijeet Bhogale, S. Bhattacharjee, M. Roy Chowdhury, Chandan Bagdia, M. F. Rojas, J. M. Monti, A. Jorge, M. Horbatsch, T. Kirchner, R. D. Rivarola, and L. C. Tribedi. (2022) *Phys. Rev. A*, **105** 062822



## A travelling-wave ion-mobility system for preparation of conformationally pure molecular targets for collision experiments

M. Goulart<sup>1</sup>, Klaas Bijlsma, Maartje Nieuwenhuis, Jente Damm, and Thomas Schlathölter<sup>1,2,\*</sup>

<sup>1</sup>University of Groningen, Zernike Institute for Advanced Materials, 9747 AG Groningen, Netherlands

<sup>2</sup>University of Groningen, University College Groningen, 9718 BG Groningen, Netherlands

For more than two decades, ion collisions with gas phase biomolecules have been investigated to improve our understanding of the molecular mechanisms of radiation therapy. Initially, collision experiments with biomolecular systems have focused on relatively small DNA or protein building blocks, that were brought into the gas-phase by evaporation. More radiobiologically relevant molecular systems such as entire DNA strands, are too fragile for this experimental approach, which is why electrospray ionization has become a widespread technique to produce gas-phase targets of complex biomolecular ions [1].

Over the last years, our team has employed a combination of electrospray ionization with radiofrequency ion guiding and trapping, to prepare targets of mass-selected trapped gas-phase DNA ions for radiobiologically relevant MeV ion collision experiments [2,3]. A recurrent problem in studies involving large molecular systems is the fact that they occupied a large conformational space, even under cryogenic conditions.

Conformational separation can be accomplished by ion-mobility techniques, where bunches of molecular ions drift through an inert gas under the influence of an electric field. The ion drift velocity can then be directly related to its geometric cross section. Typically, drift regions need to be several meters long and kV potentials are required.

We have employed an alternative ion-mobility approach that is based on traveling waves and radiofrequency ion guiding. The electrode structures are implemented on printed circuit boards (see figure). The apparatus allows for production of intense beams of protonated and deprotonated clusters of amino acids and prebiotic molecules, that are both  $m/q$  selected and conformationally pure. The entire system is

very compact and can easily be interfaced with e.g. MeV or keV ion beamlines.

In the near future, we plan to use MeV carbon ions from the IRRSUD facility at GANIL/France to investigate collisions with conformer selected DNA.

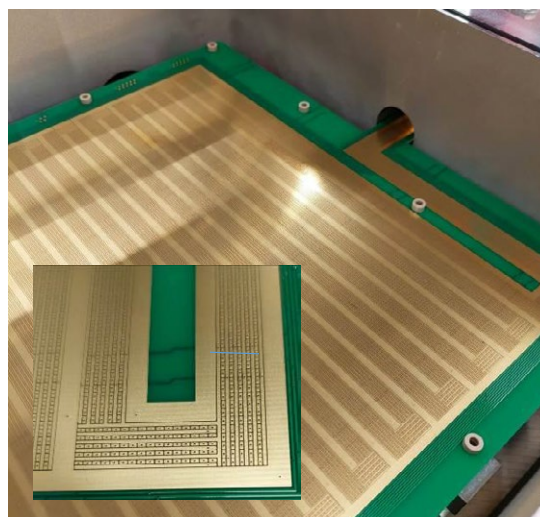


**Figure 1.** Photograph of the traveling wave PCB with zoom into the region of the last 180° turn.

### References

- [1] S. Bari, R. Hoekstra, T. Schlathölter, 2010 *Phys. Chem. Chem. Phys.* 12 3376
- [2] W. Li, O. Kavatsyuk, W. Douma, X. Wang, R. Hoekstra, D. Mayer, M. Robinson, M. Gühr, M. Lalande, M. Abdelmouleh, M. Ryszka, J.-C. Pouilly, T. Schlathölter, 2021 *Chemical Science* 12 13177
- [3] M. Lalande, M. Abdelmouleh, M. Ryszka, V. Vizcaino, J. Rangama, A. Méry, F. Durantel, T. Schlathölter, and J.-C. Pouilly, 2018 *Physical Review A* 98 062701

\* E-mail: [t.a.schlatholter@rug.nl](mailto:t.a.schlatholter@rug.nl)

## Ultrafast rotational energy transfer initiating by Coulomb explosion in two-body dissociation of $\text{CO}_2^{3+}$

Weiying Xu<sup>1\*</sup>, Ruichao Dong<sup>2,3</sup>, Xincheng Wang<sup>1†</sup>, and Yuhai Jiang<sup>1,4‡</sup>

<sup>1</sup>Center for Transformative Science, ShanghaiTech University, Shanghai 201210, China

<sup>2</sup>Shanghai Advanced Research Institute, Chinese Academy of Sciences, Shanghai 201210, China

<sup>3</sup>University of Chinese Academy of Sciences, Beijing 100049, China

<sup>4</sup>School of Physical Science and Technology, ShanghaiTech University, Shanghai 201210, China

**Synopsis** A detailed dynamics of two-body dissociation for the ground state  $\text{CO}_2^{3+}$  has been traced by an *ab initio* molecular dynamics simulation. The kinetic energy release deduced from simulation is in good agreement with the experimental one, and a considerable amount of energy transfers into the rotational degree of freedom of the  $\text{CO}^{2+}$  fragments after the C-O bond breaks up at about 60 fs.

The motion picture for the initial stages of molecular dissociation before Coulomb explosion embodies the vital structural dynamics information for molecular geometry reconstruction, which can be hardly revealed by the kinetically complete measurement experiments [1]. Meanwhile, it plays an important role for understanding the response of single molecules or biological tissue to radiolysis by various radiation sources, where charge and energy transfers will happen while the excited systems relax [2]. The two-body dissociation dynamics of the prototype system of  $\text{CO}_2^{3+}$  ions, the simplest breakage pathway, involves the rotational and vibrational degrees of freedom in the  $\text{CO}^{2+}$  fragments relative to diatomic molecules, which is common and more complex in larger systems. However, there are few detailed studies on two-body fragmentation of  $\text{CO}_2^{3+}$  in contrast to three-body channel.

Here an *ab initio* molecular dynamics simulation employing an atom-centered density matrix propagation method (ADMP) [3] has been used to snapshot the complete Coulomb explosion process of the ground state  $\text{CO}_2^{3+}$  shown in Fig. 1, in which about 73.45% of 10000 simulated trajectories are two-body dissociation events  $\text{CO}_2^{3+} \rightarrow \text{CO}^{2+} + \text{O}^+$ . Fig. 1(a) and (b) show the two C-O bond lengths versus time, respectively, which indicate the C-O bond breakage takes place at about 60 fs on average, and the vibrational period of  $\text{CO}^{2+}$  is about 23 fs. The total kinetic energy release (KER) versus time is shown in

Fig. 1(c), and the simulated KER distributions for  $\text{CO}^{2+}$ ,  $\text{O}^+$ , and  $\text{CO}^{2+} + \text{O}^+$  are in very good agreement with the experimental results shown in Fig. 1(d) [4], which suggests this simulation is valid and reliable. Fig. 1(e) and (f) show a considerable amount of energy transfers into the rotational and vibrational degrees of freedom of  $\text{CO}^{2+}$  after the Coulomb explosion happens at about 60 fs.

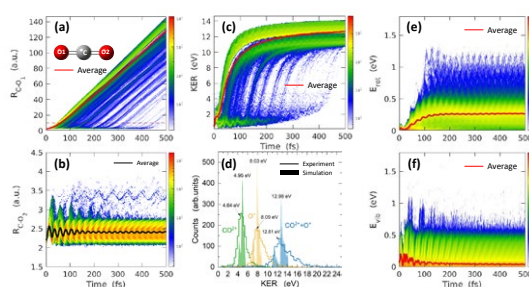


**Figure 1.** The simulated results for two-body dissociation dynamics of  $\text{CO}_2^{3+}$ .

### References

- [1] Vager Z, Naaman R and Kanter E P 1989 *Science* **244** 426
- [2] Jiang Y H, Rudenko A, Herrwerth A *et al* 2010 *Phys. Rev. Lett.* **105** 263002
- [3] Yang H J, Wang E L, Dong W X *et al* 2018 *Phys. Rev. A* **97** 052703
- [4] Zhang S, Wang X C, Jiang W B *et al* 2022 *J. Chem. Phys.* **156** 134302

\*E-mail: [xuwq1@shanghaitech.edu.cn](mailto:xuwq1@shanghaitech.edu.cn)

†E-mail: [wangxch1@shanghaitech.edu.cn](mailto:wangxch1@shanghaitech.edu.cn)

‡E-mail: [jiangyh3@shanghaitech.edu.cn](mailto:jiangyh3@shanghaitech.edu.cn)

## Statistical Analysis of X-ray Spectra of Aqueous Tripeptides

E A Eronen<sup>1\*</sup>, A Vladyka<sup>1</sup>, F Gerbon<sup>2</sup>, C J Sahle<sup>2</sup> and J Niskanen<sup>1</sup>

<sup>1</sup>University of Turku, Department of Physics and Astronomy, FI-20014 Turun yliopisto, Finland

<sup>2</sup>ESRF, The European Synchrotron, 71 Avenue des Martyrs, CS40220, 38043 Grenoble Cedex 9, France

**Synopsis** We report an analysis of extensive statistical simulations for core-level spectra of aqueous tripeptides. Our goal is to determine what kind of structural information can be deduced from X-ray spectroscopy of these systems. We discuss methods we have developed for the analysis of the relation between the structure of a molecule and its theoretical X-ray spectrum. Experimental X-ray Raman scattering confirms the overall shapes of the simulated ensemble-averaged nitrogen K-edge spectra.

The folding of proteins is a complex and complicated question [1], affected by both intramolecular and intermolecular interactions. The process is ultimately dependent on the primary order of the aminoacids and the surrounding solvent. While diffraction allows for atomistic structure determination of proteins, it requires a crystalline sample. Instead, owing to its localized mechanism, X-ray spectroscopy maintains its sensitivity to atomistic structure also in the liquid phase.

A liquid system allows for the movement of relatively strongly interacting molecules, which leads to a broad distribution of possible configurations. These individual configurations have been computationally observed to have significantly different X-ray spectra, only their ensemble mean predicting the experimentally observed spectrum. Although X-ray spectroscopy does not permit full structural reconstruction, its principles allow for discovery of structural information, especially when combined with statistical analysis [2, 3] of computational results.

In this contribution, we present our ongoing statistical analysis of computational X-ray spectra of aqueous tripeptide systems. Classical molecular dynamics was used to obtain the configuration distribution of the system (*e.g.* triglycine in Fig. 1a, visualised with the Ramachandran plot in Fig. 1b). Then, X-ray absorption spectra were calculated with density functional theory (Fig. 1c).

The main goal of our study is to determine if X-ray spectroscopy could be used to gain new structural information of aqueous tripeptides. As the systems are complex, simple tools like linear correlations between the internal coordinates of the system and its X-ray absorption spectrum do not deliver satisfying results. We approach this problem by applying neural networks and a specialized dimensionality reduction method, as already done with a different system [3]. The results are compared to X-ray Raman scattering spectra of liquid triglycine at the nitrogen K edge.

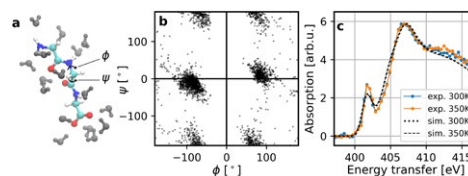


**Figure 1.** Results for the study of triglycine(aq). **a:** An example configuration and its Ramachandran angles  $\phi$  and  $\psi$ . **b:** Ramachandran plot for an MD trajectory. **c:** Experimental X-ray Raman scattering spectra and the mean of simulated X-ray absorption spectra at two temperatures.

### References

- [1] Dill HK A and MacCallum J L 2012 *Science* **338** 1042
- [2] Niskanen J *et al.* 2017 *Phys. Rev. E* **96** 013319
- [3] Vladyka A, Sahle C J and Niskanen J 2023 *Phys. Chem. Chem. Phys.* **25** 6707

\*E-mail: [eeveli.a.eronen@utu.fi](mailto:eeveli.a.eronen@utu.fi)

## The role of molecular collisions in the conversions of nuclear spin isomers of methanol gas

Z.-D. Sun<sup>1,2\*</sup>

<sup>1</sup>School of Physics, Shandong University, Jinan, 250100, China

<sup>2</sup>School of Physics and Electrical Engineering, Kashi University, Kashgar, 844006, China

**Synopsis** Molecular collisions play indirect role in a quantum relaxation process in the conversions of nuclear spin isomers of methanol (CH<sub>3</sub>OH) gas through the mixed ortho and para states caused by intramolecular magnetic hyperfine interactions.

According to identity principle in quantum mechanics, all molecules possessing identical nuclei with nonzero spin have two or more distinct nuclear spin isomers (NSIs) with different arrangements of total nuclear spin quantum numbers. The NSIs are the basic molecular species of existence in nature. They distribute in different quantum states. For example, The H<sub>2</sub> molecules have two NSIs, the ortho-H<sub>2</sub> and para-H<sub>2</sub> belong to rotational levels with odd and even rotational quantum numbers, respectively. The NSIs can be converted from one isomeric species to the other when the flipping of a nuclear spin of one of the equivalent atoms occurs. The nuclear spin conversion rate of polyatomic molecules in the gas phase depends on the collisions. It is known that, due to the steep magnetic field gradient produced by the collision partner, collisions with paramagnetic O<sub>2</sub> with a large magnetic moment  $\sim 2\mu_B$  in a <sup>3</sup>Σ state speed up ortho-para conversion in H<sub>2</sub> [1] and in CH<sub>3</sub>F [2], while it is 4 times less efficient for conversion that <sup>13</sup>CH<sub>3</sub>F itself [3], although the molecules survive some 10<sup>9</sup> collisions for <sup>13</sup>CH<sub>3</sub>F and 10<sup>11</sup> collisions for CH<sub>3</sub>F before conversion takes place. Molecular collisions play a direct role in the conversions of NSIs of these gases. Rather than magnetic intermolecular interactions, however, nonmagnetic collisions can also cause the conversions of NSIs in molecules through the mixed near-degenerate levels belonging to different NSIs. This indirect role of the collisions was demonstrated by observation of conversion rate of the NSIs in CH<sub>3</sub>OH gas.

The CH<sub>3</sub>OH molecule has the hindered internal rotation (*i.e.* torsion) of the CH<sub>3</sub> group with respect to the OH group. Different from H<sub>2</sub>, CH<sub>3</sub>F, and <sup>13</sup>CH<sub>3</sub>F molecules which have overall rotational symmetry, the CH<sub>3</sub>OH molecule

does not rotate around the overall rotational symmetry axis but the CH<sub>3</sub> axis. The identical nuclei in the CH<sub>3</sub> produce a specific type of NSIs of the ortho- and para-CH<sub>3</sub>OH isomers in methanol, which are distinguished by the torsional-symmetry quantum number and distribute in energy levels of *A*- and *E*-symmetry, respectively. Due to the multifold interactions among vibration, rotation, and torsion modes, levels in both ortho- and para-CH<sub>3</sub>OH states are so dense and close in energies that intramolecular magnetic hyperfine interactions in CH<sub>3</sub>OH can induce coherent mixings between them. We show in this talk that the decoherence is produced by molecular collisions which destroy the quantum coherence between the mixed ortho and para states in CH<sub>3</sub>OH, the ortho-para conversion in CH<sub>3</sub>OH can be induced by nonmagnetic molecular collisions in an energy relaxation process from a non-equilibrium concentration to the natural equilibrium level of their populations. Subsequent collision accounts for this relaxation in CH<sub>3</sub>OH gas, in which collisional relaxation rate is neither proportional nor anti-proportional to the pressure broadening parameter. The pressure dependence of the observed ortho-para conversion rates clearly show the inhibition of the spin interconversion between the ortho- and para-CH<sub>3</sub>OH isomers in a quantum relaxation process by frequent molecular collisions with increasing gas pressures.

### References

- [1] Farkas A, *Orthohydrogen, Parahydrogen and Heavy Hydrogen*, Cambridge University Press, London, 1935.
- [2] Nagels B *et al*, 1998 *Chem. Phys. Lett.* **294** 387
- [3] Nagels B *et al*, 1995 *J. Chem. Phys.* **103** 5161

\* E-mail: [zdsun@sdu.edu.cn](mailto:zdsun@sdu.edu.cn)

## Combining momentum-space wavefunctions and frontier orbital theory for providing predictive insights into pharmacological activity

S Long\*, Y Onitsuka, S Nagao and M Takahashi†

Institute of Multidisciplinary Research for Advanced Materials, Tohoku University, Sendai, 980-8577, Japan

**Synopsis** We propose a new pharmacological index, the similarity index of frontier orbitals in momentum space (SIFOMS), which highlights the spatial distribution of frontier electron density, far from the nuclei, being crucial in molecular reactivity and recognition. We apply SIFOMS into the toxicity prediction for carbamates that are known as electron acceptors in their toxicity mechanism. We show that SIFOMS calculations with their lowest unoccupied molecular orbitals reproduce well the experimental toxicity ratio among the carbamates studied, thereby demonstrating the novel ability of SIFOMS.

Quantitative structure activity relationship (QSAR) has widely been used in drug discovery to predict pharmacological activity through data training. On contrary, in cases where training data are insufficient, predicting activity based on reaction mechanism is a useful alternative. Such prediction was typically conducted based on lock-and-key theory [1] that assumes the structural complementarity between ligand and receptor drives chemical reactivity, while many exceptions to this have also been found [2]. To tackle this issue, Cooper and Allan proposed an idea that shapes of total electron density govern activity mechanism, and introduced molecular similarity index (MSI) of the R and T molecules:

$$I_{\text{MSI}}[\text{R}, \text{T}] = \frac{2 \int \rho^{\text{R}}(\mathbf{p}) \rho^{\text{T}}(\mathbf{p}) d\mathbf{p}}{\int [\rho^{\text{R}}(\mathbf{p})]^2 d\mathbf{p} + \int [\rho^{\text{T}}(\mathbf{p})]^2 d\mathbf{p}}$$

Here  $\rho(\mathbf{p})$  denotes electron density for all occupied molecular orbital wavefunctions in momentum space obtained by Fourier transform of the corresponding position-space one. The key behind this idea is the utilization of momentum-space wavefunction that is sensitive to the region far from nuclei governing long-range interaction. MSI can be regarded as a predictive activity ratio between reference molecule and target molecules. By using MSI concept, they predicted activity of a group of HIV inhibitors [3].

To clarify the applicable range of MSI, we apply it into several carbamates, labeled with A to F here. Their position-space wavefunctions are computed at the DFT/B3LYP 6-31G\*\* level. In Figure 1, we plot the experimental and predictive toxicity ratios between reference molecule A and target molecules A to F [4], showing the MSI does not work. We have then advanced the MSI concept into similarity index of frontier orbitals in momentum space (SIFOMS)

by introducing the frontier orbital theory [5] that chemical reaction is governed by a specific outermost orbital such as highest occupied molecular orbital (HOMO) and lowest unoccupied molecular orbital (LUMO). The results are also included in Figure 1. It is evident that SIFOMS with LUMO successfully predicts the experimental toxicity. This is consistent with the reported mechanism [6], in which carbamates act as an electron acceptor, and hence unoccupied molecular orbitals should be crucial. In the talk, further analyses of the results are discussed.

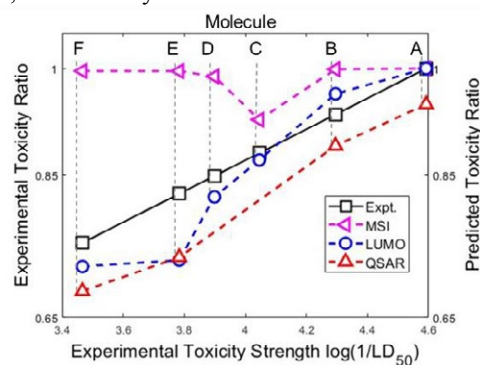


Figure 1. Toxicity ratio among several carbamates

### References

- [1] Koshland Jr DE 1995 *Angew. Chem. Int. Ed. Engl.* **33** 2375
- [2] Stumpf D and Bajorath J 2012 *J. Med. Chem.* **55** 2932
- [3] Cooper D L, Mort K A, Allan N L and et al 1993 *J. Am. Chem. Soc.* **115** 12615
- [4] Hamadache M O and et al 2016 *J. Hazard. Mater.* **303** 28
- [5] Fukui K 1982 *Science.* **218** 747
- [6] Metcalf R L 1971 *Bull. World. Health. Organ.* **44** 43

\* E-mail: [long.sihan.s7@dc.tohoku.ac.jp](mailto:long.sihan.s7@dc.tohoku.ac.jp)

† E-mail: [masahiko@tohoku.ac.jp](mailto:masahiko@tohoku.ac.jp)



## Probing the internal dynamics of homonuclear dimer anions via time-dependent electron detachment inside an electrostatic ion trap

R Chacko<sup>1\*</sup>, S Knaffo<sup>1</sup>, N Klinkby<sup>2</sup>, O Heber<sup>1</sup> and D Zajfman<sup>1</sup>

<sup>1</sup>Department of Particle Physics and Astrophysics, Weizmann Institute of Science, Rehovot 7610001, Israel

<sup>2</sup>Department of Physics and Astronomy, Aarhus University, Aarhus C, DK-8000, Denmark

**Synopsis** The internal dynamics and relaxation processes within the homonuclear dimer anions of copper ( $\text{Cu}_2^-$ ) and silver ( $\text{Ag}_2^-$ ) are investigated employing a novel experimental technique. The experimental set-up includes electrostatic ion beam trap (EIBT), laser-assisted photodetachment, and velocity map imaging spectrometry of ejected electrons. The study reveals transitions that were not reported earlier. The results give insights into the lifetime and the internal decay processes of the anion dimers of copper and silver.

Understanding the internal energy distribution and the dynamics of energy evolution is crucial in many studies of molecules in the gas phase. Homonuclear dimer anions generally possess only one bound state, and the excited states typically lie in the detachment continuum. This makes them short-lived, and experimentally that can be challenging. We study the internal structure and dynamics of silver and copper dimer anions using a novel technique developed in our lab [1].

A unique experimental setup is fashioned with a combination of laser assist photodetachment, ion beam storage, and electron spectrometry to survey the electron ejection from the molecular anions via photodetachment and autodetachment over long time scales. Anions accelerated to 4.2 keV energy are injected into an Electrostatic Ion beam Trap (EIBT), where they oscillate between the two electrostatic mirrors of the EIBT. A laser-assisted Velocity Map Imaging (VMI) spectrometer integrated into the system records the ejected electrons' position and time-of-flight [2]. The corresponding neutral fragments are recorded separately via a MCP detector mounted after the exit mirrors of the EIBT. The coincidence events between the electrons and neutrals are stored and analyzed as a function of trapping time. The internal energy dynamics can be inferred from the photoelectron spectra obtained at different storage time windows.

The internal decay processes of hot anion clusters of silver and copper over a long time scale

has been measured recently [3, 4, 5] with no direct information about the actual internal energy distribution. The present study probes the decay processes of hot anion dimers of copper and silver via electron detachment. We observe new transitions with different angular distributions which were not reported earlier. The temporal analysis allows probing the lifetime of the states. The results from this study will be presented at the conference.

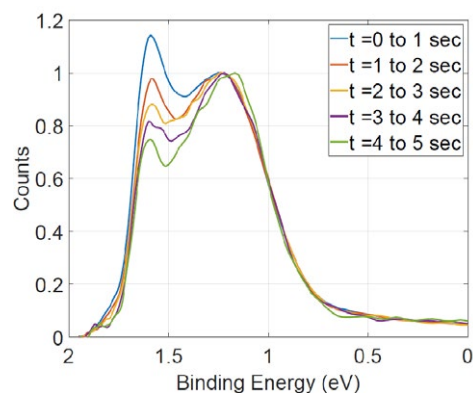


**Figure 1.** Photoelectron spectra of  $\text{Ag}_2^-$  at different storage times.

### References

- [1] Abhishek Shahi *et al.* 2022 *Sci. Rep.* **12** 22518
- [2] K. Saha *et al.* 2017 *Rev. Sci. Instrum.* **88** 053101
- [3] K. Hansen *et al.* 2017 *Phys. Rev. A* **95** 022511
- [4] E. K. Anderson *et al.* 2020 *Phys. Rev. Lett.* **124** 173001
- [5] P. Jasik *et al.* 2021 *J. Chem. Phys.* **154** 164301

\*E-mail: [robby.chacko@weizmann.ac.il](mailto:robby.chacko@weizmann.ac.il)

## Ultralong-range Rydberg Molecules: Electronic Structure and Rydberg blockade

D. Mellado-Alcedo<sup>1</sup>, J. Gacía-Garrido<sup>1</sup>, A. Guttridge<sup>2,3</sup>, D. K. Ruttley<sup>2,3</sup>, C. S. Adams<sup>2,3</sup>, S. L. Cornish<sup>2,3</sup>, H. R. Sadeghpour<sup>4</sup> and R. González-Férez<sup>1\*</sup>

<sup>1</sup>Instituto Carlos I de Física Teórica y Computacional, and Departamento de Física Atómica, Molecular y Nuclear, Universidad de Granada, 18071 Granada, Spain

<sup>2</sup> Department of Physics, Durham University, South Road, Durham, DH1 3LE, UK

<sup>3</sup> Joint Quantum Centre Durham-Newcastle, Durham University, South Road, Durham, DH1 3LE, UK

<sup>4</sup> ITAMP, Center for Astrophysics | Harvard & Smithsonian, Cambridge, MA 02138 USA

**Synopsis** We describe the electronic structure and main features of ultralong-range Rydberg molecules formed by a Rydberg atom, Rb or Cs, and the diatomic molecule RbCs. We also present the first experimental observation of the Rydberg blockade due to the charge-dipole interaction between a single Rb atom and a single RbCs molecule confined in different optical tweezers.

The exotic properties of Rydberg atoms make them unique probes of their environments. In hybrid systems, they form ultralong-range molecules when combined with ground-state atoms [1, 2], ions [3], or polar molecules [4, 5], which inherit these exciting properties.

When the diatomic polar molecule is immersed into the wave function of the excited atom, the anisotropic scattering of the Rydberg electron from the permanent electric dipole moment of the dimer is responsible for the binding mechanism in these Rydberg molecules [4, 5]. In this work, we explore the electronic structure and main properties of these exotic ultralong-range molecules, which are formed by either Rubidium or Cesium Rydberg atoms interacting with RbCs. Our focus is the regime where the charge-dipole interaction of the Rydberg electron with the diatomic polar molecule induces a coupling between the quantum defect Rydberg states and the nearest degenerate hydrogenic manifold. We present adiabatic electronic states evolving from the Rydberg degenerate manifold and from the quantum defect states, and analyze the non-adiabatic coupling between these potentials, and the decay rates and formation rates of their of the bound vibrational states. We propose a protocol to create these molecules experimentally in these electronic states from a mixture of ultra-

cold atoms and ultracold molecules [6].

In addition, we present the first experimental demonstration of the Rydberg blockade due to the charge-dipole interaction between a single Rb atom and a single RbCs molecule. The atom and molecule are confined in optical tweezers, which are used to control their relative distance. For a separation of 310(40) nm, the charge-dipole interaction between the Rydberg electron and atomic core with the dipole moment of RbCs provokes the blockade of the transition to the Rb(52s) Rydberg state. The observed excitation dynamics are in excellent agreement with the theoretical results obtained using the electronic structure of the Rydberg Molecule Rb-RbCs [7].

### References

- [1] C.H. Greene, A.S. Dickinson, and H. R. Sadeghpour, *Phys. Rev. Lett.* **85**, 2458 (2000).
- [2] V. Bendkowsky et al, *Phys. Rev. Lett.* **105**, 163201 (2010)
- [3] N. Zuber, et al. *Nature* **605**, 453–456 (2022).
- [4] S.T. Rittenhouse and H.R. Sadeghpour, *Phys. Rev. Lett.* **104**, 243002 (2010).
- [5] R. González-Férez, H.R. Sadeghpour and P. Schmelcher, *New J. Phys.* **17**, 013021 (2015).
- [6] R. González-Férez, S. T. Rittenhouse, P. Schmelcher, and H.R. Sadeghpour, *J. Phys. B: At. Mol. Opt. Phys.* **53**, 074002 (2020).
- [7] A. Guttridge et al, arXiv:2303.06126 (2023).

\*E-mail: rogonzal@ugr.es

## Inner-shells effect for positrons and electrons traversing cold matter and plasmas

C D Archubi<sup>1\*</sup>, C C Montanari<sup>1†</sup>, N R Arista<sup>2</sup>, and D G Arbó<sup>1</sup>

<sup>1</sup>Instituto de Astronomía y Física del Espacio, CONICET-UBA, Ciudad de Buenos Aires, CP1428, Argentina

<sup>2</sup>CONEA, San Carlos de Bariloche, Argentina

**Synopsis** We present theoretical calculations for stopping power, mean free path and straggling of positrons and electrons in cold targets and plasmas in a wide range of velocities. Two different dielectric models are employed and the results discussed.

We present our recent investigation on the projectile and temperature dependence of the energy loss. To that end, we present a comparative study between two dielectric approaches, which takes into account the inner-shells, and the ionization gap within the energy loss moments of protons, positrons and electrons traversing Si, Fe and Al targets, both in cold solid state and in plasma. We compare the results from the unified-wave-packet model [1, 2] (UWPM) and shellwise local plasma approximation [3] (SLPA) on an extensive range of parameters including low, intermediate, and high projectile energies and target temperatures going from that corresponding to cold solid state typical densities to plasma temperature of 60 eV. We re-formulate the SLPA in order to include light particles restrictions. We give special consideration to the case of positrons and electrons, where the inner-shells contribution had not been analyzed previously. Fig. 1 displays our results for stopping on a cold solid Si target.

The present temperature dependent calculations prove that for increasing plasma temperatures, the stopping and straggling of positrons and electrons have an increasing behavior, similar to that found for protons [1].

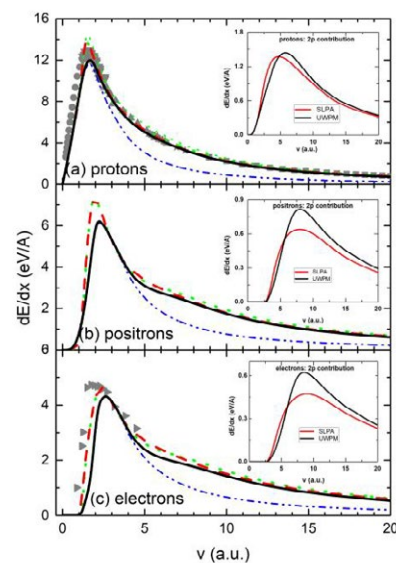


**Figure 1.** Stopping power on a cold solid-state Si target for impinging (a) protons, (b) positrons, and (c) electrons, as a function of the impact velocity. Curves: black-solid lines, total UWPM results; red-dashed lines, total SLPA results, blue-dashed-double dotted lines, FEG contribution (UWPM); green-dotted lines, total UWPM values using Lindhard FEG. Symbols: available experimental data from different works. The inserted show the results for the isolated 2p contribution.

### References

- [1] Archubi C D and Arista N R 2020, *Phys. Rev A.* **102** 052811
- [2] Archubi C D and Arista N R 2022, *Phys. Rev A.* **105** 032806
- [3] Montanari C C and Miraglia J E 2013, *Adv. Quant. Chem.* **65** Chap 7 165-201

\* E-mail: [archubi@iafe.uba.ar](mailto:archubi@iafe.uba.ar)

† E-mail: [mclaudia@iafe.uba.ar](mailto:mclaudia@iafe.uba.ar)

## Stereodynamical control of cold collisions between two aligned $D_2$ molecules

P G Jambrina<sup>1</sup> J F E Croft<sup>2</sup> J Zuo<sup>3</sup> H Guo<sup>3</sup> F J Aoiz<sup>4</sup> and N Balakrishnan<sup>5\*</sup>

<sup>1</sup>Departamento de Química Física, Universidad de Salamanca, Salamanca 37008, Spain

<sup>2</sup>The Dodd-Walls Centre for Photonic and Quantum Technologies, Dunedin, New Zealand and Department of Physics, University of Otago, Dunedin, New Zealand

<sup>3</sup>Department of Chemistry and Chemical Biology, University of New Mexico, Albuquerque, New Mexico 87131, USA

<sup>4</sup>Departamento de Química Física, Universidad Complutense, Madrid 28040, Spain

<sup>5</sup>Department of Chemistry and Biochemistry, University of Nevada, Las Vegas, Nevada 89154, USA

**Synopsis** Resonant scattering of optically state-prepared and aligned molecules in the cold regime allows the most detailed interrogation and control of bimolecular collisions. Here we report our results for collisions of two *ortho*- $D_2$  molecules prepared in the  $j = 2$  rotational level of the  $v = 2$  vibrational manifold using the Stark-induced adiabatic Raman passage technique. Key features of the experimental angular distributions are reproduced and attributed primarily to a partial wave resonance with orbital angular momentum  $\ell = 4$ .

Bimolecular collisions involving diatomic molecules are topics of active investigation due to the continuing interest in cooling and trapping of molecules and their applications in sensing, precision spectroscopy, quantum information processing, and ultracold chemistry, to name a few. By combining optical state-preparation using the Stark-induced adiabatic Raman passage (SARP) method with co-expansion of the colliding species in the same molecular beam Mukherjee and coworkers have been able to explore the stereodynamics of atom-molecule and molecule-molecule collisions at collision energies in the vicinity of 1 K [1]. In this regime, collision outcomes are dominated by isolated partial waves allowing measurements of differential cross sections (DCS) with partial wave resolution.

Recently, Mukherjee and coworkers have reported DCS for collisions between two aligned  $D_2$  molecules prepared in the  $v = 2$  vibrational level and  $j = 2$  rotational level using the SARP method. Here we provide a first principles simulation of the experiment using explicit quantum close-coupling calculations [2]. As shown in Figure 1 our calculations using a full-dimensional interaction potential for the  $H_2+H_2$  system nearly quantitatively reproduces the experimental angular distribution. However, a key difference is that our calculations show that the DCS is dominated by a  $l = 4$  shape resonance than a  $l = 2$

resonance ascribed in the experiment.

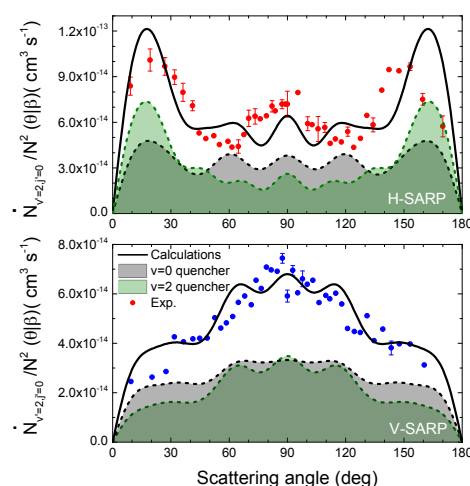


**Figure 1.** Velocity-averaged differential rates for  $D_2(v'=2, j'=0)$  production in  $D_2(v = 2, j = 2) + D_2(v = 2, j = 2)$  and  $D_2(v = 2, j = 2) + D_2(v = 0, j = 1, 2)$  collisions normalized by the square of the total density of  $D_2$ . Results of our calculations are shown in solid curves while experimental results of Zhou *et al.*[1] are shown in dots. Calculations using a H-SARP (V-SARP) preparation are shown in the top (bottom) panels. See [1, 2] for more details.

### References

- [1] Zhou H, Perreault W D, Mukherjee N and Zare R N 2022 *Nat. Chem* **14**, 658
- [2] Jambrina P G *et al.* 2023 *Phys. Rev. Lett.* **130**, 033002

\*E-mail: [naduvala@unlv.nevada.edu](mailto:naduvala@unlv.nevada.edu)

## Improved method to treat asymptotic non-adiabatic couplings in scattering processes

P Hedvall<sup>1\*</sup> and Å Larson<sup>1†</sup>

<sup>1</sup>Department of Physics, Stockholm University, Albanova University Center, S-106 91 Stockholm, Sweden

### Synopsis

The reprojection method is an approach to deal with the problem of having a non-zero asymptotic non-adiabatic coupling in heavy particle scattering. The method is here implemented in a diabatic representation with a mixing matrix to second order in  $1/R$ , resulting in a well defined convergence region for the total cross section at low energy collisions.

In the conventional Born-Oppenheimer treatment of molecules, the nuclear and electron coordinates are separated in such a way that the molecular electron structure can be solved for in a fixed nuclear configuration. However, in a strict sense, these coordinates does not give a correct description for the atom-atom (or ion-ion, ion-atom) scattering reaction in the asymptotic region. Most often the coordinate differences can be neglected for, but for some systems this issue manifest as non-zero asymptotic non-adiabatic couplings. In the reprojection method [1, 2, 3] a transformation matrix is introduced which mixes the conventional Born-Oppenheimer asymptotic solutions to give correct scattering boundary conditions in the asymptotic region. It has been successfully applied in an adiabatic representation, e.g. for inelastic Li+Na scattering [3]. However, in order to obtain a converged cross section, it is necessary to impose a cutoff for the contributing rotational quantum numbers and integrate the coupled Schrödinger equation to sufficiently large internuclear distances. This issue meets its extreme at lower collision energies where a region of convergence for the cross section may be difficult to define.

In the present study, the reprojection method is implemented in a diabatic representation and with a mixing matrix including higher order terms in  $1/R$ . A strict diabatic representation is defined such that the non-adiabatic coupling vanishes. Hence, the conventional adiabatic-to-diabatic transformation needs modification in order to implement the reprojection method. Moreover, the inclusion of higher order terms in  $1/R$  for the reprojection method makes it

possible to identify a clear convergence region for lower collision energies, with integration stop ( $R_0$ ) at a moderate internuclear distance. The method is here applied to inelastic scattering in Li+Na collisions, see Fig. 1.

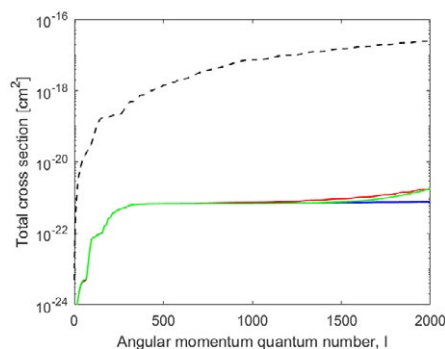


**Figure 1.** Total cross section for Li(2s)+Na(3s) → Li(2p) + Na(3s) at collision energy 5 eV, as a function of the maximum value of the angular momentum quantum number  $l$ . The dotted curve shows the cross section obtained using the conventional Born-Oppenheimer approach. The solid red curve shows the cross section when using the reprojection method to zeroth order with integration stop at  $R_0 = 280 a_0$ , the solid blue curve when using the reprojection method to second order and  $R_0 = 280 a_0$ , and the solid green curve when using the reprojection method to second order and  $R_0 = 75 a_0$ .

### References

- [1] Grosser J, Menzel T and Belyaev A K 1999 Phys Rev A **59**
- [2] Belyaev A K, Egorova D, Grosser J and Menzel T 2001 Phys. Rev. A **64** 052701
- [3] Belyaev A K 2010 Phys. Rev. A **82** 060701(R)

\*E-mail: [patrik.hedvall@fysik.su.se](mailto:patrik.hedvall@fysik.su.se)

†E-mail: [aasal@fysik.su.se](mailto:aasal@fysik.su.se)



## Low-energy collisions between two indistinguishable tritium-bearing hydrogen molecules: HT+HT and DT+DT

R A Sultanov\*

Department of Mathematics and Engineering, Odessa College, Odessa, TX, USA

**Synopsis** Elastic and rotational energy transfer collisions between two tritium-containing hydrogen molecules are computed at low- and very low energies, down to ultra-cold temperatures:  $T \simeq 10^{-8}$  K. A pure quantum-mechanical approach is applied. A high-quality global six-dimensional potential energy surface (PES) has been appropriately modified and used in these calculations. In the case of the symmetrical  $H_2+H_2$  and  $D_2+D_2$  collisions one can use the original  $H_4$  PES as it is, i.e. without transformations. However, in the case of the non-symmetrical (or symmetry-broken)  $HD+H_2/D_2$ ,  $HT+HT$ ,  $DT+DT$  scattering systems one should also apply the original  $H_4$  interaction field (PES), but the propagation (solution) of the Schrödinger equation runs, in this case, over the corrected Jacobi vector.

Tritium bearing hydrogen molecules are of a significant scientific interest, see Ref. [1] and, for instance, Tritium Laboratory Karlsruhe (TLK) reports at Karlsruhe Institute of Technology (Germany). In this work a quantum-mechanical close-coupling calculation is performed for elastic and rotational energy transfer inelastic collisions at low- and very low energies:



Here H is a hydrogen atom, D is deuterium, and T is tritium. Global six-dimensional symmetrical  $H_2-H_2$  potential energy surfaces (PESs) [2, 3] have been adopted and appropriately modified for current 4-atomic systems. Specifically, we changed the position of the center of mass in HT and DT. In this presentation a special attention will be given to different geometrical modifications of the multidimensional  $H_2-H_2$  potentials, as in Ref. [4]. State-resolved integral cross sections  $\sigma_{j_1 j_2 \rightarrow j'_1 j'_2}(\varepsilon_{kin})$  for quantum-mechanical rotational transitions  $j_1 j_2 \rightarrow j'_1 j'_2$  in HT and DT molecules and corresponding state-resolved thermal rate coefficients  $k_{j_1 j_2 \rightarrow j'_1 j'_2}(T)$  have been computed. The relationship between the rate coefficient  $k_{j_1 j_2 \rightarrow j'_1 j'_2}(T)$  and the cross section  $\sigma_{j_1 j_2 \rightarrow j'_1 j'_2}(\varepsilon)$  can be obtained through the following weighted average:

$$k_{j_1 j_2 \rightarrow j'_1 j'_2}(T) = \frac{8k_B T}{\pi \mu} \frac{1}{(k_B T)^2} \int_{\varepsilon_s}^{\infty} e^{-\varepsilon/k_B T} \times \sigma_{j_1 j_2 \rightarrow j'_1 j'_2}(\varepsilon) \varepsilon d\varepsilon, \quad (3)$$

where  $k_B$  is Boltzmann constant,  $\mu$  is reduced mass of the molecule-molecule system and  $\varepsilon_s$  is the minimum kinetic energy for the levels  $j_1$  and  $j_2$  to become accessible. Additionally, for comparison purposes,  $H_2+H_2/HD$  calculations for a few selected rotational transitions have also been performed. These energy transfer collisions are of fundamental importance in astrophysics, see for example [5, 6, 7], papers [4] and Ref. [8]. The hydrogen molecules HT and DT are treated as rigid rotors in our calculations. A pronounced isotope effect is identified in cross sections of collisions (1)-(2).

### References

- [1] Lai K -F, Hermann V, Trivikram T M, Diouf M, Schlösser M, Ubachs W, and E. J. Salumbides E J, *Phys. Chem. Chem. Phys.* 2020 **22** 8973.
- [2] Boothroyd A I, Martin P G, Keogh W J, and Peterson M J, *J. Chem. Phys.* 2002 **116**, 666.
- [3] Patkowski K, Cencek, Jankowski W P, Szalewicz K, Mehl J B, Garberoglio G, and Harvey A H, *J. Chem. Phys.* 2008 **129**, 094304.
- [4] Sultanov R A , Guster D, and Adhikari S K , *J. Phys. B: At. Mol. Opt. Phys.* 2016 **49**, 015203; *AIP Advances* 2012 **2**, 012181; *Phys. Rev. A* 2012 **85** 052702.
- [5] Balakrishnan N, Croft J F E, Yang B H, Forrey R C, and Stanci P C, *ApJ* 2018 **866**:95.
- [6] Wan Y, Balakrishnan N, Yang B H, Forrey R C, and Stanci P C, *MNRAS* 2019 **488**, 381.
- [7] Wan Yier, *PhD Dissertation 2019*, The University of Georgia, Athens, Georgia: [http://getd.libs.uga.edu/pdfs/wan\\_yier\\_201908\\_phd.pdf](http://getd.libs.uga.edu/pdfs/wan_yier_201908_phd.pdf).
- [8] Sultanov R A and Guster D, *Chem. Phys. Lett.* 2007 **436**, 19.

\*E-mail: [rsultanov@odessa.edu](mailto:rsultanov@odessa.edu); [r.sultanov2@yahoo.com](mailto:r.sultanov2@yahoo.com)

## Mutual neutralization between diatomic cation and atomic anion

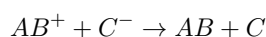
A Dochain<sup>1\*</sup>, M Poline<sup>1</sup>, Ansgar Simonsson<sup>1</sup>, Stefan Rosén<sup>1</sup>, MingChao Ji<sup>1</sup>, Henning Schmidt<sup>1</sup>, and R D Thomas<sup>1</sup>

<sup>1</sup>Stockholm University, Department of Physics, Stockholm, SE 106 91, Sweden.

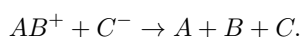
**Synopsis** We provide a sequential explanation for the mutual neutralization reaction between diatomic cation and atomic anion. This model describes well the branching ratios recently measured at the DESIREE facility.

During the last decade, significant interest has been reignited in the mutual neutralization reaction. Several groups have developed new (DESIREE [1], Hebrew University of Jerusalem) or upgraded existing (UCLouvain [2], VEN-DAMS [3]) experimental setups to focus on this reaction. This renewed interest comes from the increasingly realized importance of this reaction in stellar atmospheres [4], planetary ionospheres [2], and industrial plasmas [5].

Those measurements are combined with theoretical models which describe accurately atom-atom mutual neutralization [6, 7]. Unfortunately, the only model that exists which describes MN reaction involving molecules is a semi-empirical model [8]. This model's inaccuracy for atom-atom MN has been shown for several systems [2, 4]. Furthermore, for MN involving molecular cations, i.e.,  $AB^+ + C^-$ , this model predicts mostly



while the observed MN products for such reaction are mostly



These recent measurements, performed at the DESIREE facility [1], were allowed by a recent upgrade of the neutral particles detector, which allows simultaneous detection of many particles, with sub-mm position accuracy and ns resolution. This allows an improved detection efficiency of the 3-body particles compared to the previous detection system.

In order to improve the description of these

reactions, we propose a model which describes the reaction in a sequential way. First, the anion donates its extraneous electron to the cation at a diatom-atom distance significantly greater than the initial internuclear distance of the cationic ground-state. This assumption means that this part of the reaction can be described similarly to case of atom-atom MN, meaning that the cation is produced in a (highly) singly excited state. This excited state later decays, either by photon emission or by coupling with other excited states. In these two mechanisms, only radiative decay can stabilize the neutral molecule as a final product while all the other processes leads to complete dissociation of the molecule.

This reaction seems more selective than the dissociative recombination – due to selection rules applied by the angular momentum of the reactants and products – but less than the ion-neutral dissociative charge transfer – due to the coulomb attraction between the two reactants.

### References

- [1] Thomas R D *et al* 2011 *Rev. Sci. Instrum.* **82** 065112.
- [2] Poline M *et al* 2021 *Phys. Chem. Chem. Phys.* **23** 24607; de Ruelle *et al* 2018 *Phys. Rev. Lett.* **121** 083401.
- [3] Shuman N S *et al* 2012 *Adv. At. Mol. Opt. Phys.* **61** 209.
- [4] Launoy T *et al* 2019 *Astrophys. J.* **883** 85; Grumer J *et al* 2022 *Phys. Rev. Lett.* **128** 033401.
- [5] Poline M *et al* 2022 *Phys. Rev. A* **106** 012812.
- [6] Hörnquist, J *et al* 2022 *Phys. Rev. A* **106** 062821; and references therein.
- [7] Barklem 2016 *Phys. Rev. A* **93** 042705 and references therein.
- [8] Olson R E 1972 *J. Chem. Phys.* **56** 2979.

\*E-mail: [arnaud.dochain@fysik.su.se](mailto:arnaud.dochain@fysik.su.se)

## A new approach for measuring the reaction rates of low-energy ion–polar-molecule reactions for astrochemistry

K Okada<sup>1\*</sup>, K Sugata<sup>1</sup>, N Kimura<sup>2</sup>, K Sakimoto<sup>1, 3</sup>, and H A Schuessler<sup>3</sup>

<sup>1</sup> Department of Materials and Life Sciences, Sophia University, Tokyo, 102-8554, Japan

<sup>2</sup> Atomic, Molecular and Optical Physics Lab., RIKEN, Saitama, 351-0198, Japan

<sup>3</sup> Department of Physics and Astronomy, Texas A&M University, Texas, 77843-4242, United States

**Synopsis** We propose a new approach to measure the reaction rate constants of ion-polar molecule reactions at low energies by combining buffer-gas cooling of ions with velocity filtering of polar molecules. The proof-of-principle experiment has been done for the  $\text{Ca}^+ + \text{CH}_3\text{F}$  and  $\text{Ca}^+ + \text{C}_2\text{H}_5\text{OH}$  reactions. This new method will enable us to measure the temperature dependence of reaction rate constants and branching ratios for various ion-polar systems related to astrochemistry.

Low-energy ion–polar-molecule reactions are important chemical processes in interstellar matter. Recently, we have demonstrated a new measurement method of ion–polar-molecule reactions at low energies by combining buffer-gas cooling of ions trapped in a cryogenic ion trap with velocity filtering of polar molecules [1]. Here we report the results of the reaction rate measurements for  $\text{Ca}^+ + \text{CH}_3\text{F} \rightarrow \text{CaF}^+ + \text{CH}_3$  and  $\text{Ca}^+ + \text{C}_2\text{H}_5\text{OH} \rightarrow \text{products}$  at low energies. The experimental setup consists of a cryogenic linear Paul trap and a wavy Stark velocity filter [2]. Rotationally cooled polar molecules are produced by a temperature-variable buffer gas cell and are transported to an ion trap by the wavy Stark velocity filter. The translational temperatures of the velocity-selected  $\text{CH}_3\text{F}$  and  $\text{C}_2\text{H}_5\text{OH}$  are between 5 and 20 K. The number densities of those molecules range from  $10^4$  to  $10^6 \text{ cm}^{-3}$ . In order to cool  $\text{Ca}^+$  ions, we load the helium buffer gas of  $1.2 \times 10^{-3} \text{ Pa}$  in the ion trap chamber [1]. We selected the electronic state of  $\text{Ca}^+$  by controlling the 397 and 866 nm laser light with two shutters. We monitored the relative number of  $\text{Ca}^+$  ions by measuring the laser-induced fluorescence (LIF) intensity from the  $\text{Ca}^+$  ions to determine the reaction rates of the present reaction systems. Fig.1 (a) shows the results for the  $\text{Ca}^+ - \text{CH}_3\text{F}$  system. We separately determined the rate constants for the  $^2\text{S}_{1/2}$  and  $^2\text{D}_{3/2}$  of  $\text{Ca}^+$  at different gas cell temperatures ( $T_{\text{cell}} = 295$  or 30 K) of  $\text{CH}_3\text{F}$ . The plot points connected with lines are the PRS capture rate constants calculated for the velocity-selected  $\text{CH}_3\text{F}$  molecules, where the rotational temperature of the input fluoromethane

\*E-mail: [okada-k@sophia.ac.jp](mailto:okada-k@sophia.ac.jp)

molecules was assumed to be 295 K or 30 K (for details of the PRS theory, refer to [1]). We applied the same method to the  $\text{Ca}^+ + \text{C}_2\text{H}_5\text{OH}$  ( $\text{C}_2\text{H}_5\text{OD}$ ) reactions. As with the  $\text{Ca}^+ - \text{CH}_3\text{F}$  system, the metastable  $\text{Ca}^+$  showed higher reactivity than the ground state at the average collision energy of about 90 K (Fig.1 (b)). We have determined the reaction rate constants at different gas cell temperatures (room temperature and 150 K). The present new approach will be applied to various astrochemically important ion–polar-molecule reactions with further use of cryogenic multipole ion traps.

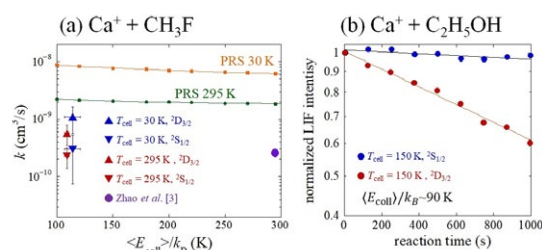


**Figure 1.** (a) Reaction rate constants of  $\text{Ca}^+ + \text{CH}_3\text{F} \rightarrow \text{CaF}^+ + \text{CH}_3$  at translational reaction temperatures of about 110 K. The present result for the  $^2\text{S}_{1/2}$  state is in good agreement with the previous room-temperature result [3]. (b) The decay curves of the normalized LIF intensity of  $\text{Ca}^+$  during the  $\text{Ca}^+ + \text{C}_2\text{H}_5\text{OH}$  reaction.

### References

- [1] Okada K *et al.* 2022 *J. Phys. Chem. A* **126** 4881
- [2] Okada K *et al.* 2017 *Rev. Sci. Instrum.* **88** 083106
- [3] Zhao X *et al.* 2006 *J. Phys. Chem. A* **110** 10607

## Observation of radiative vibrational cooling of $\text{N}_2\text{O}^+$ ions using a cryogenic electrostatic ion storage ring: contribution of Fermi resonance

S Harayama<sup>1,2\*</sup>, S Kuma<sup>2</sup>, N Kimura<sup>2</sup>, K.C Chartkunchand<sup>2</sup>,  
Y Nakano<sup>2,3</sup>, T Yamaguchi<sup>1</sup>, and T Azuma<sup>2</sup>

<sup>1</sup>Department of Physics, Saitama University, Saitama 338-8570, Japan

<sup>2</sup>Atomic, Molecular and Optical Physics Laboratory, RIKEN, Saitama 351-0198, Japan

<sup>3</sup>Department of Physics, Rikkyo University, Tokyo 171-8501, Japan

**Synopsis** The radiative cooling of a triatomic molecular ion  $\text{N}_2\text{O}^+$  was studied in the time domain of up to a few seconds using the RIKEN cryogenic ion storage ring (RICE). The population evolution of vibrational states in the NN-O stretching mode coupled with the bending mode (Fermi resonance) was observed by detecting the neutral products produced by predissociation as a function of time after laser excitation. We found that the decay lifetimes of the states in the Fermi resonance are significantly different from those in the non-resonance case.

The energy dissipation mechanism of molecules via radiative cooling is crucial to understanding the stability of hot, excited molecules and plays an important role in chemical reactions in dilute environments such as the Earth's upper atmosphere. We recently performed action spectroscopy of the linear triatomic molecular ion  $\text{N}_2\text{O}^+$  isolated in vacuum using the RIKEN cryogenic electrostatic ion storage ring RICE [1]. This molecule possesses three different vibration modes, i.e., NN-O stretching, bending, and N-NO stretching. In the present study, we focused on the coupling between these modes. Fermi resonance coupling takes place between states belonging to different modes which are close in energy [2]. We observed the Fermi resonance dynamics as reflected in changes of decay lifetimes in the time domain of a few seconds. Such observations have not been achieved before because of the lack of technical approaches to trace slow dynamics of isolated molecules in vacuum. RICE satisfies the necessary conditions; it offers a cryogenic environment of about 4 K for effective suppression of black-body radiation and an ultrahigh vacuum of less than  $10^{-10}$  Pa.

The electronic ground state of  $\text{N}_2\text{O}^+$  splits into two states,  $X^2\Pi_{1/2}$  and  $X^2\Pi_{3/2}$ , due to the spin-orbit interaction, and each has its own vibrational state. As shown in Fig. 1(a), when the vibrational quantum number of each vibration is labeled as  $(v_1 v_2 v_3)$ , the (2 0 0) and (1 2 0) vibrational states in  $X^2\Pi_{3/2}$  are coupled by Fermi

resonance, while these vibrational states are not coupled in  $X^2\Pi_{1/2}$  (Fig. 1(b)).

$\text{N}_2\text{O}^+$  ions were excited by a laser introduced in the co-propagating direction with the stored  $\text{N}_2\text{O}^+$  ions. The population evolution of vibrational states in the  $X^2\Pi$  state for each case was measured by detecting neutral N fragments produced via  $\text{N}_2\text{O}^+ \rightarrow \text{NO}^+ + \text{N}$  predissociation channels as a function of time after laser excitation.

We found a clear difference in the radiative cooling rate depending on the presence or absence of states coupled by the Fermi resonance, and these results were compared with calculations of the radiative cooling process utilizing the relevant rate equations.

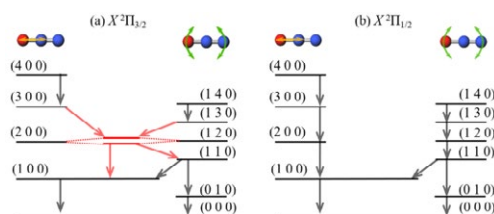


**Figure 1.** Schematic of vibrational states and pathways of radiative cooling (a) with Fermi resonance, (b) without Fermi resonance.

### References

- [1] R. Igosawa, *et al.*, J. Chem. Phys. 153, 184305 (2020).
- [2] H. Gritli, *et al.*, Chem. Phys. 178, 223–233 (1993).

\* E-mail: s.harayama.109@ms.saitama-u.ac.jp

## Mutual Neutralization in sub-eV $C_{60}^+ + C_{60}^-$ collisions

Paul R.<sup>1\*</sup>, Gatchell M.<sup>1</sup>, Ji M.C.<sup>1</sup>, Rosén S.<sup>1</sup>, Björkhage M.<sup>1</sup>, Schmidt H.T.<sup>1</sup>, Cederquist H.<sup>1</sup>, Larson Å.<sup>1</sup>, Zettergren H.<sup>1</sup>

<sup>1</sup>Department of Physics, Stockholm University, Roslagstullsbacken 21, 114 21 Stockholm

**Synopsis** We present results from studies of Mutual Neutralization in collisions of oppositely charged  $C_{60}$  ions at the DESIREE facility, and our calculated cross-sections for this reaction as well as for electron attachments to  $C_{60}$  and  $C_{60}^+$ .

The detection of fullerenes in neutral and ionic forms in several extra-terrestrial environments [1,2] has been subsequently followed by extensive research, inquiring about the factors that constitute the molecule's formation and survival in these environments. To advance the understanding of charge-transfer processes involving fullerene molecules and their importance in e.g. space, we have performed mutual neutralization (MN) studies using the cryogenic storage ring facility, DESIREE [3]. With DESIREE, we are able to study sub-eV collisions between  $C_{60}^+$  and  $C_{60}^-$  ions. We measure the kinetic-energy-release distribution for the neutral products formed in the MN process, which reveals information about the excited states being populated and their branching ratios [4]. The MN process is then modelled with the multi-state Landau-Zener method [5] using interaction potentials from [6,7] and semi-empirical coupling elements from Ref [8]. The excited states of  $C_{60}$  used in the model were computed using Time Dependent-Density Functional Theory at the PBE0/6-311++G(d,p) level of theory. The branching ratios obtained from the theoretical calculations are in good agreement with the corresponding experimental ones, supporting the use of the model for calculations of the total MN cross section as a function of the center-of-mass collision energy. The results from these calculations are shown as a solid black line in Fig. 1 together with the corresponding cross sections for electron attachment to  $C_{60}^+$  (red dashed line) and  $C_{60}$  (blue dotted line) using the model in Ref 6. These results show that MN processes may be im-

portant in certain astrophysical environments, especially in molecular clouds where complex molecules such as fullerenes are believed to be the main carriers of negative charges [9].

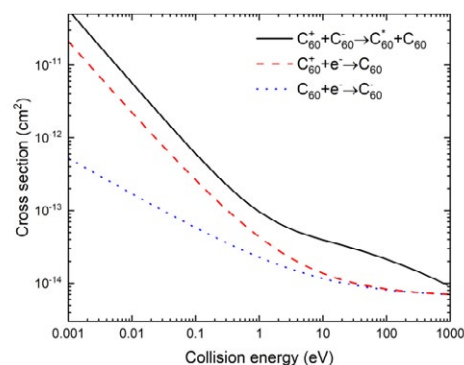


**Figure 1.** The cross sections for different processes compared as a function of their collision energies.

### References

- [1] Maier, J. P., and Campbell E.K., *Angewandte Chemie International Edition* 2017 [56 18](#)
- [2] Cami, J., et al., *Science* 2010 [329 5996](#)
- [3] Schmidt, H. T., et al., *Review of Scientific Instruments* 2013 [84 5](#)
- [4] Eklund, G. et al., *Phys Rev A* 2020 [102 1](#)
- [5] Zener, C., *Proceedings of the Royal Society of London. Series A*, 1932 [137 833](#)
- [6] Girifalco, L. A., *J. of Phys Chem* 1992 [96 2](#)
- [7] Lindén F., et al., *J. of Chem Phys* 2016 [145 19](#)
- [8] Olson, Ronald E., *J. of Chem Phys* 1972 [56 6](#)
- [9] Tielens, A.G.G.M., et al., *Astrophysics and Space Science Library* 1995 [202 315](#)

\* E-mail: [raka.paul@fysik.su.se](mailto:raka.paul@fysik.su.se)



## Slow decay processes of molecular anions during long-time storage in a cryogenic storage ring

V C Schmidt<sup>1\*</sup>, K Blaum<sup>1</sup>, R Čurík<sup>2</sup>, P Fischer<sup>3</sup>, L Gamer<sup>1</sup>, S George<sup>1</sup>, J Göck<sup>1</sup>, M Grieser<sup>1</sup>, F Grussie<sup>1</sup>, R von Hahn<sup>1</sup>, O Heber<sup>4</sup>, M A Iron<sup>4</sup>, Á Kálosi<sup>5,1</sup>, C Krantz<sup>1</sup>, H Kreckel<sup>1</sup>, E Miliordos<sup>6</sup>, P M Mishra<sup>1</sup>, D Müll<sup>1</sup>, O Novotný<sup>1</sup>, F Nuesslein<sup>1</sup>, M Ončák<sup>7</sup>, D Paul<sup>5,1</sup>, H B Pedersen<sup>8</sup>, L Schweikhard<sup>3</sup>, K Spruck<sup>1</sup>, Y Toker<sup>9</sup>, A Wolf<sup>1</sup>, A Znotins<sup>1</sup>

<sup>1</sup>Max-Planck-Institut für Kernphysik, Heidelberg, 69117, Germany

<sup>2</sup>J. Heyrovský Institute of Physical Chemistry, 18223 Prague 8, Czech Republic

<sup>3</sup>Institut für Physik, Universität Greifswald, 17487 Greifswald, Germany

<sup>4</sup>Weizmann Institute of Science, Rehovot 76100, Israel

<sup>5</sup>Columbia Astrophysics Laboratory, Columbia University, New York, New York 10027, USA

<sup>6</sup>Department of Chemistry and Biochemistry, Auburn University, Alabama 36849, USA

<sup>7</sup>Universität Innsbruck, 6020 Innsbruck, Austria

<sup>8</sup>Department of Physics and Astronomy, Aarhus University, Aarhus 8000, Denmark

<sup>9</sup>Bar-Ilan University, 529002 Ramat-Gan, Israel

**Synopsis** The decay of internally excited molecular ions through photon emission or via destructive pathways (electron detachment/dissociation) is strongly dependent on the involved states and resulting lifetimes vary vastly. Especially the investigation of slow decay mechanisms requires experimental conditions where the particles can be stored on long timescales (> 1000 s) in the gas phase with negligible residual gas collisions or black body radiation. The Cryogenic Storage Ring (CSR) offers excellent conditions for these types of experiments. A summary of recent studies on molecular anions is given.

Molecular systems offer a variety of excitation possibilities via electronic, vibrational and rotational degrees of freedom. The coupling between those modes and consequentially the corresponding decay rates range from atomic timescales to hours and beyond. The electrostatic Cryogenic Storage Ring (CSR) [1] at the Max-Planck-Institut für Kernphysik in Heidelberg, Germany, provides ideal conditions to probe processes with lifetimes on the upper end of this scale. The ring is cooled with a closed-cycle liquid helium system to temperatures below 10 K, strongly suppressing black body radiation. Additionally, its cold chambers act as a cryopump, reaching residual gas densities of  $\approx 1000$  particles/cm<sup>3</sup>. As a result, storage lifetimes of thousands of seconds can be achieved for molecular ions with kinetic energies of up to 300 keV per charge unit.

In the CSR, the internal decay processes of excited molecular anions have been studied. The hot ions, e.g., produced in a sputter source, are stored in the ring, where they deexcite almost undisturbed by background radiation or residual gas collisions. For ions produced with sufficiently high excitation, autodecay processes in

the form of either detachment or dissociation can be observed. Two separate detectors are used to record charged and neutral fragments. To probe the internal properties of the stored ions, laser excitation at specific wavelength can also be employed, recording the prompt or delayed, charged or neutral fragments. This action spectroscopy is combined with time-of-flight mass spectrometry in the CSR [2] to identify molecular species in the stored beam, such as for the isobaric doublet of CN<sup>-</sup> and C<sub>2</sub>H<sub>2</sub><sup>-</sup> at A = 26.

Here, we report on ongoing studies of very slow decay processes in anions stored for up to 2000 s. These investigations include the stability of the ground state vinylidene anion H<sub>2</sub>CC<sup>-</sup> [3], investigating its possible decay by isomerization-driven autodetachment, as well as very long lifetimes observed for infrared-inactive vibrational excitations in Al<sub>4</sub><sup>-</sup> cluster ions.

### References

- [1] von Hahn R et al 2016 *Rev. Sci. Instrum.* **87** 063115
- [2] Grieser M et al 2022 *Rev. Sci. Instrum.* **93** 063302
- [3] Jensen M J et al 2000 *Phys. Rev. Lett.* **84** 1128

\*E-mail: [viviane.schmidt@mpi-hd.mpg.de](mailto:viviane.schmidt@mpi-hd.mpg.de)

## X-ray imaging of nanostructures in superfluid helium droplets

R M P Tanyag<sup>1,2\*</sup>

<sup>1</sup>Department of Chemistry, Aarhus University, 8000 Aarhus C, Denmark

<sup>2</sup>On behalf of Imaging Quantum Vortices and Nanostructures Collaborations

**Synopsis** X-ray coherent diffractive imaging facilitated the identification of different structure formation regimes in the confined space of a self-bound superfluid helium droplet. Broadly, these regimes are: vortex-free aggregation, vortex-induced aggregation, and cluster network formation.

A self-bound superfluid helium droplet is an extremely cold and frictionless medium for growing metastable and self-organized dopant nanostructures. Their visualization offers an opportunity to identify different structure formation regimes and dissect the mechanisms driving their assembly. Using x-ray coherent diffractive imaging, three regimes have been distinguished, see Fig. 1: vortex-free aggregation, vortex-induced aggregation, and cluster network formation [1, 2, 3]. In this contribution, we point out that the regime boundaries depend on the droplet size and the amount of dopants, and how the droplet's rotational state influences the types of structure formed. Additionally, the transition between the vortex-free and vortex-induced aggregation was discovered to occur when the droplet contains about  $10^8$  atoms per droplet; only partially affected by how the droplets are generated [3]. These results not only present a means of controlling structure formation in superfluid helium droplets, but they also lay the foundation for imaging the assembly of nanostructures with different intermolecular forces for future studies.

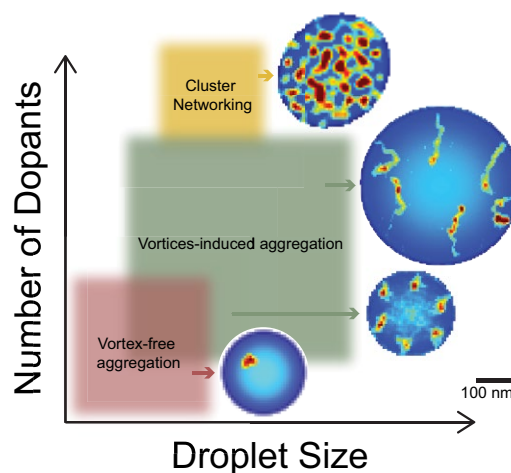


**Figure 1.** Different regimes of nanostructure formation inside an isolated superfluid helium droplet at varying droplet sizes and number of dopants. The numerically reconstructed image from the vortex-free aggregation was obtained from the European XFEL SQS 2195 beamtime [3], while the others were from the LCLS-AMO 54912 beamtime [1, 2].

### References

- [1] Jones CF, Bernando C, Tanyag RMP, Bacellar C, Ferguson KR, Gomez LF, et al. 2016 *Phys. Rev. B* **93** 180510(R)
- [2] Tanyag RMP 2018 Imaging superfluid helium droplets *University of Southern California PhD Thesis*
- [3] Ulmer A, Heilrath A, Senfftleben B, O'Connell-Lopez SMO, Kruse B, Seiffert L, et al. 2023 [ArXiv2302.07355](https://arxiv.org/abs/2302.07355)

\*E-mail: [tanyag@chem.au.dk](mailto:tanyag@chem.au.dk)

## CO<sub>2</sub> activation by Cu clusters in superfluid helium nano-droplets

Olga V. Lushchikova<sup>1\*</sup>, M. Gatchell<sup>2</sup>, J. Reichegger<sup>1</sup>, S. Kollotzek<sup>1</sup>, F. Zappa<sup>1</sup>, P. Scheier<sup>1</sup>

<sup>1</sup> Institut für Ionenphysik und Angewandte Physik, Universität Innsbruck, Technikerstr. 25, A-6020 Innsbruck, Austria

<sup>2</sup> Department of Physics, Stockholm University, SE-10691 Stockholm, Sweden

**Synopsis** The development of efficient CO<sub>2</sub> utilization methods is critical in mitigating climate change. Copper-based catalysts show potential, but their limited efficiency and selectivity necessitate a molecular-level understanding of their interaction with CO<sub>2</sub>. This study uses ultracold superfluid He nano-droplets as cryo-nano reactors to grow and investigate cationic and anionic Cu clusters and their complexes with CO<sub>2</sub>. First we verify the structure of the clusters with He tagging and then study the deformation of the CO<sub>2</sub> induced by the cluster using photo fragmentation IR spectroscopy.

Copper-based materials are among the most promising catalysts for CO<sub>2</sub> utilization. However, CO<sub>2</sub> conversion is still inefficient and requires high-energy input resulting in even more CO<sub>2</sub> emissions. Therefore, the molecular-level understanding of CO<sub>2</sub> interaction with copper is crucial for the design of more efficient catalysts. In our study, we mimic the catalyst's active site with copper clusters to study how they affect the structure of CO<sub>2</sub>.

Previously, the structure of cationic Cu clusters and its role in CO<sub>2</sub> hydrogenation has been extensively studied by IR multiple-photon dissociation spectroscopy using a free-electron laser, FELIX.[1, 2] The clusters were formed using a laser ablation source, resulting in the log-normal distribution of the cluster sizes limiting the choice of the studied cluster sizes.

In the present study, we demonstrate the possibility of forming singly charged clusters via the pickup of dopant metal into multiply charged superfluid helium nano-droplets (mc-HNDs).[3] This method allows the formation of cluster size distribution narrower than Poisson, which is much narrower than conventional gas-phase methods allow.[4] Simulation of the experimental data helped us to understand, what is the underlying mechanism of the cluster formation, and which parameters are responsible

for the cluster size distribution and selection of the most abundant cluster size.

As a next step, we implement mc-HNDs as ultracold (0.4 K) nano-reactors to study the reaction of Cu<sub>n</sub><sup>+/-</sup> with CO<sub>2</sub>. Here, we start with the verification of the cluster structure using He as a probe molecule.[5] Then, Cu<sub>n</sub><sup>+/-</sup> are reacted with CO<sub>2</sub> and structure, fragmentation patterns and energies are investigated by means of collision-induced dissociation and photo-fragmentation spectroscopy of He-tagged ions. Formation of clusters in mc-HNDs allows a substantial signal intensity stable over a long-time range of the desired cluster size and makes it possible to perform He tagging of negatively charged ions, which is impossible otherwise.

### References

- [1] Lushchikova O.V. et al. 2021 Phys Chem Chem Phys **23** 26661-26673
- [2] Lushchikova O.V. et al. 2019 J Phys Chem Lett **10** 2151-2155
- [3] Tiefenthaler L. et al. 2020 Rev. Sci. Instrum. **91** 033315
- [4] Kollotzek S. et al. 2022 Int J Mol Sci **23** 3613
- [5] Lushchikova O.V. et al. 2023 Phys Chem Chem Phys

\* E-mail: [olga.lushchikova@uibk.ac.at](mailto:olga.lushchikova@uibk.ac.at)

## A versatile ion source for cold ions using superfluid helium nanodroplets

P Martini<sup>1</sup>\*, H Zettergren<sup>1</sup>, H T Schmidt<sup>1</sup> and M Gatchell<sup>1</sup>

<sup>1</sup> Department of Physics, Stockholm University, Stockholm, 10691, Sweden

**Synopsis** Highly charged superfluid helium nanodroplets (HNDs) can be used to efficiently produce both cationic and anionic molecular or atomic clusters. These ions can then be analyzed by mass spectrometry methods and be used as precursors in collision experiments.

The cryogenic environment of helium nanodroplets can be used to study atoms, molecules and clusters at low temperatures [1]. Recent results showed that these HNDs can be highly charged [2,3]. These charges embedded in the HNDs can then be used as nucleation centers for the growth of small ionic clusters, both negatively or positively charged. To extract these ions from the droplets different methods can be used like evaporation of the HNDs or collision upon a surface. In fact, superfluid HNDs show a splashing like behavior upon collisions with a surface like classical liquids. It is so possible to liberate the ions from the HNDs [4]. Alternatively, it is also possible to liberate the ions by collisions with e.g. helium atoms at room temperature [5].

Here we show our newly developed experimental setup, which combines a helium nanodroplet ion source with a commercially available high-resolution time of flight mass spectrometer (QTOF-premier, Waters; see illustration *Figure 1*). HND are produced by supersonic expansion of precooled (below 10K) and pressurized (~20 bar) He gas of 99,9999% purity. These droplets are then highly ionized by a crossed beam electron impact source. The HNDs can pick up almost any atom or molecule by individual collisions. These dopants get attracted and ionized by the charges embedded in the HNDs. After liberating these ions, a quadrupole mass-filter allows us to select specific ions. The selected ions can be further studied by collisions with gases, or by overlapping the path of the ions with a tunable laser beam it is possible to perform messenger type action spectroscopy [6]. Additionally a reaction cell is planned to be installed for studying electron or ion bombardment induced reactions starting from mass-

selected and cryogenically cooled cluster precursors. Charged products will then be measured with the QTOF, which gives a mass resolution in excess of 20,000.

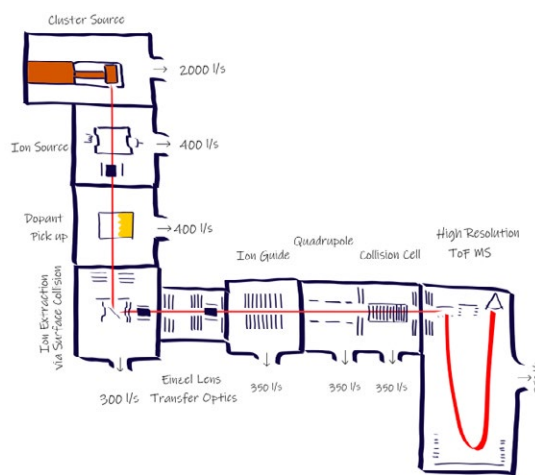


**Figure 1.** Illustration of the experimental setup, where the liberation of ions from the HNDs is achieved by collision with a polished stainless steel surface. In red, the path of the HNDs and the ions are shown from the cluster source at the top left towards the QTOF at the bottom right.

### References

- [1] Toennies J P and Vilesov A F 2004 *Angew. Chem. Int. Ed.* **43** 2622–48.
- [2] Laimer F *et al.* 2019 *Phys. Rev. Lett.* **123** 165301.
- [3] Laimer F *et al.* 2021 *Chem. Eur. J.* **27** 7283
- [4] Martini P *et al.* *Phys. Rev. Lett.* **127** 263401.
- [5] Tiefenthaler L *et al.* 2020 *Rev. Sci. Instrum.* **91** 033315.
- [6] Gatchell M *et al.* 2019 *Far. Diss.* **217** 276.

\* E-mail: [paul.martini@fysik.su.se](mailto:paul.martini@fysik.su.se)

## Mid-infrared spectroscopy of aromatic molecular cations in helium nanodroplets

A Iguchi<sup>1,2\*</sup>, S Kuma<sup>1†</sup>, H Tanuma<sup>2</sup> and T Azuma<sup>1,2</sup>

<sup>1</sup>Atomic, Molecular and Optical Physics Laboratory, Wako 351-0198, Japan

<sup>2</sup>Department Physics, Tokyo Metropolitan University, Tokyo 192-0397, Japan

**Synopsis** Superfluid helium droplets used as the cryogenic solvent for spectroscopy immediately cool captured molecules to a droplet temperature of 0.4 K. We constructed the setup to ionize neutral molecules in droplets. By electron impact ionization and mid-infrared laser light, we produced aromatic molecular cations in helium droplets and observed vibrational bands, which showed only a few  $\text{cm}^{-1}$  shifts from the gas-phase results.

In interstellar space, there are over 200 molecular species and we have not yet assigned some lines of the spectra. Aromatic molecules are thought to be responsible for the unidentified infrared bands. The observation of isolated cold molecular ions in laboratories leads to an improvement in identification. Superfluid helium droplets, which cool captured molecules immediately to the droplet temperature of 0.4 K, are an outstanding solvent for the spectroscopy of cold molecular ions. Helium droplets make the spectroscopic observation possible for the rovibrational states because of the weak perturbation from helium. Therefore the spectra of molecules in droplets have a linewidth narrower than other rare gas matrices and resemble the spectra of gas-phase molecules. The number of captured molecules per droplet can be controlled by the pressure of molecular vapor and droplet size, so that we can generate an experimental condition for isolated molecules at low temperatures. We applied this method to study aromatic molecular cations.

Superfluid helium droplets were produced in a pulsed beam by expanding in high-pressure (2 MPa) and cold ( $< 20$  K) helium gas through a solenoid valve [1]. Helium droplet beam can capture gas-phase neutral molecules by collision, and cool them down to the droplet temperature via evaporation of surface helium atoms. We installed a filament setup to ionize molecules in droplets by electron impact, which can operate with currents higher than 10 mA. The ionizer has several electrodes repelling the fragments produced after ionization, so that only the molecular cations in helium droplets can arrive downstream. To observe the infrared spectrum, we used a pulsed mid-infrared OPO laser and a time-of-flight mass spectrometer

(TOF-MS). When the molecular ion absorbs the IR photon and is excited vibrationally, all helium atoms around the ion evaporate and the bare ion is detected. The acceleration electrodes of TOF-MS with pulsed high-voltage are synchronized to the laser pulse.

In this study, we chose aniline ( $\text{C}_6\text{H}_5\text{-NH}_2$ ) as the target species. Figure 1 shows the spectrum obtained by scanning the IR laser when TOF-MS was turned to  $m/q = 93$ . The power of the IR laser was 20 mJ. We observed 2 vibrational peaks in the 3300-3560  $\text{cm}^{-1}$  range. While the peak at 3395  $\text{cm}^{-1}$  has been known as the N-H symmetric stretching band in helium droplets [2], we observed another peak at 3490  $\text{cm}^{-1}$ . This peak is assigned to the N-H antisymmetric stretching band [3]. It has only a small shift from the gas-phase peak about +4  $\text{cm}^{-1}$ .

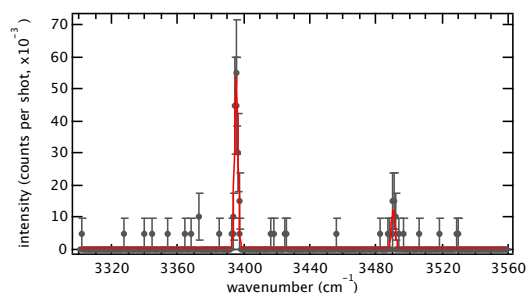


**Figure 1.** The infrared spectrum of aniline monomer cation in helium droplets. These peaks are assigned to the N-H symmetric stretching at 3395  $\text{cm}^{-1}$  and the N-H antisymmetric stretching at 3490  $\text{cm}^{-1}$ .

### References

- [1] Kuma S and Azuma T 2017 *Cryogenics* **88** 78
- [2] Smolarek S *et al* 2010 *J. Am. Chem. Soc.* **132** 14086
- [3] Honda M *et al* 2003 *J. Phys. Chem. A* **107** 3678

\* E-mail: [iguchi-arisa@ed.tmu.ac.jp](mailto:iguchi-arisa@ed.tmu.ac.jp)

† E-mail: [susumu.kuma@riken.jp](mailto:susumu.kuma@riken.jp)



## Supersolidity in a quasi-2D spinor Bose-Einstein condensate with SO-coupling

Pardeep Kaur<sup>1\*</sup>, Sandeep Gautam<sup>1†</sup> and S. K. Adhikari<sup>2#</sup>

<sup>1</sup>Department of Physics, Indian Institute of Technology Ropar, Rupnagar, Punjab 140001, India

<sup>2</sup>Instituto de Física Teórica, Universidade Estadual Paulista - UNESP, 01.140-070 São Paulo, São Paulo, Brazil

**Synopsis** We report the emergence of supersolid-like solitons in a spin-2 Bose-Einstein condensate (BEC) with spin-orbit coupling in a quasi-two-dimensional geometry. These solitons are characterized by a simultaneous presence of density and phase modulations and arise due to the interplay between the spin-orbit coupling and the spin-dependent interaction. Our results suggest a promising avenue towards the experimental realization of supersolidity in a spinor BEC with spin-orbit coupling.

We investigate the dynamics of a spin-2 BEC with spin-orbit coupling in a quasi-two-dimensional geometry. By numerically solving the Gross-Pitaevskii equation, we observe the emergence of supersolid-like solitons in the BEC, which exhibit a simultaneous presence of density and phase modulations. These solitons arise due to the interplay between the spin-orbit coupling and the spin-dependent interaction. We show that the solitons exhibit robustness against perturbations and decay, and they can be manipulated by varying the strength of the spin-orbit coupling or the trapping potential.

The phenomenon of supersolidity, where a solid can flow without resistance, has been a topic of interest in various fields of physics. While supersolidity has been experimentally observed in helium-4, its realization in a BEC has been challenging. Recently, it has been proposed that spin-orbit coupling can induce supersolid phases in dipolar BECs [1]. Our work provides further evidence of the potential of spin-orbit-coupled BECs to exhibit supersolidity.

The possible solutions are predicted by solving the non-interacting Hamiltonian and are shown in Figure 1. These solutions are also confirmed with numerical simulations by including the interactions also [3].

Moreover, our work demonstrates the importance of spin-orbit coupling in controlling the properties of ultracold atoms, which is crucial for the realization of novel quantum phases and topological states of matter.

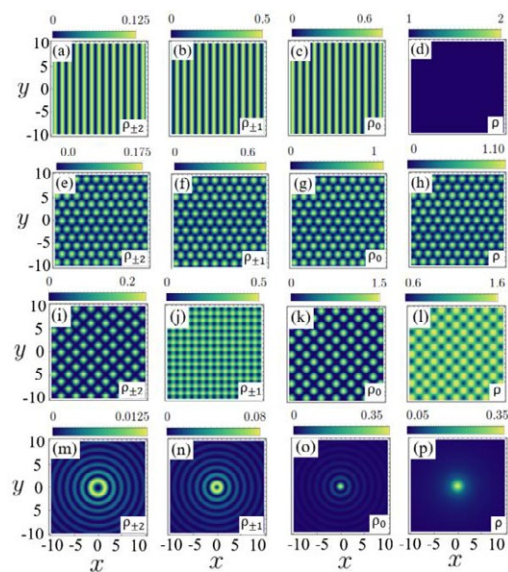


**Figure 1.** The two-dimensional contour plot of densities of the components and total density corresponding to Stripe (ST) phase in (a)-(d) for SO-coupling strength = 1. The same for triangular lattice (TL), square lattice (SL) and Multi-ring (MR) are shown in (e)-(h), (i)-(l) and (m)-(p), respectively.

### References

- [1] Kadau H, Schmitt M, Wenzel M, Wink C, Maier T, Ferrier-Barbut I and Pfau T 2016 *Nature* **530** 194
- [2] Schmitt M, Wenzel M, Böttcher F, Ferrier-Barbut I and Pfau T 2016 *Nature* **539** 259
- [3] Kaur P, Gautam S and Adhikari S.K. 2022 *Phys. Rev. A* **105** 023303

\* E-mail: [2018phz0004@iitrpr.ac.in](mailto:2018phz0004@iitrpr.ac.in)

† E-mail: [sandeep@iitrpr.ac.in](mailto:sandeep@iitrpr.ac.in)

# E-mail: [sk.adhikari@unesp.br](mailto:sk.adhikari@unesp.br)

## Waterloo/ ALLS Reaction Microscope Cold Target Recoil Ion Momentum Spectrometer Endstation

K Tian<sup>1\*</sup>, H Ibrahim<sup>2,3</sup>, R Karimi<sup>1</sup>, F Légaré<sup>3</sup>, A Staudte<sup>2</sup> and J Sanderson<sup>1†</sup>

<sup>1</sup>University of Waterloo, Waterloo, N2L 3G1, Canada

<sup>2</sup>University of Ottawa, Ottawa, K1N 6N5, Canada

<sup>3</sup>Advanced Laser Light Source Laboratory (ALLS) at the INRS, Varennes, J3X 1P7, Canada

**Synopsis** The Cold Target Recoil Ion Momentum Spectrometer Endstation at the Advanced Laser Light Source facility will soon be open to users. It is designed for studying molecular reactions, initiated by the new ALLS+ 100kHz repetition rate laser source. All electrons and ions, resulting from the multiple ionization of a single molecule are projected by a combination of electric and magnetic fields onto time and position sensitive detectors[1].

A COLTRIMS apparatus with double high precision detectors can measure the time of flight and position information of all fragment ions, electrons, and positive ions, making it possible to construct their three-dimensional momentum vectors. The system includes a supersonic thin jet system, to maintain a coincidence condition with only one molecule observed per laser shot and enable precise determination of conservation of momentum from the ions measured in coincidence.

At the Advanced Laser Light Source(ALLS): the apparatus will be combined with the Yb: YAG-pumped, Optical Parametric Chirped Pulse Amplification system [2][3] to image ultrafast dynamics. This tunable laser system can provide laser pulses of 2mJ at 100kHz or 10mJ at 20kHz. The IR pulses can be used to generate UV pulses of a few  $\mu\text{J}$ .

The COLTRIMS' supersonic thin jet unit is composed of a skimmer and a X/Y steerable gas source with 30-micron nozzle to select the central coldest part of the molecular beam. An adjustable 4 jaw slit system can further narrow the molecular beam down. The target density can be matched to different experimental needs.

The time of flight (TOF) spectrometer is the central part of the COLTRIMS experiment. The spectrometer contains two 3-layer HEX75 delay line detectors, which have zero dead time, high precision, multi-hit micro channel plates (MCP). A single drift region (5cm for ions, 30 cm for electrons, size is adjustable) is maintained by copper electrodes which are connected to each other by a resistance chain. The electric field directs the positively charged ions to the ion

detector, whereas electrons are captured by a homogeneous magnetic field and fly to the electron detector. The field strengths can be changed for individual experiments.

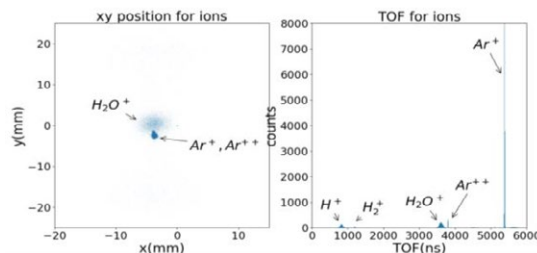


**Figure 1.** Position and time information from Ar jet irradiated by 35fs laser pulses at  $\sim 10^{15}$  W/cm<sup>2</sup>, background H<sub>2</sub>O (resulting in H<sup>+</sup> and H<sub>2</sub>O<sup>+</sup>) illustrate the high spatial and temporal precision available from the jet.

Currently, the apparatus is being characterized and will be available for user applications in the future. We will present information data showing the capabilities of the apparatus, the currently available high repetition rate laser source and likely future developments. Figure 1. shows preliminary test results obtained with an Argon jet and 35 fs laser pulses in Waterloo.

Information on how to access the instrument by applying for beamtime is available at [ALLS@inrs.ca](mailto:ALLS@inrs.ca). Informal expressions of interest are welcome and can be made to any of the authors.

### References

- [1] Dörner, R., et al., (2000) Phys Rep 330 95-192
- [2] Jeong, YG., et al. Sci Rep 8, 11794 (2018).
- [3] Ibrahim, H., et al. Nat Commun 5, 4422 (2014).

\* E-mail: [k3tian@uwaterloo.ca](mailto:k3tian@uwaterloo.ca)

† E-mail: [J3sanderson@uwaterloo.ca](mailto:J3sanderson@uwaterloo.ca)

## Present and future opportunities at the CAMP instrument at the Free-Electron Laser FLASH

B Erk<sup>1\*</sup>

<sup>1</sup>Deutsches Elektronen-Synchrotron DESY, Notkestr. 85, Hamburg, 22607, Germany

**Synopsis** The free-electron laser facility FLASH in Hamburg is undergoing a major upgrade towards an externally seeded, high-repetition-rate machine. The multi-purpose instrument CAMP at beamline BL1 at FLASH1 is tailored for pump-probe experiments on atoms, molecules, and clusters in the gas phase. Recent developments and future opportunities, in particular for AMO research, at this instrument will be discussed.

In recent years several extreme ultraviolet (XUV) and X-ray FELs came into operation around the world. The free-electron laser FLASH in Hamburg, that started user operation in 2005, is undergoing a transformational upgrade, called FLASH2020+, towards an echo-enabled high-harmonic generation (EEHG) seeded XUV and soft X-ray FEL machine with variable polarization (FLASH1 branch) [1], based on a superconducting linear accelerator, allowing for high repetition rates up to 5000 pulses per second in burst-mode.

The CAMP instrument [2] – a permanent end-station installed at beamline BL1 in the FLASH1 branch – with its modular and flexible layout allows using various detection schemes employing large-area, single-photon counting pnCCD photon-detectors and Velocity Map Imaging (VMI) electron and ion spectrometers. The instrument is tailored to study ultrafast dynamics in the gas phase, combining femtosecond optical laser pulses with intense XUV and soft x-ray pulses.

In recent years we have implemented and successfully used event-based, time-resolved camera systems – PimMS [3] and TimePix3 [4] – in a double-sided VMI spectrometer. This allows us to measure the full 3D momentum of all, individual ionic fragments as well as electrons simultaneously and enables advanced analysis methods using correlations between fragments in both yield and momentum. These novel camera systems are also fully capable of operating at high repetition rates up to MHz rates [4] and in burst.

At the same time, shot-by-shot measurements of the strongly fluctuating self-amplified spontaneous emission (SASE) photon energy spectrum can be correlated with VMI electron measurements. This enables to reach a resolution much better than the typical broad bandwidth of SASE FELs [5].

On the other hand, the CAMP instrument offers large area pnCCD imaging detectors [2], and using soft X-rays wide-angle coherent scattering experiments enable to measure the 3D shape of single in-flight particles of few 100nm diameter [6].

The upcoming upgrade of the facility, providing external seeding at photon energies up to the carbon K-edge with full coherence and high repetition rate will offer many new capabilities to users, which can be used to great advantage at the CAMP instrument.

### References

- [1] Beye M et al. 2023 *Eur. Phys. J. Plus* **138** 193
- [2] Erk B et al. 2018 *Journal of synchrotron radiation* **25(5)** 1529
- [3] Forbes R et al. 2020 *Journal of physics B* **53** 224001
- [4] Bromberger H et al. 2022 *Journal of physics B* **55** 144001
- [5] Wang J et al. 2023 *New Journal of Physics* **accepted**
- [6] Colombo A et al. 2023 *Science advances* **9(8)** eade5839

\* E-mail: [benjamin.erk@desy.de](mailto:benjamin.erk@desy.de)

## Direct measurement of few-cycle electric fields using a lock-in detection

R N Shah<sup>1</sup>\*, J Muhammad<sup>1</sup>, I Kosse<sup>1</sup>, S Bengtsson<sup>2</sup>, R Mori<sup>1</sup>, M Niebuhr<sup>1</sup>, F Frassetto<sup>3</sup>, L Poletto<sup>3</sup> and G Sansone<sup>1</sup>†

<sup>1</sup>Physikalisches Institut, Albert-Ludwigs Universitaet Freiburg, Freiburg, 79104, Germany

<sup>2</sup>Department of Physics, Lund University, PO Box 118, SE-221 00 Lund, Sweden

<sup>3</sup>Istituto di Fotonica e Nanotecnologie, CNR, Padova, Italy

**Synopsis** We present an all optical technique to measure the electric field of few cycle laser pulses via high-order harmonic generation (HHG). In our approach, the generation of an isolated attosecond pulse and the associated photon yield serves as ultrashort temporal gate to characterize the electric field of an unknown pulse. The intrinsic noise associated with the harmonic generation process is strongly reduced by using a lock-in detection, thus making our measurement technique fast, repeatable and with good signal-to-noise (SNR) ratio.

Direct measurements techniques of ultrashort laser pulses based on highly nonlinear processes, such as HHG, have recently gain increasing importance [1-4].

In our experiments, the process of isolated attosecond pulse (IAP) generation is used as a temporal tip to scan over a weak perturbing pulse to be measured in a typical Mach-Zehnder interferometer configuration. In contrast to other direct electric field measurement techniques [1-2], we use the total cut-off harmonic yield as our observable simplifying the experimental procedure and increasing the absolute signal level. In this way, we are able to measure fields having as low as tens of nanojoules of energy. Furthermore, utilizing the fundamental property that the high-order harmonic generation process is most efficient for linearly polarized driving pulses, we are able to measure the complete polarization state of a laser field by repeating the characterization for two orthogonal polarizations of the field generating the IAPs.

In our work, we used a multi-channel plate (MCP) coupled to a phosphor screen to detect the spectrally resolved harmonic supercontinuum. Due to the highly nonlinear nature of the harmonic generation and measurement process, the measurement technique is highly susceptible to noises. An effective way to strongly improve the SNR is through the use of lock-in technique. Thus, the measurement was accomplished either by (i) integrating the camera signal looking at the phosphor screen or by (ii) using current in the power lines of MCP as a signal which is locked to a reference optical chopper placed on

the optical path of the pulse to be characterized. The comparison between the two approaches at a low scan rate (1 Hz) is presented in Fig. 1a. Scan rate is the inverse of amount of time spent at each delay step. Noise levels, characterized by standard deviation in the highlighted region of Fig. 1a, has improved by a factor of 2 through the lock-in detection. Moreover, at higher scan rates (10 Hz) in Fig. 1b, compared to lock-in detection (red line) the camera acquisition fails to isolate effectively the field waveform from the noise (black line).

Our technique facilitates our future studies like polarization sensitive plasmonic resonances in nanostructures.

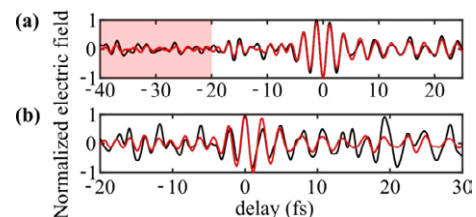


**Figure 1.** Measurement of electric field by the phosphor screen and camera summing the camera count (black) and measurement with lock-in technique (red). **(a)** At a scan rate of 1 Hz **(b)** At a scan rate of 10 Hz.

### References

- [1] Kim K. T., *et. al.* 2013, *Nature Photonics* **7**, [958–962](#)
- [2] Wyatt A. S., *et. al.* 2016, *Optica* **3**, [303-310](#)
- [3] Carpeggiani P., *et. al.* 2017, *Nature Photonics* **11**, [383-389](#)
- [4] Park S. B., *et. al.* 2018, *Optica* **5**, [402-408](#)

\* E-mail: [ronak.shah@physik.uni-freiburg.de](mailto:ronak.shah@physik.uni-freiburg.de)

† E-mail: [giuseppe.sansone@physik.uni-freiburg.de](mailto:giuseppe.sansone@physik.uni-freiburg.de)

## A hybrid mode-locking Yb: fiber laser for generations of vector dissipative solitons

K. Chen\*, T. Cao, S. Liu, Q. Xu, Z. Li and J. Peng

School of Optical and Electronic Information, Huazhong University of Science and Technology, Wuhan, 430074, China

**Synopsis** We report a novel hybrid mode-locking Yb: fiber laser based on the combination of NALM and NPR, and its rich vector dynamics are measured and analyzed by the time-stretch dispersive Fourier transform technique.

High energy Yb-doped fiber femtosecond lasers have been widely used in micro-machining [1]. One of the keys to obtain stable high-power outputs is a reliable oscillator.

Currently, all-polarization-maintaining (PM) fiber mode-locking lasers based on nonlinear amplifying loop mirror (NALM) and semiconductor absorber mirror (SESAM) are widely used in industries for their decent environmental stability. However, SESAM is easy to be damaged and needs to be moved occasionally after damage spots being formed in long-term operation [2], and the output power from an all-PM NALM mode-locking fiber laser is low. Therefore, we report a novel hybrid mode-locking Yb: fiber laser based on the combination of NALM and nonlinear polarization rotation (NPR) mechanisms, where both good self-starting mode-locking and high power with broadband spectrum are obtained simultaneously, with stable single pulse operation at 0.81 nJ and 35.3 nm bandwidth (full width at half maximum).

Furthermore, in this configuration, a strong asymmetry of the NALM enhances the differential nonlinear polarization rotation of the counter-propagating pulses in the fiber ring, so the output pulses formed by interference at the coupler possess rich vector polarization dynamic properties. This kind of laser is naturally an excellent platform capable of generating both vector solitons (NALM output) and scalar solitons (PBS output) without any additional couplers placed in the cavity. At the output, we observed significant energy exchanges between the two orthogonal polarization components at the spectral positions of Kelly sidebands. In the meantime, the time-stretch dispersive Fourier transform (TS-DFT) technique is employed to

study the formation process of mode-locking vector dissipative solitons, soliton collision and other vector transient dynamic processes.

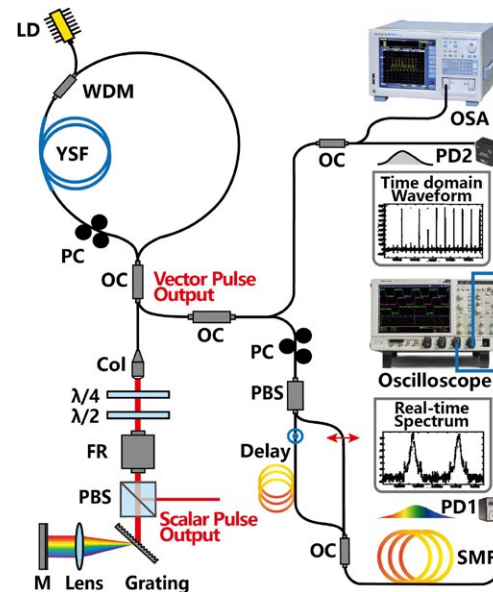


**Figure 1.** Experimental setup of the hybrid mode-locked Yb: fiber laser (on the left), and its transient dynamic measurement line (on the right). YbF: Yb-doped single clad fiber, WDM: wavelength division multiplexer, OC: optical coupler, LD: laser diode, Col: collimator, FR: Faraday rotator, PBS: polarization beam splitter, M: mirror, PC: polarization controller, PD: photodetector, SMF: standard single-mode fiber, OSA: optical spectrum analyzer.

### References

- [1] Fermann M E and Hartl I 2013 *Nat. photonics* **7** 11
- [2] Kieu K and Wise F W 2008 *Opt. Express* **16** 15

\* E-mail: [kchenn@hust.edu.cn](mailto:kchenn@hust.edu.cn)



## The CSR-ReMi – A cryogenic in-ring reaction microscope

F. Herrmann<sup>1</sup>\*, D. V. Chicharro<sup>1</sup>, R. Moshhammer<sup>1</sup>, C. D. Schröter<sup>1</sup> and T. Pfeifer<sup>1</sup>

<sup>1</sup>Max Planck Institute for Nuclear Physics, Saupfercheckweg 1, 69117 Heidelberg, Germany

**Synopsis** Report on the setup of the reaction microscope for the cryogenic storage ring CSR and presentation of the first benchmark measurements gathered at room temperature.

The CSR-ReMi is a dedicated in-ring reaction microscope to perform experiments on slow and cold molecular ions and clusters in the cryogenic storage ring CSR [1]. A reaction microscope [2] is a combined electron and ion spectrometer for energy and angular resolved particle detection created in individual collision processes. It offers multi-hit capability and provides high detection efficiency, acceptance and resolution. With coincident detection of all collision fragments, kinematically complete data sets on the reaction dynamics can be collected. This allows stringent tests of theoretical concepts for the description of molecular fragmentation and relaxation dynamics. The implementation of this first cryogenic reaction microscope worldwide will considerably extend the range of scientific applications at the CSR. In the CSR-ReMi, experiments like electron transfer, photo detachment and molecular break-up reactions are possible.

The implementation of the CSR-ReMi into the CSR started in May 2022 and its integration is expected to be finalized in spring 2023. Subsequent final checks before commissioning and first benchmark measurements at room temperature will follow. Thereafter, first fundamental experiments on the collision dynamics of neutral targets with stored cold molecular ions are planned. In addition to the incoupling for the supersonic gas jet, which supplies the neutral target beam, the CSR-ReMi is equipped with a laser incoupling line. Figure 1 shows an overview of the central chamber of the CSR-ReMi. Here, the cold ion beam (blue) of the CSR can interact with a gas jet (yellow) or a laser beam (green). The future addition of a laser system will further increase the scientific scope of the CSR-ReMi, since e.g. a high-power femtosecond laser will allow to do time-resolved experiments on state-prepared molecules using established pump-probe techniques.

\* E-mail: [felix.herrmann@mpi-hd.mpg.de](mailto:felix.herrmann@mpi-hd.mpg.de)

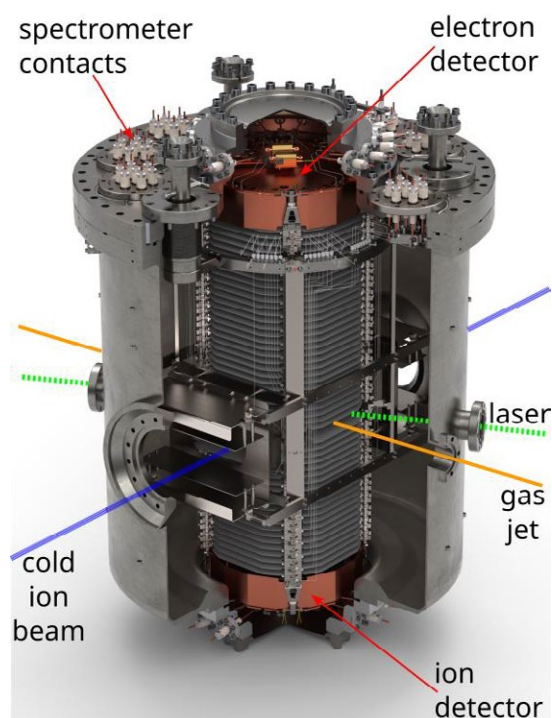


**Figure 1.** Central chamber of the CSR-ReMi containing the spectrometer, electron and ion detector.

This contribution will present the design, main components and working principle of the complete machine. Also, first test results of the benchmark measurements at room temperature will be discussed.

### References

- [1] R. von Hahn et al., The cryogenic storage ring CSR, *Rev. Sci. Instrum.* 87, 063115 (2016); <https://doi.org/10.1063/1.4953888>
- [2] J. Ullrich et al., Recoil-ion and electron momentum spectroscopy: reaction-microscopes, *Rep. Prog. Phys.* 66 (2003) 1463–1545

## The (only) way towards low-energy, heavy, highly charged ions: the HITRAP deceleration facility

N Stallkamp<sup>1,2\*</sup>, Z Andelkovic<sup>2</sup>, S Fedotova<sup>2</sup>, W Geithner<sup>2</sup>, F Herfurth<sup>2</sup>, M Horst<sup>2,3</sup>, D Neidherr<sup>2</sup>, S Rausch<sup>2,3</sup>, S Trotsenko<sup>2</sup> and G Vorobjev<sup>2</sup>

<sup>1</sup>Institute of Nuclear Physics, Goethe University Frankfurt a.M., 60439 Frankfurt a.M., Germany

<sup>2</sup>GSI Helmholtzzentrum für Schwerionenforschung GmbH, 64291 Darmstadt, Germany

<sup>3</sup>Institute of Nuclear Physics, TU Darmstadt, 64289 Darmstadt, Germany

**Synopsis** Heavy, highly charged ions (HCI) at low energies provide excellent conditions for precise studies of fundamental properties in the presence of extreme electromagnetic fields, such as laser spectroscopy of the hyperfine structure, bound-electron g-factor, surface-HCI interaction etc. Due to the complexity of their production, the availability of such systems is very limited. The aim of HITRAP is to reliably bridge the gap between high-energy HCI production and precision experiments with these systems at low energies.

The HITRAP facility, located at the GSI Helmholtzzentrum für Schwerionenforschung GmbH in Darmstadt, Germany, is designed to decelerate and cool heavy, highly charged ions (HCI) created by the GSI accelerator complex [1]. The system consists of a two-stage deceleration structure, an interdigital H-type linac (IH) and a radio-frequency quadrupole (RFQ), followed by a cryogenic Penning-Malmberg trap for subsequent ion cooling. The deceleration stages reduce the ion energy from 4 MeV/u to 500 keV/u and to 6 keV/u respectively, before forwarding a slow, but hot ion bunch towards the cooling trap. The trap is operated in a so-called nested configuration, in which the electrons, created by an external photo-electron source, are stored simultaneously with the HCI and serve as cold thermal bath. Via Coulomb-Coulomb interaction the ions transfer their energy to the electrons which are cool by continuously dissipating energy via synchrotron radiation, due to their circular motion in a strong magnetic field.

**Table 1.** Kinetic energies within HITRAP

	IH	RFQ	Trap
Energy	500 keV/u	6 keV/u	sub-eV/q

After cooling, the ions can be transported via a low-energy transfer beamline towards various attached experiments [2]. A dedicated small ion source (Dresden EBIT) is attached to the beamline and used for commissioning of the cooling

trap as well as a source of light HCI for experiments [3]. Examples of such experiments are laser spectroscopy of trapped HCI, measurements of bound-electron g-factor and surface-HCI interaction at low energies.

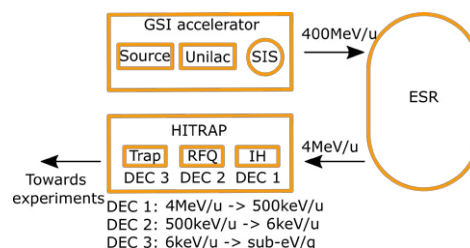


**Figure 1.** HITRAP facility within GSI complex.

So far, deceleration of heavy HCI has been regularly set up down to 6 keV/u, though the process is somewhat lengthy, hampered by a low delivery rate of a single ion bunch per 40 seconds. The subsequent electron cooling process is under development with promising results. Ions from the EBIT are regularly stored and mixed with electrons. An interaction between them has been verified, however a clear cooling effect could not be observed so far. The current status of this development as well as future aspects will be presented.

### References

- [1] Herfurth F *et al* 2015 *Phys. Scr.* **2015** 014065
- [2] Andelkovic Z *et al* 2015 *Nucl. Instrum. Methods Phys. Res. Section A* vol. 795 **2015** 055
- [3] Sokolov A *et al* 2010 *JINST* **5** C11001

\*E-mail: [n.stallkamp@gsi.de](mailto:n.stallkamp@gsi.de)

## ErUM-FSP APPA: BMBF Collaborative Research Center at FAIR

S Schippers<sup>1,2\*</sup> and T. Stöhlker<sup>3,4,5†</sup> for the APPA collaborations

<sup>1</sup>I. Physikalisches Institut, Justus-Liebig-Universität Gießen, Germany

<sup>2</sup>Helmholtz Forschungsakademie Hessen für FAIR (HFHF), Campus Gießen, Germany

<sup>3</sup>Helmholtz-Institut Jena, Germany

<sup>4</sup>GSI Helmholtzzentrum für Schwerionenforschung, Darmstadt, Germany

<sup>5</sup>Institut für Optik und Quantenelektronik, Friedrich-Schiller-Universität Jena, Germany

**Synopsis** The collaborative research center ErUM-FSP APPA joins the German university groups who contribute to the scientific instrumentation and to the scientific research at the international heavy-ion research facility FAIR under the umbrella of research pillar APPA (Atomic, Plasma Physics and Applications). It is funded by the German Ministry for Education and Research (BMBF). We will briefly present the individual projects of the current funding period 2021–2024.

The BMBF collaborative research center ErUM-FSP APPA [1] joins the German university groups (Figure 1), who have set out to perform scientific research at the future international accelerator complex FAIR under the umbrella of APPA (Atomic, Plasma Physics and Applications [2]). The FAIR installations are currently under construction at the site of the GSI Helmholtz Center for Heavy Ion Research in Darmstadt, Germany. APPA is one of the four research pillars of FAIR comprising the international research collaborations BIOMAT (biophysics and materials science [3]), FLAIR (low-energy antiprotons), HED@FAIR (plasma physics [4]), and SPARC (atomic physics [5]) who focus on investigations of (anti)matter under extreme conditions (strong fields, high densities, high pressures, and high temperatures).

The collaborative research center ErUM-FSP APPA pursues coordinated research projects in the area of accelerator based experiments with heavy ions at the future FAIR-installation. Central issues are:

- Further development of the the experimental infrastructure, in particular, research and development for enhancing the scientific capabilities of the existing installations and of the future accelerator and detector systems including the respective base technologies.
- Set-up of the APPA experiments of the modules 0-3 of the modularized start version of FAIR.

\*E-mail: [stefan.schippers@physik.uni-giessen.de](mailto:stefan.schippers@physik.uni-giessen.de)

†E-mail: [t.stoehlker@gsi.de](mailto:t.stoehlker@gsi.de)

- Realization of the APPA research program during the current FAIR Phase-0.



**Figure 1.** Map showing the locations of German university groups with APPA-related scientific activities.

### References

- [1] <http://fsp-appa.fair-center.eu>
- [2] Stöhlker T *et al* 2015 *Nucl. Instrum. Methods A* **365** 680
- [3] Durante M *et al* 2019 *Phys. Rep.* **800** 1
- [4] Schoenberg K S *et al* 2020 *Phys. Plas.* **27** 043103
- [5] Stöhlker T *et al* 2014 *Hyperfine Interact.* **227** 45

## A real-time gas monitoring system based on ion mobility spectrometry for high concentration

K Takaya<sup>1\*</sup>, M Hagiwara<sup>1</sup>, S Matoba<sup>2</sup>, M Takaya<sup>1</sup> and N Shibata<sup>1</sup>

<sup>1</sup>National Institute of Occupational Safety and Health, Kanagawa, 2148585, Japan

<sup>2</sup>A High Energy Accelerator Research Organization, KEK, Ibaraki, 3191106, Japan

**Synopsis** Ion-mobility spectrometry (IMS) can perform qualitative and quantitative analysis of multi-component chemical mixtures in real time, which is difficult for commonly used instruments such as gas chromatography–mass spectrometry and photo-ionization detectors. IMS is commonly applied in microanalytical (ppb) sensing of toxic gases. Thus, its application to quantitative analyses of chemical substances with a high proton affinity is generally not possible at high concentrations because multimeric complexes are generated. In this study, we found that calibration curves derived from shifts in nominal arrival-time spectra of chemical substances overlapping with water clusters enables quantitative analysis at high concentrations.

In this study, An IMS device available in the work environment was developed for real-time measurement of chemicals. Experiments were conducted to examine the performance of the device using methyl ethyl ketone (MEK) which is widely used in factories as a test sample. The response time of this device was 10 s or less, suggesting that real-time monitoring can be performed in the work environment.

MEK may exist high concentration in factories to dissolve paints, inks, and adhesives, and to perform various types of cleaning of acrylic, urethane, and epoxy resins. However, the concentration cannot be estimated based on the ion intensity of the spectrum because saturation has already occurred at a certain high concentration. Therefore, this study estimated the concentration based on the degree of the shift from the peak of the water clusters (RIP). Since the peak of MEK overlaps with the peak of RIP, the peak observed in this study is a nominal peak. It is assumed that if the concentration of MEK increases, the concentration of water cluster ions will decrease, and the nominal peak shifts from the peak position of RIP. The concentration was estimated from the peak shift amount, and calibration curves between the arrival time and the concentration of MEK was obtained from the two different ambient conditions. Although the

difference in the ambient conditions resulted in an arrival time shift, the same correlation between the arrival time and the concentration of MEK was obtained from the two different ambient conditions (Figure 1). As a result, calibration curves under the two different conditions could be obtained with high accuracy ( $R^2$ , 0.997 and 0.998, respectively). It was confirmed that MEK could be adequately monitored in real-time by using this device.

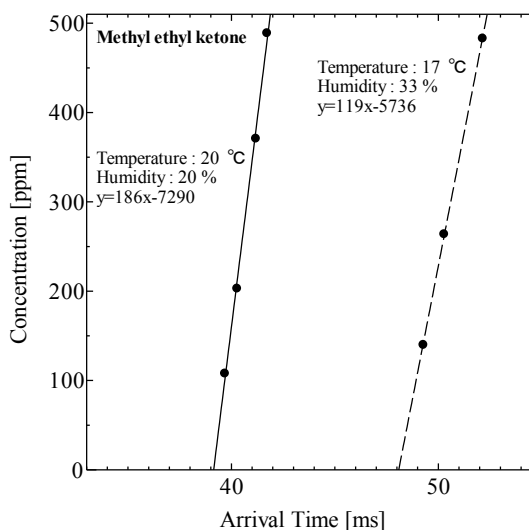


**Figure 1.** Relationship between arrival time and concentration at methyl ethyl ketone. Solid line is the calibration at Temperature : 20 ° C , Humidity : 20 %RH. Dotted line is the calibration at Temperature : 17 ° C, Humidity : 33 %RH. The measurement error of the flow rate at the permeator used in this study was estimated to be about 3 %.

\* E-mail: takaya-k@h.jniosh.johas.go.jp



## Development of an universal in-ring COLTRIMS Reaction Microscope for CRYRING@ESR

G. Kastirke<sup>1</sup>, L. Ph. H. Schmidt<sup>1</sup>, T. Jahnke<sup>1</sup>, R. Dörner<sup>1</sup> and M. S. Schöffler<sup>1\*</sup>

<sup>1</sup>Institut für Kernphysik, Goethe University, Max-von-Laue-Str. 1, 60438 Frankfurt, Germany

**Synopsis:** Here we report on the current status designing and constructing a universal and versatile COLTRIMS Reaction Microscope for the CRYRING storage ring at the FAIR userfacility.

In order to study ion-atom, ion-molecule collisions in great detail an instrument that measures the momenta of all emitted charged particles is essential. A COLTRIMS (Cold Target Recoil Ion Momentum Spectroscopy) Reaction Microscope is such an instrument. The target is provided by a super sonic gas jet that is multiple times differentially pumped and shaped with skimmers and movable slits. The total length is about 1 m, but can be shortened to less than half. Under such conditions a very cold target is provided with variable target density and basically no residual gas intake into the interaction chamber.

As the study of possible reactions covers direct target ionization, electron transfer and projectile ionization for atomic, molecular and cluster targets, the imaging unit (spectrometer and detectors) has to be versatile as well. For example, studying electron transfer processes [1,2] requires a high resolution in longitudinal direction. This favours an extraction geometry rather parallel to the ion-beam direction, similarly as the investigation of ECC (electron capture to the continuum) or the short-time formation of molecular orbitals during saddle-point ionization [3]. Experiments that result in a Coulomb explosion [4] of the multiple ionized target molecule [5] or cluster [6] require a short spectrometer, which therefore has to be mounted transversally. For the detectors, hexagonal delayline anodes with reduced inner layer size of 80 and 150 mm diameter equipped with microchannel plates (regular and efficiency enhanced [7]) are going to be used.

The COLTRIMS Reaction Microscope will be placed in the experimental section of the CRYRING@ESR of the FAIR user facility. Therefore a vacuum base pressure of low

$10^{-11}$  mbar is anticipated. As outlined the spectrometer can be placed in longitudinal configuration with an angle of  $\sim 20^\circ$  with respect to the ion beam. Alternatively the spectrometer can also be mounted in the widespread transversal extraction geometry. The design is in both cases most flexible in the exact electric field geometry (length, plate diameters).

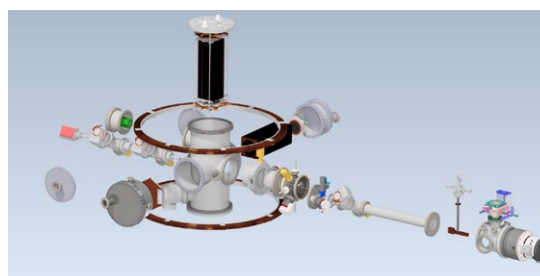


**Figure 1.** Sketch of the COLTRIMS Reaction microscope for CRYRING with a spectrometer that can be used either in a longitudinal or transversal extraction geometry. The ion beam from CRYRING enters/exits through the large flange on the left/right.

### References

- [1] H.-K. Kim et al., Phys. Rev. A, **85**, 022707 (2012)
- [2] Y. Xue et al., Phys. Rev. A., **90**, 052720 (2014)
- [3] L. Ph. H. Schmidt et al., Phys. Rev. A., **76**, 012703 (2007)
- [4] L. Ph. H. Schmidt et al., Phys. Rev. Lett., **108**, 073202, (2012)
- [5] D. Misra et al., Phys. Rev. Lett., **102**, 153201, (2009)
- [6] J. Titze et al., Phys. Rev. Lett., **106**, 033201, (2011)
- [7] K. Fehre et al., Rev. Sci. Instr., **89**, 045112, (2018)

\* E-mail: [schoeffler@atom.uni-frankfurt.de](mailto:schoeffler@atom.uni-frankfurt.de)



## Novel High Harmonic Beamline Design for Ultrafast X-ray Spectroscopy

P Burden<sup>1\*</sup>, P Elten<sup>1</sup>, A E Boguslavskiy<sup>1</sup>, C Marceau<sup>2</sup>, I Wilkinson<sup>3</sup>, A Rouzée<sup>4</sup>, P Corkum<sup>1</sup>, A Stolow<sup>1</sup>

<sup>1</sup>University of Ottawa, Ottawa, K1N 6N5, Canada

<sup>2</sup>National Research Council Canada, Ottawa, K1N 5A2, Canada

<sup>3</sup>Helmholtz-Zentrum Berlin, Berlin, 14109, Germany

<sup>4</sup>Max-Born-Institut, Berlin, 12489, Germany

**Synopsis** Advances in ultrafast X-ray pulses have given birth to the field of Time Resolved X-ray Absorption Spectroscopy (TRXAS). The use of high power short-wave infrared lasers has opened a ‘table-top’ route to ultrafast soft X-ray pulses via High Harmonic Generation (HHG). The University of Ottawa has recently installed a 550 W ytterbium disk laser system, currently the highest average power ultrafast laser in Canada. This light source will pump a novel beamline providing X-rays beyond the oxygen K-edge. The design of this beamline is the main focus of this poster.

The advent of ultrafast X-ray pulses of light has given birth to the new fields of Time Resolved X-ray Diffraction (TRXRD) and Time Resolved X-ray Absorption Spectroscopy (TRXAS), recognized by the U.S. Department of Energy as important future research directions [1]. The ultrafast coupling of electronic and vibrational dynamics is of global importance, as it underlies key processes such as photosynthesis [2], vision [3] and solar energy conversion [4]. TRXAS probes both electronic and vibrational dynamics in a way which allows for atom-specific characterization.

Ultrafast X-ray pulses (~1-5 keV @ 10-100 fs) have, to date, been available only at large scale (~\$1 billion) X-ray Free Electron Laser (XFEL) facilities, such as those located in the U.S., Germany, Italy, and Japan. However, developments in high power infrared ultrafast lasers have opened a “table-top” route to ultrafast soft X-ray pulses (~0.1-0.7 keV @ 0.1-10 fs) via the process of High Harmonic Generation (HHG) [5]. This recent development has permitted the first TRXAS experiments to be performed in labs rather than at XFEL facilities [6].

With the University of Ottawa’s recent installation of a high-power industrial Yb disk laser system (550 W, < 900 fs pulses, 1030 nm, 10 kHz), we aim to generate, via HHG, intense and stable soft X-ray continua out to beyond 500 eV. This 1  $\mu\text{m}$  laser system will pump an Optical Parametric Chirped Pulse Amplifier (OPCPA) chain to produce high energy few-cycle pulses of light at 2  $\mu\text{m}$  with actively stabilized Carrier-Envelope Phase (CEP).

UV (pump) pulses will be generated from a 2-stage fibre compressor & resonant dispersive wave fibre. Then, the soft X-ray (probe) pulses will be recombined with bright UV (pump) pulses via a “holey” mirror. The pump and probe are then directed towards the sample, where we aim to study samples in the gas phase.

A unique flat-field X-ray spectrometer has been specifically designed by Helmholtz-Zentrum Berlin for our beamline. It will consist of 4 sets of variable line spacing gratings on a concave ultrahigh precision Si substrate, diffracting and re-focussing the x-rays simultaneously with high resolution (> 3000) and high transmission (>20% at 300 eV). This optic will be combined with a large 40 $\times$ 40 mm soft X-ray enhanced CMOS sensor. The use of such a large sensor compounded with a flat focal field, will allow for simultaneous (single-shot) measurement of several atomic edges. Such simultaneous measurements will result in reduced signal acquisition time and will permit covariance and correlation between fluctuations at different atomic edges, removing common-mode noise.

### References

- [1] Heinz T et al. U.S. Department of Energy 2017 *Basic Energy Sciences Roundtable: Opportunities for Basic Research at the Frontiers of XFEL Ultrafast Science*
- [2] Higgins J S et al. 2021 *PNAS* **118**
- [3] Oliveira-Brett A M 2017 *Reference Module in Chemistry, Molecular Sciences and Chemical Engineering*
- [4] Romero E et al. 2014 *Nat Phys* **10** 676
- [5] Popmintchev D et al. 2018 *Phys Rev Lett* **120**
- [6] Pertot Y et al. 2017 *Science* **355**

\* E-mail: [pburd055@uottawa.ca](mailto:pburd055@uottawa.ca)

## The development of marking system of secondary battery anode and cathode using nanosecond laser with *in situ* tracking module.

Seungsik Ham<sup>1\*</sup>, Jaesung Park<sup>2\*</sup>, Taeho Jun<sup>1</sup> and Ho Lee<sup>2,3,4†</sup>

<sup>1</sup>R&D center, JY engineering, Pyeongtaek,17712, Republic of Korea

<sup>2</sup>Institute for Nanophotonics Applications, Kyungpook National University, Daegu, 41566, Republic of Korea

<sup>3</sup>School of Convergence, Department of Robot and Smartsystem engineering, Kyungpook National University, Daegu, 41566, Republic of Korea

<sup>4</sup>Laser Application center, Kyungpook National University, Daegu, 41566, Republic of Korea

**Synopsis** The secondary battery, which has recharging qualities, is focused on different industrial industries, especially electric automobiles. Recently, several problems, such as fires, have been attributed to defects, therefore it is important to keep an eye out for them. Due to the intricate manufacturing process, tracking defects is difficult. Therefore, we suggested that barcodes be printed on the electrodes to enable tracking throughout the whole production cycle and to create an integrated system for barcode printing and reading. On anode material, we used our technique to barcode marking and reading.

A secondary battery is a type of energy storage that may be recharged after being discharged. As more people switch to electric cars, the need for auxiliary batteries as a power source is rising quickly. However, a variety of problems, including fire and explosion, are occurring because of faulty batteries, and a response through product tracking is becoming more and more necessary.

In this study, an integrated barcode marking and tracking system was suggested. In the first production process, each secondary battery cell was conceptually identified with a distinct barcode. The electrode procedure and a system capable of tracking each product through barcode recognition were also used.

The system consists of a barcode marking module with a nanosecond laser integrated with a BCR (barcode reader) for rearrangement. Our system is made up of laser optics for barcode marking that includes a nanosecond pulsed laser, which is a 532 nm central wavelength and a 2-axis galvanometer mirror for scanning, a mechanical region for sample in-and-out processes, and a barcode reading zone for recognition.

Furthermore, we used laser marking to optimize the laser's parameters, and we were able to obtain 100% recognition. A detailed parameter is described in Table 1.

† E-mail: [hlee@knu.ac.kr](mailto:hlee@knu.ac.kr)

\* S. Ham and J.Park equally contributed to this paper

**Table 1.** Optimal laser parameter for barcode marking.

Wavelength(nm)	532
Repetition rate(kHz)	240
Power(W)	4.2
Scan speed(mm/s)	3,000
Pulse width(ns)	10

Surface morphology, such as marking depth, was examined using confocal microscopy. Here, we discovered that the ideal depth for barcode recognition is between 1 and 2 micrometers (Figure 1).

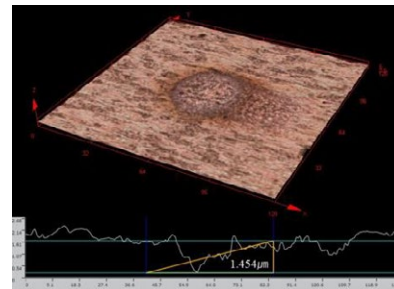


**Figure 1.** Representative image and profile of laser marking spot.

### Acknowledgement

This work was supported by the Technological Innovation R&D Program (S3236367) funded by the Ministry of SMEs and Startups (MSS, Korea)

### References

- [1] Euhduck J, Deongsoo P and Yoonbo S, 1994 *Energy Engg.J.* **32**
- [2] Janez D, Drago B, Ales G and Janez M, 2011, *Optics and laser in engineering.* **49 2**

## Development of Polymer Dispersed Liquid Crystal (PDLC)-based switchable spatial filter using femtosecond laser micro-patterning

Jaesung Park<sup>1\*</sup>, JongWook Park<sup>2\*</sup>, and Ho Lee<sup>1,2,3†</sup>

<sup>1</sup>Institute for Nanophotonics Applications, Kyungpook National University, Daegu, 41566, Republic of Korea  
<sup>2</sup>School of Convergence, Department of Robot and Smartsystem engineering, Kyungpook National University, Daegu, 41566, Republic of Korea

<sup>3</sup>Laser Application center, Kyungpook National University, Daegu, 41566, Republic of Korea

**Synopsis** A spatial filter is a kind of optical part that can filter a beam's frequency information. These spatial filters let light pass through an active area. The fact that the active region cannot be moved is a drawback of most spatial filters. This work used PDLC and femtosecond laser micropatterning to construct a spatial filter that allows the active region's position to be changed to tackle this issue.

A spatial filter is a sort of optical component that filters the frequency data from a laser beam by selectively allowing or preventing the laser beam from passing through a certain point.

The region of the spatial filter through which light travels is referred to as the active area, and most commercial spatial filters are unable to alter the active area's position. Additionally, because it is made of liquid crystal (LC), there are drawbacks such as the difficulty of changing the form when using a premade mask and the issue of significant light loss caused by the polarizer.

To solve these issues, this work created a switchable spatial filter utilizing PDLC (Polymer-Dispersed Liquid Crystal) and femtosecond laser micropatterning. This experiment used a femtosecond laser for microfabrication so that independent voltages could be applied to the ITO layer. Commercial PDLC (QPDL-7, Qingdao liquid crystal, China) that combines liquid crystal and pre-polymer was employed in the experiment.

An empty cell was created by injecting the PDLC into ITO, and its characteristics are reported in Table 1.

**Table 1.** Physical properties of PDLC

Operating Temperature	Viscosity [1/S]	Birefringence (@589nm)
-10 ~60 [°C]	56	0.227
index	(@ 1kHz, 20°C)	(@ 1kHz, 20°C)
1.52	18.3	5.6

\* E-mail: sung\_e@knu.ac.kr

† E-mail: holee@knu.ac.kr

As illustrated in Figure 1, the cell created for this study is a device that modifies the PDLC's transparency by turning the voltage on and off.

This acts as a spatial filter, switching between an opaque state for an area where voltage is not applied and a transparent state for which voltage is applied.

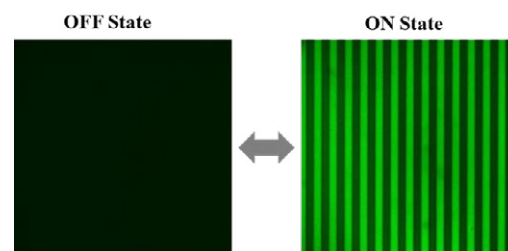


**Figure 1.** The image of a PDLC-based switchable spatial filter

This work created a switchable PDLC cycle spatial filter with a transmittance of roughly 80 to 85%.

### Acknowledgement

This research was supported by Basic Science Research Program through the National Research Foundation of Korea (NRF) funded by the Ministry of Education (NRF-2022R111A3063490)

### References

- [1] Klug A. and Pinnell J. 2020 American Journal of Physics 88 12
- [2] LeGrange J. D. and Carter S. A. 1997 Journal of Applied Physics 81 9

## Ultrafast electron-stimulated desorption to form ion pulses for time-resolved ion surface collision experiments

M.C. Chirita Mihaila<sup>1</sup>, G.L. Szabo<sup>1</sup>, A. Redl<sup>1</sup>, M. Goldberger<sup>1</sup>, and R. A. Wilhelm<sup>1\*</sup>,

<sup>1</sup>TU Wien, Institute of Applied Physics, Vienna, 1040, Austria, EU

**Synopsis** We present a design for picosecond ion pulse generation based on electron-stimulated desorption of a water film. We use UV femtosecond laser pulses to produce ultrafast electron pulses and their impact on a high-voltage biased electrode leads to the formation of ions with a picosecond timing precision well-synchronized to the laser. First results are presented as well.

In contrast to electrons or photons, ion pulses are currently not available in the range of picoseconds or below. The main reason is the large initial momentum given by the ion mass, which limits the achievable timing precision of an ion impact on a surface or molecule [1, 2].

We use a femtosecond laser system with UV light in order to trigger ultrafast electron emission from a photocathode in the linear emission regime. Optimizing for highest electron intensity per pulse ( $> 1000$  electrons per pulse), we propagate the electrons through a set of high-voltage electrostatic lenses and a strong axial magnetic field. Electron impact ionization of atoms and molecules in the gas phase leads to the formation of ions. Interestingly, due to over-focussing by the magnetic field, electrons can impact the positively-biased electrostatic lens optics and trigger ultrafast electron-stimulated desorption (incl. ionization) which is seen by measuring short ( $< 100$  ps) proton pulses independent of gas background pressure. In this case the initial momentum distribution of the molecular or atomic species to be ionized is not isotropic anymore breaking potentially the present pulse width barrier.

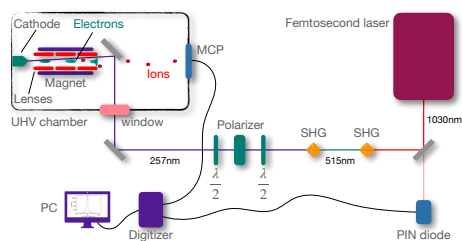


**Figure 1.** Principal layout of the laser-triggered ion source which delivers picosecond ion pulses over macroscopic distances.

\*E-mail: [wilhelm@iap.tuwien.ac.at](mailto:wilhelm@iap.tuwien.ac.at)

Figure 1 shows the design layout of our experiment including a self-build second harmonic generation, polarizer and the laser-triggered electron beam ion source.

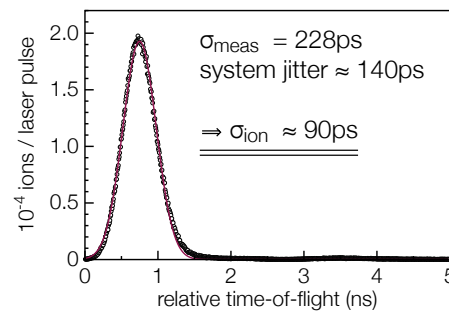


**Figure 1.** Relative time-of-flight spectrum of  $H^+$  ions at 8.5 keV kinetic energy. The measured pulse width is  $\sigma = 228$  ps with a total system jitter of  $\sim 140$  ps.

Figure 2 shows a preliminary result for protons produced by electron-stimulated desorption from a high voltage biased electrode. The measured pulse width is 228 ps with a total system jitter of about 140 ps. From this we can estimate that the ion pulse jitter is below 100 ps. Currently we can produce about  $10^{-2}$  ions per laser pulse (integral of peak in Fig. 2), which translates into about  $10^4$  ions/s using 1 MHz laser repetition rate. Further optimization of both pulse width reduction (and system jitter reduction) as well as output current is underway.

### References

- [1] Moshhammer R 2000 *Phys. Rev. Lett.* **84** 447
- [2] Golombek A *et al.* 2021 *New J. Phys.* **23** 033023

## Development of portable Electron Beam Ion Traps at NIST

J N Tan<sup>1\*</sup>, D La Mantia<sup>1</sup>, A S Naing<sup>1</sup>, A Henins<sup>1</sup>, A Banducci<sup>2</sup>, SM Brewer<sup>2</sup>

<sup>1</sup>National Institute of Standards & Technology, Gaithersburg, MD 20874, USA

<sup>2</sup>Department of Physics, Colorado State University, Fort Collins, CO 80523, USA

**Synopsis** An electron beam ion trap (EBIT) uses electron impact ionization to produce highly charged ions for many applications. Calculable transition energies in few electron ions, for example, can be useful for evaluating and calibrating novel quantum sensors. A room-temperature, portable EBIT with a 0.29 T peak field has been built at the National Institute of Standards and Technology (NIST). We briefly present the performance of this extremely compact prototype, and report on the progress in building a new portable EBIT that is designed to provide a peak magnetic field approaching 0.7 T.

Electron beam ion sources and traps[1,2] are used to generate highly charged ions (HCIs) for various applications. Highly ionized atoms are produced and trapped within an accelerated beam of electrons that is magnetically compressed to very high current density in the trapping region.

The advent of the EBIT opened up many atomic physics experiments, including investigations of quantum electrodynamics (QED), ion-ion collisions, ion-surface interactions, laboratory astrophysics and plasma diagnostics.[3] It is an important tool for spectroscopic studies across a wide region of the electromagnetic spectrum, from the visible, to EUV, to the X-ray domain.

At high energies, superconductive magnets have been used to produce the strong magnetic field (3T & higher) needed to attain very high electron current densities, exemplified by spectroscopic measurements on H-like uranium ( $U^{91+}$ ) to test QED and nuclear size effects that are greatly enhanced by the large nuclear charge (thus, very small orbital)[4]. At low energies, a number of compact EBITs have been built to produce HCIs with low ionization thresholds for charge states of interest; in particular, recent theoretical studies propose that some HCIs with forbidden optical transitions (e.g.,  $Pr^{10+}$  or  $Nd^{10+}$ ) have properties that are advantageous in searching for time-variation in the fine-structure constant, and in developing very stable atomic clocks[5]. Metrologically, the calculable transition energies in H-like and He-like ions can be useful in providing natural-linewidth limited

spectral lines for the evaluation of novel quantum sensors (such as transition-edge sensors) as well as for calibration that is traceable to the revised International System of Units (quantum SI) based on fundamental constants.

At NIST, a room-temperature EBIT with a peak magnetic field of 0.29 T was built using a pair of axially magnetized NdFeB rings. The strong magnets are embedded in the drift tubes, resulting in a very compact architecture. We briefly present the performance of this prototype [6,7] and report on the progress in building a new portable EBIT designed to provide a higher peak magnetic field (approaching 0.7 T) using a larger number of radially magnetized NdFeB rings.

This work is supported by NIST Grants #70NANB19H1162 and #70NANB15H046.

### References

- [1] Donets E 1997 *Physica Scripta* **T71** 5.
- [2] Levine MA, Marrs RE, Henderson JR, Knapp DA, and Schneider MG 1988 *Physica Scripta* **1988** 157
- [3] Beyer H and Shevelko V 2003 *Introduction to the Physics of Highly Charged Ions* (Institute of Physics).
- [4] Beiersdorfer P 2009 *Canadian J. Physics* **87** 9.
- [5] Kozlov MG, Safronova MS, Crespo Lopez-Urrutia and Schmidt PO 2018 *Rev. Mod. Phys.* **90** 045005.
- [6] Naing AS 2021 *Ph.D. Thesis*, U. of Delaware
- [7] Naing AS, Norrgard EB, Foo BC and Tan JN, manuscript in preparation

\* E-mail: [joseph.tan@nist.gov](mailto:joseph.tan@nist.gov)



## Toward a new type of gas phase spectroscopy for complex organic ions

S. Knaffo<sup>1\*</sup>, M.L. Rappaport<sup>1</sup>, H. Kreckel<sup>2</sup>, K. Blaum<sup>2</sup>, A. Wolf<sup>2</sup>, Th. Henning<sup>3</sup>,  
Y. Toker<sup>4</sup>, S.Sunil Kumar<sup>5</sup>, O. Heber<sup>1</sup>, D. Zajfman<sup>1</sup>

<sup>1</sup>Department of Particle Physics, Weizmann Institute of Science, Rehovot 76100, Israel

<sup>2</sup>Max-Planck-Institut für Kernphysik, Saupferchweg 1, 69117 Heidelberg, Germany

<sup>3</sup>Max-Planck-Institut für Astronomie, Königstuhl 17, 69117 Heidelberg, Germany

<sup>4</sup>Department of Physics and Institute of Nanotechnology and Advanced Materials, Bar-Ilan University, 529002 Ramat-Gan, Israel

<sup>5</sup>Department of Physics and Center for Atomic, Molecular, and Optical Sciences and Technologies, IISER Tirupati, Tirupati 517507, Andhra Pradesh, India

**Synopsis** One of the most sensitive spectroscopic methods in existence is Laser-Induced-Fluorescence (LIF), with applications ranging from environmental studies to genomic sequencing. Current limitations arise from the fact that larger molecular ions often do not exhibit electronic fluorescence, but re-distribute and emit the absorbed energy through vibrational transitions in the mid-infrared. We intend to exploit this mid-infrared emission - and thus extend the LIF technique toward more complex molecules - using a cryogenic ion trap combined with an ultra-sensitive mid-infrared detection scheme.

More than 270 molecules have been detected in interstellar space to date, and modern telescopes continue to add entries to the catalog of identified species at a steady pace [1]. In recent years the detection frequency of complex organic molecules (COMs) with clear pre-biotic relevance has picked up in pace, with important implications for open questions such as the possible delivery of organic material to Earth and the origin of life. However, there is currently no established technique to obtain gas phase spectra of large molecular ions.

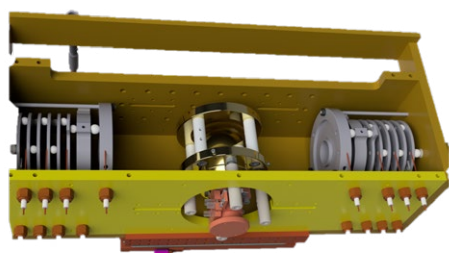


**Figure 1.** The CEBIT with BIB detectors modification

We propose to develop a novel spectroscopy technique that is based on laser excitation of electronic transitions in complex molecules, followed by internal re-distribution of the energy among vibrational states and finally the emission of mid-infrared photons [2]. We intend to detect these photons using a sensitive mid-infrared detector. To this end we will combine an existing cryogenic electrostatic ion trap with a mid-infrared detector module based on blocked-impurity-band (BIB) arsenic-doped silicon diodes. The ion trap and the detector have been developed and tested separately. Here, we present the challenges and goals to combine these two techniques in the laboratory and the current design stage of the experiment.

### References

- [1] Brett A. McGuire (2022), *Astrophys. J. Suppl.* **295** 30
- [2] L. J. Allamandola, A. G. G. M. Tielens, M and J. R. Barker (1989), *Astrophys. J. Suppl.* **71** 733

\*E-mail: [stav.knaffo@Weizmann.ac.il](mailto:stav.knaffo@Weizmann.ac.il)

## Recent progress of muon catalyzed fusion study: IV. Nuclear reaction processes in the dt $\mu$ molecule

M Kamimura<sup>1</sup>, Y Kino<sup>1\*</sup>, T Yamashita<sup>1</sup>

<sup>1</sup>RIKEN, Wako, 351-0198, Japan

<sup>2</sup>Tohoku University, Sendai 980-8578, Japan

**Synopsis** The coupled channel Schrödinger equation for the intramolecular nuclear fusion reaction ( $dt\mu \rightarrow \alpha + n + \mu + 17.6$  MeV) is solved, satisfying the exact boundary condition and the low energy  $d + t \rightarrow \alpha + n$  reaction cross section. The dynamics of the muon released after the reaction, for the muonic molecule  $(dt\mu)_{J=0}$  as the initial state and the outgoing wave in the  $\alpha n\mu$  channel.

Muon catalyzed fusion ( $\mu$ CF) is a process in which nuclear fusion reactions are facilitated by muons which are similar to electrons but are about 207 times more massive [1]. A muon injected into the mixture of deuterium (D) and tritium (T) forms a muonic molecule with a deuteron d and a triton t, namely,  $dt\mu$ . Due to the average nuclear distance of about 700 fm, the wave function of the relative motion of the two nuclei has a non-zero amplitude around the origin where nuclear interaction occurs. Consequently, an intramolecular nuclear fusion reaction,  $dt\mu \rightarrow \alpha + n + \mu + 17.6$  MeV, occurs instantly with a rate six orders of magnitude higher than the muon decay rate.  $\mu$ CF holds the potential to be a highly efficient and clean energy source. However, the input energy required to practically produce muons ( $\sim 5$  GeV/muon) exceeds the output energy obtained from nuclear fusion ( $\sim 3$  GeV/muon). Despite this,  $\mu$ CF has recently attracted significant interest due to various new developments [2] and applications.

We employ a coupled three-body model that includes the  $dt\mu$ - and  $\alpha n\mu$ -channels. The coupled-channel Schrödinger equation

$$\begin{aligned} (H_{dt\mu} - E)[\Psi_0^{(C)}(dt\mu) + \Psi^{(N)}(dt\mu)] \\ = -V_{dt-\alpha n}\Psi^{(+)}(\alpha n\mu) \\ (H_{\alpha n\mu} - (E + 17.6 \text{ MeV}))\Psi^{(+)}(\alpha n\mu) \\ = -V_{\alpha n-dt}[\Psi_0^{(C)}(dt\mu) + \Psi^{(N)}(dt\mu)] \end{aligned}$$

is solved for the reaction with a total spin-angular momentum quantum number of 3/2, which involves the  ${}^5\text{He}(3/2^+)$  compound nucleus. The boundary condition is satisfied for the initial state of the muonic molecule  $(dt\mu)_{J=0}$ , and for the outgoing wave in the  $\alpha n\mu$  channel. The Hamiltonians  $H_{dt\mu}$  and  $H_{\alpha n\mu}$  represent the initial  $dt\mu$  channel and the final  $\alpha n\mu$  channel, respectively.  $\Psi_0^{(C)}(dt\mu)$ ,  $\Psi^{(N)}(dt\mu)$ , and  $\Psi^{(+)}(\alpha n\mu)$

are the fixed source term of the  $(dt\mu)_{J=0}$  wave function, the nuclear wave function that describes the d-t relative motion due to the nuclear interaction, and the outgoing wave function that describes both the  $\alpha + n + \mu$  and  $(\alpha\mu)_n + n$  channels.  $V_{dt,\alpha n}$  and  $V_{\alpha n-dt}$  are non-local coupling potentials that precisely reproduce the energy dependence of the low energy cross section for the nuclear reaction. The details of the calculation are shown in the references [3,4].

The resulting  $dt\mu$  fusion rate is  $1.15 \times 10^{12} \text{ s}^{-1}$ . By substituting the obtained total wave function into the  $T$  matrix based on the Lippmann-Schwinger equation, we have calculated the fusion rates  $\lambda_r^b$  and  $\lambda_r^c$ , corresponding to the bound and continuum states of the outgoing  $\alpha$ - $\mu$  pair, respectively. We then derived an initial  $\alpha$ - $\mu$  sticking probability of 0.857%, which can explain the recent observations. We have much improved the sticking-probability calculation. We also calculate the absolute values for the energy spectra of the muons released after the fusion reaction. The most important result is that the peak energy is 1.1 keV, while the mean energy is 9.5 keV owing to the long higher-energy tail. This is a crucial result for the ongoing experimental project aimed at developing an ultraslow muon by utilizing  $\mu$ CF for various applications, such as a scanning muon microscope and an injection source for the muon collider.

### References

- [1] Nagamine K and Kamimura M 1998 *Adv. Nucl. Phys.* **24** 151
- [2] Yamashita T *et al.*, 2022 *Sci Rep.* **12** 6393
- [3] Kamimura M *et al.* 2023 *Phys. Rev. C* **107** 034607
- [4] Hiyama E *et al.*, 2003 *Prog. Part. Nucl. Phys.* **51**, 223

\* E-mail: y.k@tohoku.ac.jp

# Index

Last name	First name	Abstract Title	Abstract Topic (Projectile)	Abstract Topic (Target)	Poster #
Abdul Jalil	Sohail	Controlling the polarization and phase of high-order harmonics with a plasmonic metasurface	Photon	Atom	<a href="#">We057</a>
Abul Kalam Azad Siddiki	Md	Probing the fragmentation pathways of an Argon dimer in slow ion-dimer collisions	Heavy	Cluster	<a href="#">Th102</a>
Al-Hagan	Ola	Electron Impact Induced Fragmentation of ND <sub>3</sub> <sup>+</sup>	N/A	Ion	<a href="#">Mo075</a>
Alarcon	Miguel	Estimating Rare Gas Spectra with a New Theoretical Model for Pump-Probe Spectroscopy	Photon	Atom	<a href="#">Th013</a>
Antoine Hervieux	Paul	Collective effects in positronium formation from rare gas atoms	Lepton	Atom	<a href="#">Th062</a>
Antonio	Nicholas	Wave-packet continuum discretisation approach to dressed carbon ion collisions with atomic hydrogen	Heavy	Atom	<a href="#">Mo086</a>
Arbó	Diego	Quantum Holography in Above Threshold Ionization	Photon	Atom	<a href="#">Fr003</a>
Arbó	Diego	Inner-shells effect for positrons and electrons traversing cold matter and plasmas	Lepton	-Other-	<a href="#">Mo108</a>
Arbó	Diego	A time-dependent theory for RABBIT	Photon	Atom	<a href="#">Th010</a>
Arbó	Diego	Atomic phase delays in $w - 2w$ above-threshold ionization	Photon	Atom	<a href="#">We026</a>
Ariel Fojon	Omar	Cross sections for ionization of liquid water by electron impact	Lepton	Molecule	<a href="#">Fr095</a>
Armstrong	Gregory	R-matrix with time dependence theory for double photoionization of general atoms	Photon	Atom	<a href="#">Fr022</a>
Arthur-Baidoo	Eugene	Positron annihilation spectra and binding energies for heterocyclic molecules	Lepton	Molecule	<a href="#">Th071</a>
Arun	Subramani	On the role of isomerisation in the photo dissociation of PANHs : A casestudy with methyl amidogen abstraction	Photon	Molecule	<a href="#">Fr052</a>
Astigarreta	Moana	Temperature of H <sub>3</sub> <sup>+</sup> produced in the H <sub>2</sub> + H <sub>2</sub> <sup>+</sup> reaction	N/A	Molecule	<a href="#">Fr106</a>
Attia	Maroua	Electron impact ionization of atoms and molecules: an improved BBK model	Lepton	Atom	<a href="#">Fr078</a>
Aumayr	Friedrich	Collisions between solar wind ions and the lunar surface	Heavy	Surface	<a href="#">Fr111</a>
Ayasli	Atilay	Ion molecule reaction dynamics of the radical anion O <sup>-</sup> with deuterated methane CD <sub>4</sub> and methyl iodide CH <sub>3</sub> I	Heavy	Molecule	<a href="#">Th108</a>
Ayuso	David	Ultrafast imaging of molecular chirality via low-order nonlinear interactions	Photon	Molecule	<a href="#">Fr032</a>
Babette Menz	Esther	Measurement of Dielectronic Recombination of Ne <sup>2+</sup> at CRYRING@ESR	Lepton	Ion	<a href="#">Fr075</a>
Badhan	Vipul	Design and Underlying Concepts of a Python Based Quantum Package for High Precision Atomic Structure Calculations	N/A	Atom	<a href="#">Fr135</a>
Badnell	Nigel	Plasma screening effects on dielectronic satellites	Lepton	Ion	<a href="#">Fr072</a>
Badnell	Nigel	Quadrupole l-changing collisions	Heavy	Atom	<a href="#">Mo090</a>
Banas	Dariusz	Nanostructures formed on a gold crystal surface by the impact of slow highly charged xenon ions.	Heavy	Surface	<a href="#">Fr122</a>
Bandurin	Yu	Photoluminescence of L-valine irradiated with 12.5 MeV electrons	Lepton	Molecule	<a href="#">AF002</a>
Bandurin	Yu	Investigation of photoluminescence of glucose and fructose in the powder form	Lepton	Molecule	<a href="#">AF003</a>

Last name	First name	Abstract Title	Abstract Topic (Projectile)	Abstract Topic (Target)	Poster #
Barrachina	Raul	Quantum vortices in the fully differential cross section for the ionization of atoms by the impact of protons and positrons	N/A	Atom	<a href="#">Mo088</a>
Barrachina	Raul	Three-particle one-dimensional model for ionization collisions: A simple laboratory to test perturbative approximations	Heavy	Atom	<a href="#">Th098</a>
Barrachina	Raul	Time evolution of Migdal electrons	N/A	Atom	<a href="#">We105</a>
Bartschat	Klaus	Multi-sideband interference structures observed via high-order photon-induced continuum-continuum transitions in helium	Photon	Atom	<a href="#">Fr018</a>
Bastani	Parnia	Laser-based processing of dielectric chips for the generation of nano focused XUV radiation	Photon	Surface	<a href="#">We064</a>
Baumann	Thomas	Soft x-ray spectroscopy on non-linear interaction of x-rays with matter at the Small Quantum Systems instrument of European XFEL	Photon	Atom	<a href="#">Mo006</a>
Beatriz Monteiro-Carvalho	Ana	Production of O <sub>2</sub> <sup>+</sup> following the double ionization of CO <sub>2</sub>	Lepton	Molecule	<a href="#">Th075</a>
Beatriz Monteiro-Carvalho	Ana	Absolute cross sections for ionization and fragmentation of CO <sub>2</sub> by electron impact	Lepton	Molecule	<a href="#">We093</a>
Behera	Nihar	Intermolecular coulombic decay in an unbound substituted benzene	Photon	Molecule	<a href="#">We038</a>
Ben Ltaief	Ltaief	Efficient indirect interatomic Coulombic decay induced by photoelectron im-pact excitation in large pure He nanodroplets	Photon	Cluster	<a href="#">Fr028</a>
Benda	Jakub	Polarization-induced molecular photoionization delays and equivalence of RABITT and streaking dipole-laser coupling	Photon	Molecule	<a href="#">Mo037</a>
Benredjem	Djamel	Ionization cross section and plasma density effects	Lepton	Ion	<a href="#">Th066</a>
Bernard	Jérôme	Recurrent fluorescence rates of tetracene cations C <sub>18</sub> H <sub>12</sub> <sup>+</sup> measured at two electrostatic Storage Rings: DESIREE and Mini-Ring.	Photon	Molecule	<a href="#">Fr026</a>
Biela-Nowaczyk	Weronika	Recombination processes in He-like oxygen ions measured at CRYRING@ESR electron cooler	Heavy	Ion	<a href="#">Fr071</a>
Bin Zhang	Song	Carrier-envelope-phase measurement of sub-cycle UV pulses using angular photofragment distributions	Photon	Molecule	<a href="#">Fr030</a>
Bin Zhang	Song	Time-resolved resonant Auger scattering clocks distortion of a molecule	Photon	Molecule	<a href="#">Mo028</a>
Bin Zhang	Song	Electron-rotation coupling in diatomics by intense UV pulses	Photon	Molecule	<a href="#">Th033</a>
Bin Zhang	Song	Ultraviolet Pump-Probe Photodissociation Spectroscopy of Electron-Rotation Coupling in Diatomics	Photon	Molecule	<a href="#">We031</a>
Bohachov	H	Studies of the VUV luminescence excited by electron impact on the gas-phase glycine and alanine	Lepton	Molecule	<a href="#">AF004</a>
Bolognesi	Paola	Ion-neutral coincidence experiments to characterize the photofragmentation of cyclo-dipeptides	Photon	Molecule	<a href="#">Mo034</a>
Bolognesi	Paola	Photofragmentation of cyclo-dipeptides in the gas-phase and routes to the for-mation of peptide chains	Photon	Molecule	<a href="#">Th029</a>
Bondy	Aaron	A comparison study for high-order harmonic generation in helium	Photon	Atom	<a href="#">Mo019</a>
Bondy	Aaron	High precision theory for the Rydberg states of helium up to n = 24: test of a 7 $\sigma$ discrepancy with experiment	N/A	N/A	<a href="#">Th129</a>
Bondy	Aaron	Charge-state distributions after beta decay of <sup>6</sup> He	Lepton	Atom	<a href="#">We077</a>
Borbély	Sándor	Photoelectron holography: an interplay between difference interference mechanisms.	Photon	Atom	<a href="#">Mo005</a>

Last name	First name	Abstract Title	Abstract Topic (Projectile)	Abstract Topic (Target)	Poster #
Borovik	Oleksandr	Electron-impact ionization of the 5p6 subshell in barium	Lepton	Ion	<a href="#">AF001</a>
Bossaer	Chandler	Orbital perspective of high-harmonic generation in ReS2	Photon	Surface	<a href="#">Mo061</a>
Bouloufa-Maafa	Nadia	Two-photon optical shielding of collisions between ultracold polar molecules	Photon	Molecule	<a href="#">Th122</a>
Brédy	Richard	XUV-induced dynamics in complex molecular ions in the gas phase	Photon	Molecule	<a href="#">Fr048</a>
Brédy	Richard	Ultrafast dynamics in tryptophan-based peptides controlled by micro-environment	Photon	Molecule	<a href="#">Mo042</a>
Brédy	Richard	Fragmentation and dynamics of protonated reserpine induced by femtosecond laser excitation	Photon	Molecule	<a href="#">We043</a>
Brienza	Robert	Microwave Spectroscopy of high-n low-l 84Sr Rydberg states in a cold gas	N/A	Atom	<a href="#">Th113</a>
Buckman	Stephen	Electron Atom/Molecule Scattering and its Applications: A Tribute to Michael Brunger	Lepton	N/A	<a href="#">AF010</a>
Buckman	Stephen	Electron Swarms as a Bridge Between Atom/Molecule Collisions and Gas Discharges: A Tribute to Robert W. Crompton	Lepton	Atom	<a href="#">AF011</a>
Burden	Philippe	Novel High Harmonic Beamline Design for Ultrafast X-ray Spectroscopy	N/A	Molecule	<a href="#">Mo135</a>
Burgt	Peter	Fragmentation of pyrene molecules following double ionization by 70 eV electron impact	Lepton	Molecule	<a href="#">We137</a>
Cao	Shiquan	Interaction between highly charged ions near the Bohr velocity energy region and laser-produced plasmas	Heavy	Ion	<a href="#">Mo093</a>
Carlini	Laura	Aromatic cyclo-dipeptides in the gas-phase: photoemission and state-selected fragmentation	Photon	Molecule	<a href="#">We046</a>
Cassidy	Jack	Many-body theory calculations of positron binding to halogenated hydrocarbons	Lepton	Molecule	<a href="#">Mo070</a>
Chacko	Roby	Probing the internal dynamics of homonuclear dimer anions via time-dependent electron detachment inside an electrostatic ion trap	Photon	Ion	<a href="#">Mo106</a>
Chacko	Roby	A 22-pole RF ion trap experimental setup to study the ion-neutral and ion-photon interactions relevant to astrophysical environments.	Heavy	Ion	<a href="#">Th096</a>
Chakraborty	Himadri	DFT study of d-electron photoionization of x@C60 with x = Cu+, Cu, Cu-, Zn	Photon	Cluster	<a href="#">Th028</a>
Chakraborty	Himadri	Shone and driven, they cool down in femtoseconds but scoot off in attoseconds	Photon	Cluster	<a href="#">We032</a>
Chao Jiang	Wei	Multi-photon double ionization of helium by ultrashort XUV pulses: probing the role of electron correlations	Photon	Atom	<a href="#">Fr007</a>
Chao Jiang	Wei	Strong-field Effects on Time Delays in Correlated Ionization	Photon	Atom	<a href="#">Th016</a>
Charlotte Schmidt	Viviane	Slow decay processes of molecular anions during long-time storage in a cryogenic storage ring	Photon	Molecule	<a href="#">Mo116</a>
Chen	Dongyang	Laser cooling experiments at the CSRe: explanation for the observed wide deceleration range on a coasting ion beam by a cw laser	Photon	Ion	<a href="#">Fr002</a>
Chen	Keyu	UV-induced ring-opening dynamics investigated by time-resolved Coulomb explosion imaging	Photon	Molecule	<a href="#">Fr045</a>
Chen	Guangqing	Tracing the expansion of molecular plasma with electron collision	Photon	Molecule	<a href="#">Mo078</a>
Chen	Kun	A hybrid mode-locking Yb: fiber laser for generations of vector dissipative solitons	Photon	-Other-	<a href="#">Mo128</a>
Chicharro Vacas	David	Probing conical intersection dynamics in the dissociative photoionization of formaldehyde at FLASH	Photon	Molecule	<a href="#">Th031</a>



Last name	First name	Abstract Title	Abstract Topic (Projectile)	Abstract Topic (Target)	Poster #
Ciappina	Marcelo	Twisted attosecond pulse trains driven by amplitude-polarization pulses	Photon	Atom	<a href="#">Fr010</a>
Ciappina	Marcelo	Isomer effects and orbital features in the ellipticity dependence of high-order harmonics from C <sub>20</sub> isomers	Photon	Cluster	<a href="#">Mo027</a>
Ciappina	Marcelo	Spatially dependent laser assisted photoionization of He	Photon	Atom	<a href="#">Th005</a>
Ciappina	Marcelo	Pulse length effects in long wavelength driven non-sequential double ionization	Photon	Atom	<a href="#">We010</a>
Cornetta	Lucas	Chemical shifts in the carbon core-level of ethanol in water-ethanol mixtures	Photon	Molecule	<a href="#">We121</a>
Cote	Robin	Resonant processes and their impact in many-body dynamics	Heavy	Atom	<a href="#">Th124</a>
Cui	Shucheng	State-selective single-electron capture in 1 keV/u Ar 2+ -Ar collisions	Heavy	Atom	<a href="#">Th091</a>
Cunningham	Brian	Many-body theory and calculations of spectra for low-energy positron annihilation in polyatomic molecules	Lepton	Molecule	<a href="#">Mo069</a>
D. Borisova	Gergana	Visualisation and laser-induced modification of a vibrational wave-packet revival in the excited H <sub>2</sub> molecule	Photon	Molecule	<a href="#">Mo035</a>
Da Costa	Cintia	Amorphous and crystalline pyridine ices irradiated by MeV ions	Heavy	Surface	<a href="#">Fr115</a>
Dahlstroem	Jan Markus	Photoelectron signature of dressed-atom stabilization in intense XUV field	Photon	Atom	<a href="#">We134</a>
Das	Nirmallya	Dissociation dynamics in Tetrachloromethane molecule induced by ion impact	N/A	Molecule	<a href="#">Fr109</a>
Das	Nirmallya	Dissociation dynamics in Chloroform molecule induced by ion impact.	N/A	Molecule	<a href="#">Mo098</a>
De	Ruma	Ultrafast non-adiabatic relaxation of C60: In search of efficient MD model	Photon	Cluster	<a href="#">We035</a>
De Barros	Ana	Swift heavy ion irradiation of water, carbon monoxide, and methanol mixture in the solid phase	Heavy	Molecule	<a href="#">Th101</a>
De Barros	Ana	Synthesis of N-O-H bearing species in HONO2 and H2O: an infrared spectroscopic study using heavy-ion irradiation of solid samples	Heavy	Molecule	<a href="#">We120</a>
Derlikiewicz	Julia	Carrier-phase envelope control of nondipole effects in ionization	Photon	Atom	<a href="#">Fr014</a>
Diaz-Tendero	Sergio	Efficient molecular oxidation in collisions with superoxide anions	Heavy	Molecule	<a href="#">We119</a>
Ding	Xiaobin	Indirect ionization of the Mo <sup>14+</sup> ion in EBIT	Lepton	Ion	<a href="#">Th068</a>
Dinger	Mareike	Modelling of the (e,2e) binary collision of water using the distorted wave Born approximation with single center expansion	Lepton	Molecule	<a href="#">We090</a>
Dochain	Arnaud	Mutual neutralization between diatomic cation and atomic anion	Heavy	Molecule	<a href="#">Mo112</a>
Dong	Chenzhong	Theoretical investigation of dielectronic satellite spectra of Au <sup>69+</sup> -Au <sup>65+</sup> ions	Photon	Ion	<a href="#">Fr076</a>
Dong	Ruichao	First commissioning results of the AMO endstation at the Shanghai soft X-ray free-electron laser facility	Photon	Atom	<a href="#">We013</a>
Dong	Chenzhong	EUV spectra of Ge <sup>4+</sup> - Ge <sup>13+</sup> ions in laser-produced plasmas	Photon	Ion	<a href="#">We126</a>
Dong Sun	Zhen	The role of molecular collisions in the conversions of nuclear spin isomers of methanol gas	Photon	Molecule	<a href="#">Mo104</a>
Dorn	Alexander	Electron-electron-ion coincidence studies for electron impact ionization of small water clusters	Lepton	Cluster	<a href="#">Fr094</a>

Last name	First name	Abstract Title	Abstract Topic (Projectile)	Abstract Topic (Target)	Poster #
Drescher	Markus	Collective electron dynamics in large ultracold atomic ensembles	Heavy	Ion	<a href="#">Th111</a>
Drouillard	Nathan	Studying the Optical Properties of 1-decanol for Ultrashort Pulse Generation	Photon	-Other-	<a href="#">Fr062</a>
Dutta	Saurav	Photoexcited Polycyclic Aromatic Hydrocarbon undergoes Intermolecular Coulombic Decay	Photon	Molecule	<a href="#">We039</a>
Dvorak	Jan	Vibrational patterns in dissociative photoionization of H <sub>2</sub> and D <sub>2</sub> molecules by VUV + NIR absorption	Photon	Molecule	<a href="#">Mo044</a>
Erdmann	Ewa	Fragmentation upon collision-induced activation of cysteine–water cluster cations	Heavy	Molecule	<a href="#">Th100</a>
Erk	Benjamin	Present and future opportunities at the CAMP instrument at the Free-Electron Laser FLASH	Photon	Molecule	<a href="#">Mo125</a>
Eronen	Eemeli	Statistical Analysis of X-ray Spectra of Aqueous Tripeptides	Photon	Molecule	<a href="#">Mo103</a>
Esponda	Nicolás	An improved short-range description for CDW-EIS model with dressed projectiles.	Heavy	Atom	<a href="#">Th089</a>
Fabrikant	Ilya	Low-energy positronium scattering from O <sub>2</sub>	Lepton	Atom	<a href="#">Th074</a>
Fabrikant	Ilya	Near-threshold collisional dynamics in the e <sup>-</sup> -e <sup>+</sup> +p system	Lepton	Atom	<a href="#">We079</a>
Farizon	Michel	Formation and elongation of polyglycine via unimolecular reactions in the gas phase	N/A	Cluster	<a href="#">Fr108</a>
Fernanda Rojas Barillas	Maria	Ionization of molecules by bare ions impact: dynamic effective charge in the residual-target continuum state	N/A	Molecule	<a href="#">Mo100</a>
Fernández-Villoria	Francisco	Time-Resolved Images of Intramolecular Charge Transfer in Organic Molecules	Photon	Molecule	<a href="#">Fr034</a>
Fernández-Villoria	Francisco	Ultrafast Dynamics in Donor-Acceptor Prototype Molecules by XUV-IR Attosecond Spectroscopy	Photon	Molecule	<a href="#">Mo029</a>
Florin	Naemi	Survival of Interstellar Carbon Knockout Fragments	Heavy	Molecule	<a href="#">Th109</a>
Frederike Schmidt-May	Alice	Mutual neutralization of H <sub>2</sub> <sup>+</sup> with Li <sup>+</sup> , O <sup>+</sup> , N <sup>+</sup> and C <sup>+</sup> at DESIREE	Heavy	Ion	<a href="#">Th117</a>
Fritzsche	Stephan	Modeling and computation of atomic cascades	Heavy	Ion	<a href="#">Fr128</a>
Fritzsche	Stephan	Separation of the inner and outer electrons for two-electron atoms near the critical bound limit	Heavy	Atom	<a href="#">Fr129</a>
Fritzsche	Stephan	A community platform for just atomic computations	Lepton	Atom	<a href="#">Fr130</a>
Fritzsche	Stephan	Nondipole effects in strong-field ionization using few-cycle laser pulse	Photon	Atom	<a href="#">Mo009</a>
Fritzsche	Stephan	Nonsequential double ionization of Ne with elliptically polarized laser pulses	Photon	Atom	<a href="#">Mo010</a>
Fritzsche	Stephan	Accurate molecular ab initio calculations in support of strong-field attosecond physics experiments	Photon	Molecule	<a href="#">Th053</a>
Fritzsche	Stephan	Effect of the Breit interaction on the angular distribution of Auger electrons following electron-impact excitation of Be-like ions	Heavy	Ion	<a href="#">Th054</a>
Fritzsche	Stephan	Linear polarization and angular distribution of the Lyman- $\alpha$ line following electron-impact excitation of H-like ions	Heavy	Ion	<a href="#">Th055</a>
Fritzsche	Stephan	Lorentz-force shifts in strong-field ionization with mid-IR laser fields	Photon	Atom	<a href="#">We007</a>
Fritzsche	Stephan	An atomic magnetometer to detect the oscillating magnetic field based on twisted light atom interaction	Photon	Atom	<a href="#">We008</a>
Fukuzaki	Rihito	Observation of recurrent fluorescence from excited anthracene cations	Heavy	Molecule	<a href="#">We118</a>

Last name	First name	Abstract Title	Abstract Topic (Projectile)	Abstract Topic (Target)	Poster #
Gan	Ziyan	Probing Photoelectron Dynamics by Coulomb-distorted Terahertz Radiation	Photon	Atom	<a href="#">Mo025</a>
Gao	Yong	Experimental study of single electron capture in 150 keV O <sup>5+</sup> + He collisions	Heavy	Ion	<a href="#">We102</a>
Ge	Peipei	Attosecond Delays in Vibrationally Resolved Dissociation of Molecules	N/A	Molecule	<a href="#">We030</a>
Génévriez	Matthieu	The planetary states of the Sr atom	Photon	Atom	<a href="#">Th132</a>
Gervasoni	Juana	Neutron spectra in nuclear hybrid reactors	N/A	Surface	<a href="#">Fr127</a>
Geyer	Angelina	Experimental fingerprint of the electron's longitudinal momentum at the tunnel exit in strong field ionization	Photon	Atom	<a href="#">Th017</a>
Ghosh	Raju	Theoretical investigation of bound and resonant states of imidogen radical NH.	Lepton	Molecule	<a href="#">We083</a>
Gi	Hiroki	First principles simulation of high harmonic generation using quantum computer	Photon	Atom	<a href="#">Fr004</a>
Giovannetti	Gaia	Realtime tracking of ultrafast dynamics in liquid water	Photon	Molecule	<a href="#">Fr056</a>
Gochitashvili	Malkhaz	Excitation processes in collisions of He <sup>+</sup> ions with N <sub>2</sub> , O <sub>2</sub> molecules	N/A	Molecule	<a href="#">Mo099</a>
Gombosuren	Zorigt	DIRECT DETERMINATION OF THE FULLY DIFFERENTIAL CROSS SECTION OF THE IONIZATION BY THE WAVE FUNCTION	N/A	Atom	<a href="#">Mo089</a>
Gomonai	A	The near-threshold electron-impact resonance excitation of the In <sup>+</sup> ion	Lepton	Ion	<a href="#">AF005</a>
Gong	Xiaochun	Attosecond time-resolved photoemission dynamics in atoms and molecules	Photon	Atom	<a href="#">Th004</a>
Gonzalez-Ferez	Rosario	Ultralong-range Rydberg Molecules: Electronic Structure and Rydberg blockade	Lepton	Molecule	<a href="#">Mo107</a>
Gope	Krishnendu	Ultrafast competition between H <sub>2</sub> <sup>+</sup> and H <sub>3</sub> <sup>+</sup> formation via roaming H <sub>2</sub> mechanism	Photon	Molecule	<a href="#">Fr036</a>
Gorczyca	Thomas	Energy variation of double K-shell photoionization of Ne	Photon	Atom	<a href="#">Fr021</a>
Gorczyca	Thomas	Photoionization of Atomic Sodium Near Threshold	Photon	Atom	<a href="#">Mo024</a>
Gorfinkiel	Jimena	Resonances in electron scattering from SO <sub>2</sub>	Lepton	Molecule	<a href="#">Th082</a>
Graves	Vincent	Computed total and partial cross sections for direct electron and positron impact ionisation	Lepton	Molecule	<a href="#">Fr085</a>
Graves	Vincent	R-Matrix investigations of low-energy positron scattering from biomolecules	Lepton	Molecule	<a href="#">We097</a>
Grell	Gilbert	First principle approach to the simulation of attosecond XUV pump XUV probe spectra for small organic molecules	Photon	Molecule	<a href="#">Fr043</a>
Grell	Gilbert	Impact of the XFEL shot-to-shot variation onto soft X-Ray pump-probe studies of attosecond charge migration in molecules	Photon	Molecule	<a href="#">Mo047</a>
Guan	Bowen	Quantification of Pressure-Enhanced Electron-Phonon Coupling in Bi <sub>2</sub> S <sub>3</sub> via Femtosecond Pump-Probe Spectroscopy	No	Yes	<a href="#">We136</a>
Guerrero	Alfonso	Observation of the ions CH <sub>3</sub> <sup>+</sup> , SH <sup>+</sup> , SH <sub>2</sub> <sup>+</sup> and CH <sub>3</sub> S <sup>+</sup> from thiophene and tetrathiophene by laser radiation at 532,355 and 266 nm	Photon	Molecule	<a href="#">Mo043</a>
Guilherme Falkowski	Alan	An iterative negative imaginary potential applied to the Schwinger multichannel method to model ionization effects	Lepton	Molecule	<a href="#">We098</a>
Gumberidze	Alexandre	Towards determination of absolute cross sections for excitation of hydrogen-like uranium in collisions with neutral atoms	Heavy	Atom	<a href="#">Mo091</a>

Last name	First name	Abstract Title	Abstract Topic (Projectile)	Abstract Topic (Target)	Poster #
Guo	Dalong	Two- and three-body dissociations of $C_{3}H_{6}$ isomer dications investigated by 4 keV/u $Ar^{8+}$ impact	Heavy	Molecule	<a href="#">Fr099</a>
Guo	Yipan	Emission of x rays in collisions of xenon ions with metal surfaces	Heavy	Surface	<a href="#">Fr126</a>
Hack	Szabolcs	Diatomic molecular vibrations in a strong infrared laser field: an analytic treatment of the laser-dressed Morse potential	Photon	Molecule	<a href="#">Fr053</a>
Hainge	Joshua	Momentum of Light in an Atom	Photon	Atom	<a href="#">Mo003</a>
Hammond	Tj	Supercontinuum amplification for nonlinear optics	Photon	-Other-	<a href="#">Fr063</a>
Hans	Andreas	The role of non-local processes in the decay of X-ray induced electronic inner-shell vacancies in weakly bound systems	Photon	Cluster	<a href="#">We045</a>
Hansen	Thomas	Doping effects in high-harmonic generation from correlated systems	Photon	-Other-	<a href="#">We058</a>
Hanus	Václav	Nonadiabatic Tunneling of Photoelectrons Induced by Few-Cycle Near-Fields	Photon	-Other-	<a href="#">Fr058</a>
Hanus	Václav	Carrier envelope phase sensitivity of photoelectron circular dichroism	Photon	Molecule	<a href="#">Th046</a>
Harayama	Sakumi	Observation of radiative vibrational cooling of $N_{2}^{+}$ ions using a cryogenic electrostatic ion storage ring: contribution of Fermi resonance	Heavy	Ion	<a href="#">Mo114</a>
Harries	James	A new pulsed superfluid helium droplet machine for experiments at a free-electron laser beamline	Photon	Cluster	<a href="#">Mo033</a>
Harries	James	Direct confirmation of 164-nm-wavelength superfluorescence from a dense sample of helium ions.	Photon	Atom	<a href="#">Th006</a>
Harris	Allison	Probing electron projectile coherence with twisted electron collisions	Lepton	Molecule	<a href="#">Fr087</a>
Harris	Allison	Strong field phenomena with sculpted laser pulses	Photon	Atom	<a href="#">Mo011</a>
Hatada	Keisuke	Dissociation of methanol molecules excited by XFEL studied with molecular frame photoelectron diffraction	Photon	Molecule	<a href="#">We054</a>
He	Lanhai	Attosecond time delay during resonance-enhanced multiphoton ionization of noble gases in strong laser fields	Photon	Atom	<a href="#">We018</a>
Heber	Oded	Molecular ion time-dependent rotational relaxation dynamics probed by photo-electron in an ion trap	Photon	Molecule	<a href="#">Th138</a>
Hedvall	Patrik	Improved method to treat asymptotic non-adiabatic couplings in scattering processes	Heavy	Molecule	<a href="#">Mo110</a>
Hedvall	Patrik	Charge transfer in Sodium Iodide collisions	Heavy	Molecule	<a href="#">Th119</a>
Herrmann	Felix	The CSR-ReMi – A cryogenic in-ring reaction microscope	Heavy	Atom	<a href="#">Mo130</a>
Hill	Christian	CollisionDB: An online repository of plasma collisional data sets	N/A	-Other-	<a href="#">Th143</a>
Hishikawa	Akiyoshi	Orbital effects in laser tunneling ionization of Ar and H <sub>2</sub> studied by electron-ion coincidence momentum imaging	Photon	Atom	<a href="#">Th020</a>
Hofmann	Max	Sub-cycle resolved tunnel ionization of chiral molecules	Photon	Molecule	<a href="#">Fr044</a>
Høgh Albrechtsen	Simon	The primary steps of ion solvation in helium nanodroplets	Photon	Cluster	<a href="#">Fr029</a>
Høj Kristensen	Henrik	Femtosecond timed imaging of rotation and vibration of alkali dimers on the surface of helium nanodroplets	Photon	Molecule	<a href="#">We042</a>
Holenak	Radek	Stopping power of heavy ions under channeling condition	Heavy	Surface	<a href="#">Fr140</a>
Holenak	Radek	A versatile 3D transmission setup for ion-solid interaction studies using keV ion energies at Uppsala University	Heavy	Surface	<a href="#">Fr118</a>
Holzmeier	Fabian	Ionization Dynamics in H <sub>2</sub> by Interference of One- and Two-Photon Pathways employing VUV FEL Pulses	Photon	Molecule	<a href="#">Fr037</a>

Last name	First name	Abstract Title	Abstract Topic (Projectile)	Abstract Topic (Target)	Poster #
Holzmeier	Fabian	Dissociative Photoionization of EUV Lithography Photoresist Models	Photon	Molecule	<a href="#">Th052</a>
Hörnquist	Johan	Theoretical studies of reactive scattering processes involving the H <sub>2</sub> reaction complex	Heavy	Atom	<a href="#">Th116</a>
Hoshino	Masamitsu	VUV photoelectron spectroscopy of vibrationally-excited CO <sub>2</sub> molecules	Photon	Molecule	<a href="#">Th044</a>
Hu	Zhimin	Breit effect on radiative transition rates of highly charged heavy ions	Lepton	Ion	<a href="#">We131</a>
Huang	Zhongkui	Development of particle detectors for electron-ion collision spectroscopy with highly charged ions at the storage ring CSRe	Heavy	Ion	<a href="#">We073</a>
Huck	Saiva	AEGIS Phase II: Upgrading for collinear antihydrogen production	Heavy	Atom	<a href="#">We109</a>
Hui Zhu	Jian	Oscillator strengths and cross sections of the valence-shell excitations of HBr studied by fast electron impact	Lepton	Molecule	<a href="#">Mo079</a>
Hutcheson	Lynda	Core-resonance line-shape analysis of atoms undergoing strong-field ionization	Photon	Ion	<a href="#">Th008</a>
Iacob	Felix	Reactive collisions of electrons with NS <sup>+</sup> cation in interstellar media	Heavy	Molecule	<a href="#">We138</a>
Ibrahim	Heide	The Big, the Small & the Shoulder: Controlling OCS post-ionization Dynamics	Photon	Molecule	<a href="#">Fr039</a>
Iguchi	Arisa	Mid-infrared spectroscopy of aromatic molecular cations in helium nanodroplets	Photon	Ion	<a href="#">Mo120</a>
Iida	Shimpei	Experimental determination of thermal electron detachment rates of C <sub>7</sub> <sup>-</sup>	Photon	Cluster	<a href="#">We052</a>
Ilchen	Markus	Metrology of Attosecond Soft X-ray Pulses at European XFEL	Photon	Atom	<a href="#">Fr047</a>
Indrajith	Suvasthika	Scaling laws for the cooling dynamic of catacondensed PAH cations.	Photon	Molecule	<a href="#">Mo031</a>
Ingólfsson	Oddur	FEBID of [(CH <sub>3</sub> ) <sub>2</sub> AuCl] <sub>2</sub> and its fragmentation through low energy electron in-teraction under single collision conditions.	Lepton	Molecule	<a href="#">Fr083</a>
Ingólfsson	Oddur	Comparison of electron induced reactions of (CH <sub>3</sub> ) <sub>3</sub> AuP(CH <sub>3</sub> ) <sub>3</sub> under single col-lision conditions and its deposition composition in UHV FEBID.	Lepton	Molecule	<a href="#">Th083</a>
Ingólfsson	Oddur	Low energy electron interaction with the potential extreme ultraviolet resist material component 2-(trifluoro-methyl) acrylic acid.	Lepton	Molecule	<a href="#">We094</a>
Isberner	Leonard	First Dielectronic Recombination Measurements at the Cryogenic Storage Ring	Lepton	Ion	<a href="#">We074</a>
Ishikawa	Kenichi	Electron excitation dynamics in silicon irradiated by femtosecond double pulses of different wavelength combination	Photon	-Other-	<a href="#">Mo059</a>
Ismail	Iyas	Unexpected pathway to double-core-hole states in atoms and molecules	Photon	Molecule	<a href="#">We024</a>
Jana	Kamalesh	Ultrafast THz Magnetic Field Generation Using Quantum Interference Control of Semiconductor Currents	Photon	Surface	<a href="#">Mo056</a>
Jeng	Hao	New methods for implementing photon addition with postselection and swift electrons	Photon	-Other-	<a href="#">Fr137</a>
Ji	Xh	Laser-assisted positron-H scattering in reduced quantum mode	Lepton	Atom	<a href="#">Th060</a>
Jiang	Jun	The QED correction of the transition energy of Ne 7 <sup>+</sup> and Ca 17 <sup>+</sup> ions	Photon	Ion	<a href="#">We132</a>
Jolly	Mariette	Upcoming atomic physics studies of ion-ion collisions	Heavy	Ion	<a href="#">Th097</a>



Last name	First name	Abstract Title	Abstract Topic (Projectile)	Abstract Topic (Target)	Poster #
Jun Li	Xian	Low-energy elastic scattering of positrons by helium	Lepton	Atom	<a href="#">Th059</a>
Kahvedzic	Resad	Impact of nondipole corrections on photoelectron rescattering off atomic targets in intense midinfrared laser pulses	Photon	Atom	<a href="#">Fr005</a>
Kalosi	Abel	Dissociative recombination of ArH <sup>+</sup> at the Cryogenic Storage Ring	Lepton	Molecule	<a href="#">Fr097</a>
Kamp	Denise	Dynamical instabilities and macroscopic quantum self-trapping in a rotating Bose-Einstein condensate	N/A	Atom	<a href="#">Th125</a>
Kanaya	Satoru	Development of atomic momentum spectroscopy of polyatomic molecules	Lepton	Molecule	<a href="#">Th077</a>
Kaneyasu	Tatsuo	Tracking Few-Femtosecond Auger Decay by Synchrotron Radiation	Photon	Atom	<a href="#">Th014</a>
Kang	Huipeng	Determination of ionic polarizability by nonsequential double ionization	Photon	Atom	<a href="#">Th001</a>
Kanti	Deeksha	Laser-assisted radiative attachment in short laser pulses	Lepton	Atom	<a href="#">Th070</a>
Kanya	Reika	Observation of THz-wave-assisted electron scattering by Ar atoms	Lepton	Atom	<a href="#">We068</a>
Karls	Julia	Radiative lifetimes in atomic negative ions	Photon	Ion	<a href="#">We129</a>
Kartashov	Daniil	High-order harmonic generation and confinement in artificial atoms	Photon	-Other-	<a href="#">Fr061</a>
Katsoulis	Georgios	Novel semiclassical model for accurate spectra and nondipole effects in multielectron ionization of strongly driven atoms	Lepton	Atom	<a href="#">We027</a>
Kaur	Pardeep	Supersolidity in a quasi-2D spinor Bose-Einstein condensate with SO-coupling	Heavy	-Other-	<a href="#">Mo121</a>
Kelemen	V	Ramsauer-Townsend minima in the low-energy integral cross sections of elastic electron scattering by Sb, Xe and Bi, Rn atoms	Lepton	Atom	<a href="#">AF006</a>
Kelemen	V	High-energy critical minima in differential cross sections of elastic electron scattering by Sb, Xe and Bi, Rn atoms	Lepton	Atom	<a href="#">AF007</a>
Khoma	Mykhaylo	Elastic and charge transfer cross sections for low energy H <sup>+</sup> + H collisions: Quantal and semiclassical calculations	Heavy	Atom	<a href="#">AF008</a>
Kidane	Yitbarek	Laser-assisted reduction of graphene oxide coated on melamine sponge for advanced application in electromagnetic interference shielding	Heavy	Surface	<a href="#">We135</a>
Kiefer	Nils	Strong evidence for neighbor-induced recapture obtained by electron-photon-coincidence spectroscopy	Photon	Cluster	<a href="#">Th030</a>
Kimura	Naoki	Continuous injection of metallic elements into an electron-beam ion trap using an electron-beam evaporator	Heavy	Ion	<a href="#">Fr070</a>
Kimura	Naoki	Hyperfine-induced transition in highly charged Ne-like ions studied with the cryogenic electrostatic ion storage ring RICE	Heavy	Ion	<a href="#">We123</a>
Kino	Yasushi	Recent progress of muon catalyzed fusion study: III. Alternative measurement of nuclear fusion reaction in muonic molecule	Lepton	Molecule	<a href="#">Mo066</a>
Kino	Yasushi	Recent progress of muon catalyzed fusion study: IV. Nuclear reaction processes in the dt molecule	Lepton	Molecule	<a href="#">Mo142</a>
Kircher	Max	Ion and Electron Momentum Distributions from Single and Double Ionization of Helium Induced by Compton Scattering	Photon	Atom	<a href="#">We022</a>
Kirchner	Tom	Classical-trajectory Monte Carlo calculations for ionizing proton-ammonia-molecule collisions: the role of multiple ionization	Heavy	Molecule	<a href="#">Fr101</a>

Last name	First name	Abstract Title	Abstract Topic (Projectile)	Abstract Topic (Target)	Poster #
Knaffo	Stav	Toward a new type of gas phase spectroscopy for complex organic ions	Heavy	Ion	<a href="#">Fr133</a>
Knaffo	Stav	Toward a new type of gas phase spectroscopy for complex organic ions	Photon	Ion	<a href="#">Mo140</a>
Ko	Donghyuk	Time-domain investigation of strong-field recollision to measure recombination time delay	Photon	Atom	<a href="#">Mo017</a>
Kolorenč	Přemysl	Fano-ADC(2,2) method for multi-electron decay processes	Photon	Atom	<a href="#">Mo007</a>
Korobenko	Aleksey	Momentum-resolved dynamics of femtosecond laser ablation with a pump-probe technique	Heavy	Ion	<a href="#">We061</a>
Korolev	Viacheslav	Selective enhancement of even order harmonics in a monolayer TMDC	Photon	-Other-	<a href="#">We056</a>
Kossoski	Fábris	Electronic excitation of benzene by electron impact: a theoretical and experimental investigation	Lepton	Molecule	<a href="#">Mo073</a>
Kotian	Akshit	Single-electron capture and ionisation in He <sup>2+</sup> - H <sub>2</sub> collisions	Heavy	Molecule	<a href="#">Th103</a>
Krishnadas	Anirudh	Comparison of Theoretical Methods to Calculate Electron-Impact Ionization Cross-Sections of Benzene Derivatives	Lepton	Molecule	<a href="#">Fr092</a>
Kübel	Matthias	Late recollisions in dissociative strong-field ionization of D <sub>2</sub>	Photon	Molecule	<a href="#">Mo051</a>
Kumar	Kamal	Development of electrospray ion source and setup for collision induced dissociation experiments of large molecules	N/A	N/A	<a href="#">Mo097</a>
Kumar	Sarvesh	Valence photo double ionization of CH <sub>3</sub> OD: Insights into Molecular Dynamics and Electron Correlation	Photon	Molecule	<a href="#">Th038</a>
Kumar	Kamal	Role of different electron capture mechanisms in fragmentation of CO <sub>2</sub> <sup>3+</sup> into O <sup>+</sup> + C <sup>+</sup> + O <sup>+</sup>	Heavy	Molecule	<a href="#">Th105</a>
Kumar	Akshay	Quantum coherence induced by incoherent free electron scattering	Heavy	Molecule	<a href="#">We088</a>
Küstner-Wetekam	Catmarna	Investigation of Interatomic Coulombic Decay after inner-shell ionization in heterogeneous rare gas clusters by multi-coincidence spectroscopy	Photon	Cluster	<a href="#">Th027</a>
La Mantia	David	Progress on observation of radiative double-electron capture (RDEC) with F <sub>9,8+</sub> on graphene	Heavy	Ion	<a href="#">Fr117</a>
La Mantia	David	Selective field ionization of Rydberg atoms in a room-temperature vapor	Photon	Atom	<a href="#">Mo002</a>
Laforge	Aaron	Time-resolved imaging of an elusive molecular reaction: hydrogen roaming in acetonitrile	Photon	Molecule	<a href="#">Th037</a>
Laforge	Aaron	Time-Resolved Dynamics on the Giant Plasmon Resonance of C <sub>60</sub>	Photon	Cluster	<a href="#">We034</a>
Lai	Xuanyang	Revealing the wave-function-dependent zeptosecond birth time delay in molecular photoionization	Photon	Molecule	<a href="#">Fr033</a>
Larouze	Alexandre	Alpha particle transport modeling in a biological environment with TILDA-V	Heavy	Molecule	<a href="#">Fr102</a>
Laurent	Guillaume	Tailoring the spectral phase of attosecond pulse trains generated by intense, femtosecond, two-color fields	Photon	Atom	<a href="#">Fr011</a>
Laurent	Guillaume	Complete reconstruction of an electron wavepacket generated by absorption of an attosecond pulse	Photon	Atom	<a href="#">Mo016</a>
Lei	Jianting	Asymmetry parameters in single ionization of Ne by XUV pulse	Photon	Atom	<a href="#">Th024</a>
Lemell	Christoph	Theory of molecular photoionization time delays	Photon	Molecule	<a href="#">Fr035</a>
Lemell	Christoph	Attosecond chronoscopy of the photoemission of a layered system	Photon	Surface	<a href="#">Mo054</a>

Last name	First name	Abstract Title	Abstract Topic (Projectile)	Abstract Topic (Target)	Poster #
Lemieux	Samuel	The spectrum of the vacuum as a primary reference for radiometry	Photon	-Other-	<a href="#">Fr136</a>
Leon M Petersson	C	Relativistic calculations of electron--parent ion entanglement using the KRAKEN protocol	Photon	Atom	<a href="#">Th012</a>
Li	Zhou	Quantitative broadband coherent anti-Stokes Raman scattering microscopy based on a simple laser source	Photon	Molecule	<a href="#">Mo053</a>
Li	Xuefeng	Internal collision double ionization of Ar driven by co-rotating two-color circularly polarized laser fields.	Photon	Atom	<a href="#">Th003</a>
Li	Xiaokai	Coulomb focusing in attosecond angular streaking measurement of strong field tunneling ionization	Photon	Atom	<a href="#">Th021</a>
Lin	Jingquan	Visualization of ultrafast plasmon by nonlinear multi-photon photoemission electron microscopy	Photon	Surface	<a href="#">Mo060</a>
Lin	Kang	Time-resolved Kapitza-Dirac effect	Photon	Atom	<a href="#">We009</a>
Lin	Kaizhao	Three-body fragmentation dynamics of cyclopropane induced by high-energy ion collisions	Heavy	Molecule	<a href="#">We112</a>
Lindroth	Eva	Extended RPAE method for cross sections and delays	Photon	Atom	<a href="#">Fr019</a>
Linek	Adam	AEgIS: Synthesis of mid-heavy antiprotonic atoms at CERN	Heavy	Atom	<a href="#">Th087</a>
Lino	Jorge	Scaled Born approximation for electron impact excitations of N <sub>2</sub> molecule	N/A	Molecule	<a href="#">Mo074</a>
Litvinyuk	Igor	Attosecond delays of high harmonic emissions from isotopes of molecular hydrogen measured by Gouy phase XUV interferometer	Photon	Molecule	<a href="#">We051</a>
Liu	Kunlong	Spin-polarized electron vortices generated in single-photon ionization of atoms	Photon	Atom	<a href="#">Fr016</a>
Liu	Aihua	Resonance-Enhanced Electron Capture in the Laser-Assisted Proton-Hydrogen Collision	Photon	Atom	<a href="#">Mo096</a>
Liu	Jialin	Precise determinations of the energy of the 4s24p 2P <sub>3/2</sub> -2P <sub>1/2</sub> transition and the lifetime of the 4s24p 2P <sub>3/2</sub> level in Ga-like Mo <sup>11+</sup>	Lepton	Ion	<a href="#">We124</a>
Liu	Xin	Precision Measurements of the 2P <sub>1/2</sub> -2P <sub>3/2</sub> fine-structure splitting in B-like S <sup>11+</sup> and Cl <sup>12+</sup> at SH-HtscEBIT	Photon	Ion	<a href="#">We125</a>
Lochmann	Christine	Cold collisions of atomic and molecular hydrogen with astrochemically relevant anions	Heavy	Ion	<a href="#">Th114</a>
Lu	Xuanhui	Observation of Sequential Tunneling in Driven Optical Lattices	N/A	Atom	<a href="#">Th126</a>
Luo	Xuan	Enhancement and Suppression of Nonsequential Double Ionization by Spatially Inhomogeneous Field	Photon	Atom	<a href="#">Th002</a>
Lushchikova	Olga	CO <sub>2</sub> activation by Cu clusters in superfluid helium nano-droplets	Heavy	Cluster	<a href="#">Mo118</a>
M	Salvi	Absolute photodetachment cross-section of deprotonated indole using a 16-pole ion trap	Photon	Ion	<a href="#">Mo050</a>
Ma	Lili	Theoretical investigation of electron-impact ionization of W <sup>6+</sup> ion	Heavy	Ion	<a href="#">We070</a>
Ma	Wanlu	The state-resolved integral cross sections for atomic krypton studied by fast electron scattering	Heavy	Atom	<a href="#">We072</a>
Ma	Pufang	Measurements of Absolute Electron Capture Cross Sections in He <sup>2+</sup> - He and Ne <sup>8+</sup> - O <sub>2</sub> Collisions	Heavy	Molecule	<a href="#">We114</a>
Maclot	Sylvain	Mass spectrometry at the limits of biological objects: viruses, bacteria and amyloid fibers	Photon	Molecule	<a href="#">Fr049</a>
Magunia	Alexander	Time-resolving molecular tunneling dynamics with Free-Electron-Laser-pump and High-Harmonics-Generated-probe transient absorption spectroscopy	Photon	Molecule	<a href="#">We040</a>

Last name	First name	Abstract Title	Abstract Topic (Projectile)	Abstract Topic (Target)	Poster #
Mairesse	Yann	Laser-induced electron diffraction in chiral molecules	Lepton	Molecule	<a href="#">We029</a>
Majczak	Mateusz	Carrier-envelope-phase and helicity control of electron vortices and spirals in photodetachment	Photon	Ion	<a href="#">Th009</a>
Majima	Takuya	Fast heavy-ion-induced anion–molecule reactions on the droplet surface	Heavy	Surface	<a href="#">Fr114</a>
Major	Balazs	Analytical Guidelines to Choose the Right Pressure Profile for High-harmonic Generation in Gas Targets	Photon	Atom	<a href="#">Mo020</a>
Mandal	Aditi	MsSpec-DFM (Dielectric function module): Towards a multiple scattering approach to plasmon description	Photon	Surface	<a href="#">Mo057</a>
Manson	Steven	Angular Distributions of Attosecond Time Delay in the Photoionization of ns Subshells of Atomic Systems: Relativistic and Nondipole Effects	Photon	Atom	<a href="#">Fr023</a>
Manson	Steven	Relativistic and correlation effects in np photoionization Cooper minima of high-Z atoms	Photon	Atom	<a href="#">We002</a>
Marante	Carlos	Photoionization of polyatomic molecules with ASTRA: a scalable wave-function approach	Photon	Molecule	<a href="#">We048</a>
Marcel Ngoko Djiokap	Jean	Multiphoton ionization and detachment of atoms and negative ions: A tribute to Anthony F. Starace	Photon	Atom	<a href="#">AF012</a>
Marcus	Gilad	Polarization Dependence of Laser Induced recollision and inner-shell excitations	Lepton	Atom	<a href="#">We025</a>
Marder	Lutz	Competition of photon and electron emission in the decay of doubly ionized ArKr clusters	Photon	Cluster	<a href="#">Th035</a>
Maria Mootheril Thomas	Deepthy	Signatures of ICD from heterocycle dimers and heterocycle-water complexes	Lepton	Cluster	<a href="#">We095</a>
Martini	Paul	A versatile ion source for cold ions using superfluid helium nanodroplets	N/A	Cluster	<a href="#">Mo119</a>
Márton	István	Study of the effect of higher-order dispersions on photoionisation induced by ultrafast laser pulses	Photon	Atom	<a href="#">Fr012</a>
Márton	István	Angular distribution and energy spectra of photoelectrons from tetrahydrofuran illuminated by VUV photon source	Photon	Molecule	<a href="#">Mo039</a>
Maruyama	Haruka	Spin-dependent metastable He (23S) atom scattering from Fe3O4(100) surfaces	Heavy	Surface	<a href="#">Fr116</a>
Mayro Tanyag	Rico	X-ray imaging of nanostructures in superfluid helium droplets	Heavy	Cluster	<a href="#">Mo117</a>
Mayro Tanyag	Rico	NIR-induced fragmentation of VUV-generated molecular cations	Photon	Molecule	<a href="#">We047</a>
Maxwell	Andrew	Ultrafast Imaging of Molecular Chirality with Photoelectron Vortices	Photon	Atom	<a href="#">Th135</a>
Meng	Tianming	Measurements of the single and double electron capture cross sections in O6+ + He collisions	Heavy	Atom	<a href="#">We103</a>
Meyer	Michael	Circular Dichroism in Multiphoton Ionization of Resonantly Excited Helium Ions near Channel Closing	Photon	Atom	<a href="#">Mo014</a>
Mezei	Zsolt	Novel results for the electron-impact recombination and excitation of molecular cations: the role of the core-excited bound resonances	Lepton	Ion	<a href="#">Fr096</a>
Mi	Yonghao	Observation of H3+ formation from molecular hydrogen dimers	Photon	Molecule	<a href="#">Fr050</a>
Mihelic	Andrej	Multiphoton ionization cross sections and photoelectron angular distributions of the helium atom	Photon	Atom	<a href="#">Th007</a>
Modak	Paresh	Geometry dependence of photoionization asymmetry parameter of CH3I	Photon	Molecule	<a href="#">Th137</a>
Mokhtari	Saadat	Characterizing high harmonics using frequency resolved optical switching	Photon	Surface	<a href="#">Mo062</a>

Last name	First name	Abstract Title	Abstract Topic (Projectile)	Abstract Topic (Target)	Poster #
Moreira	Giseli	Low-energy positron collisions with tetrachloroethylene (C <sub>2</sub> Cl <sub>4</sub> ) molecule	Lepton	Molecule	<a href="#">Mo071</a>
Mori	Nicolas	Convergent close-coupling calculations of positron scattering from carbon	Lepton	Atom	<a href="#">Th058</a>
Mori	Nicolas	Convergent close-coupling calculations of positron scattering from atomic oxygen	Lepton	Atom	<a href="#">We080</a>
Morini	Filippo	A study of the valence photoelectron spectrum of uracil and mixed water-uracil clusters.	Photon	Cluster	<a href="#">We041</a>
Mukherjee	Jibak	State selective electron capture study with NO <sub>2</sub> <sup>+</sup> using Cold Target Recoil Ion Momentum Spectroscopy	Heavy	-Other-	<a href="#">We110</a>
Naduvath	Balakrishnan	Stereodynamical control of cold collisions between two aligned D <sub>2</sub> molecules	Heavy	Molecule	<a href="#">Mo109</a>
Nagase	Kenta	Suppression of three-body loss near a p-wave Feshbach resonance in a quasi-1D ultracold fermionic system	N/A	Atom	<a href="#">Th140</a>
Nakano	Yuji	Far-ultraviolet (FUV) emission from laser-produced plasma of Al, Fe, Cu and Inconel	Photon	Surface	<a href="#">Mo064</a>
Nakao	Tomohiko	Lifetime measurement of collision-induced delayed fragmentation from singly charged intermediate ions	Heavy	Molecule	<a href="#">Th107</a>
Namangalam	Uma	Characterization of collision-induced dissociation of deprotonated dAMP in an ion funnel	Heavy	Ion	<a href="#">Fr105</a>
Nandi	Saikat	Isotope labelling as a tool for atto-chemistry	Photon	Molecule	<a href="#">Th036</a>
Nandi	Dhananjay	Velocity slice imaging probed for kinematically complete measurements of dissociative electron attachment to OCS molecule	Lepton	Molecule	<a href="#">Th079</a>
Nanos	Stefanos	Cusp-electron production in collisions of open-shell O <sub>6</sub> <sup>+</sup> (1s <sub>2</sub> s) ions with He	Heavy	Ion	<a href="#">Th139</a>
Narendra Shah	Ronak	Direct measurement of few-cycle electric fields using a lock-in detection	Photon	N/A	<a href="#">Mo127</a>
Nauta	Janko	Ultra-high precision laser spectroscopy of anti-hydrogen	Photon	Atom	<a href="#">We127</a>
Navarro Navarrete	José Eduardo	Precise measurement of the electron affinity of C <sub>60</sub>	Photon	Molecule	<a href="#">Th141</a>
Neha	Neha	Laser-assisted ionization of atomic hydrogen by the impact of an electron vortex beam	N/A	Atom	<a href="#">Fr079</a>
Newson	Donovan	Secondary electron emission & detection of low-energy charged particles impacting channel electron multipliers	Lepton	Surface	<a href="#">Mo082</a>
Newson	Donovan	Low-energy total cross-sections of positronium scattering from the inert atoms	Lepton	Atom	<a href="#">Th061</a>
Newson	Donovan	Differential positronium-formation cross-sections around zero degrees from atoms and molecules	Lepton	Atom	<a href="#">We081</a>
Niggas	Anna	A numerical approach to the deexcitation of a hollow atom	Heavy	Surface	<a href="#">Fr139</a>
Niikura	Hiromichi	Visualization of a complex electron wavefunction in momentum space using an attosecond pulse	Photon	Atom	<a href="#">We012</a>
Noor	Atia	Ionization dynamics of CO <sub>2</sub> in intense XUV and strong IR pump/probe at REMI end station FLASH2	Photon	Molecule	<a href="#">Th136</a>
Odagiri	Takeshi	Singlet/triplet branching ratios in core-valence double photoionization of neon	Photon	Atom	<a href="#">Fr024</a>
Okada	Kunihiro	A new approach for measuring the reaction rates of low-energy ion--polar-molecule reactions for astrochemistry	Heavy	Molecule	<a href="#">Mo113</a>
Olsson	Emelie	Double ionization of S <sub>2</sub>	Photon	Molecule	<a href="#">We037</a>
Omar Segovia Guzman	Miguel	XUV absorption spectroscopy of Ti-doped iron oxide	Photon	-Other-	<a href="#">We063</a>



Last name	First name	Abstract Title	Abstract Topic (Projectile)	Abstract Topic (Target)	Poster #
Onitsuka	Yuuki	Development of a new molecular spectroscopy technique: mapping atomic motions and elemental composition analysis of a molecule	Lepton	Molecule	<a href="#">Th078</a>
Orel	Ann	Theoretical Studies of Mutual Neutralization	Heavy	Ion	<a href="#">Th115</a>
Orimo	Yuki	Real-time first-principles simulations of molecules in intense laser fields using the erf-gau potential	Photon	Molecule	<a href="#">Mo049</a>
Orimo	Yuki	First-principles simulations of multielectron dynamics in strong laser pulses using the hardware-efficient ansatz on quantum computers	Photon	Atom	<a href="#">Th011</a>
Osaku	Chihiro	Exploring Electron-Nuclear Entangled Dynamics in Hydrogen Molecular Ions using Quantum Computer	Photon	Ion	<a href="#">We049</a>
Ott	Christian	Measuring the photoelectron angular distribution after nonlinear interaction of two photons with two active electrons in helium	Photon	Atom	<a href="#">Fr017</a>
P	Madhusudhan	Intensity variation of N <sub>2</sub> and CO in the presence of two-color ultrafast pulses.	Photon	Molecule	<a href="#">Th134</a>
Pagowska	Karolina	Investigation of the evolution of defect in Si ion implanted GaN after UHPA by means of RBS/channeling and HR-XRD methods	N/A	Ion	<a href="#">Fr125</a>
Pajek	Marek	Clocking ultrafast relaxation of Rydberg hollow atoms at surfaces by x-rays	Heavy	Surface	<a href="#">Fr121</a>
Pajek	Marek	X-ray studies of atomic processes in the EBIT plasma	Lepton	Ion	<a href="#">We067</a>
Pan	Shengzhe	An ultrafast stopwatch to clock and manipulate molecular dynamics	Photon	Molecule	<a href="#">Th039</a>
Pandey	Alpana	Electron and Positron impact ionisation of few biologically relevant molecules for coplanar and perpendicular plane emission of electrons	Lepton	Molecule	<a href="#">Mo072</a>
Parambath Safvan	Cholakka	Measurements of subrotational lifetimes of molecular ions: a new experimental technique	Heavy	Molecule	<a href="#">We113</a>
Park	Jaesung	The development of marking system of secondary battery anode and cathode using nanosecond laser with in situ tracking module	N/A	-Other-	<a href="#">Mo136</a>
Park	Jongwook	Development of Polymer Dispersed Liquid Crystal (PDLC)-based switchable spatial filter using femtosecond laser micro-patterning	Photon	-Other-	<a href="#">Mo137</a>
Park	Yeunsoo	Effects and data of electron collisions on various molecules for medical applications	N/A	Molecule	<a href="#">Mo080</a>
Paul	Raka	Mutual Neutralization in sub-eV C <sub>60</sub> <sup>+</sup> + C <sub>60</sub> <sup>-</sup> collisions	Heavy	Molecule	<a href="#">Mo115</a>
Pelimanni	Eetu	Resonant Double-Core Excitation of N <sub>2</sub>	Photon	Molecule	<a href="#">Fr046</a>
Peralta	Jesica	Stopping power in lanthanides, from Ce to Lu	Heavy	Atom	<a href="#">We106</a>
Pfäfflein	Philip	Precision X-Ray Spectroscopy of He-like Uranium employing Metallic Magnetic Calorimeter Detectors	Heavy	-Other-	<a href="#">Fr134</a>
Phelps	Zane	Investigating the UV-Induced Dynamics of Methylated Cyclopentadiene with XUV Photoelectron Spectroscopy at FLASH	Photon	Molecule	<a href="#">Th032</a>
Pier	Andreas	Chiral photoelectron angular distributions from ionization of achiral atomic and molecular species	Photon	Molecule	<a href="#">Fr038</a>
Pihlava	Lassi	Photodissociation of halogen-substituted nitroimidazole radiosensitizers – A pathway towards new radiosensitizer drugs?	Photon	Molecule	<a href="#">We036</a>
Pinheiro	Joel	XPS Study in situ of the Diluted Perovskite Nanocrystals Surface's Stability Stoichiometry	Photon	Surface	<a href="#">We065</a>

Last name	First name	Abstract Title	Abstract Topic (Projectile)	Abstract Topic (Target)	Poster #
Piwinski	Mariusz	Helical structures of alignment angle function in the electron-atom collision studies	Photon	Atom	<a href="#">Fr080</a>
Plowman	Corey	Differential ionisation in proton collisions with molecular hydrogen	Heavy	Molecule	<a href="#">Th104</a>
Powell	Jeffrey	Generating Ultrafast MeV Electrons with a mJ-class Laser	Photon	Atom	<a href="#">Mo001</a>
Purschke	David	High-order wavemixing during high-harmonic generation in solids	Photon	Surface	<a href="#">We060</a>
Quan	Wei	Ultrafast excitation dynamics for noble gas atoms subject to intense femtosecond laser fields	Photon	Atom	<a href="#">We011</a>
Rajput	Jyoti	Dissociation pathways of methane dication	Heavy	Molecule	<a href="#">Th099</a>
Rangan	Chitra	A theoretical model of depolarized scattering in molecular clusters	Photon	Cluster	<a href="#">We055</a>
Reich	Bianca	The ARTEMIS experiment: Towards high precision g-factor measurements on highly charged ions	Photon	Ion	<a href="#">Fr131</a>
Ren	Xueguang	Triple ionization and fragmentation of benzene trimers following ultrafast intermolecular Coulombic decay	Lepton	Cluster	<a href="#">Fr084</a>
Ren	Xueguang	Triple-differential cross sections in three-dimensional kinematics for electron-impact-ionization dynamics of tetrahydrofuran at 250-eV	Lepton	Molecule	<a href="#">Mo067</a>
Ren	Xueguang	Observation of ultrafast proton and energy transfer in hydrated pyrrole dimers induced by electron impact	Lepton	Cluster	<a href="#">Th076</a>
Ren	Xueguang	Cold-target electron-ion-coincidence momentum-spectroscopy study of electron-impact single and double ionization of N <sub>2</sub> and O <sub>2</sub> molecules	Lepton	Molecule	<a href="#">We089</a>
Ren	Baihui	Isomerized dissociation dynamics of hydrocarbon dications induced by slow highly charged ion impact	Heavy	Molecule	<a href="#">We111</a>
Ringleb	Stefan	Efficiency enhancement of the dynamical capture of ion bunches by instantaneous ion-mode coupling	N/A	Ion	<a href="#">Mo095</a>
Rivera Dean	Javier	Non-classical properties of light after strong-laser field processes in atomic and solid-state systems	Photon	Atom	<a href="#">We005</a>
Rogers	Joshua	Low to intermediate energy (e,2e) measurements from Krypton in the perpendicular plane	Lepton	Atom	<a href="#">Fr082</a>
Rogers	Joshua	Progress on a new toroidal spectrometer to measure multiple-path interference from Rb excited and ionized by laser radiation	Photon	Atom	<a href="#">We023</a>
Roman	Viktoria	Ionization of outer shells in the K atom by electron impact	Lepton	Atom	<a href="#">AF009</a>
Romans	Kevin	Photoionization of Rydberg atoms out of an optical dipole trap	Photon	Atom	<a href="#">Mo023</a>
Roy Chowdhury	Madhusree	Photoionization dynamics of cyano substituted PAHs in the Vacuum-Ultraviolet range	Photon	Molecule	<a href="#">Th040</a>
Ruan	Shushu	Magneto-optical trap reaction microscope for strontium atoms	Photon	Atom	<a href="#">Th112</a>
Ruivo	Julio	Photoionization and Resonance Formation in Formic Acid Monomer and Dimer	Photon	Molecule	<a href="#">Mo038</a>
S	Muthuamirthambal	Exploration of VUV photodissociation of aniline as a source of astronomically important HC <sub>2</sub> N	Photon	Molecule	<a href="#">Fr040</a>
S	Suriyaprasanth	Electron impact ionization cross sections of tyrosine	Lepton	Molecule	<a href="#">Fr093</a>
Sa'adeh	Hanan	Fragmentation of methanol molecules after valence photoexcitation studied by negative-ion positive-ion coincidence spectroscopy	Photon	Molecule	<a href="#">Fr054</a>
Sa'adeh	Hanan	Towards understanding the electronic structure of essential medicines: a photoemission study of aspirin, paracetamol, and ibuprofen in the gas phase	Photon	Molecule	<a href="#">Mo026</a>

Last name	First name	Abstract Title	Abstract Topic (Projectile)	Abstract Topic (Target)	Poster #
Sahoo	Aloka	Electron impact excitation of Na-like Ar7+, Kr25+ and Xe43+	Lepton	Ion	<a href="#">Th064</a>
Sánchez	Rodolfo	Observation of the hyperfine transition in hydrogen-like 208Bi82+	Heavy	Ion	<a href="#">We122</a>
Sang	Robert	Carrier-Envelope-Phase Effects for Multiphoton and Tunnel Excitation of Ar-gon	Photon	Atom	<a href="#">We017</a>
Sato	Takeshi	Time-dependent multicomponent optimized coupled-cluster method for nonadiabatic electro-nuclear dynamics	Photon	Molecule	<a href="#">Mo052</a>
Savin	Daniel	Merged-beams reactive scattering studies of N2 + D3 <sup>+</sup> → N2D <sup>+</sup> + D2	Heavy	Molecule	<a href="#">We116</a>
Scarlett	Liam	Convergent close-coupling calculations of electrons scattering on HeH <sup>+</sup>	Lepton	Molecule	<a href="#">Fr086</a>
Scarlett	Liam	Elastic scattering and rotational excitation of H2 by electron impact: Convergent close-coupling calculations	Lepton	Molecule	<a href="#">Th081</a>
Schippers	Stefan	Commissioning of a new energy-scan system for electron-impact ionization experiments and first results for La1+	Lepton	Ion	<a href="#">Fr067</a>
Schippers	Stefan	High-resolution dielectronic recombination of Pb78+ ions at the ultra-cold electron cooler of the CRYRING@ESR storage ring	Lepton	Ion	<a href="#">Fr068</a>
Schippers	Stefan	ErUM-FSP APPA: BMBF Collaborative Research Center at FAIR	N/A	Ion	<a href="#">Mo132</a>
Schippers	Stefan	K-shell photodetachment of carbon, oxygen, and silicon anions	Photon	Ion	<a href="#">Th025</a>
Schippers	Stefan	Vibrationally resolved inner-shell photoexcitation of the molecular anion C2 <sup>-</sup>	Photon	Ion	<a href="#">Th026</a>
Schippers	Stefan	Inner-shell ionization of low-charged silicon and iron ions	Photon	Ion	<a href="#">We001</a>
Schlathölter	Thomas	Gas-phase collision studies as a tool to investigate molecular mechanisms underlying radiation damage	Heavy	Molecule	<a href="#">Fr104</a>
Schlathölter	Thomas	A travelling-wave ion-mobility system for preparation of conformationally pure molecular targets for collision experiments	N/A	Molecule	<a href="#">Mo101</a>
Schneider	Barry	AMOS Gateway: A Portal for Research and Education in Atomic, Molecular, and Optical Science	Lepton	Molecule	<a href="#">Fr098</a>
Schöffler	Markus	Development of an universal in-ring COLTRIMS Reaction Microscope for CRYRING@ESR	Heavy	Atom	<a href="#">Mo134</a>
Schulz	Michael	Fully Differential Study of Non-PCI Higher-Order Contributions to Ionization of Helium by Proton Impact	Heavy	Atom	<a href="#">Th093</a>
Schulz	Michael	Fully Differential Study of Dissociative Capture in p + H2 Collisions	Heavy	Molecule	<a href="#">We117</a>
Segui	Silvina	Oscillator model applied to calculations of energy loss in anisotropic 2D materials	Lepton	Surface	<a href="#">Mo081</a>
Segui	Silvina	L- and M-subshell ionization cross sections of heavy atoms	N/A	Atom	<a href="#">We140</a>
Segui	Silvina	M $\beta$ photon self-attenuation across the M5 edge for elements with $70 \leq Z \leq 80$	Lepton	Atom	<a href="#">Th067</a>
Sen	Arnab	Imaging the nuclear wavepacket dynamics of multiply charged Ar2 using a two-color laser field	Photon	Molecule	<a href="#">Th045</a>
Sen	Sanket	Camphor: Dynamics post C 1s ionisation and interaction with shaped laser pulses	Photon	Molecule	<a href="#">Th050</a>
Shah	Ronak	Table-top setup for independent phase and timing control of XUV pulse pairs	Photon	Atom	<a href="#">Th133</a>
Shan	Xu	Absolute Electron Impact Ionization Cross Sections of Carbon Dioxide	Lepton	Molecule	<a href="#">Fr090</a>

Last name	First name	Abstract Title	Abstract Topic (Projectile)	Abstract Topic (Target)	Poster #
Shao	Caojie	Target atomic number dependence of the electron capture and excitation process for the relativistic hydrogen-like Cs ions	Heavy	Ion	<a href="#">Th090</a>
Sharma	Lalita	Electron impact excitation of Ar-like Kr XIX	Lepton	Ion	<a href="#">Th065</a>
Sharma	Deepak	Ion-ion collision-induced longitudinal emittance preservation in RF bunching of ions in an electrostatic ion beam trap	Heavy	Ion	<a href="#">We108</a>
Shi	Hongyu	Streaked angle-resolved shake-up photoemission from He	Photon	Atom	<a href="#">Mo013</a>
Shinpaugh	Jefferson	Fast-ion induced electron emission from nano-structured gold: applications as a radiosensitizer for cancer cell killing in hadron therapy	Heavy	Surface	<a href="#">Fr138</a>
Sigaud	Lucas	Isotopic selectivity in the metastable dication production of benzene	Lepton	Molecule	<a href="#">We092</a>
Sihan	Long	Combining momentum-space wavefunctions and frontier orbital theory for providing predictive insights into pharmacological activity	N/A	Molecule	<a href="#">Mo105</a>
Singh	Jasmeet	R-matrix calculation of electron collisions with interhalogen compounds	Lepton	Molecule	<a href="#">Fr091</a>
Singh	Balwinder	M X-ray Production Cross-Sections in Yb Induced by Nitrogen Ions	N/A	Atom	<a href="#">Mo092</a>
Singor	Adam	Photoionisation, Rayleigh, and Raman scattering cross sections for the ground and excited vibrational levels of H <sub>2</sub> <sup>+</sup>	Photon	Molecule	<a href="#">We050</a>
Sinha	Surbhi	H assisted Shape Resonance in Negative ion formation of Acetaldehyde	Lepton	Molecule	<a href="#">We139</a>
Sinha	Surbhi	Dynamics of Dissociative Electron Attachment to Acetylacetone	Lepton	Molecule	<a href="#">Th085</a>
Smolyanskiy	Vladimir	Features of the grazing interaction of microfocal bremsstrahlung with the surface edge	Photon	-Other-	<a href="#">Mo055</a>
Sokell	Emma	In memoriam of past ICPEAC chairs and stalwarts	N/A	N/A	<a href="#">AF013</a>
Sommerlad	Laura	PCI effects following 2p double ionization of argon atoms	Photon	Atom	<a href="#">We014</a>
Spicer	Kade	Energy and angular distributions of electrons produced in intermediate-energy proton-helium collisions	Heavy	Atom	<a href="#">Th094</a>
Stallkamp	Nils	The (only) way towards low-energy, heavy, highly charged ions: the HITRAP deceleration facility	Heavy	Ion	<a href="#">Mo131</a>
Stenquist	Axel	Gauge-invariant absorption of light by coherent superposition states	Photon	Atom	<a href="#">We015</a>
Steydli	Sebastien	Effect of the accelerator-related materials preparation on the ion stimulated desorption yield	Heavy	Surface	<a href="#">Fr123</a>
Su	Maogen	Application of LIBS spectral data fusion in quantitative analysis of Astragalus	Photon	Atom	<a href="#">Fr064</a>
Su	Maogen	Experimental and theoretical study on the extreme ultraviolet radiation behavior of laser-produced Al-Sn alloy plasmas	Photon	Atom	<a href="#">Fr065</a>
Su	Maogen	Analysis of 4p-5s spectral characteristics in laser-produced Ag plasmas in the EUV region	Photon	Atom	<a href="#">Fr066</a>
Sullivan	James	Measurements of positron and electron scattering from biomolecules	Lepton	Molecule	<a href="#">Th072</a>
Sultanov	Renat	Low-energy collisions between two indistinguishable tritium-bearing hydrogen molecules: HT+HT and DT+DT	Heavy	Molecule	<a href="#">Mo111</a>
Sun	Qiang	Valence-shell electronic excitations of nitrogen dioxide studied by fast electron scattering	Lepton	Molecule	<a href="#">Fr088</a>
Suster	Mihai	Nondipole study of backward emission of electrons in ionization driven by high-frequency laser pulses	Photon	Atom	<a href="#">Mo018</a>

Last name	First name	Abstract Title	Abstract Topic (Projectile)	Abstract Topic (Target)	Poster #
Swami	Deepak	Study of charge state distribution for Si projectile with carbon target	Heavy	Ion	<a href="#">Fr113</a>
Tachikawa	Masanori	Quantum Monte Carlo study on positron binding to atomic anion dimers	Lepton	Molecule	<a href="#">Th073</a>
Tahouri	Rezvan	Relativistic treatment of hole alignment due to autoionization processes and Cooper minima in noble gas atoms	Photon	Atom	<a href="#">Th022</a>
Takaya	Kazunari	A real-time gas monitoring system based on ion mobility spectrometry for high concentration	Heavy	Ion	<a href="#">Mo133</a>
Tamura	Yoshiaki	Higher multipolar terms on core-level photoemission time delay of homonuclear diatomic molecules	Photon	Molecule	<a href="#">We053</a>
Tanaka	Takumi	Development of microwave system for a high-precision Lamb shift spectroscopy of antihydrogen atoms	Heavy	Atom	<a href="#">We128</a>
Tan	Joseph	Development of portable Electron Beam Ion Traps at NIST	Lepton	Ion	<a href="#">Mo139</a>
Tan	Joseph	X-ray spectra of highly charged Nd in an EBIT plasma: line identifications and effect of metastable states on ionization balance	Lepton	Ion	<a href="#">Th142</a>
Tani	Mizuki	Theory for ionization rate of dielectrics in two-color strong laser fields	Photon	-Other-	<a href="#">We062</a>
Tarrant	James	Formation of Breathing Ions via Coherent Shake-Up	Photon	Atom	<a href="#">Mo048</a>
Tayal	Vikas	Fine-structure energy levels, oscillator strengths and lifetimes in chromium	N/A	Atom	<a href="#">We141</a>
Thumm	Uwe	Enhanced cutoff energies in strong-field photoelectron emission of plasmonic nanoparticles	Photon	-Other-	<a href="#">Fr057</a>
Thumm	Uwe	Strong-field-driven dissociation dynamics in CO <sub>2</sub> <sup>+</sup>	Photon	Molecule	<a href="#">Mo041</a>
Thümmeler	Martin	Modelling high-harmonic generation in quantum dots using a tight-binding approach	Photon	Surface	<a href="#">We059</a>
Tian	Kaili	Waterloo/ ALLS Reaction Microscope Cold Target Recoil Ion Momentum Spectrometer Endstation	Photon	Molecule	<a href="#">Mo123</a>
Tokesi	Karoly	Effect of vanadium implantation on the structure of glassy carbon	Photon	Surface	<a href="#">Fr110</a>
Tokesi	Karoly	Determination of Electron Inelastic Mean Free Path and Stopping Power of Hafnium Dioxide	Lepton	Surface	<a href="#">Mo083</a>
Tokesi	Karoly	Energy Loss Function of Samarium determined from the reflection electron energy loss spectroscopy spectra	Lepton	Surface	<a href="#">Mo084</a>
Tokesi	Karoly	Classical description of the ionization of carbon by electron impact	Lepton	Atom	<a href="#">Th056</a>
Tokesi	Karoly	Impact Parameter and Kinematic Information for Differential Ionization of Argon by 1 keV Positrons and Electrons	Lepton	Atom	<a href="#">Th057</a>
Tokesi	Karoly	Interaction of Singly Charged Sodium Ion with Nitrogen Atom: Total and Differential Ionisation Cross Sections	Heavy	Atom	<a href="#">We100</a>
Tokesi	Karoly	Interaction of Protons with Noble Gas Atoms: Total and Differential Ionisation Cross Sections	Heavy	Atom	<a href="#">We101</a>
Tomio	Lauro	Two-Dimensional Turbulence in dipolar Bose-Einstein condensate	Heavy	Atom	<a href="#">Th127</a>
Tong	Xiaomin	Electronic K x rays emitted from muonic atoms: an application of density functional theory	Heavy	Atom	<a href="#">Th128</a>
Toyama	Yuichi	Recent progress of muon catalyzed fusion study II) new muonic x-ray spectroscopy	Lepton	Molecule	<a href="#">We133</a>
Trabert	Daniel	Nonadiabatic Strong Field Ionization of Atomic Hydrogen	Photon	Atom	<a href="#">Mo008</a>
Trassinelli	Martino	Detecting sample surface magnetism with highly charged ions	Heavy	Surface	<a href="#">Fr120</a>



Last name	First name	Abstract Title	Abstract Topic (Projectile)	Abstract Topic (Target)	Poster #
Tribedi	Lokesh	Ionization of oxygen in collisions with 2.5-MeV/u Si <sup>12+</sup> ions	Heavy	Molecule	<a href="#">Fr100</a>
Tribedi	Lokesh	Giant quadrupole plasmon resonance in C <sub>60</sub> in high perturbation collisions	Heavy	Molecule	<a href="#">Th106</a>
Trinter	Florian	Shake-up and shake-off satellites as probe of ultrafast charge delocalization in liquid water	Photon	Molecule	<a href="#">Fr060</a>
Trinter	Florian	Ultrafast temporal evolution of interatomic Coulombic decay in NeKr dimers	Photon	Molecule	<a href="#">Mo036</a>
Tsitsonis	Dimitrios	Chiral Molecular Frame Photoelectron Angular Distributions in achiral formic acid	Photon	Molecule	<a href="#">Fr031</a>
Turnšek	Janez	Characterization of the longitudinal gas density profile in the microfluidic gas cell	Photon	Atom	<a href="#">Fr001</a>
Tyagi	Rohit	L-MM Auger electron emission in Arq <sup>+</sup> - Ar Collision	Heavy	Atom	<a href="#">We104</a>
Ugo Ancarani	Lorenzo	Molecular ionization cross-sections using complex Gaussian representations of the continuum	Lepton	Molecule	<a href="#">Mo068</a>
Ugo Ancarani	Lorenzo	Single ionization of helium by protons in the parabolic quasi-Sturmians approach	Heavy	Atom	<a href="#">Th095</a>
Umer	Haadi	Electron Scattering Cross Sections for Neutral and Doubly-Charged Tin	Lepton	Atom	<a href="#">Fr077</a>
Urbain	Xavier	Mutual neutralization in collision of Na <sup>+</sup> with O <sup>-</sup> and S <sup>-</sup>	Heavy	Ion	<a href="#">Th118</a>
Vallières	Simon	High Dose-Rate MeV Electron Beam from a Tightly-Focused Femtosecond IR Laser in Ambient Air: A Radiation Safety Issue	Photon	Molecule	<a href="#">Th041</a>
Van Sa Lam	Huynh	Differentiating Molecular Structures using Laser-induced Coulomb Explosion Imaging	Photon	Molecule	<a href="#">Fr041</a>
Van Sa Lam	Huynh	Direct signatures of coherent bending vibrations observed using laser-induced Coulomb explosion imaging	Photon	Molecule	<a href="#">Mo040</a>
Varma Ravi	Hari	Resonant intercluster Coulombic decay in the photoionization of Na <sub>20</sub> confined inside C <sub>240</sub>	N/A	Cluster	<a href="#">Fr027</a>
Varma Ravi	Hari	Elucidating geometrical features of e-C <sub>60</sub> interaction from their elastic scattering spectra	N/A	Cluster	<a href="#">Mo076</a>
Varma Ravi	Hari	Angular distribution, spin polarisation and time delay studies of the potassium 4s orbital in the vicinity of Cooper minimum	N/A	Atom	<a href="#">We003</a>
Vasconcelos	Debora	How does the solvation affect molecular ultrafast dissociation ?	Photon	Molecule	<a href="#">Mo045</a>
Verma	Punita	Probing the formation of quasi-molecules in collisions of Krq <sup>+</sup> -ion with Pb and Bi	Heavy	Atom	<a href="#">Mo094</a>
Wang	Yanlan	Precise control of intracycle interference with a phase-stabilized polarization-gated laser pulse	Photon	Atom	<a href="#">Fr008</a>
Wang	Tian	Disentangling interferences in the photoelectron momentum distribution from strong-field ionization	Photon	Atom	<a href="#">Fr020</a>
Wang	Yuan	Tunable spectral shift of high-order harmonic generation in atoms by a plasmon-assisted shaping pulse	Photon	Atom	<a href="#">Mo063</a>
Wang	Kedong	Photoionization dynamical parameter for the radicals using B-spline R-matrix method	Lepton	Molecule	<a href="#">We028</a>
Wang	Enliang	Isomerization dynamics of triatomic molecules driven by the electron-impact	Lepton	Molecule	<a href="#">We087</a>
Wang	Jiarong	Sequential deprotonation of the allene trication produced by He <sup>2+</sup> impact	Heavy	Molecule	<a href="#">We115</a>
Wang	Shuxing	Precise determination of 2s <sub>2</sub> 2p <sub>5</sub> → 2s 2p <sub>6</sub> transition energy in fluorine-like nickel utilizing a low-lying dielectronic resonance	Lepton	Ion	<a href="#">We130</a>

Last name	First name	Abstract Title	Abstract Topic (Projectile)	Abstract Topic (Target)	Poster #
Wanie	Vincent	Capturing electron-driven molecular chirality	Photon	Molecule	<a href="#">Th047</a>
Watanabe	Noboru	Theoretical electronic excitation cross sections of $\text{CCl}_4$	Lepton	Molecule	<a href="#">Fr089</a>
Watanabe	Noboru	Symmetry breaking in dissociative ionization of symmetric molecules by electron impact	Lepton	Molecule	<a href="#">We086</a>
Weber	Anne	Optical tunnelling without a barrier?	Photon	Atom	<a href="#">Mo012</a>
Wei Nie	Zhi	Investigation of the valence-shell excitations of $\text{CS}_2$ by high-energy electron scattering	Heavy	Molecule	<a href="#">We091</a>
Wells	Eric	Initial-site characterization of hydrogen migration in ethanol	Photon	Molecule	<a href="#">Th034</a>
Wesley Walter	C	Lifetimes of excited states of the lanthanum negative ion	Photon	Ion	<a href="#">Fr132</a>
Wilhelm	Richard	Can the ion charge state be observed while travelling within a solid?	Heavy	Surface	<a href="#">Fr112</a>
Wilhelm	Richard	Ultrafast electron-stimulated desorption to form ion pulses for time-resolved ion surface collision experiments	Heavy	Ion	<a href="#">Mo138</a>
Wong	Nicholas	Coincidence Measurements of Photodouble Ionization of Thiophene	Photon	Molecule	<a href="#">Fr051</a>
Wu	Ruiqi	Pressure-dependent Photoluminescence of 0D/2D Heterostructures	Photon	Surface	<a href="#">Mo058</a>
Xie	Luyou	Theoretical study on Dielectronic recombination process and X-ray line polarization of B-like Ar ion	Photon	Ion	<a href="#">Fr074</a>
Xie	Luyou	Theoretical investigation of KLL dielectronic-recombination processes of highly charged Cu ions	Photon	Ion	<a href="#">Th069</a>
Xie	Kevin	Emergent s-wave dimers near a p-wave Feshbach resonance in a strongly confined Fermi gas	Heavy	Atom	<a href="#">Th123</a>
Xing	Da	State-selective single electron capture in 9 keV $\text{N}^+-\text{He}$ collisions	Heavy	Atom	<a href="#">Th092</a>
Xu	Weiqing	Ultrafast rotational energy transfer initiating by Coulomb explosion in two-body dissociation of $\text{CO}_2^{3+}$	Photon	Molecule	<a href="#">Mo102</a>
Xu	Qi	Femtosecond laser assisted chemical ionization mass spectrometry	Photon	Molecule	<a href="#">Th043</a>
Xu Du	Jin	Quasi-chirp-free isolated attosecond pulse generation from atoms by optimized two near-infrared pulses and their second harmonic fields	Photon	Atom	<a href="#">Mo015</a>
Yadav	Jatin	Exploring Three Body Fragmentation of Acetylene Trication	N/A	Molecule	<a href="#">Fr107</a>
Yamashita	Takuma	Recent progress of muon catalyzed fusion study: I. new kinetics model with muonic molecular resonances	Lepton	Atom	<a href="#">Mo065</a>
Yamashita	Takuma	Calculation and Wigner law analysis of scattering cross sections for collisions of antihydrogen atom with excited positronium	Lepton	Atom	<a href="#">Th063</a>
Yamazaki	Masakazu	A binary (e, 2e) study on Ne at incident electron energies up to 4 keV: Asymptotic behavior of the (e, 2e) cross section to its high energy limits	Lepton	Atom	<a href="#">Fr081</a>
Yamazaki	Kaoru	Scaling law on the x-ray induced nonadiabatic transition in aromatic molecules	Photon	Molecule	<a href="#">We044</a>
Yang	Yugang	Photoionization of H Debye plasmas in strong field approximation	Photon	-Other-	<a href="#">Fr059</a>
Yang	Bian	Nonradiative electron capture in collisions of fast $\text{Xe}^{54+}$ with Kr and Xe	Heavy	Atom	<a href="#">Th088</a>
Yasuda	Runa	Characterization of a double torsion pendulum for detecting torque exerted by the spins of gaseous atoms	Heavy	Surface	<a href="#">Fr119</a>
Yip	Frank	Fully differential double photoionization of linear molecules beyond $\text{H}_2$	Photon	Molecule	<a href="#">Fr042</a>

Last name	First name	Abstract Title	Abstract Topic (Projectile)	Abstract Topic (Target)	Poster #
Yoshida	Shuhei	Autoionization of two-electron-excited 88Sr 5pn <sub>l</sub> j states	Photon	Atom	<a href="#">We021</a>
Yu Ma	Huan	Few-photon single ionization of cooled rubidium in the over-the-barrier regime	Photon	Atom	<a href="#">We016</a>
Yuan	Hang	Fragmentation Dynamics of a Carbon Dioxide Dication Produced by Ion Impact	Heavy	Molecule	<a href="#">Fr103</a>
Yuan	Jianmin	Intensity dependence of the double ionization dissociation of argon dimers in the fields of femtosecond laser pulses	Photon	Molecule	<a href="#">We033</a>
Yuan Lin	Chih	High-order harmonic generation of alkali metals in few-cycle laser pulses	Photon	Atom	<a href="#">Mo021</a>
Z Msezane	Alfred	Electron elastic scattering by Bk and Cf atoms: polarization effects	Lepton	Atom	<a href="#">We082</a>
Zeng	Jiaolong	Effect of transient spatial localization on electron impact excitation and ionization processes in dense plasmas	Heavy	Ion	<a href="#">We066</a>
Zhang	Shaofeng	Photoionization of a quantum grating formed by a single atom	Photon	Atom	<a href="#">Fr025</a>
Zhang	Chunyu	The effect of electron correlation on trielectronic recombination rate coefficients for Be-like argon	N/A	Atom	<a href="#">Fr073</a>
Zhang	Susu	Investigation of the spatial distribution of atomic high-order harmonic generation using the bohmian trajectories scheme	Photon	Atom	<a href="#">Mo022</a>
Zhang	Hongqiang	Focusing an electron beam by the self-arranged formation of a quadrupole-like electrostatic field inside a quartz capillary of square cross section	Lepton	Surface	<a href="#">Mo085</a>
Zhang	Weiyu	Time-resolved Imaging of CH <sub>4</sub> Fragmentation in Strong Laser Fields	Photon	Molecule	<a href="#">Th049</a>
Zhang	Xuemei	Theoretical study on radii of neutral atoms and singly charged negative ions	Heavy	Ion	<a href="#">Th130</a>
Zhang	Dongdong	New source for tuning the effective Rabi frequency in multiphoton ionization	Lepton	Atom	<a href="#">We004</a>
Zhang	Shiping	Theoretical investigation of electron-impact ionization of W <sup>8+</sup> ion	Heavy	Ion	<a href="#">We069</a>
Zhang	Fangjun	Theoretical study on the electron collision ionization of Sn <sup>11+</sup> ions	Heavy	Ion	<a href="#">We071</a>
Zhang (万凯李)	Dongdong	Phase-resolved photoelectron-imaging of potassium atoms in two-color laser fields	Photon	Atom	<a href="#">Th015</a>
Zhao	Jingjing	Unexpected enhanced terahertz radiation in two-foci cascading plasmas	Photon	Atom	<a href="#">Fr055</a>
Zhao	Wenchao	Fragmentation dynamics of BrCN <sub>q</sub> <sup>+</sup> (q = 2-6) induced by 1-keV electron impact	Lepton	Molecule	<a href="#">Th080</a>
Zhou	Yueming	Attosecond-resolved Non-dipole Electron Dynamics	Photon	Atom	<a href="#">Fr006</a>
Zhou	Lianrong	Cold molecular dynamics and chemical reactions of H <sub>2</sub> (D <sub>2</sub> ) in strong laser fields	Photon	Molecule	<a href="#">Th110</a>
Zhu	Binghui	Radiative Recombination Studies for Bare Lead Ions Interacting with Low-Energy Electrons	Heavy	Atom	<a href="#">We076</a>
Žitnik	Matjaž	Interferences due to Auger decay of a doubly excited atomic state	Photon	Atom	<a href="#">Th023</a>
Znotins	Aigars	Electron recombination of deuterated triatomic hydrogen ions at the Cryogenic Storage Ring	Lepton	Ion	<a href="#">We075</a>
Zoltán	Juhász	Irradiation of Oxygen-Bearing Ices on Top of Elemental Sulphur Layers: Implications for Astrophysical Sulphur Chemistry	Heavy	-Other-	<a href="#">Fr124</a>
Zoltán	Juhász	Molecular-rotation-induced splitting of the binary ridge in the velocity map of sub-eV H <sup>+</sup> (D <sup>+</sup> ) ions ejected from H <sub>2</sub> (D <sub>2</sub> ) molecules by ion impact	Heavy	Molecule	<a href="#">Th120</a>

Last name	First name	Abstract Title	Abstract Topic (Projectile)	Abstract Topic (Target)	Poster #
Zou	Zhihan	Rescattering sequential multiple ionization of cold Rb	Photon	Ion	<a href="#">We020</a>